POROSITY IN GRAPHITES

Thesis submitted

for the

degree of

Doctor of Philosophy

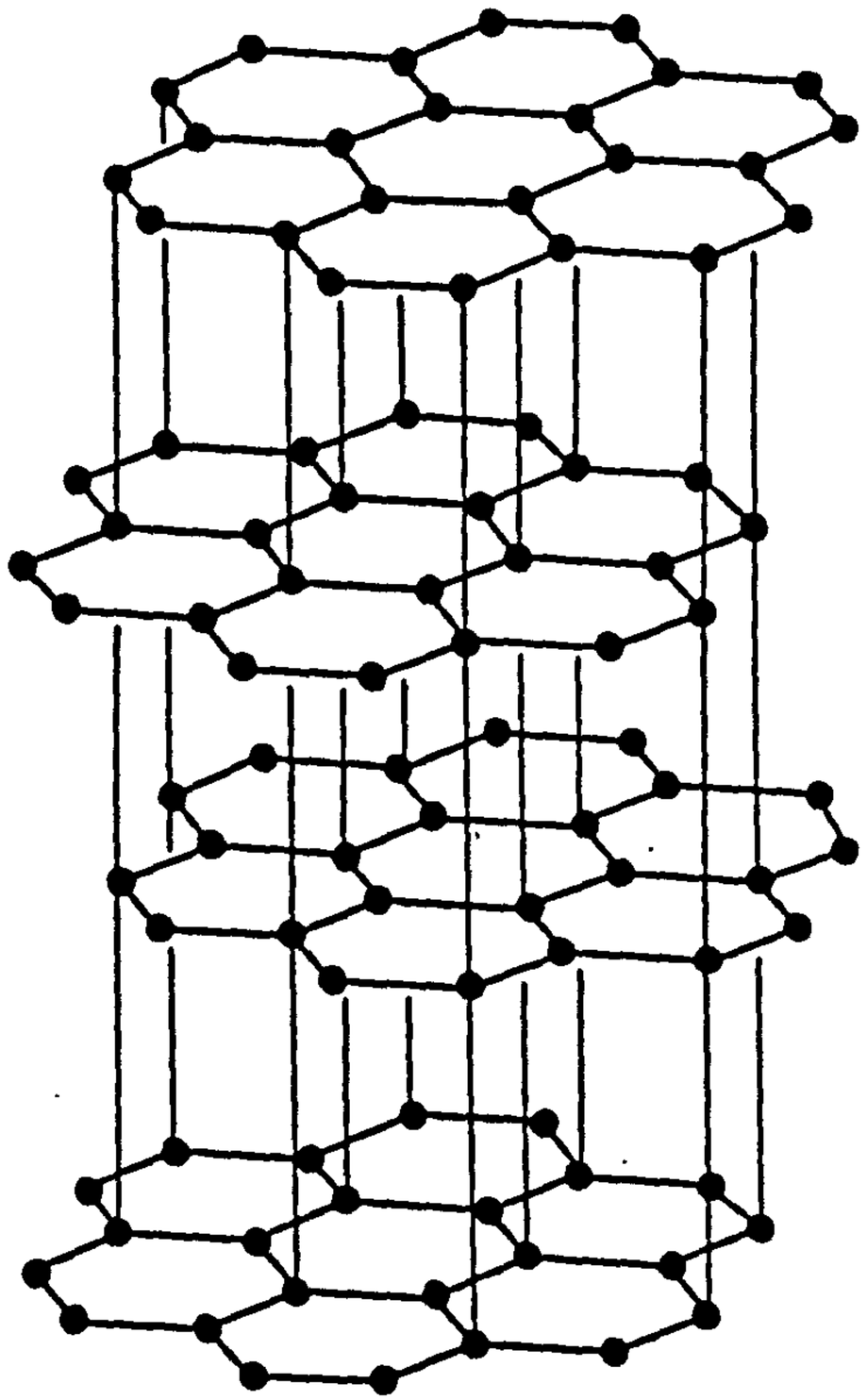
at the

University of Newcastle upon Tyne

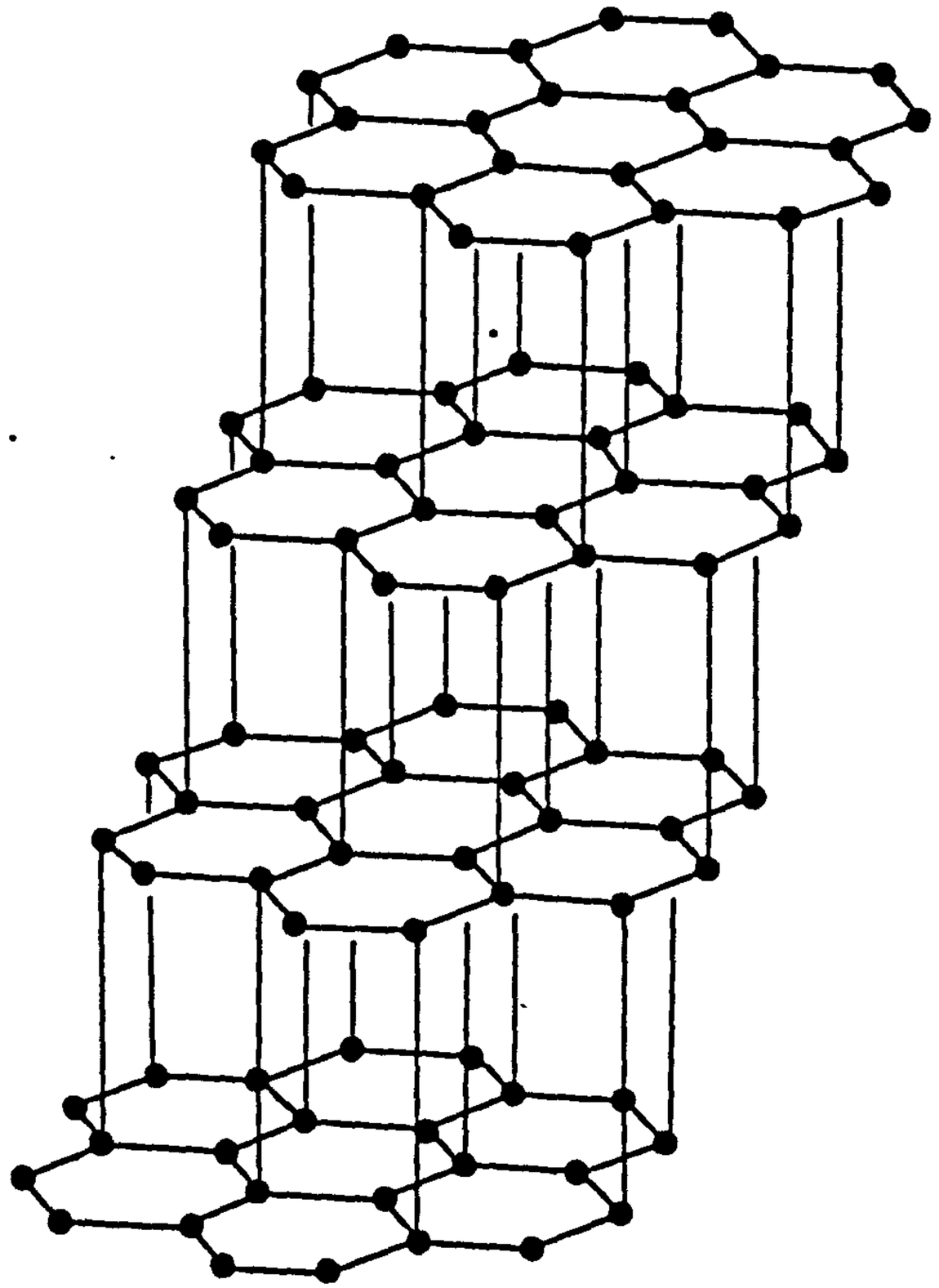
by

MARGARET EVANS (B.Sc)

November, 1978.



a) Hexagonal



b) Rhombohedral

Figure A1. The structure of graphite.

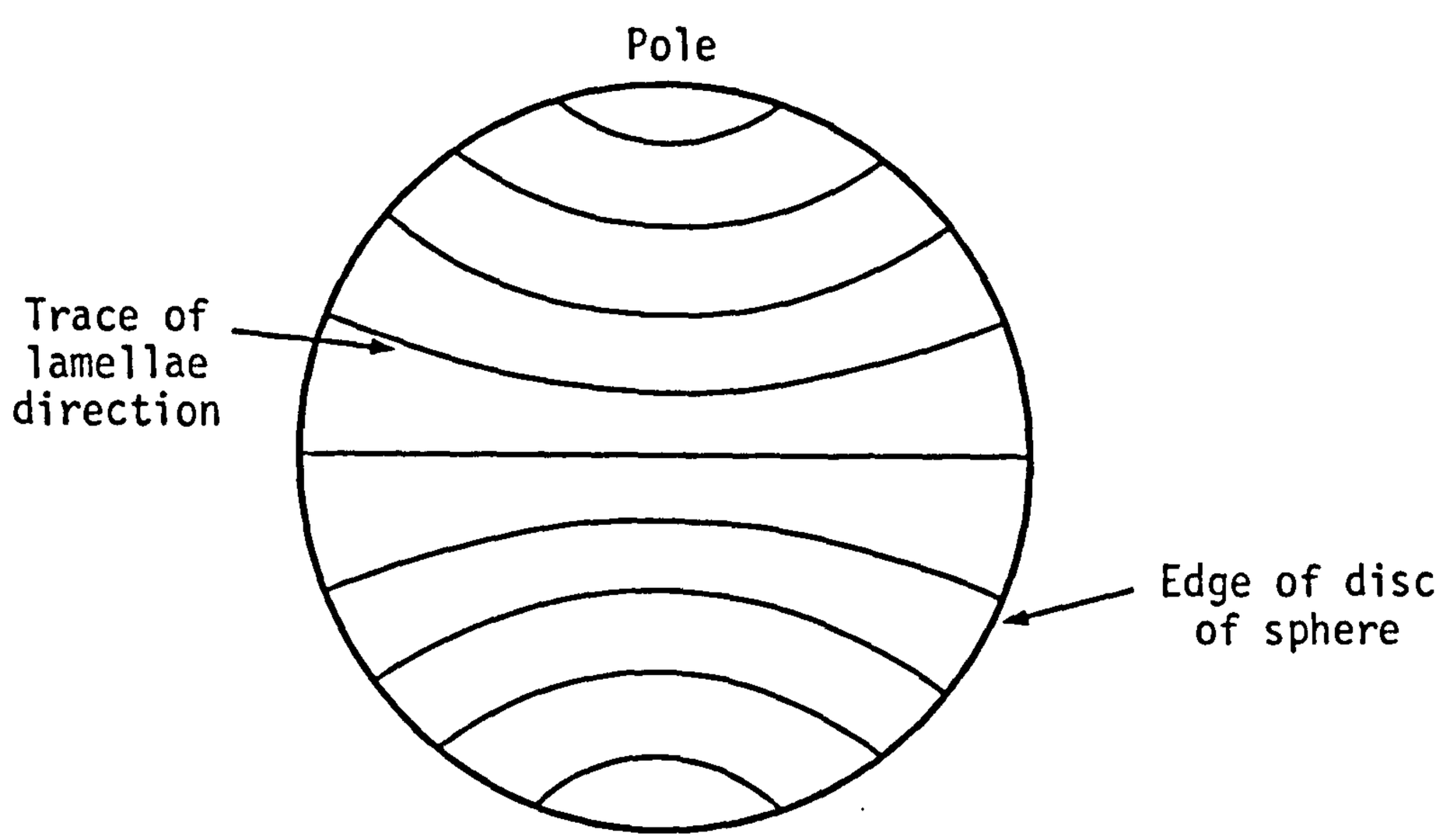


Figure A2. Layer plane arrangement in mesophase sphere.

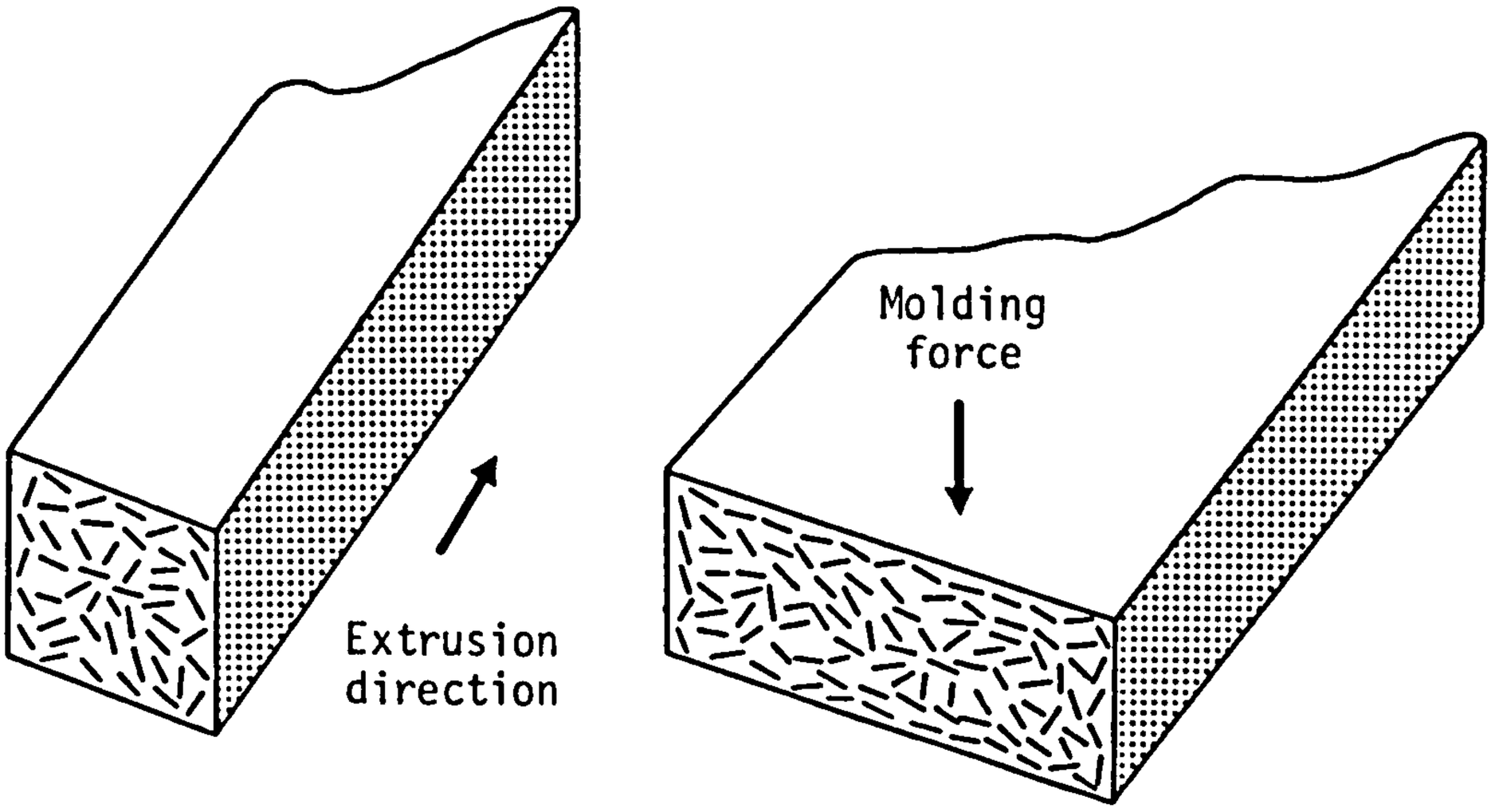


Figure A3. Schematic representation of preferred grain orientation.

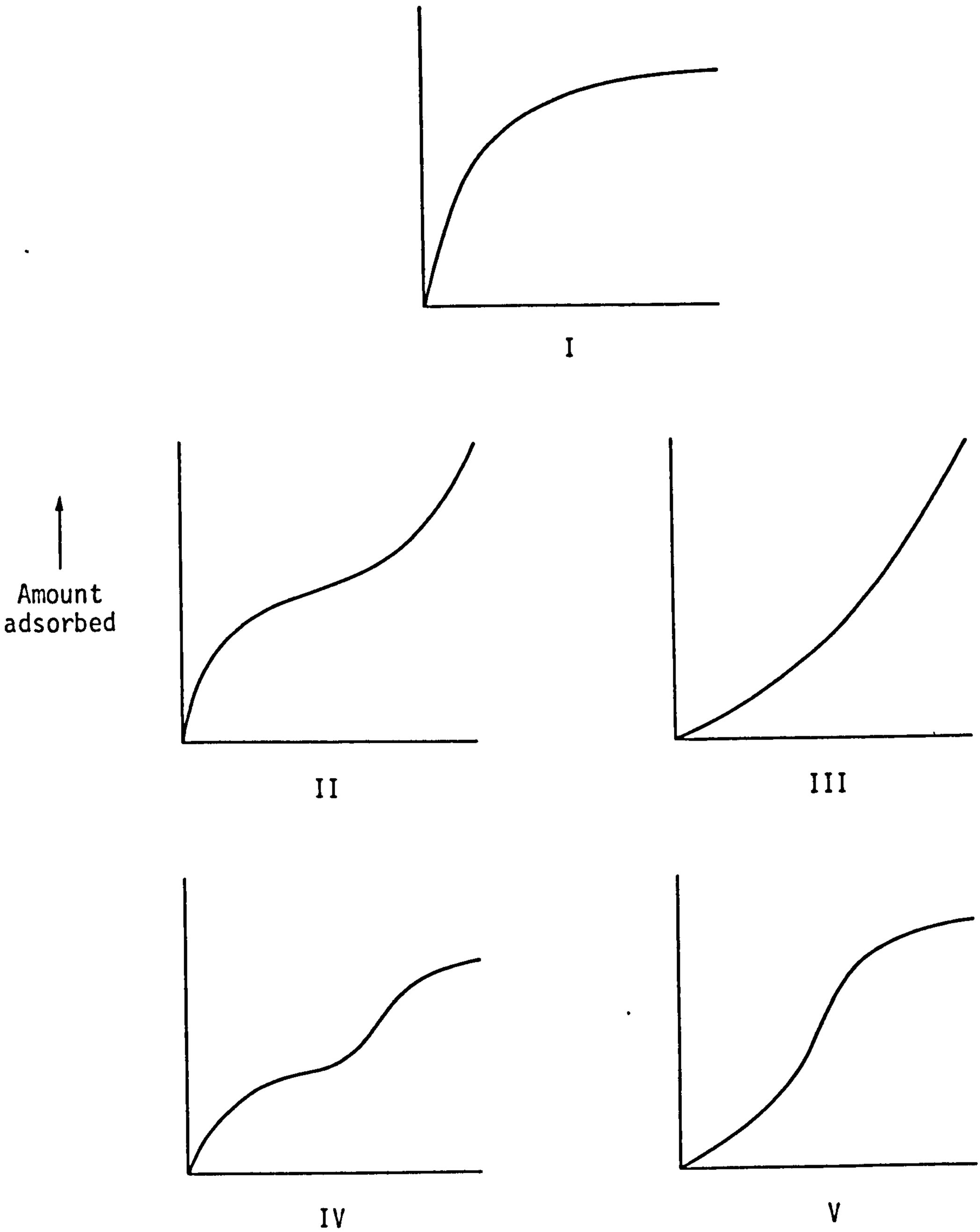


Figure A4. The five types of adsorption isotherms.[51,52]

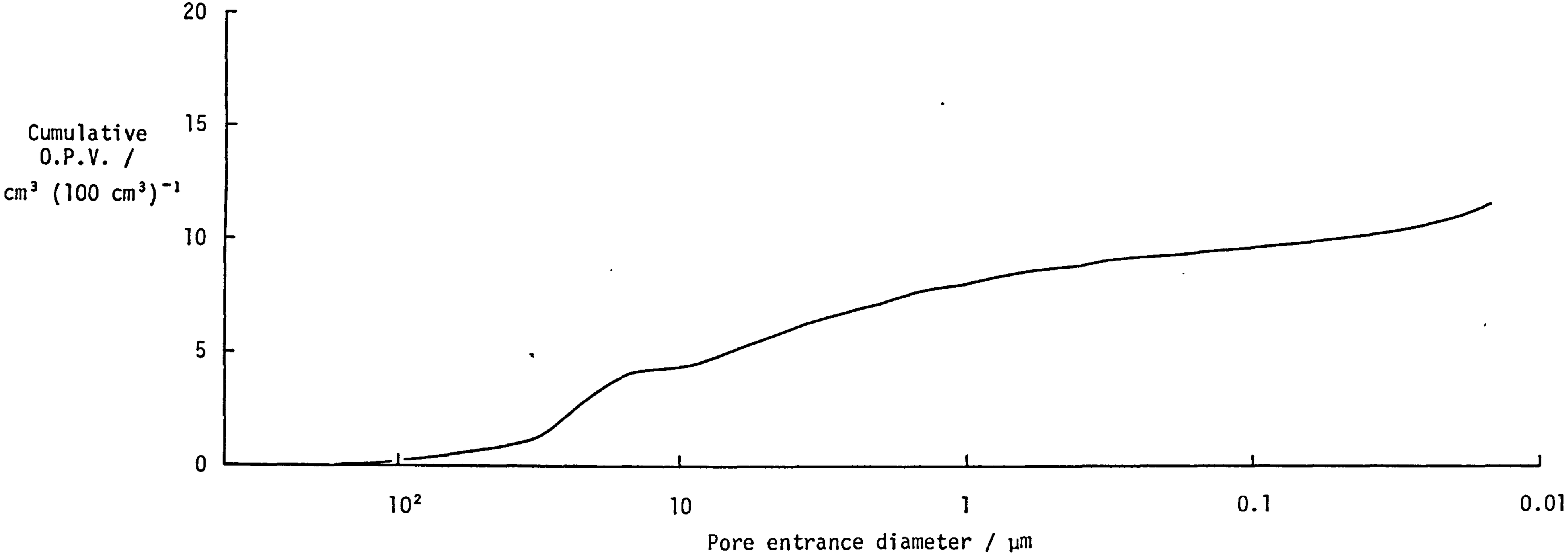


Figure A5. Mercury pore size distribution of virgin AGLMP graphite. Variation of cumulative open pore volume with pore entrance diameter.

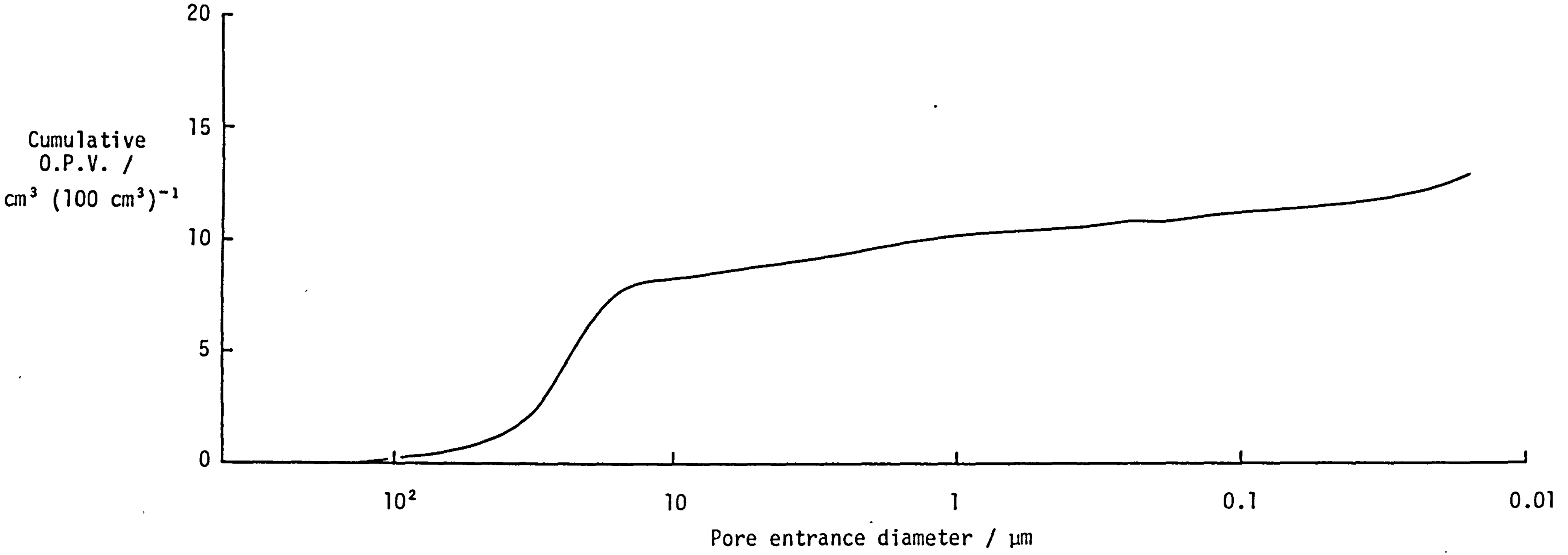


Figure A6. Mercury pore size distribution of virgin BAEL GCMB graphite. Variation of cumulative open pore volume with pore entrance diameter.

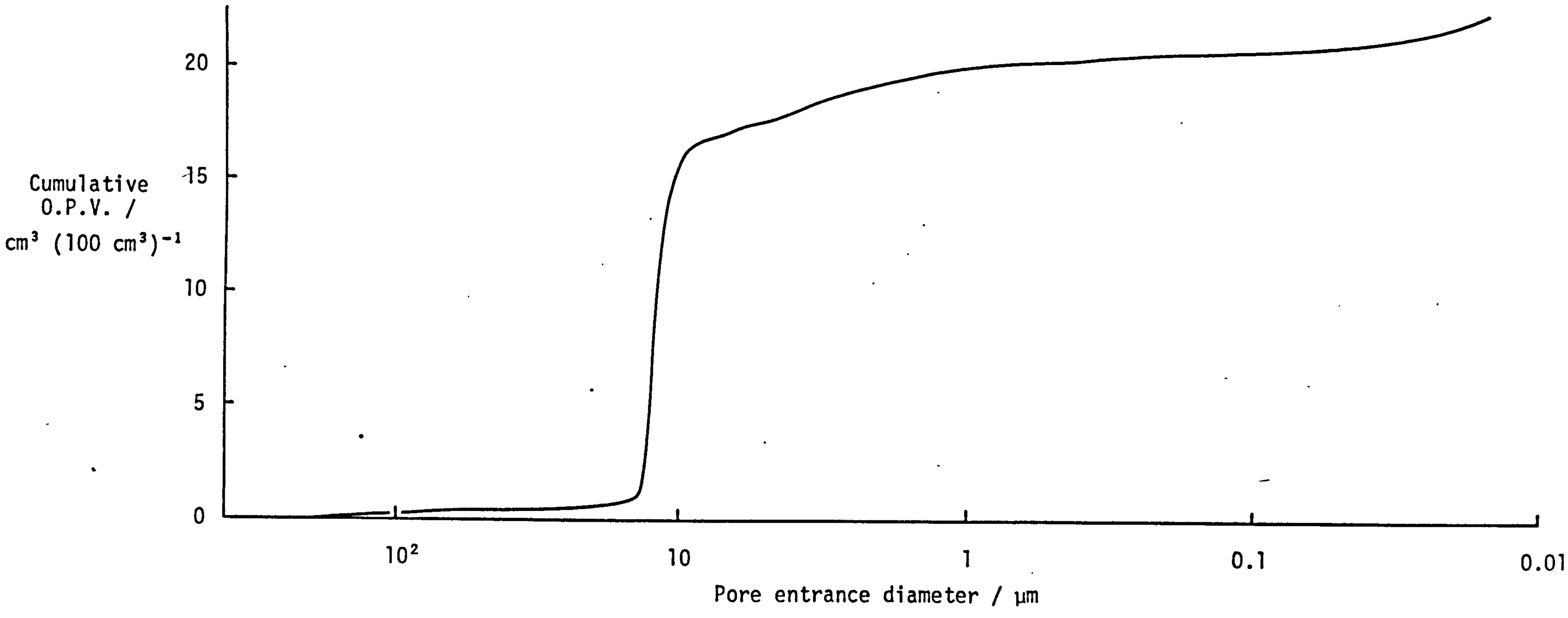


Figure A7. Mercury pore size distribution of virgin AGLHP graphite. Variation of cumulative open pore volume with pore entrance diameter.

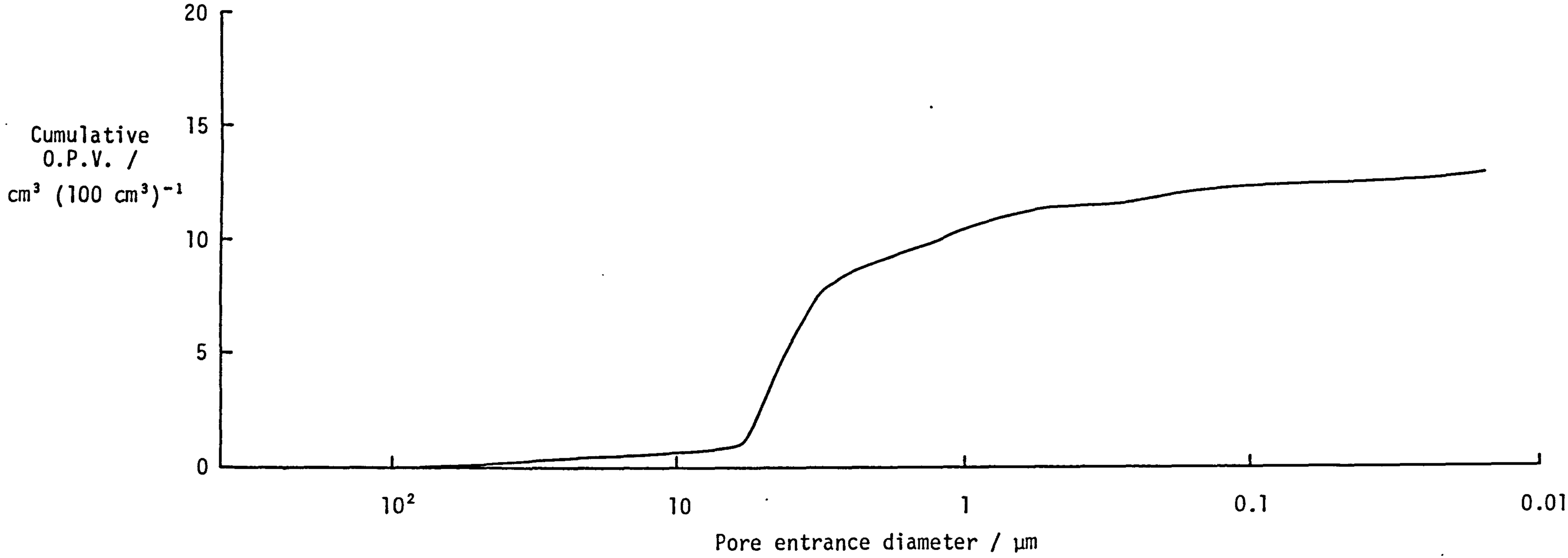


Figure A8. Mercury pore size distribution of virgin Morgans EYC 9106 graphite. Variation of cumulative open pore volume with pore entrance diameter.

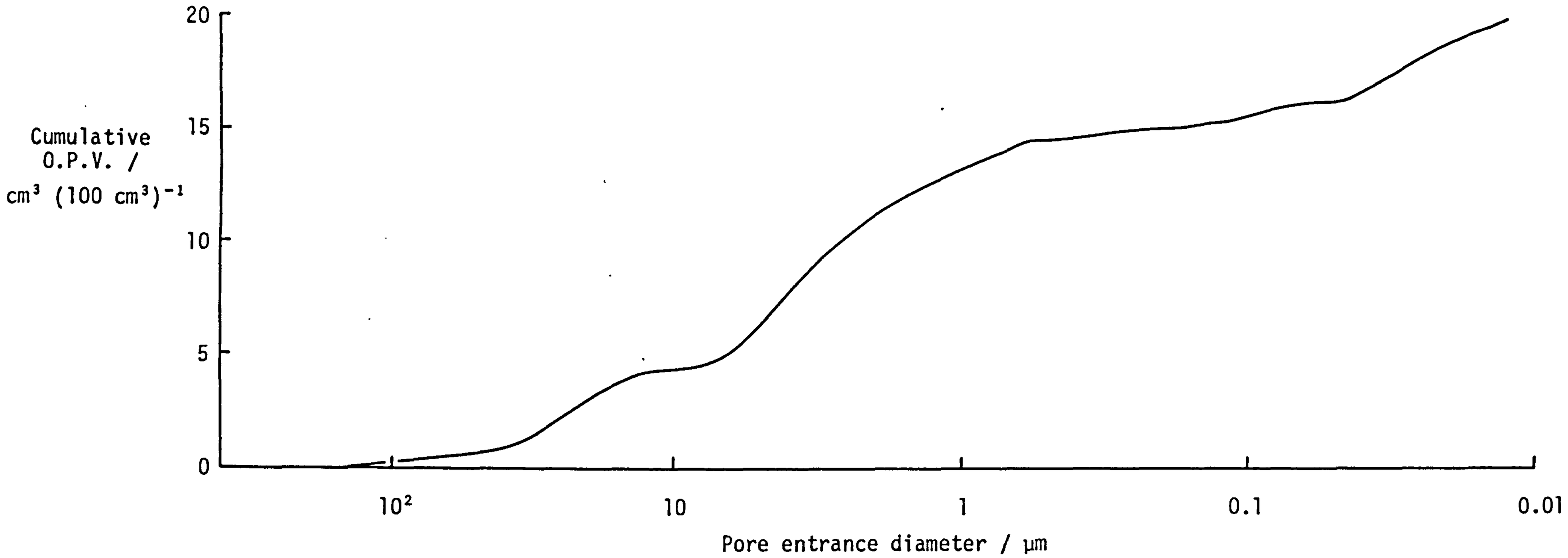


Figure A9. Mercury pore size distribution of virgin Lima graphite. Variation of cumulative open pore volume with pore entrance diameter.

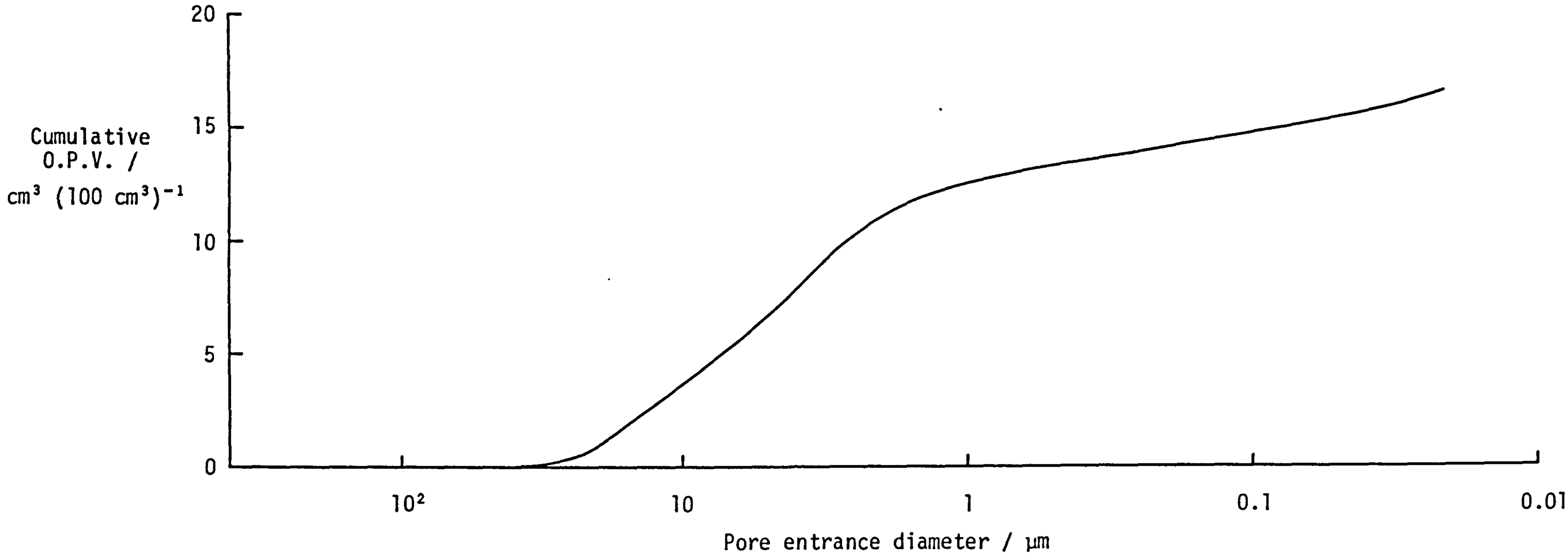


Figure A10. Mercury pore size distribution of virgin PGA L18 graphite. Variation of cumulative open pore volume with pore entrance diameter.

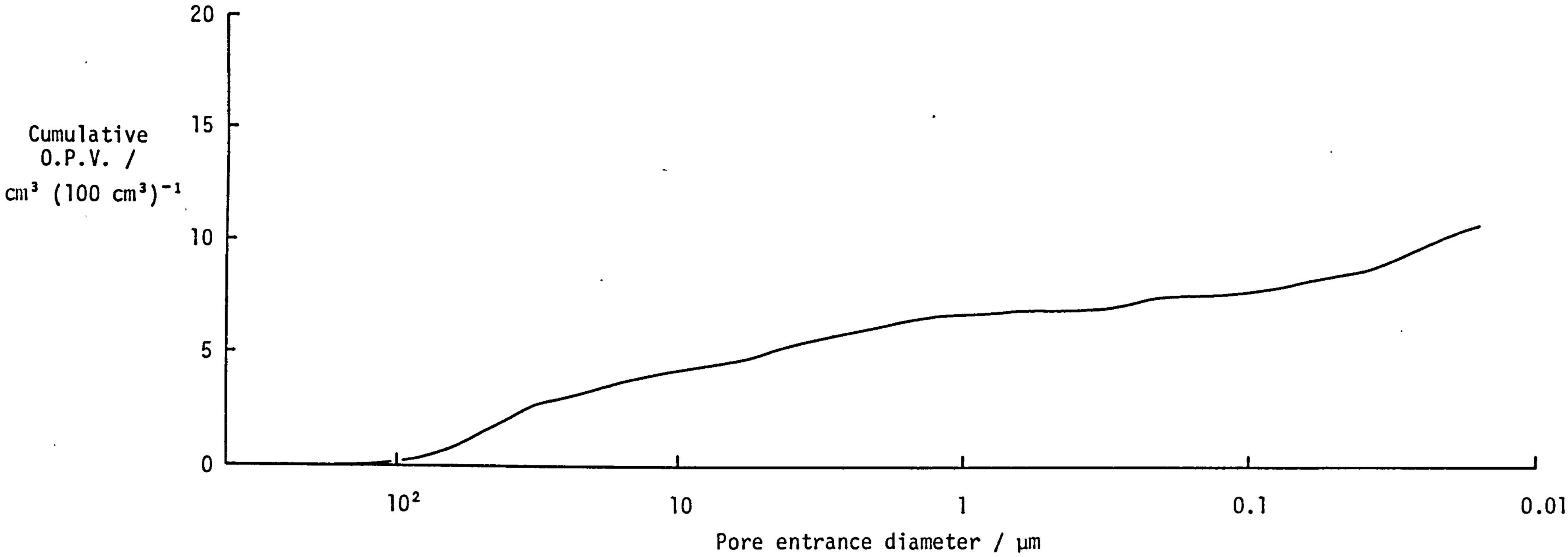


Figure A11. Mercury pore size distribution of virgin BAEL VQMB graphite. Variation of cumulative open pore volume with pore entrance diameter.

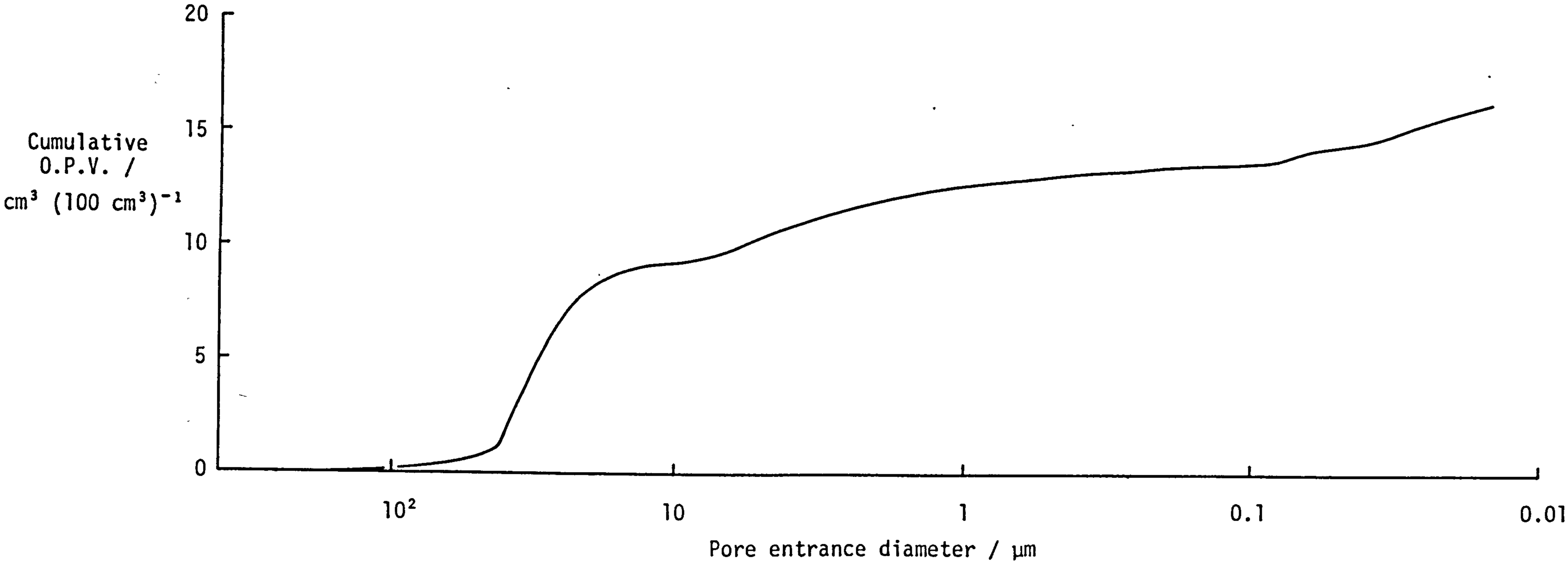
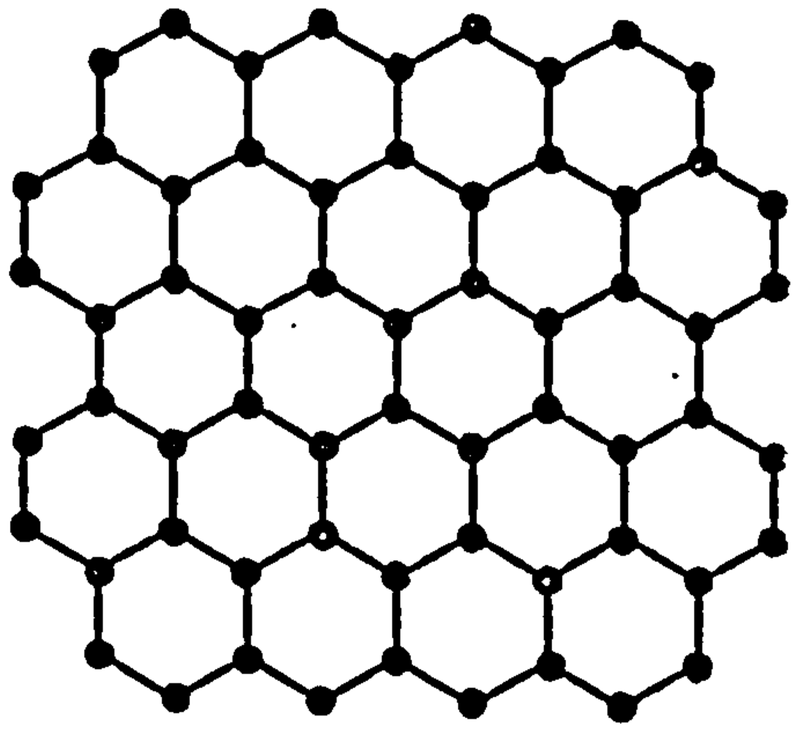
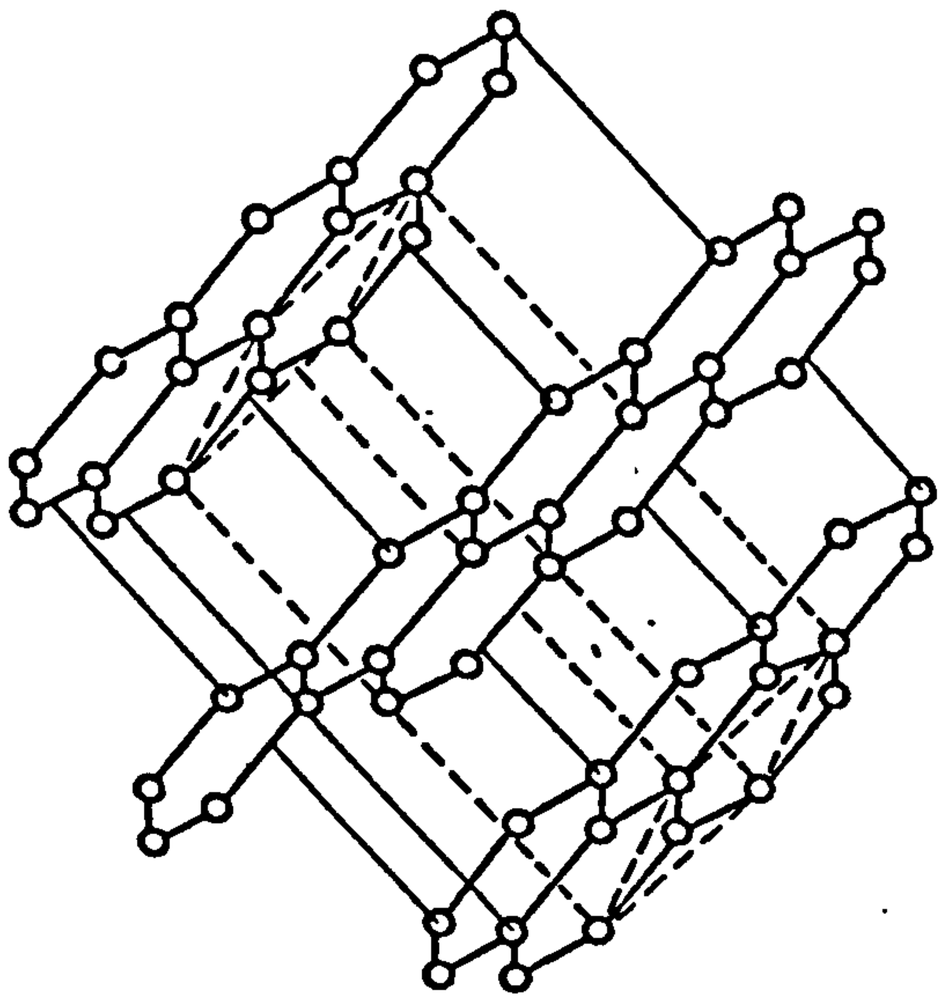


Figure A12. Mercury pore size distribution of virgin BAEL VNMC graphite. Variation of cumulative open pore volume with pore entrance diameter.



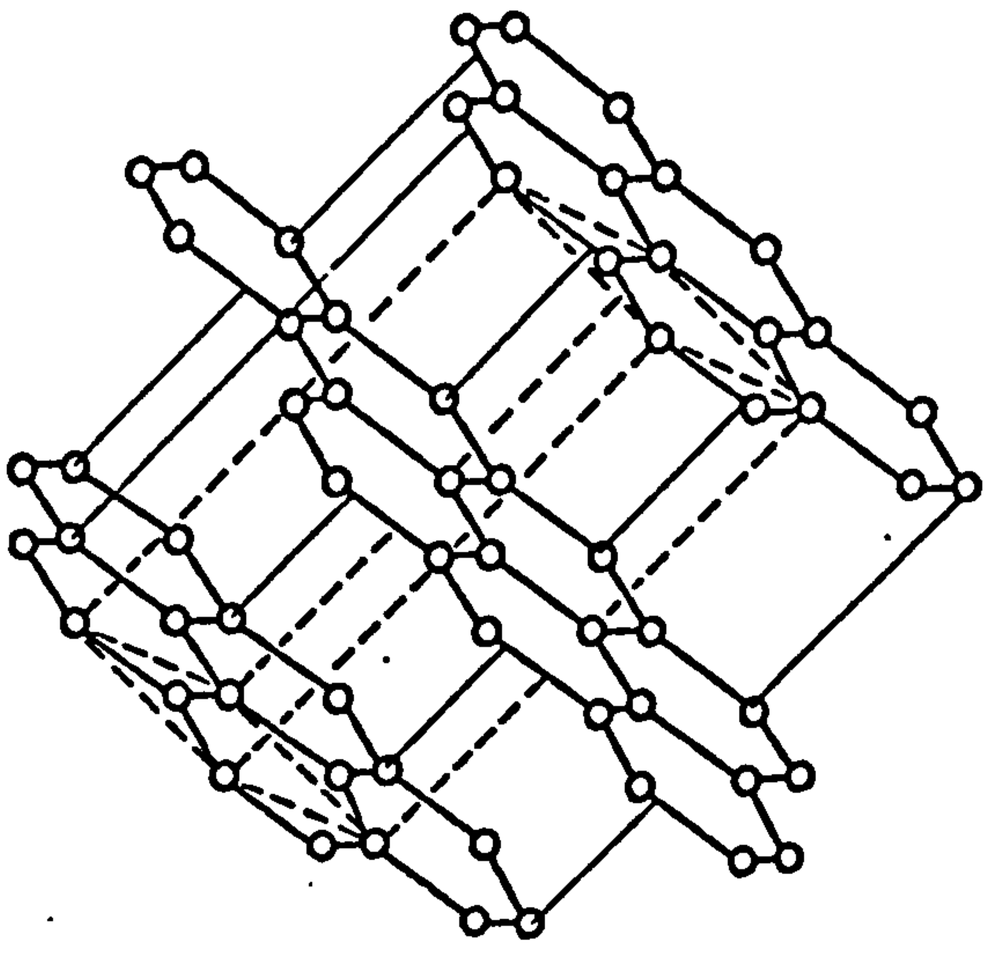
BASAL PLANE (ISOTROPIC)

PURPLE COLOURATION



PRISMATIC EDGE (ANISOTROPIC)

YELLOW COLOURATION.



PRISMATIC EDGE (ANISOTROPIC)

BLUE COLOURATION.

IN EACH CASE THE PLANE OF LIGHT IS PERPENDICULAR TO THE PLANE OF THE PAPER.

Figure 1. Relation between colours produced in an optical microscope using plane polarized light, and the orientation of the graphite planes.

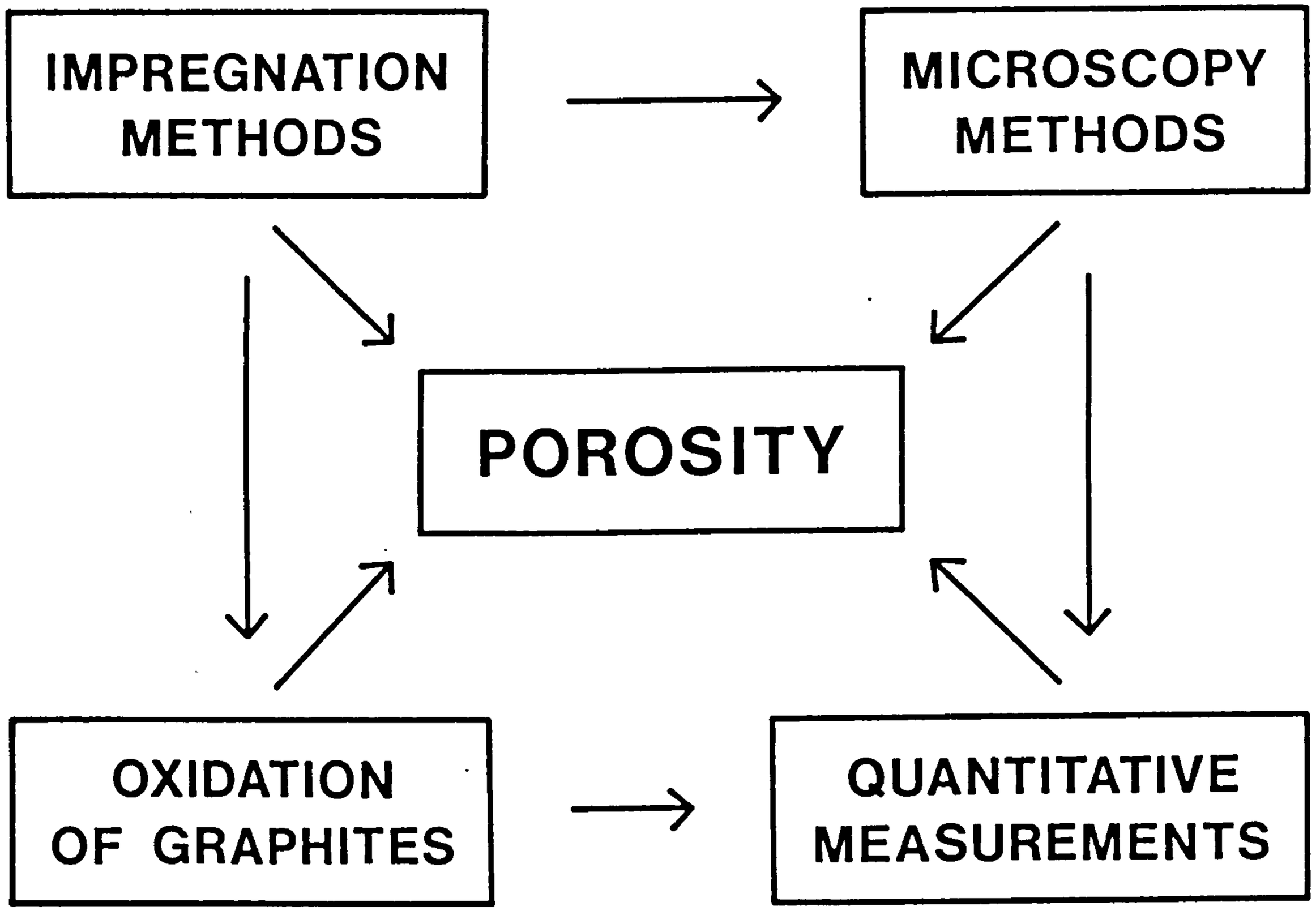


Figure 2. Methods of Assessment of the Porosity in Graphite.

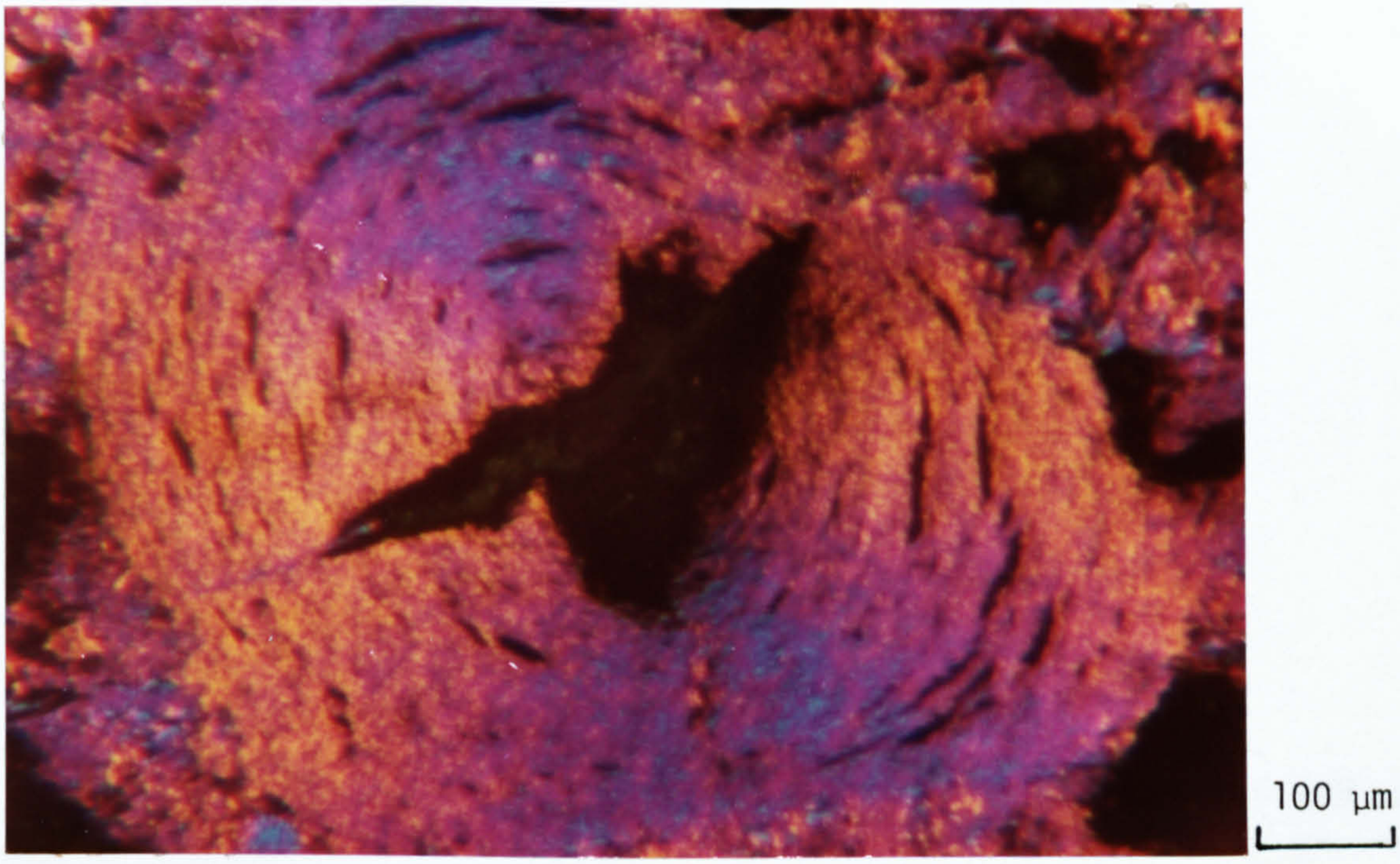


Figure 3. Optical micrograph of virgin AGLMP graphite.

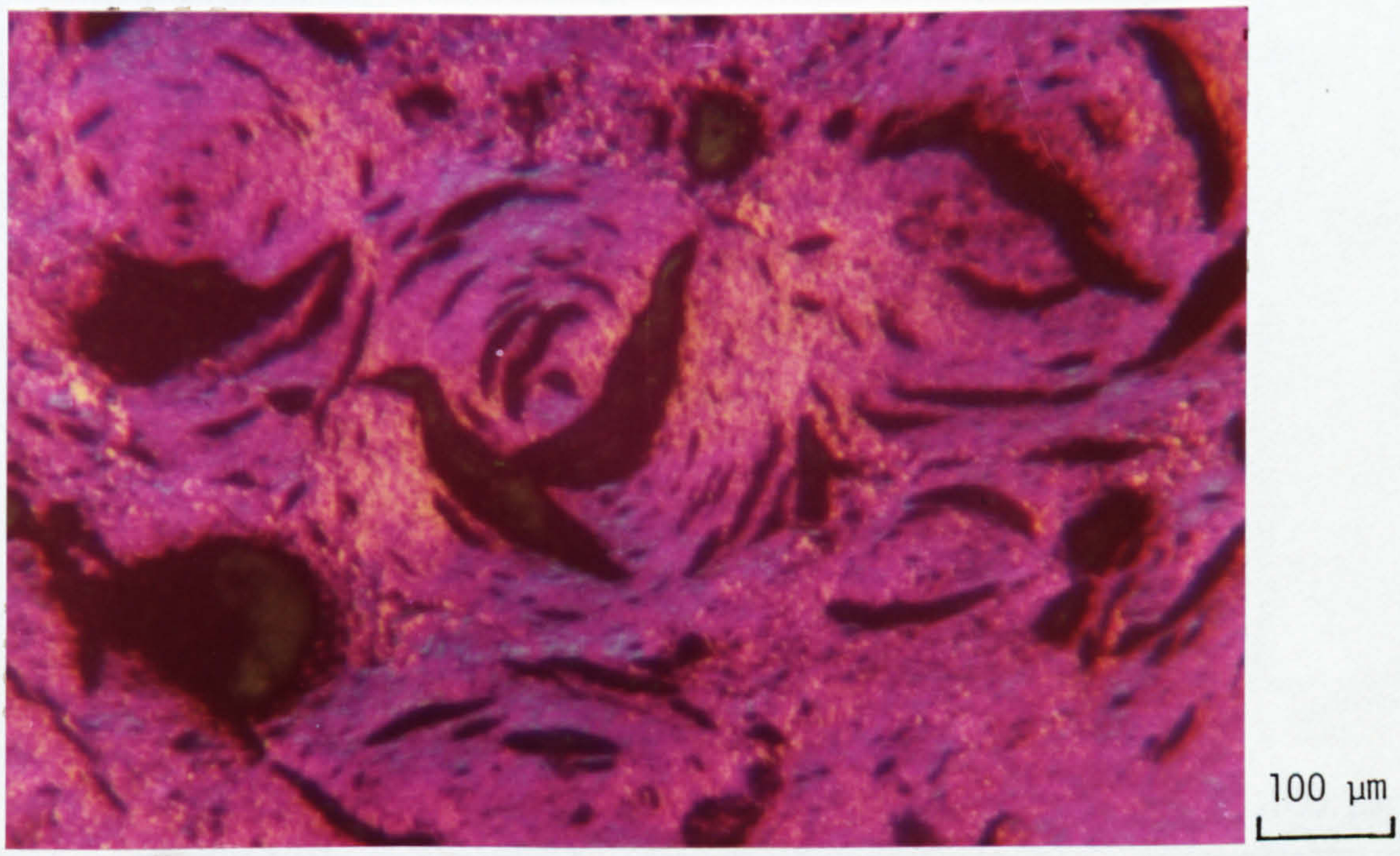


Figure 4. Optical micrograph of virgin GCMB graphite.

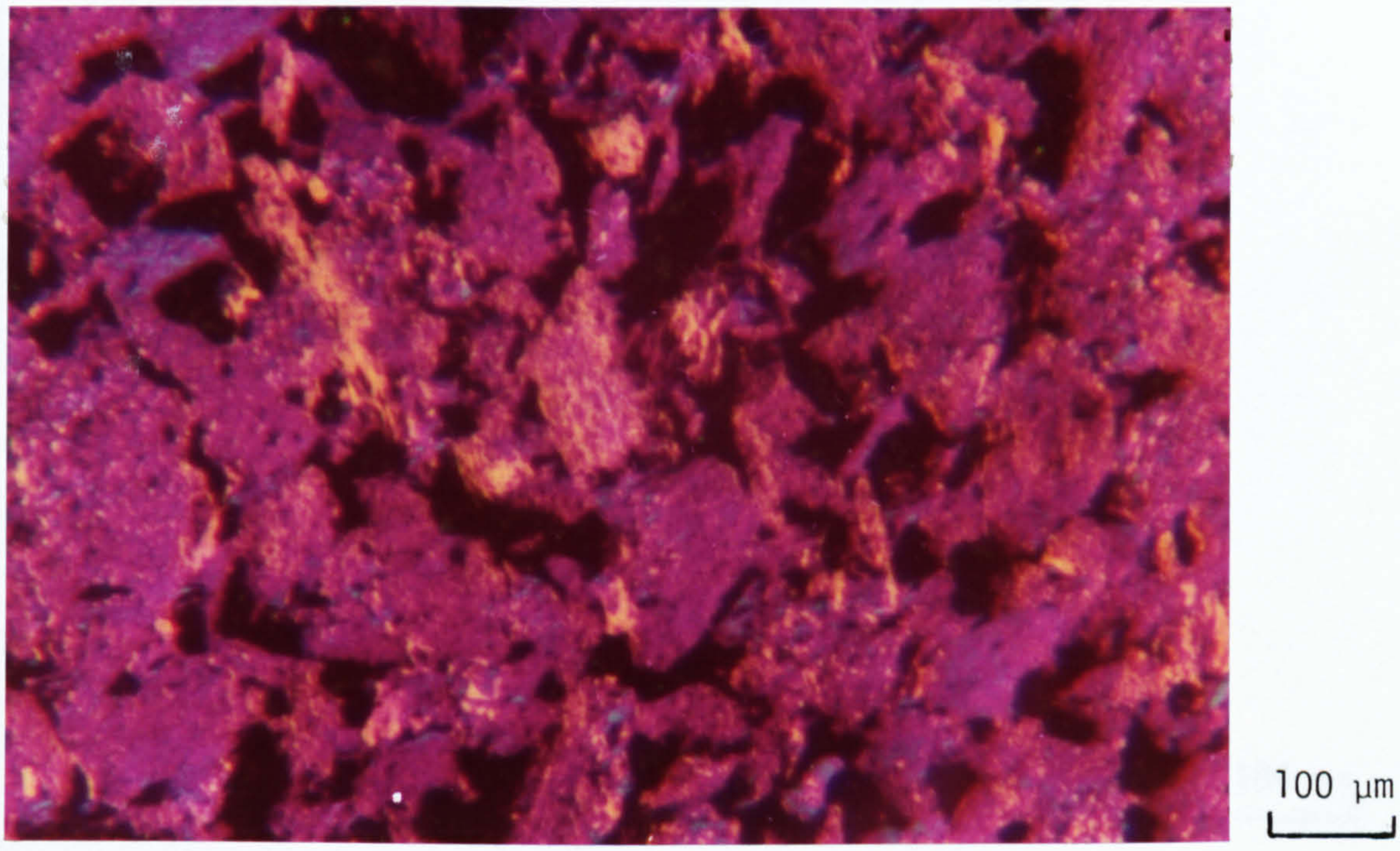


Figure 5. Optical micrograph of virgin AGLHP unipore graphite.

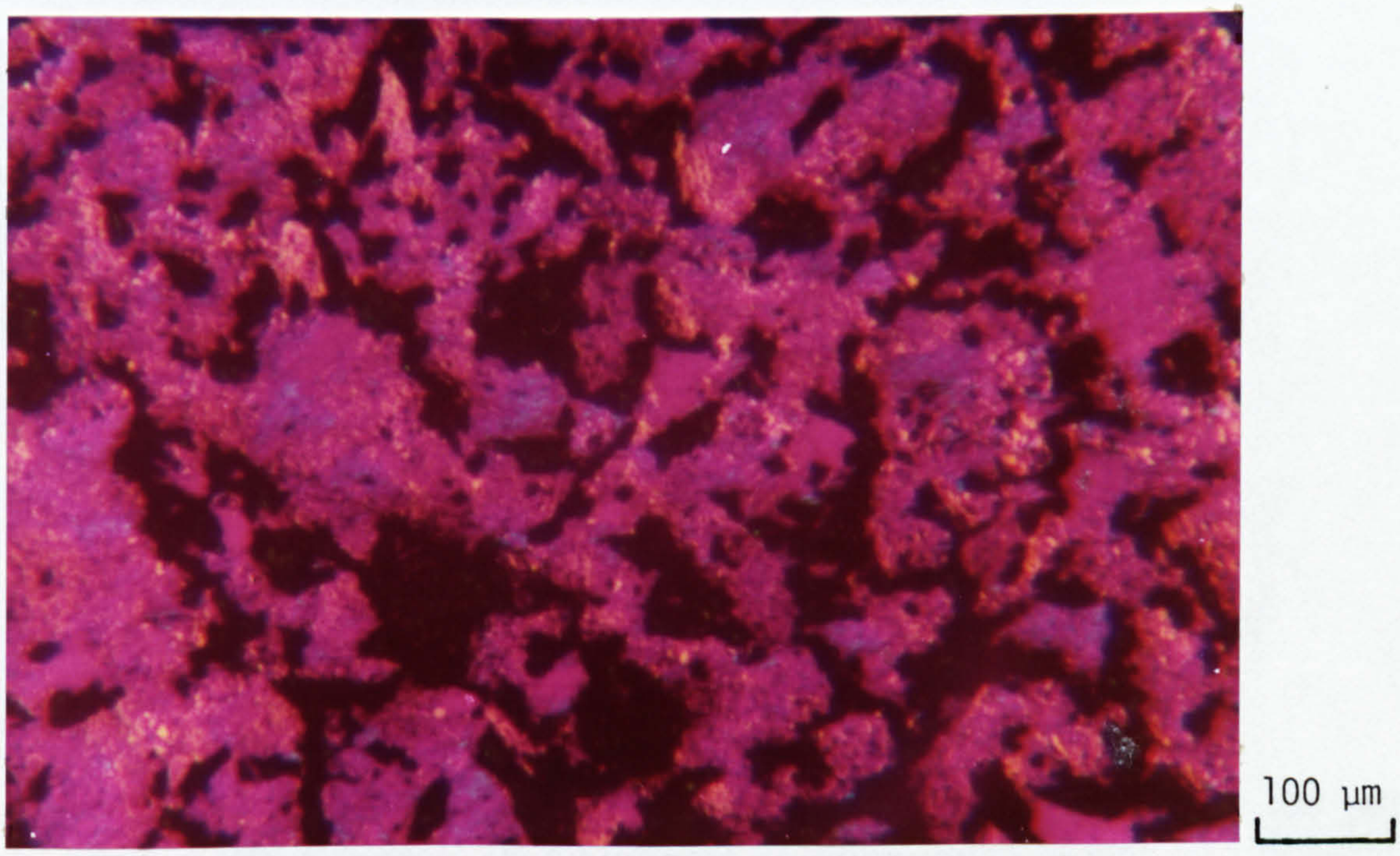


Figure 6. Optical micrograph of virgin Morgans EYC 9106 unipore graphite.

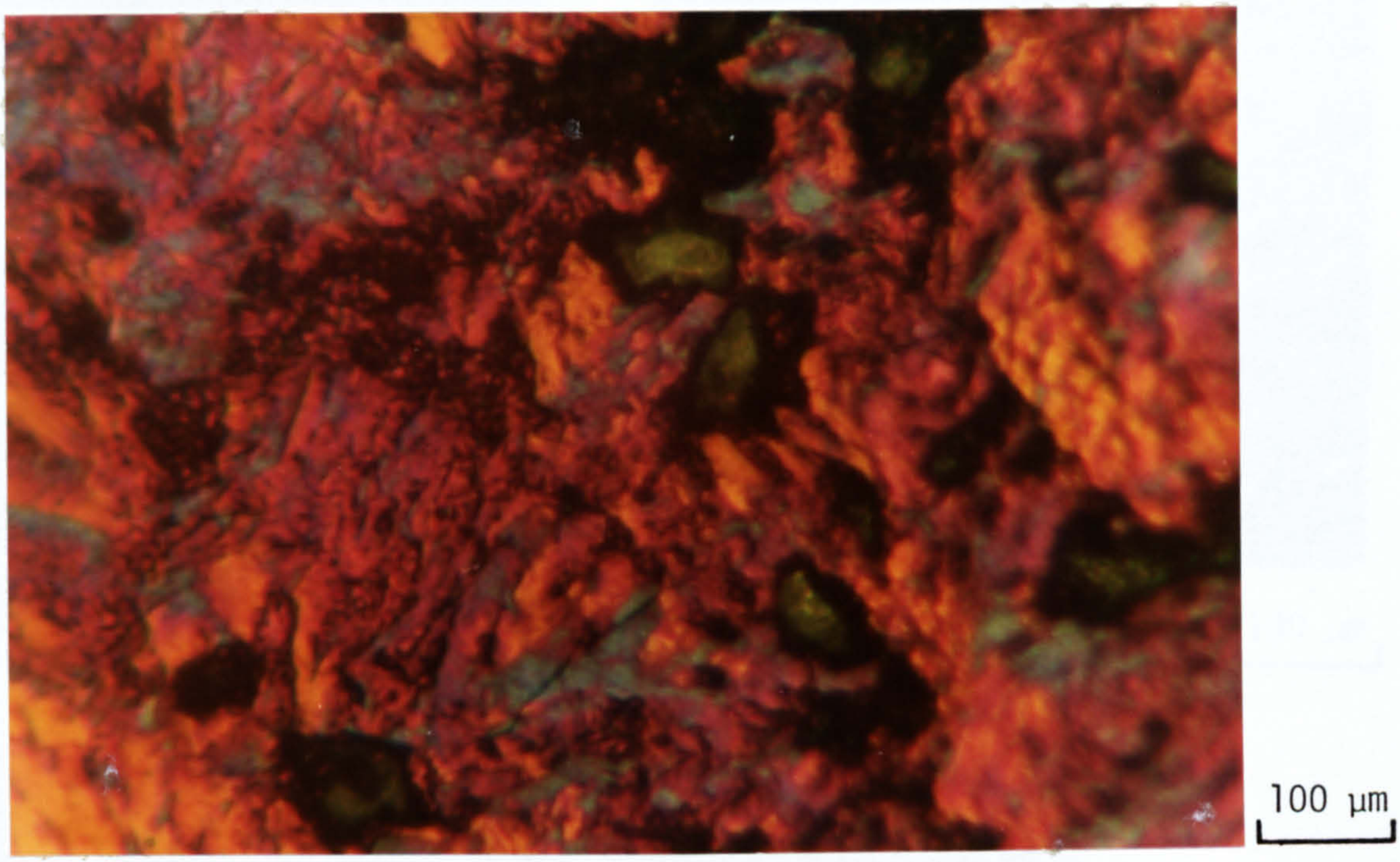


Figure 7. Optical micrograph of virgin Lima graphite.

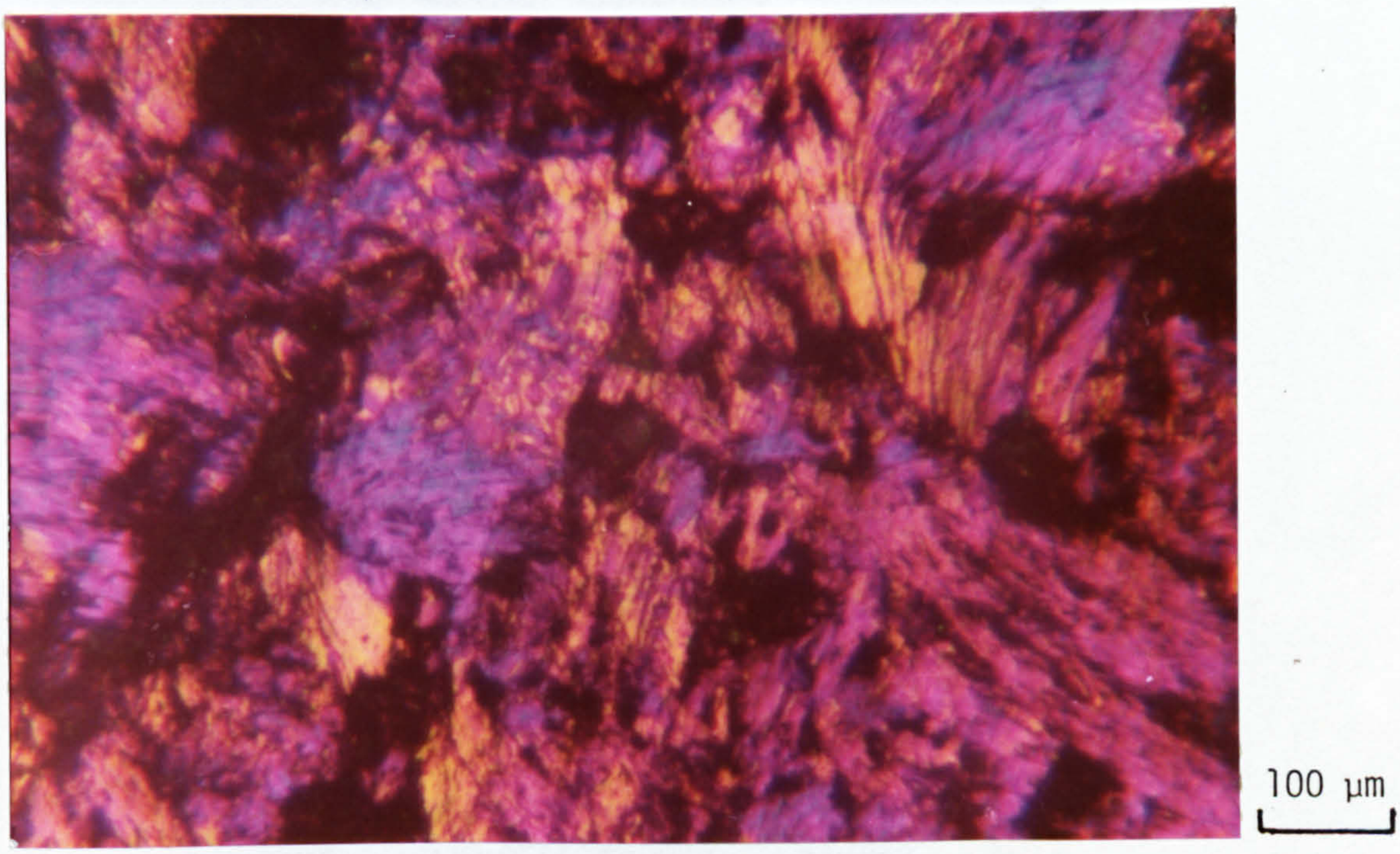
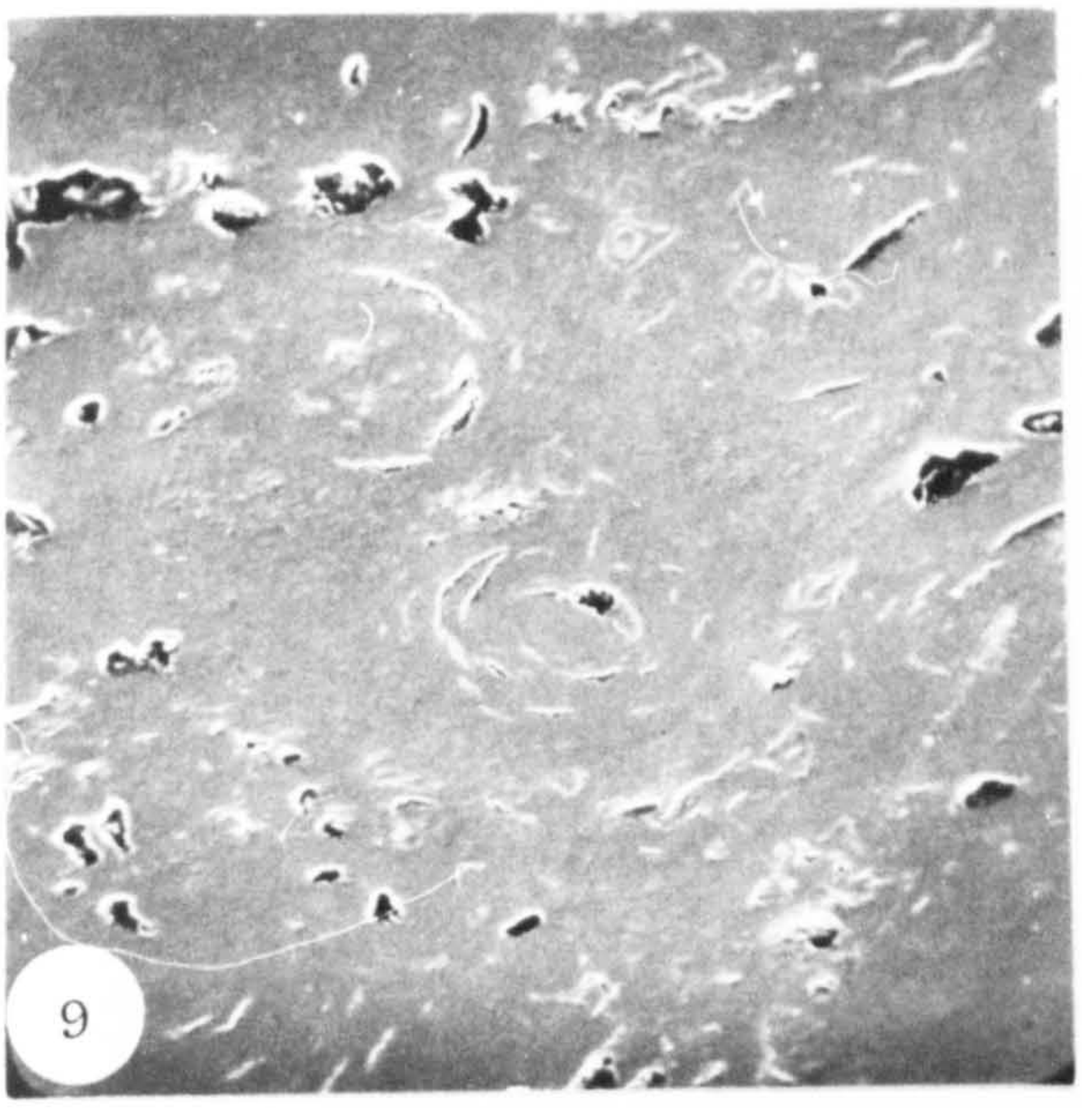
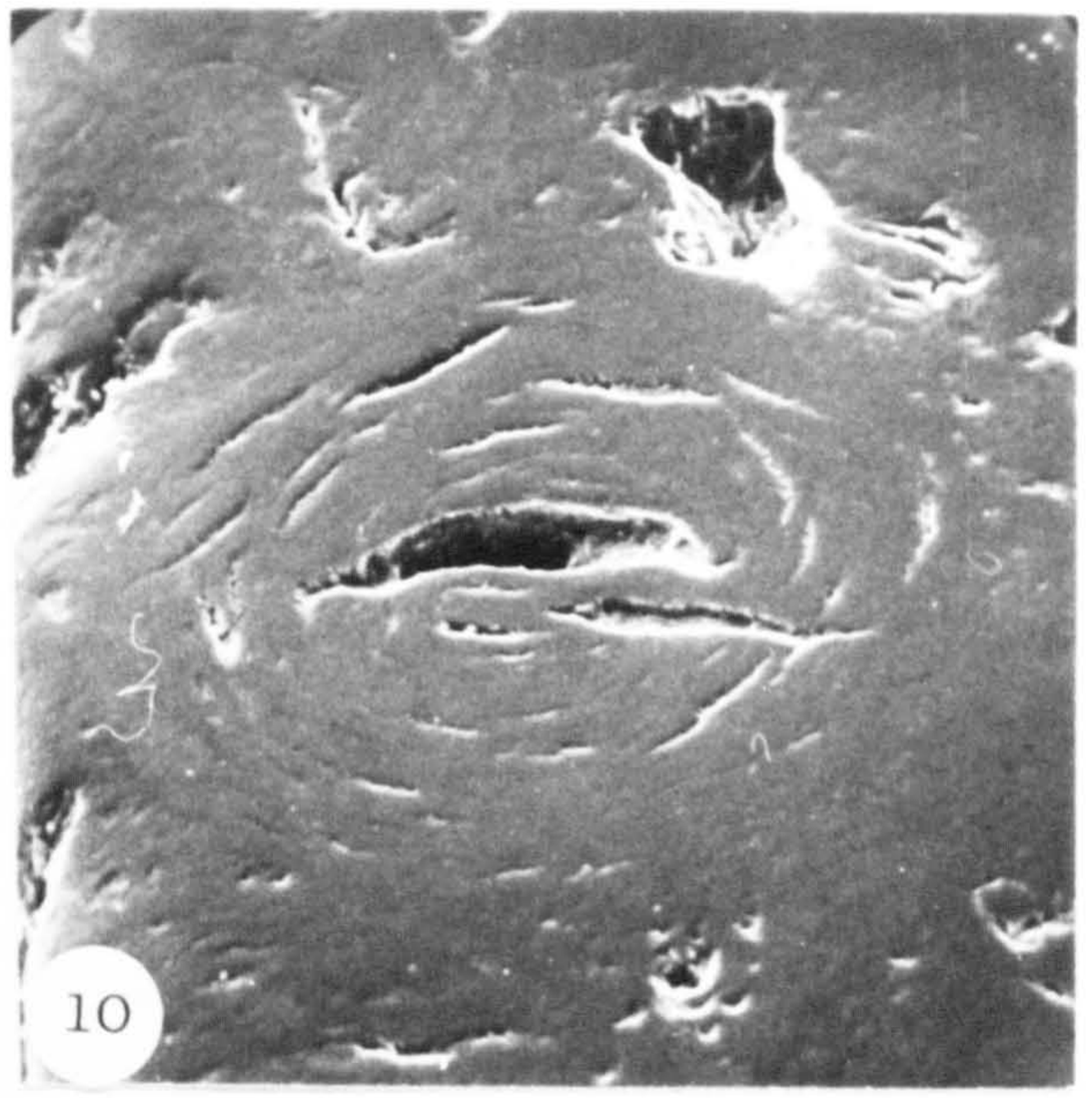


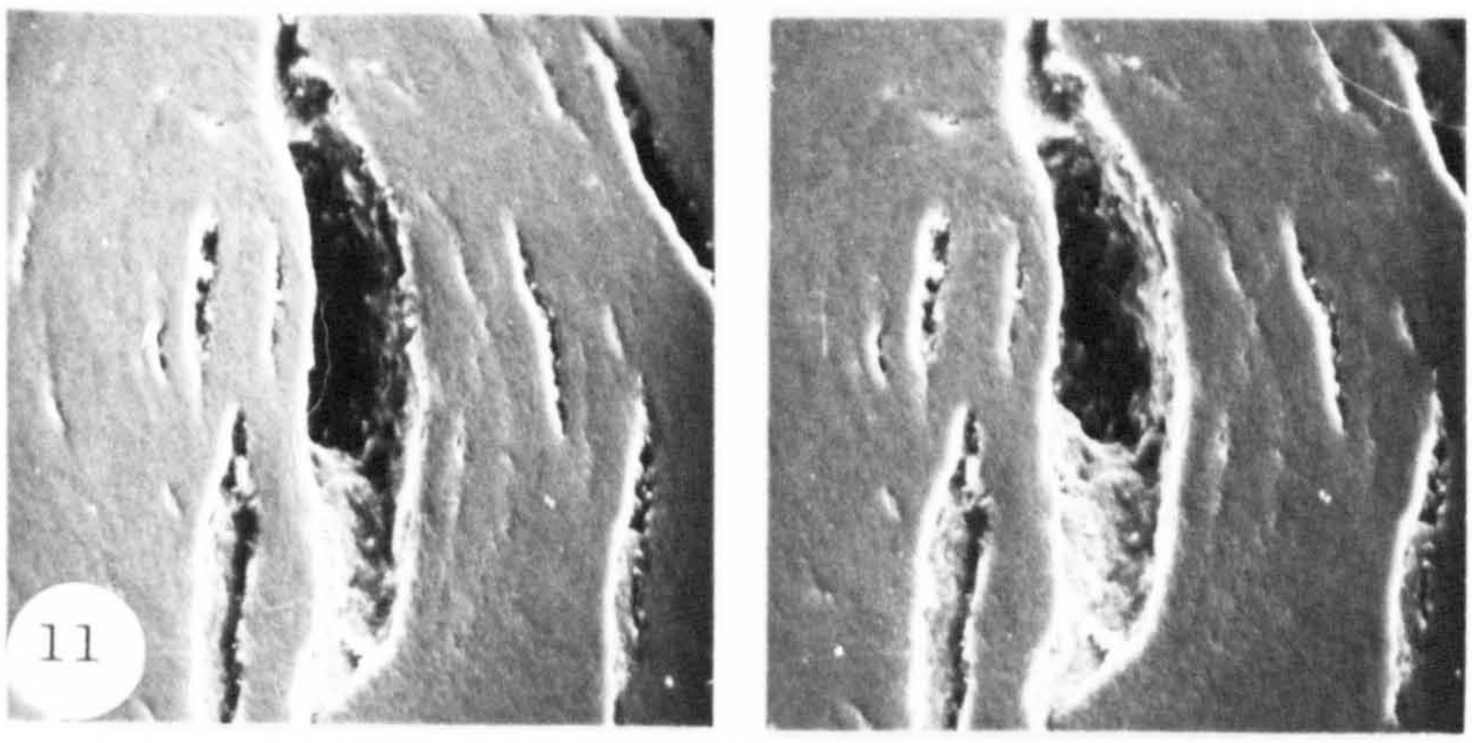
Figure 8. Optical micrograph of virgin PGA L18 graphite.



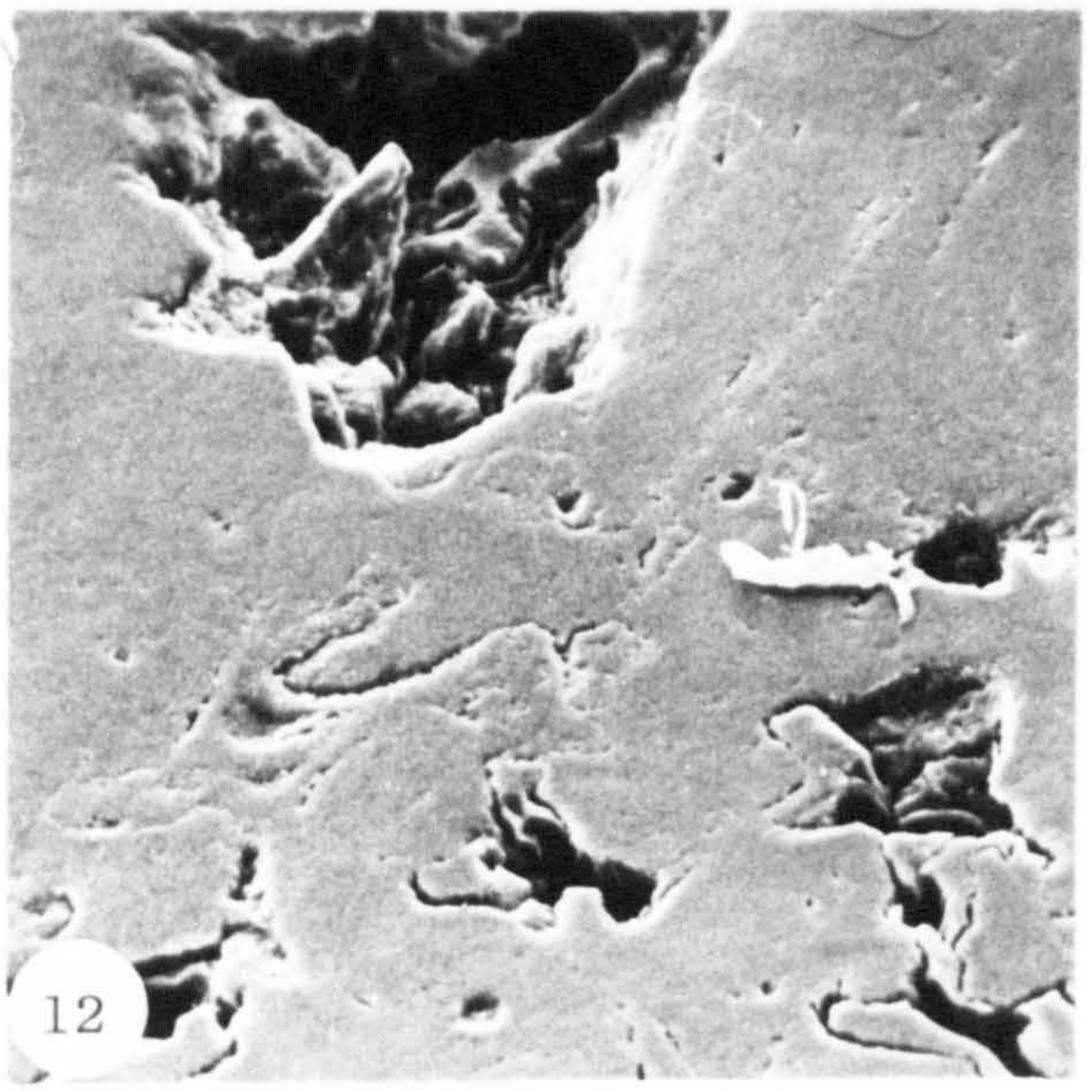
AGLMP GRAPHITE 200 µm



AGLMP GRAPHITE 100 µm

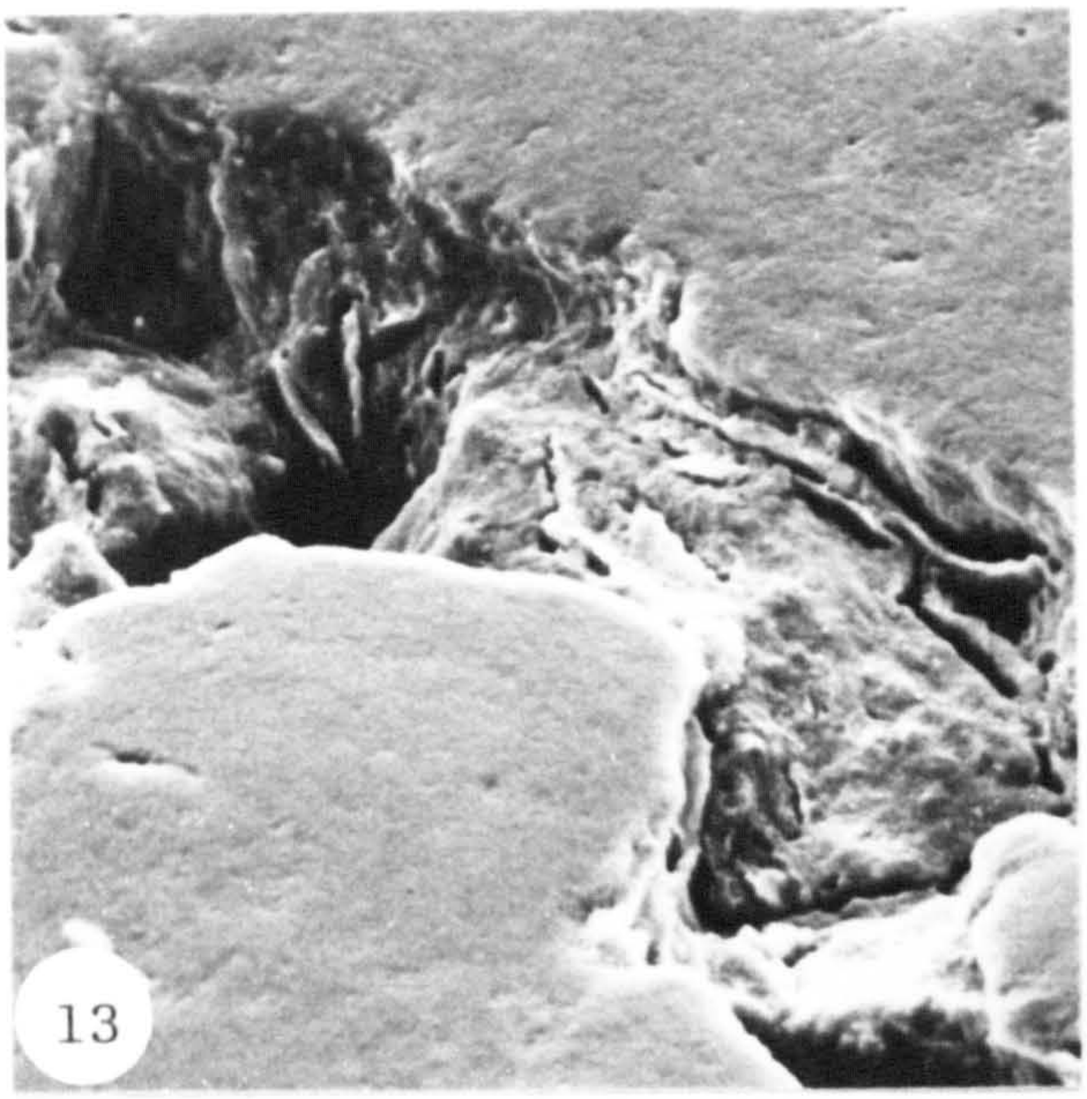


AGLMP GRAPHITE 50 µm

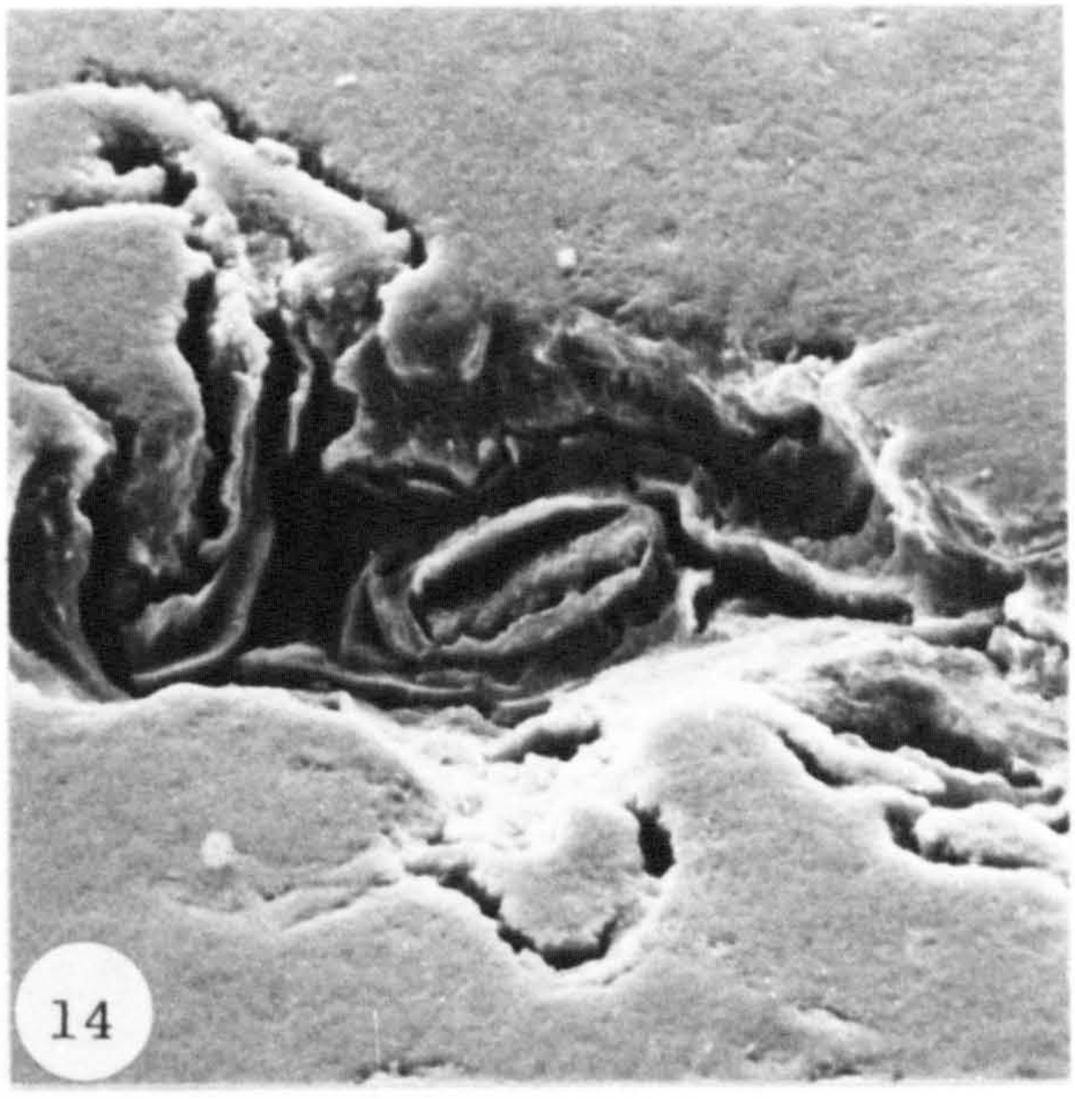


AGLMP GRAPHITE 50 µm

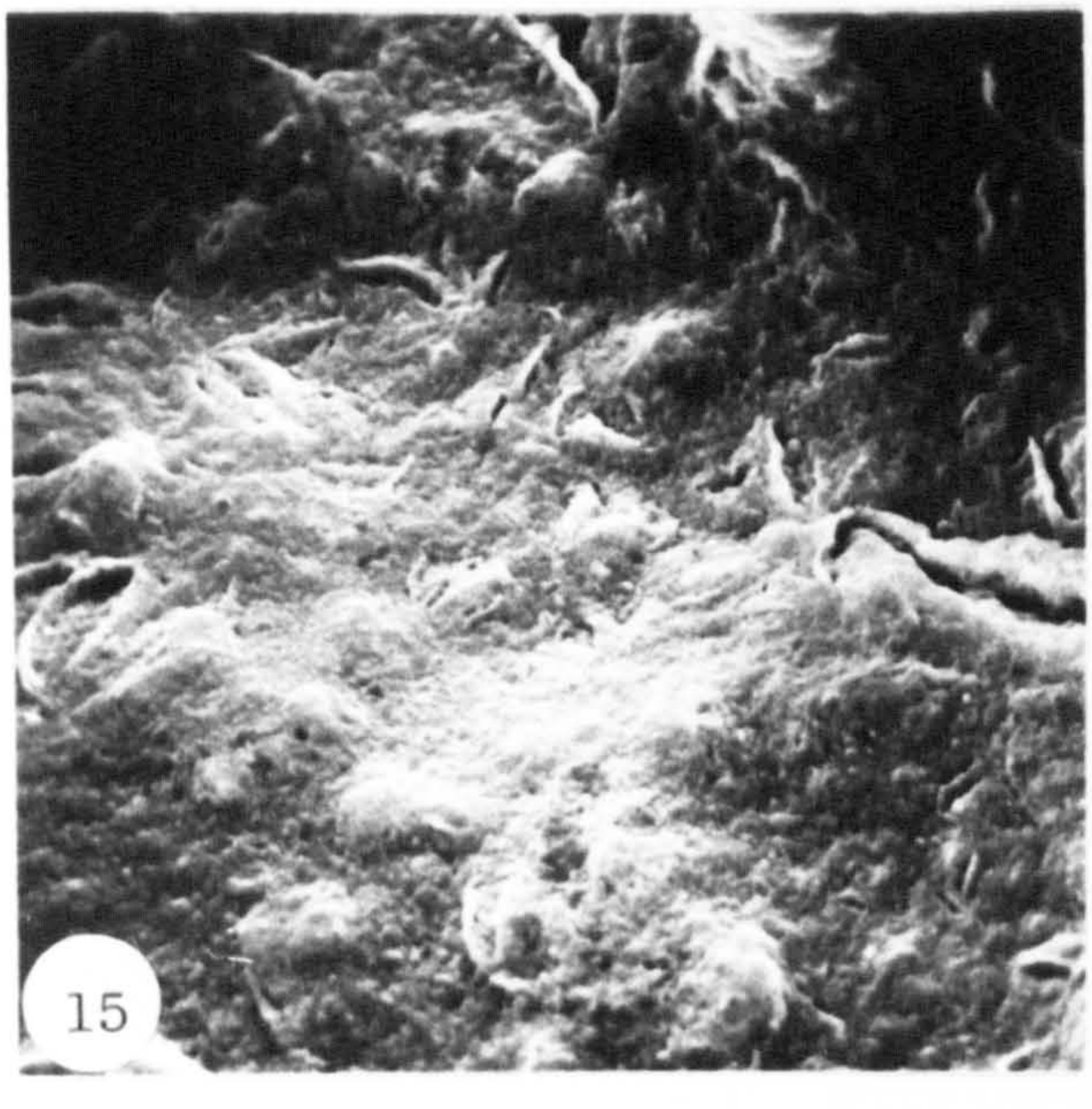
Figures 9 to 12. Scanning electron micrographs (stereoscan) of virgin AGLMP graphite.



AGLMP GRAPHITE 20 µm



AGLMP GRAPHITE 20 µm



AGLMP GRAPHITE 10 µm

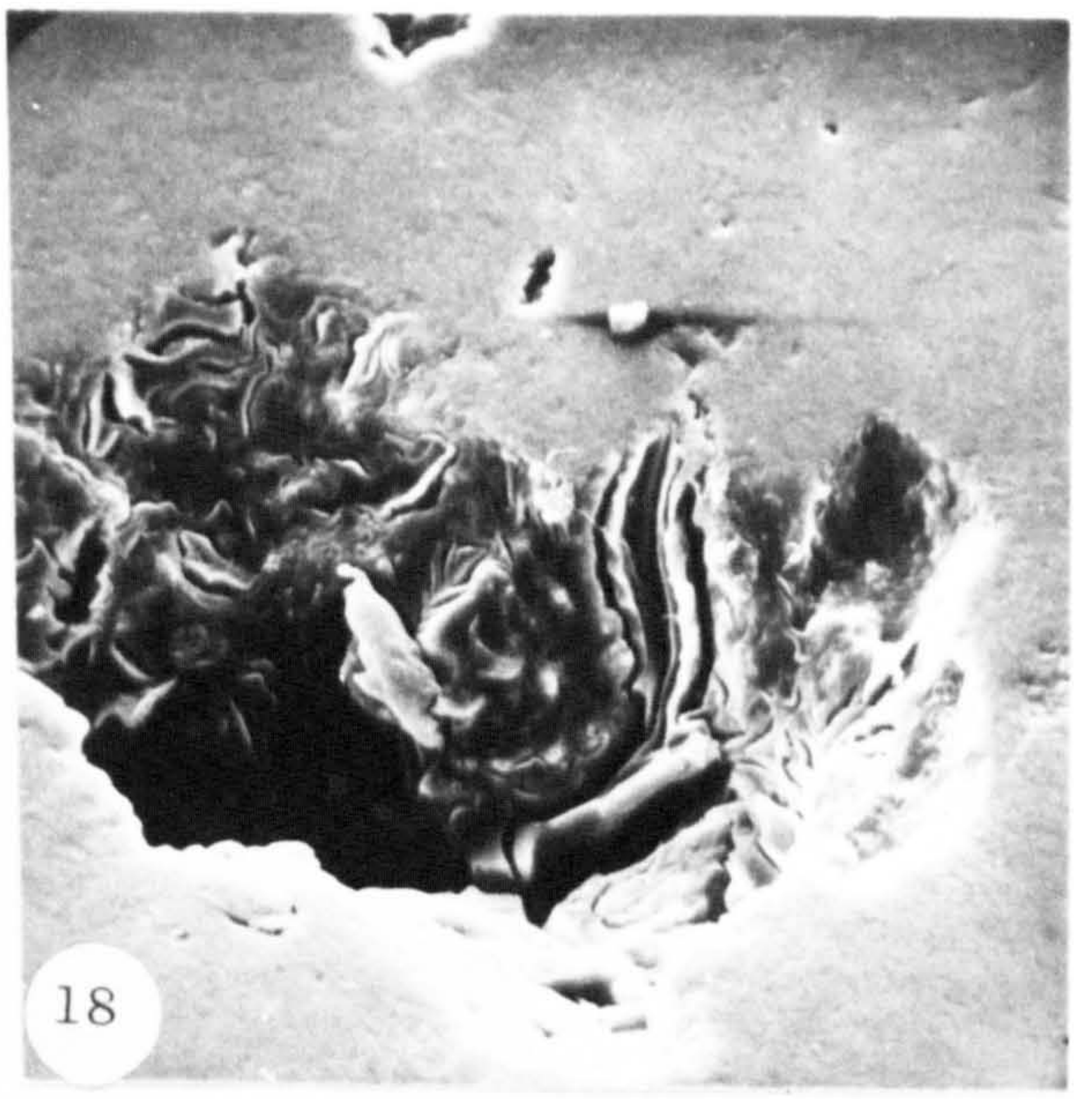


AGLMP GRAPHITE 5 µm

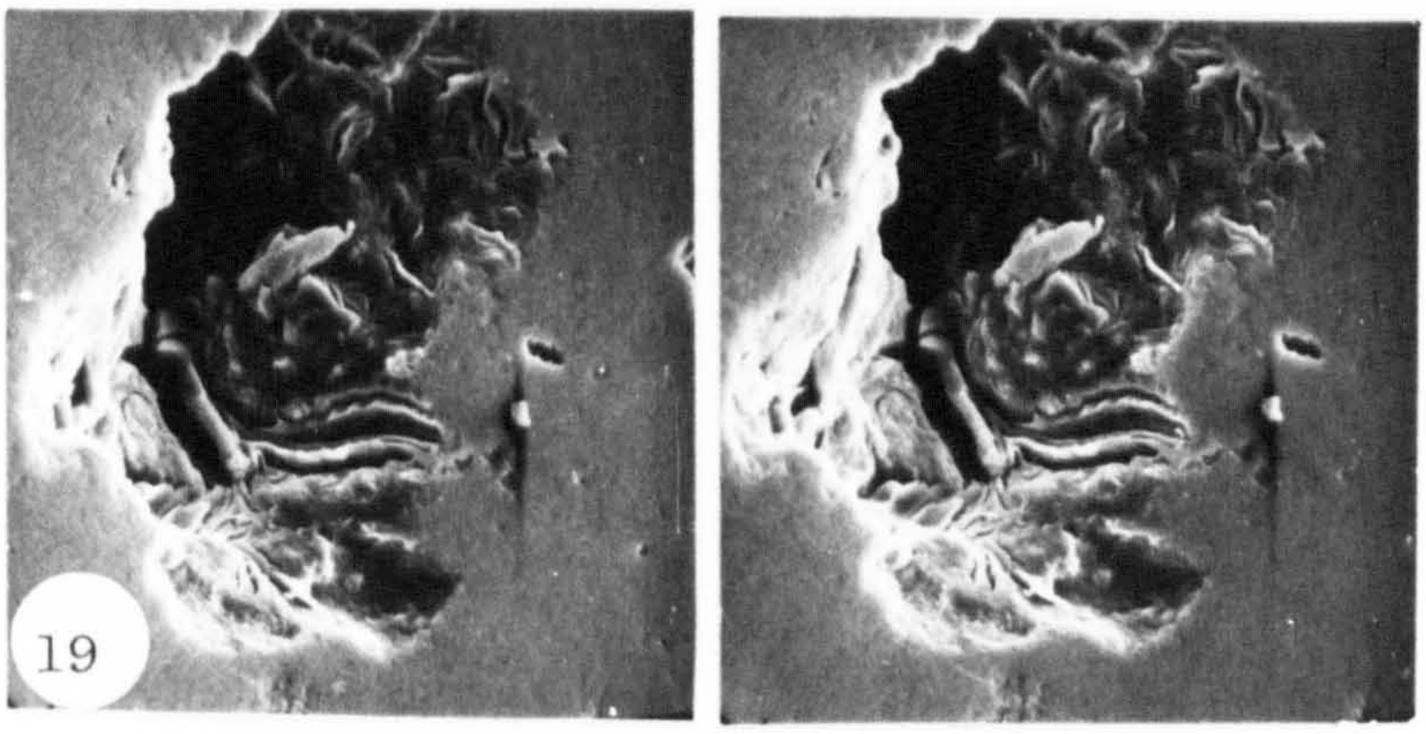
Figures 13 to 16. Scanning electron micrographs (stereoscan) of virgin AGLMP graphite.



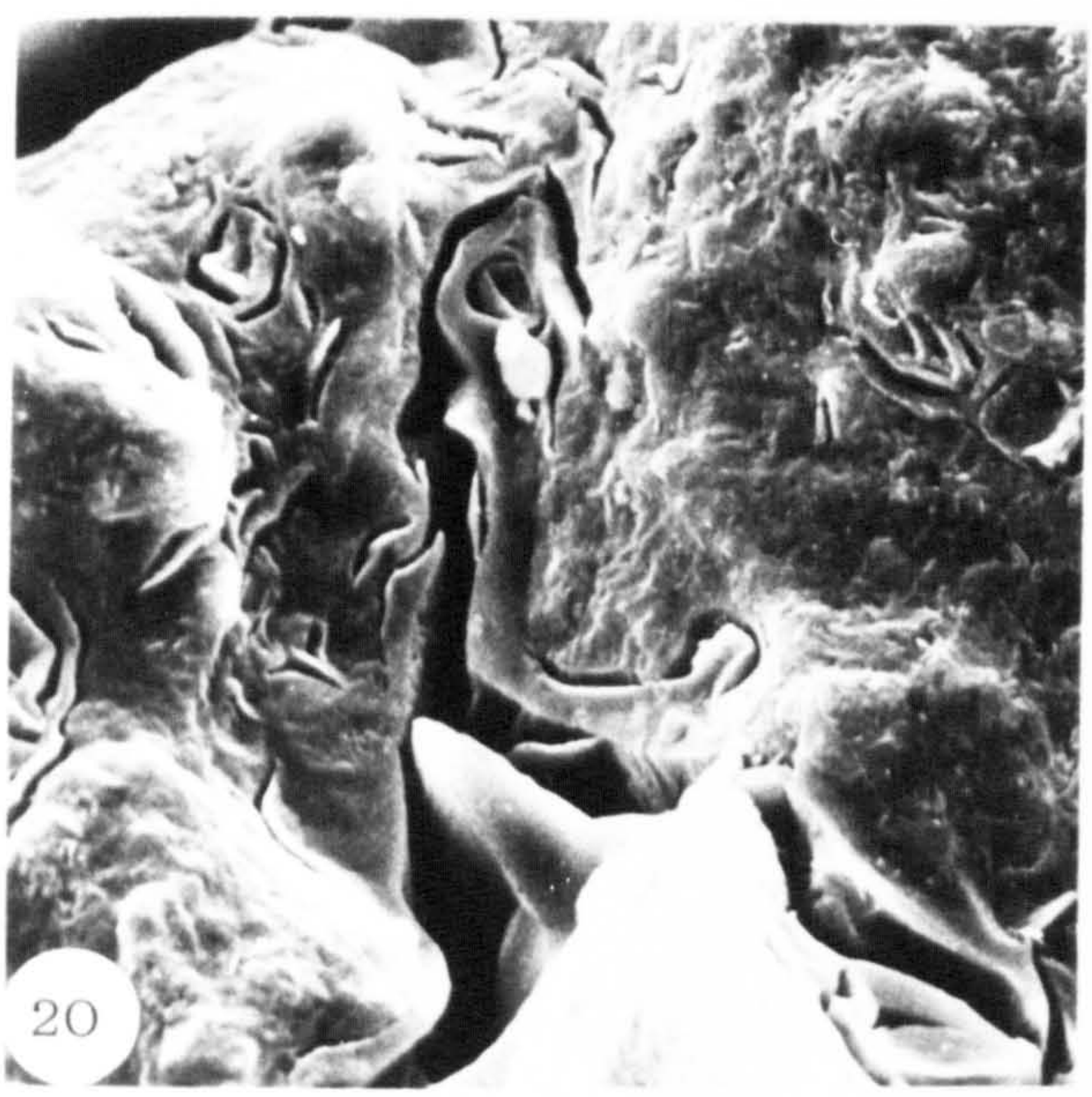
GCMB GRAPHITE 50 µm



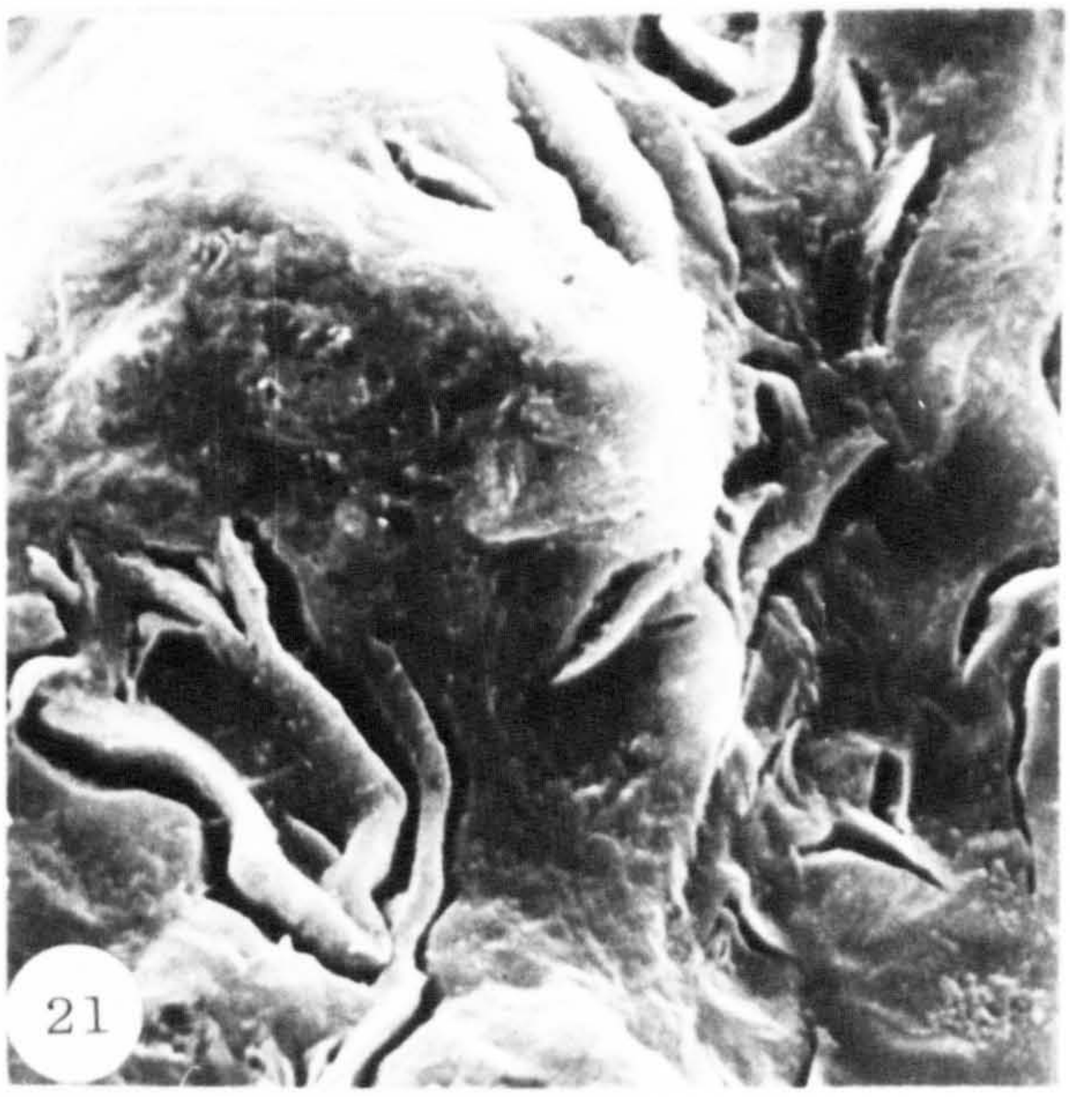
GCMB GRAPHITE 20 µm



GCMB GRAPHITE 50 µm

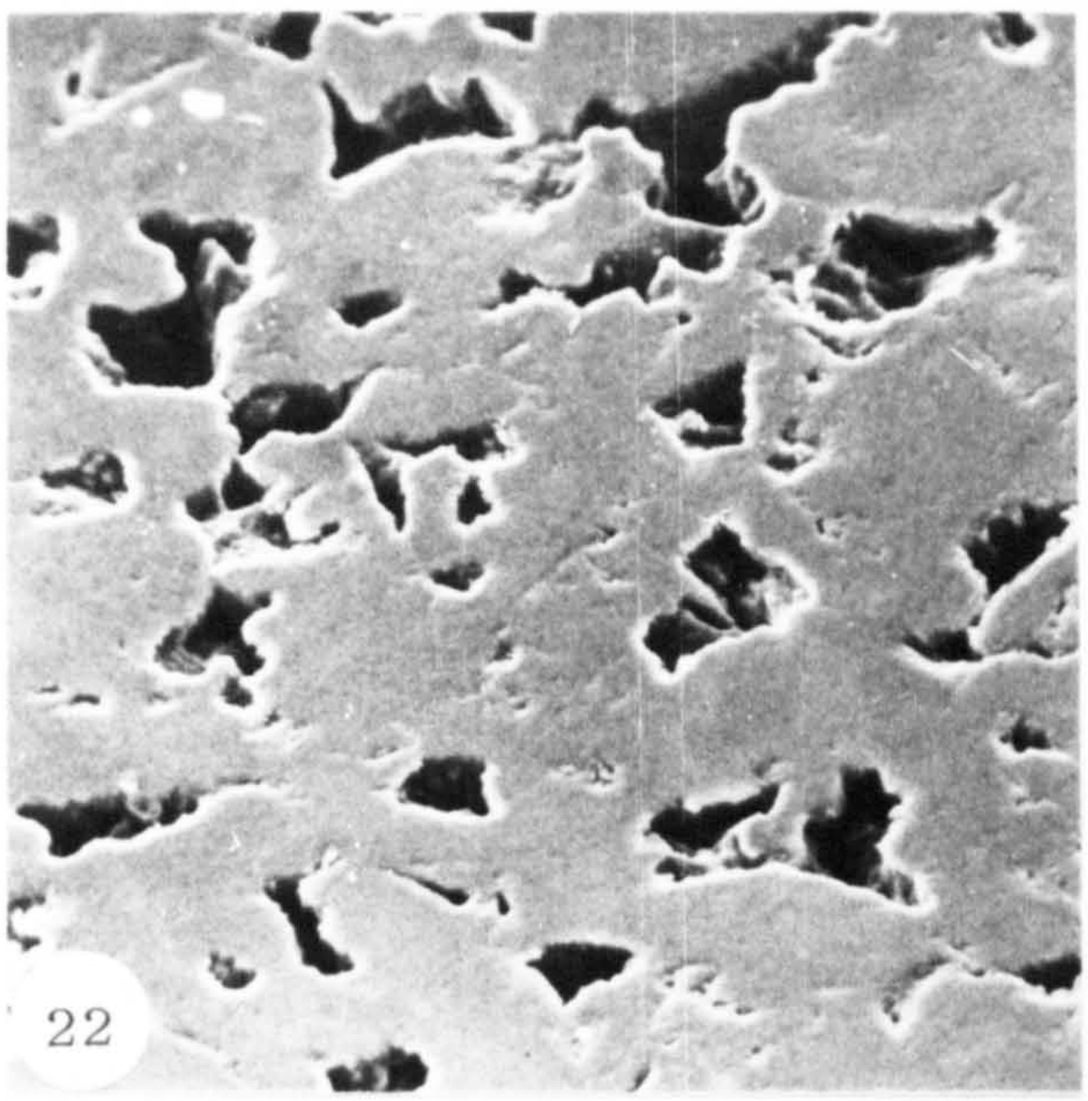


GCMB GRAPHITE 10 µm

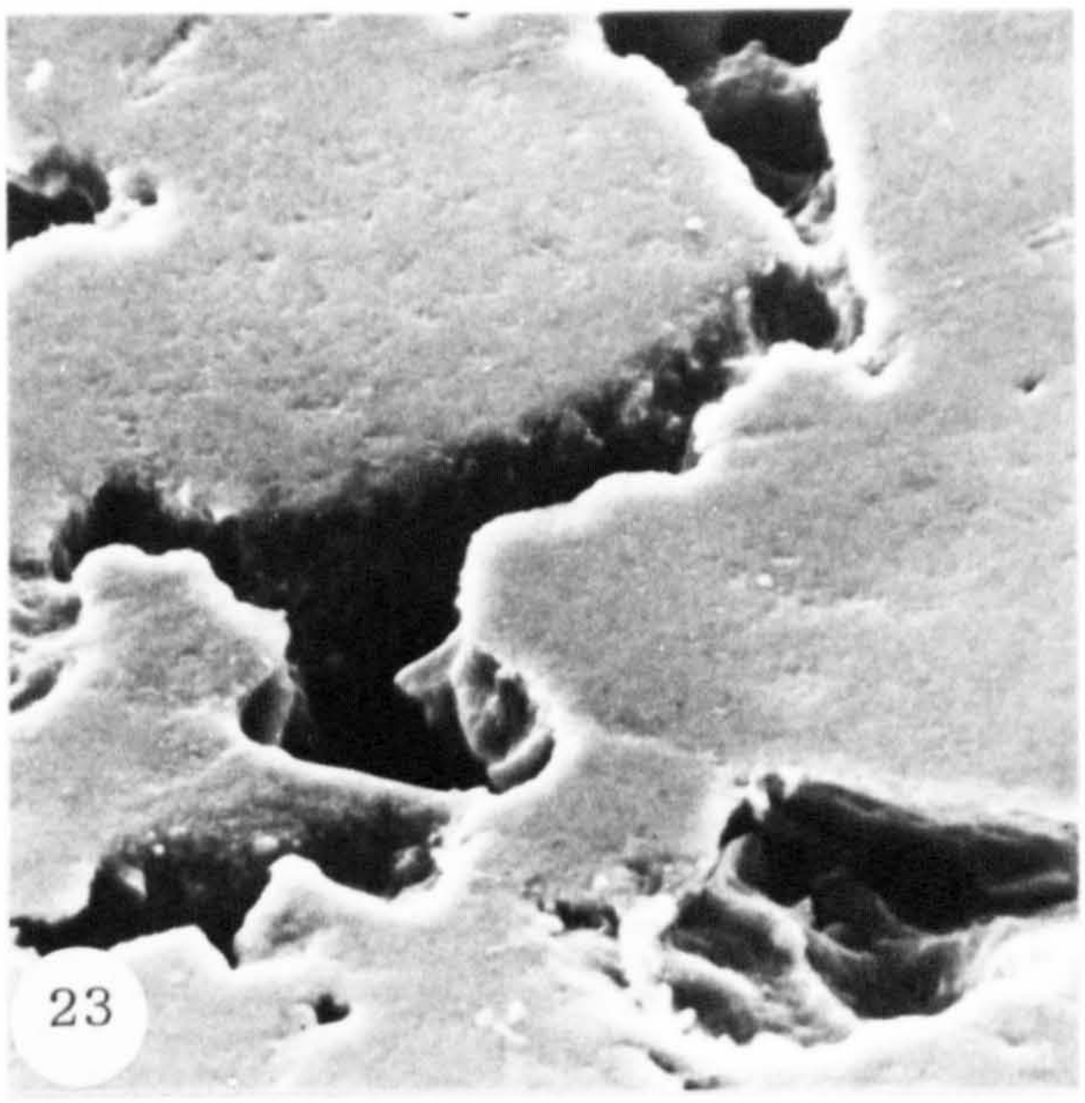


GCMB GRAPHITE 5 µm

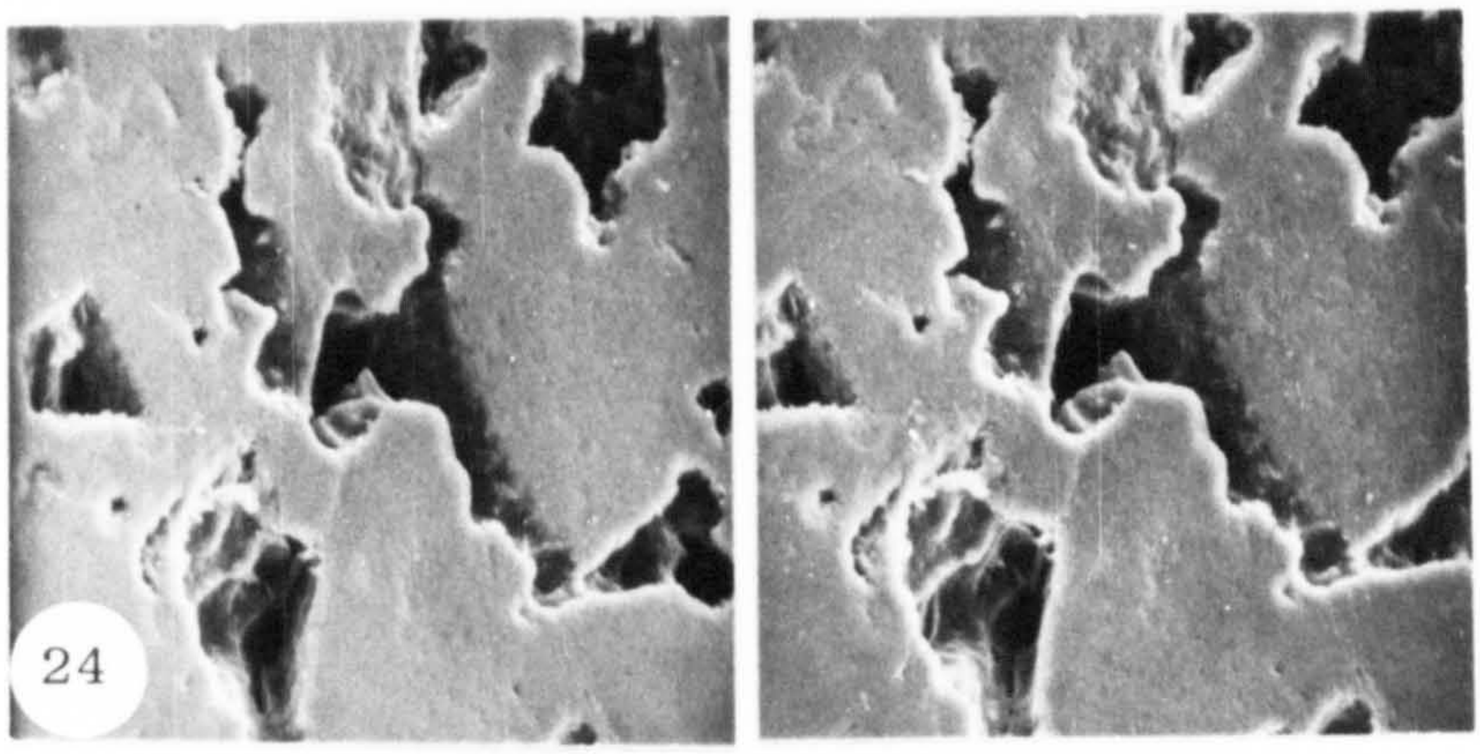
Figures 17 to 21. Scanning electron micrographs (stereoscan) of virgin GCMB graphite.



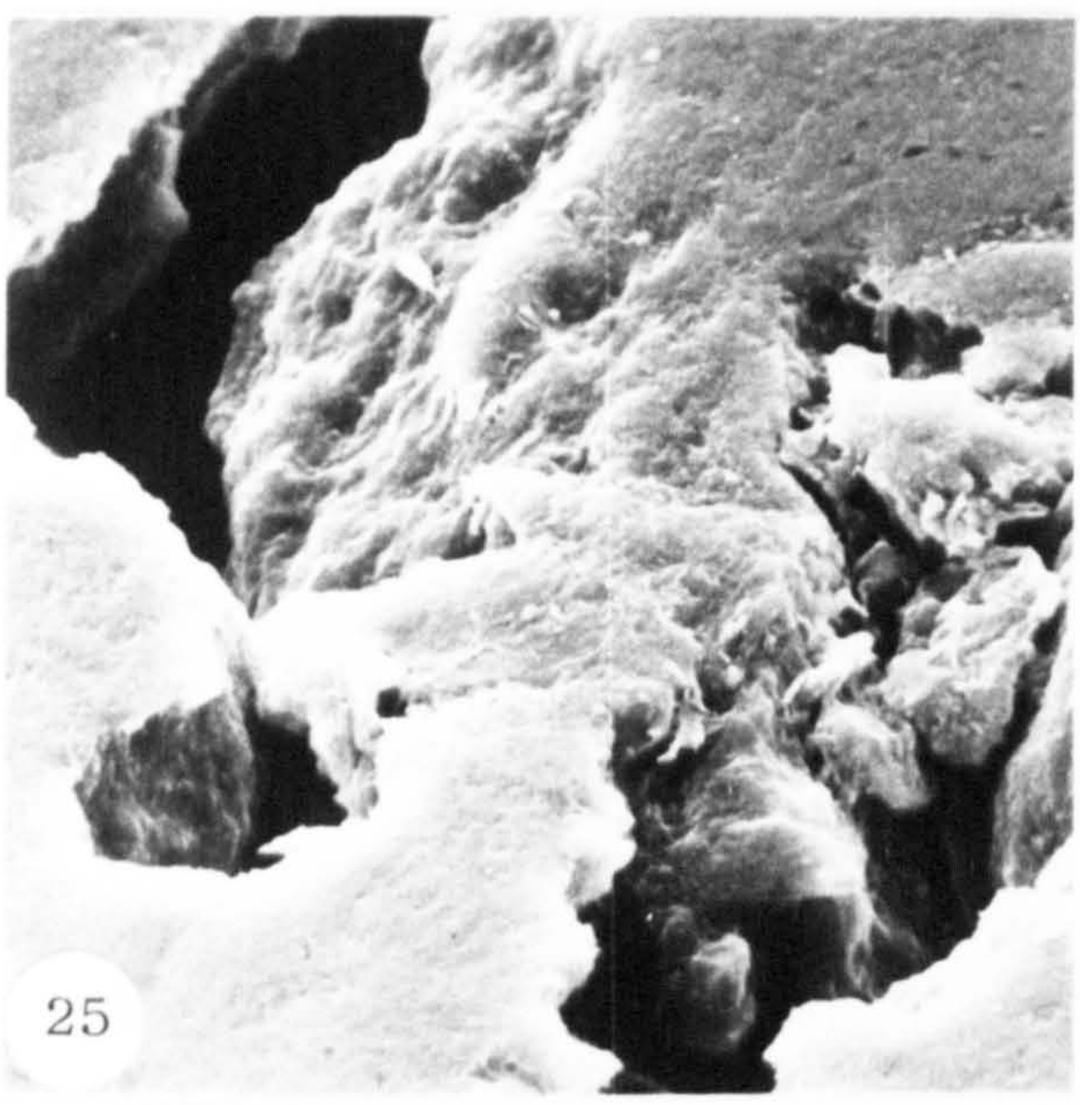
AGLHP GRAPHITE 50 µm



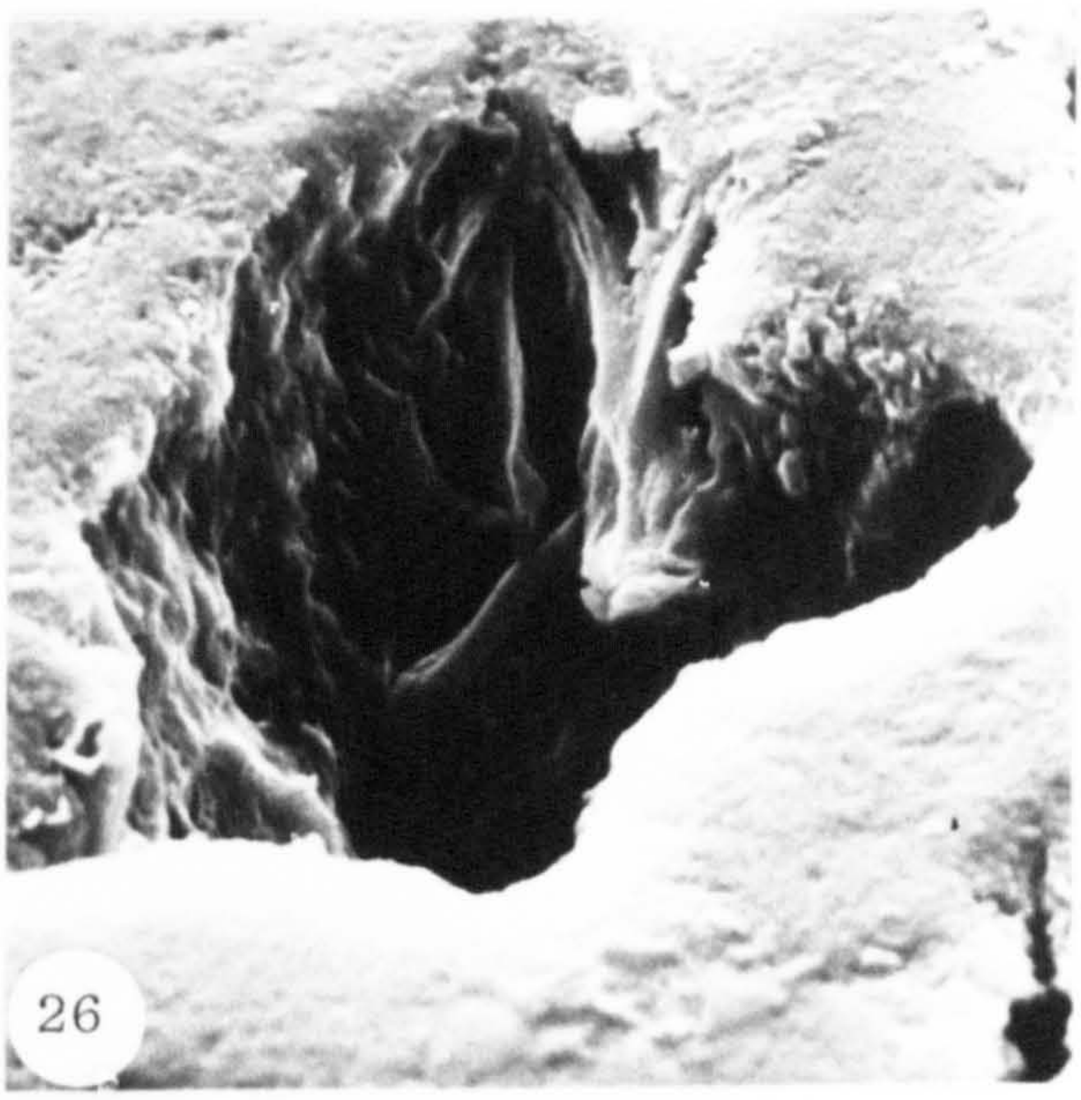
AGLHP GRAPHITE 20 µm



STEREOPAIR OF AGLHP GRAPHITE 50 µm

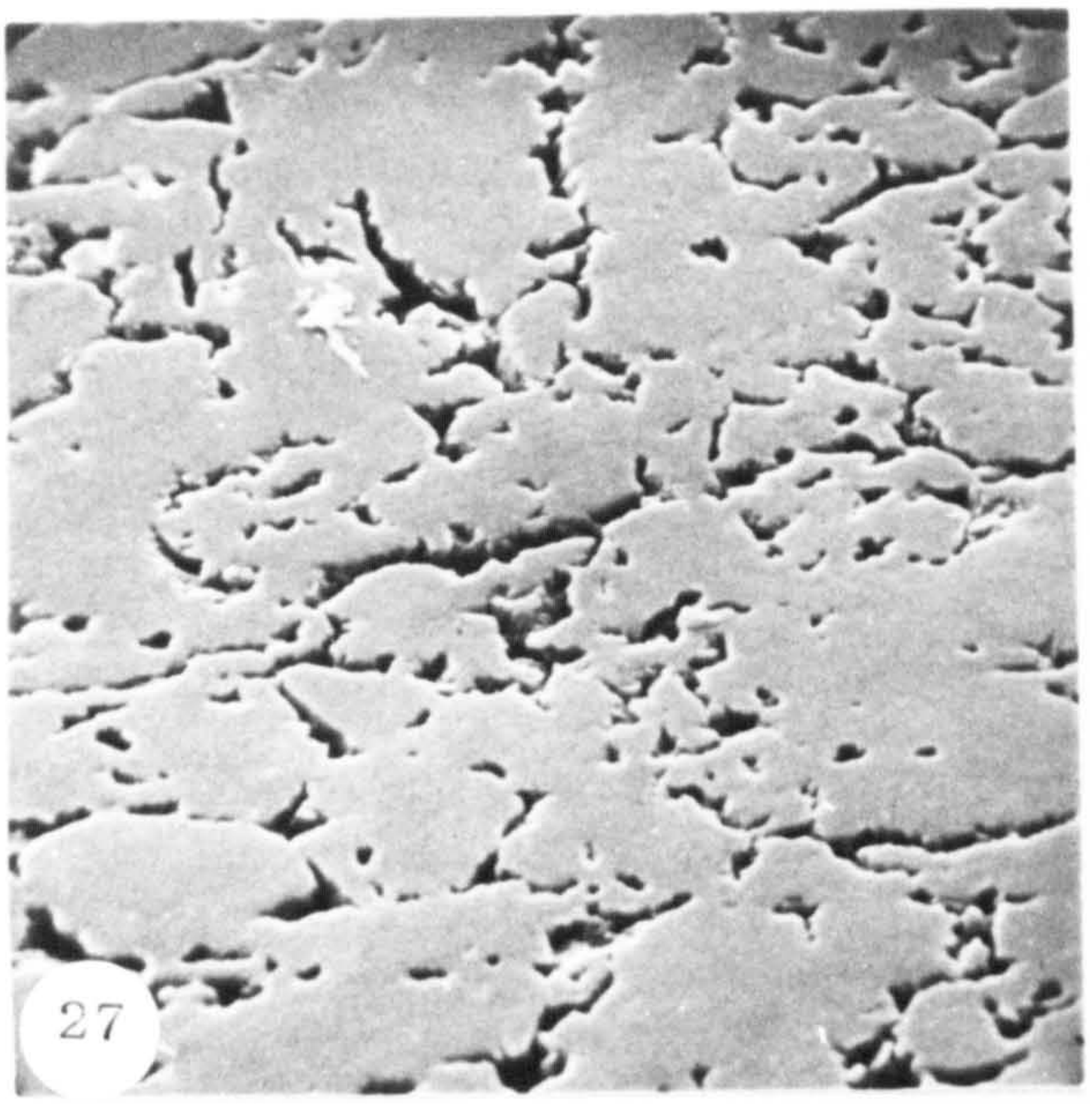


AGLHP GRAPHITE 10 µm



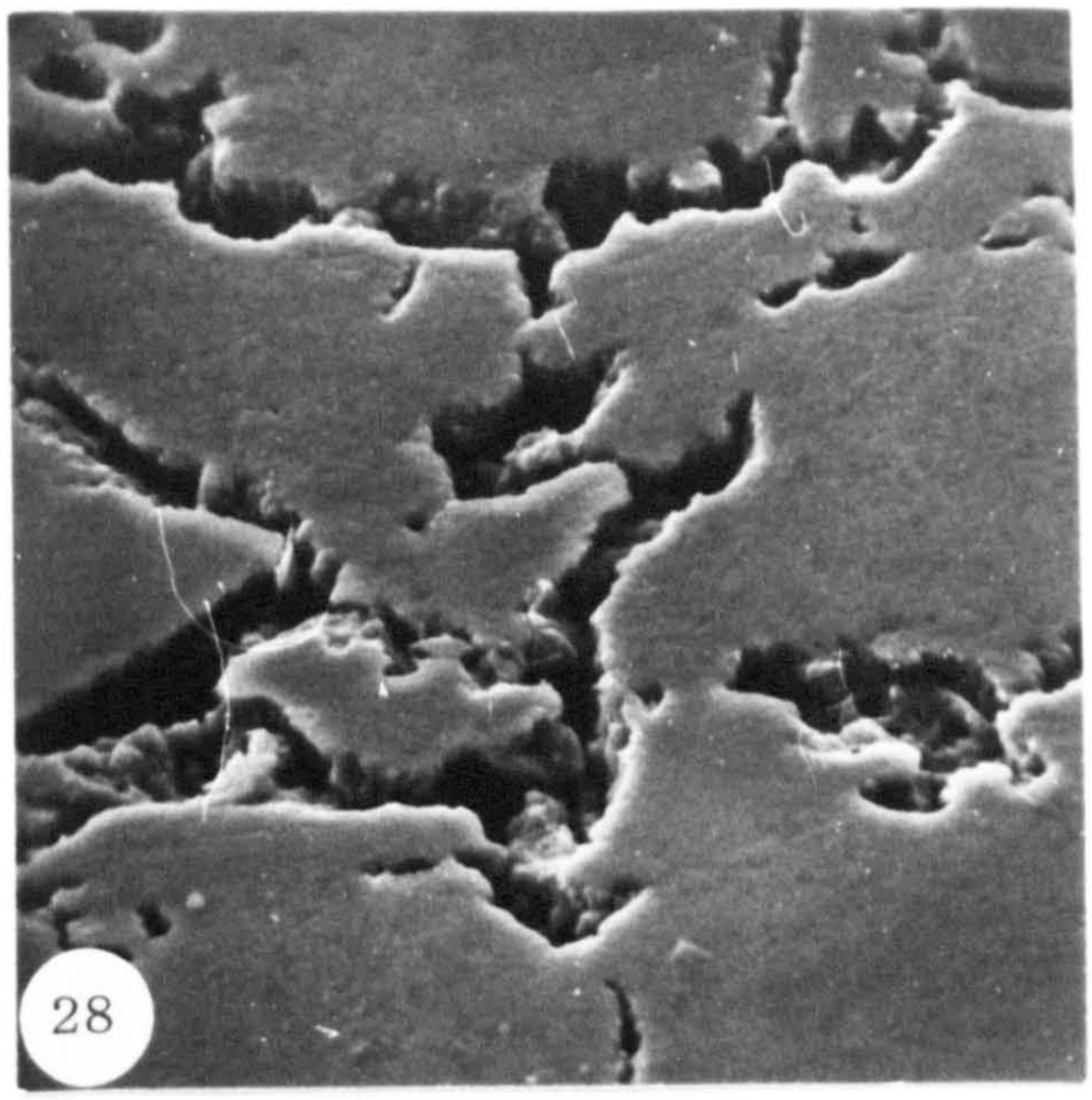
AGLHP GRAPHITE 5 µm

Figures 22 to 26. Scanning electron micrographs (stereoscan) of virgin AGLHP unipore graphite.



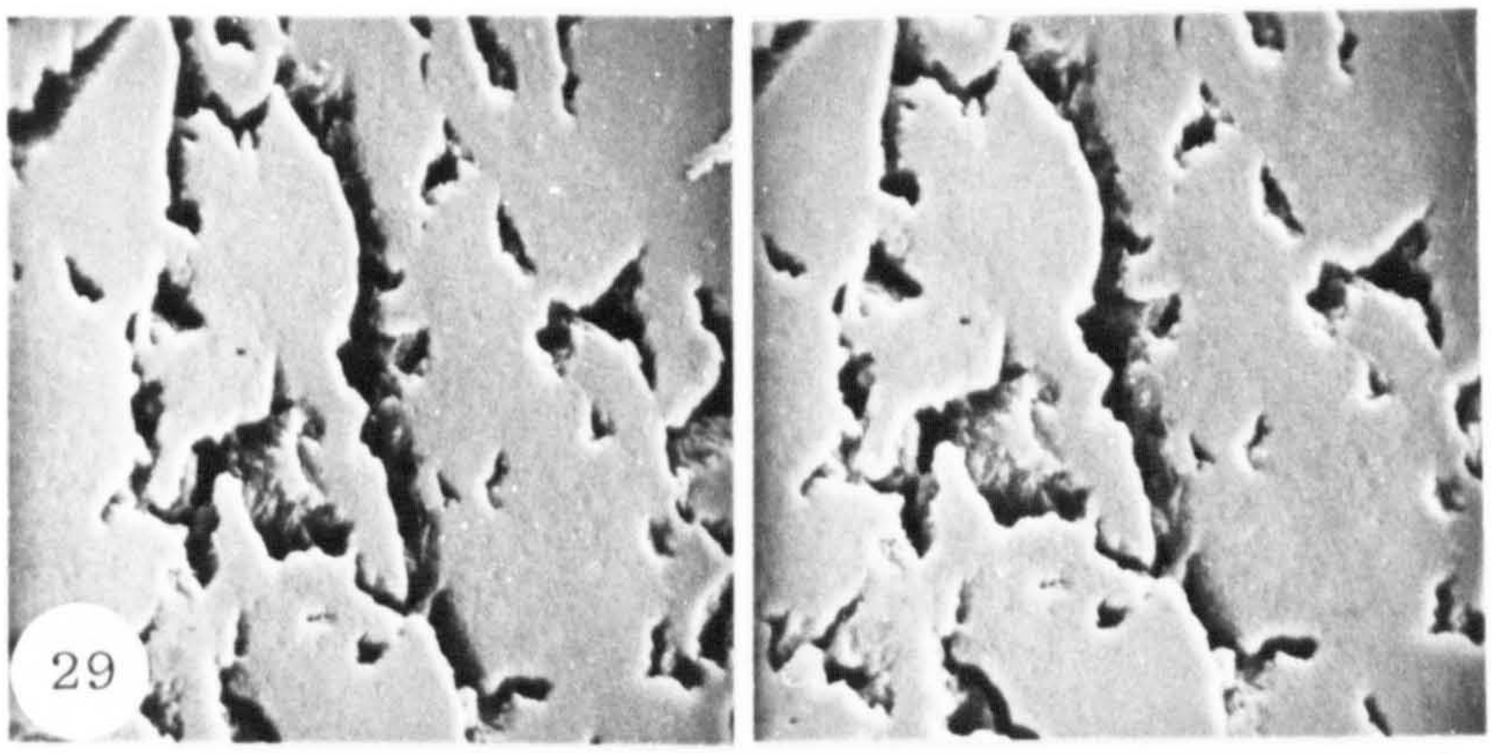
27

MORGANS EYC 9106 GRAPHITE 50 µm



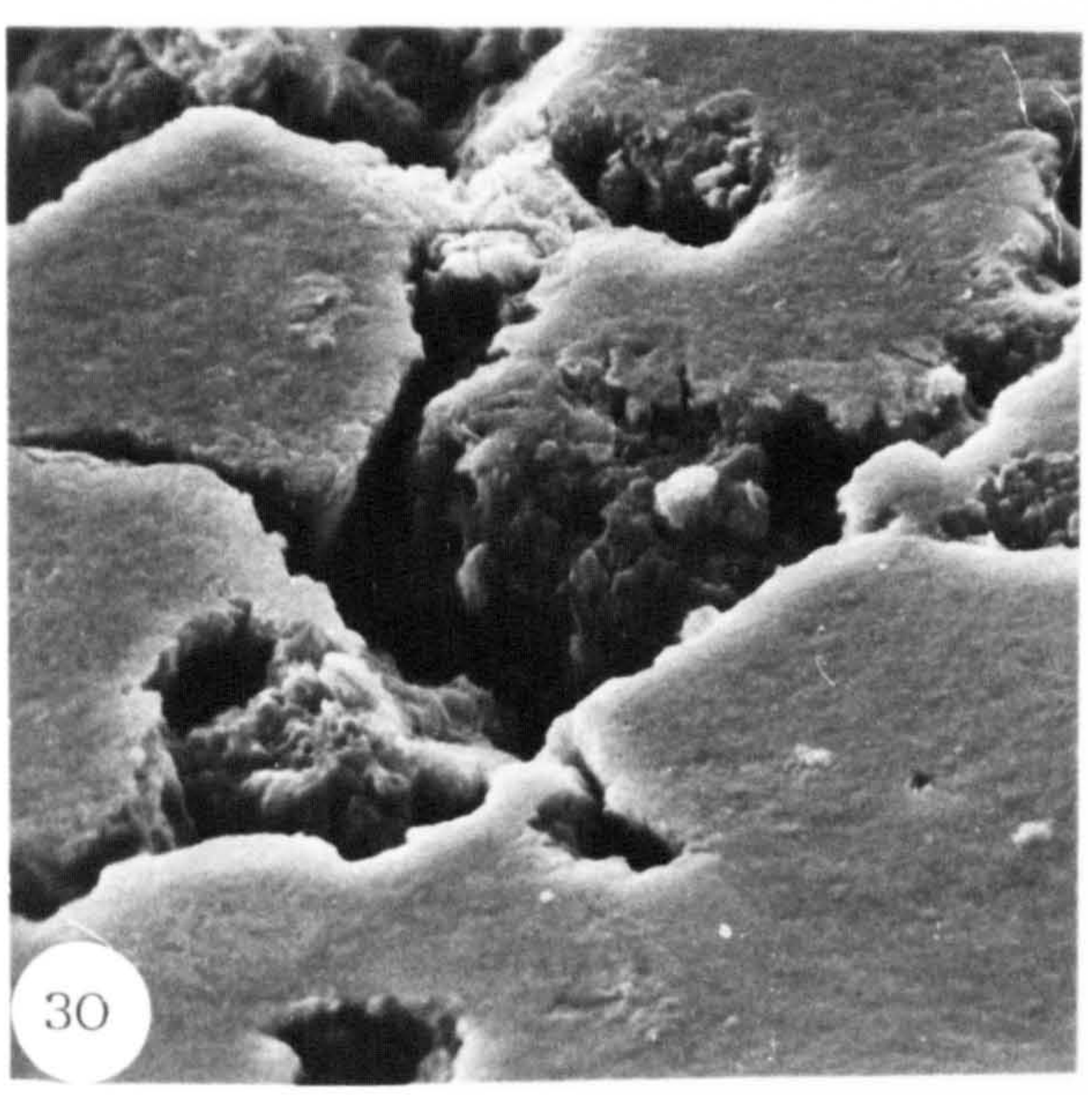
28

MORGANS EYC 9106 GRAPHITE 20 µm



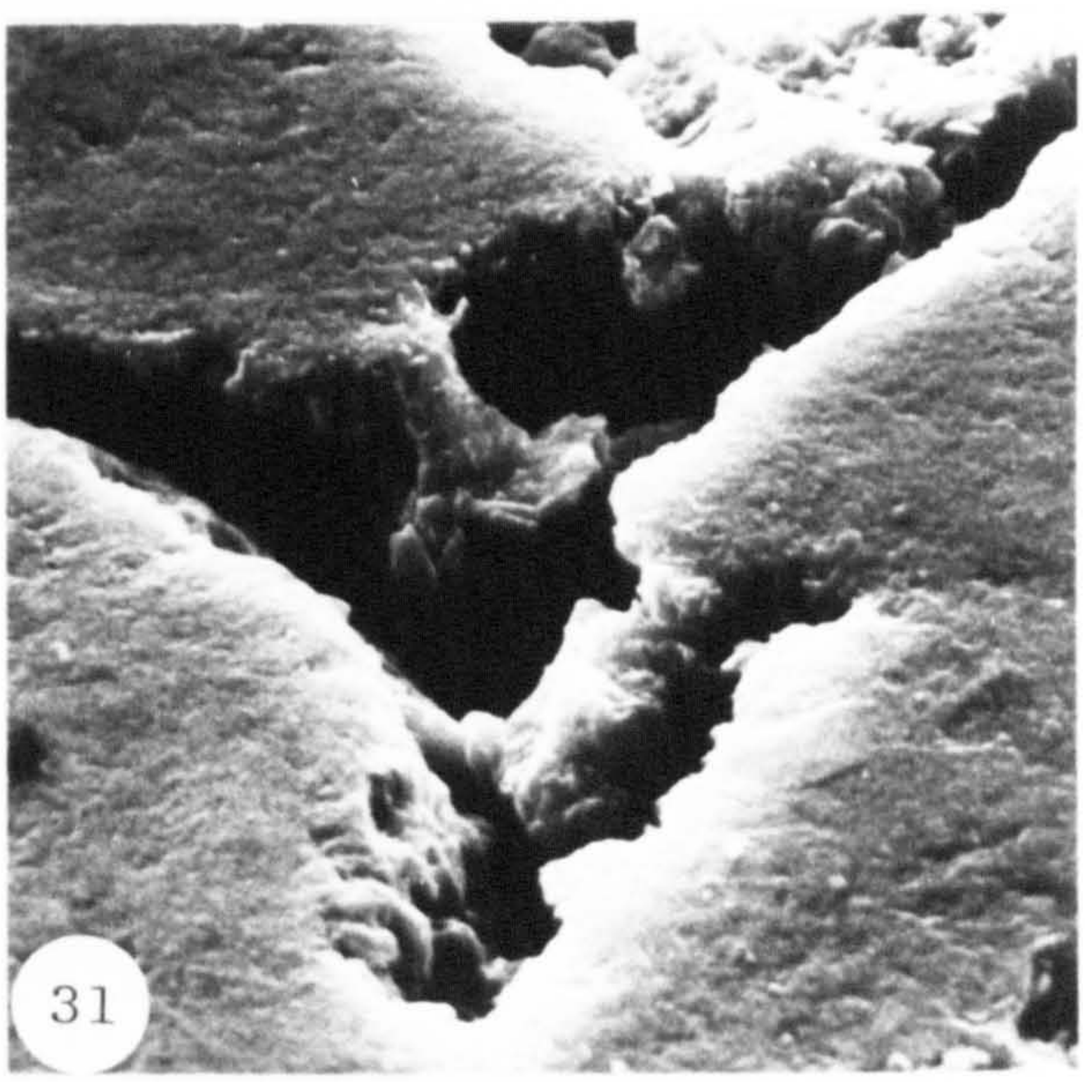
29

STEREOPAIR OF MORGANS EYC 9106 GRAPHITE 50 µm



30

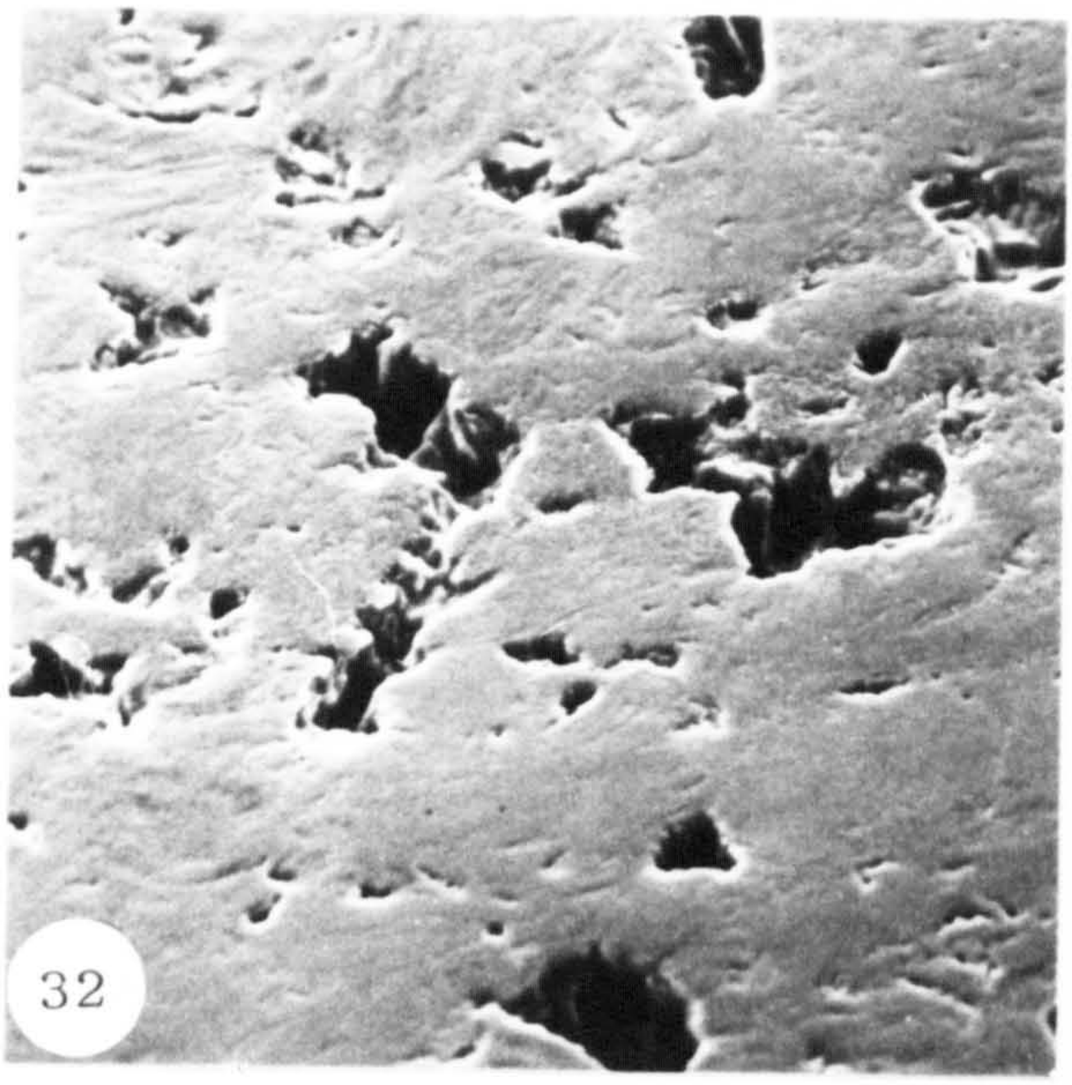
MORGANS EYC 9106 GRAPHITE 10 µm



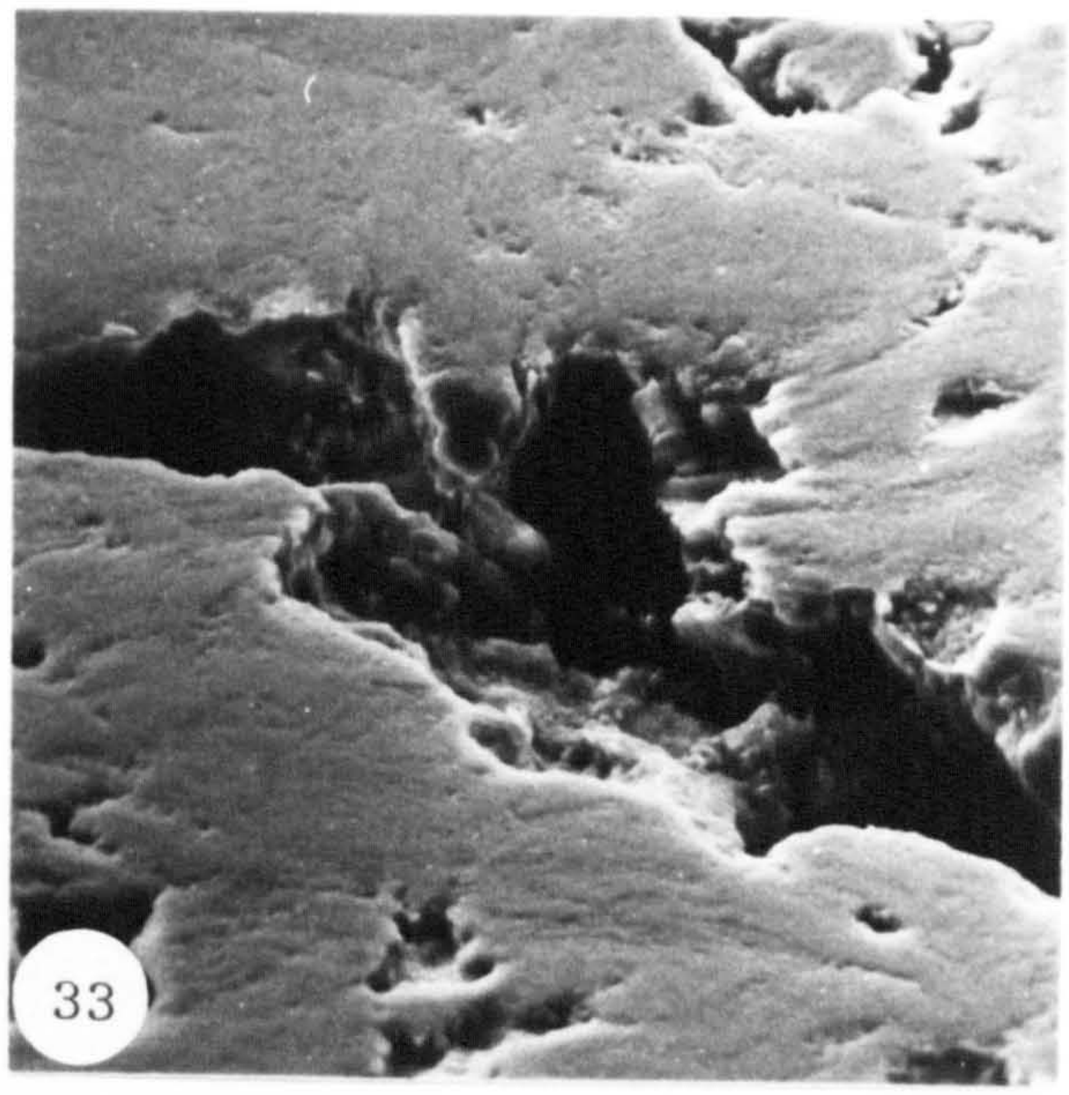
31

MORGANS EYC 9106 GRAPHITE 5 µm

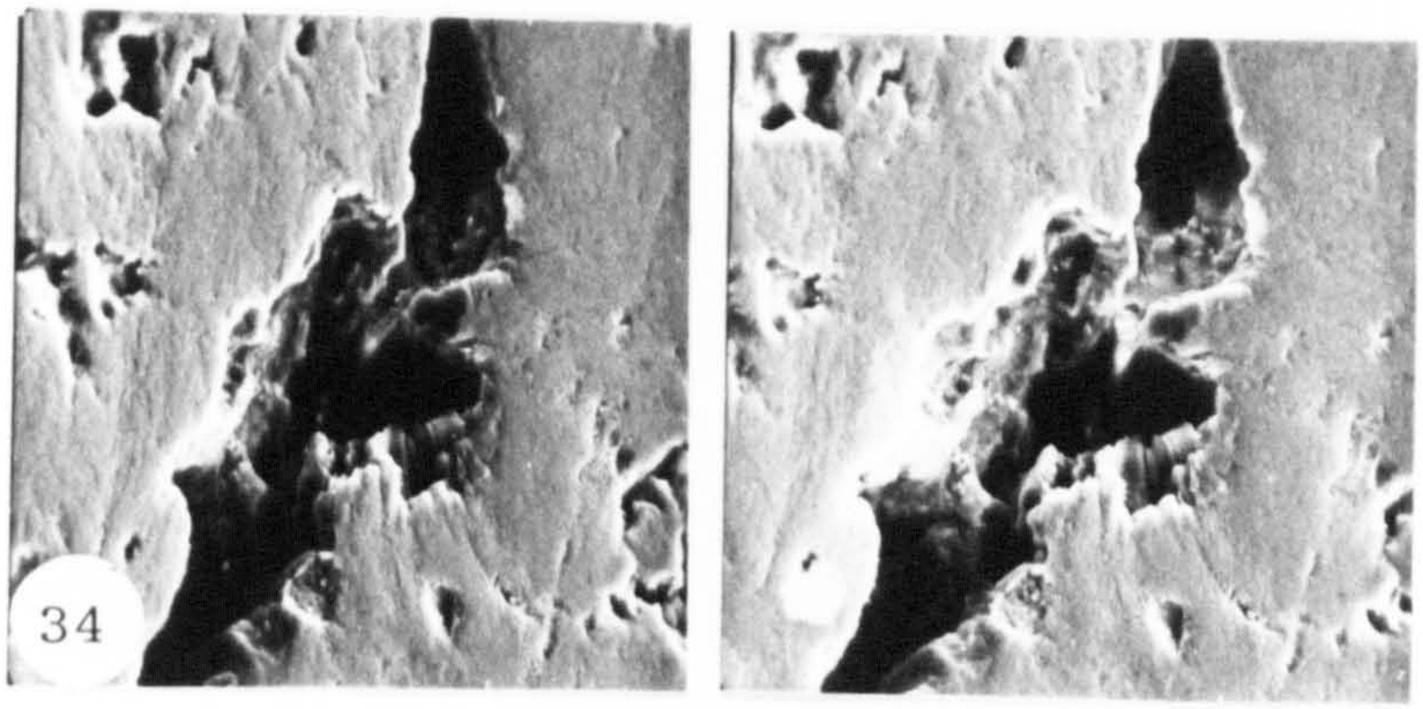
Figures 27 to 31. Scanning electron micrographs (stereoscan) of virgin Morgans EYC 9106 unipore graphite.



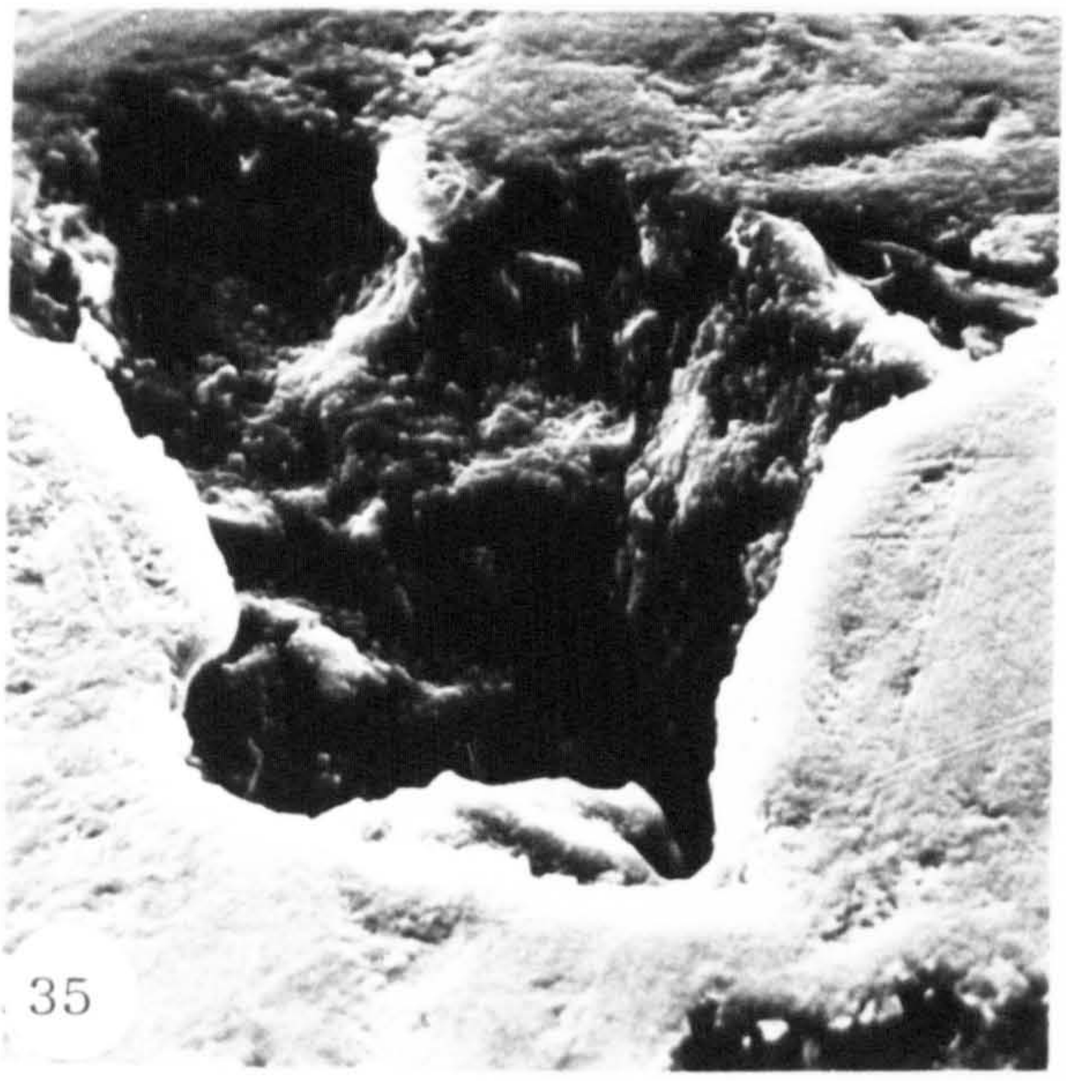
LIMA GRAPHITE 50 µm



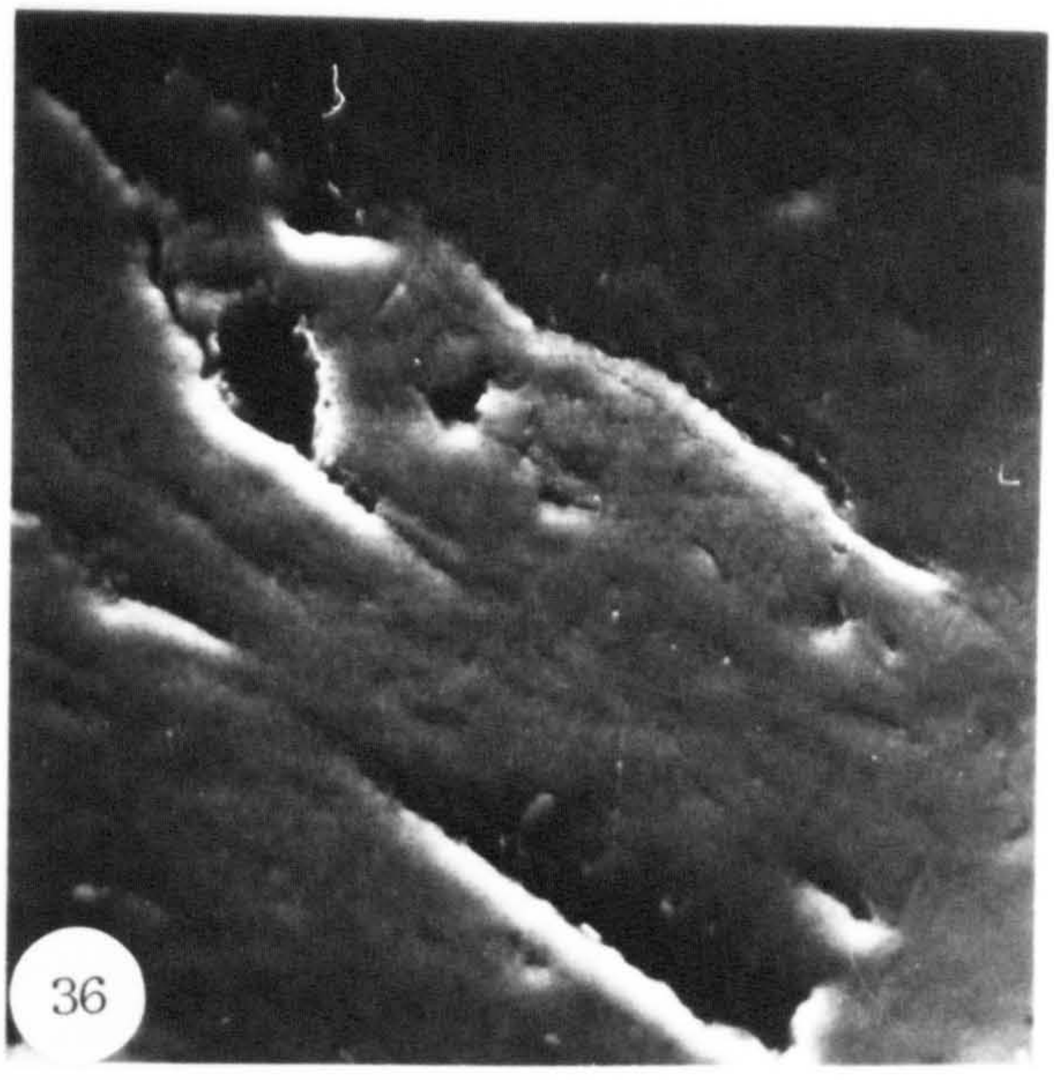
LIMA GRAPHITE 30 µm



STEREOPAIR OF LIMA GRAPHITE 50 µm

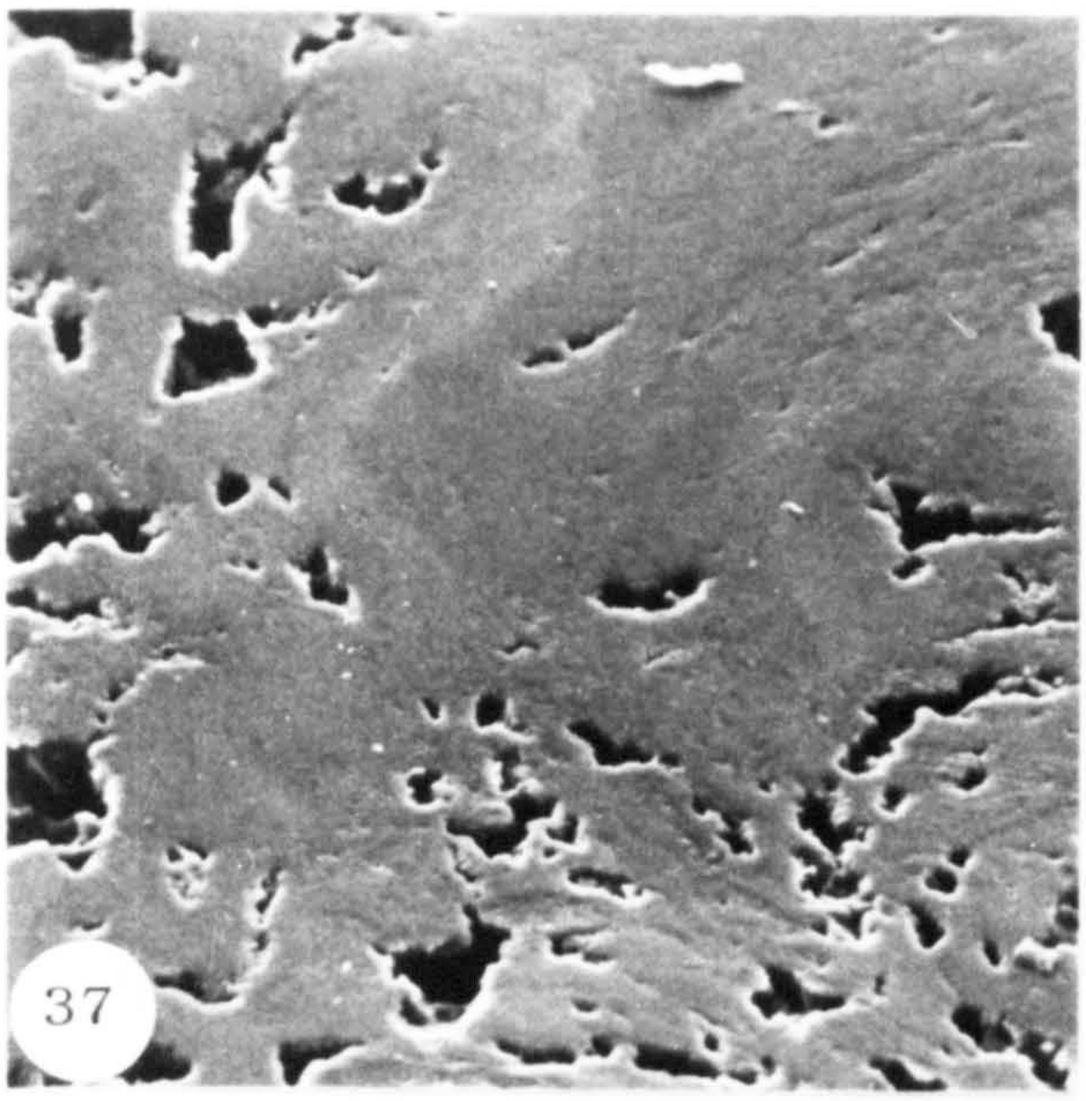


LIMA GRAPHITE 10 µm

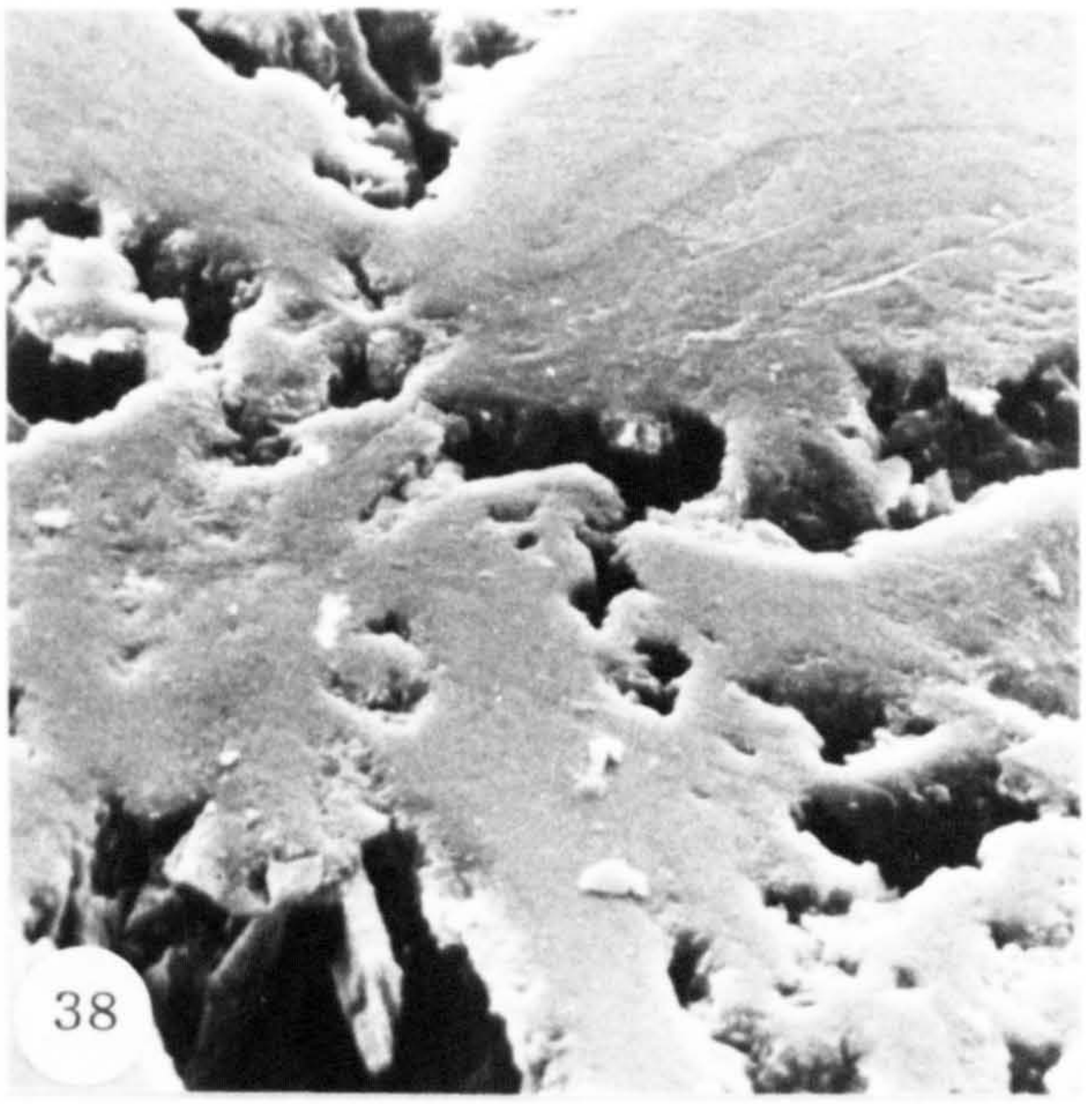


LIMA GRAPHITE 5 µm

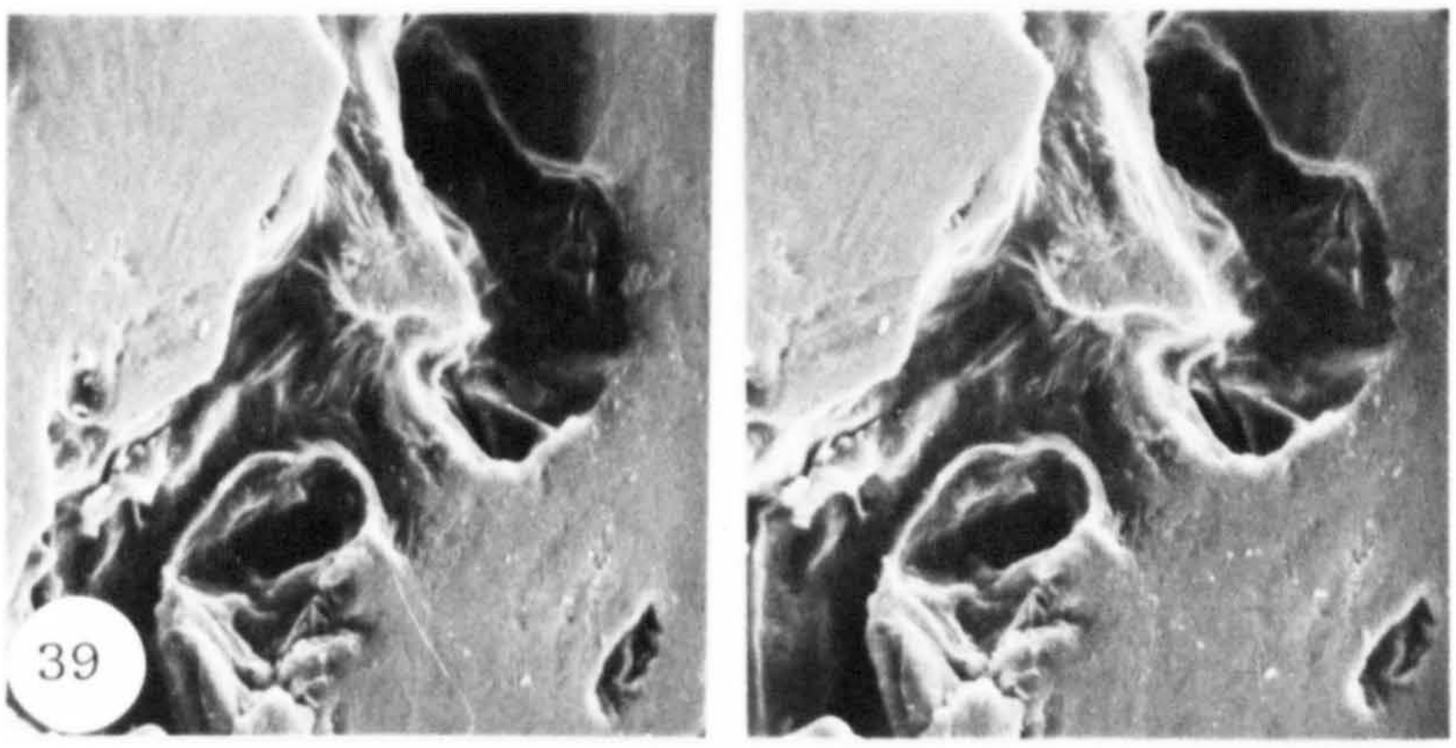
Figures 32 to 36. Scanning electron micrographs (stereoscan) of virgin Lima graphite.



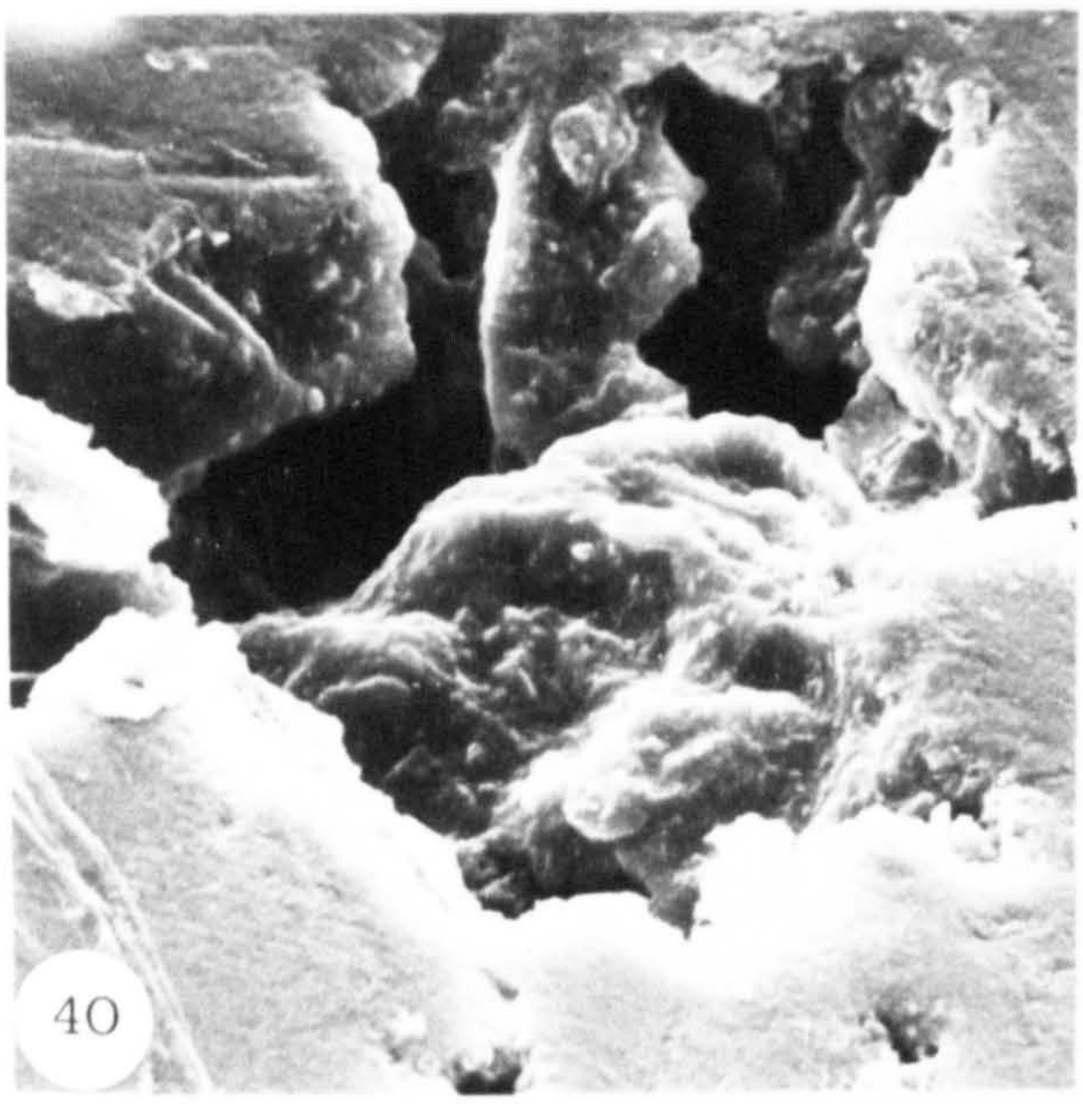
PGA L18 GRAPHITE 50 µm



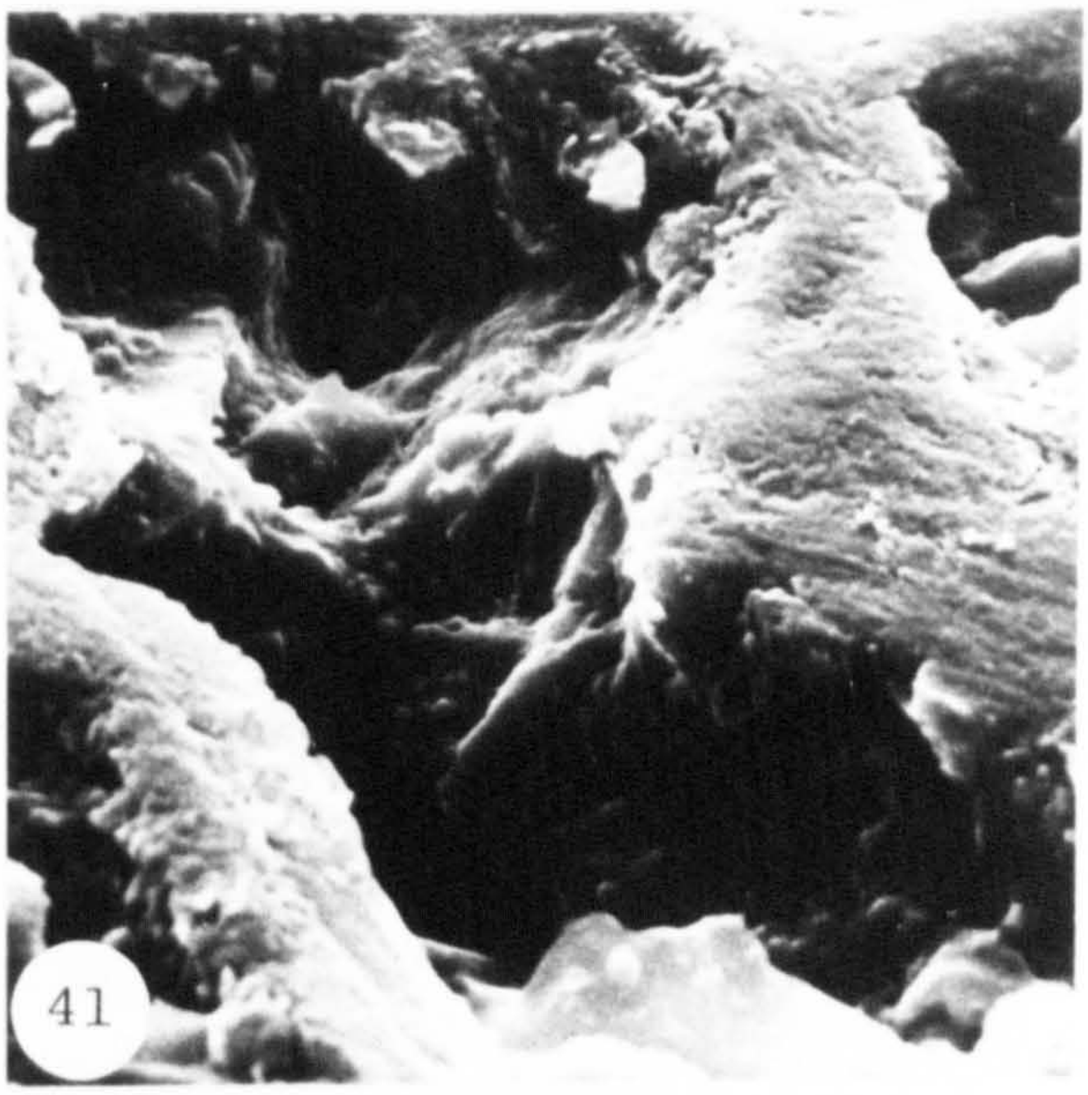
PGA L18 GRAPHITE 20 µm



STEREOPAIR OF PGA L18 GRAPHITE 50 µm

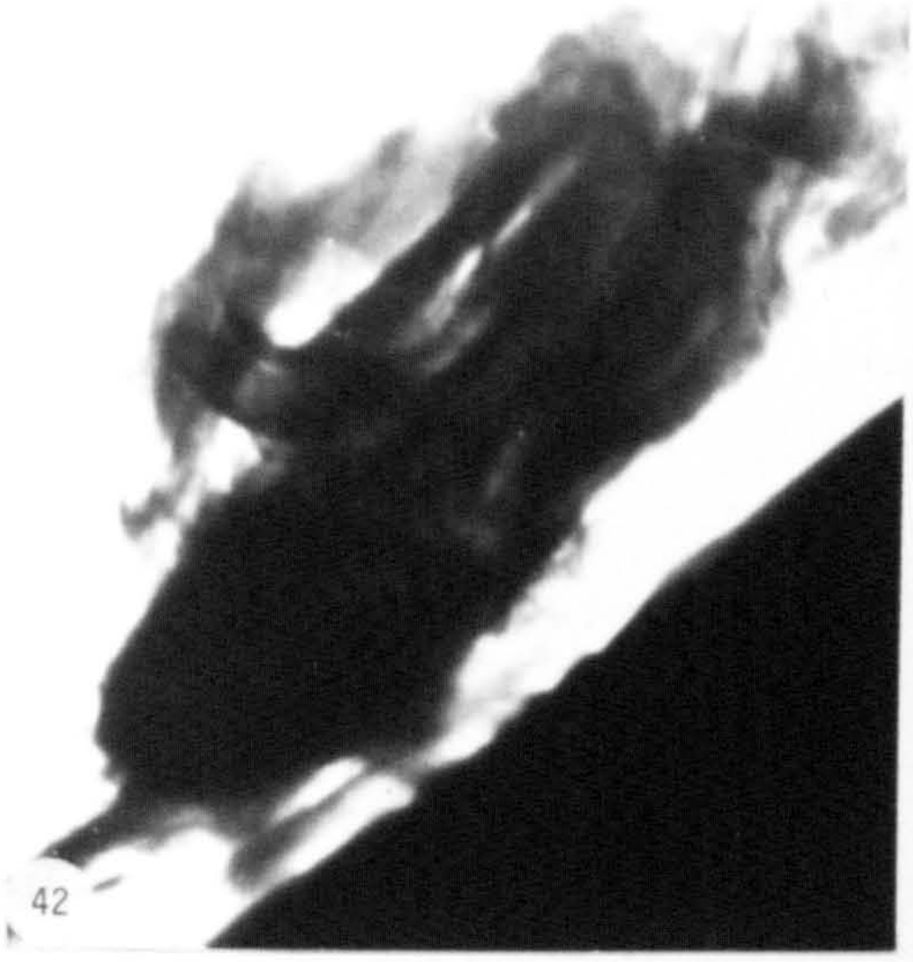


PGA L18 GRAPHITE 10 µm



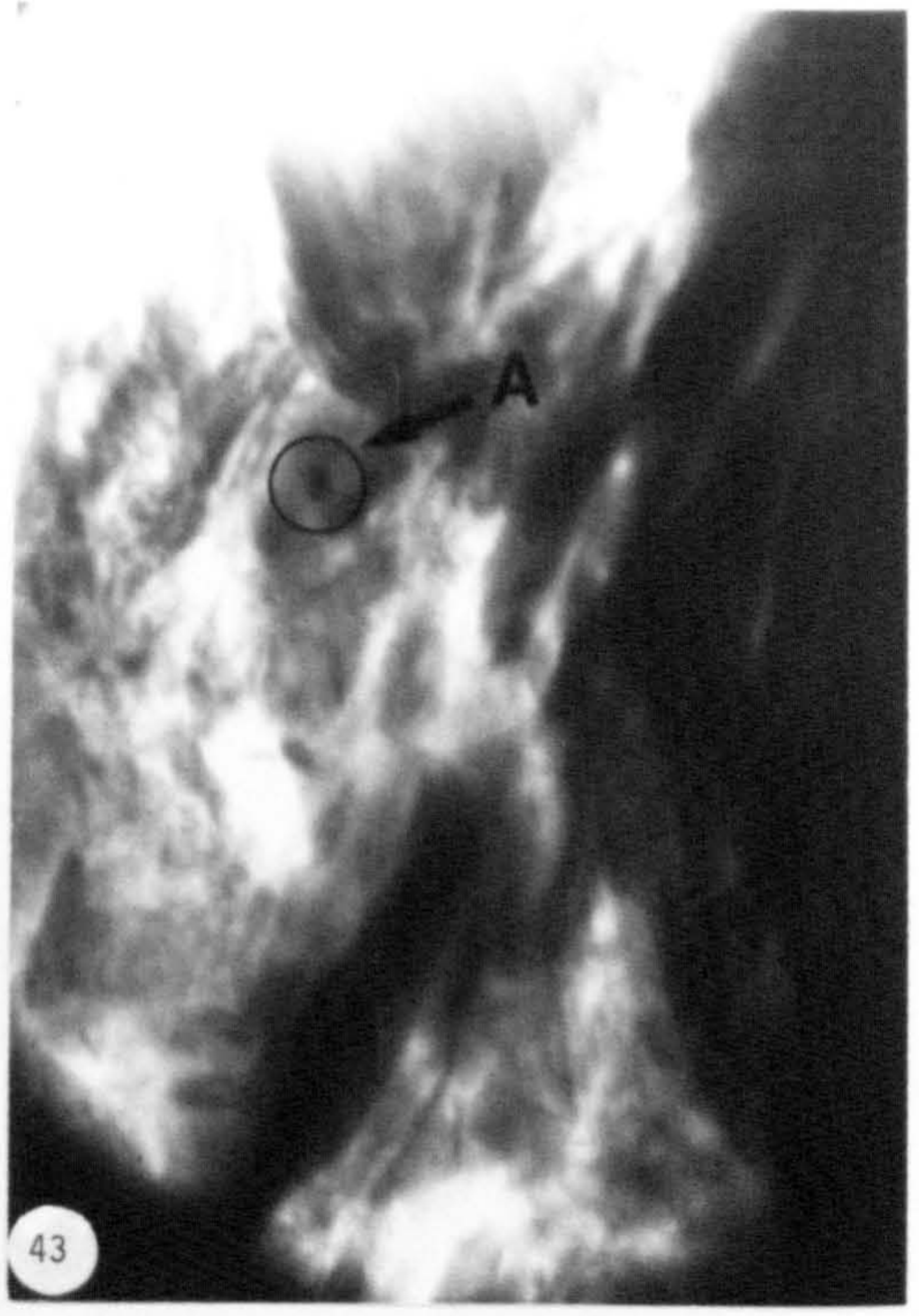
PGA L18 GRAPHITE 5 µm

Figures 37 to 41. Scanning electron micrographs (stereoscan) of virgin PGA L18 graphite.



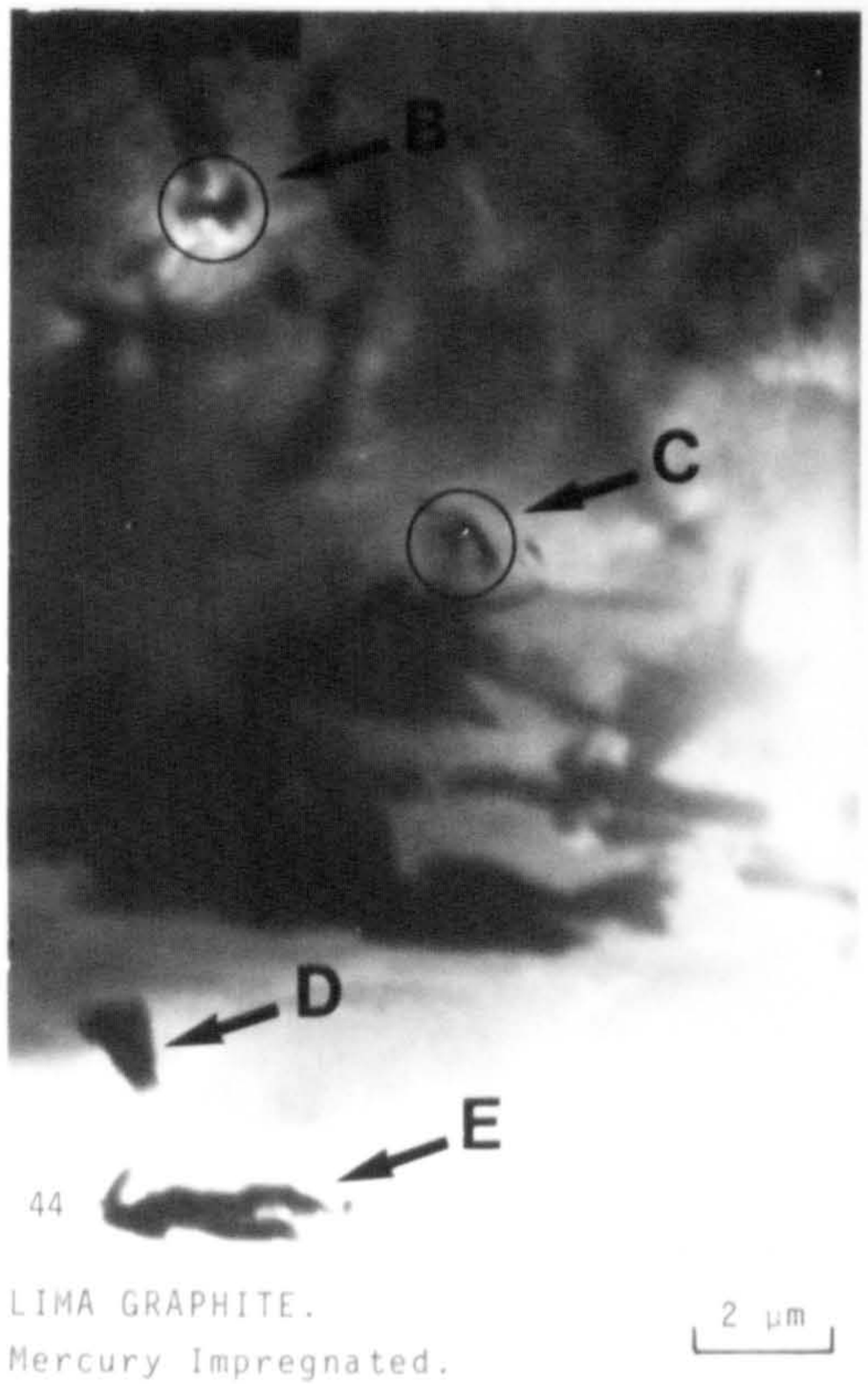
LIMA GRAPHITE.
Mercury Impregnated.

1 µm



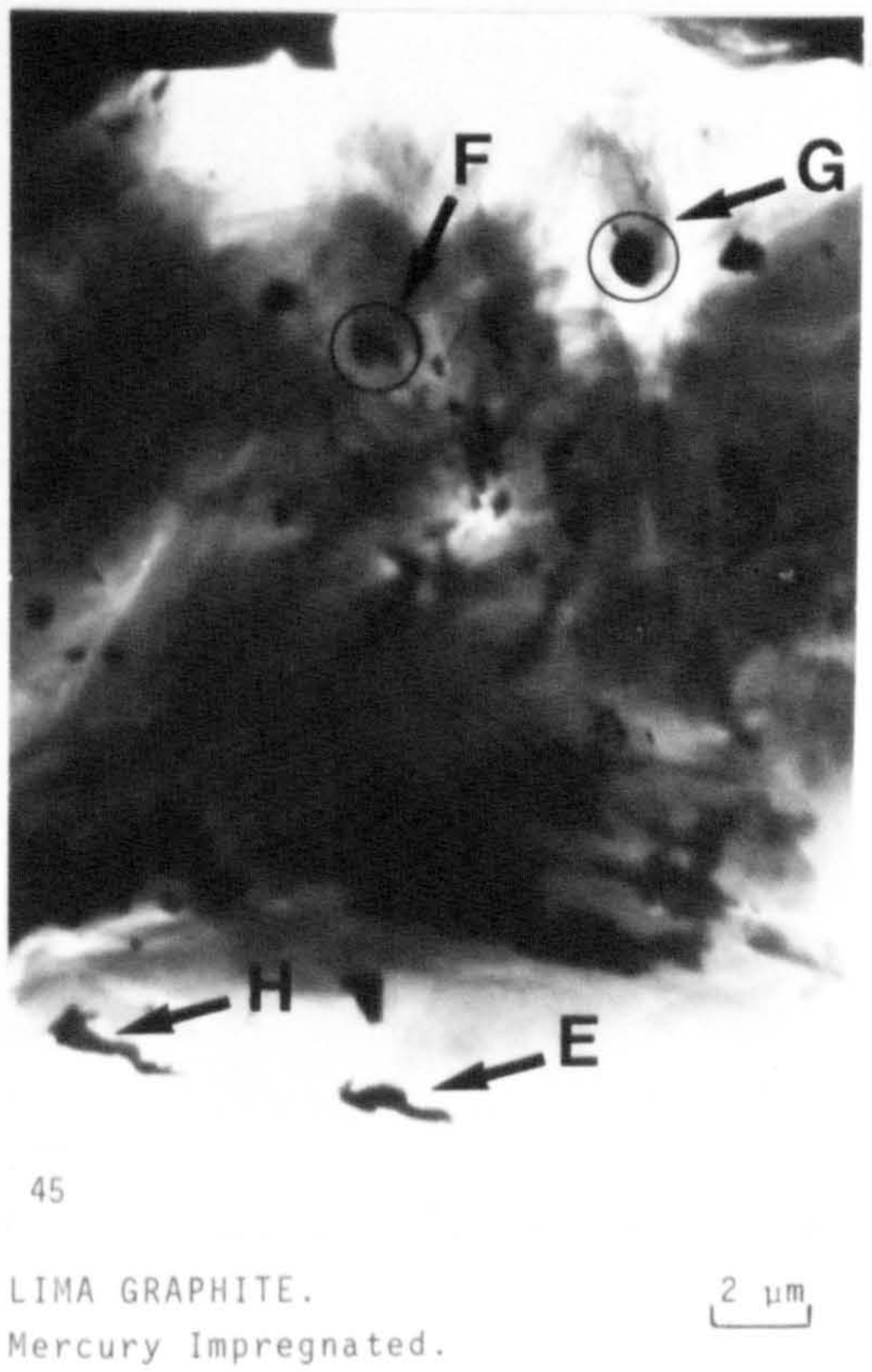
LIMA GRAPHITE.
Mercury Impregnated.

2 µm



LIMA GRAPHITE.
Mercury Impregnated.

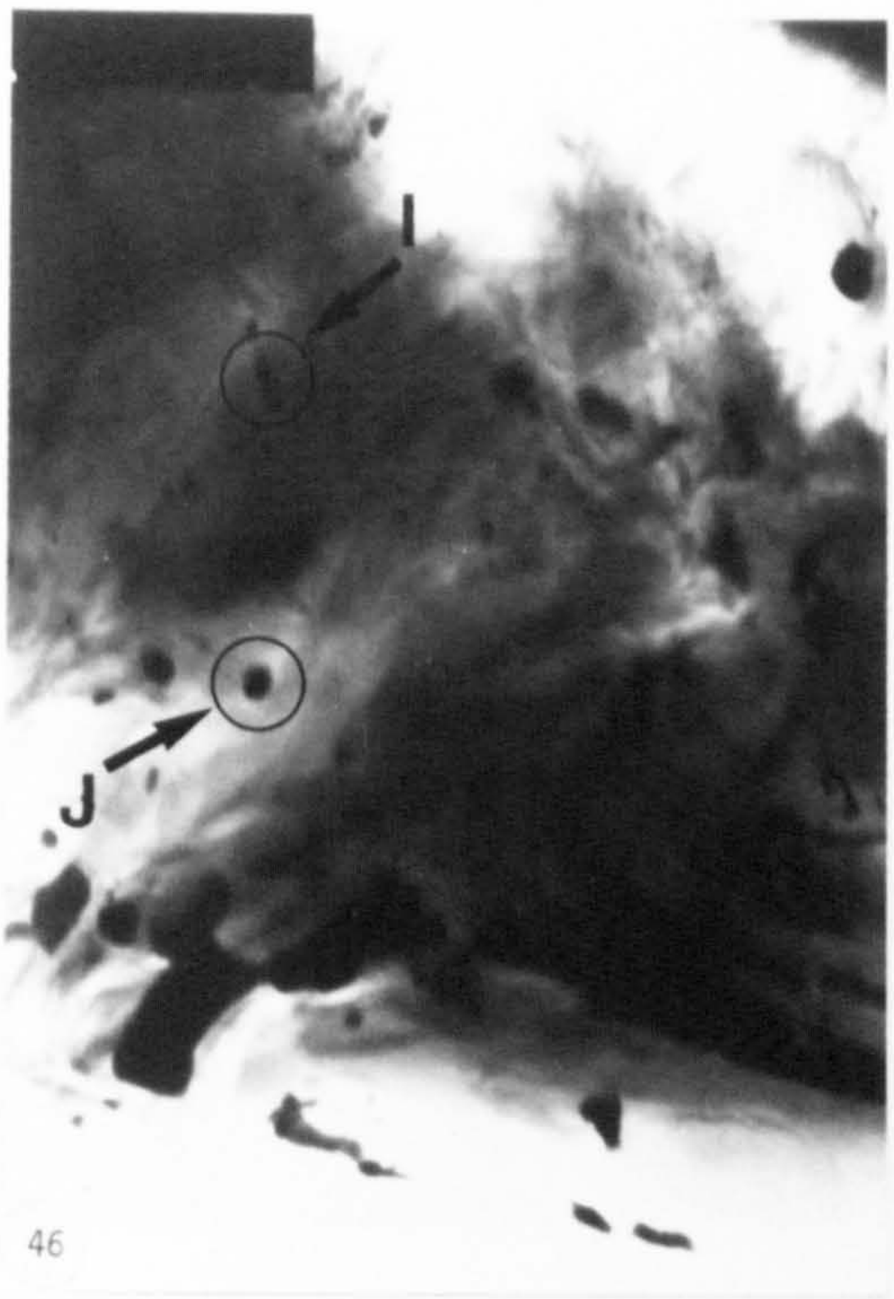
2 µm



LIMA GRAPHITE.
Mercury Impregnated.

2 µm

Figures 42 to 45. Transmission electron micrographs (1,000 kV E.M.) of a ground sample of mercury impregnated Lima Graphite.



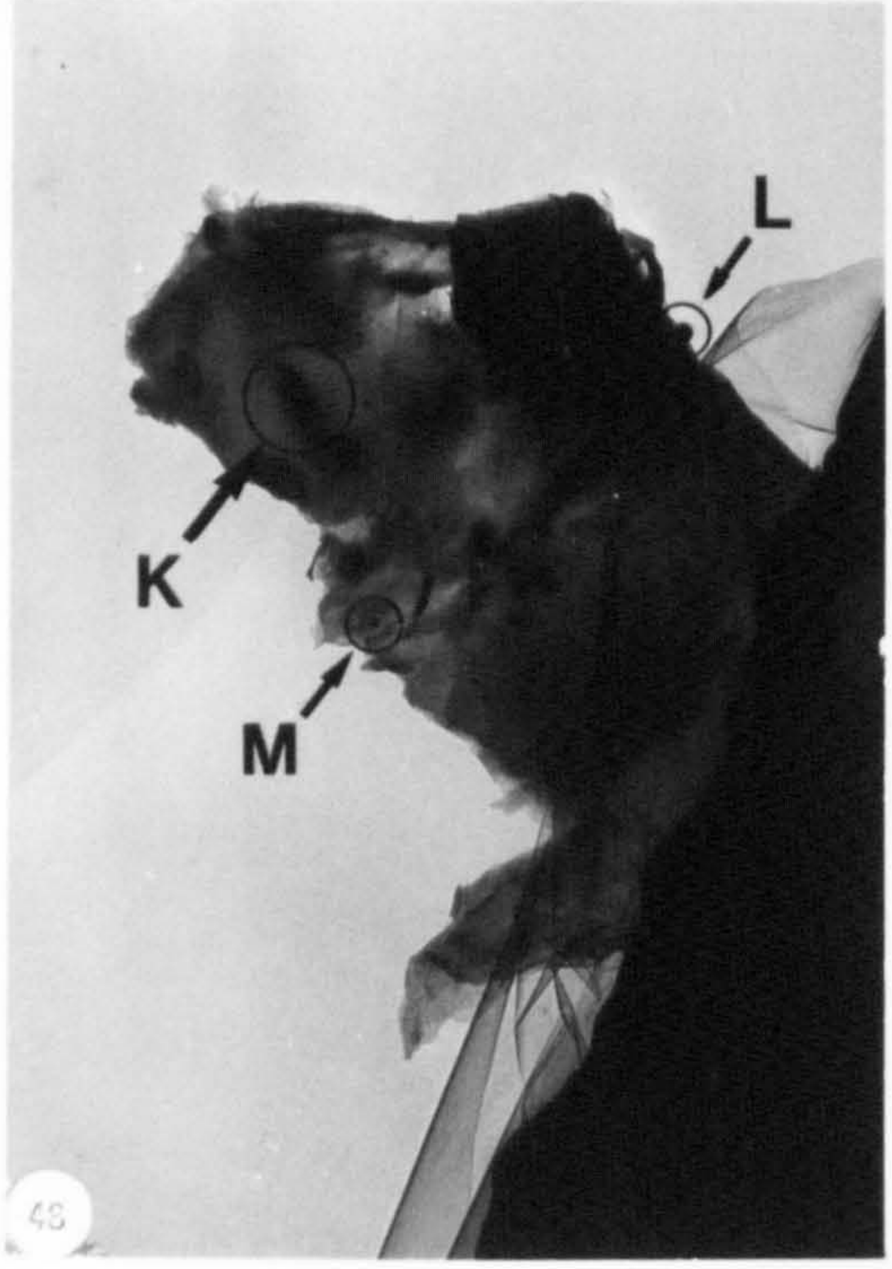
LIMA GRAPHITE.
Mercury Impregnated.

2 µm



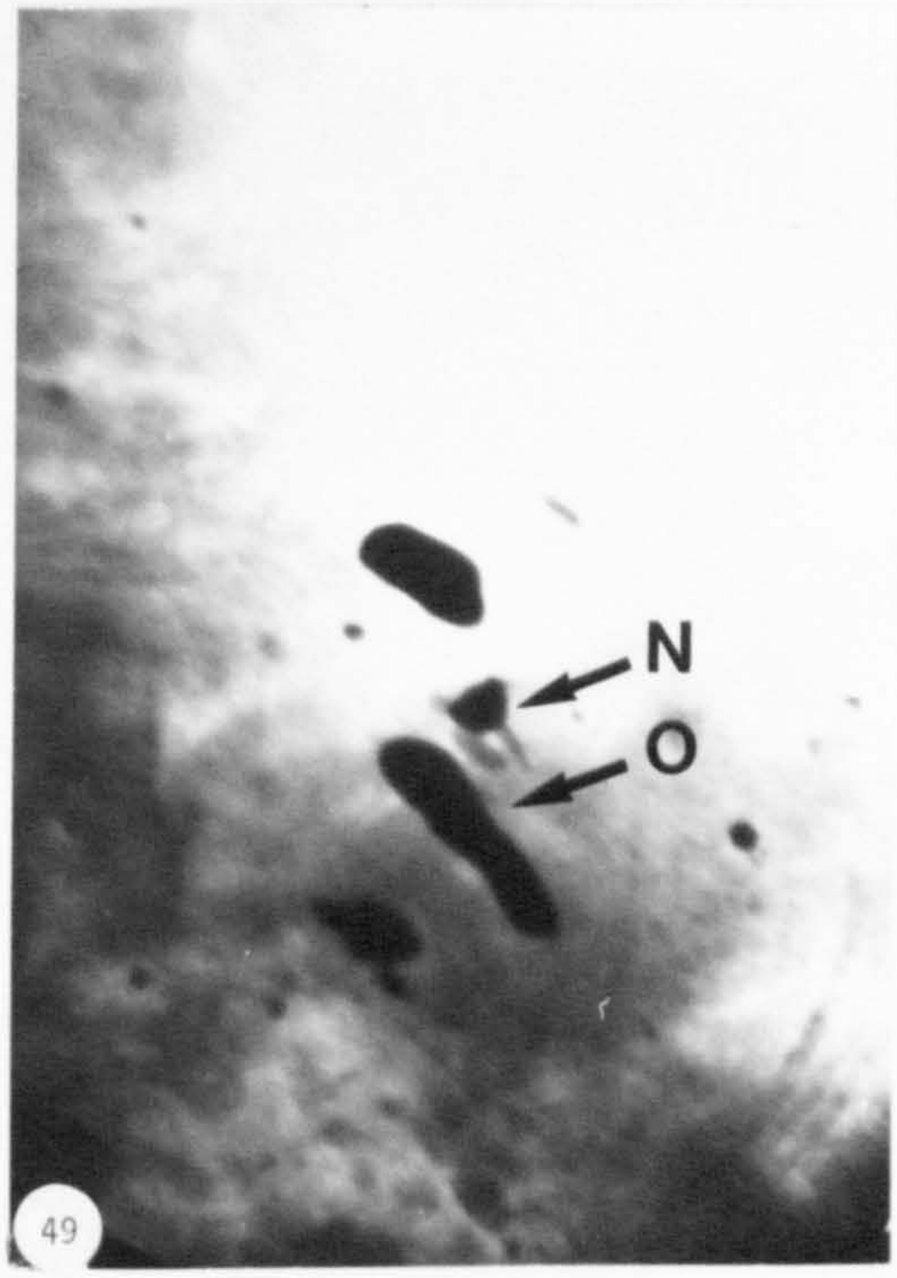
LIMA GRAPHITE.
Mercury Impregnated.
(Stereopair, 10° tilt).

2 µm



LIMA GRAPHITE.
Mercury Impregnated.

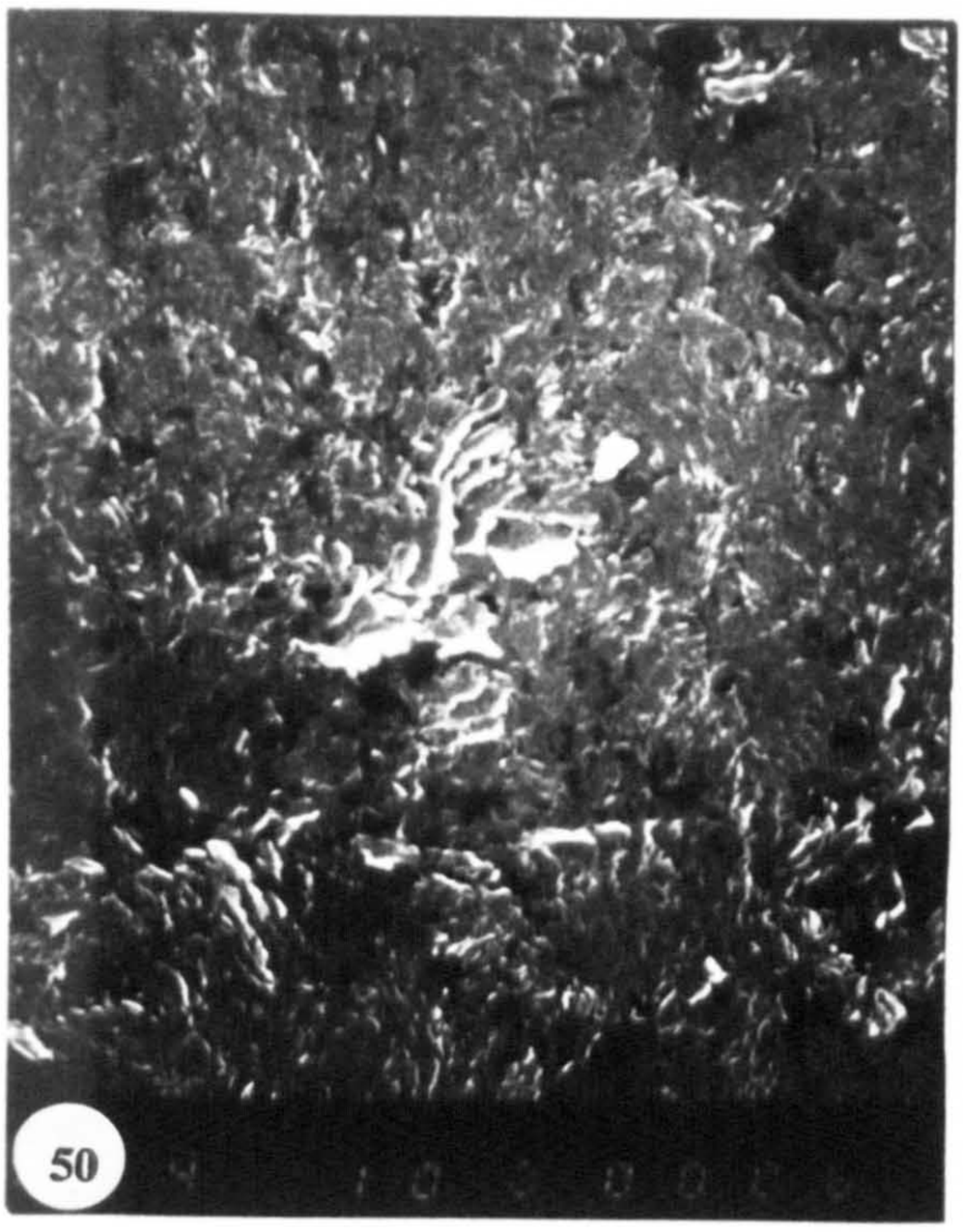
1 µm



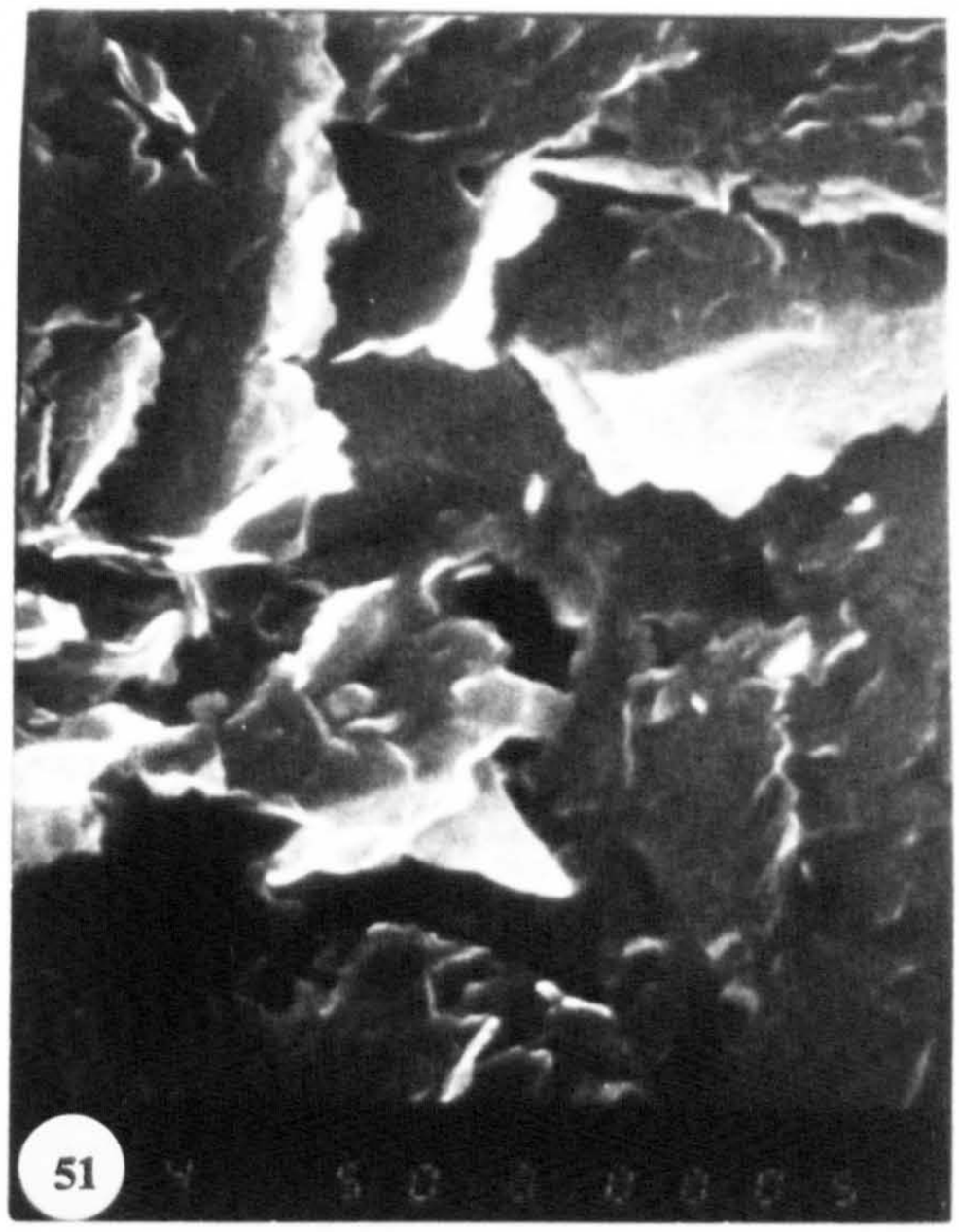
LIMA GRAPHITE.
Mercury Impregnated.

1 µm

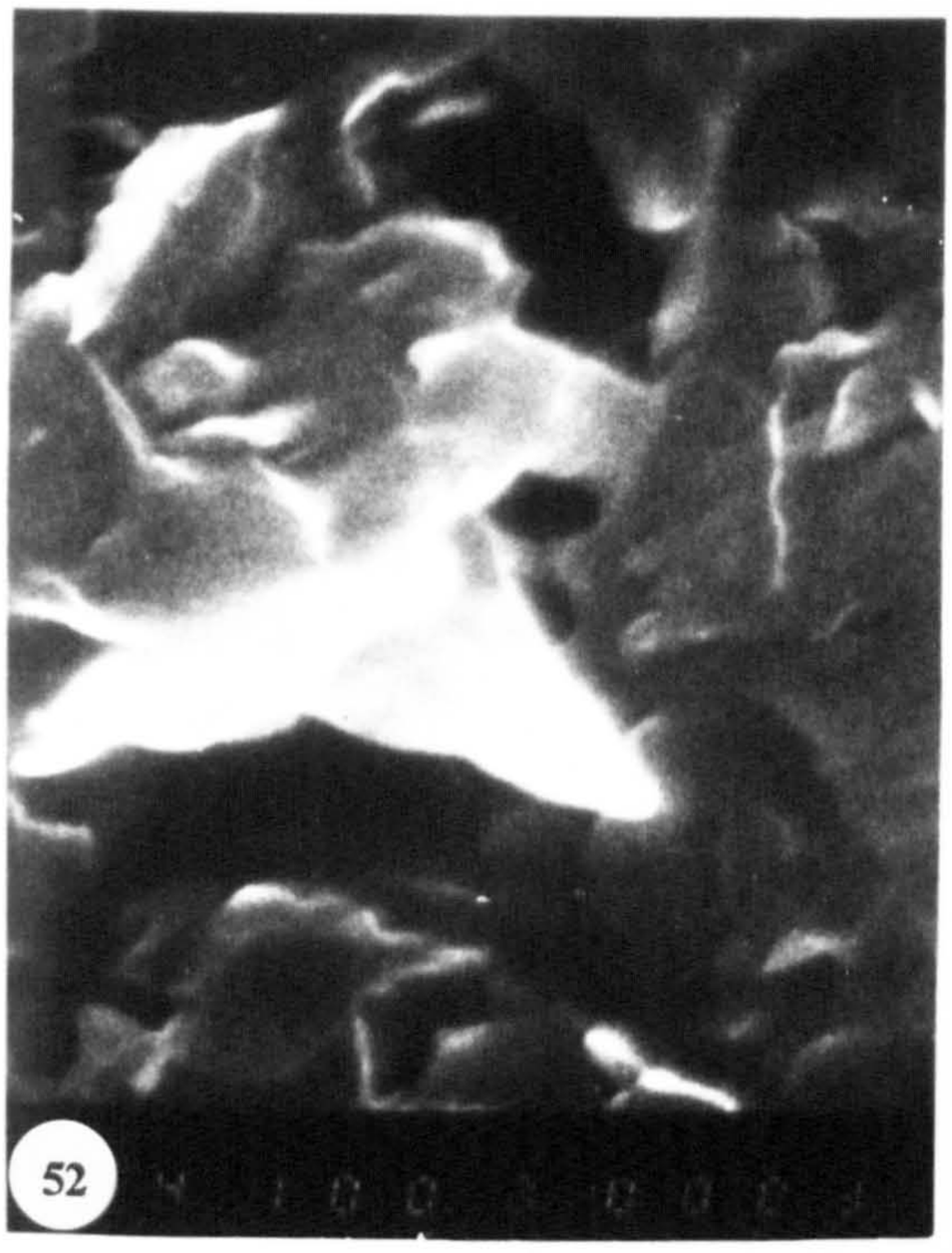
Figures 46, 47 and 48. Ground sample of mercury impregnated Lima Graphite.
Figure 49. Thin slice of mercury impregnated Lima Graphite.
Transmission electron micrographs (1,000 kV E.M.).



LIMA GRAPHITE. 1000 nm



LIMA GRAPHITE. 200 nm

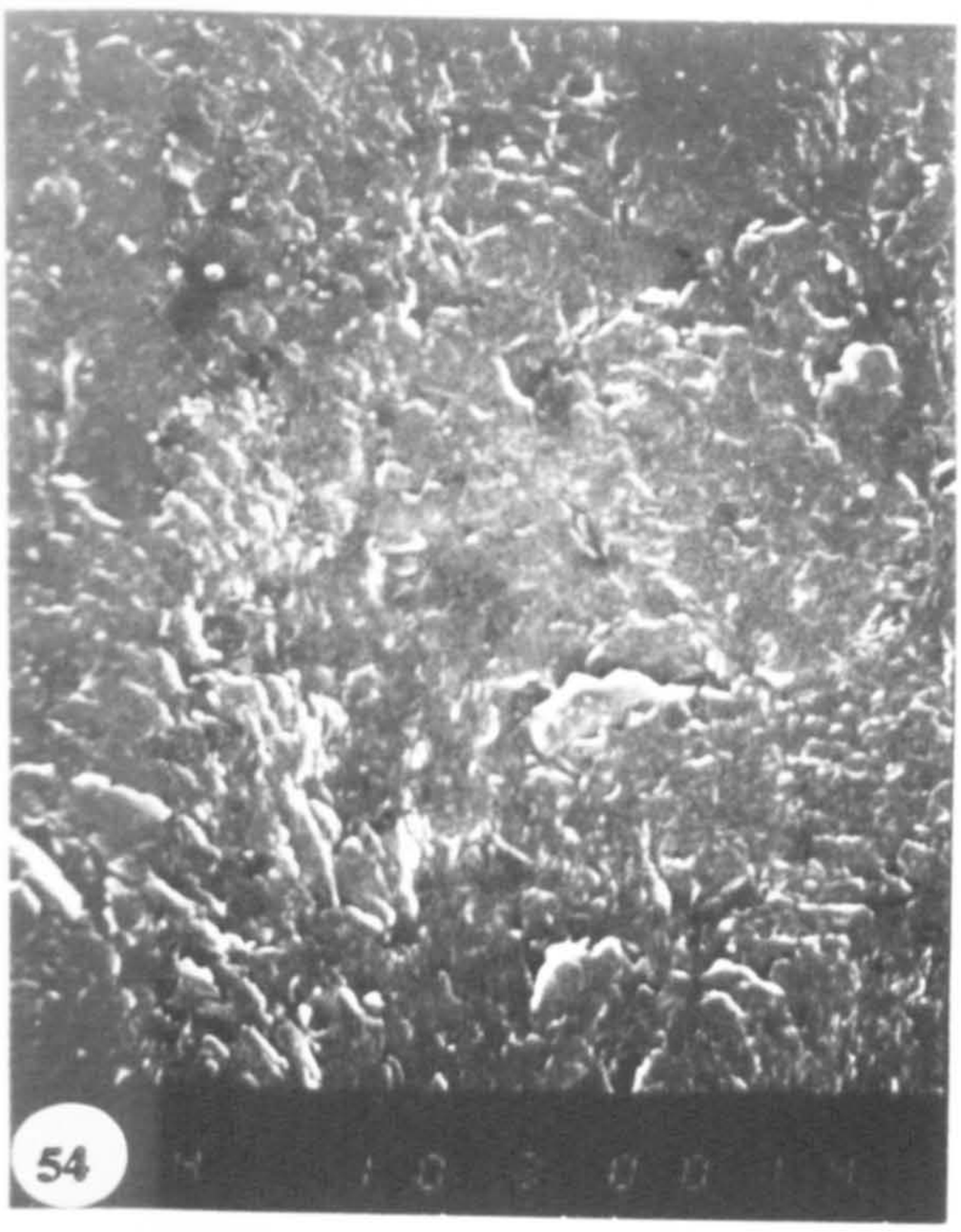


LIMA GRAPHITE. 100 nm



LIMA GRAPHITE. 50 nm

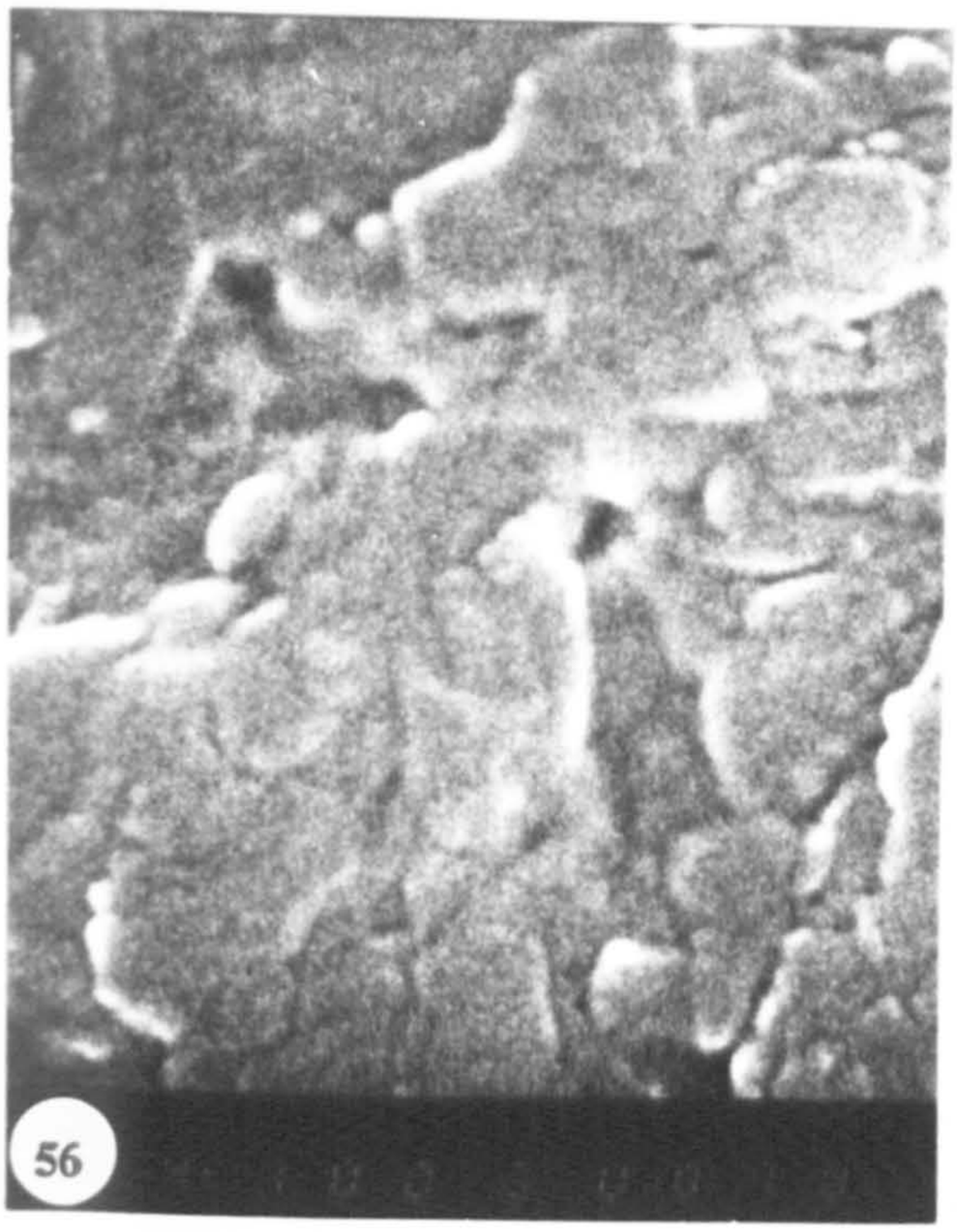
Figures 50 to 53. Scanning electron micrographs (JEOL 100C - ASID-4D) of Lima Graphite, coated with Pt/Pd.



LIMA GRAPHITE. 1000 nm



LIMA GRAPHITE. 200 nm



LIMA GRAPHITE. 100 nm



LIMA GRAPHITE. 50 nm

Figures 54 to 57. Scanning electron micrographs (JEOL 100C - ASID-4D) of Lima graphite, coated with Pt/Pd.



LIMA GRAPHITE. 50 nm



AGL HP UNIPORE GRAPHITE. 200 nm



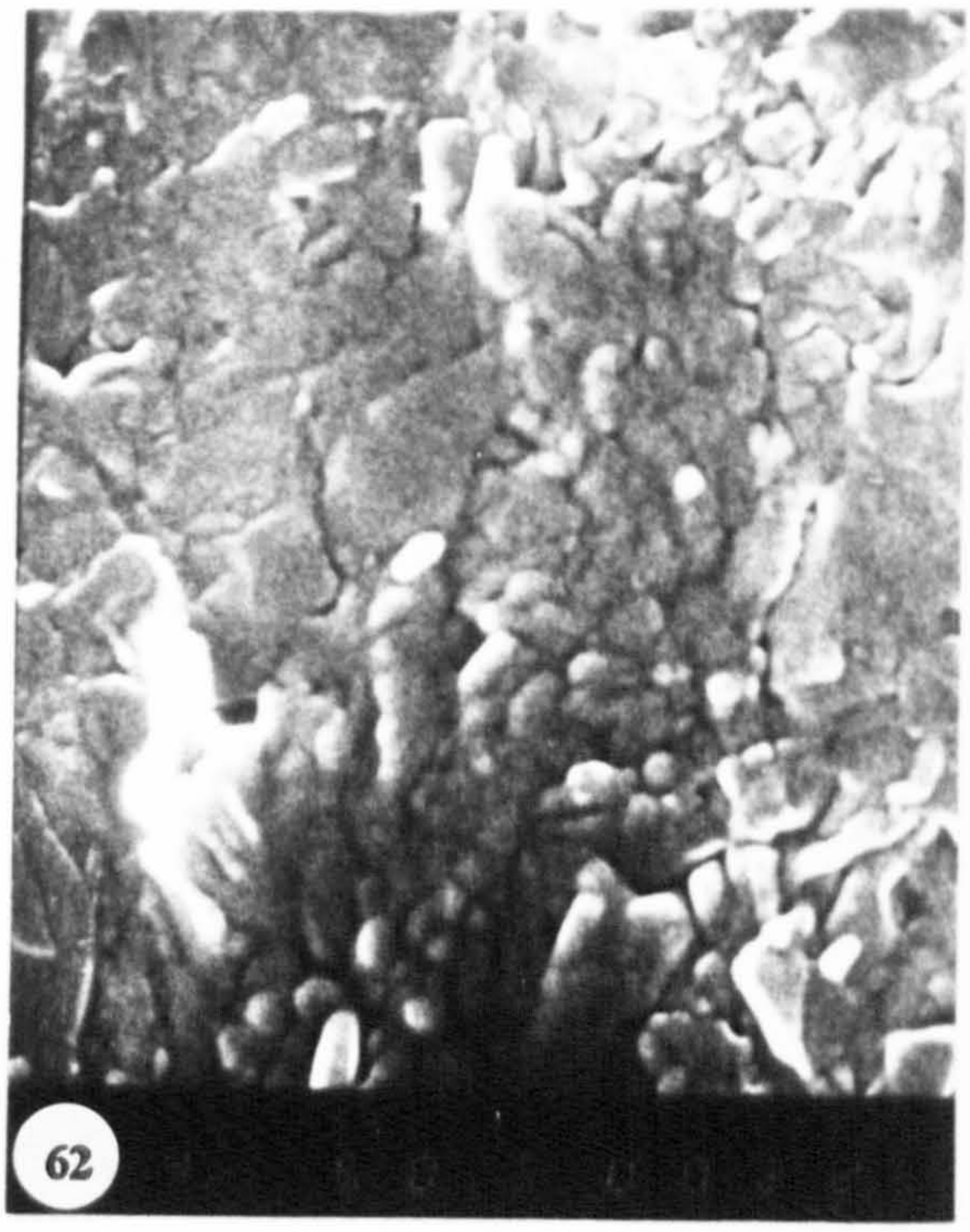
AGL HP UNIPORE GRAPHITE. 200 nm

Figure 58.
Figures 59 to 60.

Lima Graphite
AGL HP Unipore Graphite
Scanning electron micrographs (JEOL 100C - ASID-4D) coated with Pt/Pd.



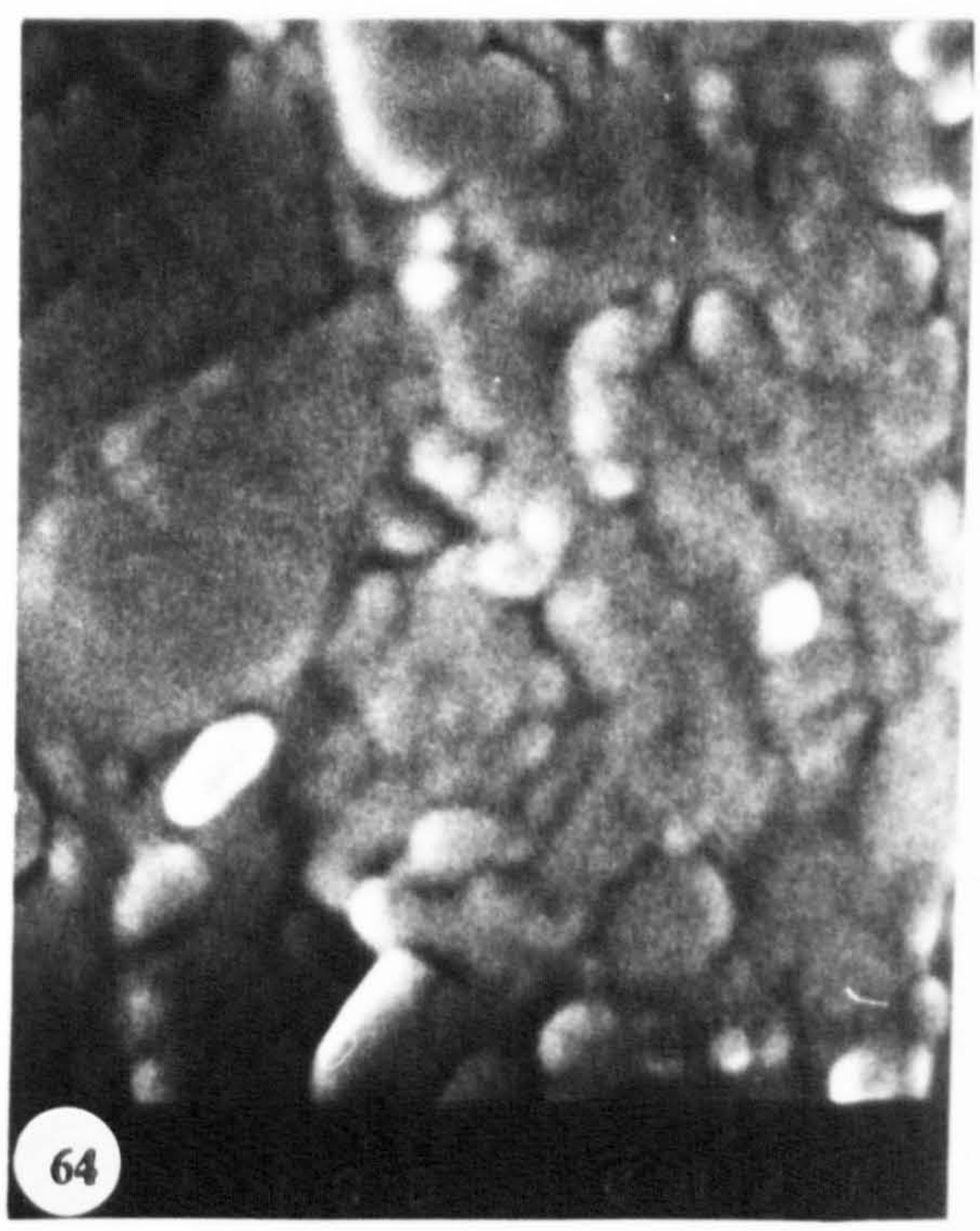
AGL HP UNIPORE GRAPHITE. 1000 nm



AGL HP UNIPORE GRAPHITE. 200 nm



AGL HP UNIPORE GRAPHITE. 100 nm



AGL HP UNIPORE GRAPHITE. 100 nm

(Stereopair of the adjacent micrograph, 12° tilt).

Figures 61 to 64. Scanning electron micrographs (JEOL 100C - ASID-4D) of AGL HP Unipore Graphite, coated with Pt/Pd.



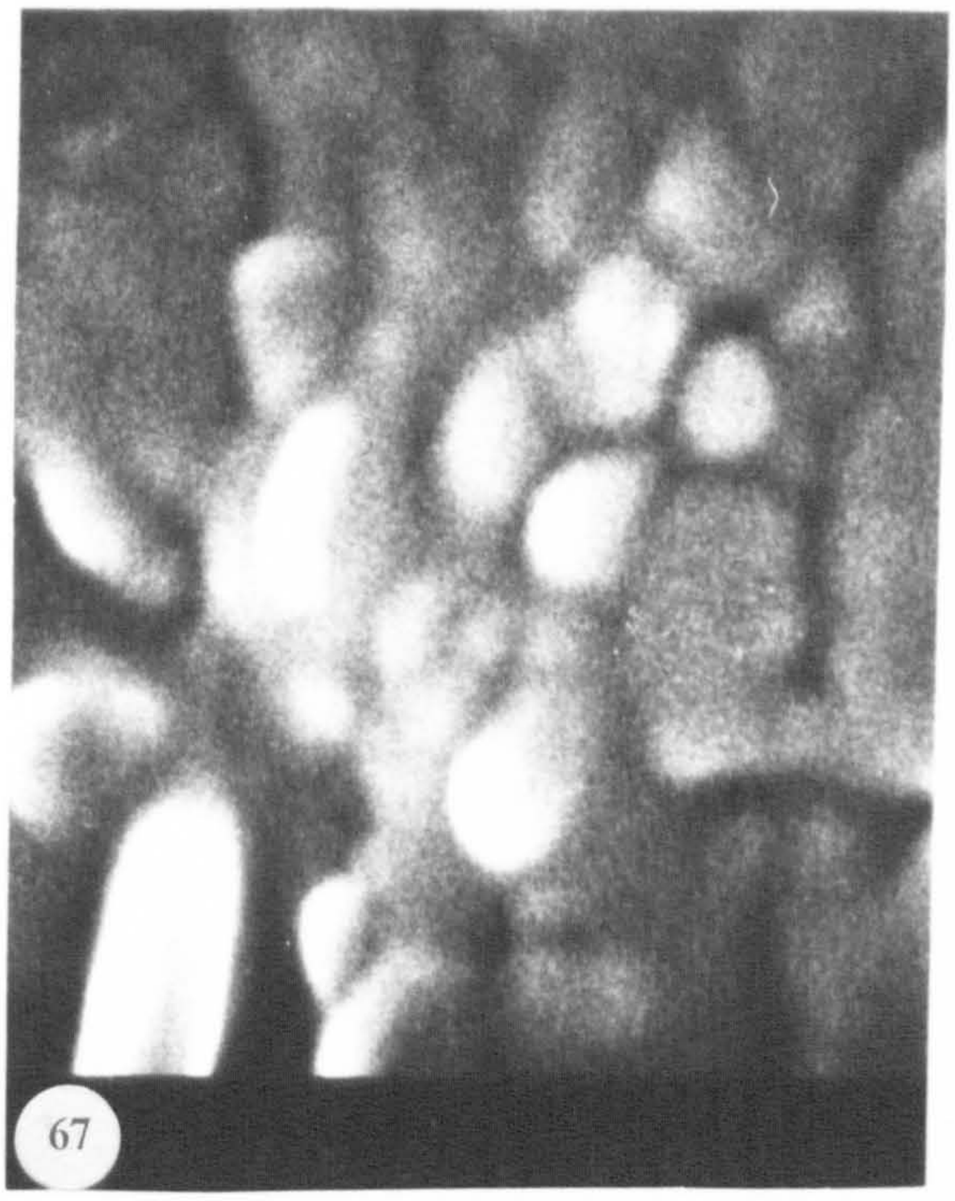
65

AGL HP UNIPORE GRAPHITE. 200 nm



66

AGL HP UNIPORE GRAPHITE. 100 nm



67

AGL HP UNIPORE GRAPHITE. 50 nm

Figures 65 to 67. Scanning electron micrographs (JEOL 100C - ASID-4D) of AGL HP Unipore Graphite, coated with Pt/Pd.

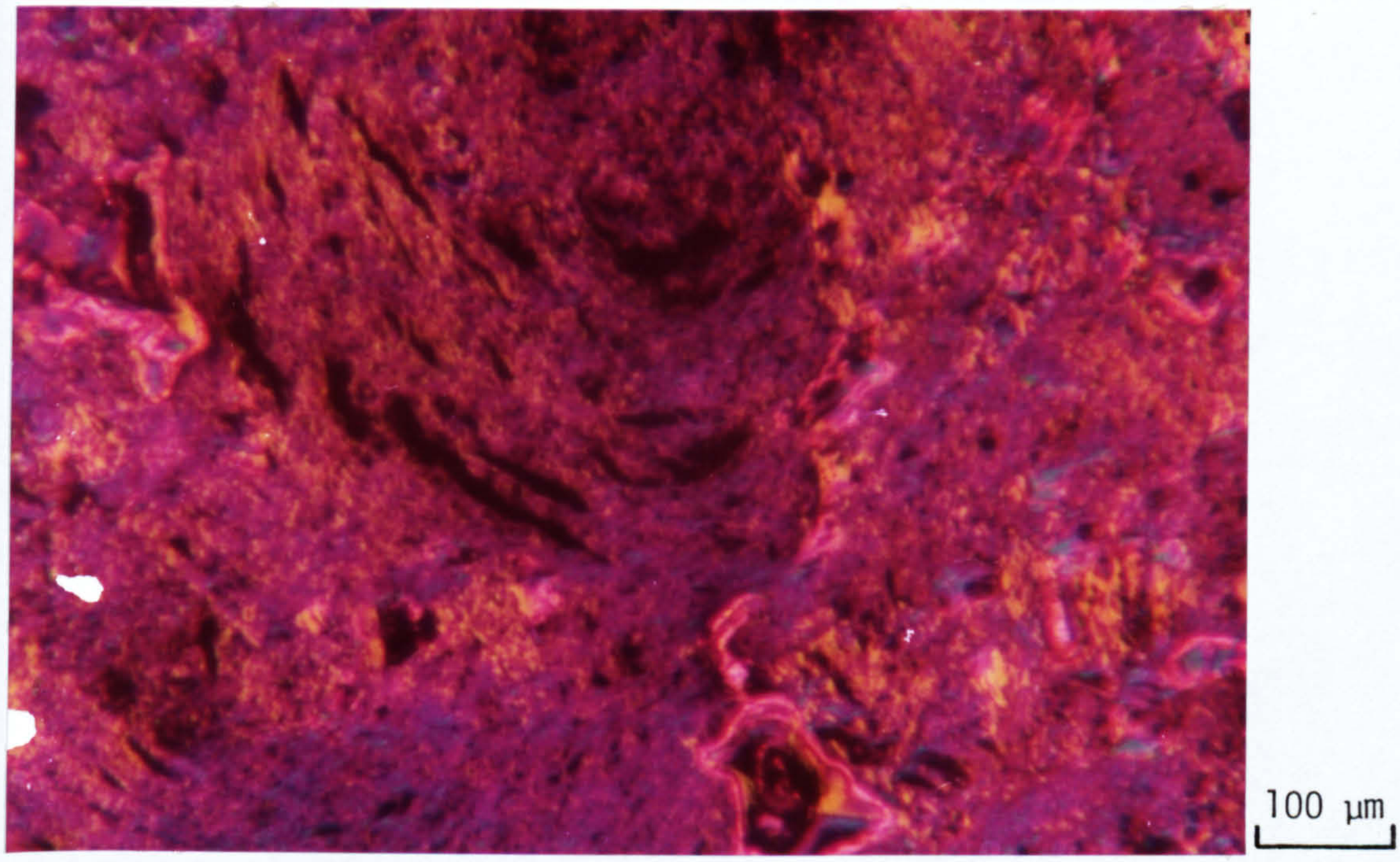


Figure 68. Optical micrograph of AGLMP graphite impregnated with gold.

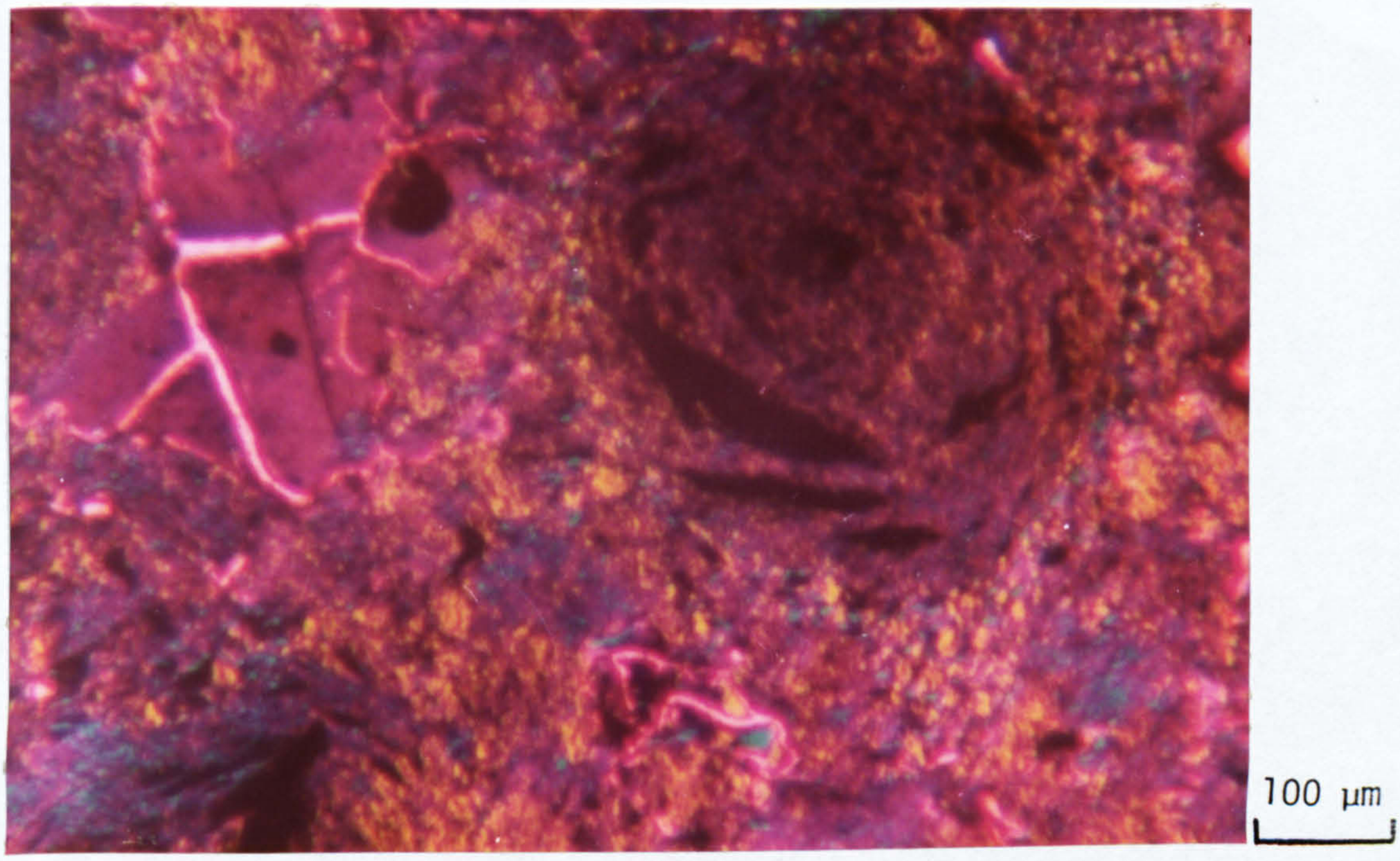


Figure 69. Optical micrograph of GCMB graphite impregnated with gold.

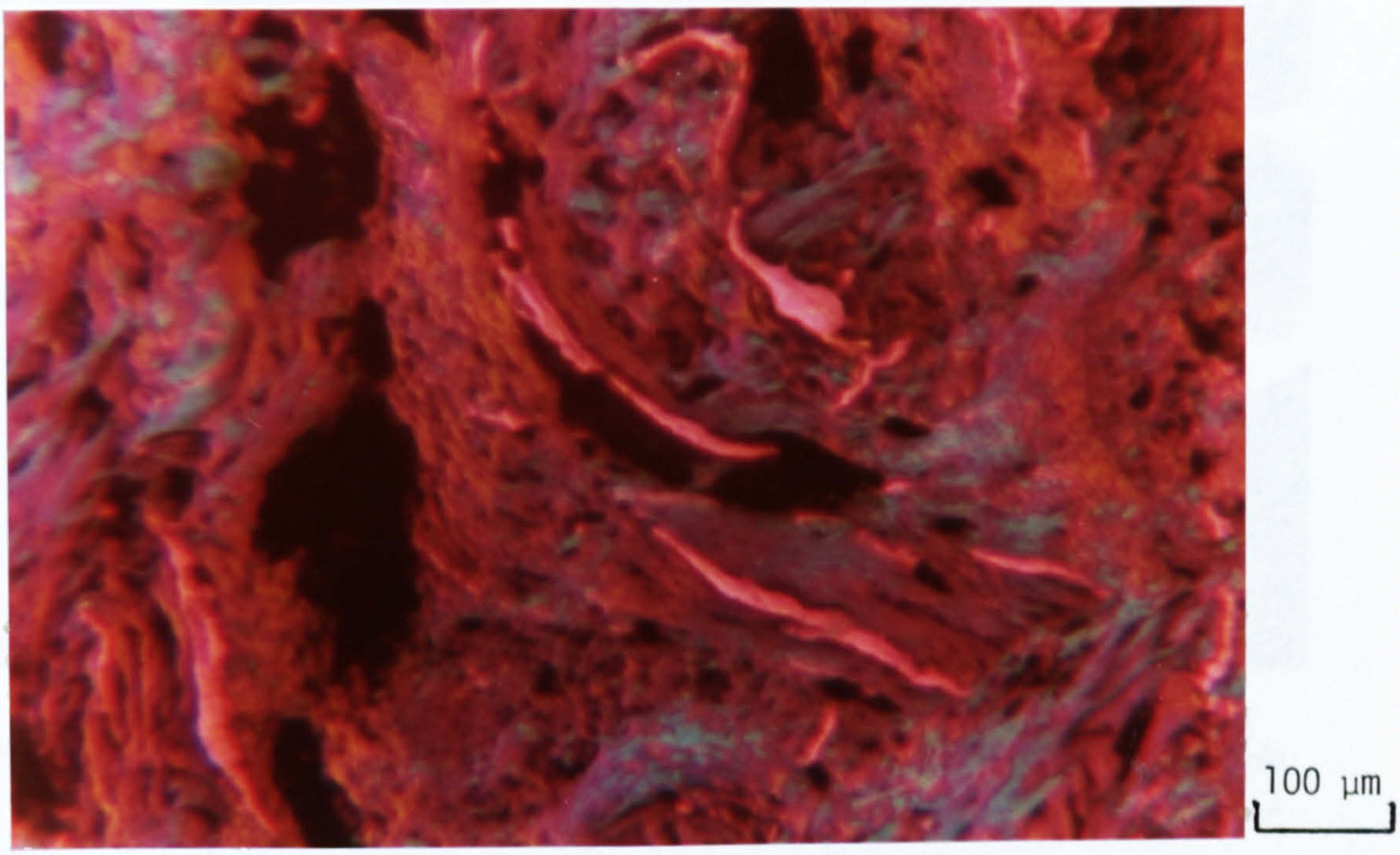


Figure 70. Optical micrograph of Lima graphite impregnated with gold.

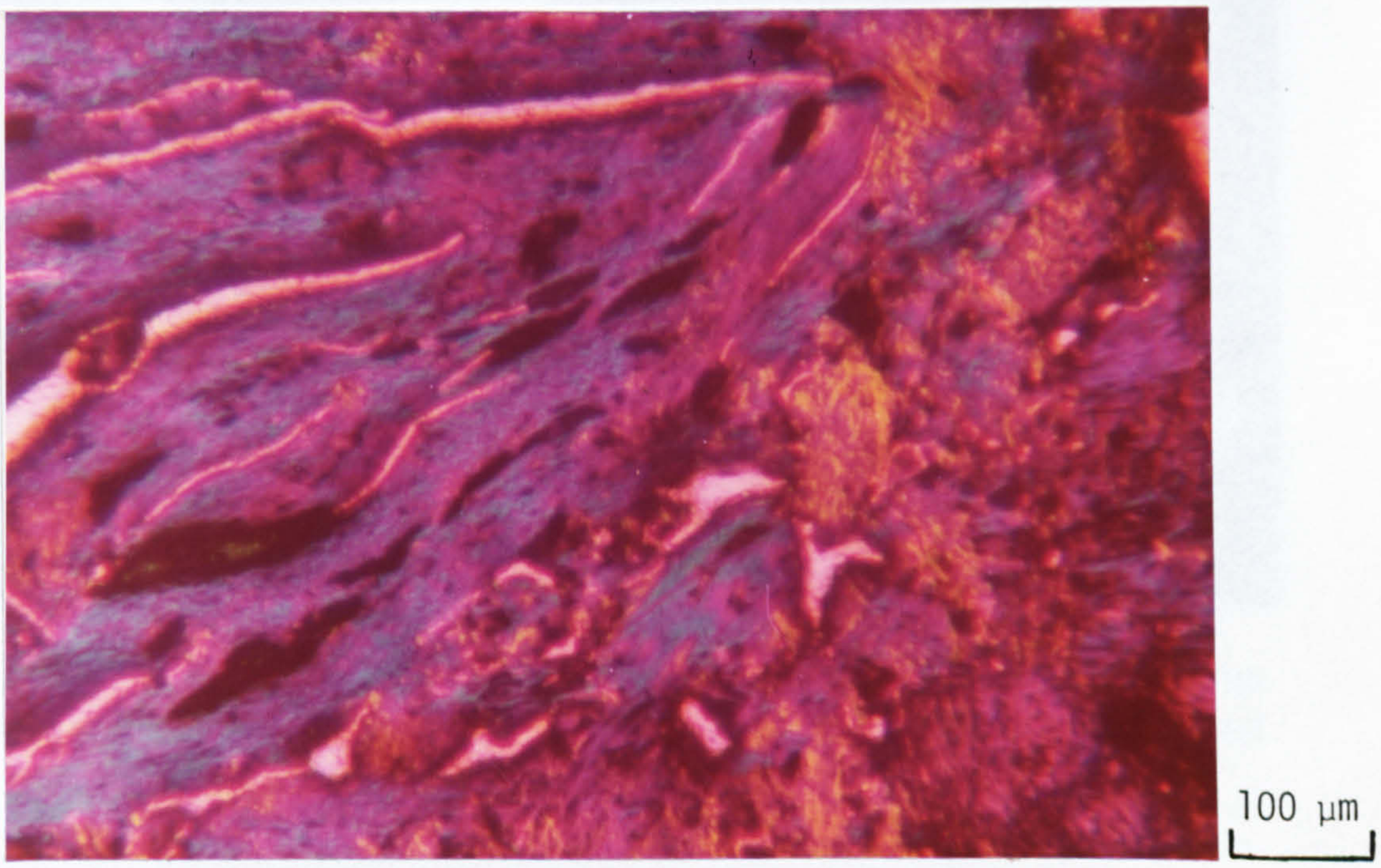
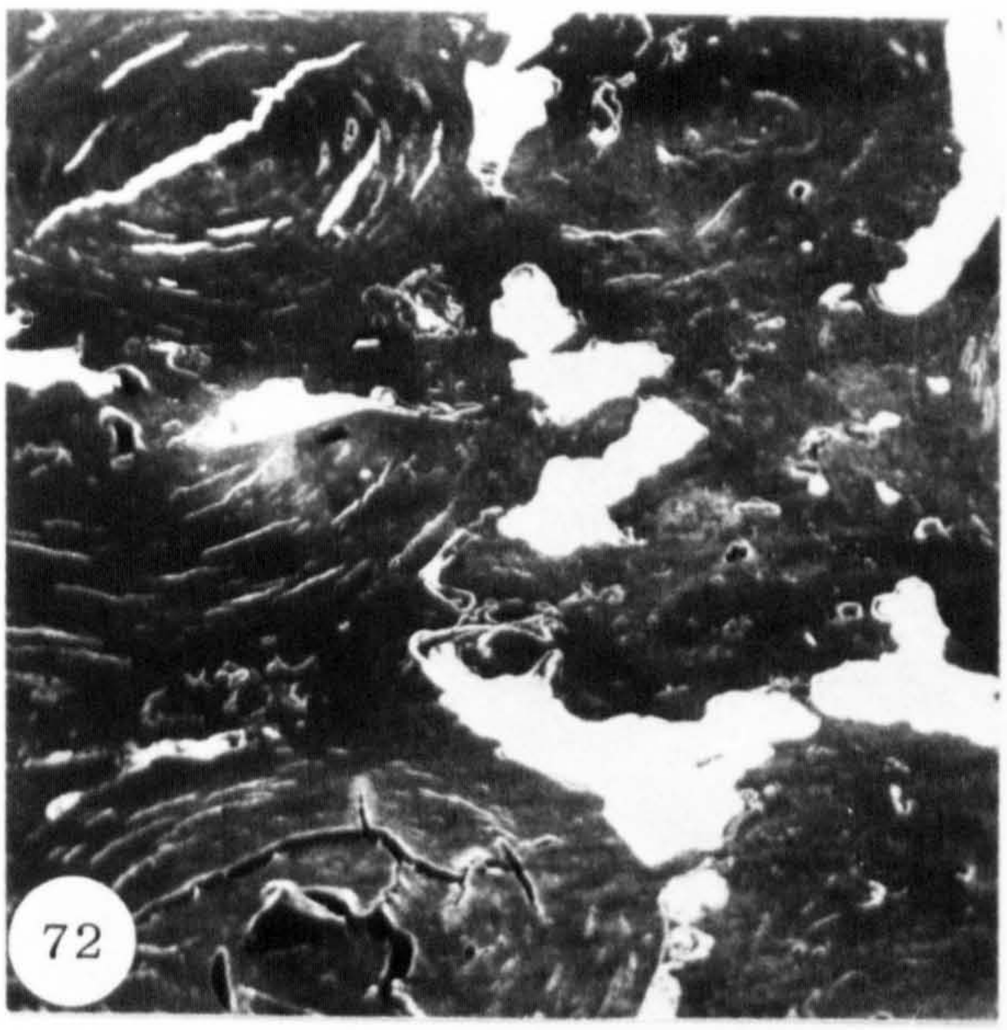
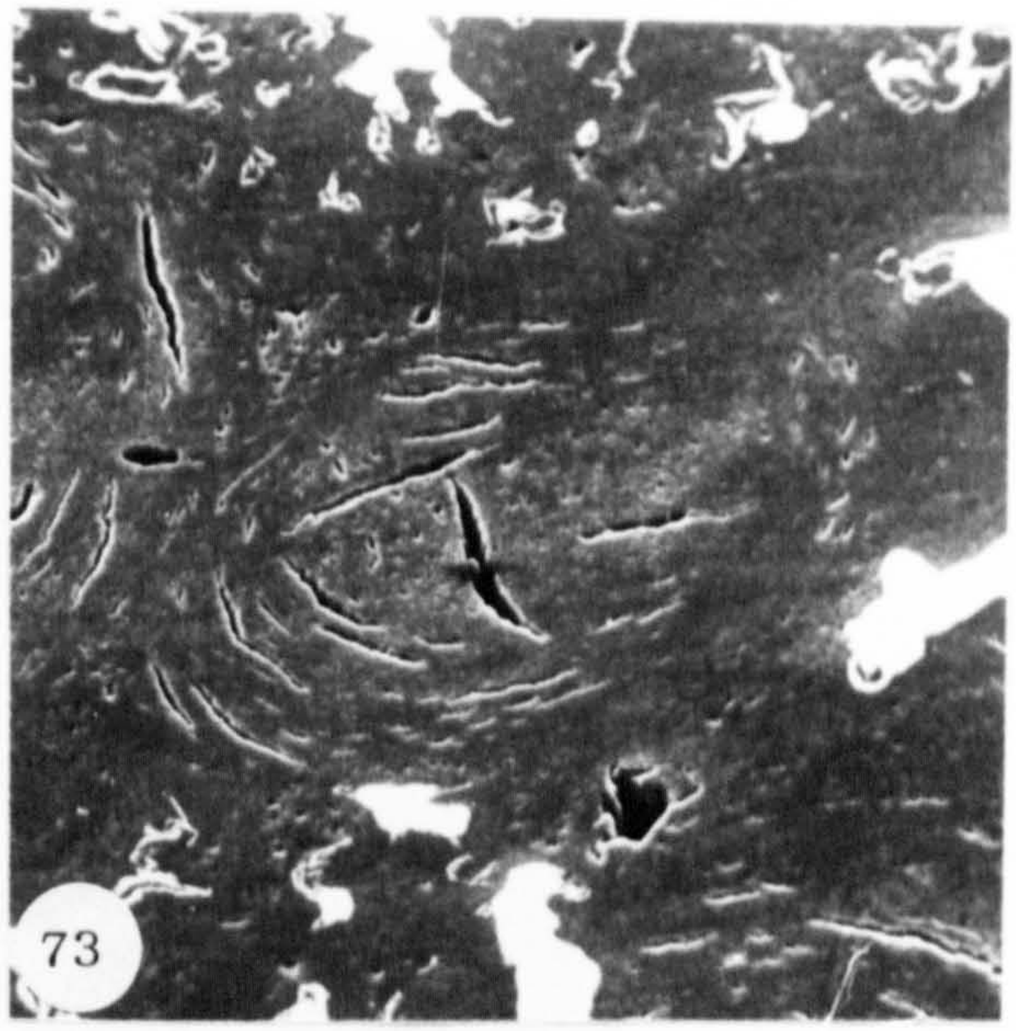


Figure 71. Optical micrograph of PGA L18 graphite impregnated with gold.



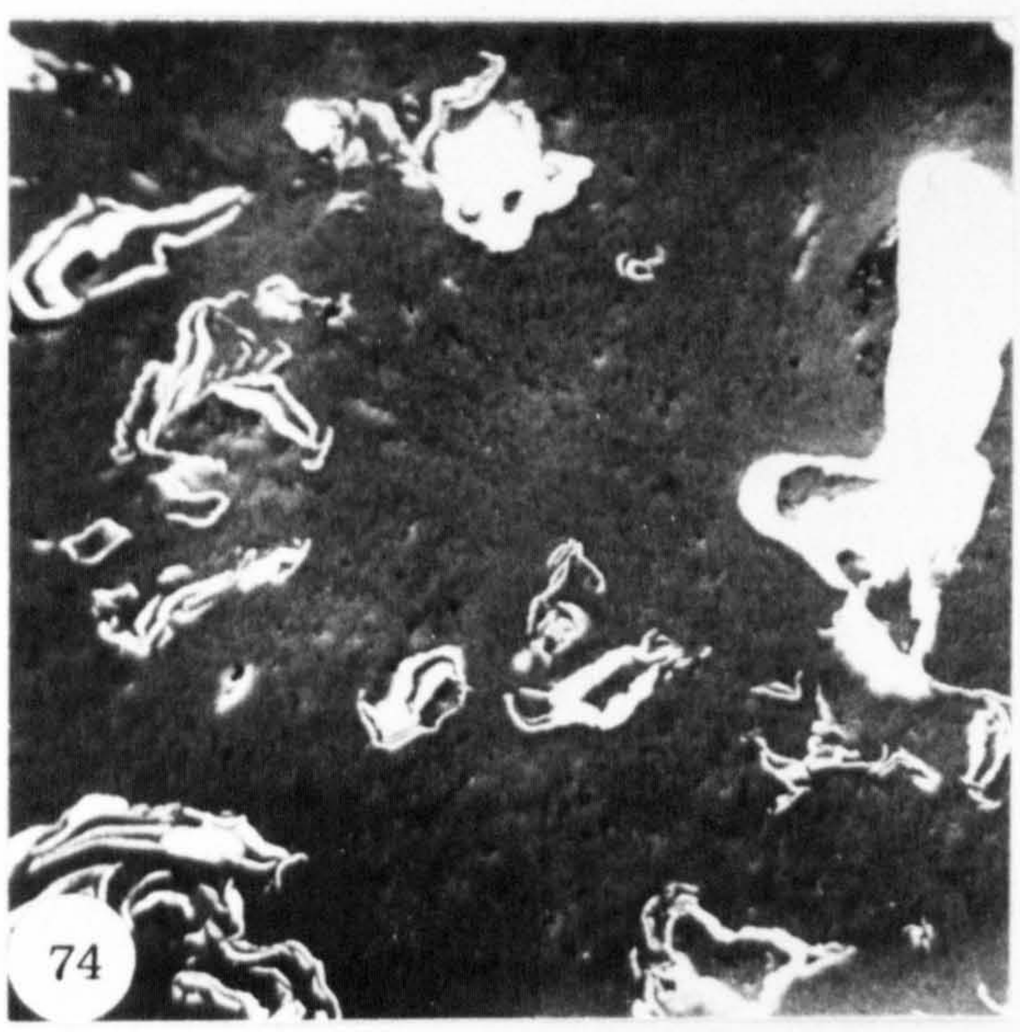
AGLMP GRAPHITE
Gold impregnated

200 µm



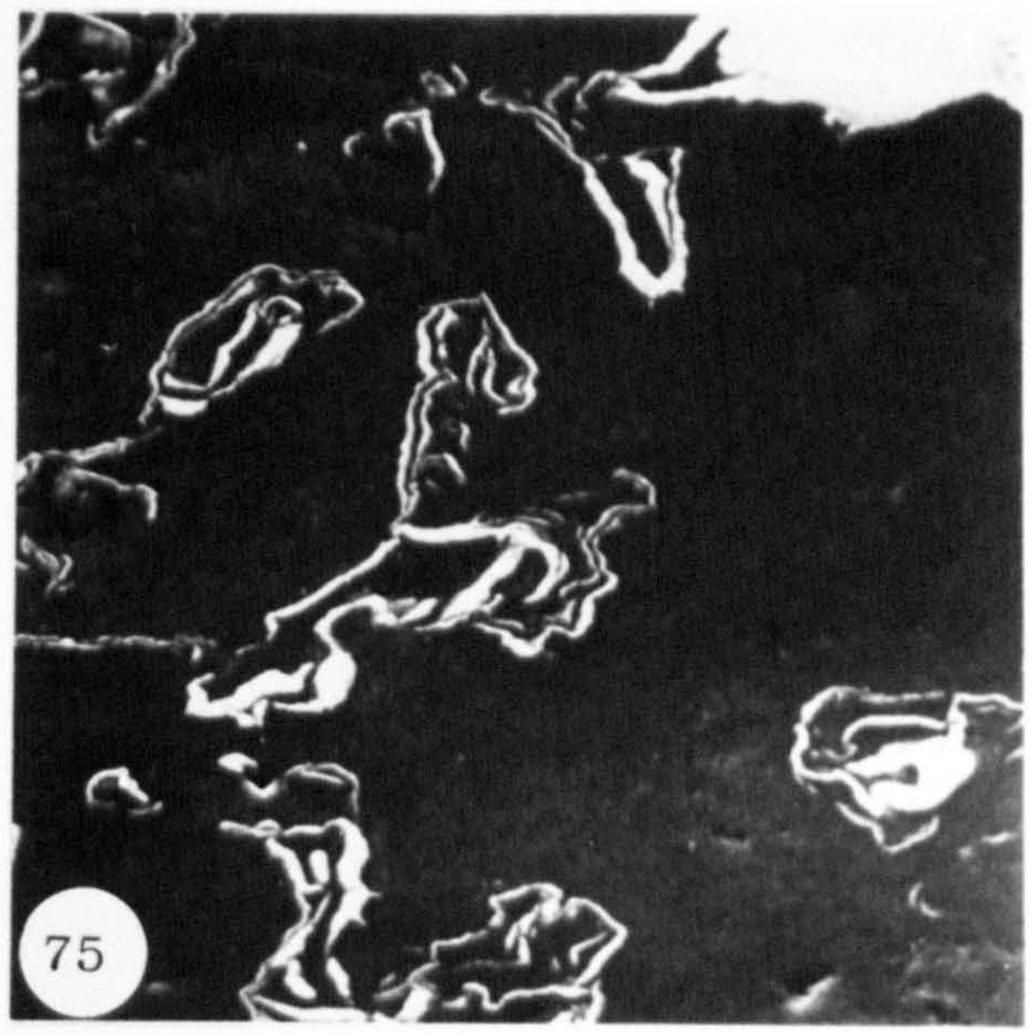
AGLMP GRAPHITE
Gold impregnated

100 µm



AGLMP GRAPHITE
Gold impregnated

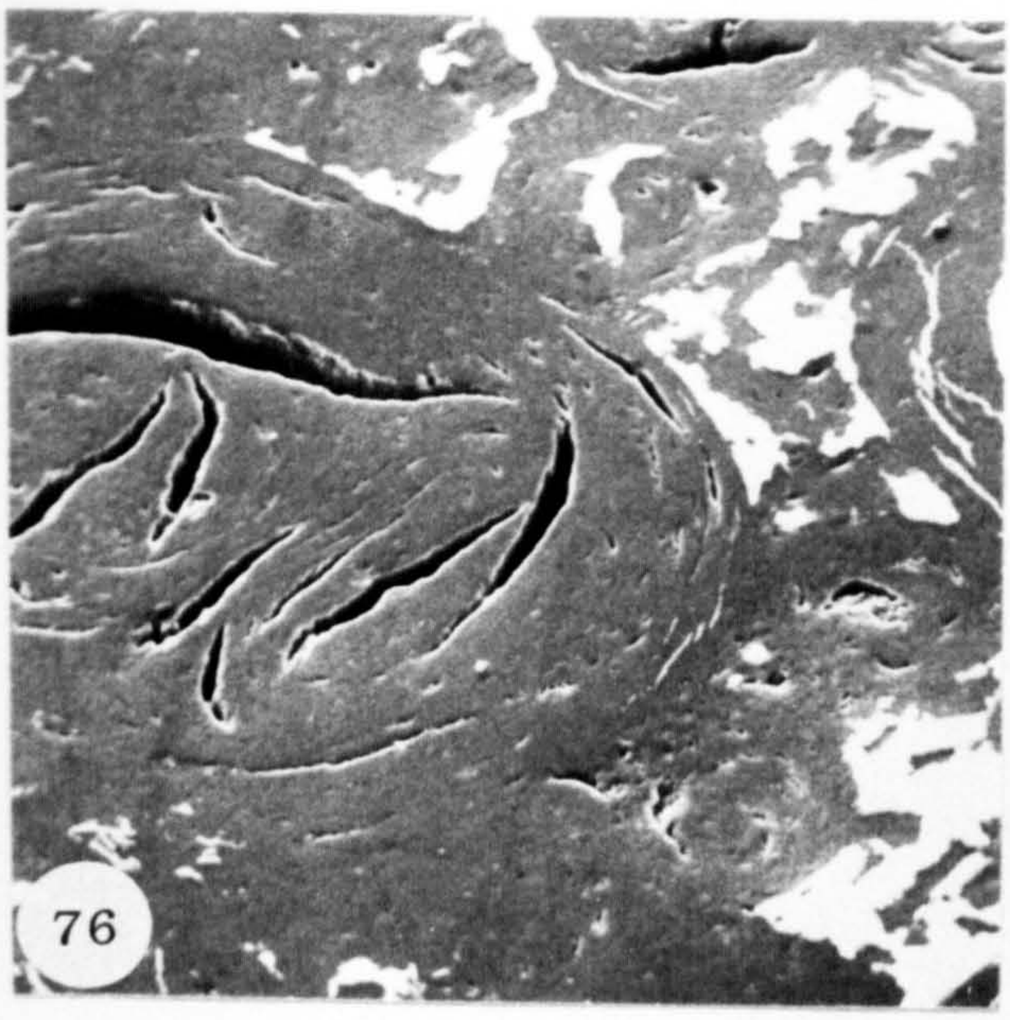
50 µm



AGLMP GRAPHITE
Gold impregnated

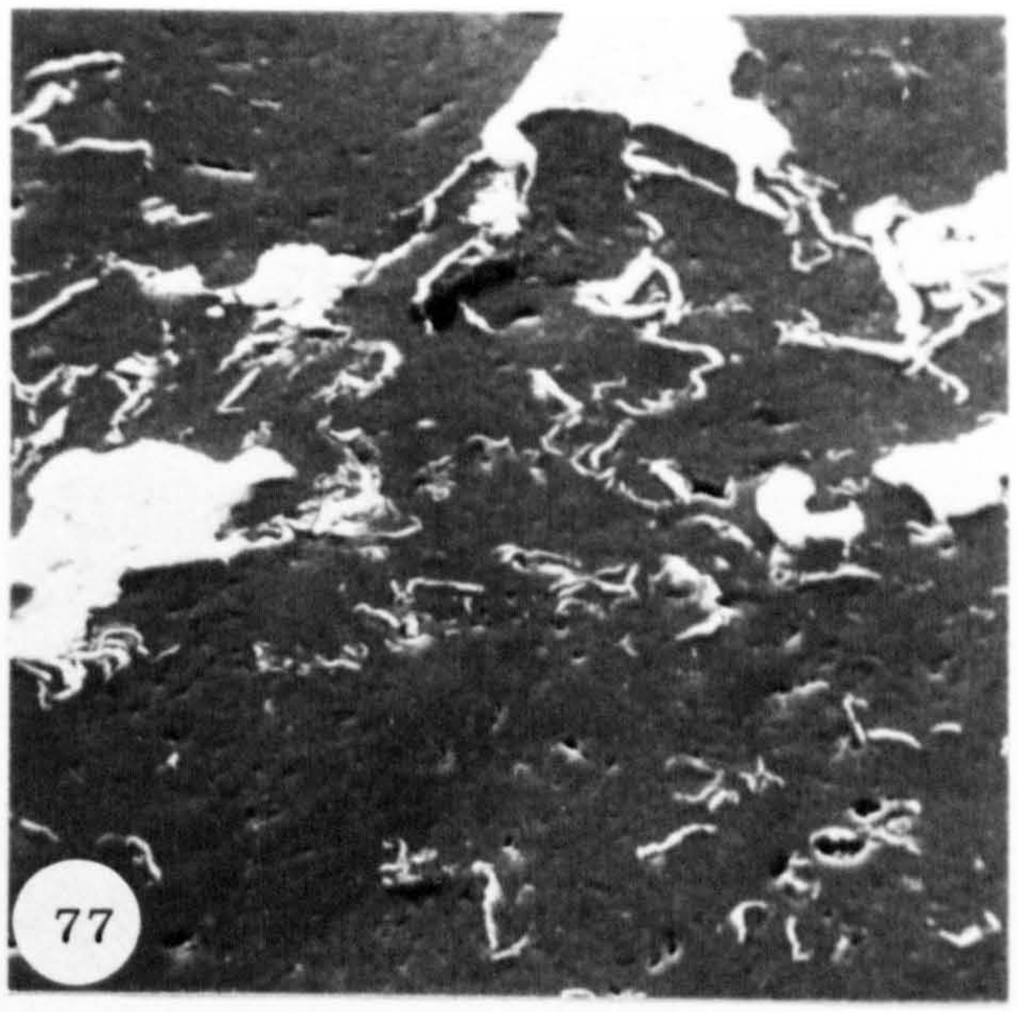
20 µm

Figures 72 to 75. Scanning electron micrographs (stereoscan) of gold impregnated AGLMP graphite.



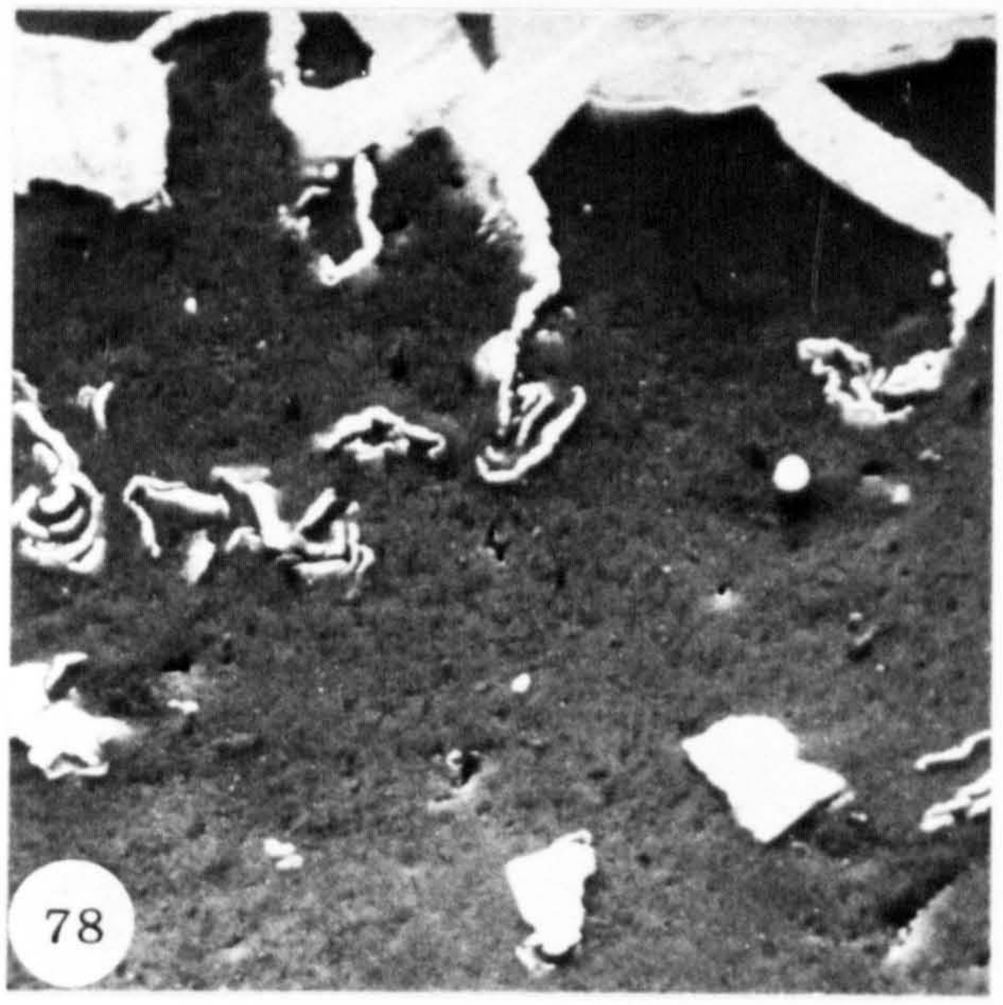
GCMB GRAPHITE
Gold impregnated

100 µm



GCMB GRAPHITE
Gold impregnated

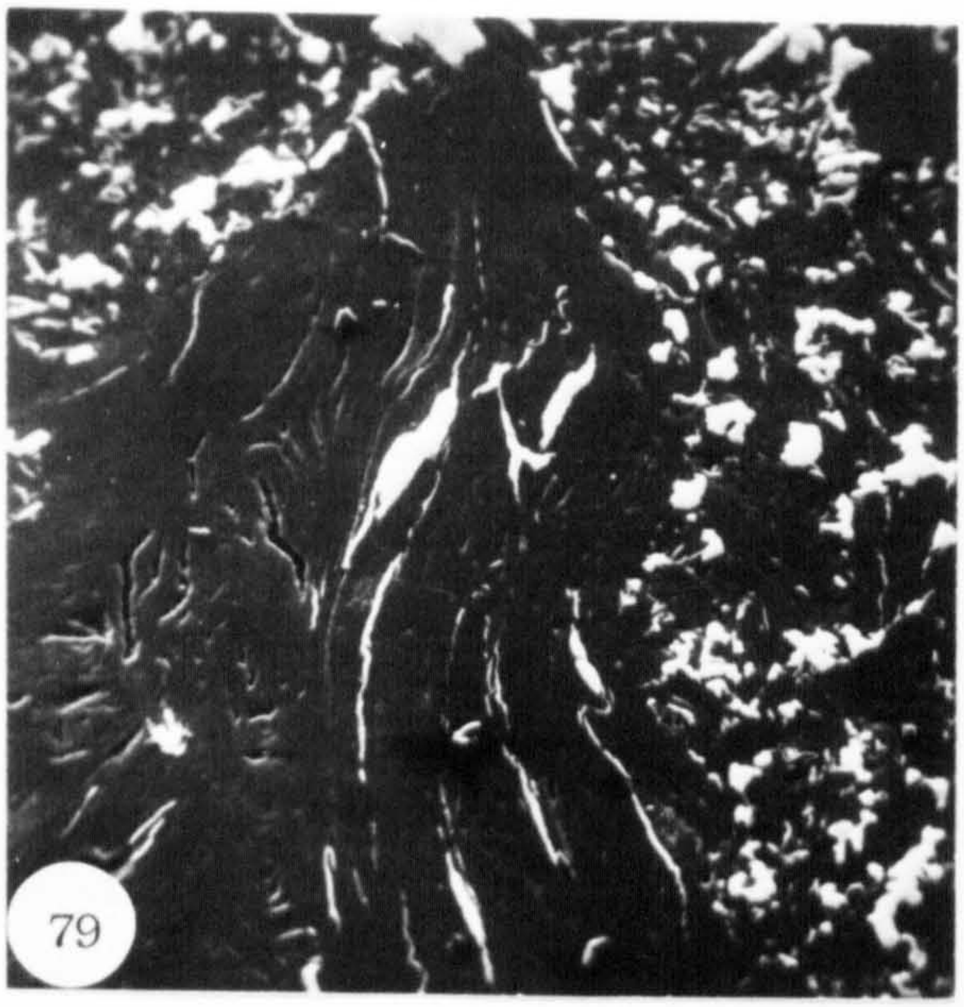
50 µm



GCMB GRAPHITE
Gold impregnated

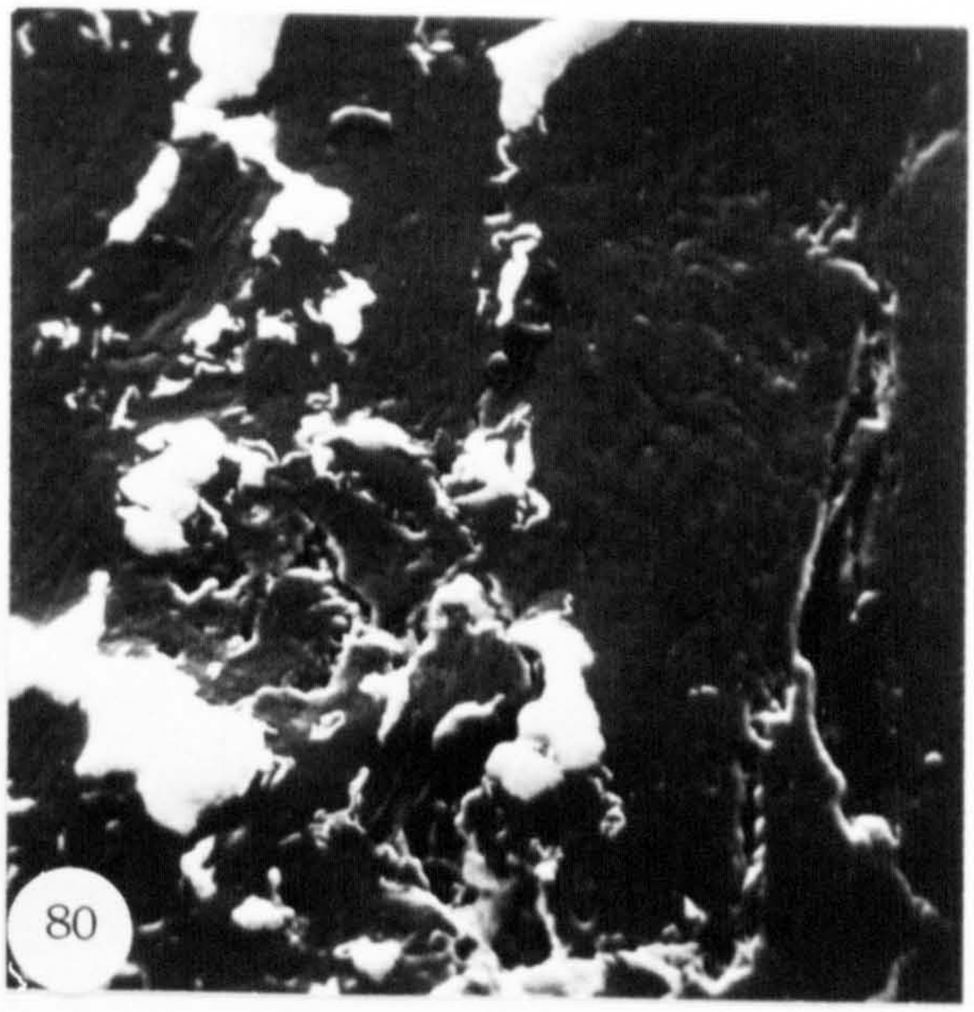
20 µm

Figures 76 to 78. Scanning electron micrographs (stereoscan) of gold impregnated GCMB graphite.



LIMA GRAPHITE
Gold impregnated

100 µm



LIMA GRAPHITE
Gold impregnated

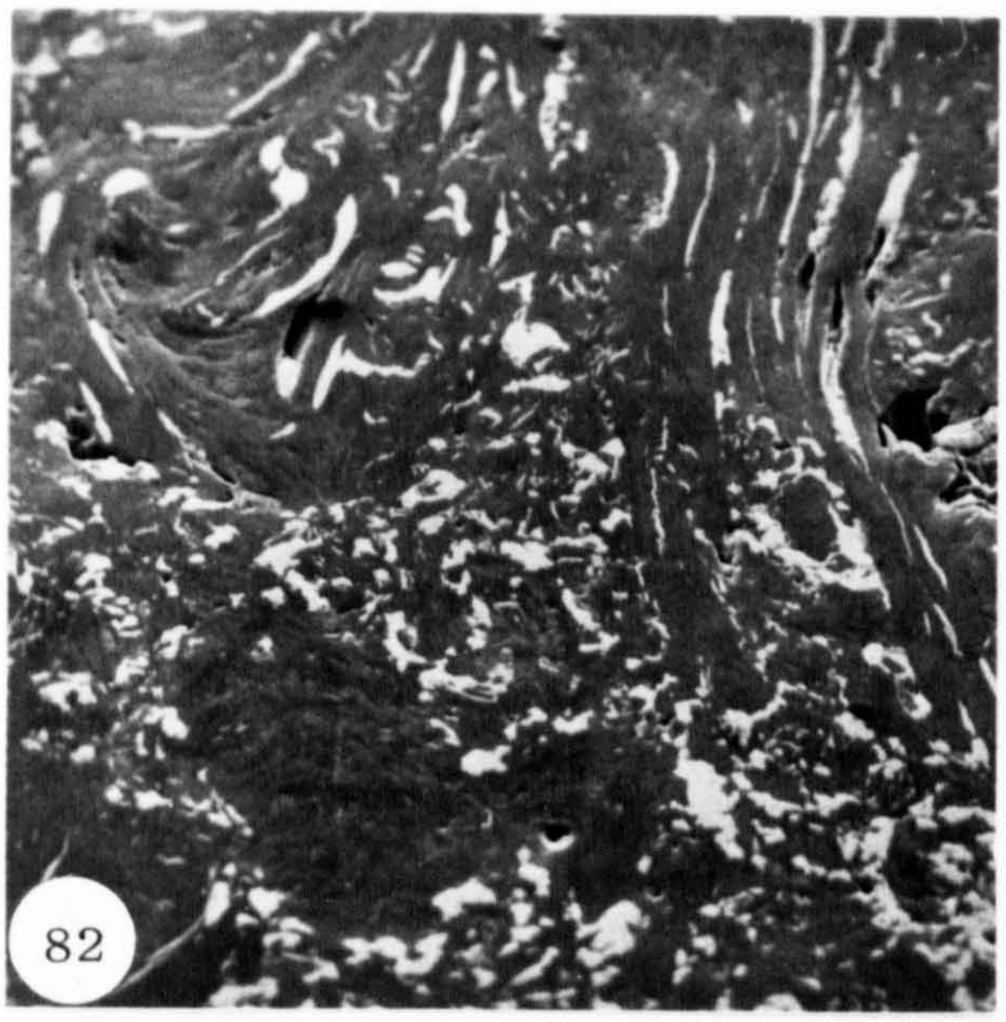
50 µm



LIMA GRAPHITE
Gold impregnated

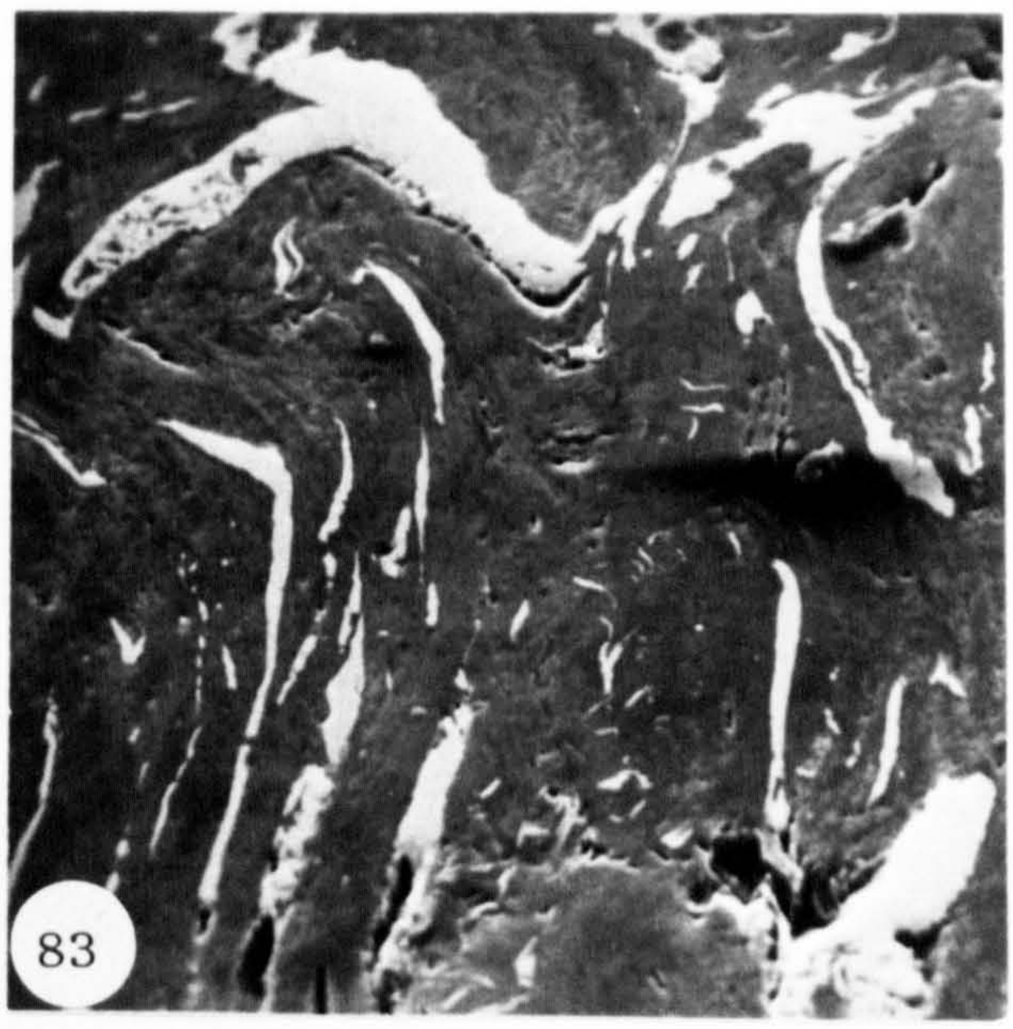
20 µm

Figures 79 to 81. Scanning electron micrographs (stereoscan) of gold impregnated Lima graphite.



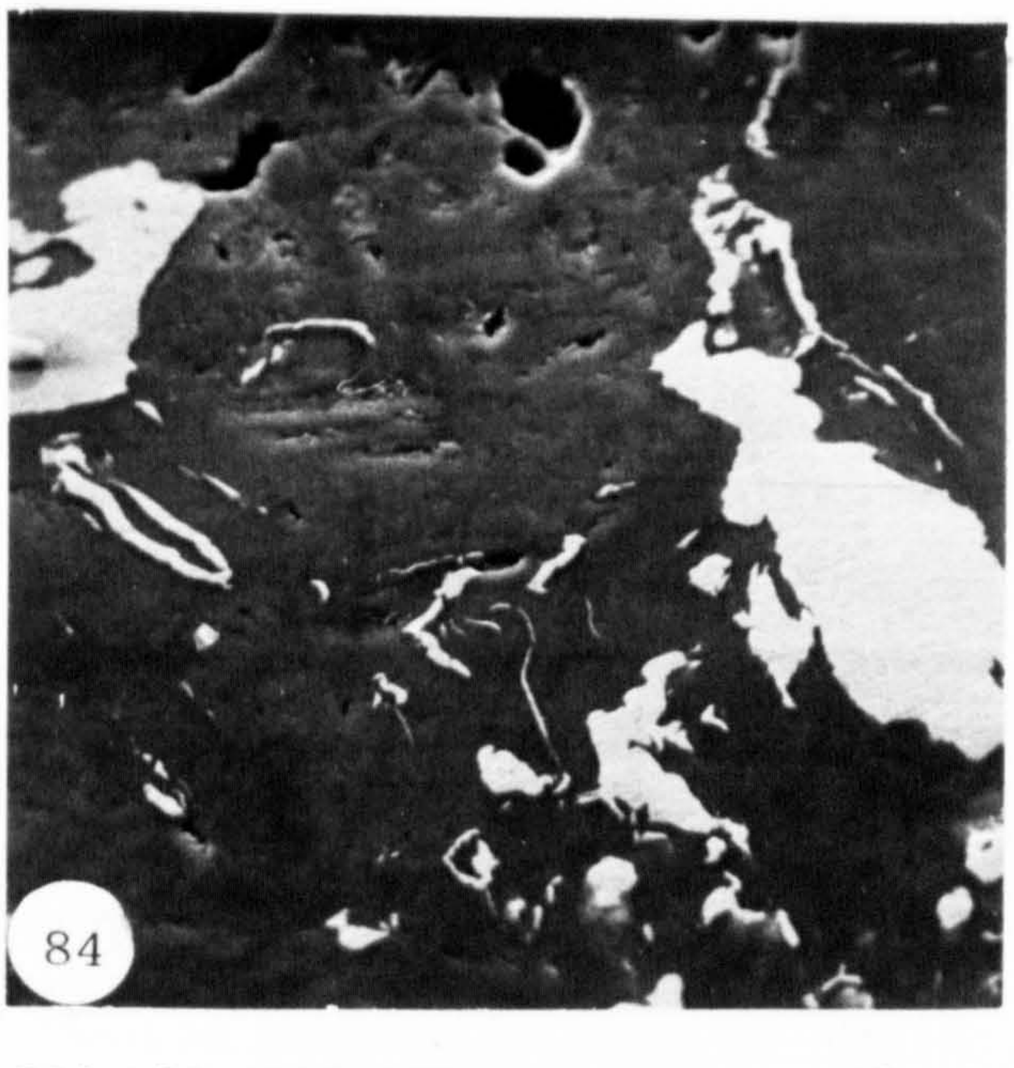
PGA L18 GRAPHITE
Gold impregnated

100 µm



PGA L18 GRAPHITE
Gold impregnated

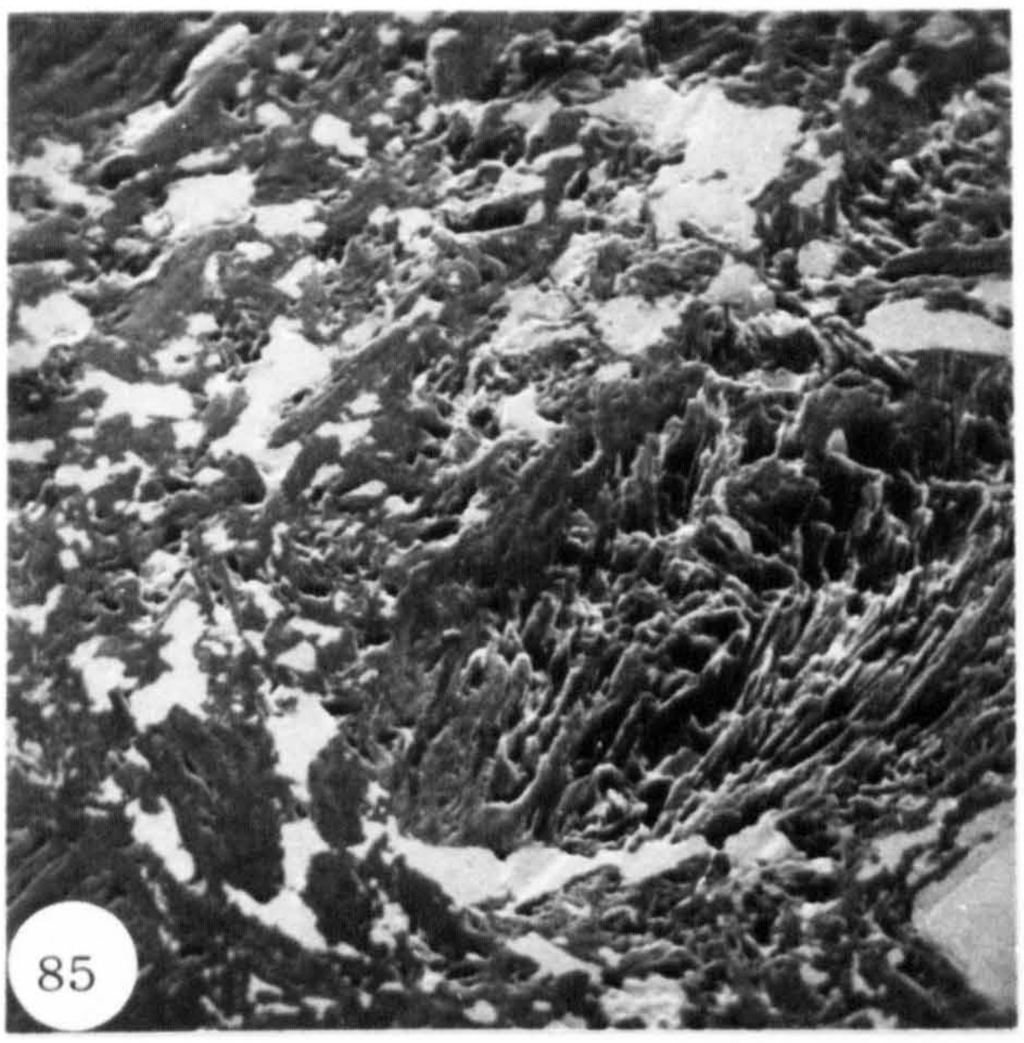
50 µm



PGA L18 GRAPHITE
Gold impregnated

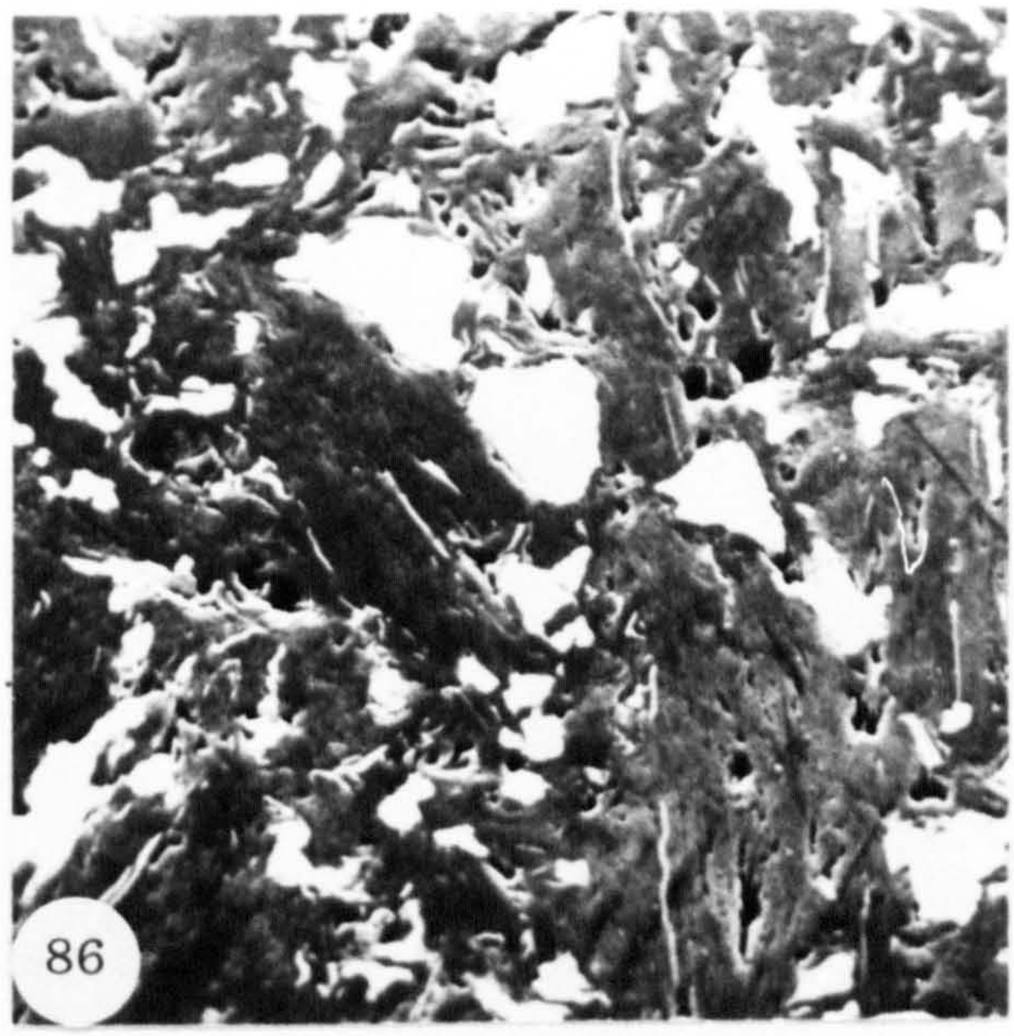
20 µm

Figures 82 to 84. Scanning electron micrographs (stereoscan) of gold impregnated PGA L18 graphite.



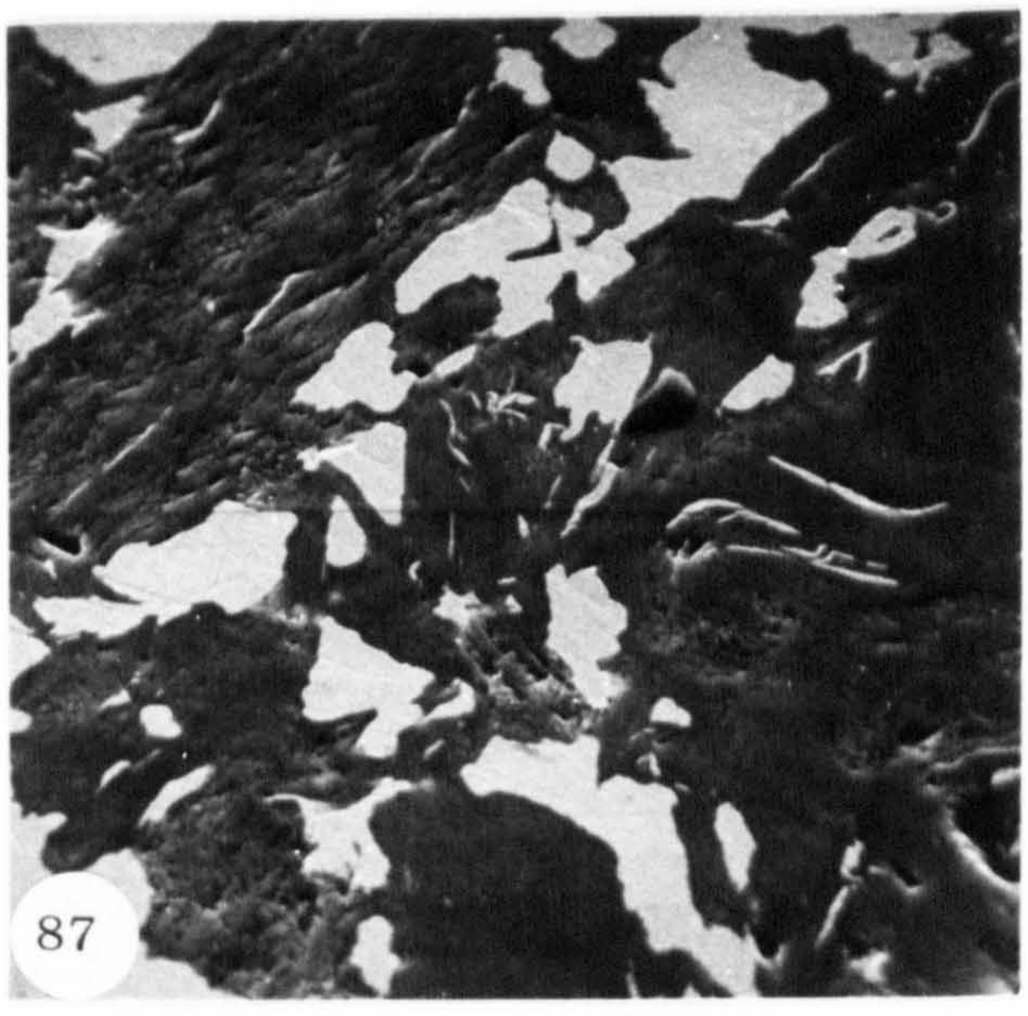
PGA L18 GRAPHITE
Bismuth impregnated

100 µm



PGA L18 GRAPHITE
Bismuth impregnated

50 µm



PGA L18 GRAPHITE
Bismuth impregnated

20 µm

Figures 85 to 87. Scanning electron micrographs (stereoscan) of bismuth impregnated PGA L18 graphite.

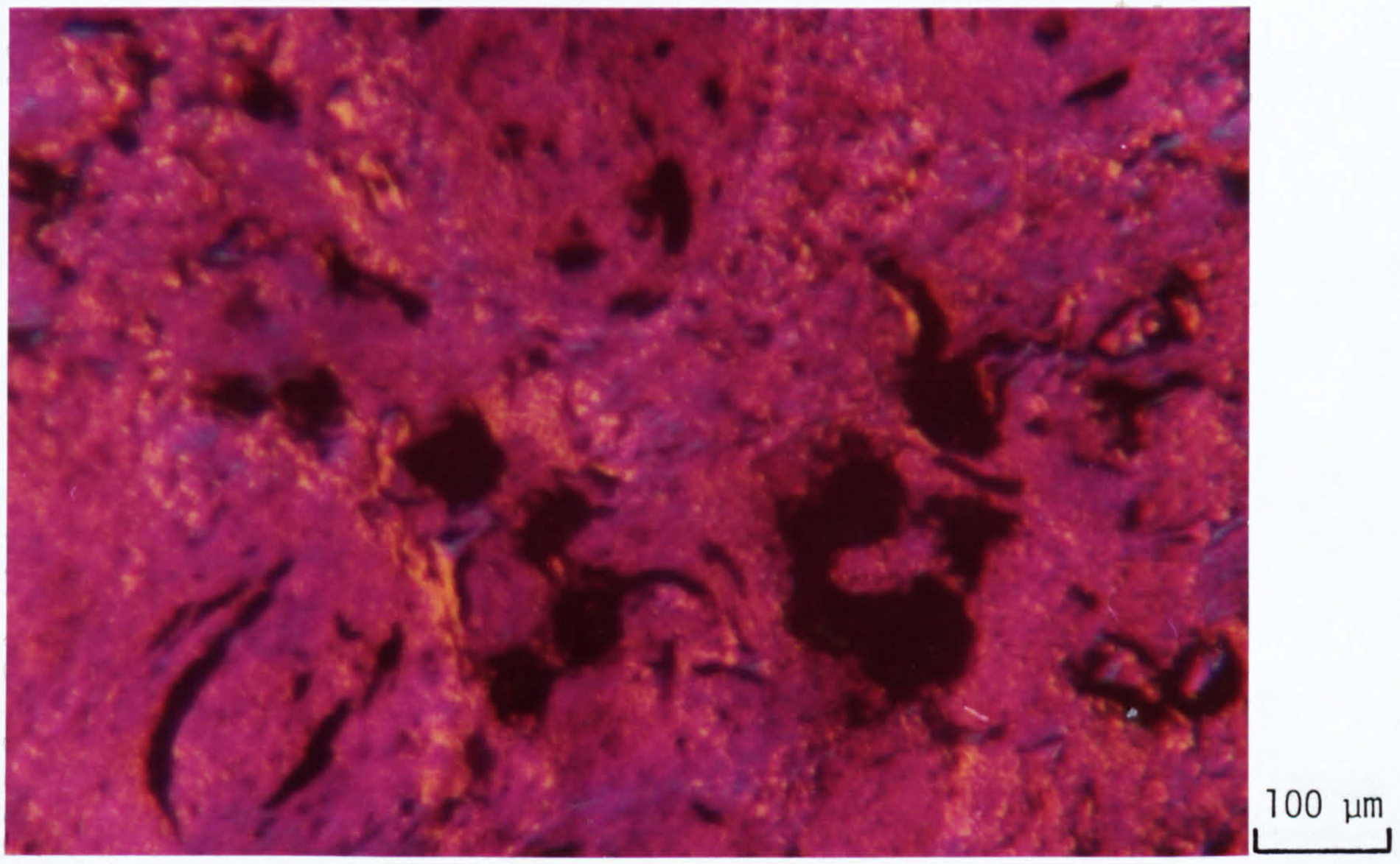


Figure 88(a). Optical micrograph of virgin AGLMP graphite.

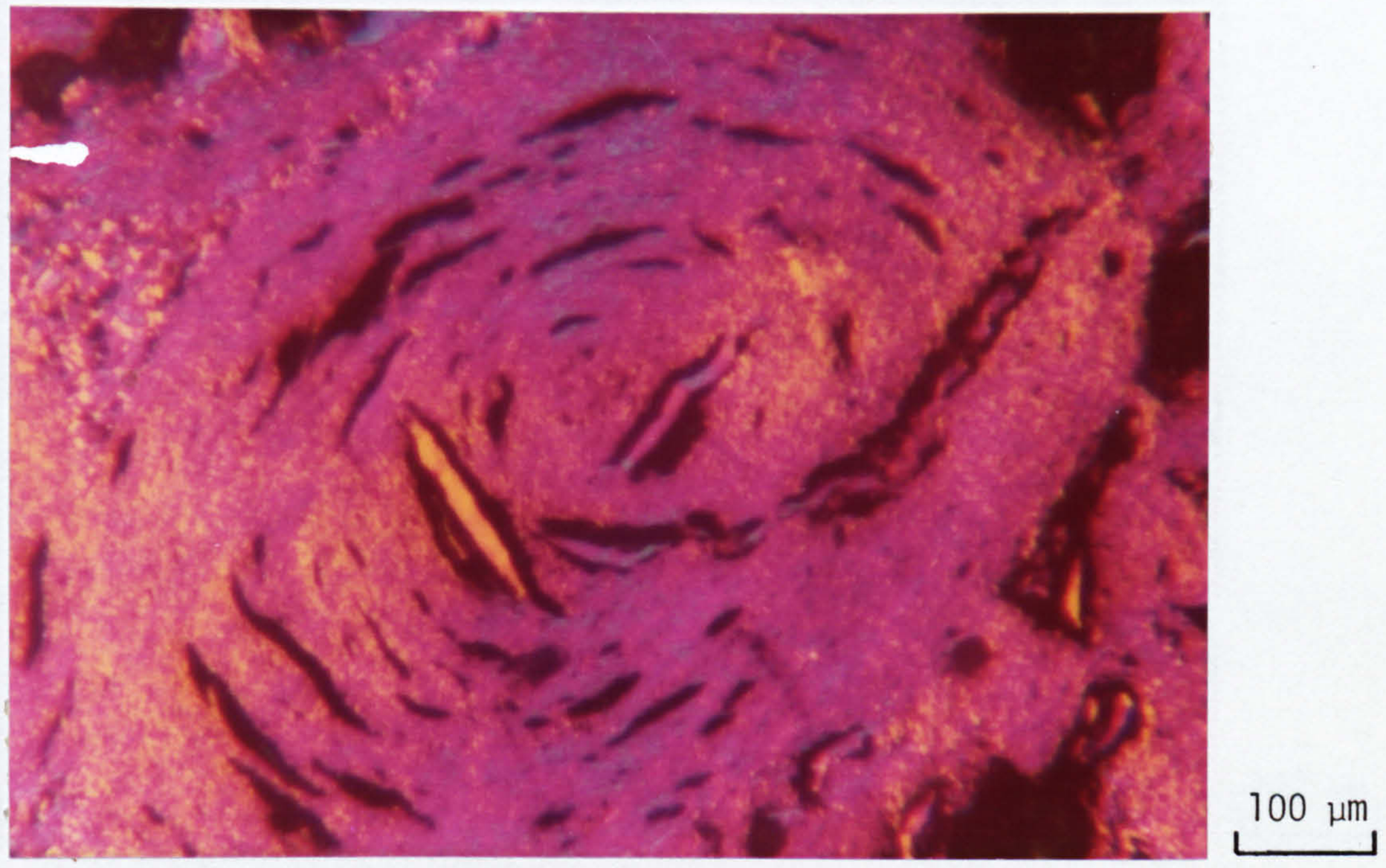


Figure 88(b). Optical micrograph of virgin AGLMP graphite.

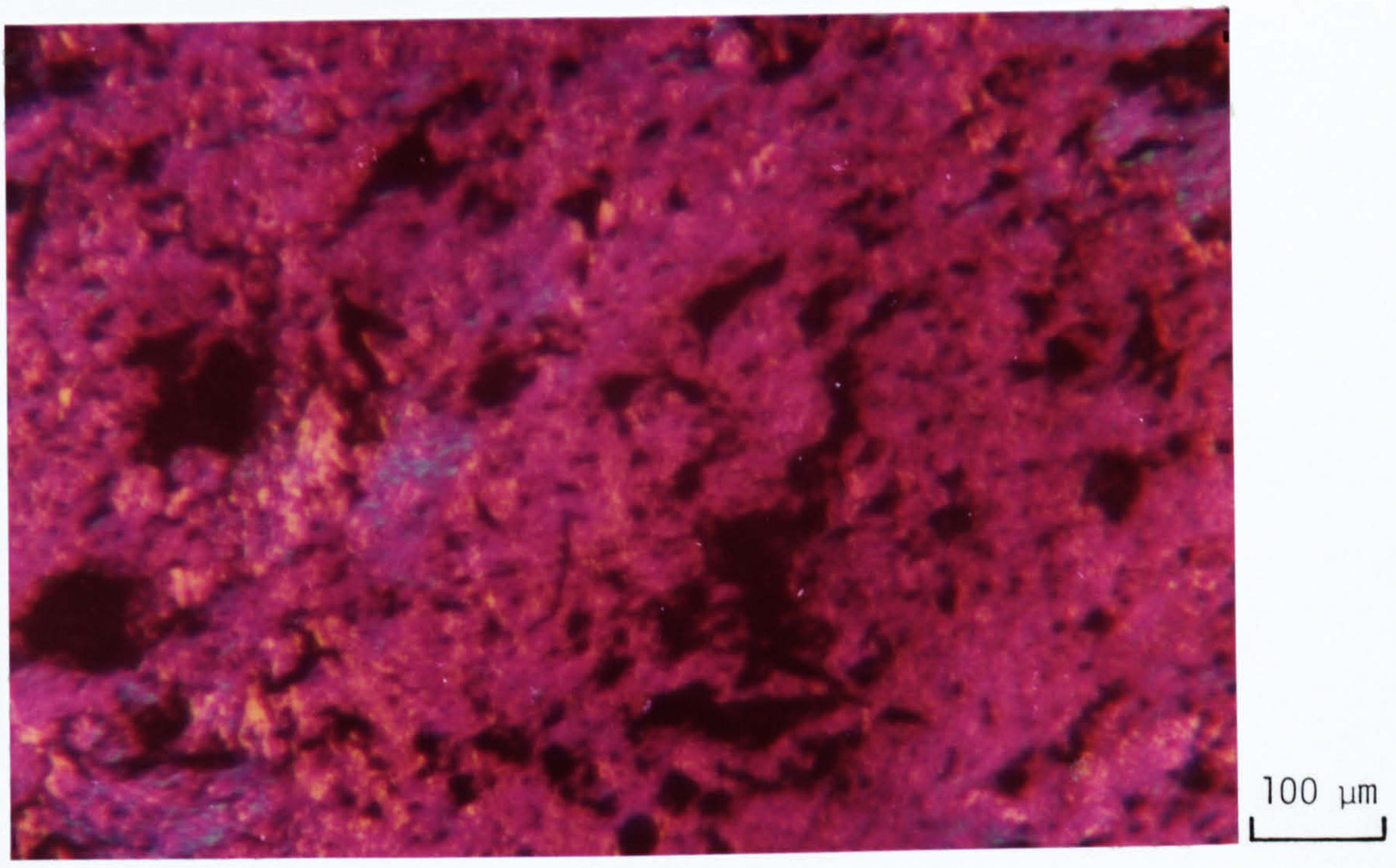


Figure 89(a). Optical micrograph of AGLMP graphite thermally oxidised to 5.4% weight loss.

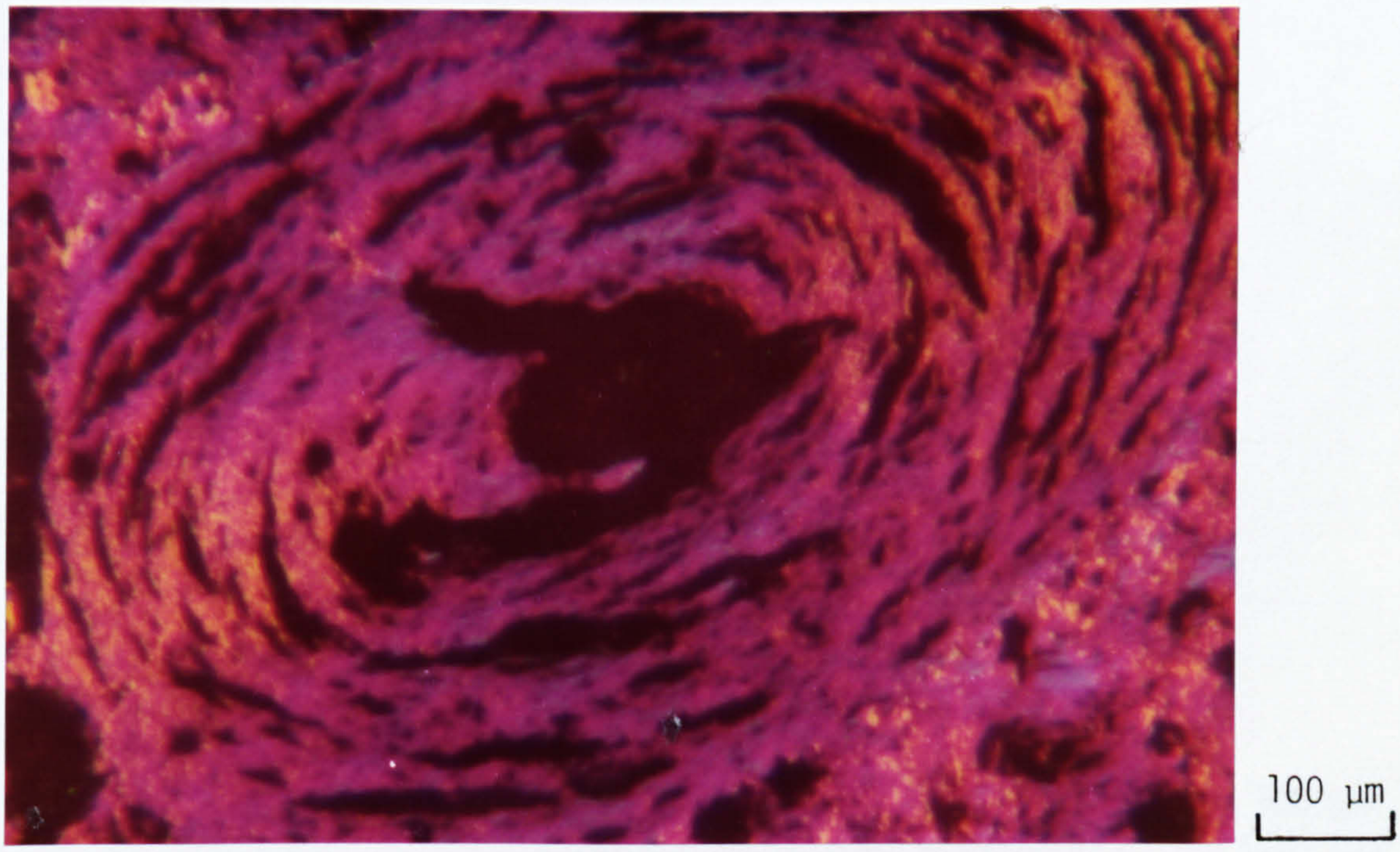


Figure 89(b). Optical micrograph of AGLMP graphite thermally oxidised to 5.4% weight loss.

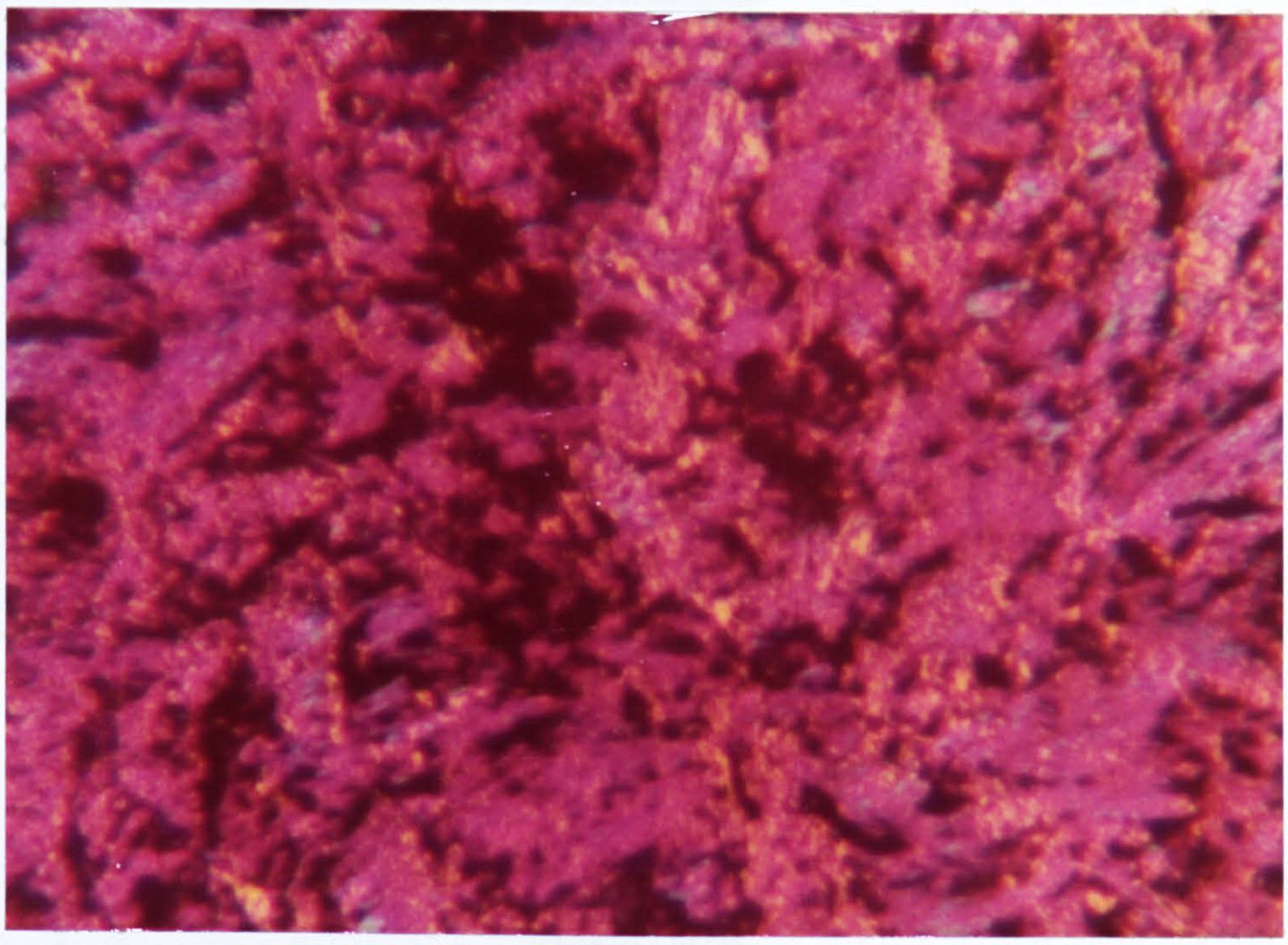


Figure 90(a). Optical micrograph of AGLMP graphite thermally oxidised to 10.5% weight loss.

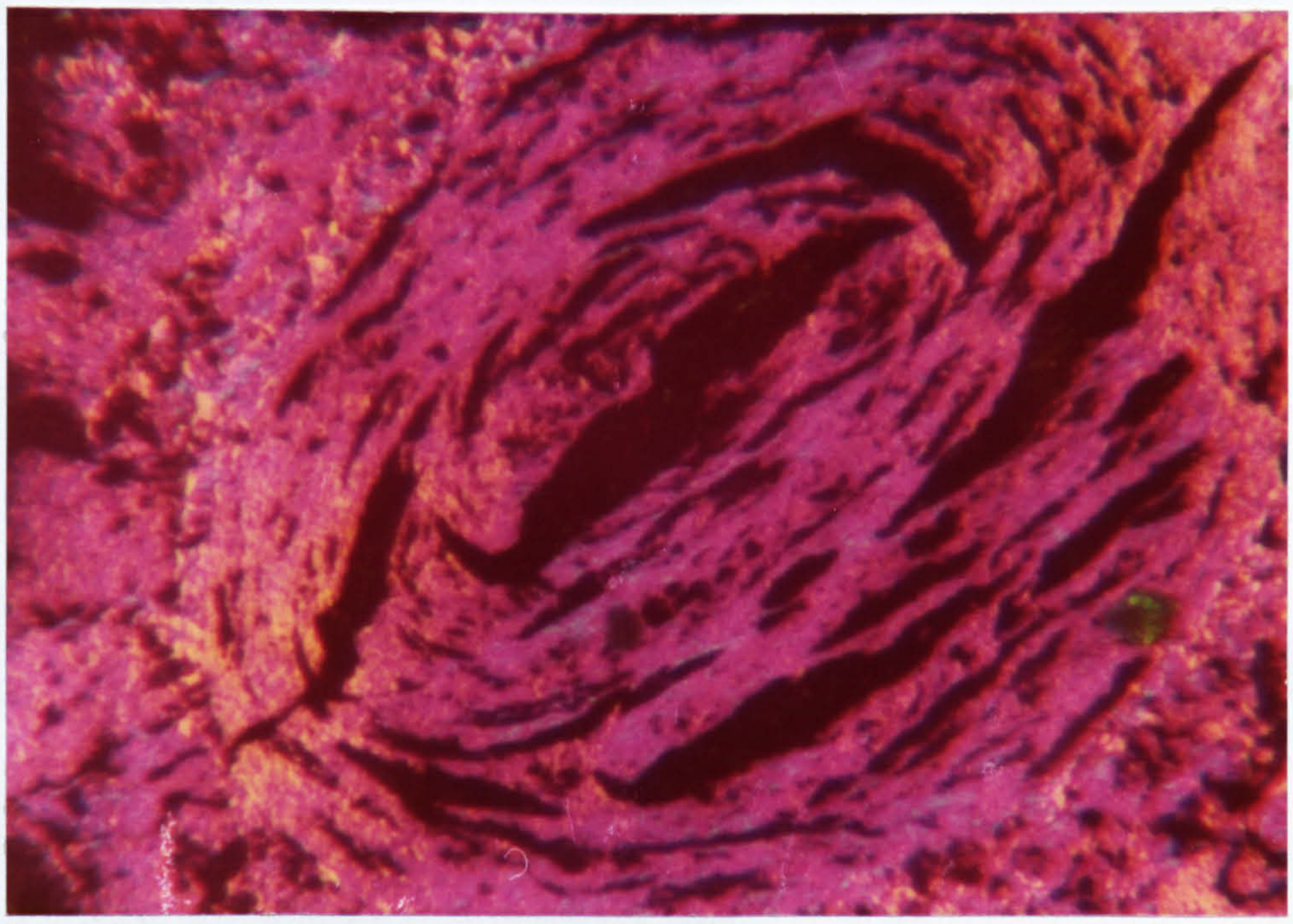
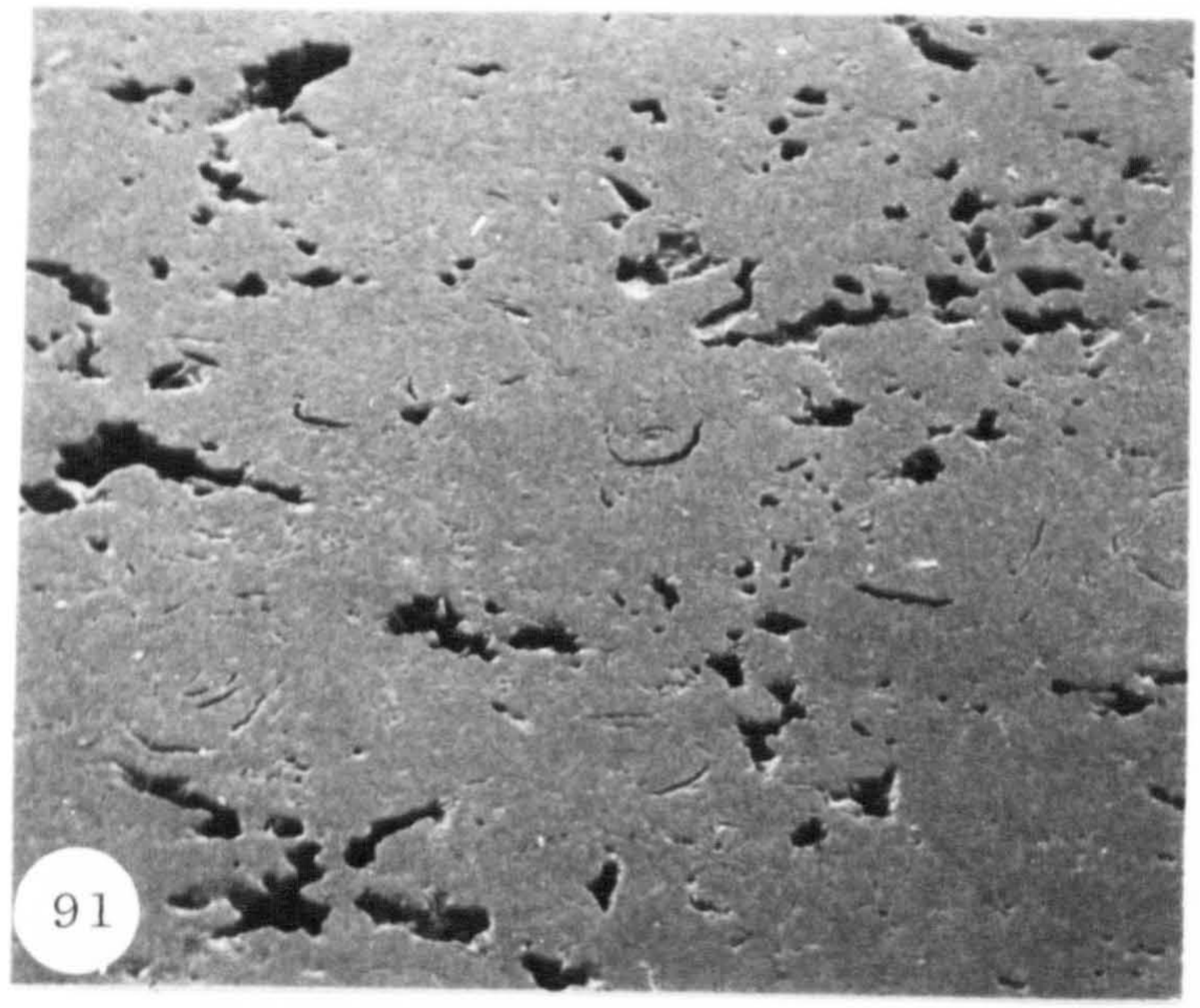
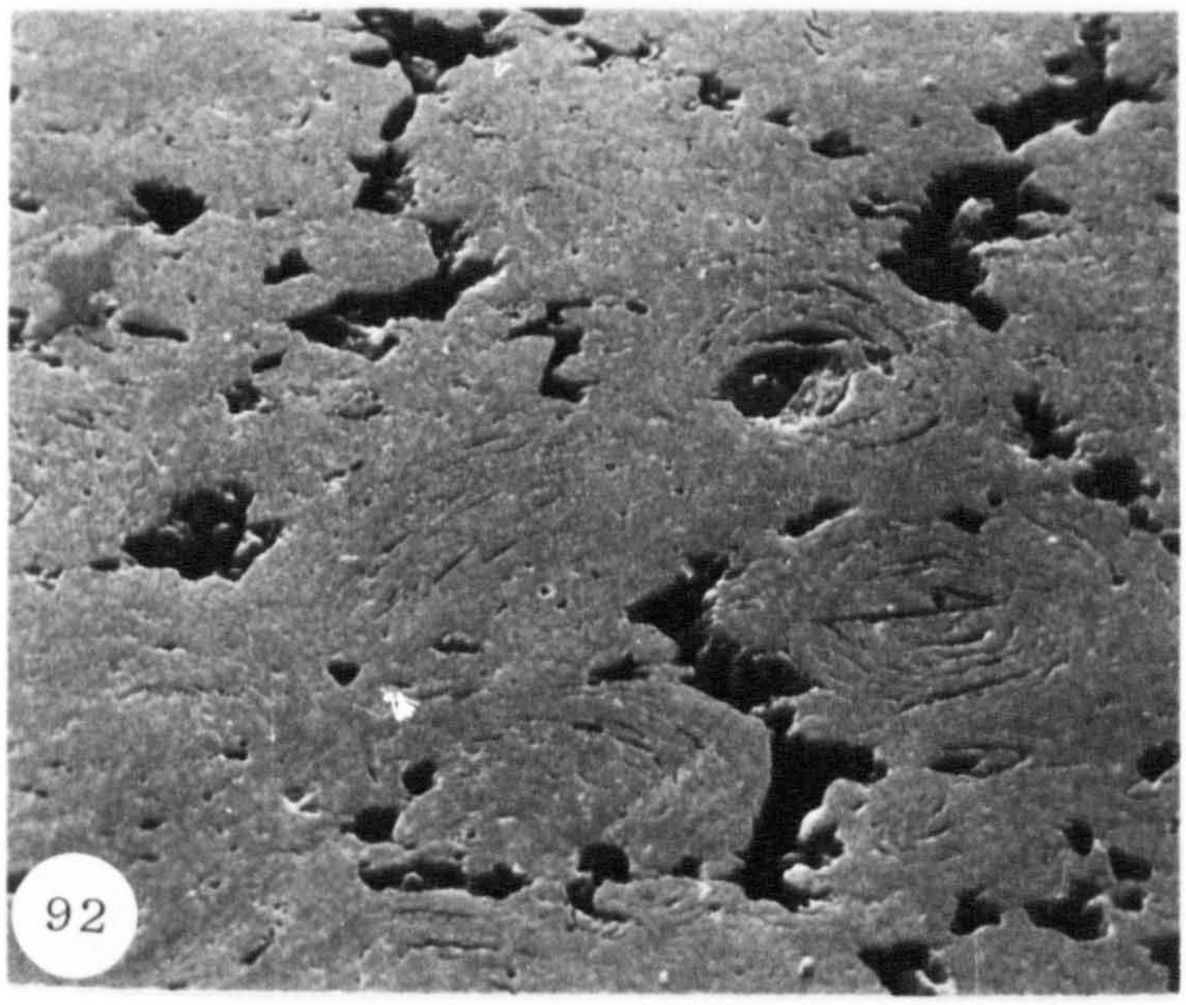


Figure 90(b). Optical micrograph of AGLMP graphite thermally oxidised to 10.5% weight loss.



VIRGIN AGLMP GRAPHITE

200 µm



AGLMP GRAPHITE THERMALLY OXIDISED TO 5.4% WEIGHT LOSS

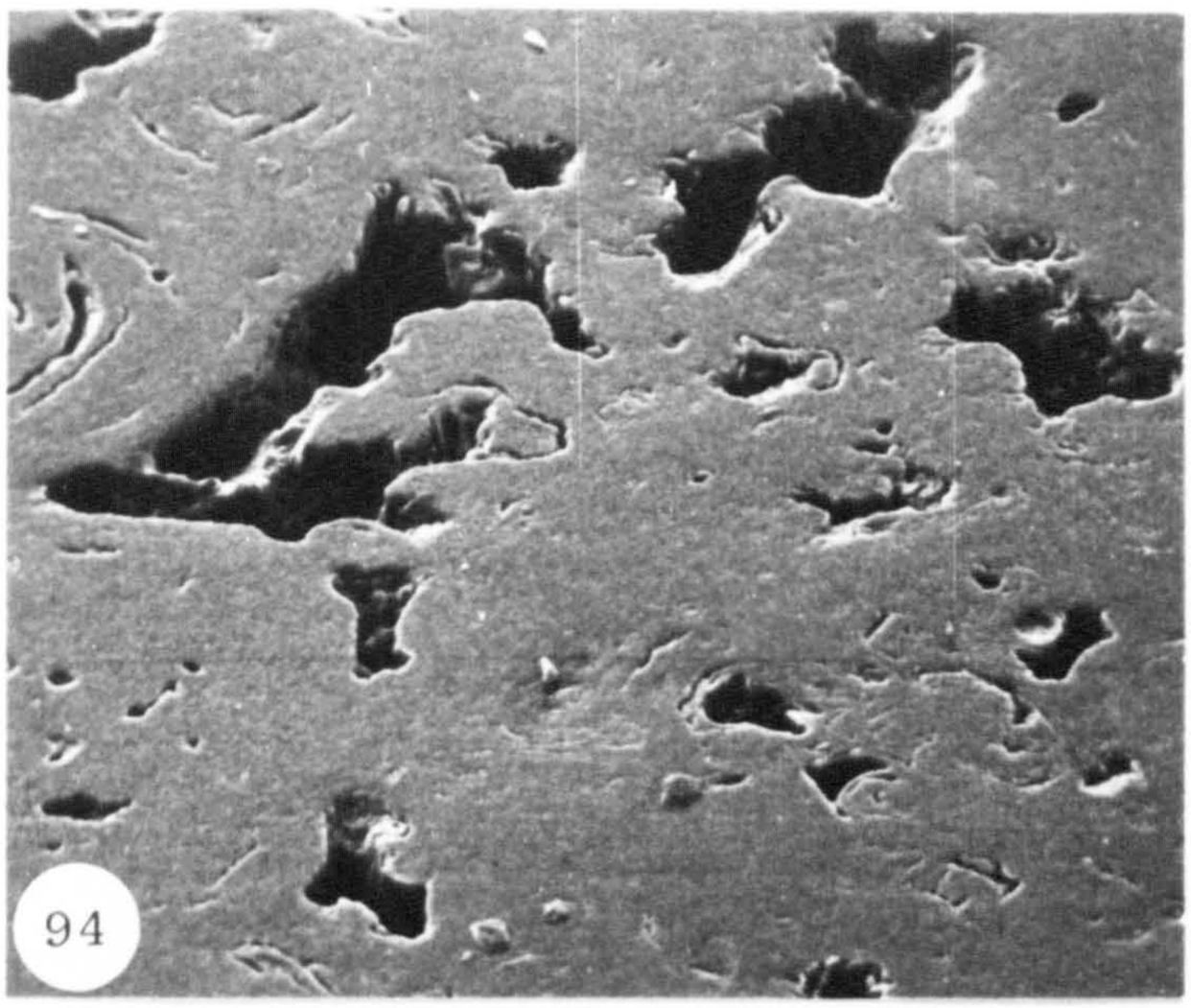
200 µm



AGLMP GRAPHITE THERMALLY OXIDISED TO 10.5% WEIGHT LOSS

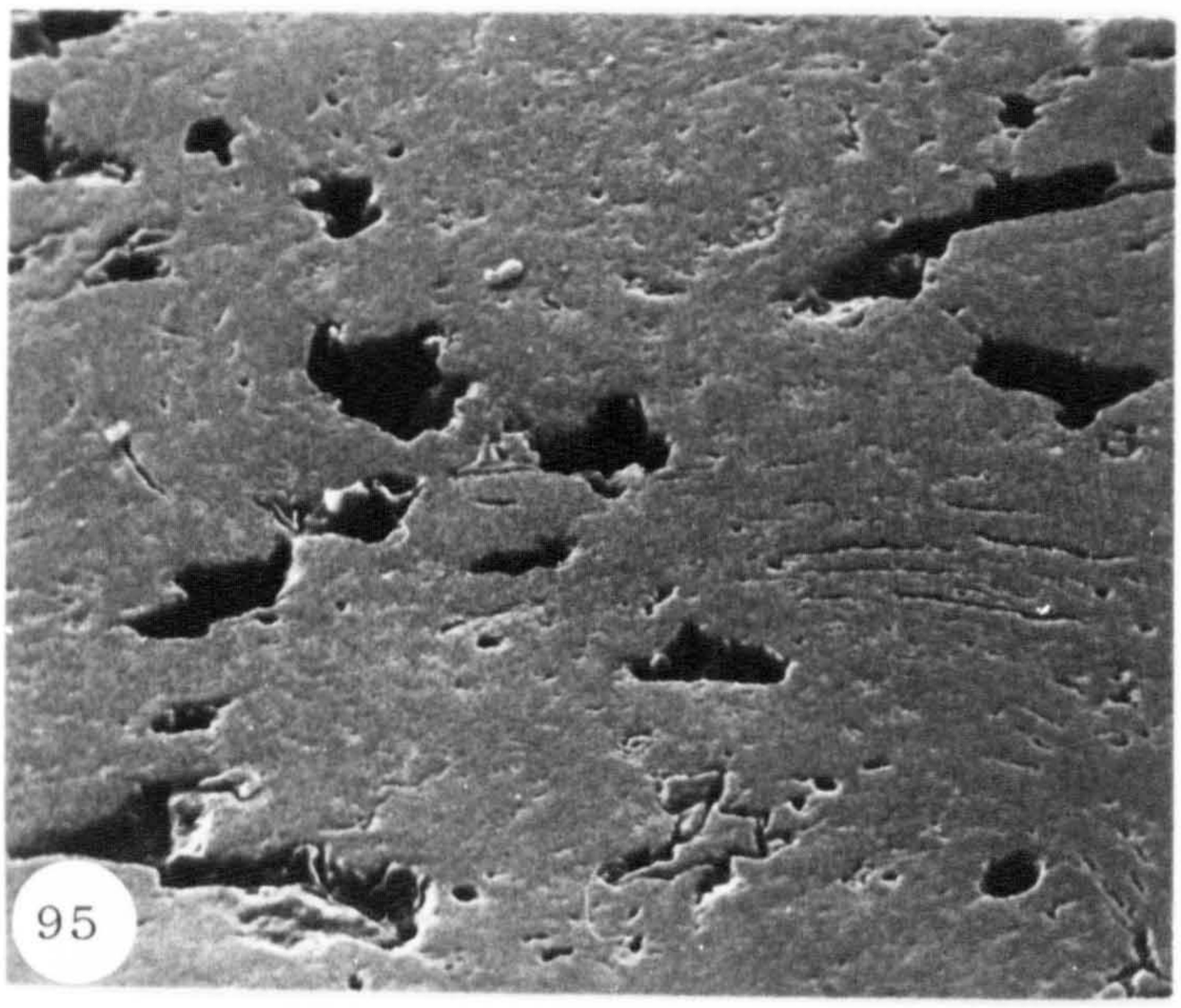
200 µm

Figures 91 to 93. Scanning electron micrographs (stereoscan) of AGLMP graphite virgin and thermally oxidised in air.



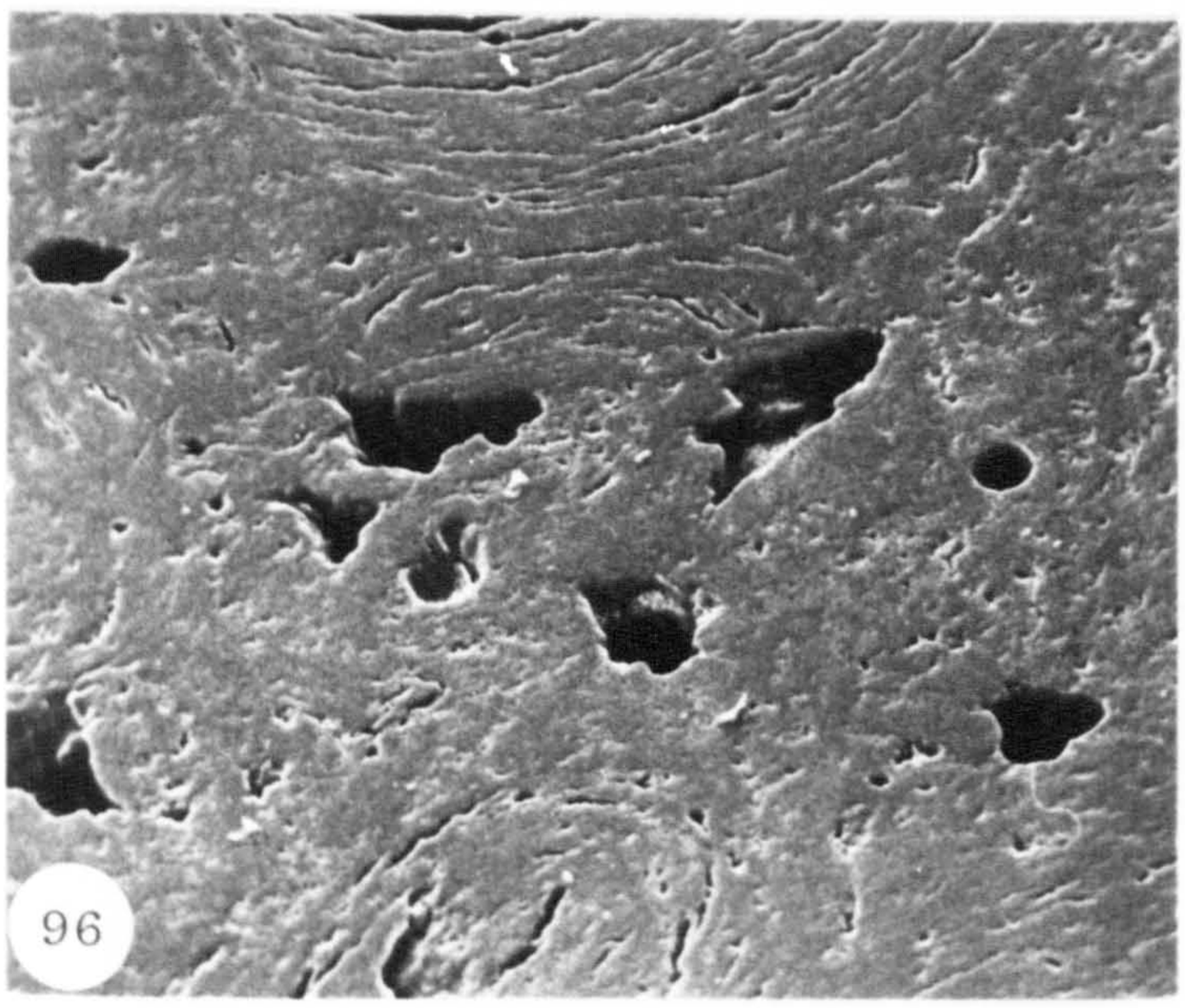
VIRGIN AGLMP GRAPHITE

100 µm



AGLMP GRAPHITE THERMALLY OXIDISED TO 5.4% WEIGHT LOSS

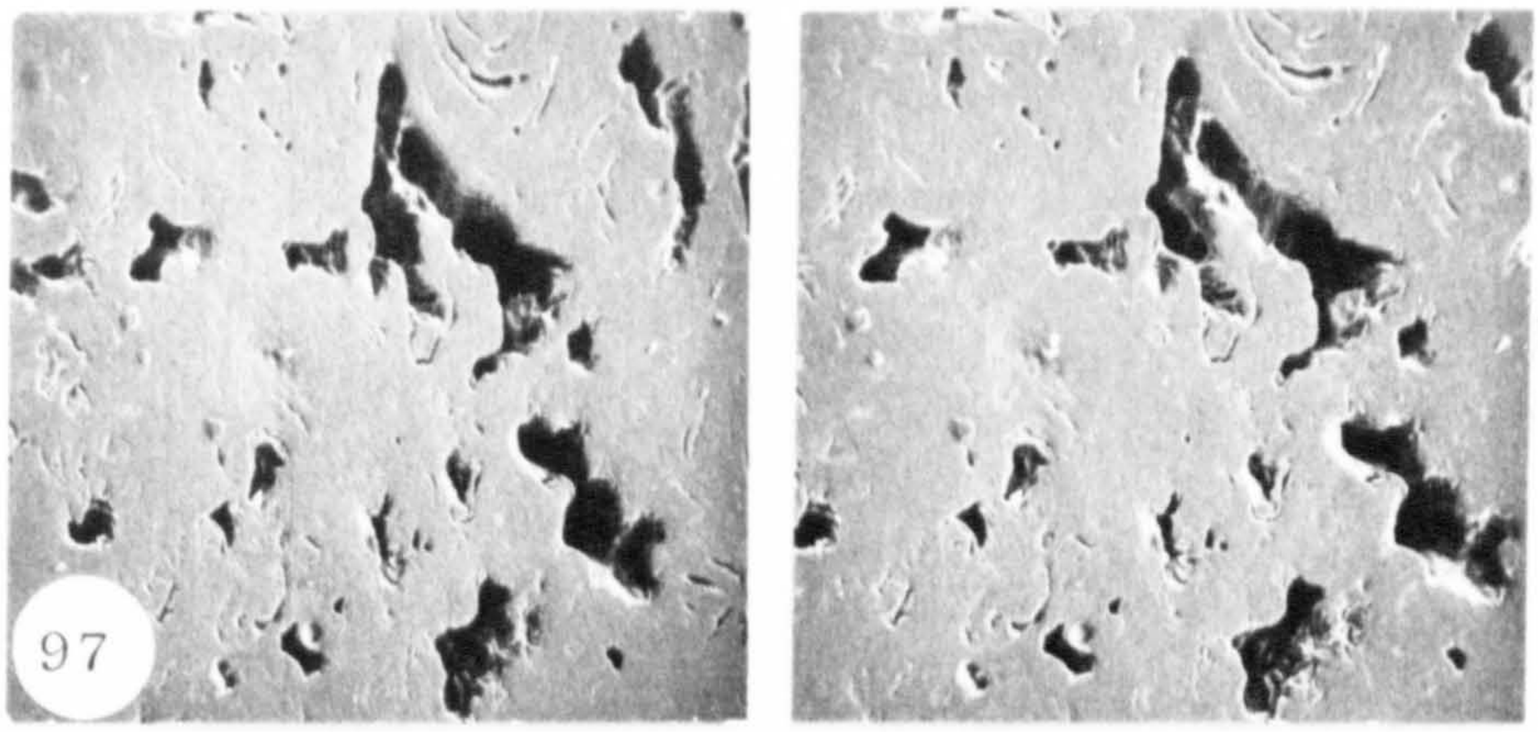
100 µm



AGLMP GRAPHITE THERMALLY OXIDISED TO 10.5% WEIGHT LOSS

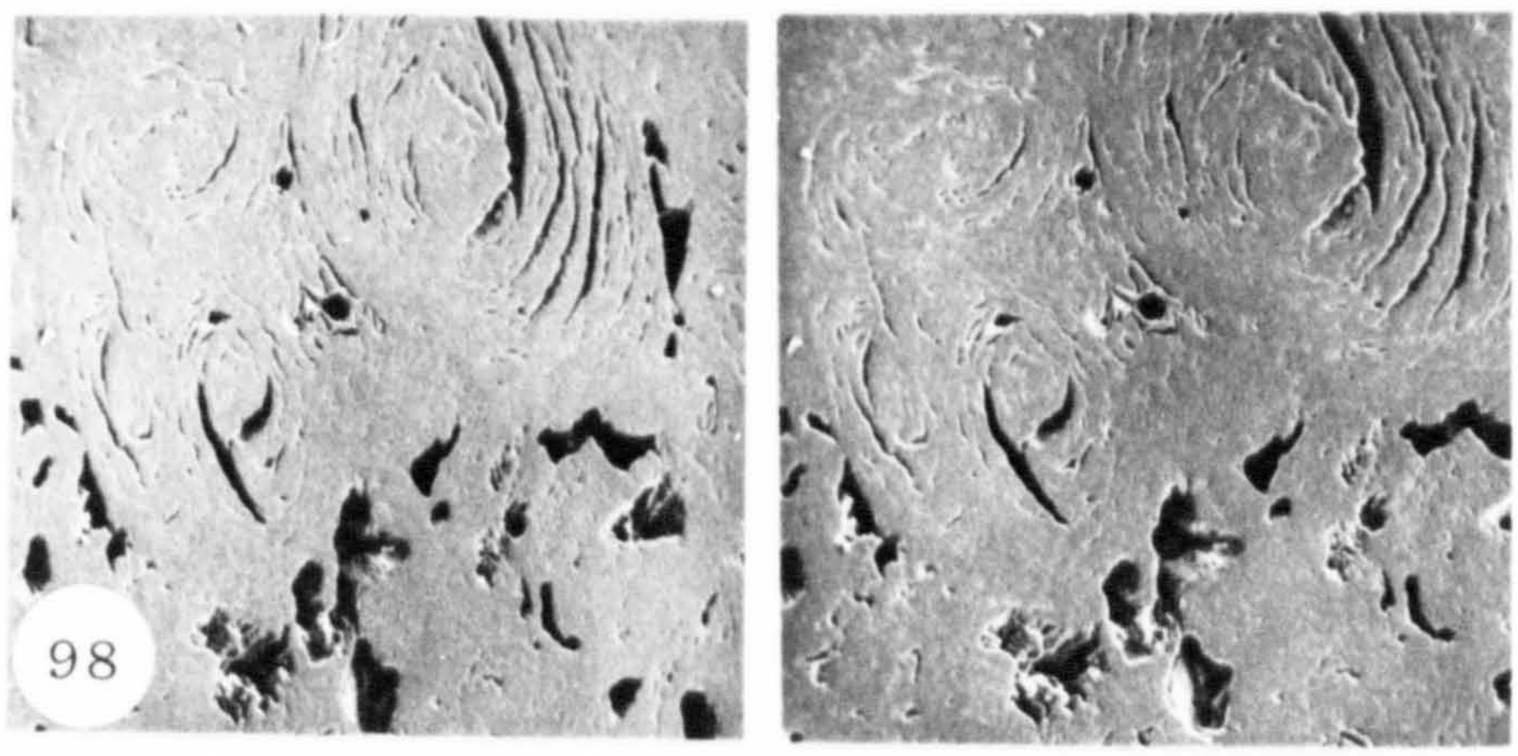
100 µm

Figures 94 to 96. Scanning electron micrographs (stereoscan) of AGLMP graphite virgin and thermally oxidised in air.



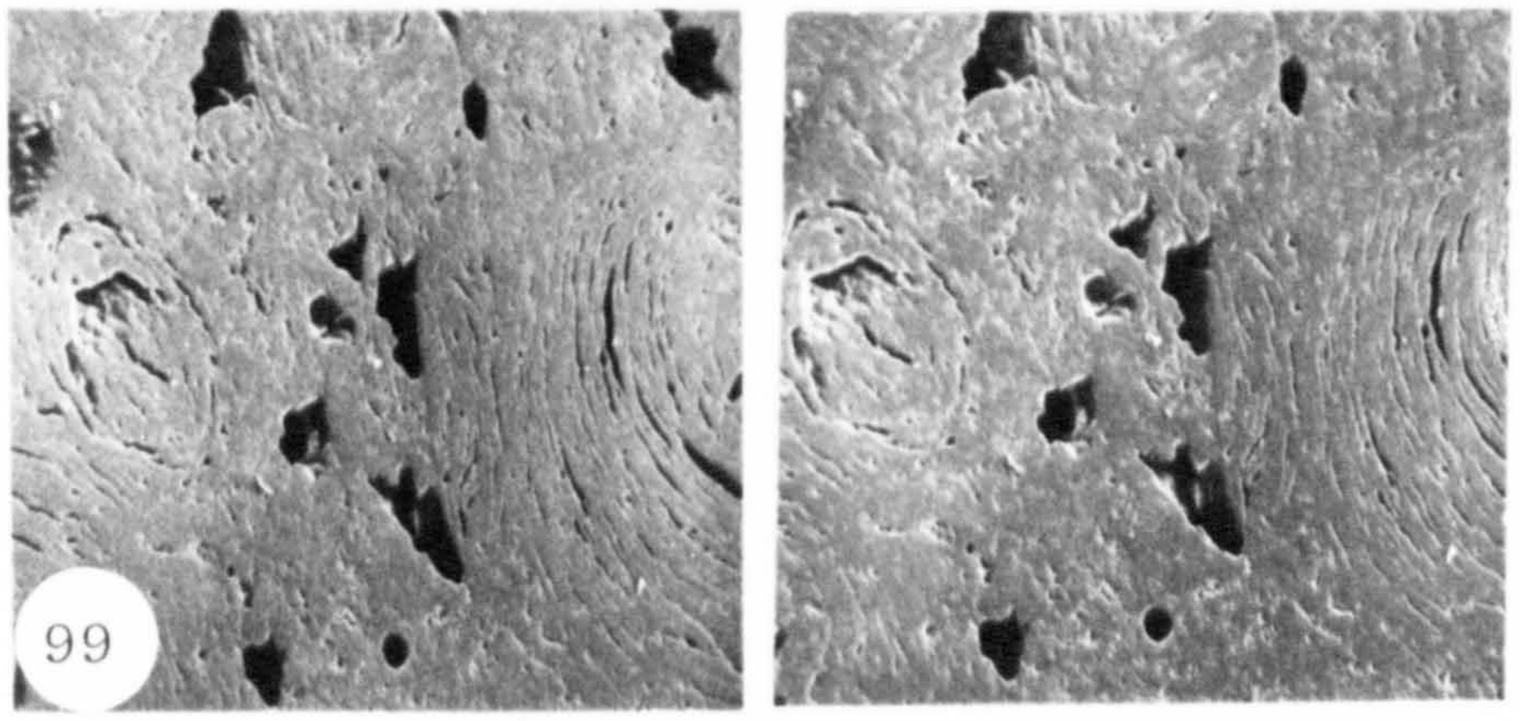
VIRGIN AGLMP GRAPHITE

200 µm



AGLMP GRAPHITE THERMALLY OXIDISED
TO 5.4% WEIGHT LOSS

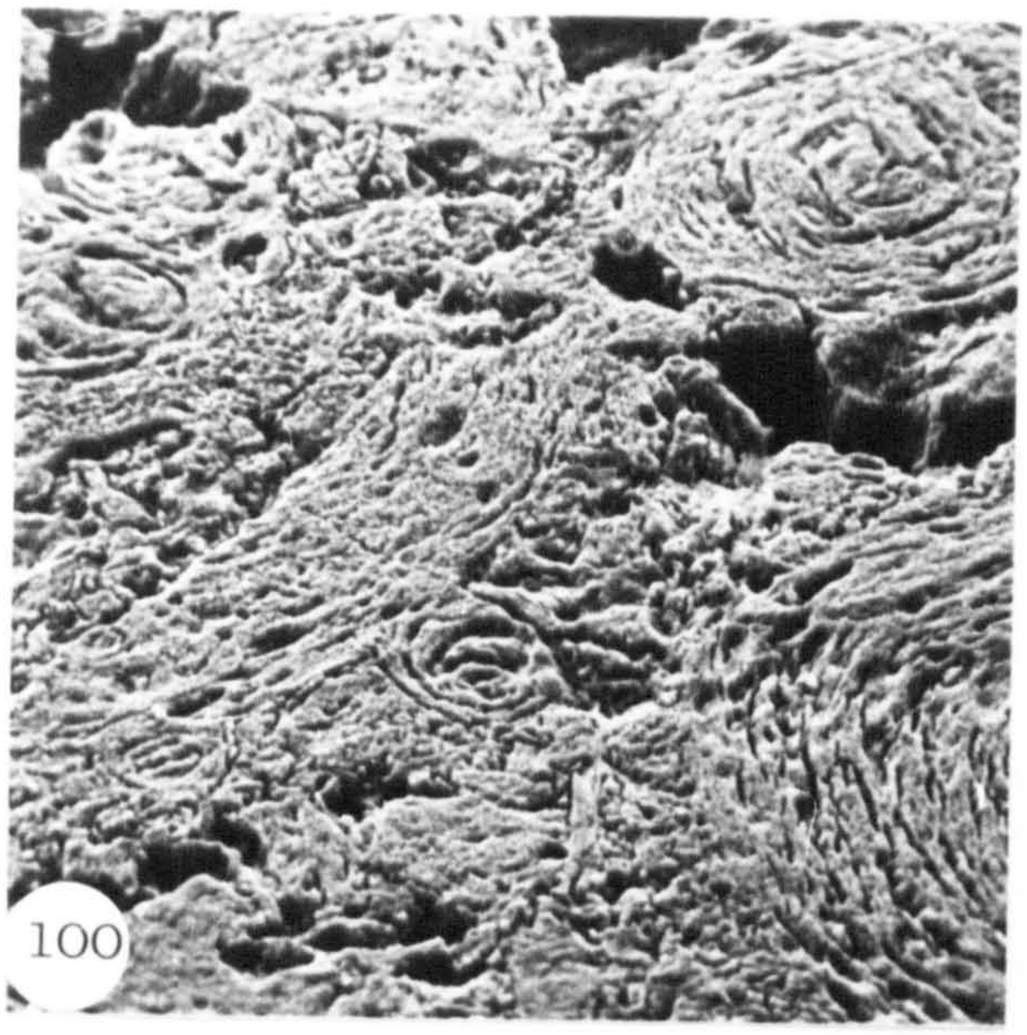
200 µm



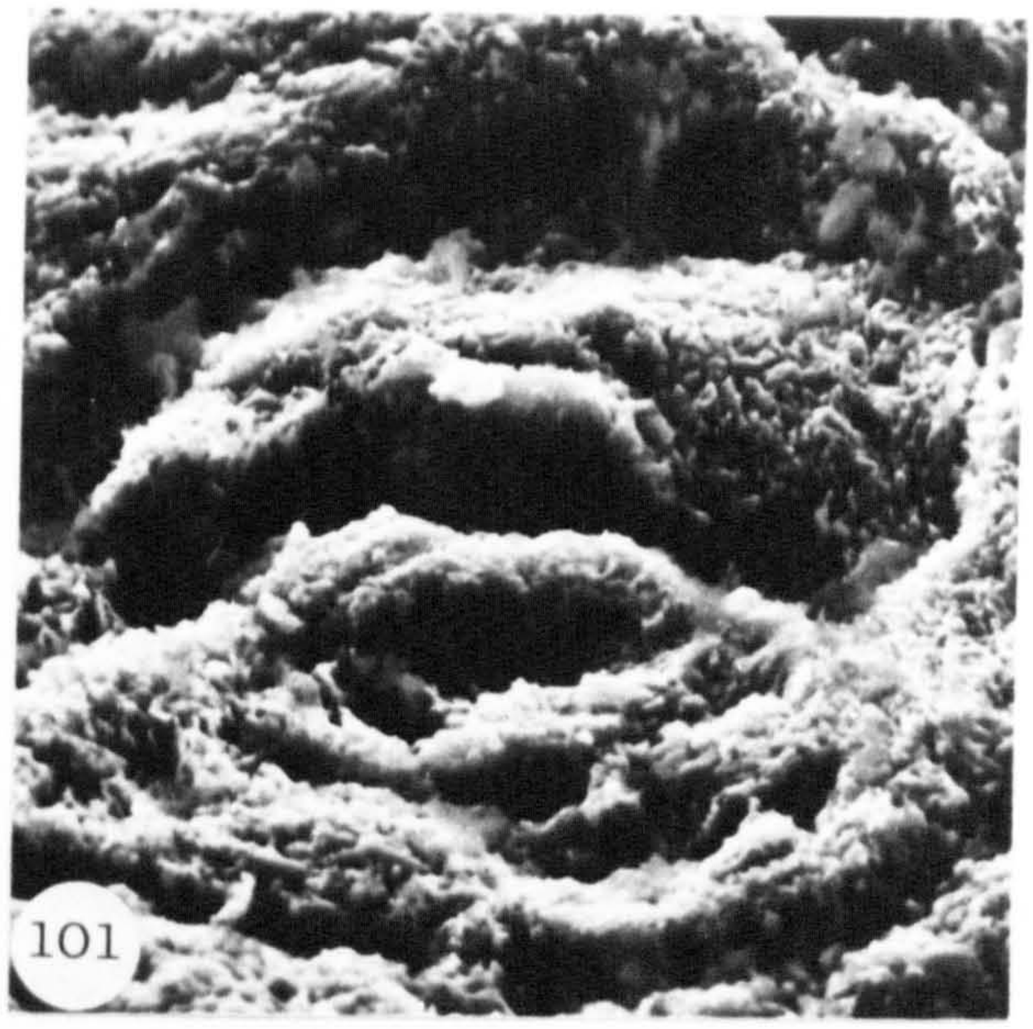
AGLMP GRAPHITE THERMALLY OXIDISED
TO 10.5% WEIGHT LOSS

200 µm

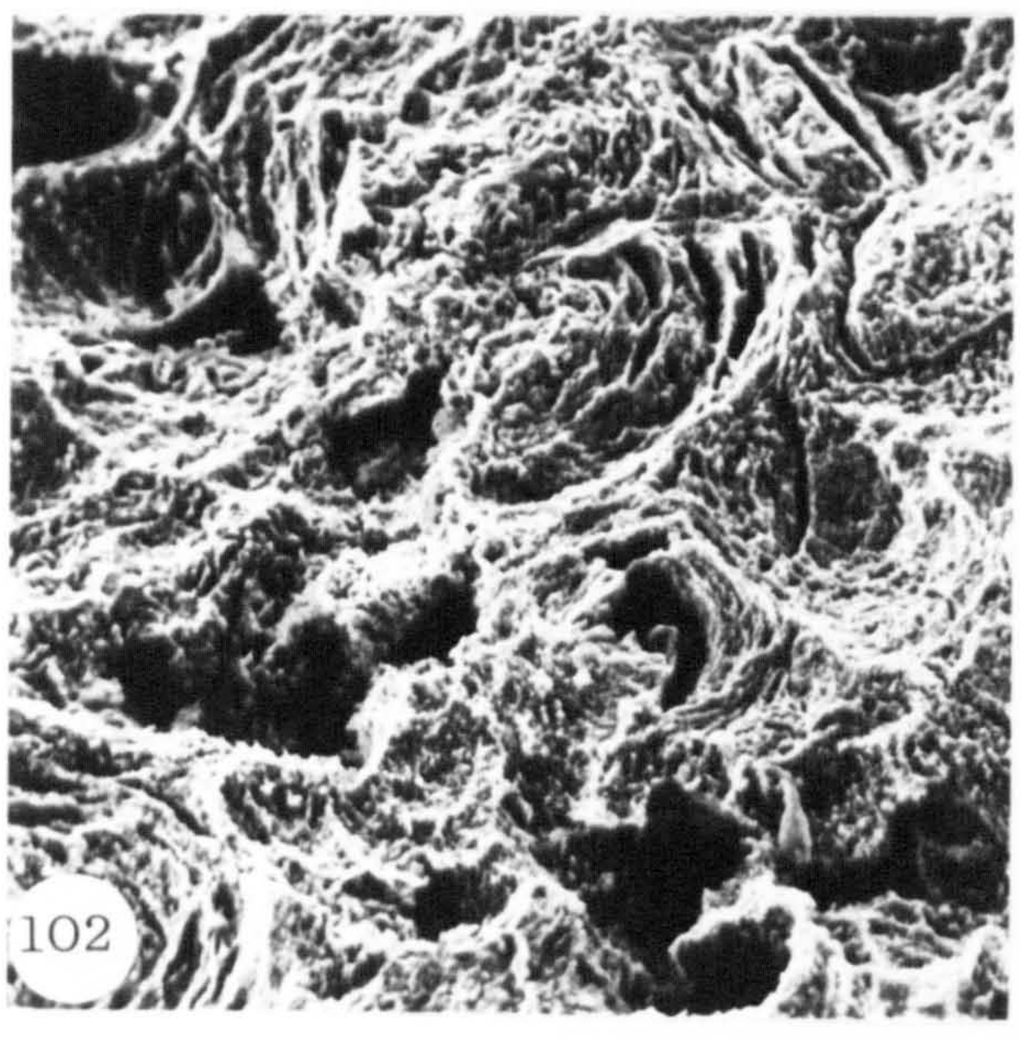
Figures 97 to 99. Stereopairs (stereoscan) of AGLMP graphite virgin and thermally oxidised in air.



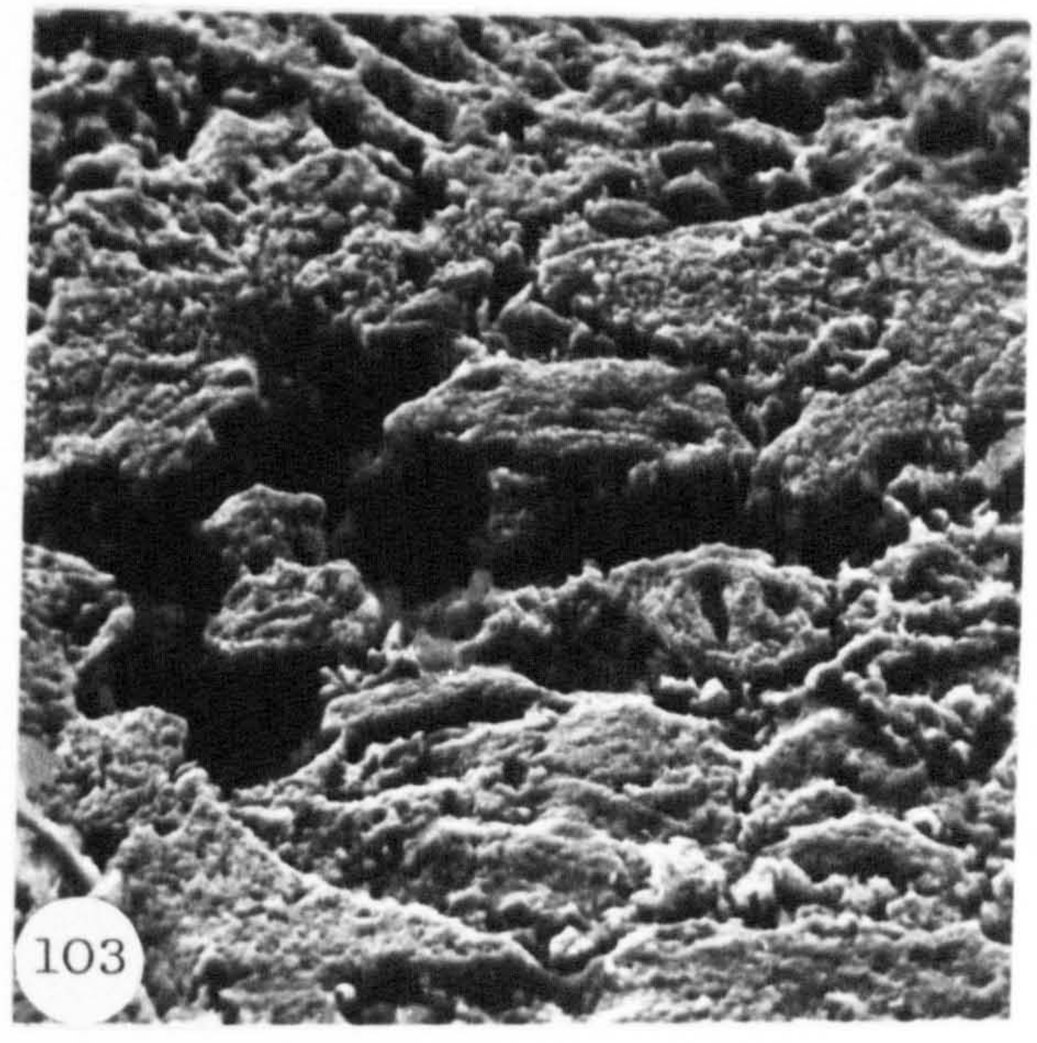
OXIDISED AGLMP GRAPHITE 100 µm



OXIDISED AGLMP GRAPHITE 10 µm

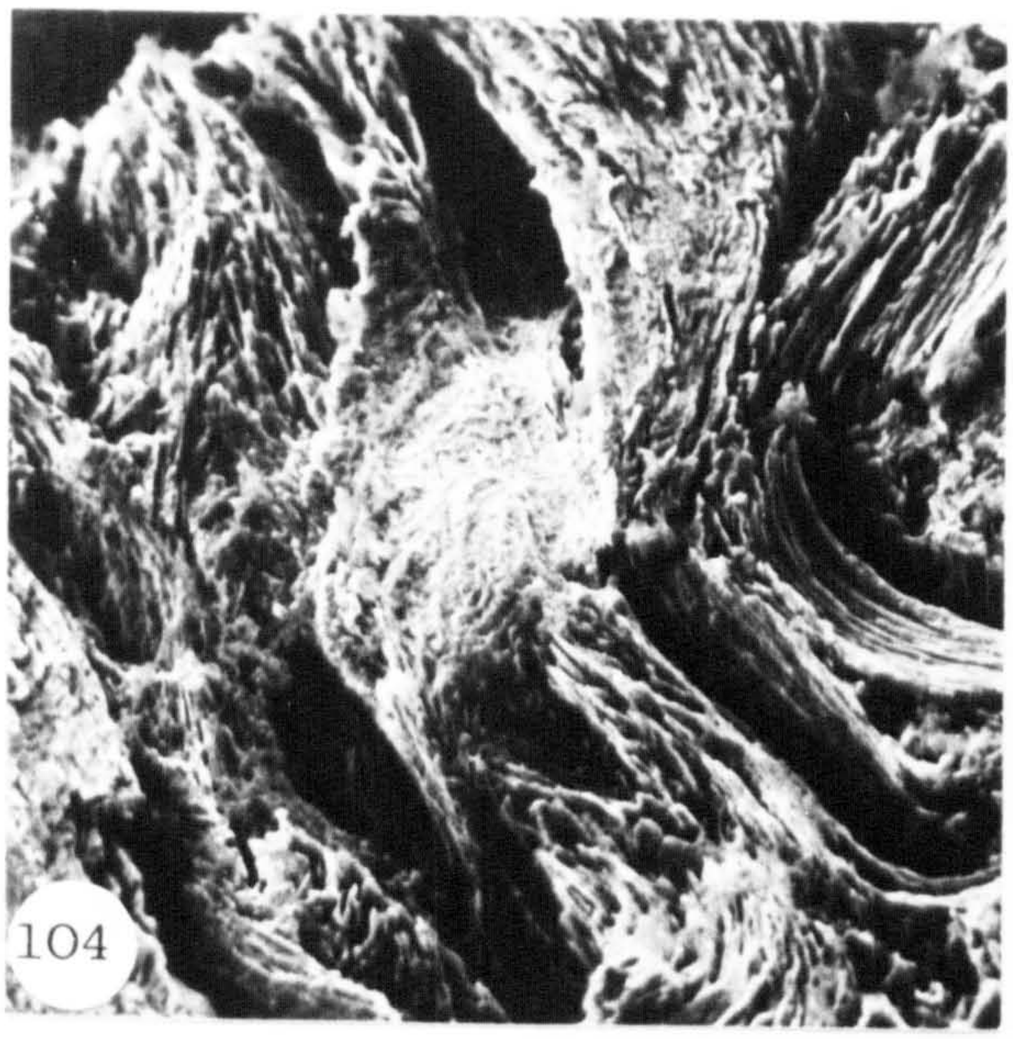


OXIDISED AGLMP GRAPHITE 100 µm

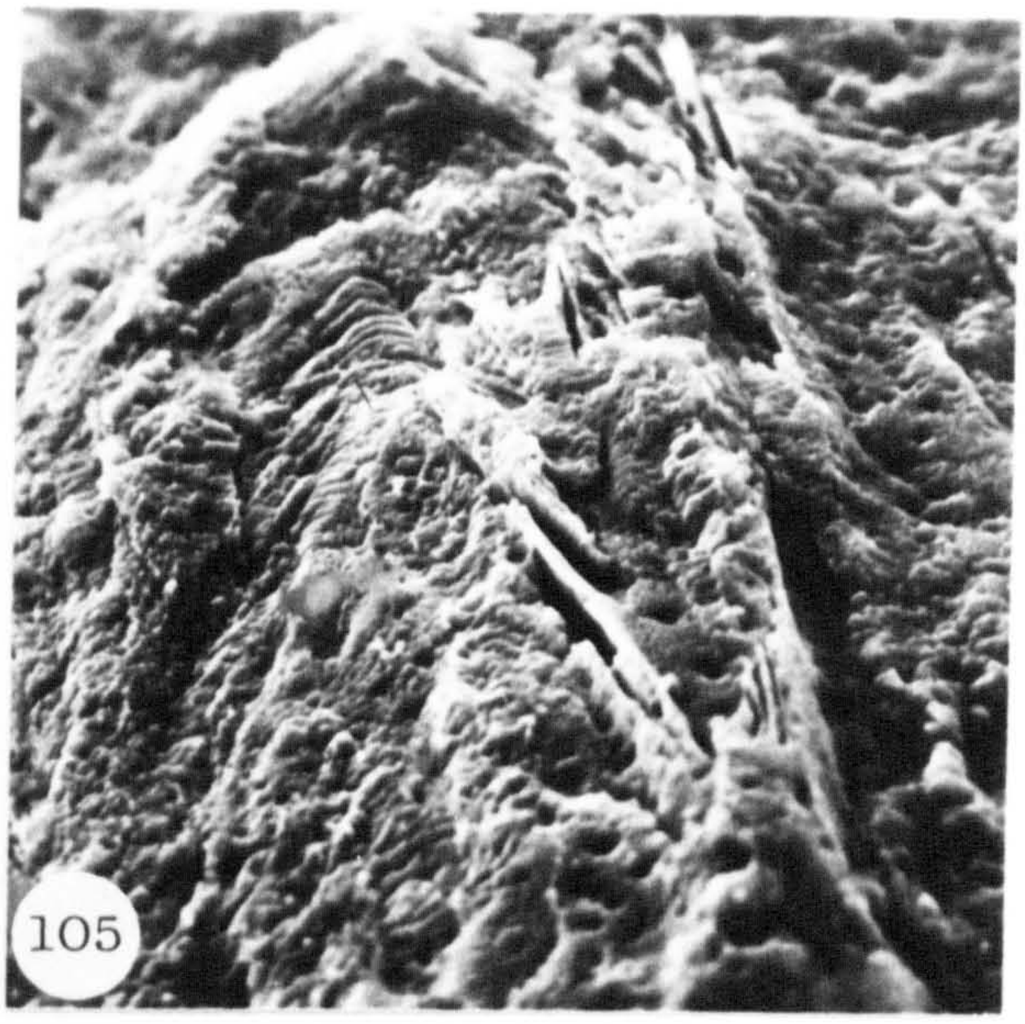


OXIDISED AGLMP GRAPHITE 50 µm

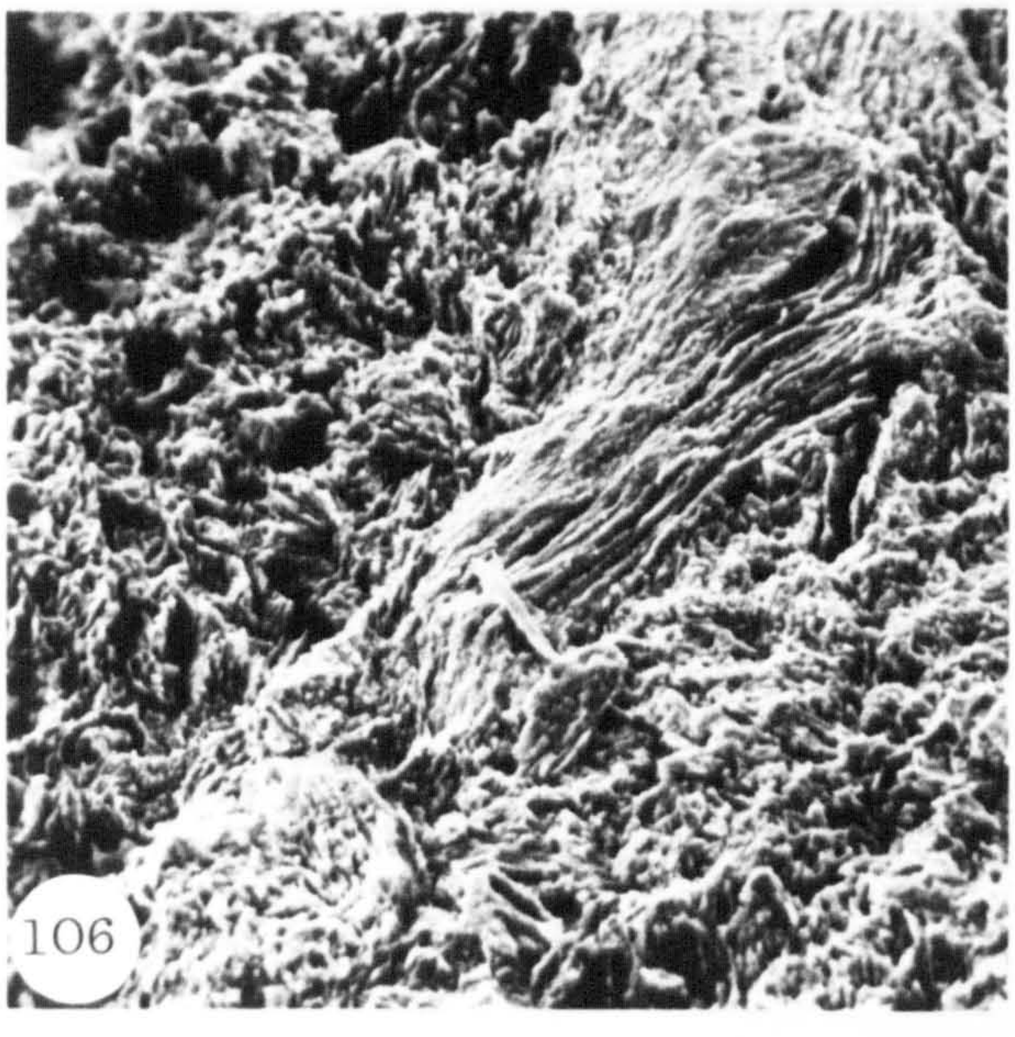
Figures 100 to 103. Scanning electron micrographs (stereoscan) of AGLMP graphite oxidised with atomic oxygen in the Plasmod apparatus.



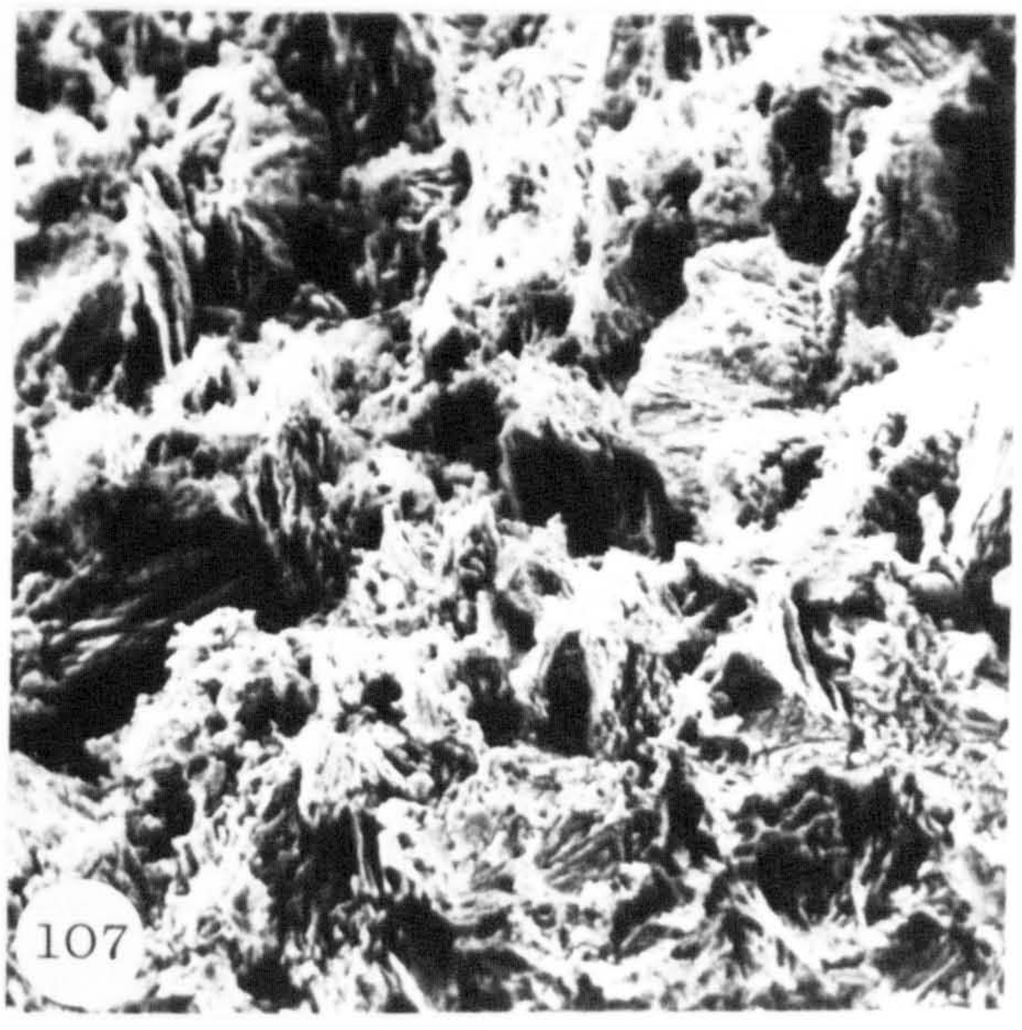
OXIDISED LIMA GRAPHITE 100 µm



OXIDISED LIMA GRAPHITE 10 µm

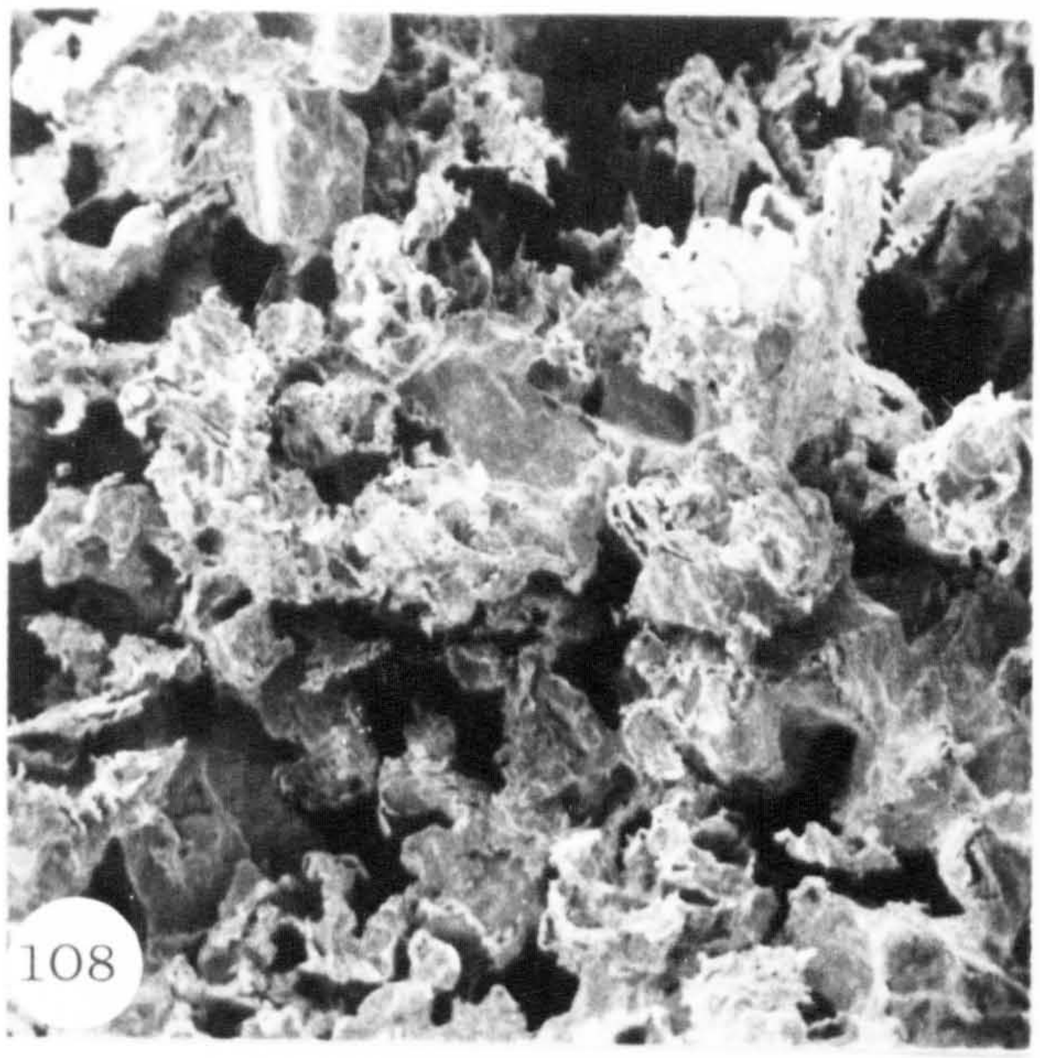


OXIDISED LIMA GRAPHITE 100 µm



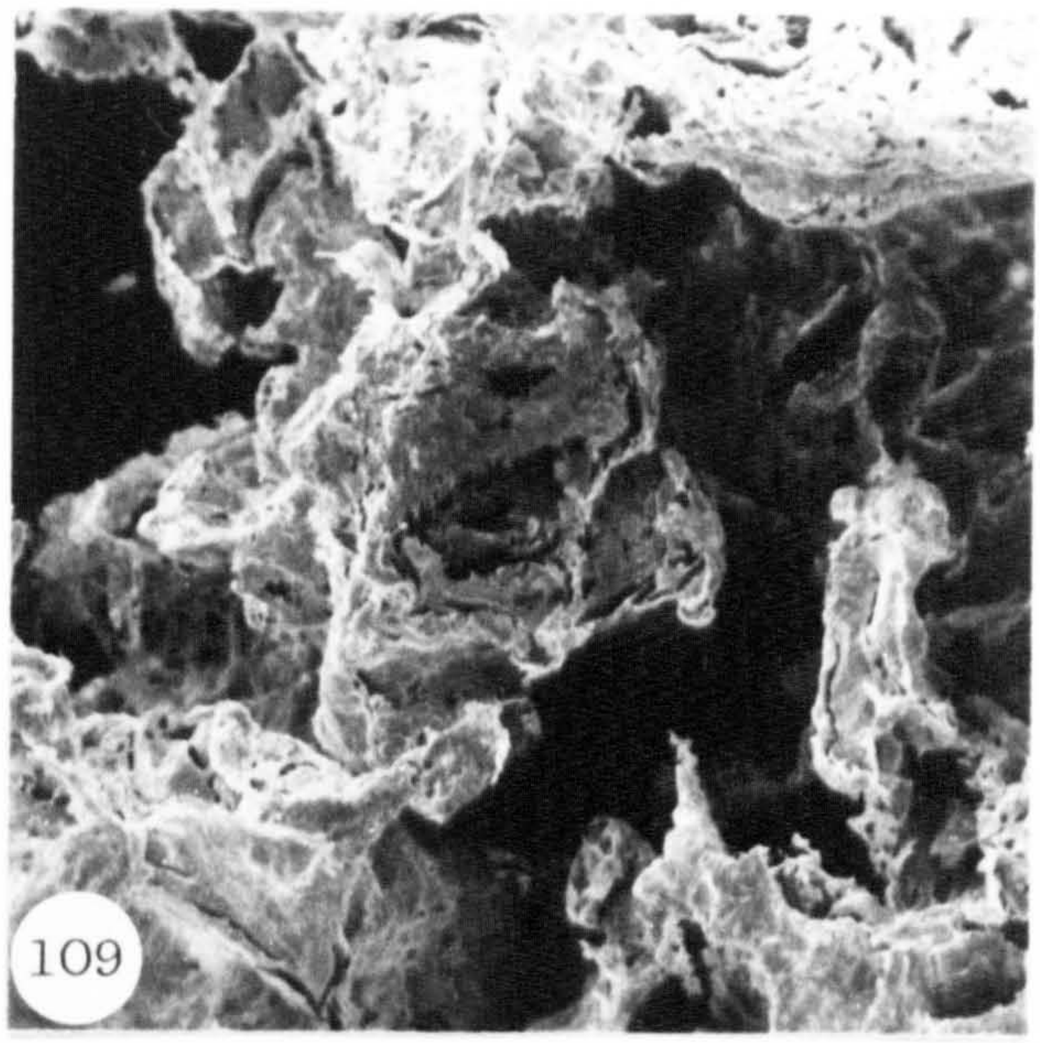
OXIDISED LIMA GRAPHITE 100 µm

Figures 104 to 107. Scanning electron micrographs (stereoscan) of Lima graphite oxidised by atomic oxygen in the Plasmod apparatus.



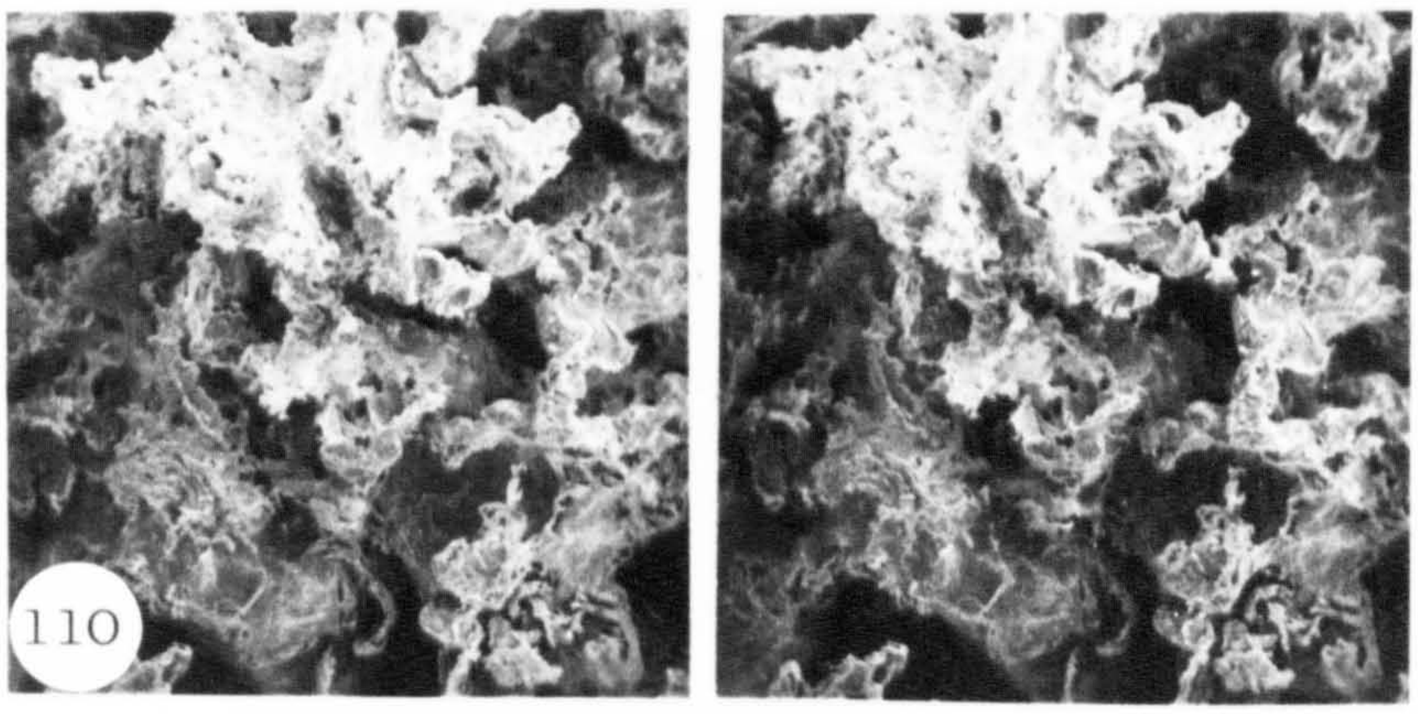
AGLMP GRAPHITE
Gold pore shape

100 µm



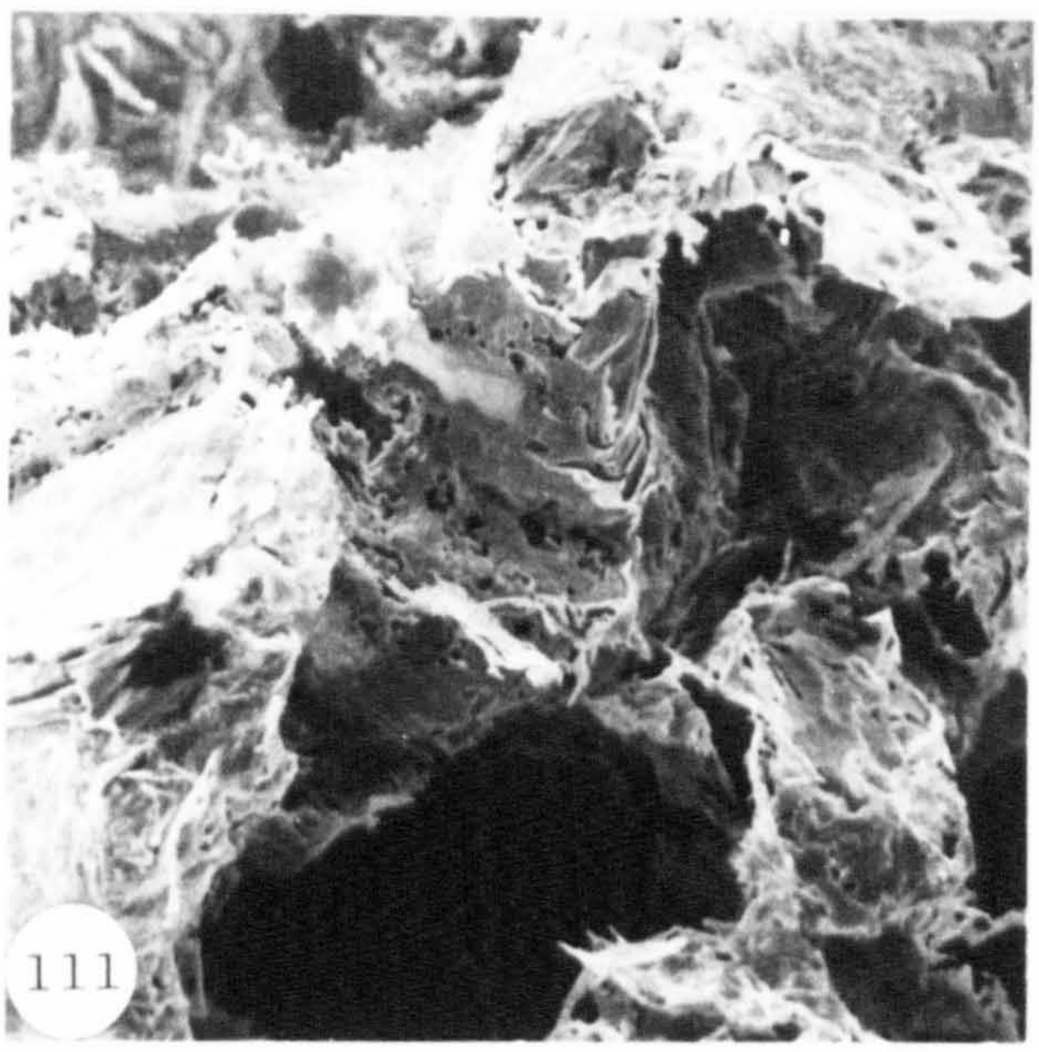
AGLMP GRAPHITE
Gold pore shape

50 µm



STEREOPAIR OF AGLMP GRAPHITE
Gold pore shape

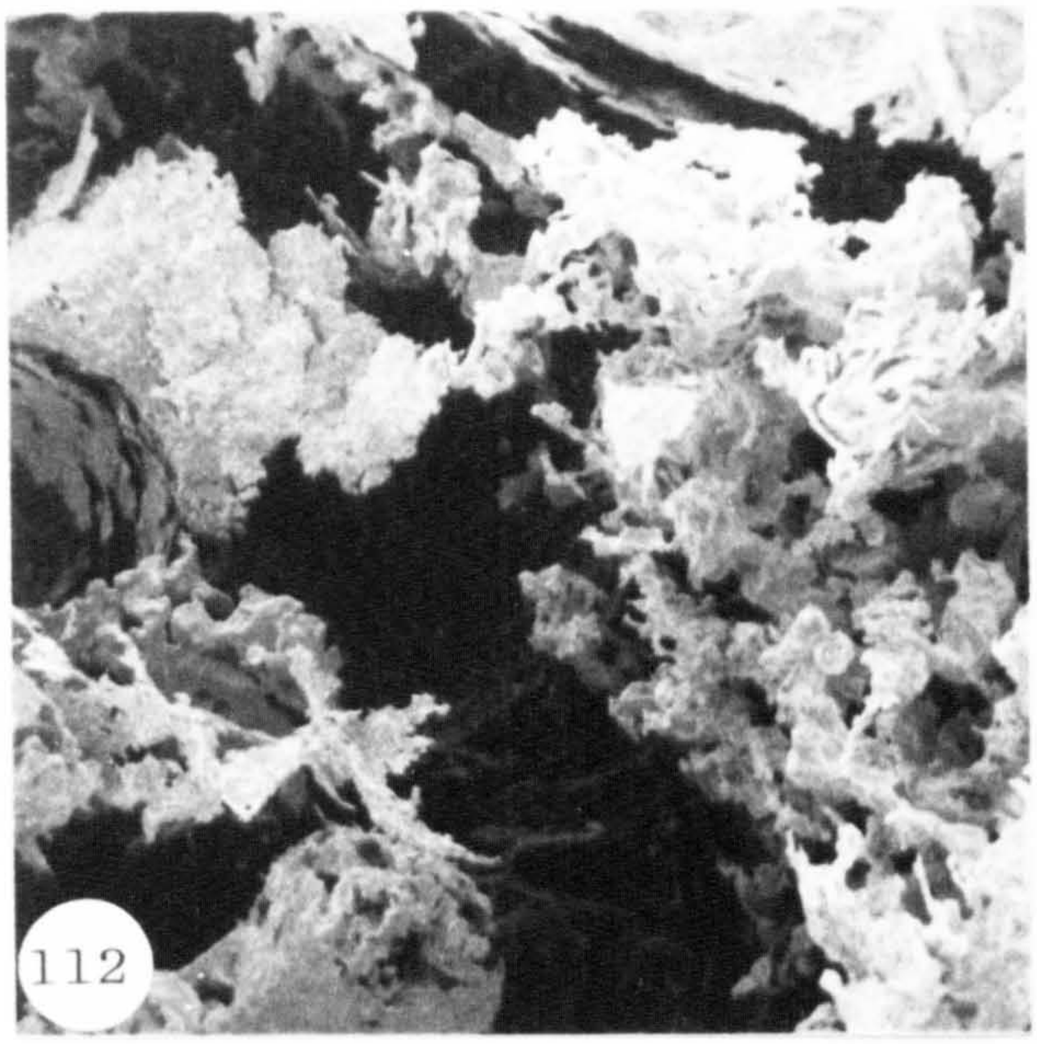
100 µm



AGLMP GRAPHITE
Gold pore shape

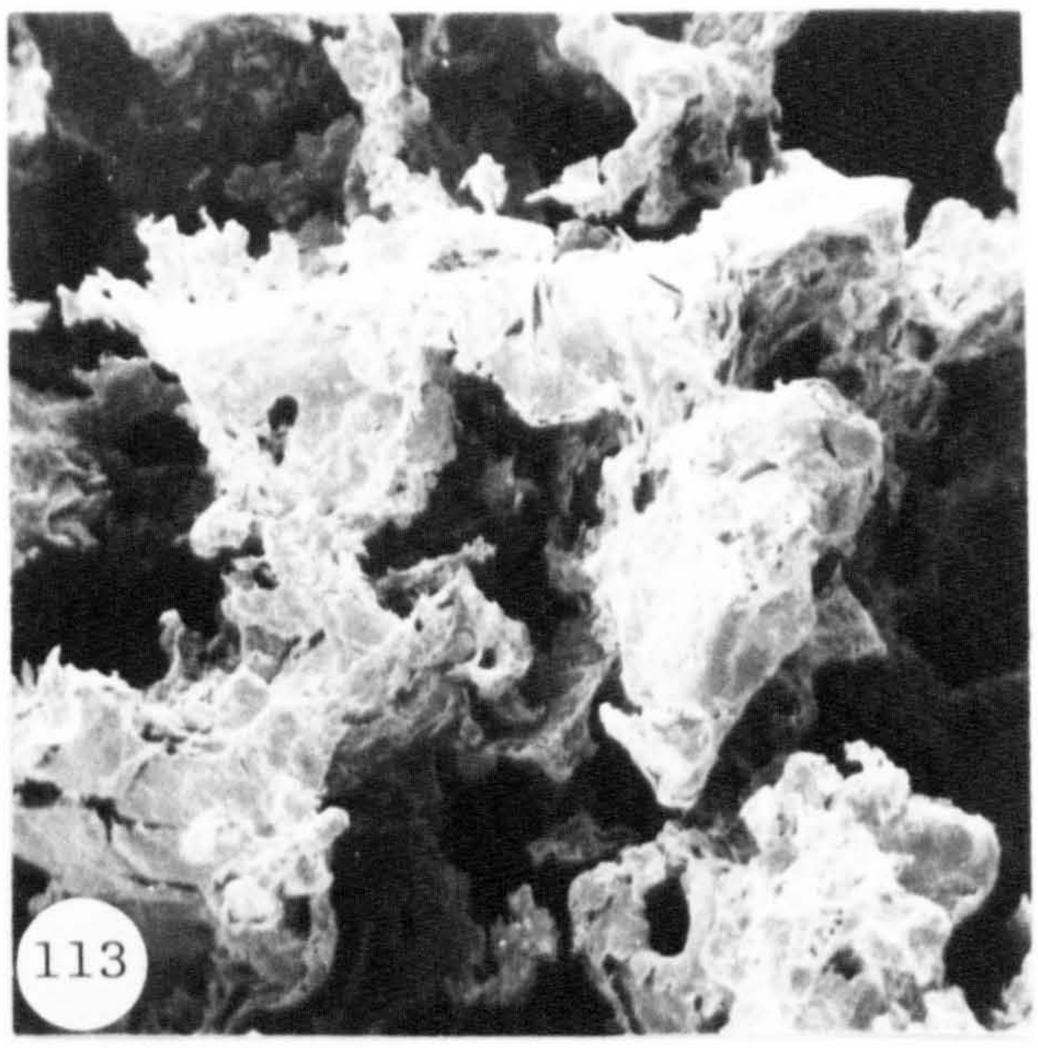
20 µm

Figures 108 to 111. Scanning electron micrographs (stereoscan) of gold pore shape after oxidation of AGLMP graphite.



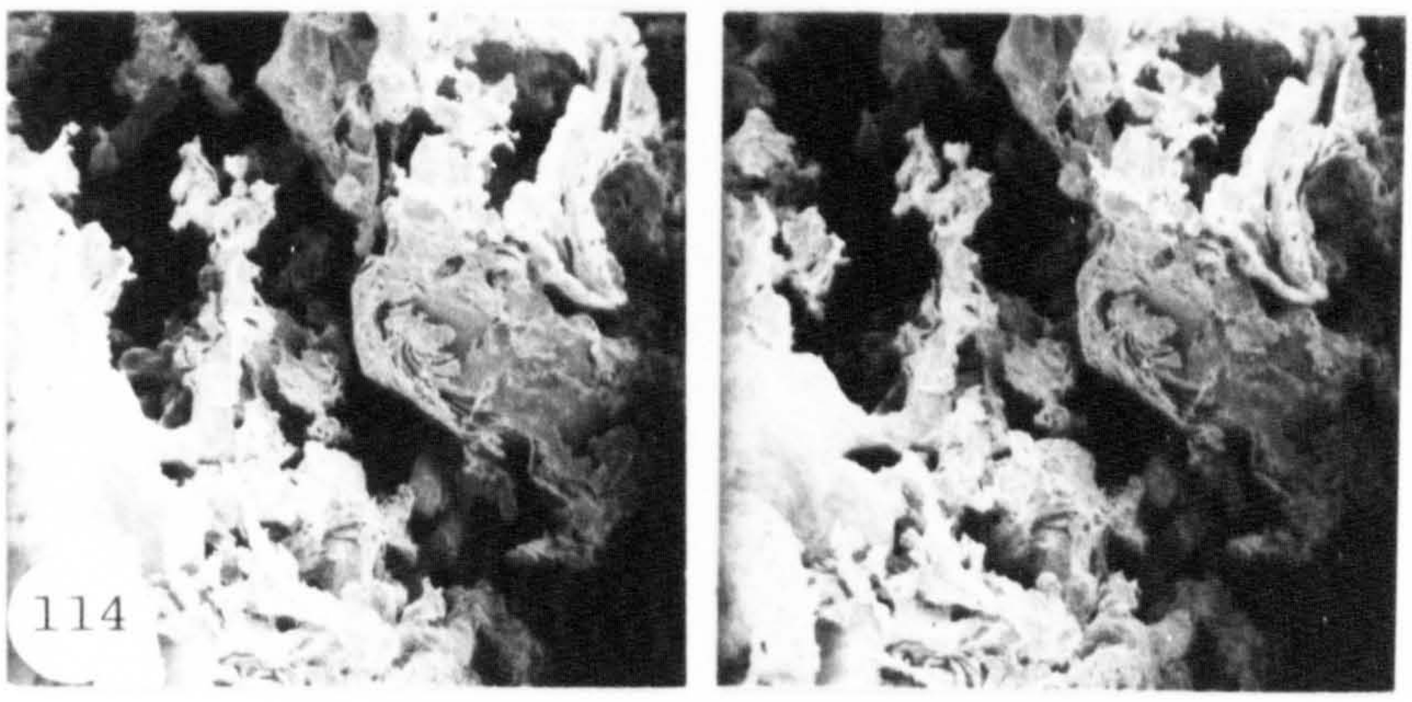
GCMB GRAPHITE
Gold pore shape

100 µm



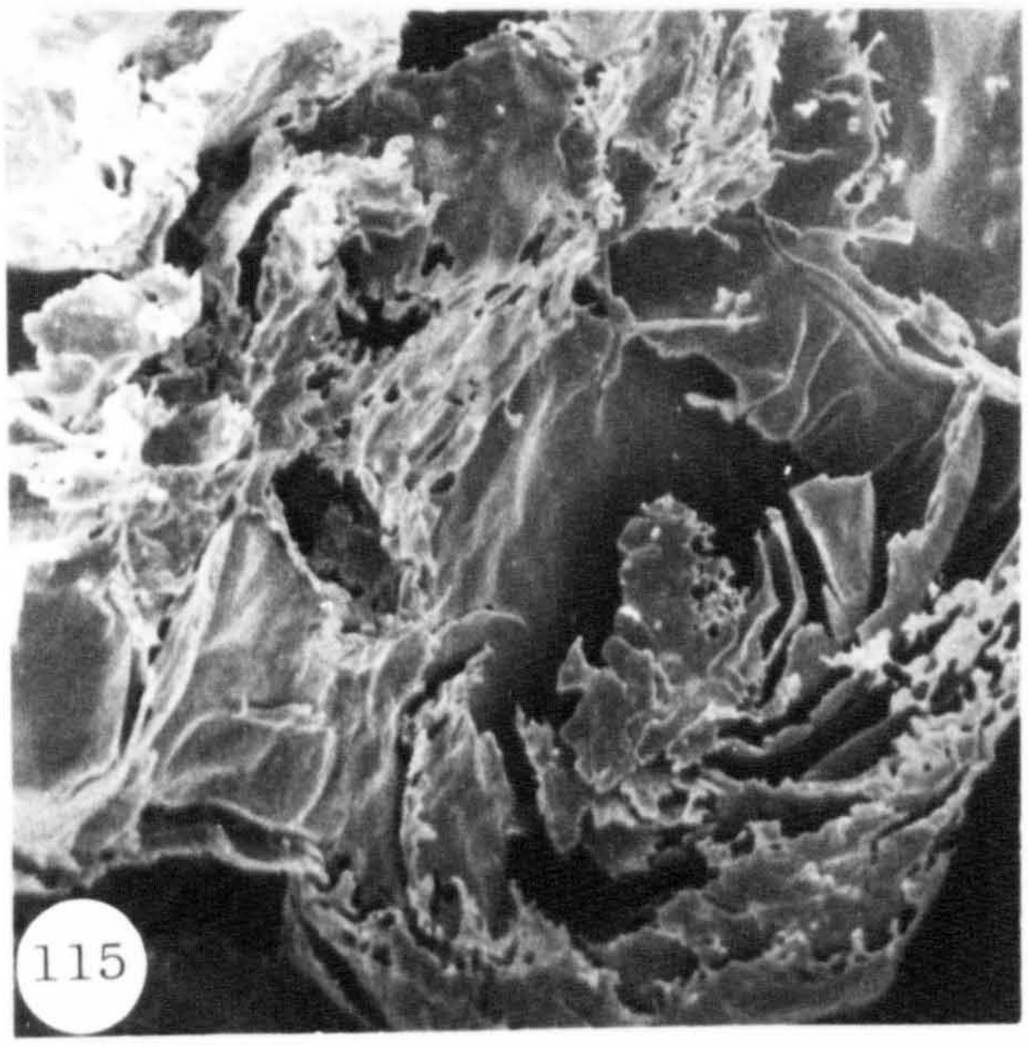
GCMB GRAPHITE
Gold pore shape

50 µm



STEREOPAIR OF GCMB GRAPHITE
Gold pore shape

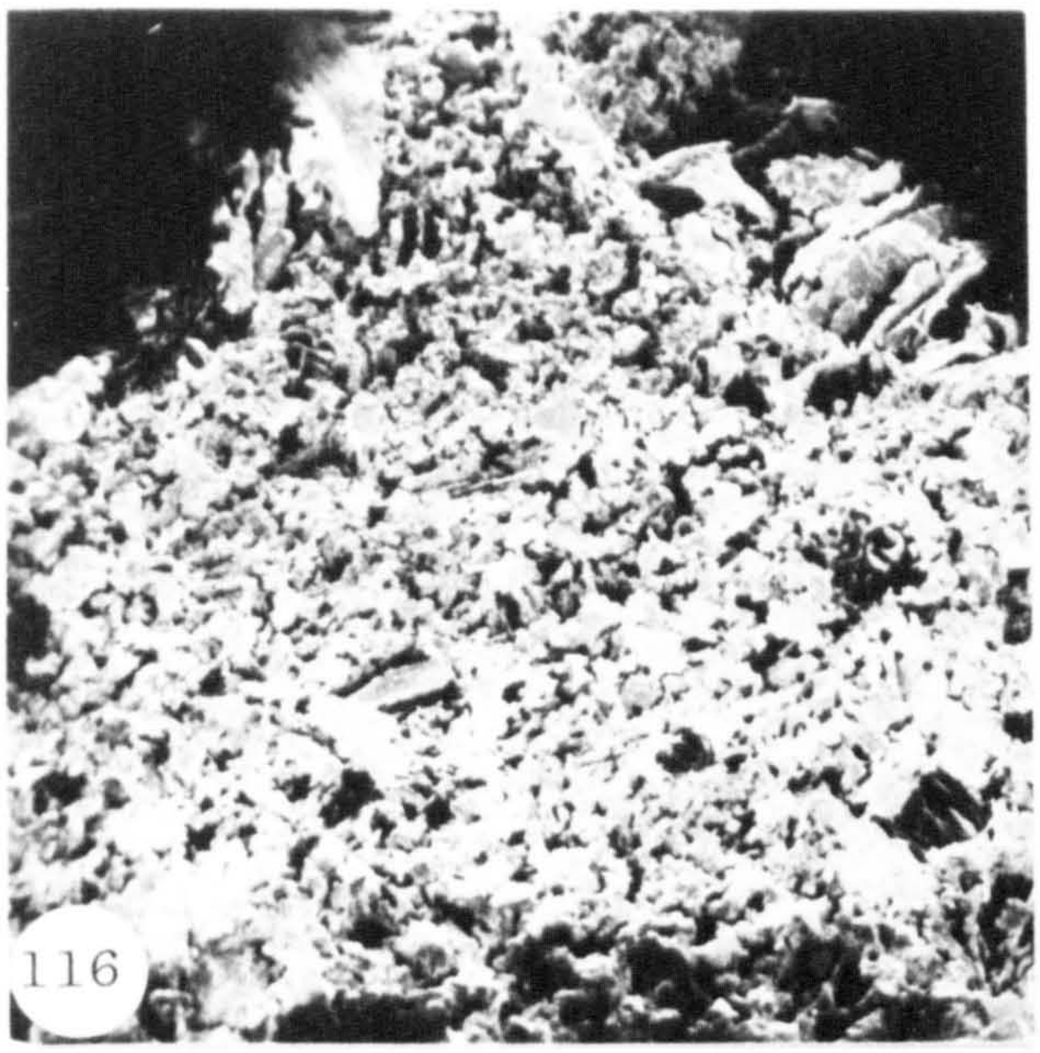
100 µm



GCMB GRAPHITE
Gold pore shape

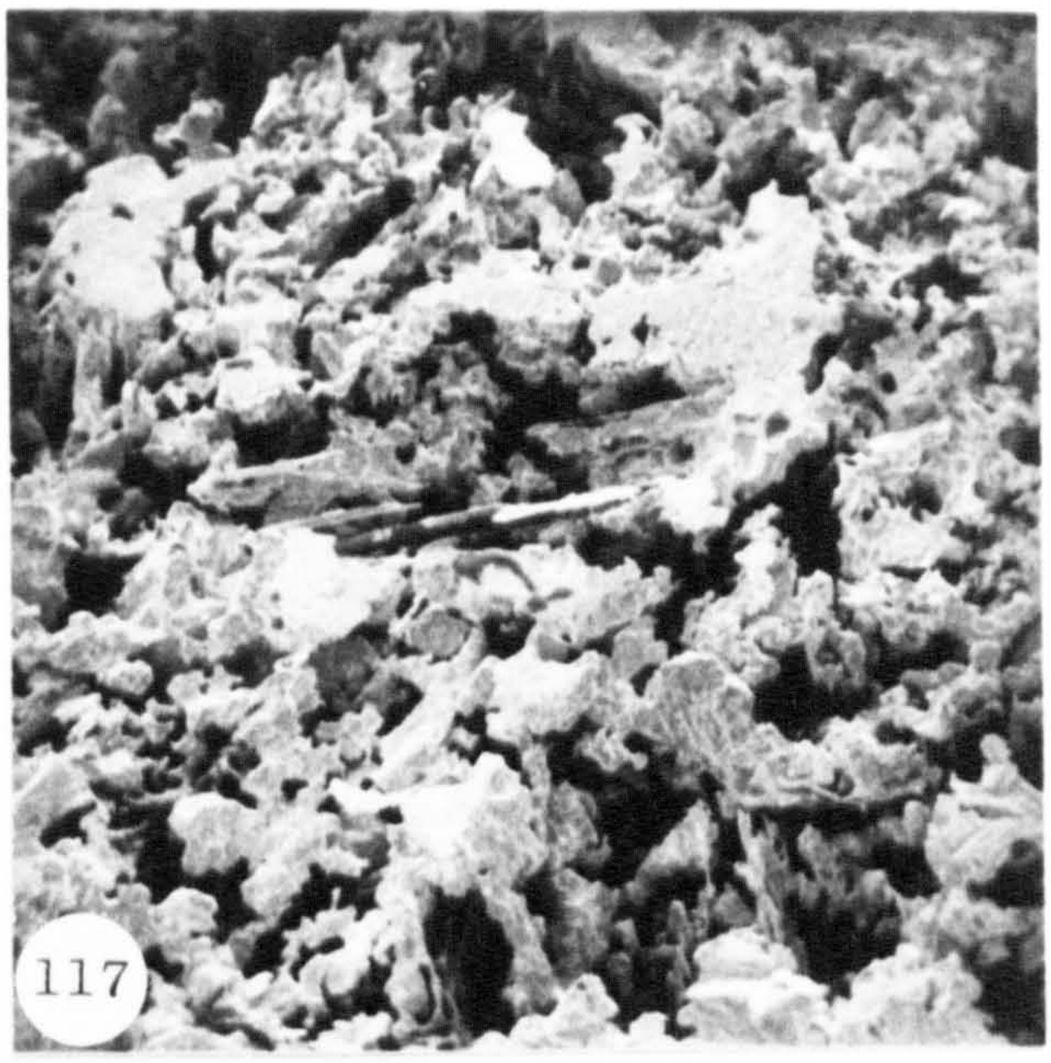
20 µm

Figures 112 to 115. Scanning electron micrographs (stereoscan) of gold pore shape after oxidation of GCMB graphite.



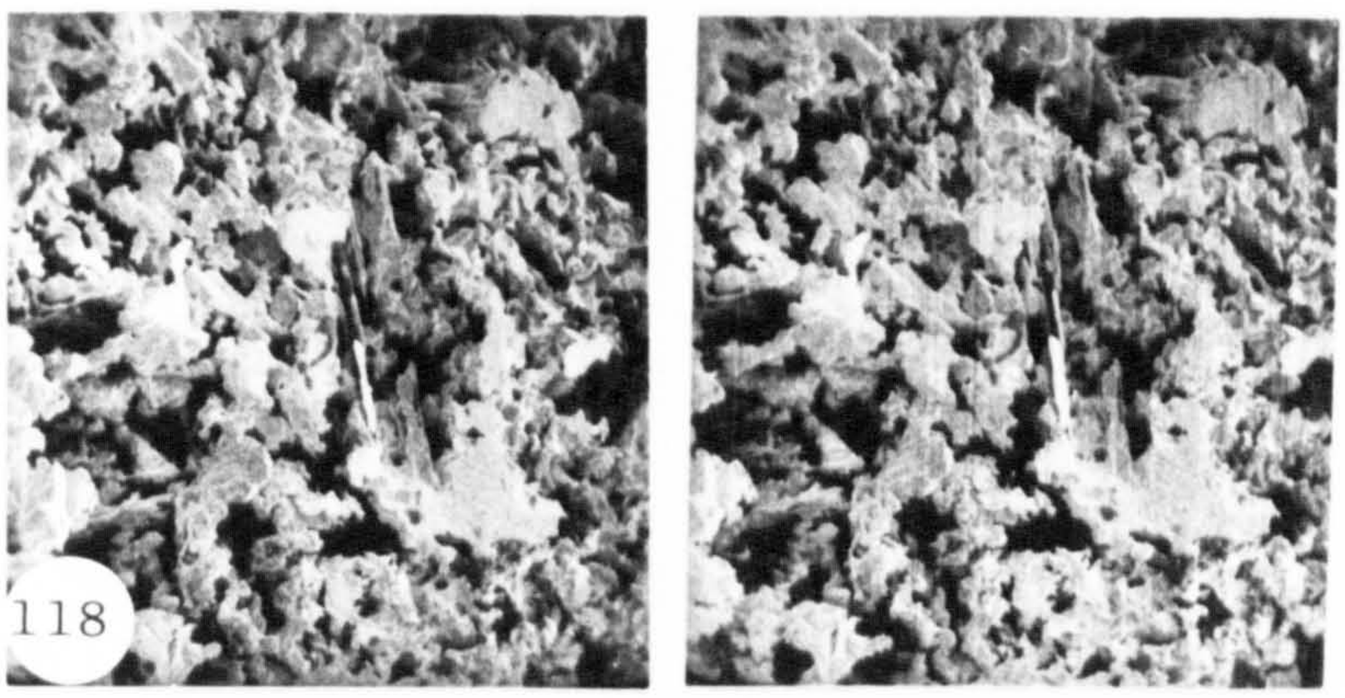
LIMA GRAPHITE
Gold pore shape

200 µm



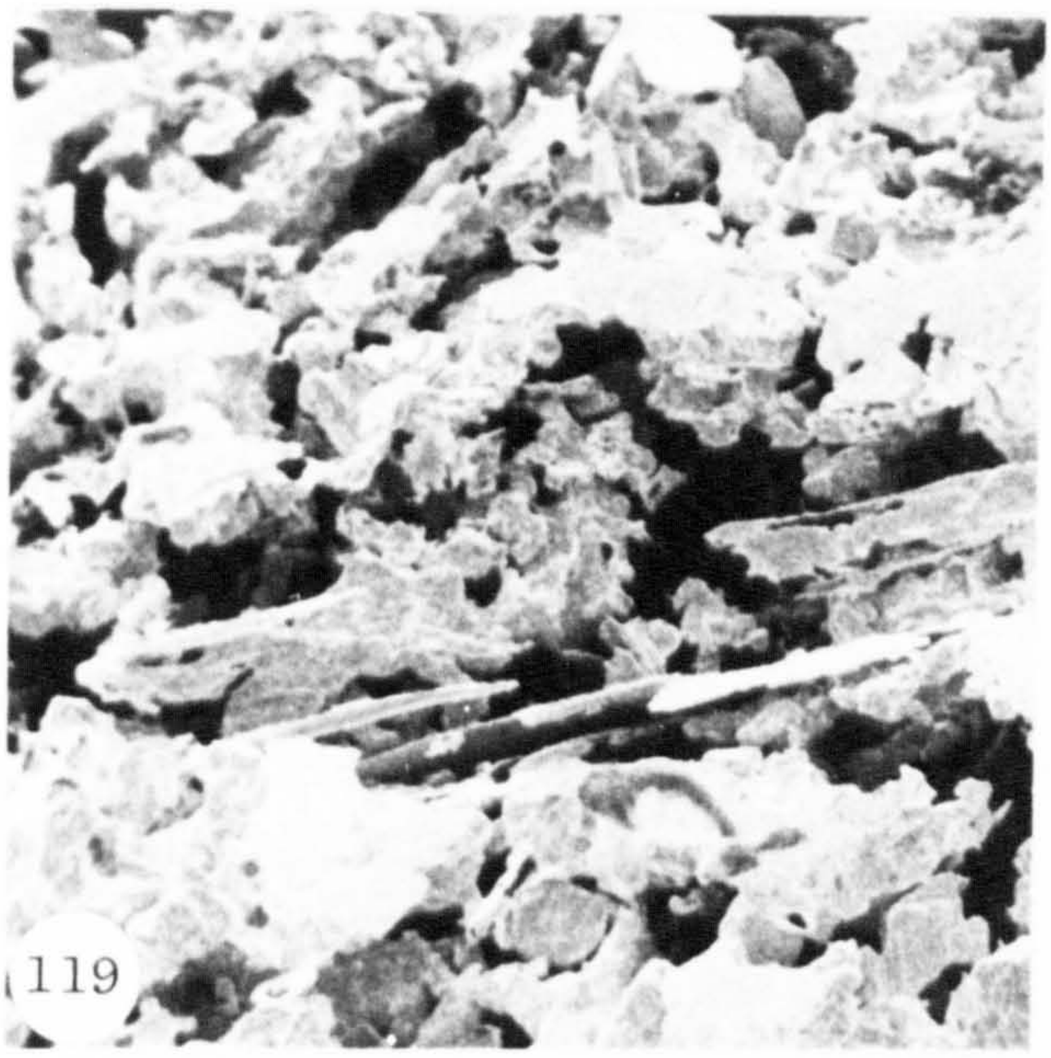
LIMA GRAPHITE
Gold pore shape

100 µm



STEREOPAIR OF LIMA GRAPHITE
Gold pore shape

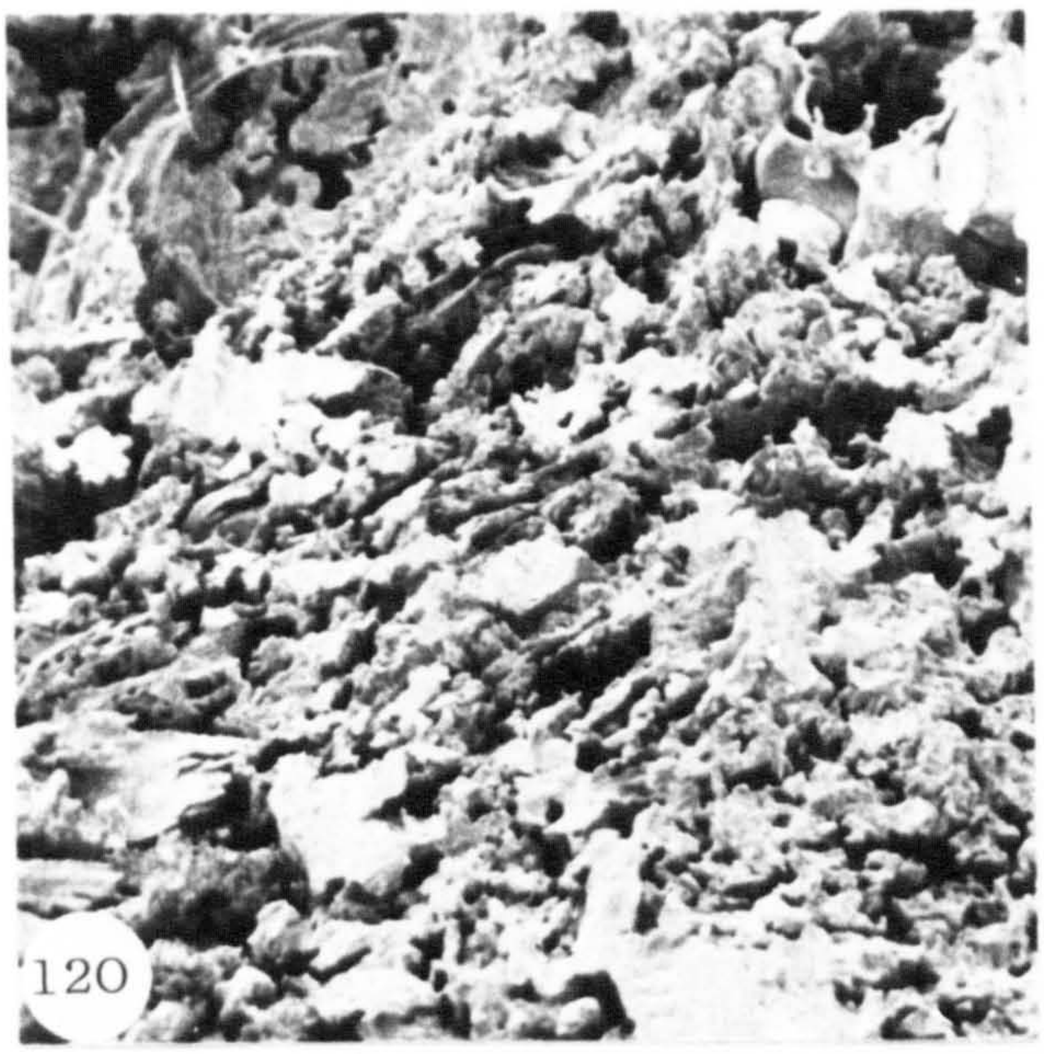
100 µm



LIMA GRAPHITE
Gold pore shape

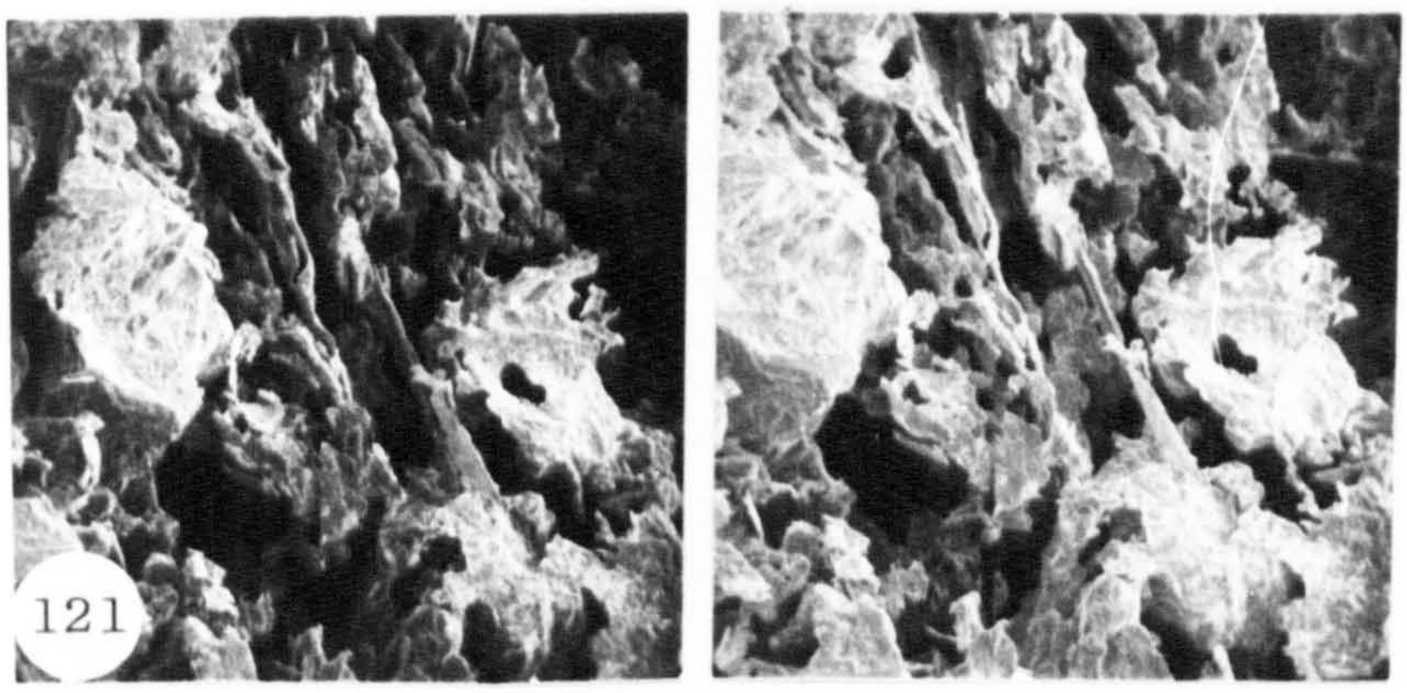
30 µm

Figures 116 to 119. Scanning electron micrographs (stereoscan) of gold pore shape after oxidation of Lima graphite.



PGA L18 GRAPHITE
Gold pore shape

100 µm



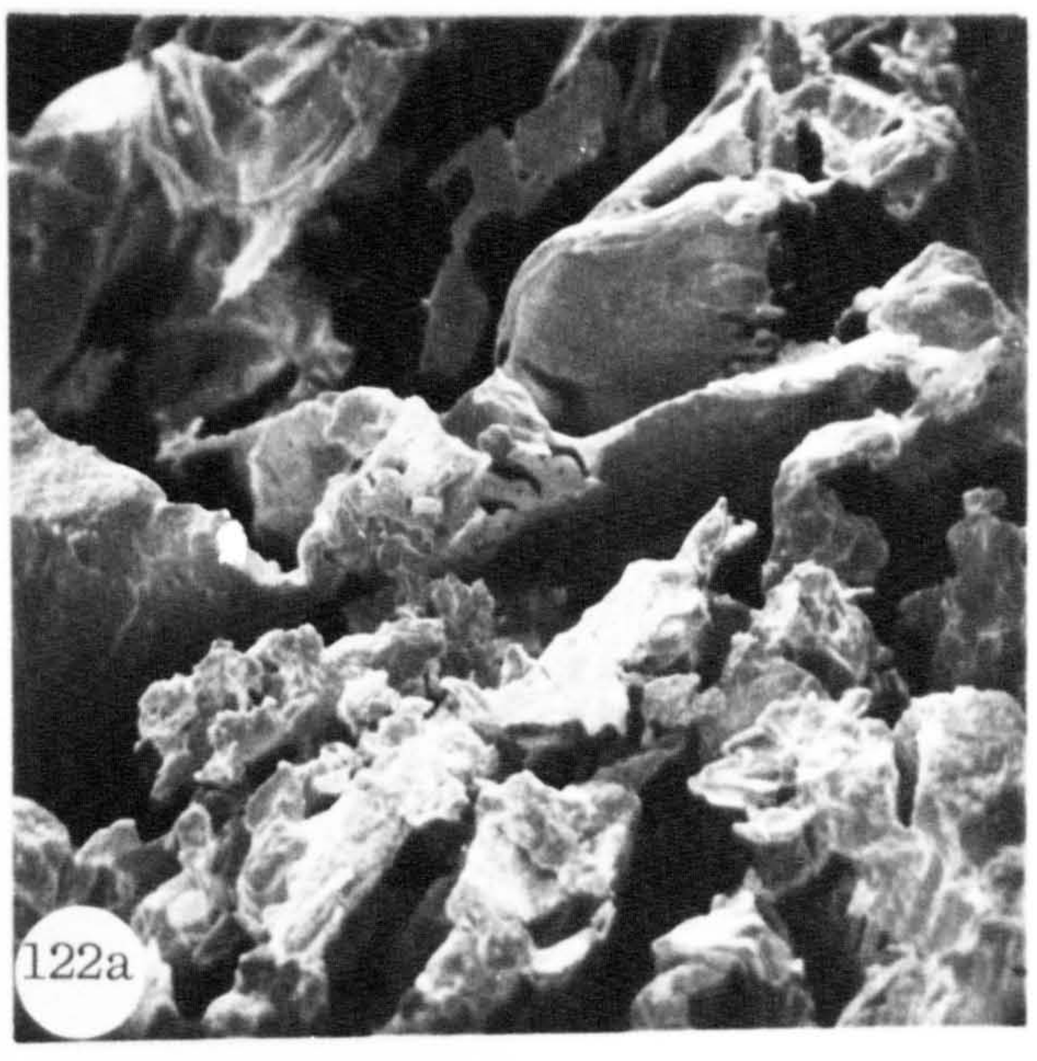
STEREOPAIR OF PGA L18 GRAPHITE
Gold pore shape

50 µm



PGA L18 GRAPHITE
Gold pore shape

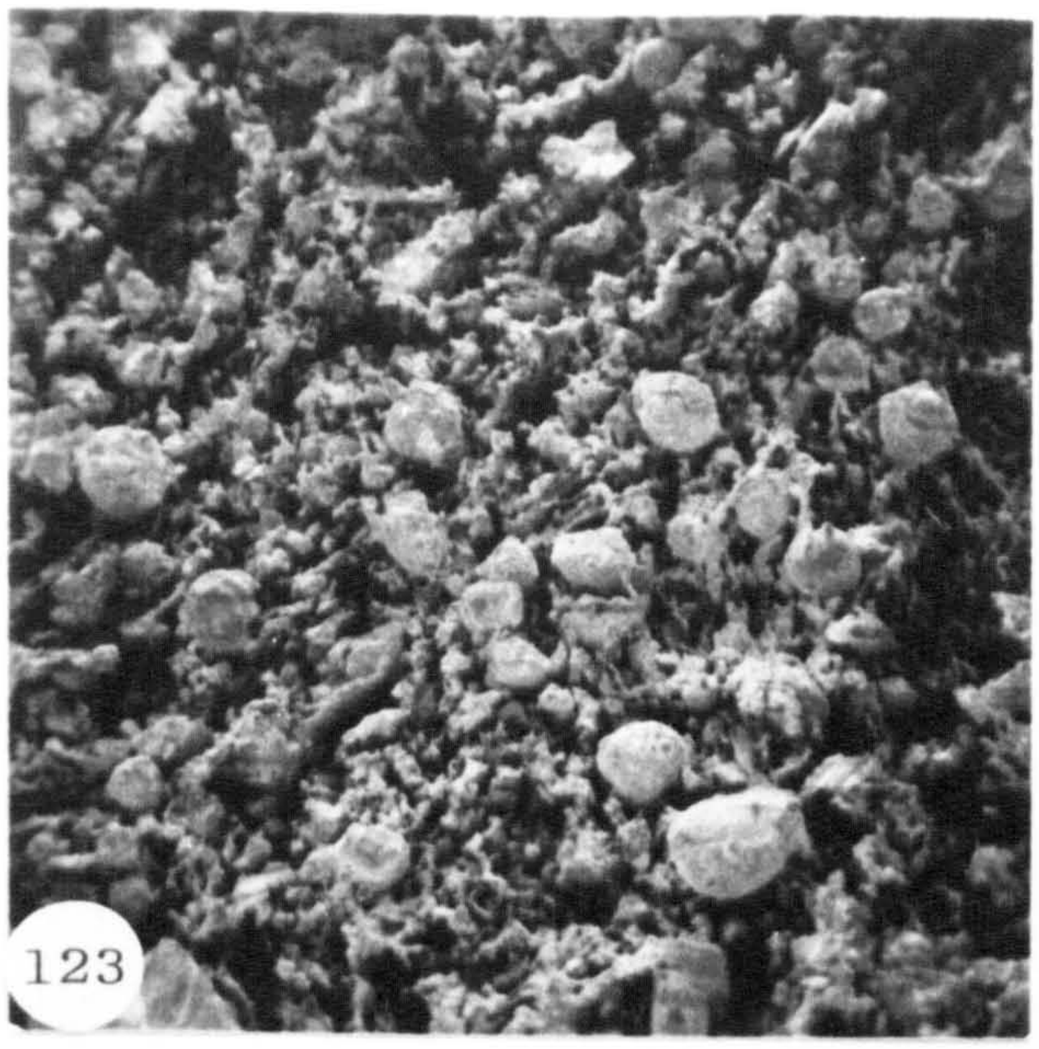
20 µm



PGA L18 GRAPHITE
Gold pore shape

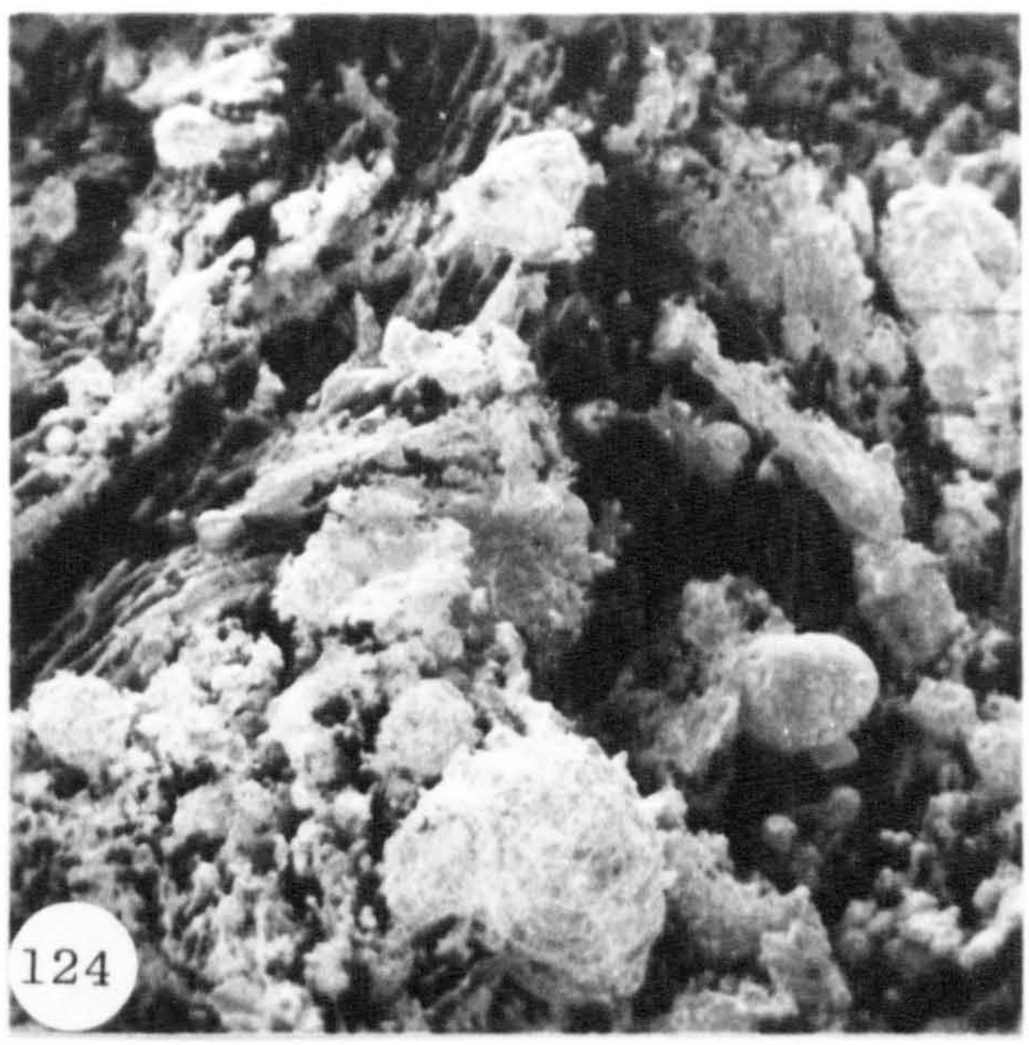
20 µm

Figures 120 to 122. Scanning electron micrographs (stereoscan) of gold pore shape after oxidation of PGA L18 graphite.



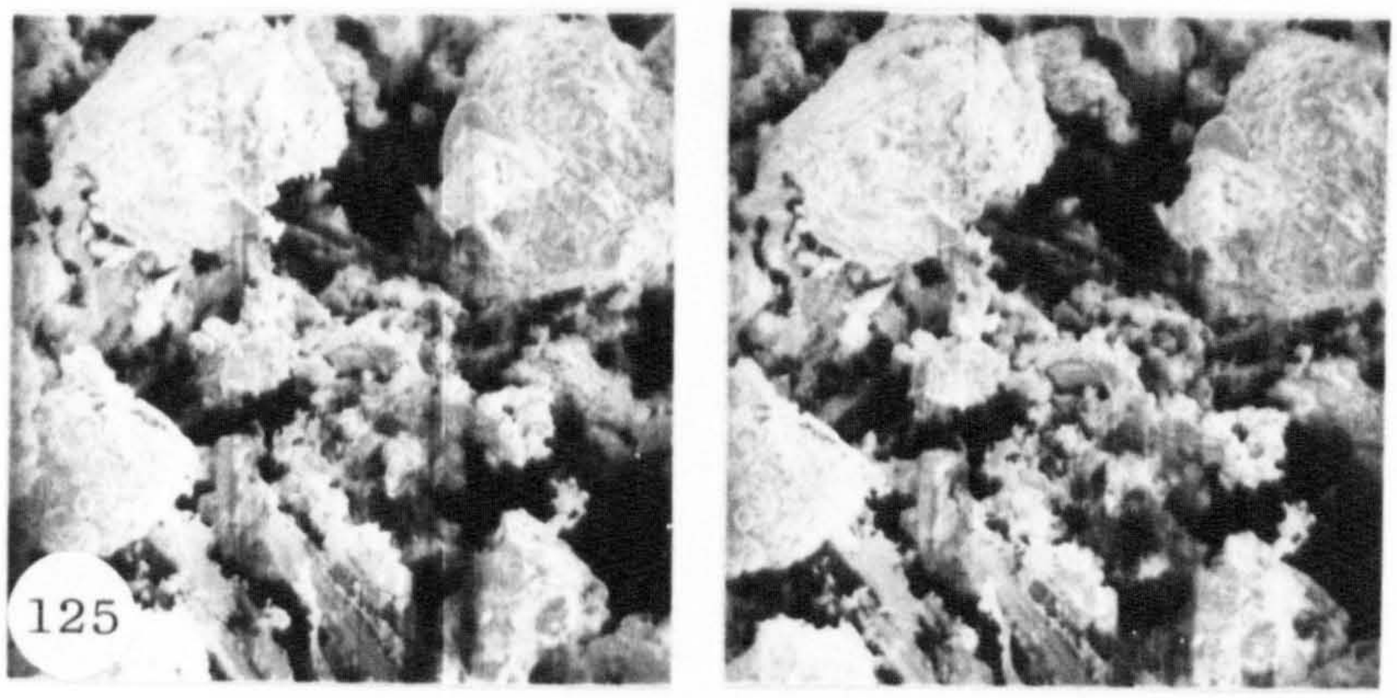
PGA L18 GRAPHITE
Bismuth pore shape

100 µm



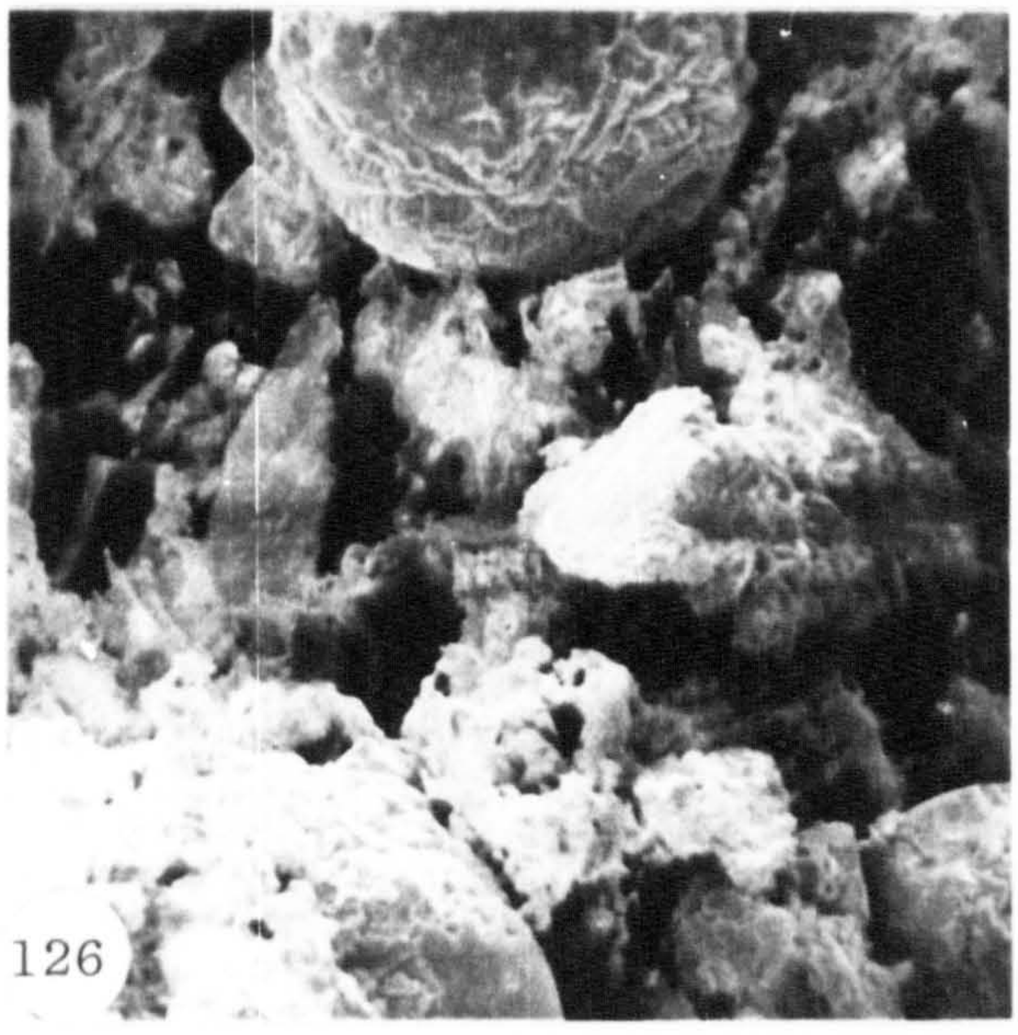
PGA L18 GRAPHITE
Bismuth pore shape

50 µm



STEREOPAIR OF PGA L18 GRAPHITE

50 µm



PGA L18 GRAPHITE
Bismuth pore shape

20 µm

Figures 123 to 126. Scanning electron micrographs (stereoscan) of bismuth pore shapes left after oxidation of PGA L18 graphite.

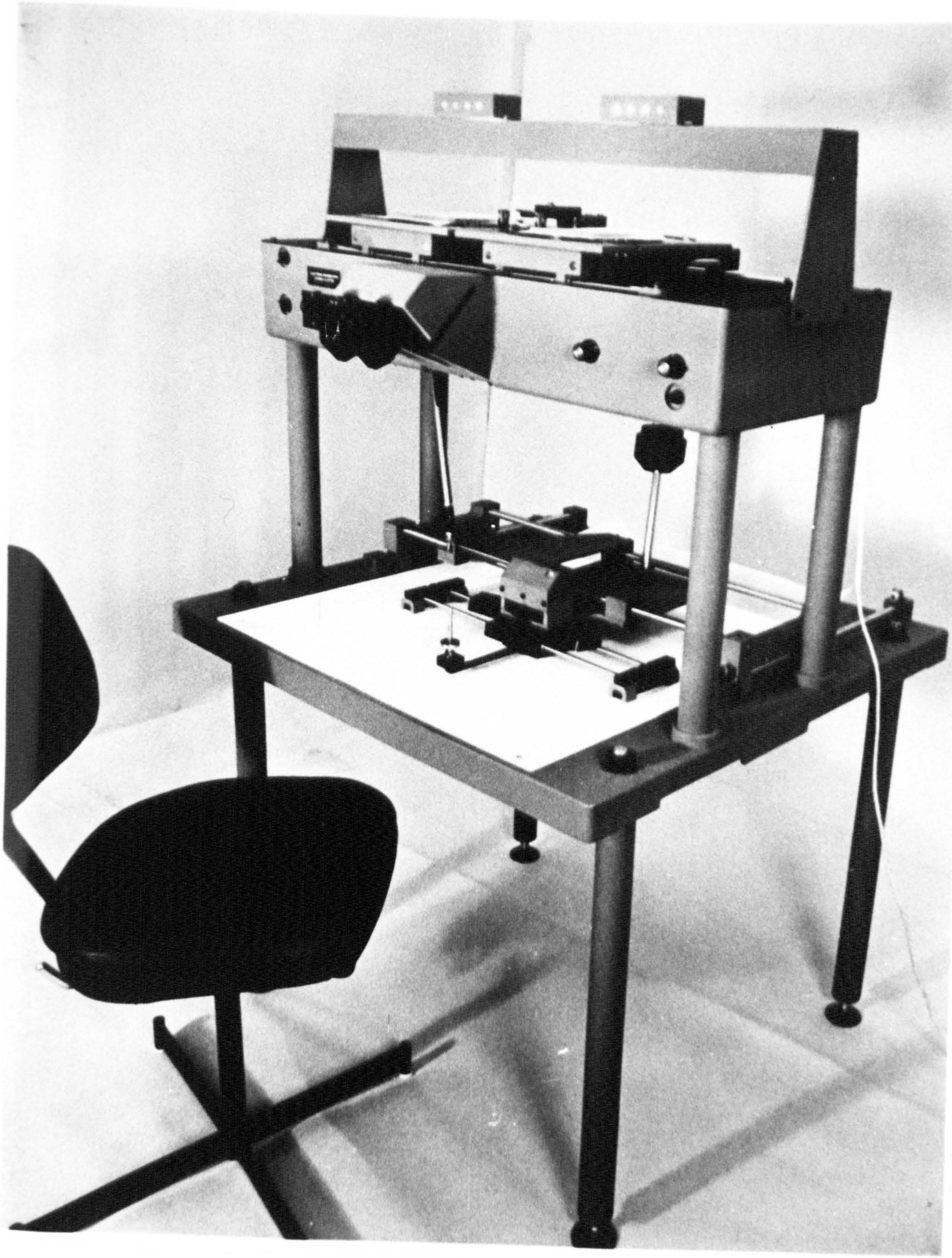
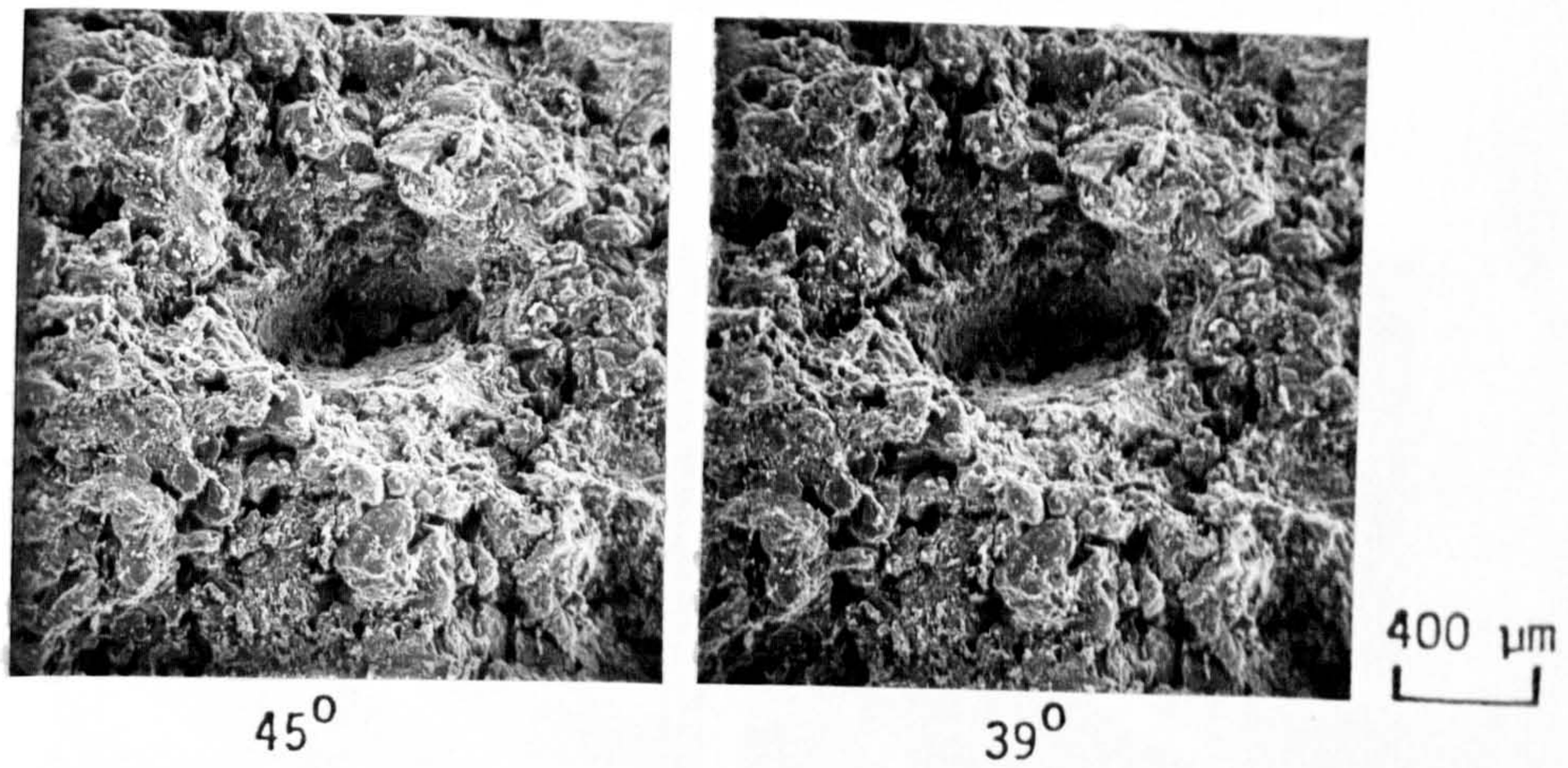
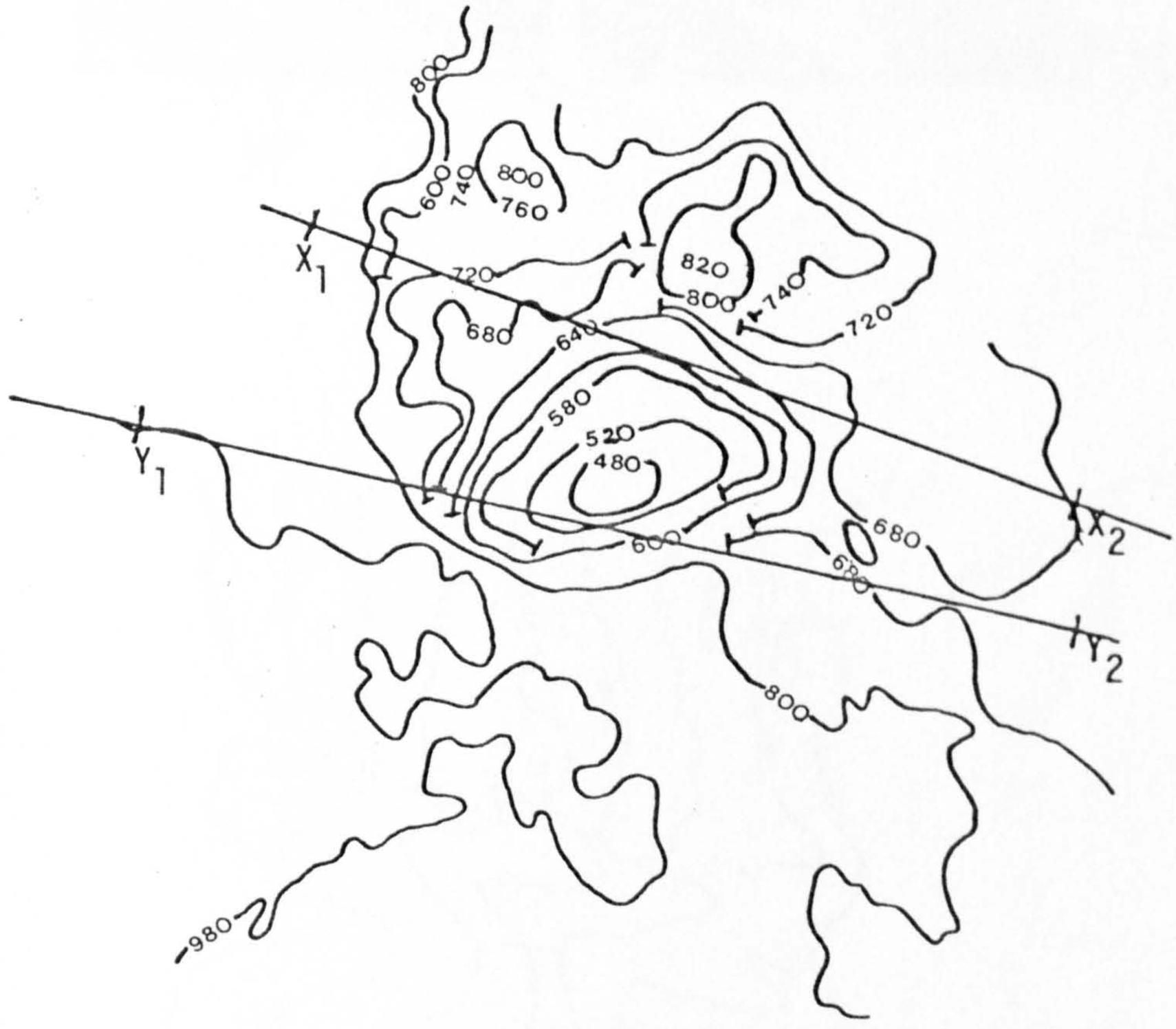


Figure 126a. The electron micrograph plotting device.



CONTOURS



PROFILES

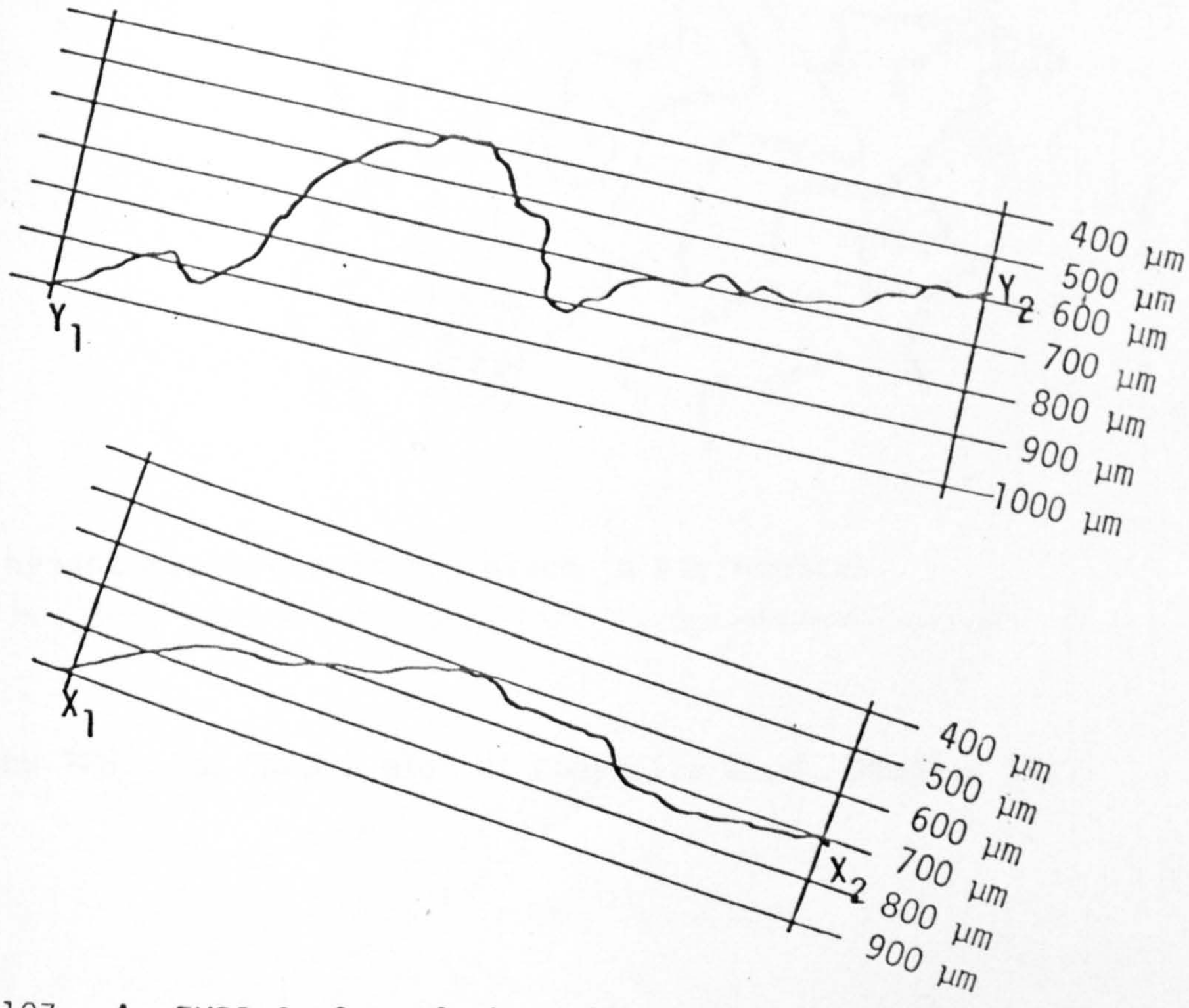
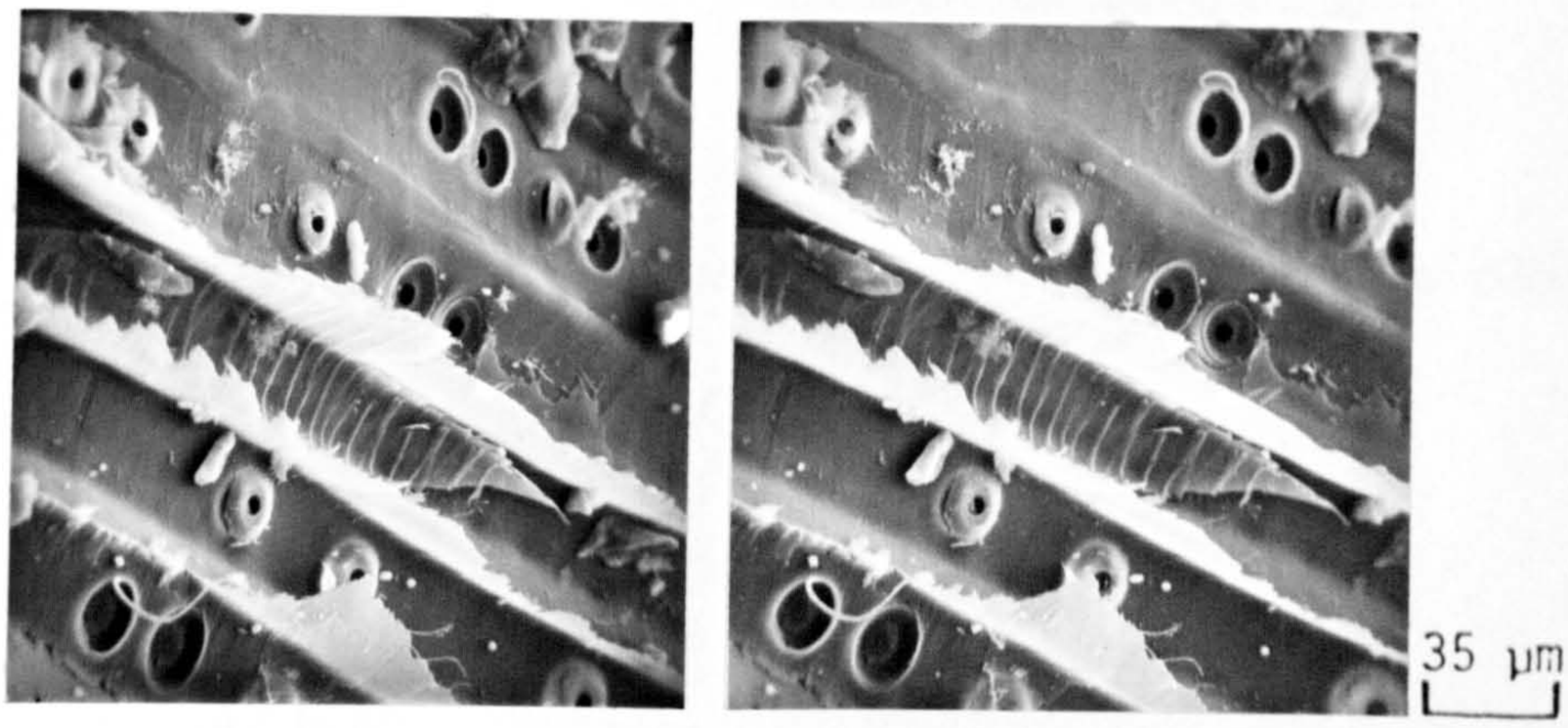
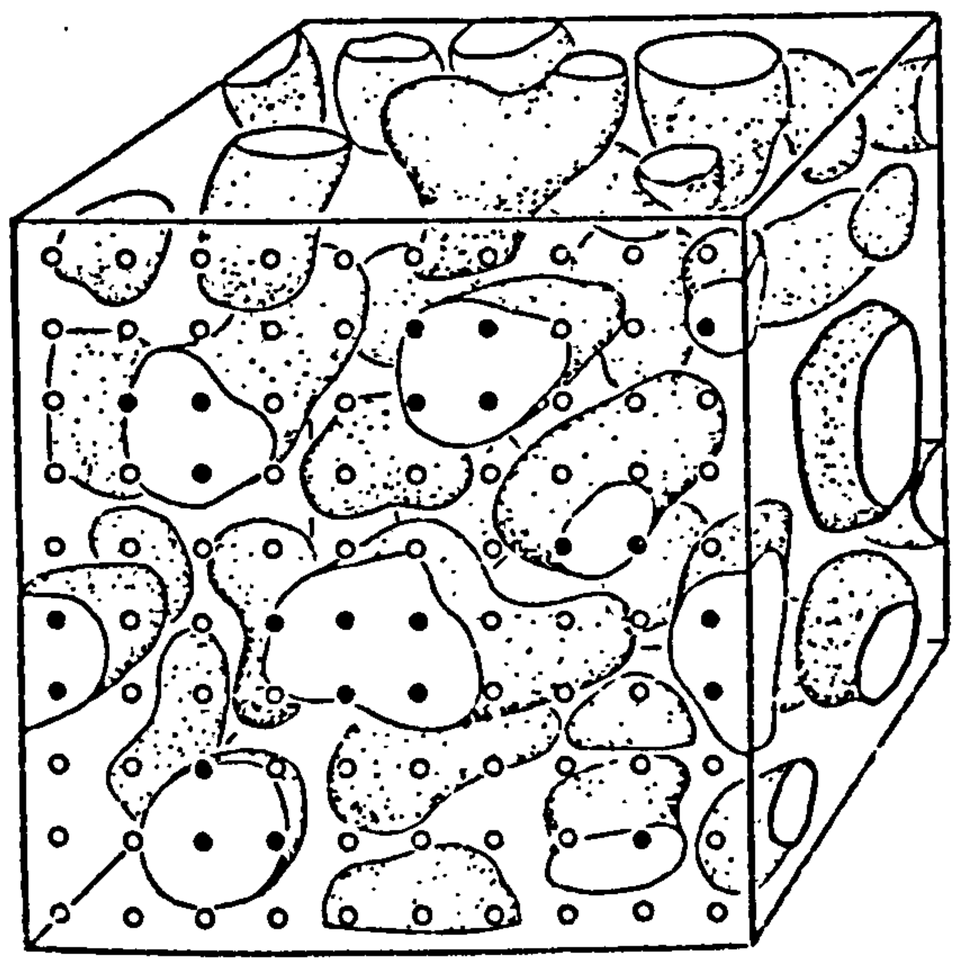


Figure 127. An EMPD 2 plot of thermally oxidised AGLMP graphite.

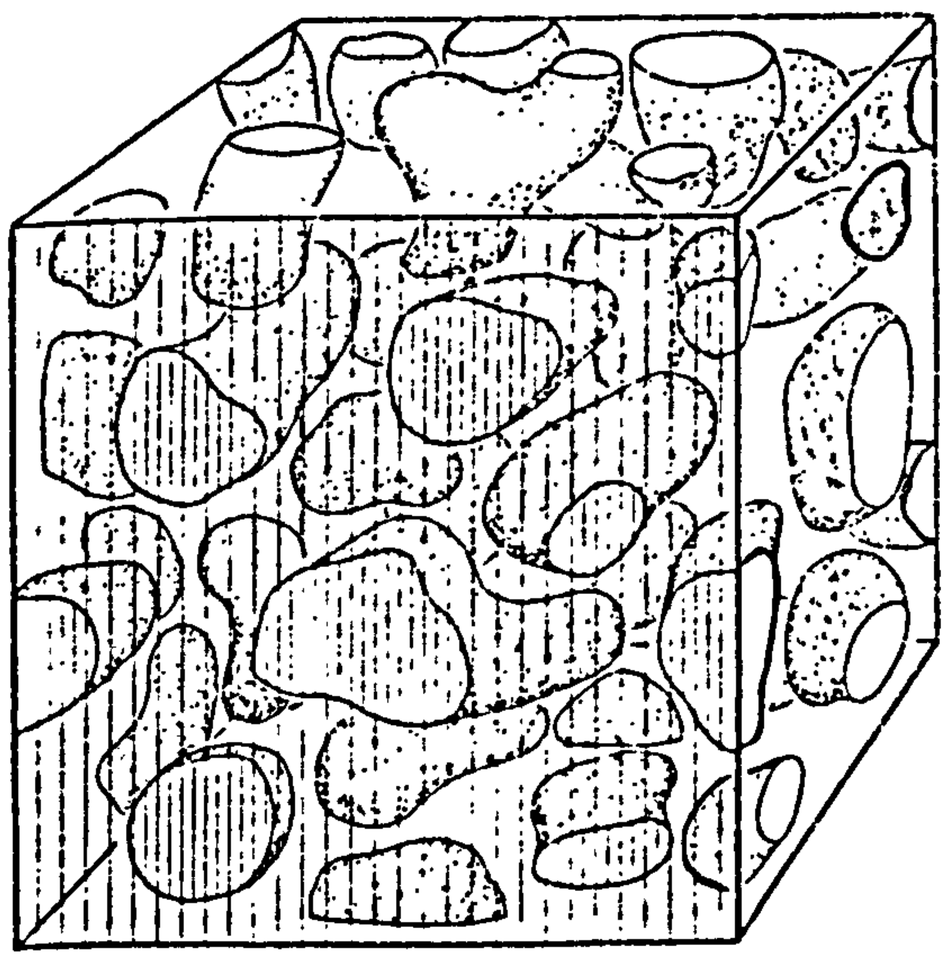


All height measurements are given in micrometres.

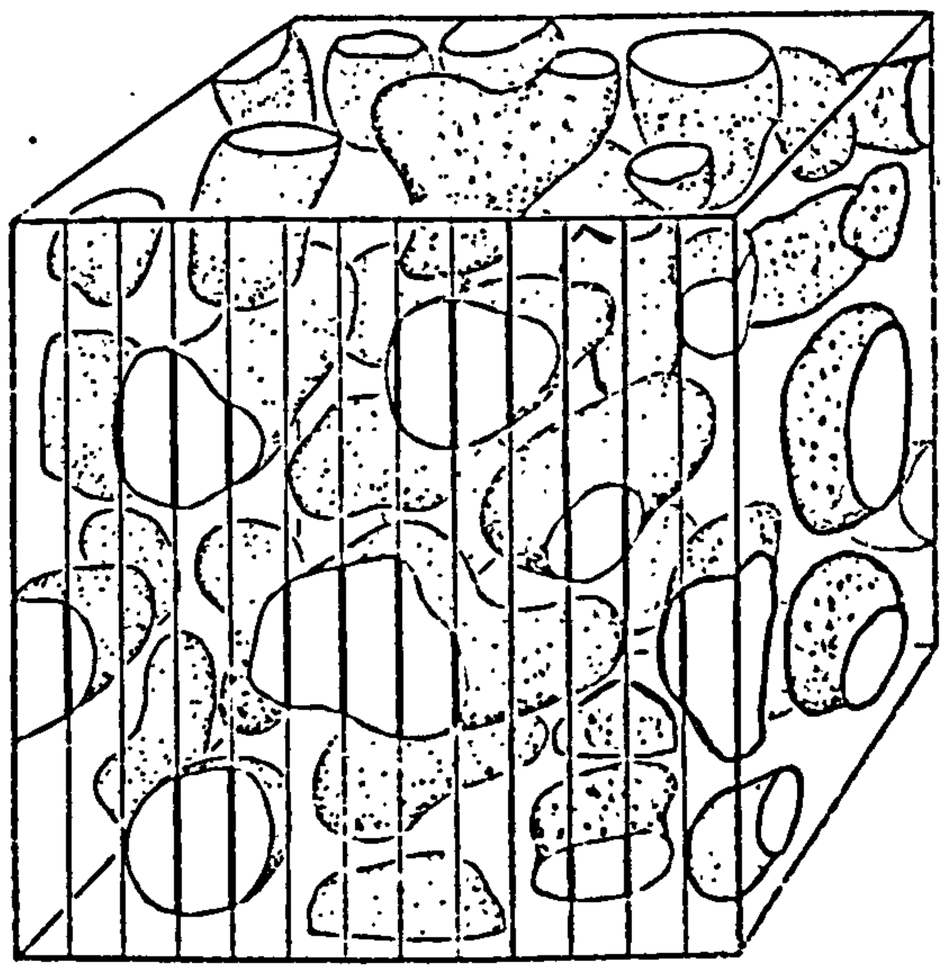
Figure 128. An EMPD 2 plot of composite wood, Douglas Fir.



(a) Analysis by point counting.

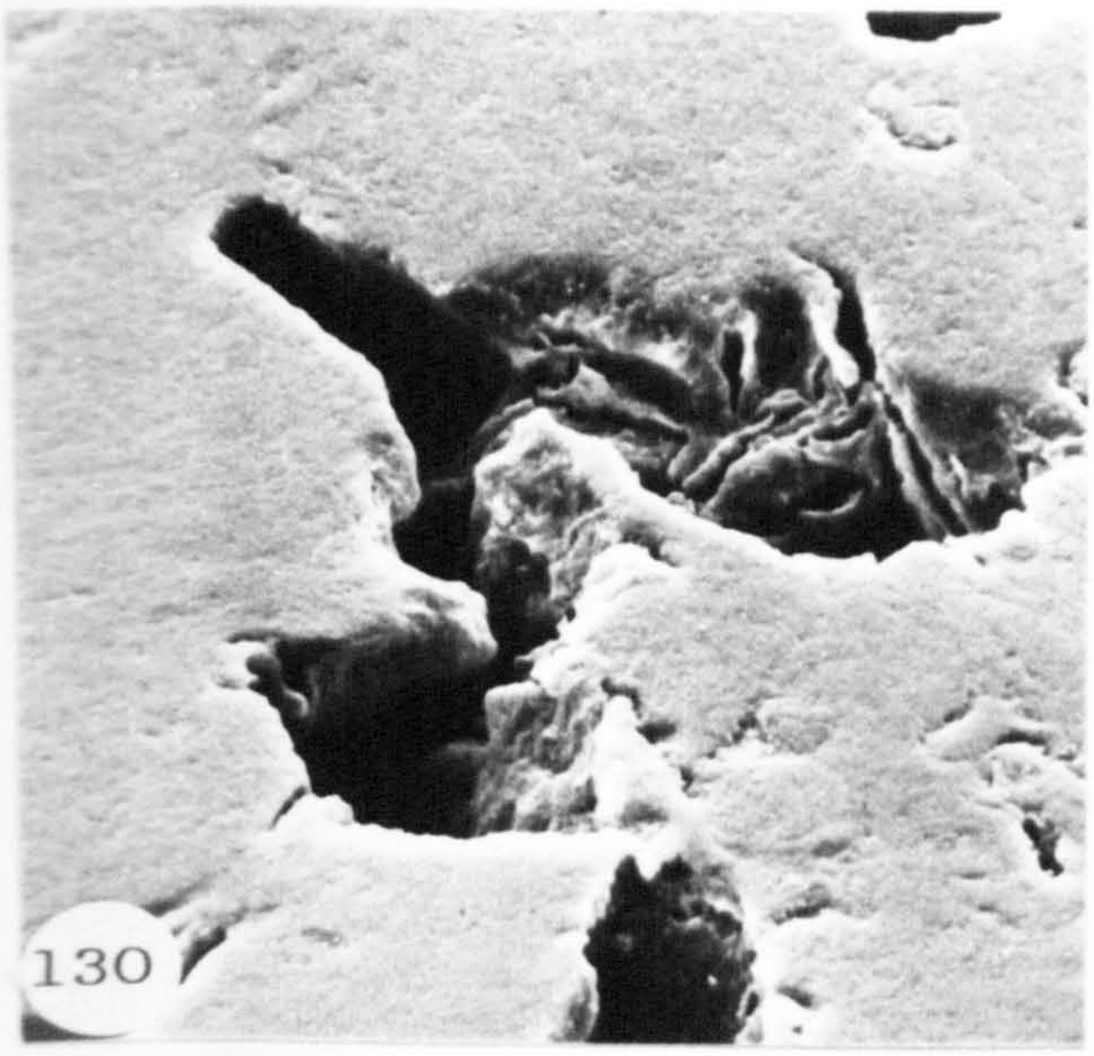


(b) Analysis by planimetry.



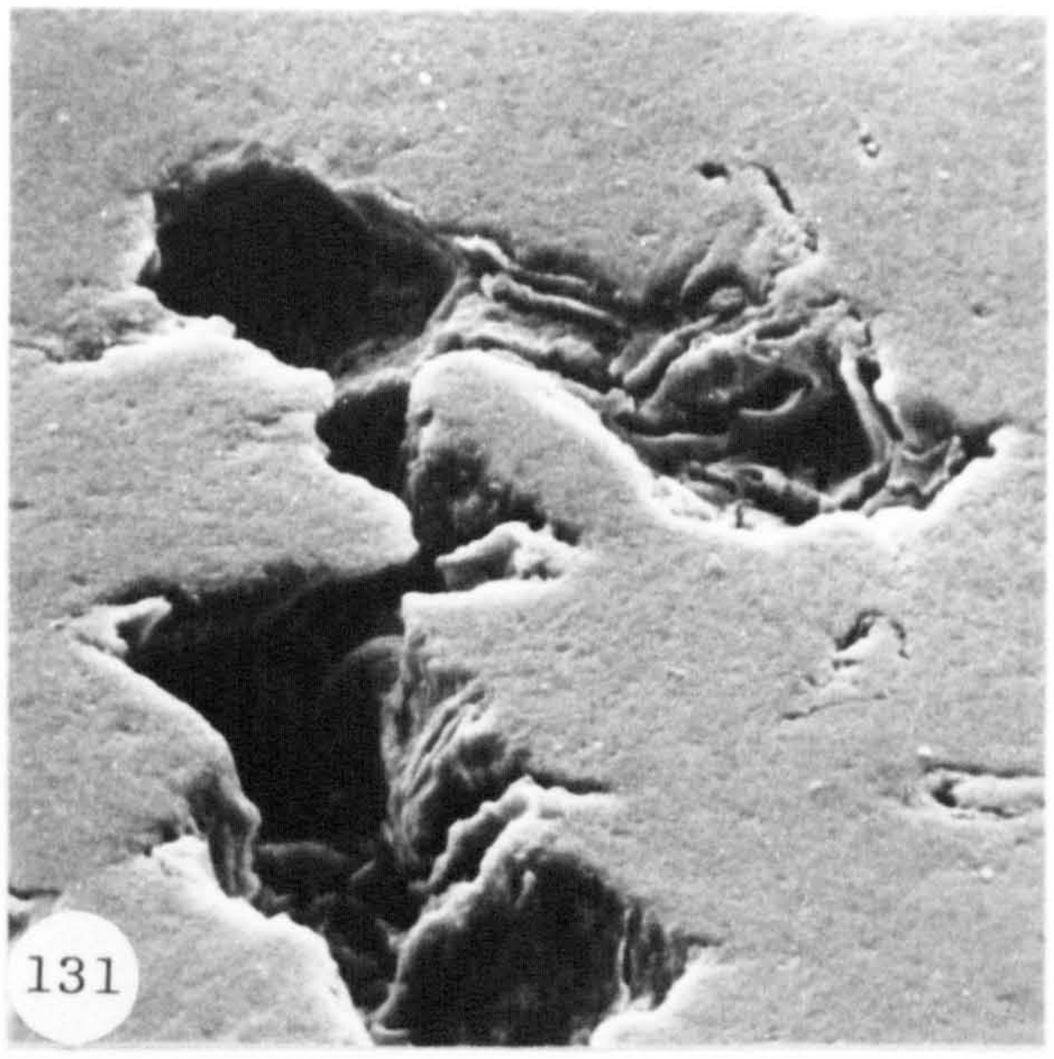
(c) Analysis by lineal integration.

Figure 129. Volumetric analysis by stereology.



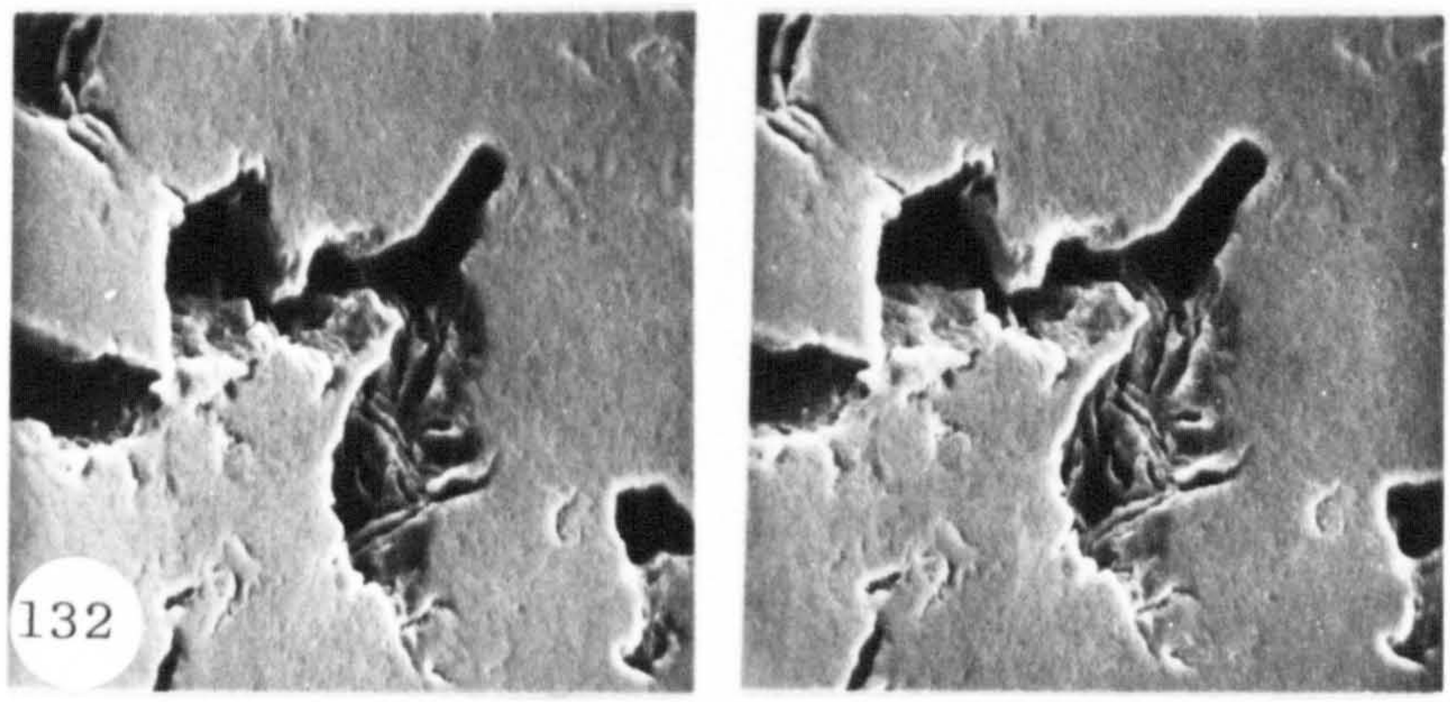
AGLMP GRAPHITE

20 µm



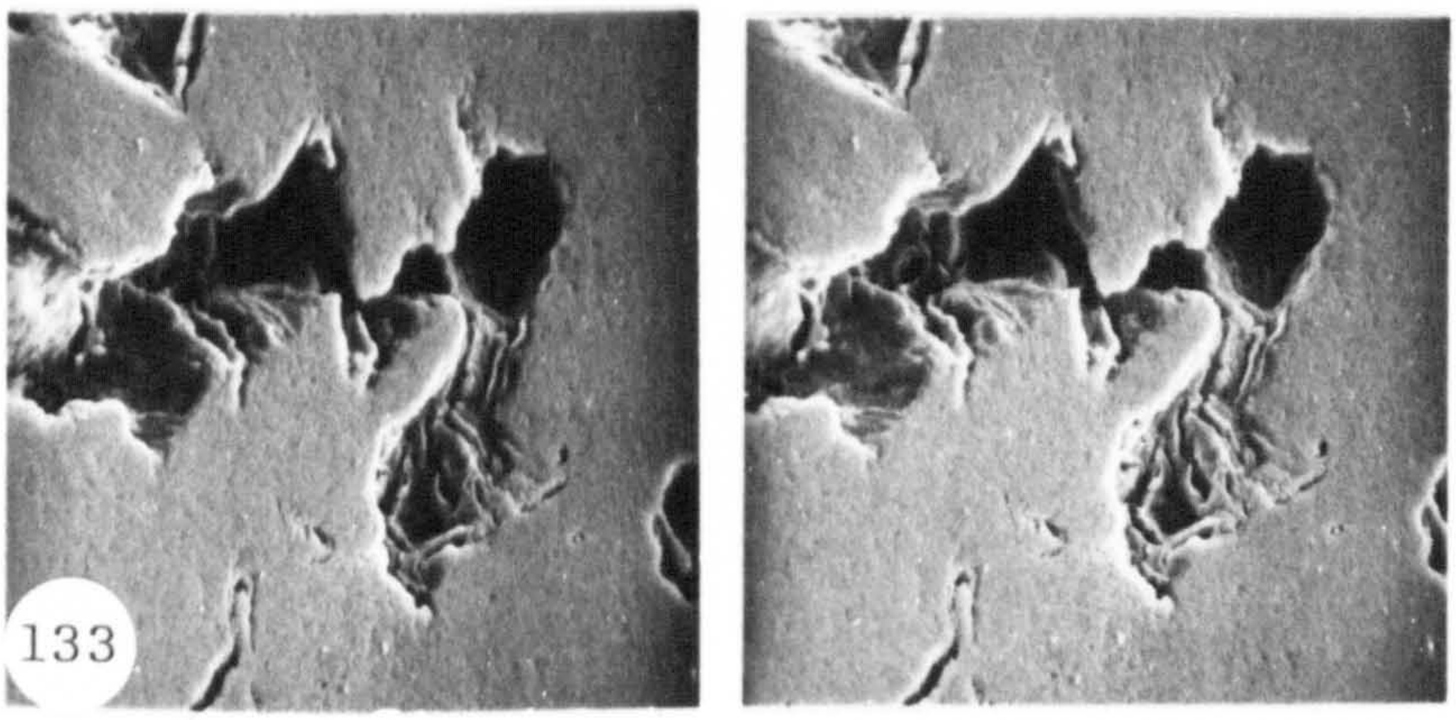
AGLMP GRAPHITE AFTER REMOVING THE SURFACE BY POLISHING

20 µm



STEREOPAIR OF AGLMP GRAPHITE

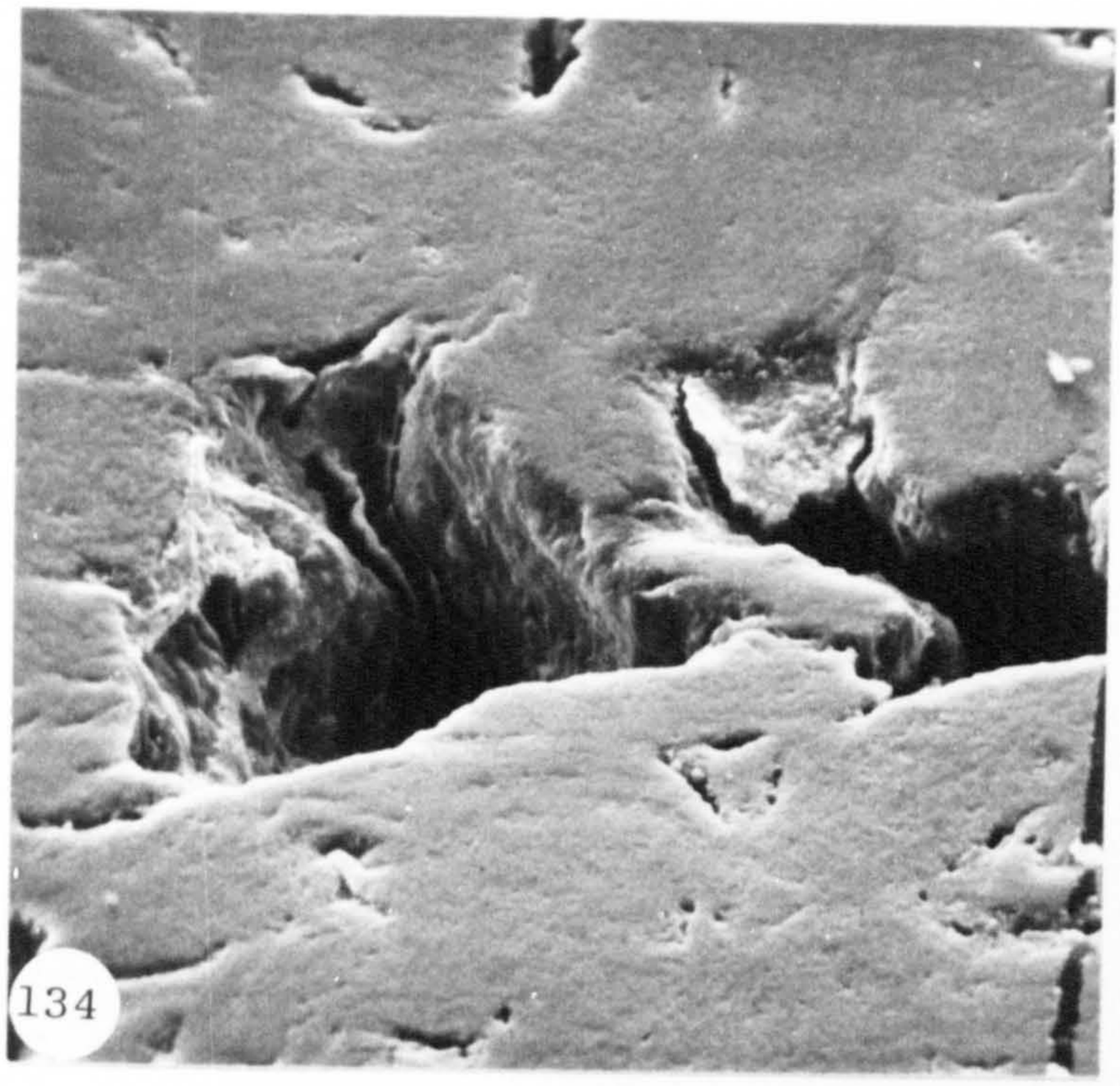
50 µm



STEREOPAIR OF AGLMP GRAPHITE AFTER REMOVING THE SURFACE BY POLISHING

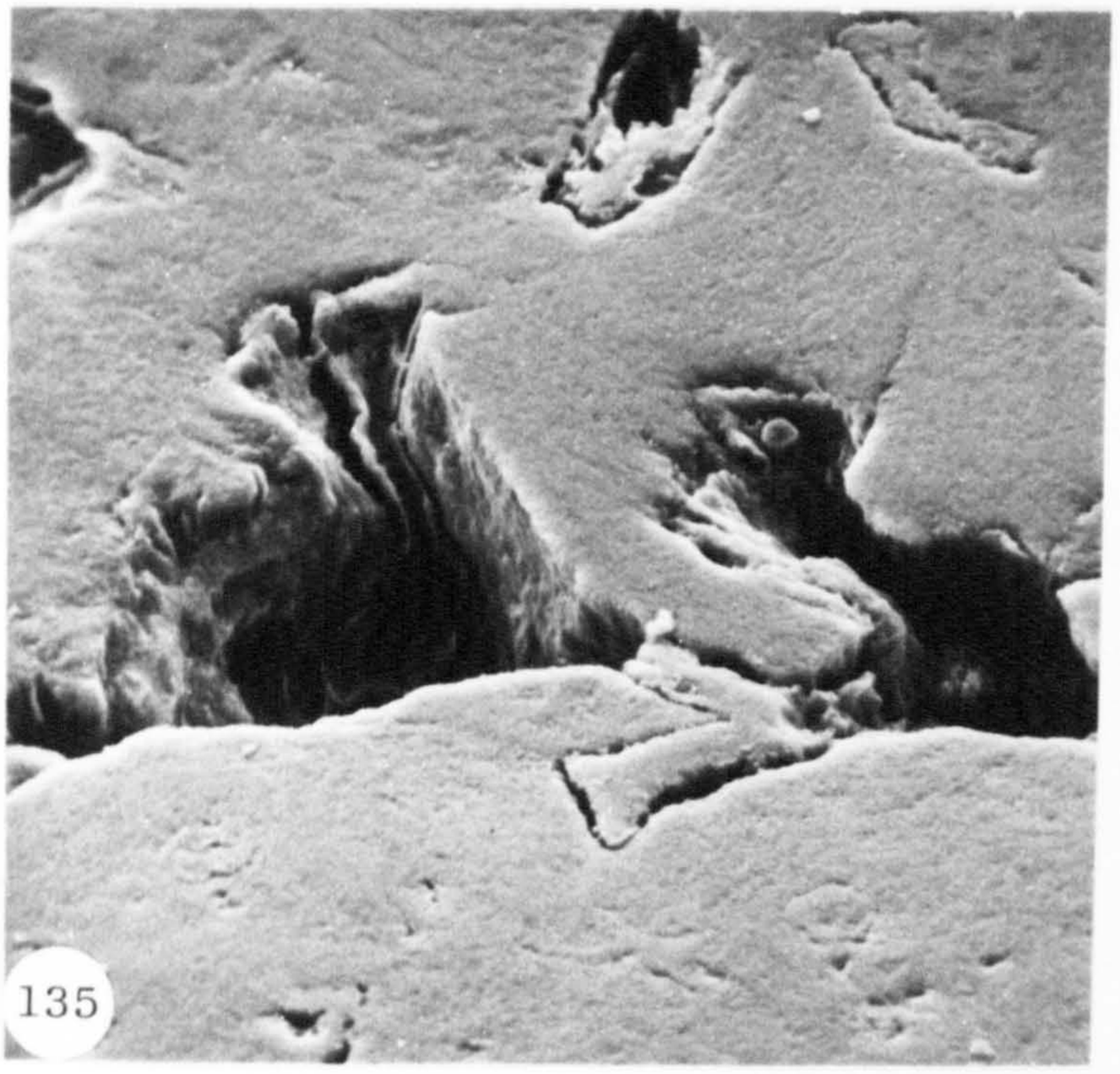
50 µm

Figures 130 to 133. Scanning electron micrographs (stereoscan) of AGLMP graphite before and after polishing the surface to observe the pores through the graphite.



AGLMP GRAPHITE

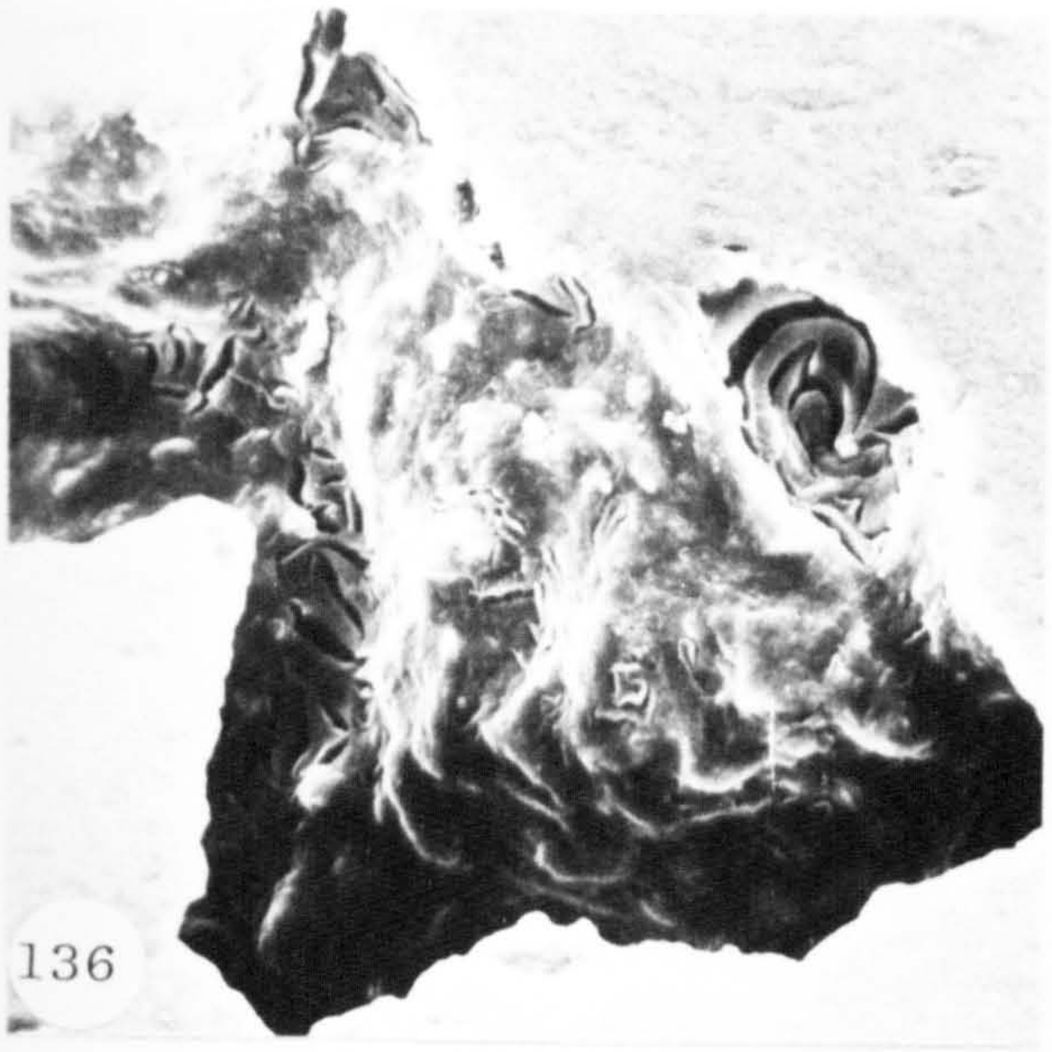
20 µm



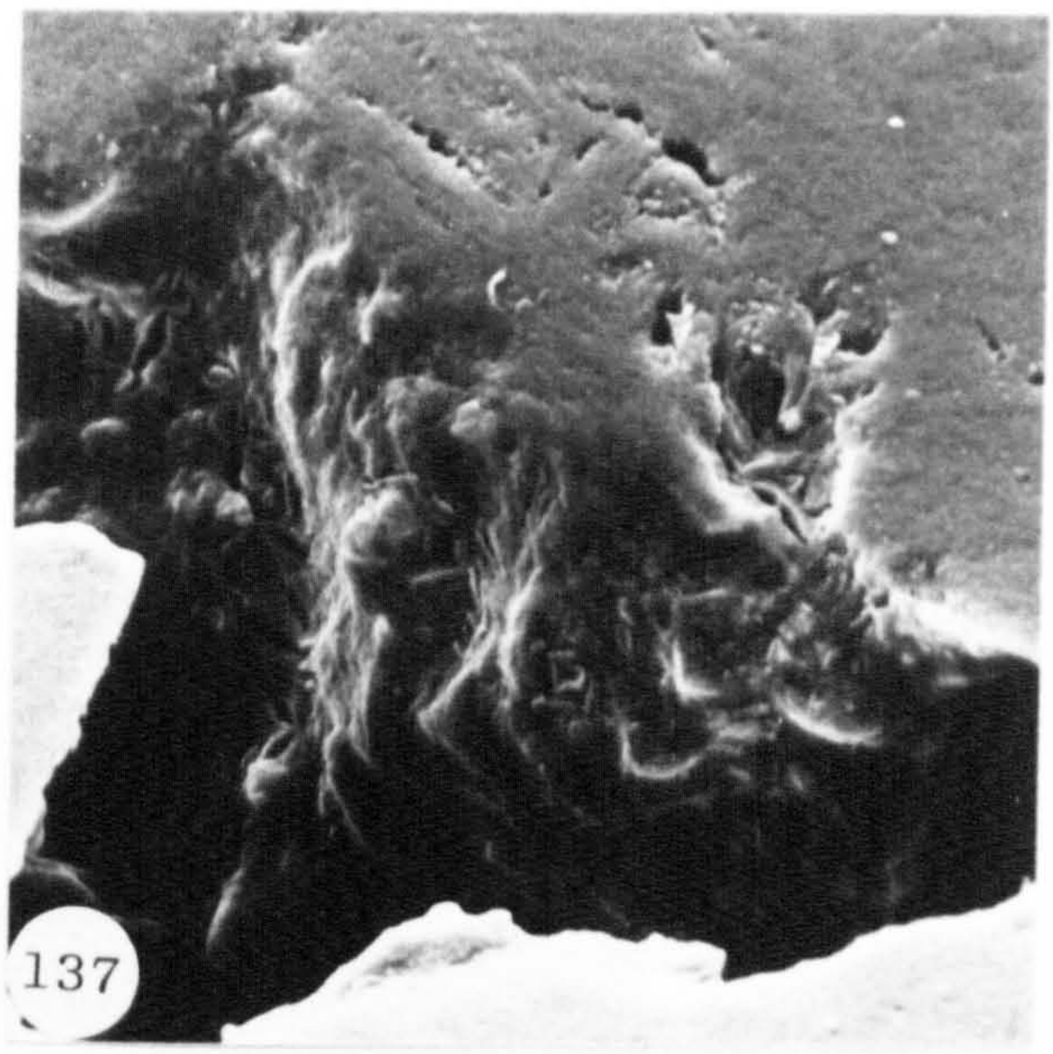
AGLMP GRAPHITE AFTER REMOVING THE SURFACE BY POLISHING

20 µm

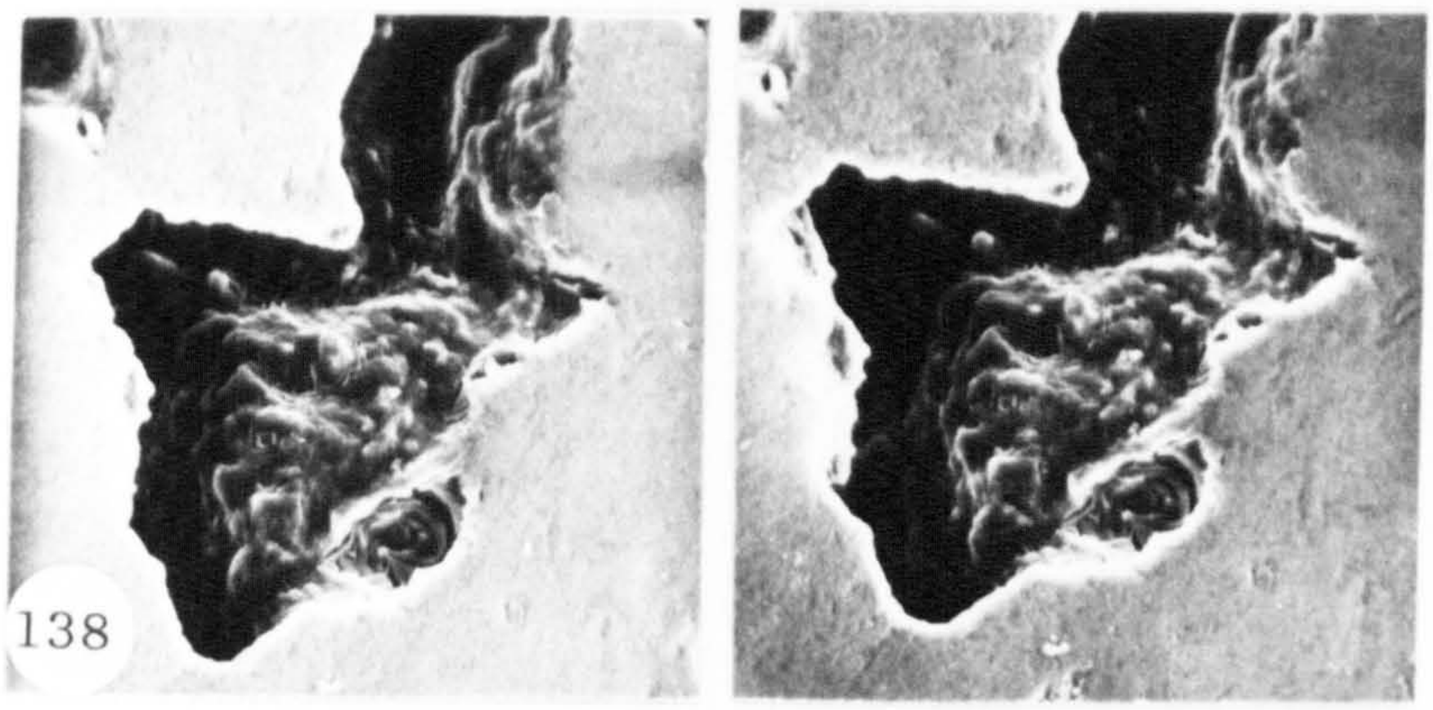
Figures 134 and 135. Scanning electron micrographs (stereoscan) of AGLMP graphite before and after polishing the surface to observe the pores through the graphite.



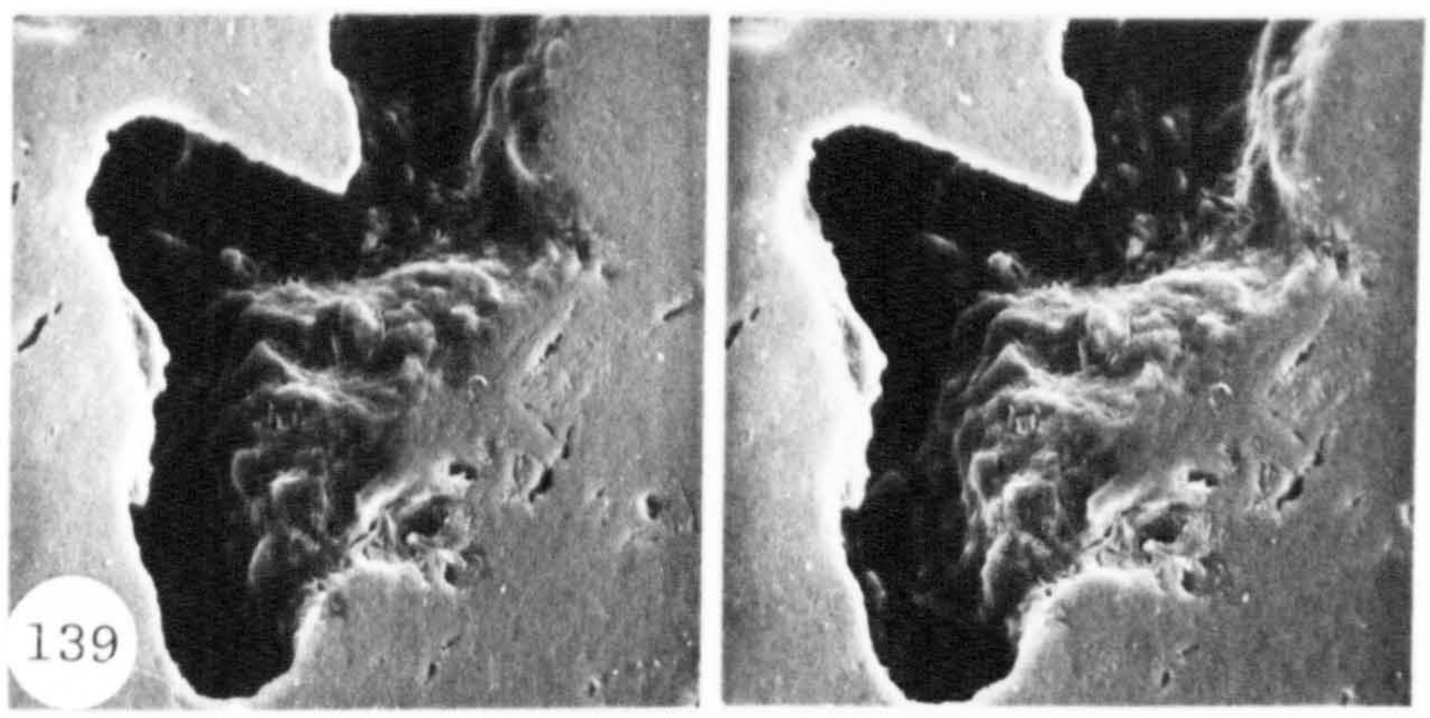
GCMB GRAPHITE 20 μm



GCMB GRAPHITE AFTER REMOVING THE SURFACE BY POLISHING 20 μm

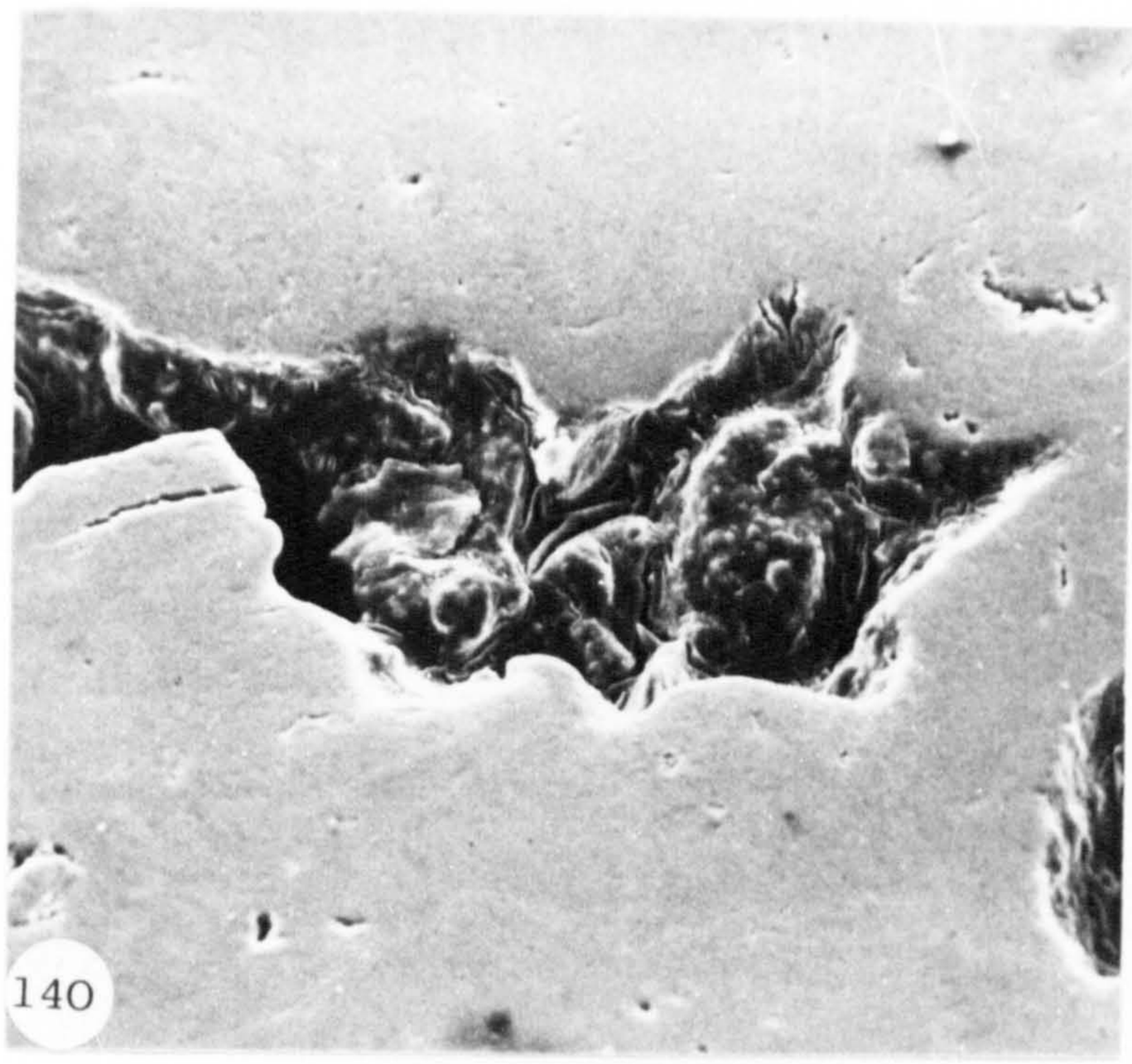


STEREOPAIR OF GCMB GRAPHITE 50 μm



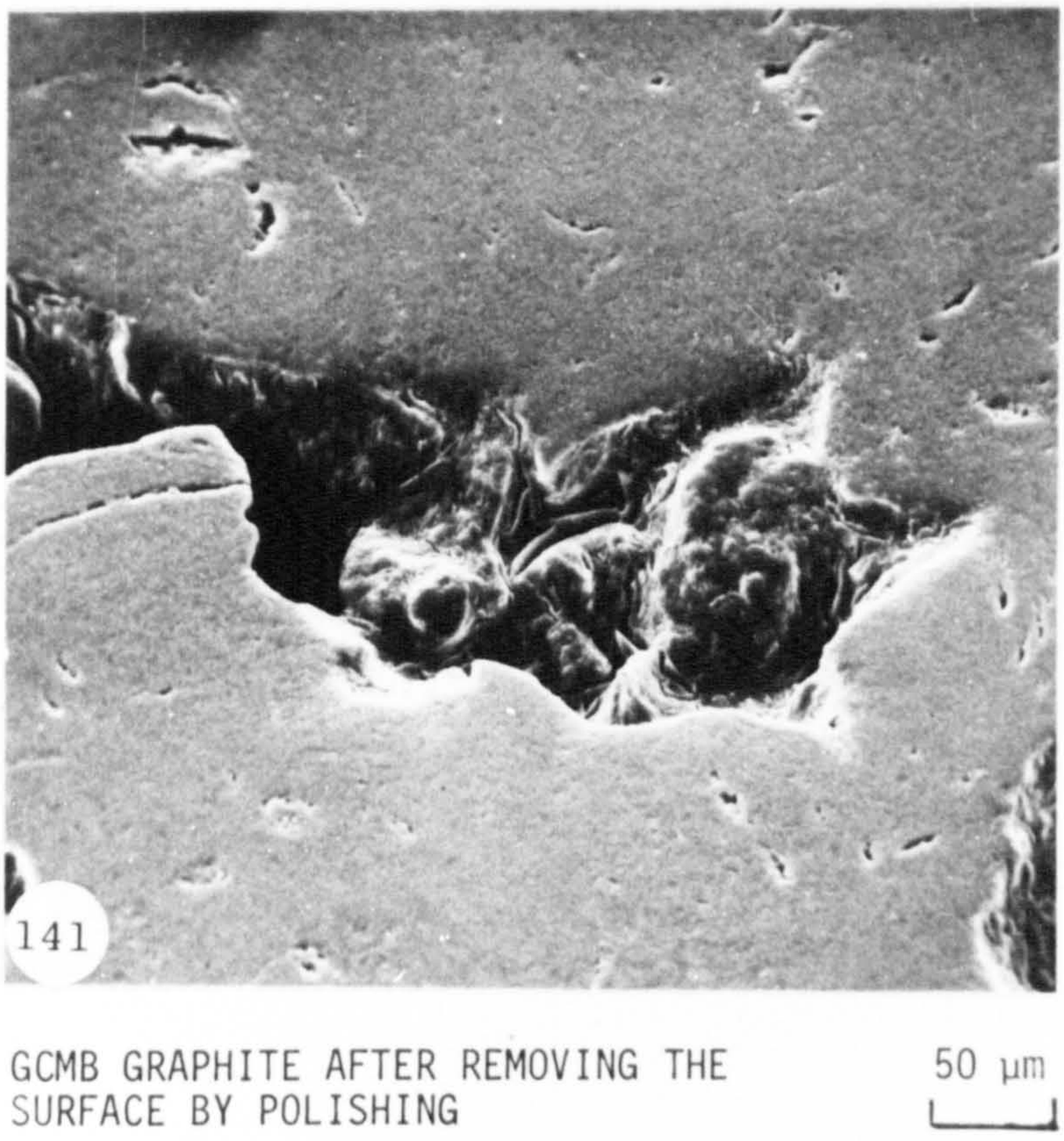
STEREOPAIR OF GCMB GRAPHITE AFTER REMOVING THE SURFACE BY POLISHING 50 μm

Figures 136 to 139. Scanning electron micrographs (stereoscan) of GCMB graphite before and after polishing the surface to observe the pores through the graphite.



GCMB GRAPHITE

50 µm



GCMB GRAPHITE AFTER REMOVING THE SURFACE BY POLISHING

50 µm

Figures 140 and 141. Scanning electron micrographs (stereoscan) of GCMB graphite before and after polishing the surface to observe the pores through the graphite.

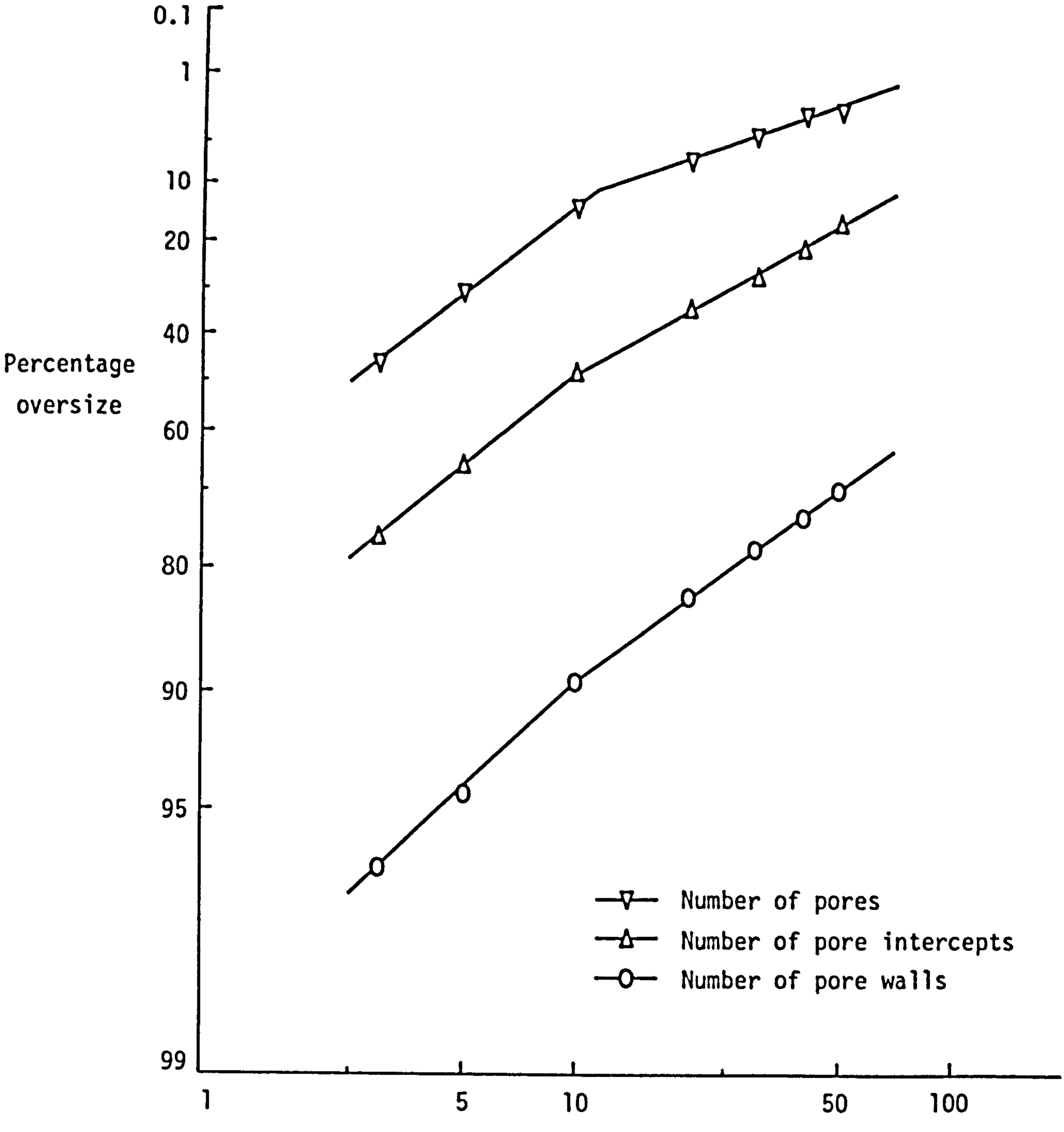


Figure 142. Pore distribution obtained from the Quantimet of AGLMP graphite.

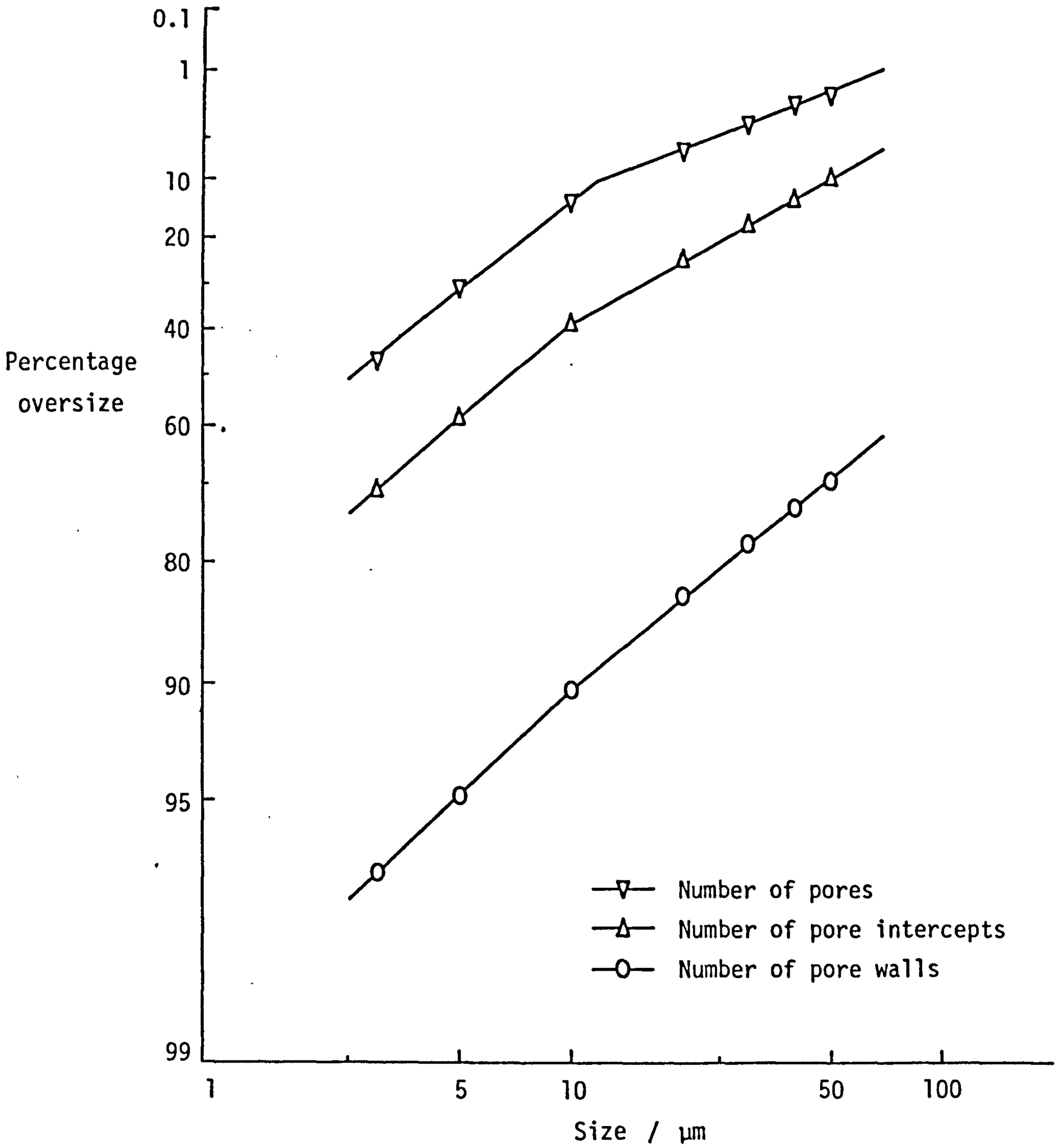


Figure 143. Pore distribution obtained from the Quantimet of BAEL GCMB graphite.

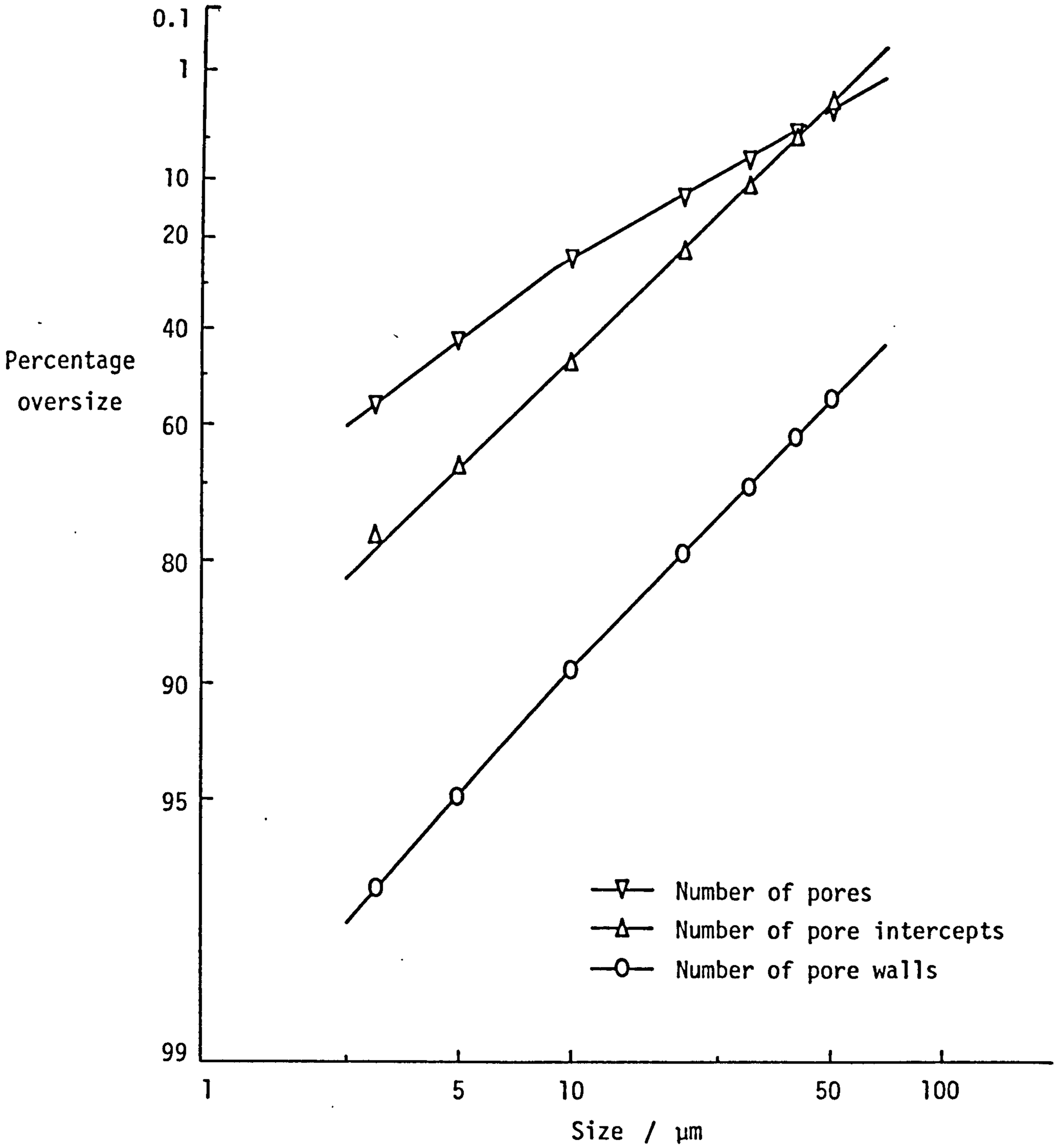


Figure 144. Pore distribution obtained from the Quantimet of AGLHP (unipore) graphite.

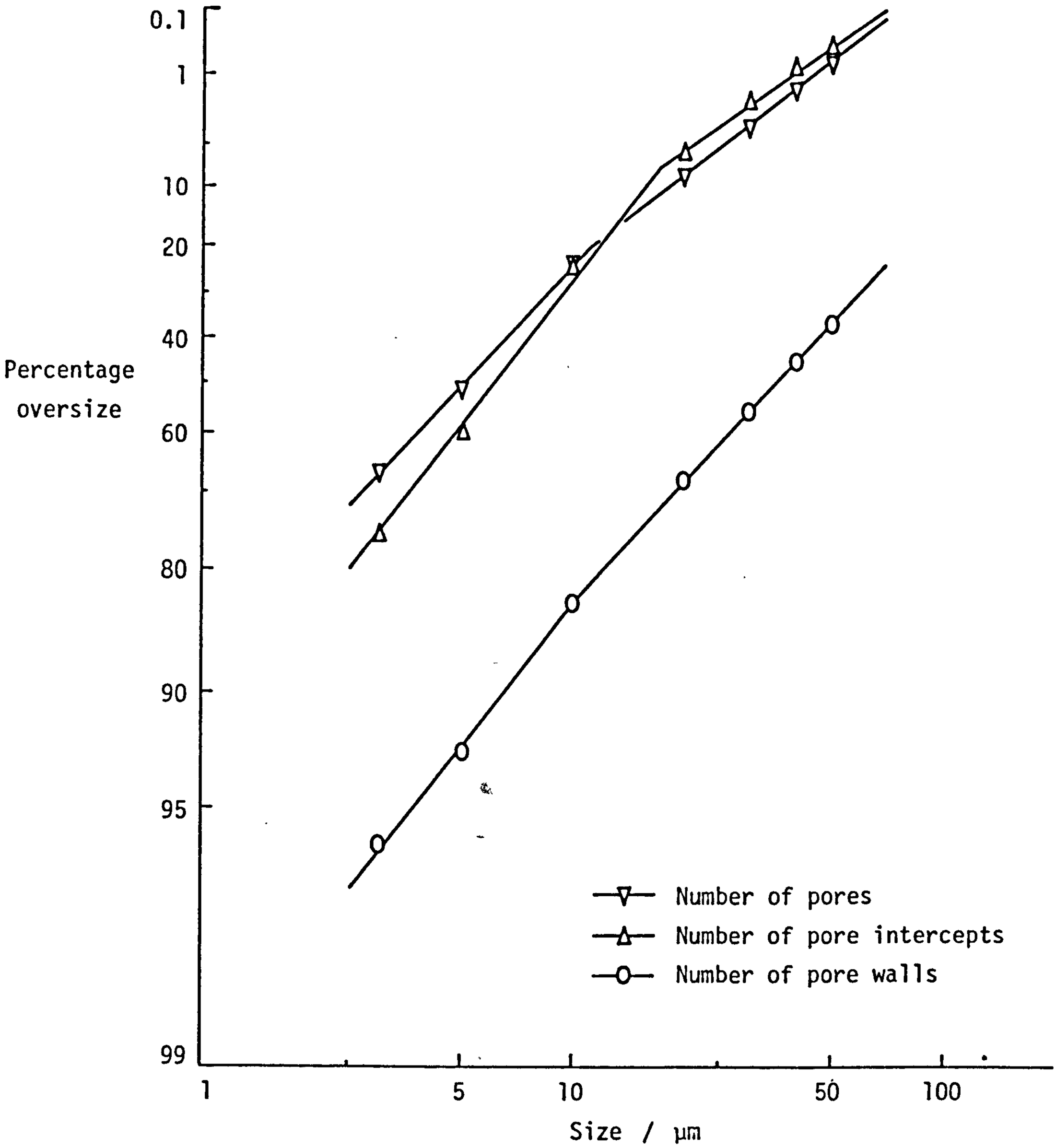


Figure 145. Pore distribution obtained from the Quantimet of Morgans EYC 9106 (unipore) graphite.

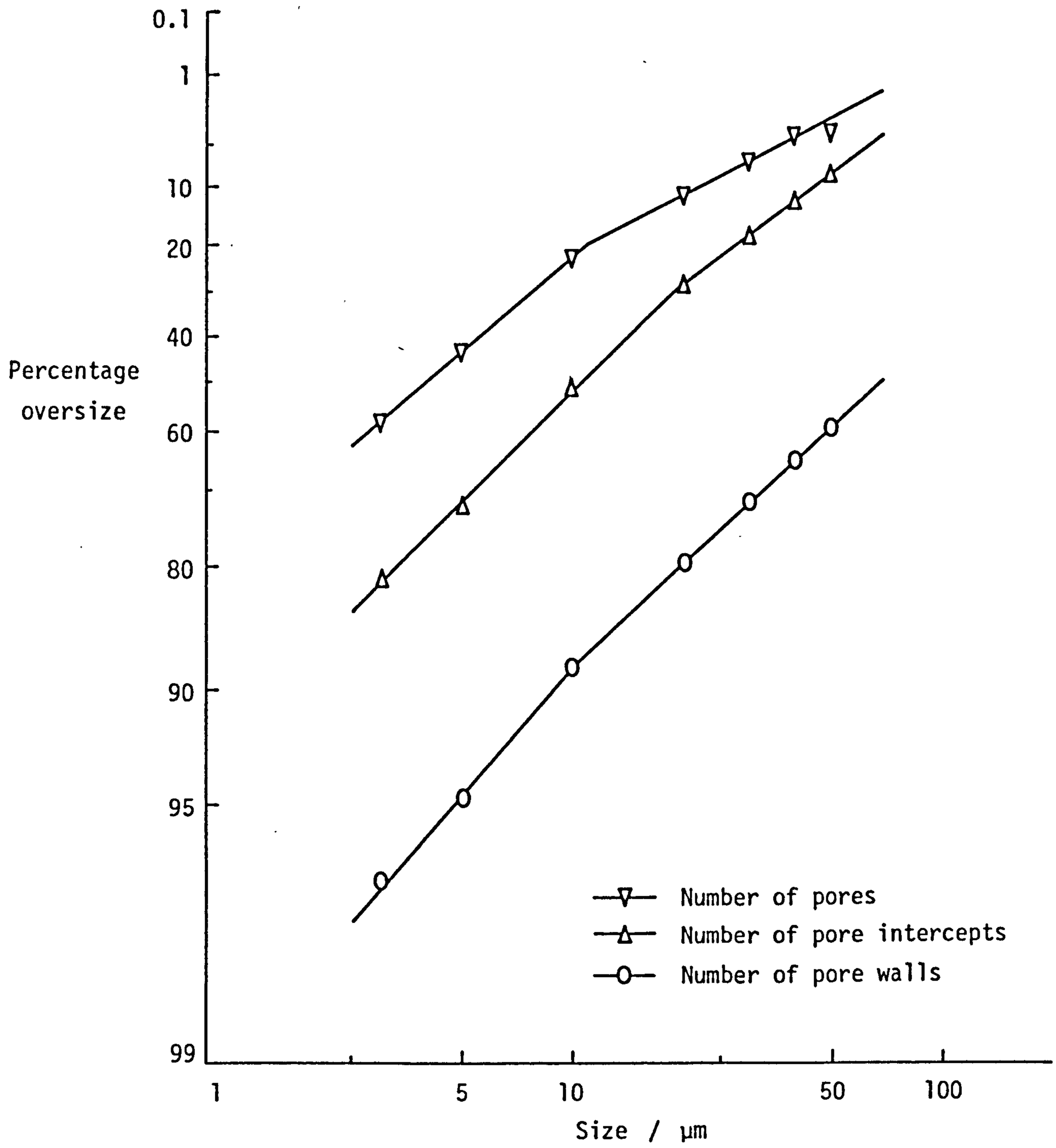


Figure 146. Pore distribution obtained from the Quantimet of Lima graphite.

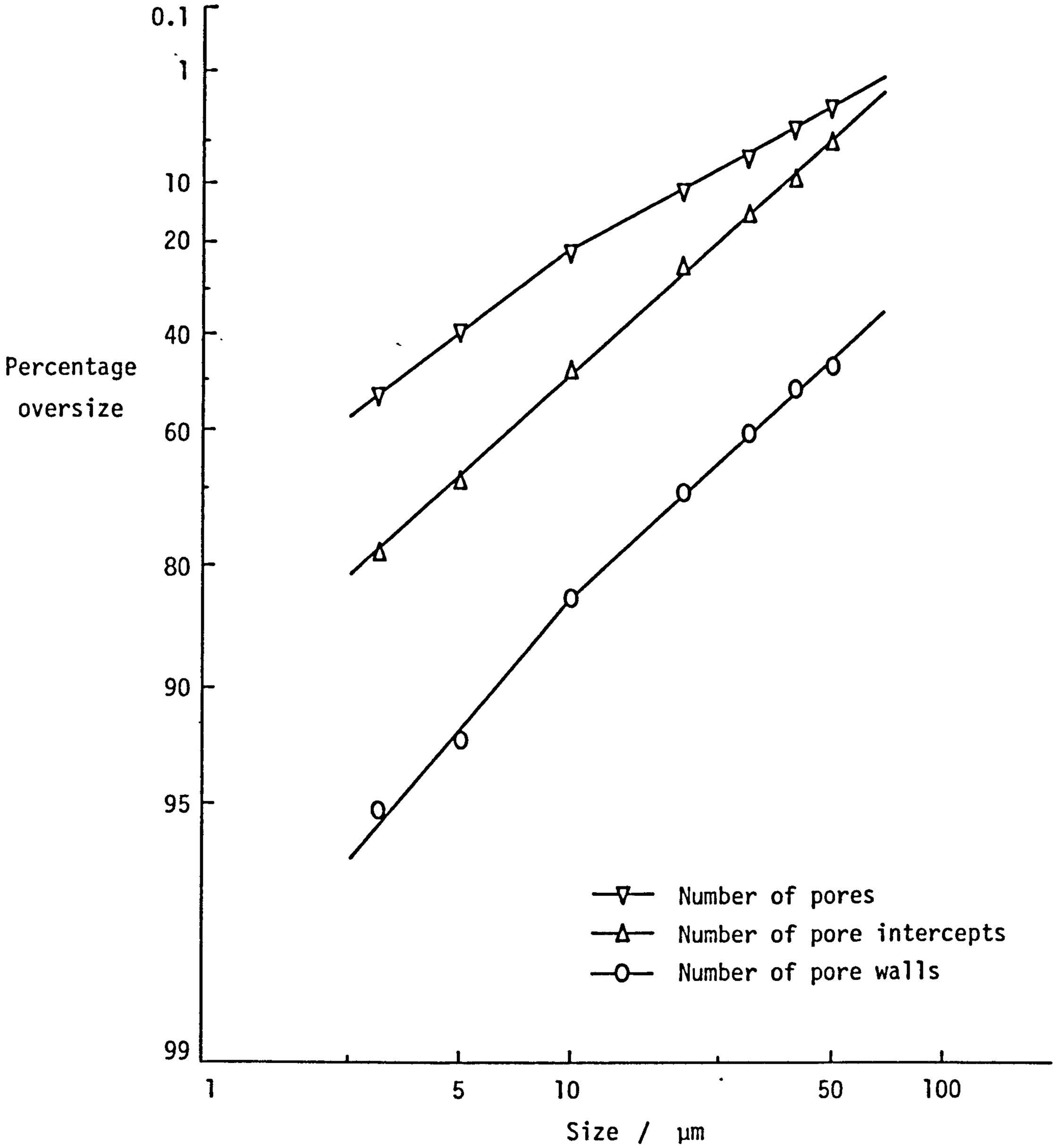


Figure 147. Pore distribution obtained from the Quantimet of PGA L18 graphite.

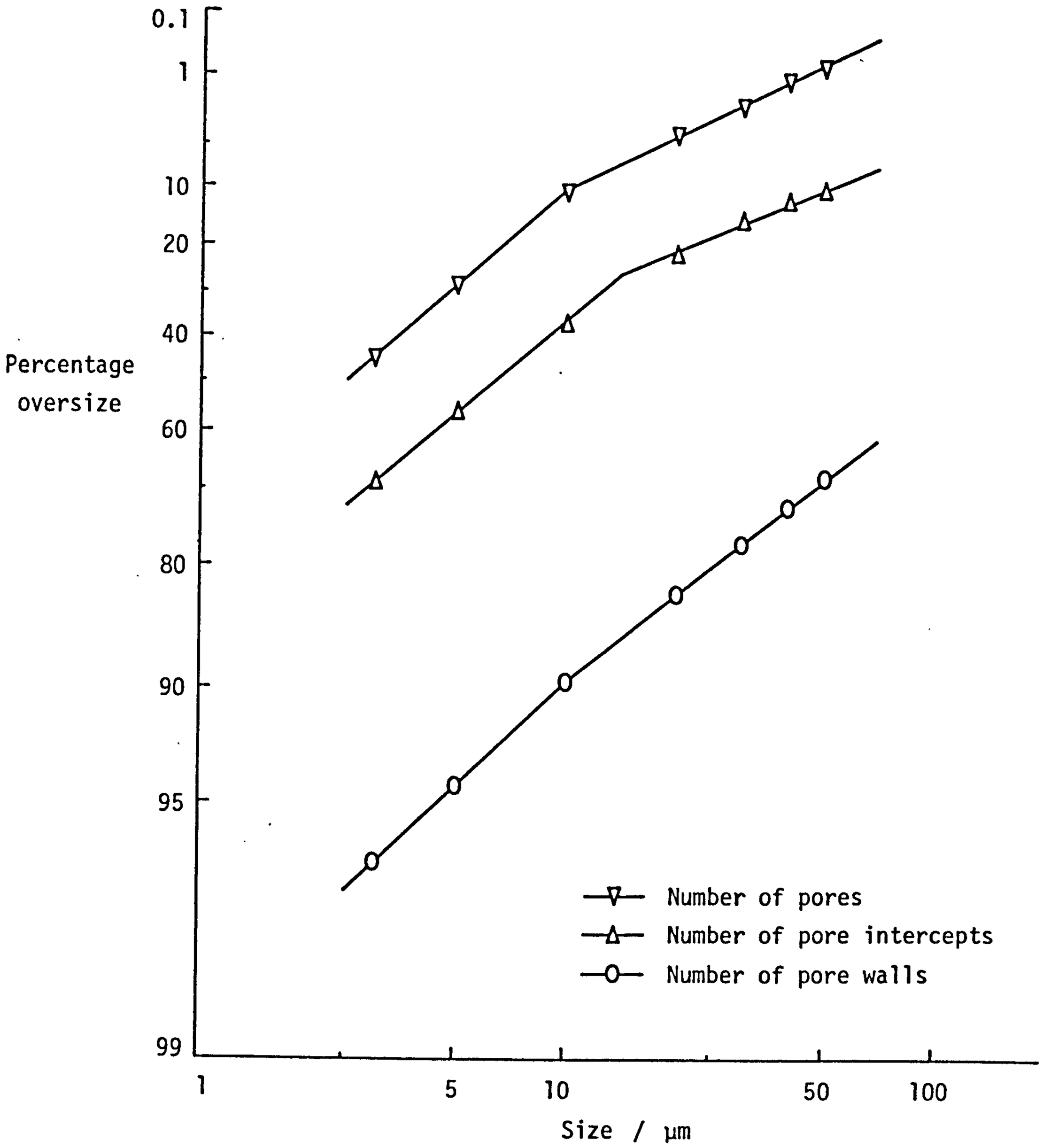


Figure 148. Pore distribution obtained from the Quantimet of BAEL VQMB graphite.

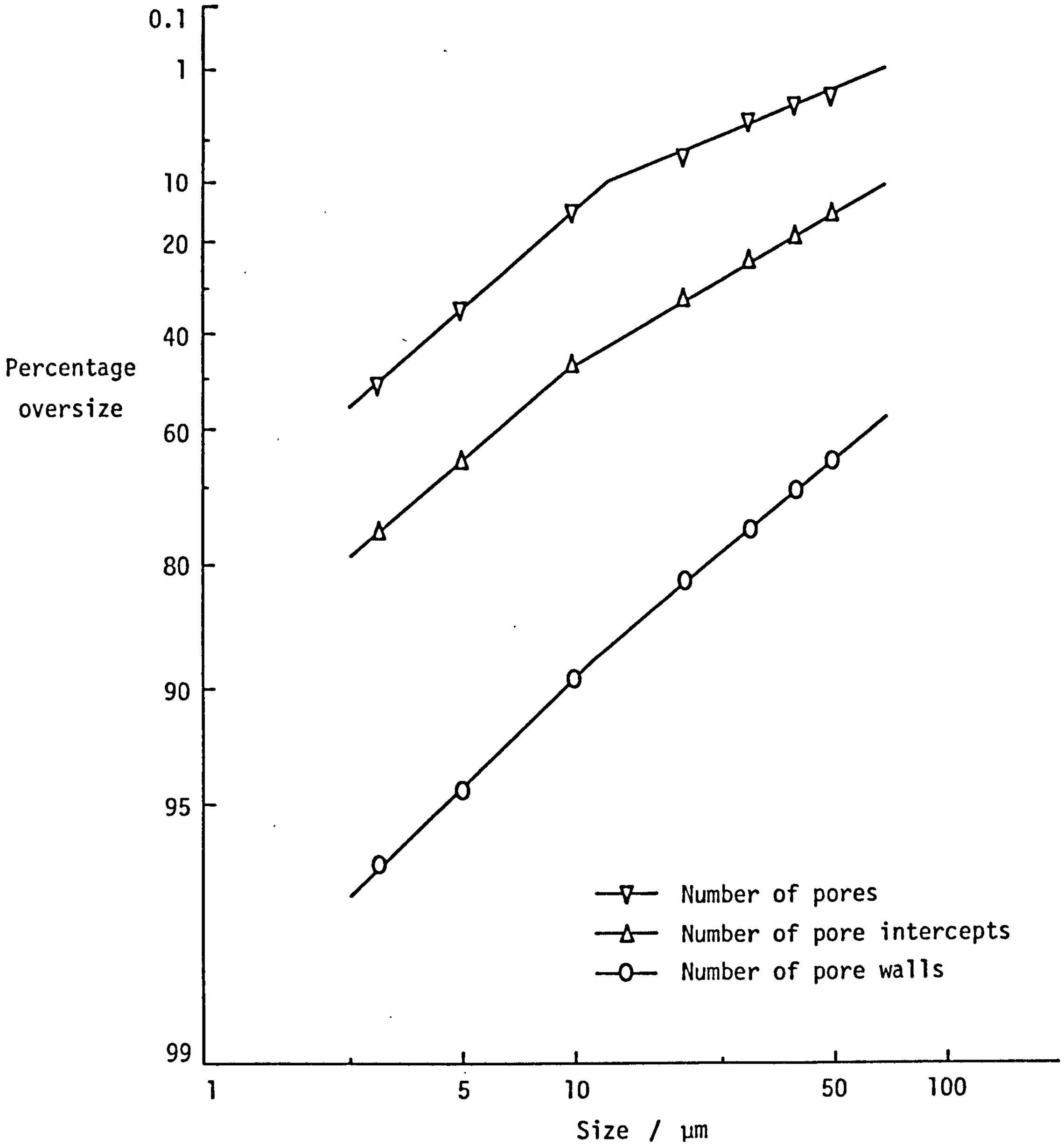
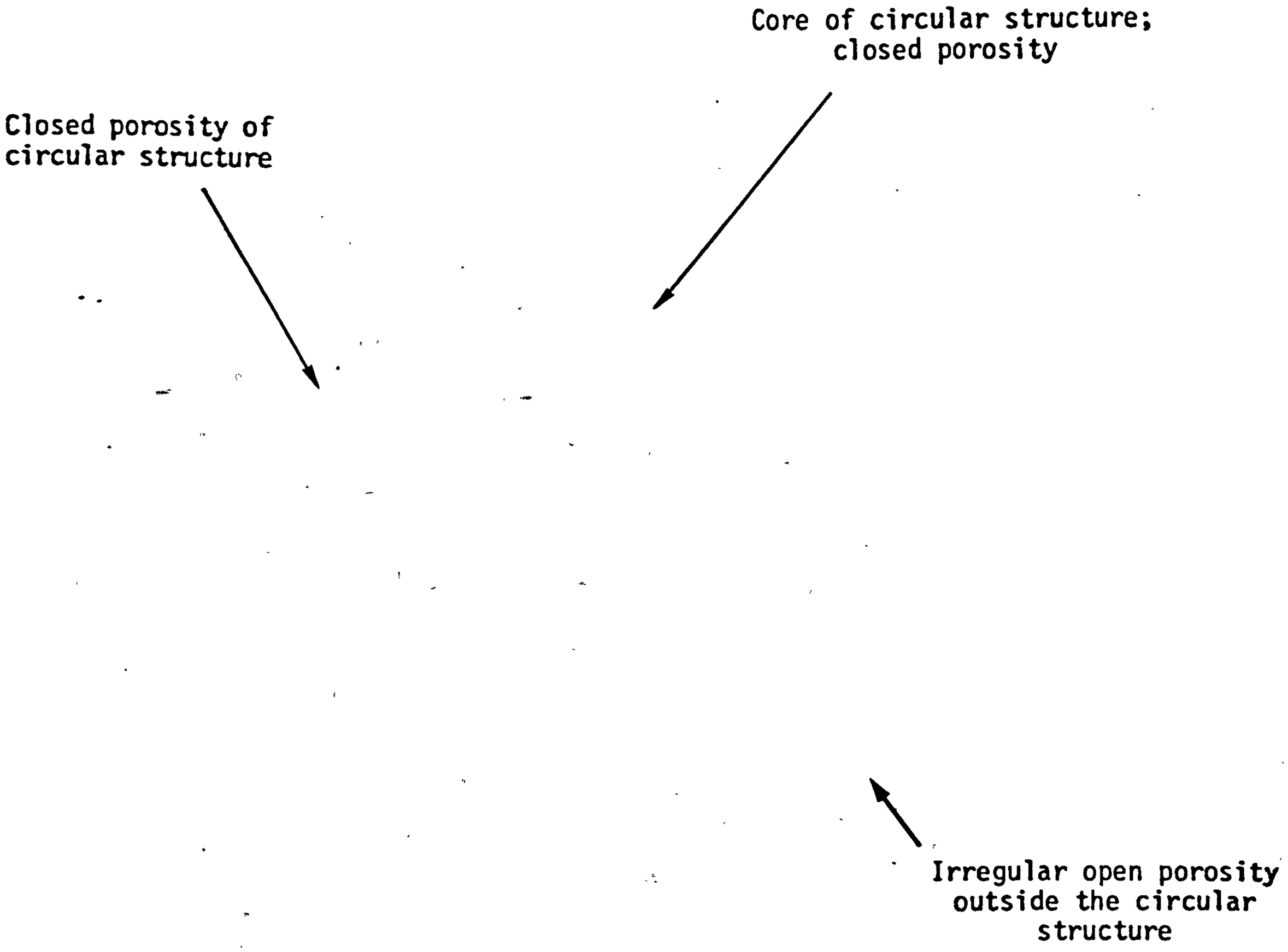


Figure 149. Pore distribution obtained from the Quantimet of BAEL VNMC graphite.


Core of circular structure; closed porosity
Closed porosity of circular structure
Irregular open porosity outside the circular structure

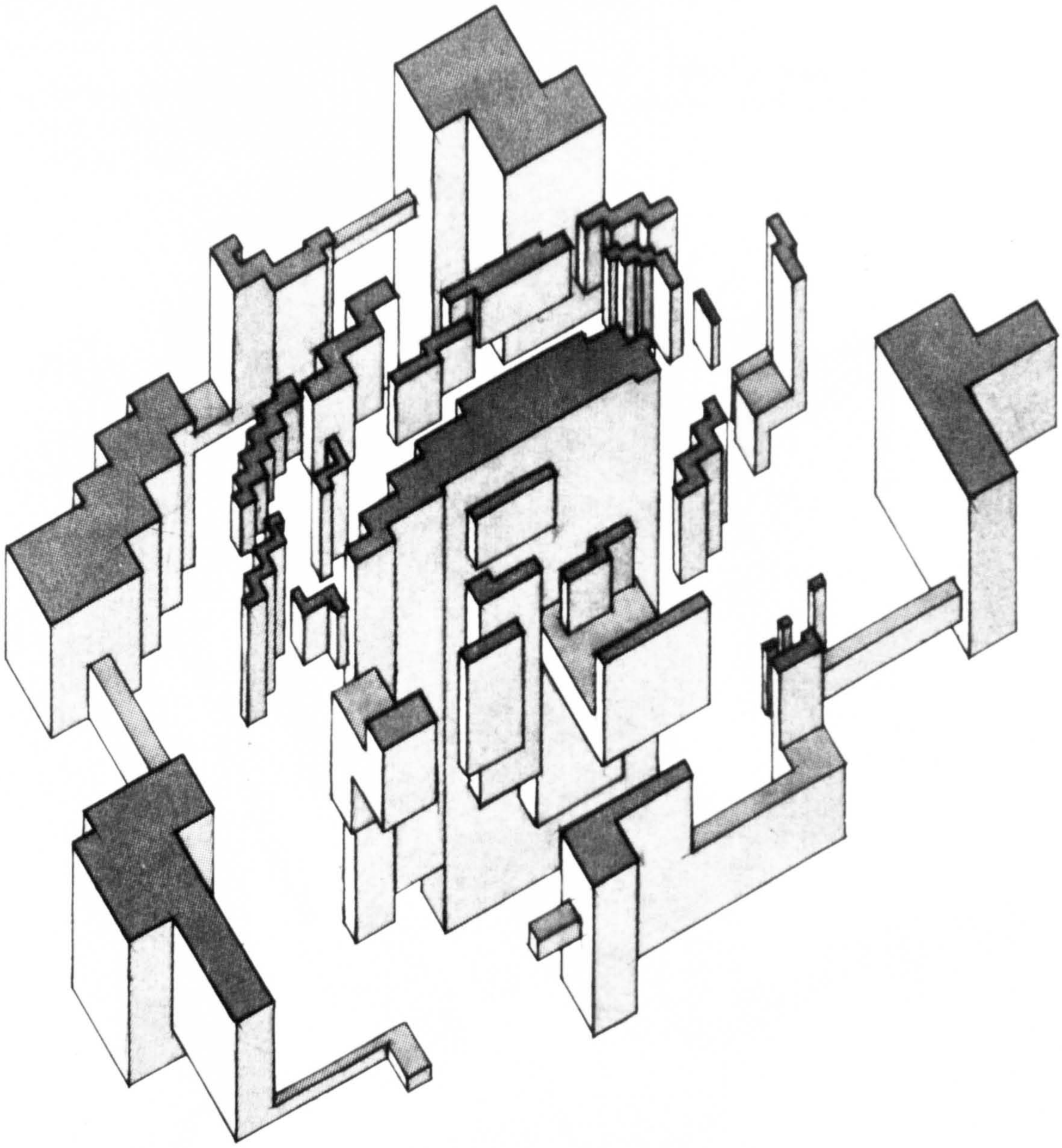


Figure 150. Diagrammatic Model of a Gilso-carbon Graphite.

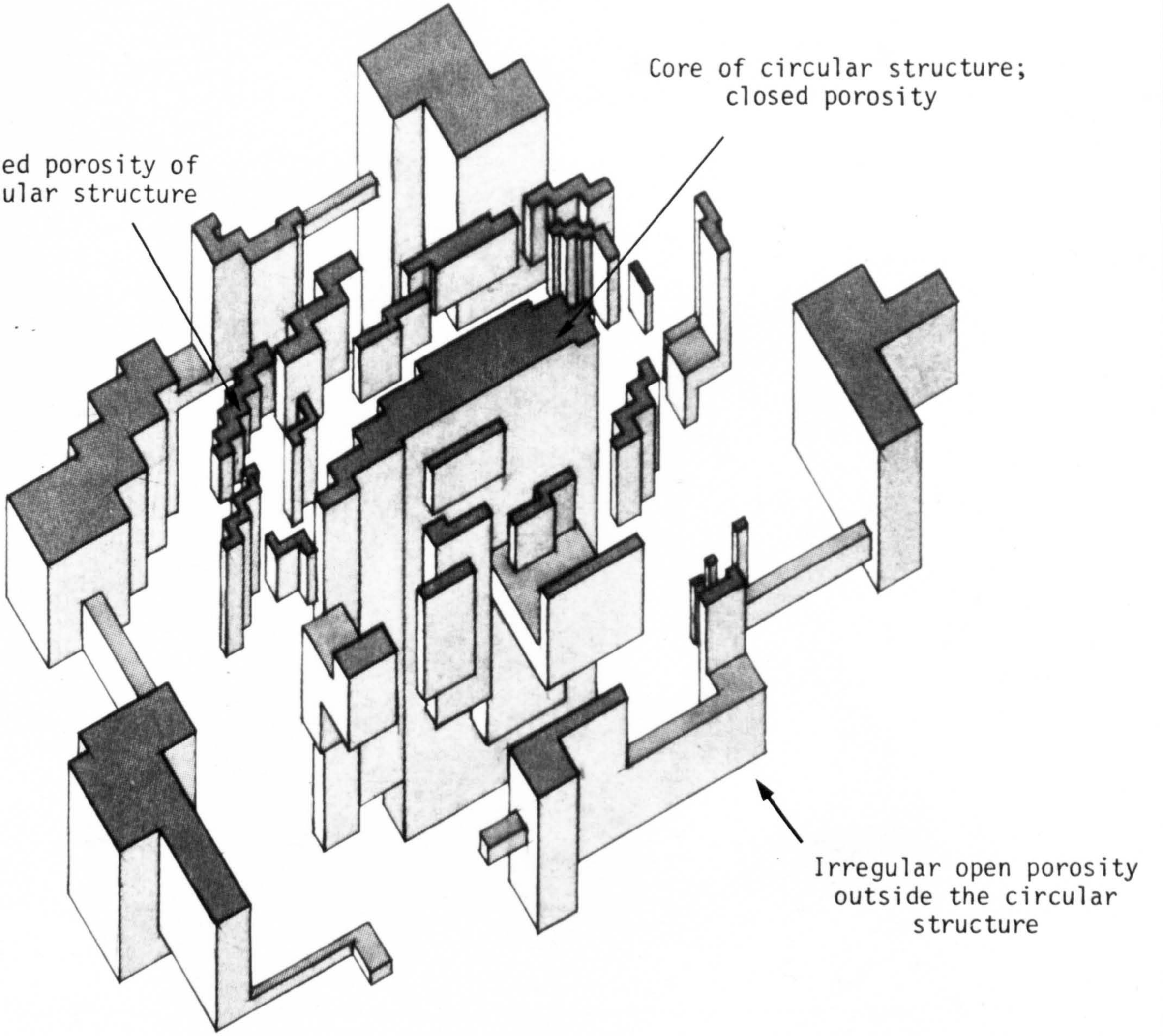


Figure 150. Diagrammatic Model of a Gilso-carbon Graphite.

Open and closed porosity associated with flow-type anisotropy

Mostly open irregular porosity associated with volatile evolution

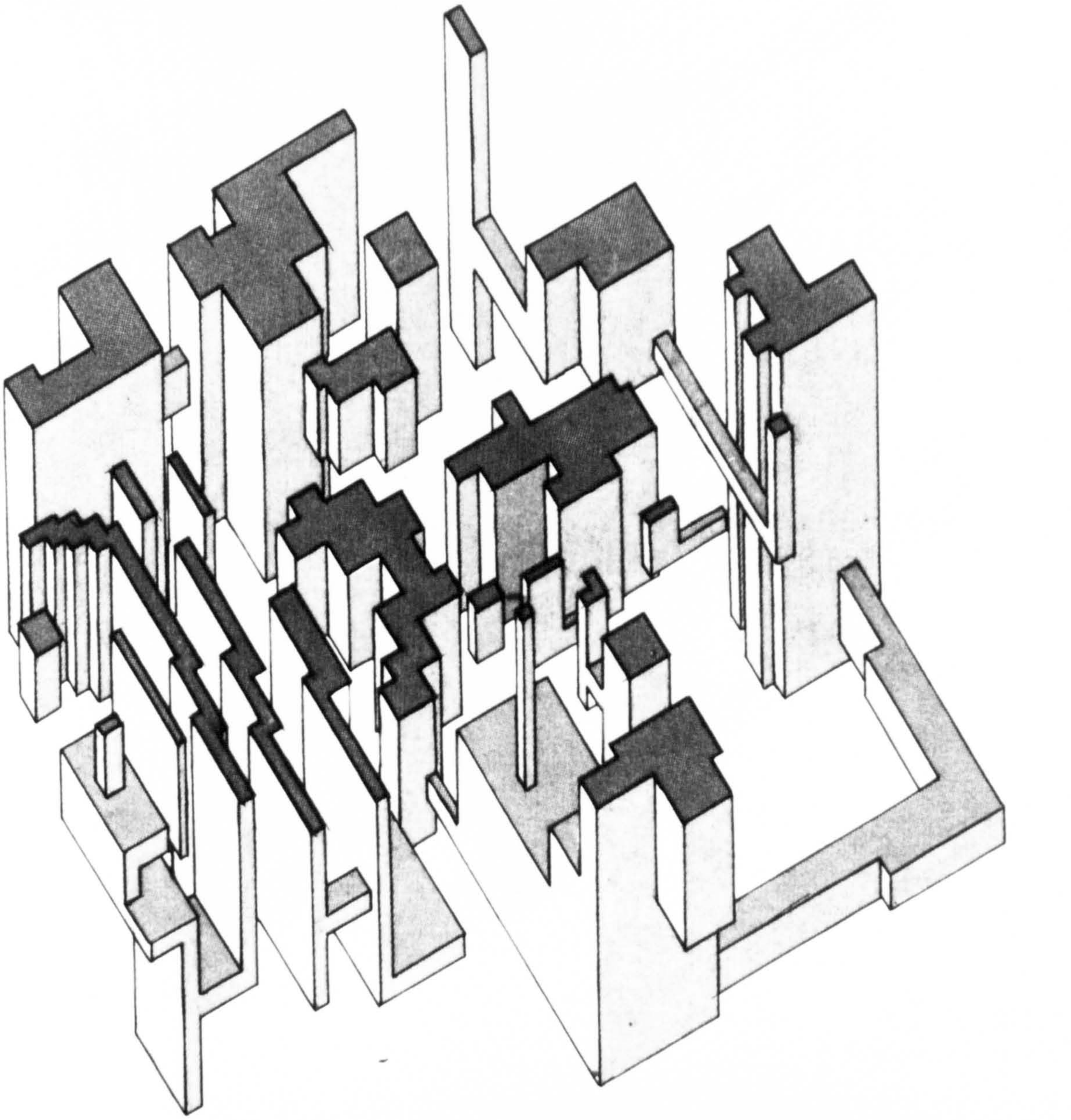


Figure 151. Diagrammatic Model of a Petroleum Coke Graphite.

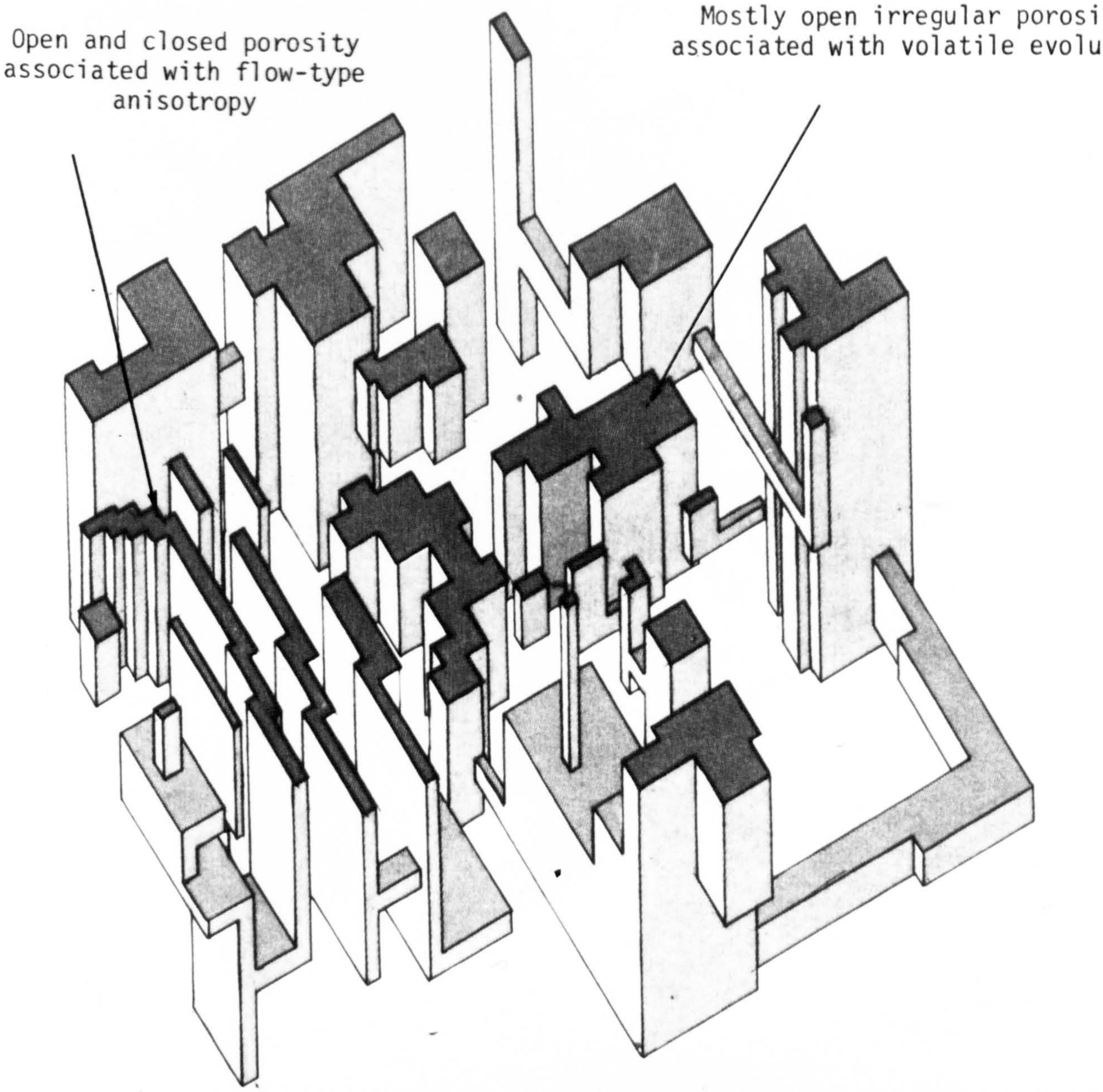


Figure 151. Diagrammatic Model of a Petroleum Coke Graphite.

Mostly open
uniform porosity

Closed
uniform porosity

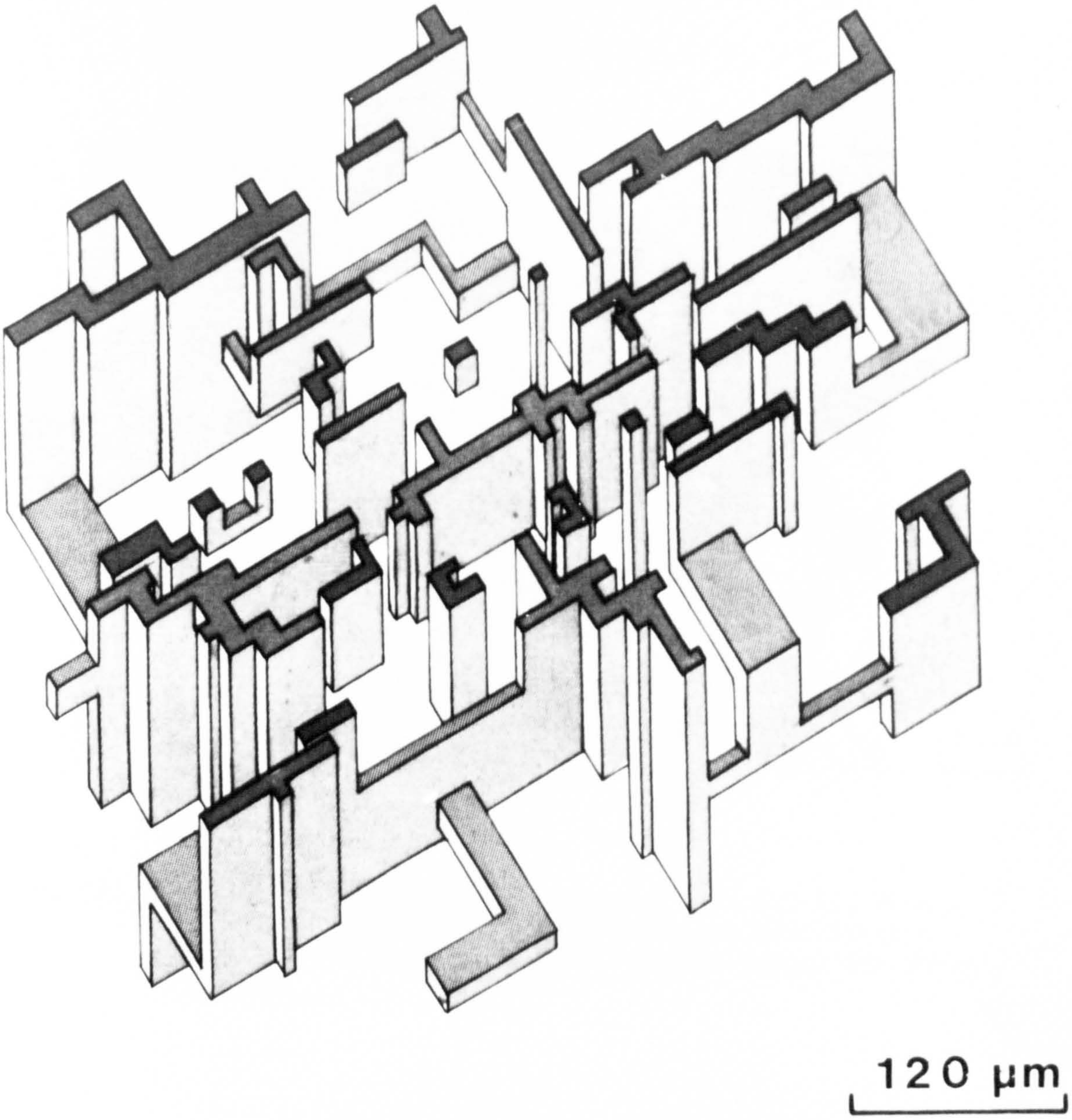


Figure 152. Diagrammatic Model of a Unipore Graphite.

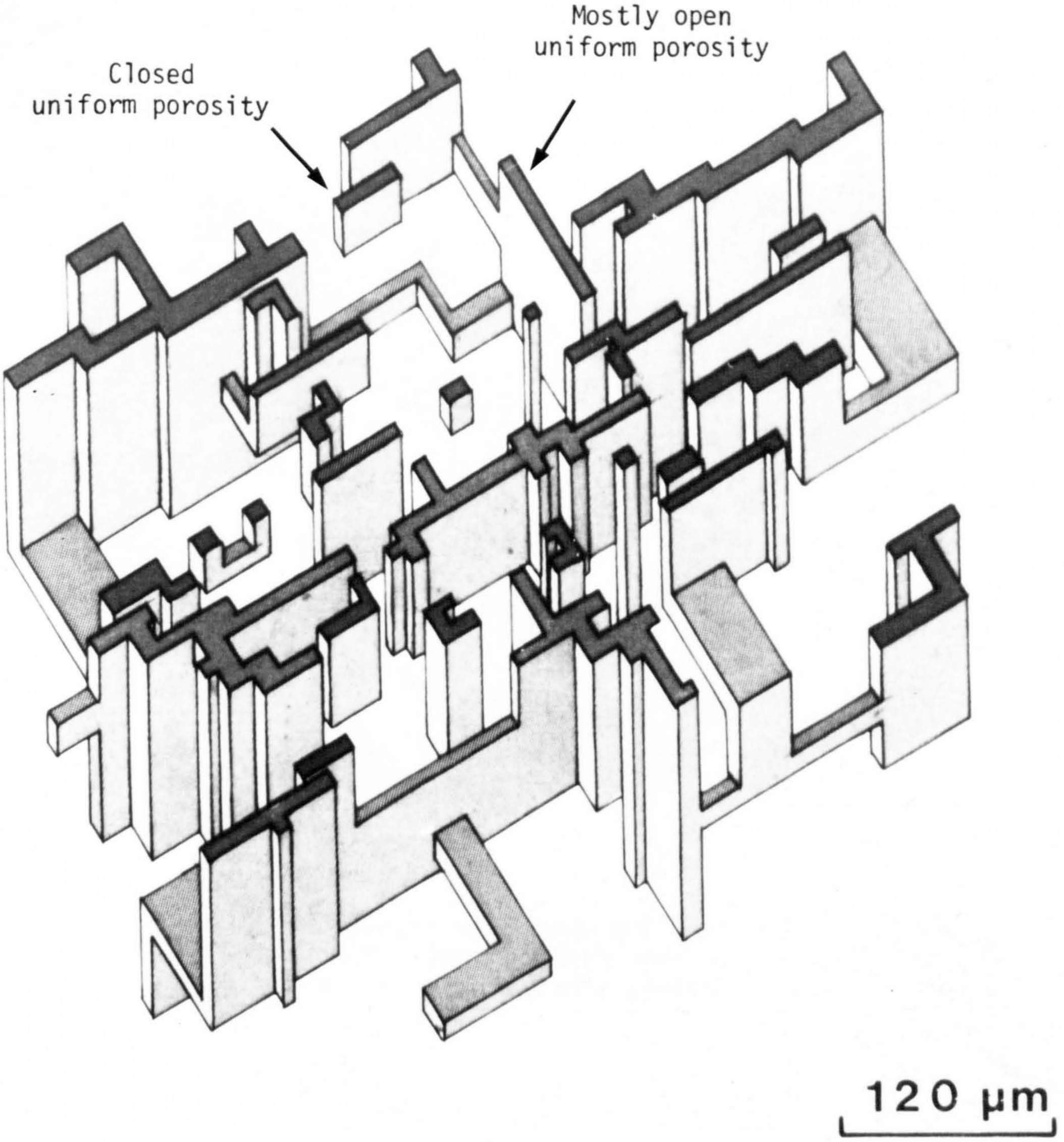


Figure 152. Diagrammatic Model of a Unipore Graphite.

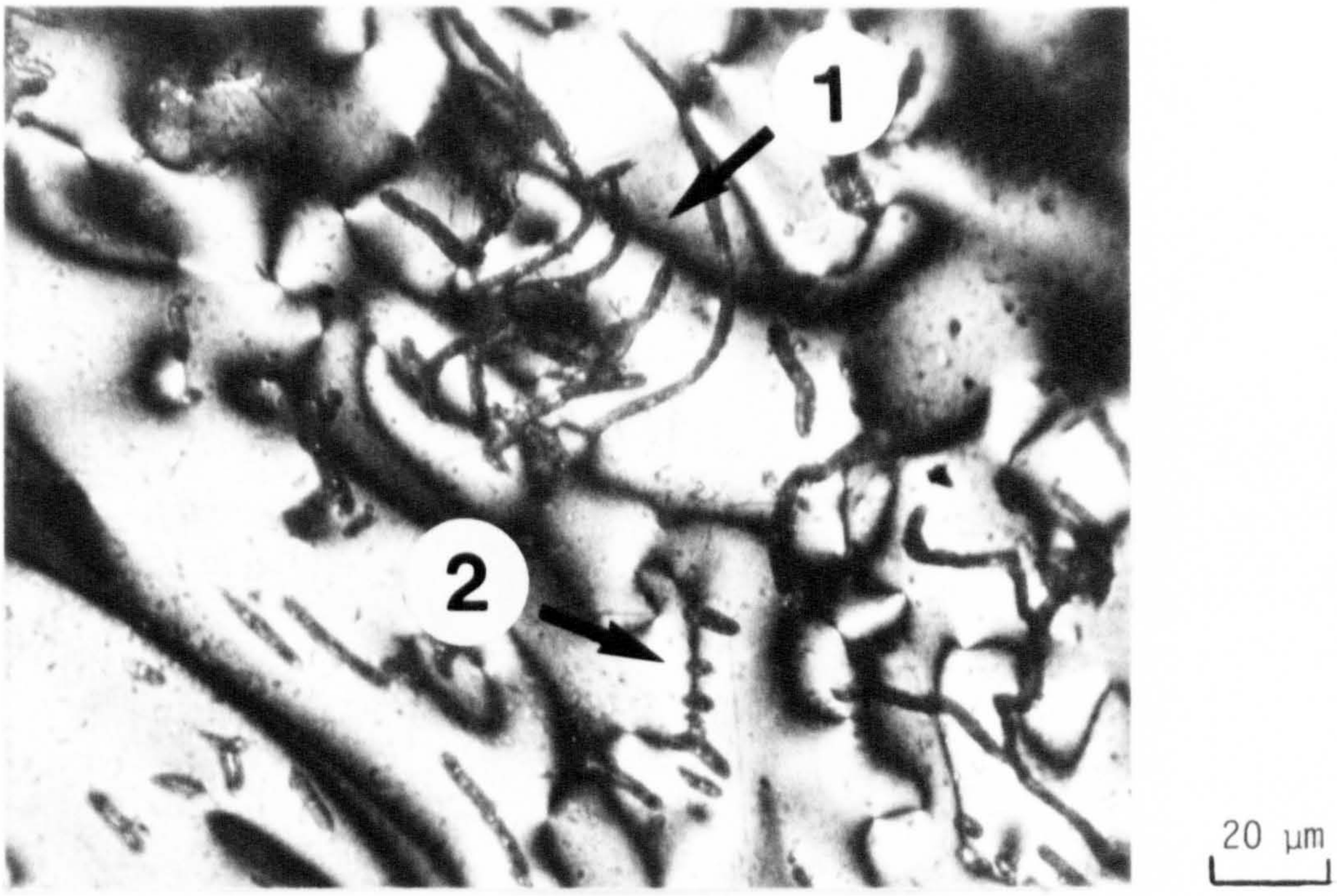
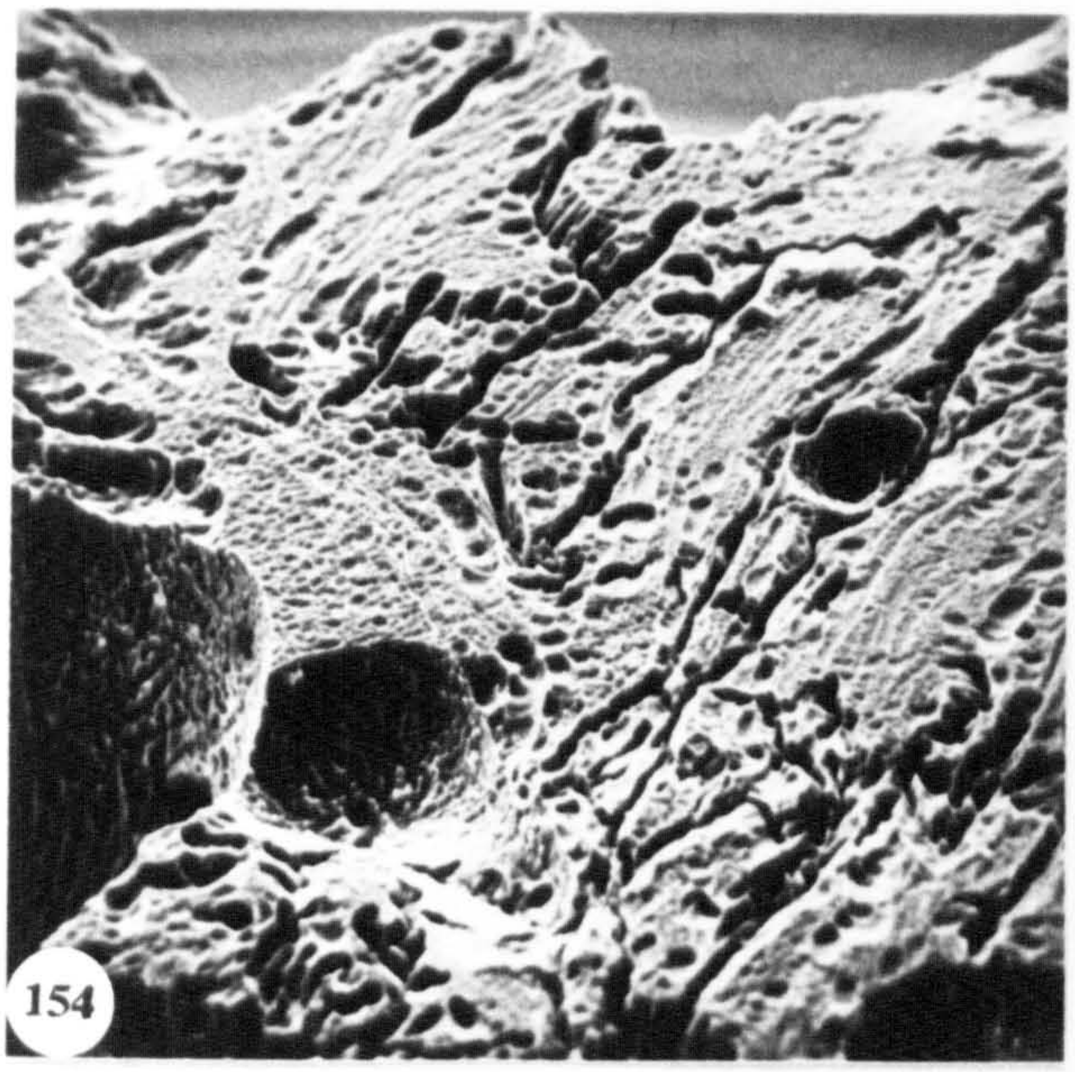
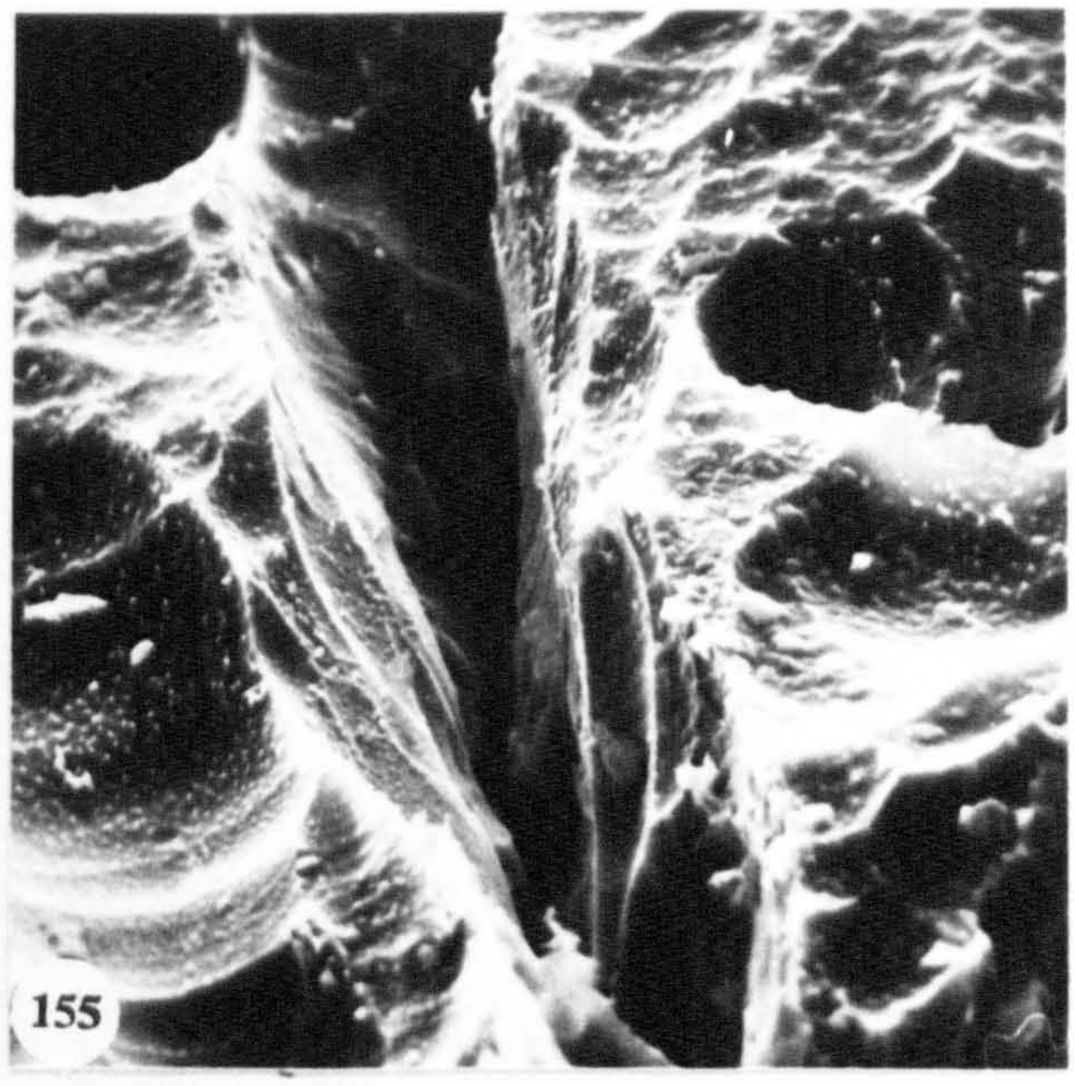
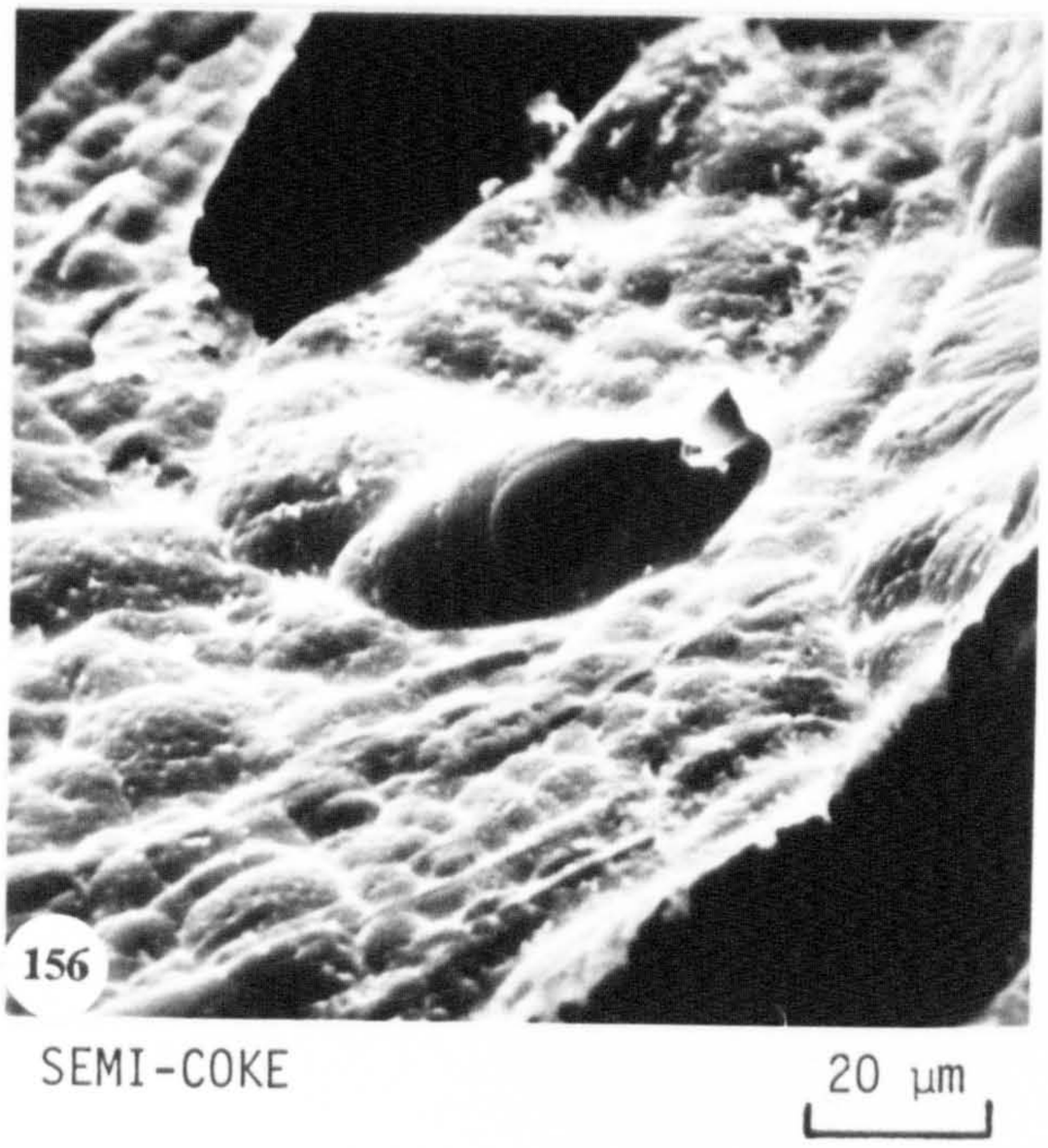


Figure 153. Optical micrograph of a semi-coke (HTT 800 K), from a mixture of 50% Gilsonite Pitch and 50% A200 Ashland Petroleum Pitch, oxidized with atomic oxygen for three minutes.







Figures 154 to 156. Scanning electron micrographs (stereoscan) of semi-coke (HTT 800 K) from a mixture of 75% Ashphaltine and 25% A200 Ashland Petroleum Pitch, oxidized with atomic oxygen for fourteen minutes.

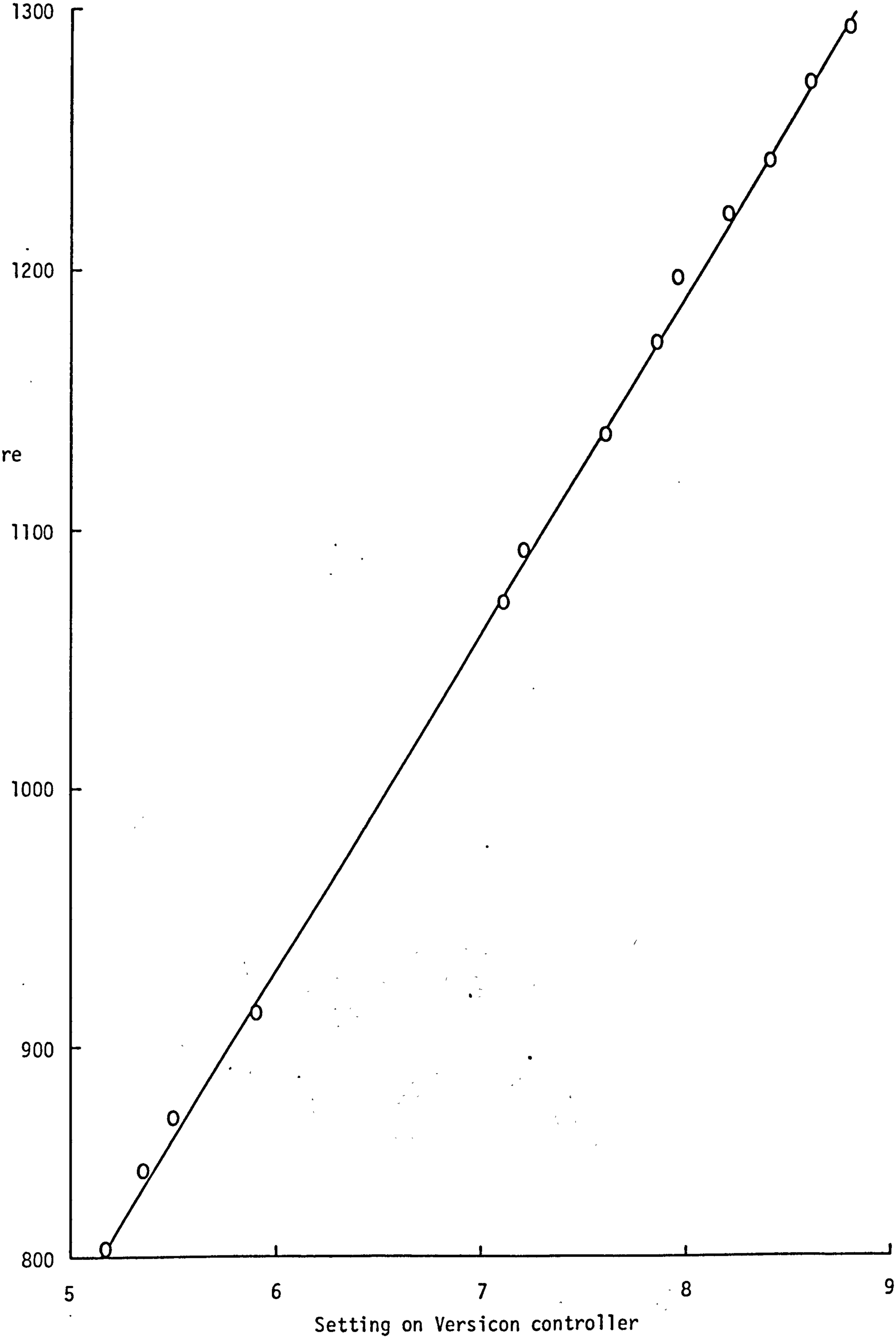
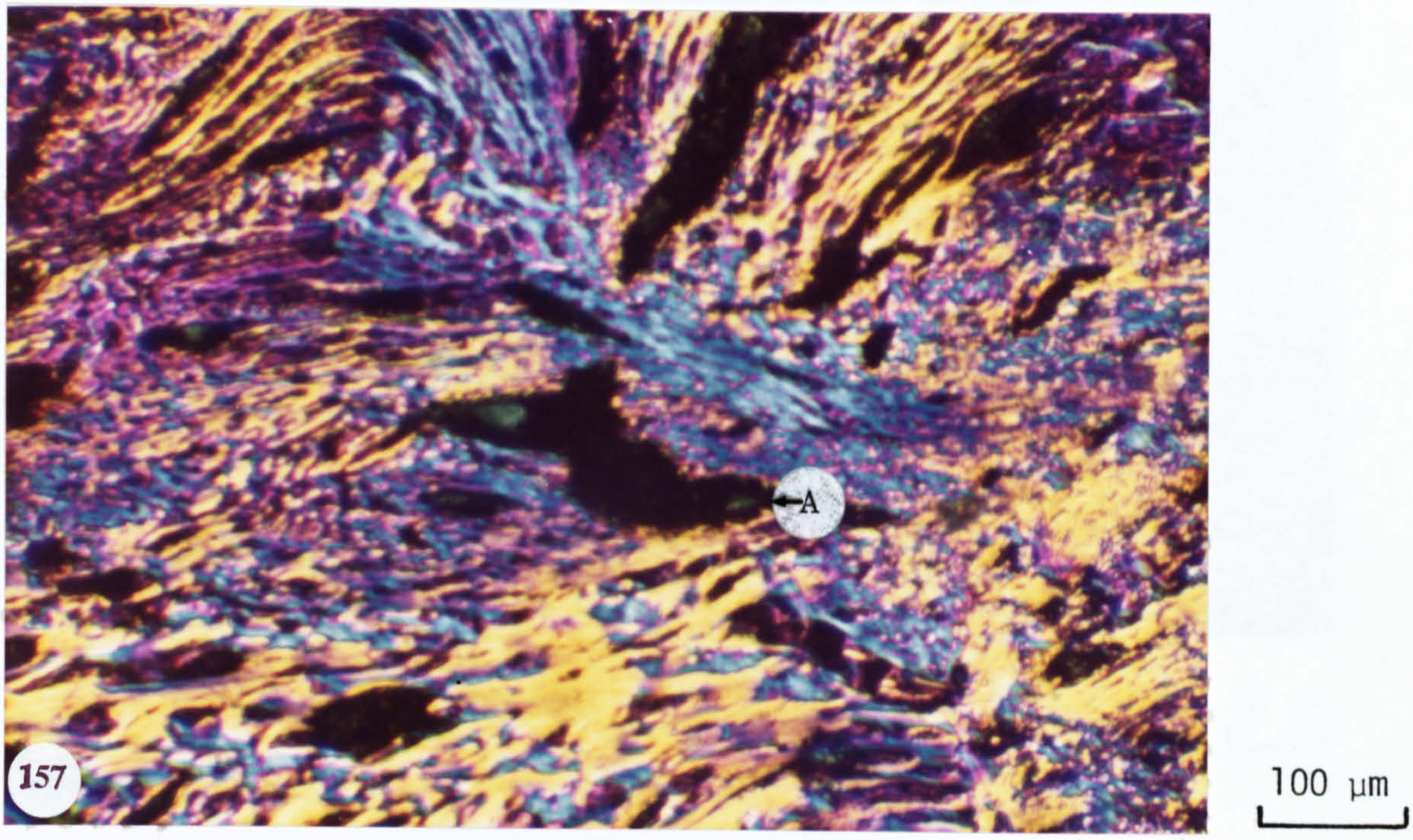
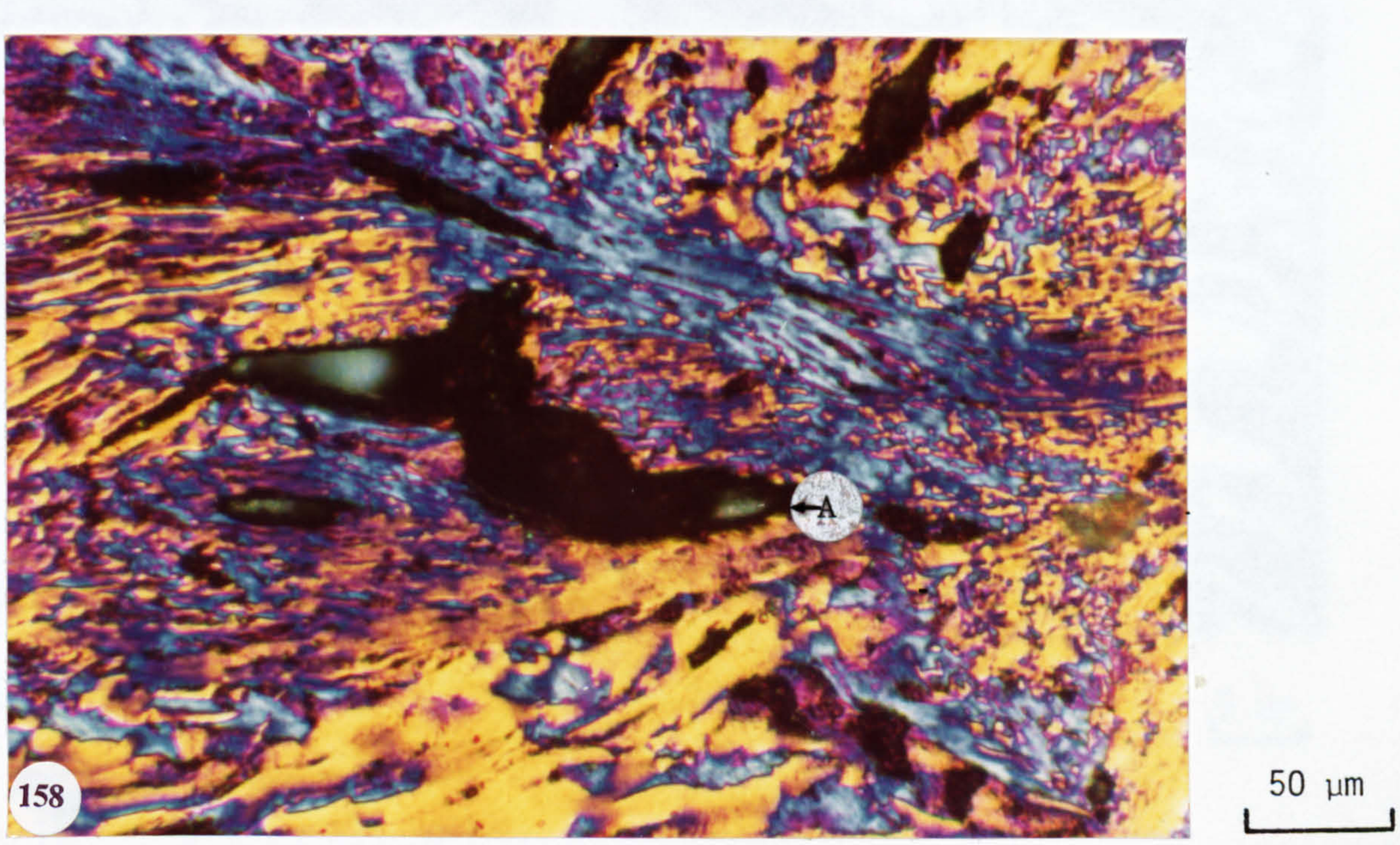


Figure 156.1. Calibration of gasification furnace.

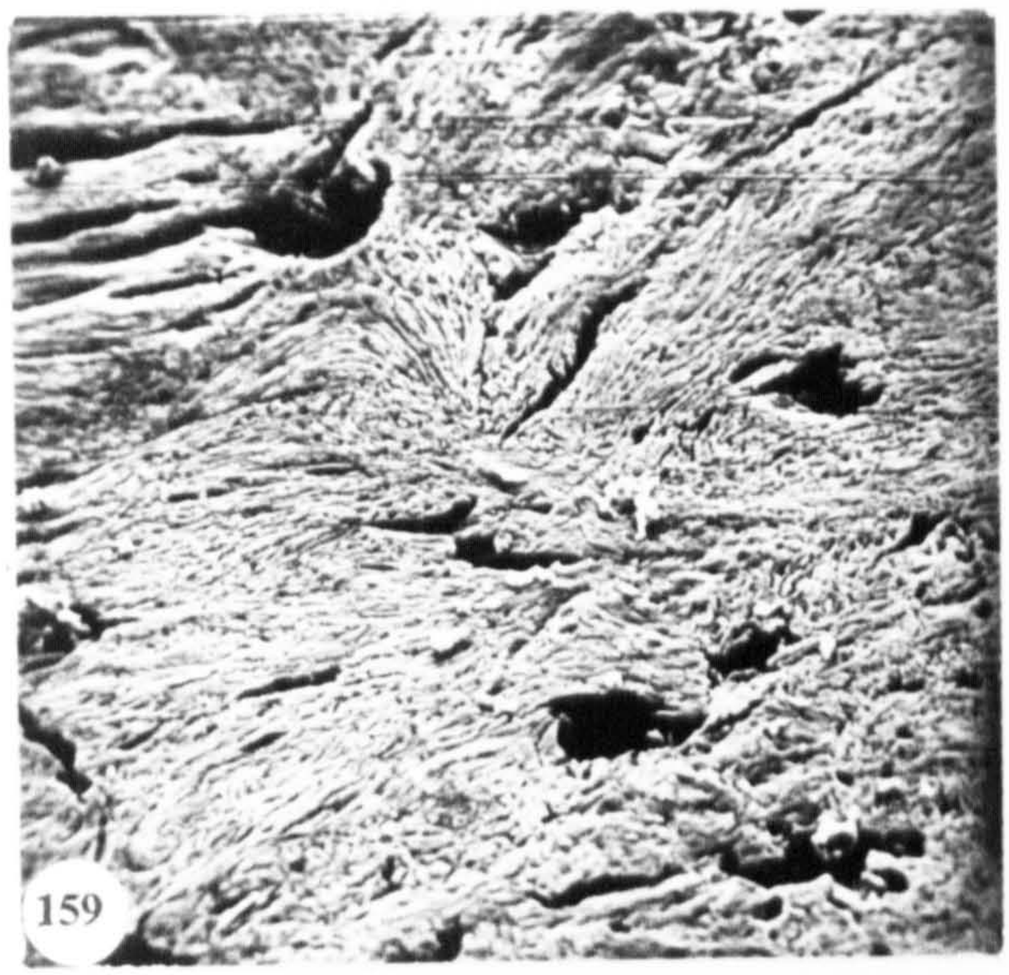


LIMA GRAPHITE

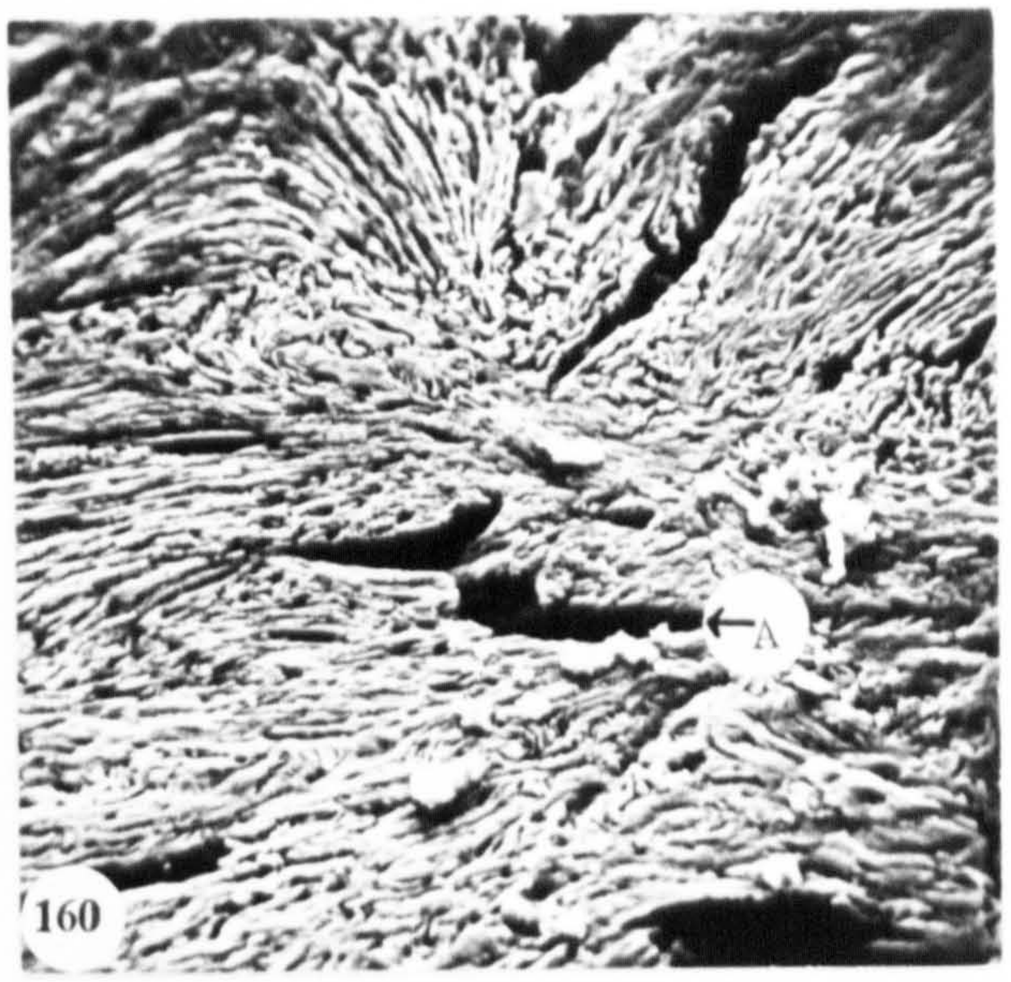


LIMA GRAPHITE

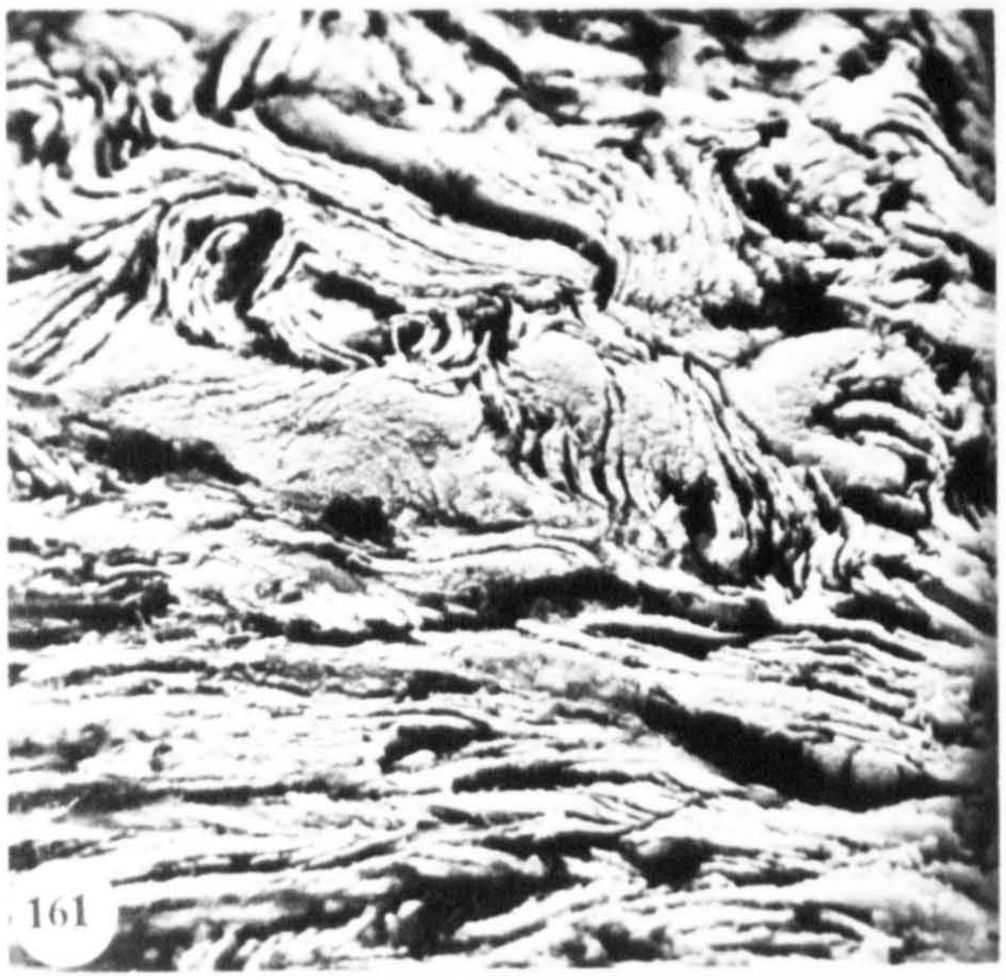
Figures 157 and 158. Optical micrographs of Lima Graphite (LG1) before gasification.



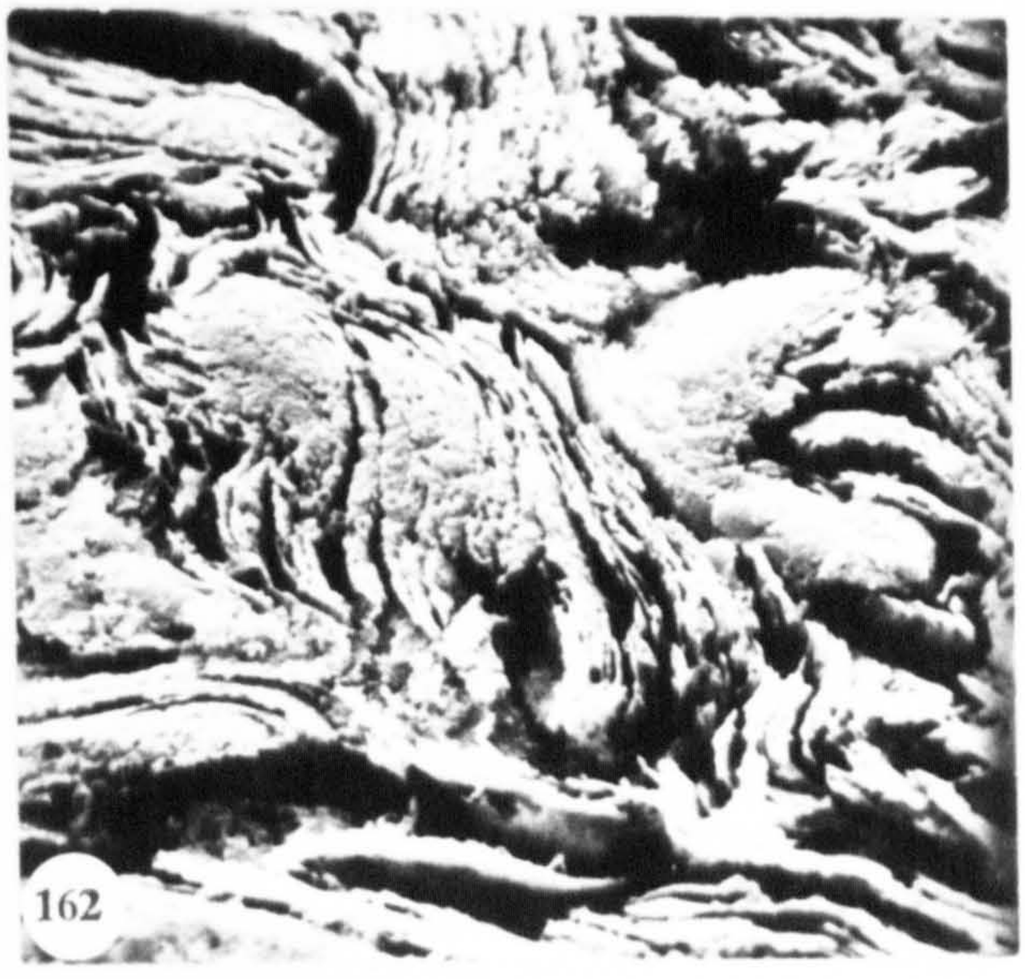
LIMA GRAPHITE 100 μm



LIMA GRAPHITE 50 μm

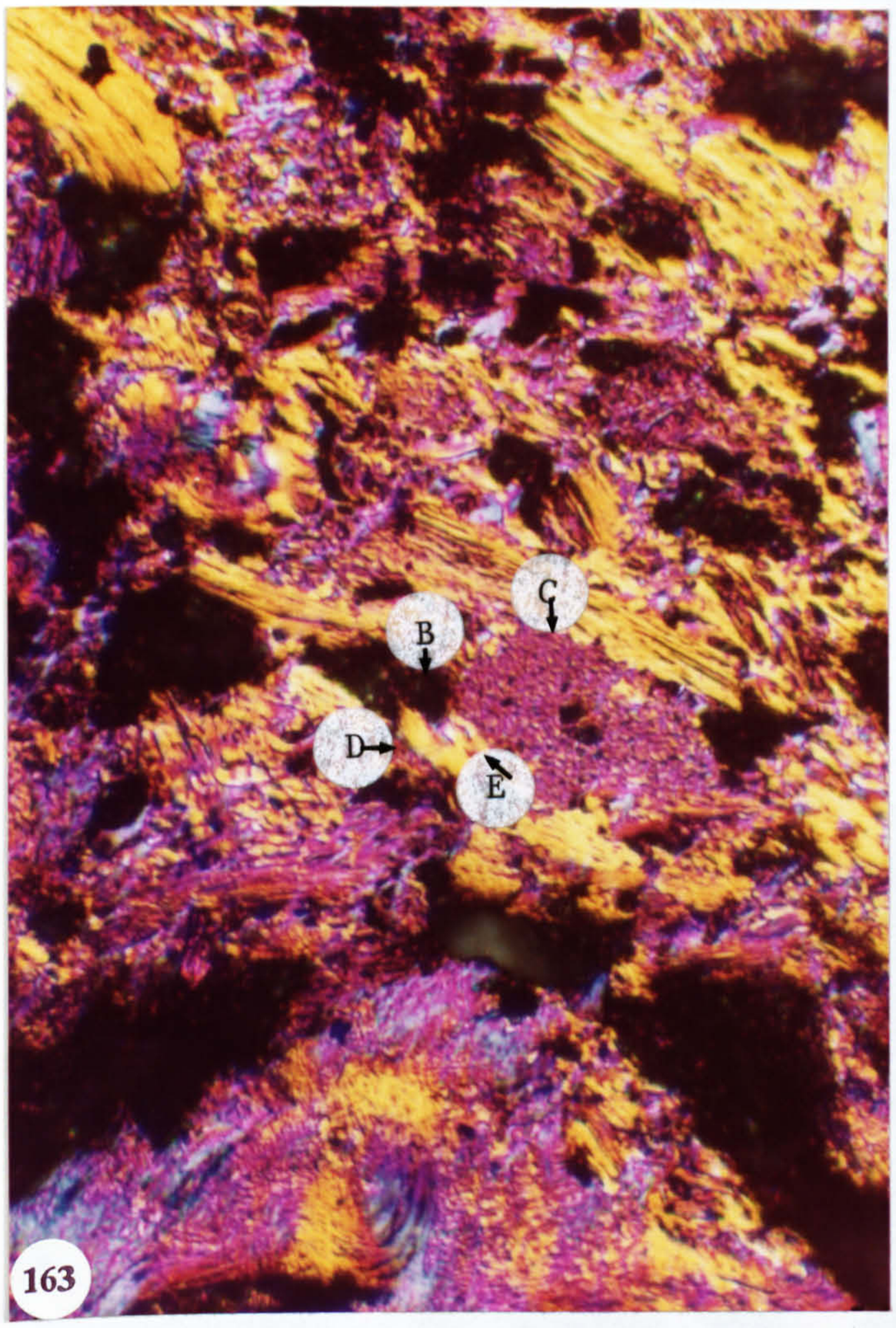


LIMA GRAPHITE 10 μm



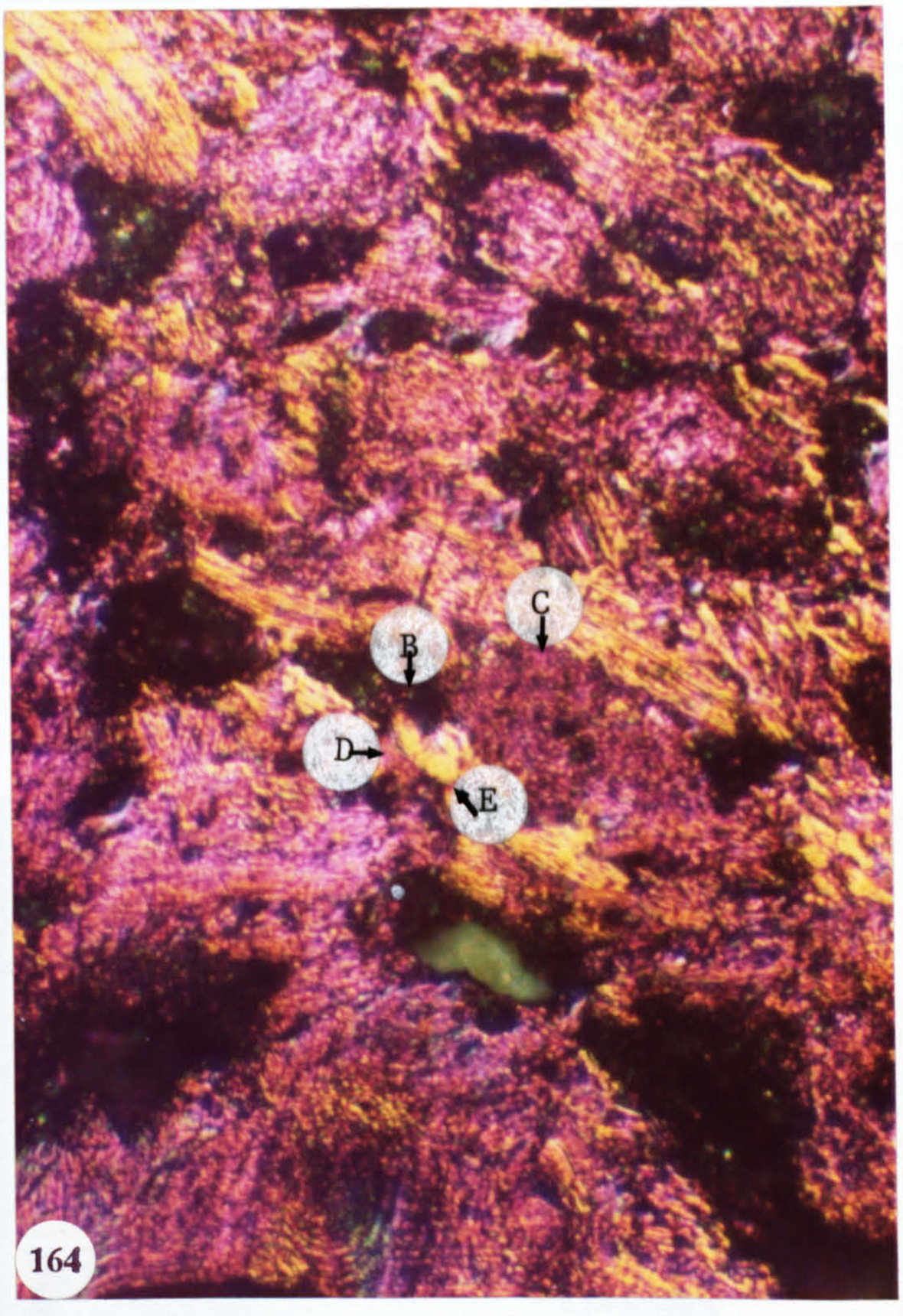
LIMA GRAPHITE 5 μm

Figures 159 to 162. Scanning electron micrographs (stereoscan) of Lima graphite (LG1) gasified in air at 973 K for 1 hour. Weight loss 16.67%.



LIMA GRAPHITE

100 µm



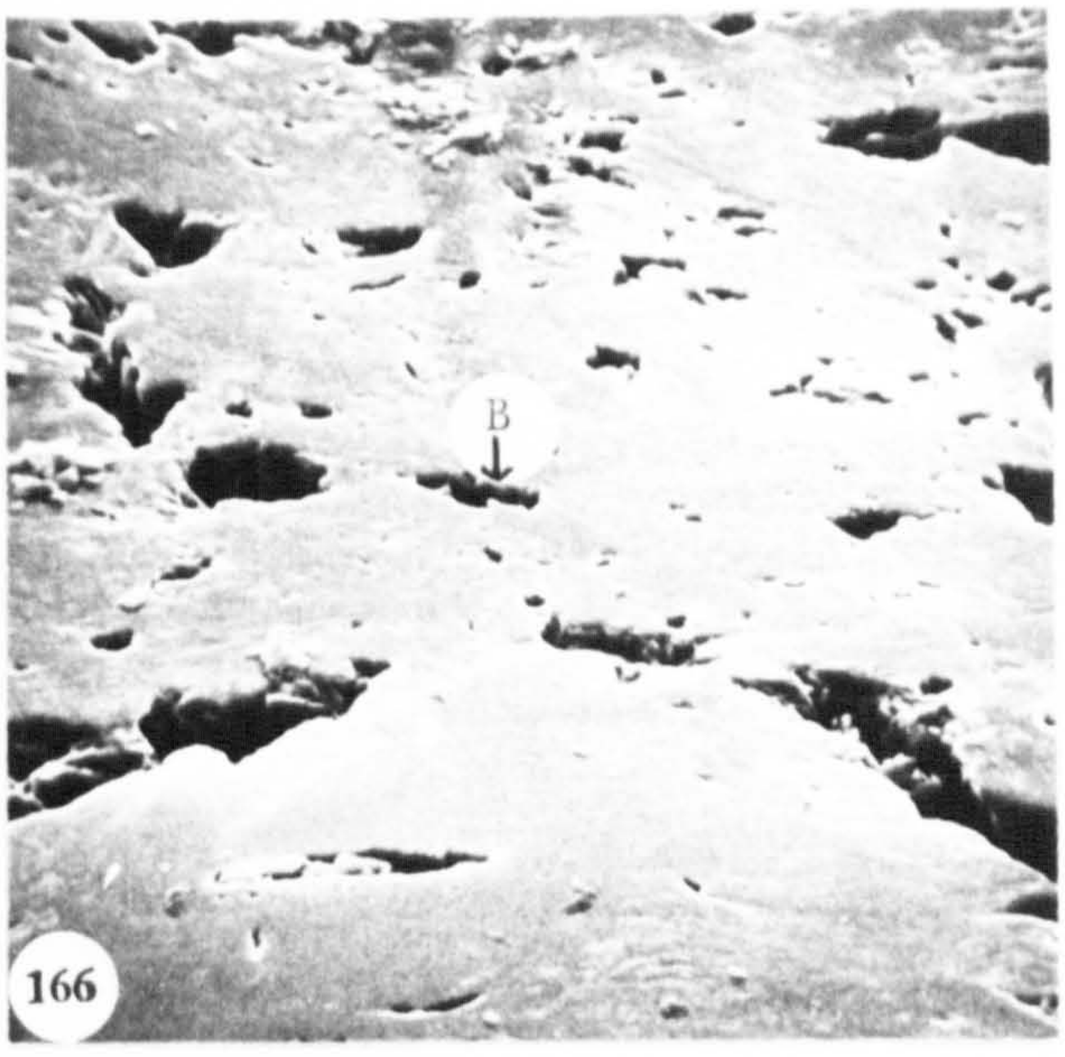
LIMA GRAPHITE

100 µm

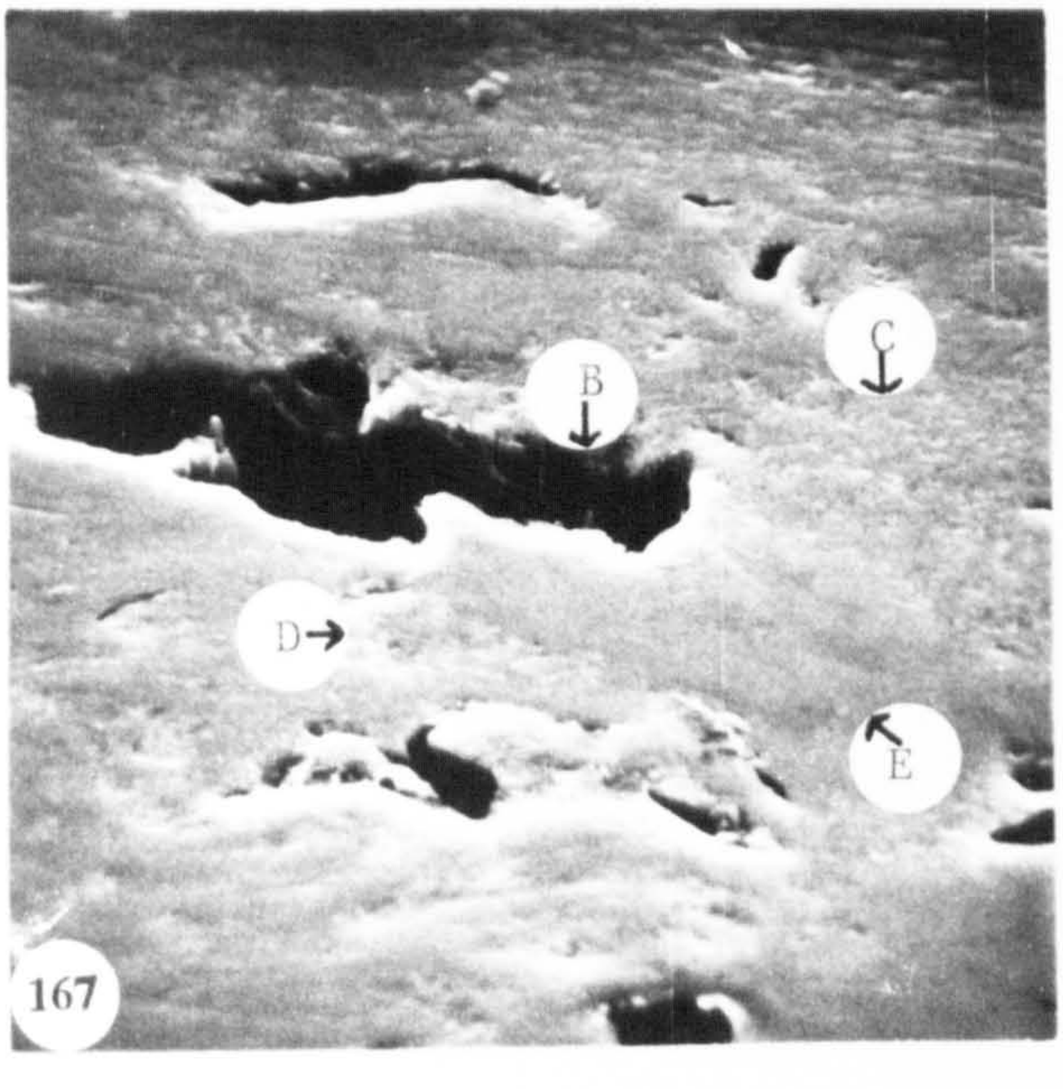
Figures 163 and 164. Optical micrographs of Lima Graphite (LG2) before and after gasification in air at 873 K for 1 hour. Weight loss 2.35%.



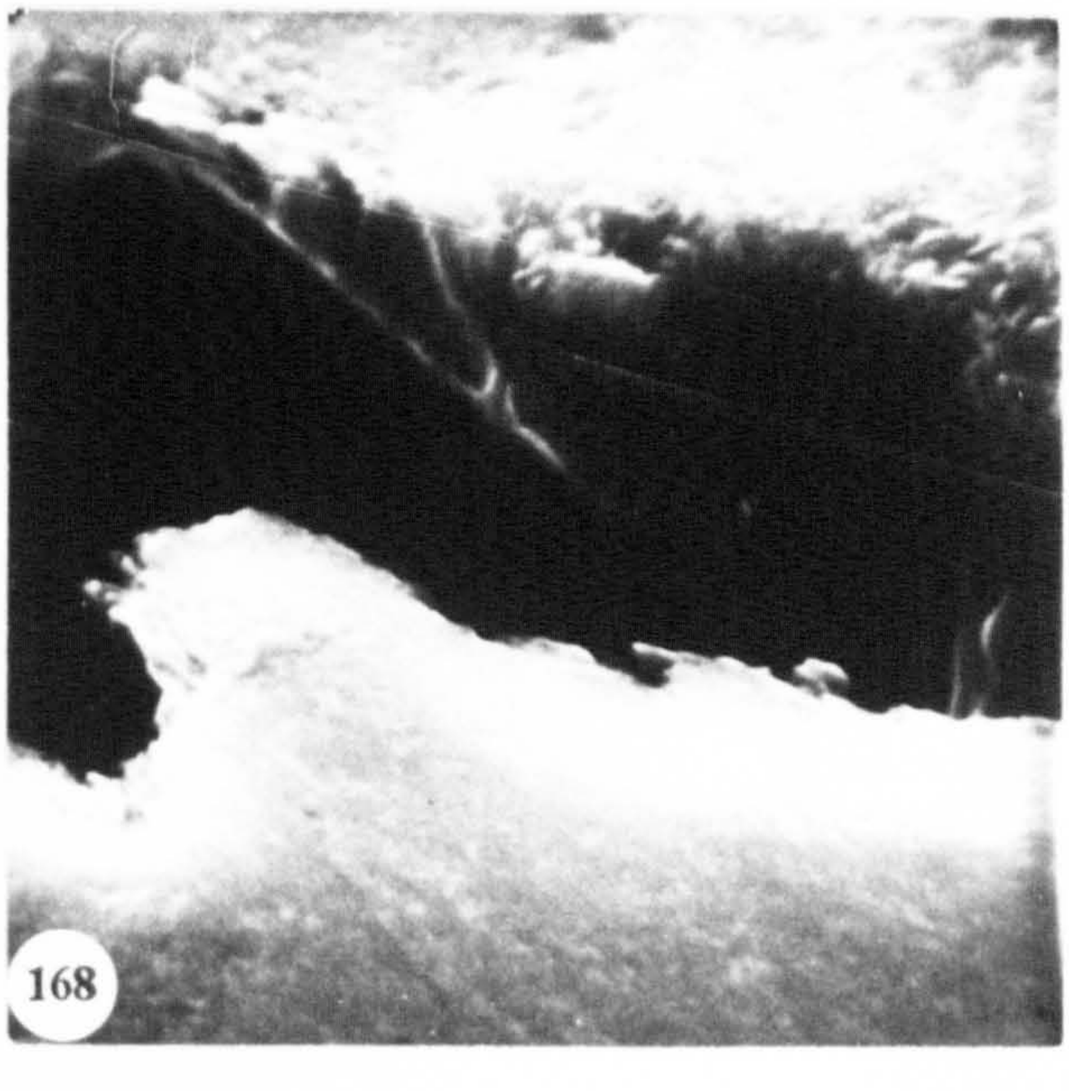
VIRGIN LIMA GRAPHITE 100 µm



VIRGIN LIMA GRAPHITE 50 µm

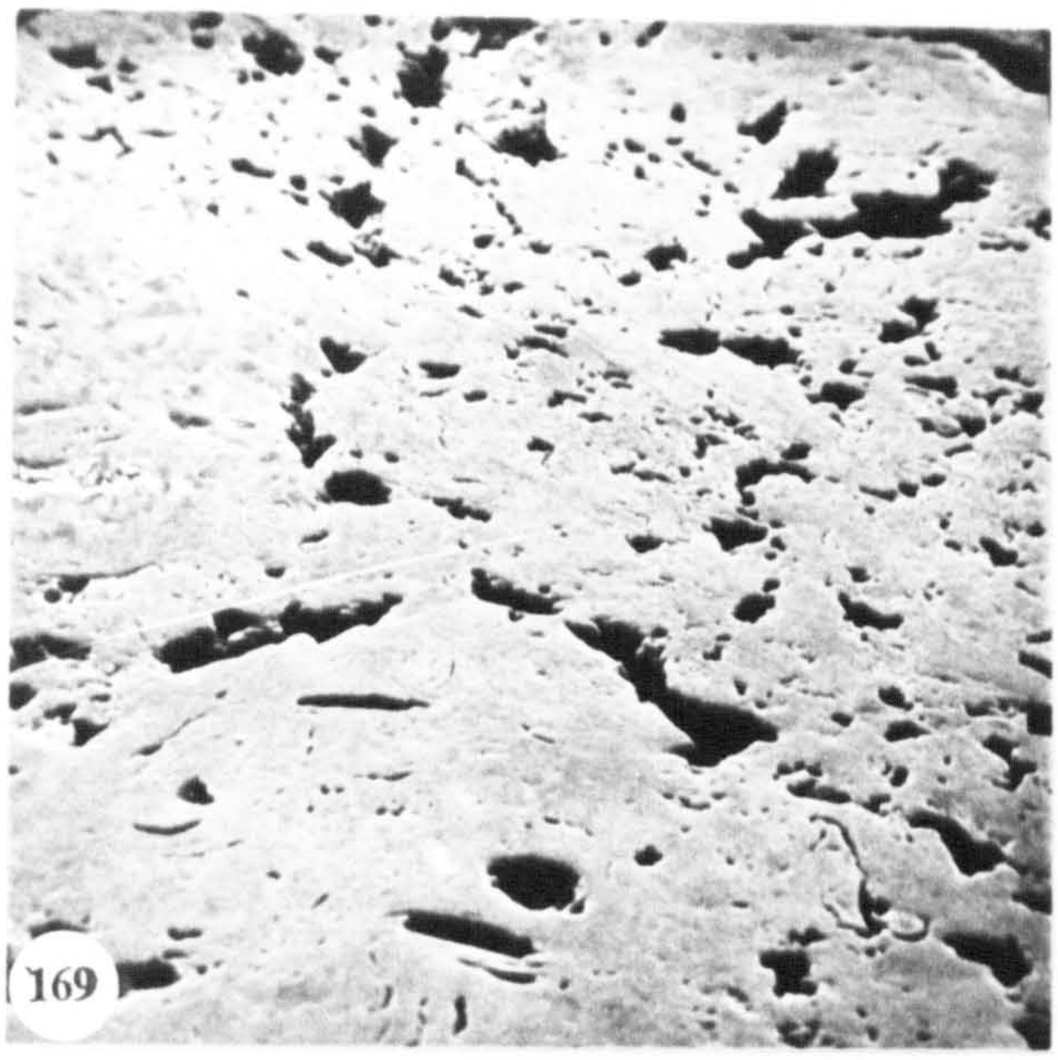


VIRGIN LIMA GRAPHITE 10 µm

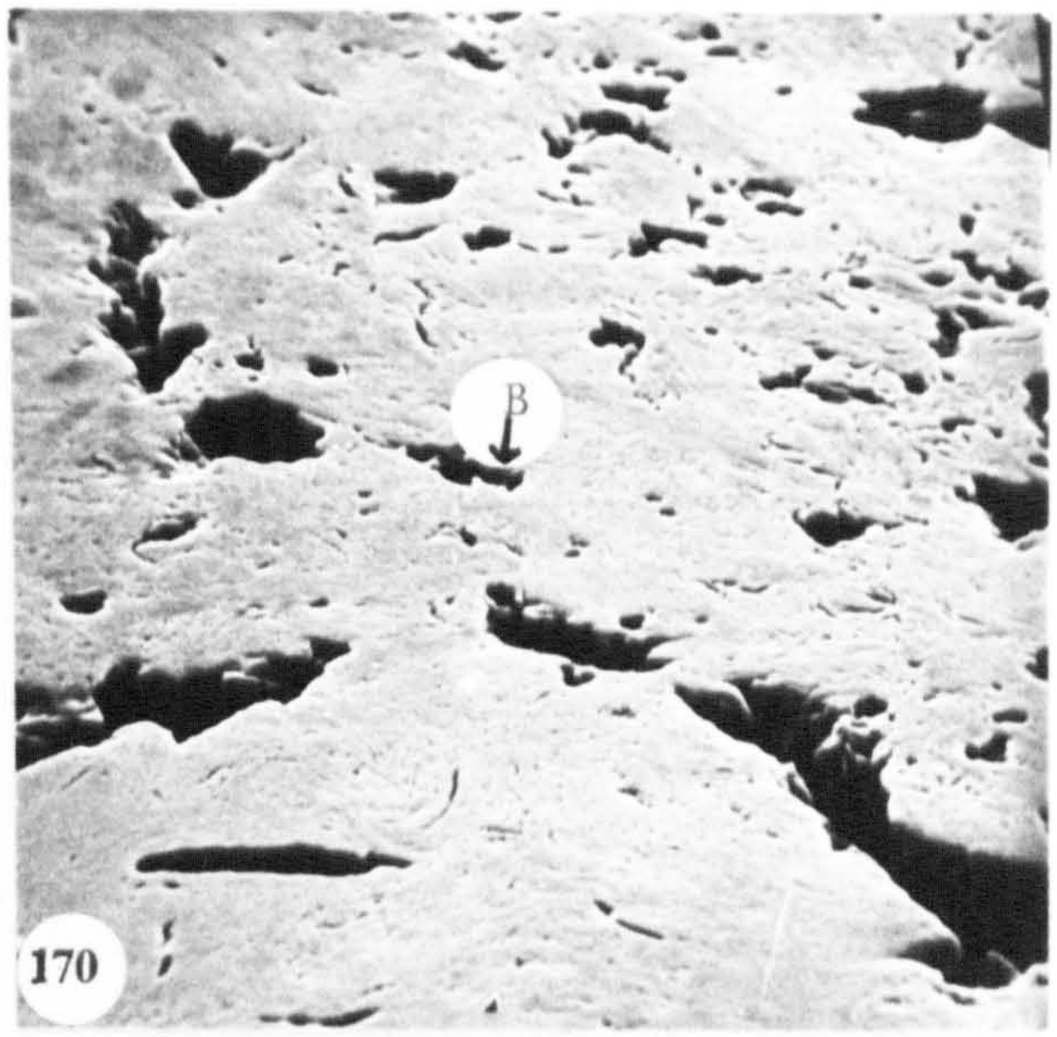


VIRGIN LIMA GRAPHITE 2 µm

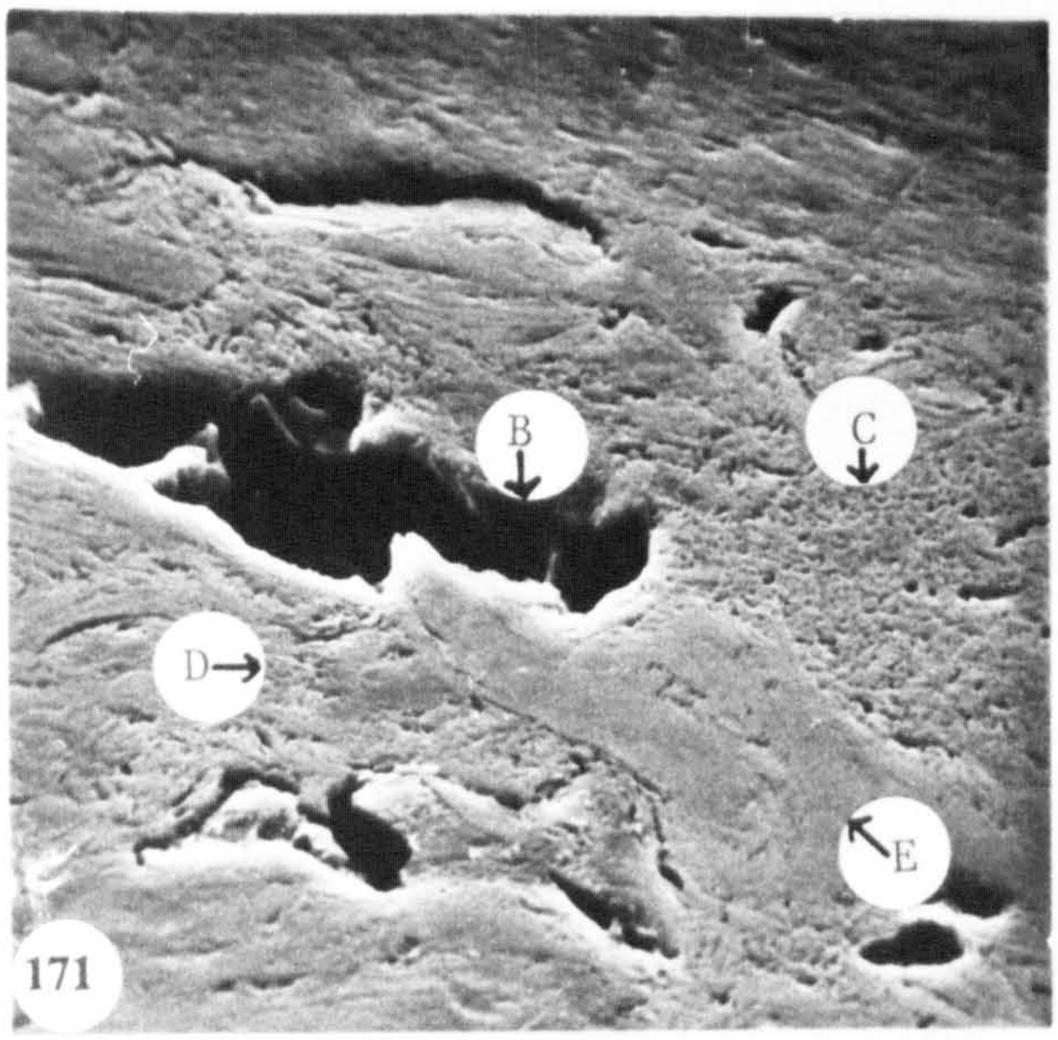
Figures 165 to 168. Scanning electron micrographs (stereoscan) of Lima graphite (LG2) before gasification.



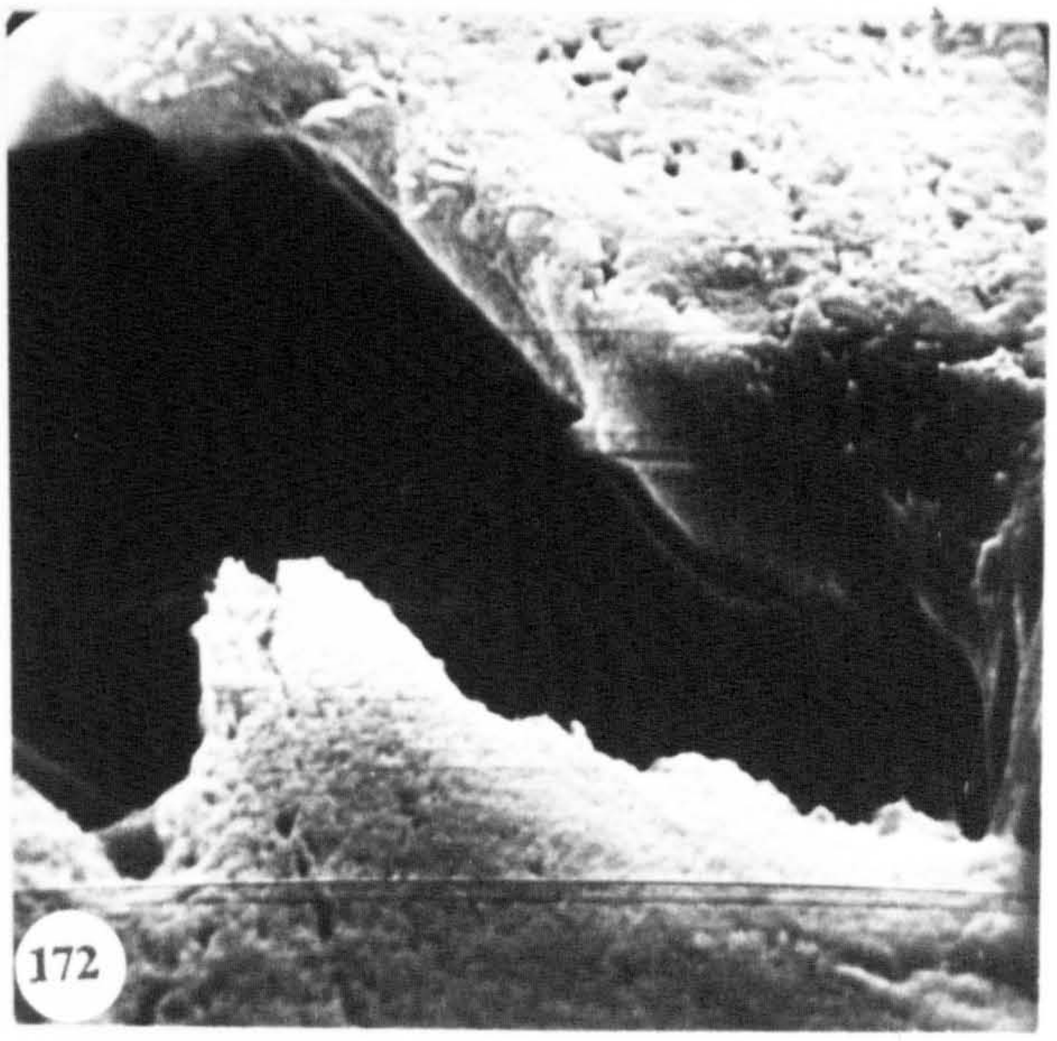
LIMA GRAPHITE 100 µm



LIMA GRAPHITE 50 µm

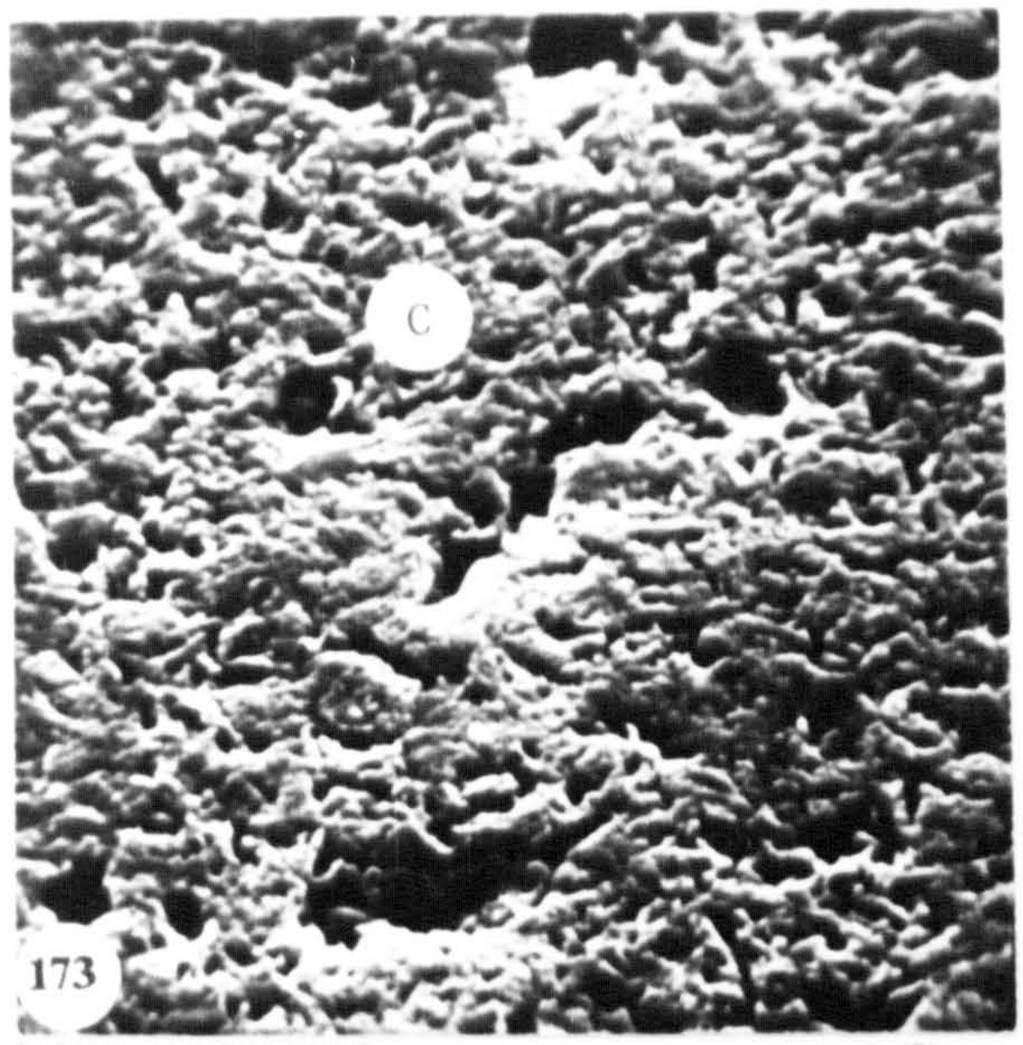


LIMA GRAPHITE 10 µm

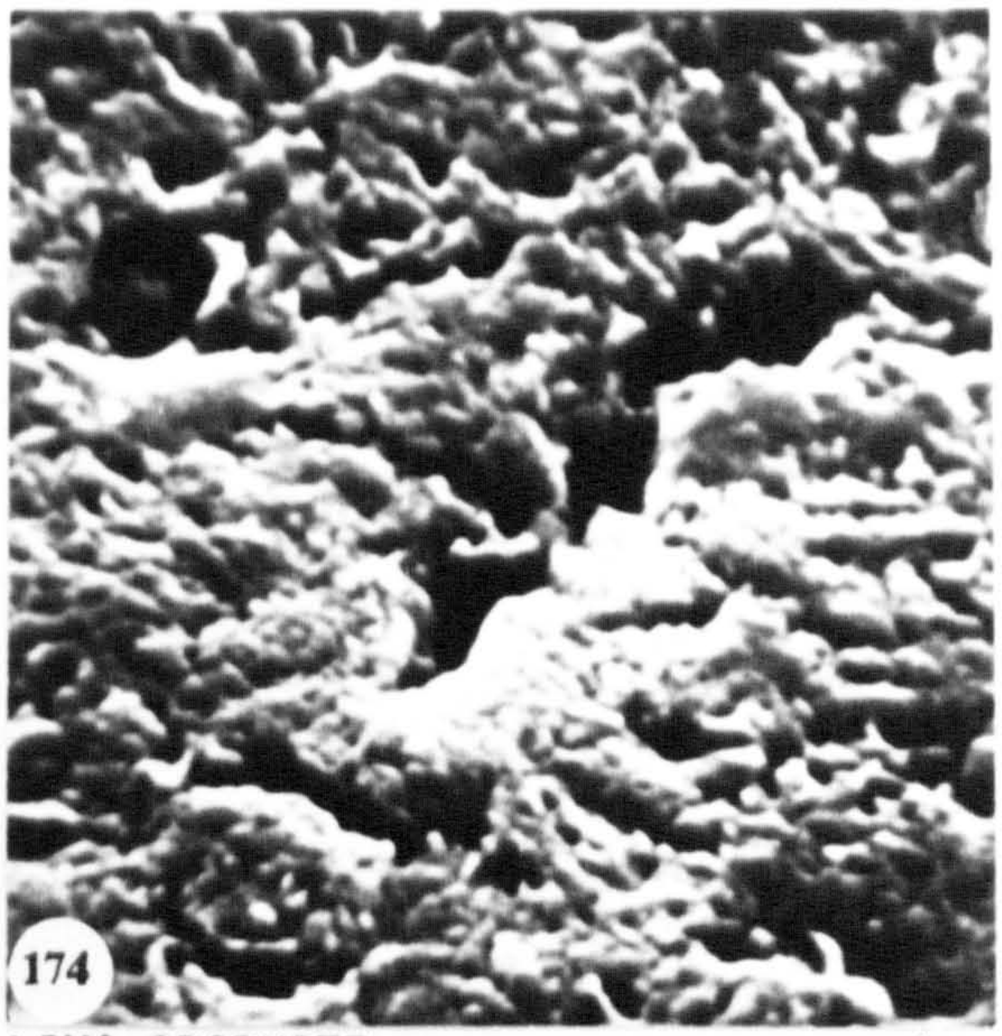


LIMA GRAPHITE 2 µm

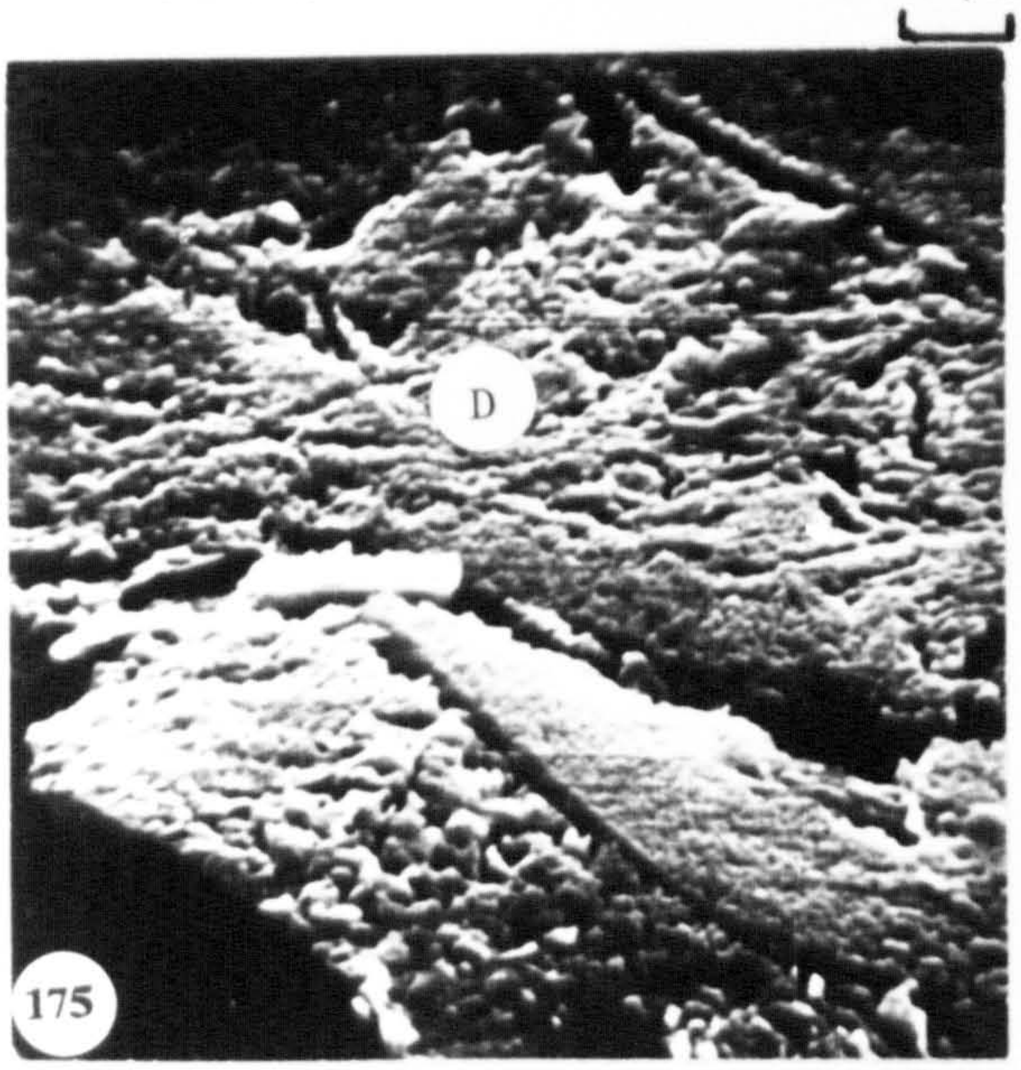
Figures 169 to 172. Scanning electron micrographs (stereoscan) of Lima graphite (LG2) gasified in air at 873 K for 1 hour. Weight loss 2.35%.



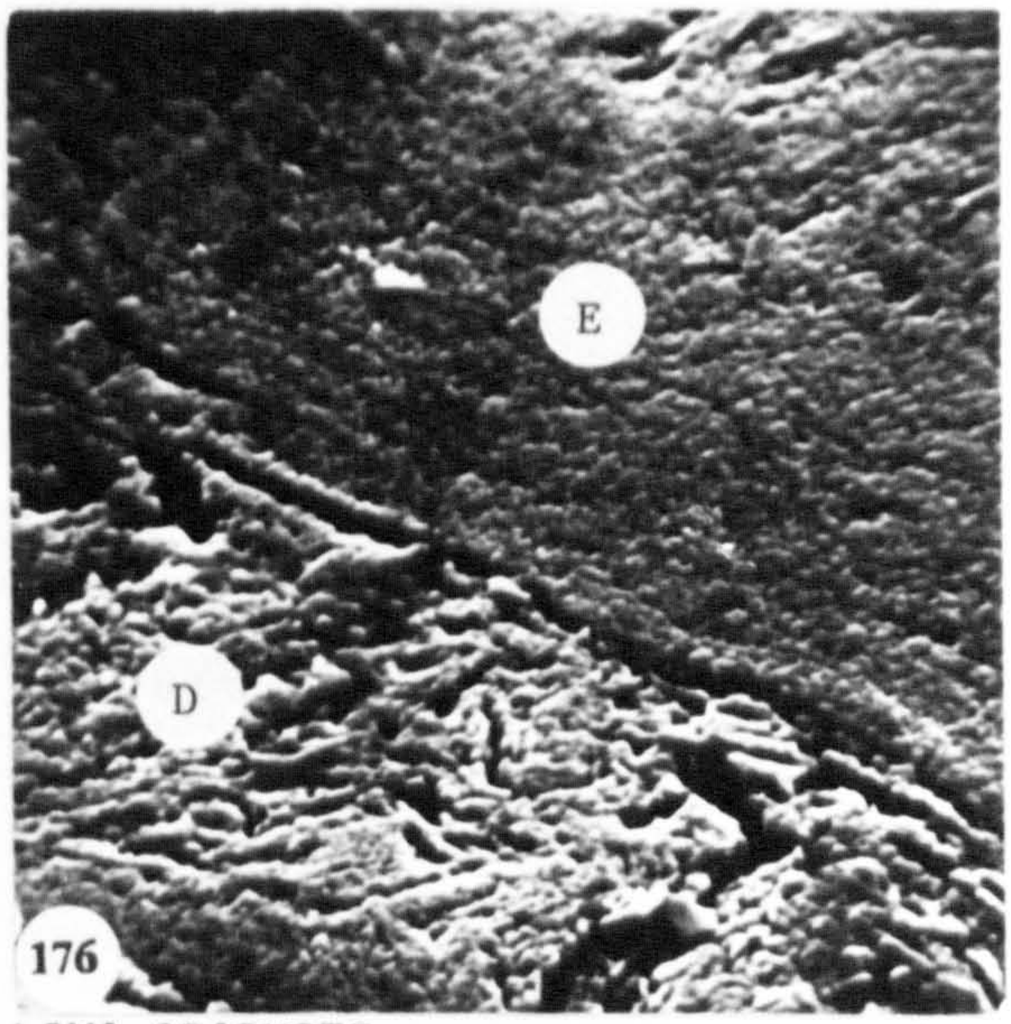
LIMA GRAPHITE 2 μm



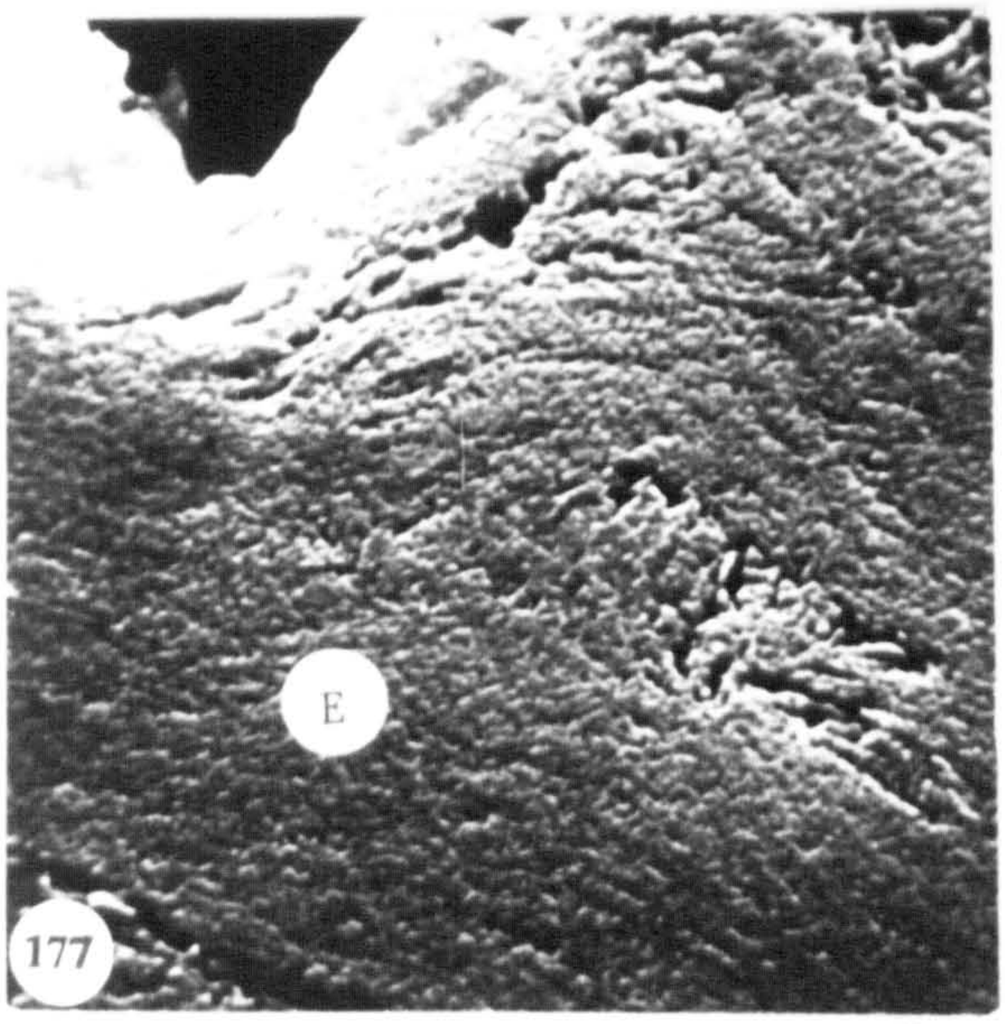
LIMA GRAPHITE 1 μm



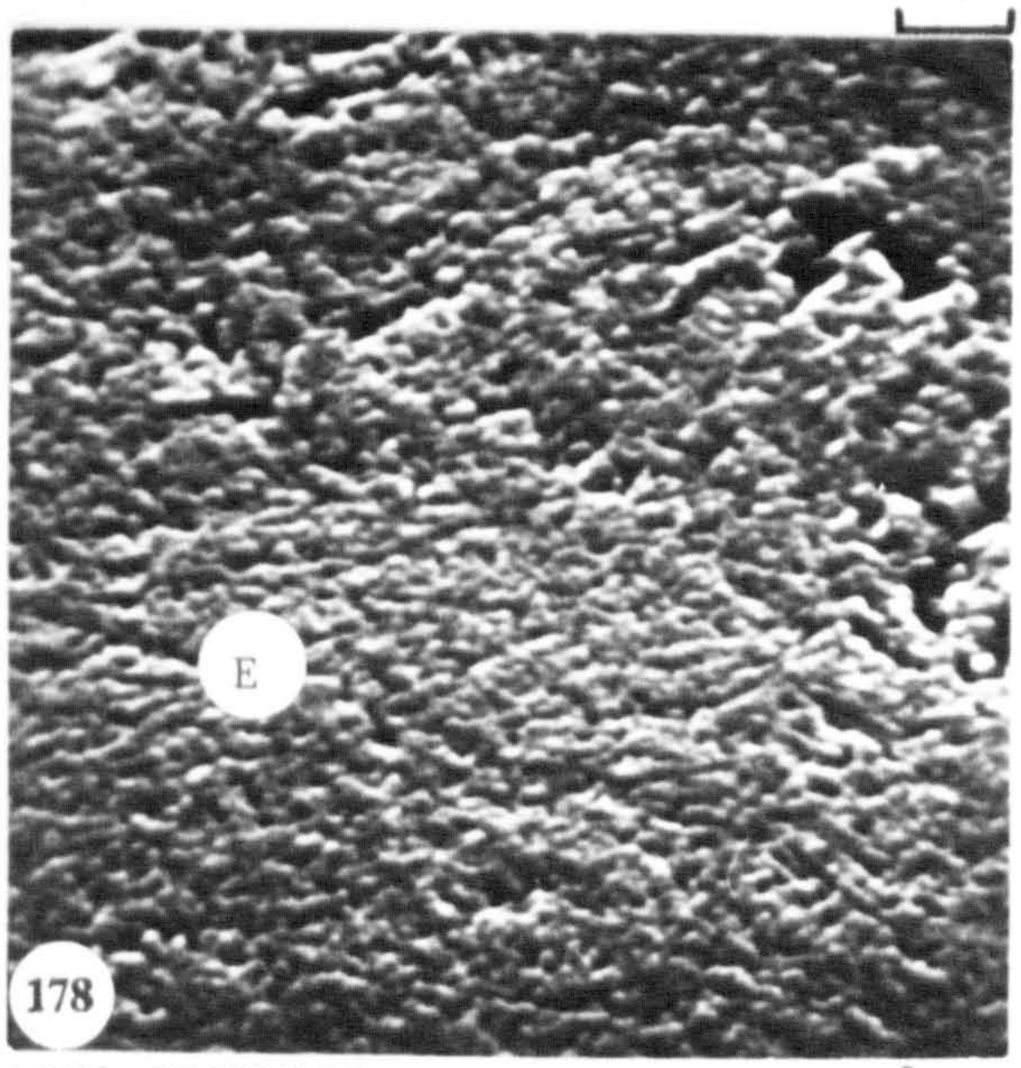
LIMA GRAPHITE 2 μm



LIMA GRAPHITE 2 μm

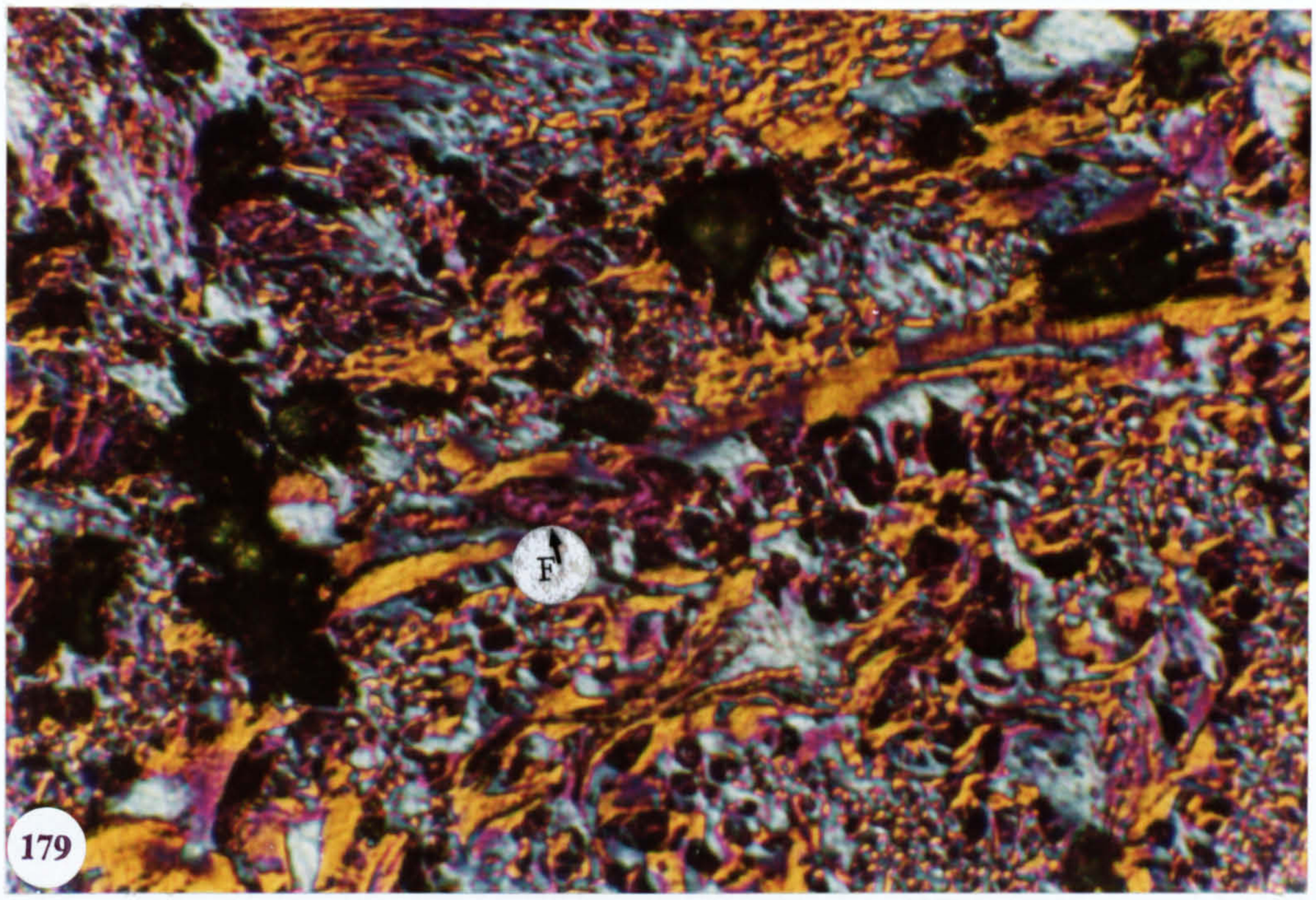


LIMA GRAPHITE 2 μm

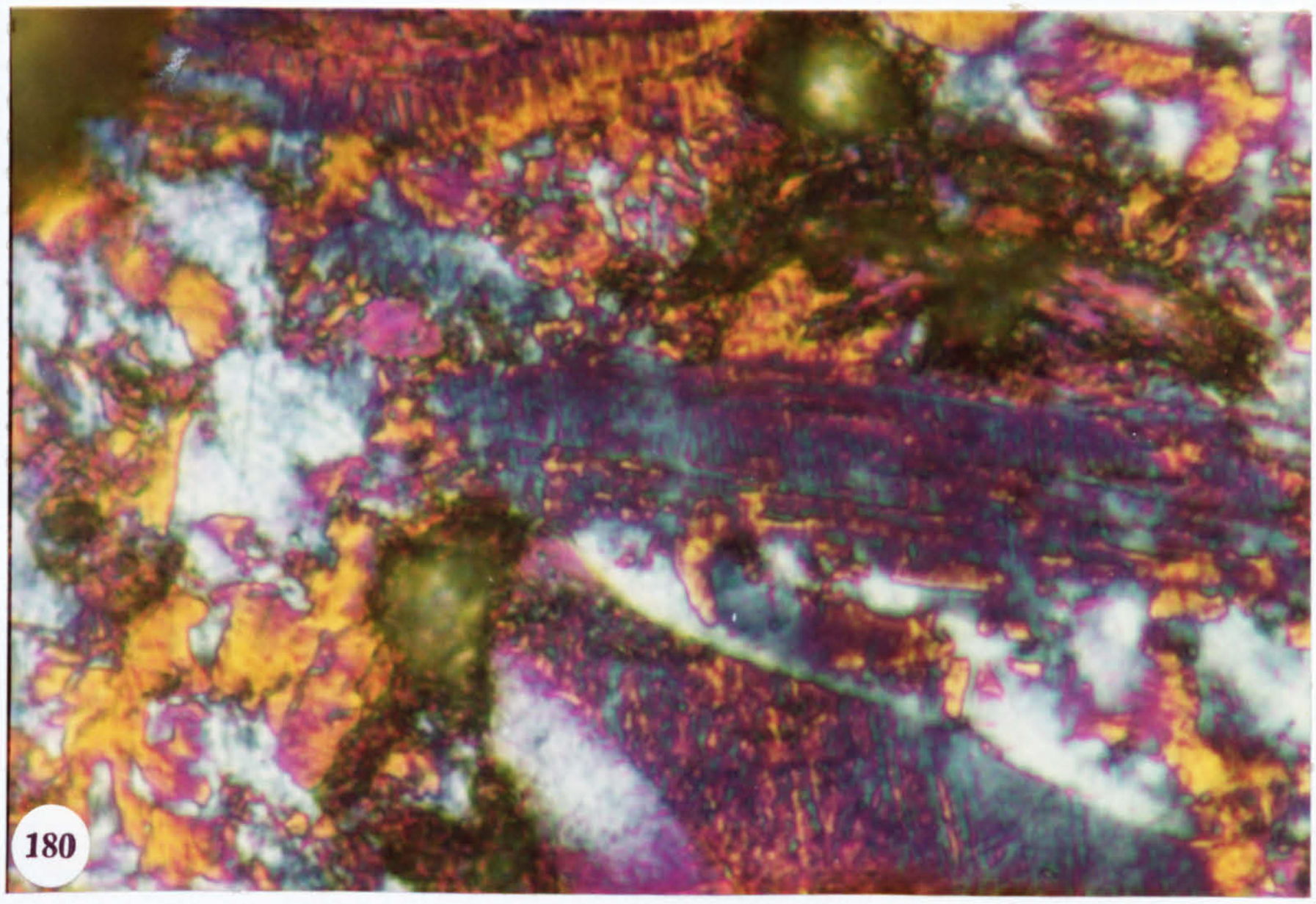


LIMA GRAPHITE 1 μm

Figures 173 to 178. Scanning electron micrographs (stereoscan) of Lima Graphite (LG2) gasified in air at 873 K for 1 hour. Weight loss 2.35%.

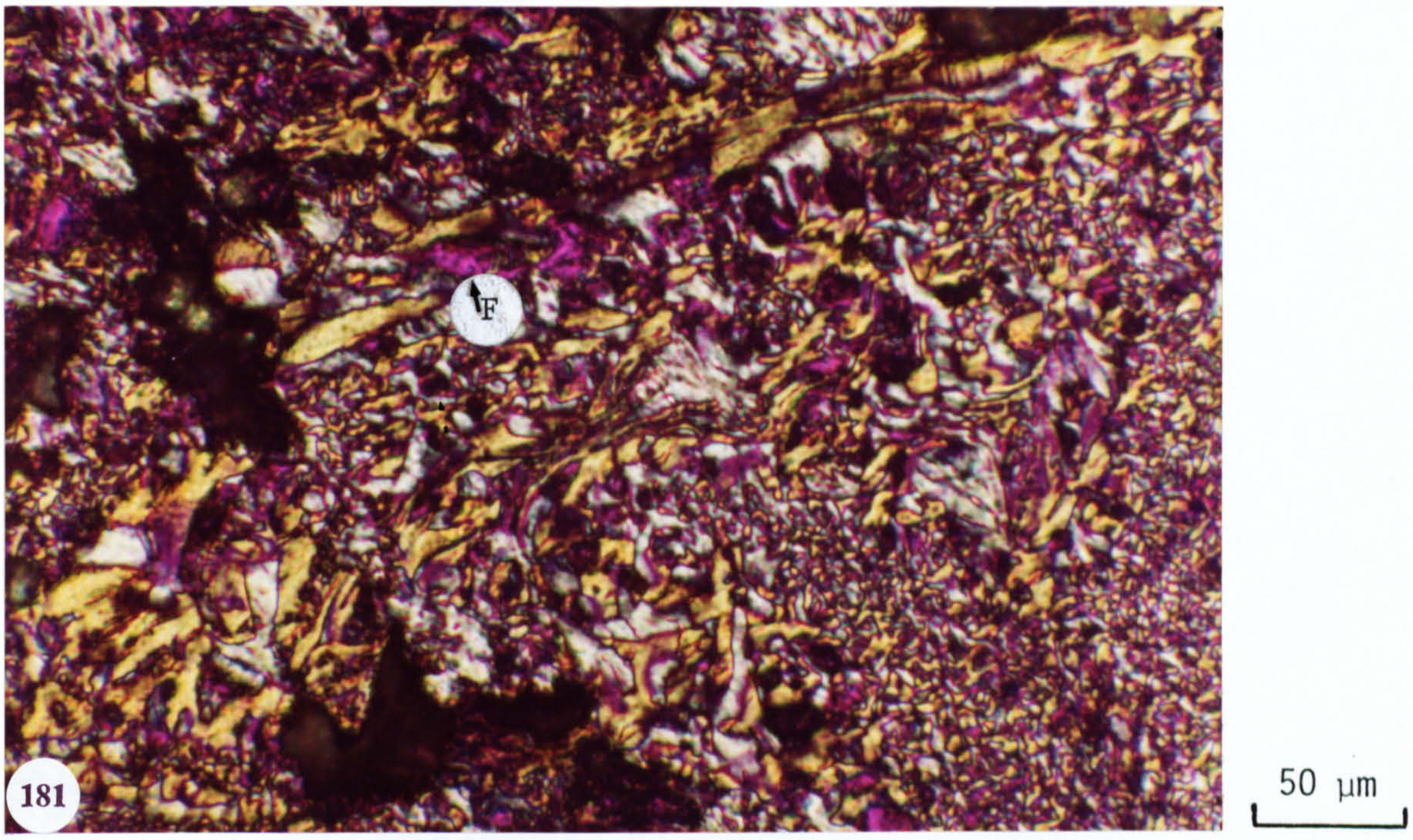


LIMA GRAPHITE

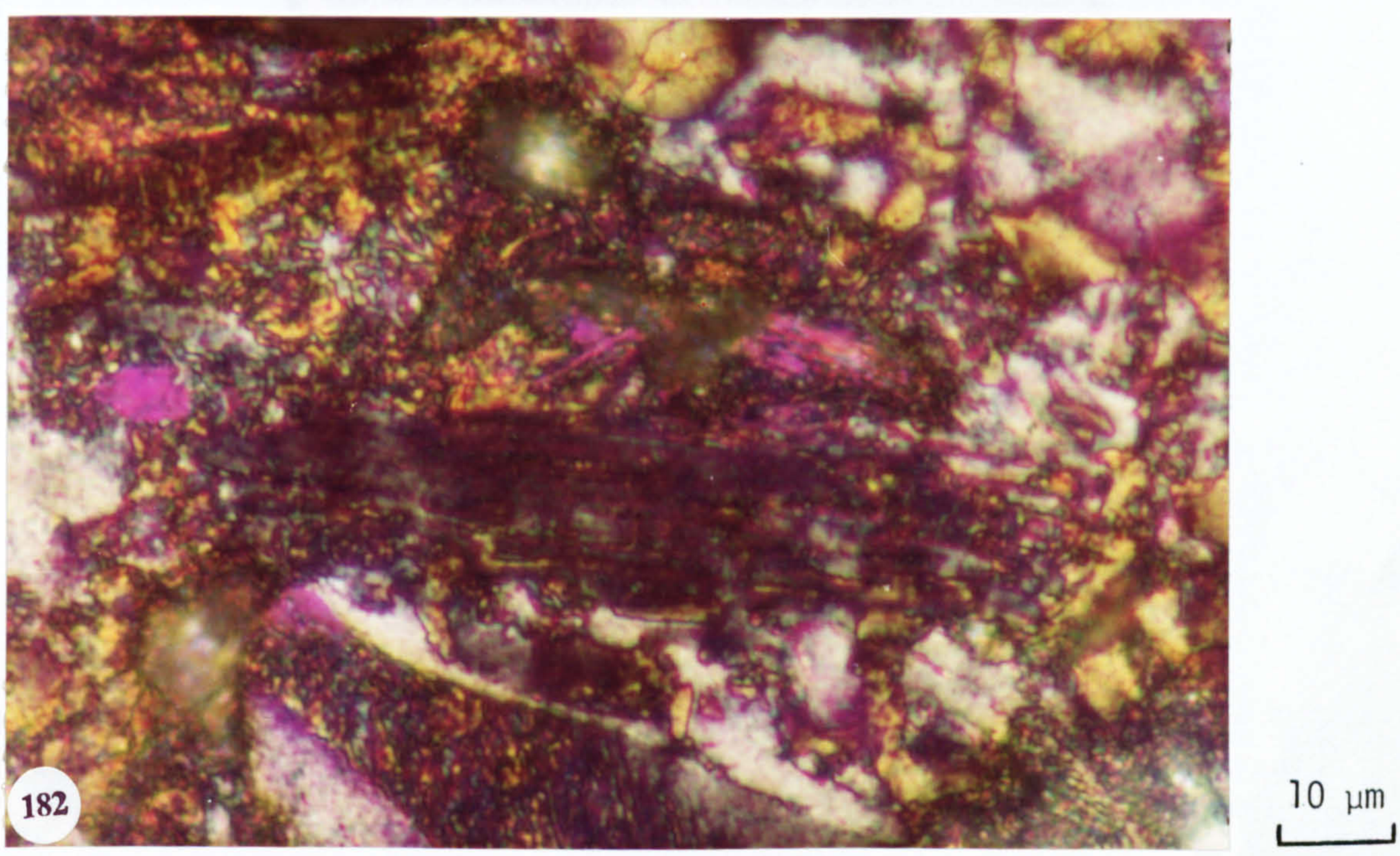


LIMA GRAPHITE

Figures 179 and 180. Optical micrographs of Lima Graphite (LG3) before gasification.

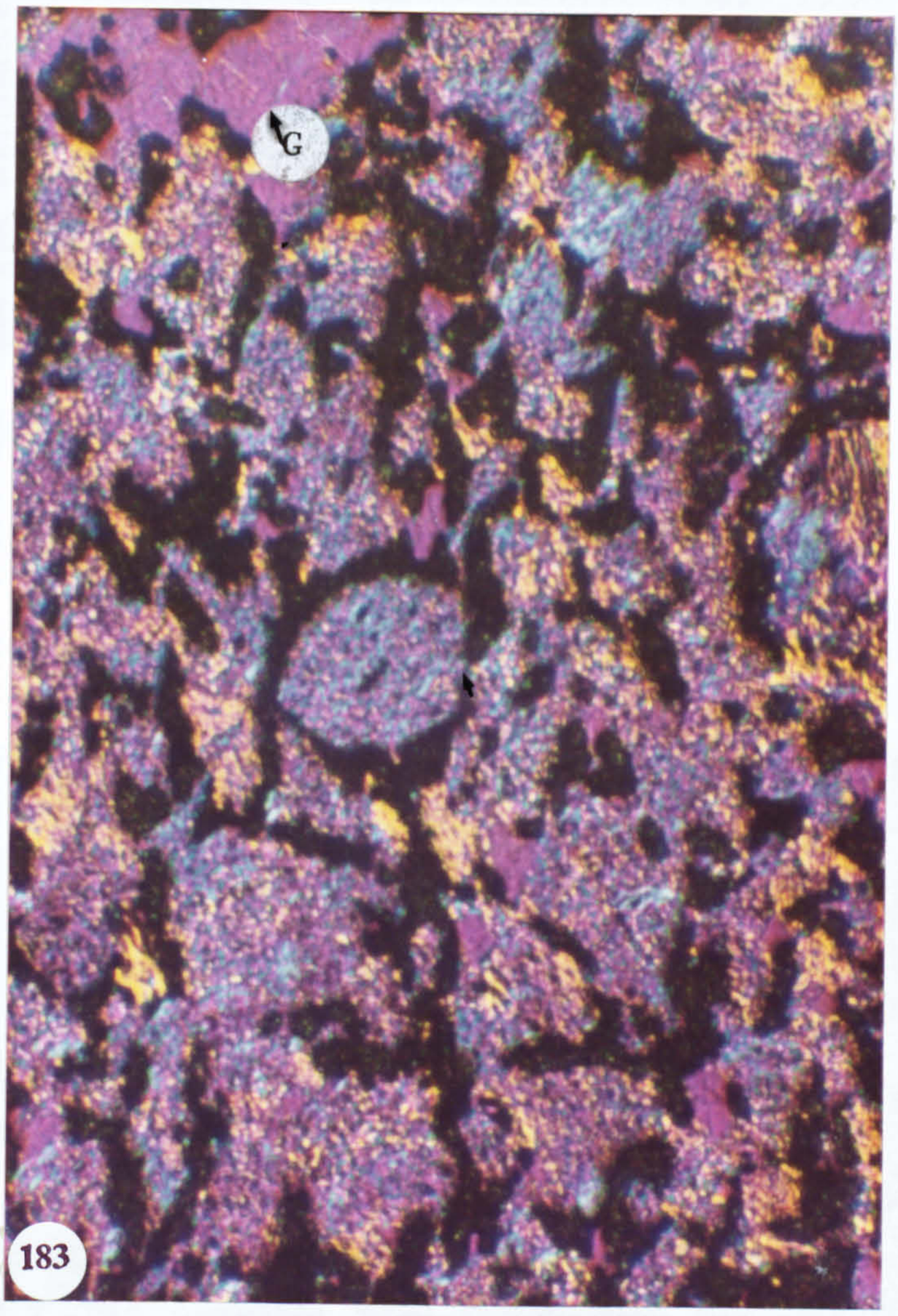


LIMA GRAPHITE



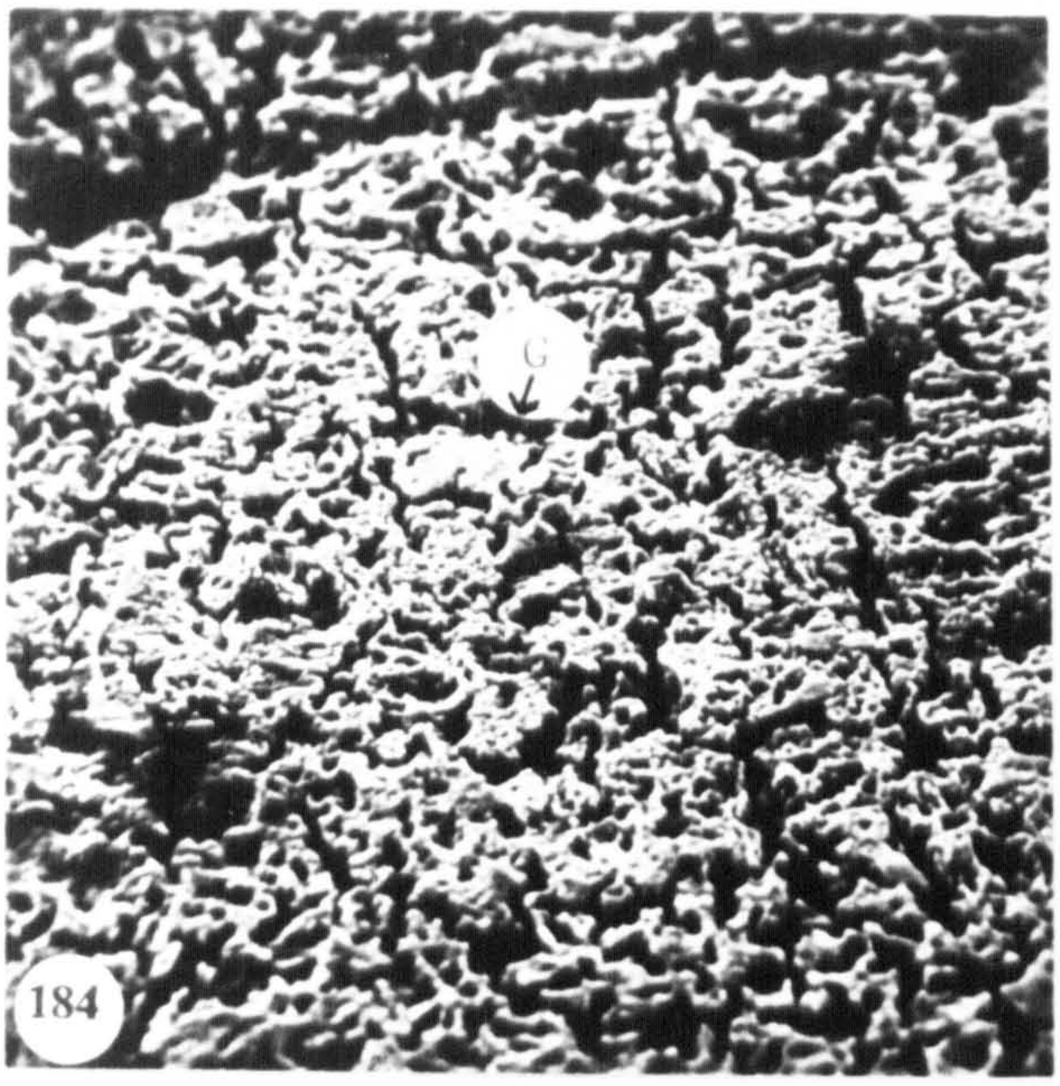
LIMA GRAPHITE

Figures 181 and 182. Optical micrographs of Lima Graphite (LG3) after gasification in air at 823 K for 1 hour. Weight loss 0.38%.

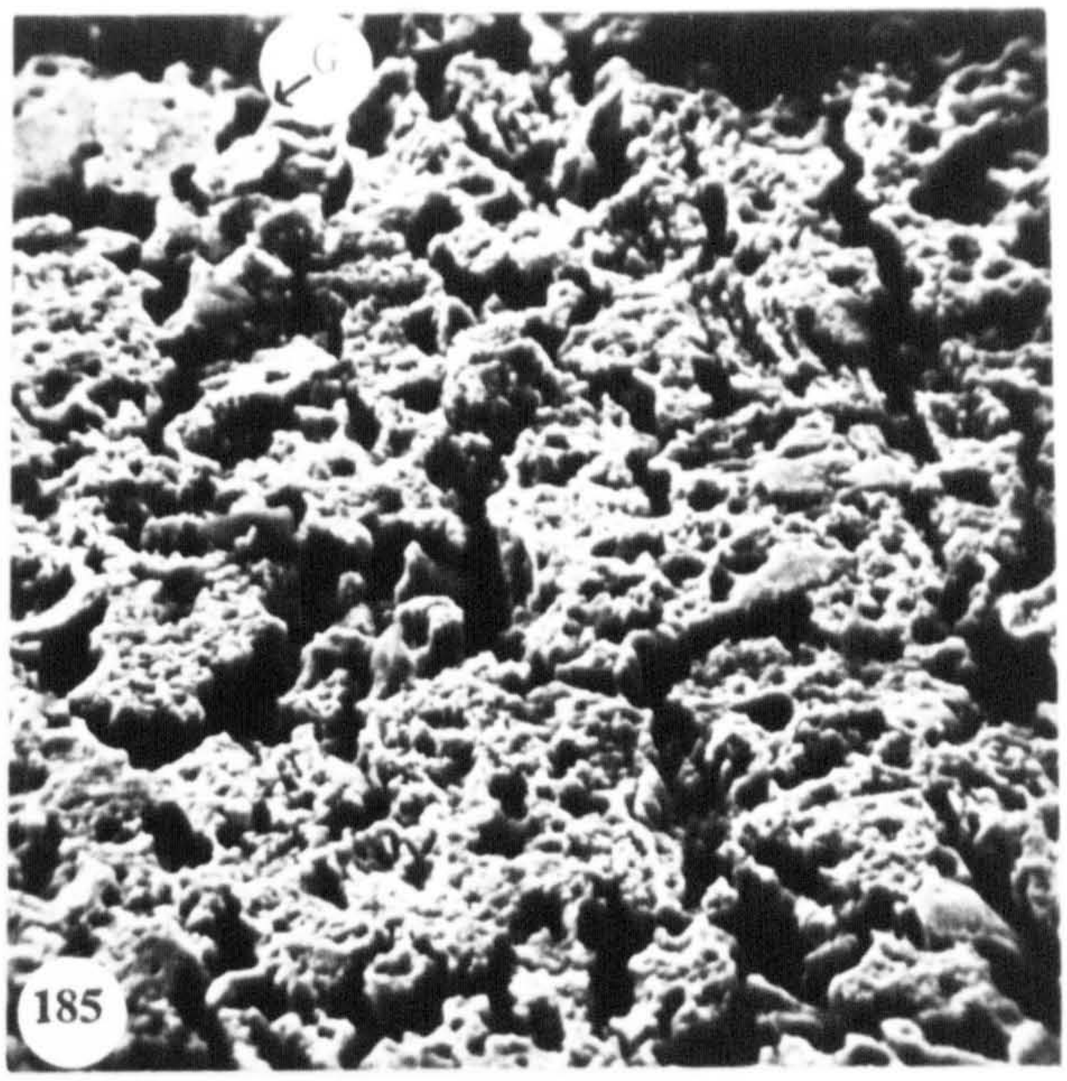


MORGANS UNIPORE GRAPHITE 100 µm

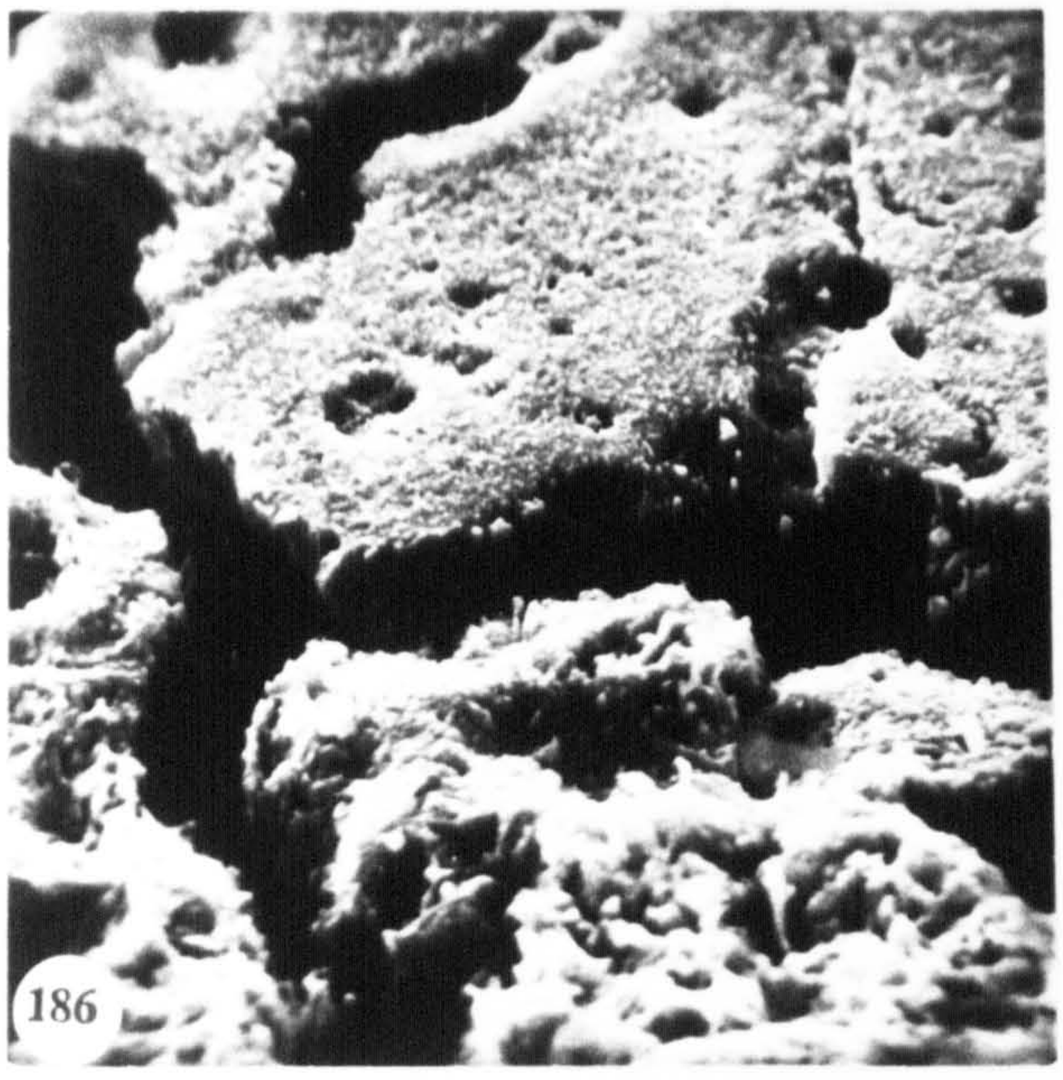
Figure 183. Optical micrograph of Morgans Unipore Graphite (MG1) before gasification.



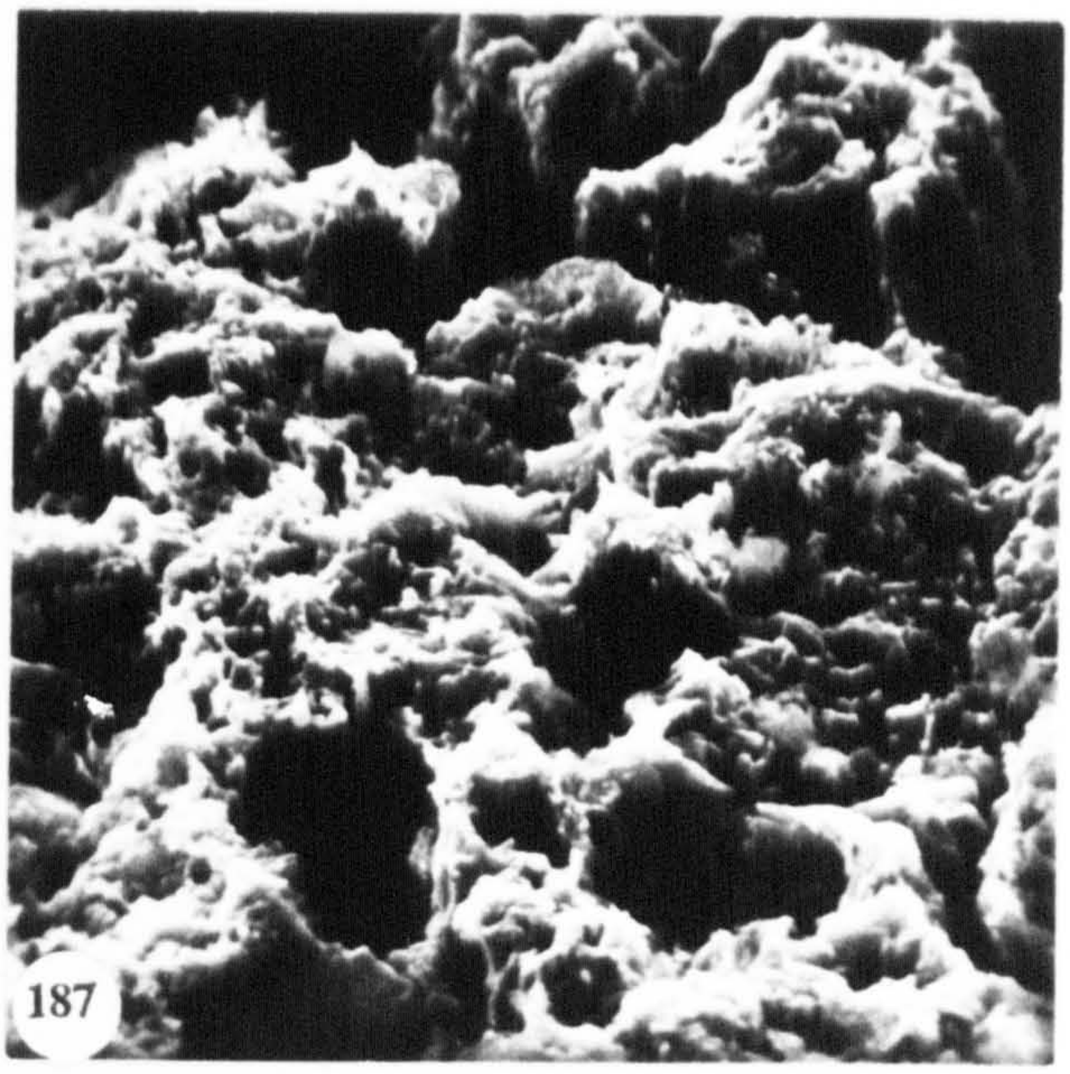
MORGANS UNIPORE GRAPHITE 100 µm



MORGANS UNIPORE GRAPHITE 50 µm

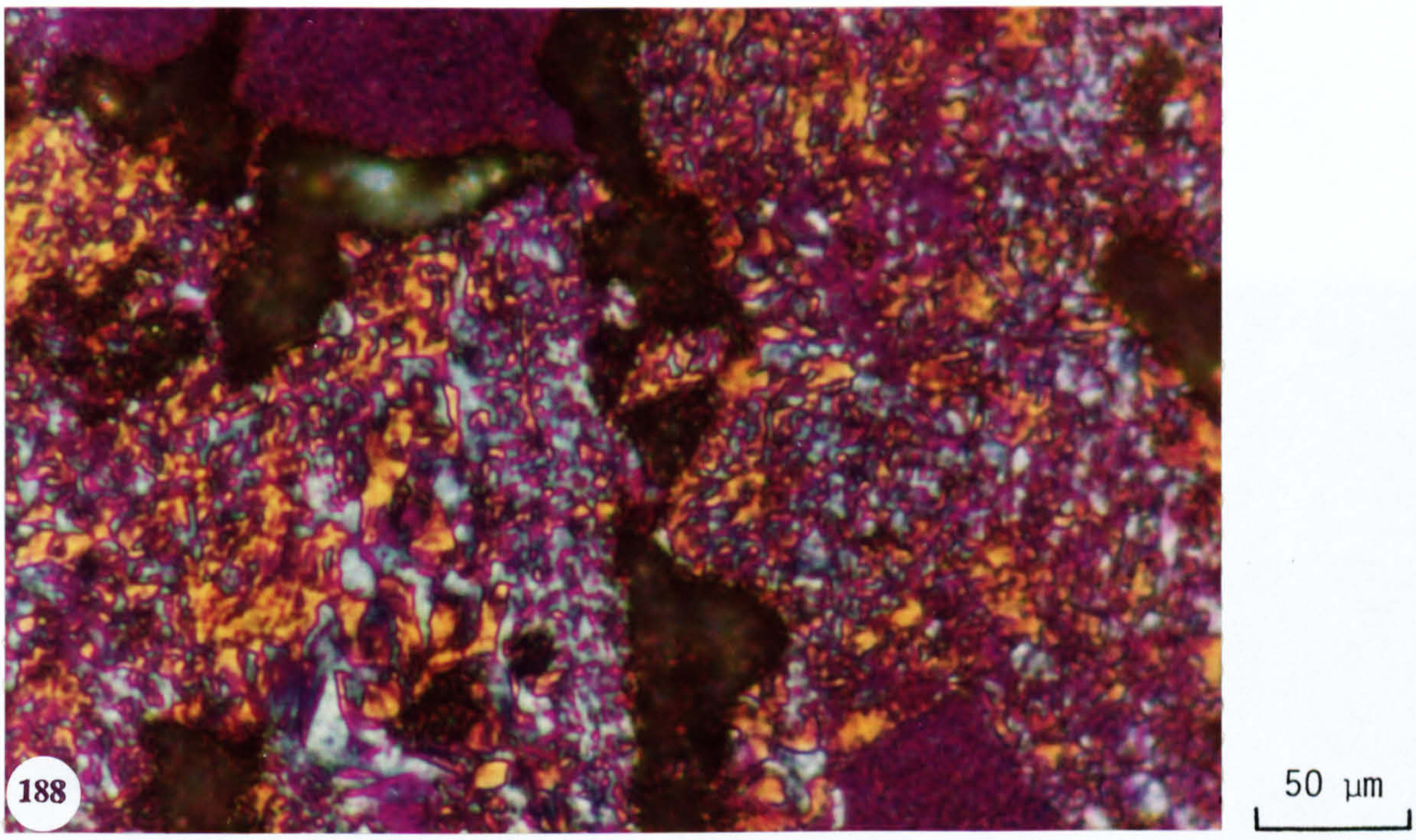


MORGANS UNIPORE GRAPHITE 10 µm

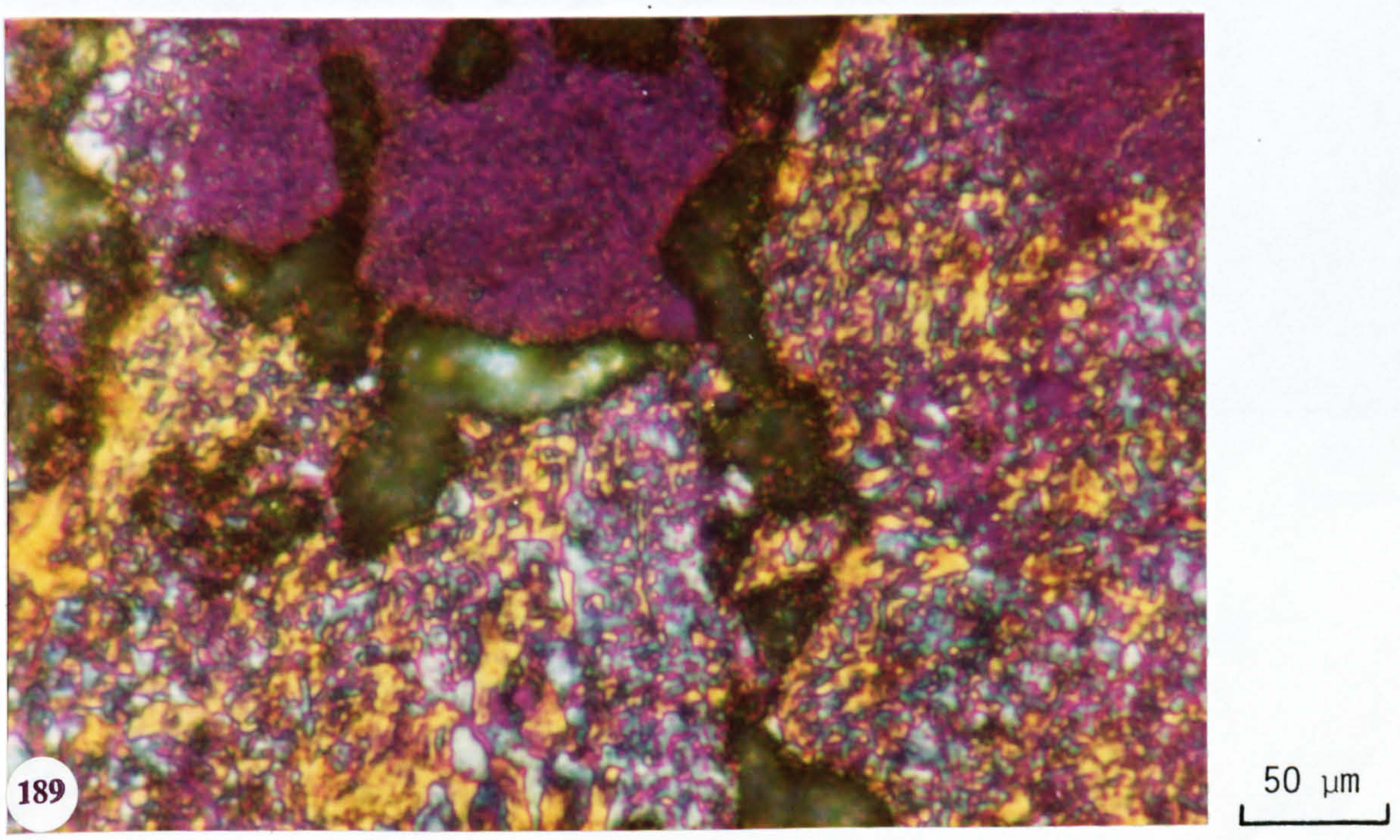


MORGANS UNIPORE GRAPHITE 10 µm

Figures 184 to 187. Scanning electron micrographs (stereoscan) of Morgans Graphite (MG1) gasified in air at 973 K for 1 hour. Weight loss 9.22%.

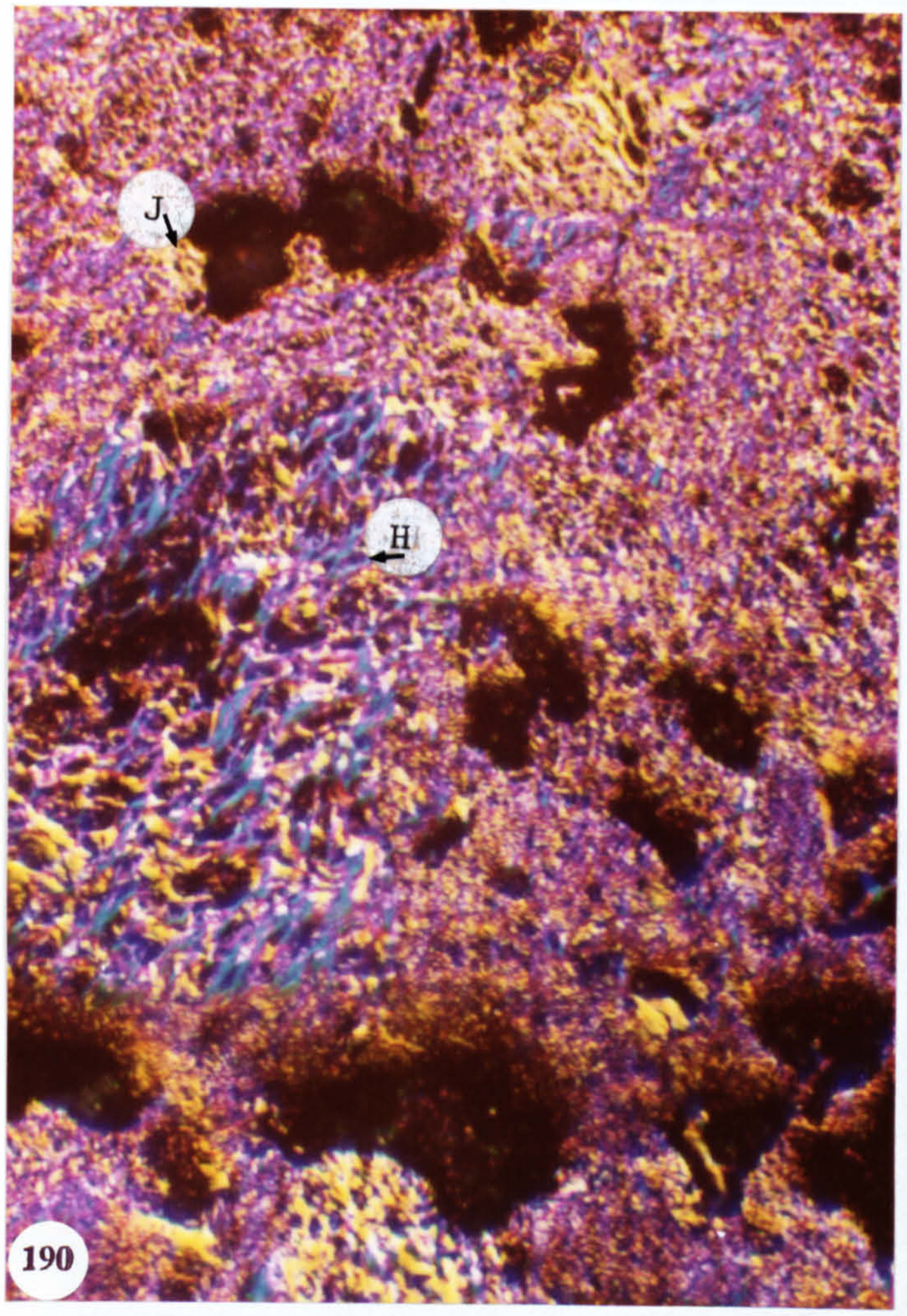


MORGANS UNIPORE GRAPHITE



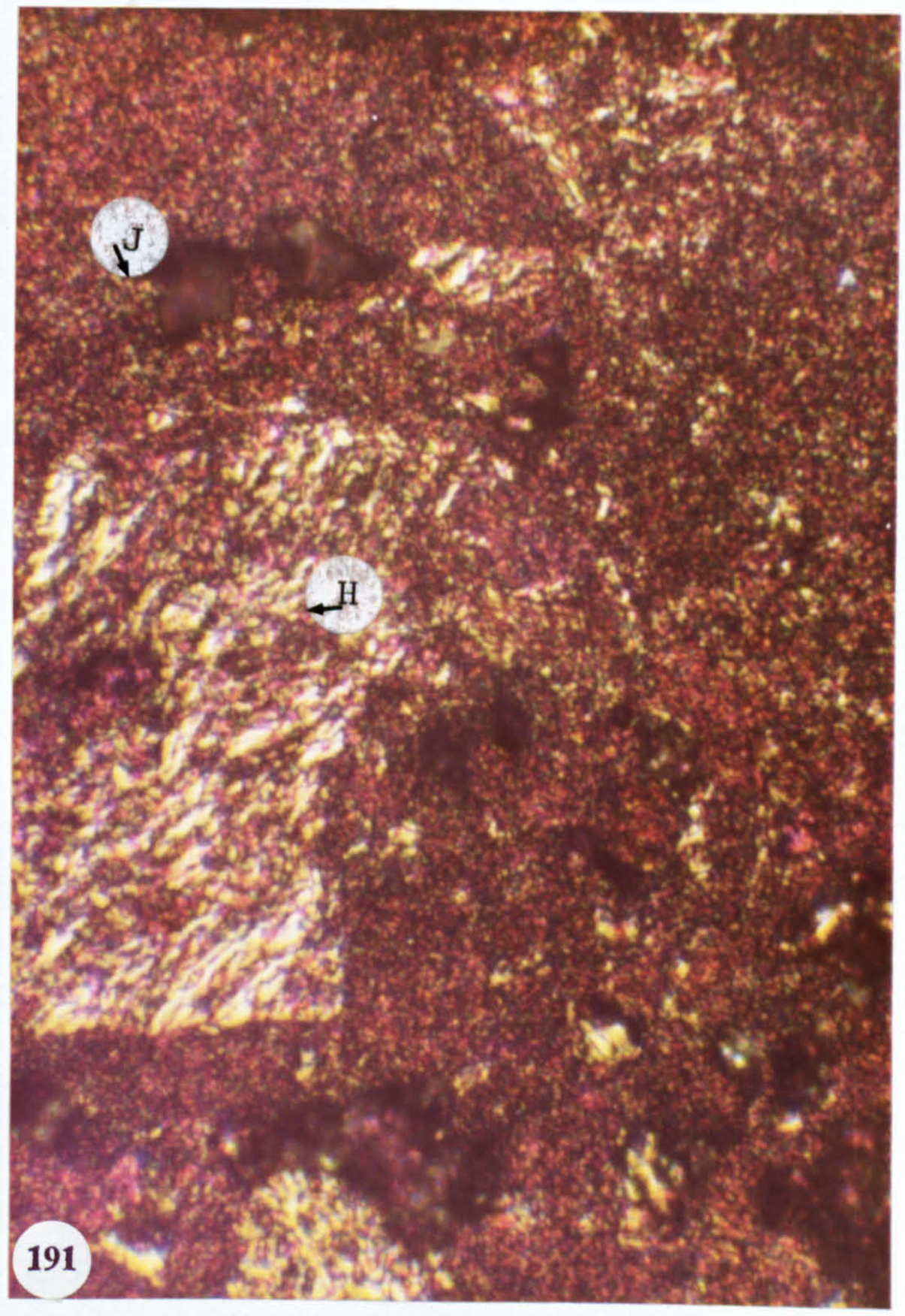
MORGANS UNIPORE GRAPHITE

Figures 188 and 189. Optical micrographs of Morgans Unipore Graphite (MG3), before and after gasification in air at 823 K for 1 hour. Weight loss 0.11%.



AGLMP GRAPHITE

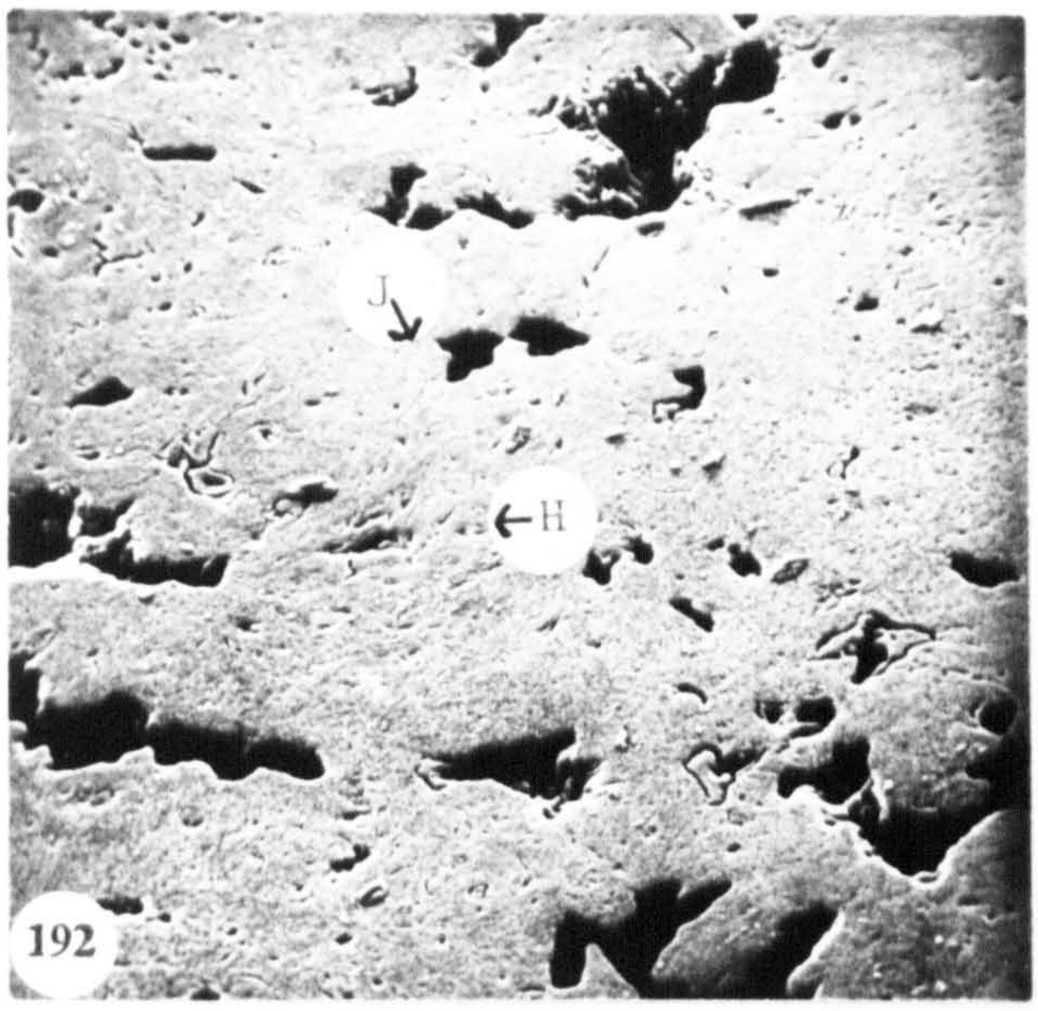
100 μm



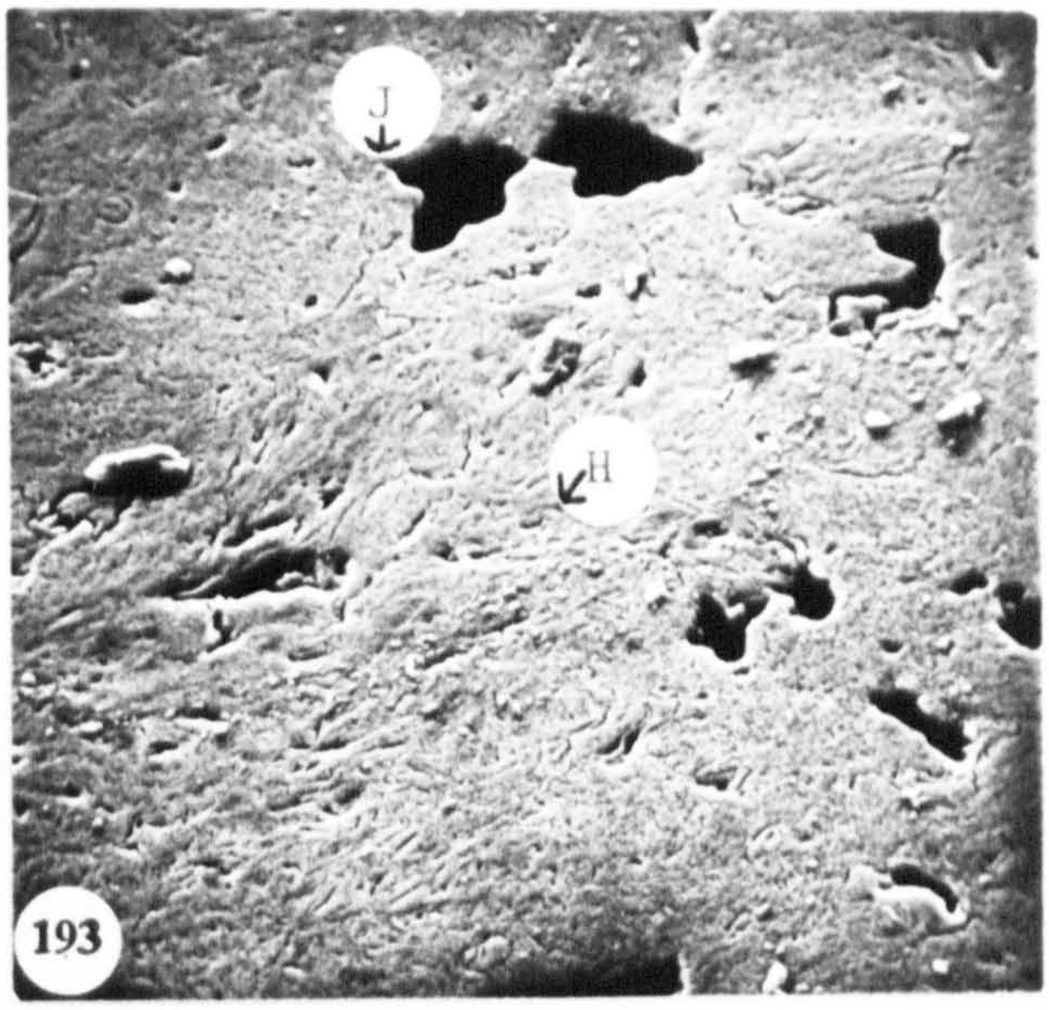
AGLMP GRAPHITE

100 μm

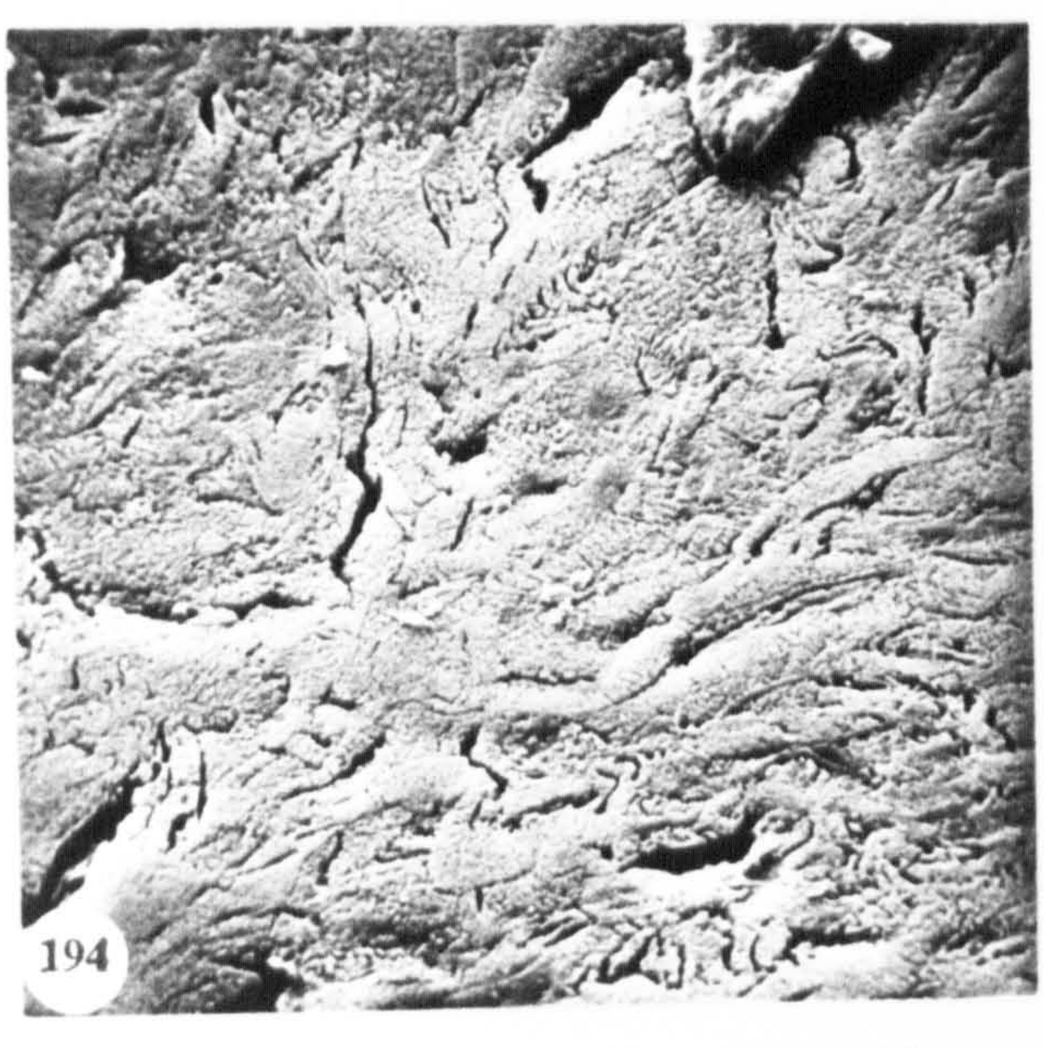
Figures 190 and 191. Optical micrographs of AGLMP Graphite (AG1) before and after gasification in air at 873 K for 1 hour. Weight loss 0.48%.



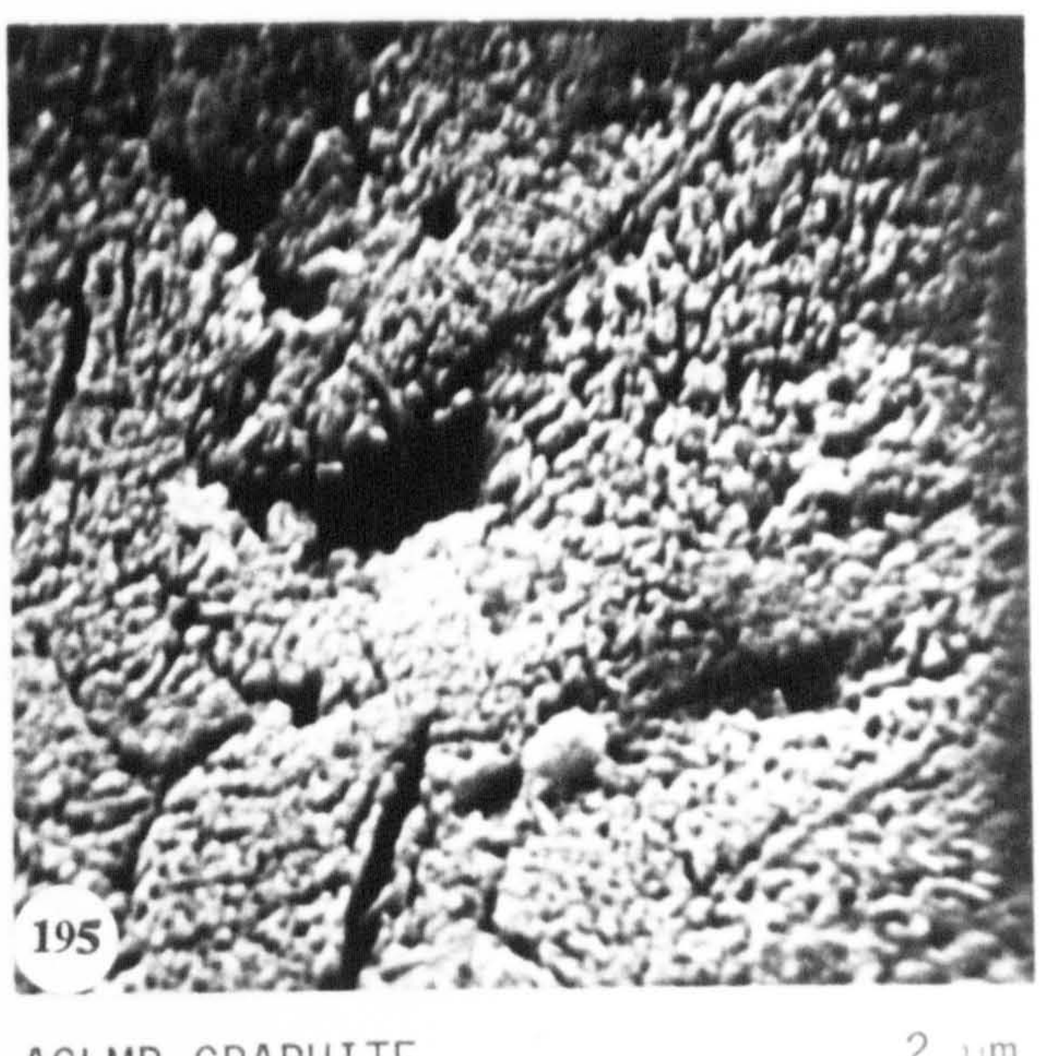
AGLMP GRAPHITE 100 µm



AGLMP GRAPHITE 50 µm

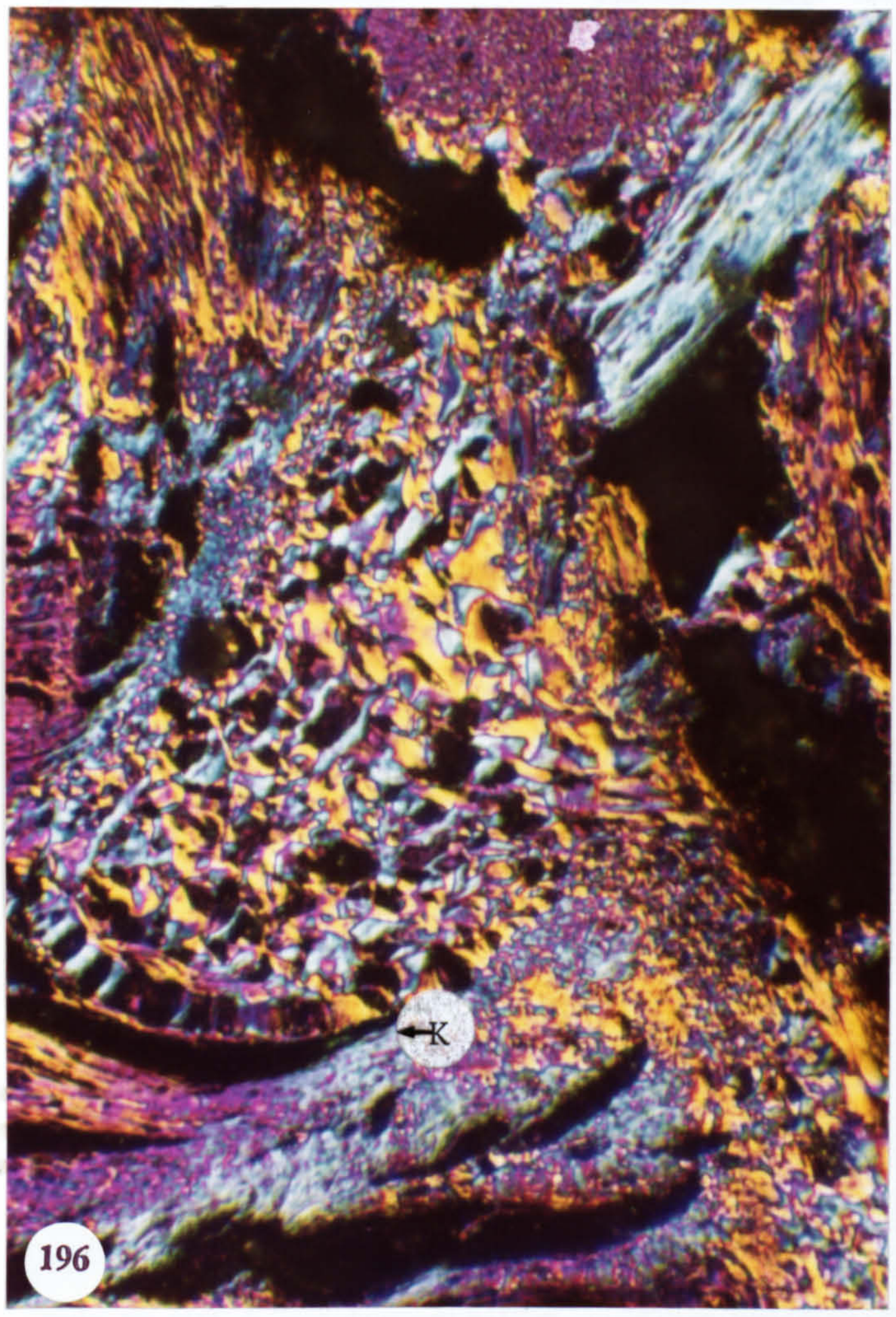


AGLMP GRAPHITE 10 µm

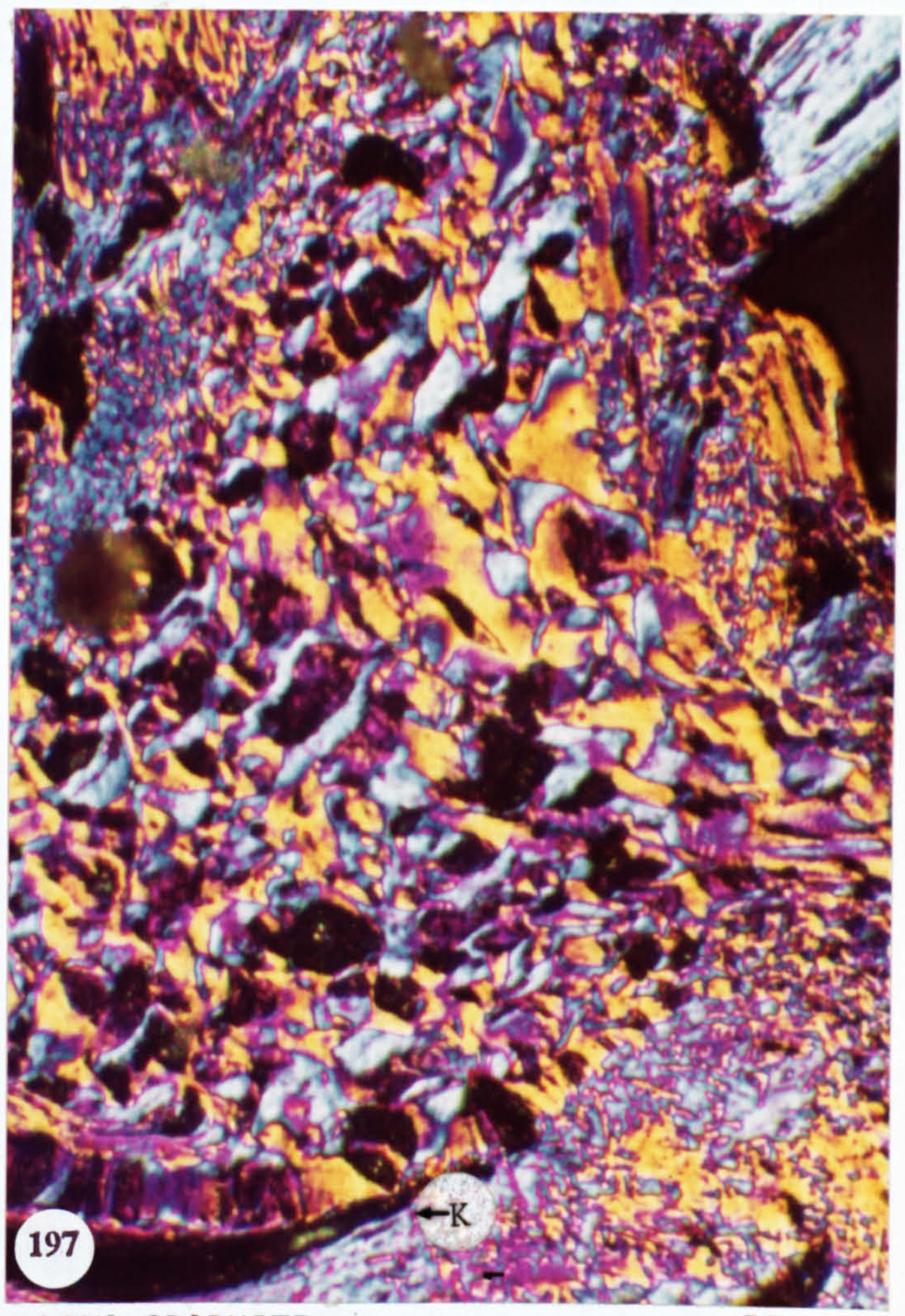


AGLMP GRAPHITE 2 µm

Figures 192 to 195. Scanning electron micrographs (stereoscan) of AGLMP Graphite (AG1) after gasification in air at 873 K for 1 hour. Weight loss 0.48%.

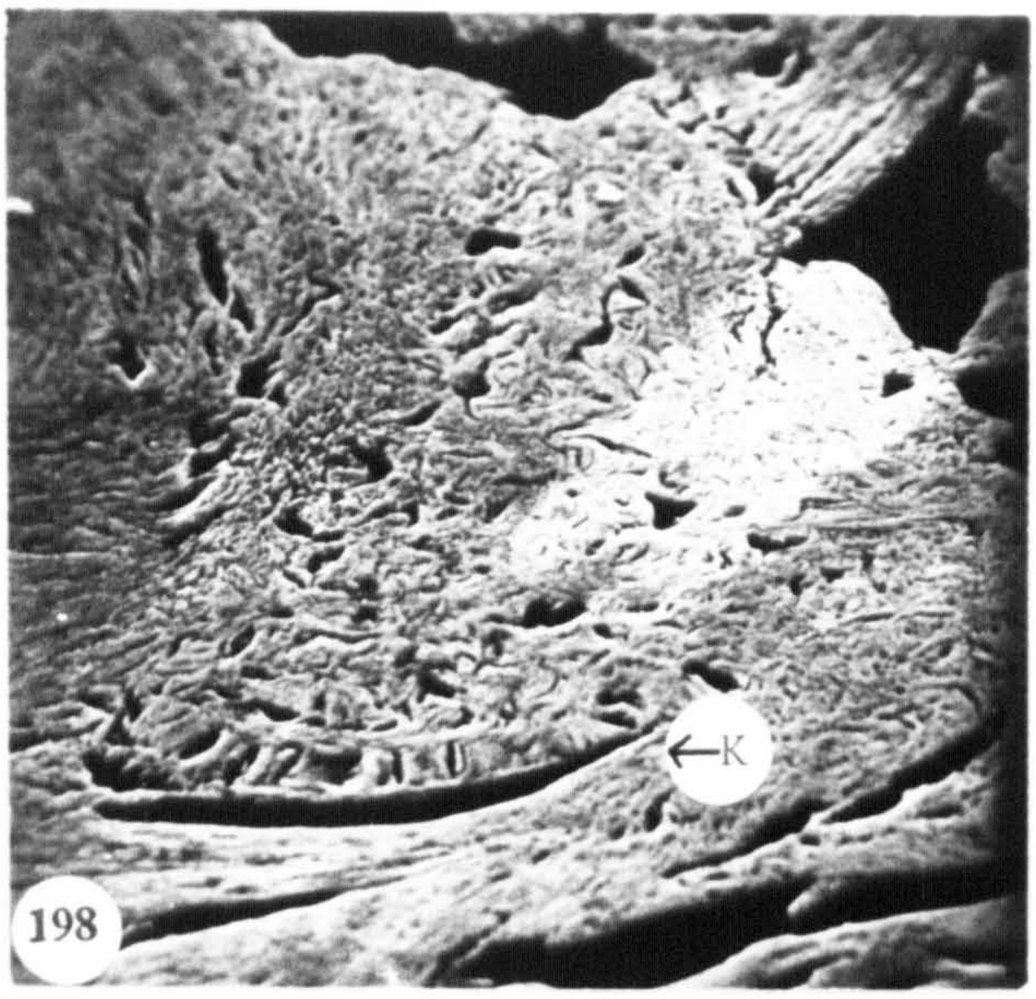


LIMA GRAPHITE 100 µm



LIMA GRAPHITE 50 µm

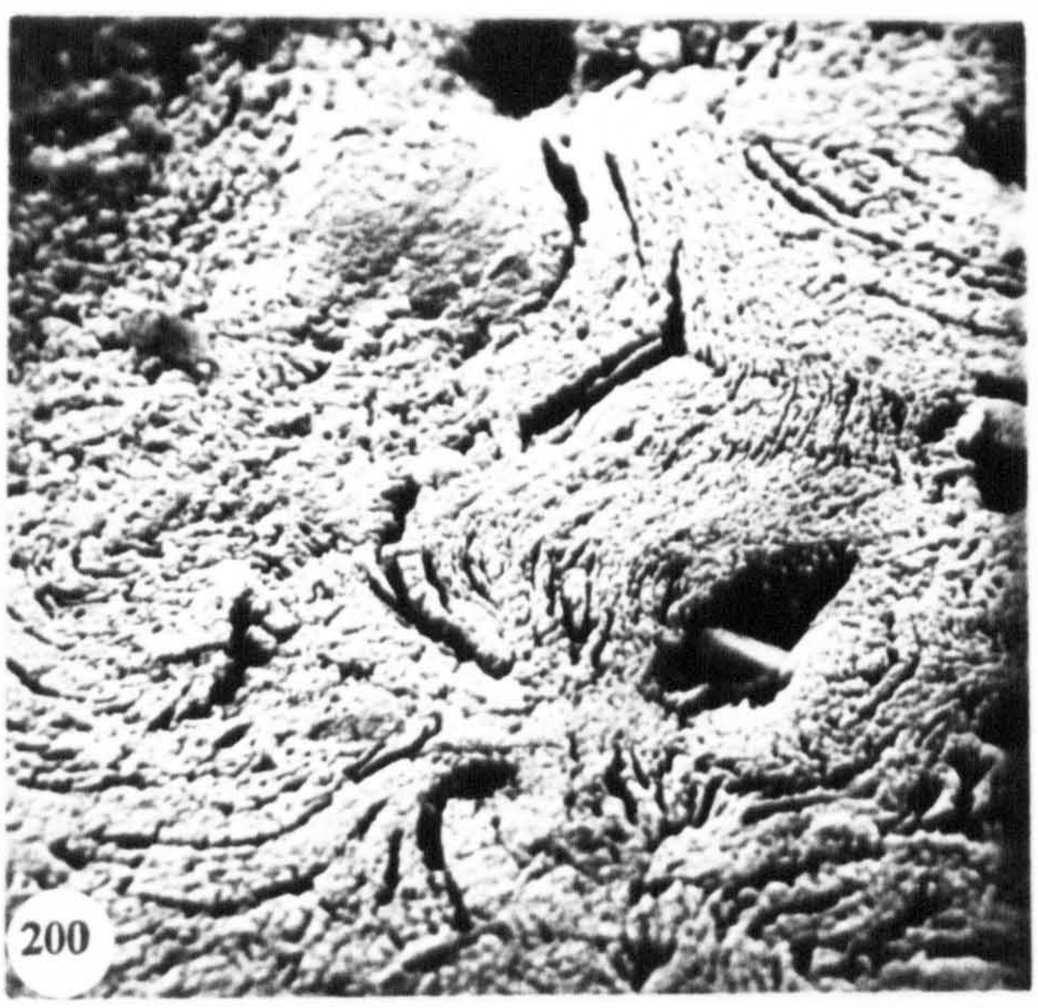
Figures 196 and 197. Optical micrographs of Lima Graphite (LG4) before gasification.



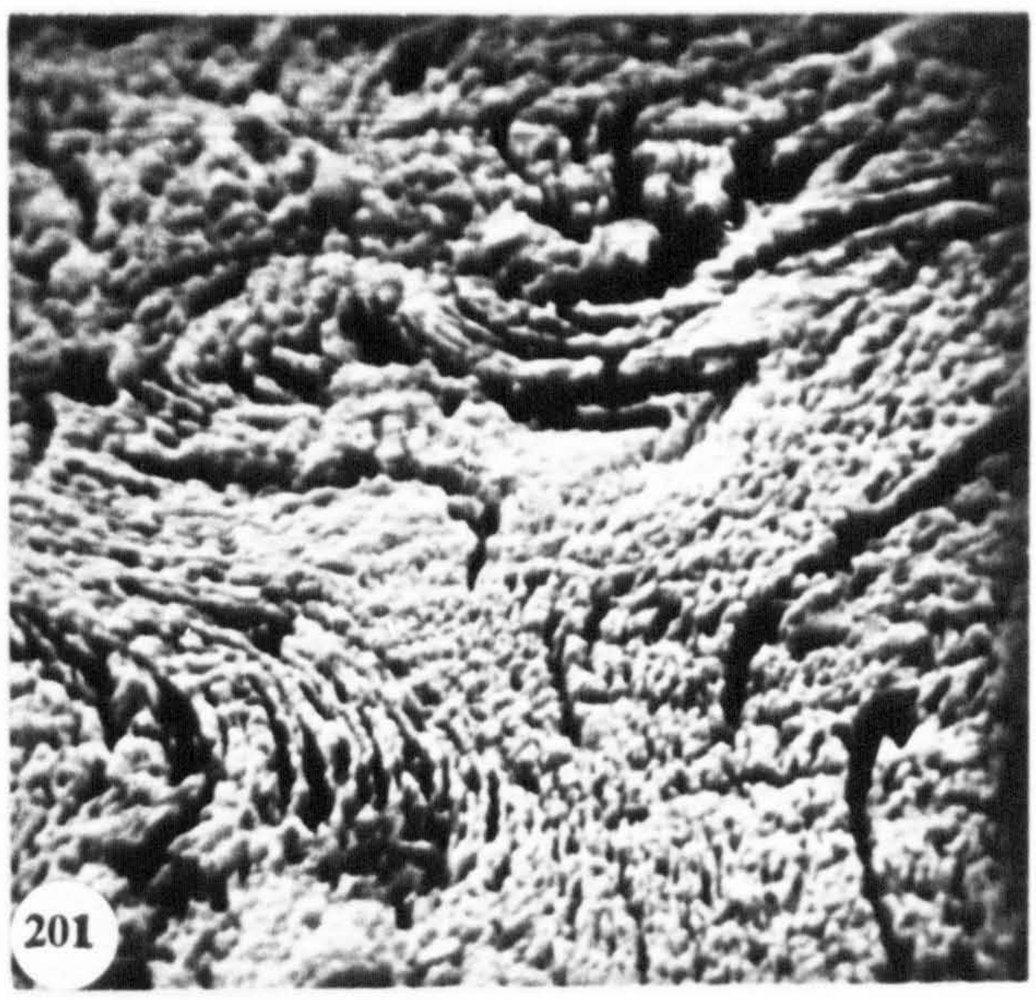
LIMA GRAPHITE 50 μm



LIMA GRAPHITE 10 μm

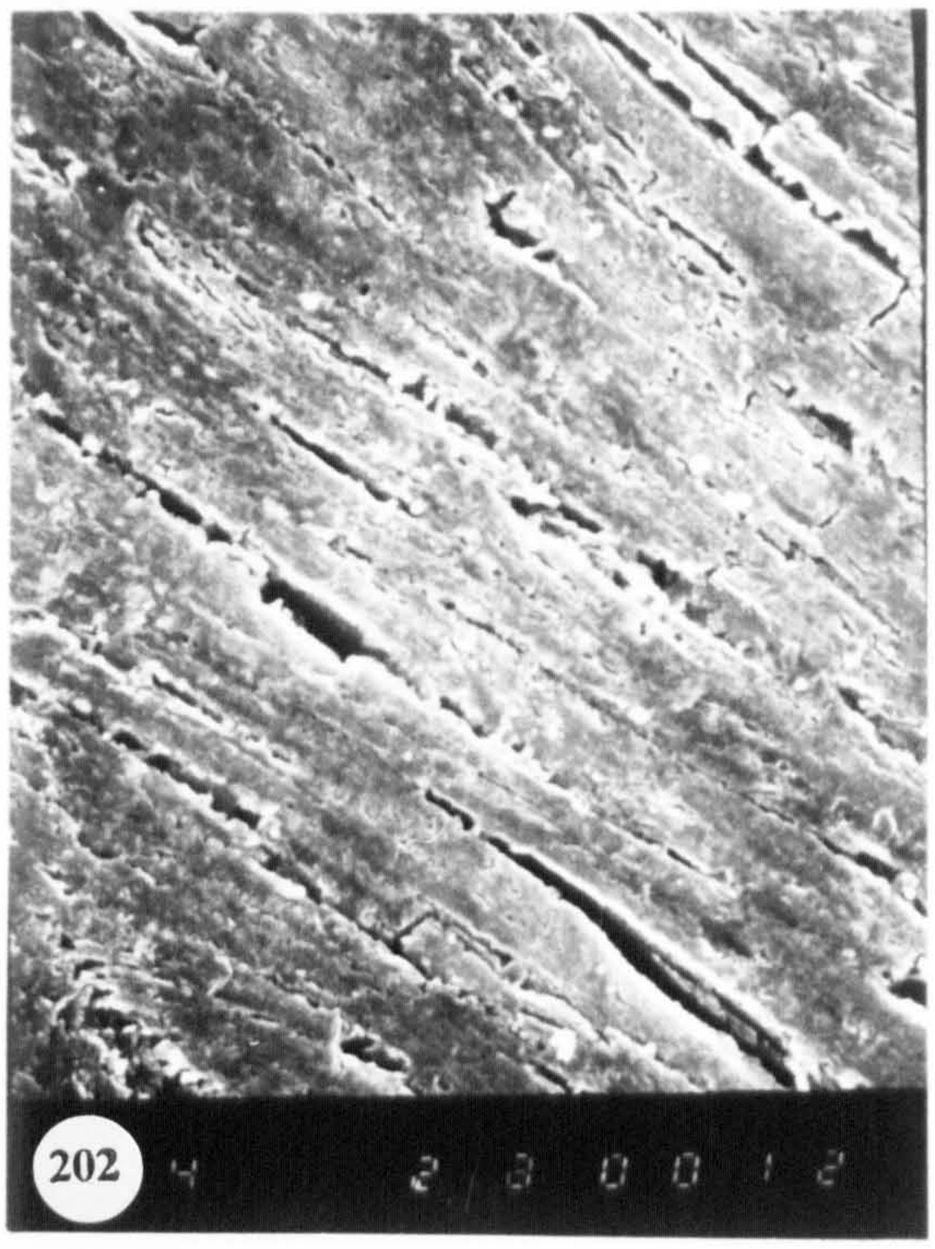


LIMA GRAPHITE 5 μm

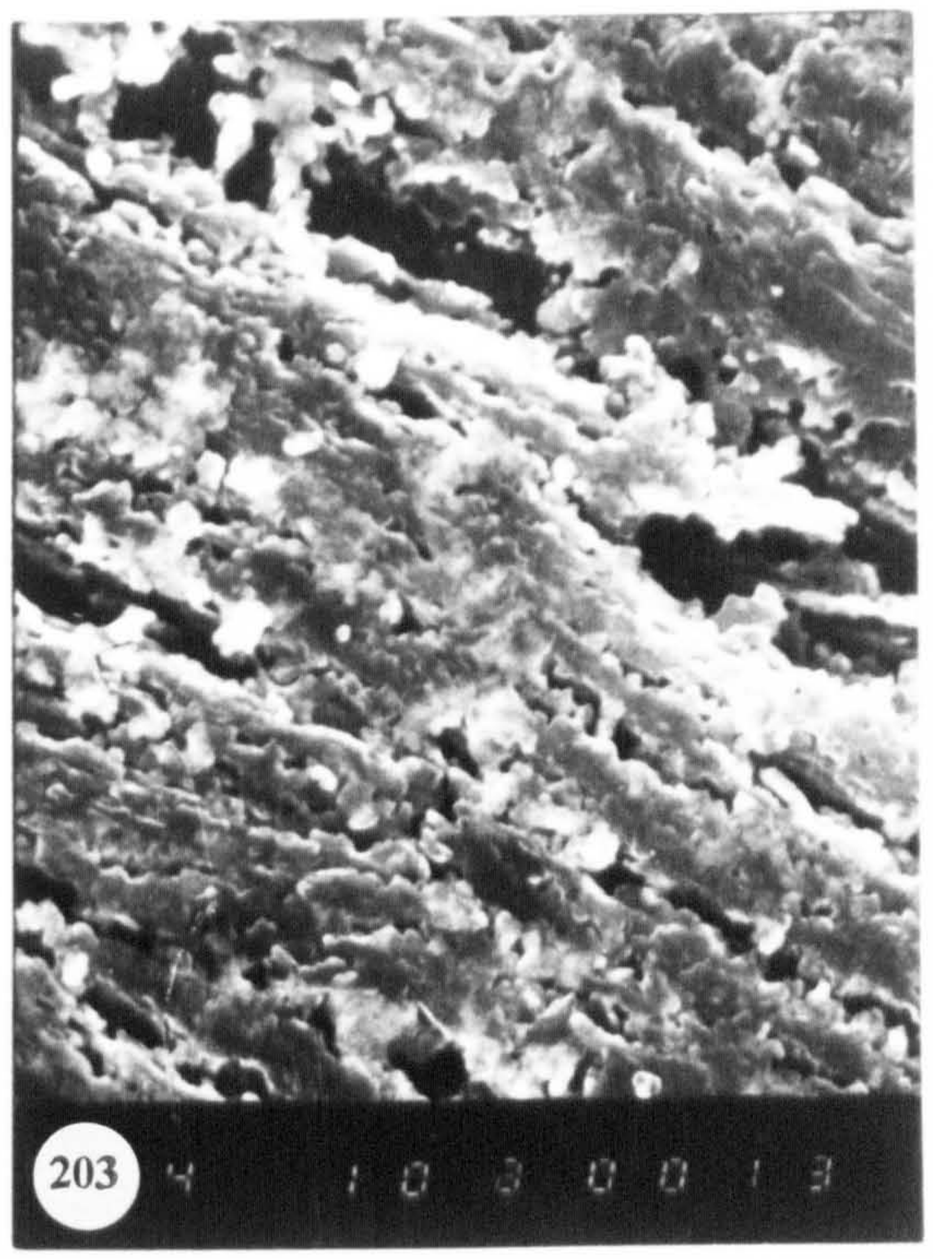


LIMA GRAPHITE 2 μm

Figures 198 to 201. Scanning electron micrographs (stereoscan) of Lima Graphite (LG4) gasified in carbon dioxide at 973 K for 16 hours. Weight loss 0.83%.



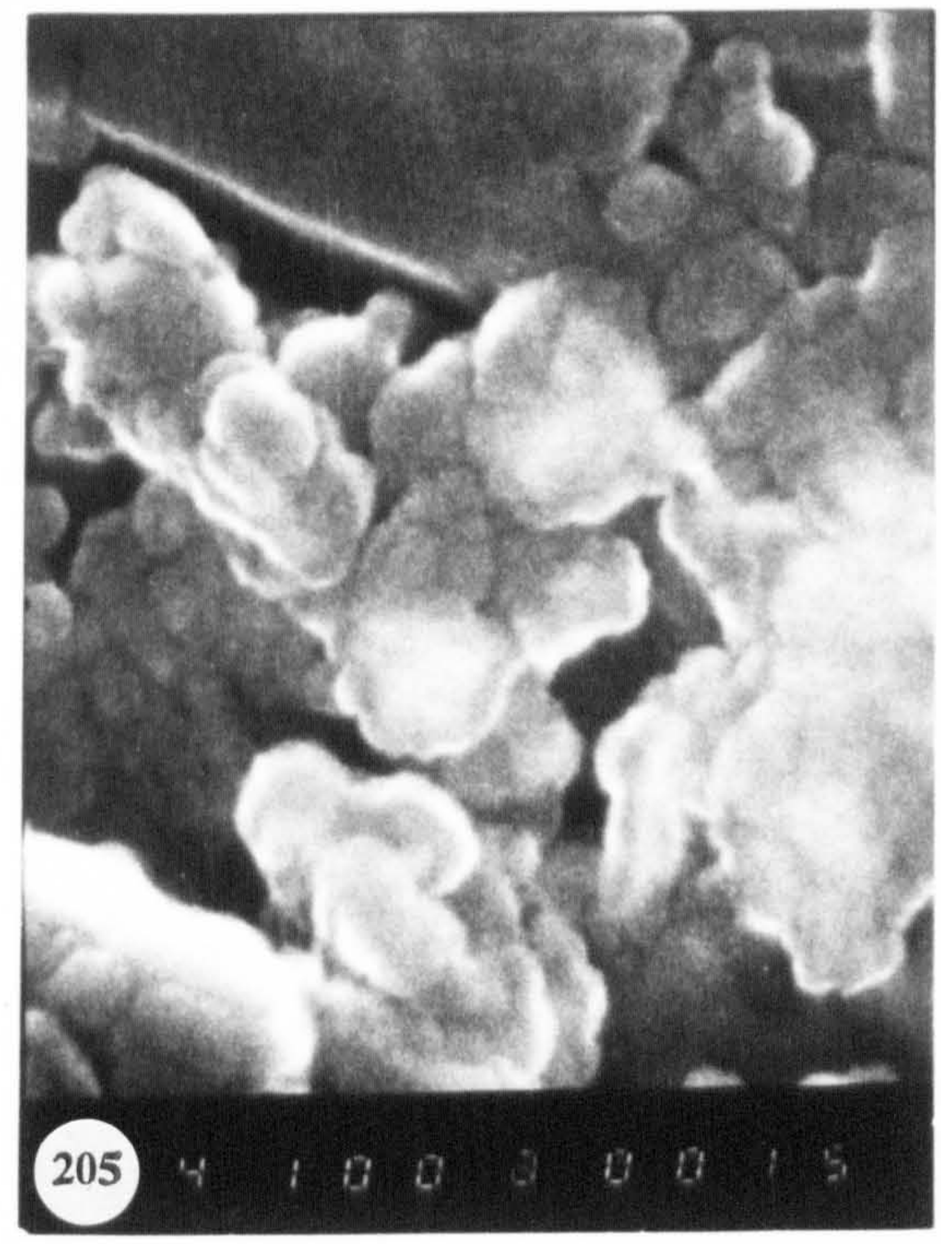
LIMA GRAPHITE. 5 µm



LIMA GRAPHITE. 1 µm

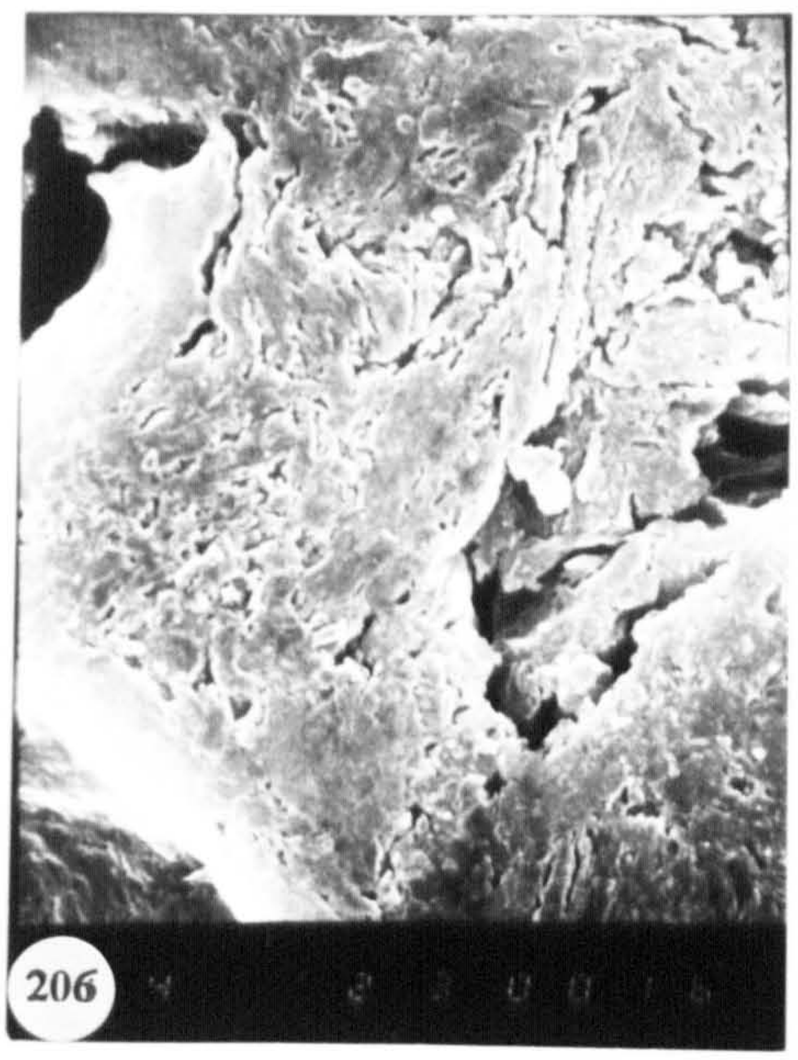


LIMA GRAPHITE. 200 nm

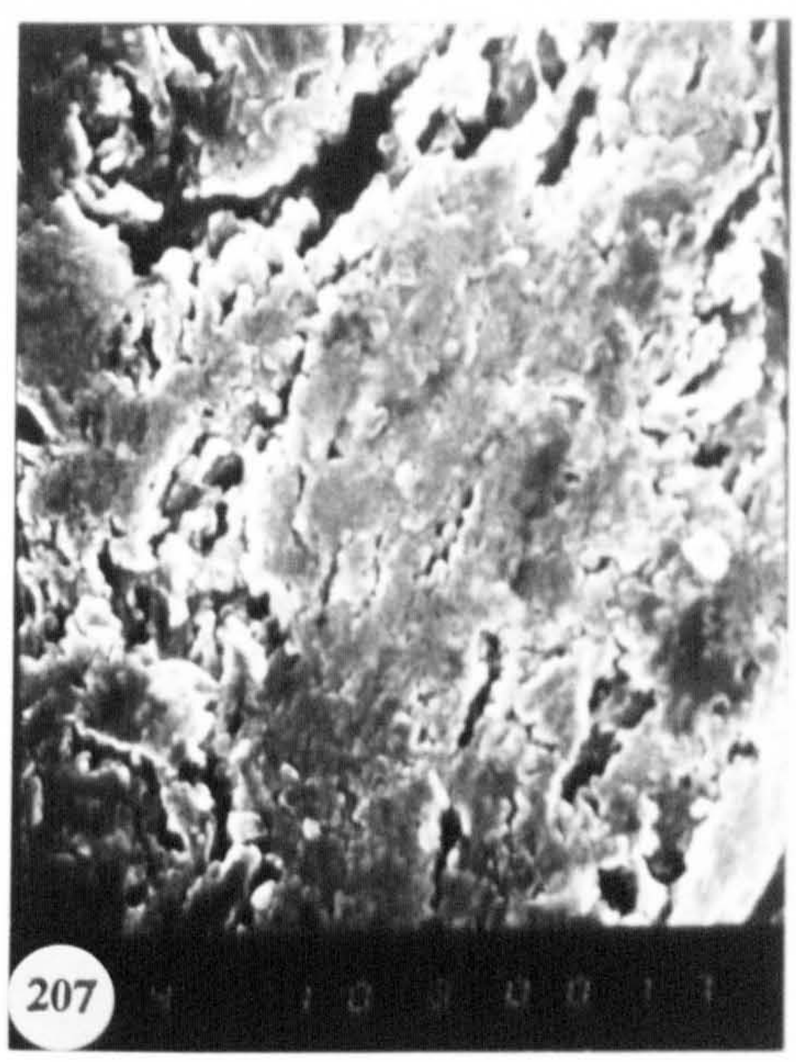


LIMA GRAPHITE. 100 nm

Figures 202 to 205 Scanning electron micrographs (JEOL 100C - ASID-4D) of Lima graphite oxidised in carbon dioxide at 700°C for 16 hours, weight loss 0.83%.

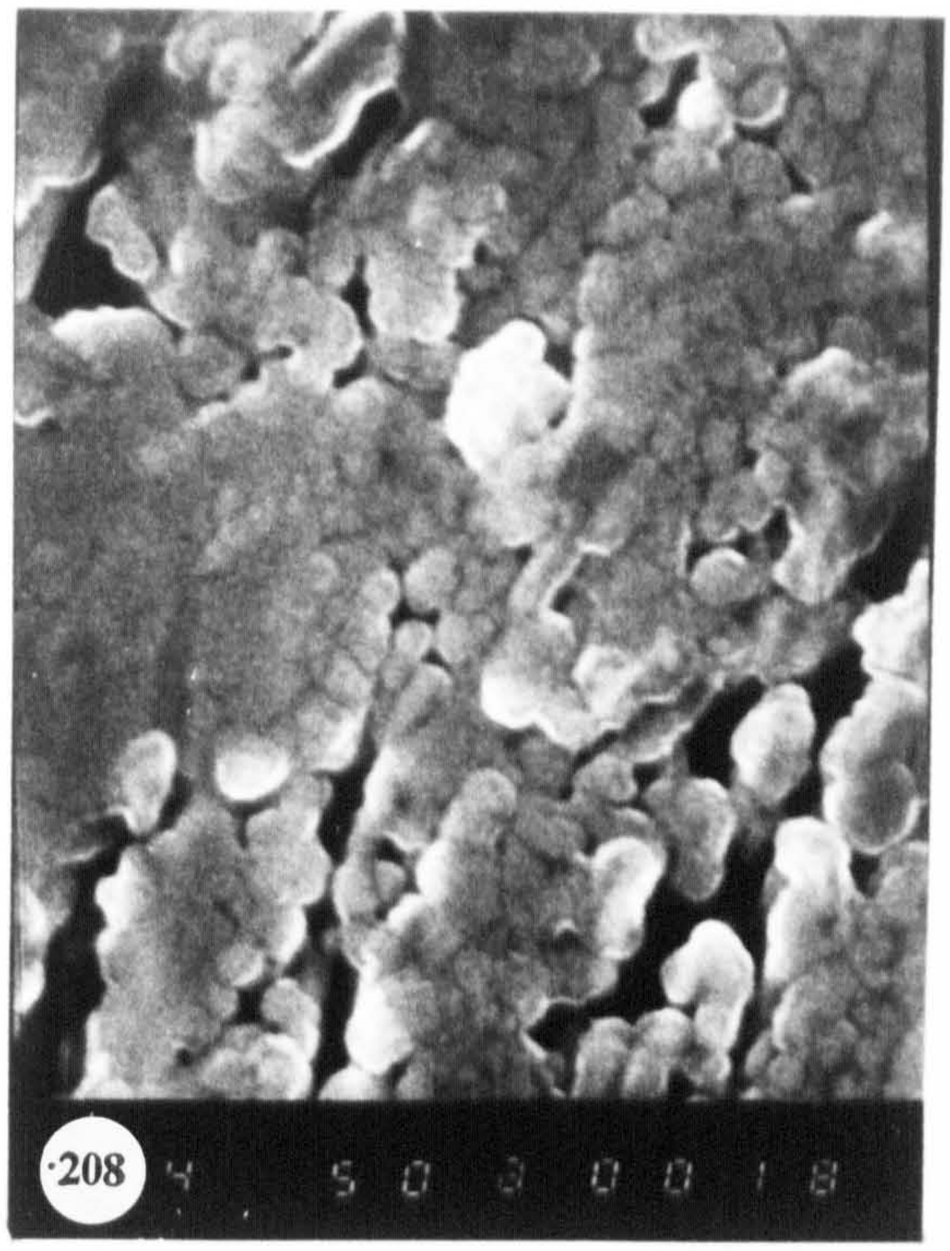


LIMA GRAPHITE. 5 µm

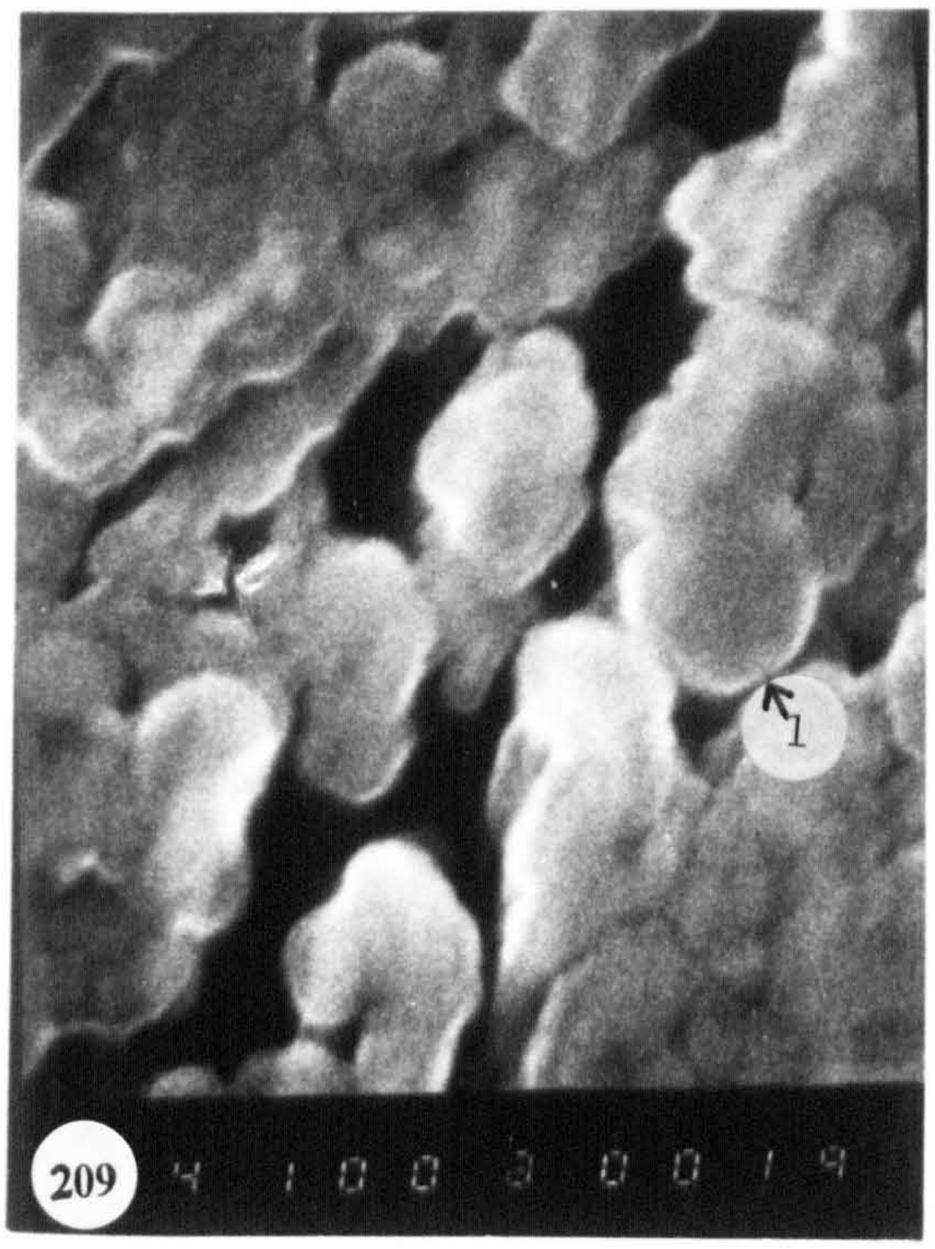


LIMA GRAPHITE. 1 µm

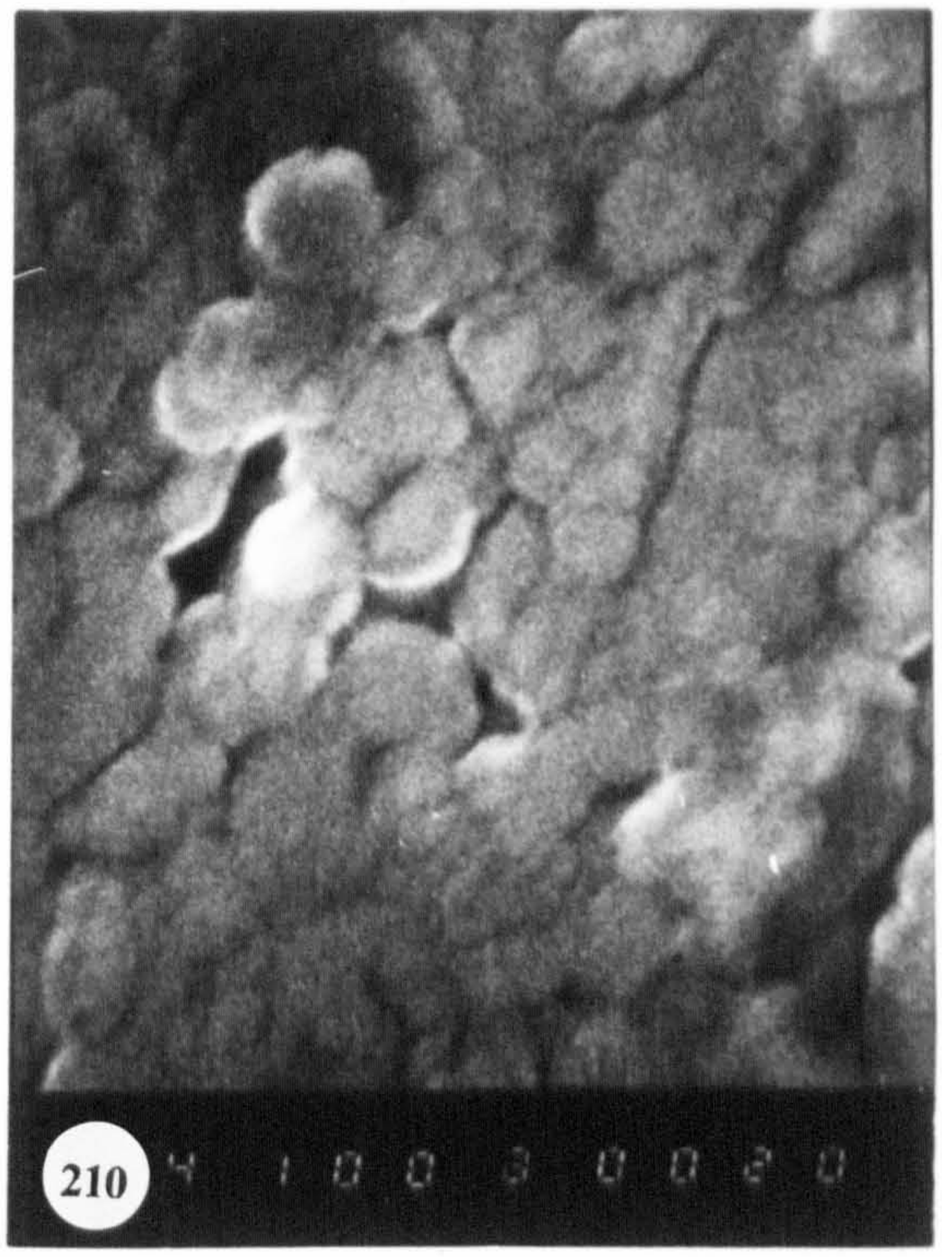
Figures 206 and 207 Scanning electron micrographs (JEOL 100C - ASID-4D) of Lima graphite oxidised in carbon dioxide at 700°C for 16 hours, weight loss 0.83%.



LIMA GRAPHITE. 200 nm

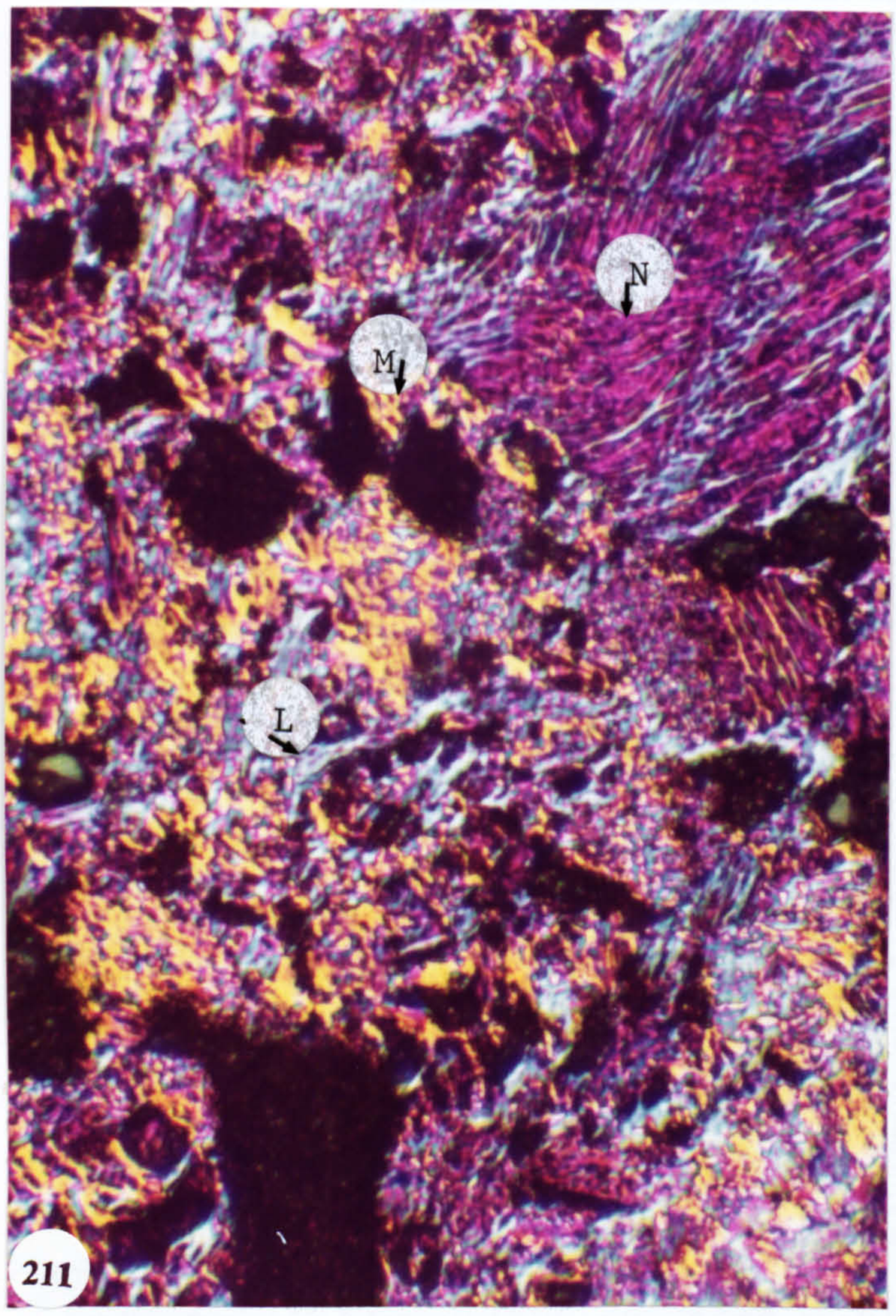


LIMA GRAPHITE. 100 nm



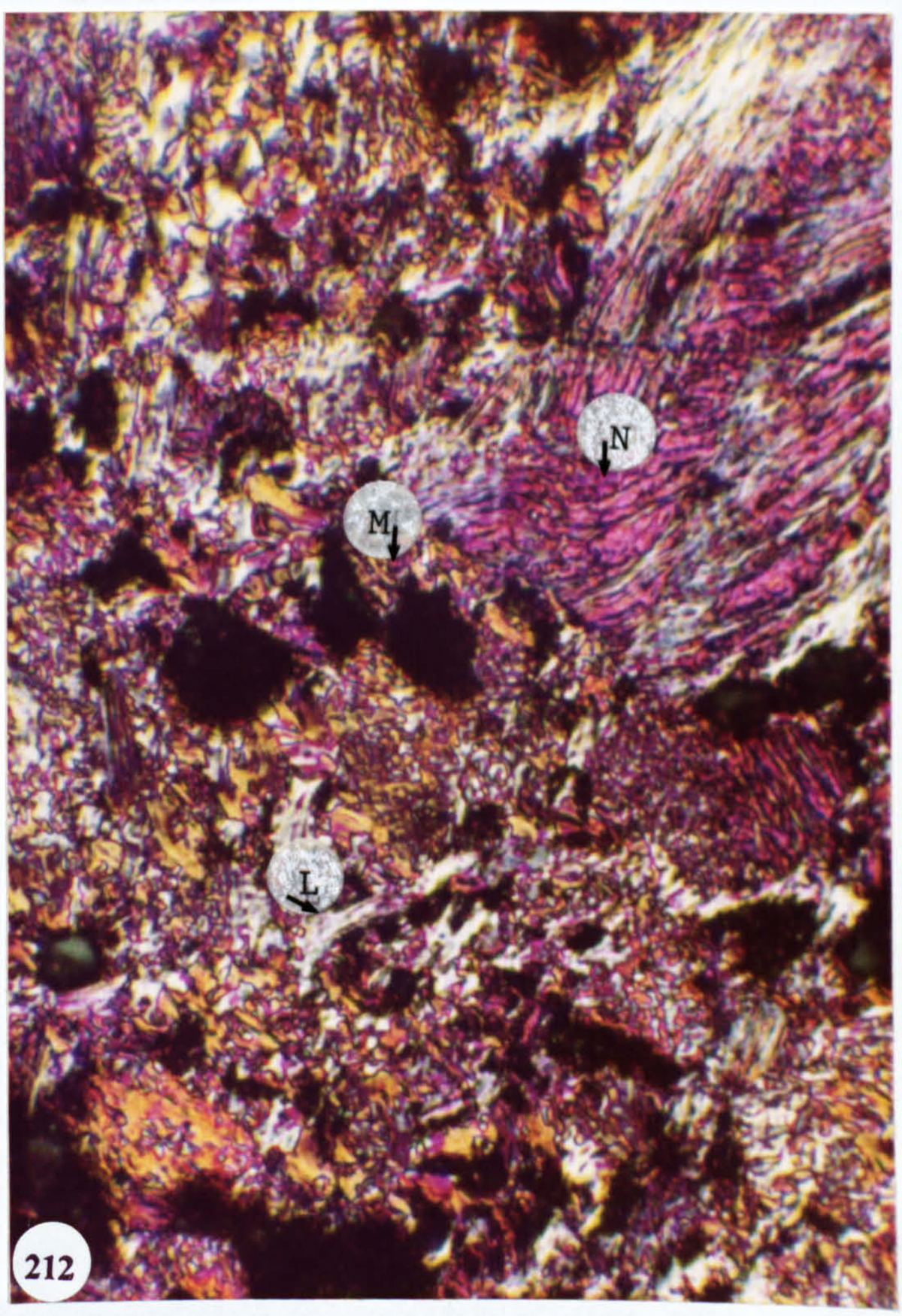
LIMA GRAPHITE. 100 nm

Figures 208 to 210 Scanning electron micrographs (JEOL 100C - ASID-4D) of Lima graphite oxidised in carbon dioxide at 700°C for 16 hours, weight loss 0.83%.



LIMA GRAPHITE

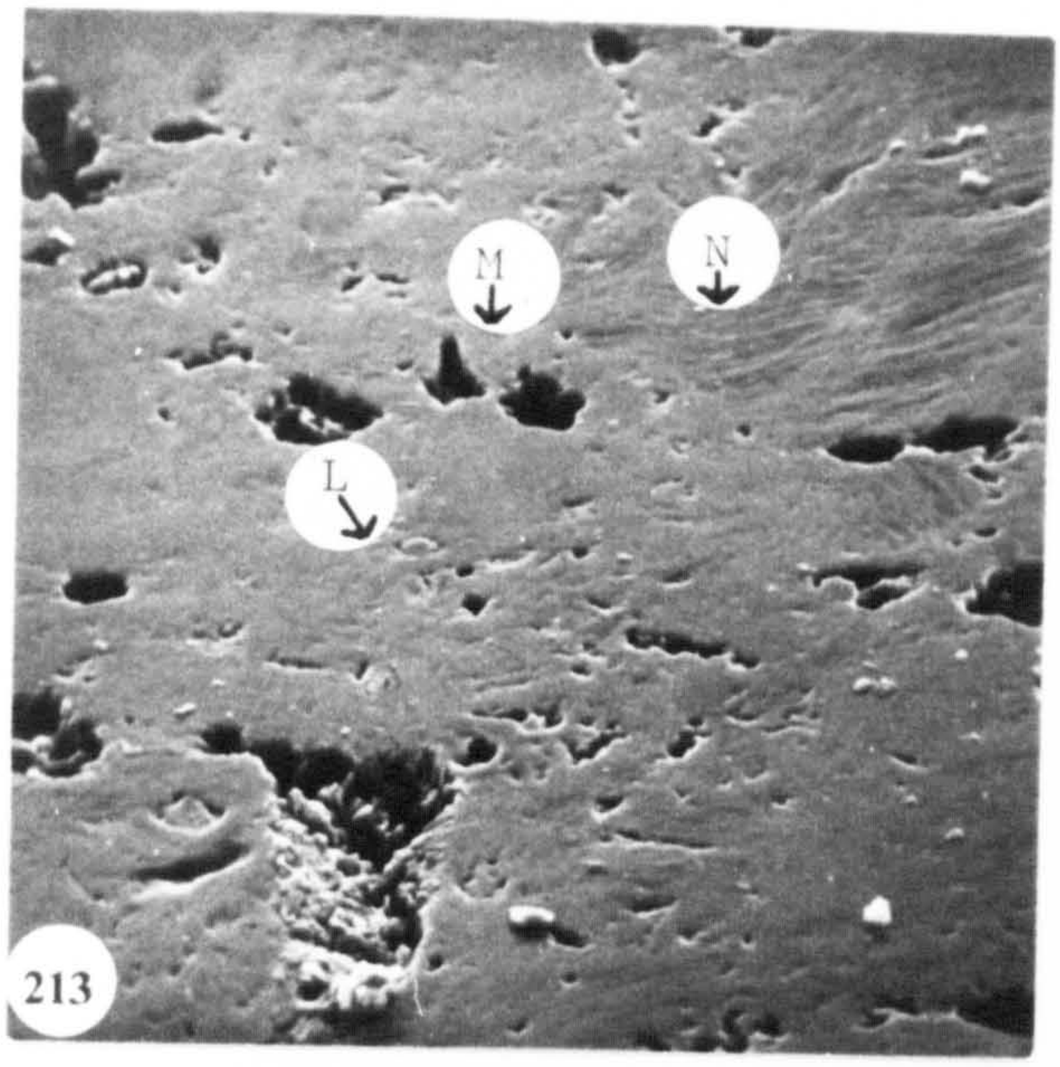
100 µm



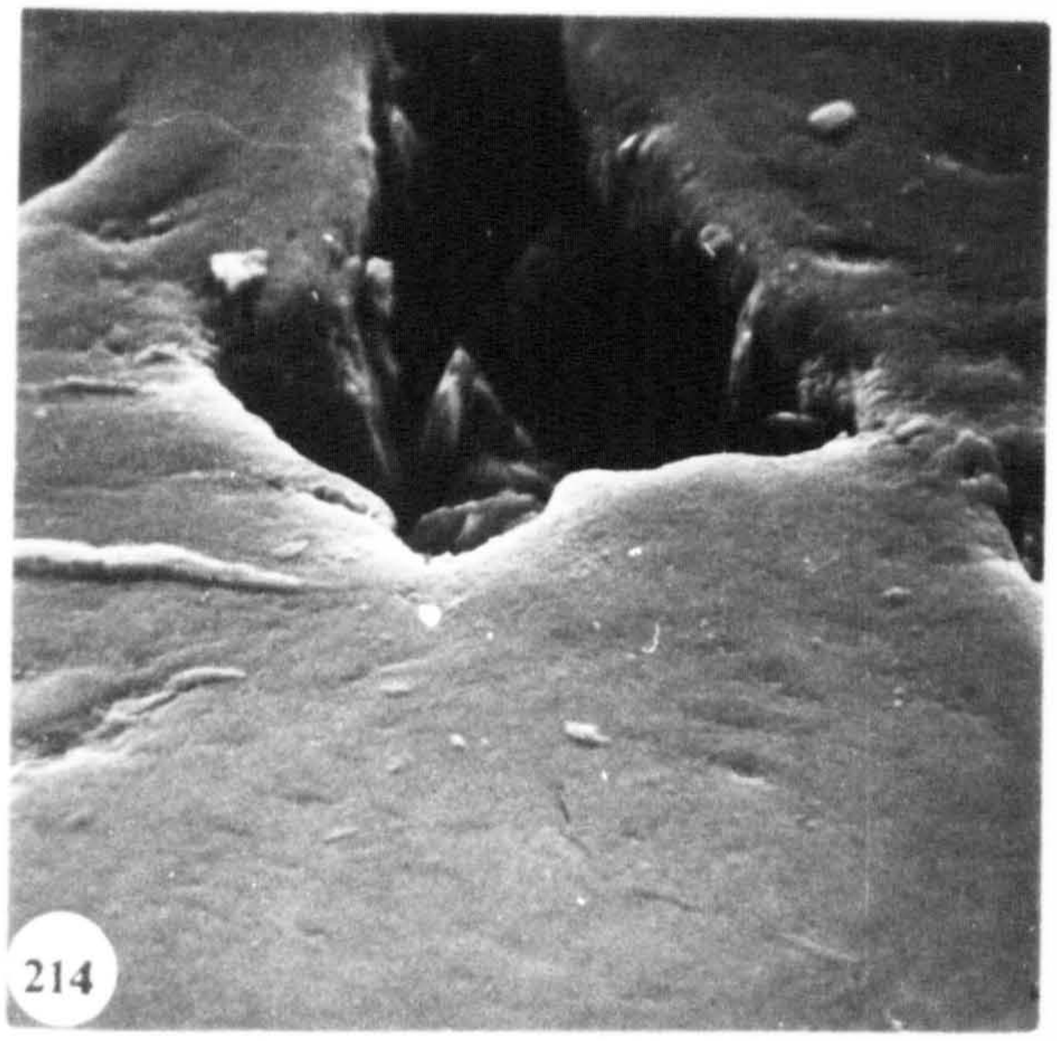
LIMA GRAPHITE

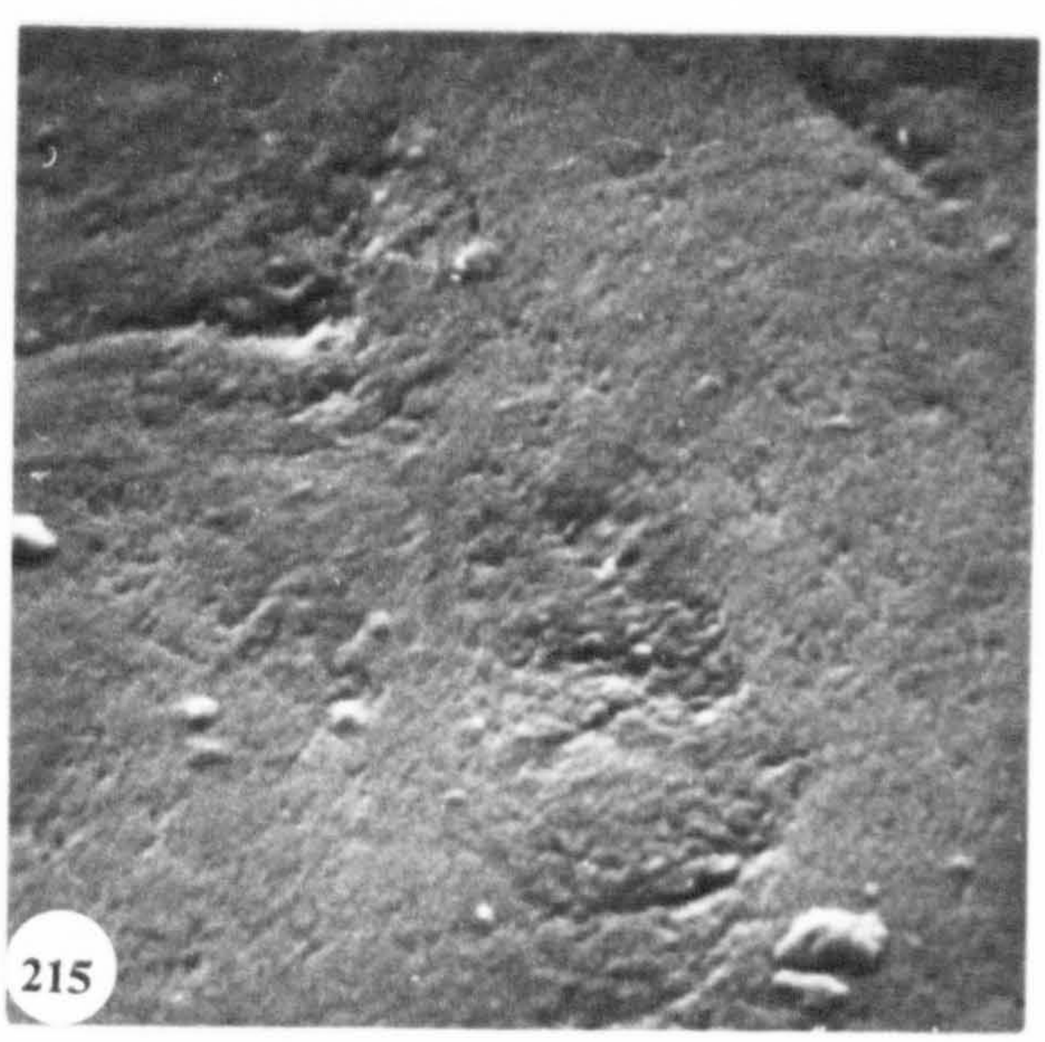
100 µm

Figures 211 and 212. Optical micrographs of Lima Graphite (LG6) before and after gasification in carbon dioxide at 873 K for 25 hours. Weight loss 0.03%.



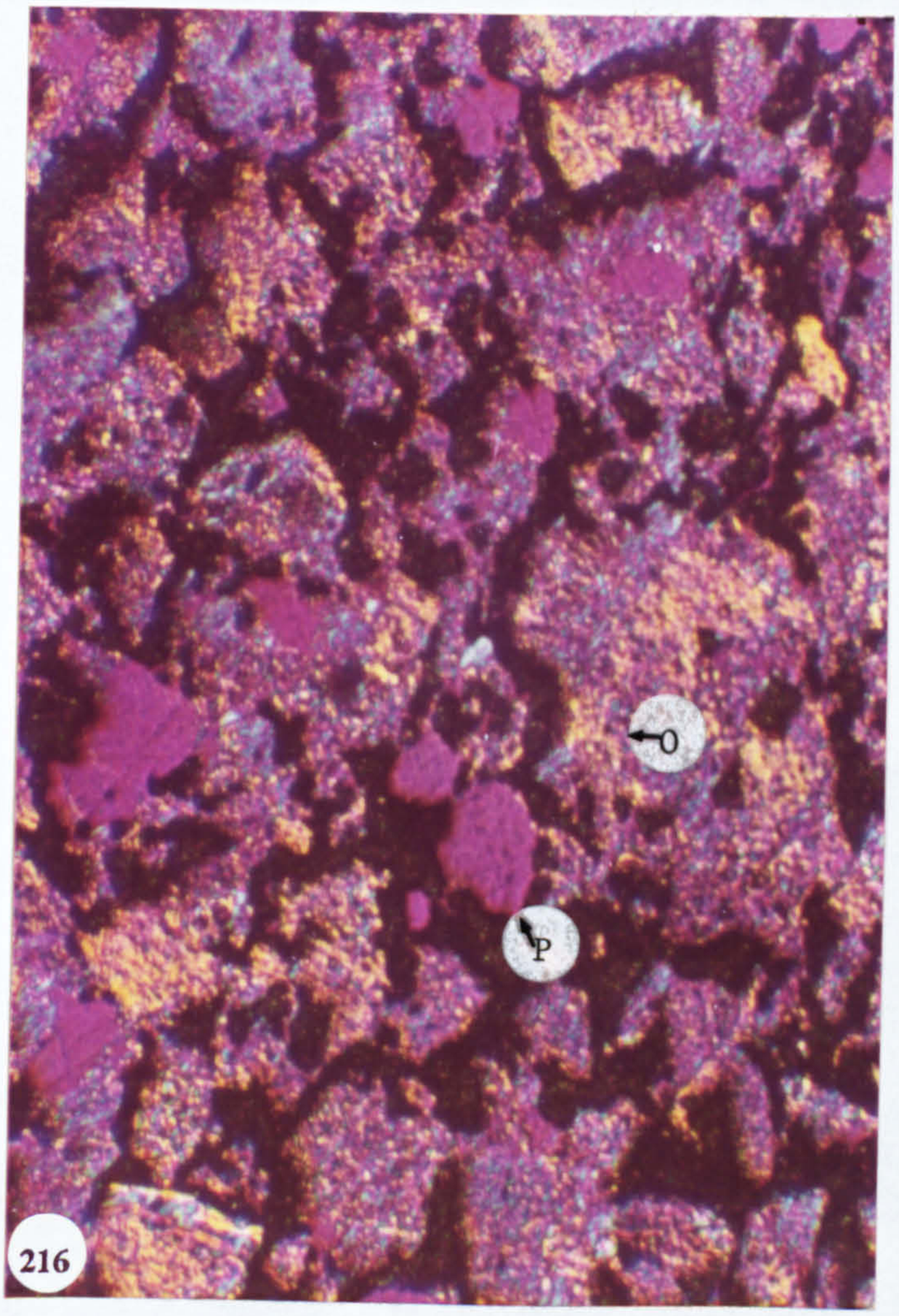
LIMA GRAPHITE 50 μm





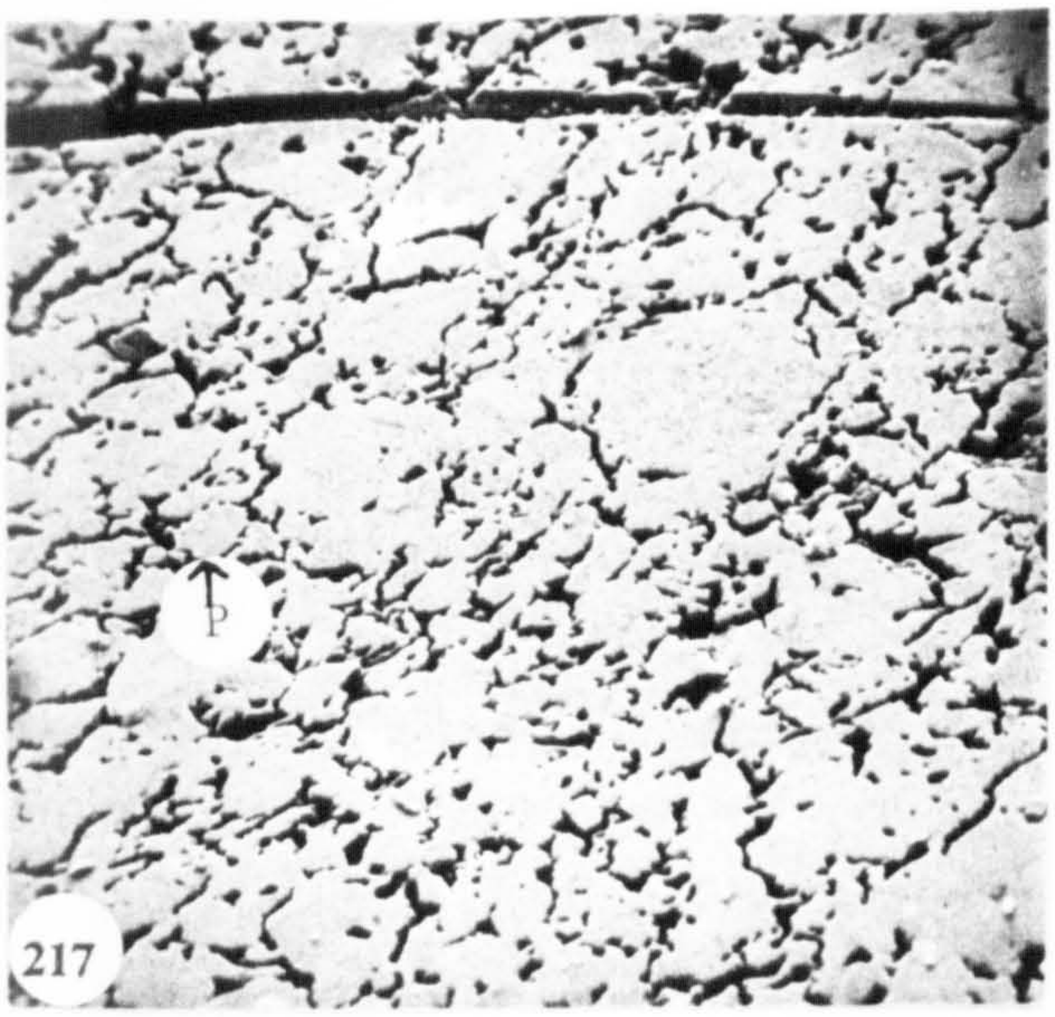
LIMA GRAPHITE 5 μm LIMA GRAPHITE 1 μm

Figures 213 to 215. Scanning electron micrographs (stereoscan) of Lima Graphite (LG6) after gasification in carbon dioxide at 873 K for 25 hours. Weight loss 0.03%.

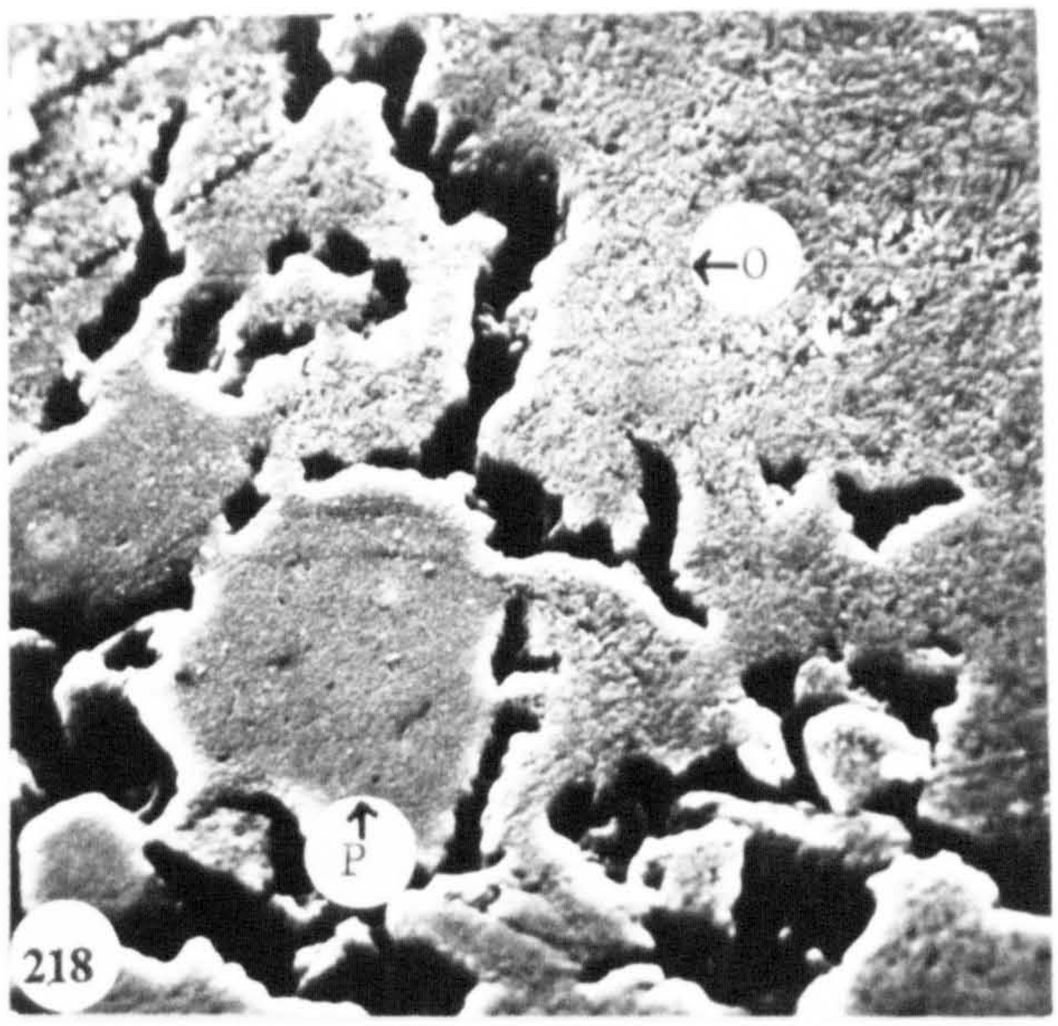


MORGANS UNIPORE GRAPHITE 100 µm

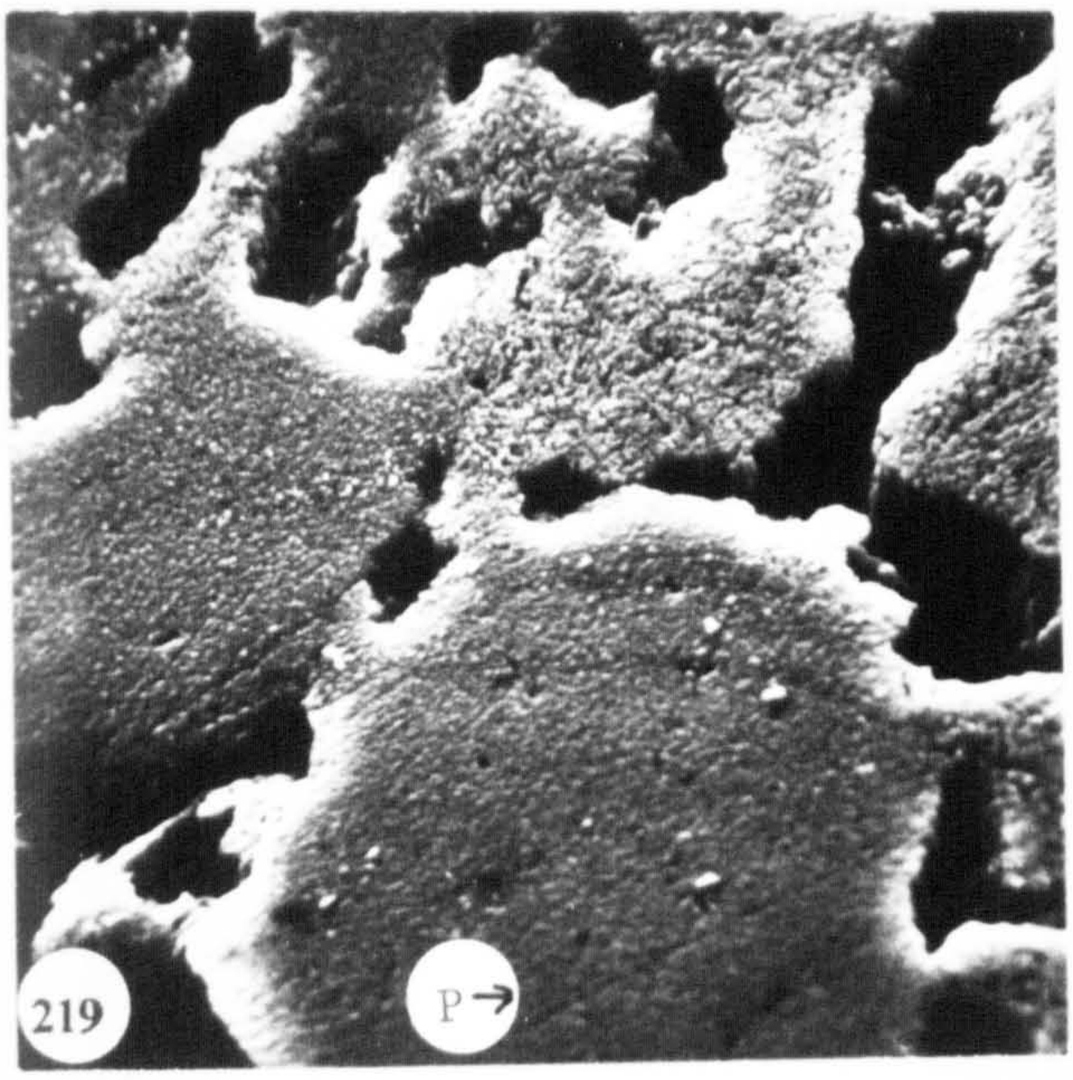
Figure 216. Optical micrograph of Morgans Unipore Graphite (MG4) before gasification.



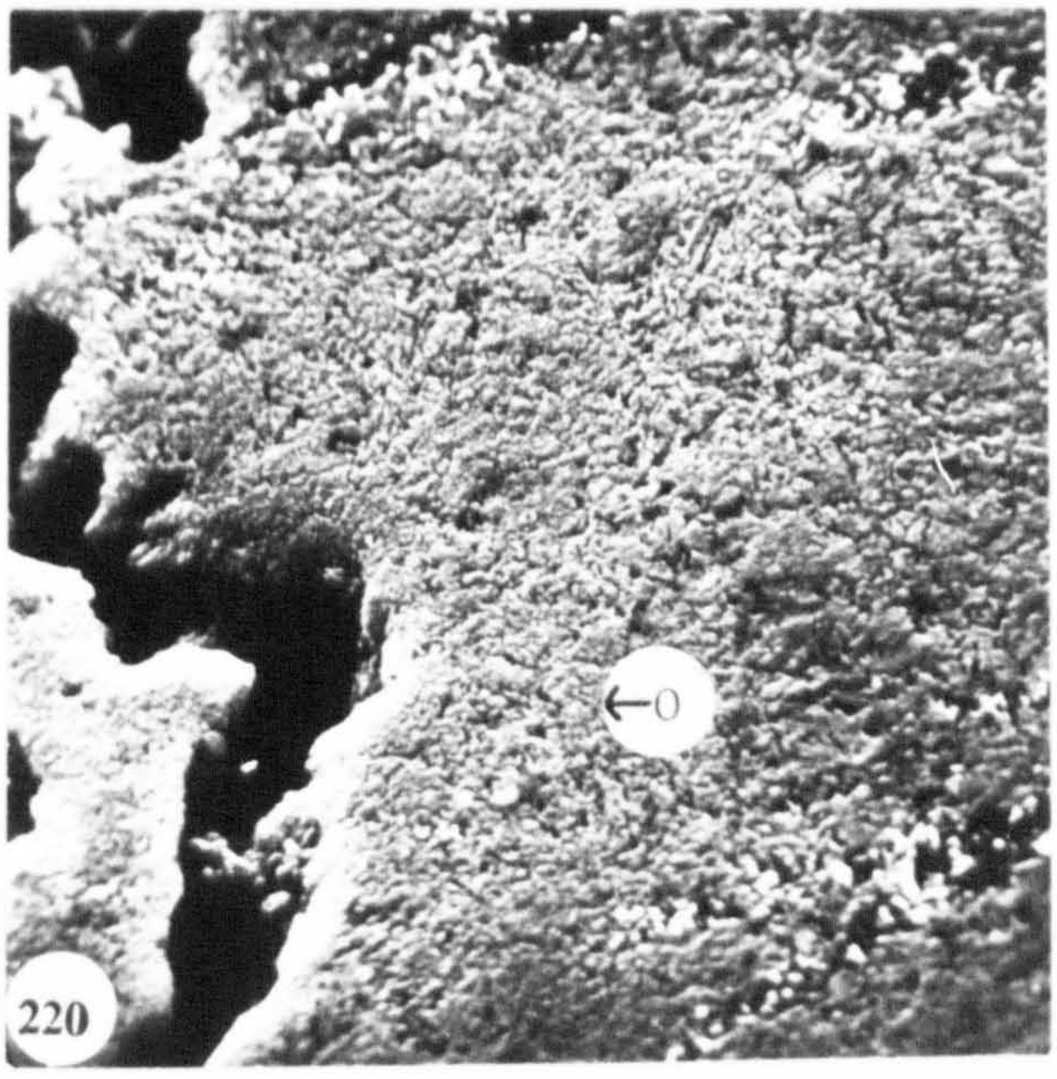
MORGANS UNIPORE GRAPHITE 100 µm



MORGANS UNIPORE GRAPHITE 20 µm

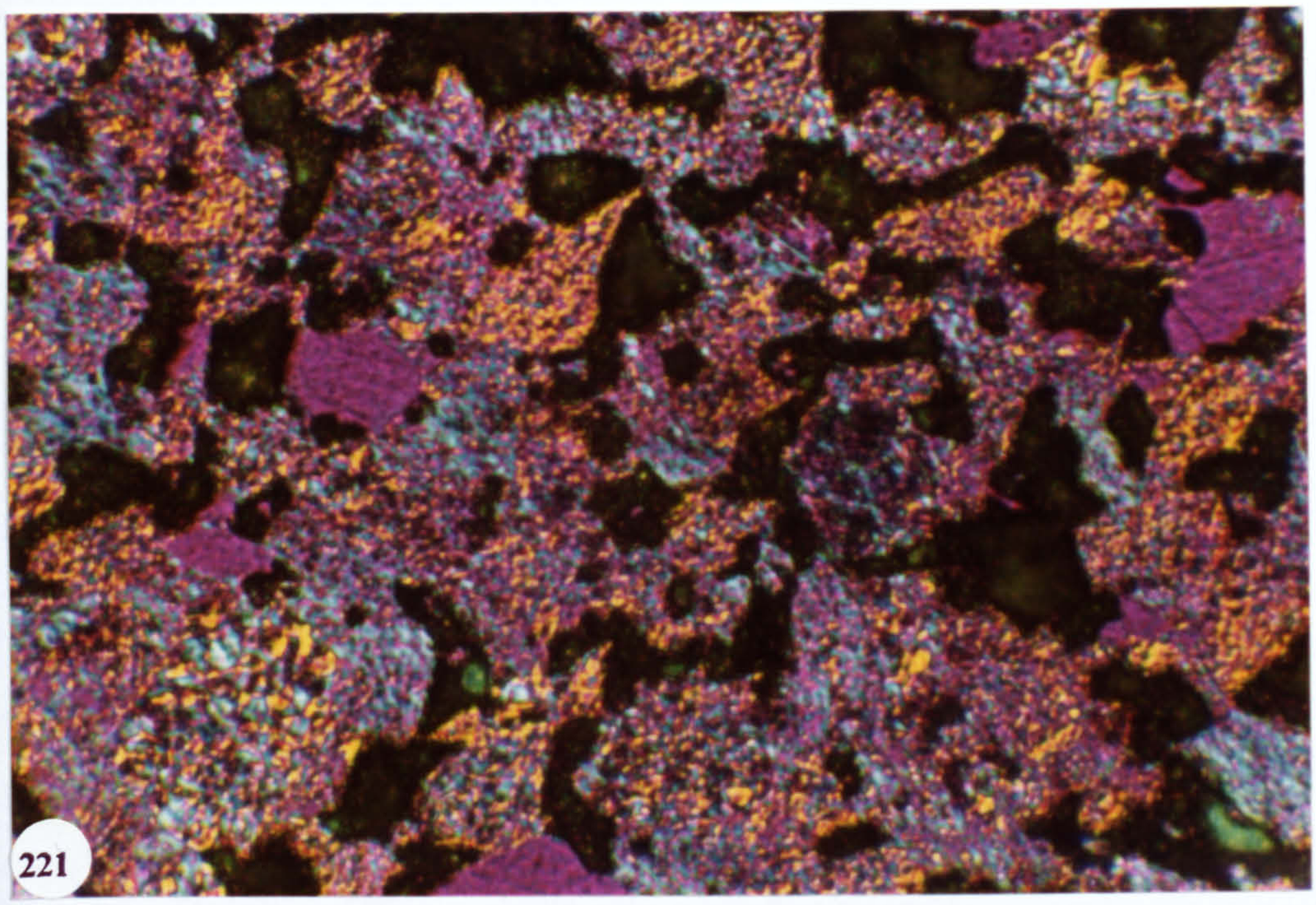


MORGANS UNIPORE GRAPHITE 10 µm

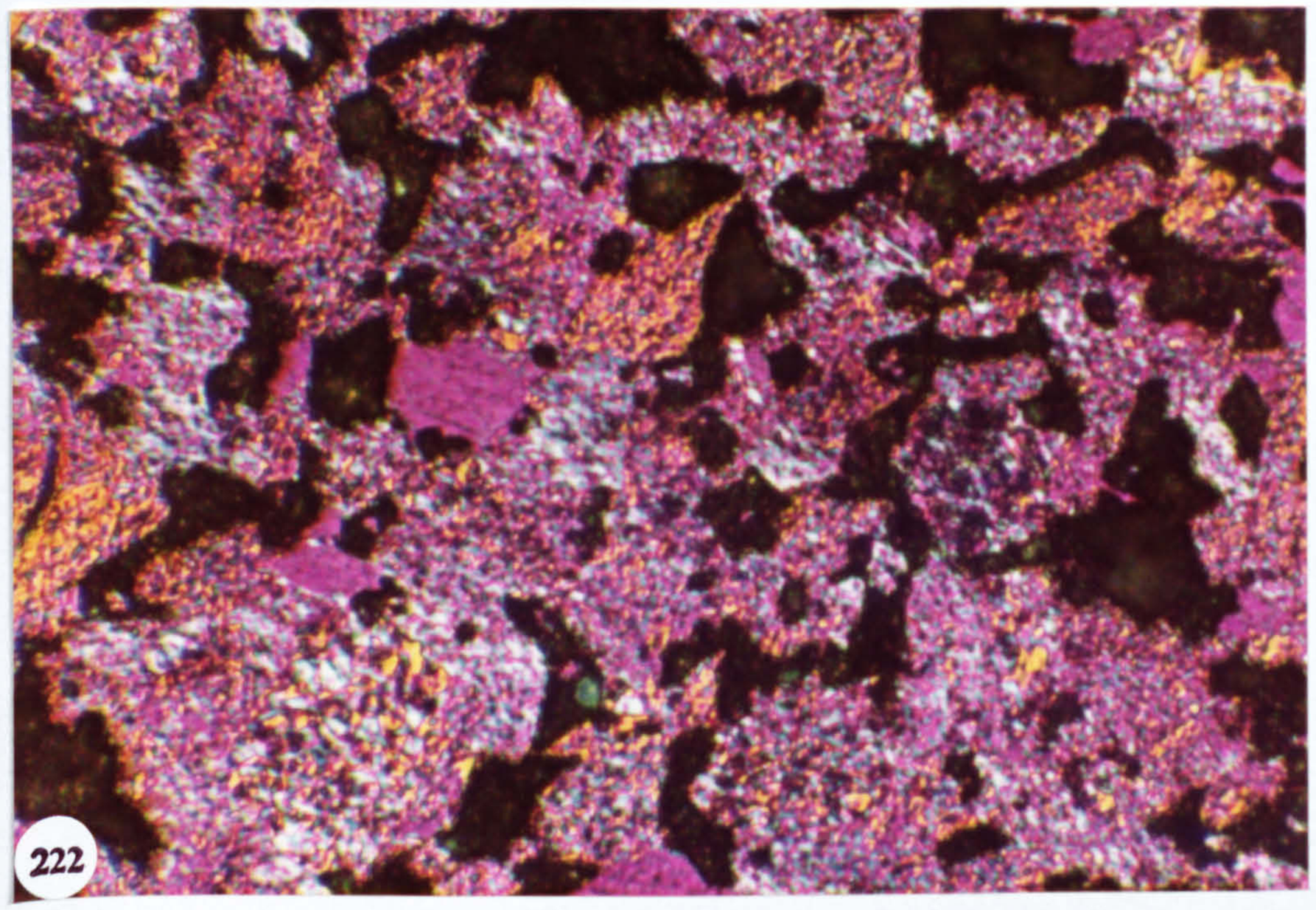


MORGANS UNIPORE GRAPHITE 10 µm

Figures 217 to 220. Scanning electron micrographs (stereoscan) of Morgans Unipore Graphite (MG4) gasified in carbon dioxide at 973 K for 16 hours. Weight loss 0.67%.

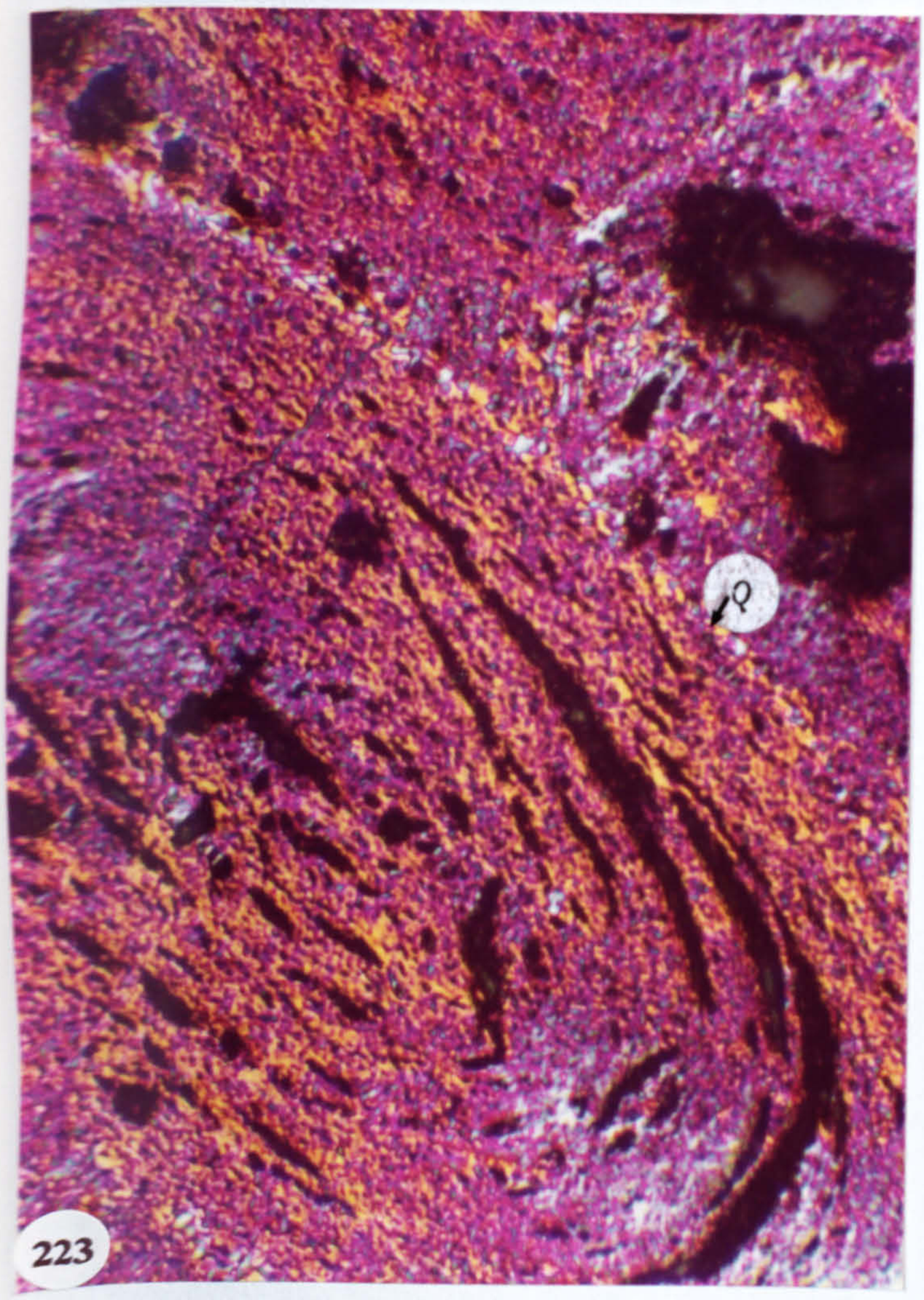


MORGANS UNIPORE GRAPHITE



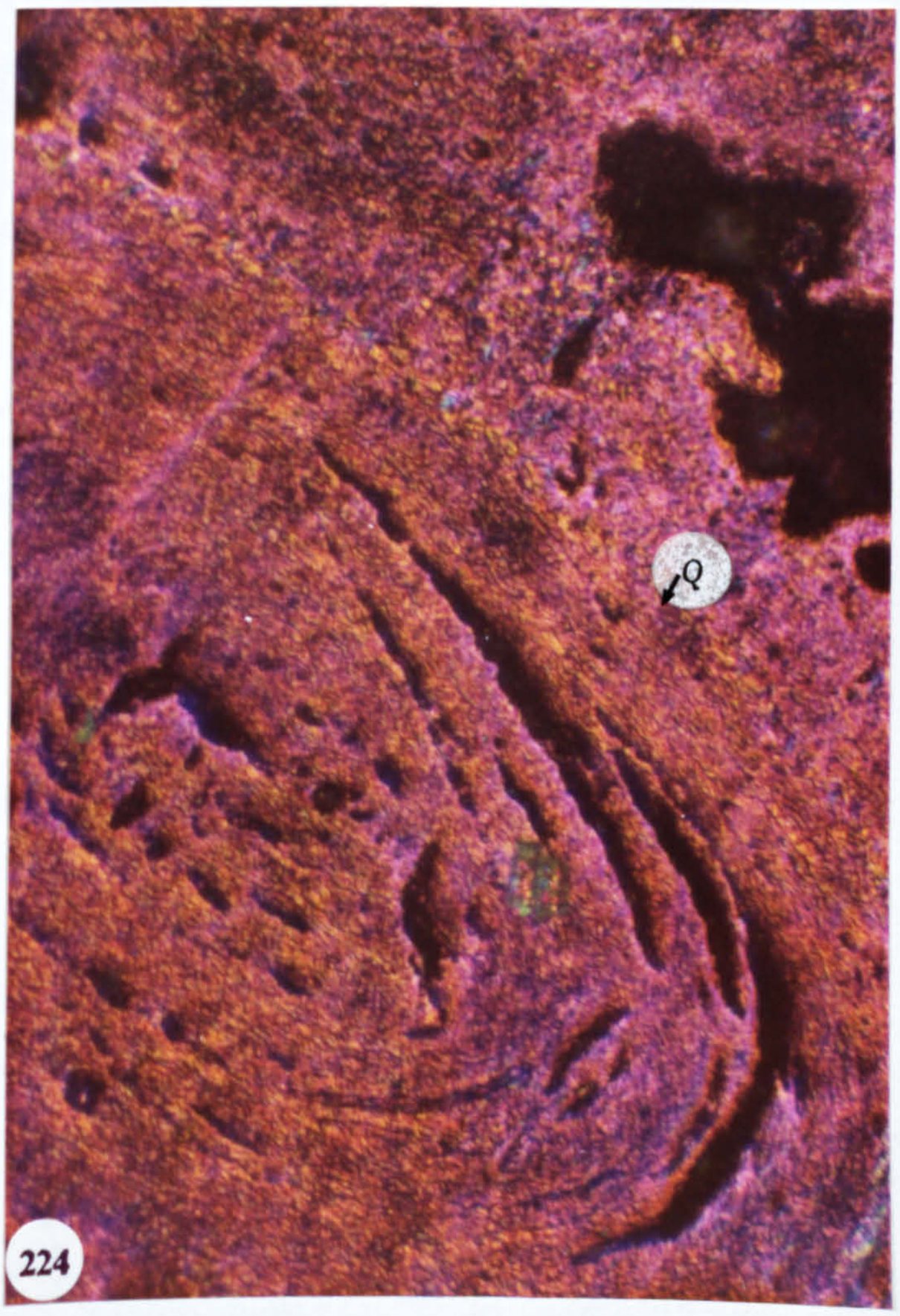
MORGANS UNIPORE GRAPHITE

Figures 221 and 222. Optical micrographs of Morgans Unipore Graphite (MG6) before and after gasification in carbon dioxide at 873 K for 25 hours. Weight loss, 0.02%.



AGLMP GRAPHITE

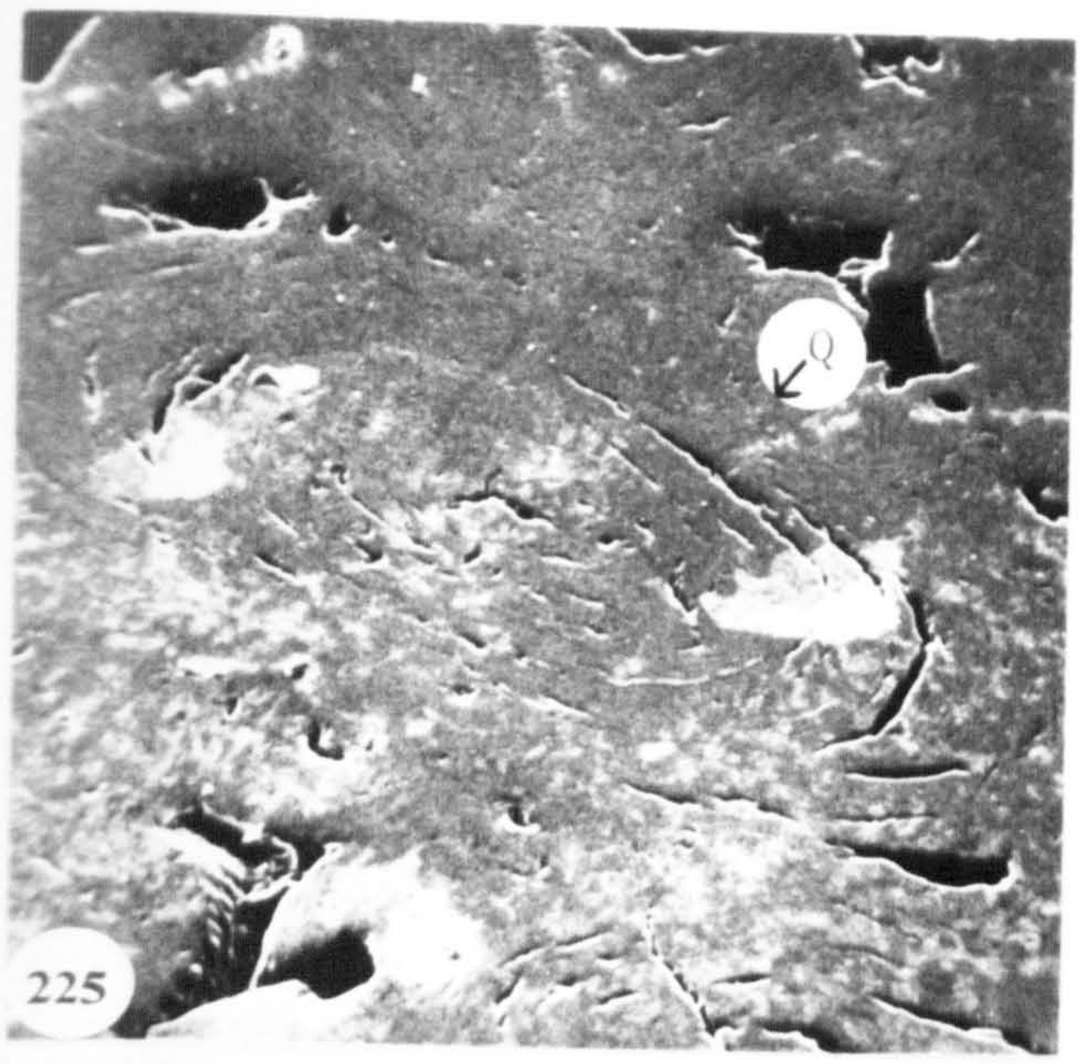
100 μm



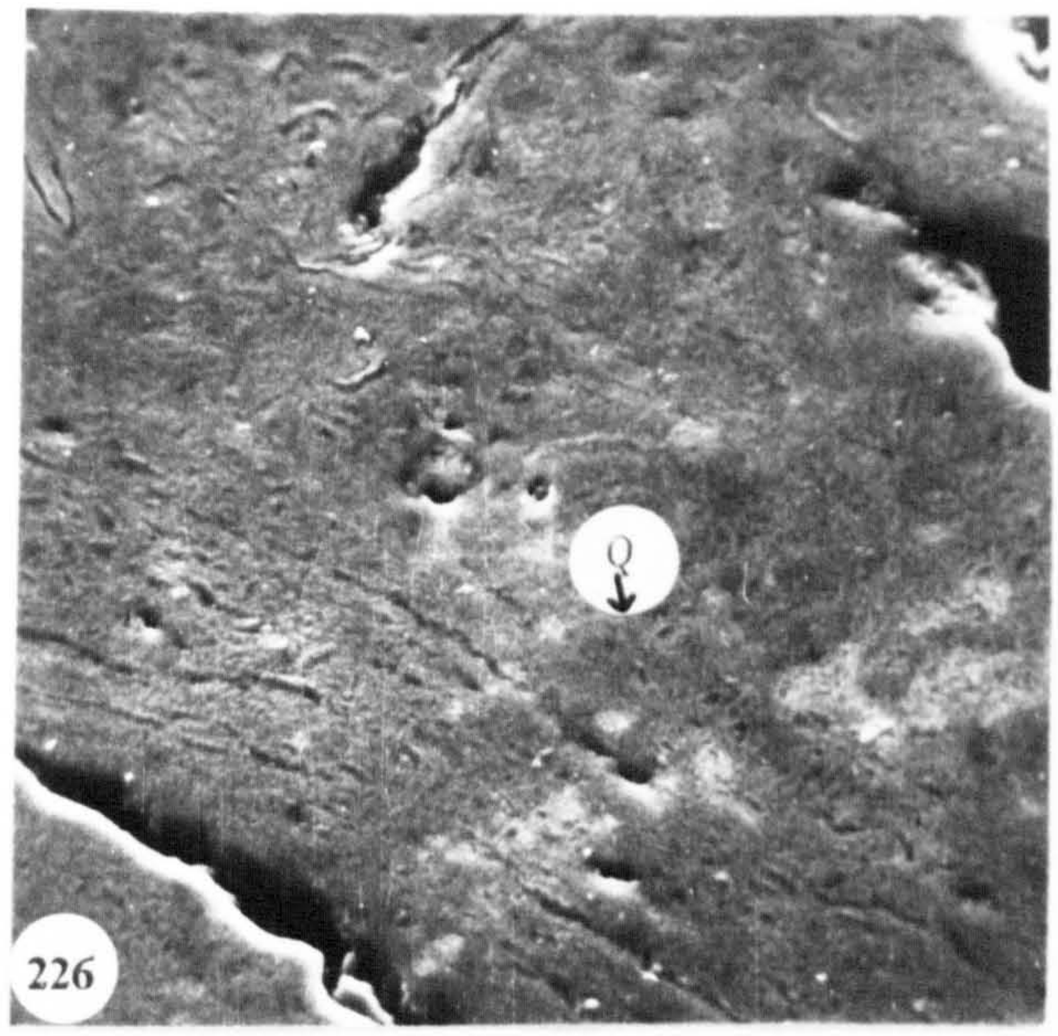
AGLMP GRAPHITE

100 μm

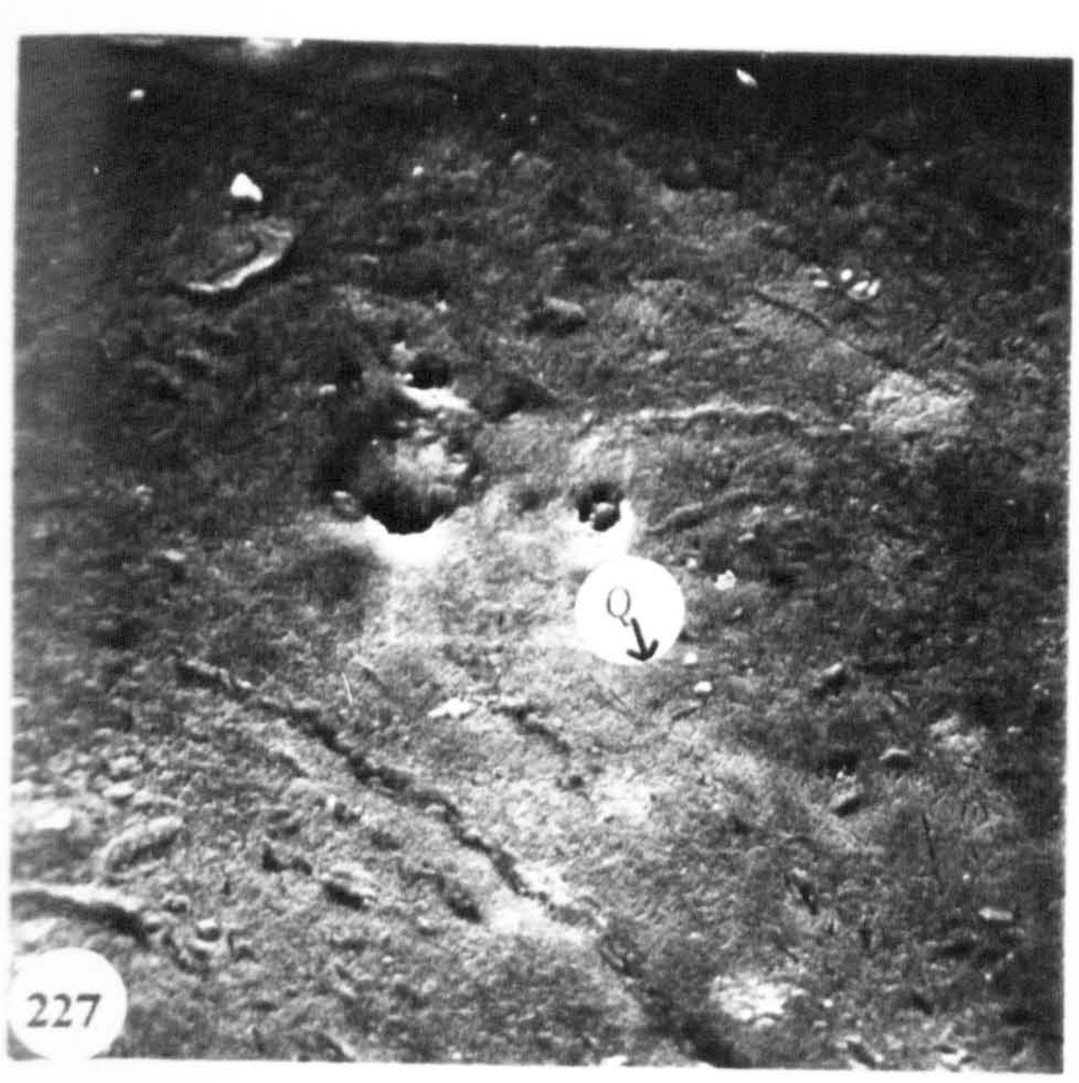
Figures 223 and 224. Optical micrographs of AGLMP Graphite (AG2) before and after gasification in carbon dioxide at 973 K for 16 hours. Weight loss 0.40%.



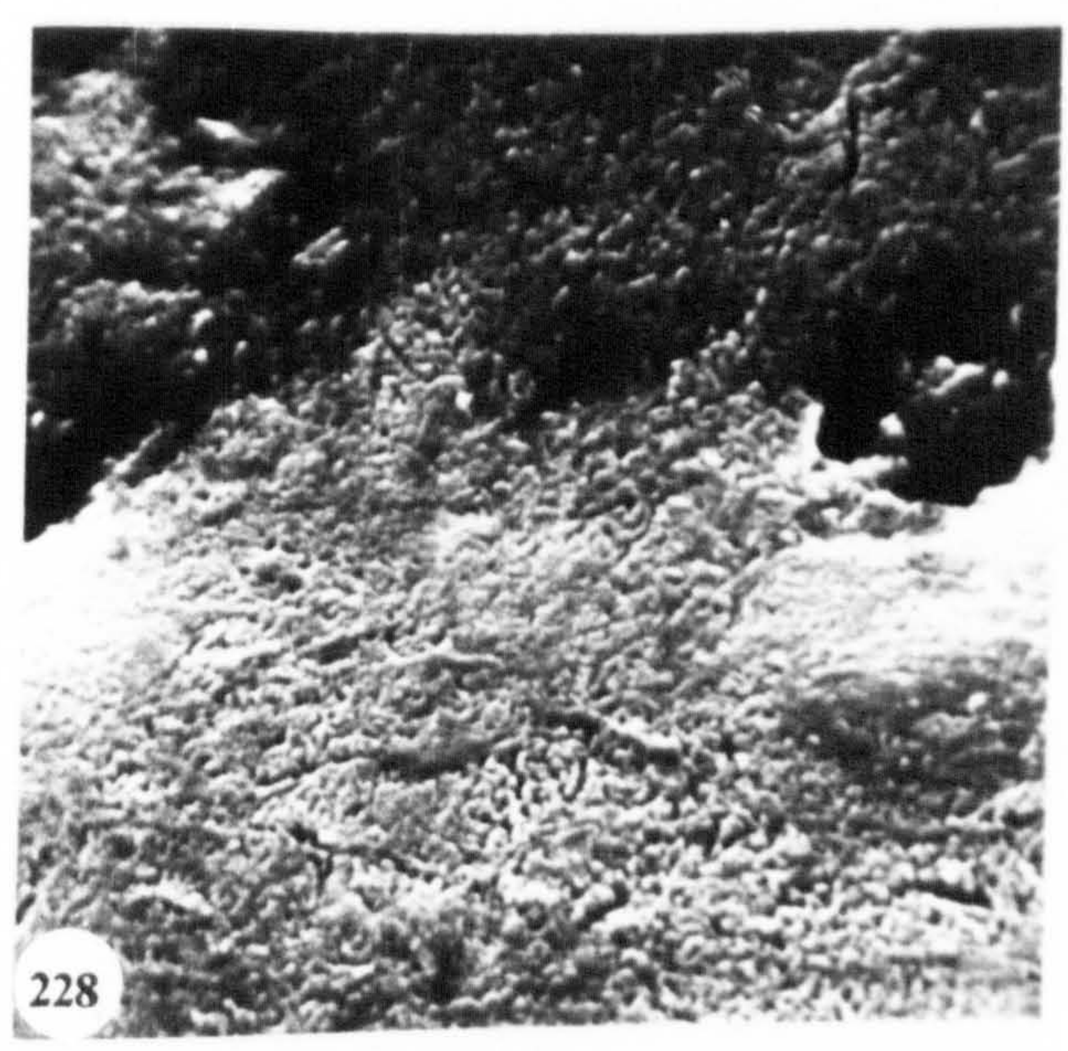
AGLMP GRAPHITE 100 µm



AGLMP GRAPHITE 20 µm

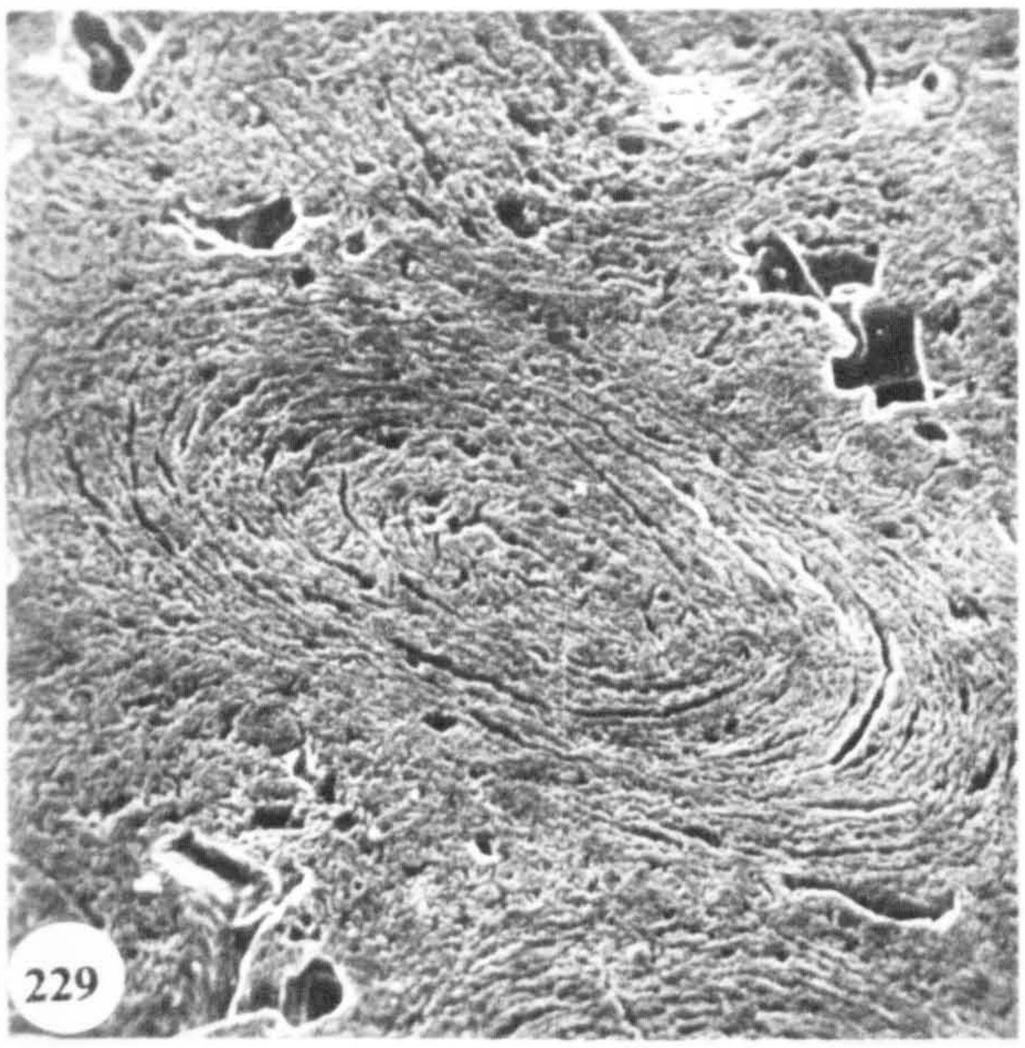


AGLMP GRAPHITE 10 µm

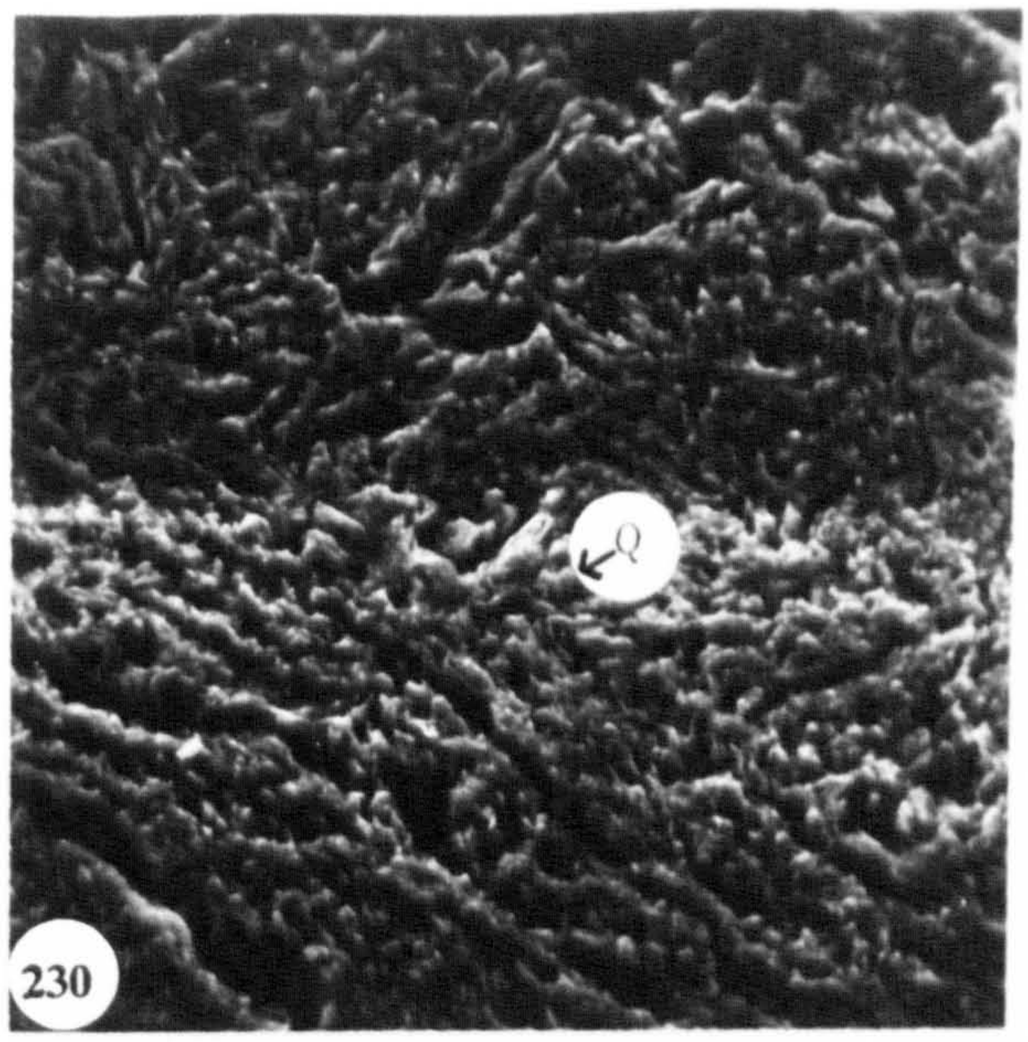


AGLMP GRAPHITE 2 µm

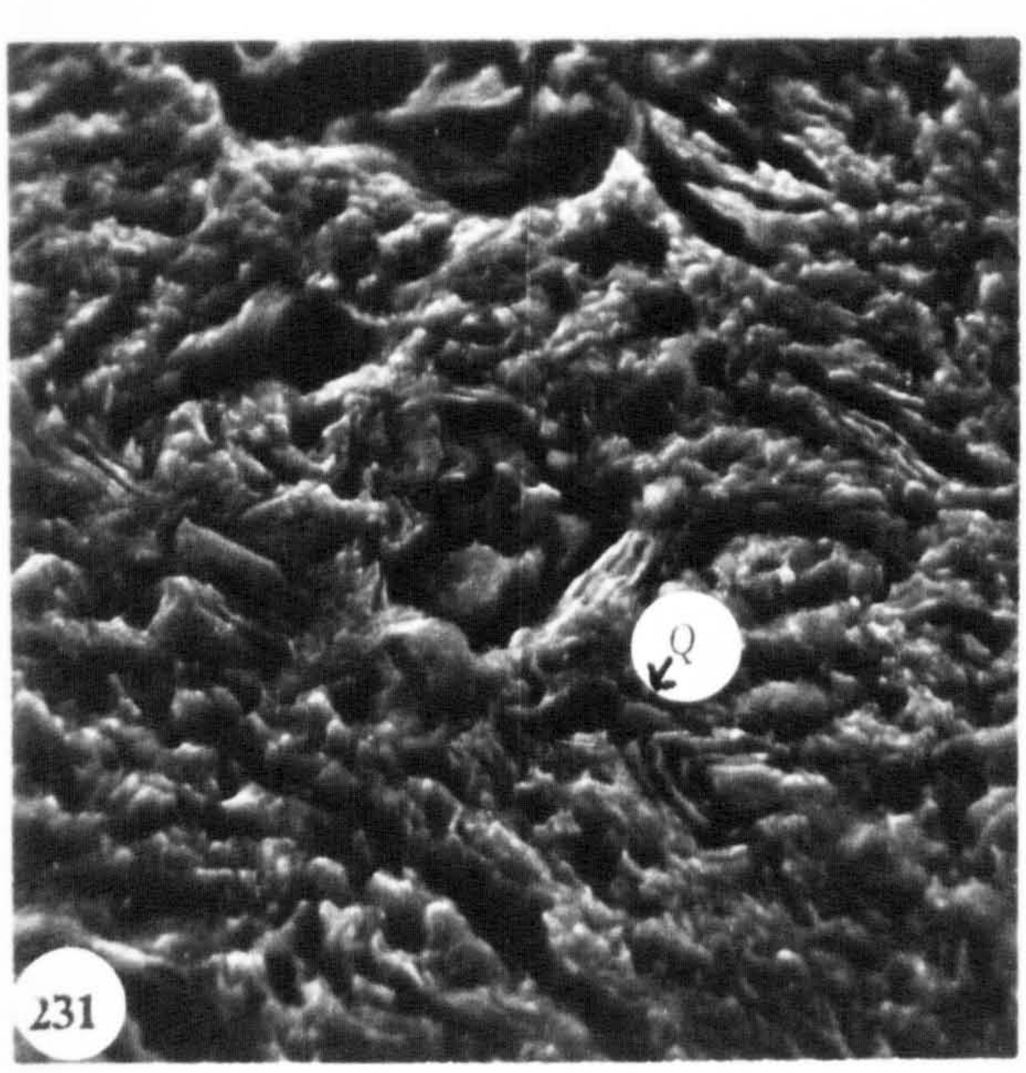
Figures 225 to 228. Scanning electron micrographs (stereoscan) of AGLMP Graphite (AG2) after gasification in carbon dioxide at 973 K for 16 hours. Weight loss 0.40%.



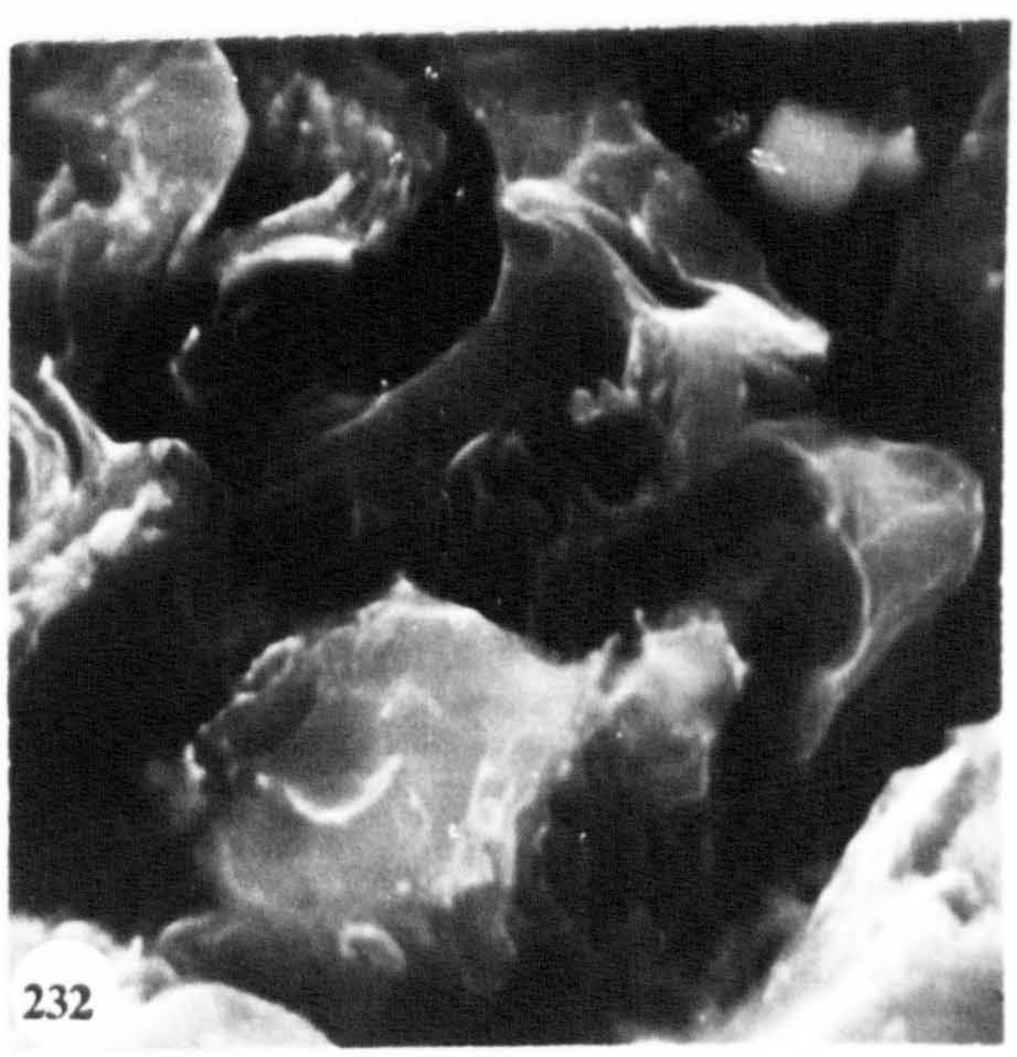
AGLMP GRAPHITE 100 µm



AGLMP GRAPHITE 20 µm

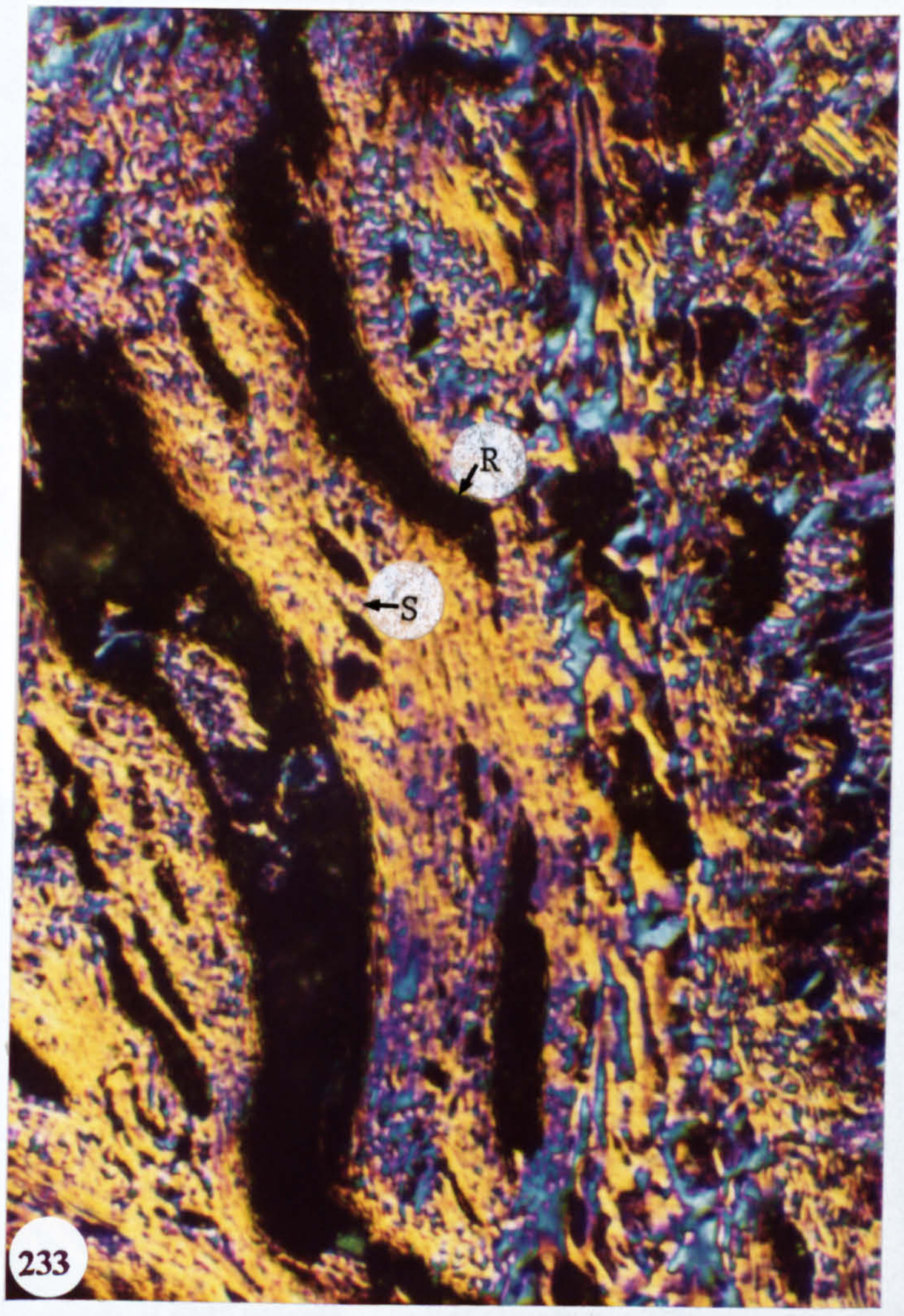


AGLMP GRAPHITE 10 µm



AGLMP GRAPHITE 2 µm

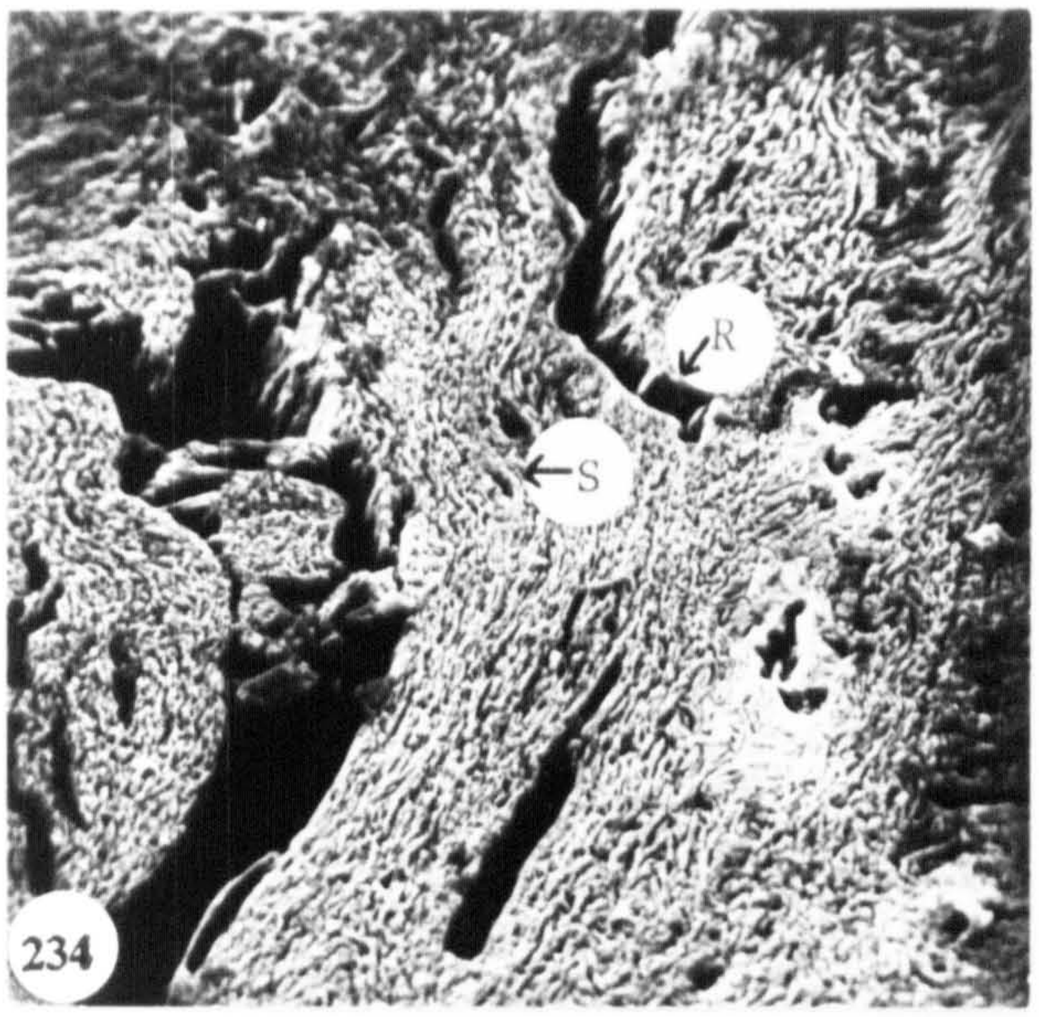
Figures 229 to 232. Scanning electron micrographs (stereoscan) of AGLMP Graphite (AG2) after gasification in carbon dioxide at 1073 K for 16 hours. Weight loss 0.76%.



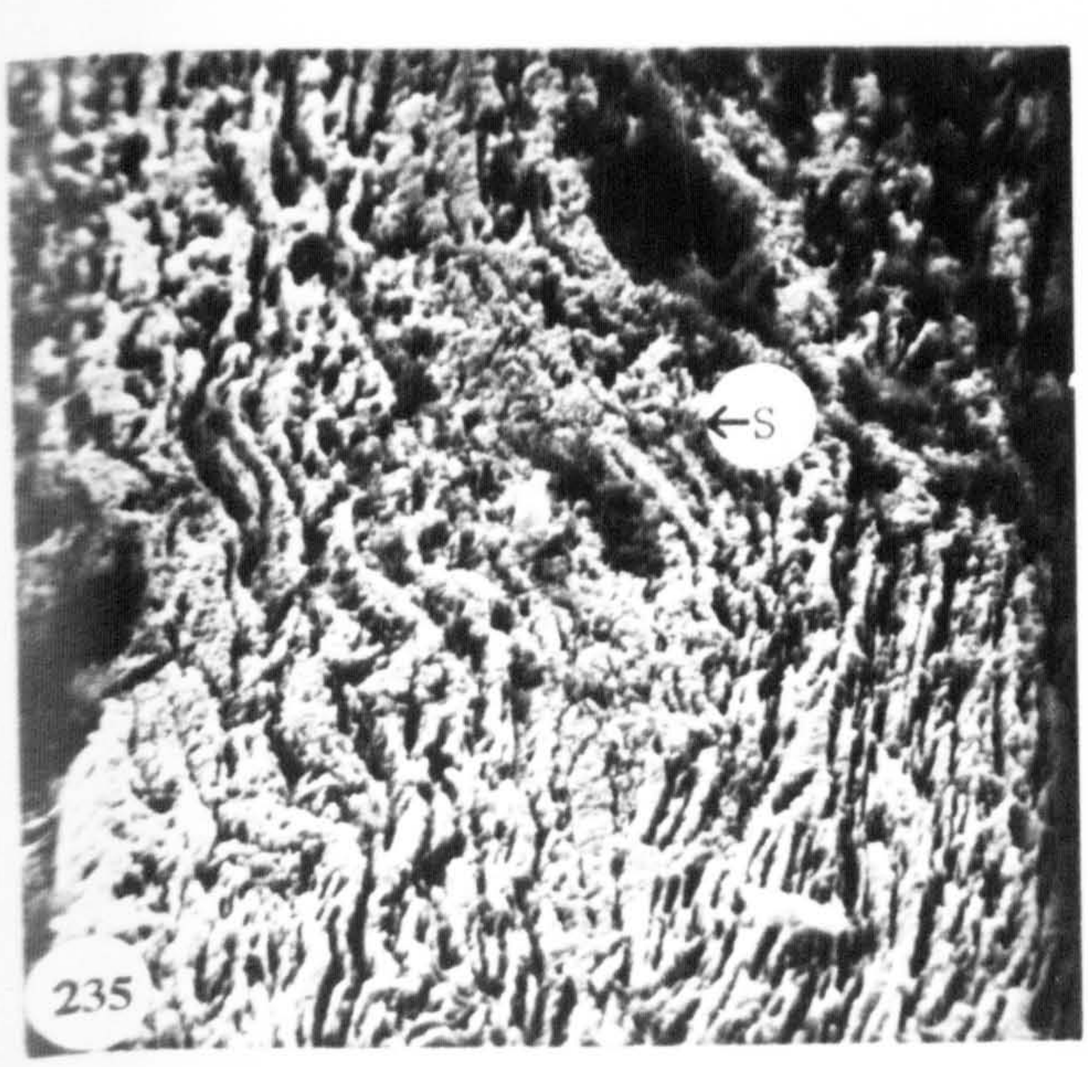
LIMA GRAPHITE

100 µm

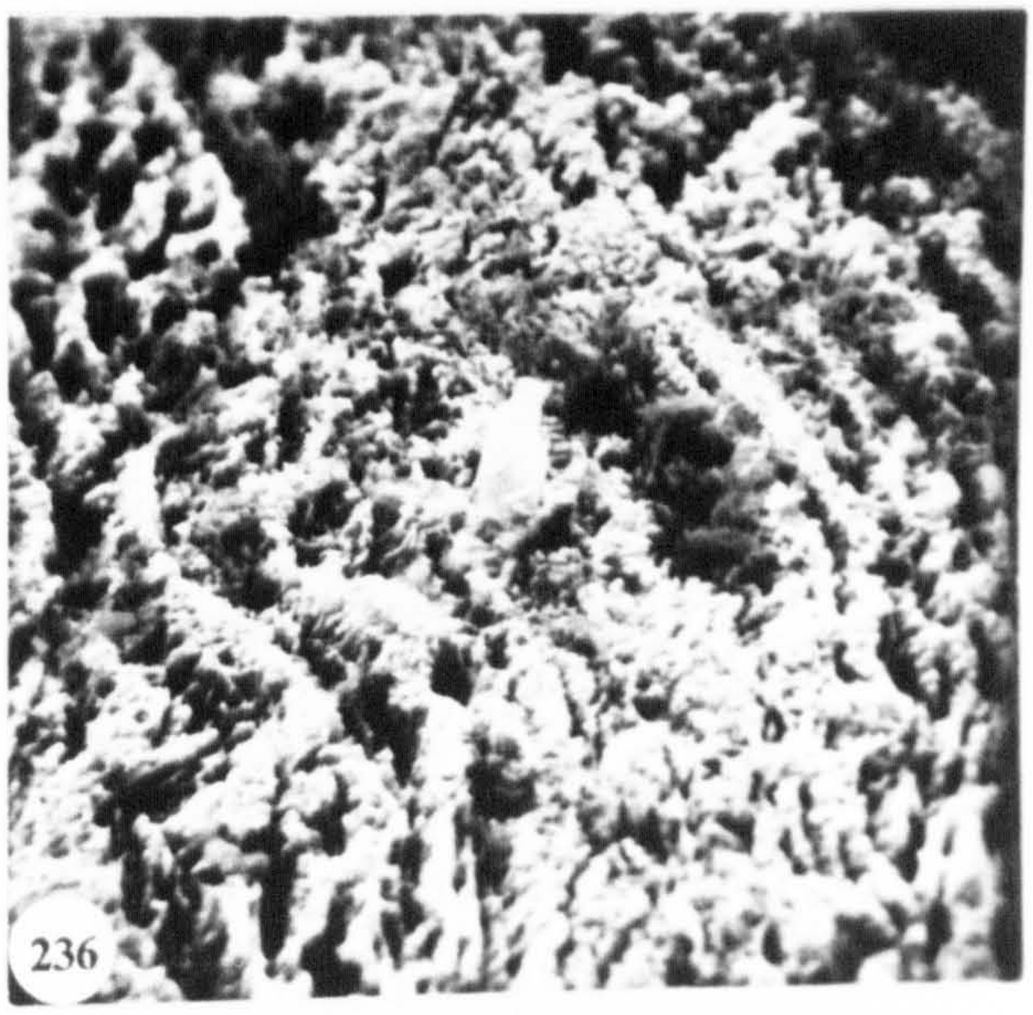
Figure 233. Optical micrograph of Lima Graphite (AG7) before gasification.



LIMA GRAPHITE 50 µm

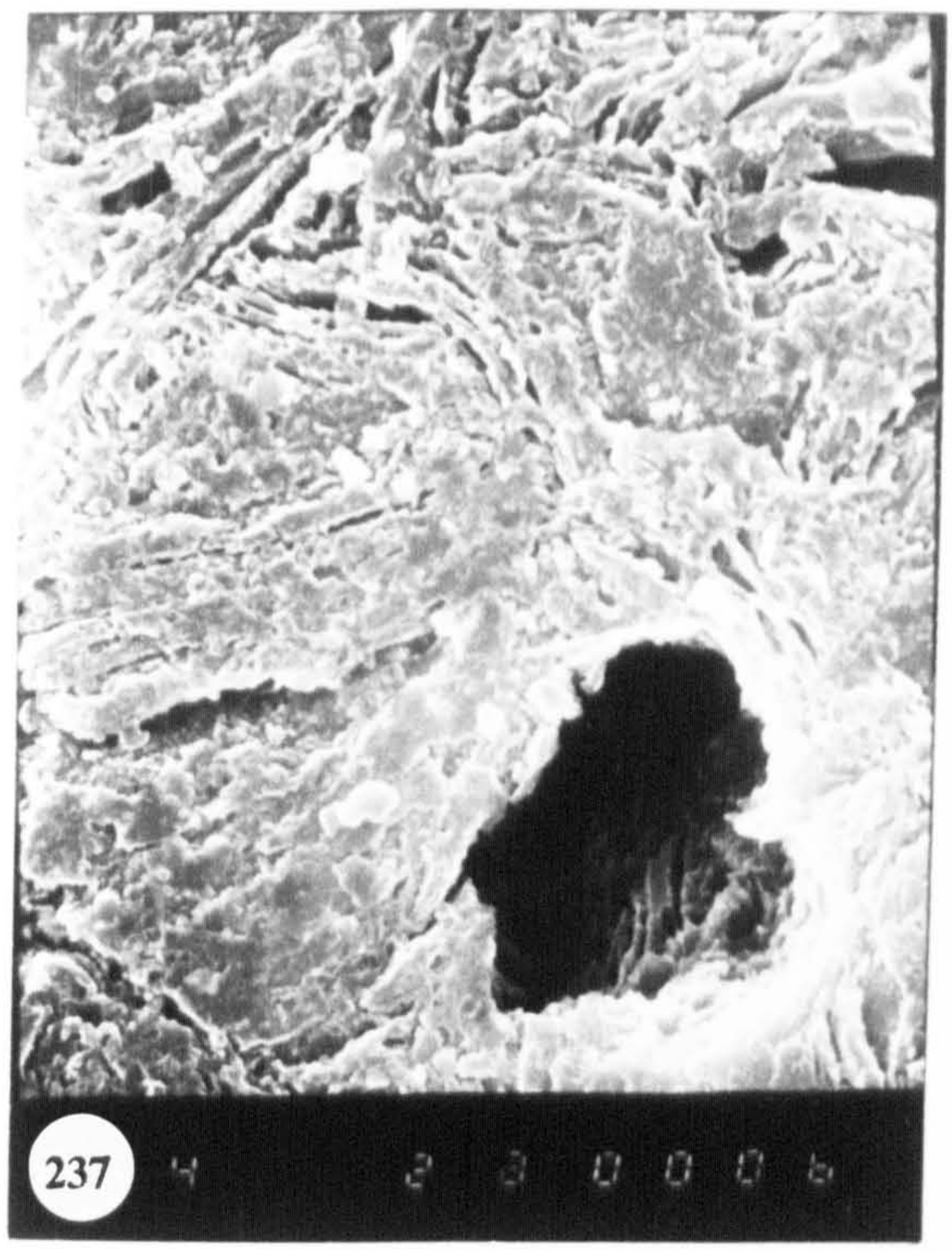


LIMA GRAPHITE 10 µm



LIMA GRAPHITE 5 µm

Figures 234 to 236. Scanning electron micrographs (stereoscan) of Lima Graphite (LG7) after gasification in atomic oxygen at~300 K for 5 minutes. Weight loss 0.98%.



LIMA GRAPHITE. 5 µm

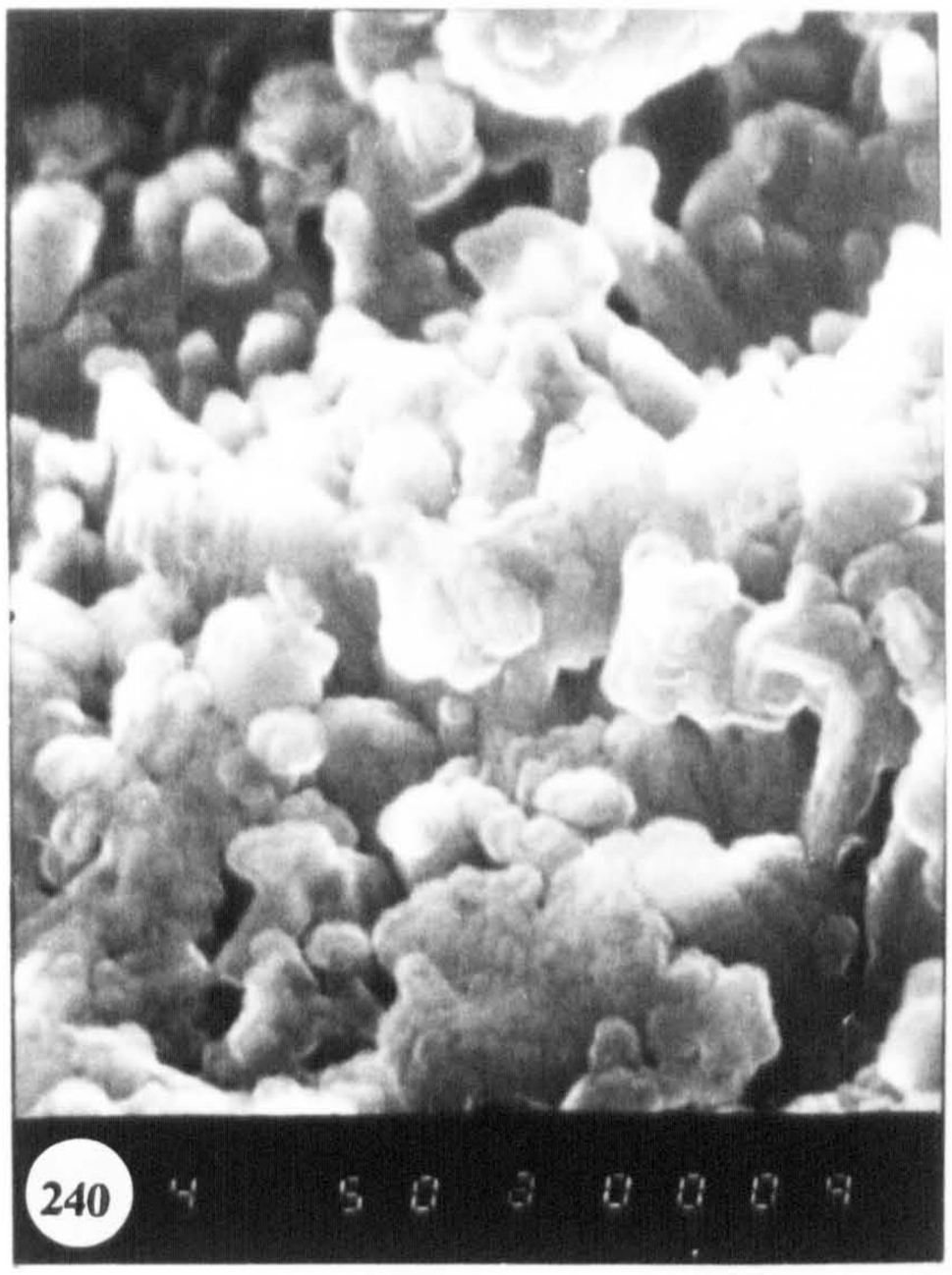


LIMA GRAPHITE. 1 µm

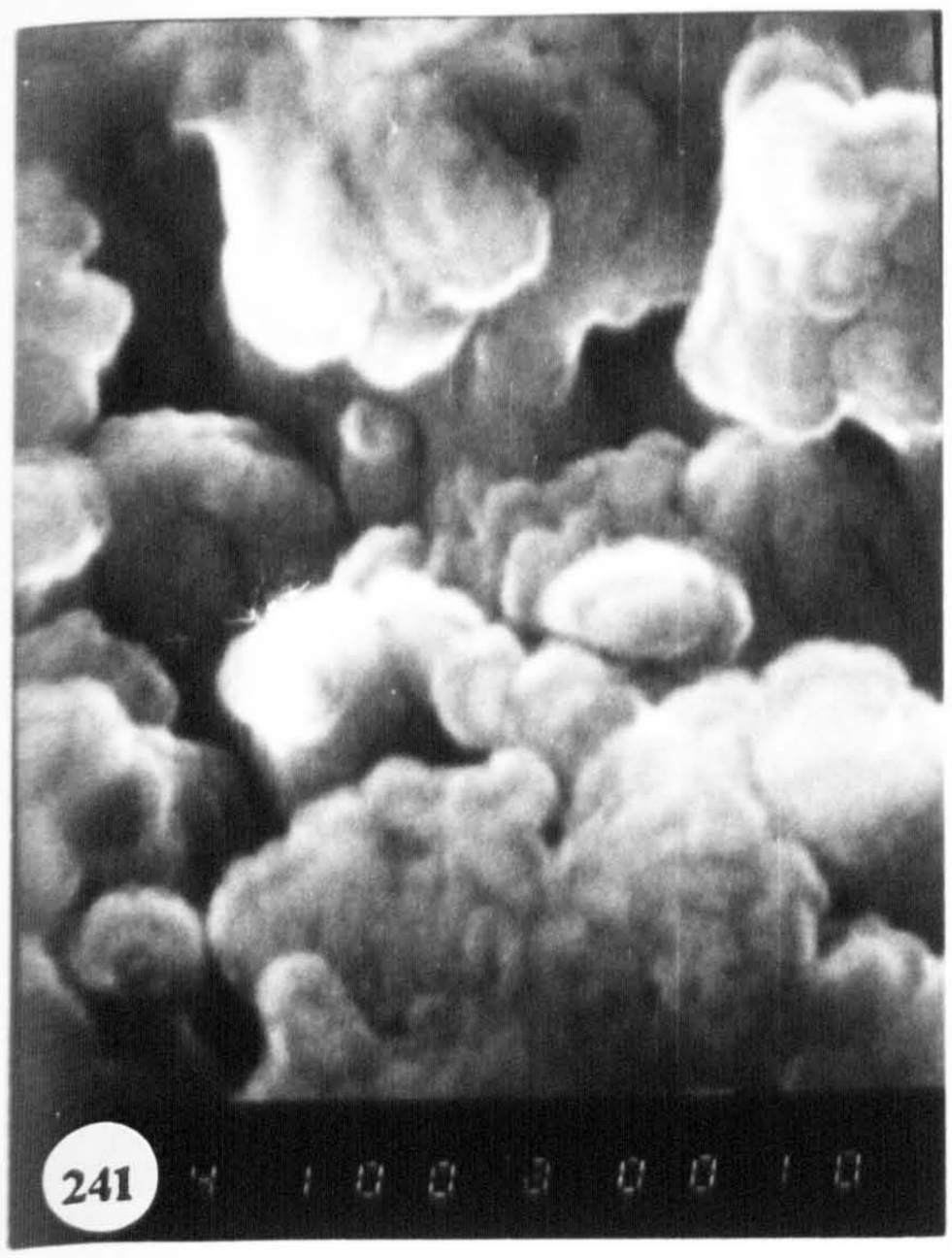


LIMA GRAPHITE. 200 nm

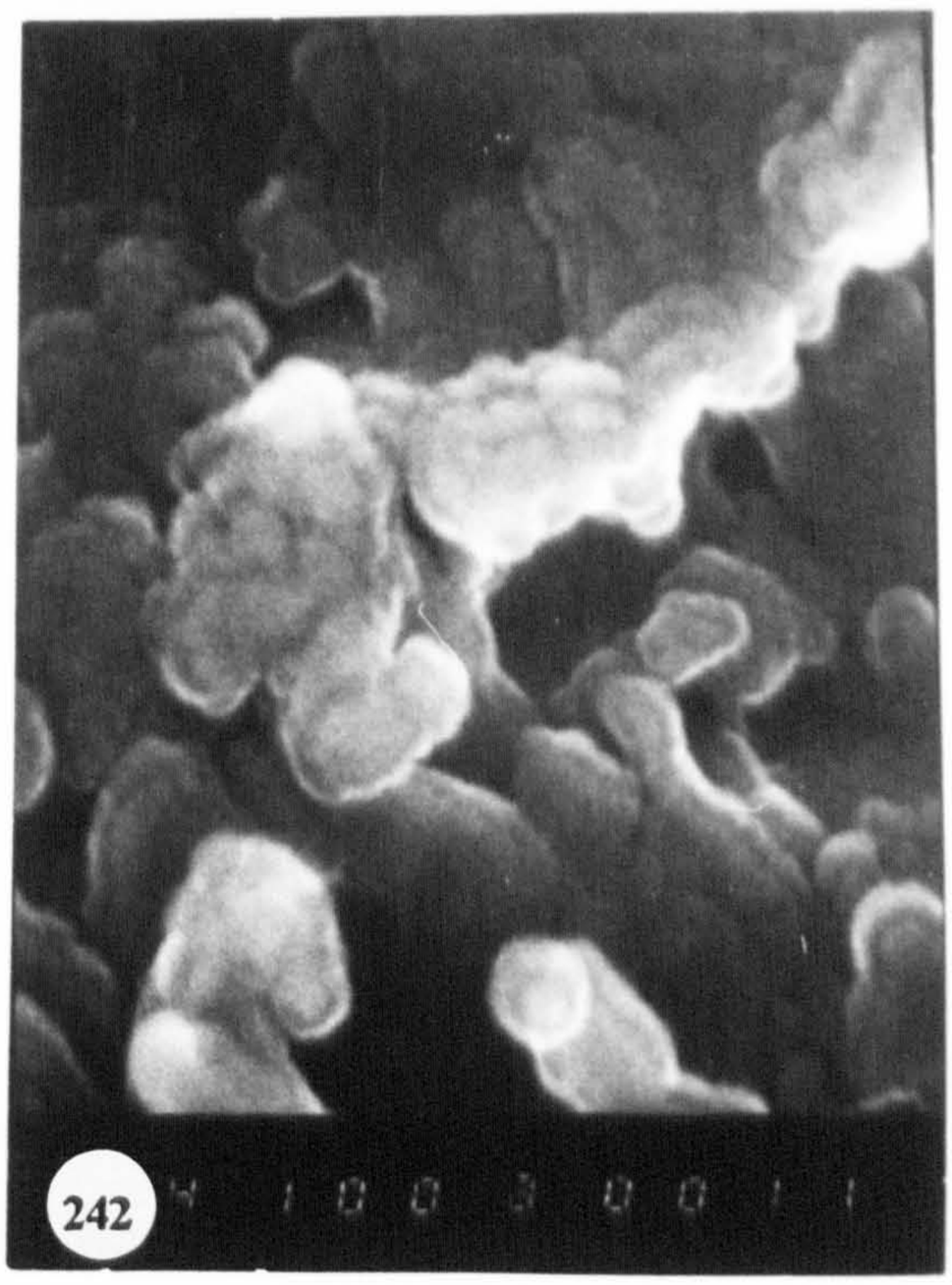
Figures 237 to 239 Scanning electron micrographs (JEOL 100C - ASID-4D) of Lima graphite oxidised in atomic oxygen at room temperature for 5 minutes, weight loss 0.98%.



LIMA GRAPHITE. 200 nm

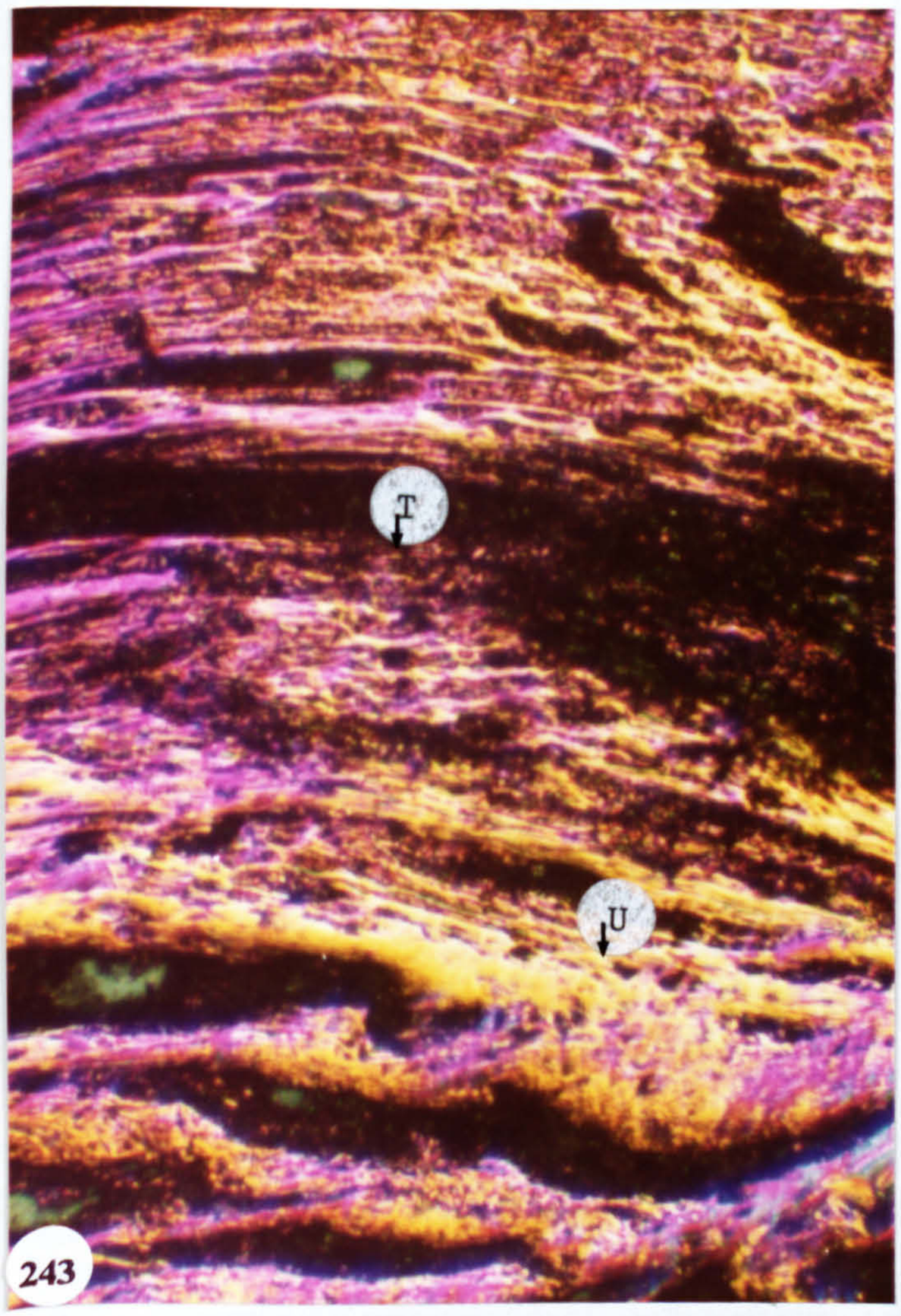


LIMA GRAPHITE. 100 nm



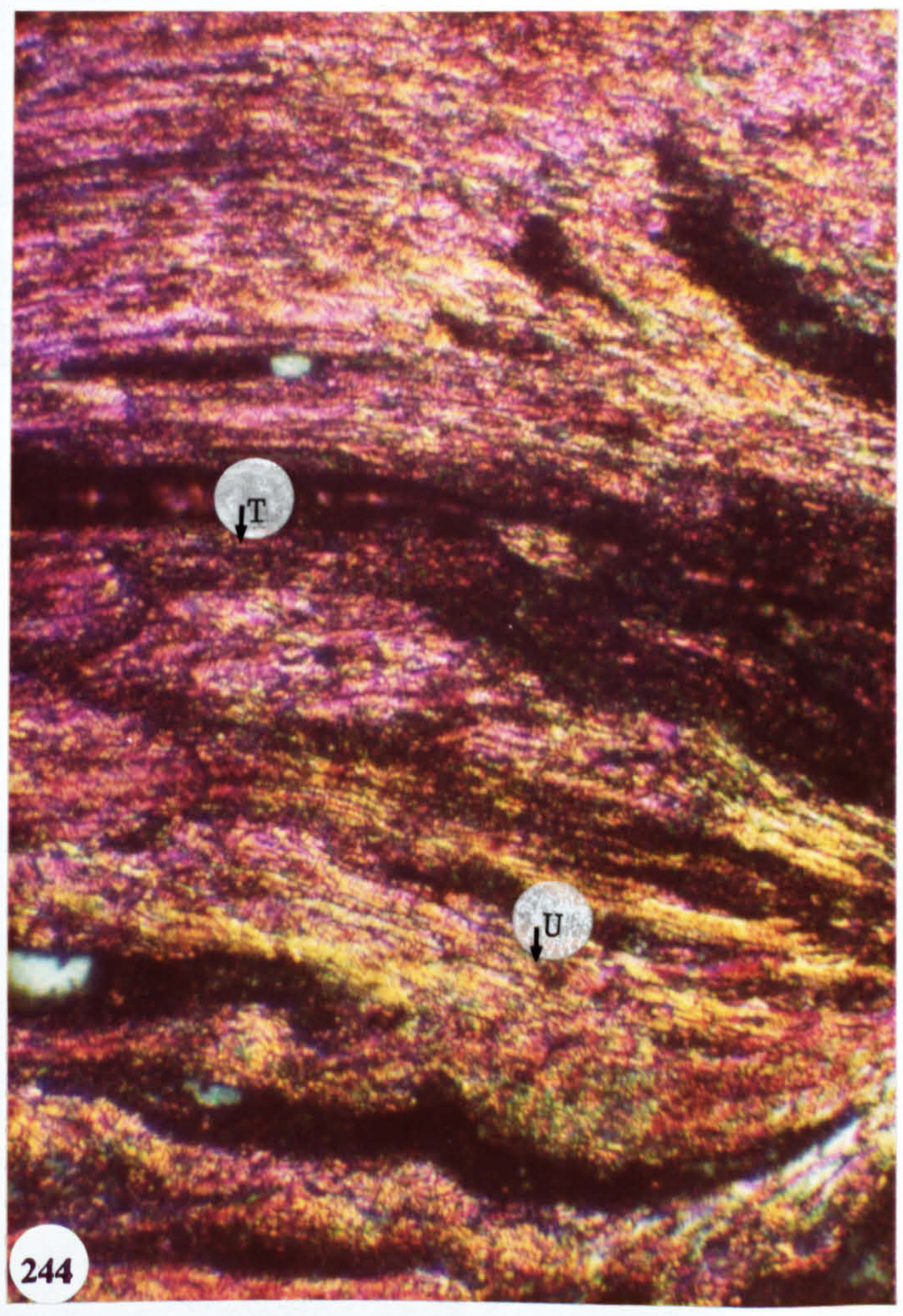
LIMA GRAPHITE. 100 nm

Figures 240 to 242 Scanning electron micrographs (JEOL 100C - ASID-4D) of Lima graphite oxidised in atomic oxygen at room temperature for 5 minutes, weight loss 0.98%.



LIMA GRAPHITE

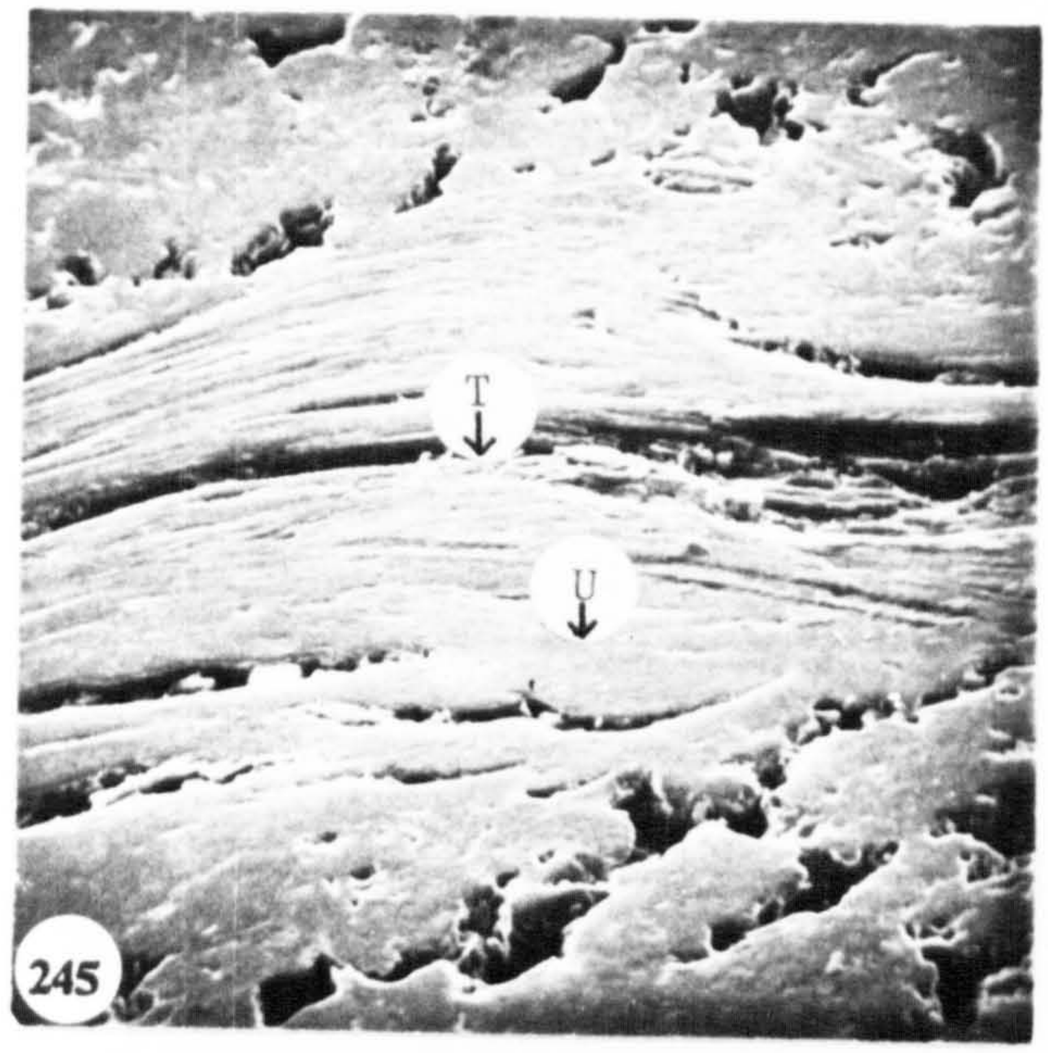
100 μm



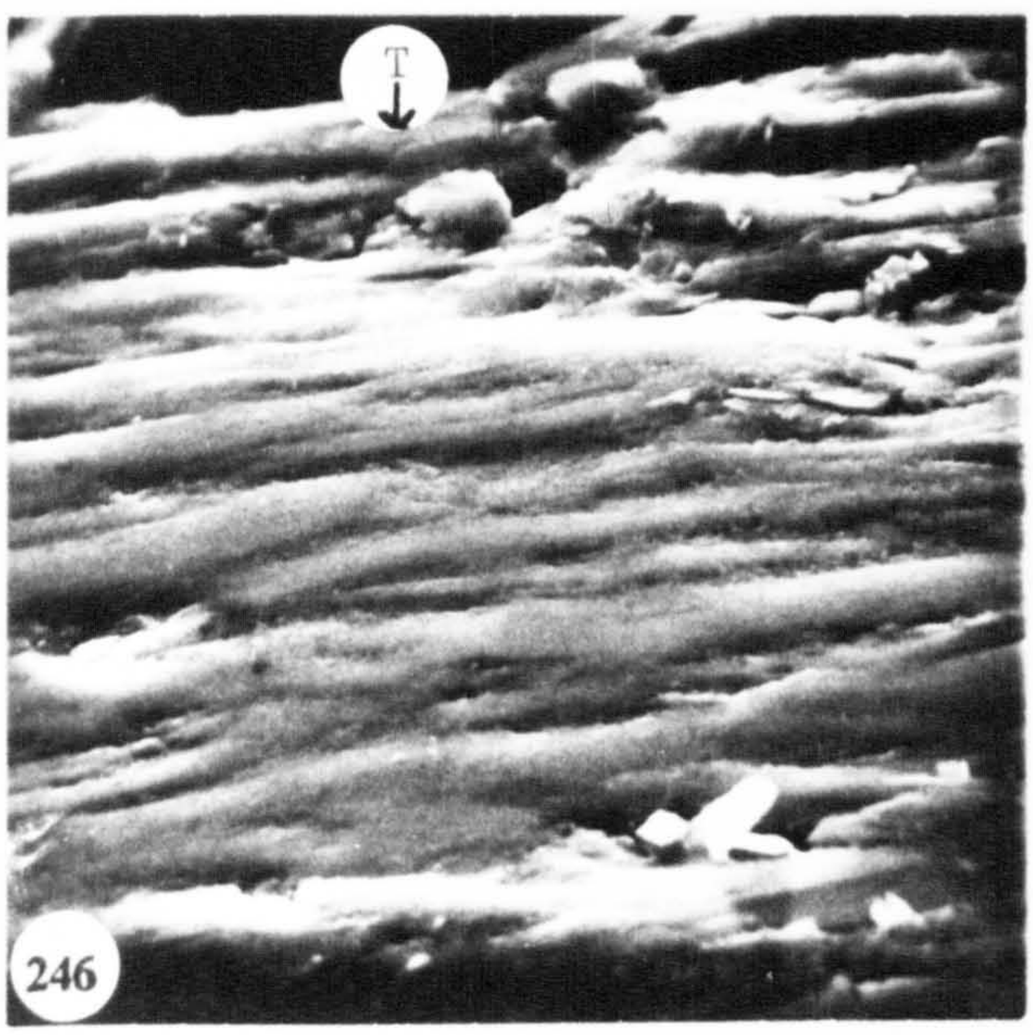
LIMA GRAPHITE

100 μm

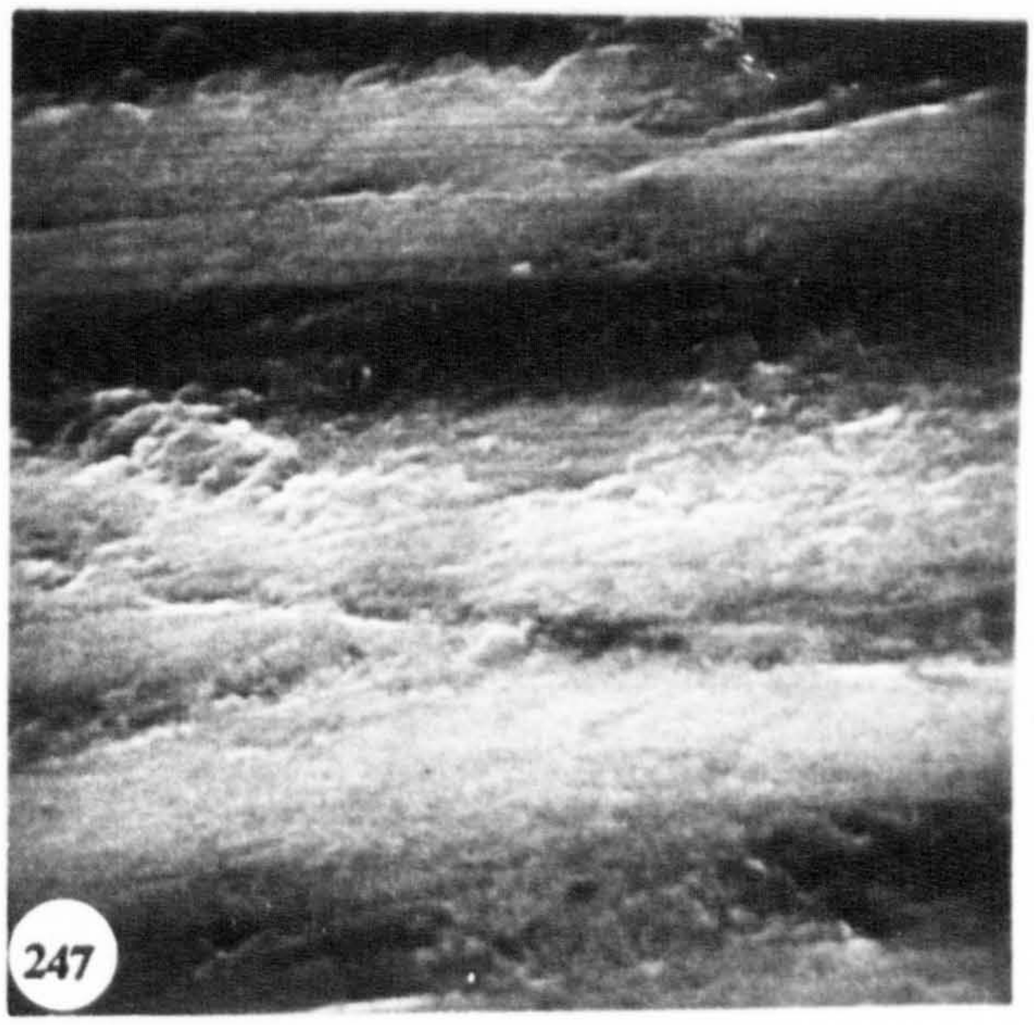
Figures 243 and 244. Optical micrographs of Lima Graphite (LG8) before and after gasification in atomic oxygen at~300 K for 3 minutes. Weight loss 0.57%.



LIMA GRAPHITE 100 µm

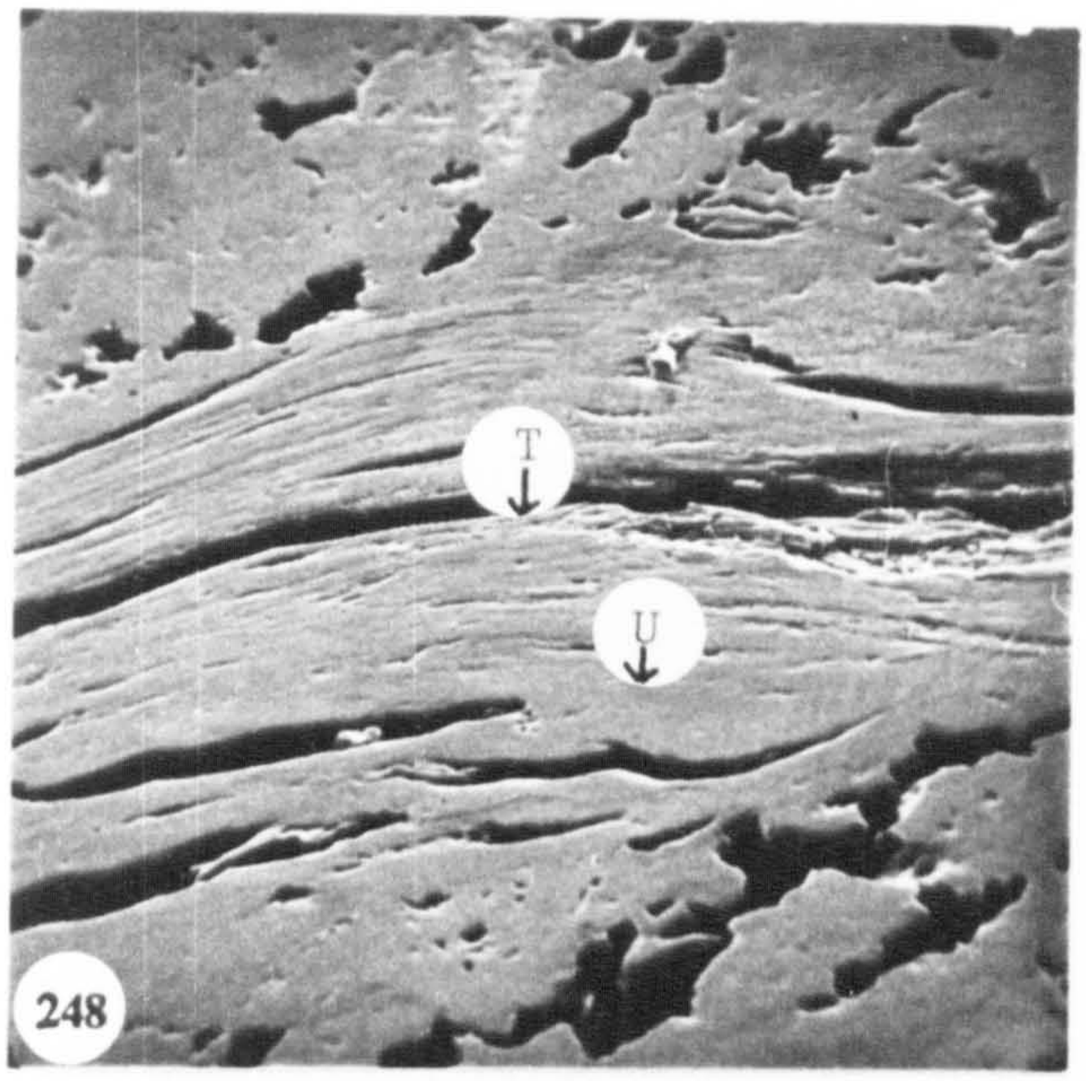


LIMA GRAPHITE 10 µm

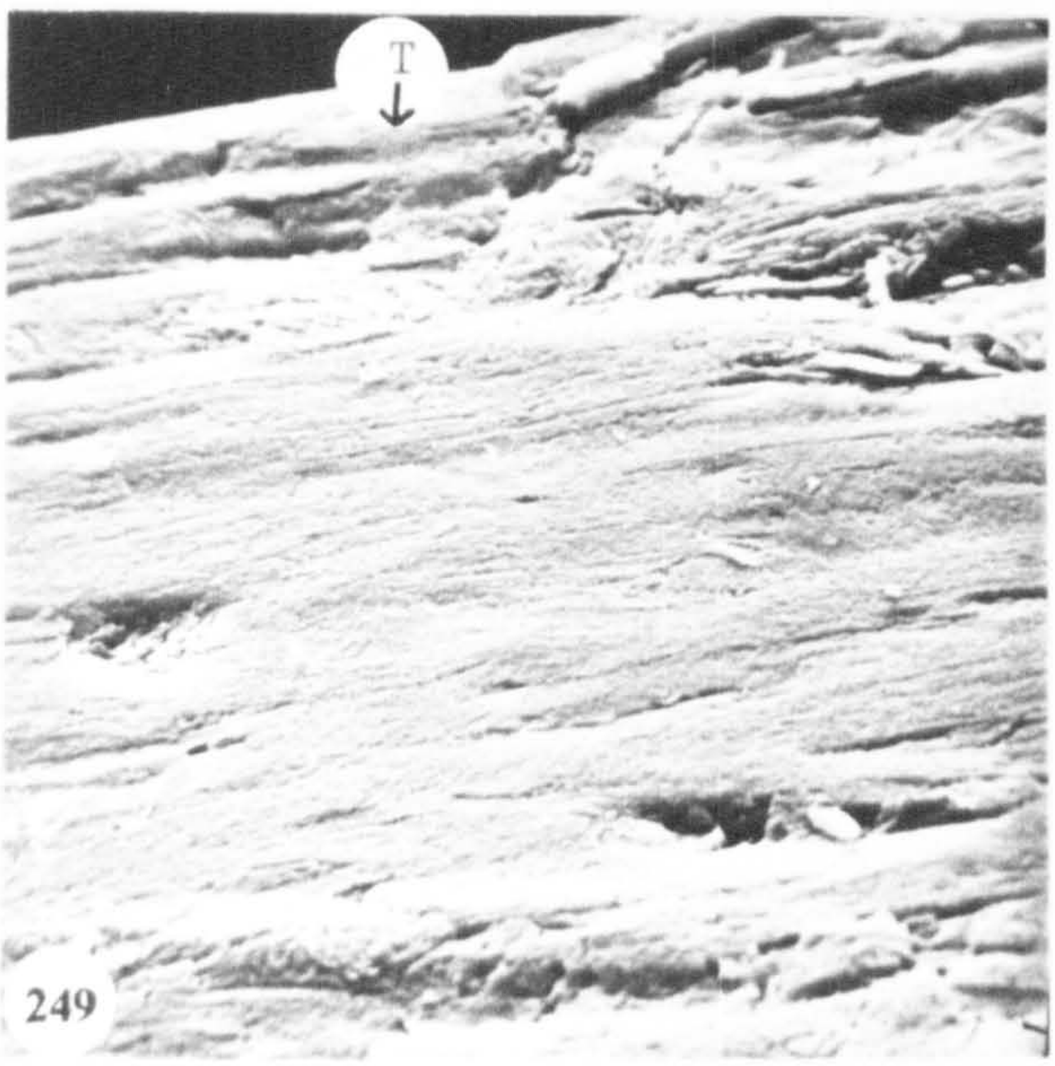


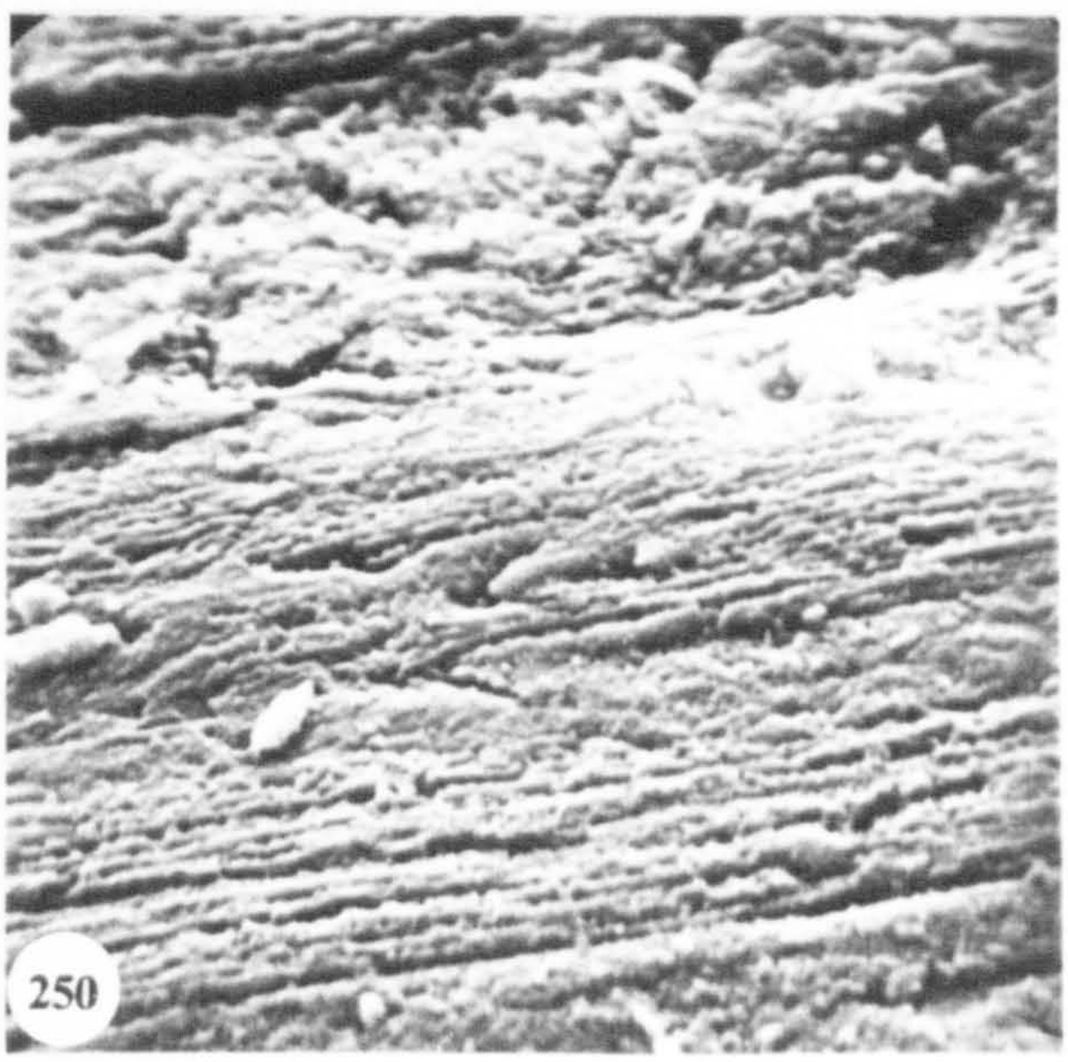
LIMA GRAPHITE 2 µm

Figures 245 to 247. Scanning electron micrographs (stereoscan) of Lima Graphite (LG8) before gasification.



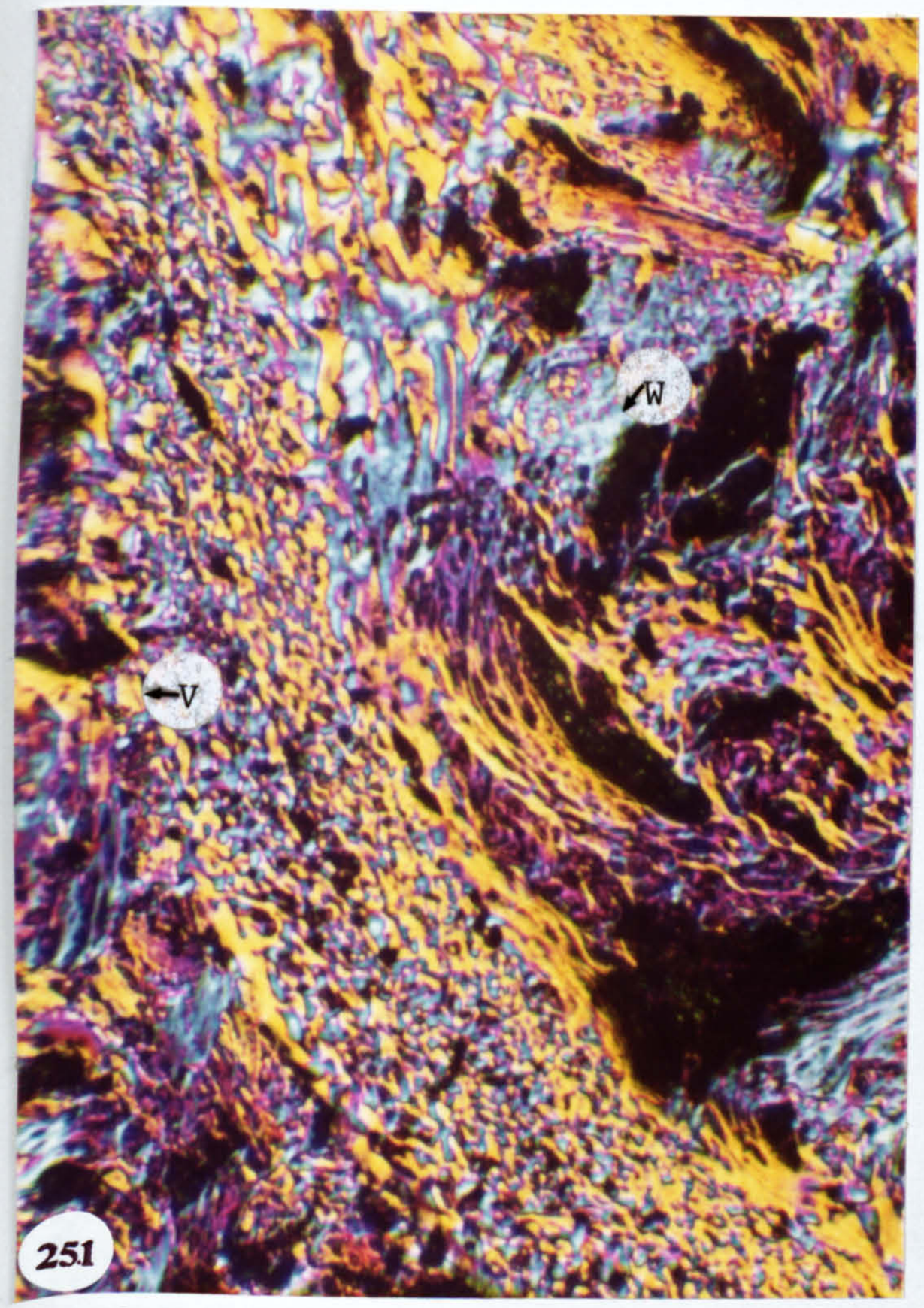
LIMA GRAPHITE 100 µm





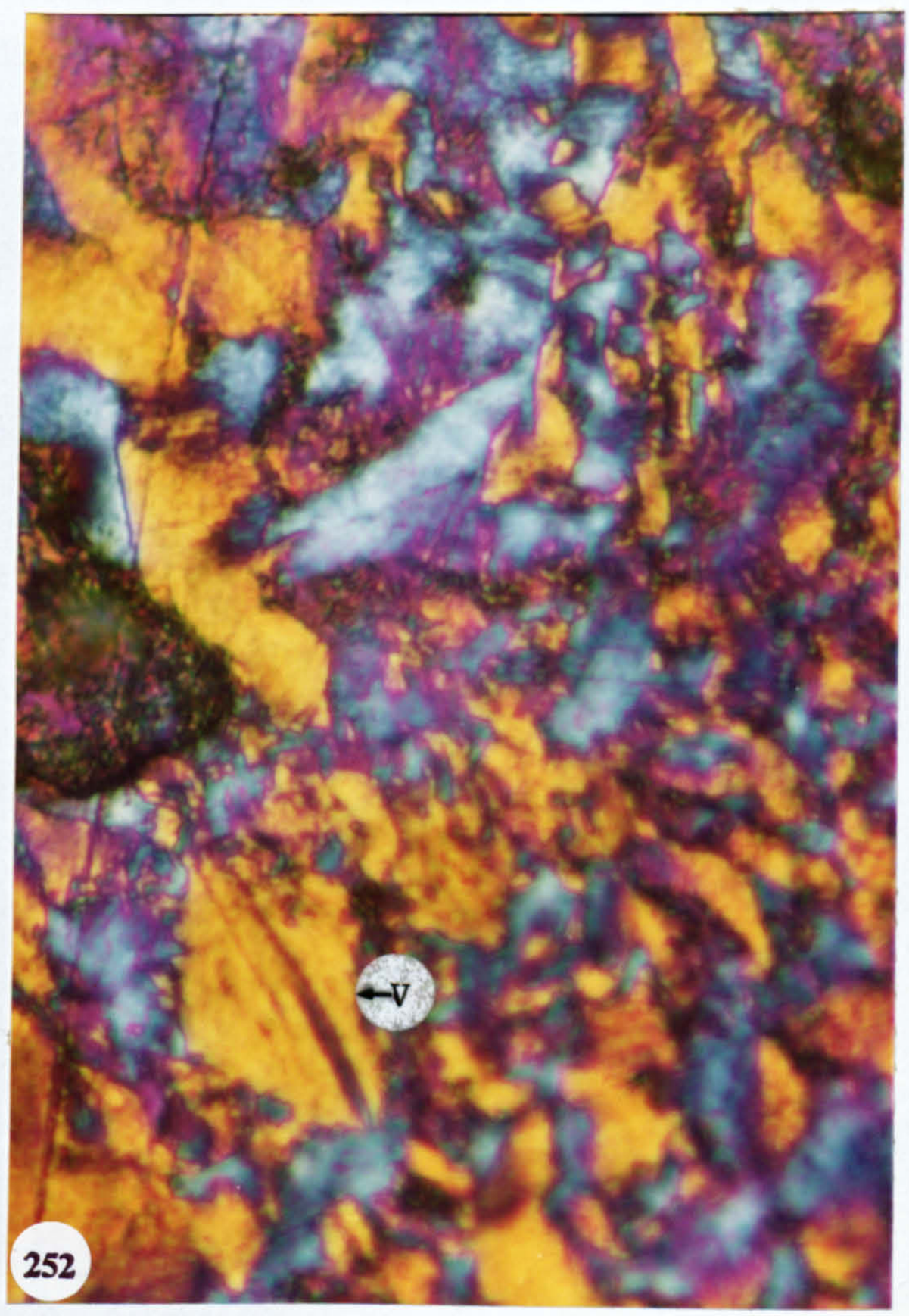
LIMA GRAPHITE 10 µm LIMA GRAPHITE 2 µm

Figures 248 to 250. Scanning electron micrographs (stereoscan) of Lima Graphite (LG8) after gasification in atomic oxygen at ~300 K for 3 minutes. Weight loss 0.57%.



LIMA GRAPHITE

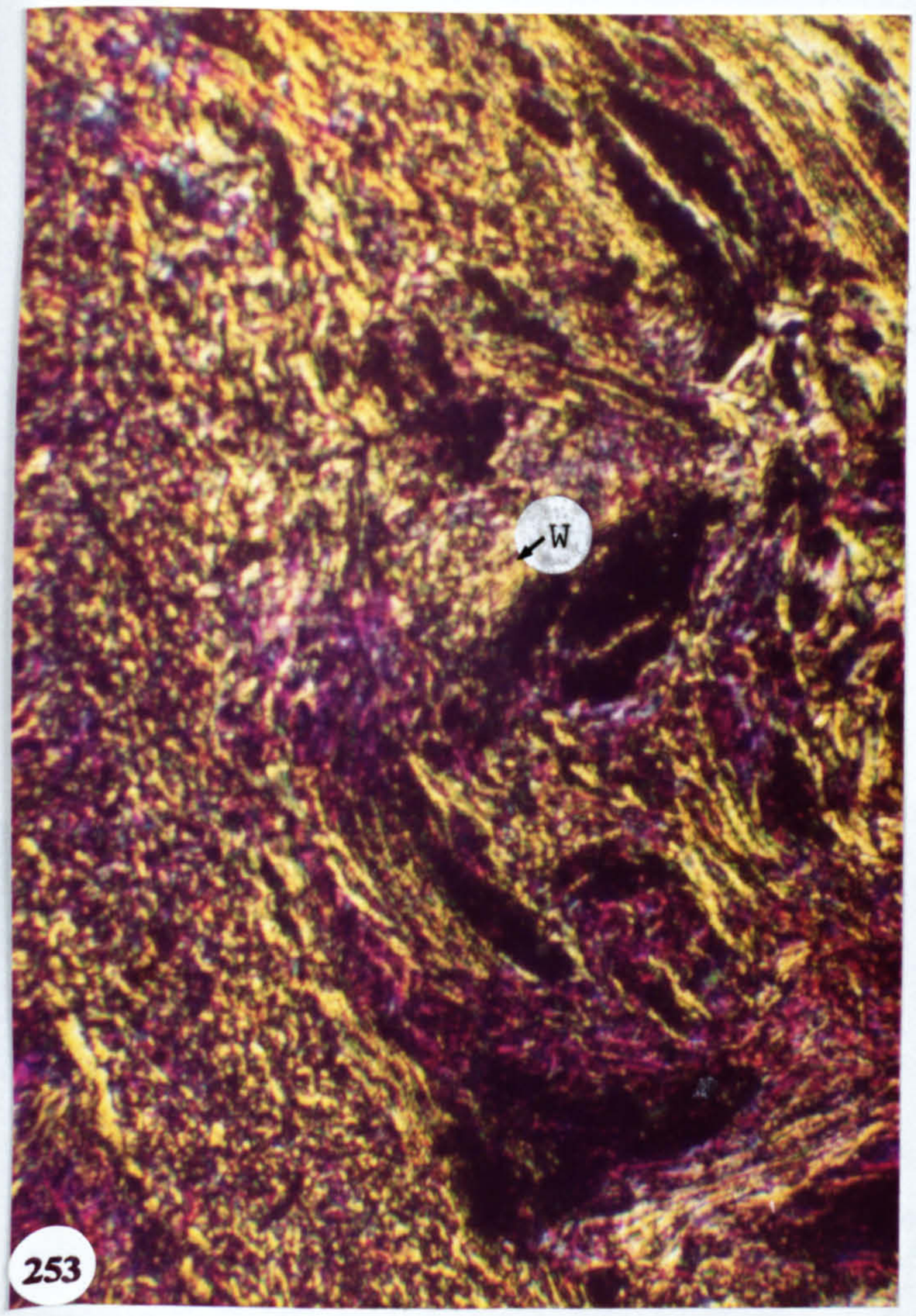
100 µm



LIMA GRAPHITE

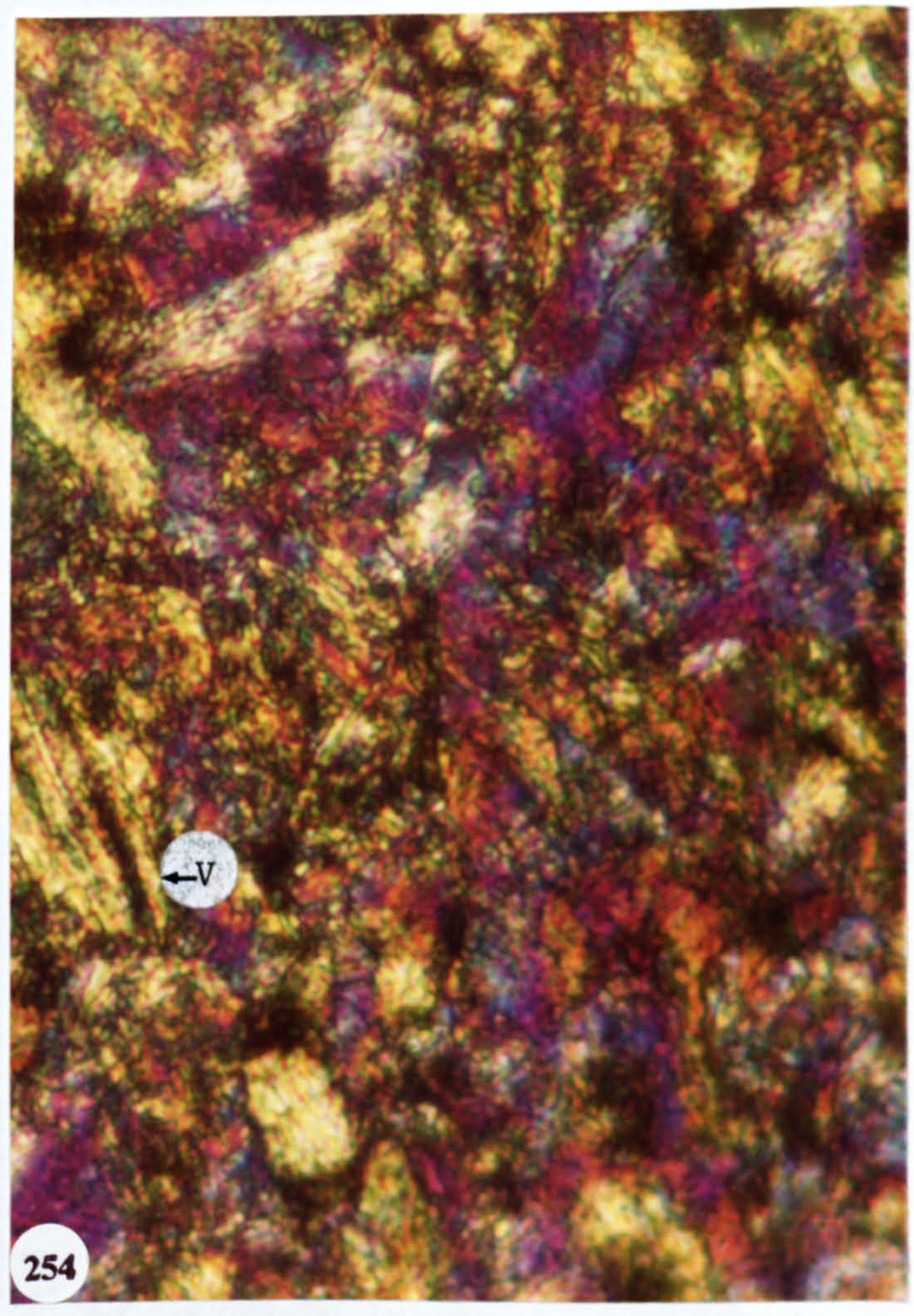
10 µm

Figures 251 and 252. Optical micrographs of Lima Graphite (LG9) before gasification.



LIMA GRAPHITE

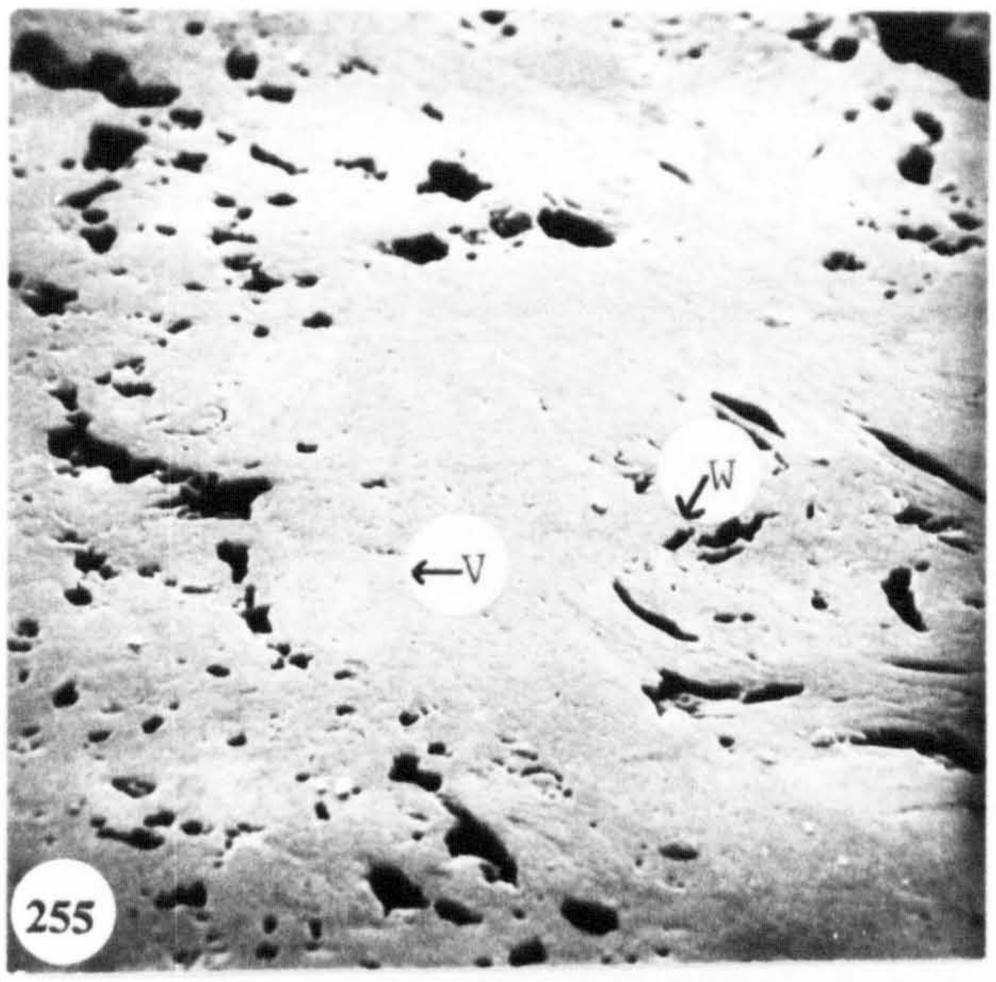
100 μm



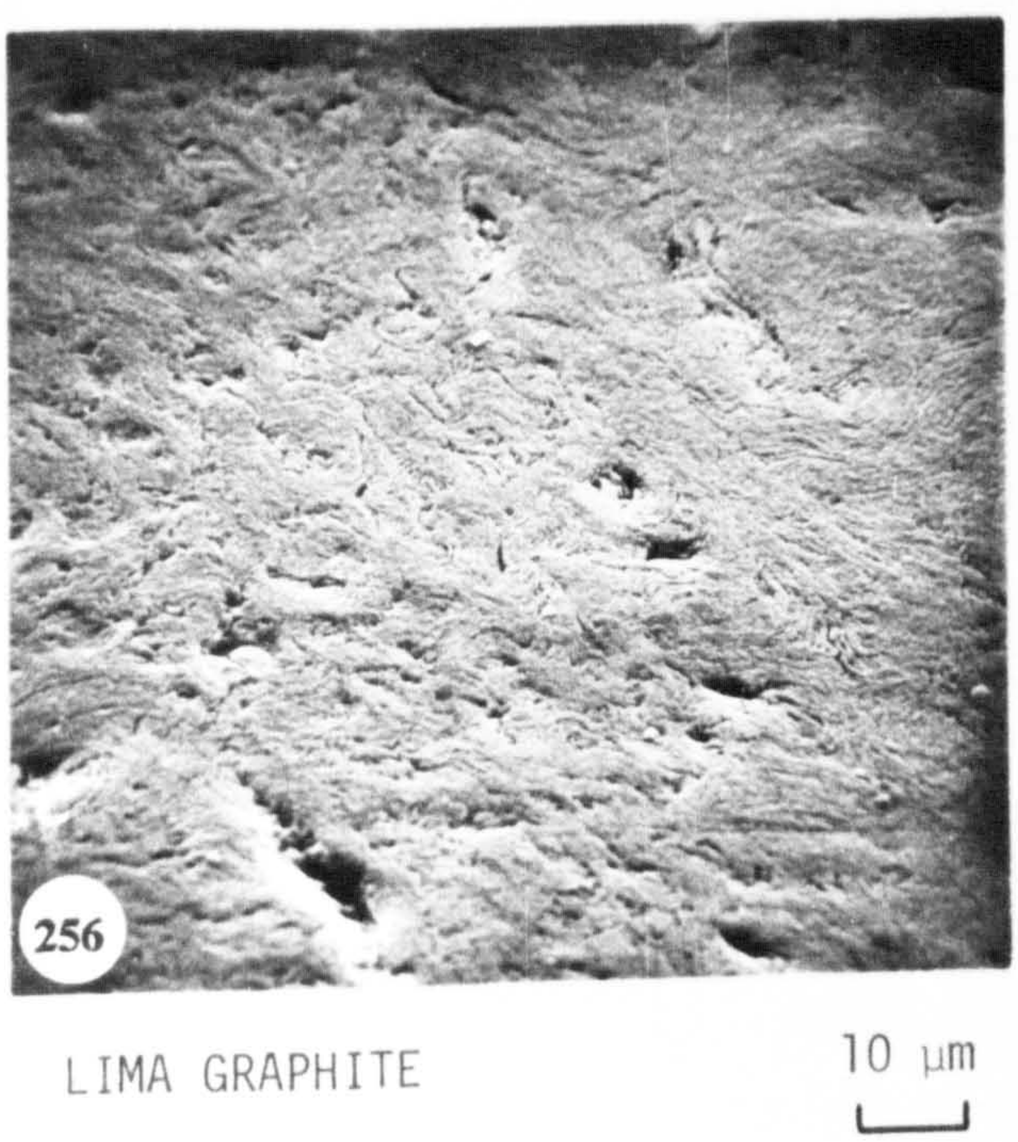
LIMA GRAPHITE

10 μm

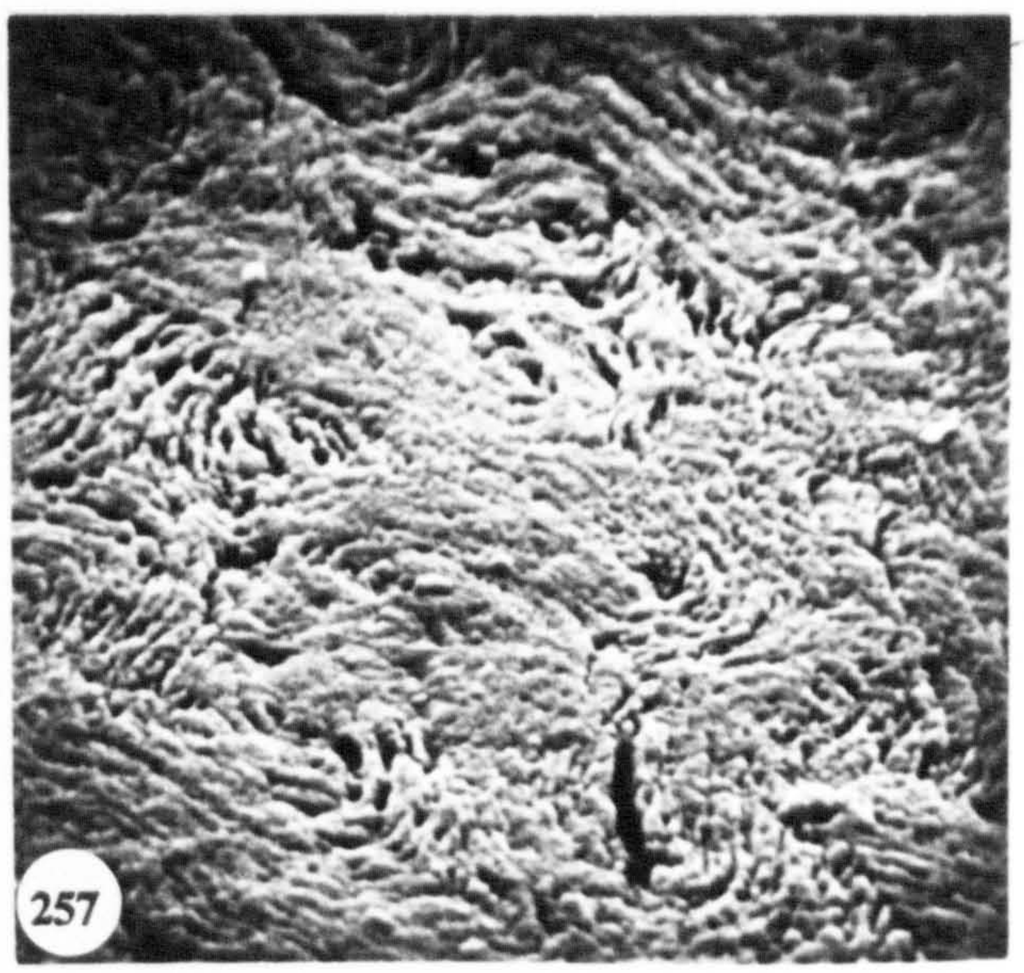
Figures 253 and 254. Optical micrographs of Lima Graphite (LG9) after gasification in atomic oxygen at ~300 K for 2 minutes. Weight loss 0.15%.



LIMA GRAPHITE 100 µm

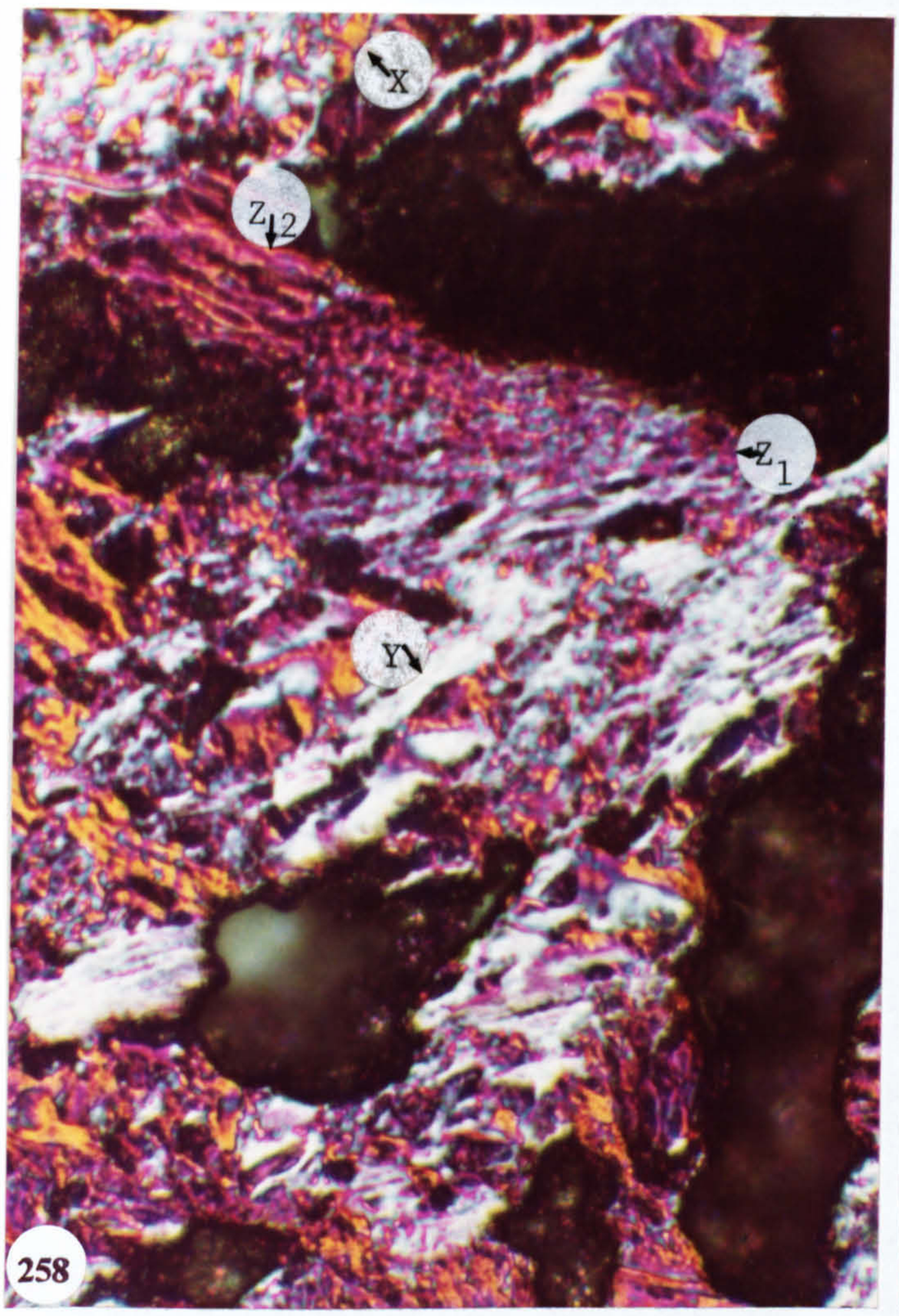


LIMA GRAPHITE 10 µm



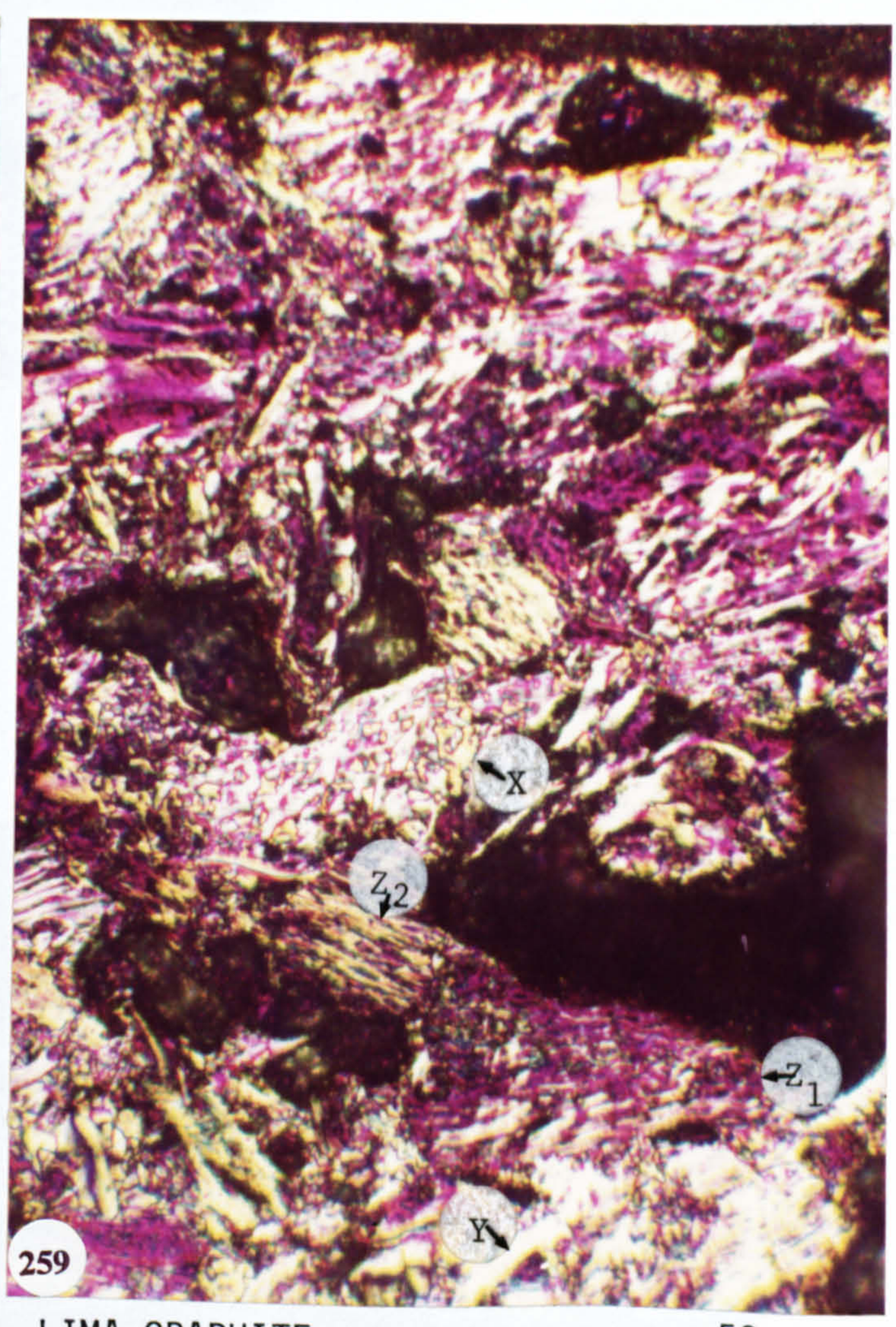
LIMA GRAPHITE 2 µm

Figures 255 to 257. Scanning electron micrographs (stereoscan) of Lima Graphite (LG9) after gasification in atomic oxygen at~300 K for 2 minutes. Weight loss 0.15%.



LIMA GRAPHITE

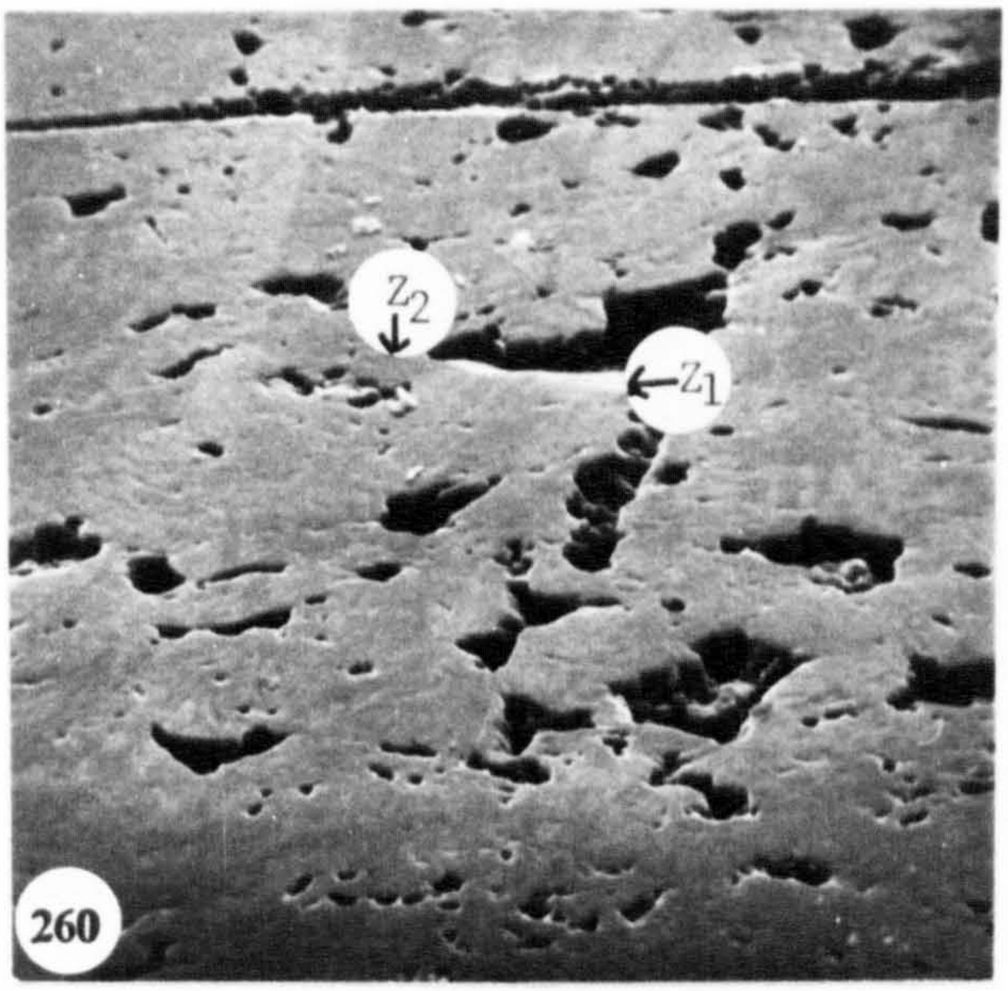
50 μm



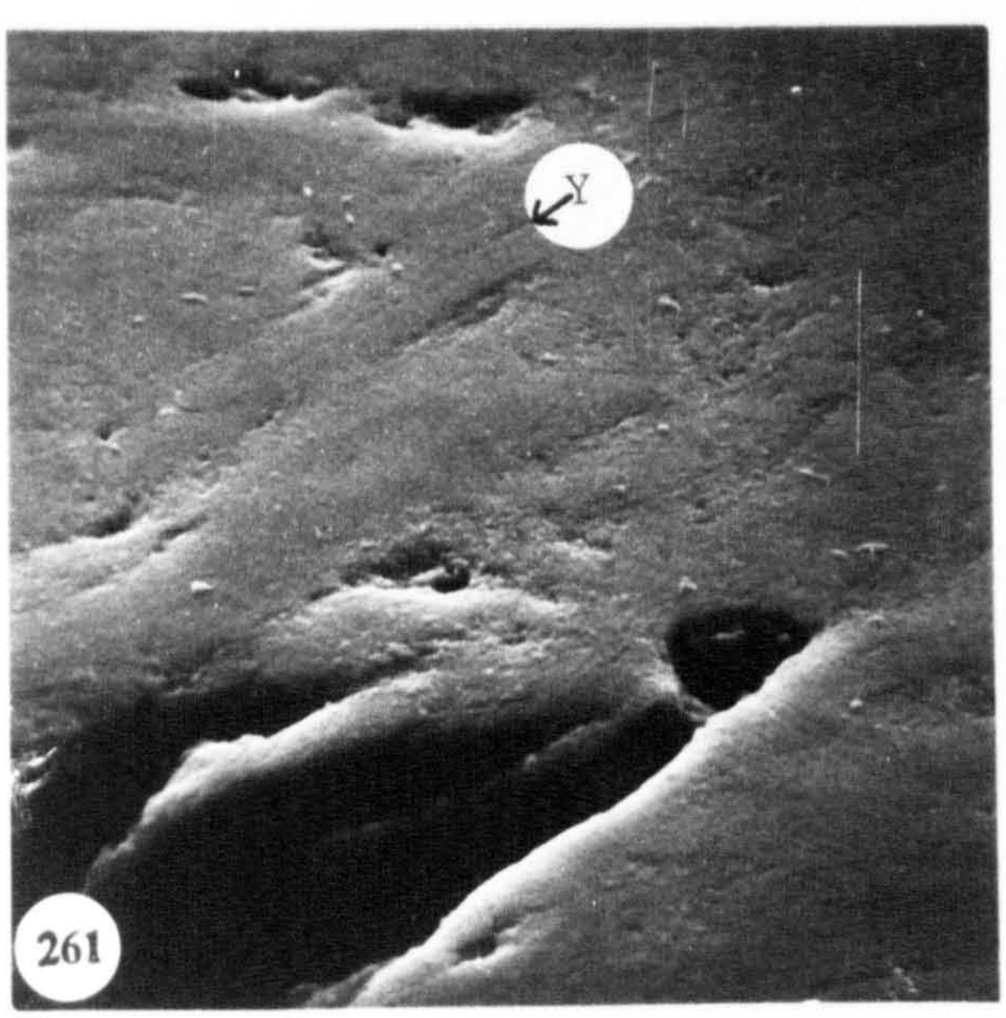
LIMA GRAPHITE

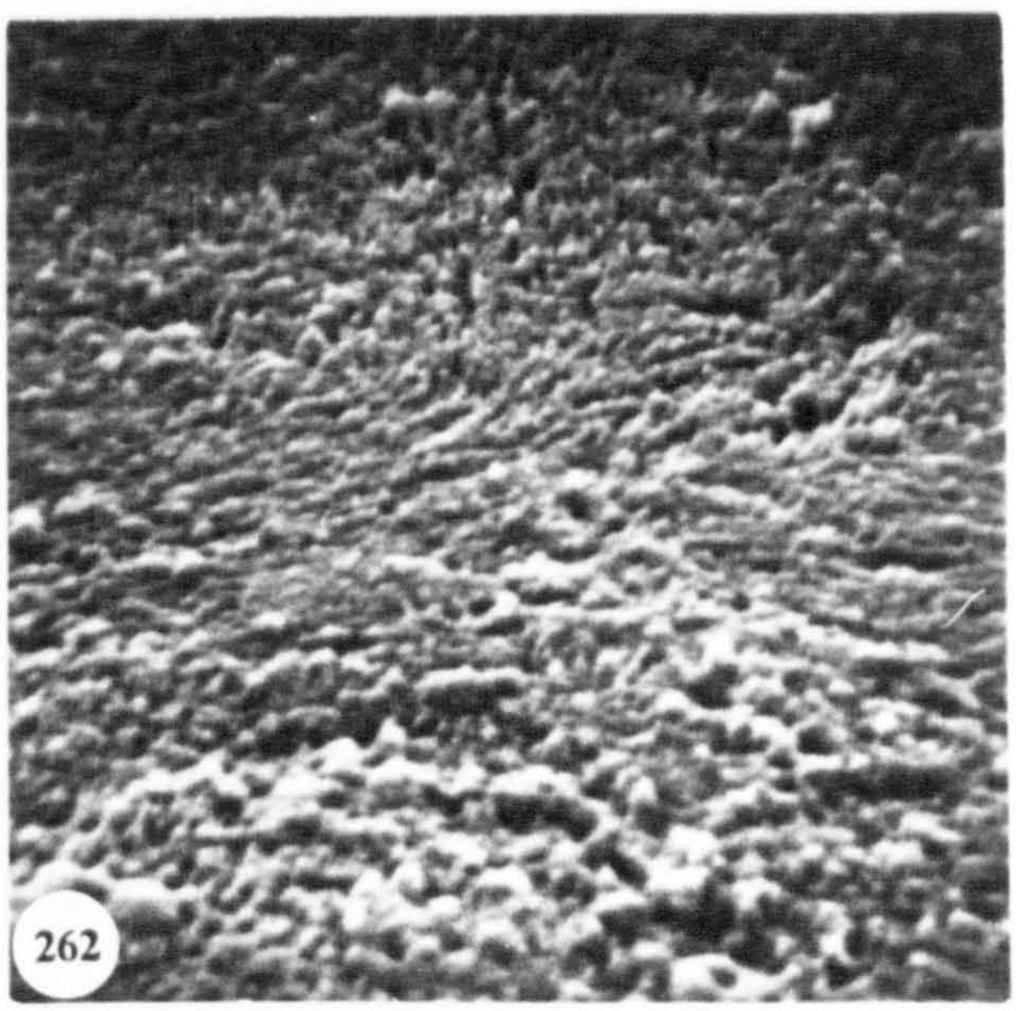
50 μm

Figures 258 and 259. Optical micrographs of Lima Graphite (LG10) before and after gasification in atomic hydrogen at~300 K for 20 minutes. Weight loss 0.08%.



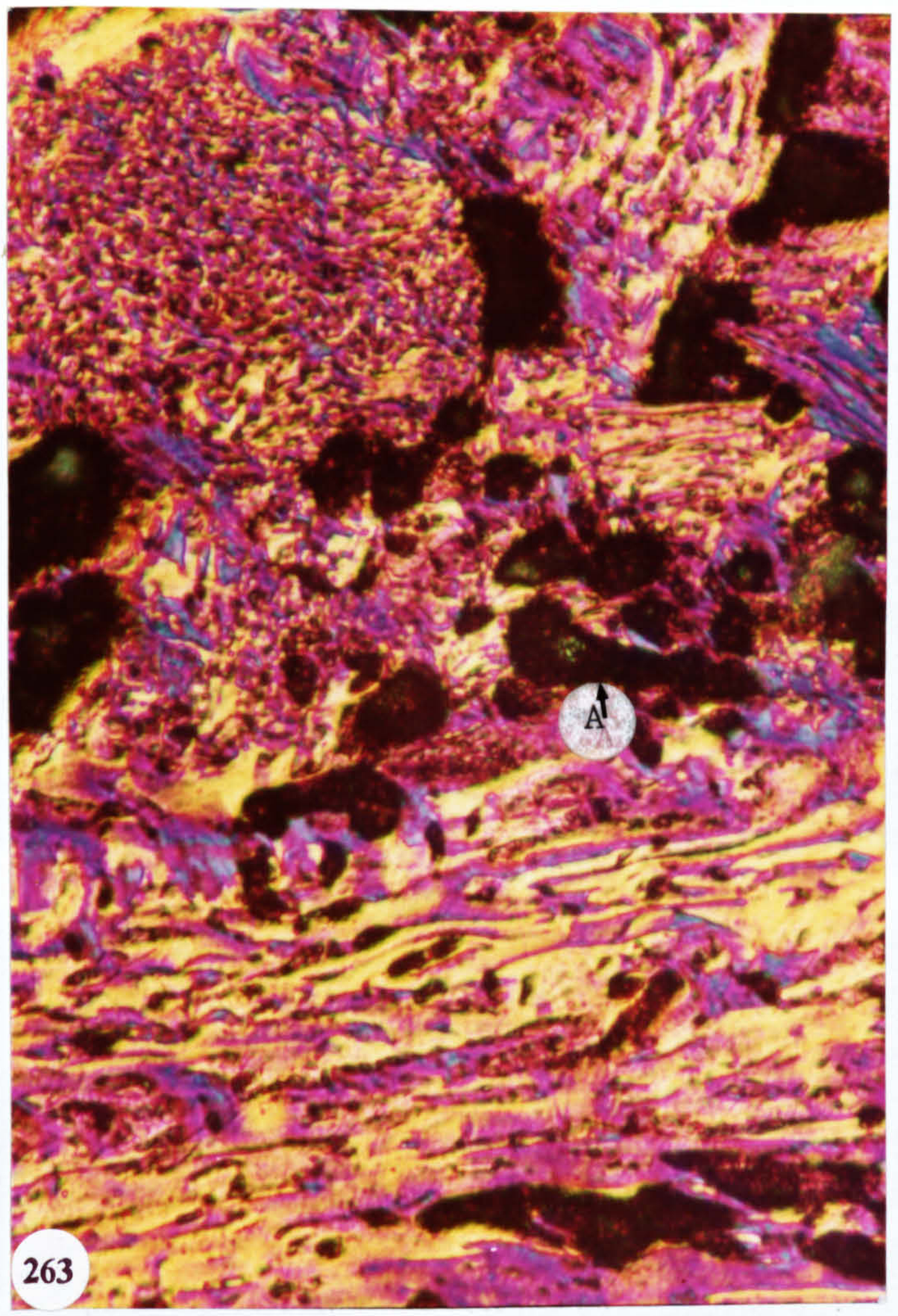
LIMA GRAPHITE 100 μm





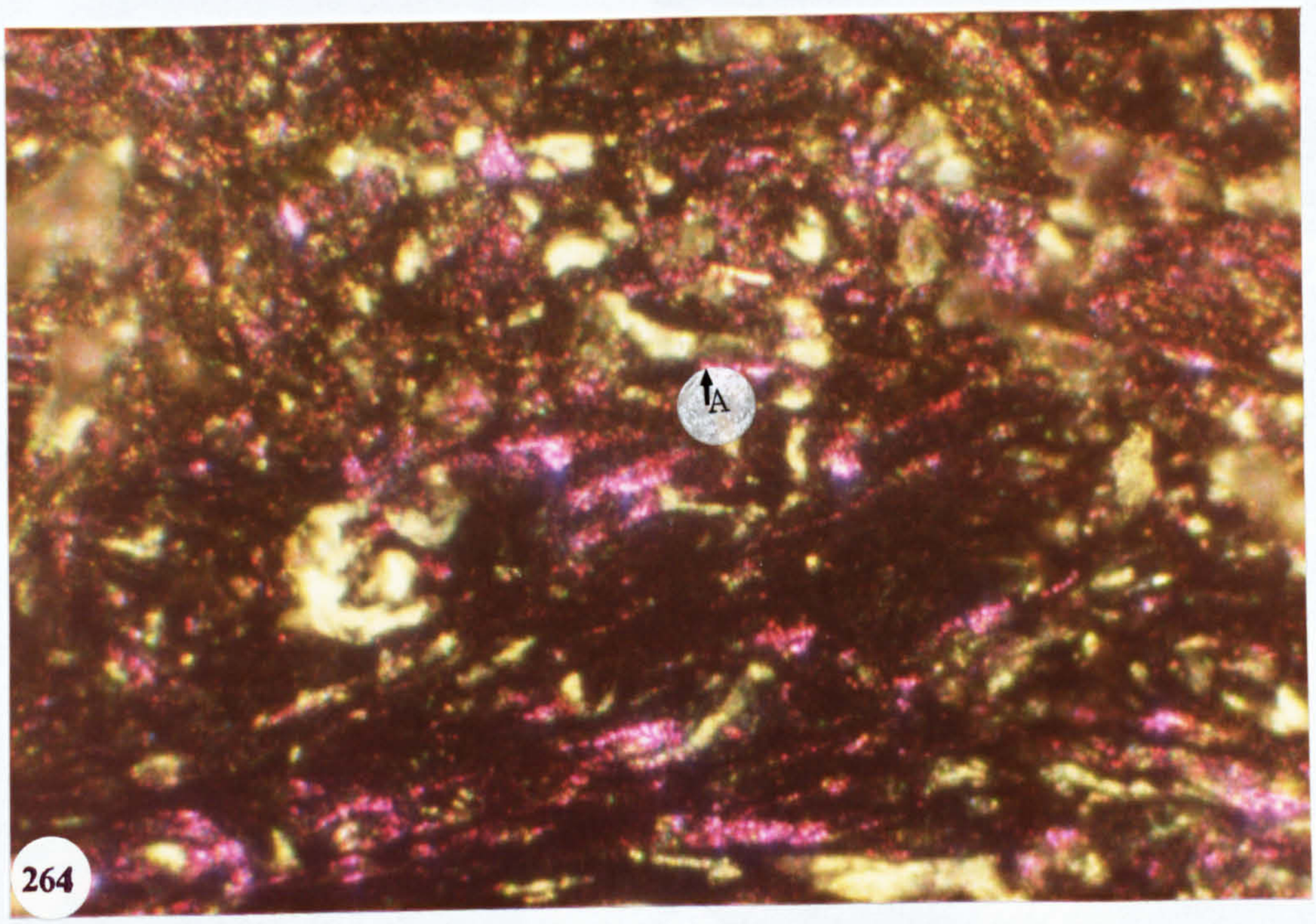
LIMA GRAPHITE 10 μm LIMA GRAPHITE 1 μm

Figures 260 to 262. Scanning electron micrographs (stereoscan) of Lima Graphite (LG10) after gasification in atomic hydrogen at ~300 K for 20 minutes.
Weight loss 0.08%.



LIMA GRAPHITE

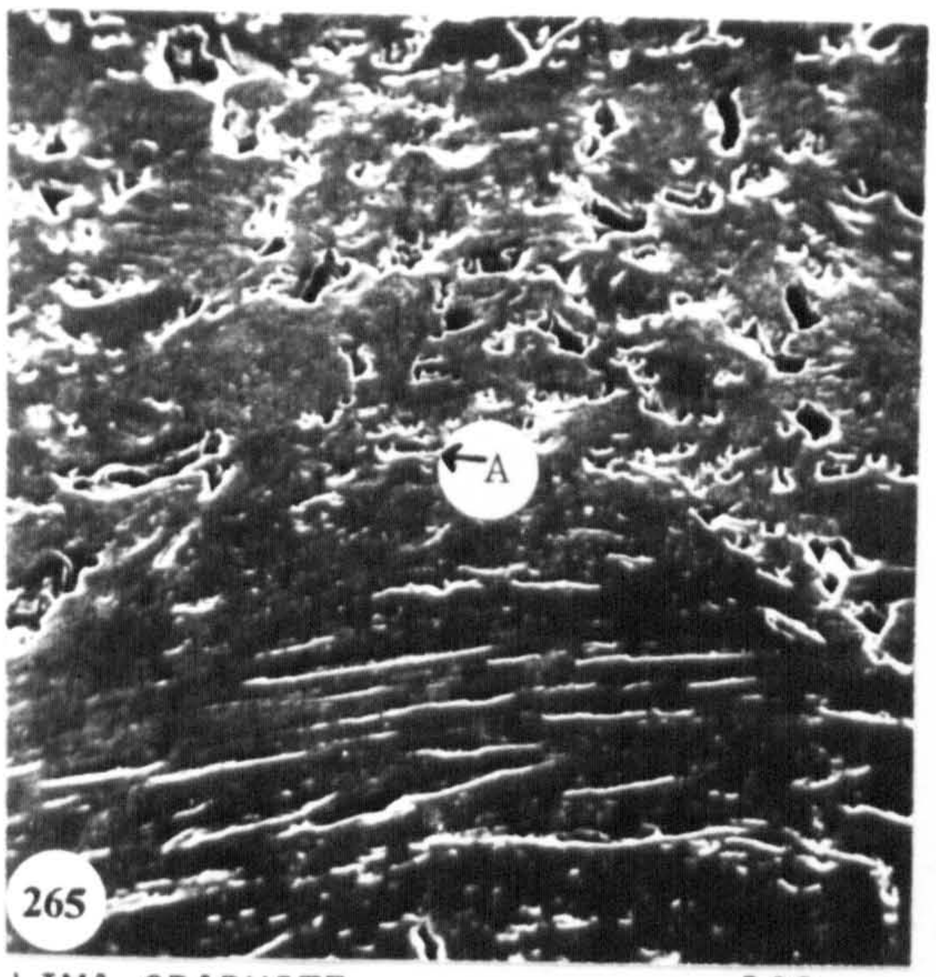
50 μm



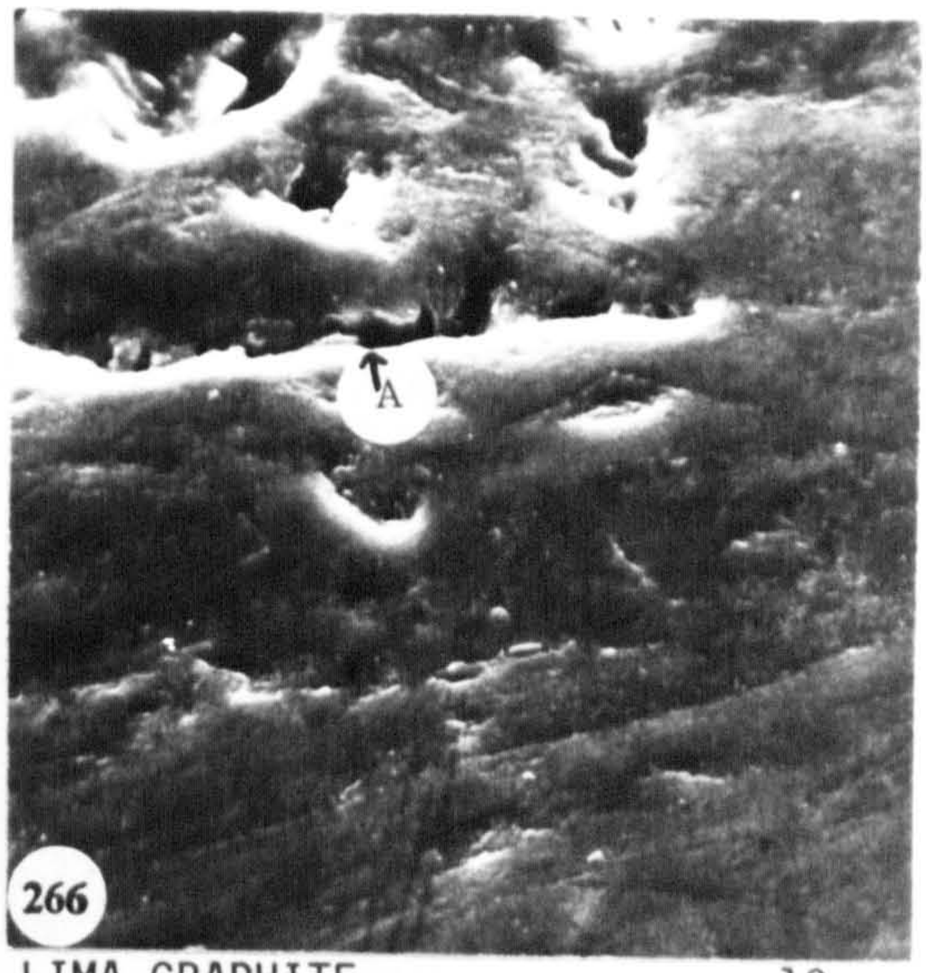
50 μm

LIMA GRAPHITE

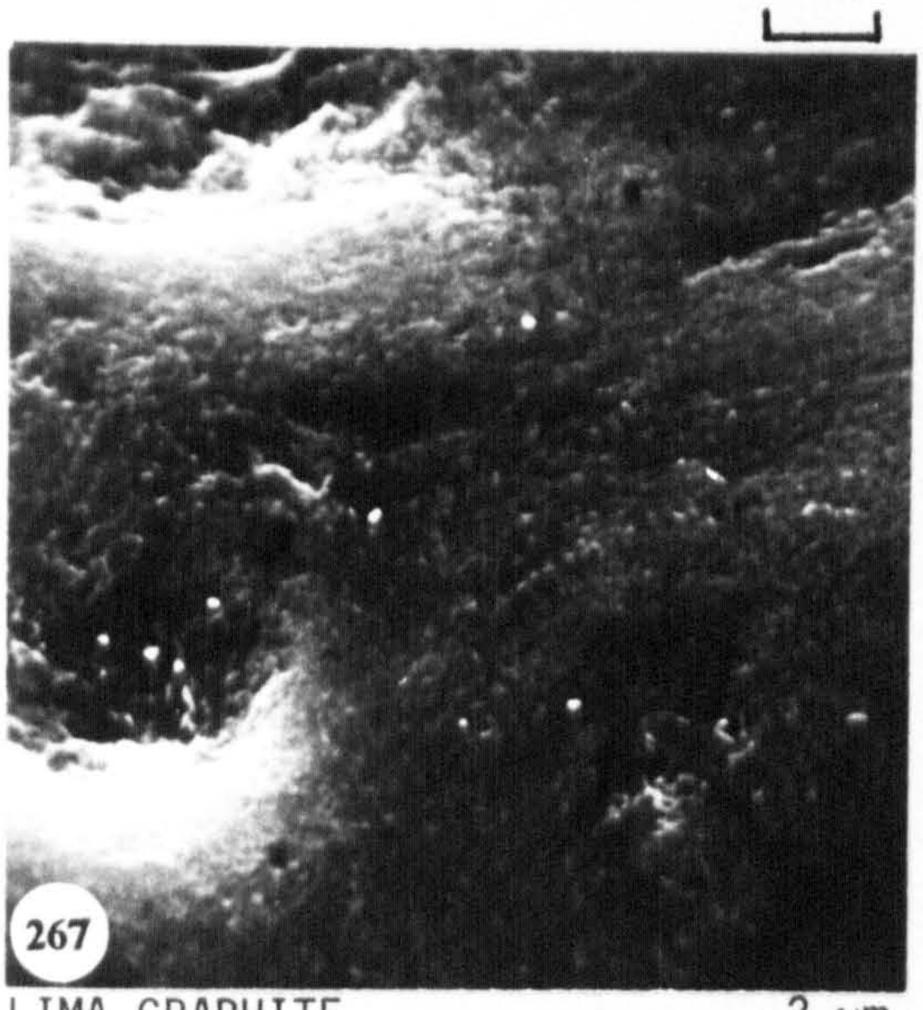
Figures 263 and 264. Optical micrographs of Lima Graphite (LG12) before and after gasification in carbon dioxide at 1073 K for 16 hours. Weight loss 1.64%.



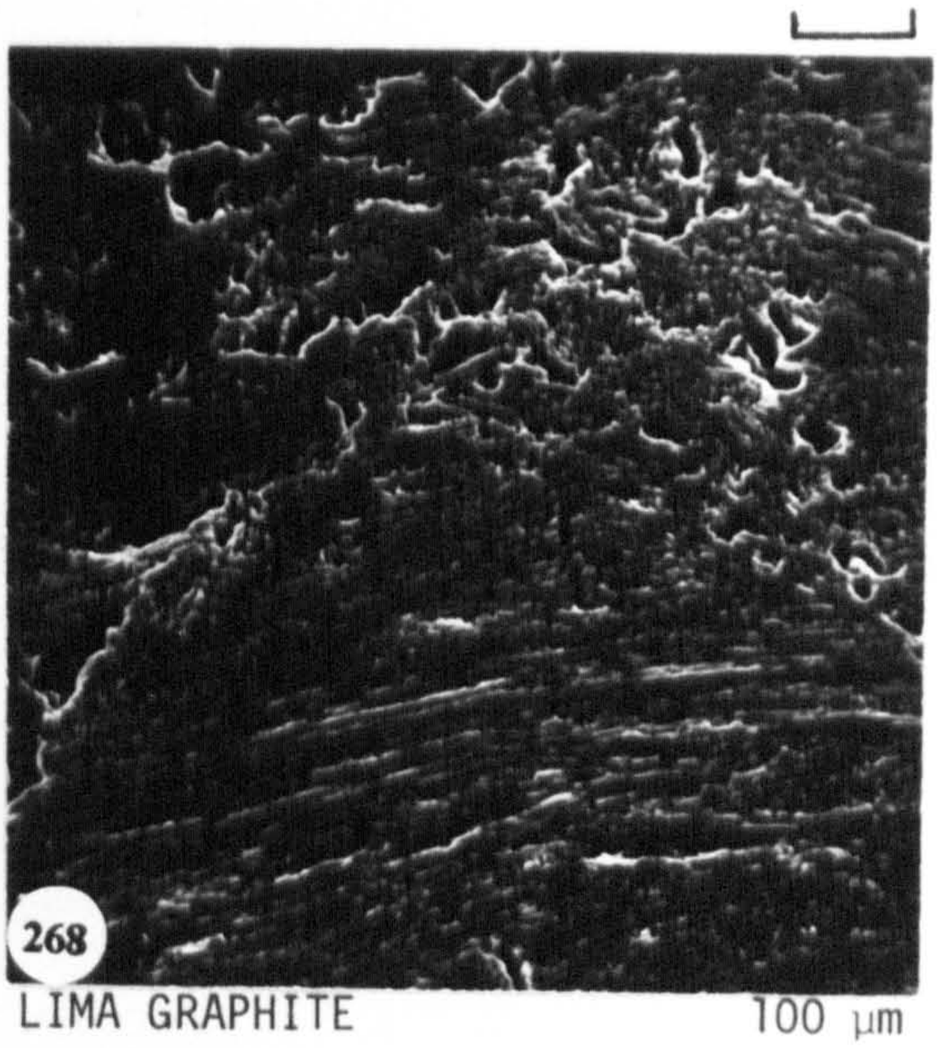
LIMA GRAPHITE 100 µm



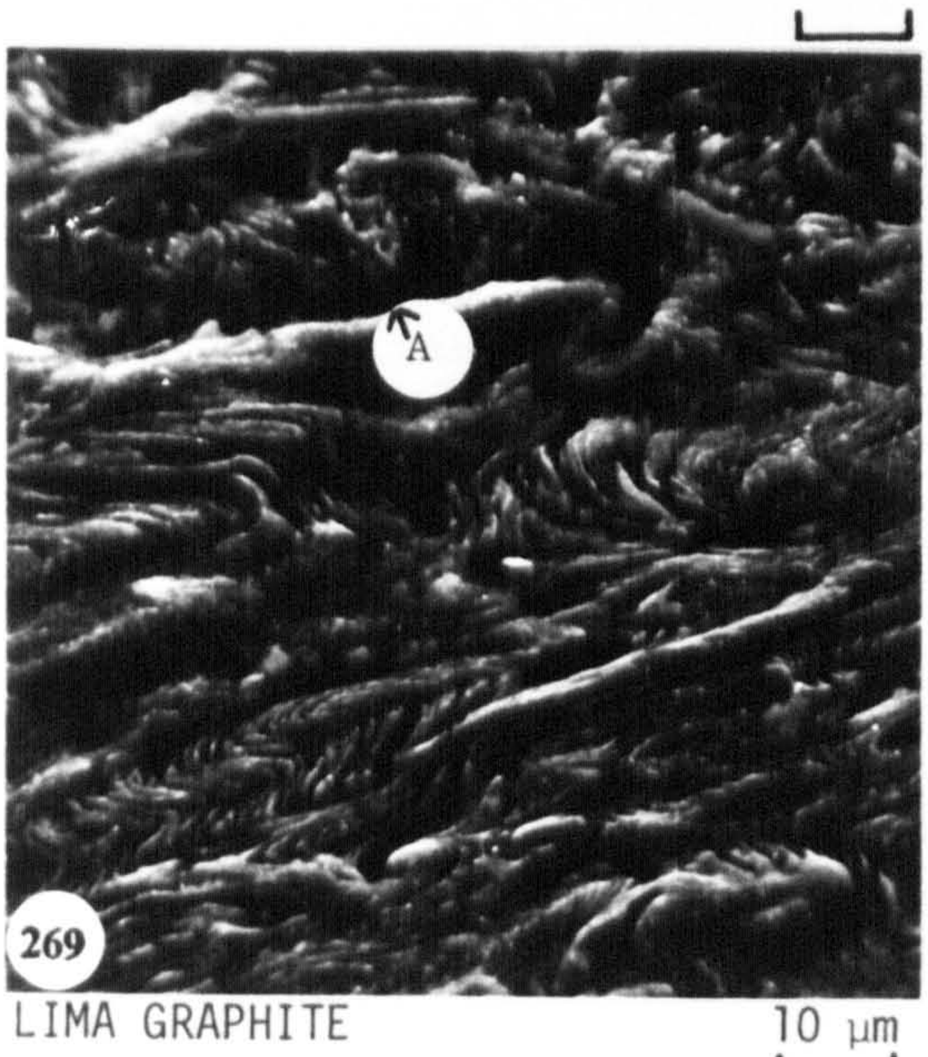
LIMA GRAPHITE 10 µm



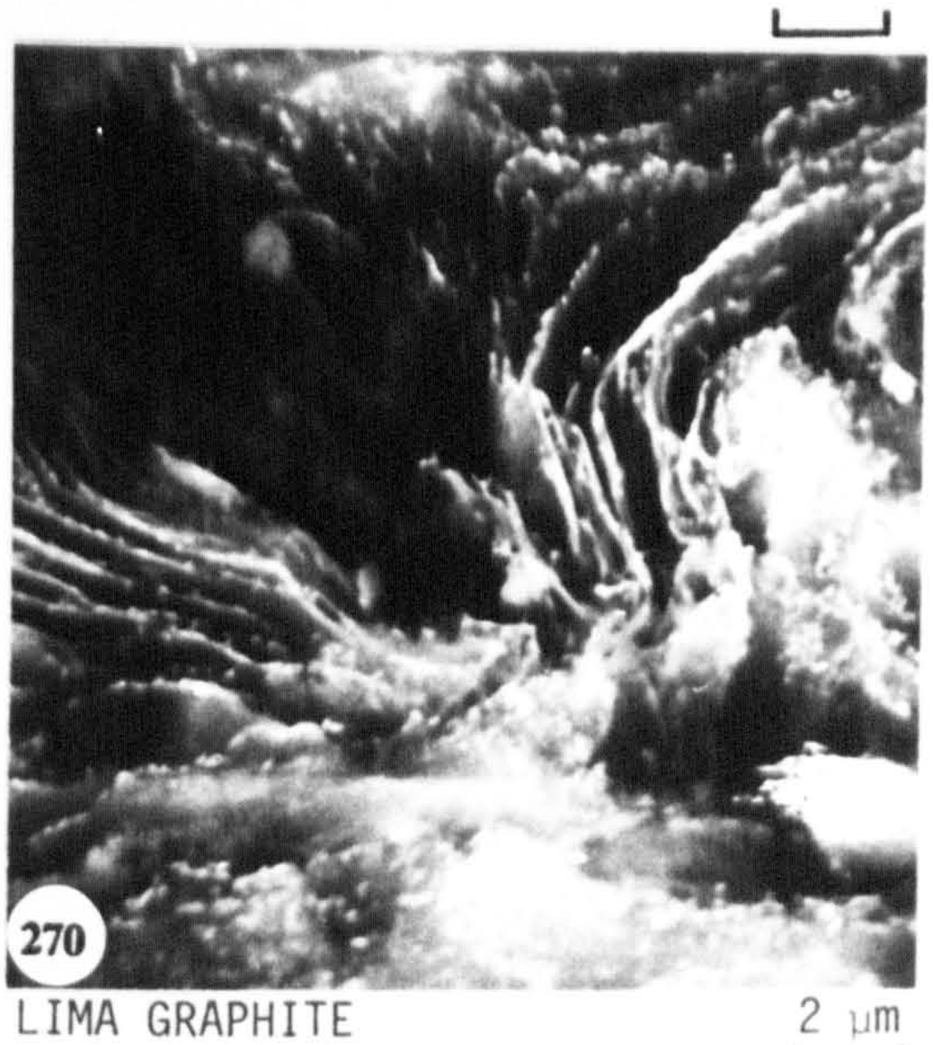
LIMA GRAPHITE 2 µm



LIMA GRAPHITE 100 µm



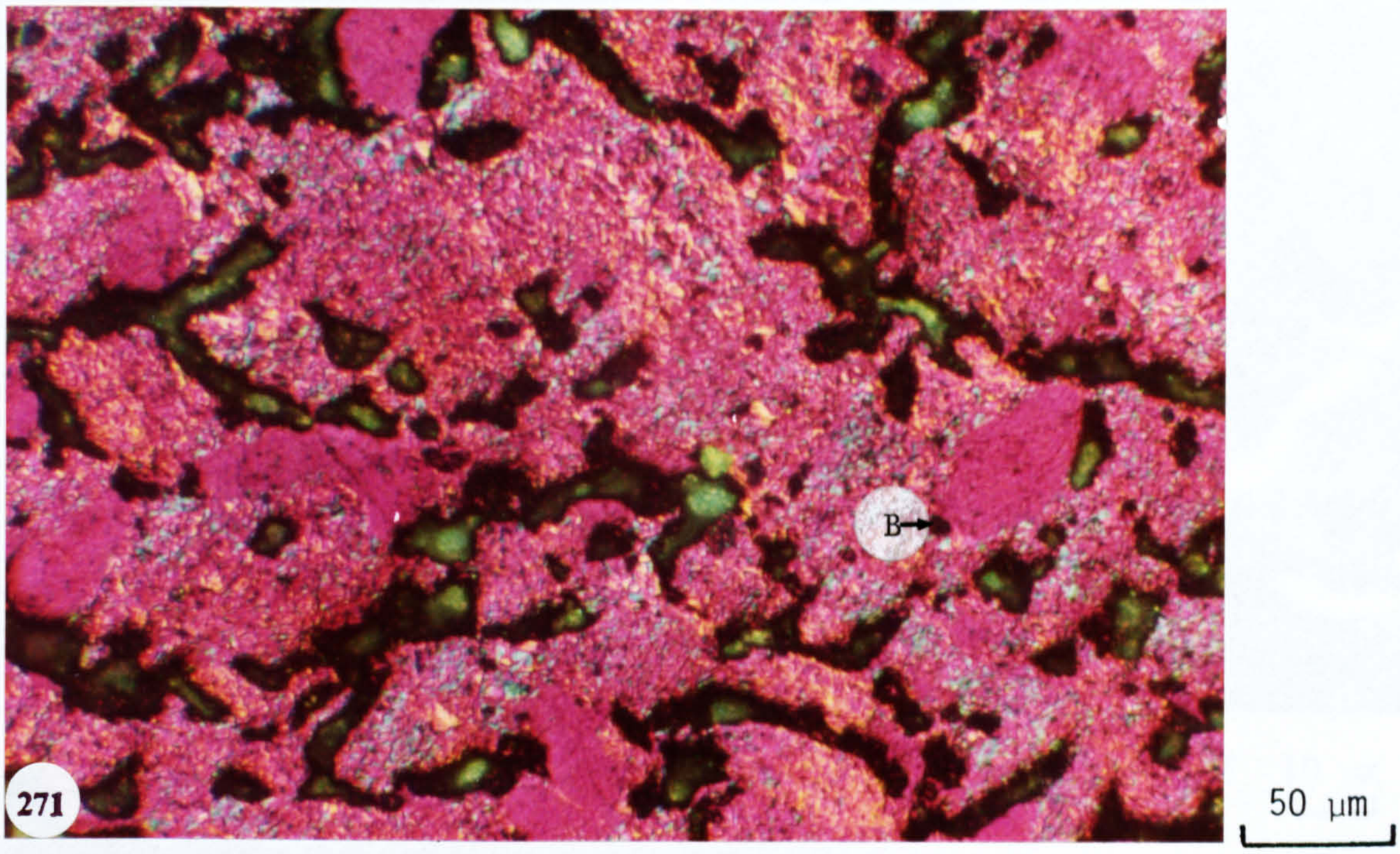
LIMA GRAPHITE 10 µm



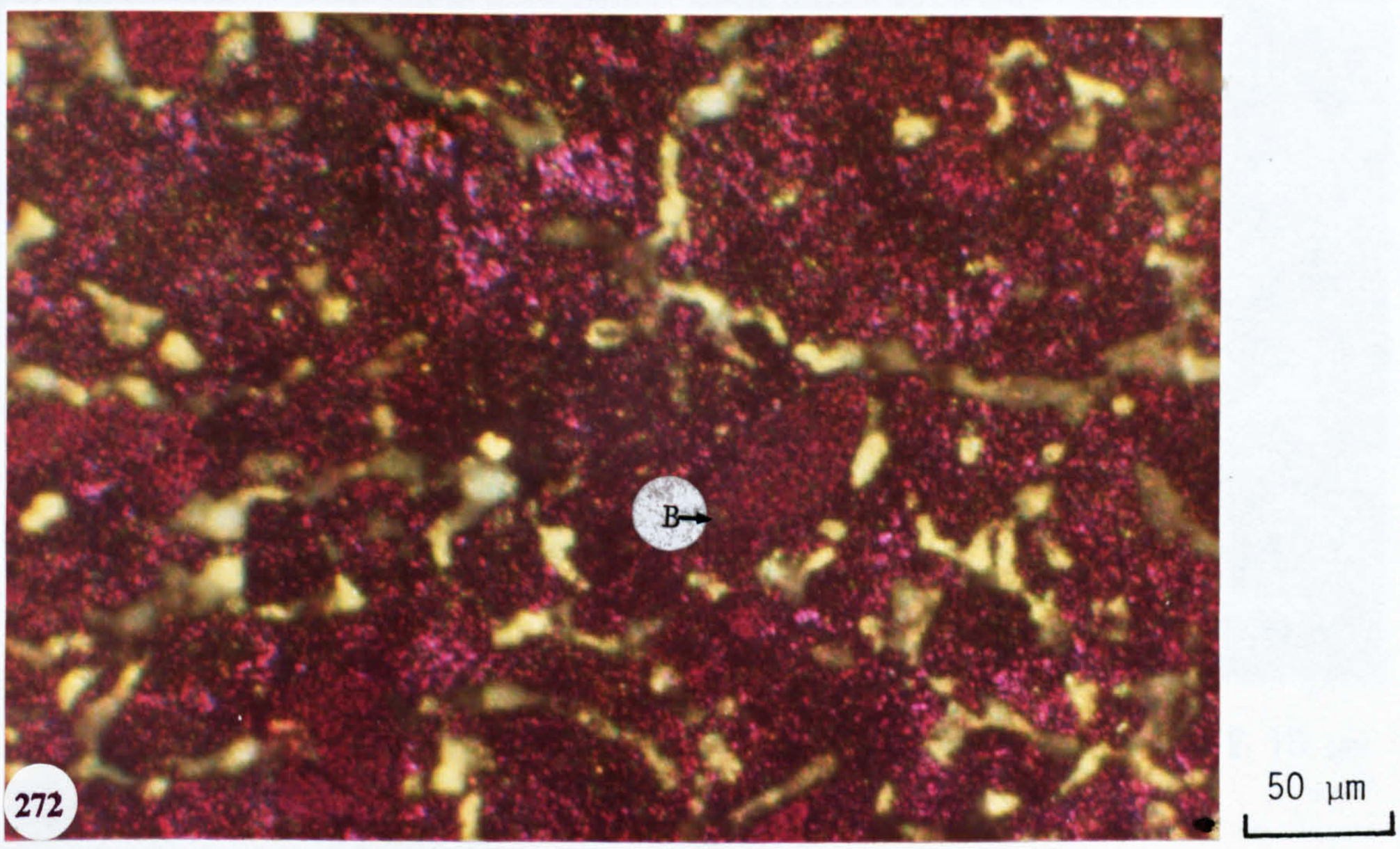
LIMA GRAPHITE 2 µm

Figures 265 to 270. Scanning electron micrographs (stereoscan) of Lima Graphite (LG12) before (Figures 265 to 267) and after (Figures 268 to 270) gasification in carbon dioxide at 1073 K for 16 hours.

Weight loss 1.64%.

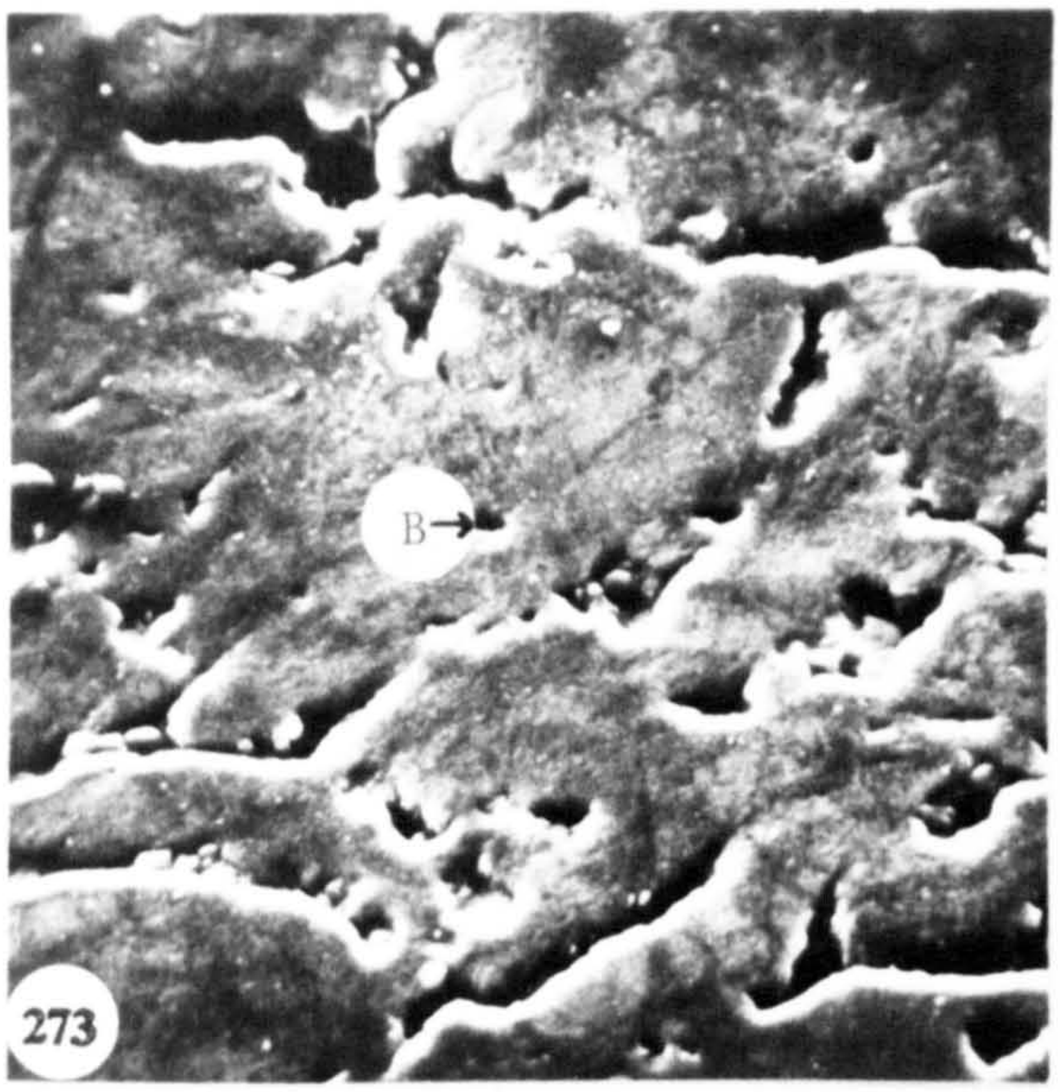


MORGANS UNIPORE GRAPHITE

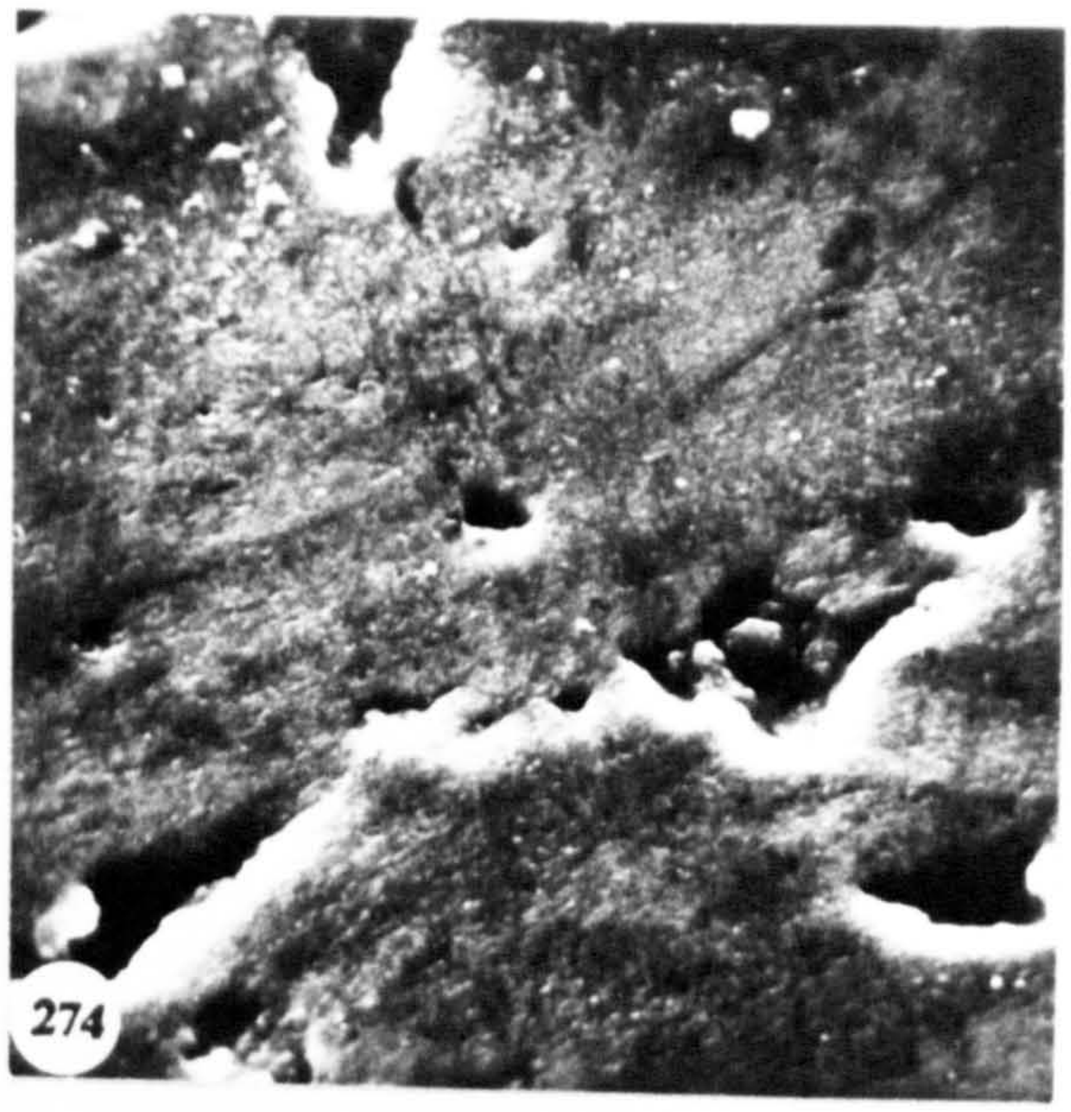


MORGANS UNIPORE GRAPHITE

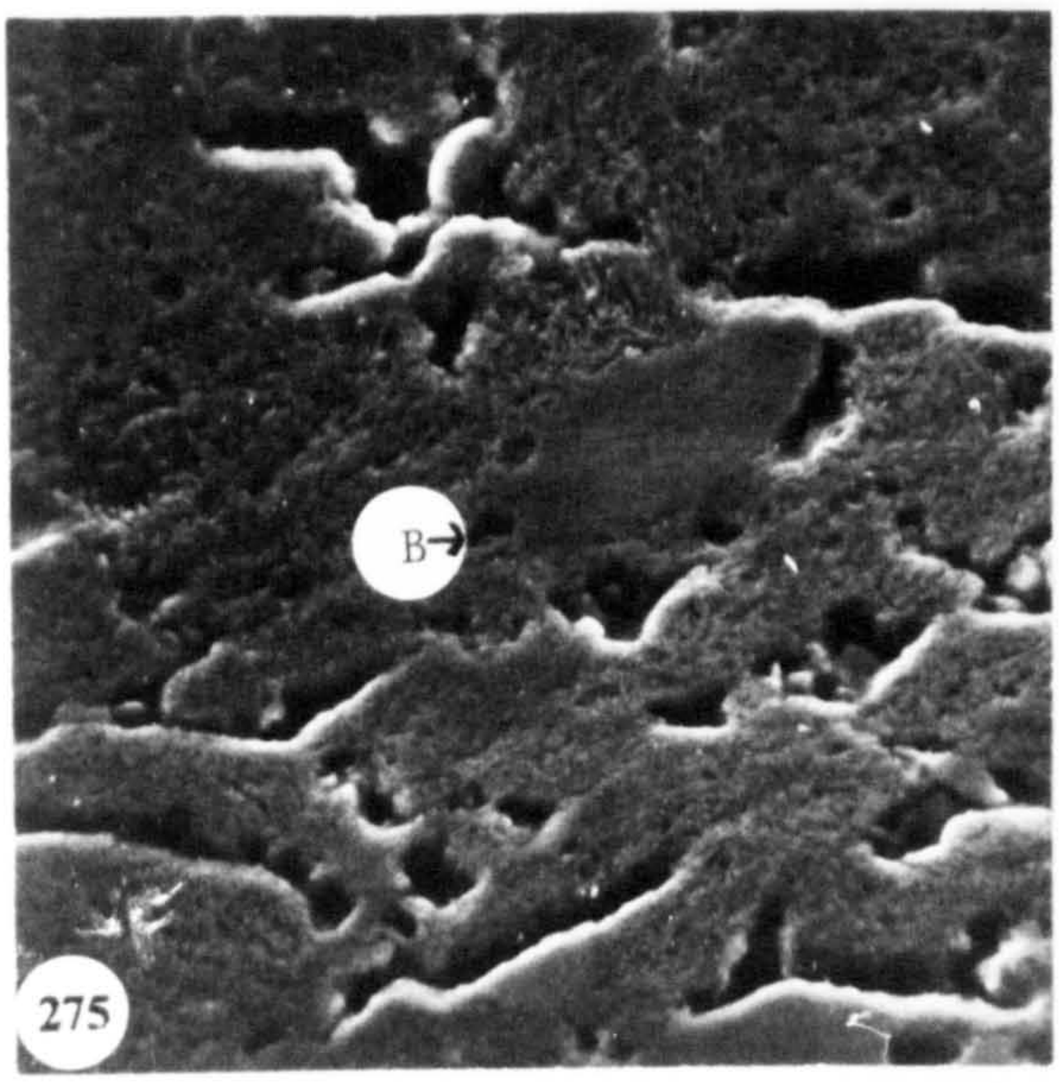
Figures 271 and 272. Optical micrographs of Morgans Unipore Graphite (MG7) before and after gasification in carbon dioxide at 1073 K for 16 hours.
Weight loss 0.60%.



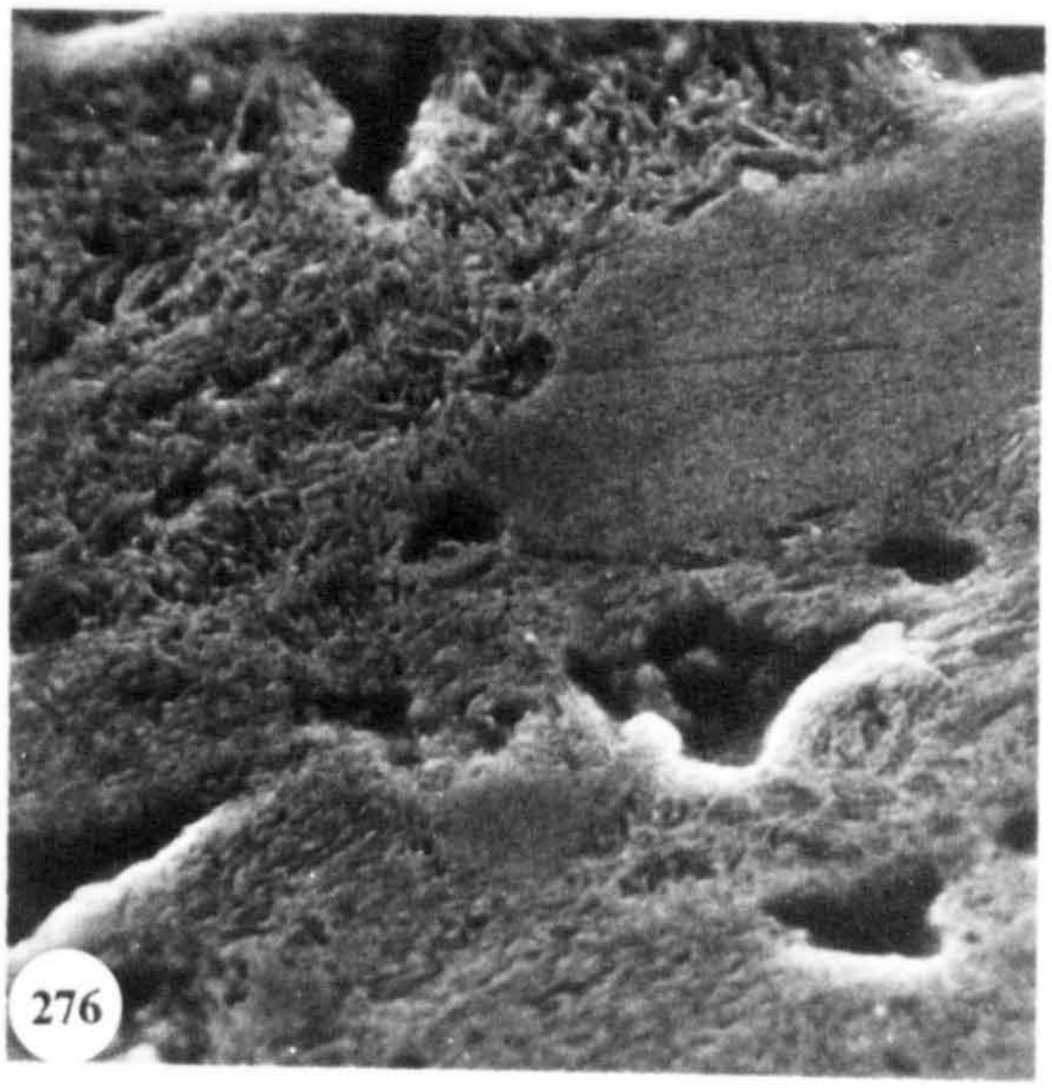
MORGANS UNIPORE GRAPHITE 40 μm



MORGANS UNIPORE GRAPHITE 10 μm

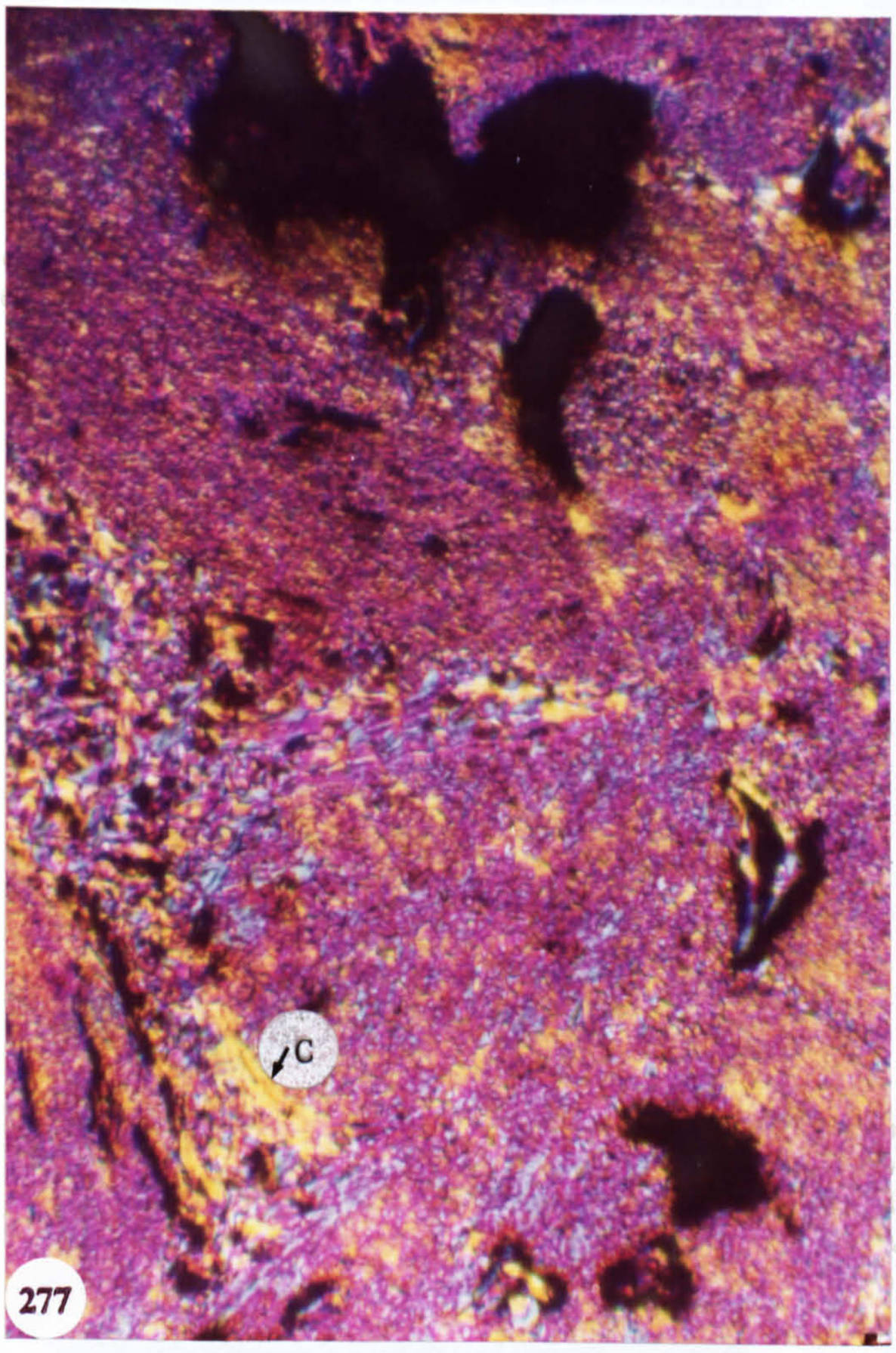


MORGANS UNIPORE GRAPHITE 40 μm



MORGANS UNIPORE GRAPHITE 10 μm

Figures 273 to 276. Scanning electron micrographs (stereoscan) of Morgans Unipore Graphite (MG7) before (Figures 273 and 274) and after (Figures 275 and 276) gasification in carbon dioxide at 1073 K for 16 hours. Weight loss 0.60%.



AGLMP GRAPHITE

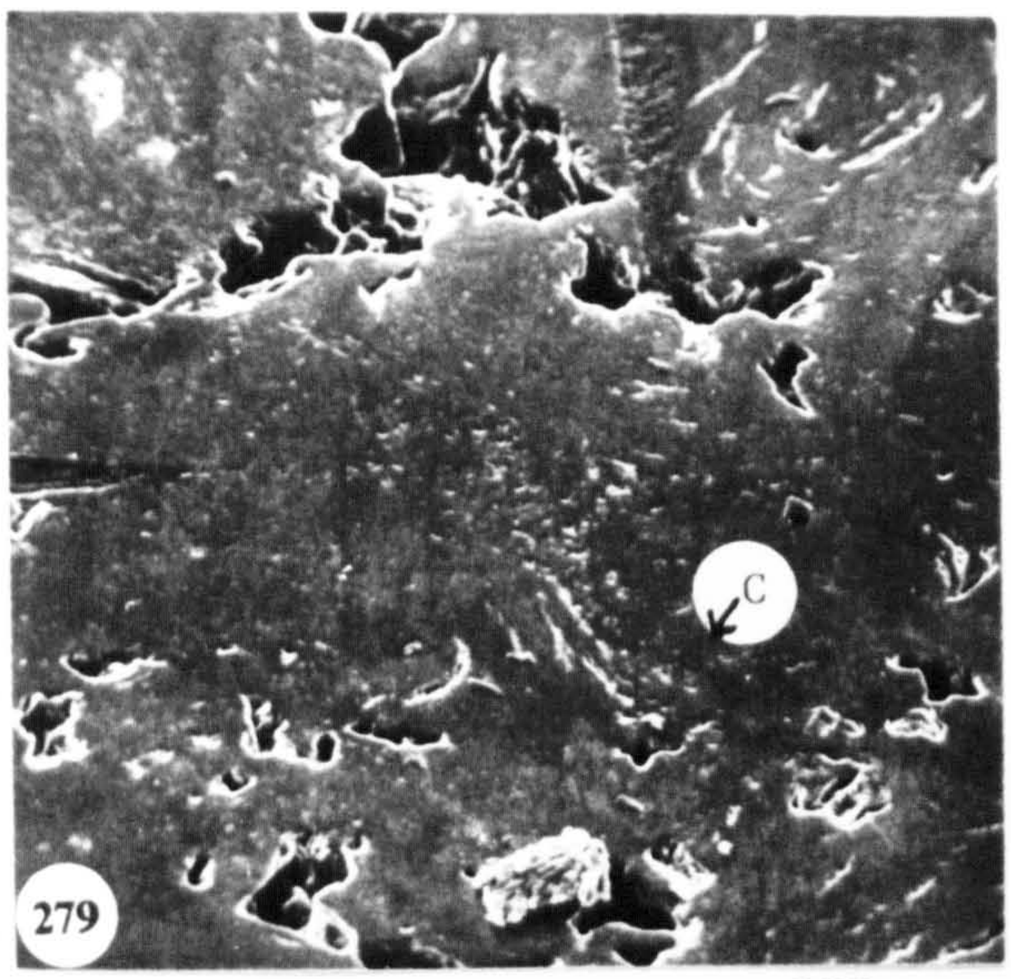
100 μm



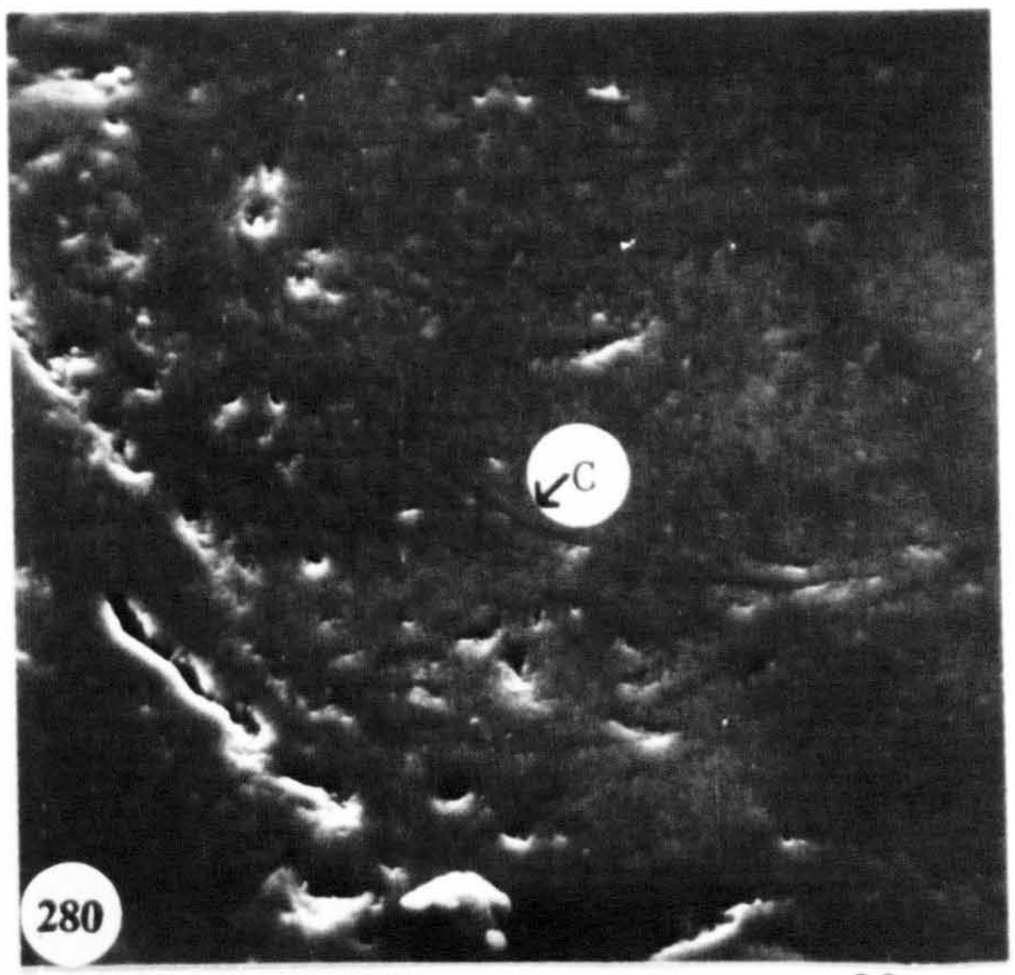
AGLMP GRAPHITE

100 μm

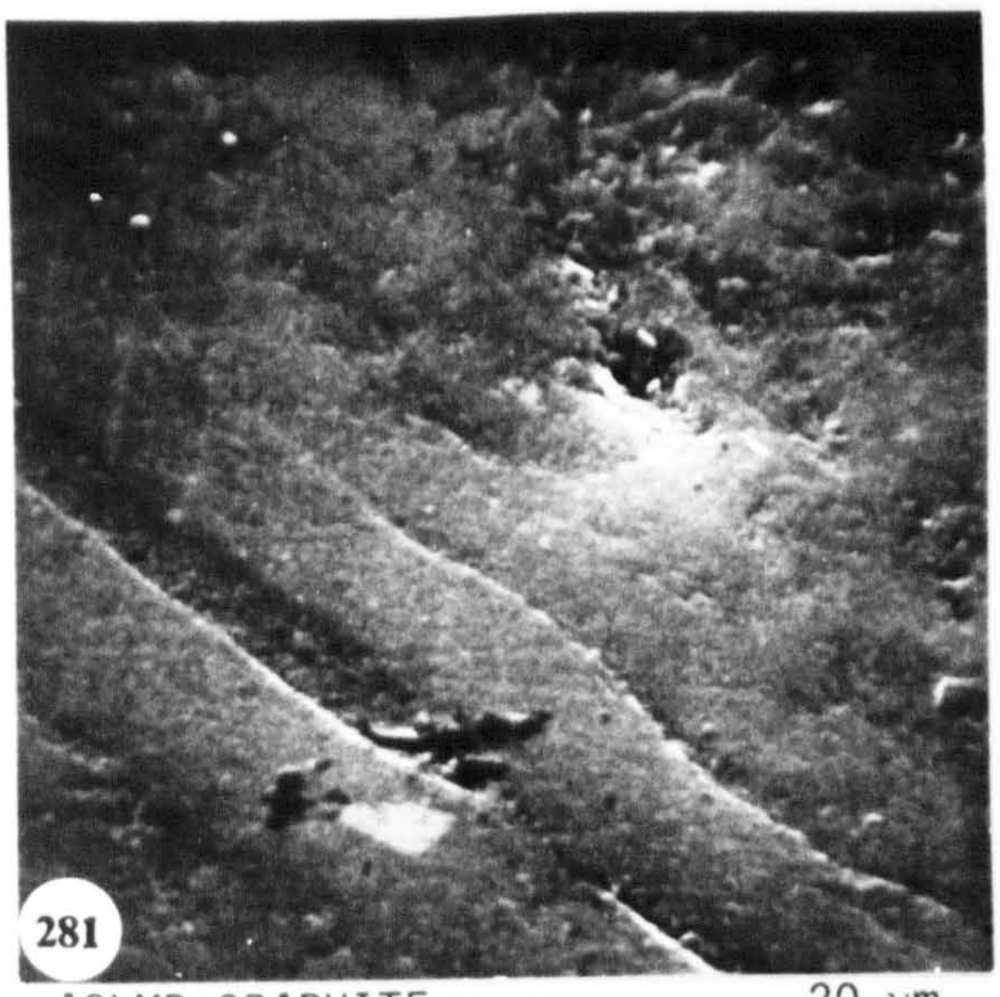
Figures 277 and 278. Optical micrographs of AGLMP Graphite (AG5) before and after gasification in carbon dioxide at 1073 K for 16 hours. Weight loss 1.34%.



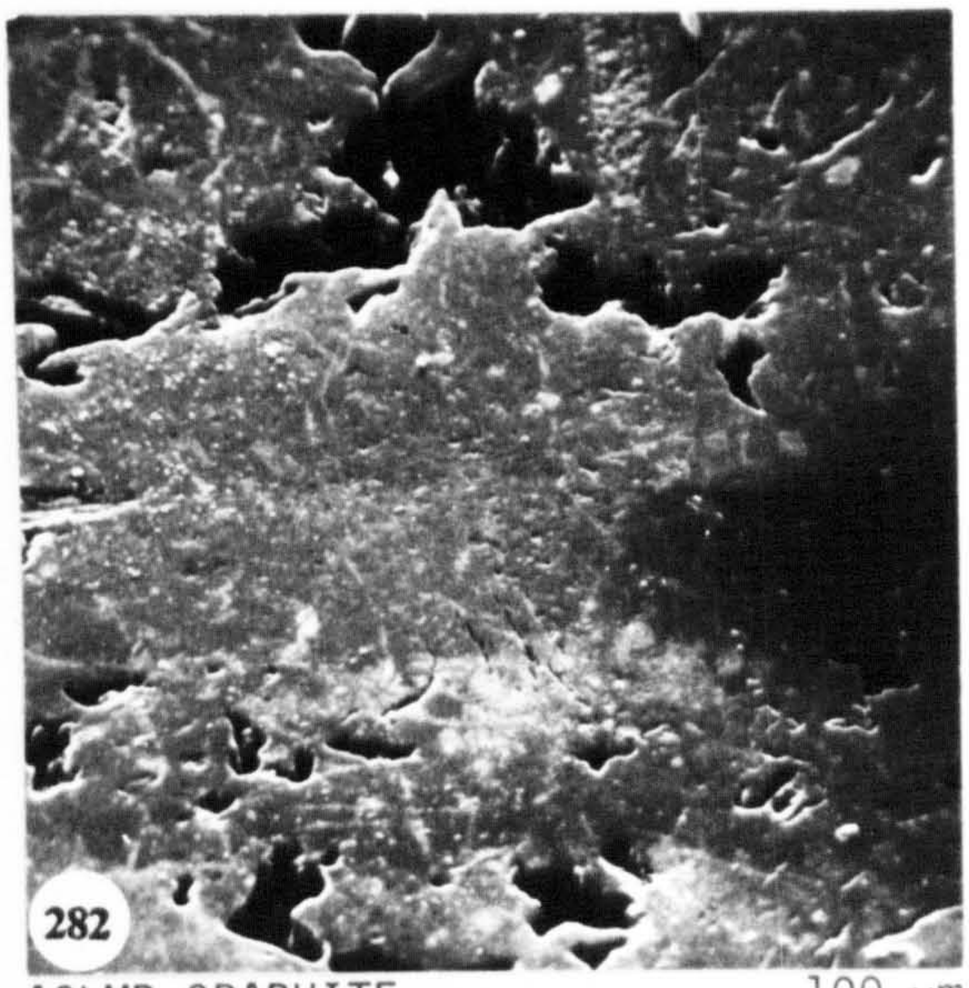
AGLMP GRAPHITE 100 µm



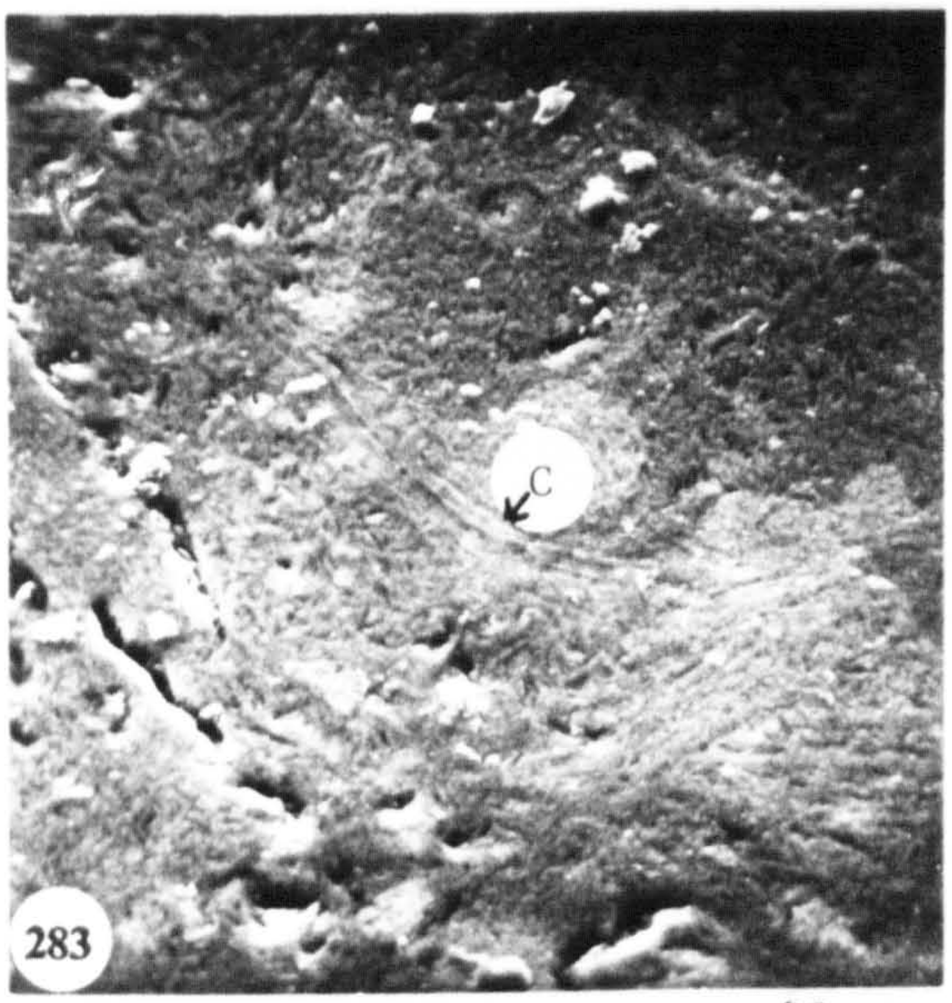
AGLMP GRAPHITE 20 µm



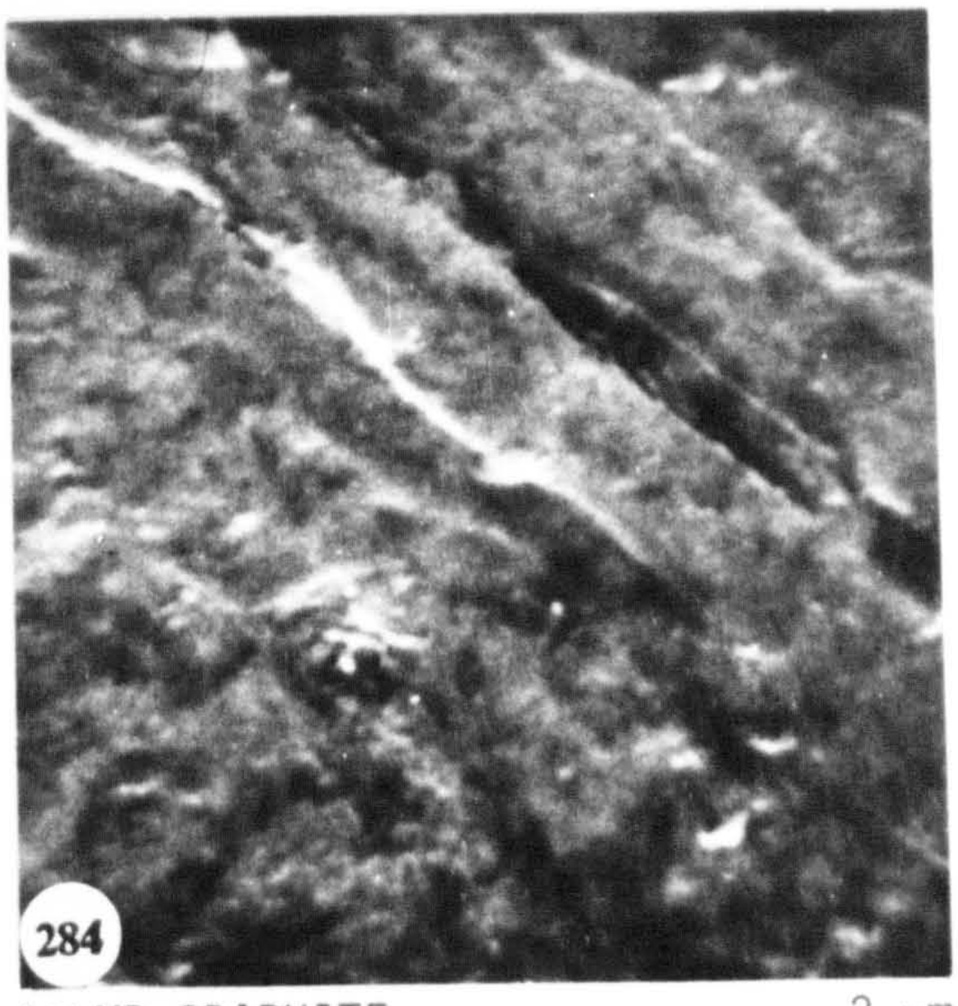
AGLMP GRAPHITE 20 µm



AGLMP GRAPHITE 100 µm

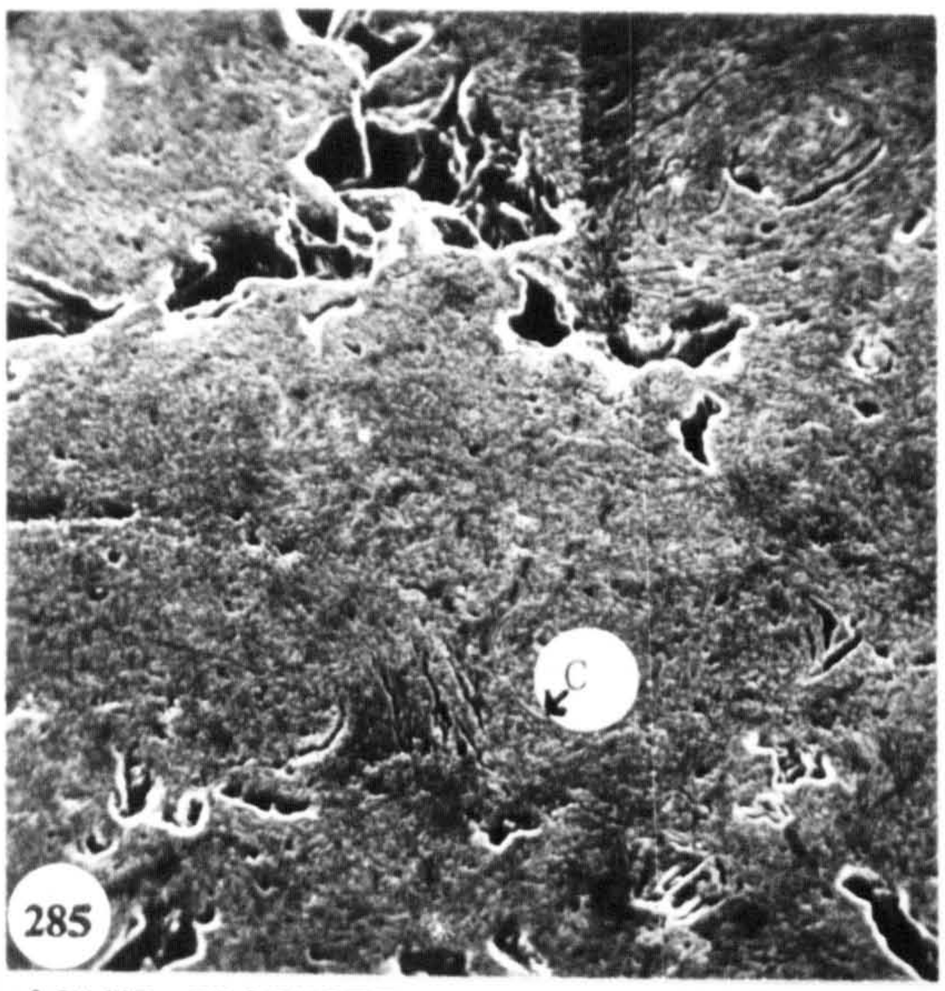


AGLMP GRAPHITE 20 µm

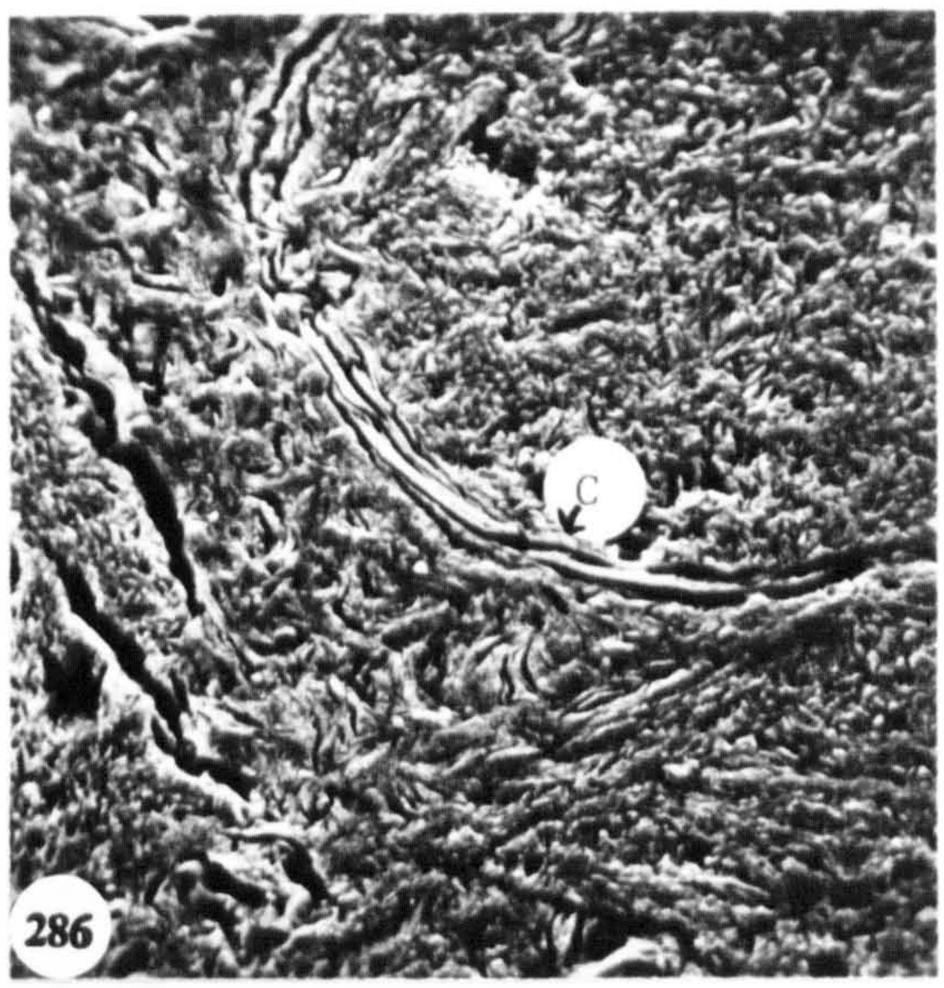


AGLMP GRAPHITE 2 µm

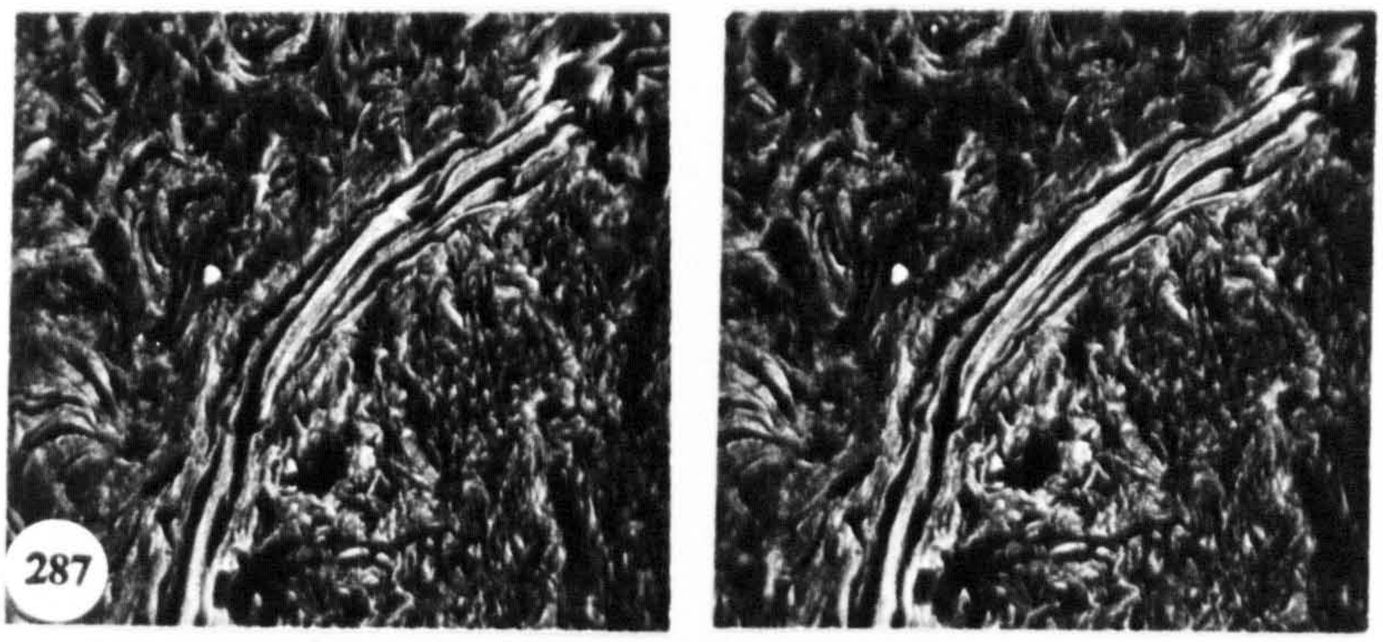
Figures 279 to 284. Scanning electron micrographs (stereoscan) of AGLMP Graphite (AG5) before (Figures 279 to 281) and after (Figures 282 to 284) gasification in carbon dioxide at 1073 K for 16 hours. Weight loss 1.34%.



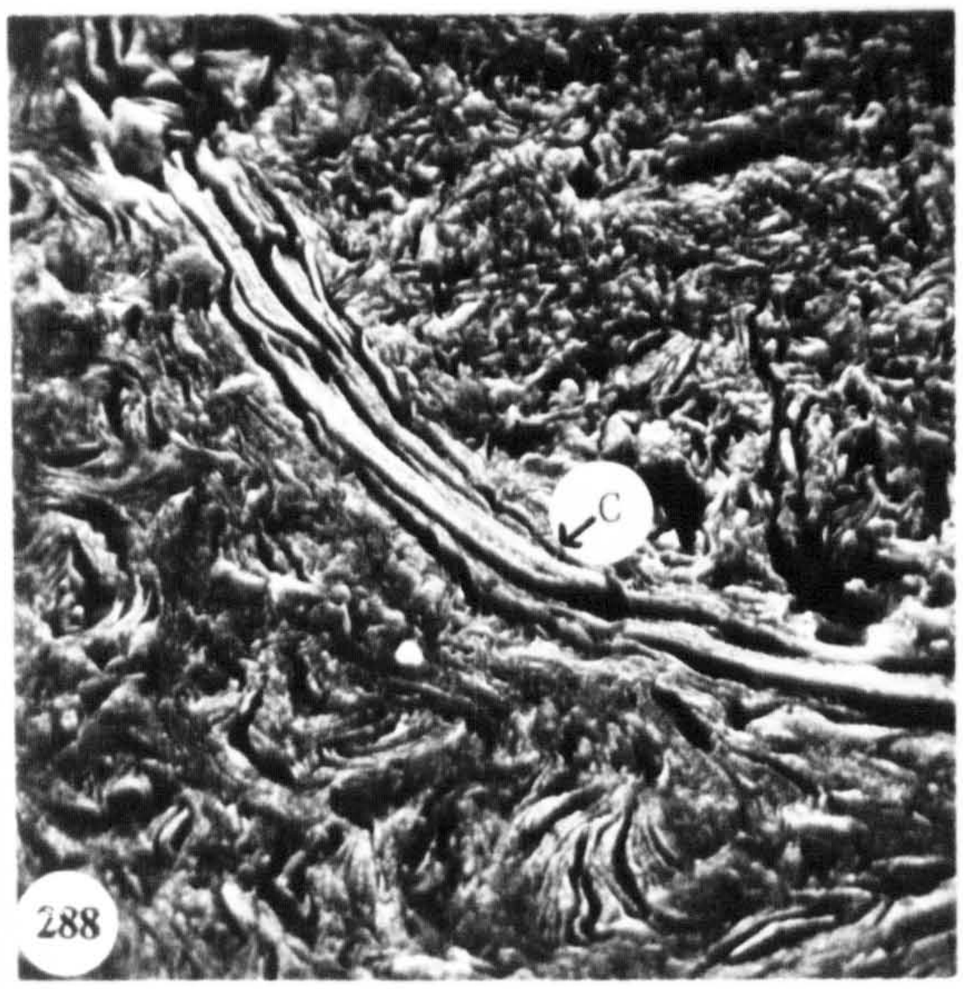
AGLMP GRAPHITE 100 µm



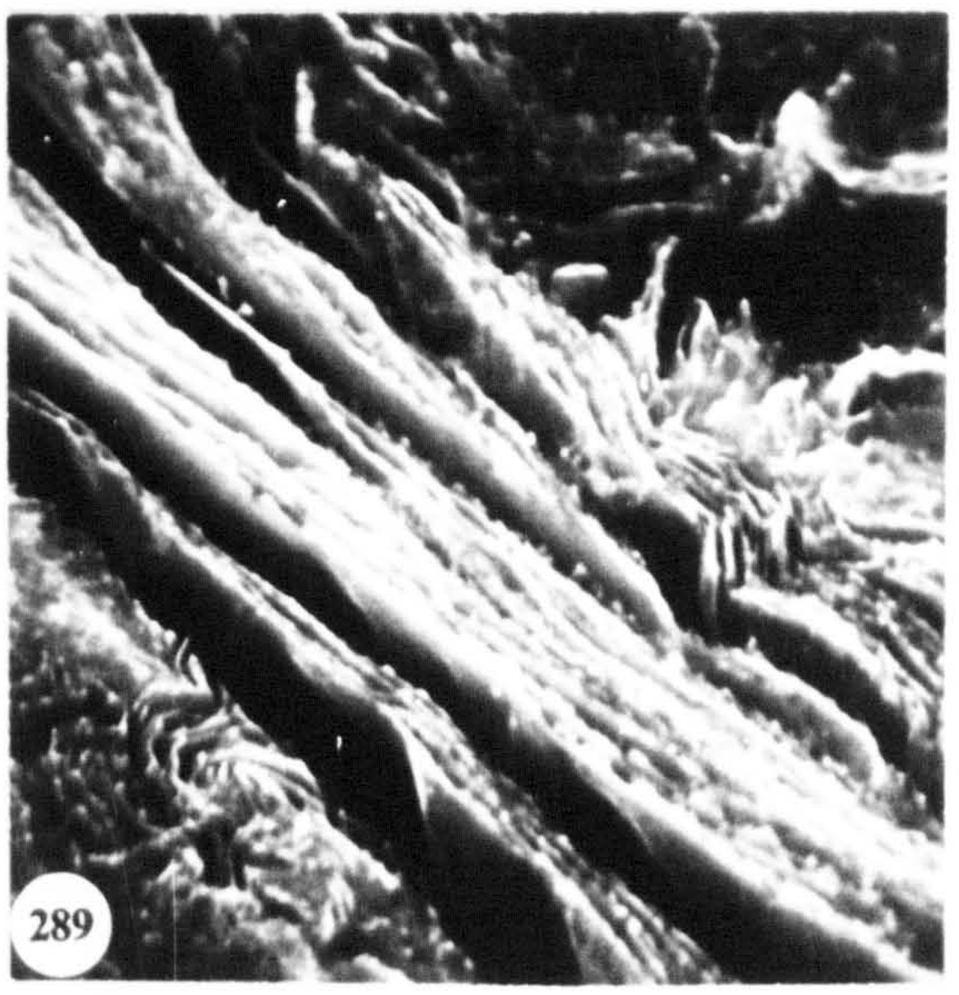
AGLMP GRAPHITE 20 µm



AGLMP GRAPHITE (Stereopair) 20 µm

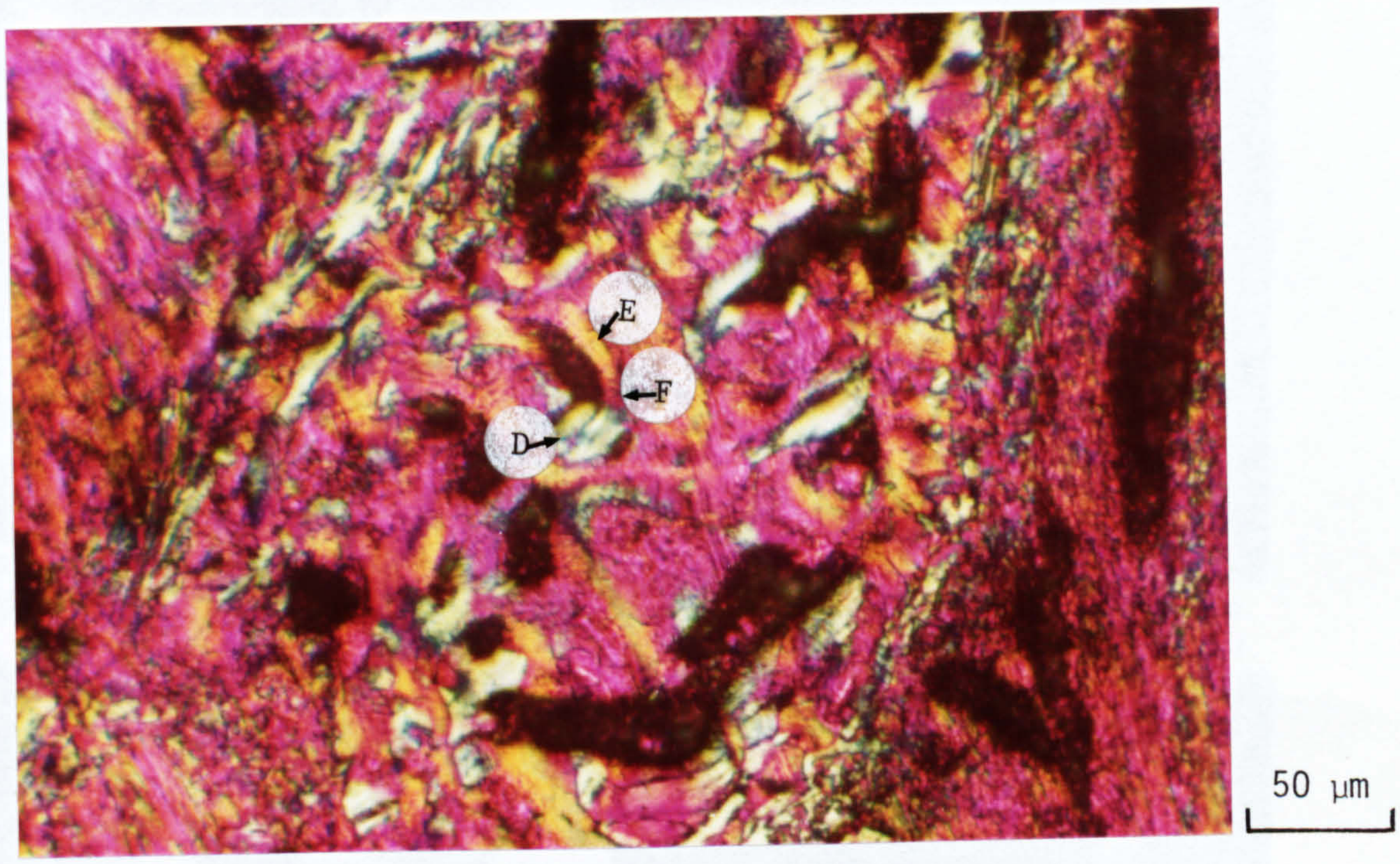


AGLMP GRAPHITE 10 µm



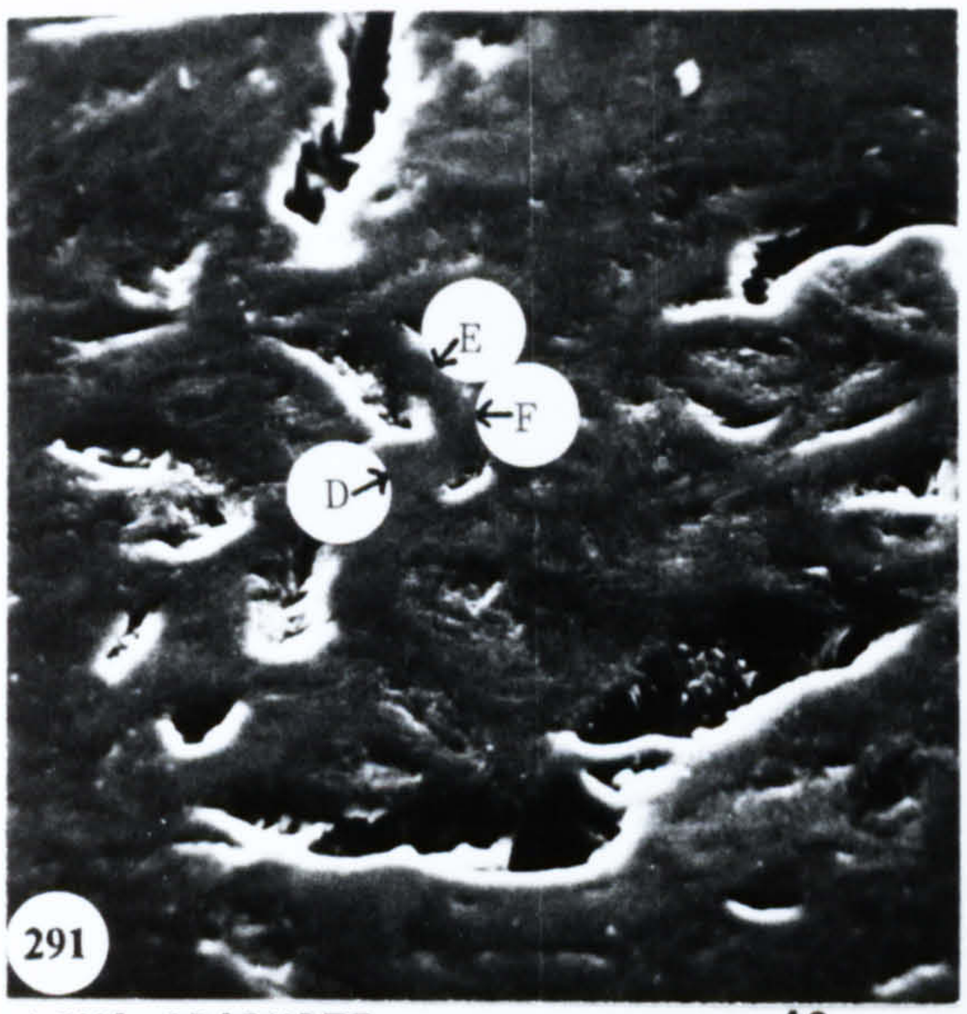
AGLMP GRAPHITE 2 µm

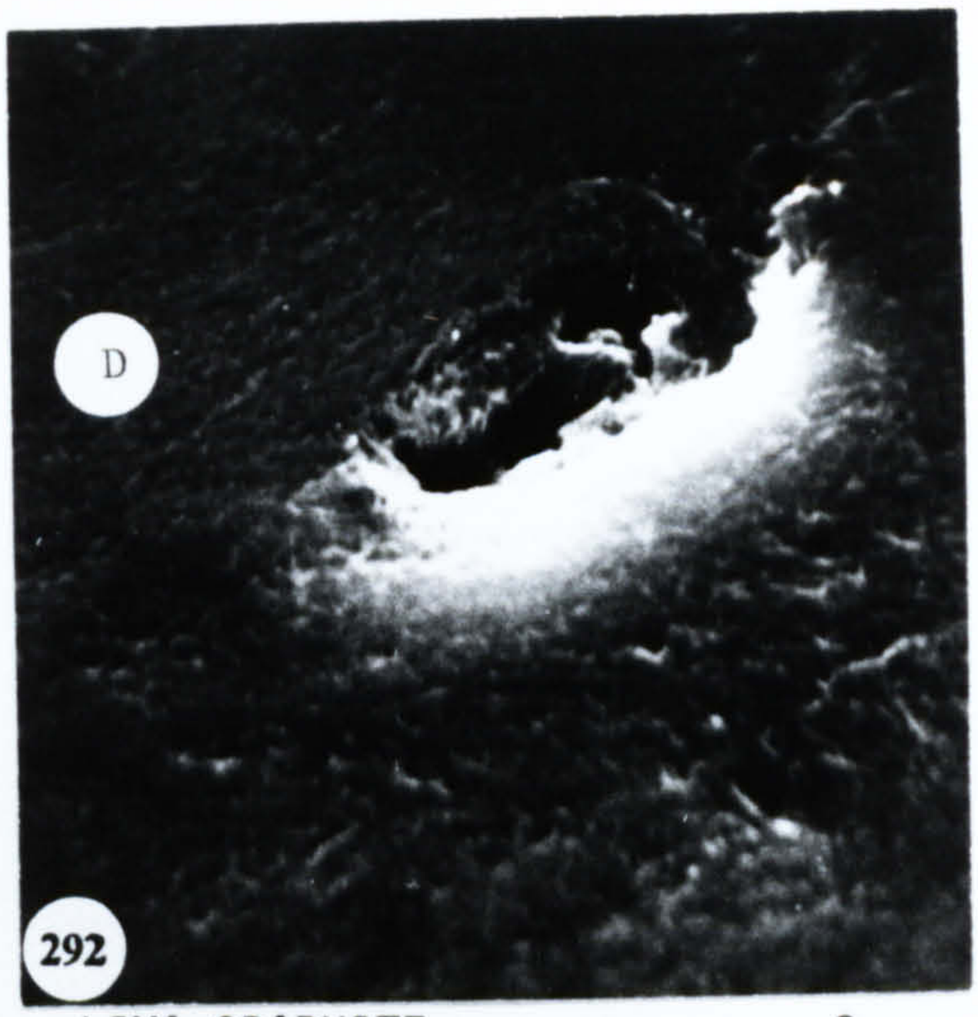
Figures 285 to 289. Scanning electron micrographs (stereoscan) of AGLMP Graphite (AG5) after gasification in carbon dioxide at 1198 K for 16 hours. Weight loss 3.44%.

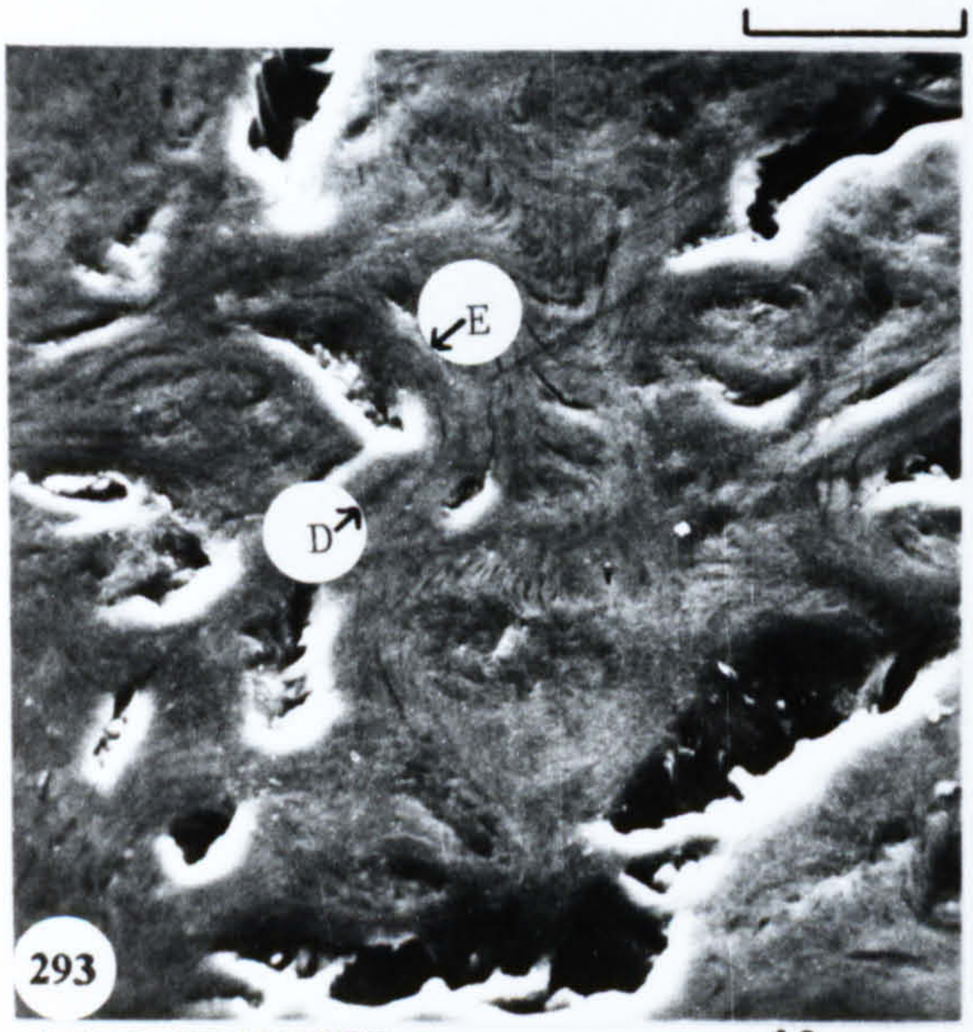


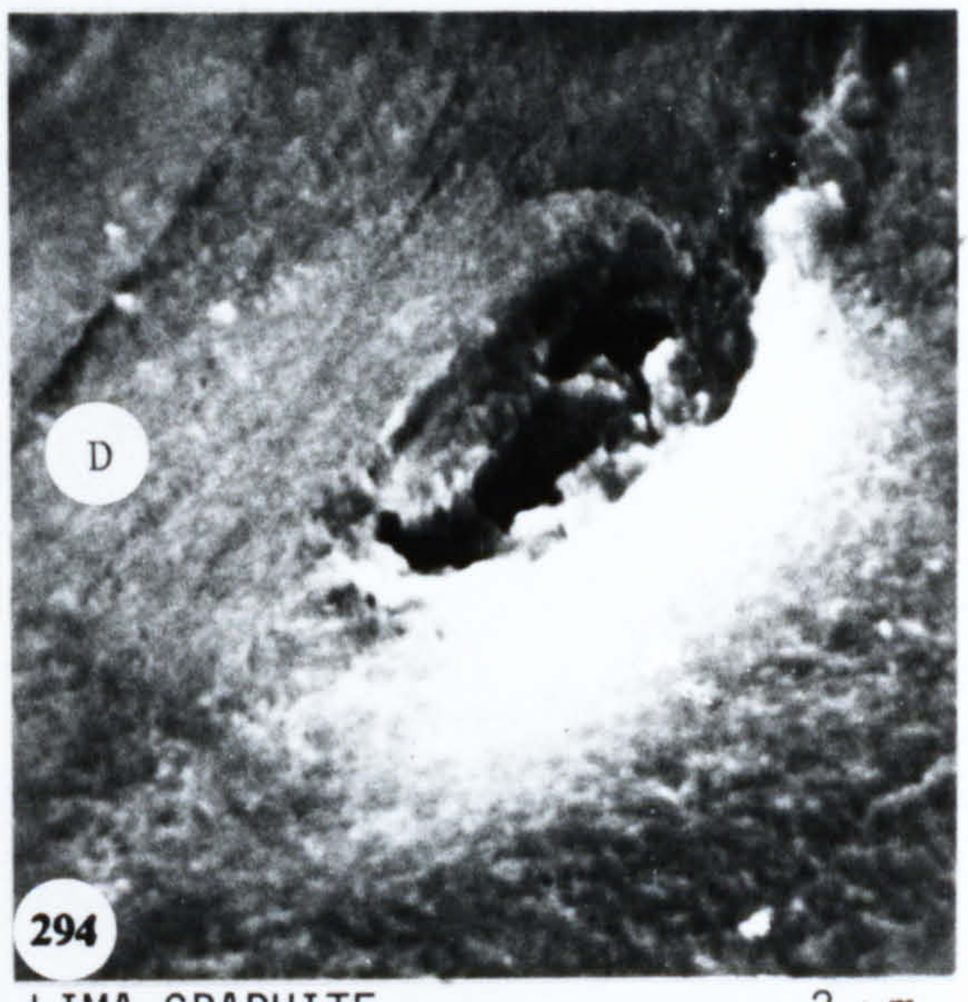
LIMA GRAPHITE

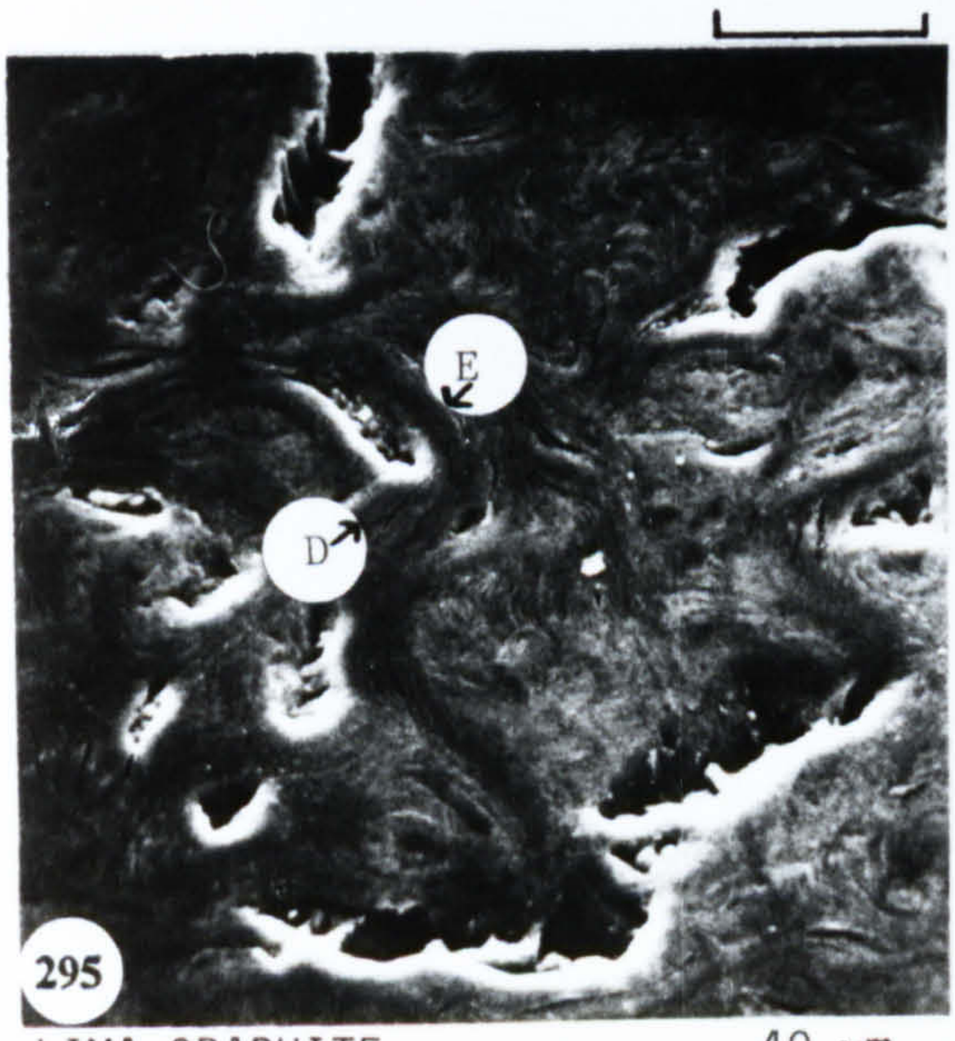
Figure 290. Optical micrograph of Lima Graphite (LG13) after gasification in carbon dioxide at 1088 K for 48 hours. Weight loss 1.42%.







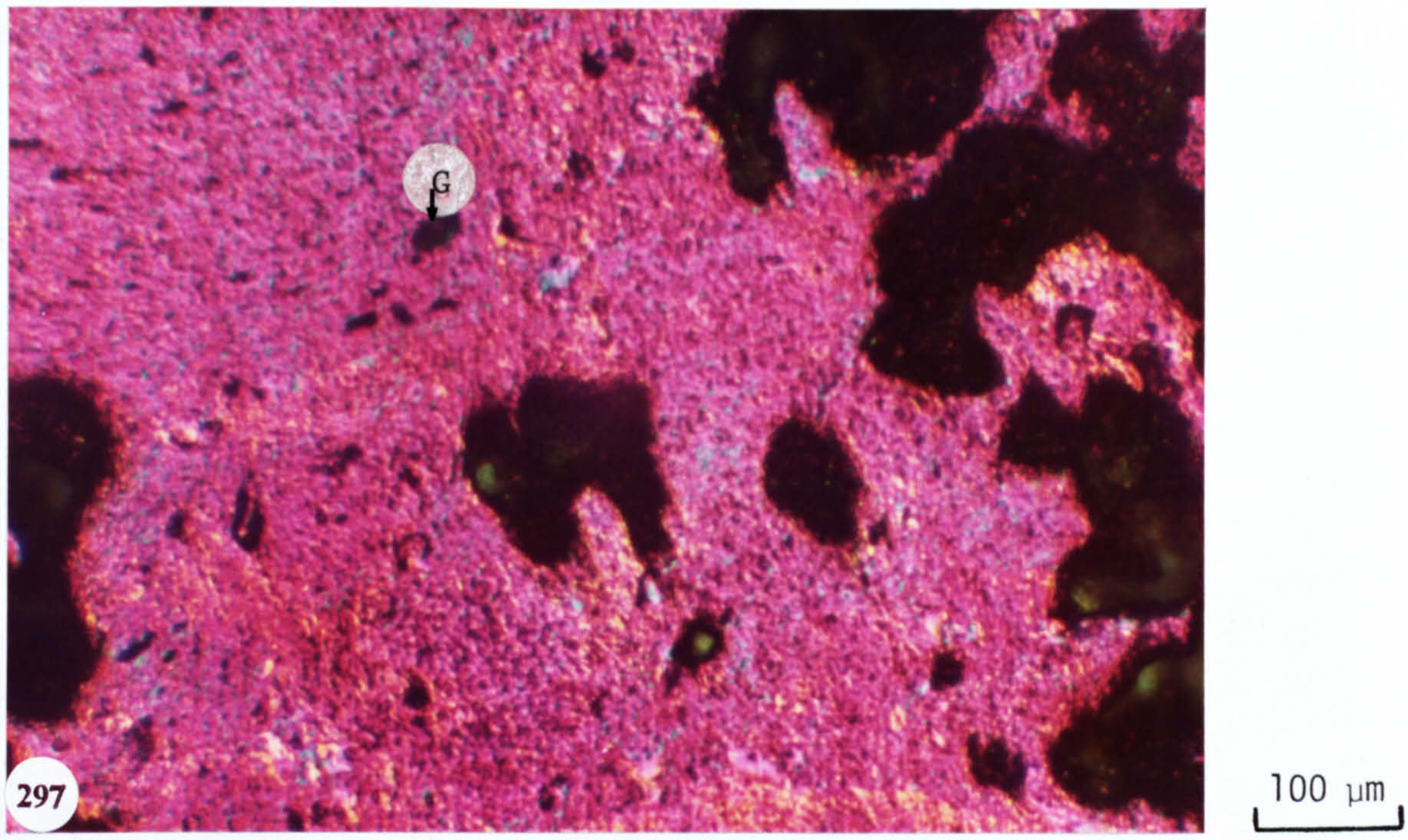




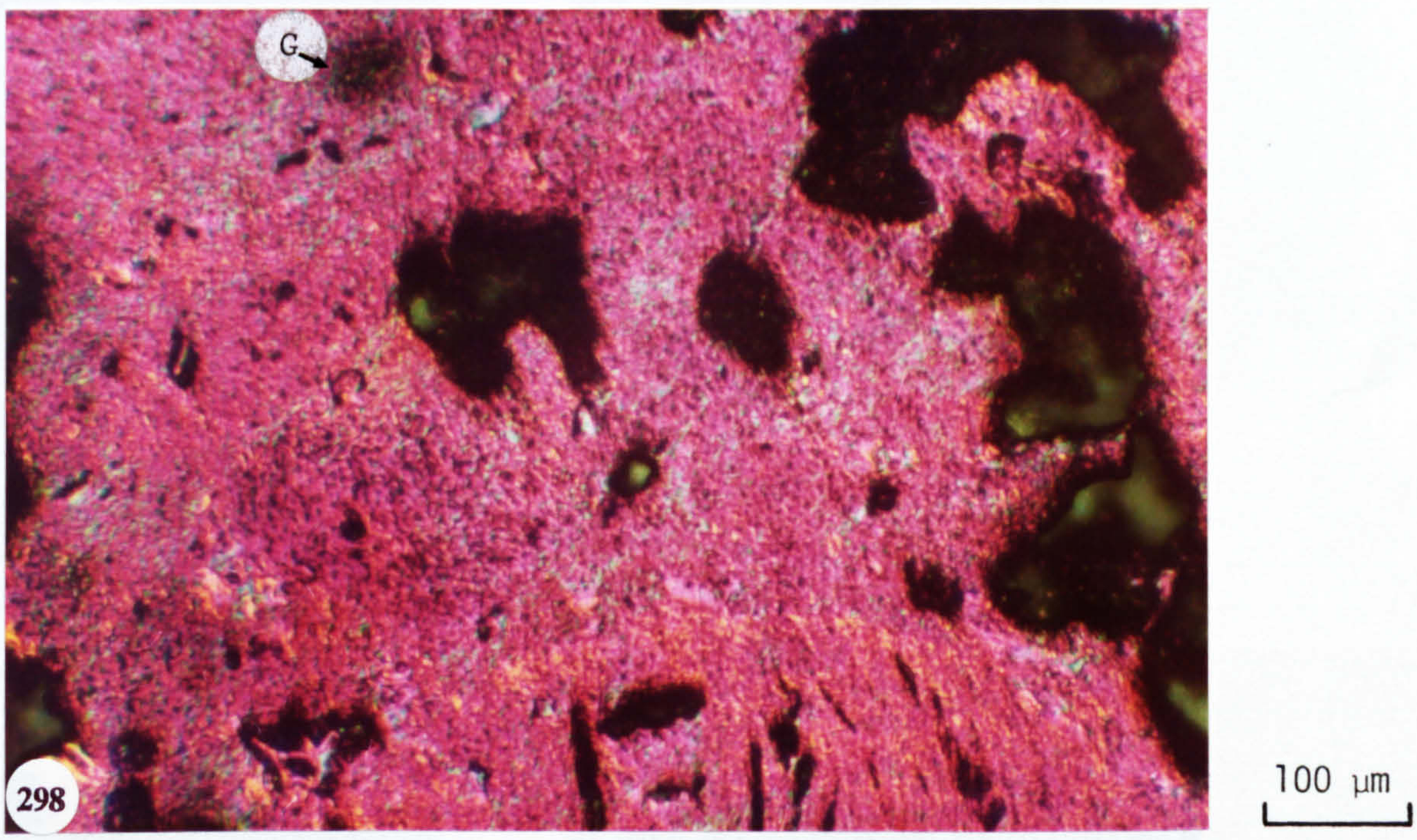


Figures 291 to 296. Scanning electron micrographs (stereoscan) of Lima Graphite (LG13) before (Figures 291 and 292) and after gasification in carbon dioxide at 1088 K (Figures 293 and 294) for 48 hours and 1173 K (Figures 295 and 296) for 16 hours.

Weight losses 1.42% and 2.63%.



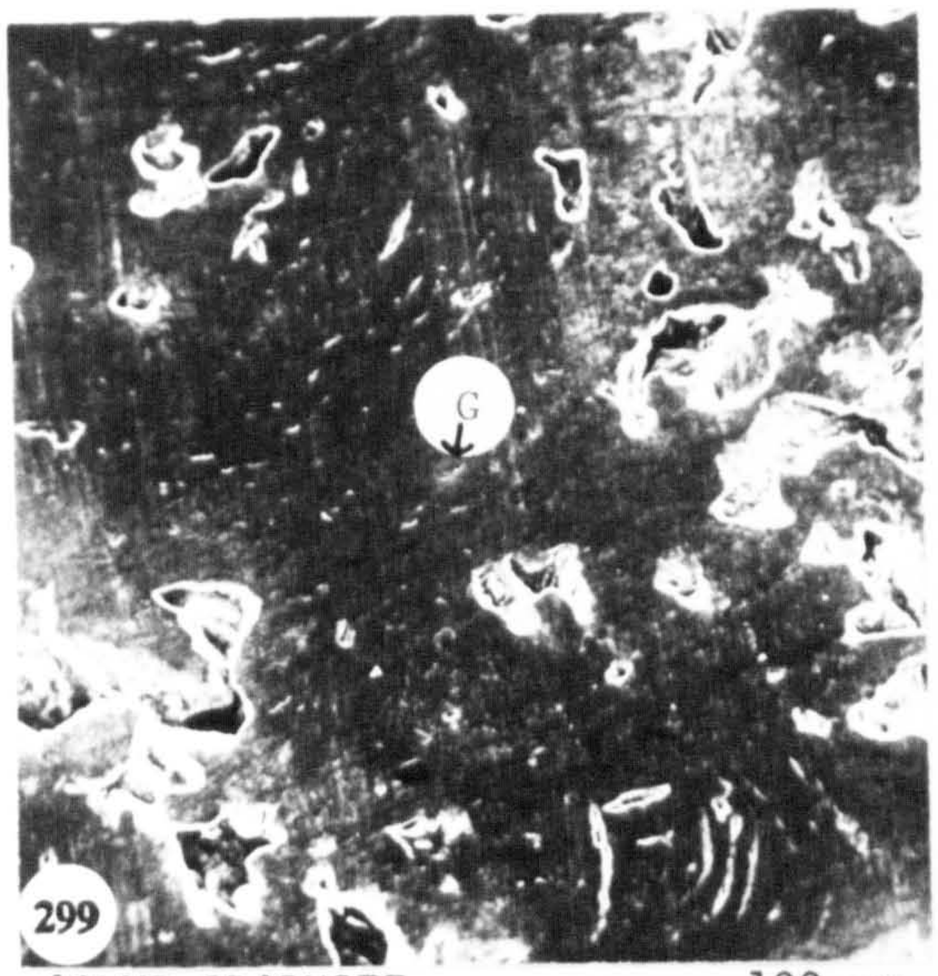
AGLMP GRAPHITE

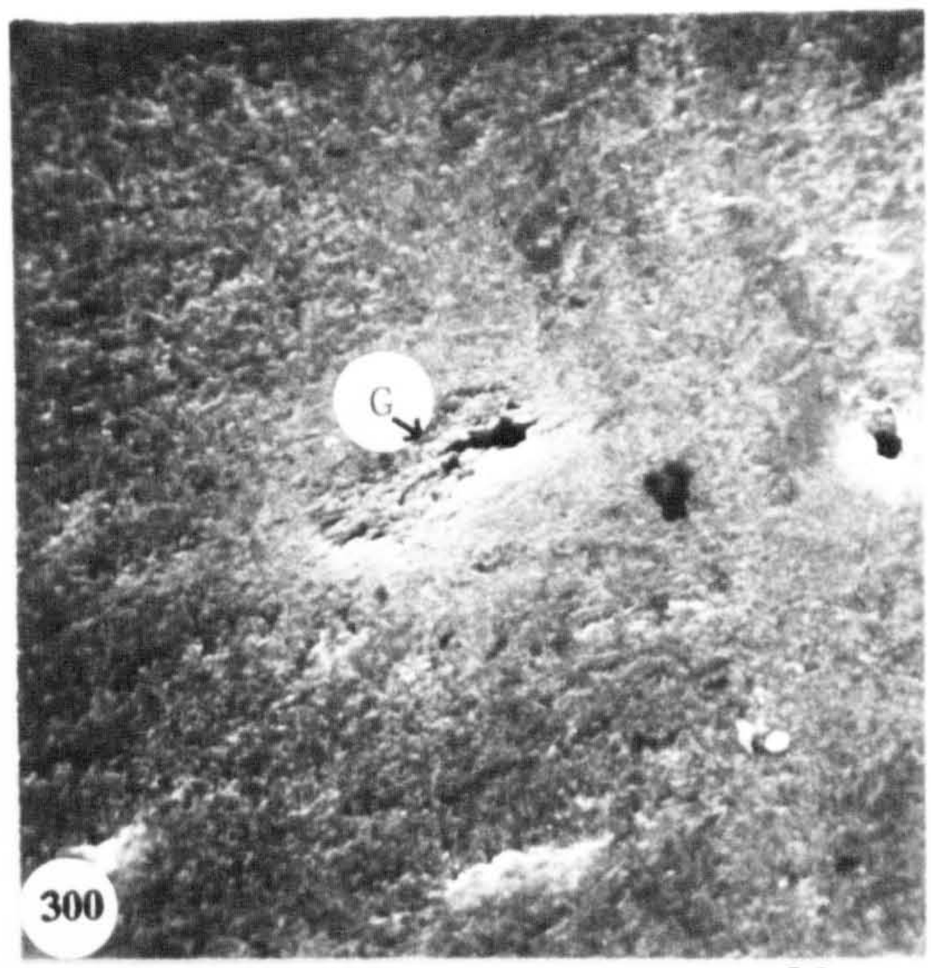


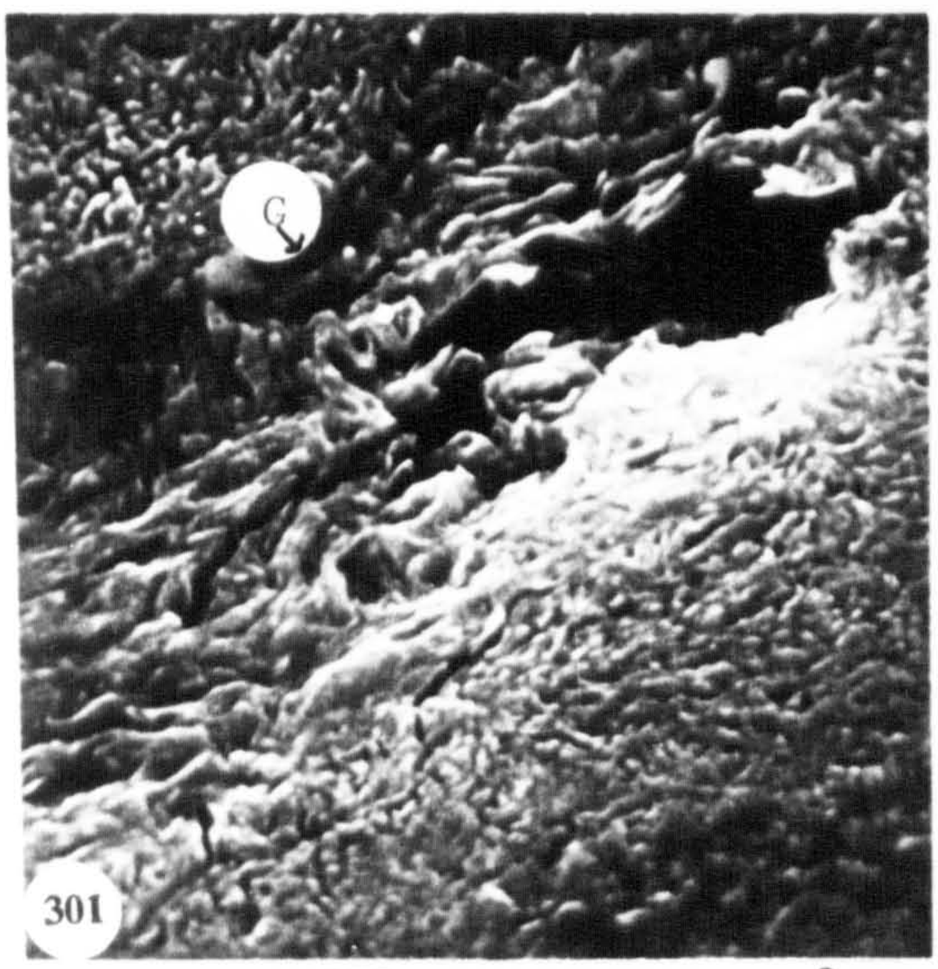
AGLMP GRAPHITE

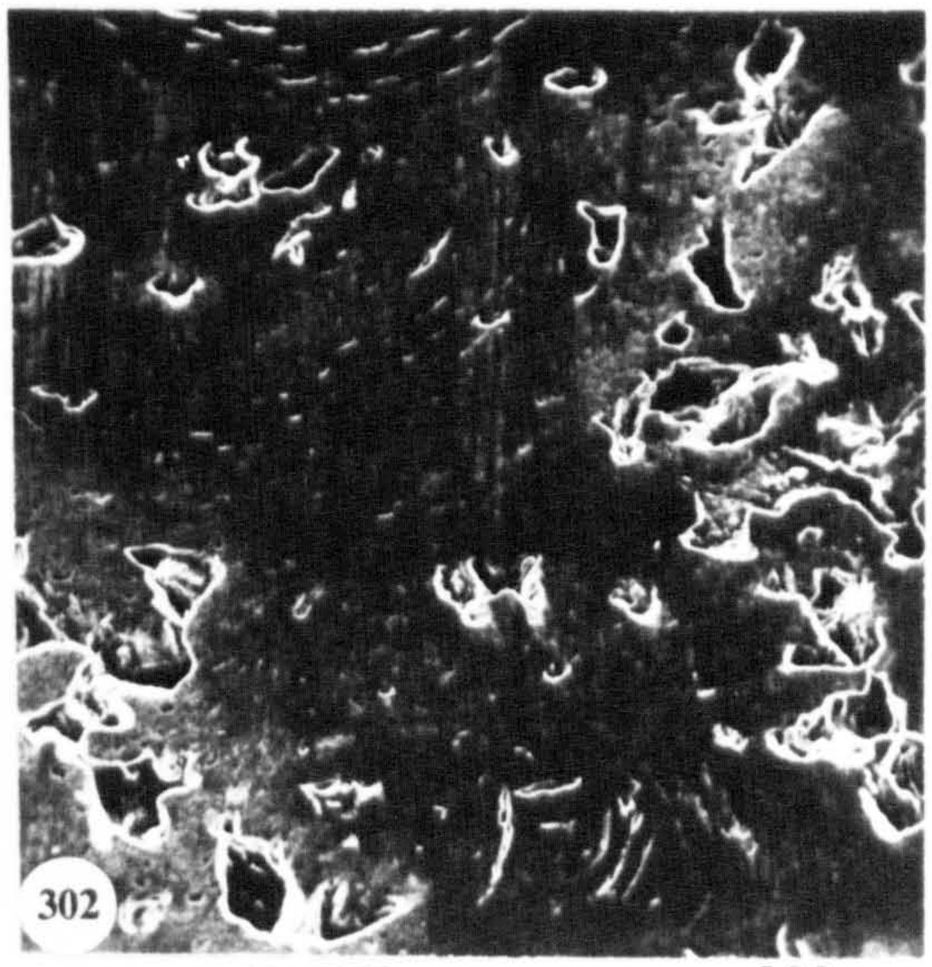
Figures 297 and 298. Optical micrographs of AGLMP Graphite (AG6) before and after gasification in carbon dioxide at 1088 K for 48 hours.

Weight loss 0.48%.

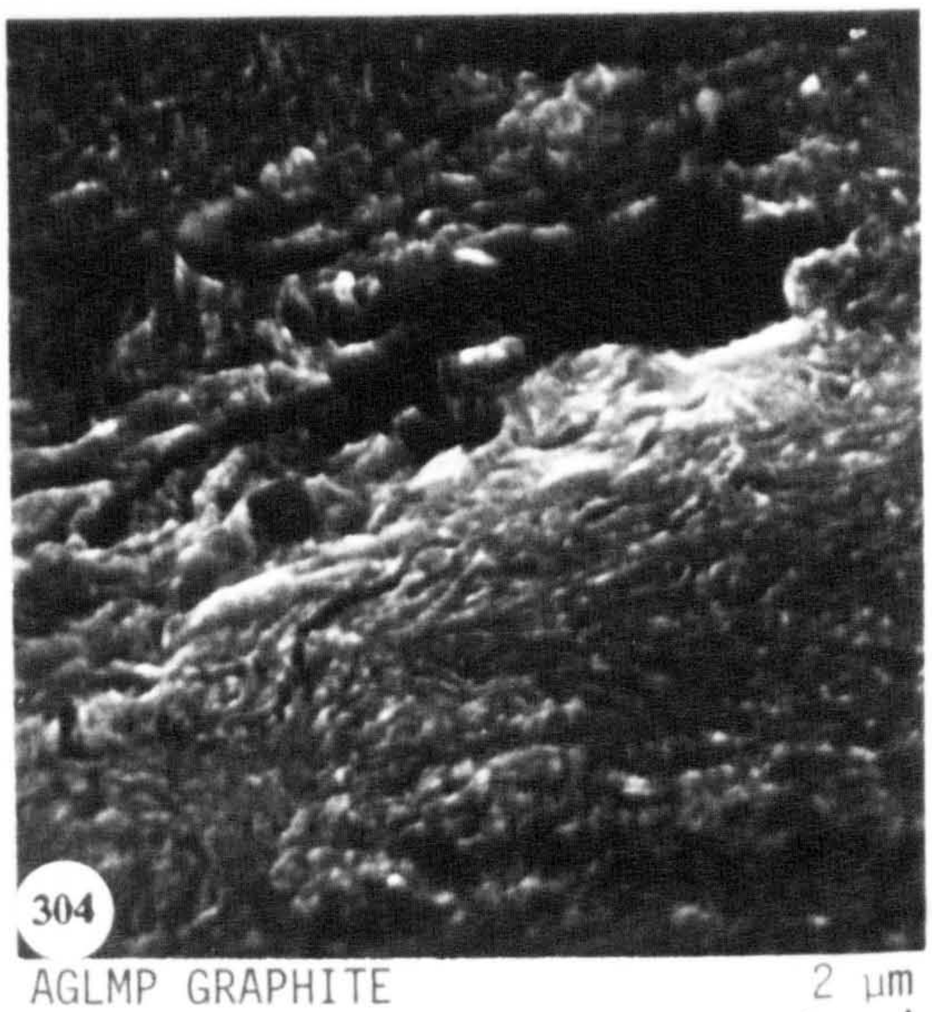




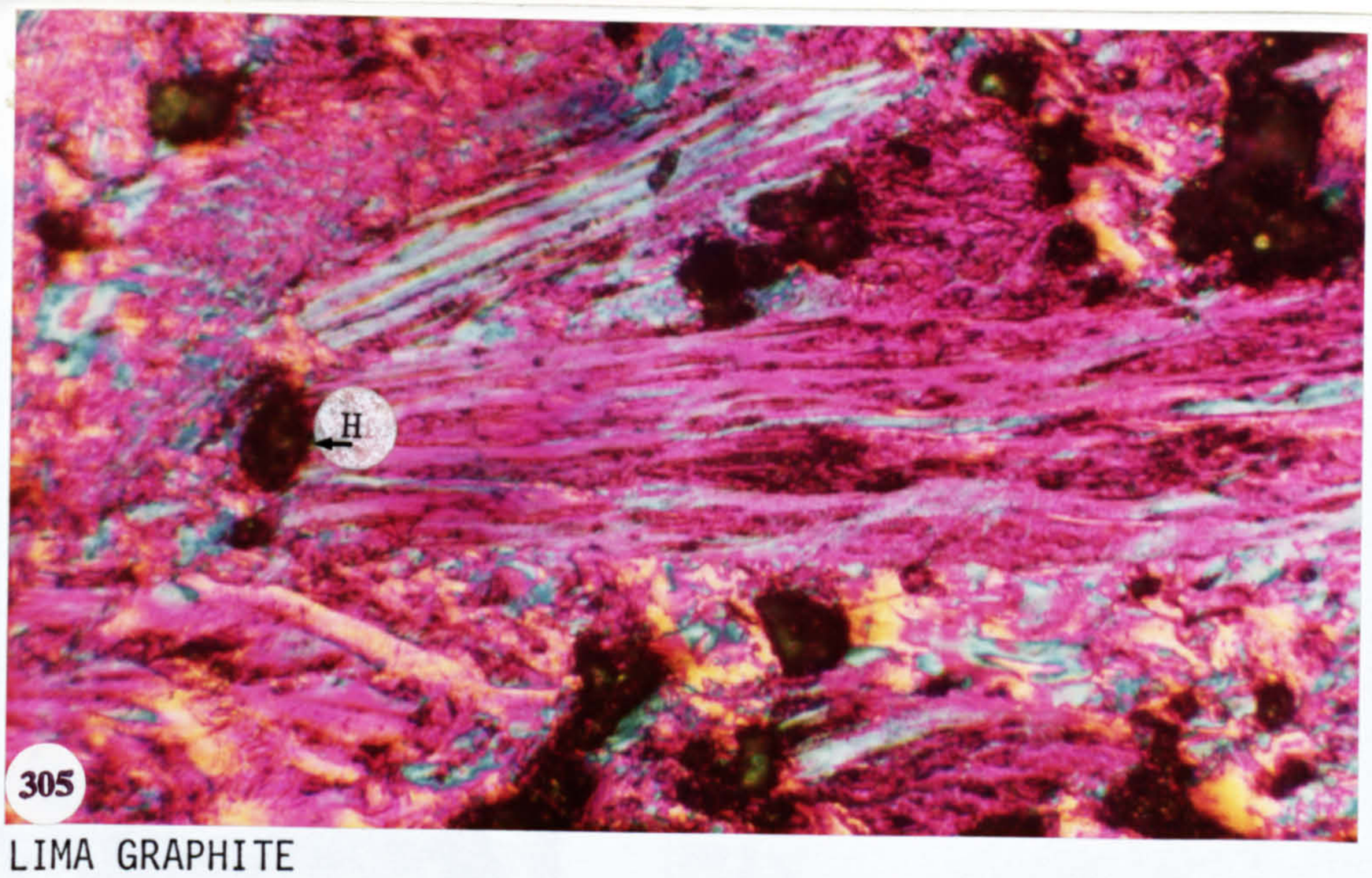




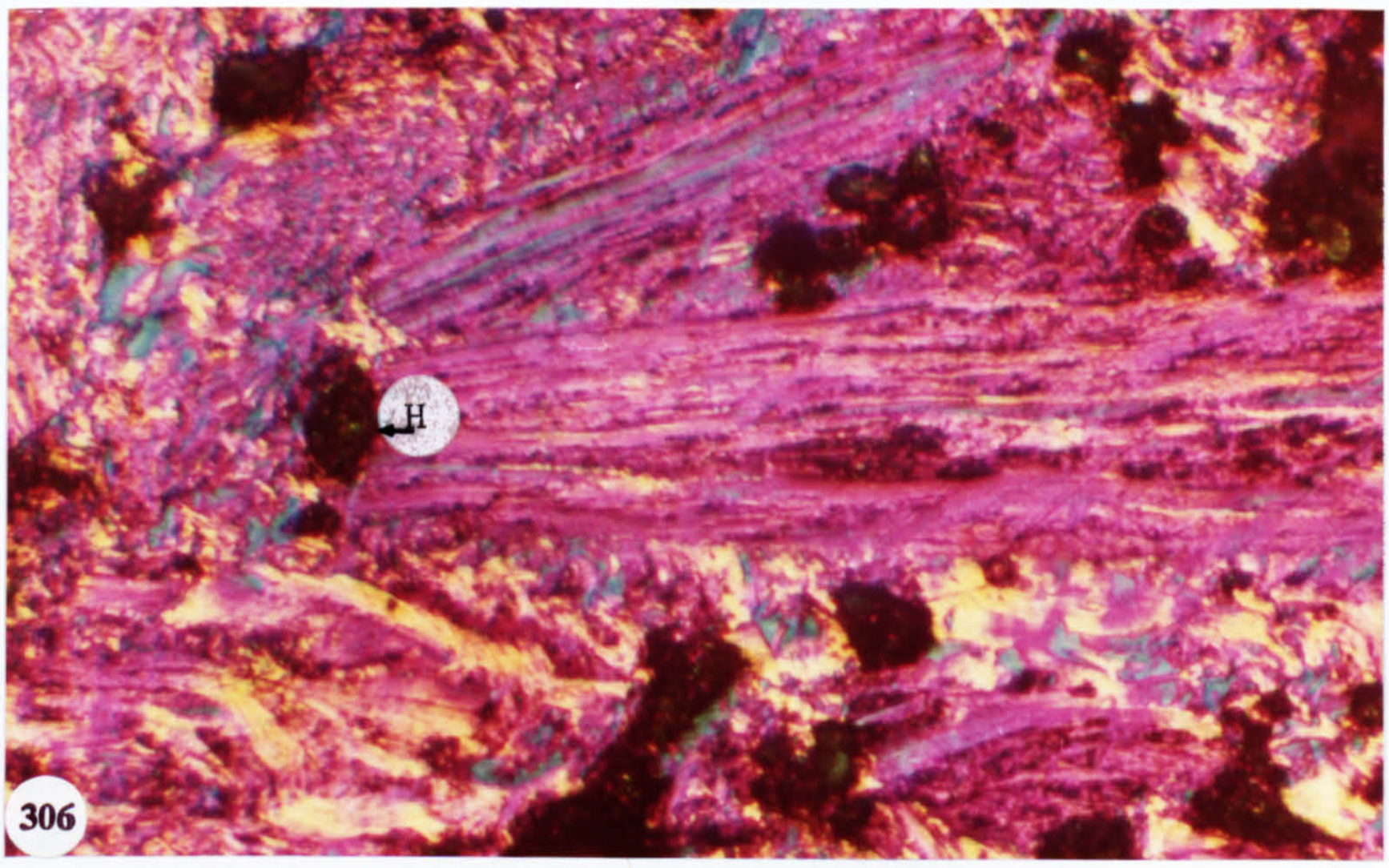




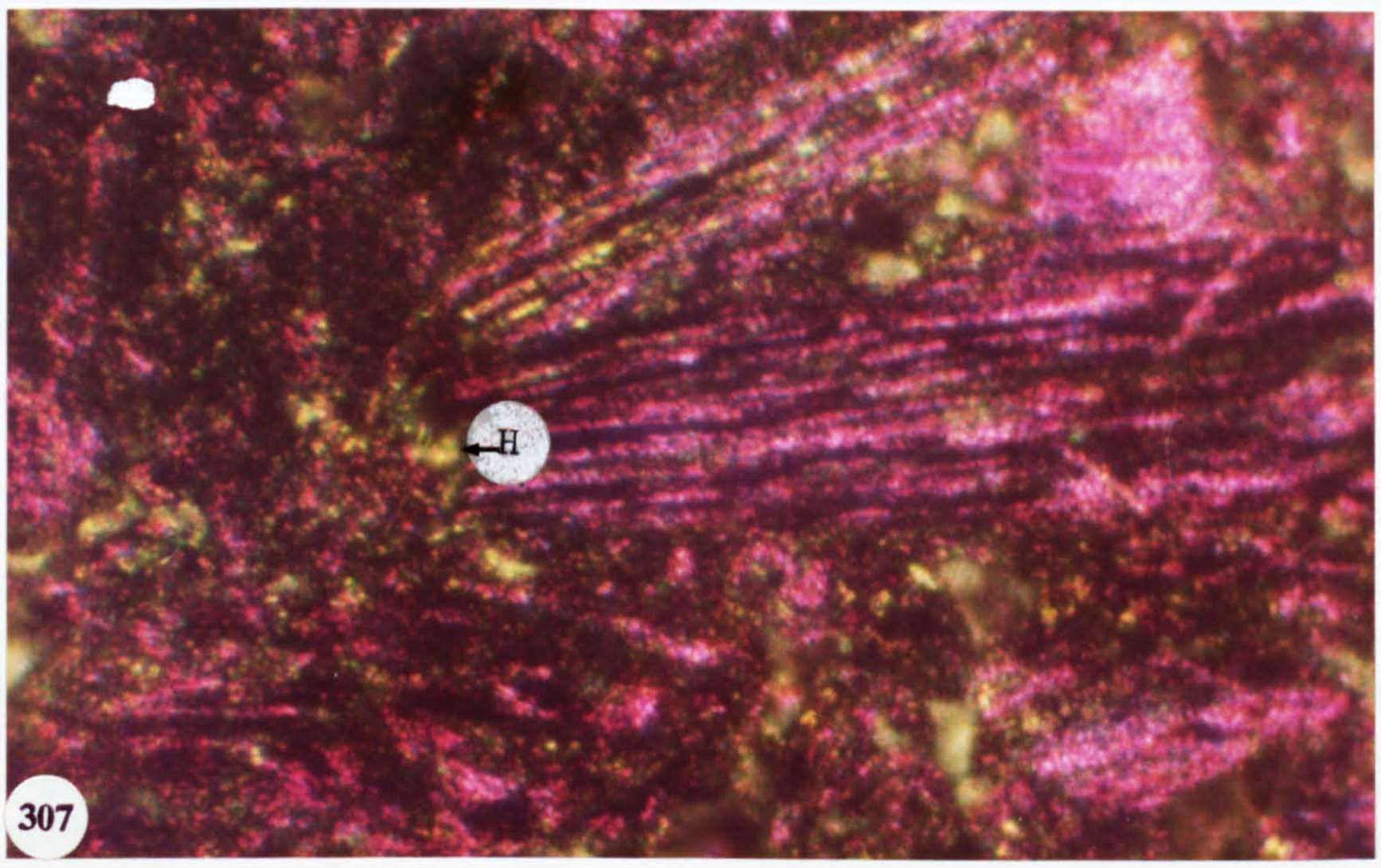
Figures 299 to 304. Scanning electron micrographs (stereoscan) of AGLMP Graphite (AG6) before (Figures 299 to 301) and after (Figures 302 to 304) gasification in carbon dioxide at 1088 K for 48 hours. Weight loss 0.48%.



LIMA GRAPHITE

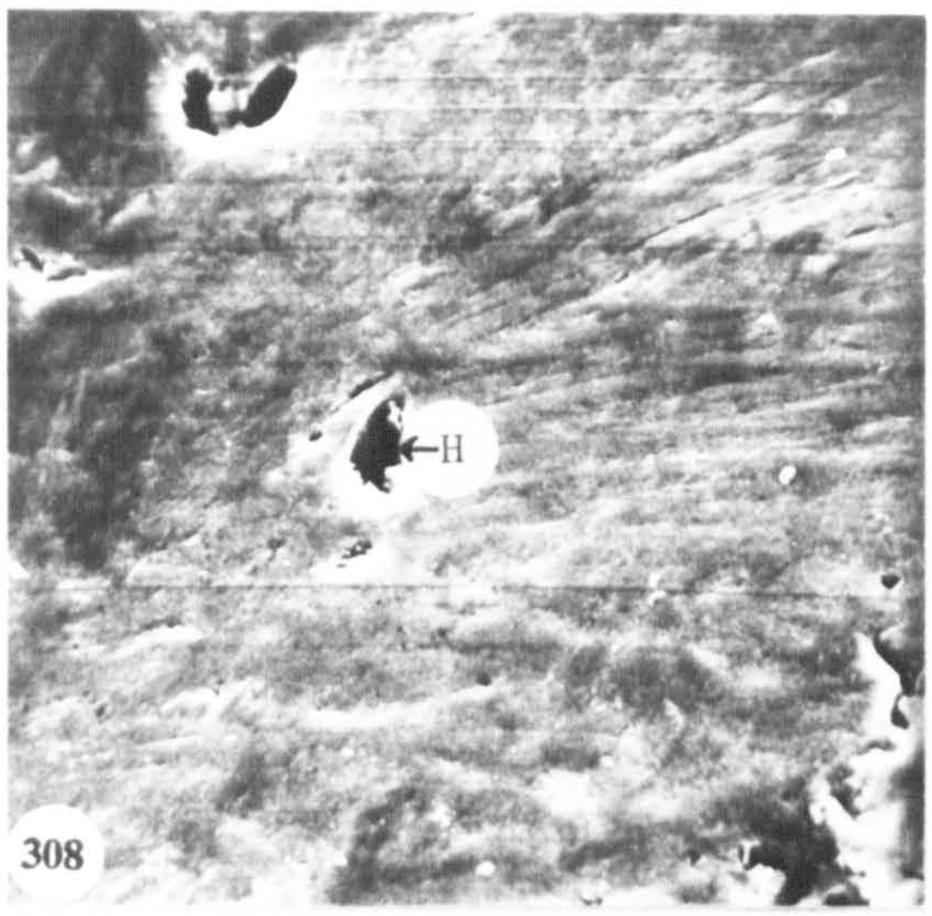


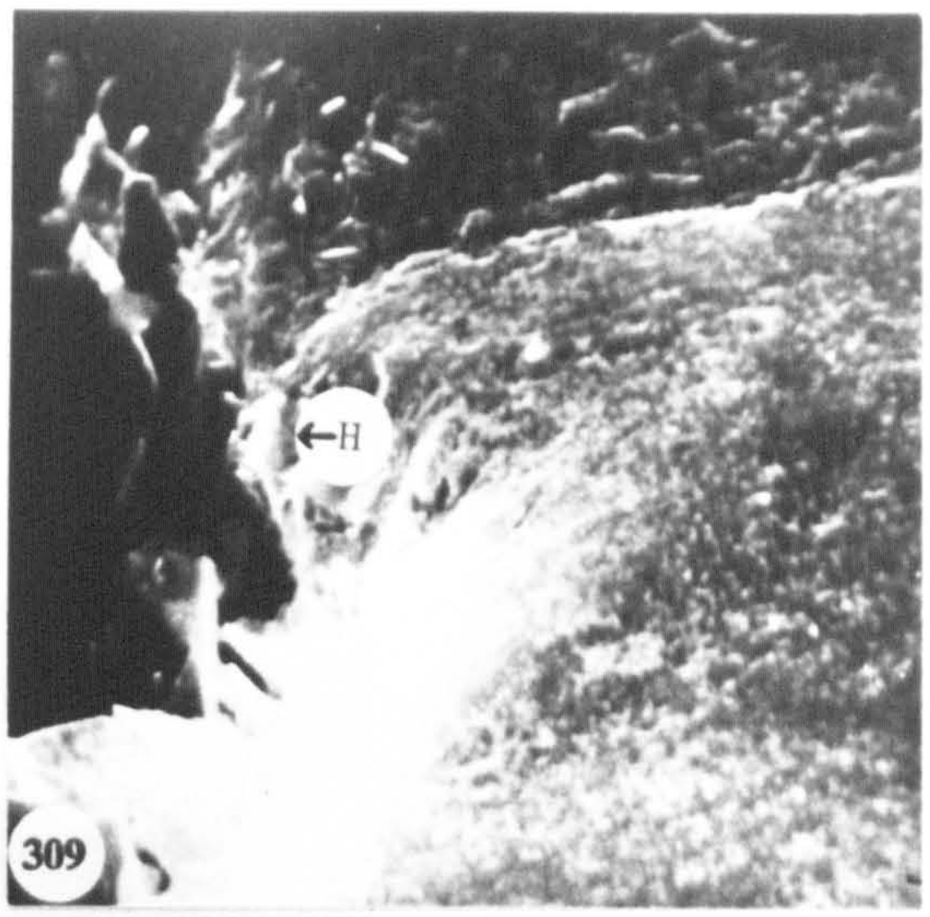
LIMA GRAPHITE

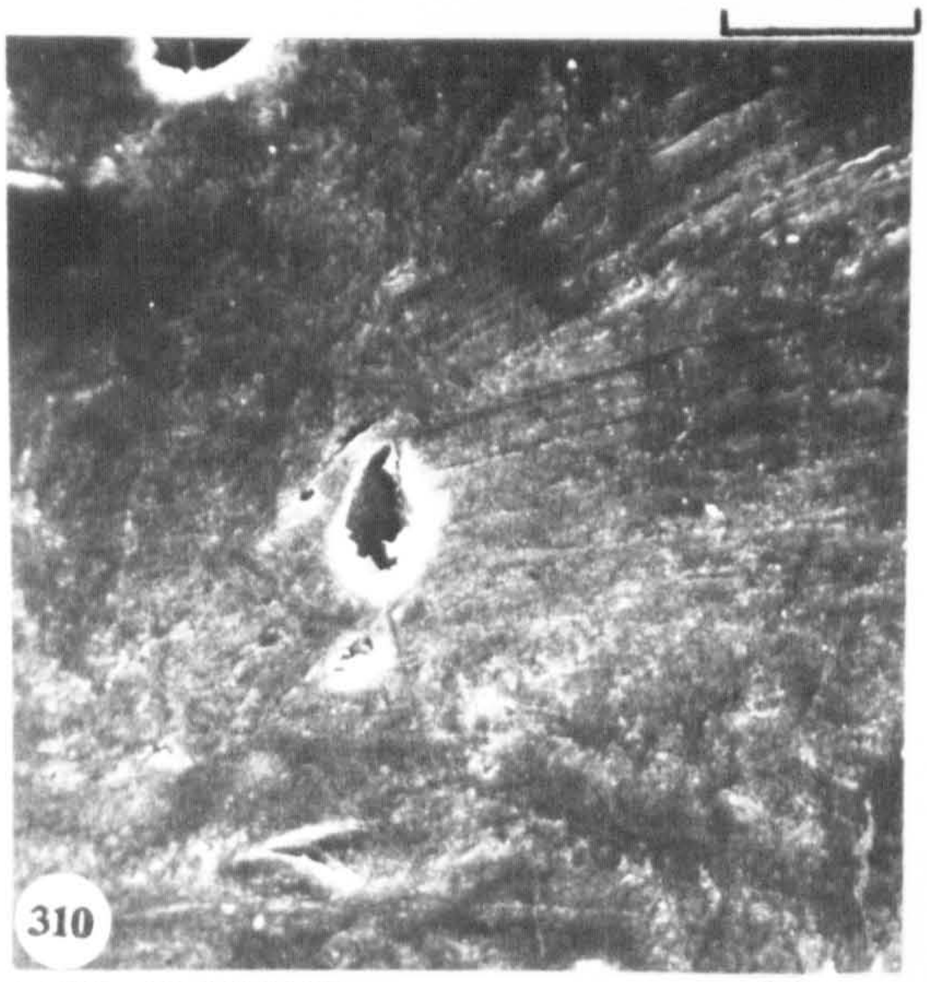


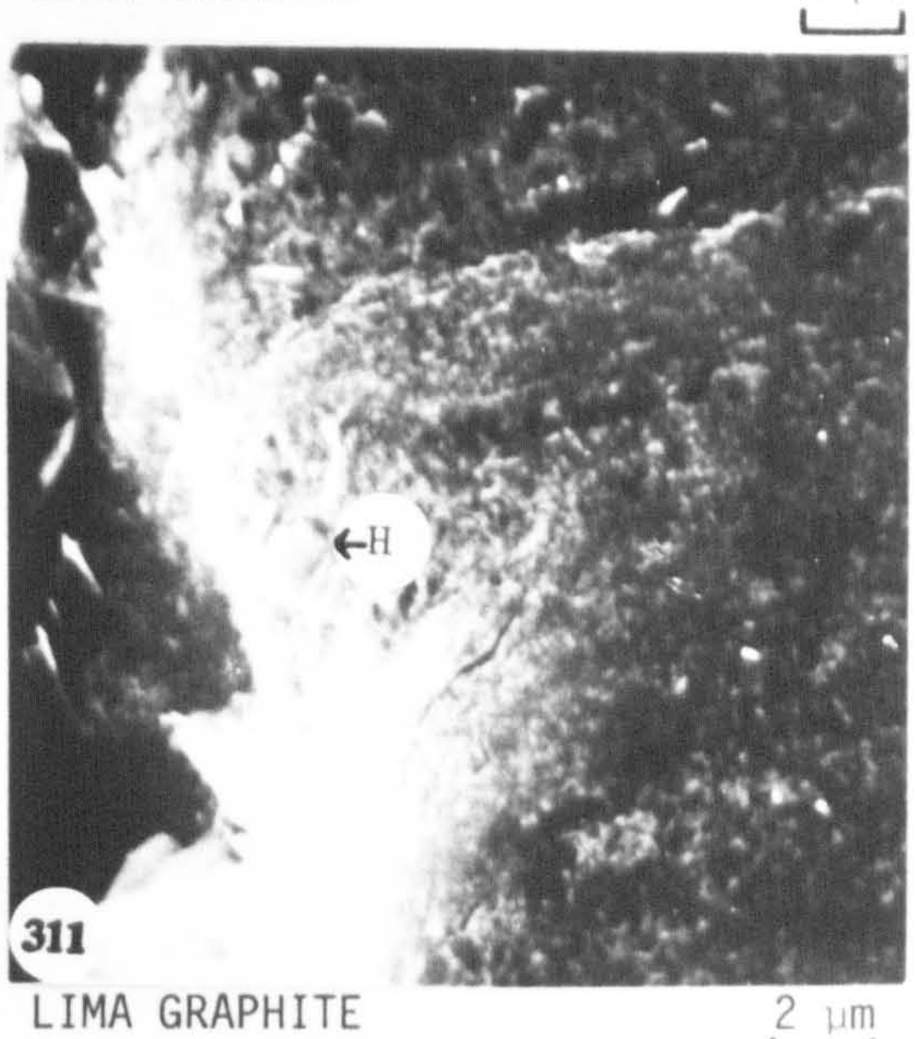
LIMA GRAPHITE

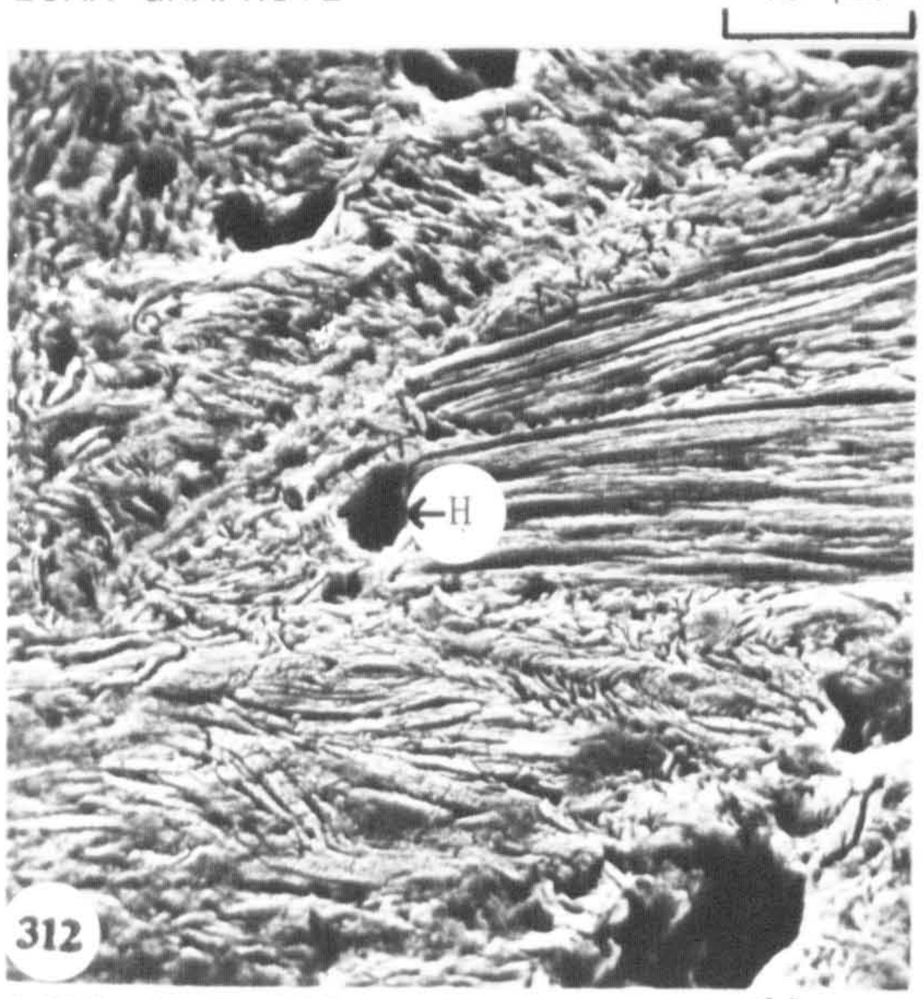
Figures 305 to 307. Optical micrographs of Lima Graphite (LG14) before (Figure 305) and after gasification in carbon dioxide at 1138 K (Figure 306) and 1223 K (Figure 307) for 16 hours each. Weight losses 2.00% and 9.40%.

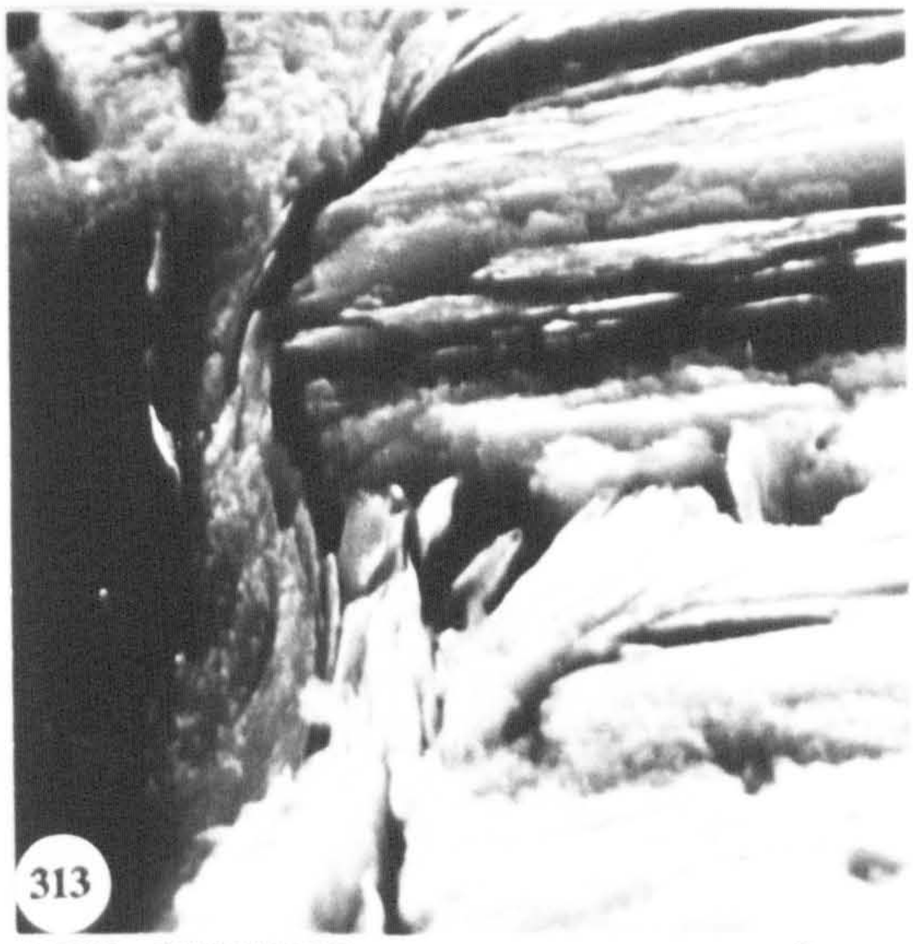




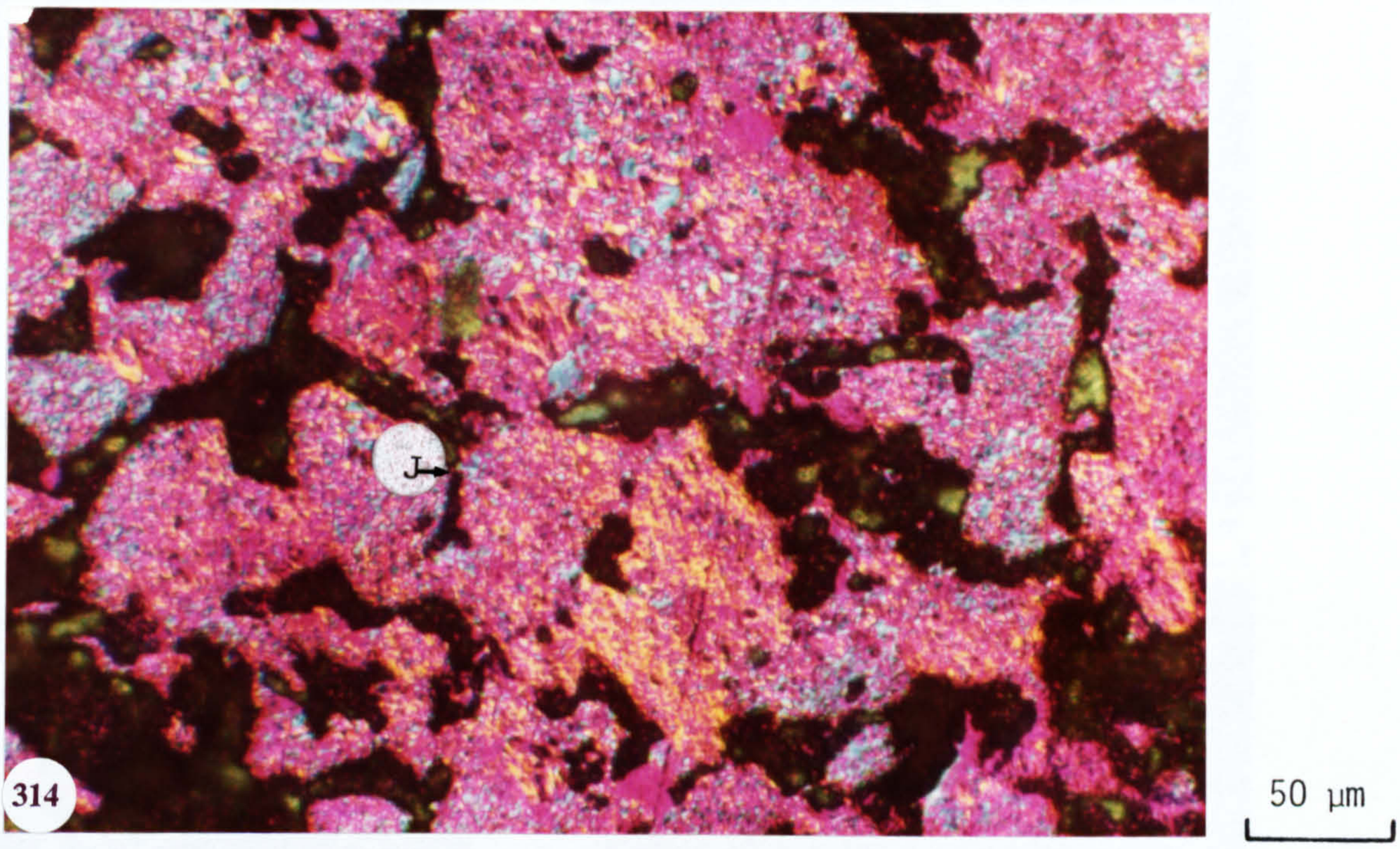




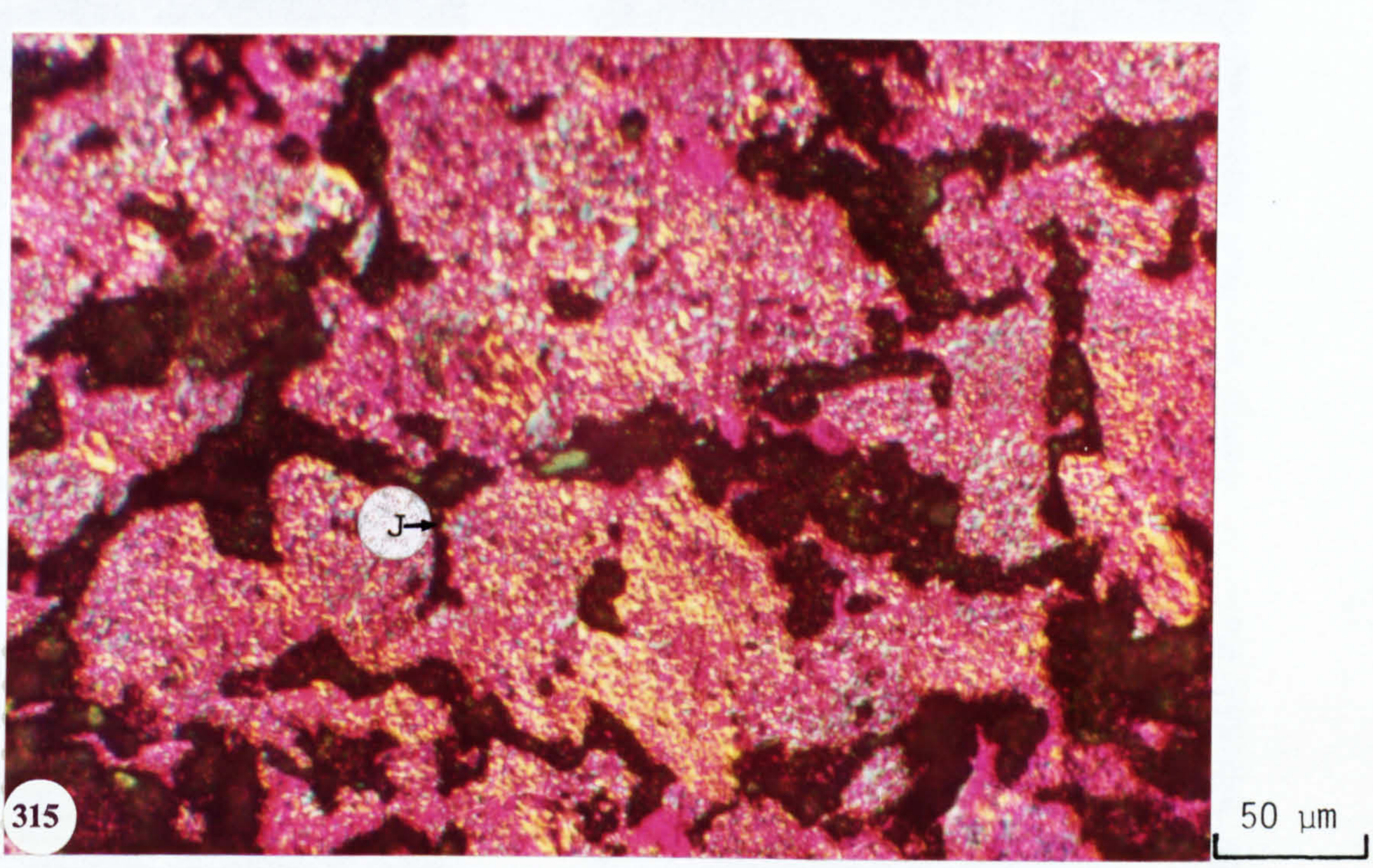




Figures 308 to 313. Scanning electron micrographs (stereoscan) of Lima Graphite (LG14) before (Figures 308 and 309) and after gasification in carbon dioxide at 1138 K (Figures 310 and 311) and 1223 K (Figures 312 and 313) for 16 hours each. Weight losses 2.00 % and 9.40%.

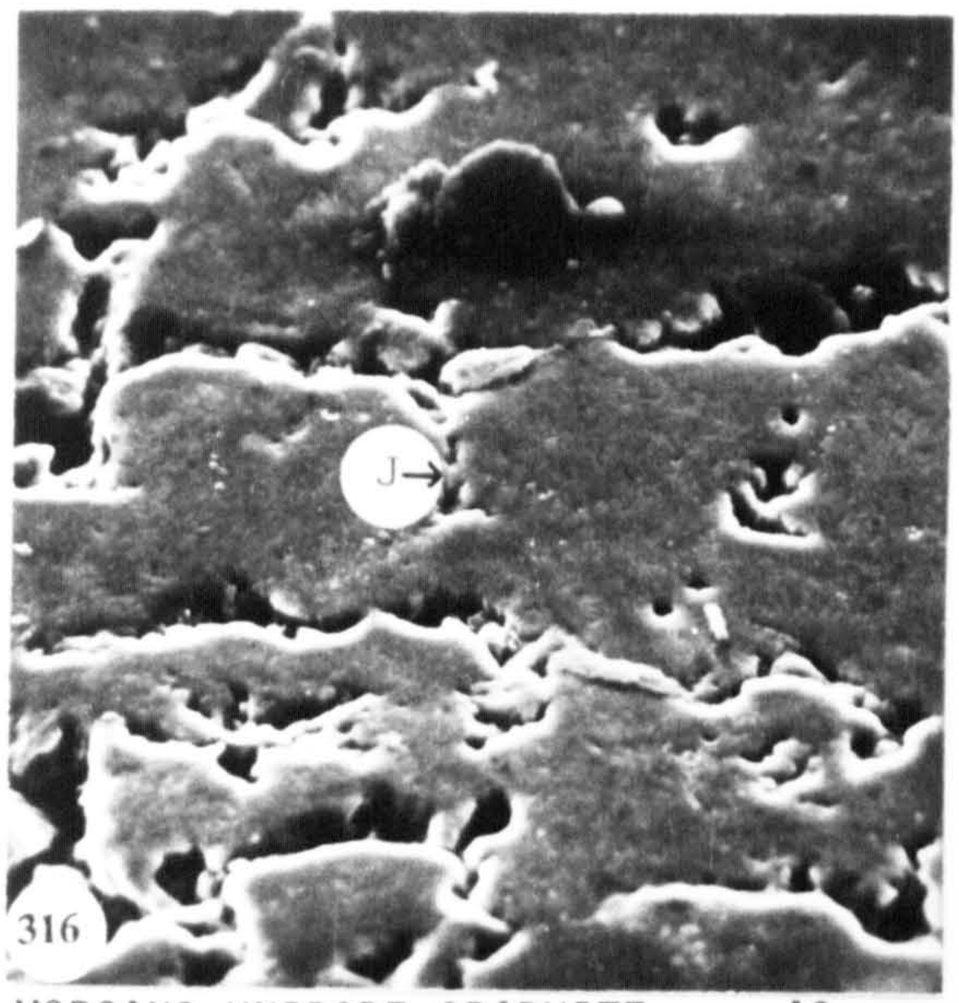


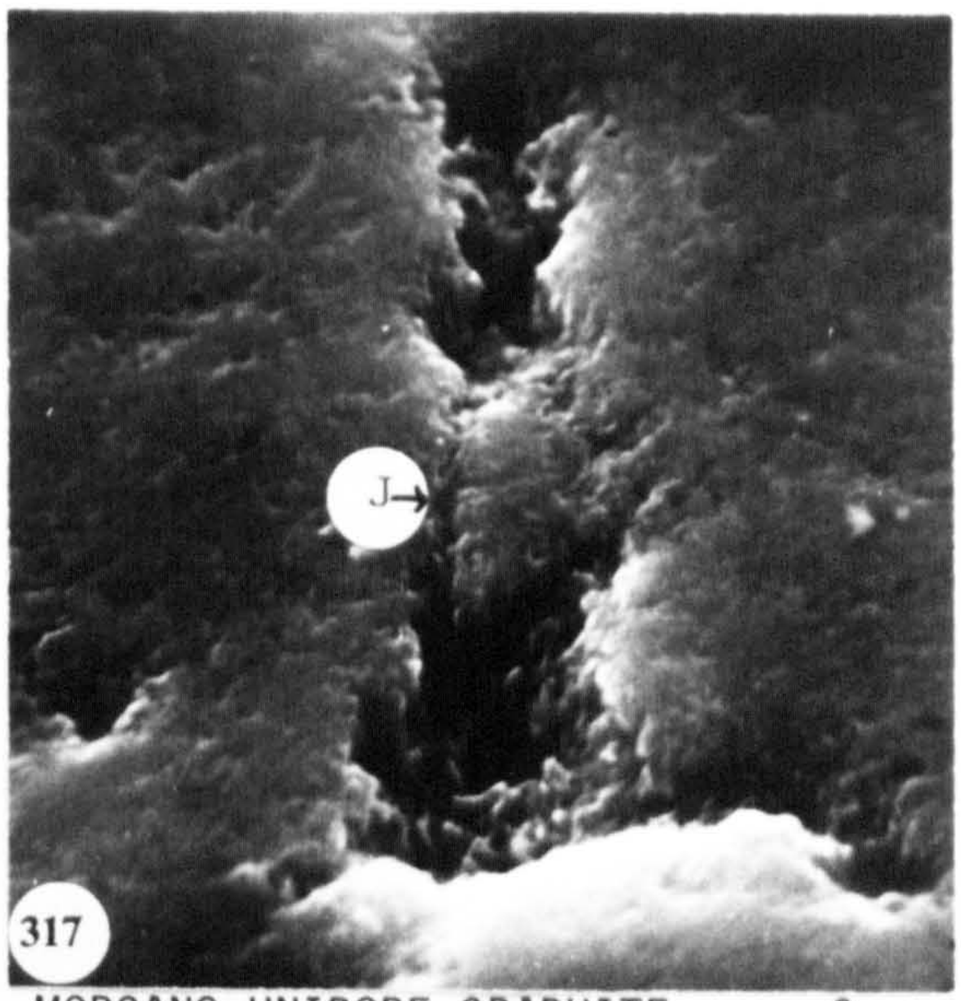
MORGANS UNIPORE GRAPHITE

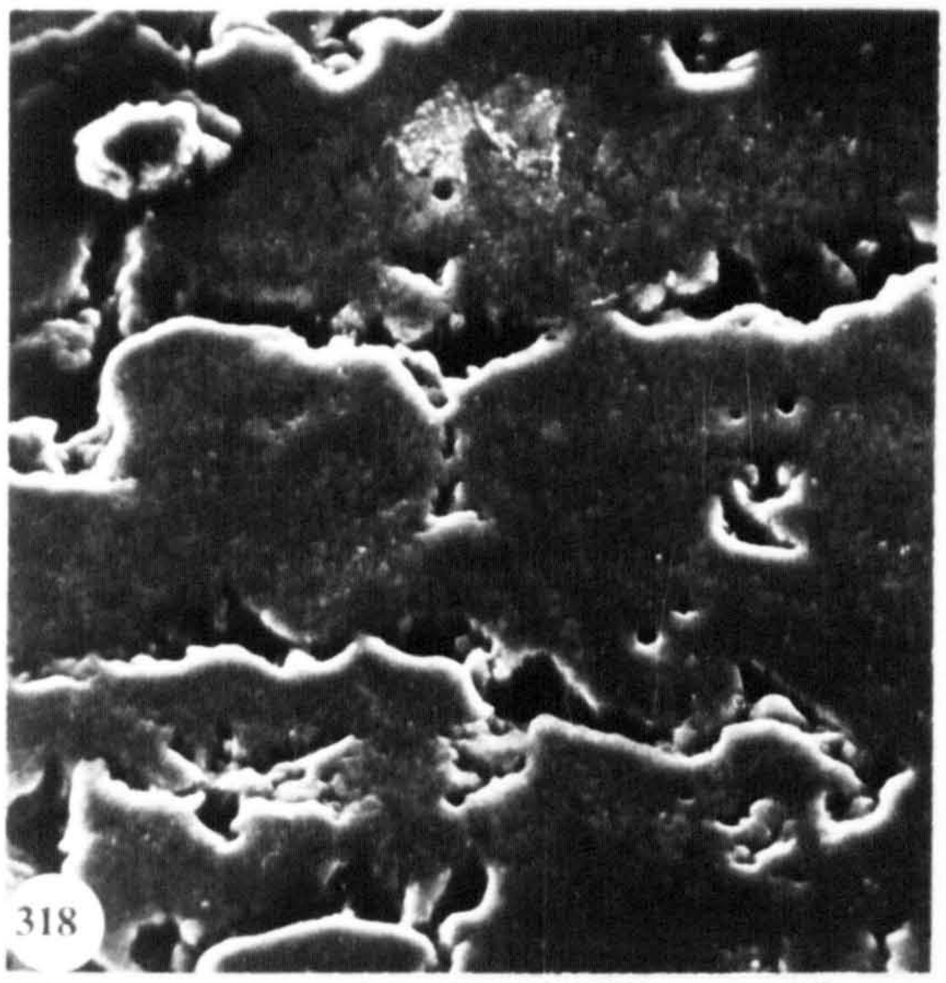


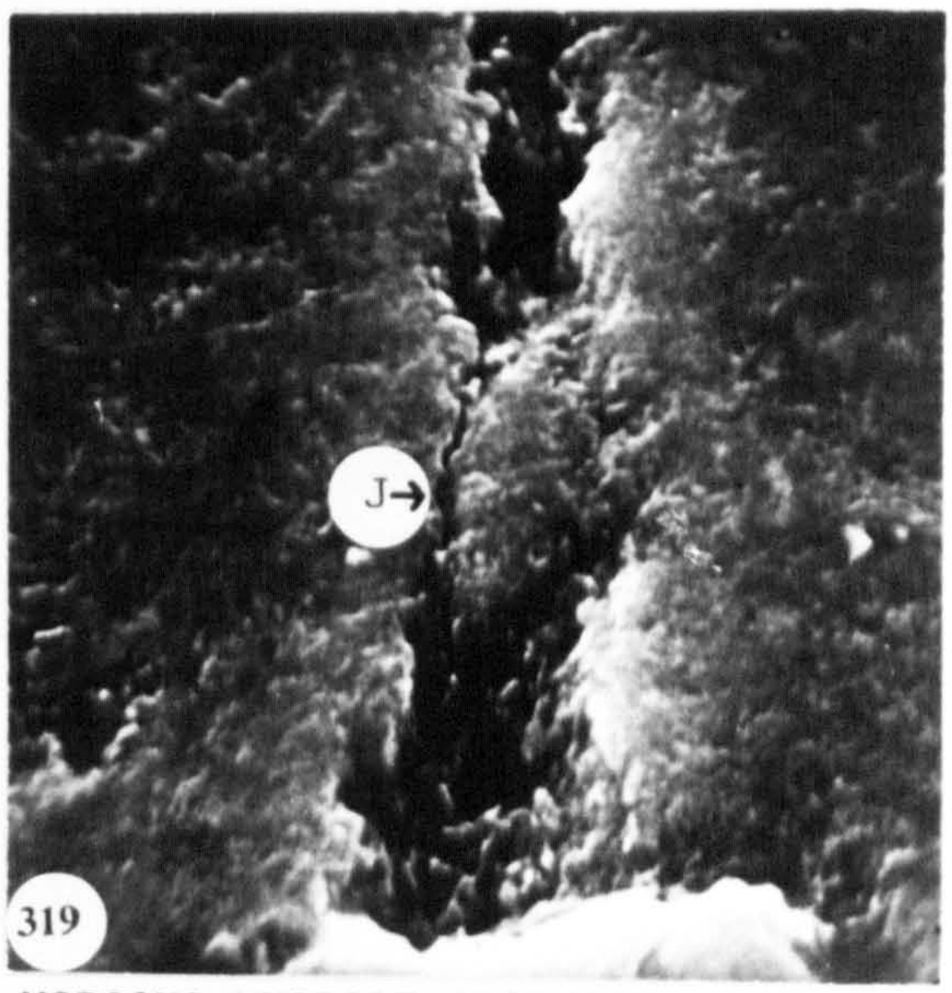
MORGANS UNIPORE GRAPHITE

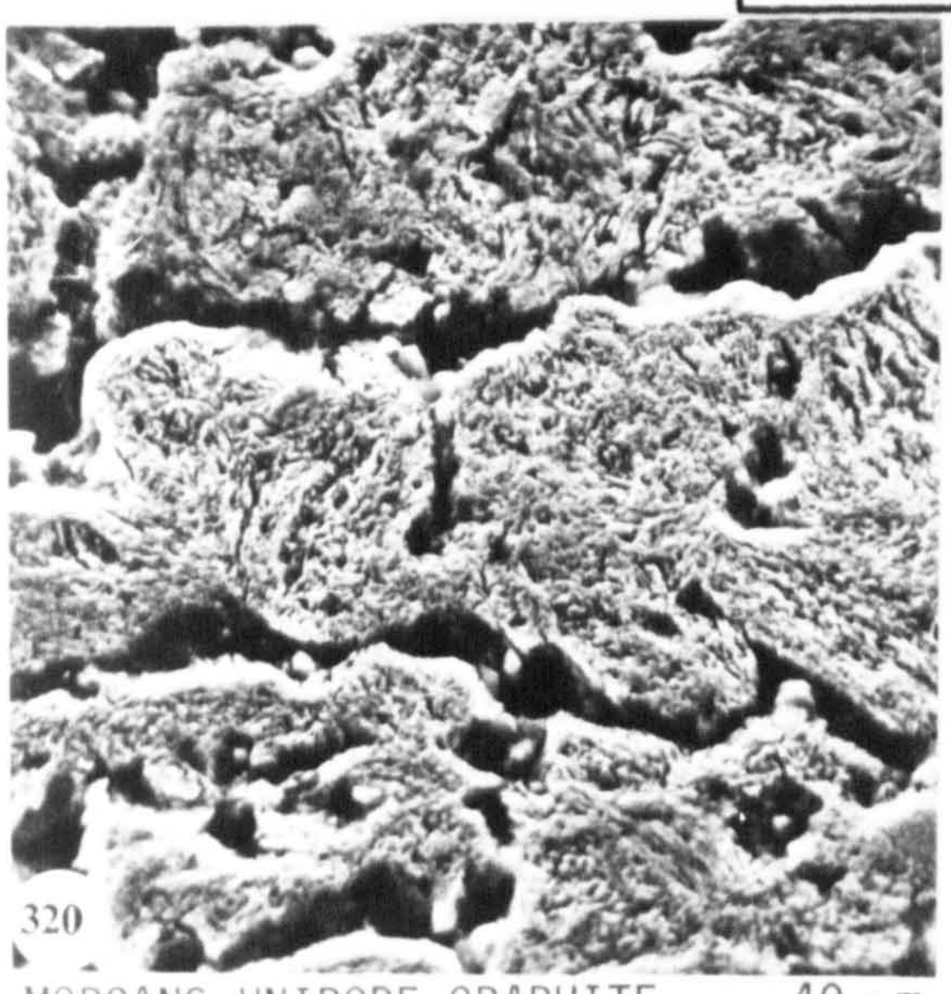
Figures 314 and 315. Optical micrographs of Morgans Unipore Graphite (MG8) before and after gasification in carbon dioxide at 1138 K for 16 hours.
Weight loss 0.85%.

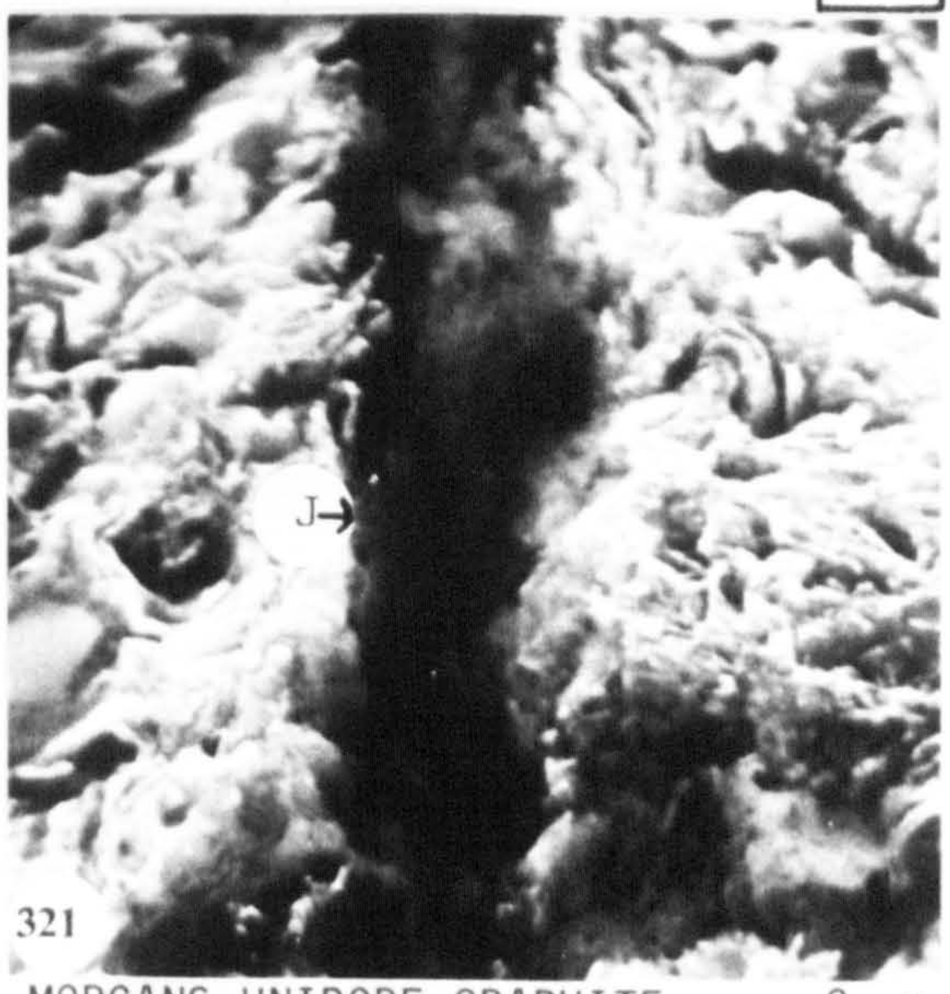




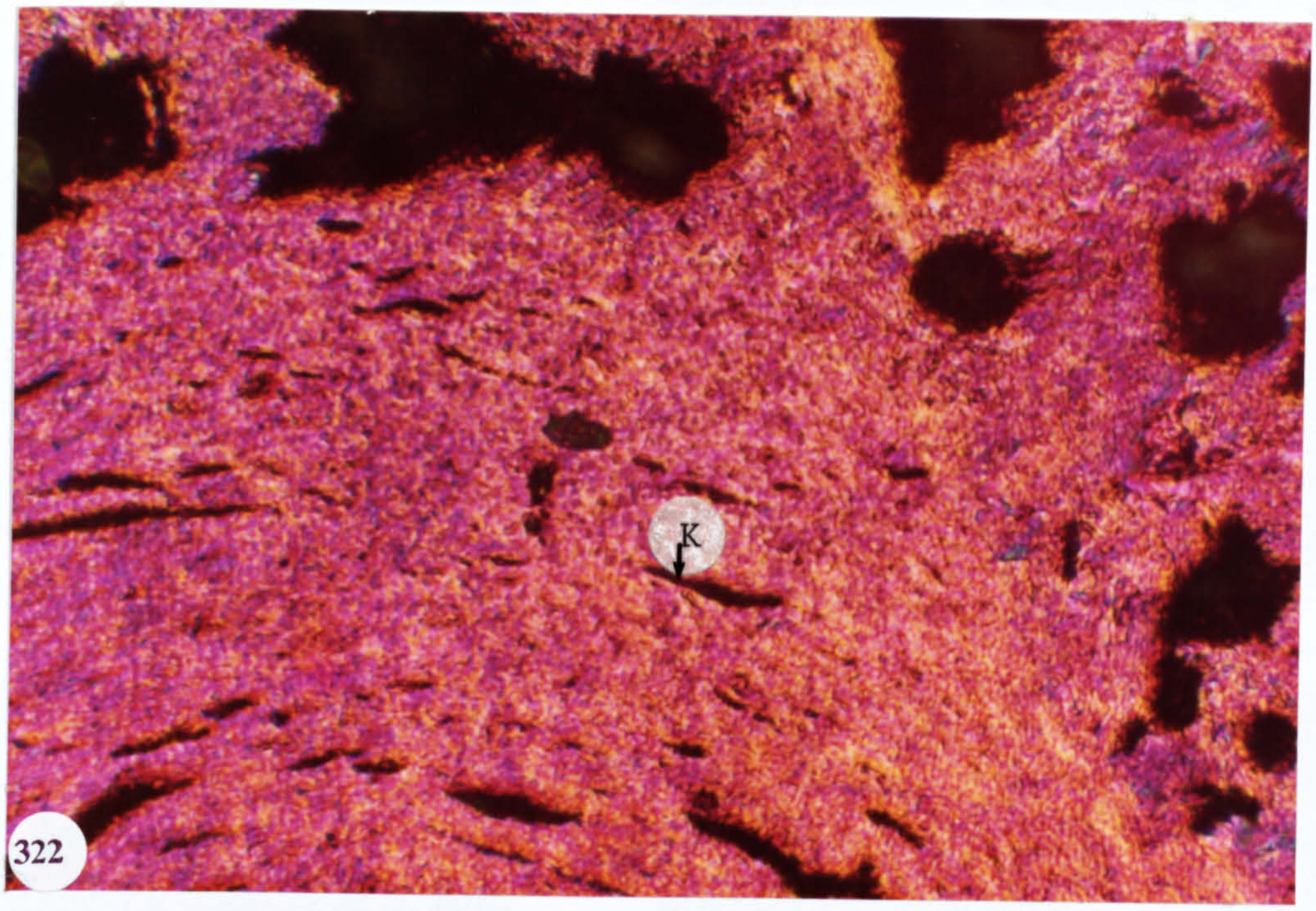




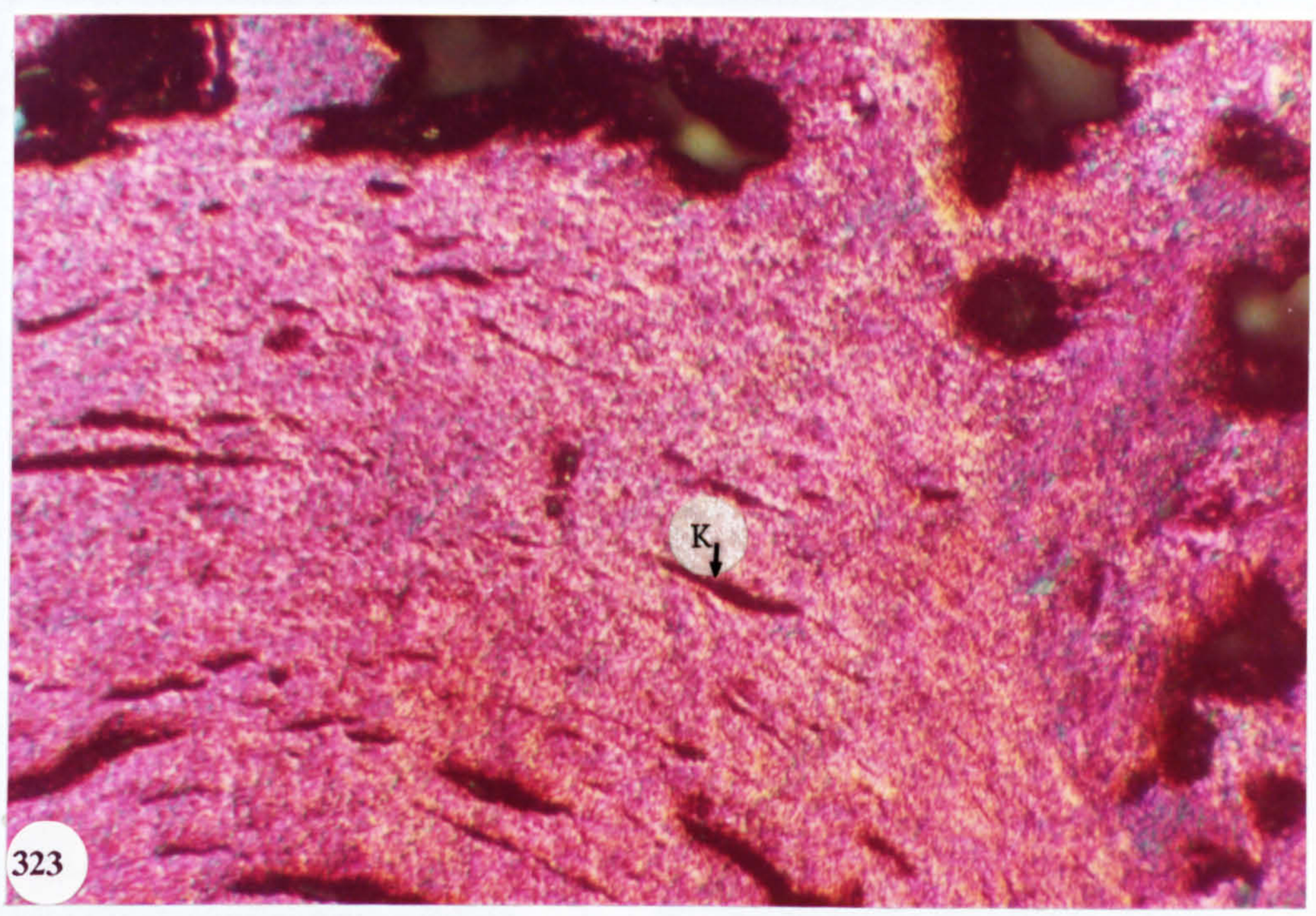




Figures 316 to 321. Scanning electron micrographs (stereoscan) of Morgans Unipore Graphite (MG8) before (Figures 316 and 317) and after gasification in carbon dioxide at 1138 K (Figures 318 and 319) and 1223 K (Figures 320 and 321) for 16 hours each. Weight losses 0.85% and 7.57%.

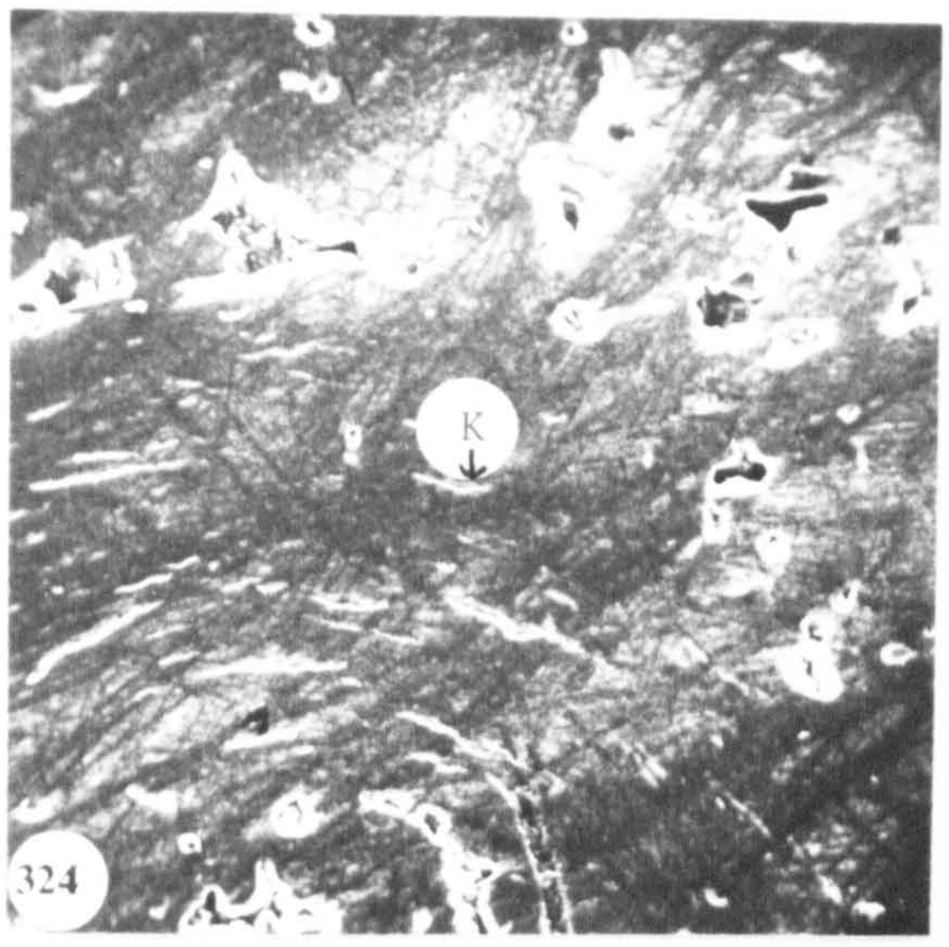


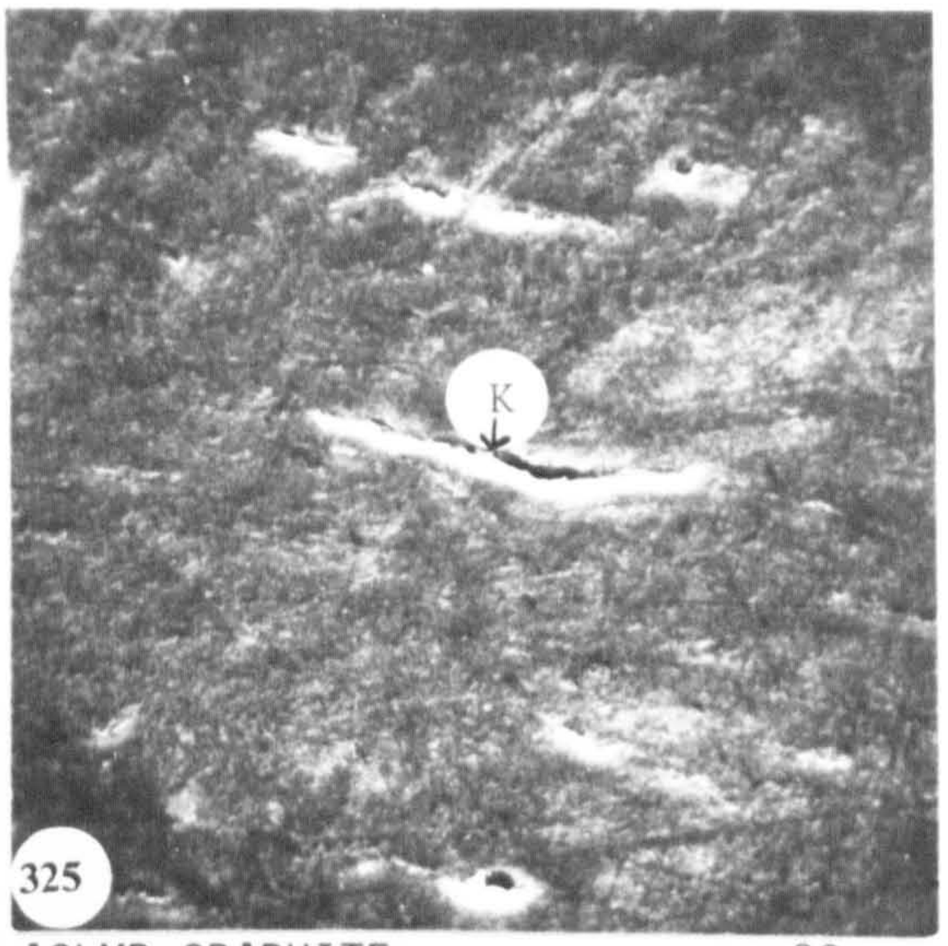
AGLMP GRAPHITE

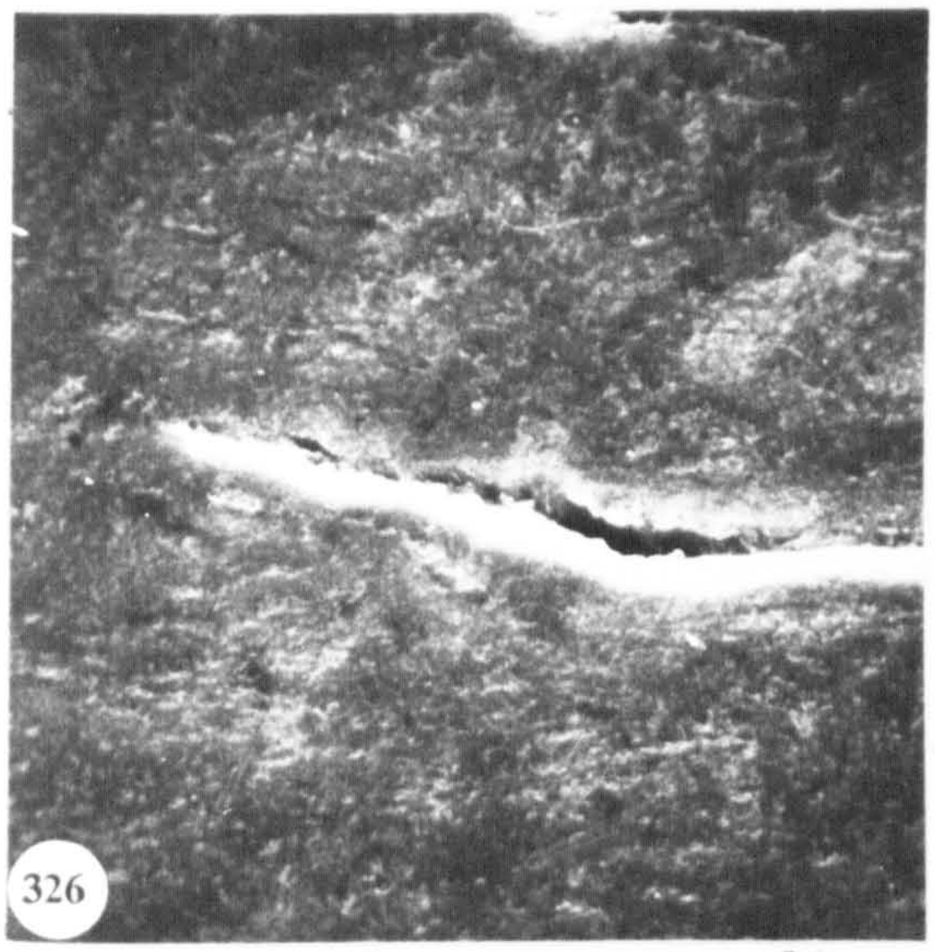


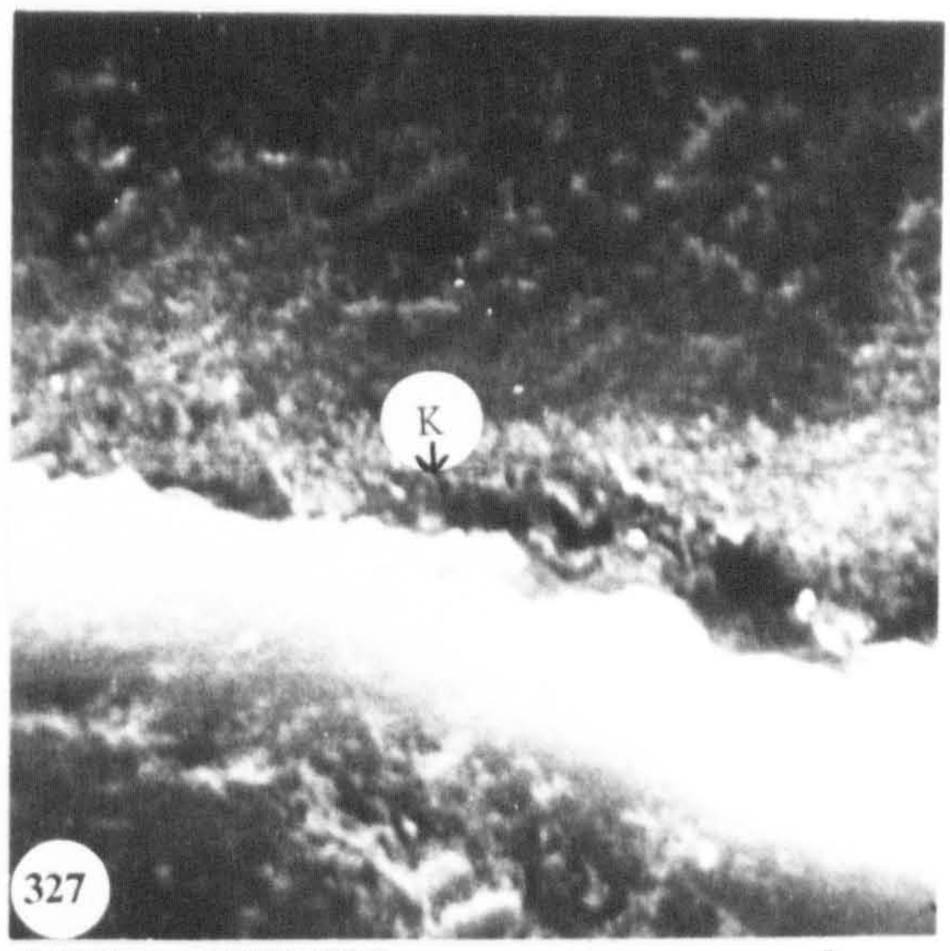
AGLMP GRAPHITE

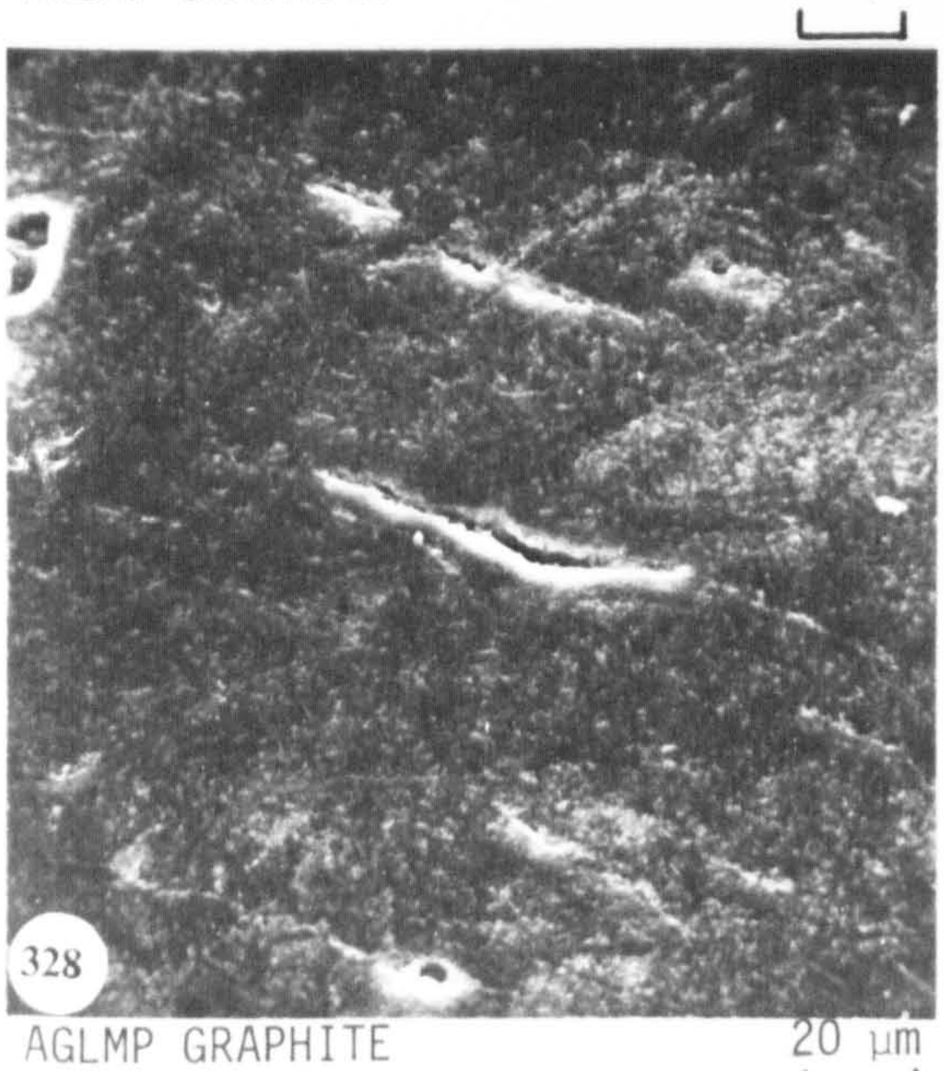
Figures 322 and 323. Optical micrographs of AGLMP Graphite (AG7) before and after gasification in carbon dioxide at 1138 K for 16 hours. Weight loss 0.81%.

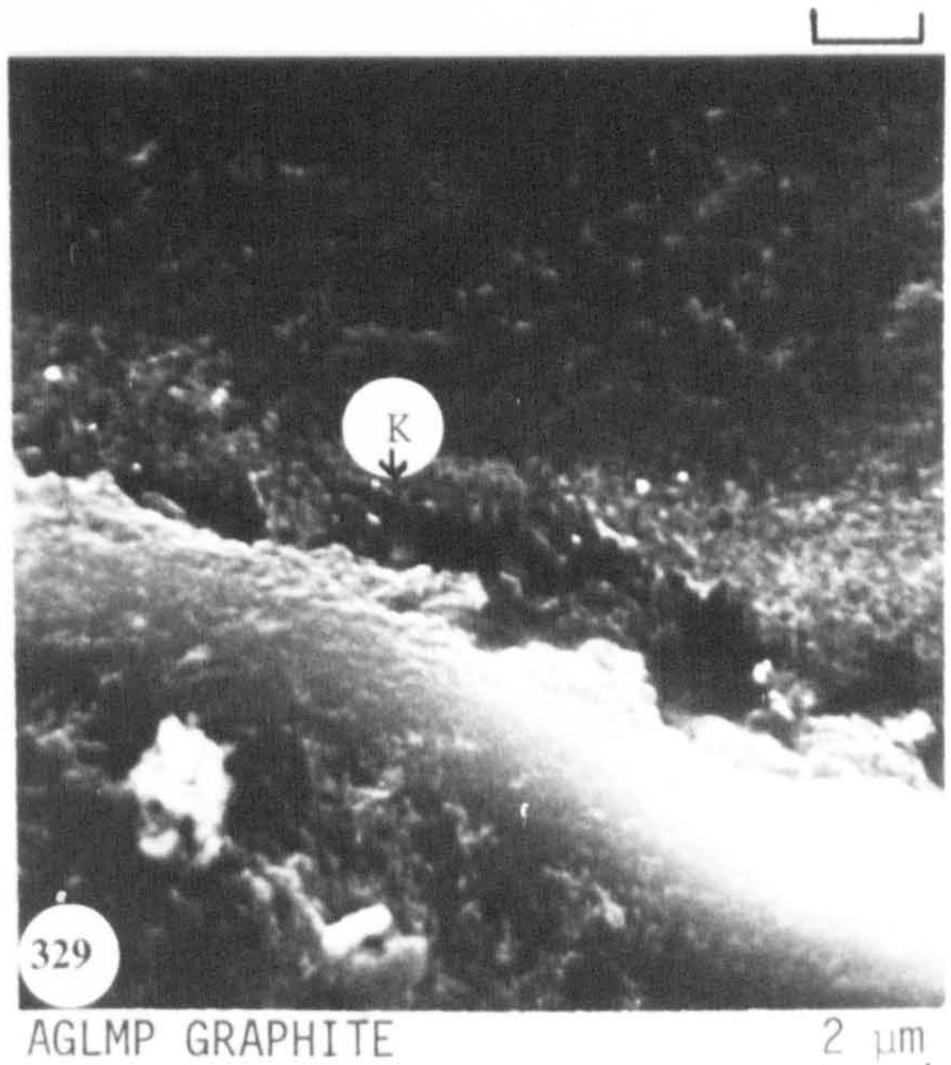






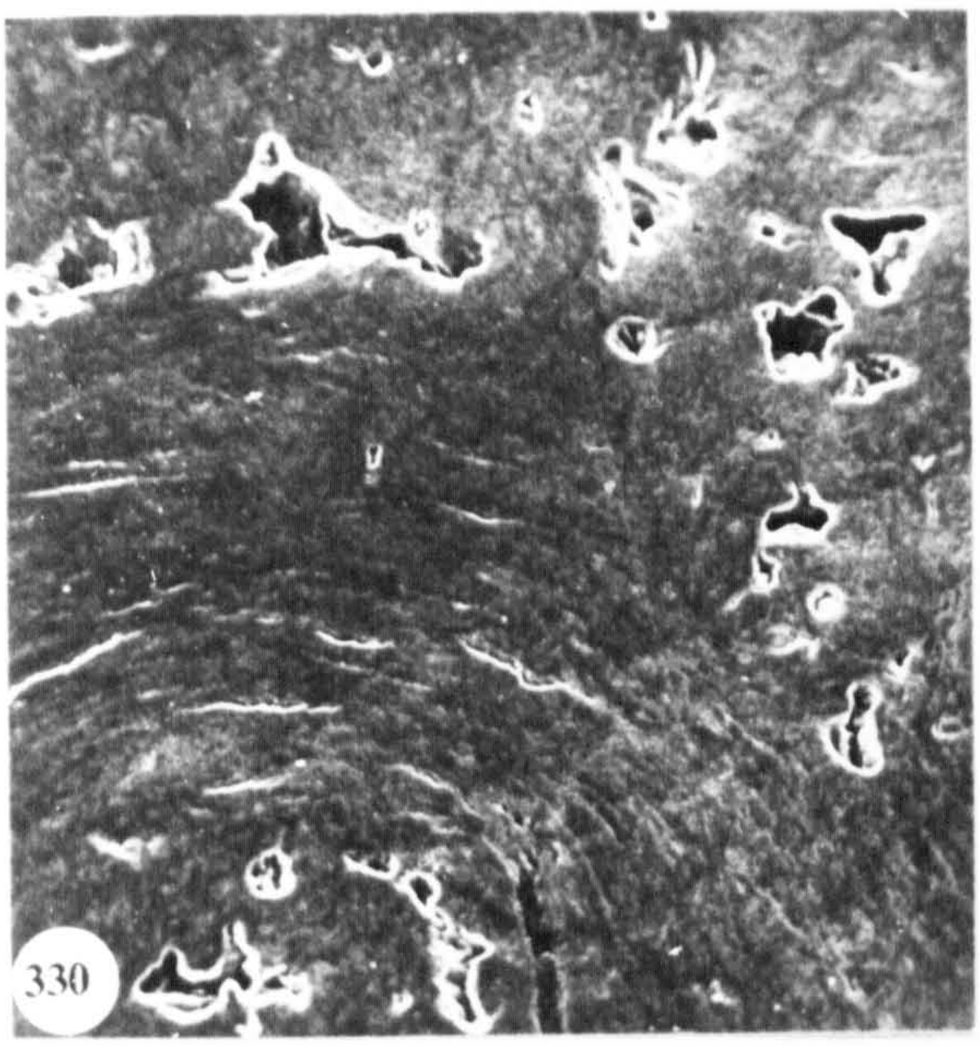




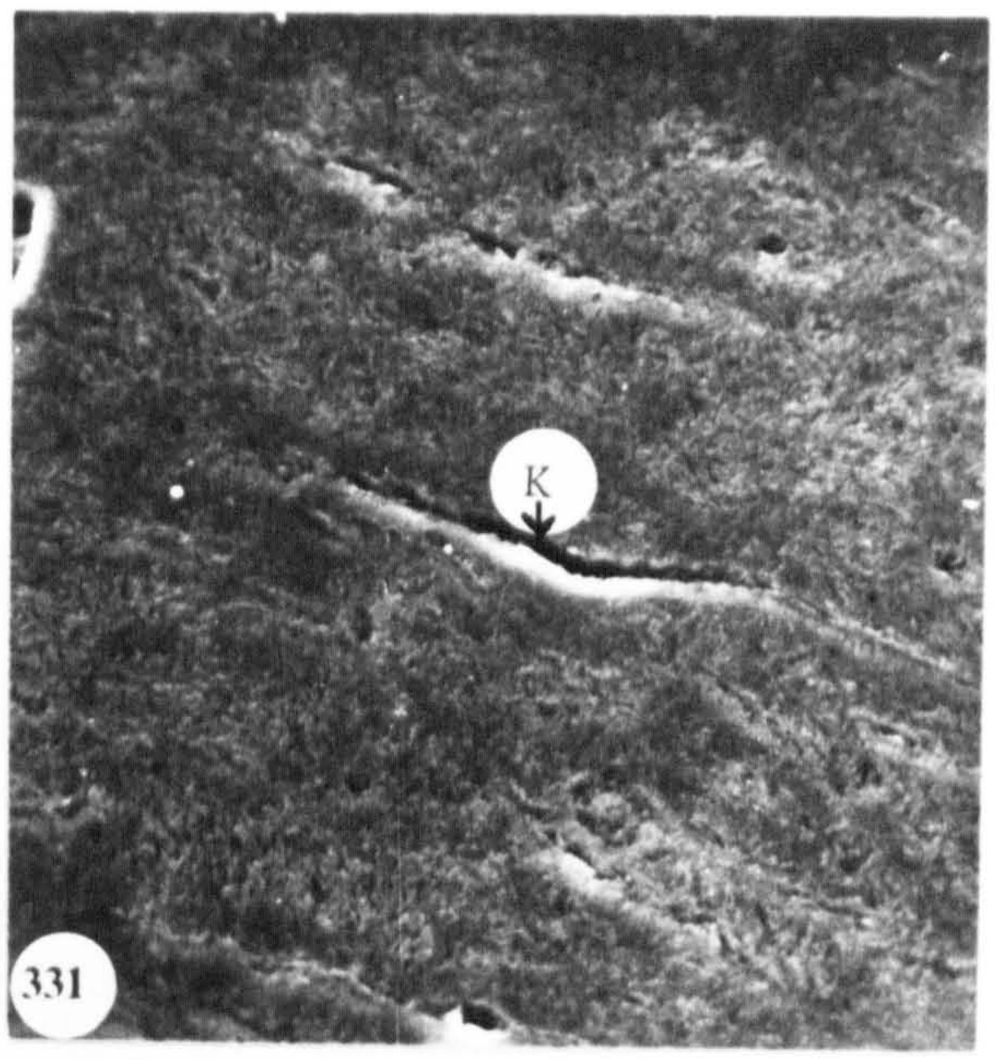


Figures 324 to 329. Scanning electron micrographs (stereoscan) of AGLMP Graphite (AG7) before (Figures 324 to 327) and after (Figures 328 and 329) gasification in carbon dioxide at 1138 K for 16 hours.

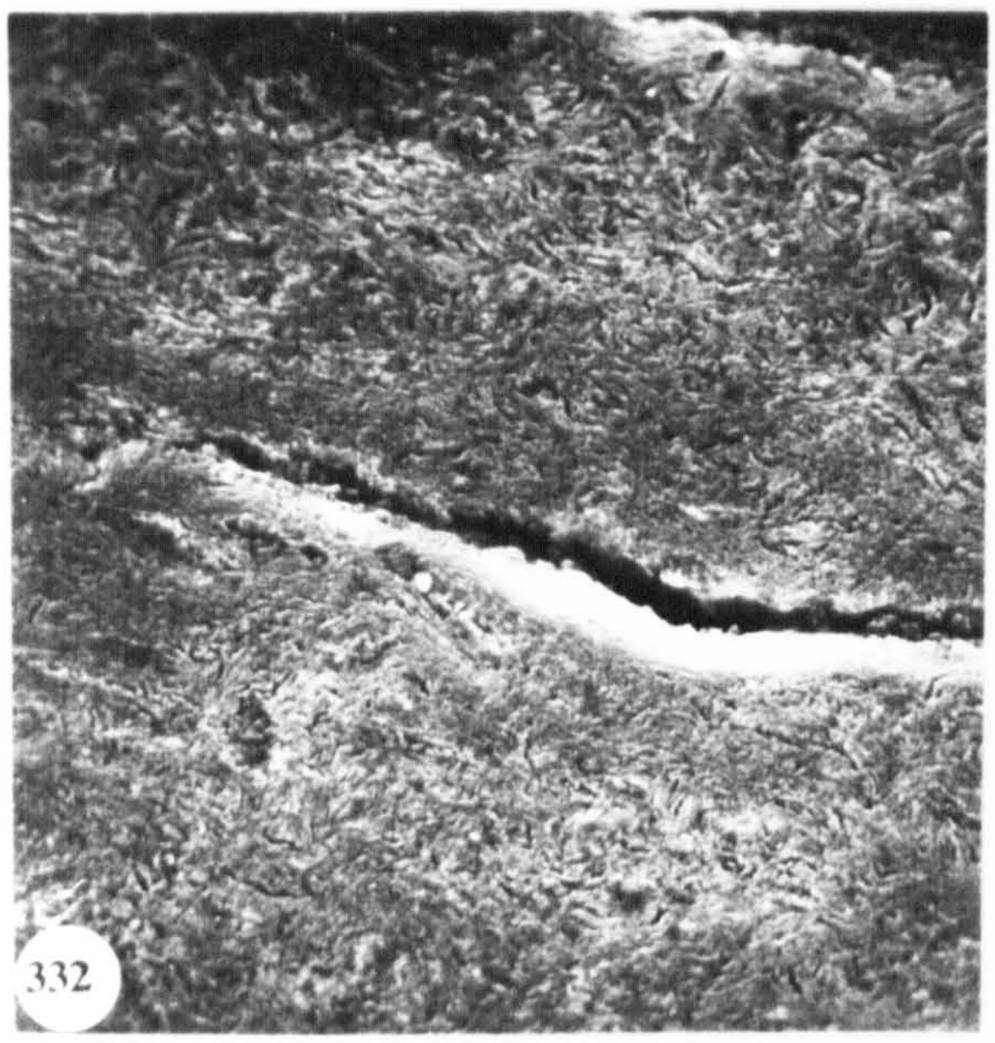
Weight loss 0.81%.



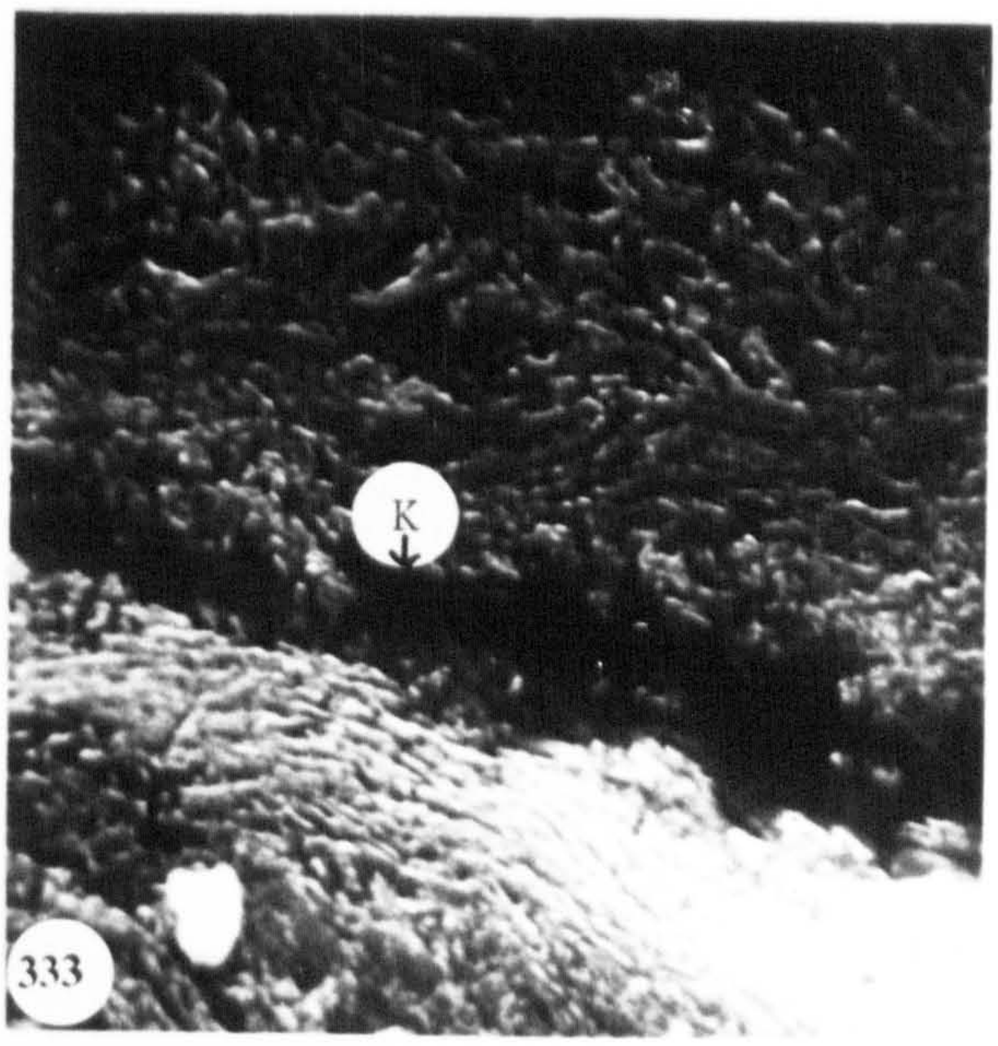
AGLMP GRAPHITE 100 µm



AGLMP GRAPHITE 20 µm

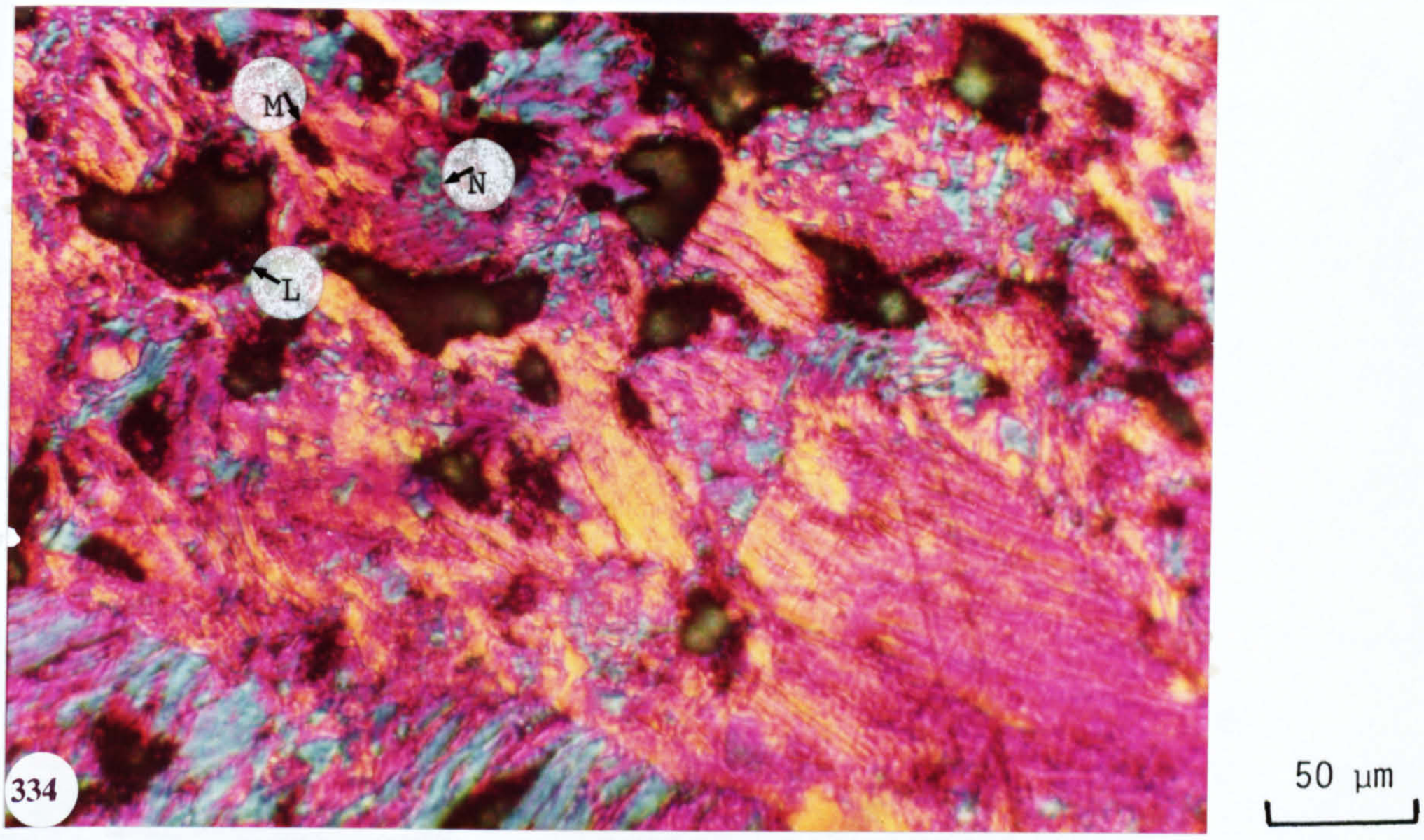


AGLMP GRAPHITE 10 µm

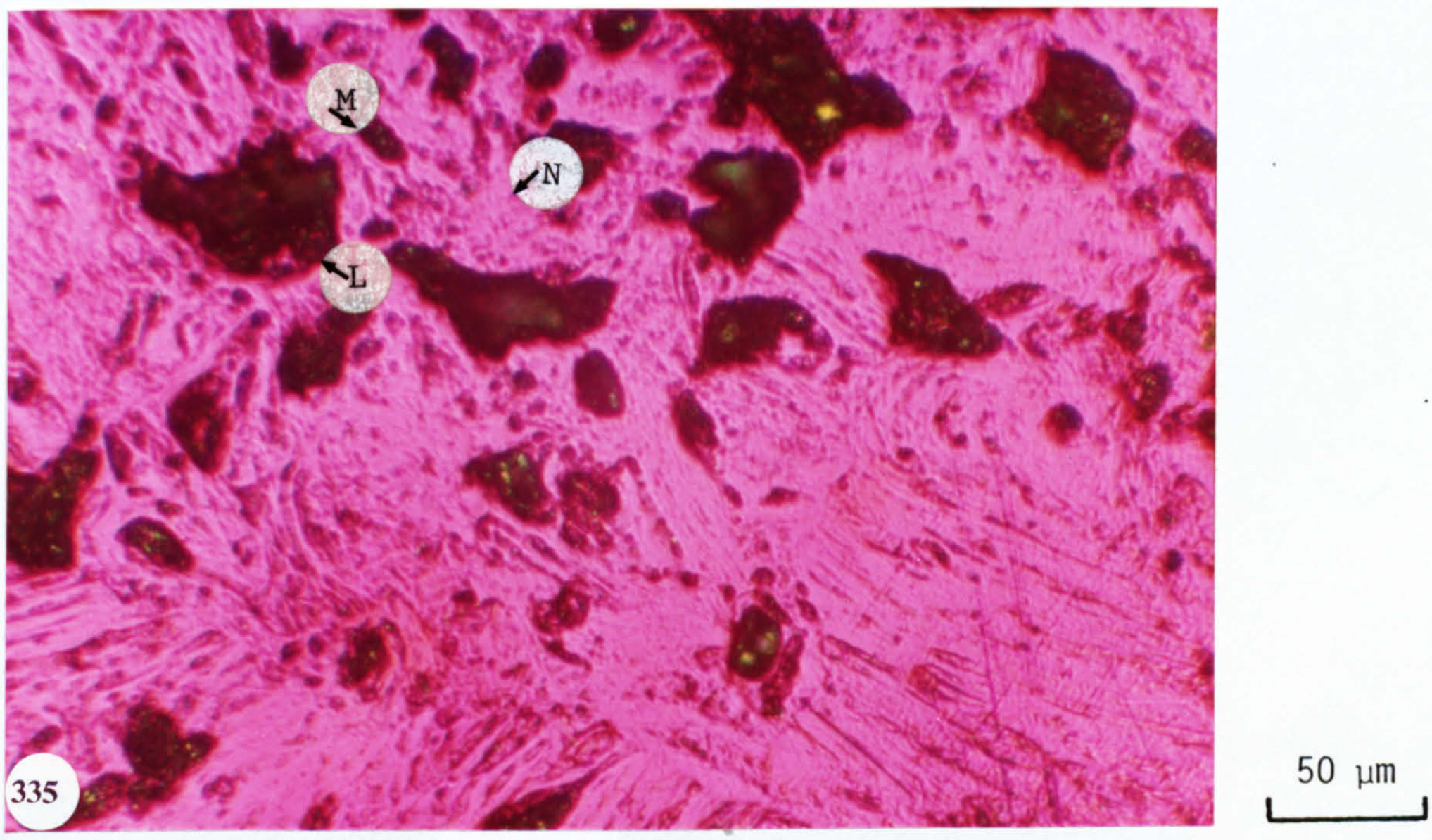


AGLMP GRAPHITE 2 µm

Figures 330 to 333. Scanning electron micrographs(stereoscan) of AGLMP Graphite (AG7) after gasification in carbon dioxide at 1223 K for 16 hours. Weight loss 2.28%.

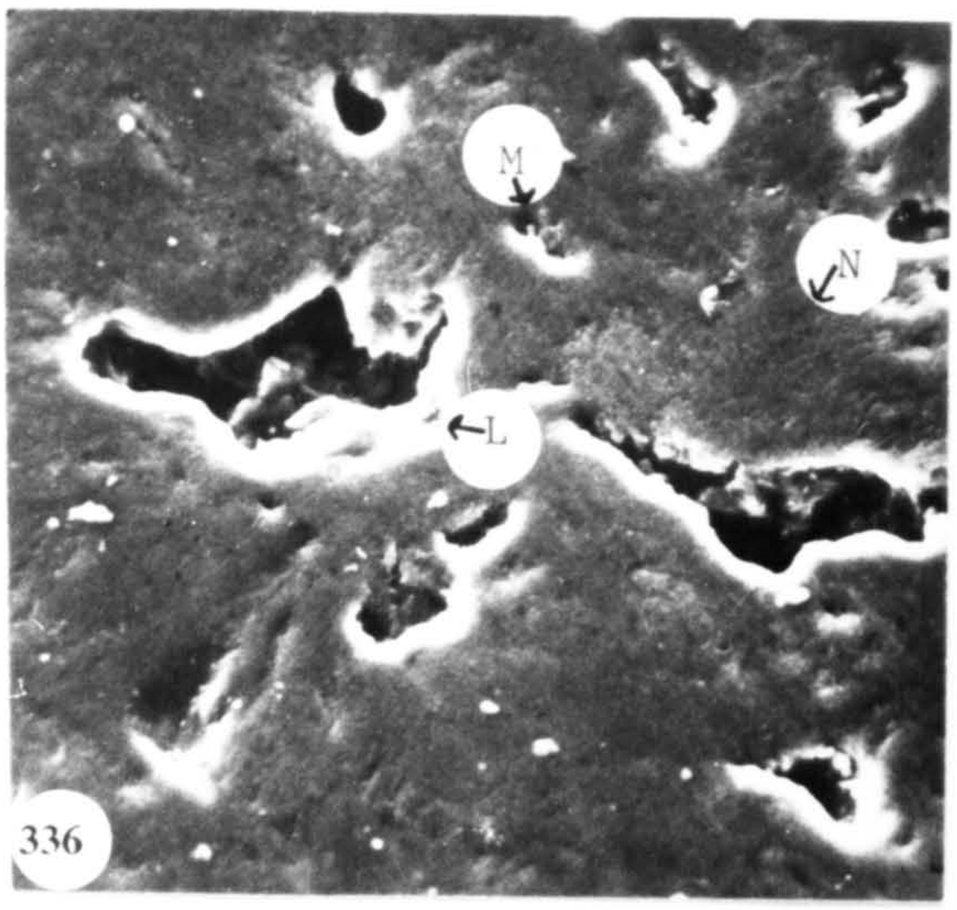


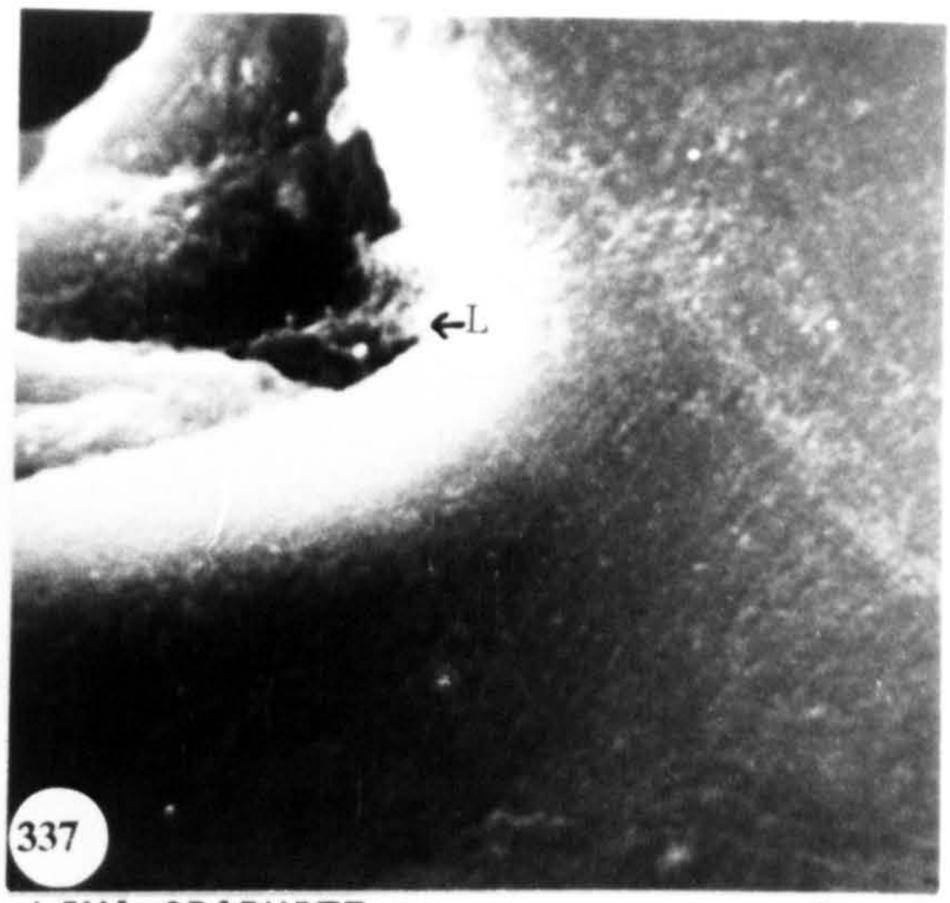
LIMA GRAPHITE

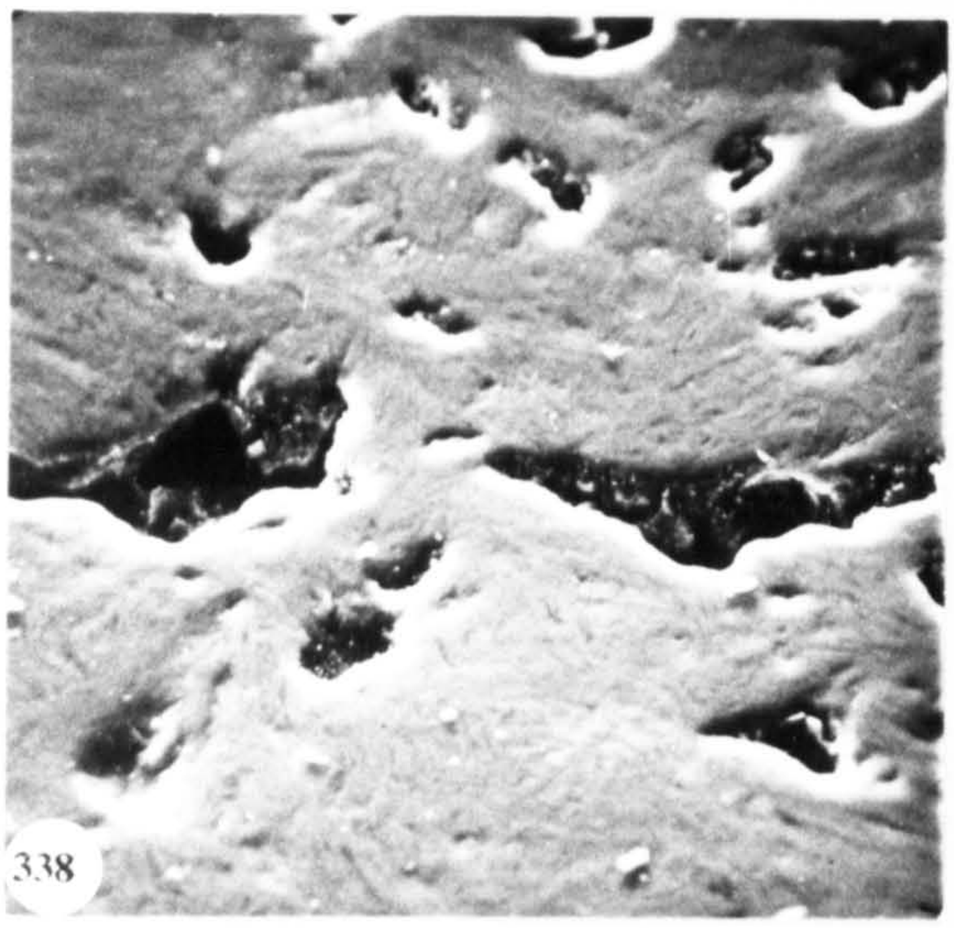


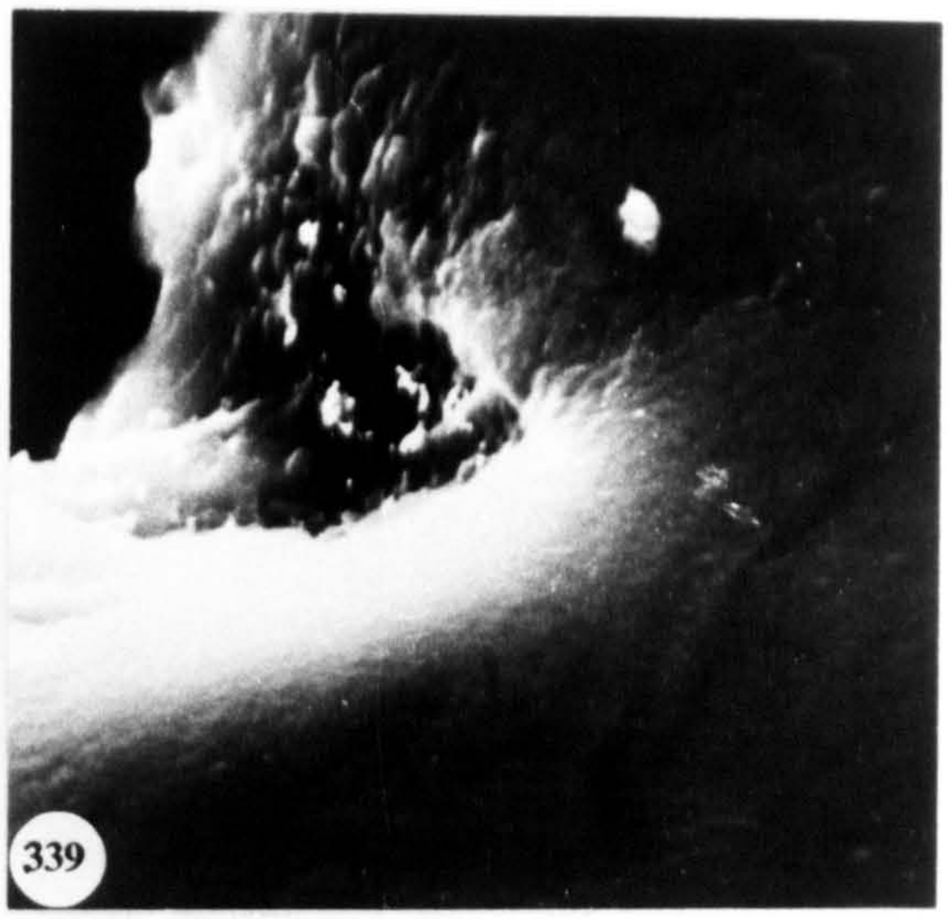
LIMA GRAPHITE

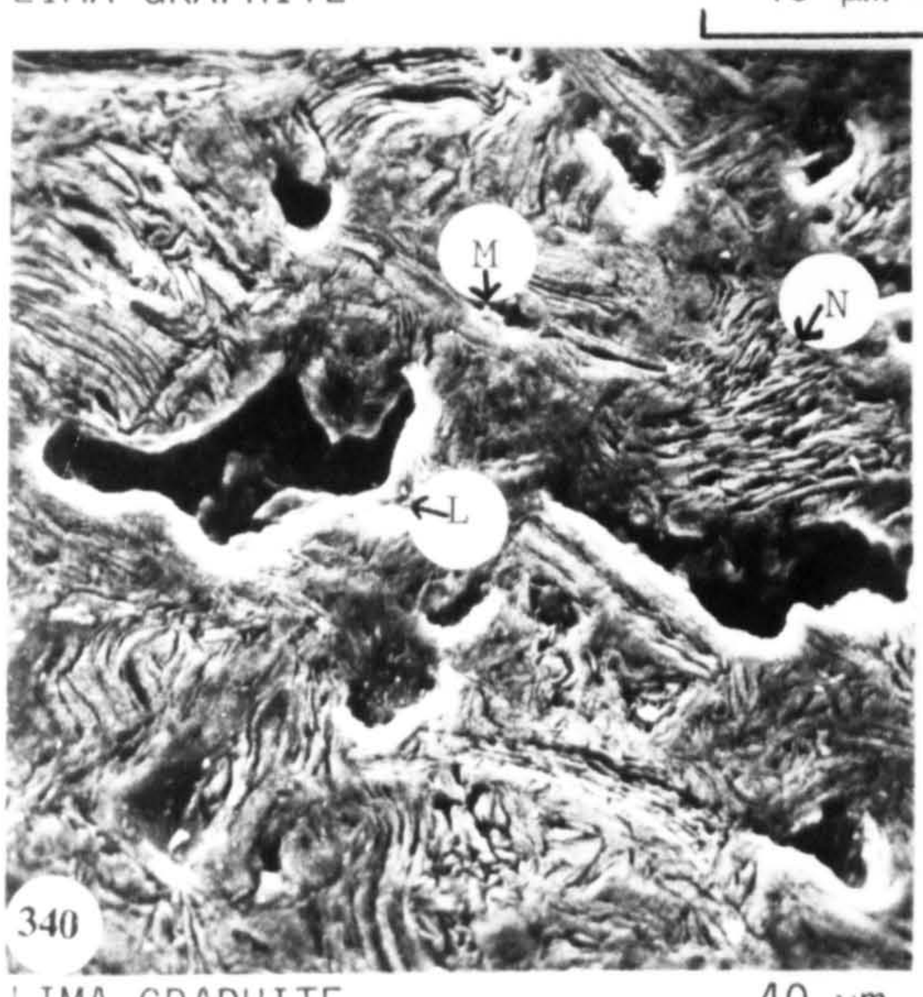
Figures 334 and 335. Optical micrographs of Lima Graphite (LG15) before and after gasification in carbon dioxide at 1173 K for 16 hours.
Weight loss 3.65%.

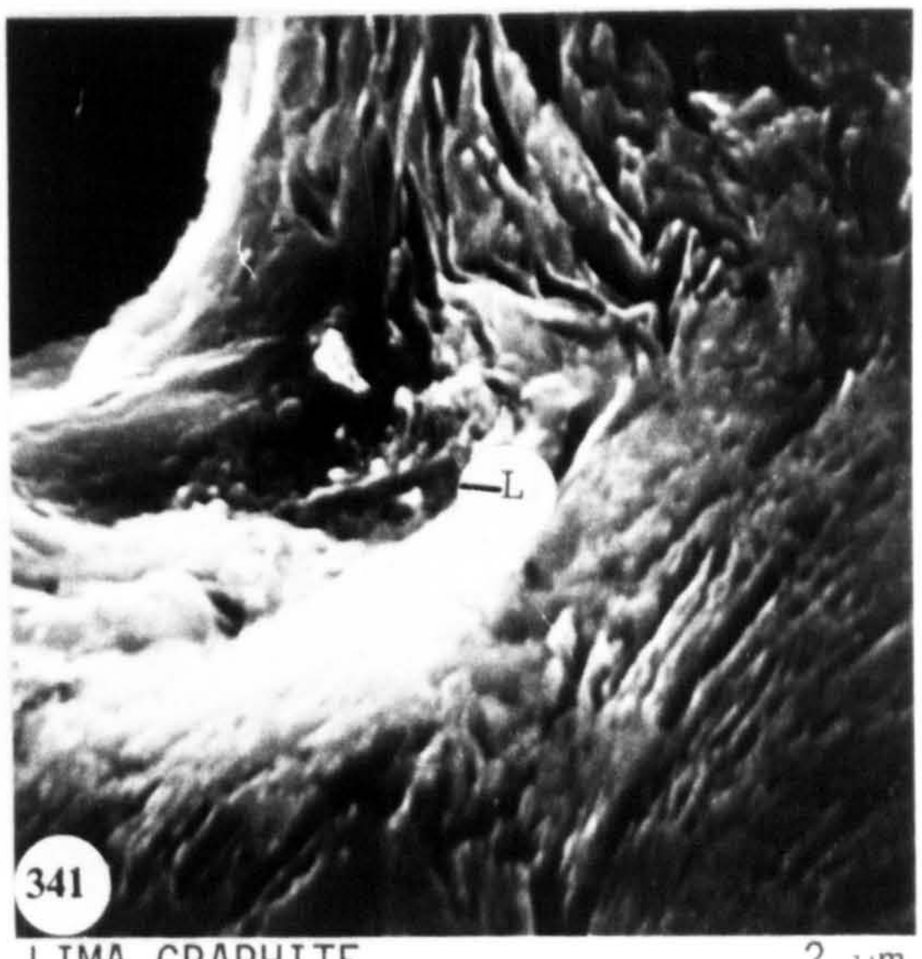




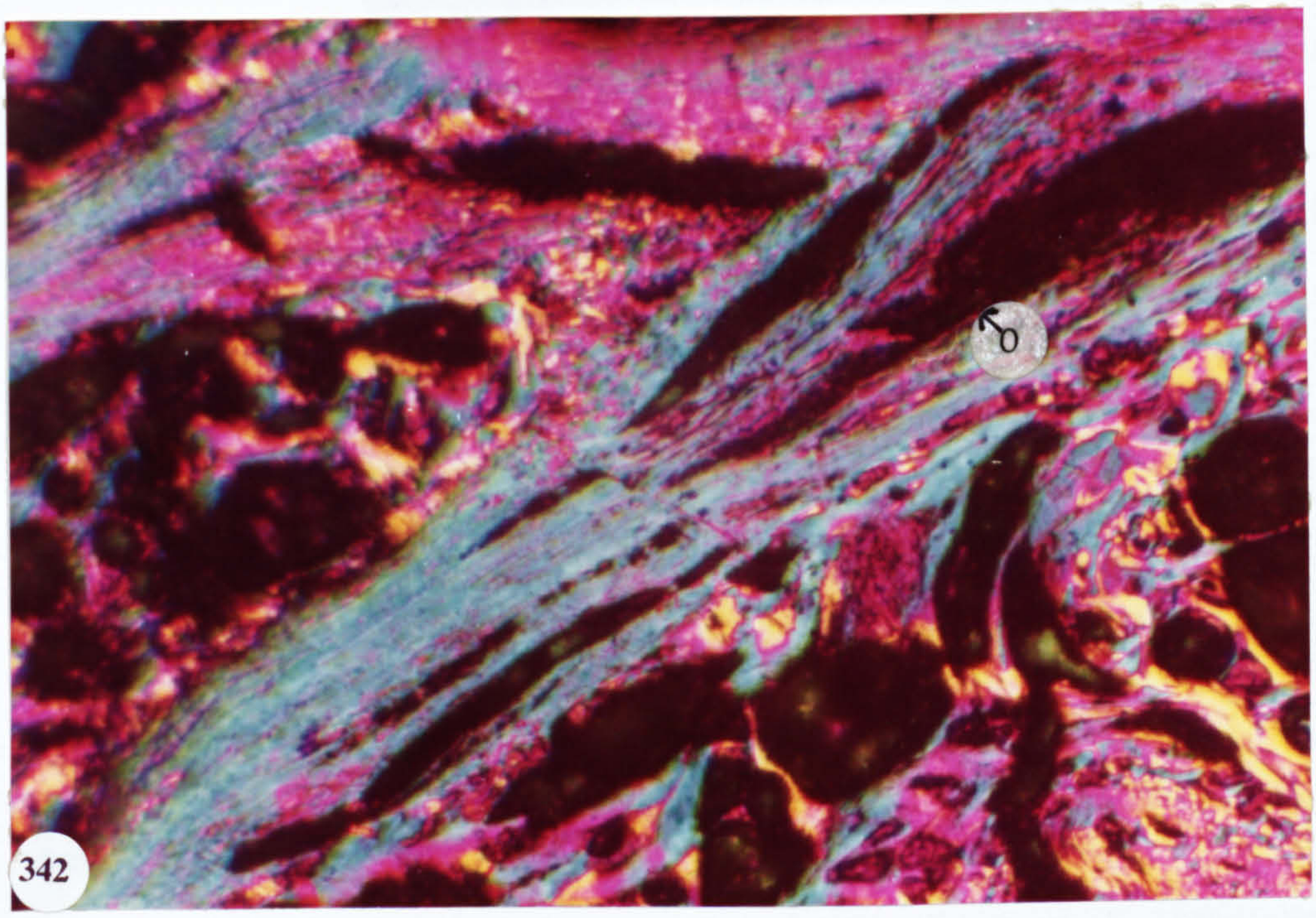




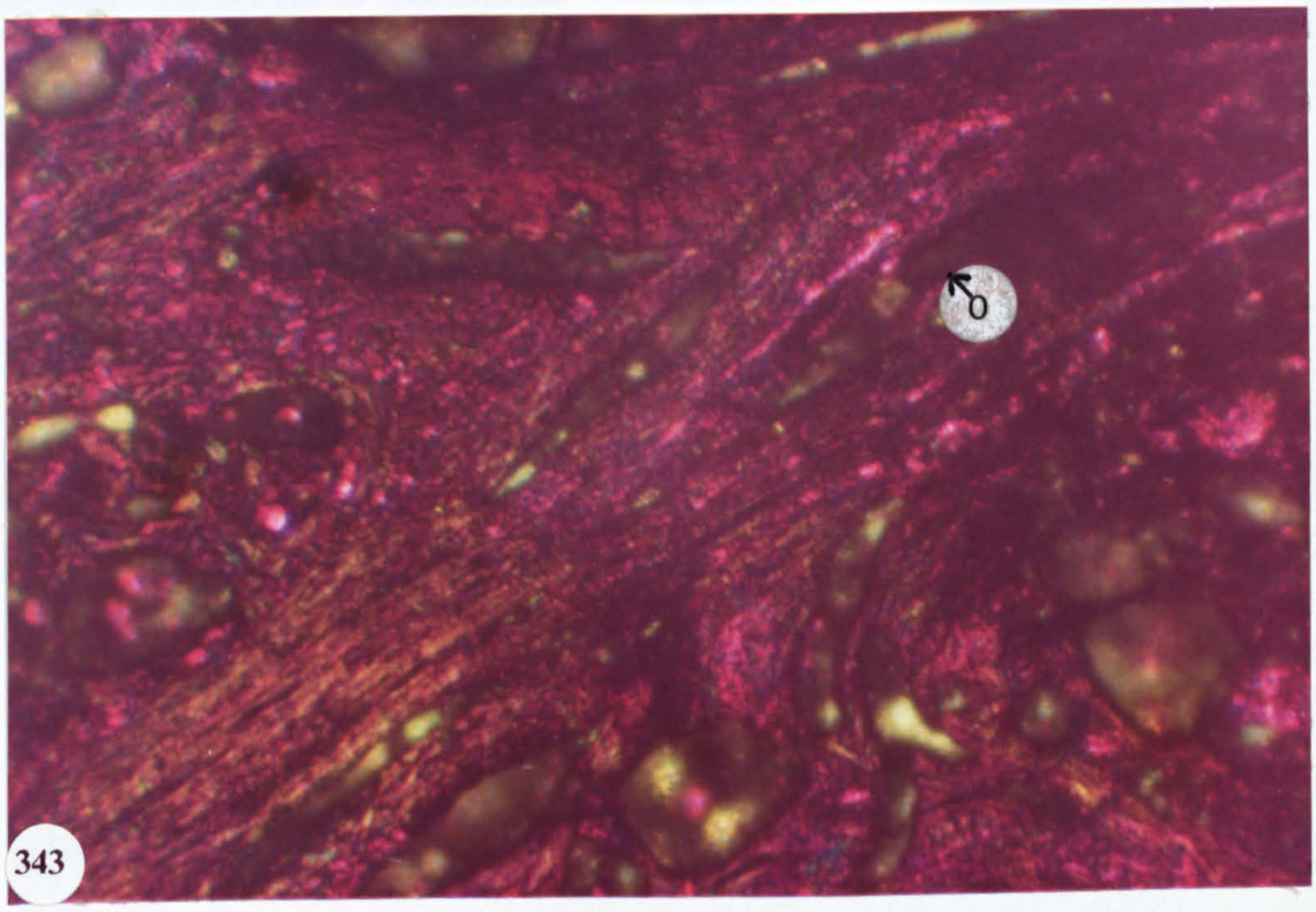




Figures 336 to 341. Scanning electron micrographs (stereoscan) of Lima Graphite (LG15) before (Figures 336 and 337) and after gasification in carbon dioxide at 1173 K (Figures 338 and 339) and 1223 K (Figures 340 and 341) for 16 hours each. Weight losses 3.65% and 9.29%.

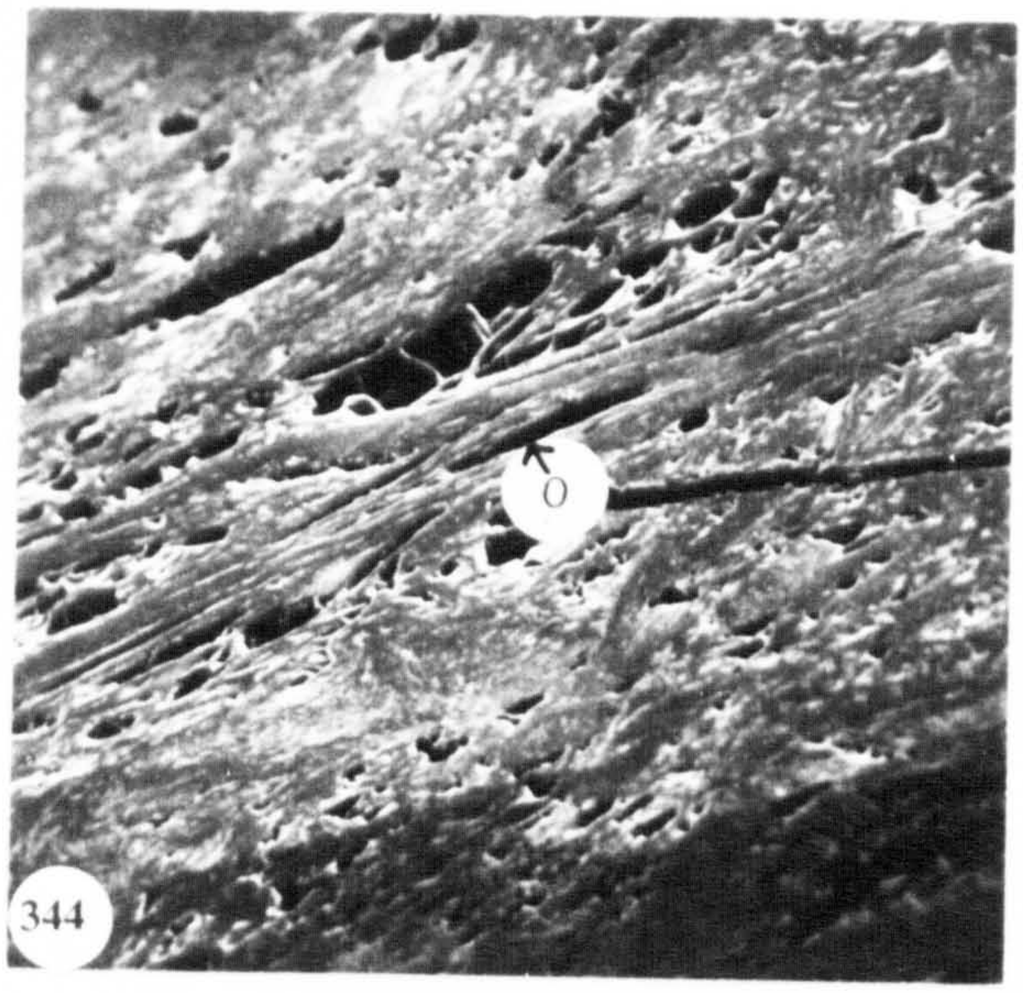


LIMA GRAPHITE

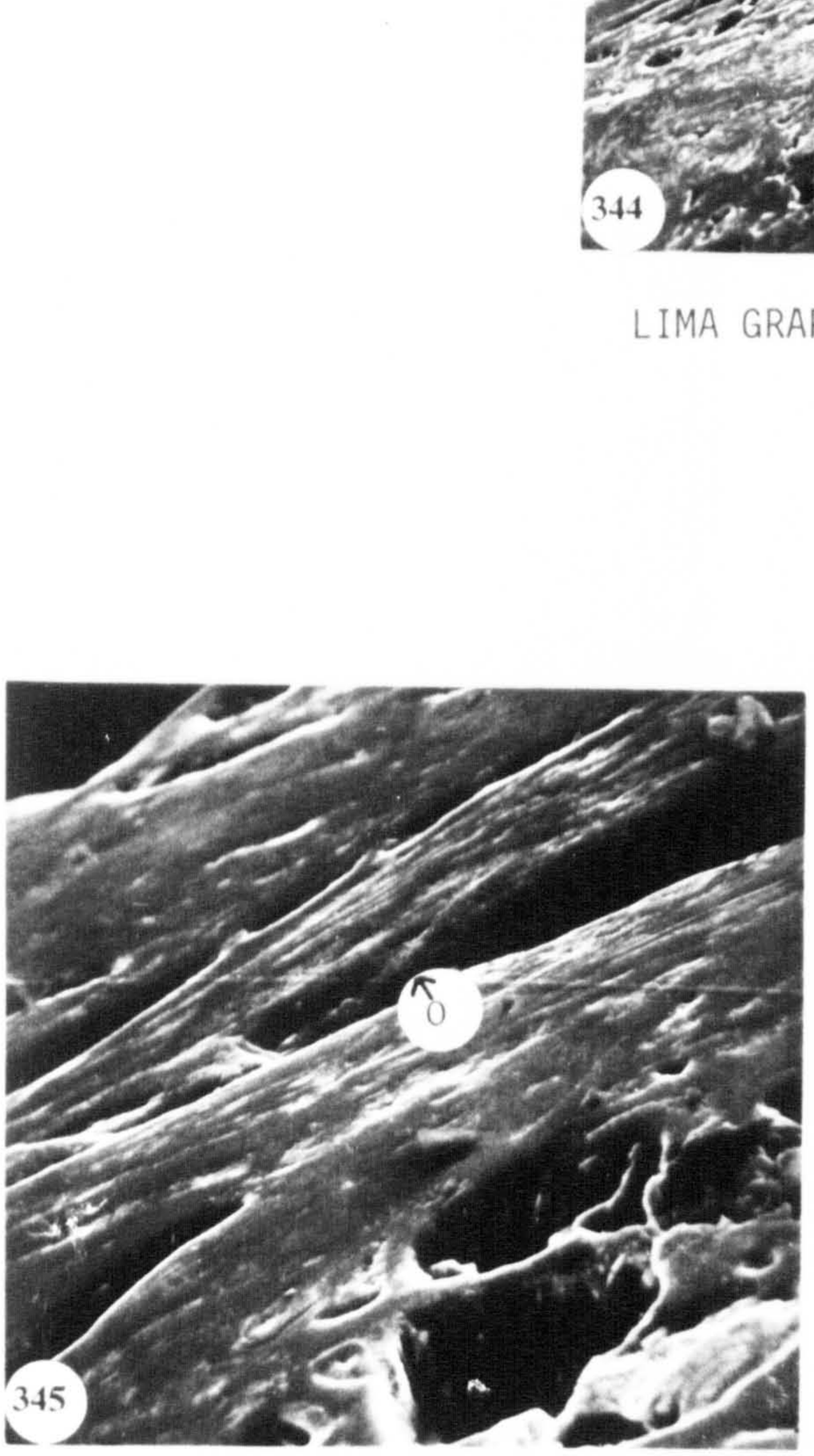


LIMA GRAPHITE

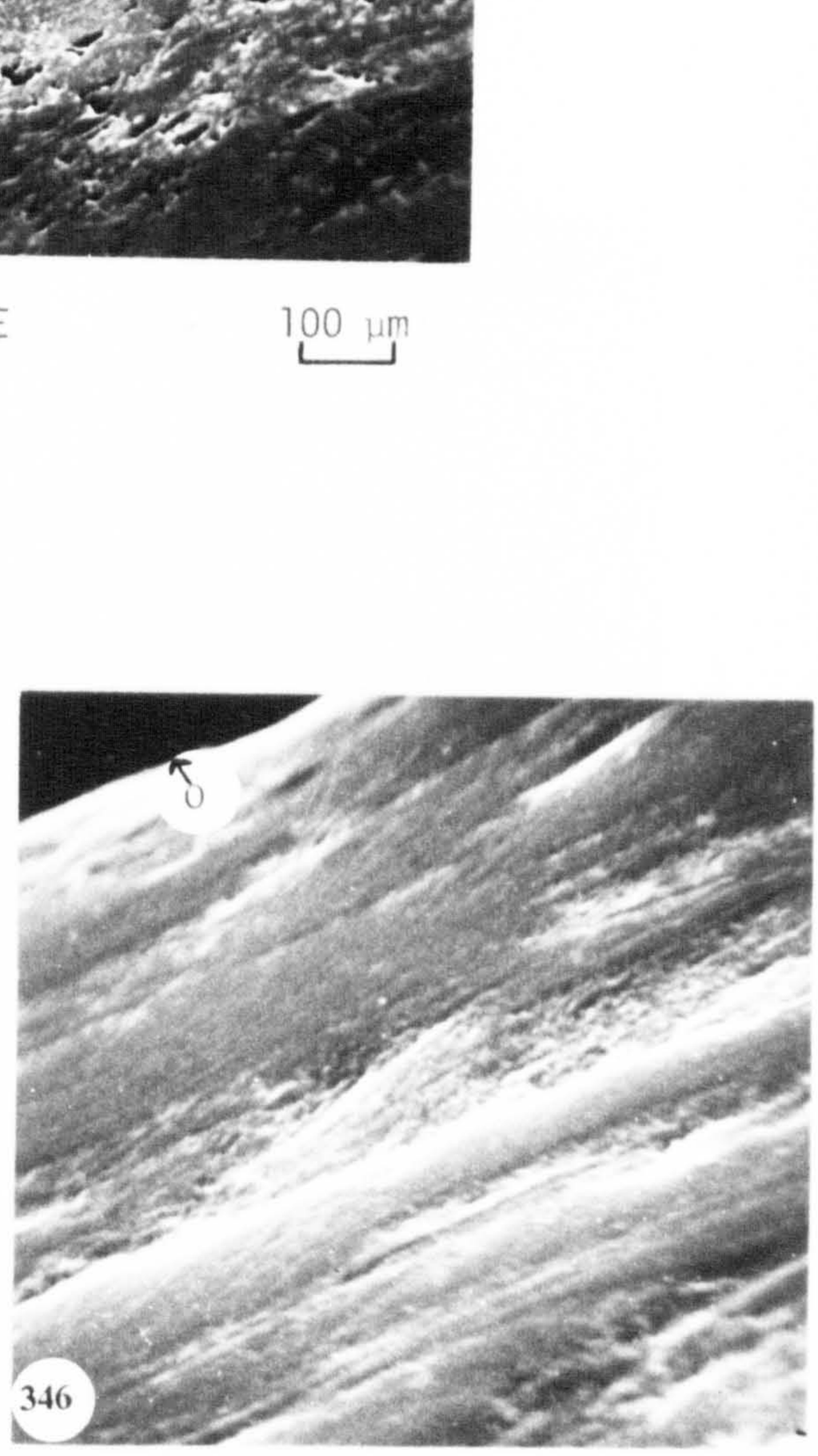
Figures 342 and 343. Optical micrographs of Lima Graphite (LG16) before and after gasification in carbon dioxide at 1198 K for 16 hours.
Weight loss 5.31%.



LIMA GRAPHITE 100 µm

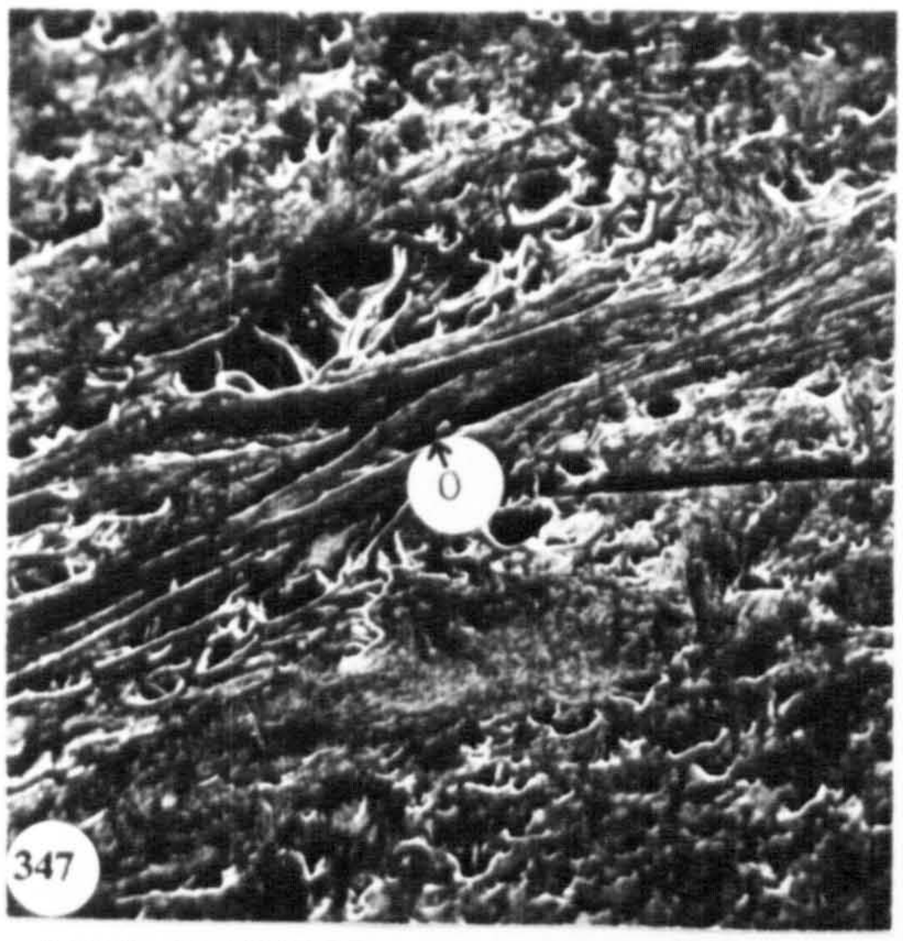


LIMA GRAPHITE 20 µm

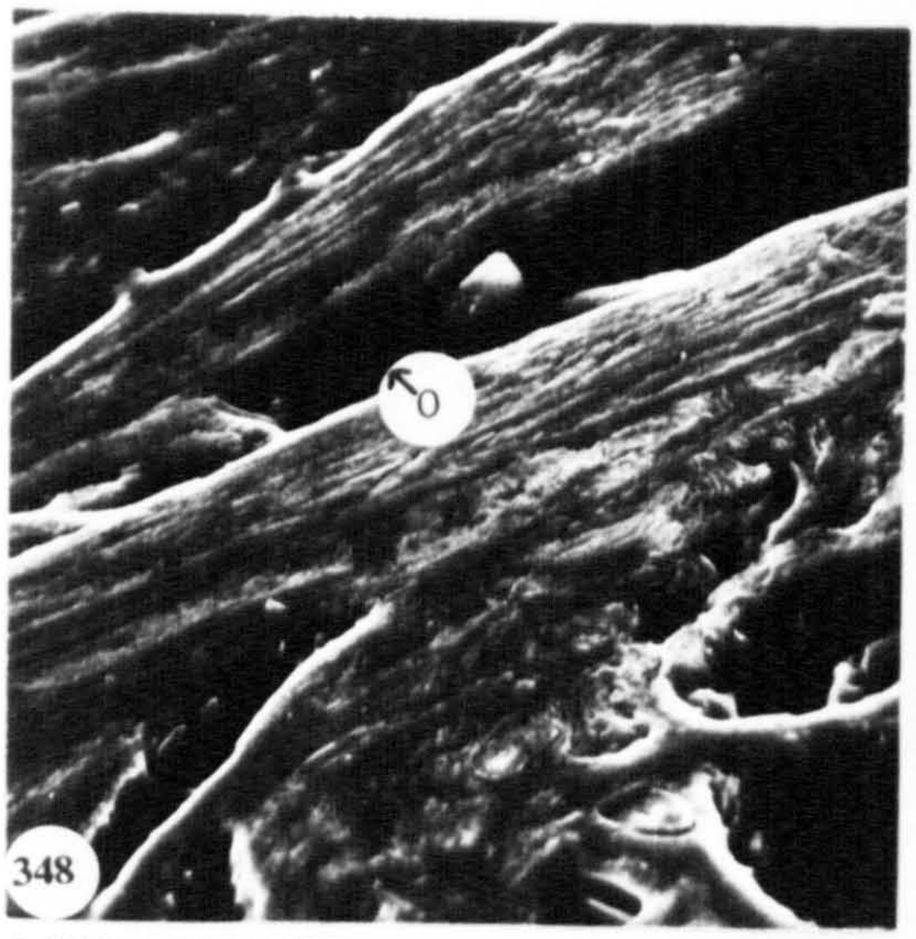


LIMA GRAPHITE 2 µm

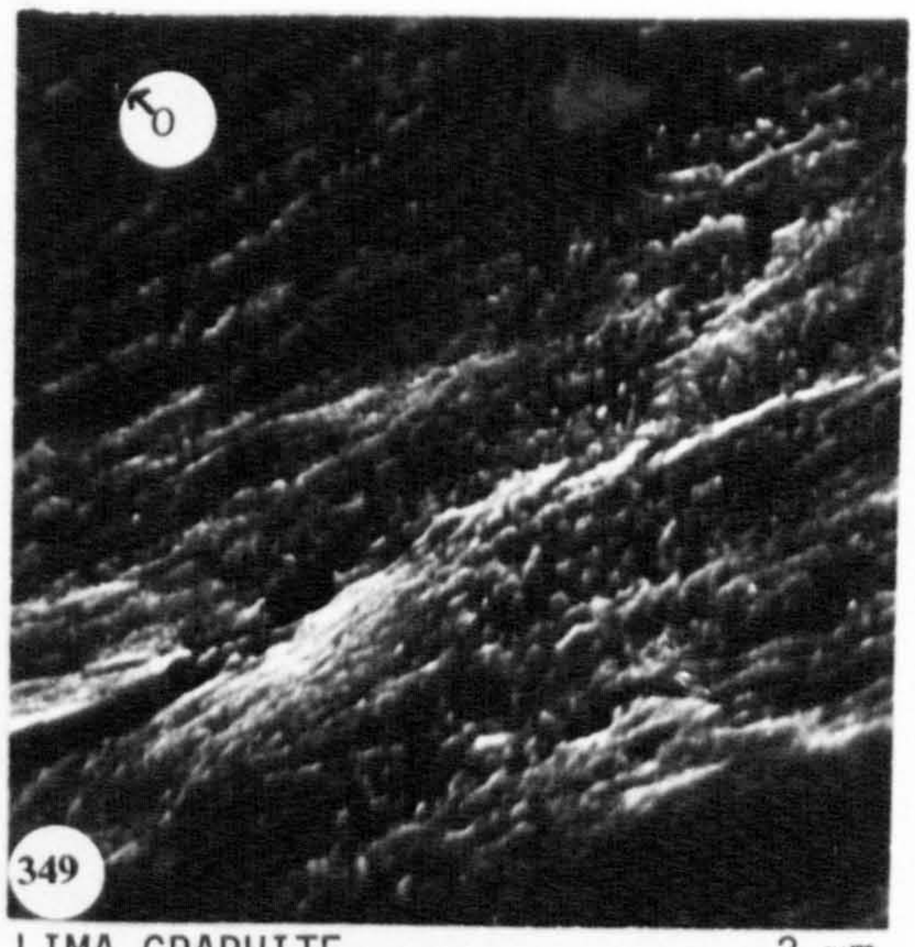
Figures 344 to 346. Scanning electron micrographs (stereoscan) of Lima Graphite (LG16) before gasification.



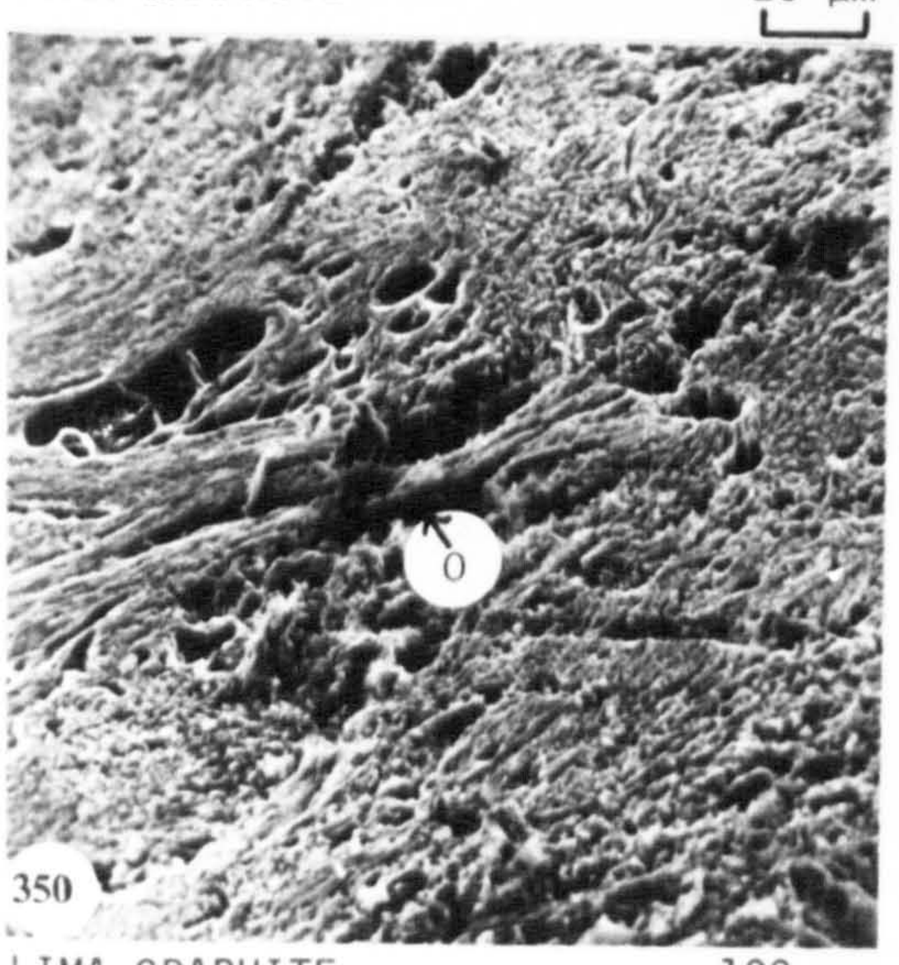
LIMA GRAPHITE 100 µm



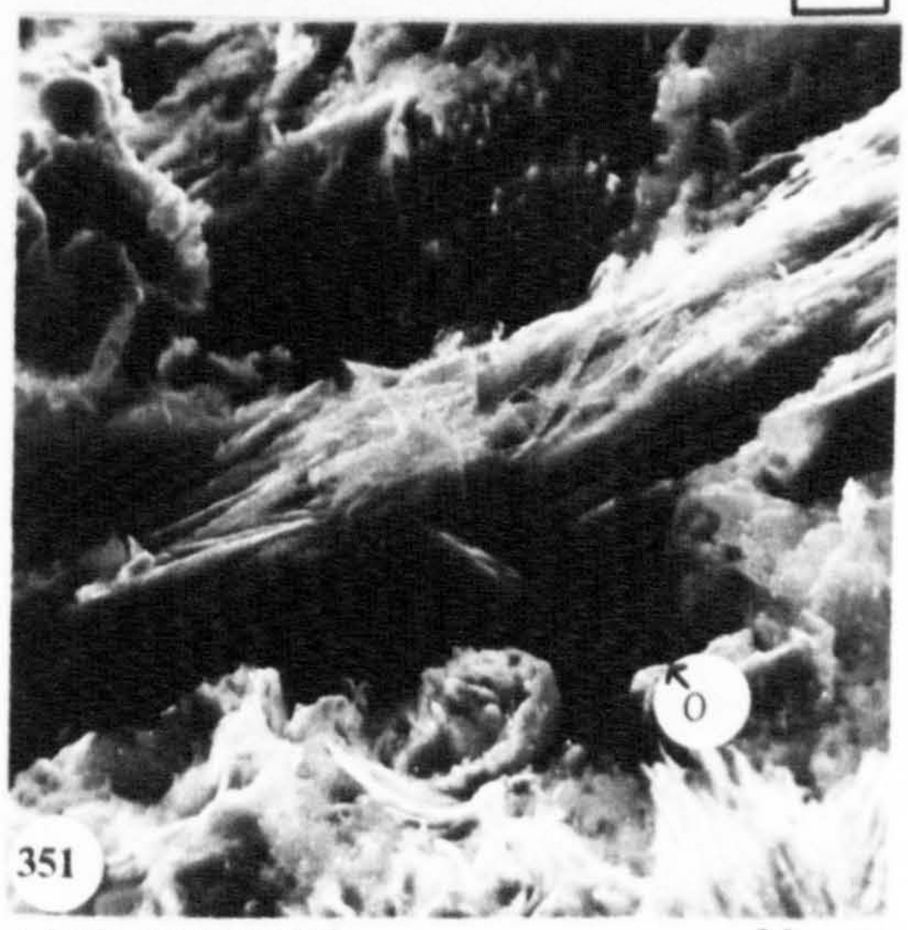
LIMA GRAPHITE 20 µm



LIMA GRAPHITE 2 µm

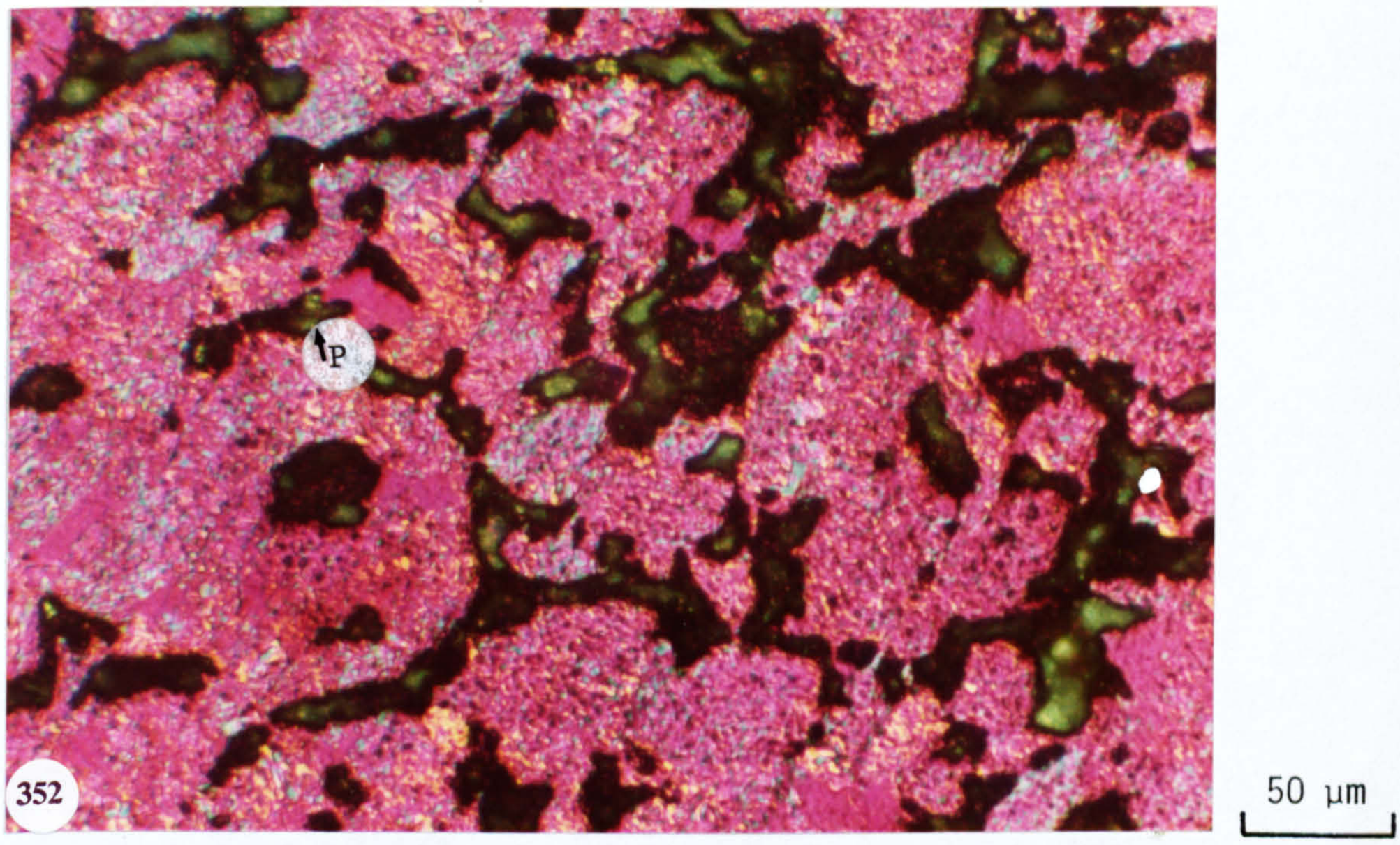


LIMA GRAPHITE 100 µm

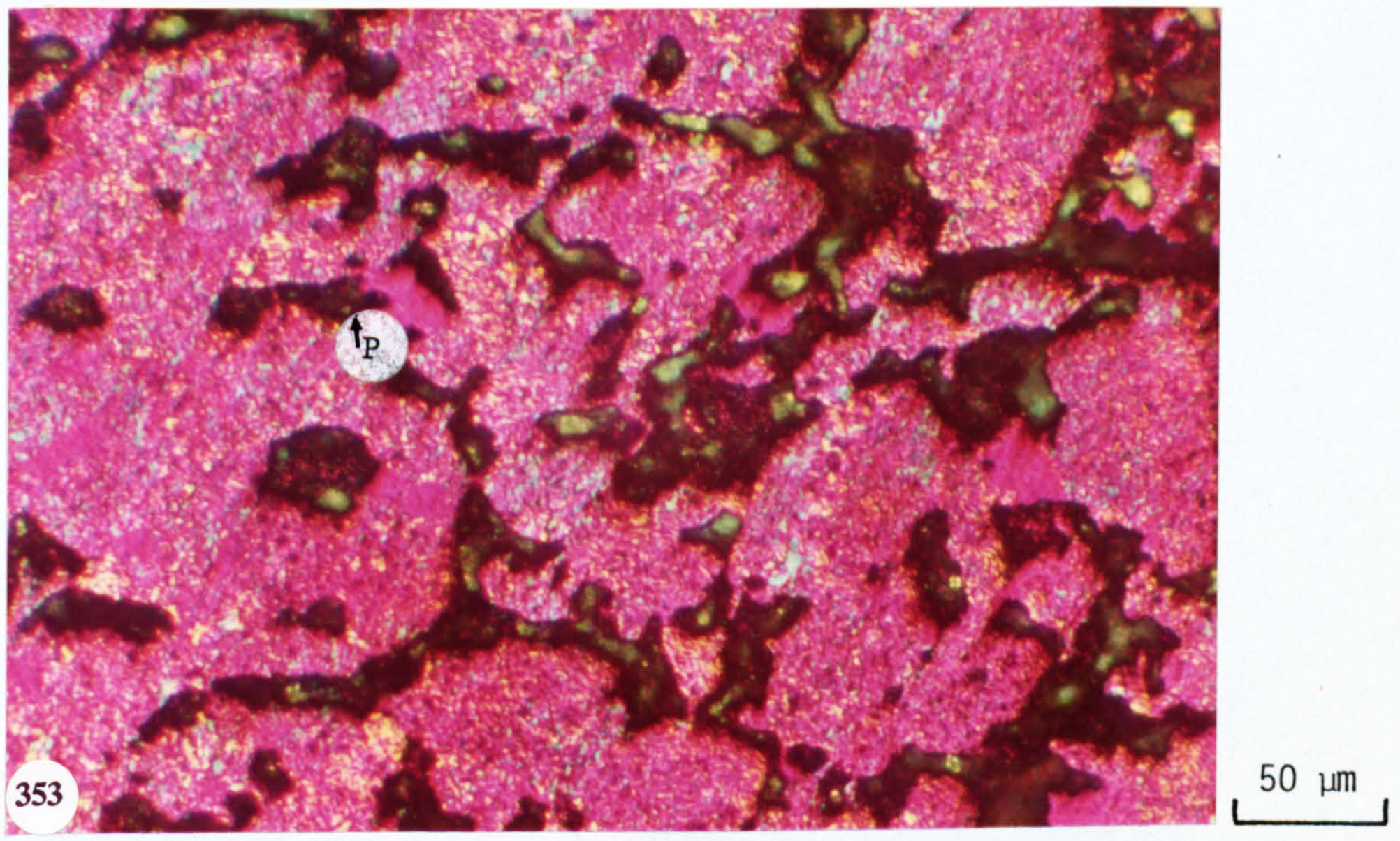


LIMA GRAPHITE 20 µm

Figures 347 to 351. Scanning electron micrographs (stereoscan) of Lima Graphite (LG16) after gasification in carbon dioxide at 1198 K (Figures 347 to 349) and 1273 K (Figures 350 to 351) for 16 hours each. Weight losses 5.31% and 37.65%.

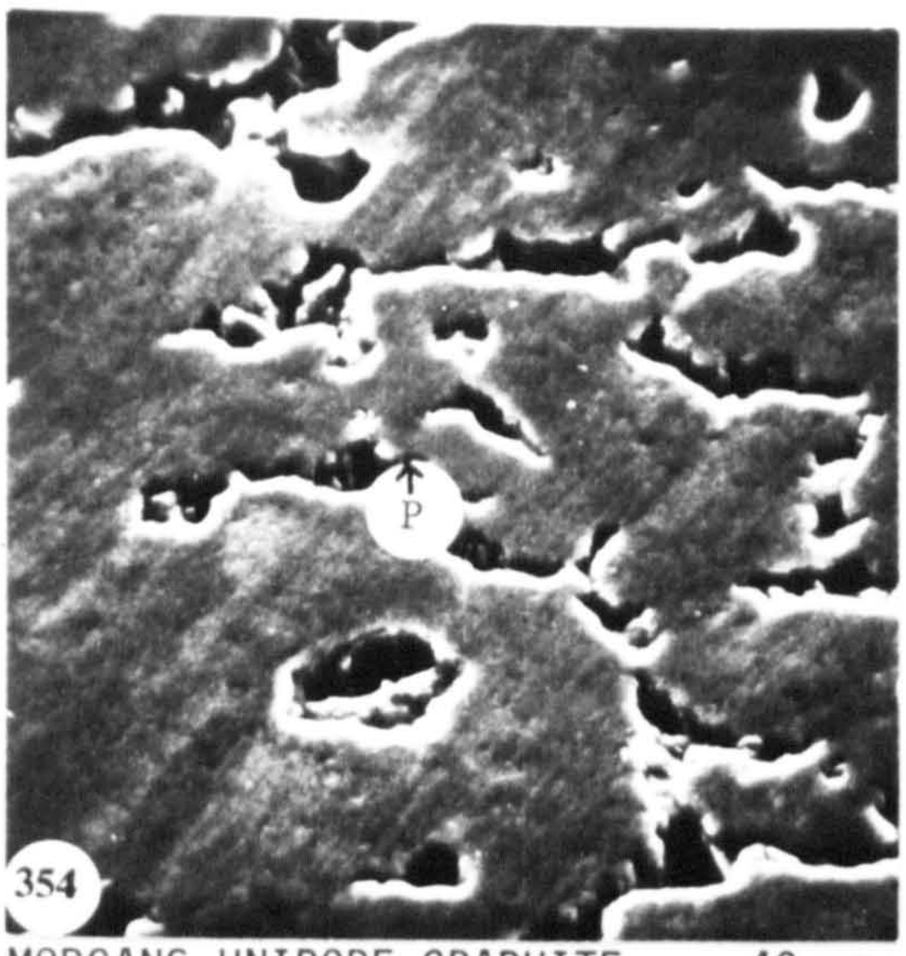


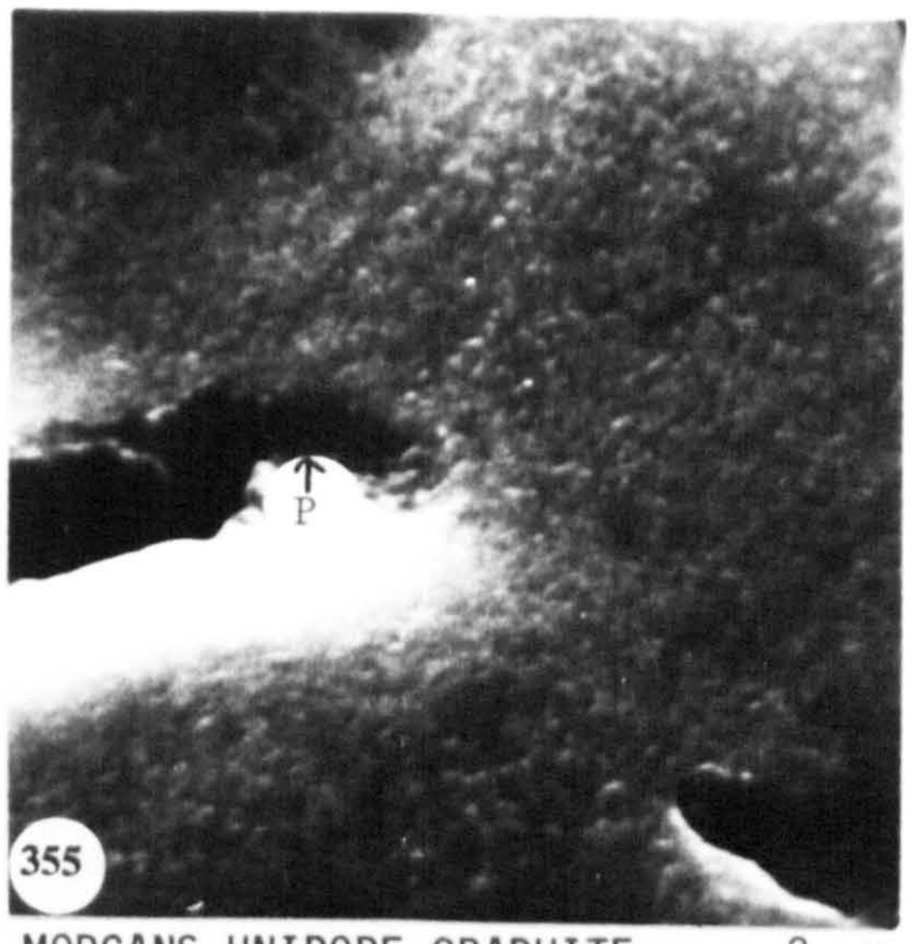
MORGANS UNIPORE GRAPHITE

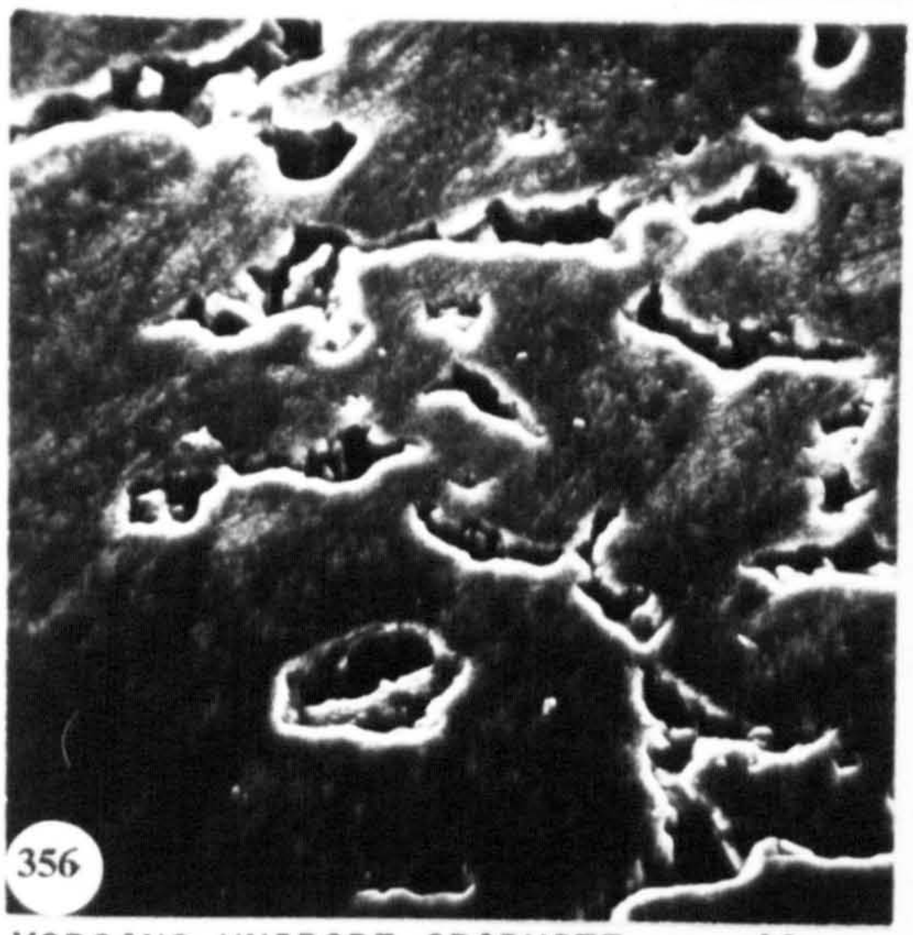


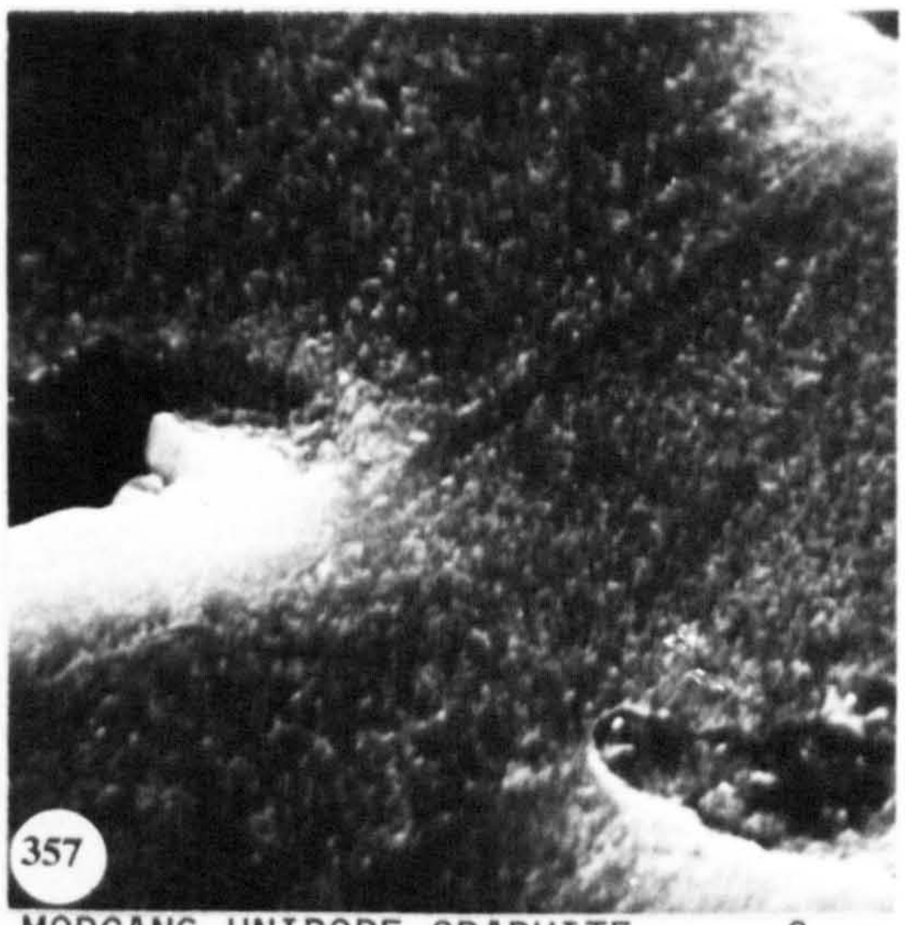
MORGANS UNIPORE GRAPHITE

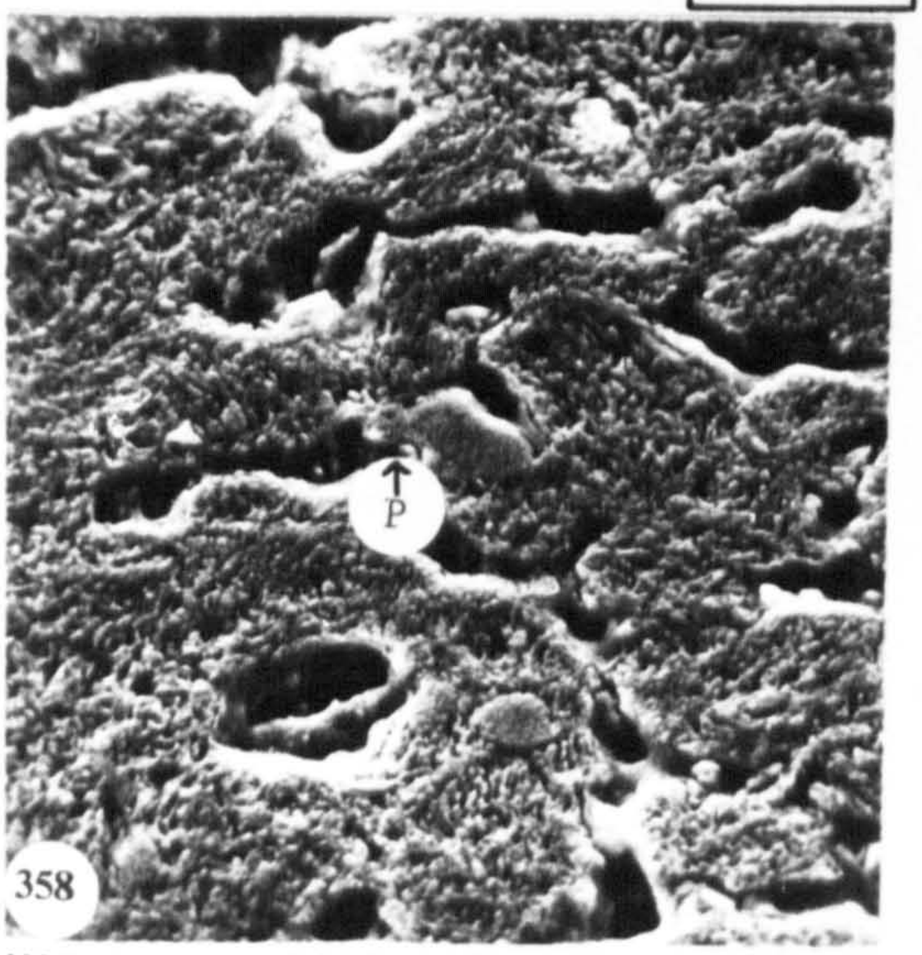
Figures 352 and 353. Optical micrographs of Morgans Unipore Graphite (MG9) before and after gasification in carbon dioxide at 1198 K for 16 hours. Weight loss 1.40%.

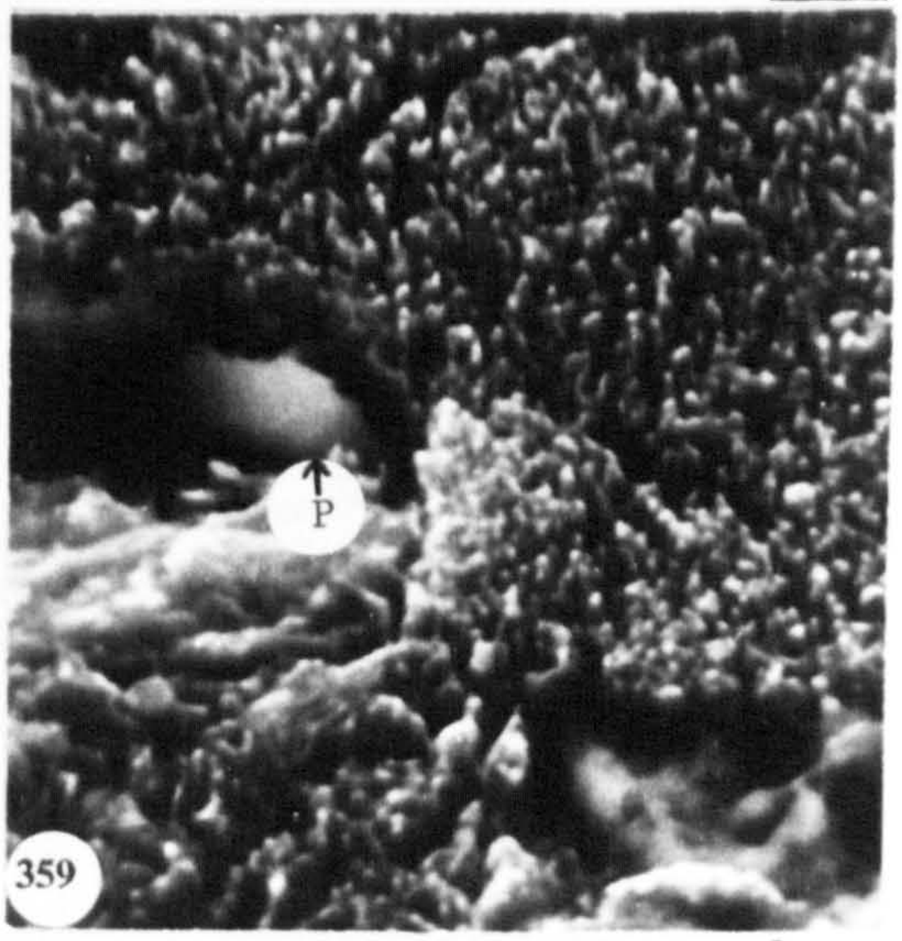




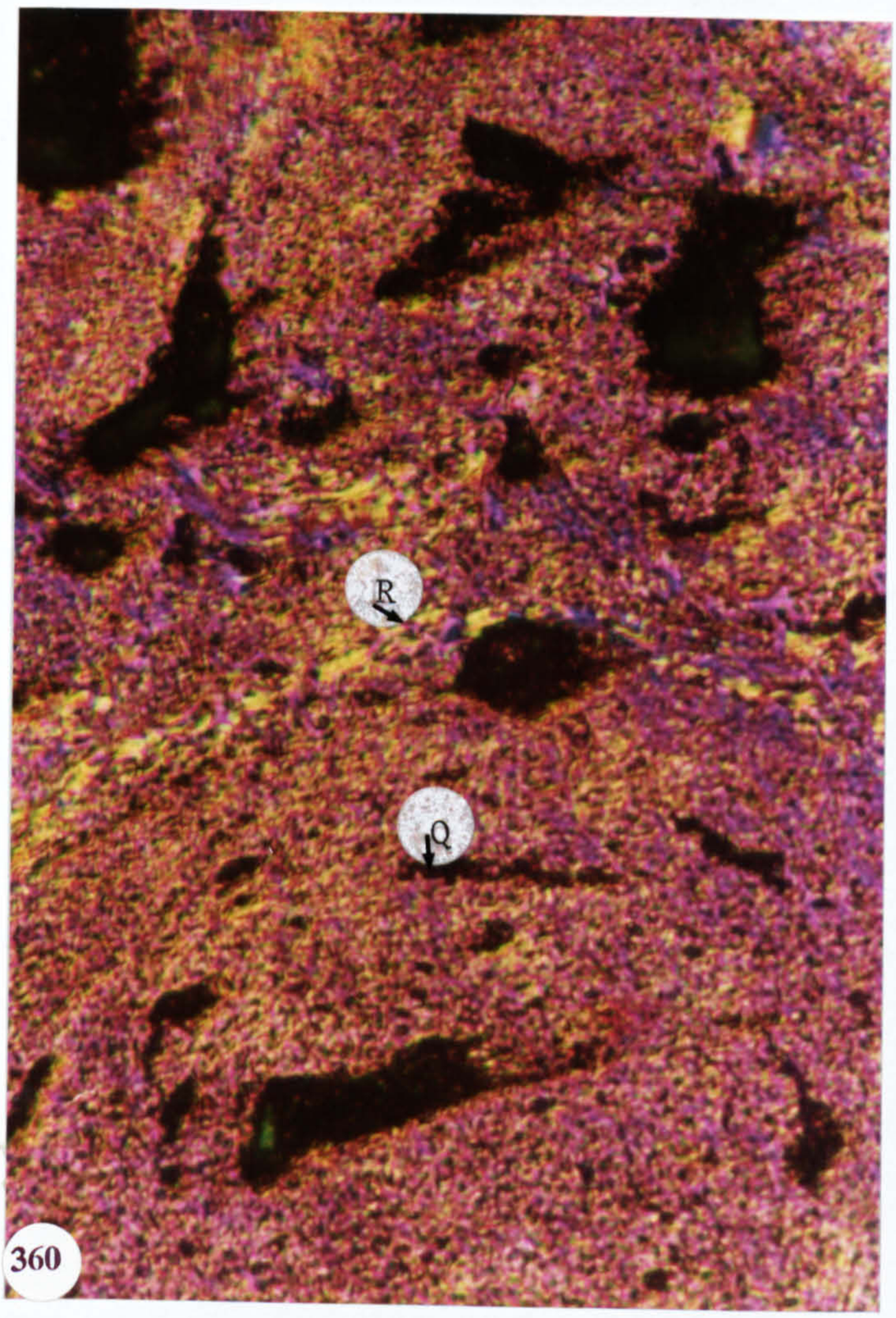




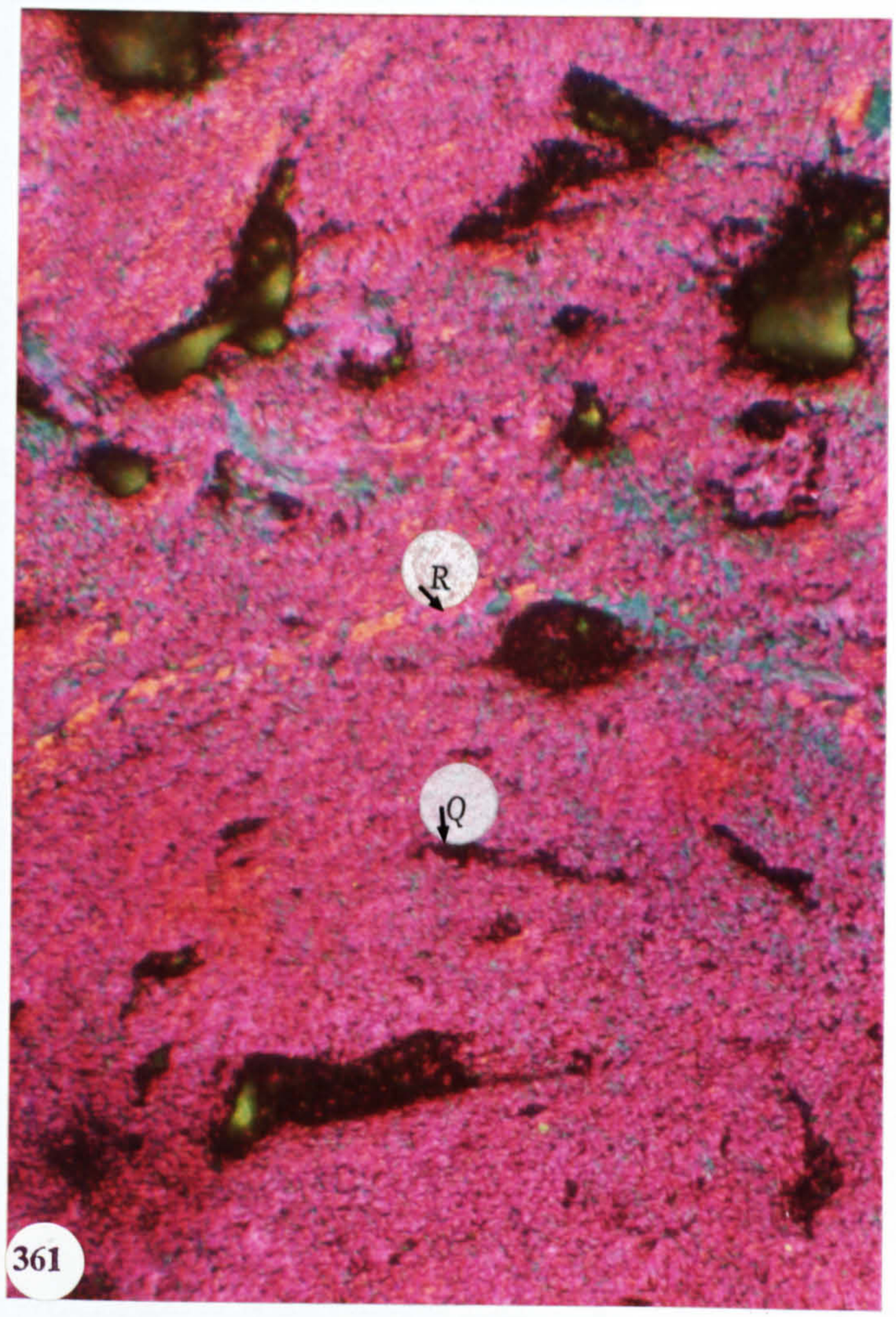




Figures 354 to 359. Scanning electron micrographs (stereoscan) of Morgans Unipore Graphite (MG9) before (Figures 354 and 355) and after gasification in carbon dioxide at 1198 K (Figures 356 and 357) and 1273 K (Figures 358 and 358) for 16 hours each. Weight losses 1.40% and 16.19%.

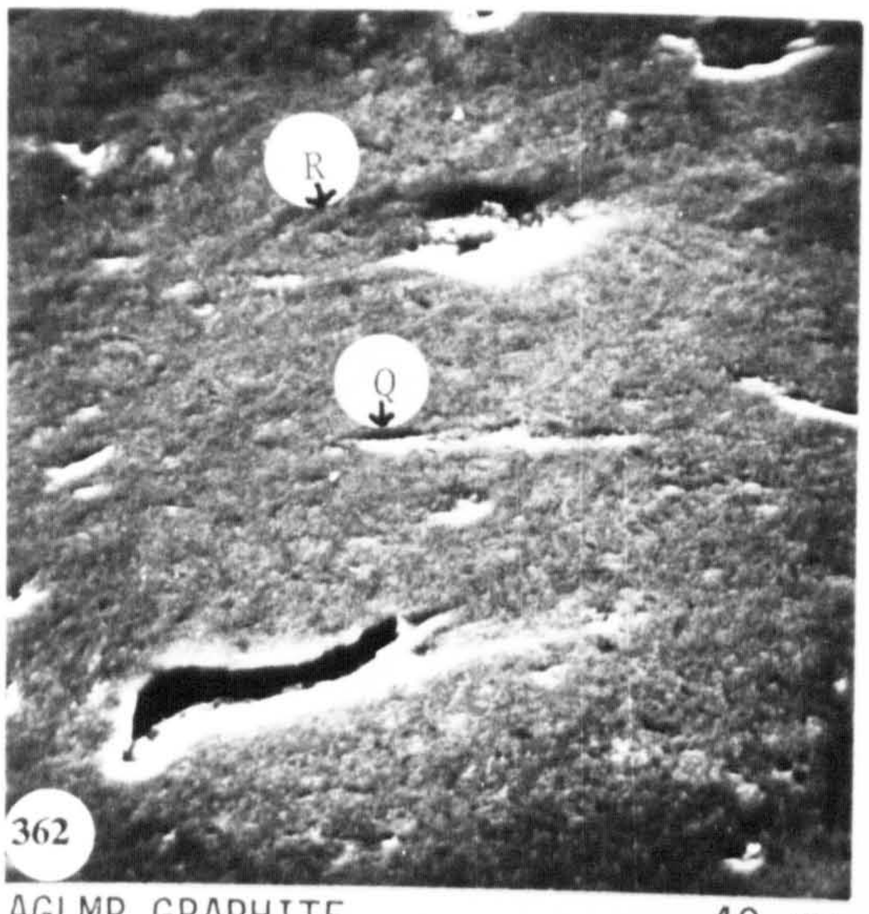


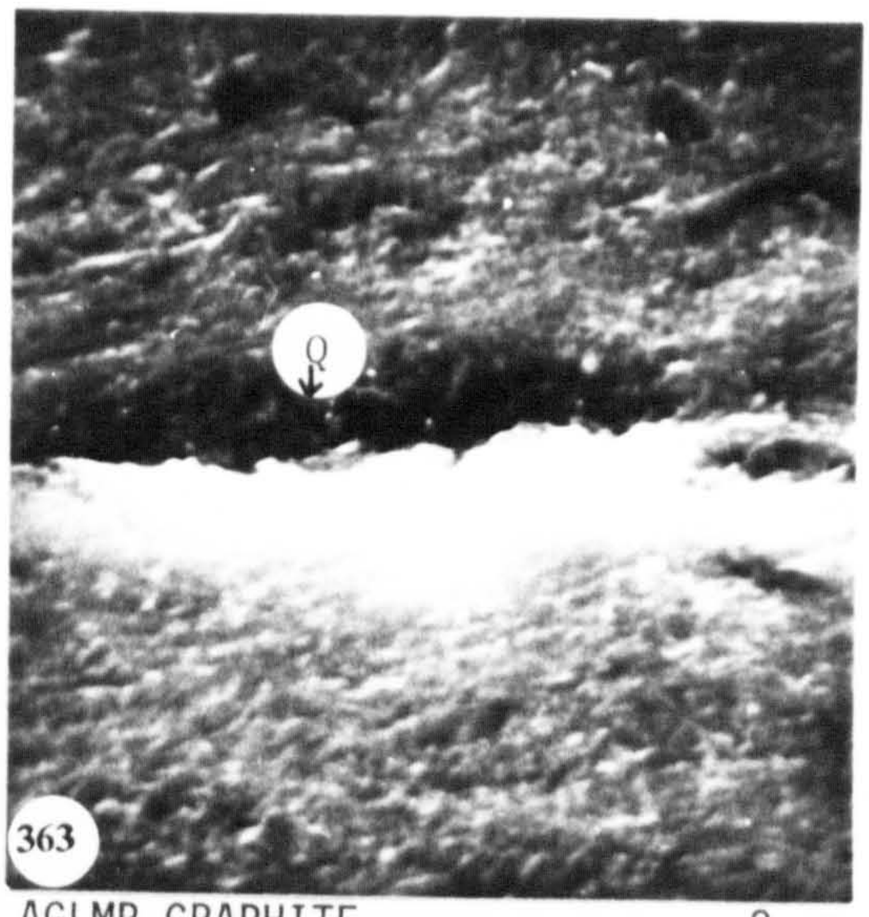
AGLMP GRAPHITE 50 μm

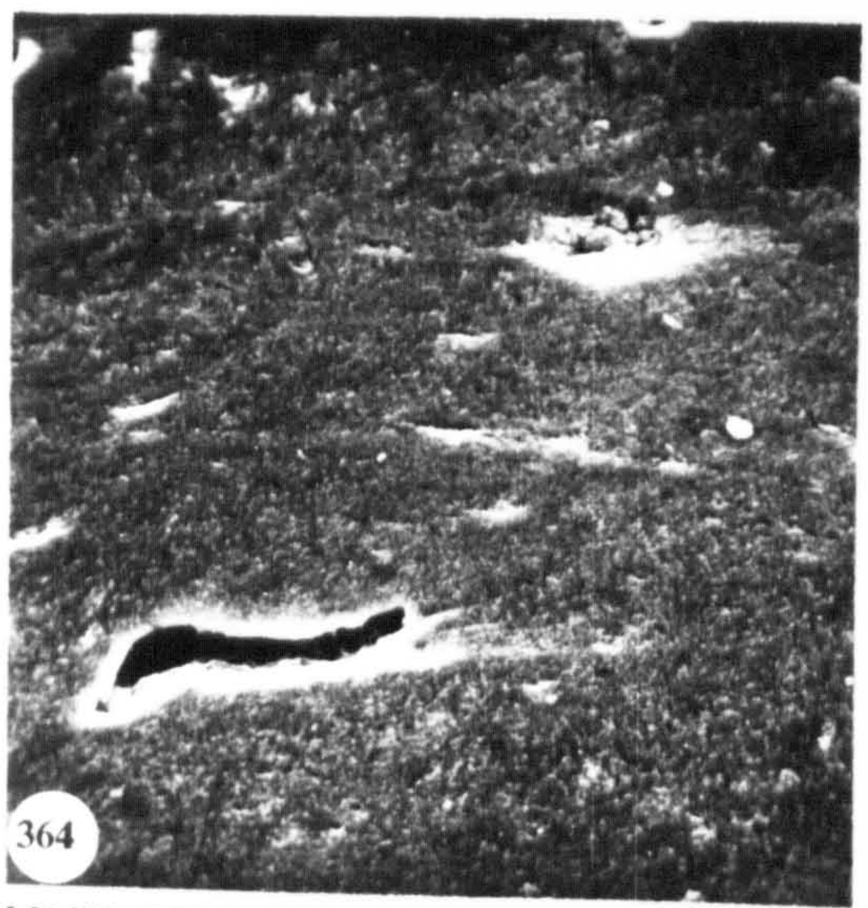


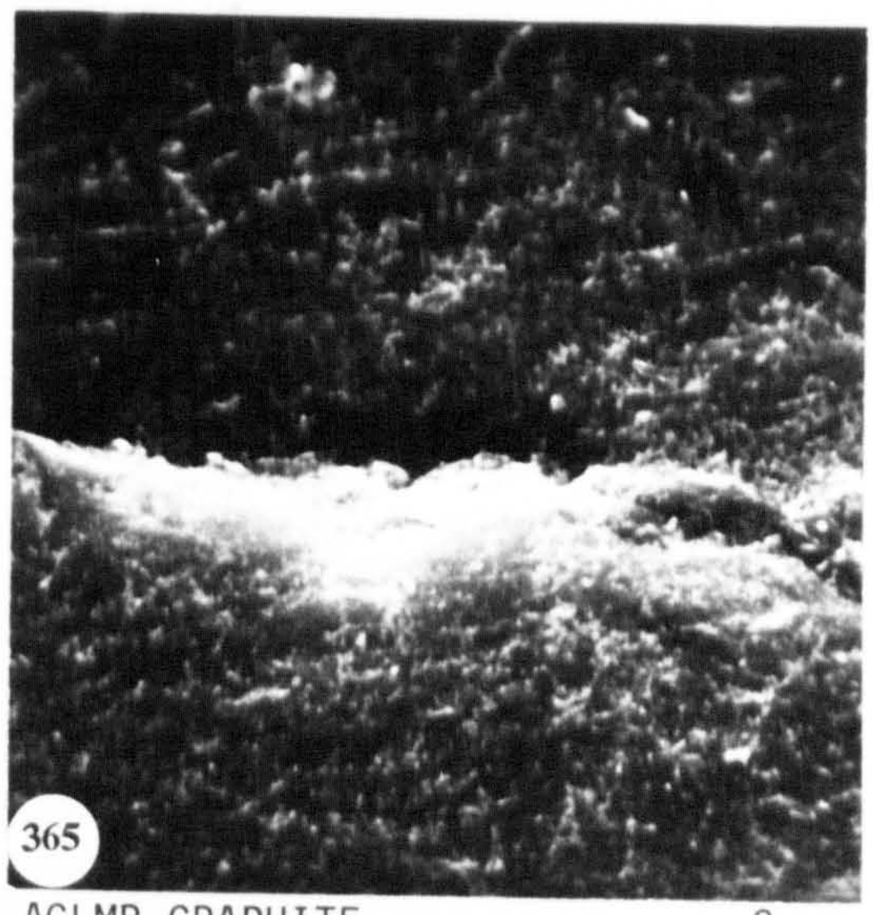
AGLMP GRAPHITE 50 μm

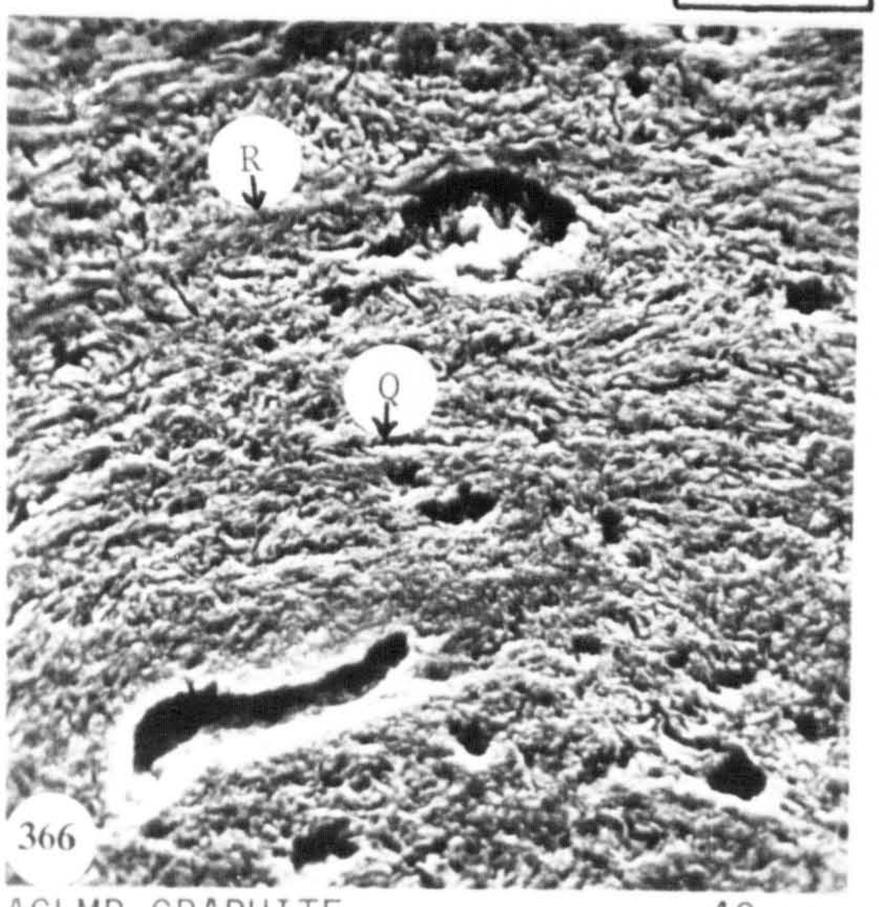
Figures 360 and 361. Optical micrographs of AGLMP Graphite (AG8) before and after gasification in carbon dioxide at 1198 K for 16 hours. Weight loss 1.07%.

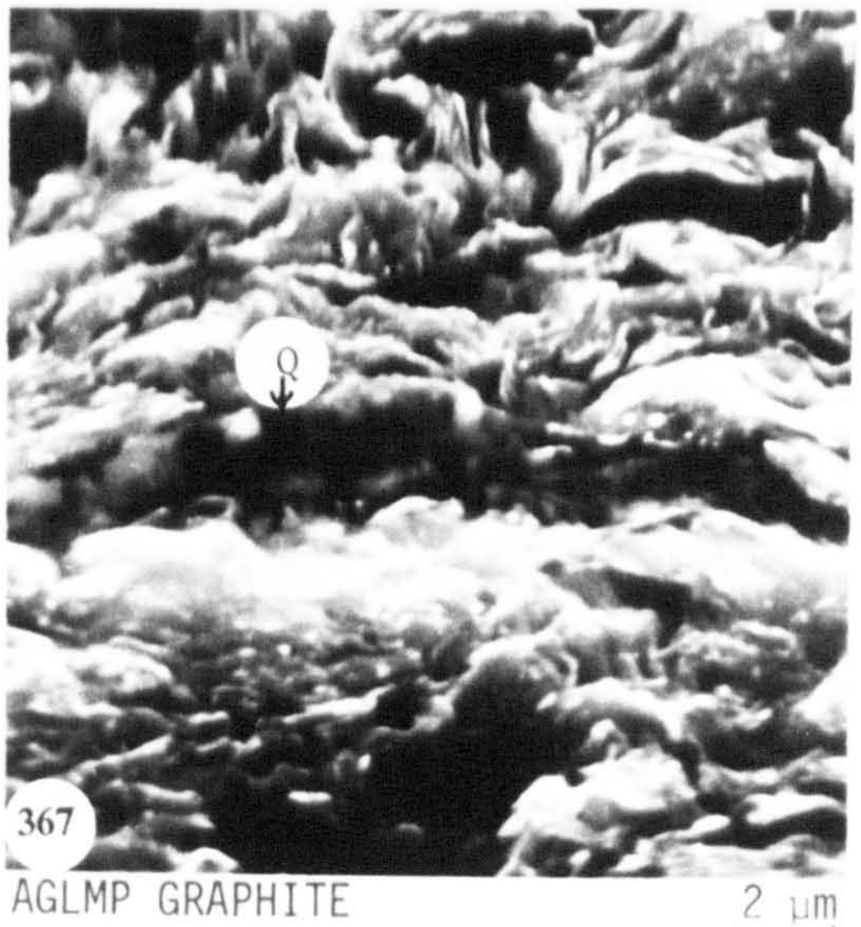




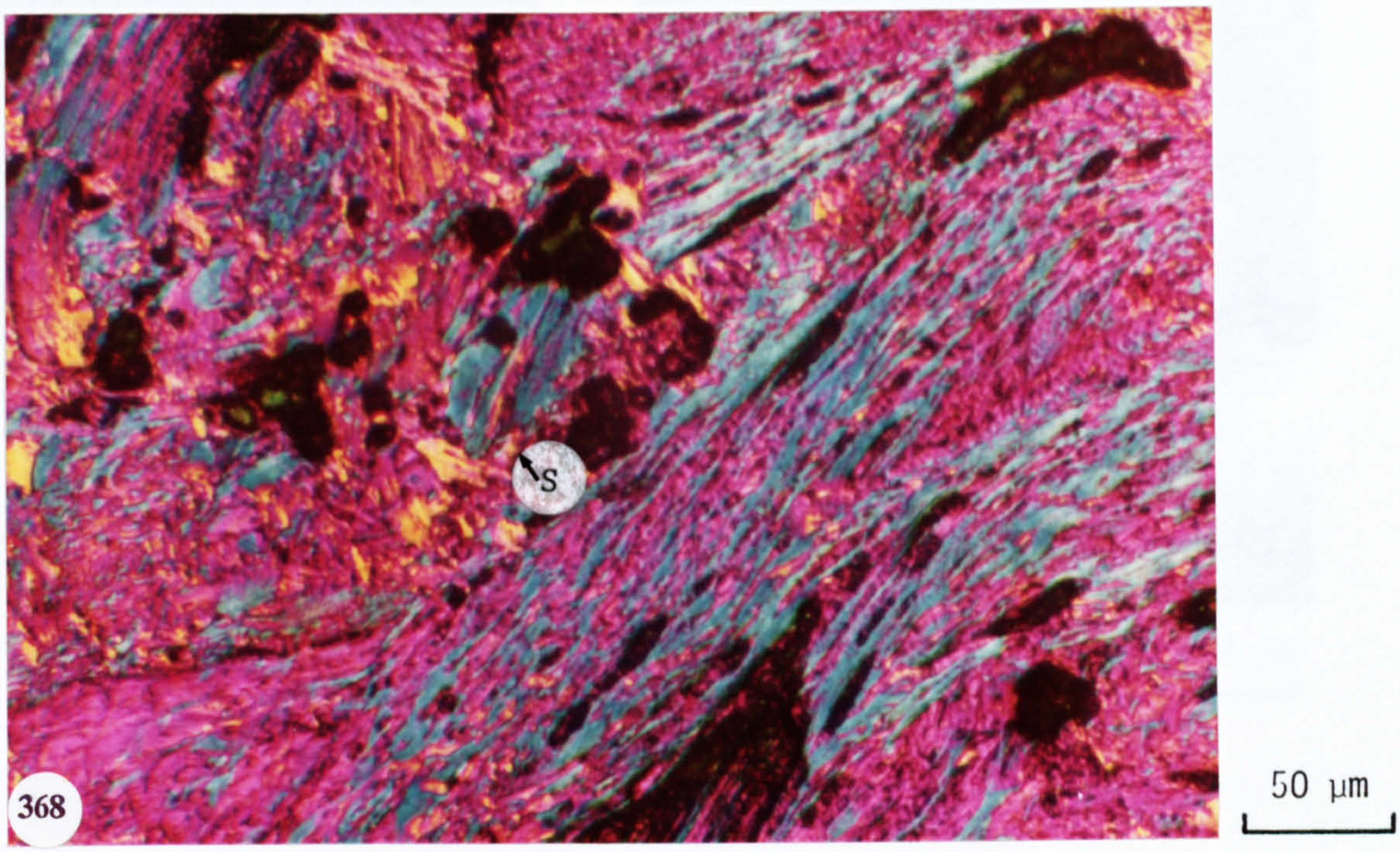




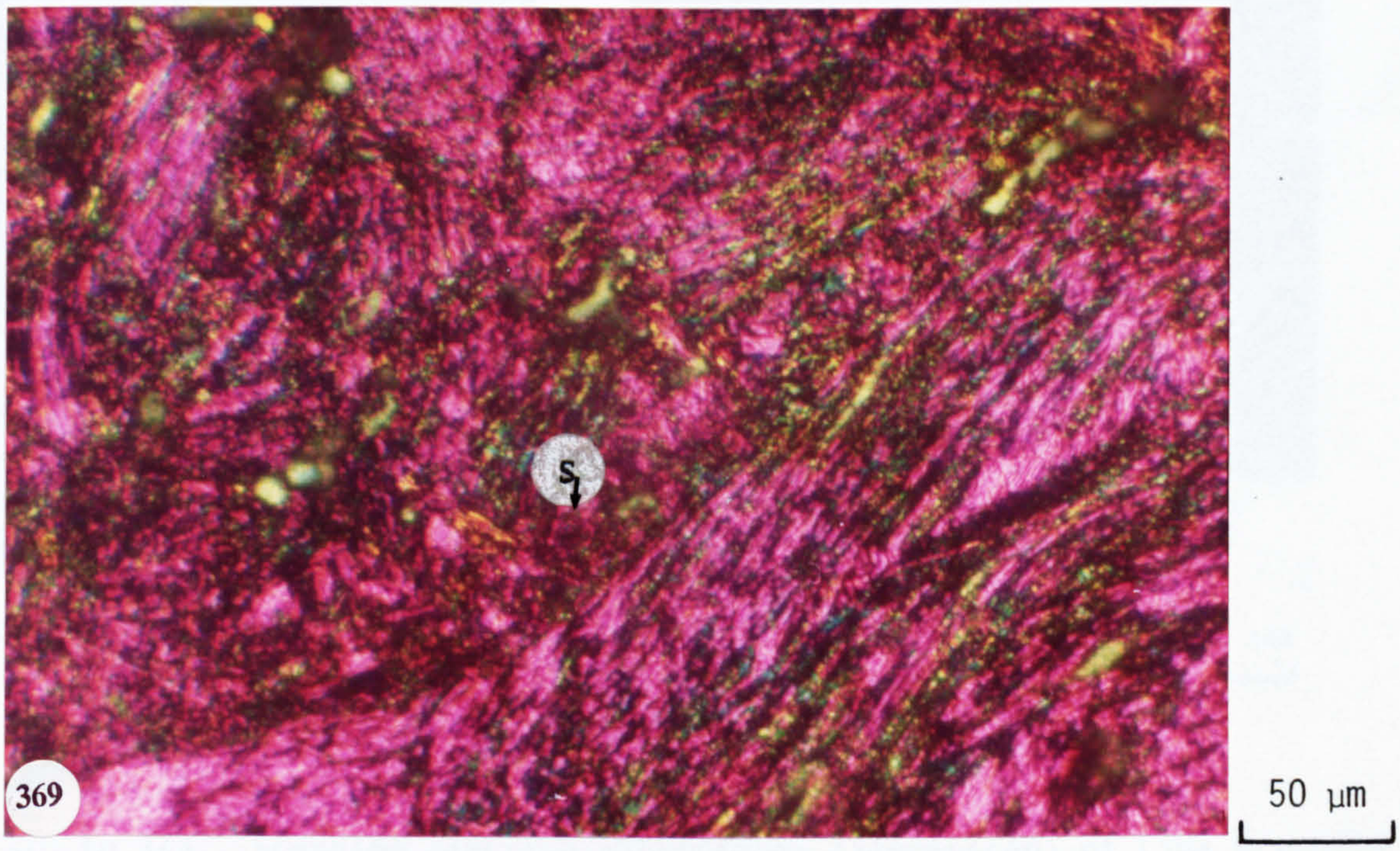




Figures 362 to 367. Scanning electron micrographs (stereoscan) of AGLMP Graphite (AG8) before (Figures 362 and 363) and after gasification in carbon dioxide at 1198 K (Figures 364 and 365) and 1273 K (Figures 366 and 367) for 16 hours each. Weight losses 1.07% and 8.12%.

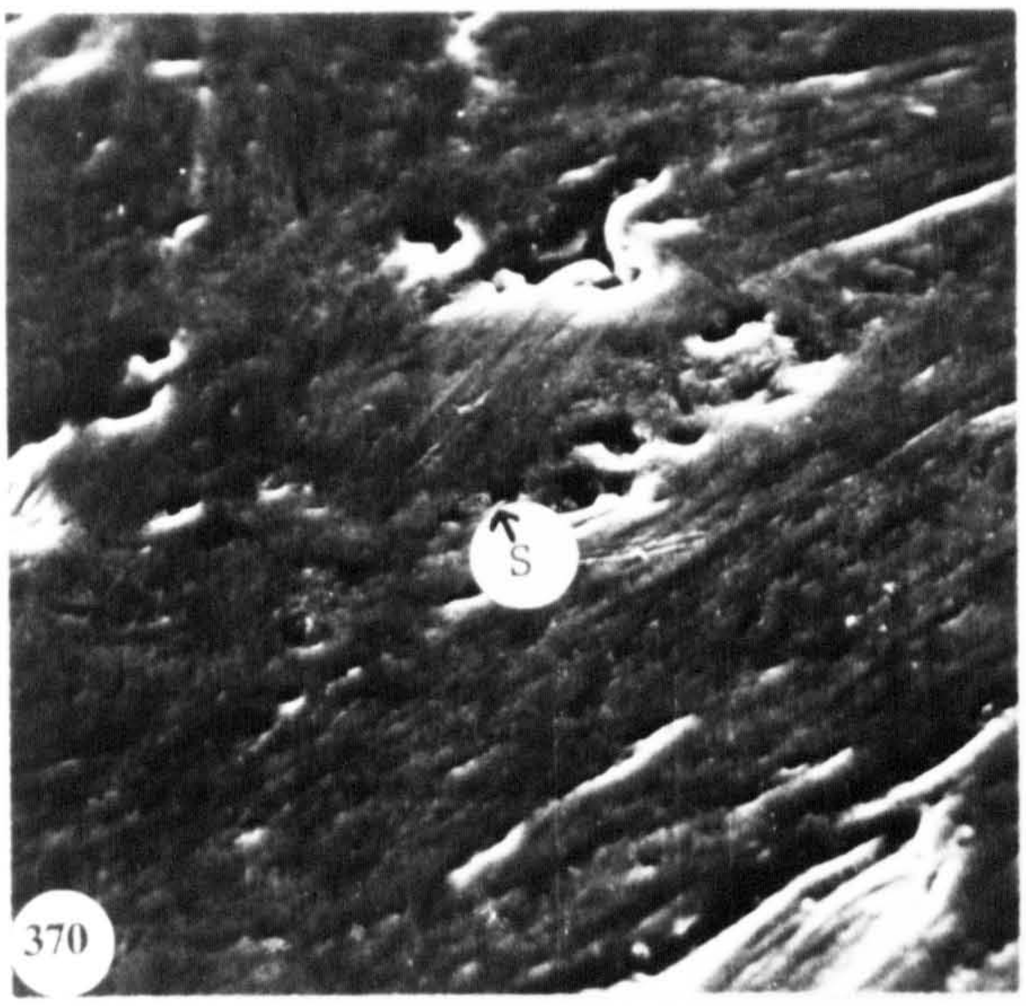


LIMA GRAPHITE



LIMA GRAPHITE

Figures 368 and 369. Optical micrographs of Lima Graphite (LG17) before and after gasification in carbon dioxide at 1243 K for 16 hours. Weight loss 5.99%.



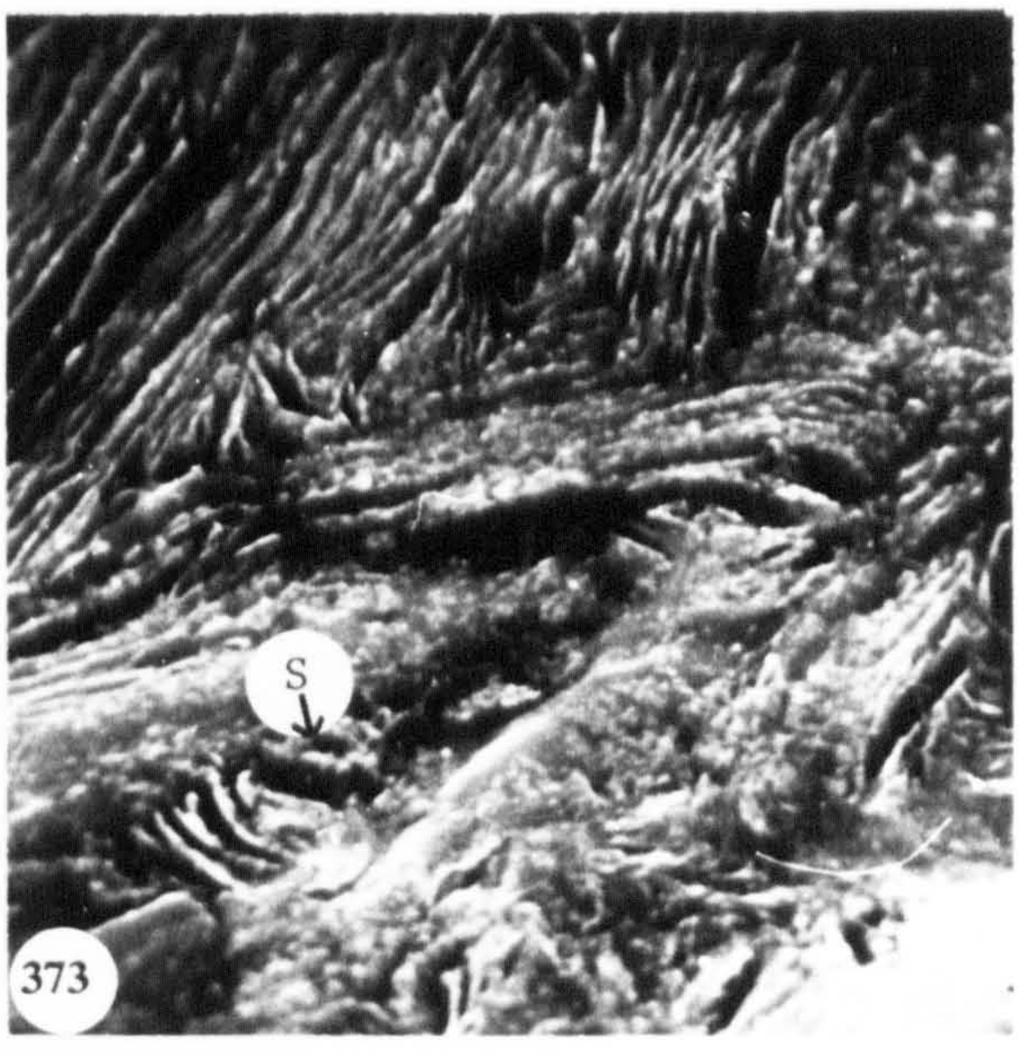
LIMA GRAPHITE 40 μm



LIMA GRAPHITE 2 μm

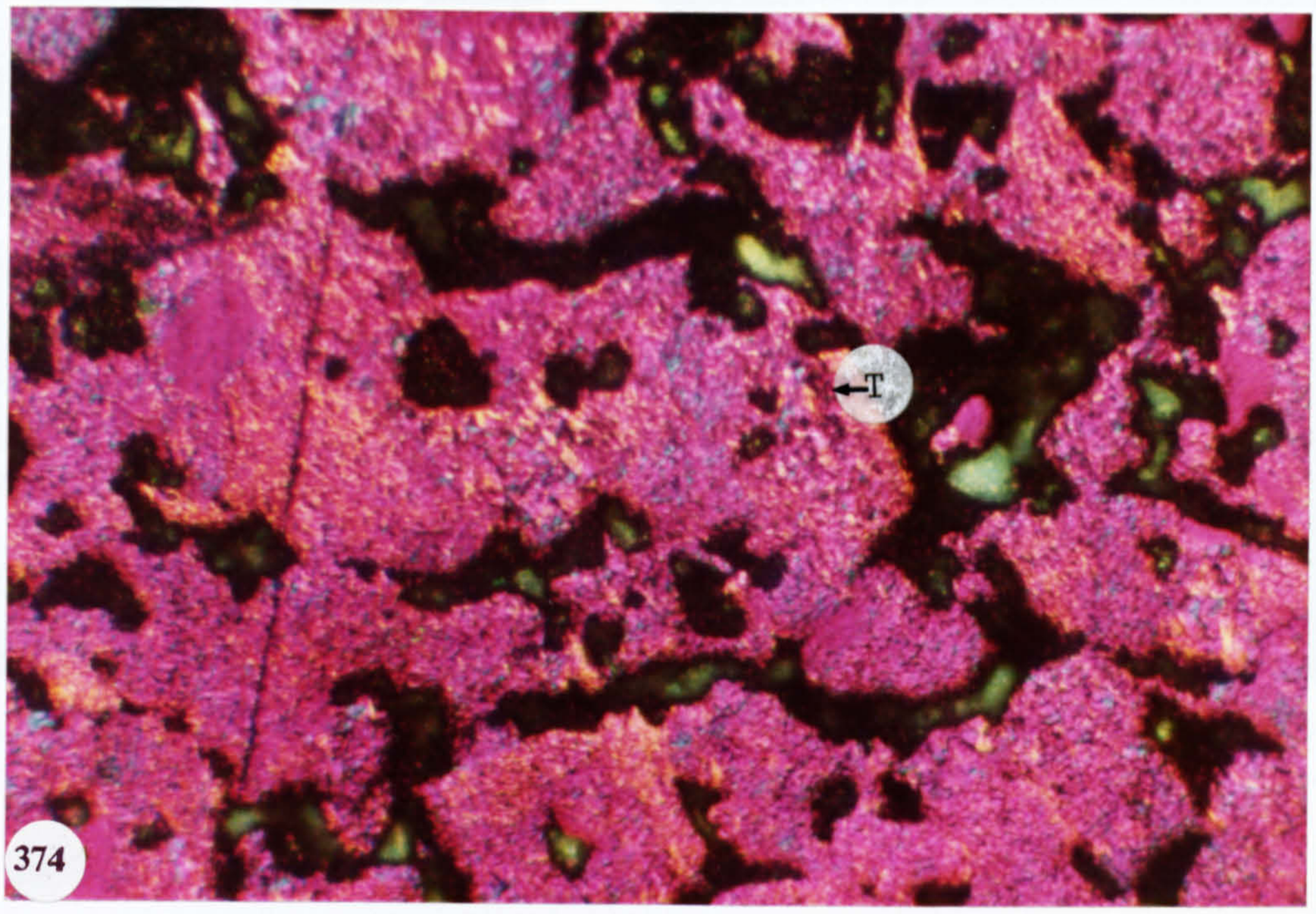


LIMA GRAPHITE 40 μm

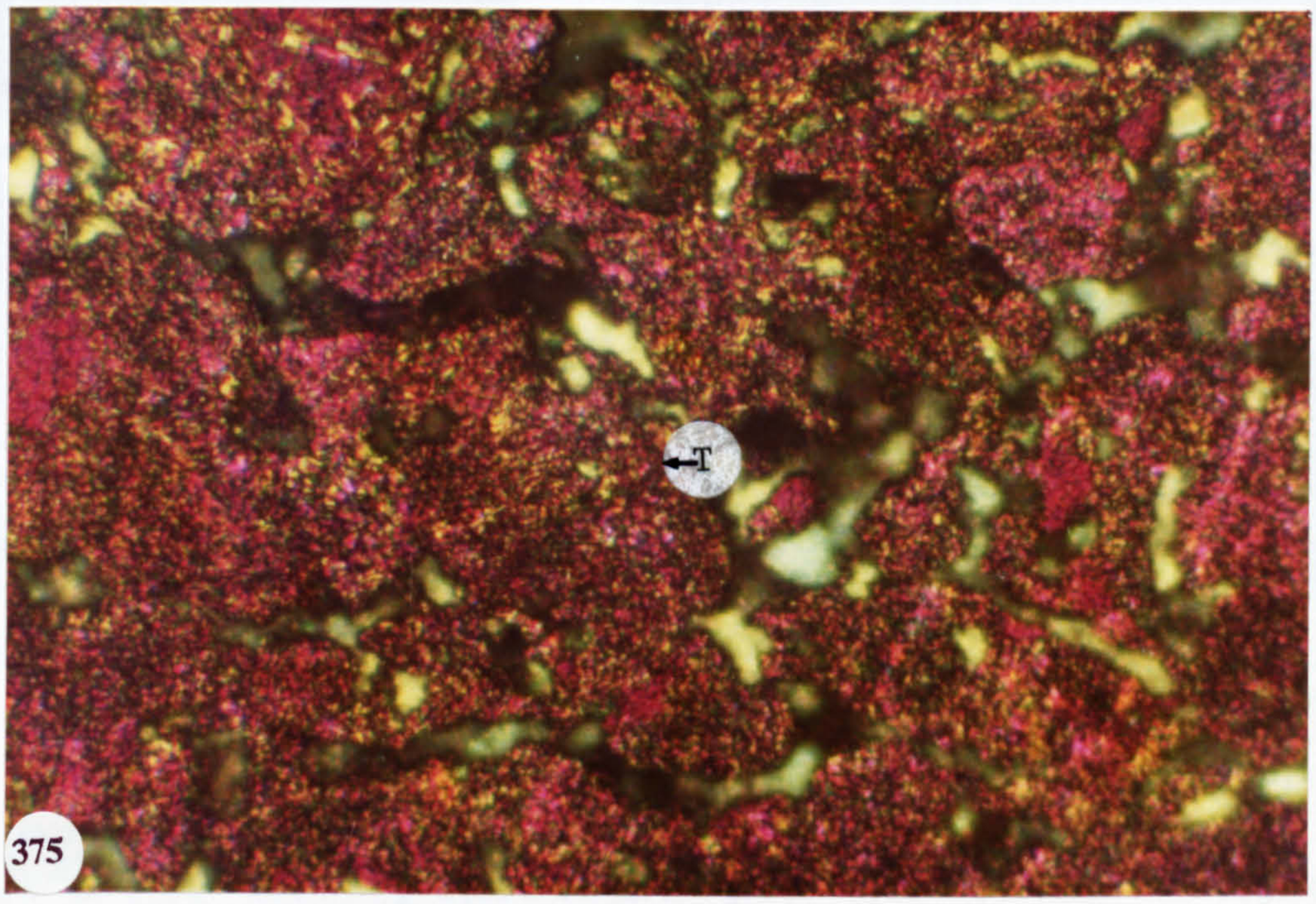


LIMA GRAPHITE 2 μm

Figures 370 to 373. Scanning electron micrographs (stereoscan) of Lima Graphite (LG17) before (Figures 370 and 371) and after (Figures 372 and 373) gasification in carbon dioxide at 1243 K for 16 hours. Weight loss 5.99%.

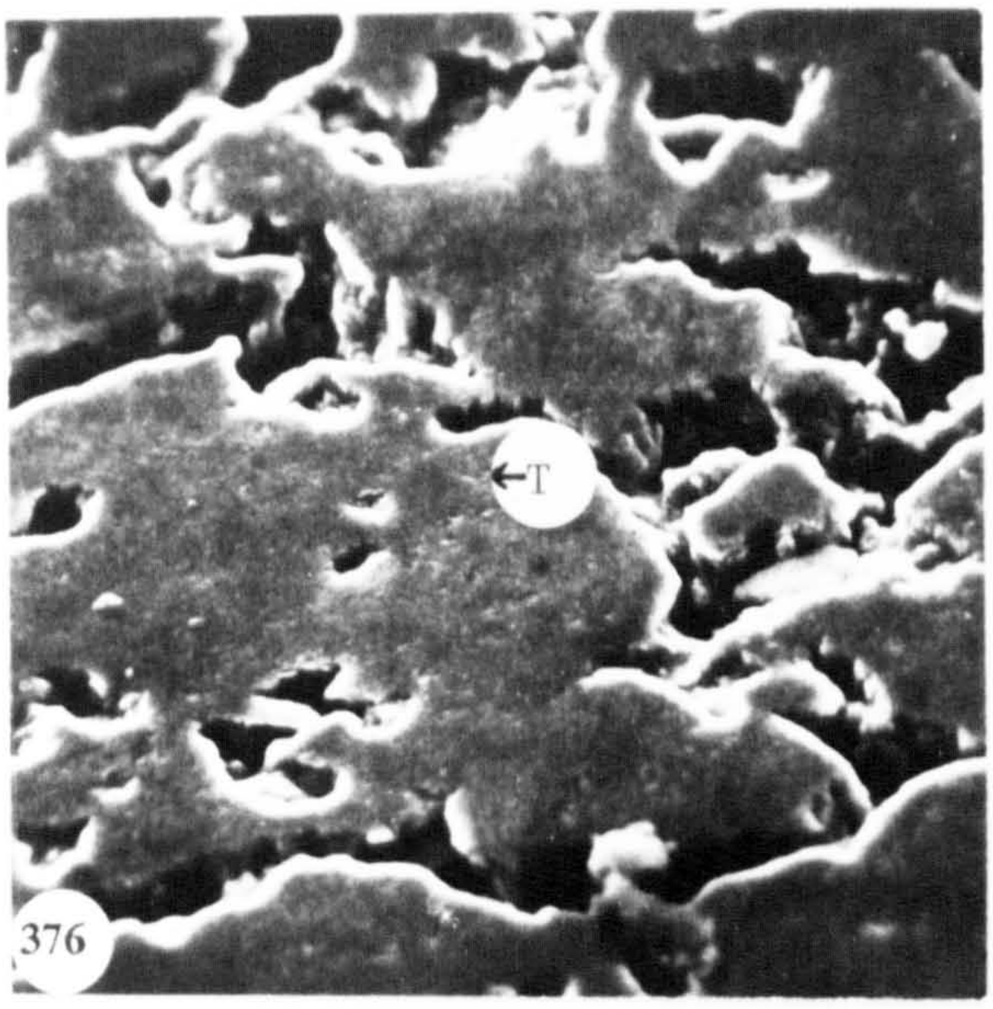


MORGANS UNIPORE GRAPHITE

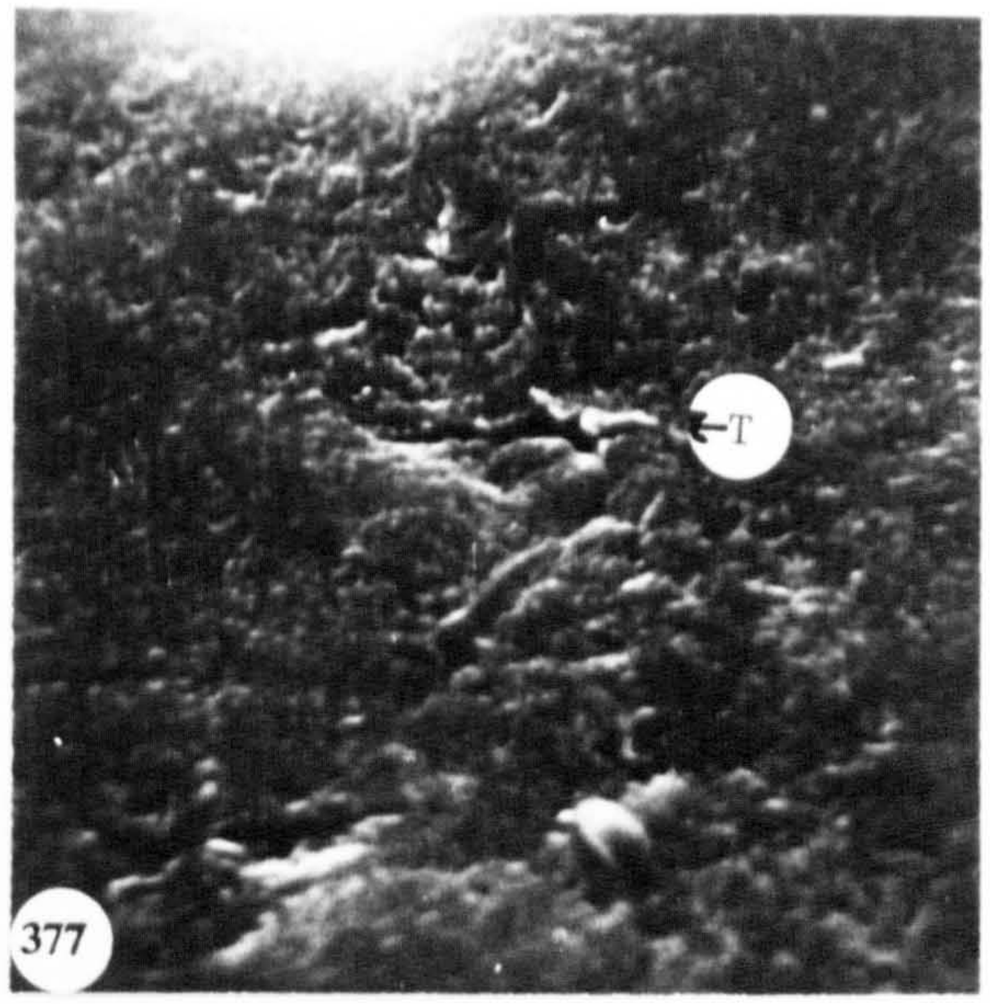


MORGANS UNIPORE GRAPHITE

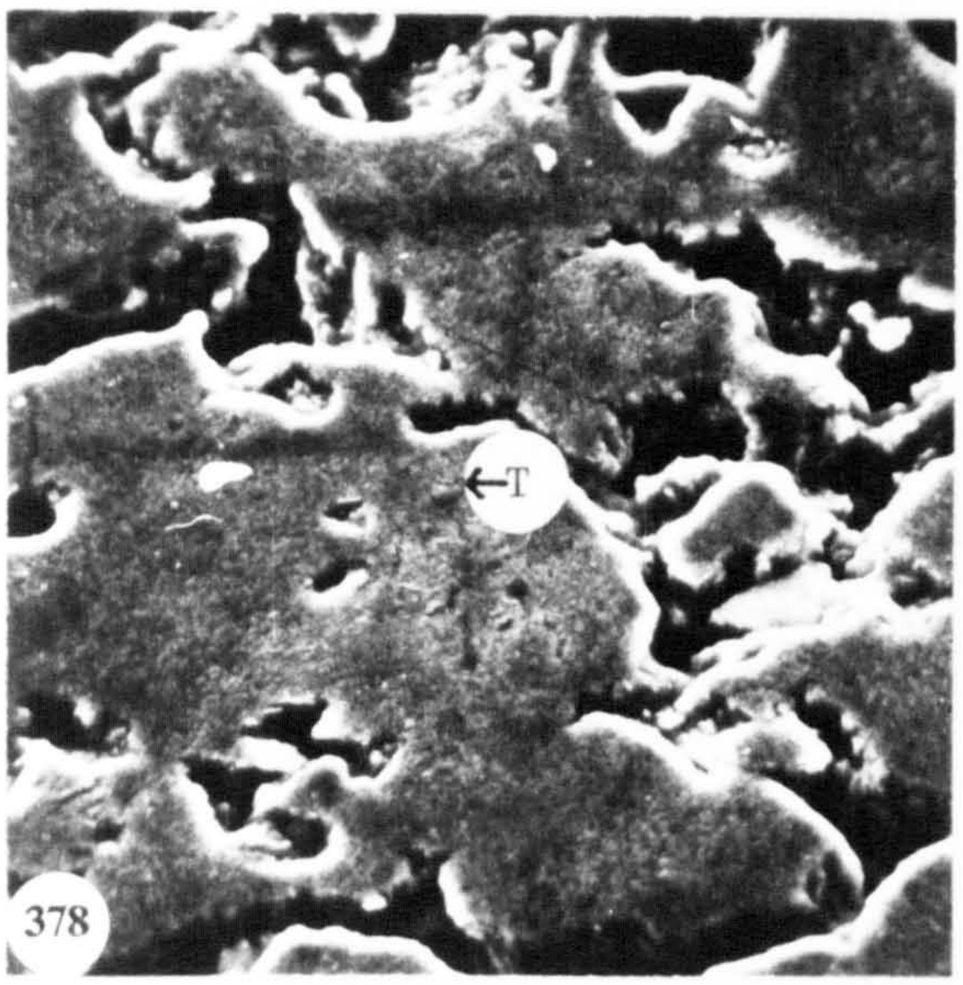
Figures 374 and 375. Optical micrographs of Morgans Unipore Graphite (MG10) before and after gasification in carbon dioxide at 1243 K for 16 hours. Weight loss 6.04%.



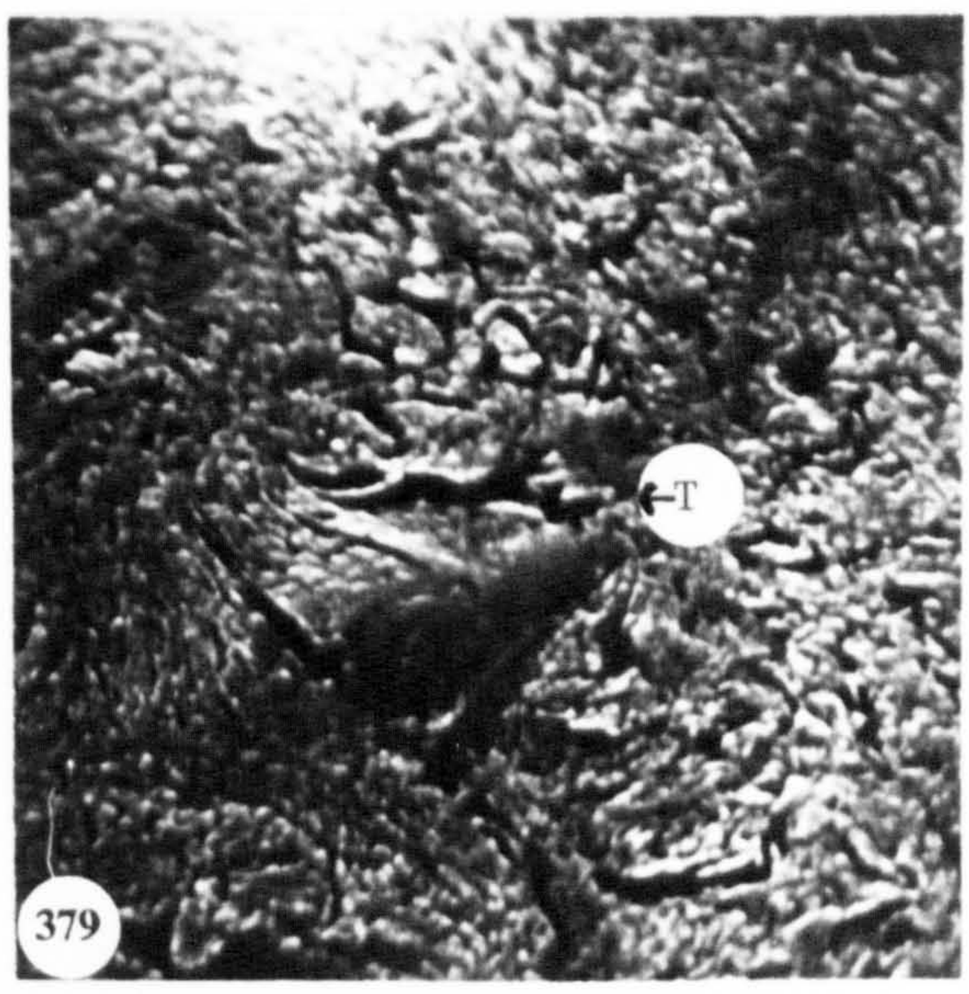
MORGANS UNIPORE GRAPHITE 40 µm



MORGANS UNIPORE GRAPHITE 2 µm

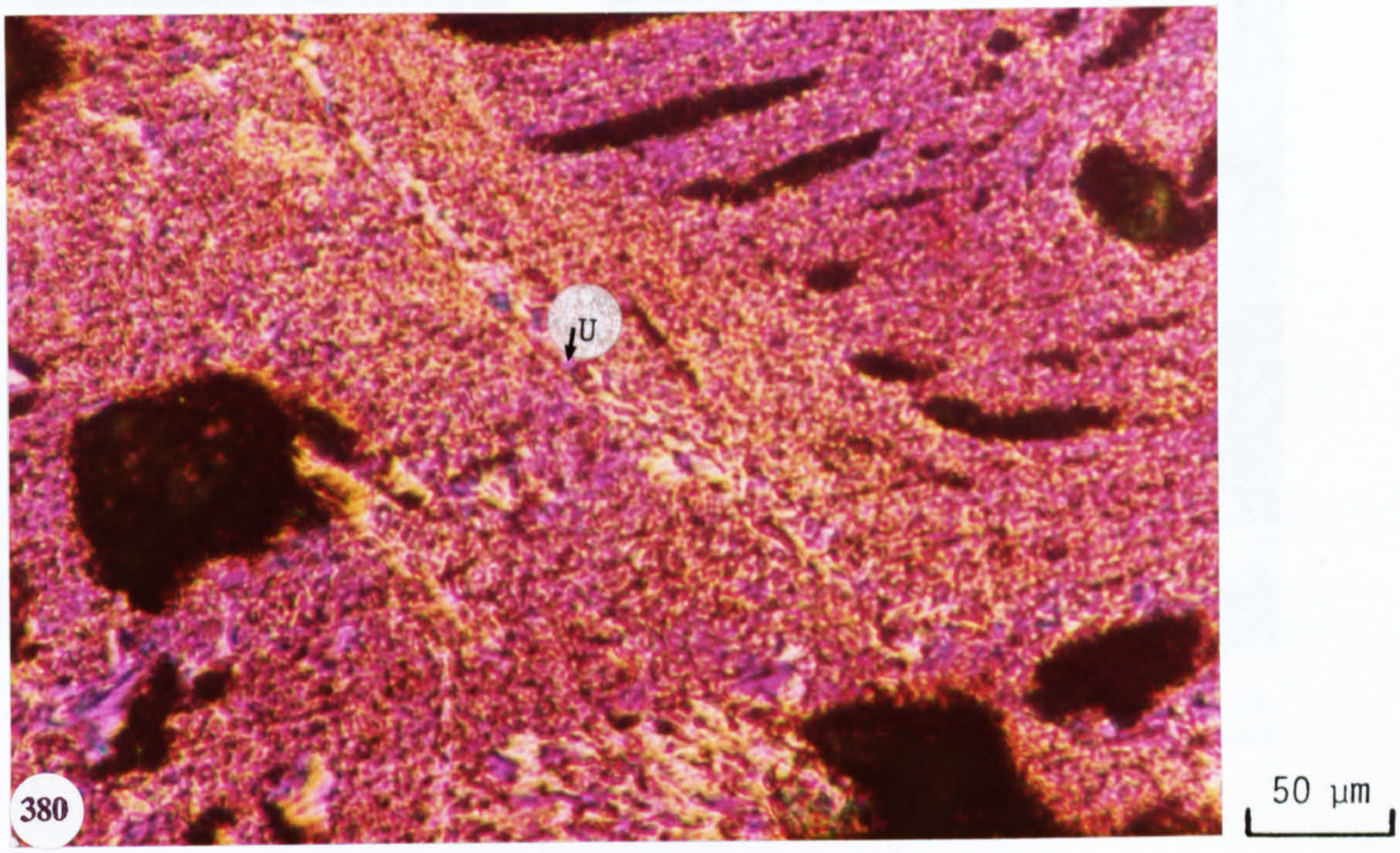


MORGANS UNIPORE GRAPHITE 40 µm

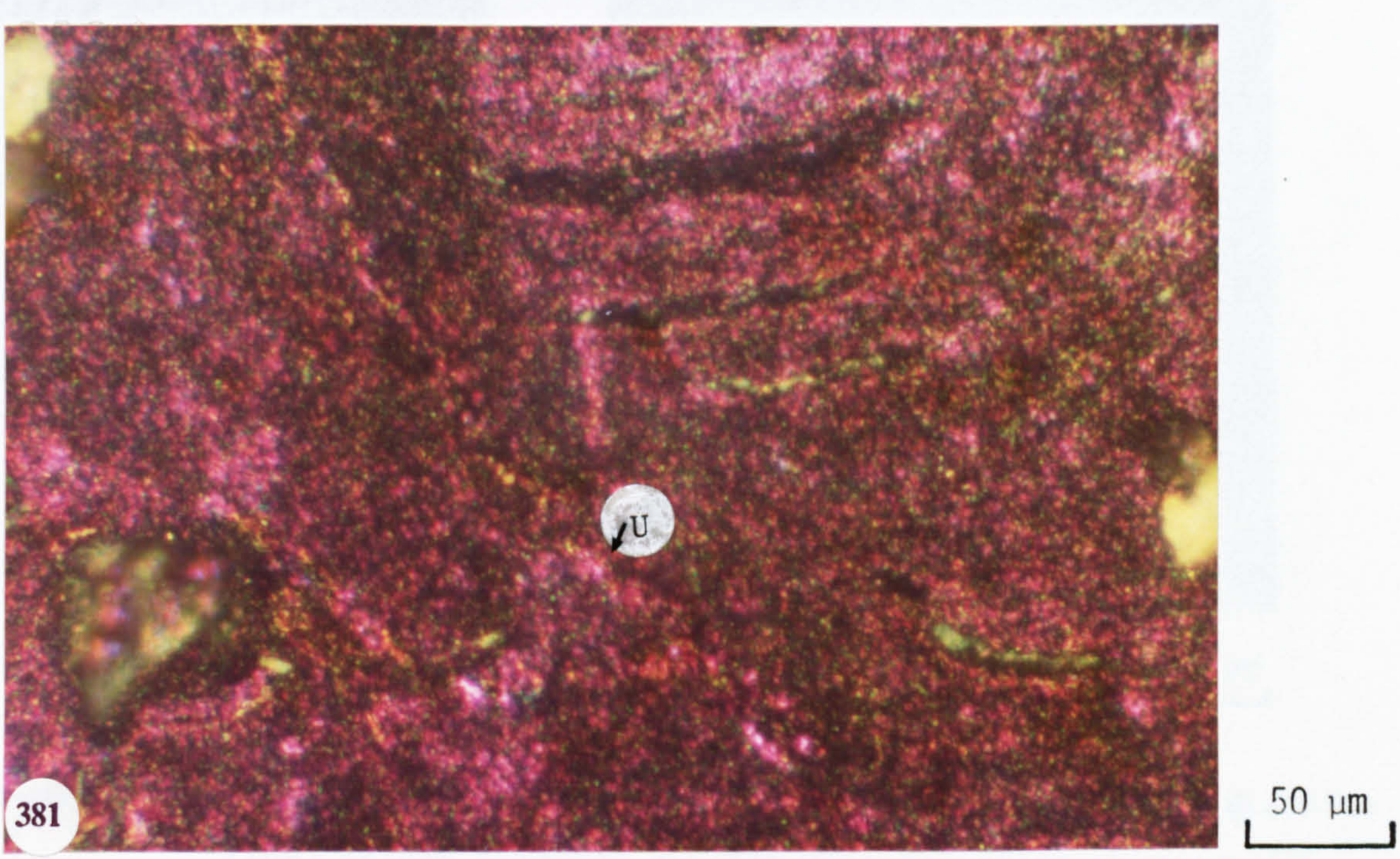


MORGANS UNIPORE GRAPHITE 2 µm

Figures 376 to 379. Scanning electron micrographs (stereoscan) of Morgans Unipore Graphite (MG10) before (Figures 376 and 377) and after (Figures 378 and 379) gasification in carbon dioxide at 1243 K for 16 hours. Weight loss 6.04%.

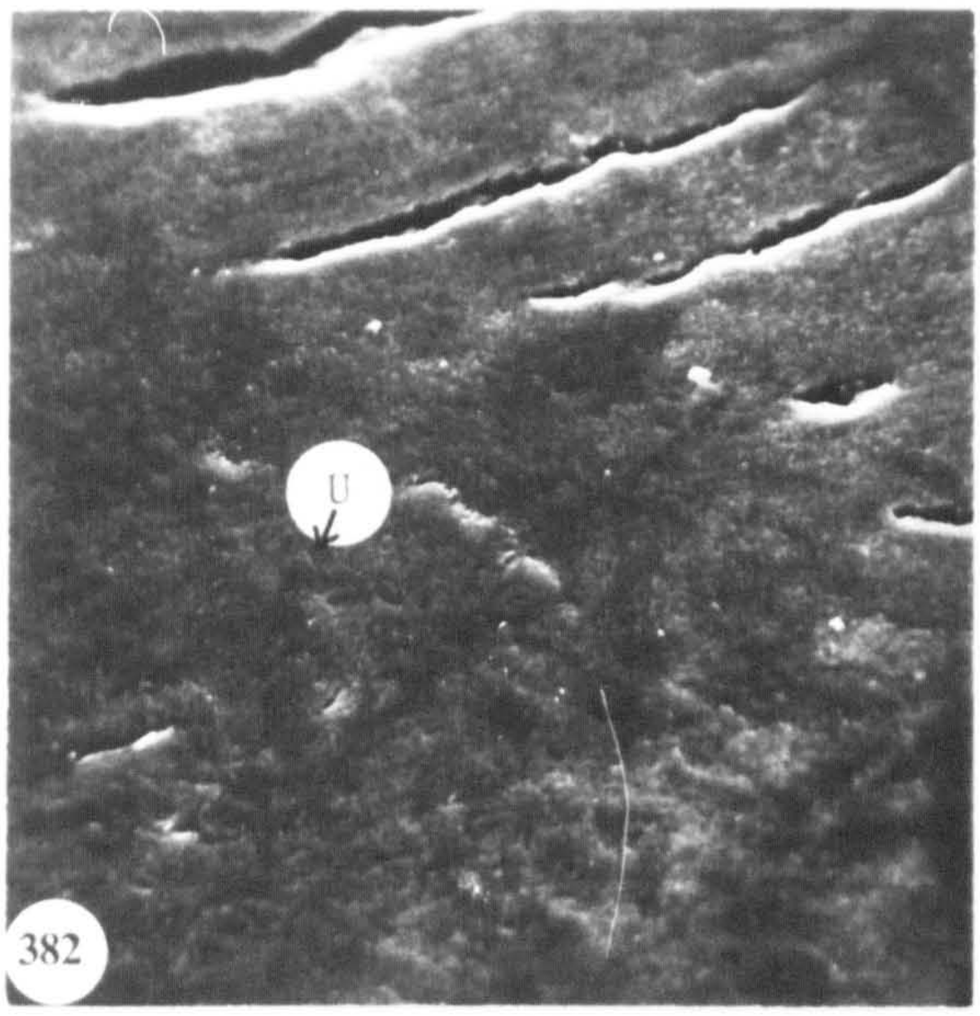


AGLMP GRAPHITE

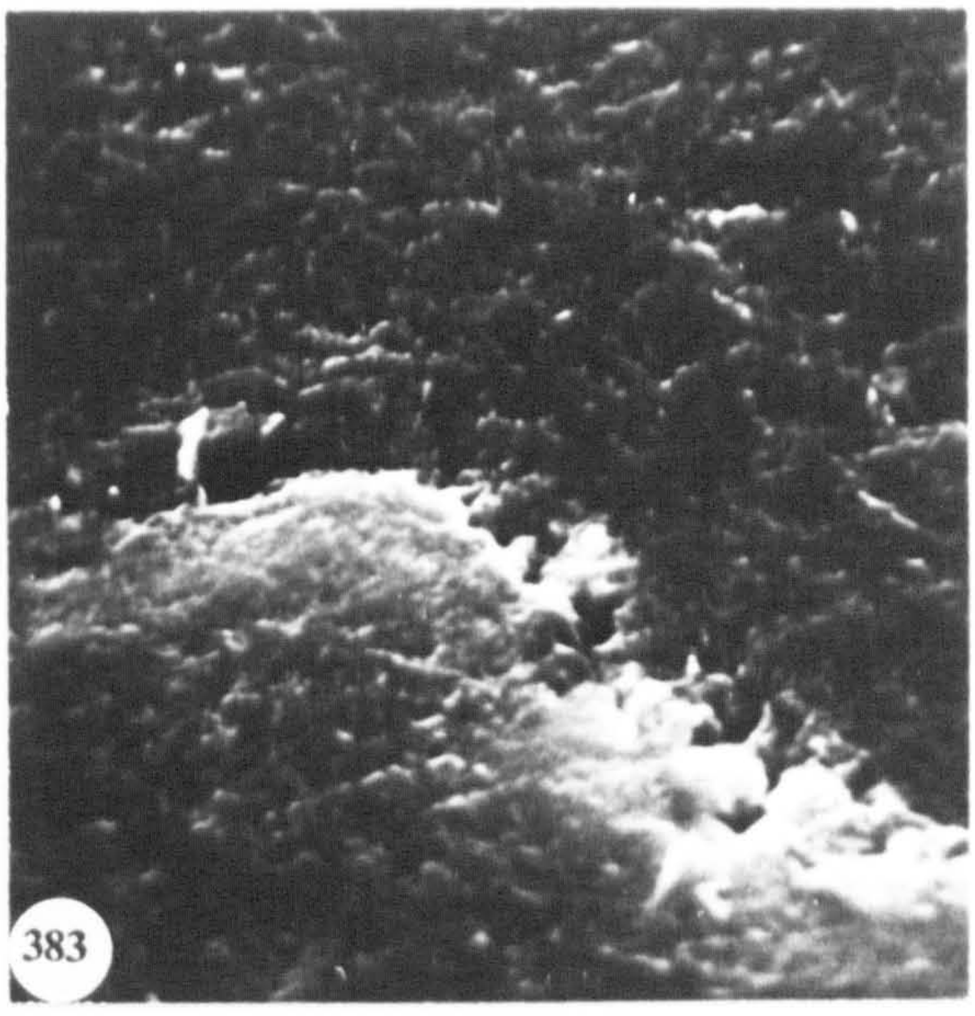


AGLMP GRAPHITE

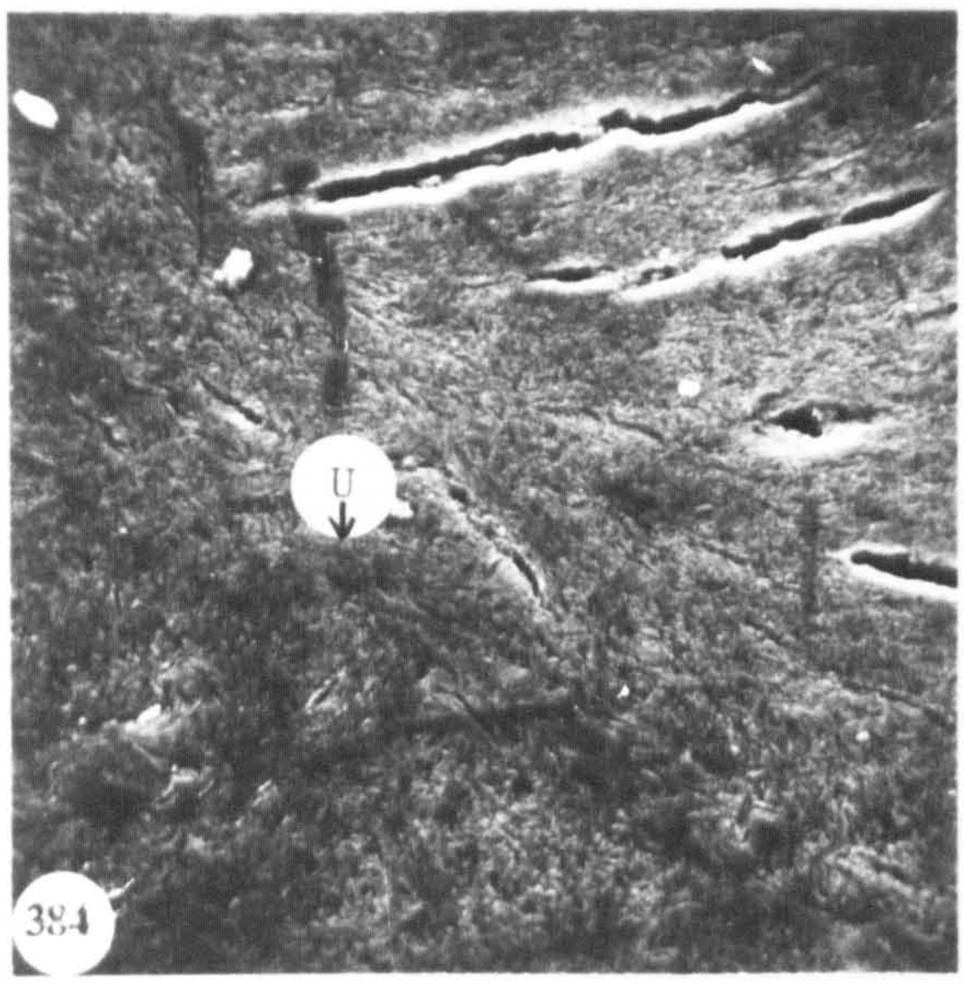
Figures 380 and 381. Optical micrographs of AGLMP Graphite (AG9) before and after gasification in carbon dioxide at 1243 K for 16 hours. Weight loss 3.30%.



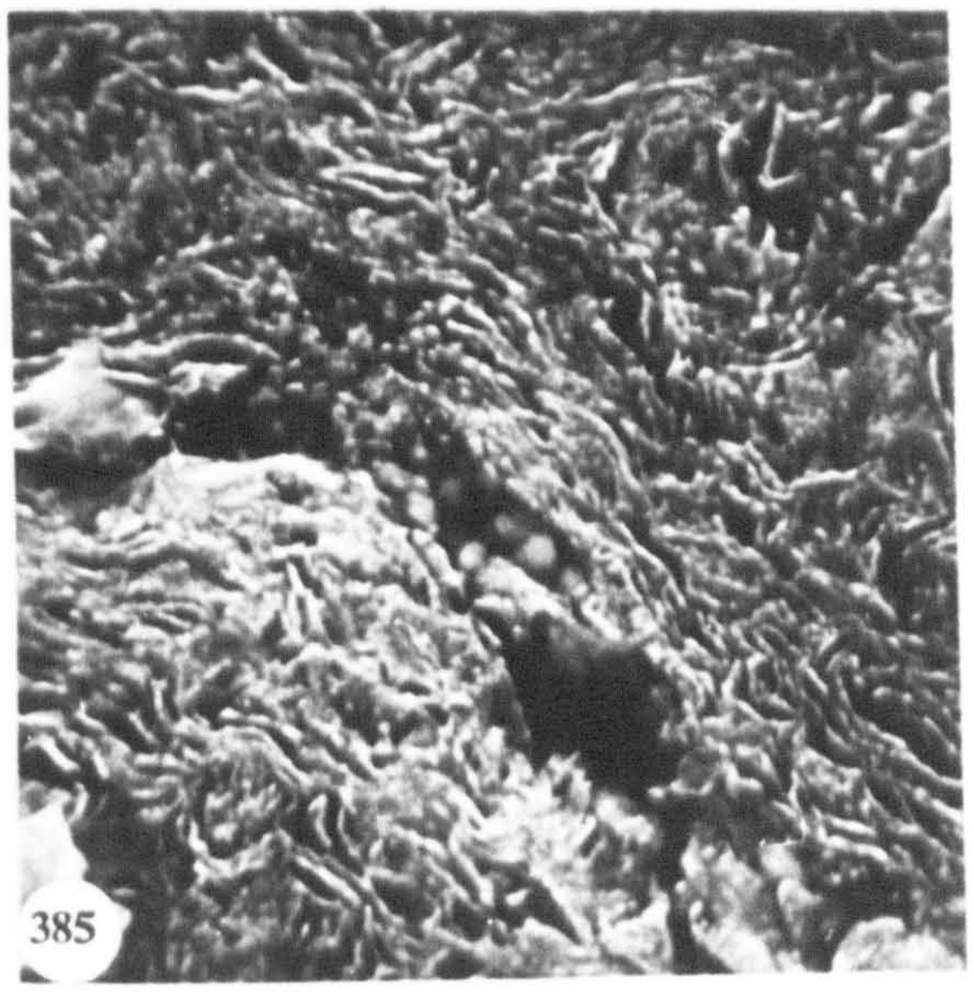
AGLMP GRAPHITE 40 μm



AGLMP GRAPHITE 2 μm

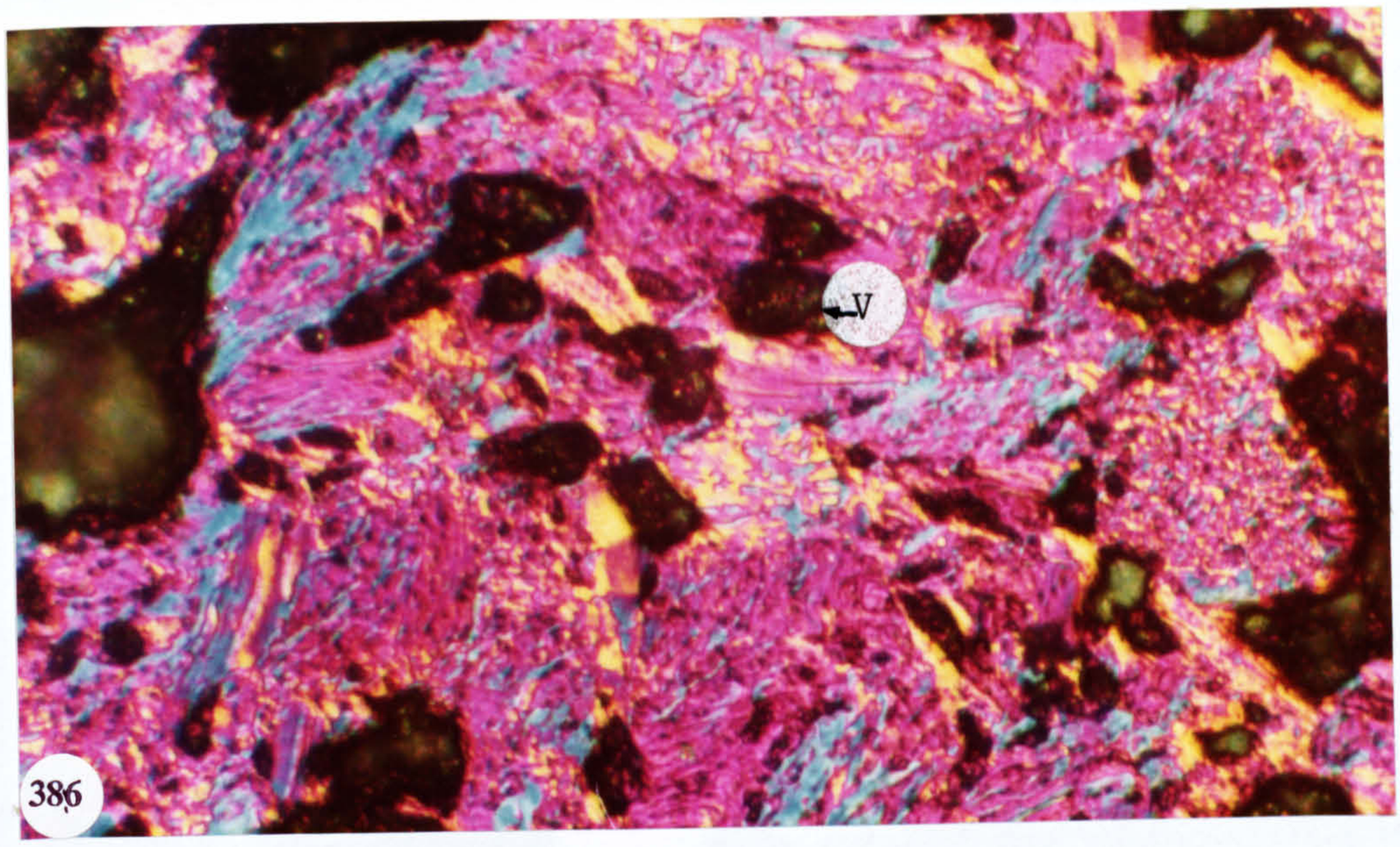


AGLMP GRAPHITE 40 μm



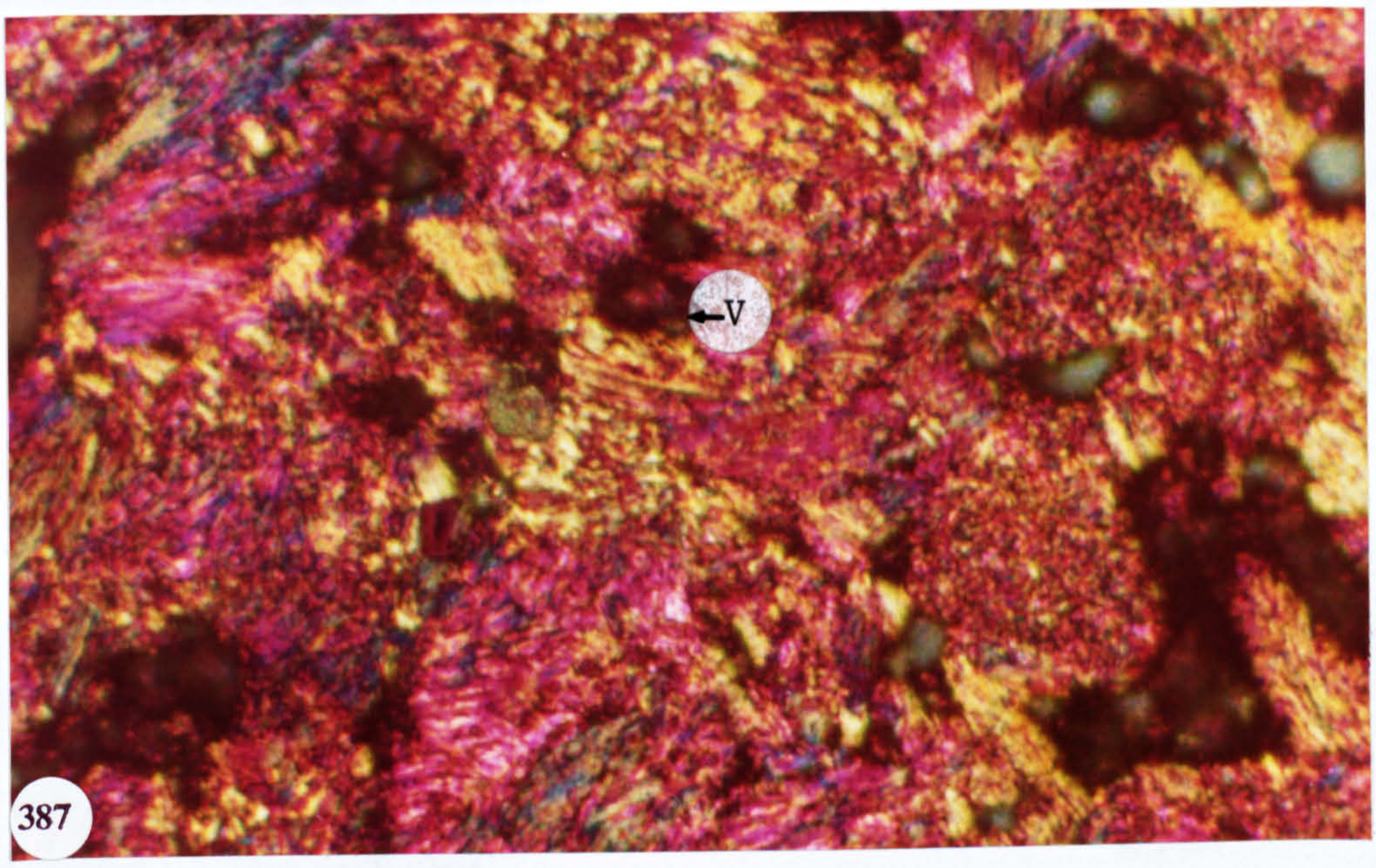
AGLMP GRAPHITE 2 μm

Figures 382 to 385. Scanning electron micrographs (stereoscan) of AGLMP Graphite (AG9) before (Figures 382 and 383) and after (Figures 384 385) gasification in carbon dioxide at 1243 K for 16 hours. Weight loss 3.30%.



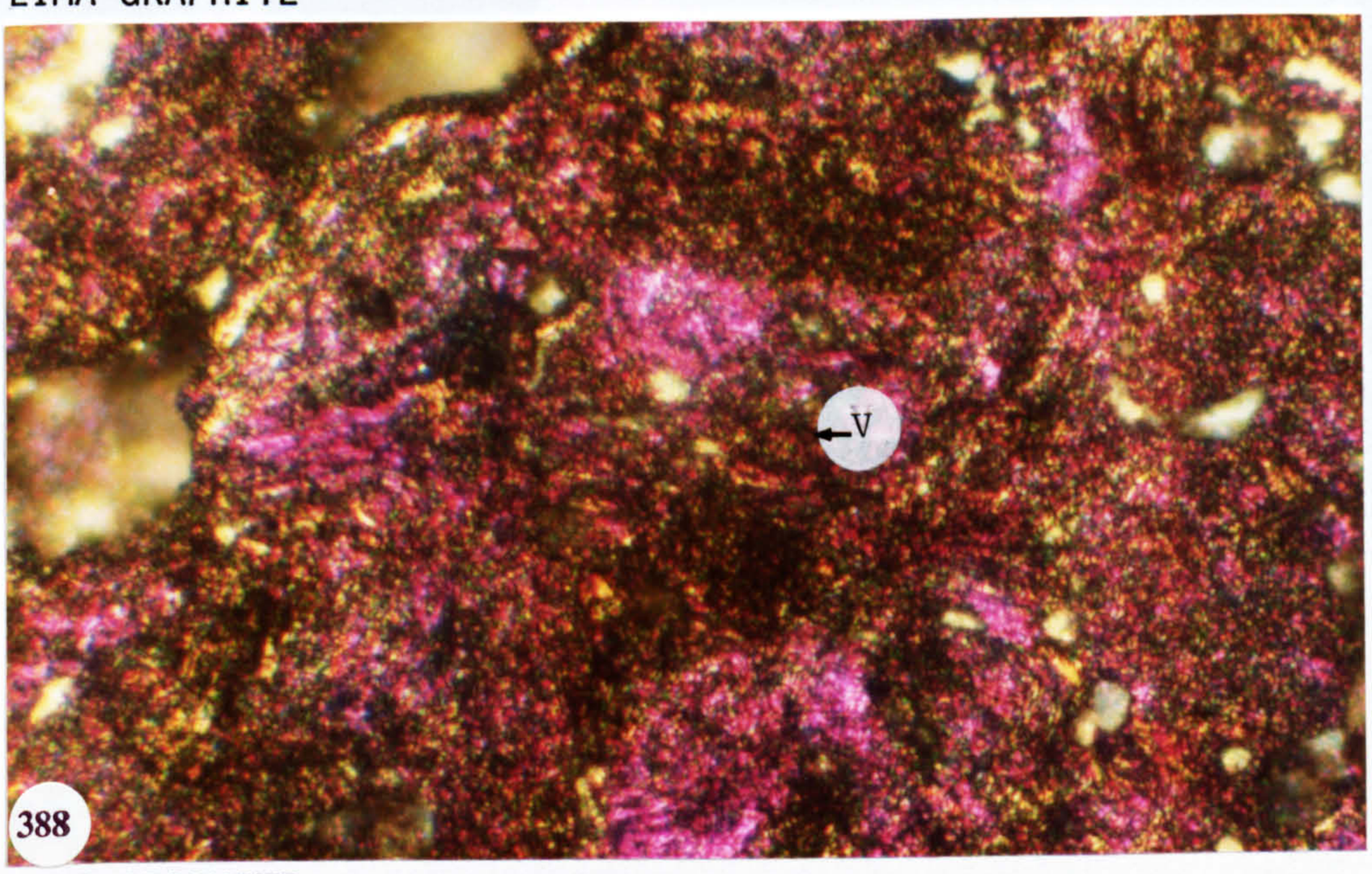
LIMA GRAPHITE

50 µm



LIMA GRAPHITE

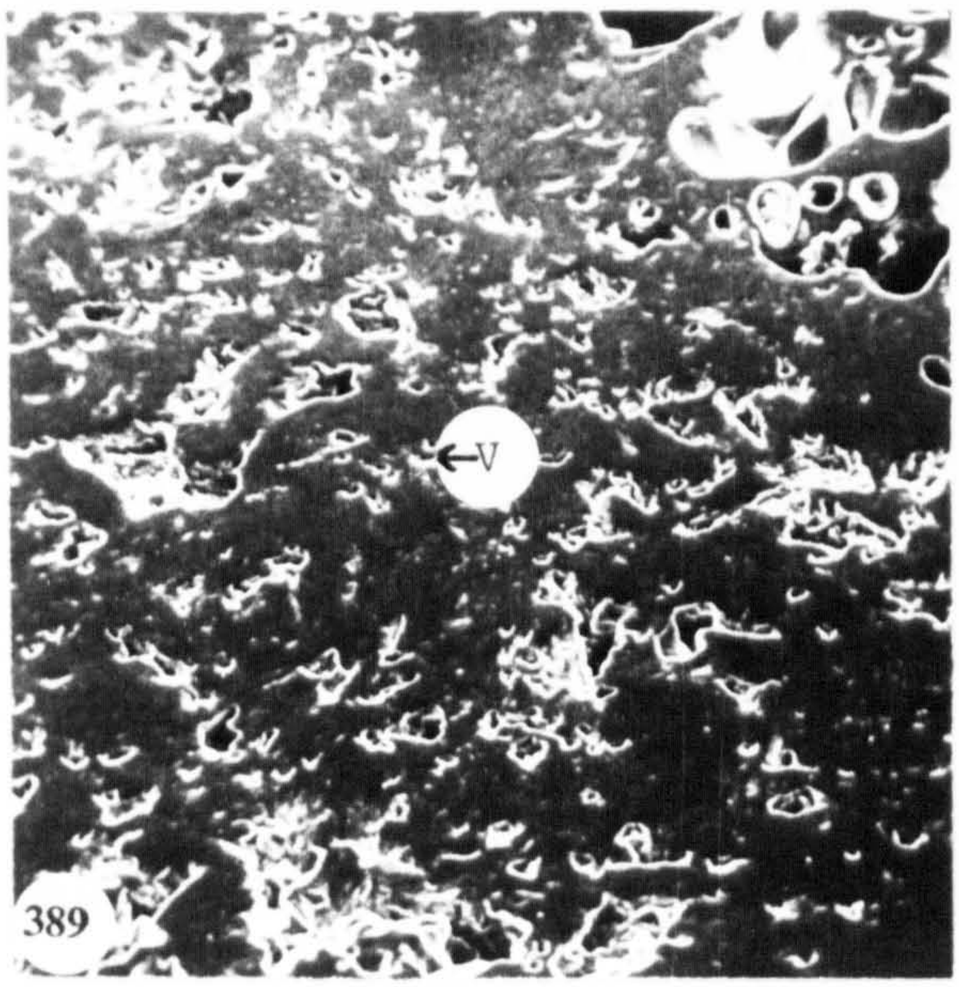
50 µm



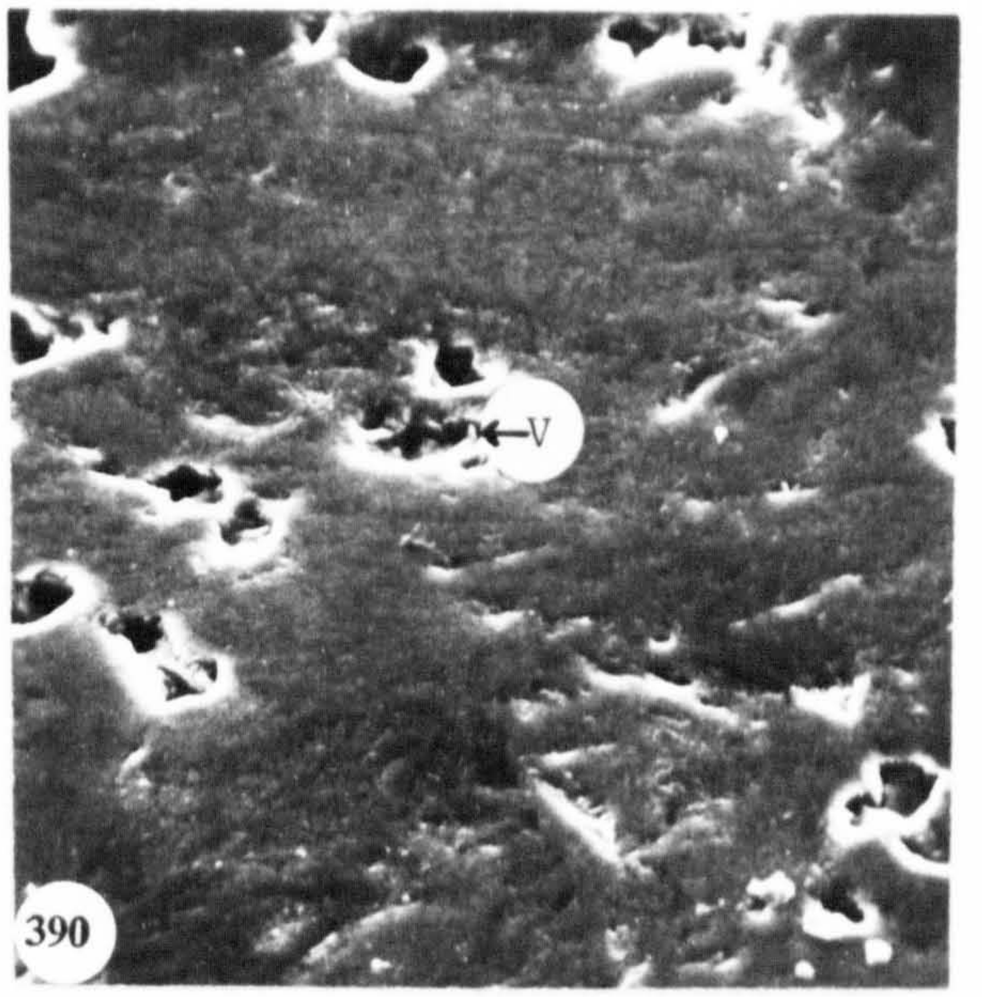
LIMA GRAPHITE

50 µm

Figures 386 to 388. Optical micrographs of Lima Graphite (LG18) before (Figure 386) and after gasification in carbon dioxide at 873 K for 16 hours (Figure 387) and 873 K for 80 hours (Figure 388). Weight losses 0.45% and 3.23%.



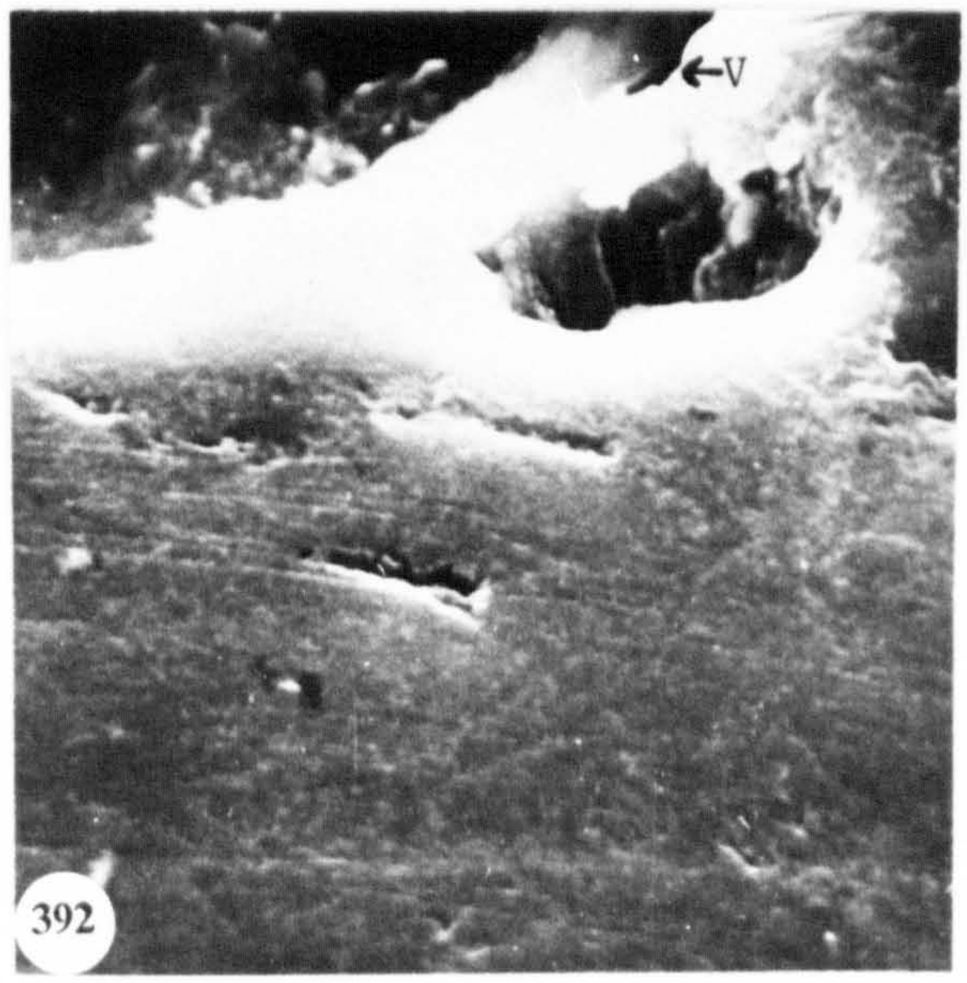
LIMA GRAPHITE 100 µm



LIMA GRAPHITE 40 µm

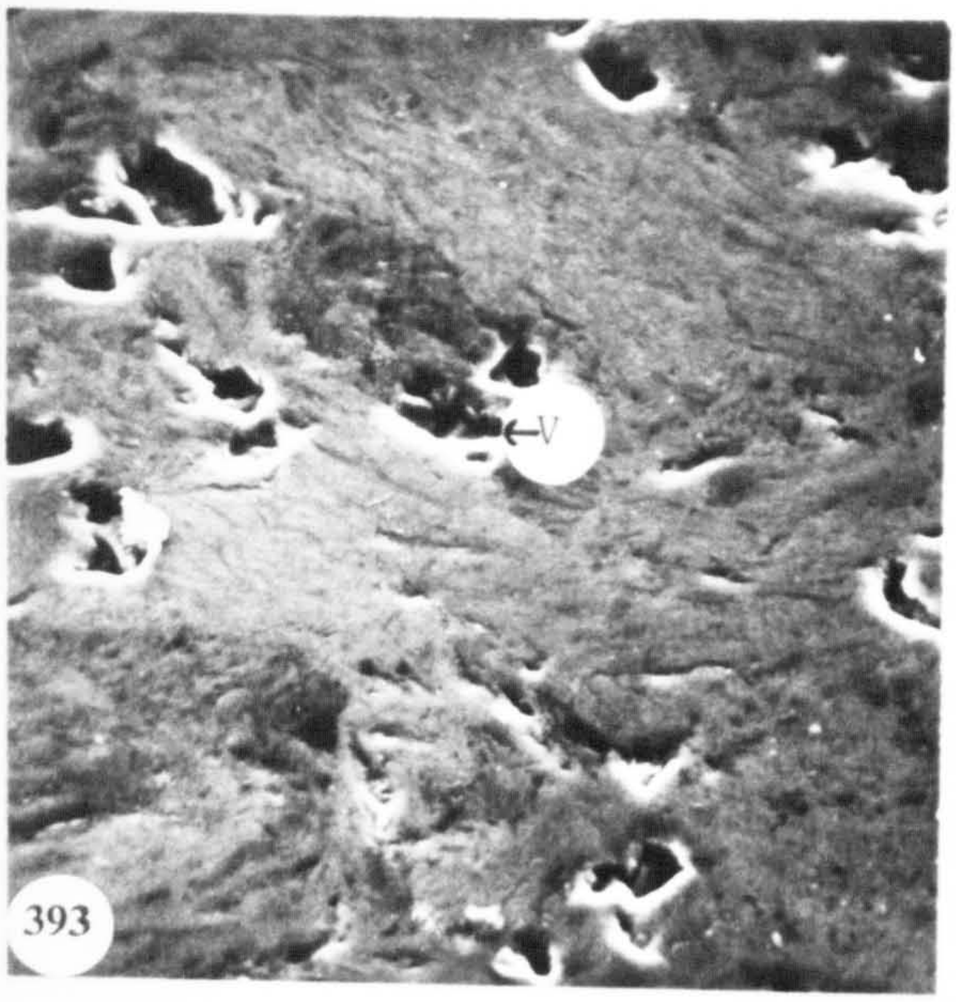


LIMA GRAPHITE 10 µm

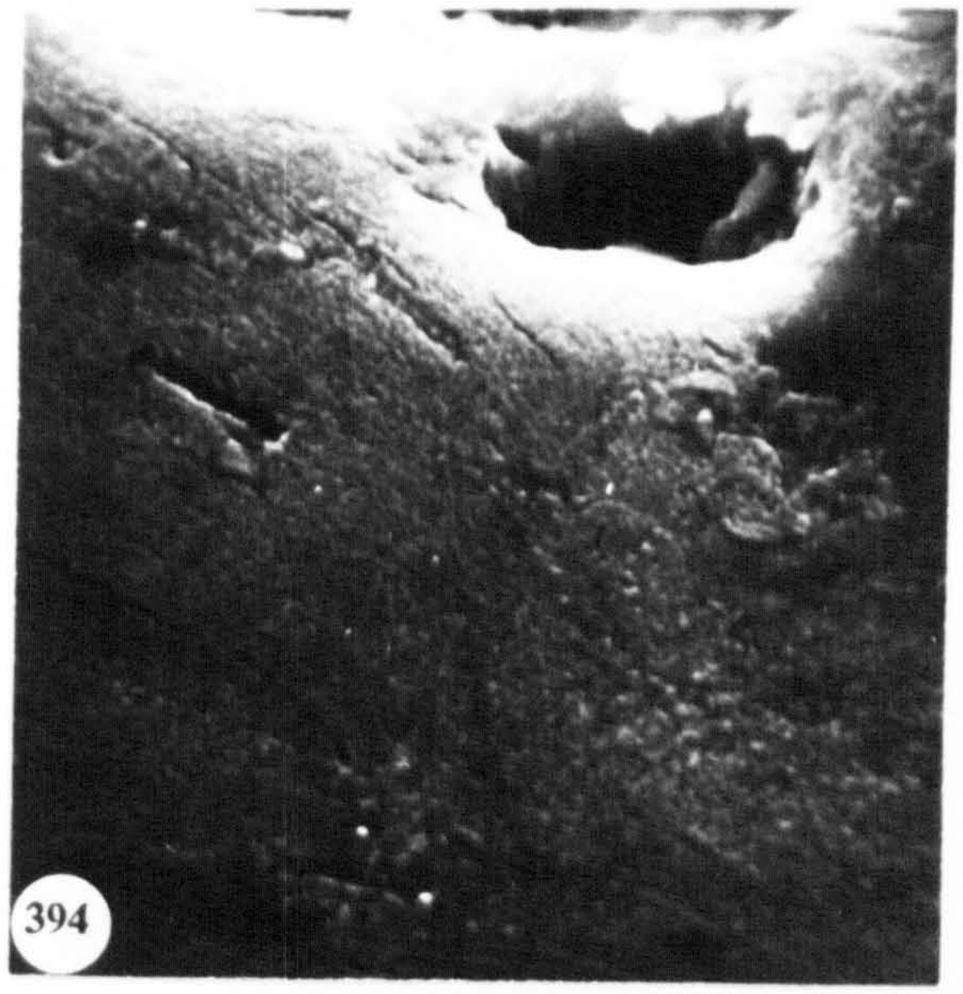


LIMA GRAPHITE 2 µm

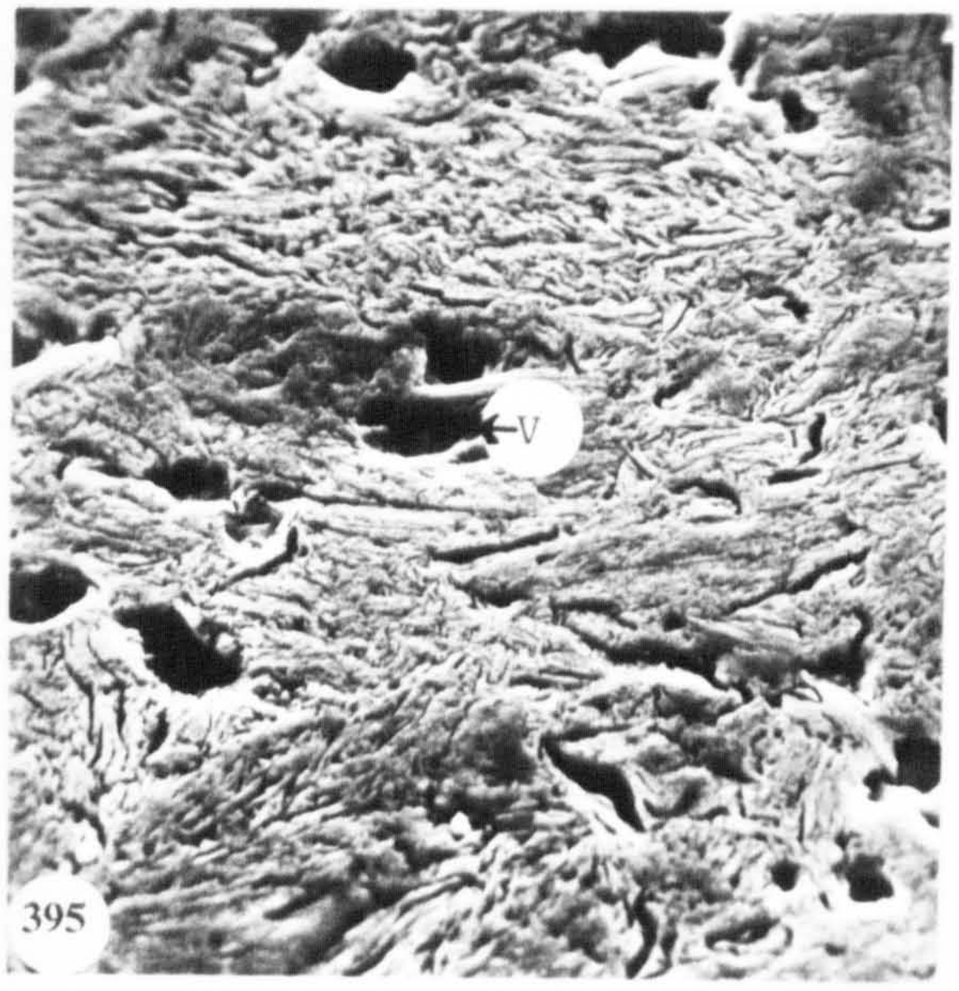
Figures 389 to 392. Scanning electron micrographs(stereoscan) of Lima Graphite (LG18) before gasification.



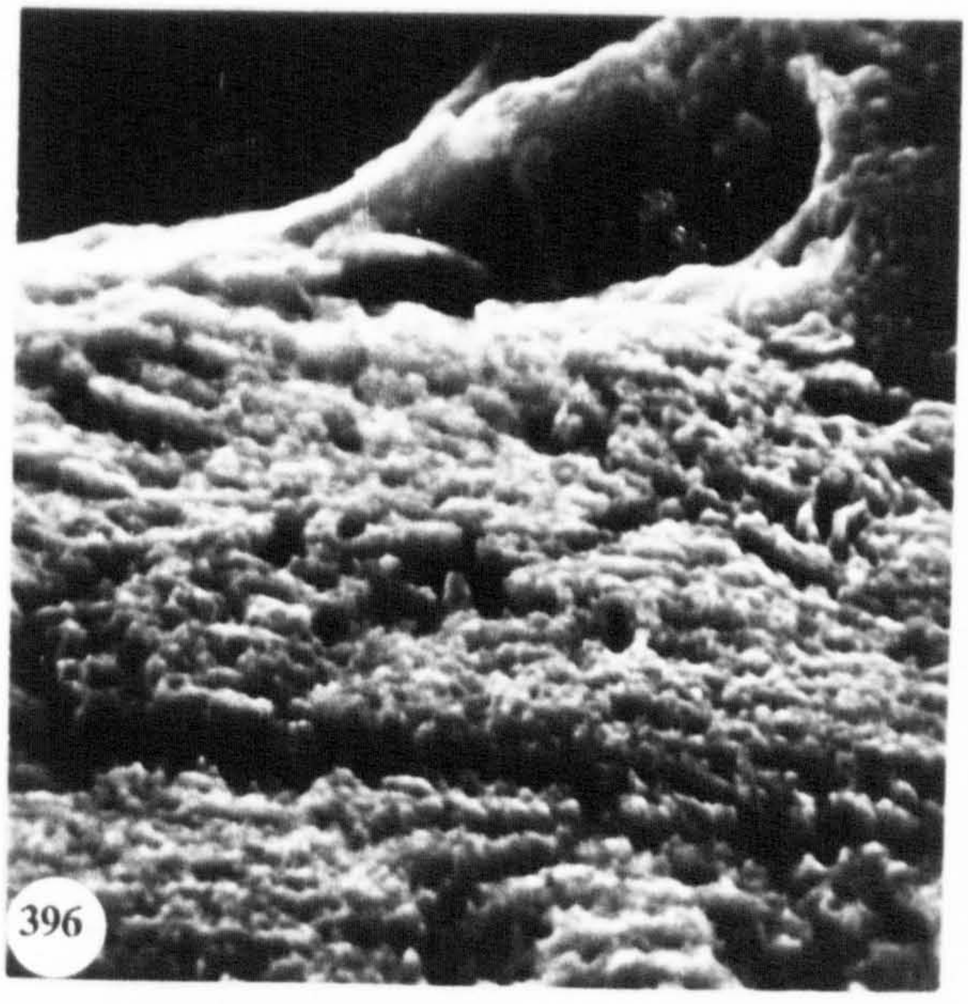
LIMA GRAPHITE 40 μm



LIMA GRAPHITE 2 μm

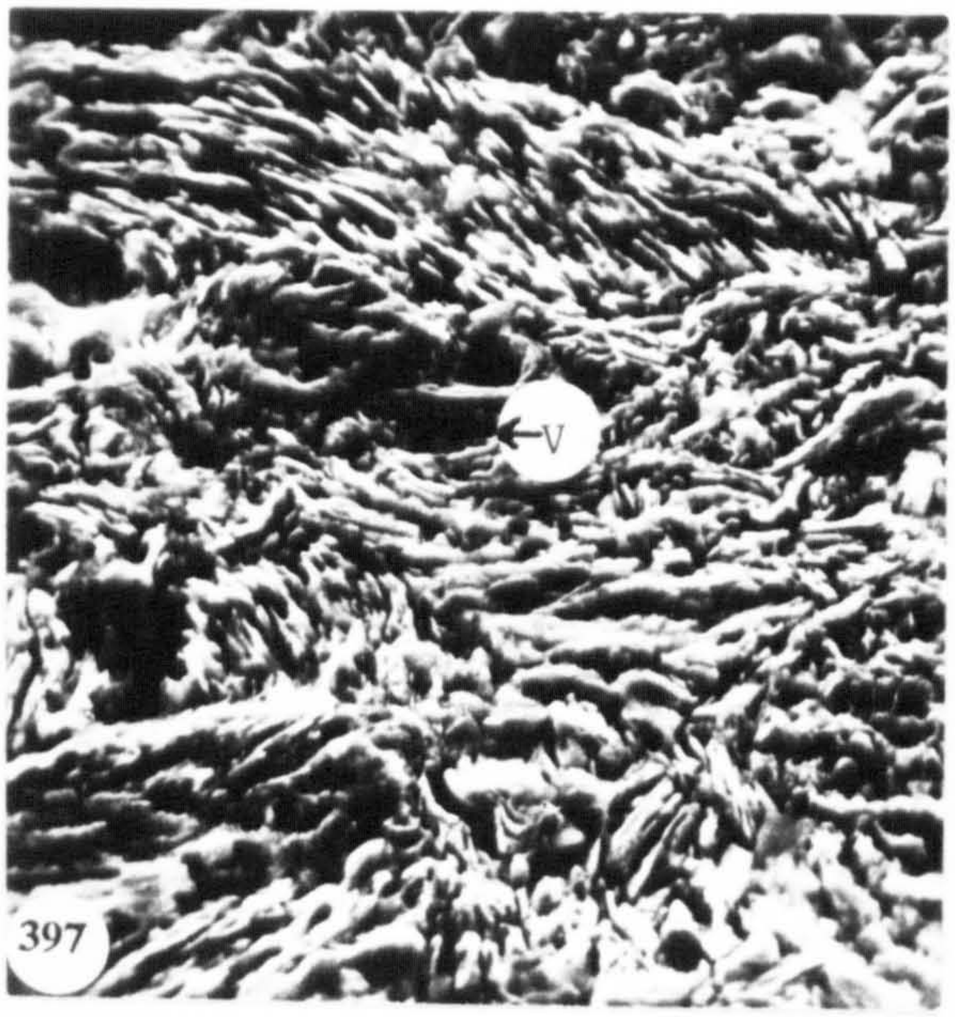


LIMA GRAPHITE 40 μm

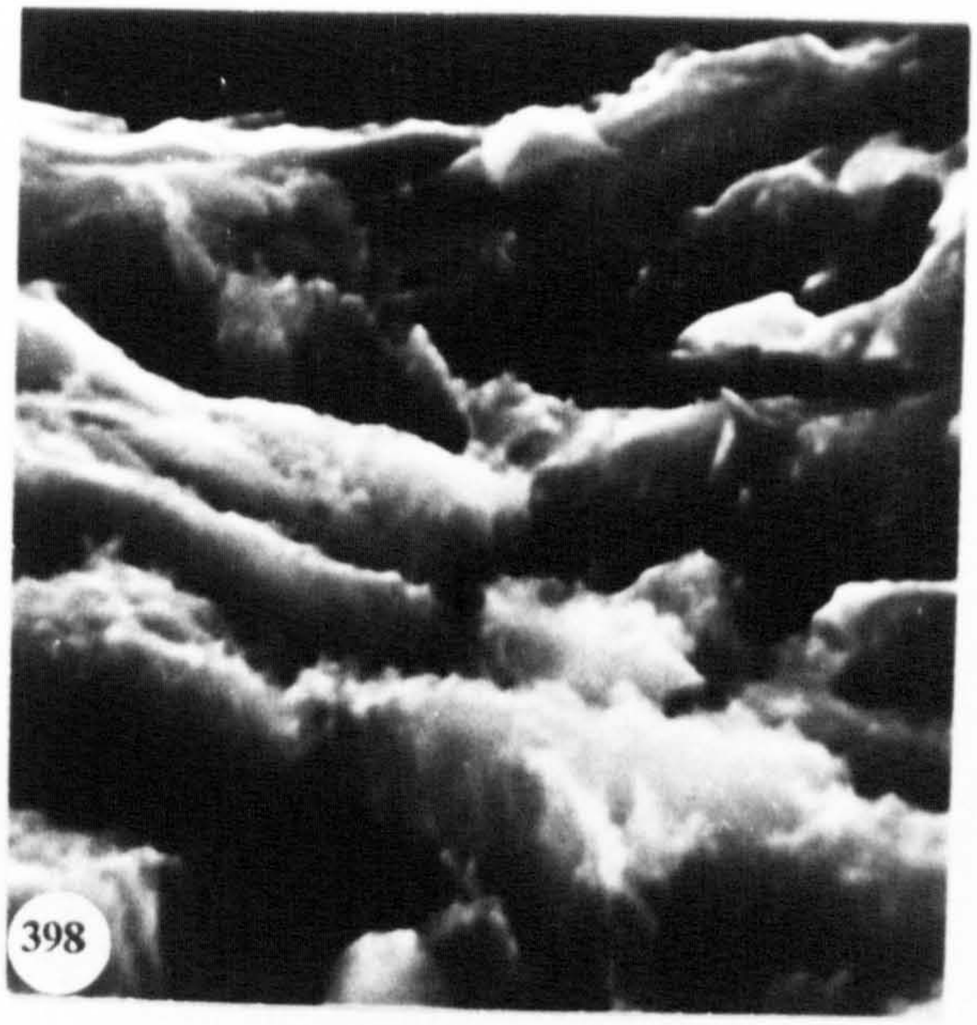


LIMA GRAPHITE 2 μm

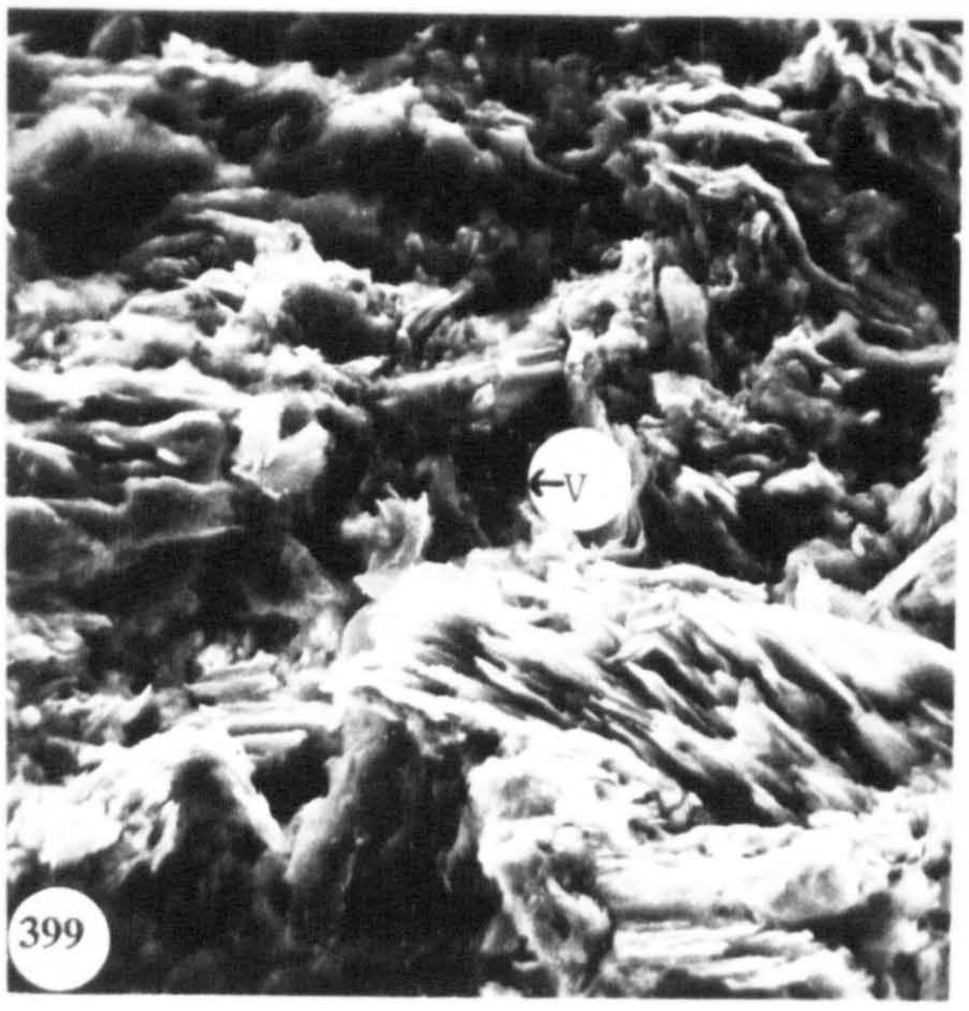
Figures 393 to 396. Scanning electron micrographs (stereoscan) of Lima Graphite (LG18) after gasification in carbon dioxide at 873 K for 16 hours (Figures 393 and 394) and 873 K for 80 hours (Figures 395 and 396). Weight losses 0.45% and 3.23%.



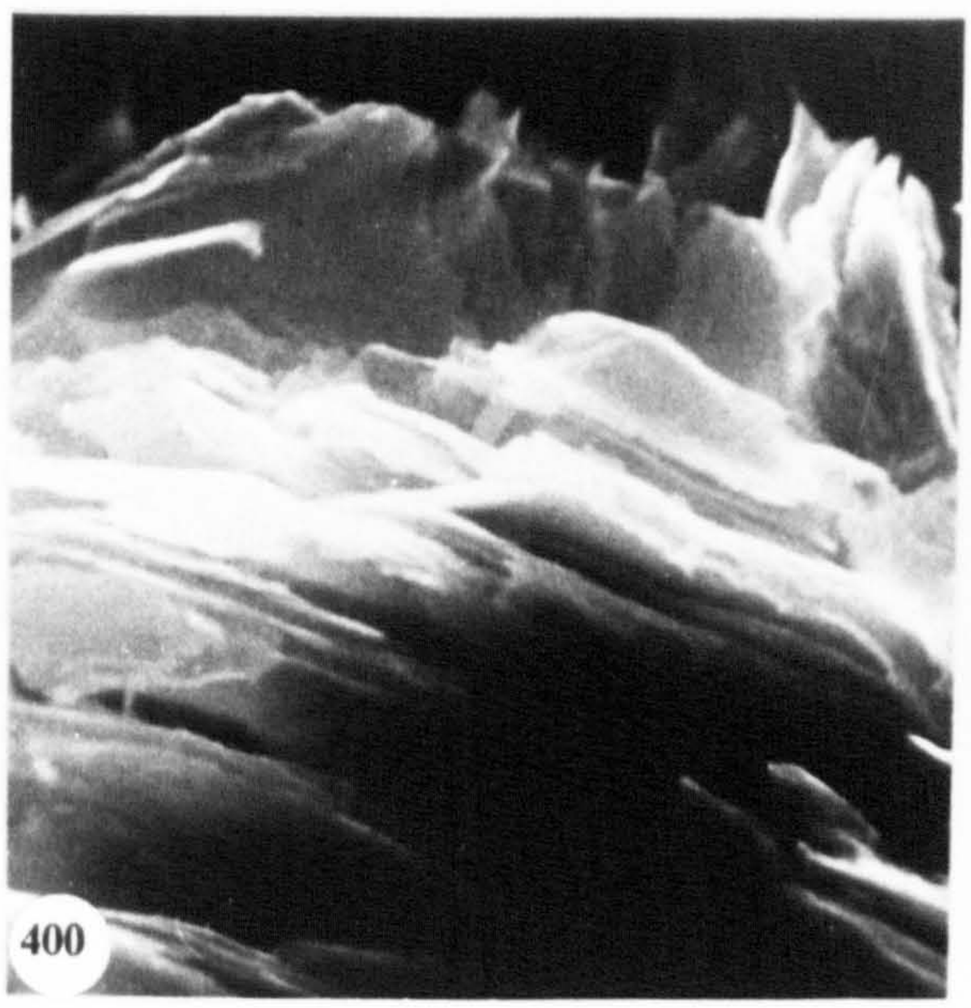
LIMA GRAPHITE 40 μm



LIMA GRAPHITE 2 μm

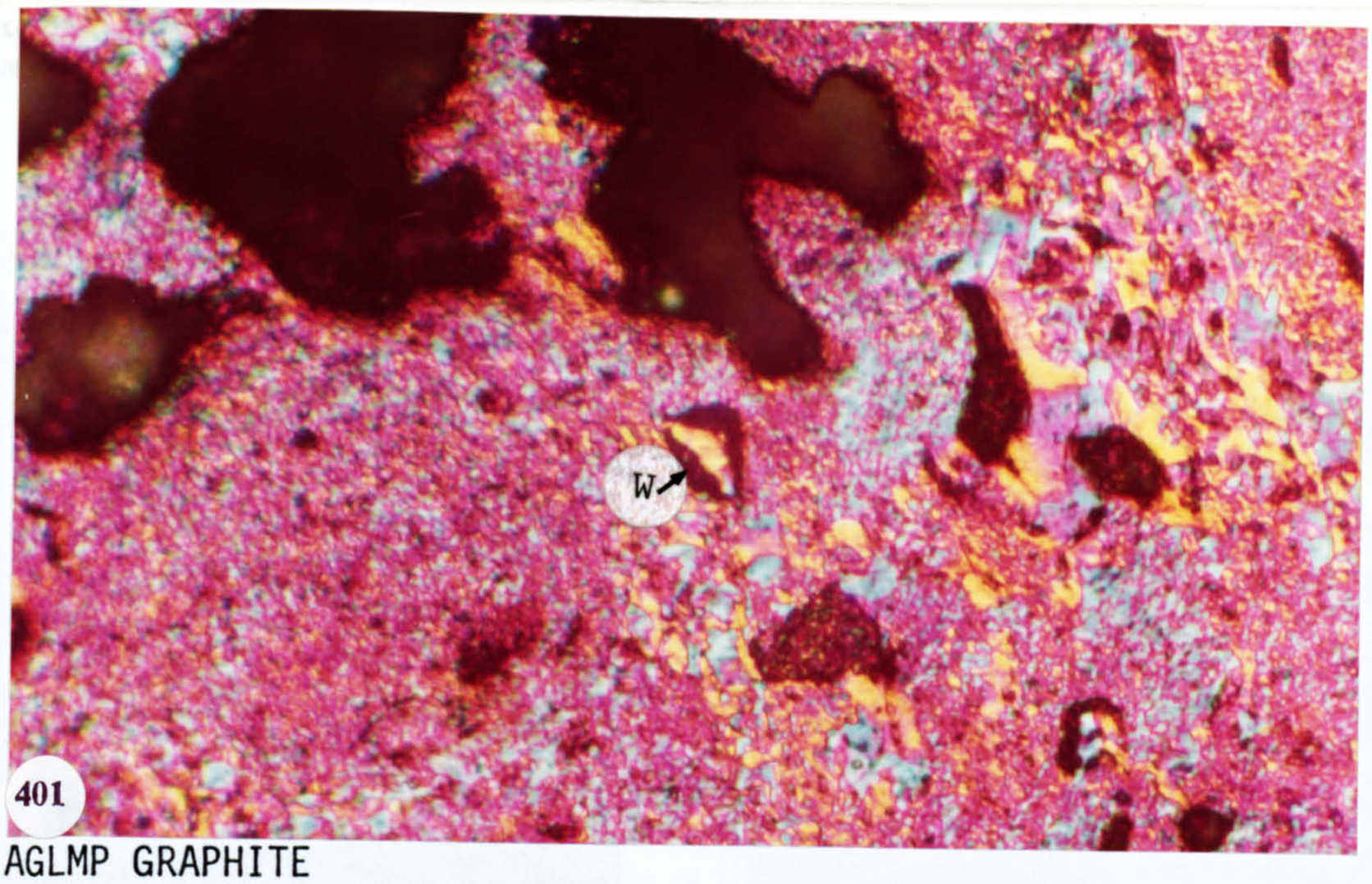


LIMA GRAPHITE 40 μm

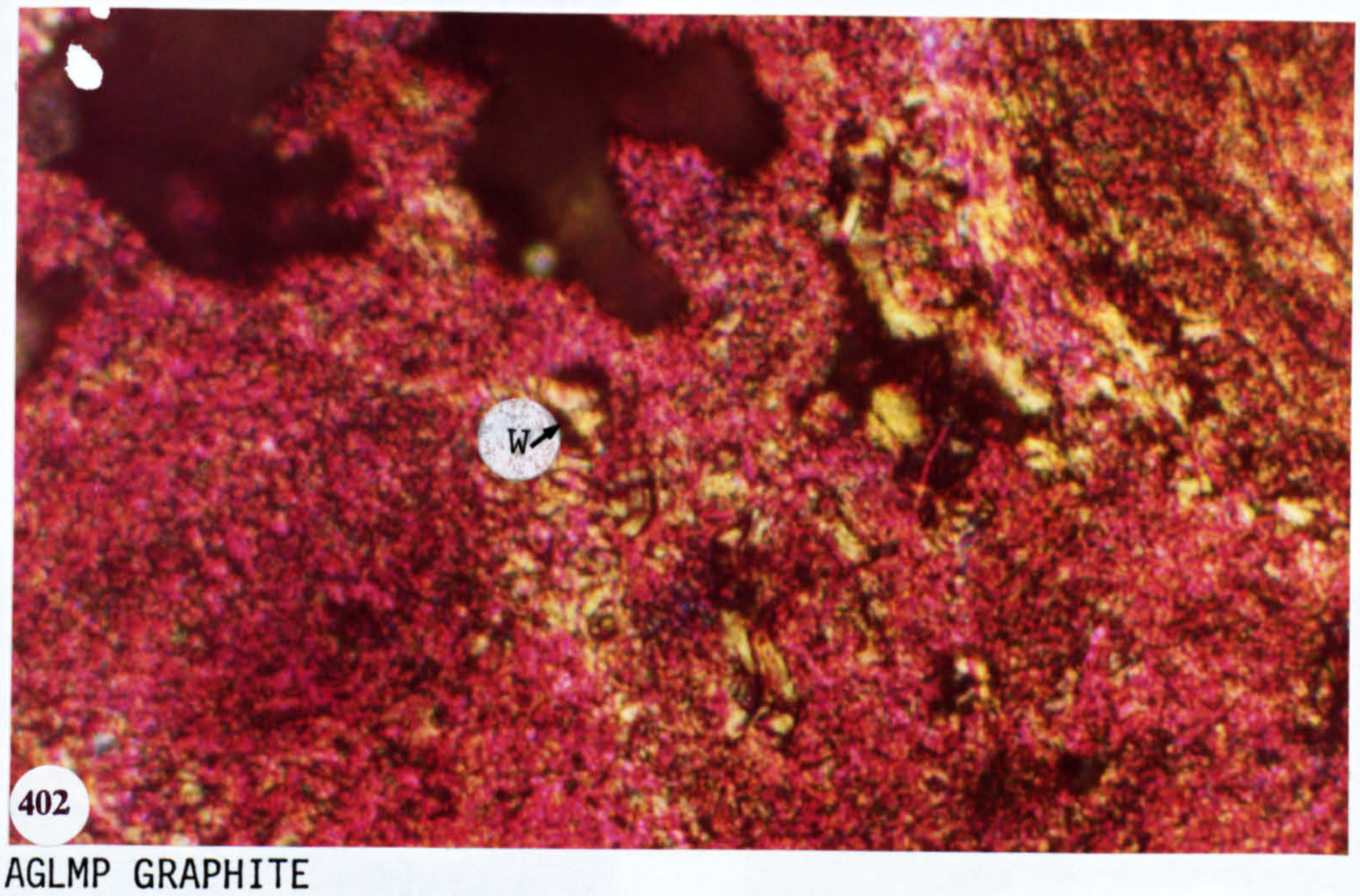


LIMA GRAPHITE 2 μm

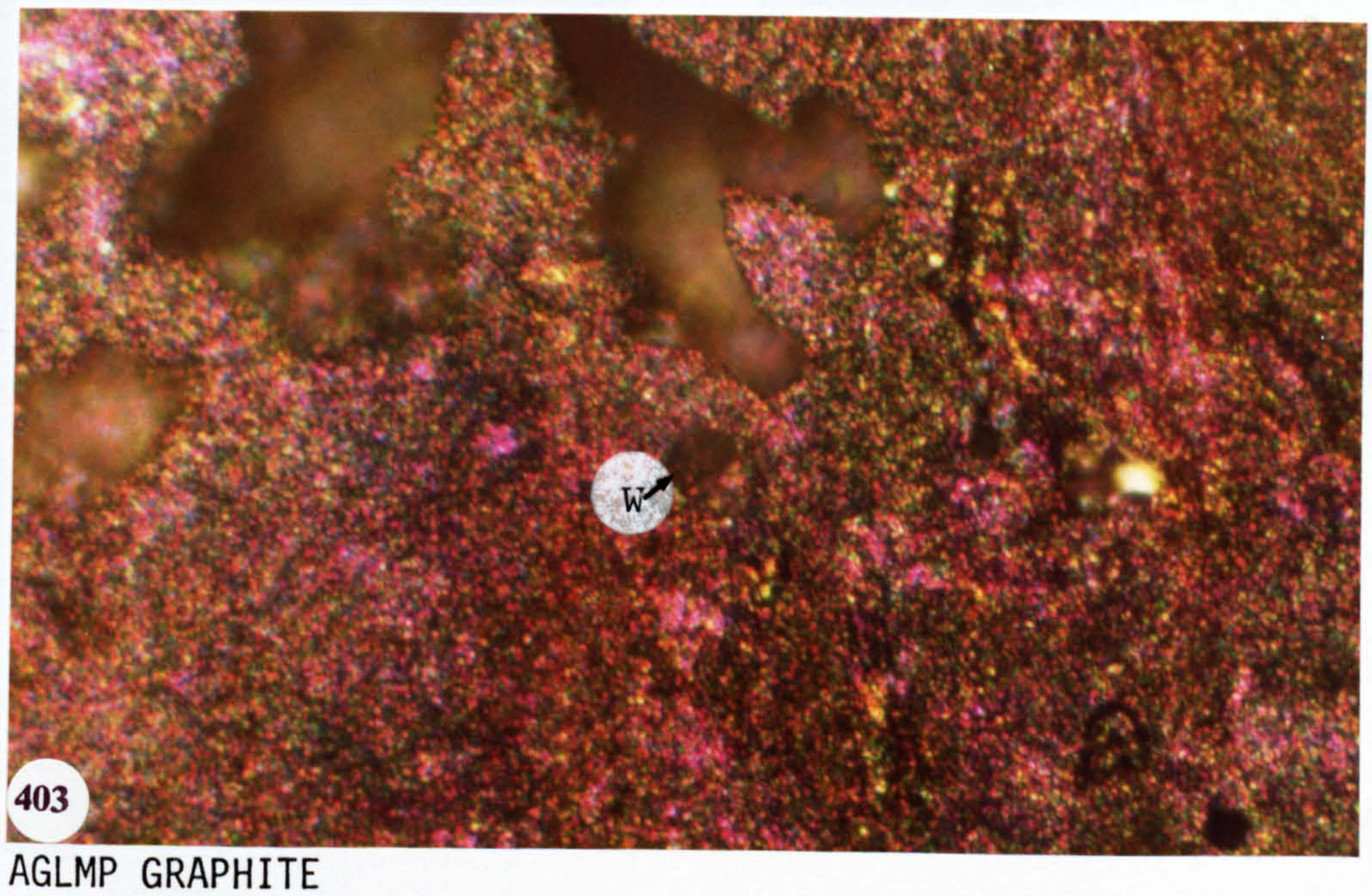
Figures 397 to 400. Scanning electron micrographs (Stereoscan) of Lima Graphite (LG18) after gasification in carbon dioxide at 973 K (Figures 397 and 398) and 1073 K (Figures 399 and 400) for 96 hours each. Weight losses 1.34% and 4.69%.



AGLMP GRAPHITE

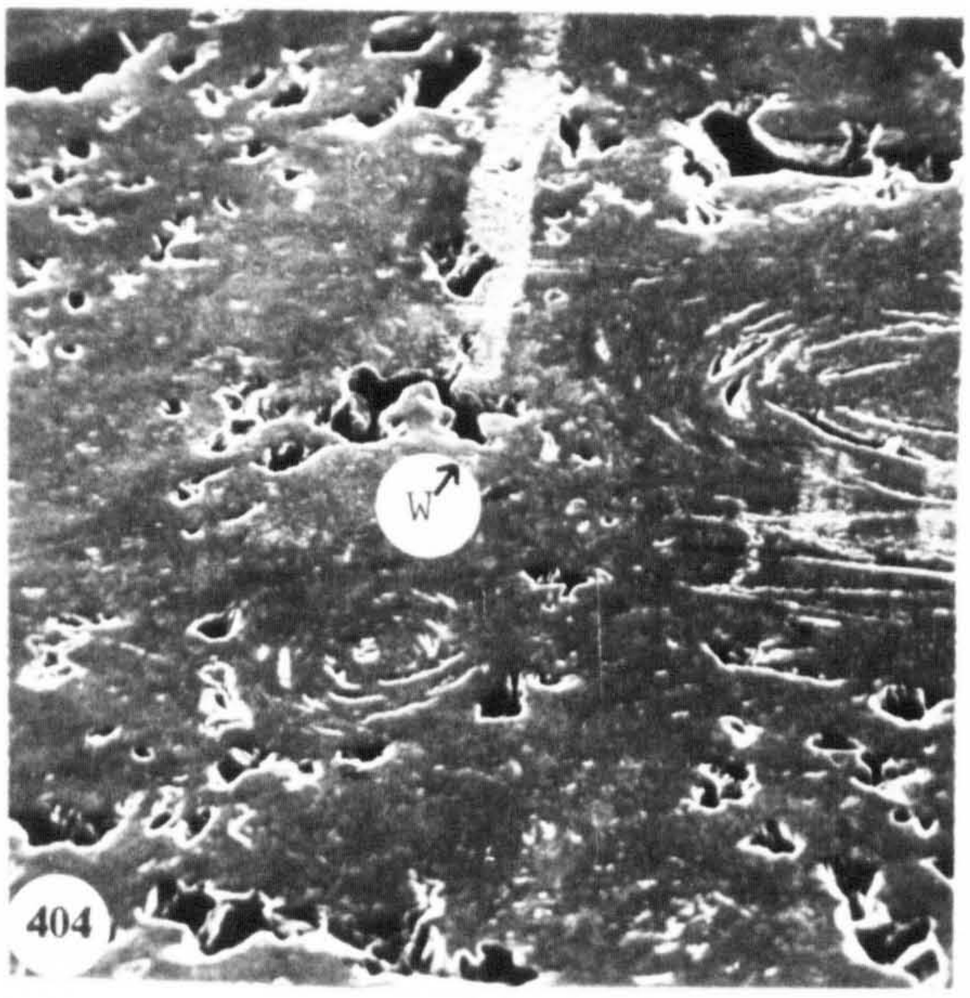


AGLMP GRAPHITE

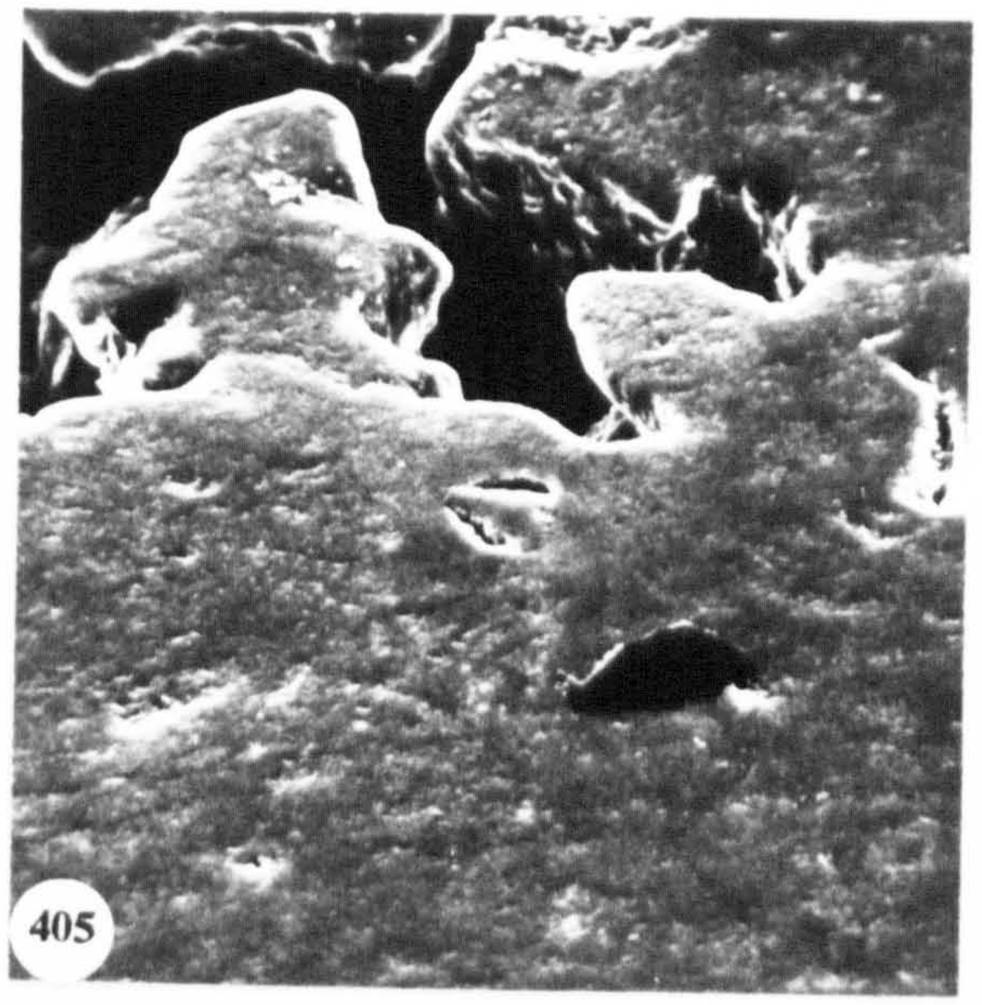


AGLMP GRAPHITE

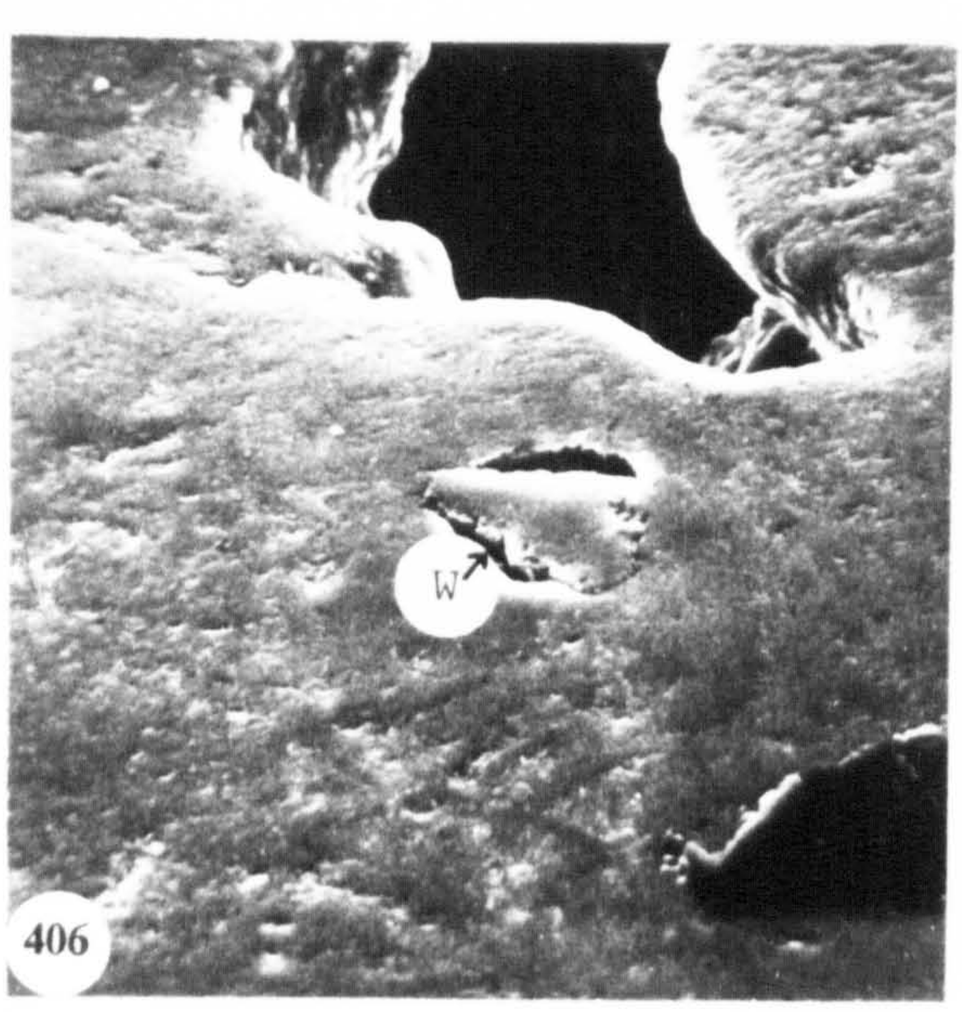
Figures 401 to 403. Optical micrographs of AGLMP Graphite (AG10) before (Figure 401) and after gasification in carbon dioxide at 873 K for 16 hours (Figure 402) and 873 K for 80 hours (Figure 403). Weight losses 0.67% and 4.29%.



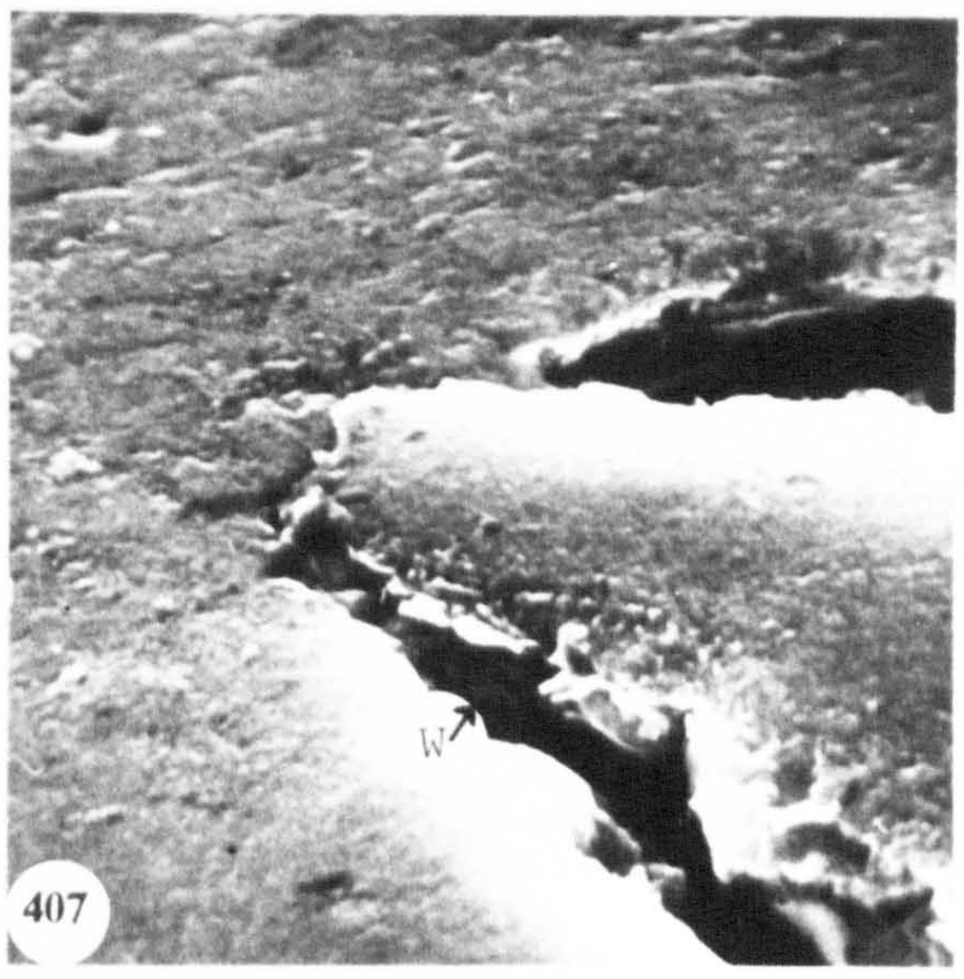
AGLMP GRAPHITE 100 μm



AGLMP GRAPHITE 40 μm

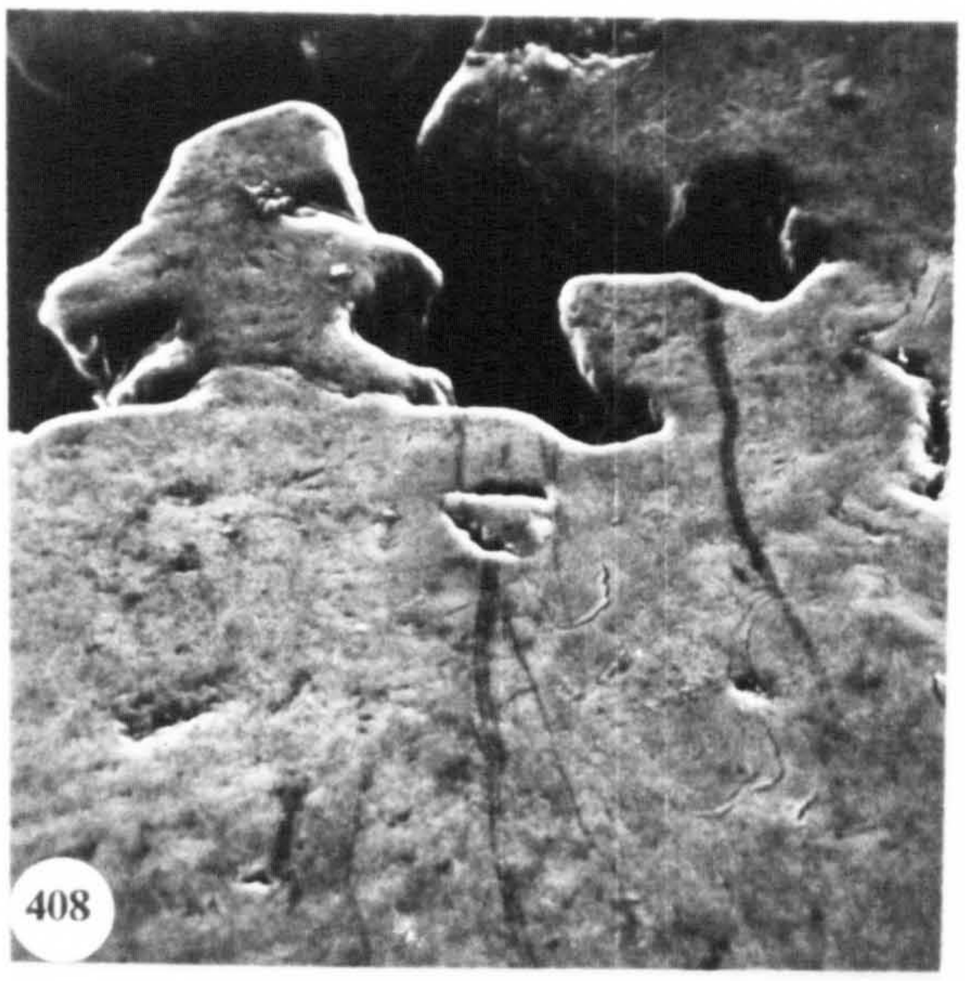


AGLMP GRAPHITE 10 μm

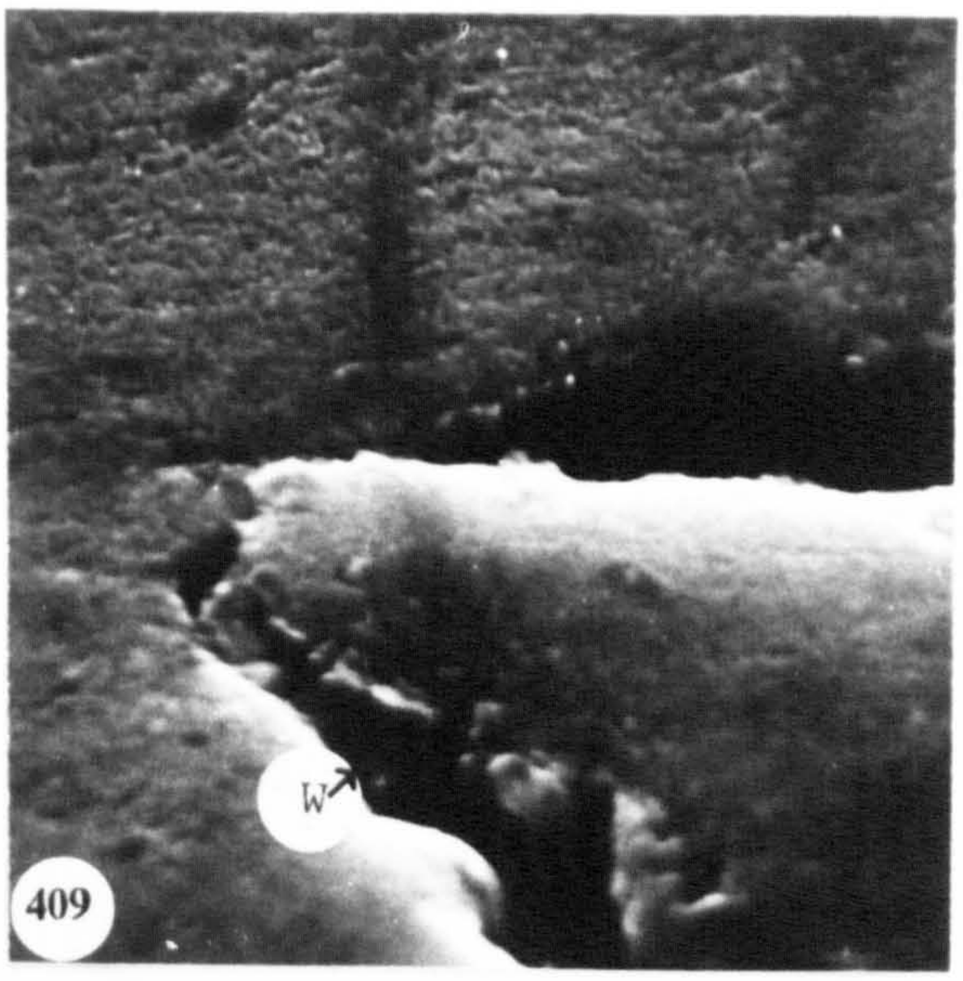


AGLMP GRAPHITE 2 μm

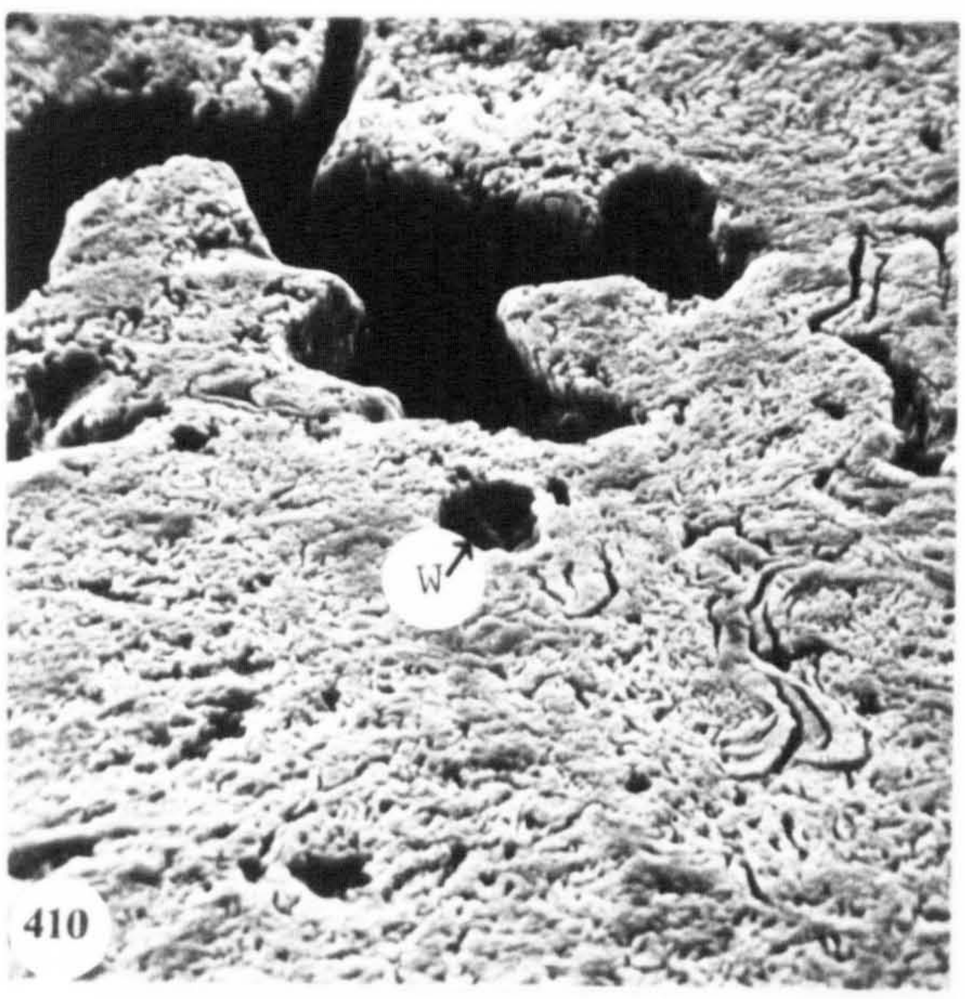
Figures 404 to 407. Scanning electron micrographs (stereoscan) of AGLMP Graphite (AG10) before gasification.



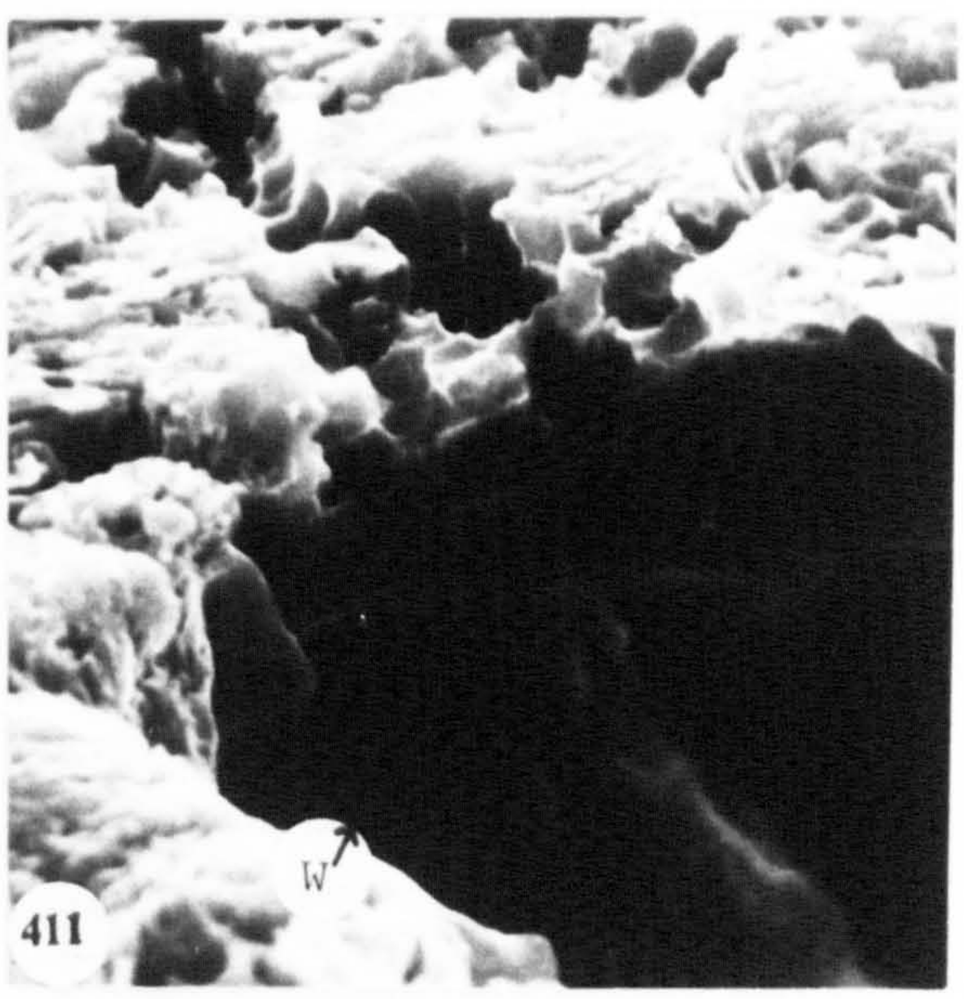
AGLMP GRAPHITE 40 μm



AGLMP GRAPHITE 2 μm

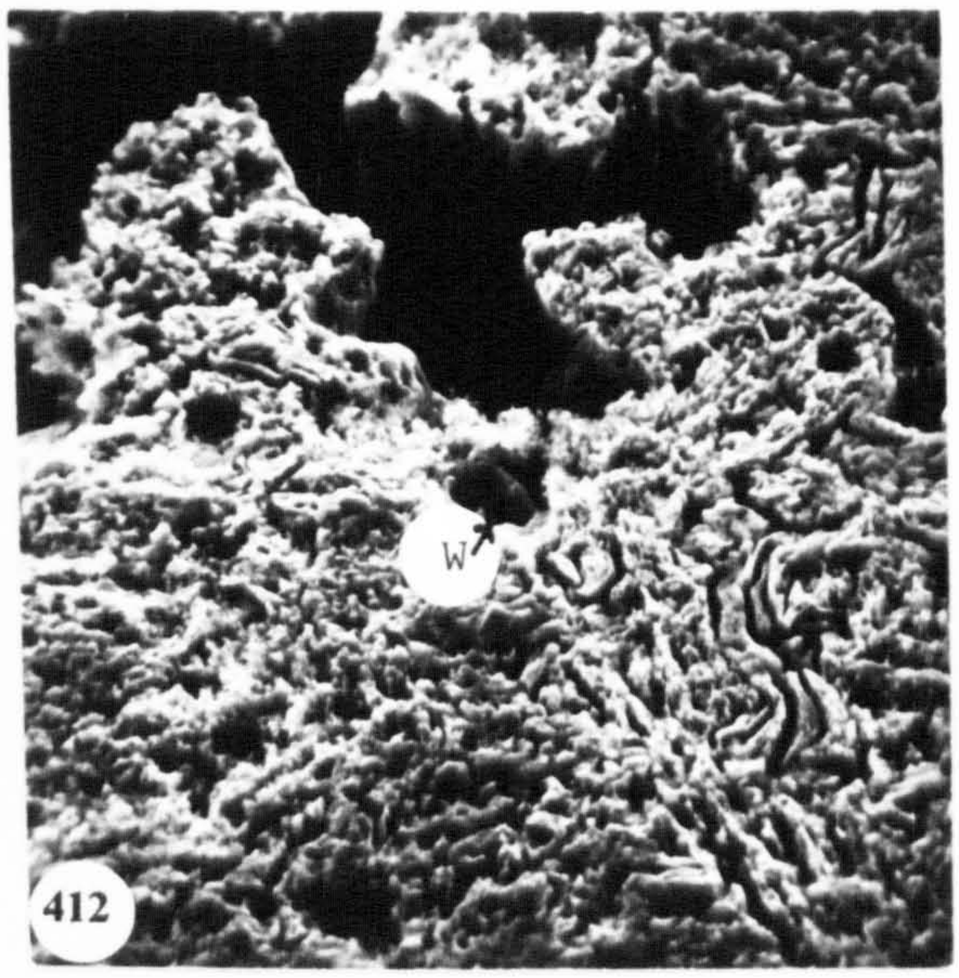


AGLMP GRAPHITE 40 μm

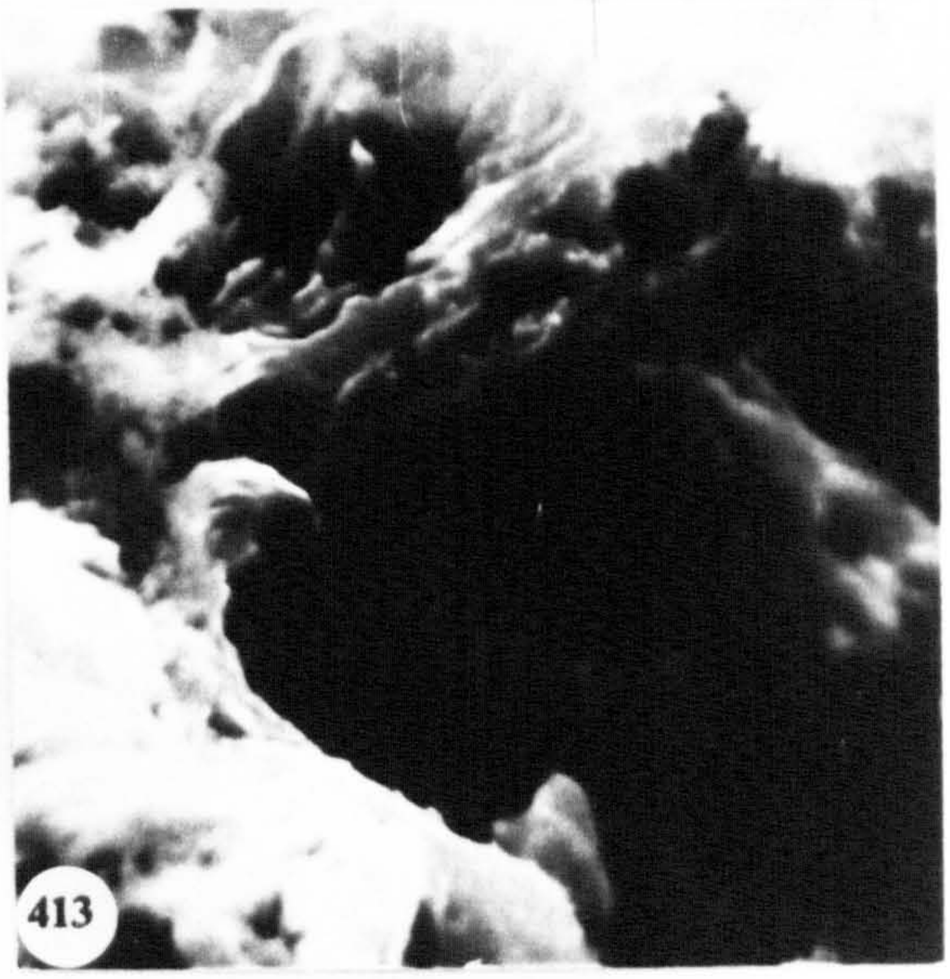


AGLMP GRAPHITE 2 μm

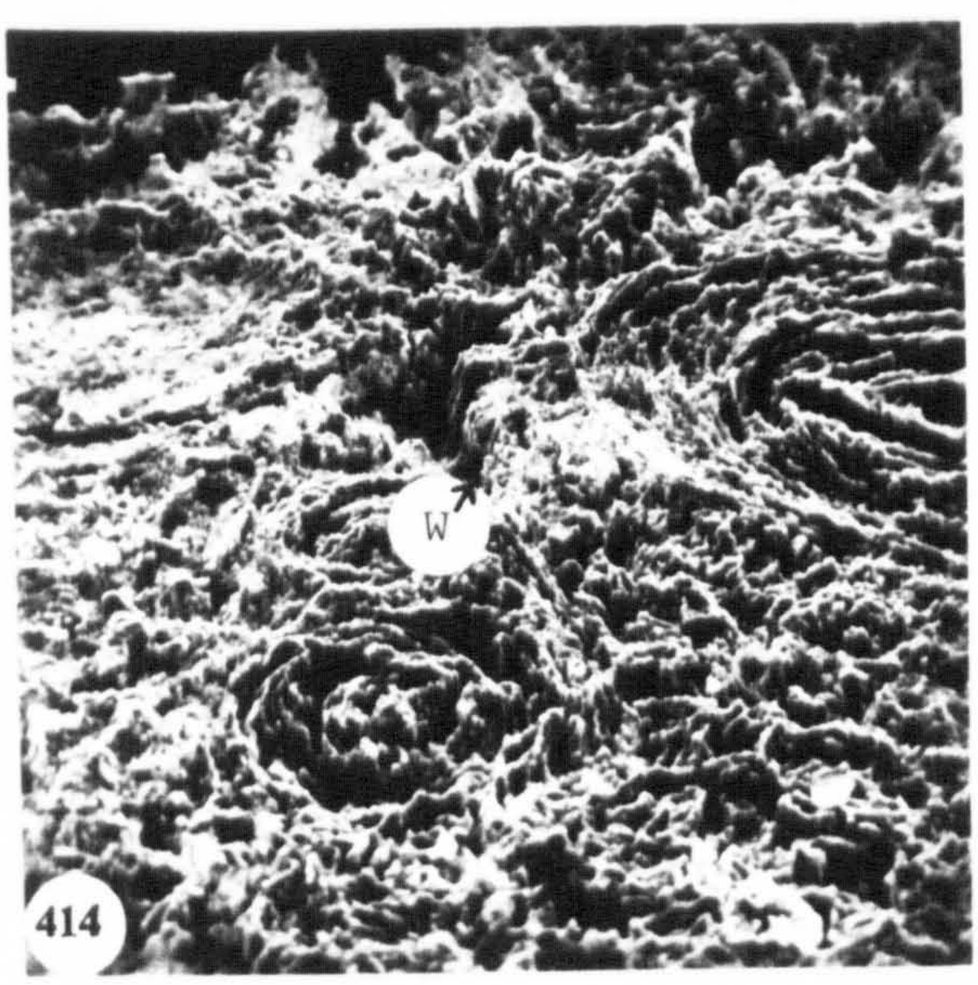
Figures 408 to 411. Scanning electron micrographs (stereoscan) of AGLMP Graphite (AG10) after gasification in carbon dioxide at 873 K for 16 hours (Figures 408 and 409) and 873 K for 80 hours (Figures 410 and 411). Weight losses 0.67% and 4.29%.



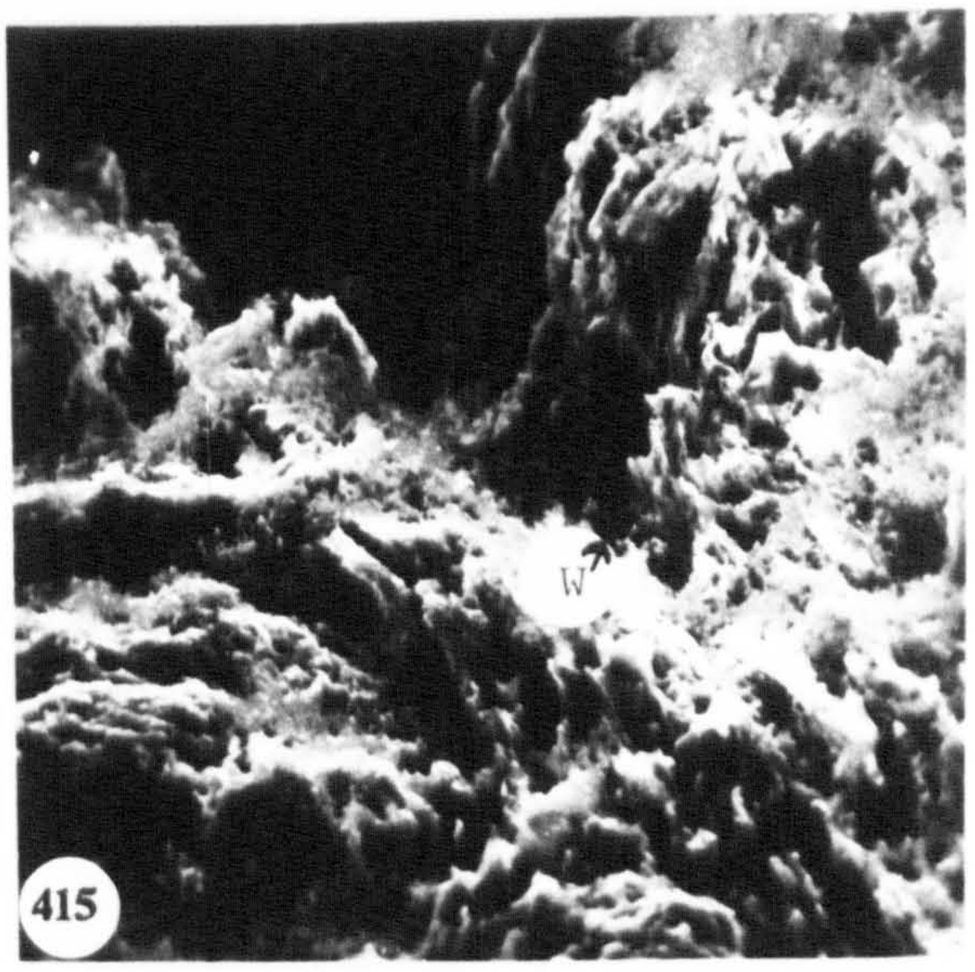
AGLMP GRAPHITE 40 μm



AGLMP GRAPHITE 2 μm

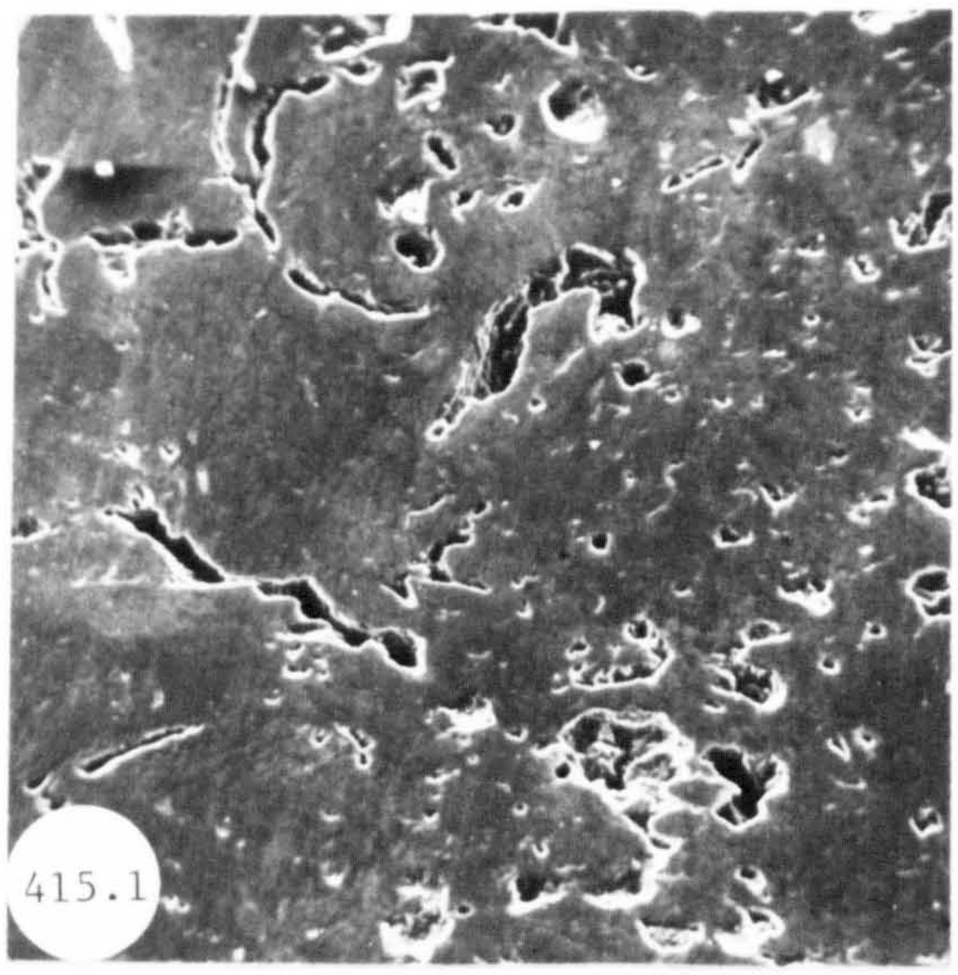


AGLMP GRAPHITE 100 μm

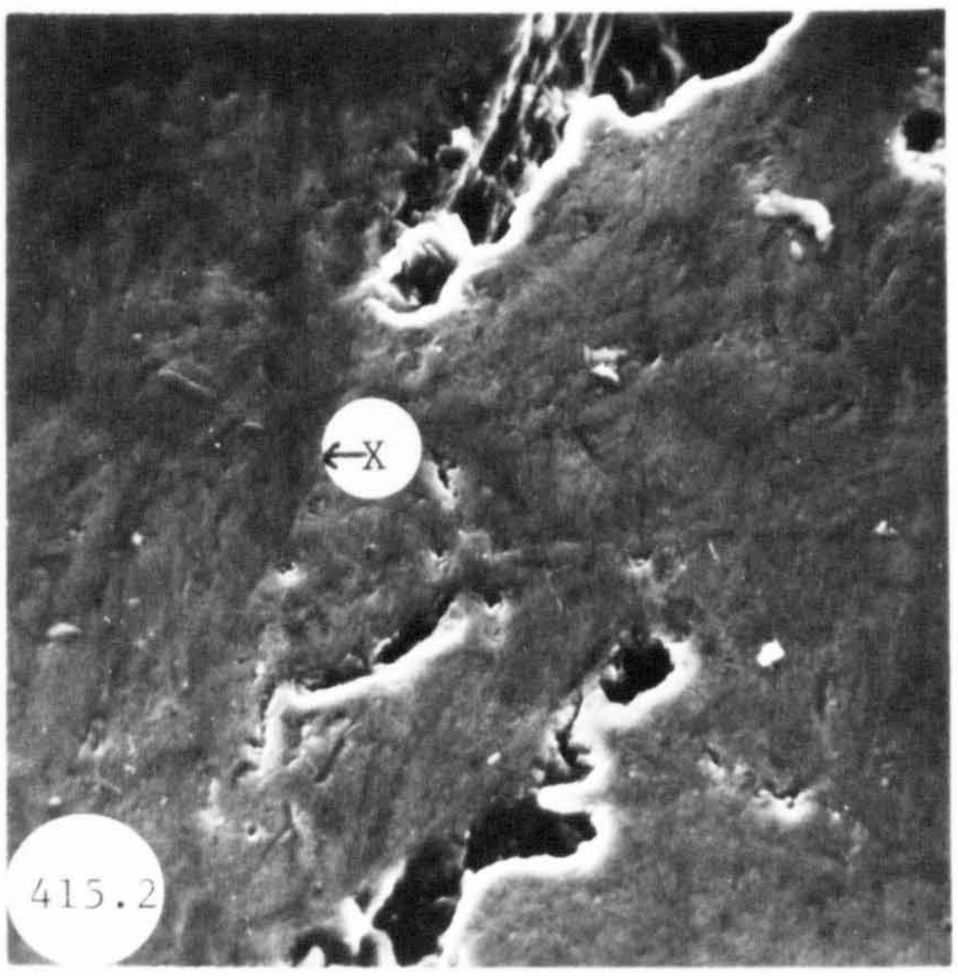


AGLMP GRAPHITE 40 μm

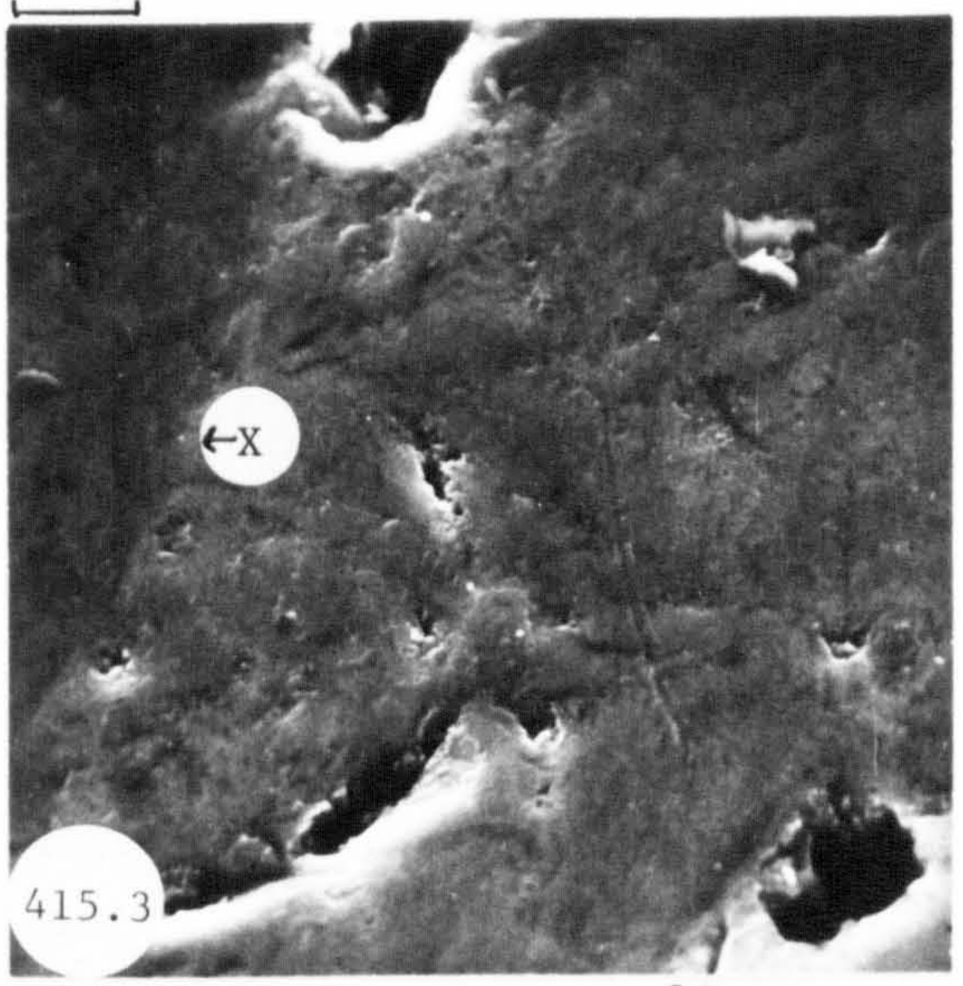
Figures 412 to 415. Scanning electron micrographs (stereoscan) of AGLMP Graphite (AG10) after gasification in carbon dioxide at 973 K (Figures 412 and 413) and 1073 K (Figures 414 and 415) for 96 hours each. Weight losses 1.83% and 5.23%.



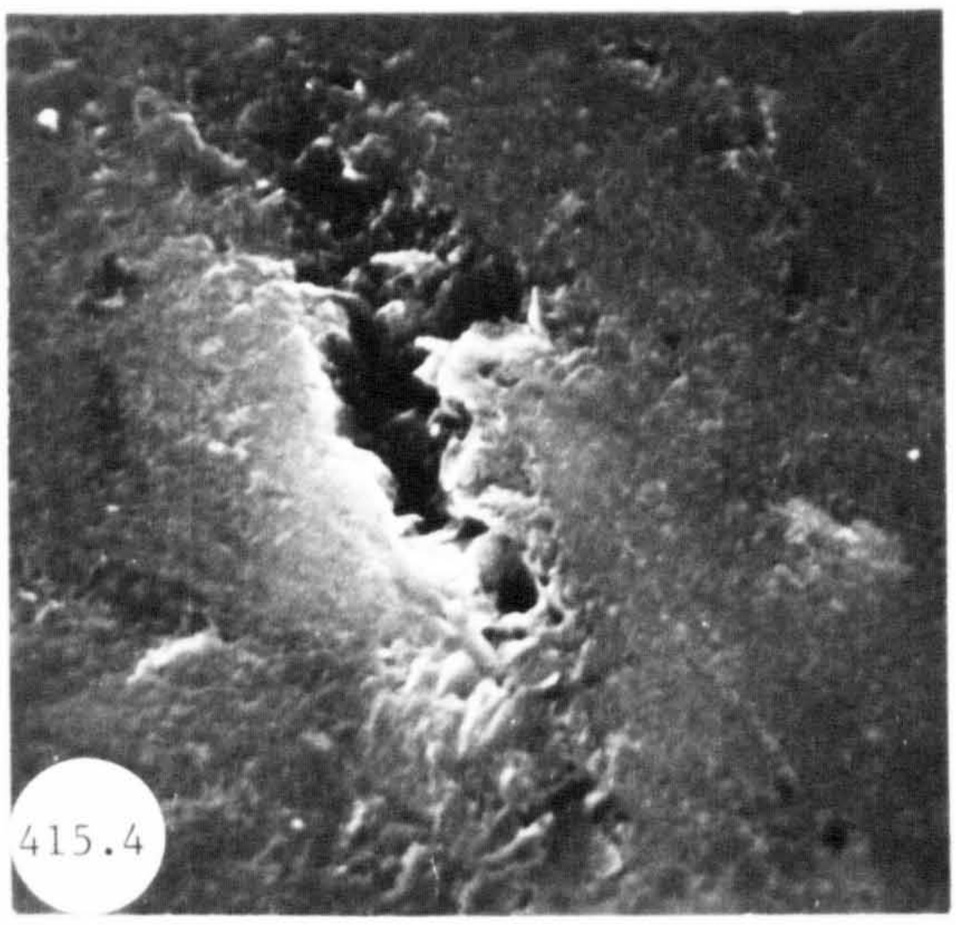
LIMA GRAPHITE 100 µm



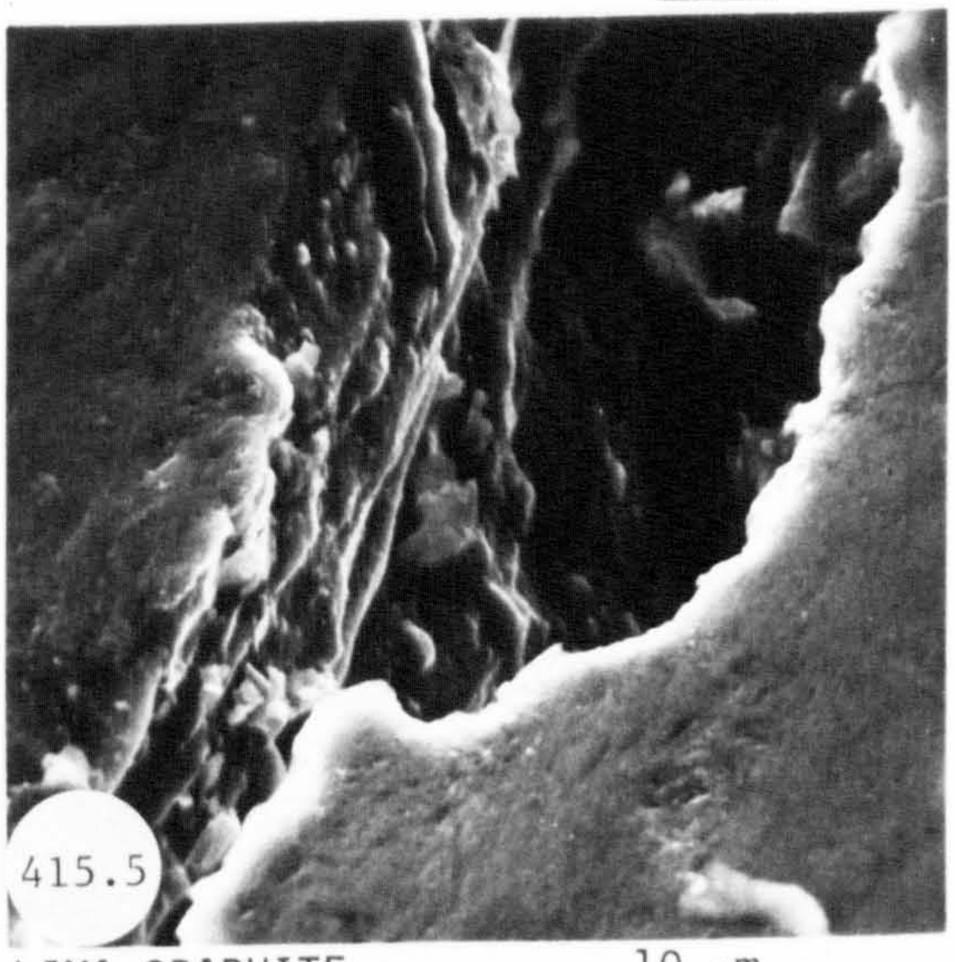
LIMA GRAPHITE 20 µm



LIMA GRAPHITE 10 µm

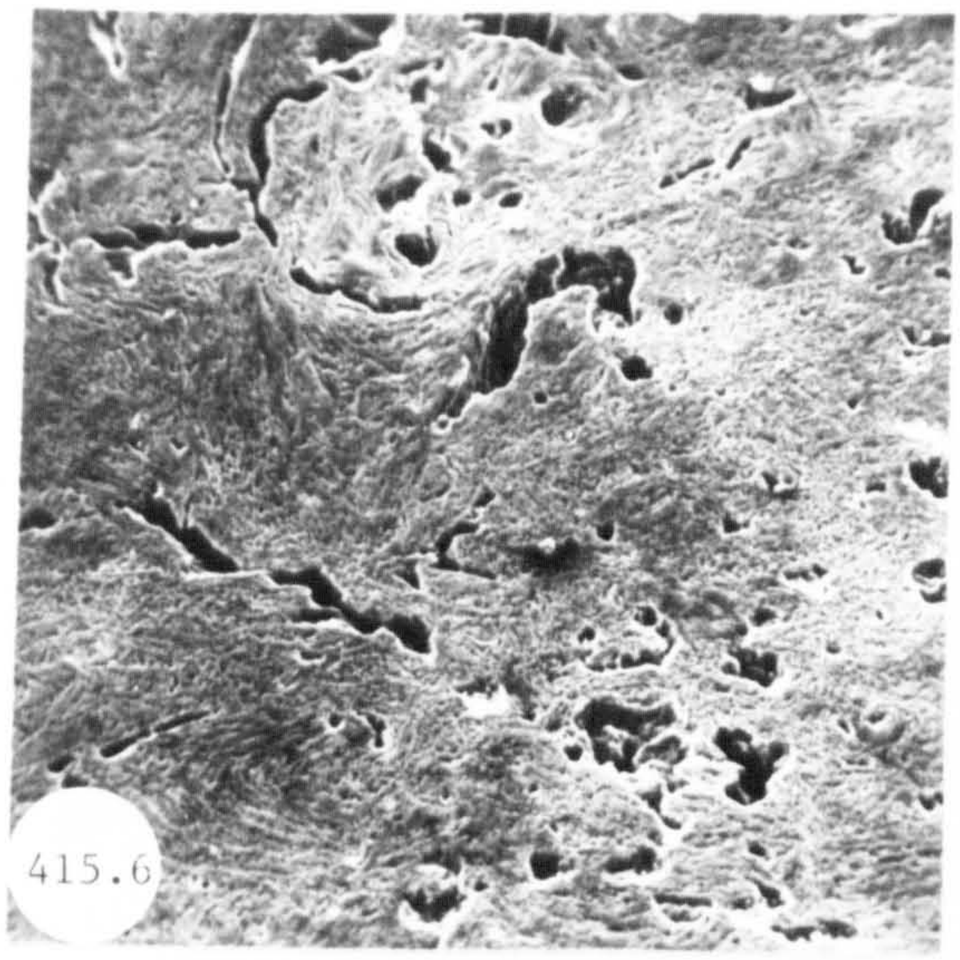


LIMA GRAPHITE 2 µm

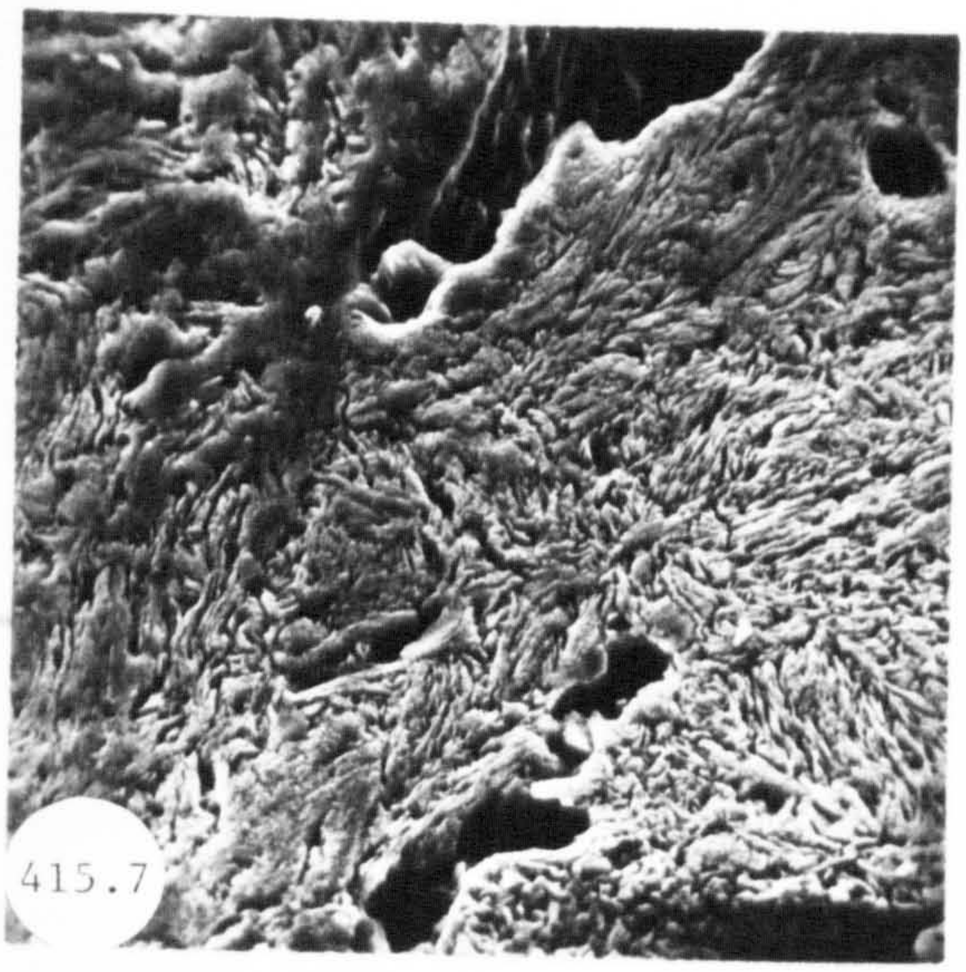


LIMA GRAPHITE 10 µm

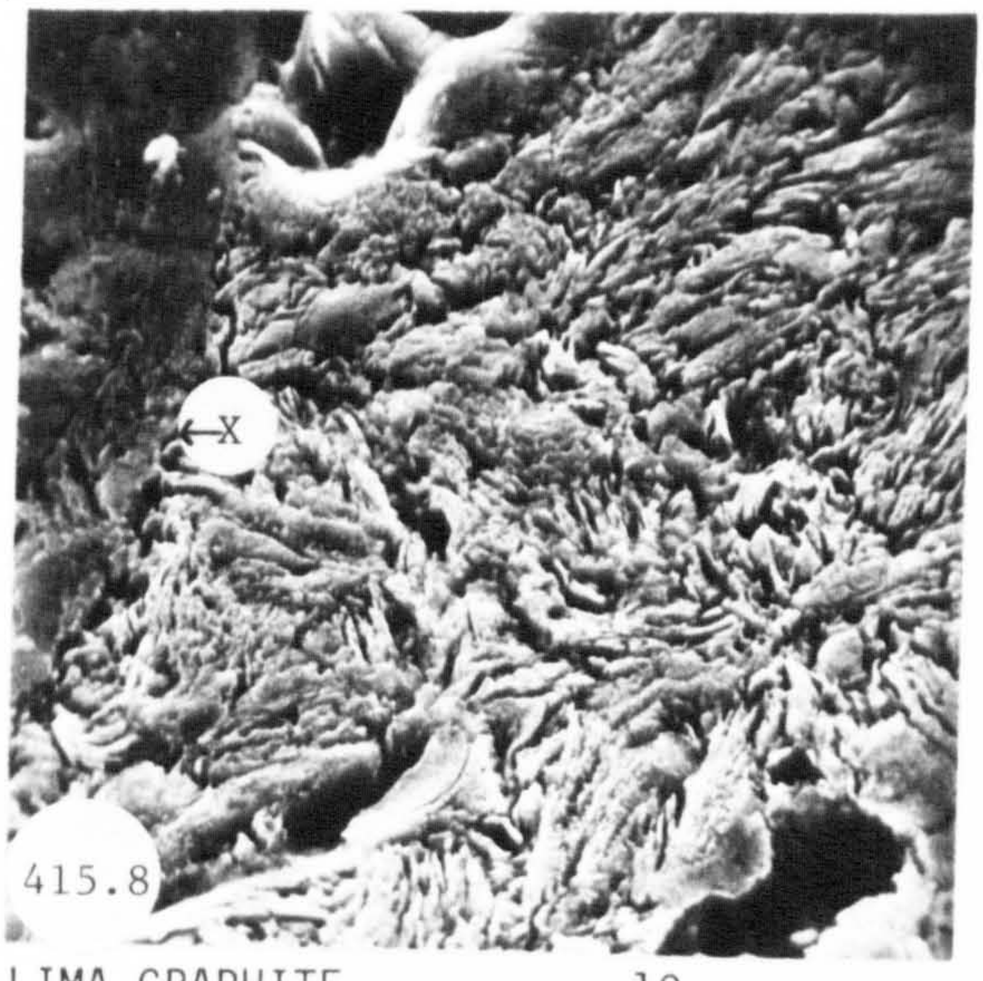
Figures 415.1 to 415.5. Scanning electron micrographs (stereoscan) of Lima Graphite (LG19) before gasification.



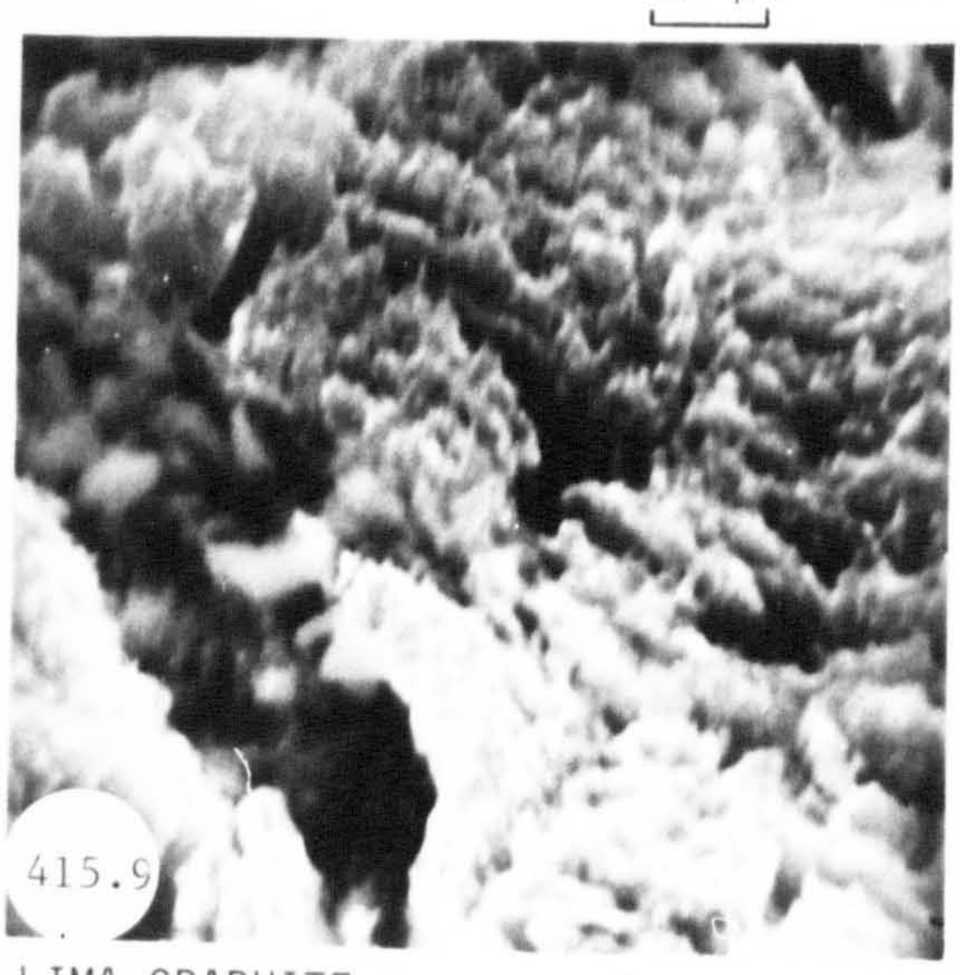
LIMA GRAPHITE 100 µm



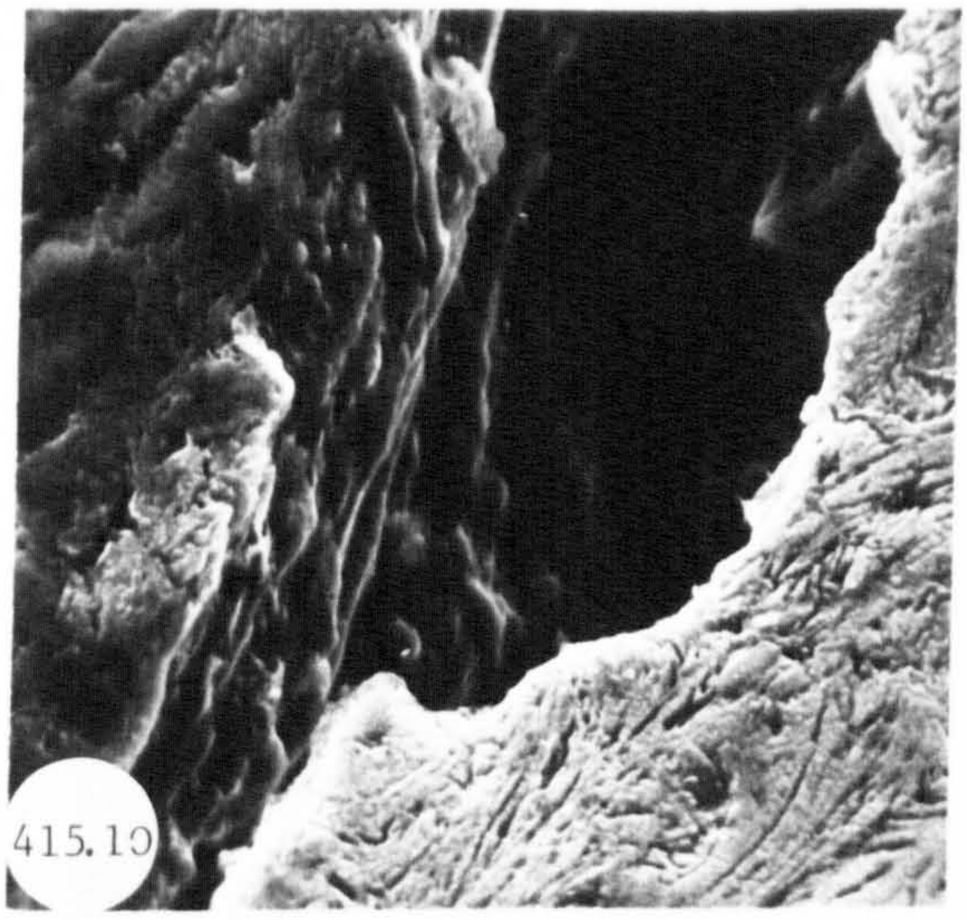
LIMA GRAPHITE 20 µm



LIMA GRAPHITE 10 µm

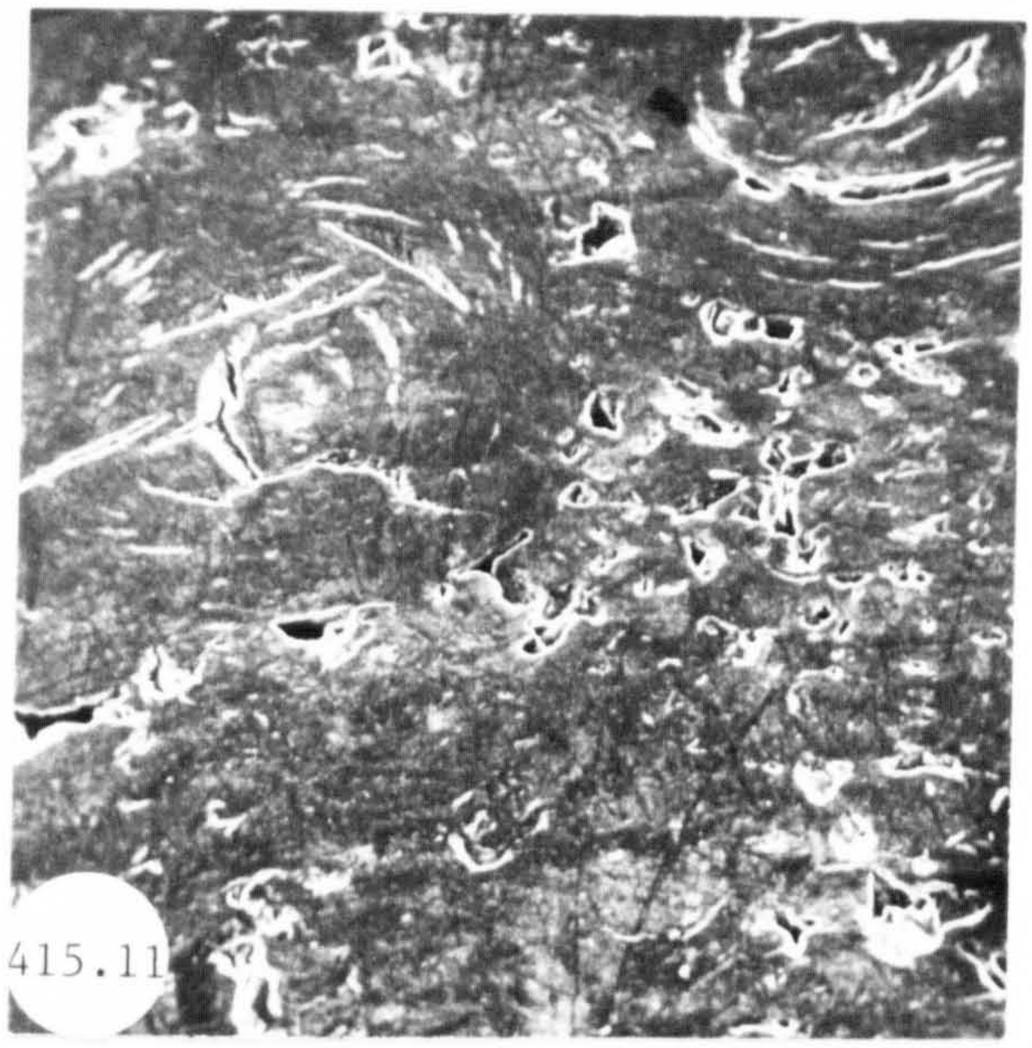


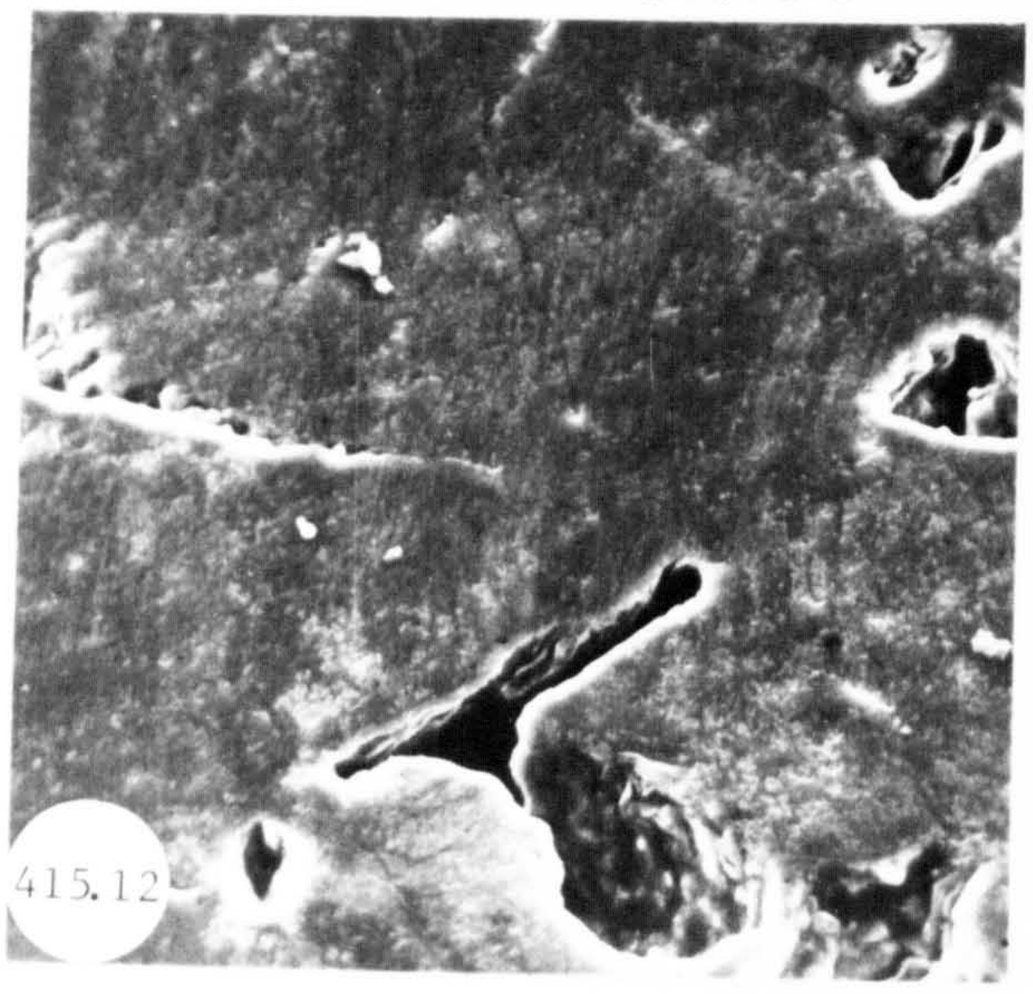
LIMA GRAPHITE 2 µm

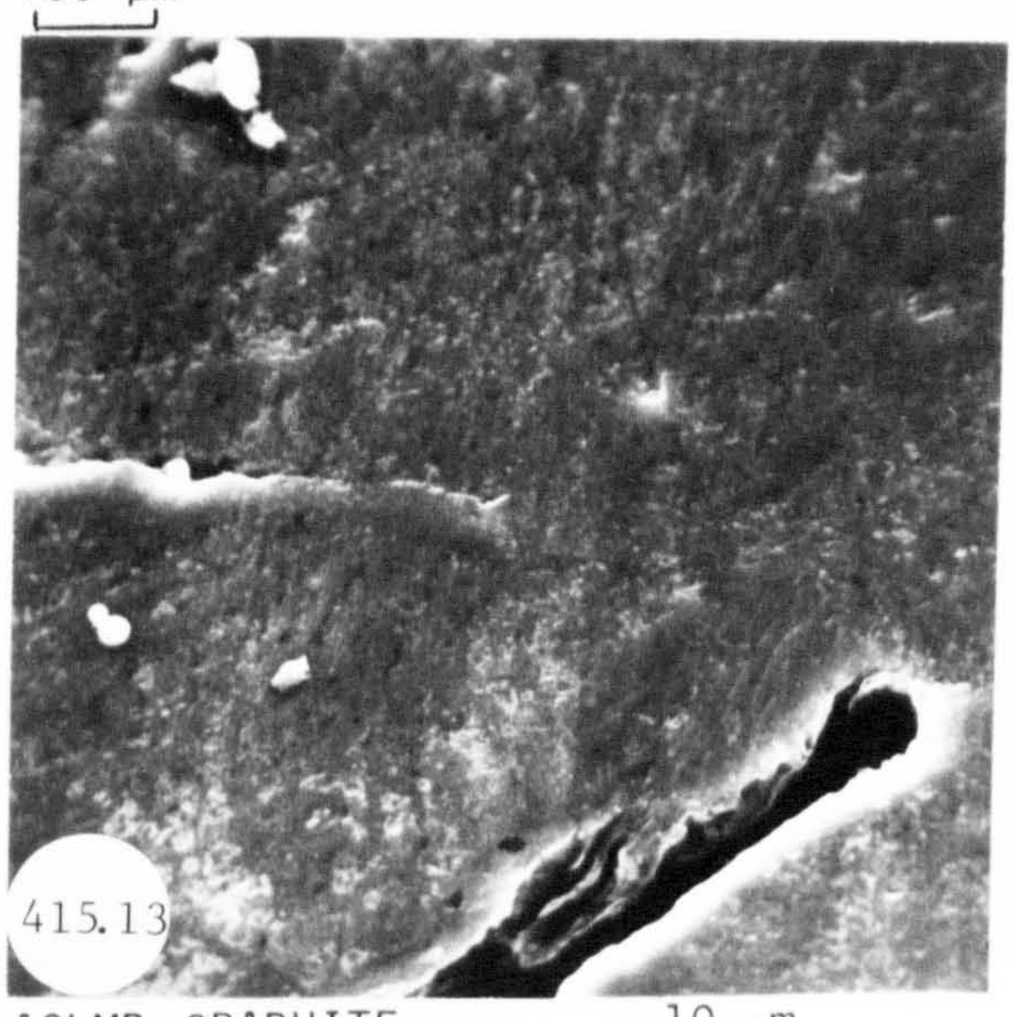


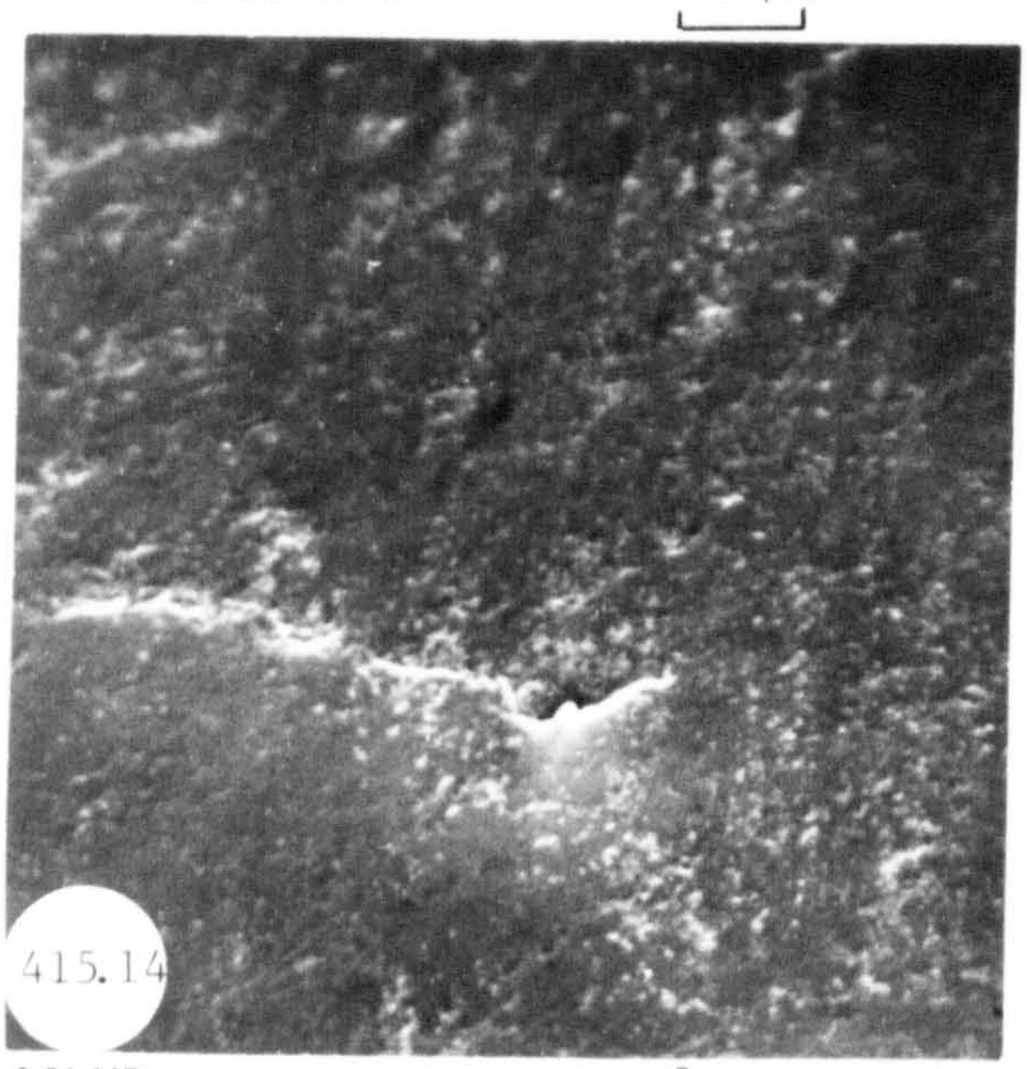
LIMA GRAPHITE 10 µm

Figures 415.6 to 415.10. Scanning electron micrographs (stereoscan) of Lima Graphite (LG19) after gasification in carbon dioxide at 913 K for 16 hours. Weight loss 1.48%.



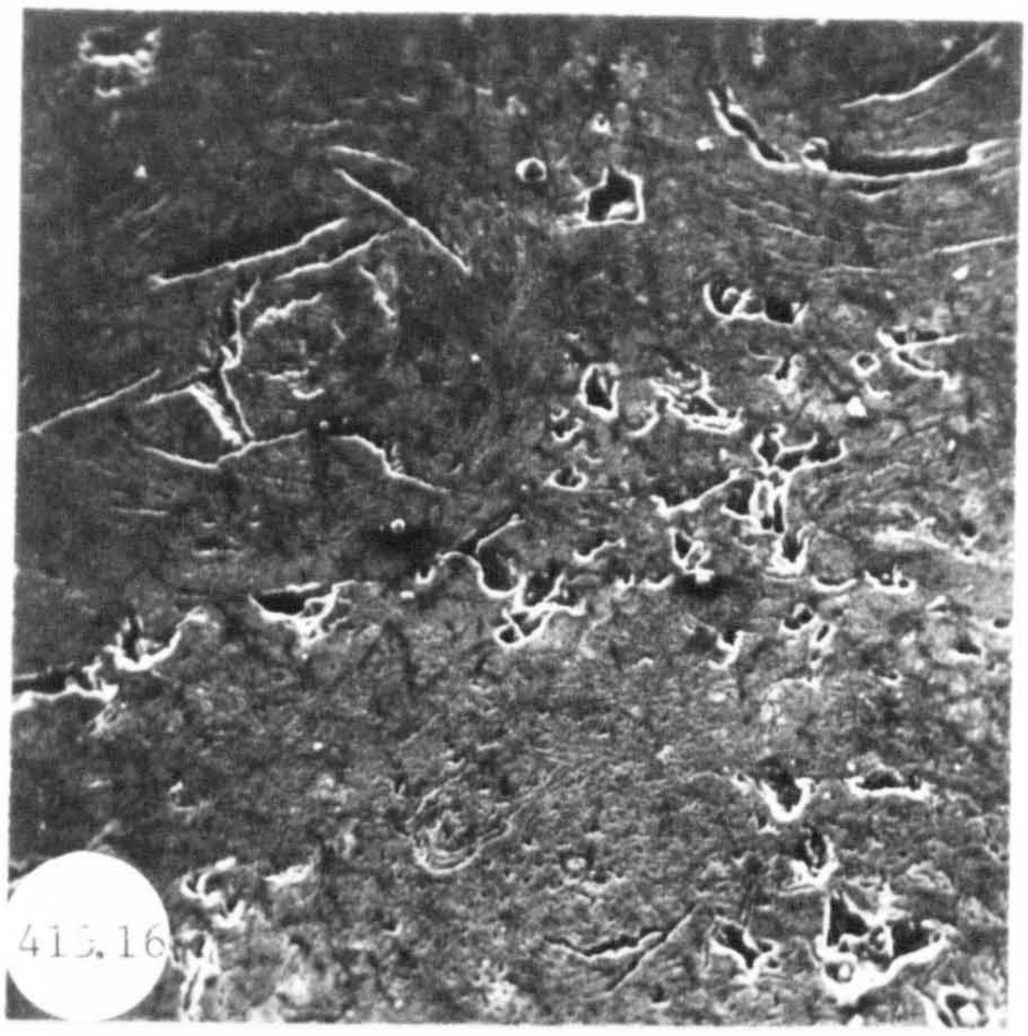


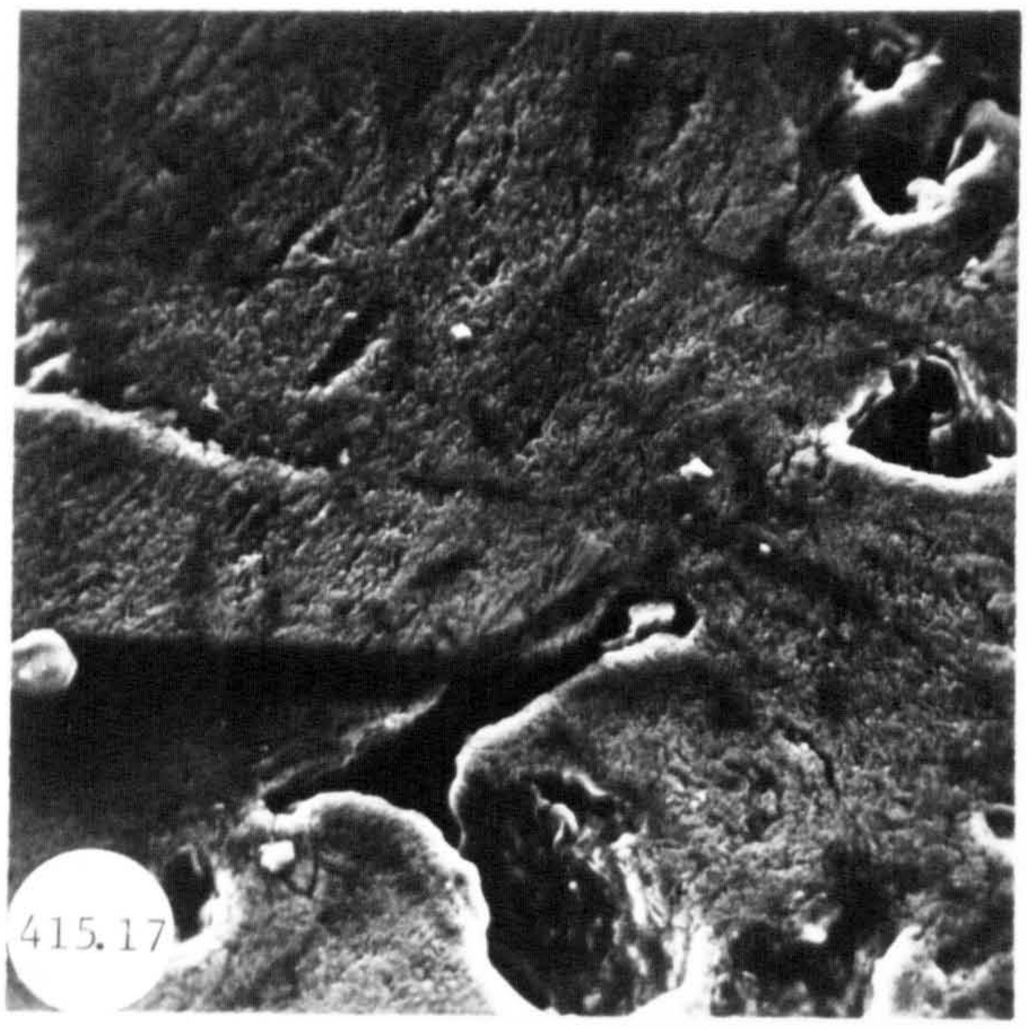


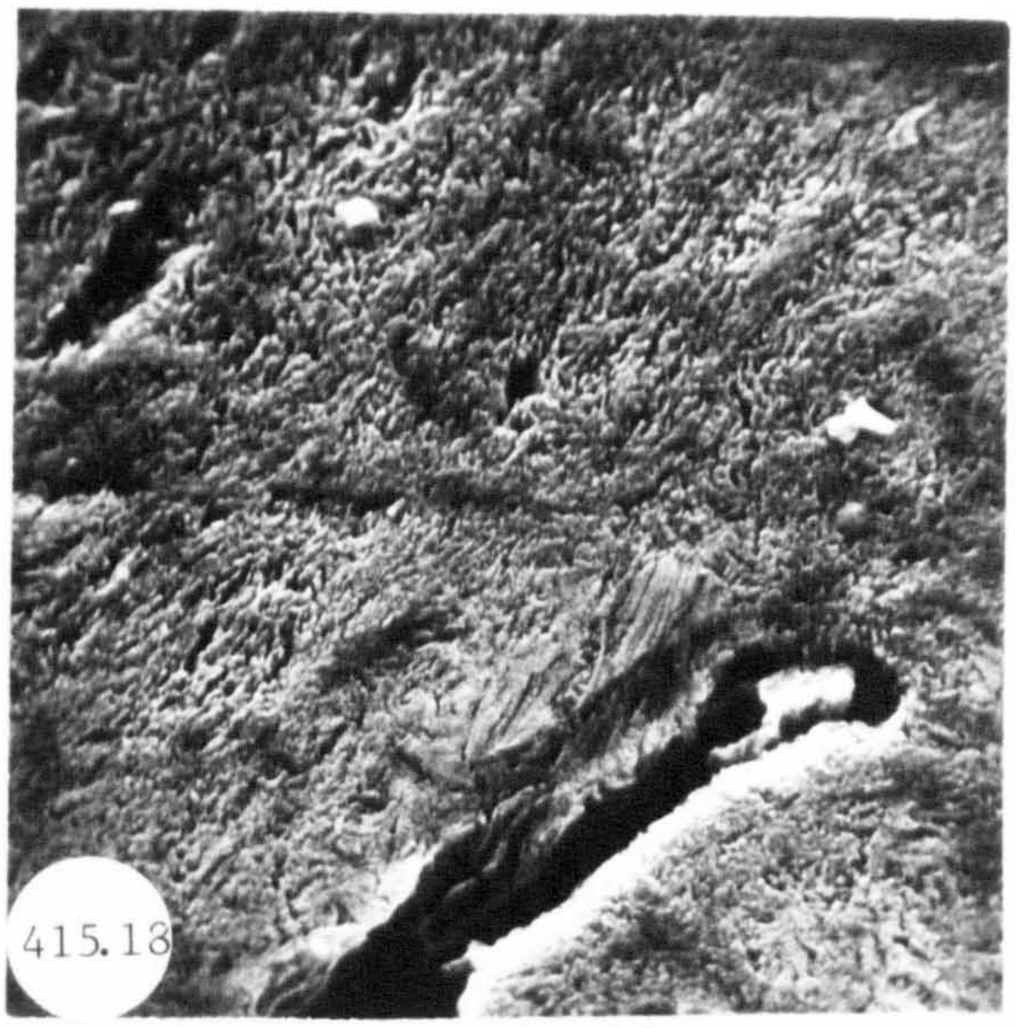


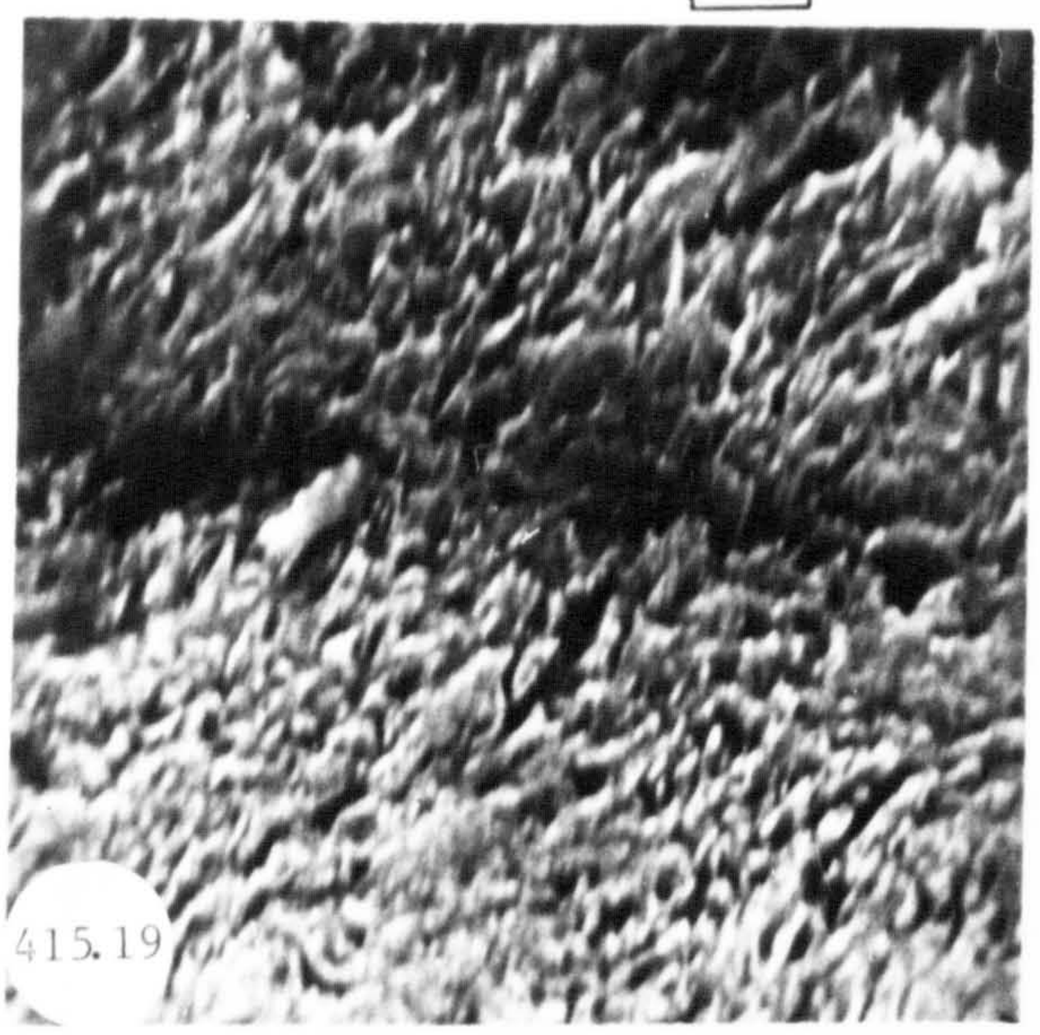


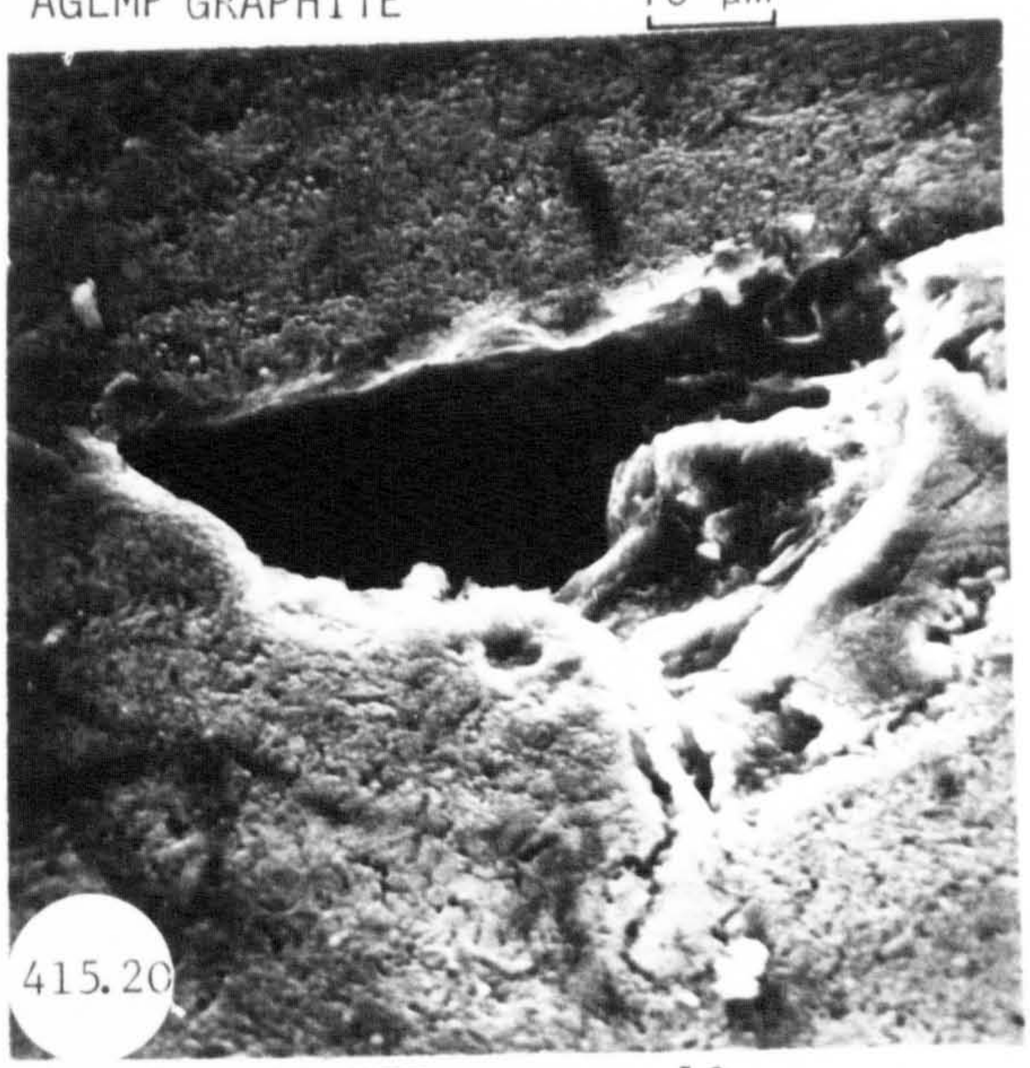
Figures 415.11 to 415.15. Scanning electron micrographs (stereoscan) of AGLMP Graphite (AG11) before gasification.





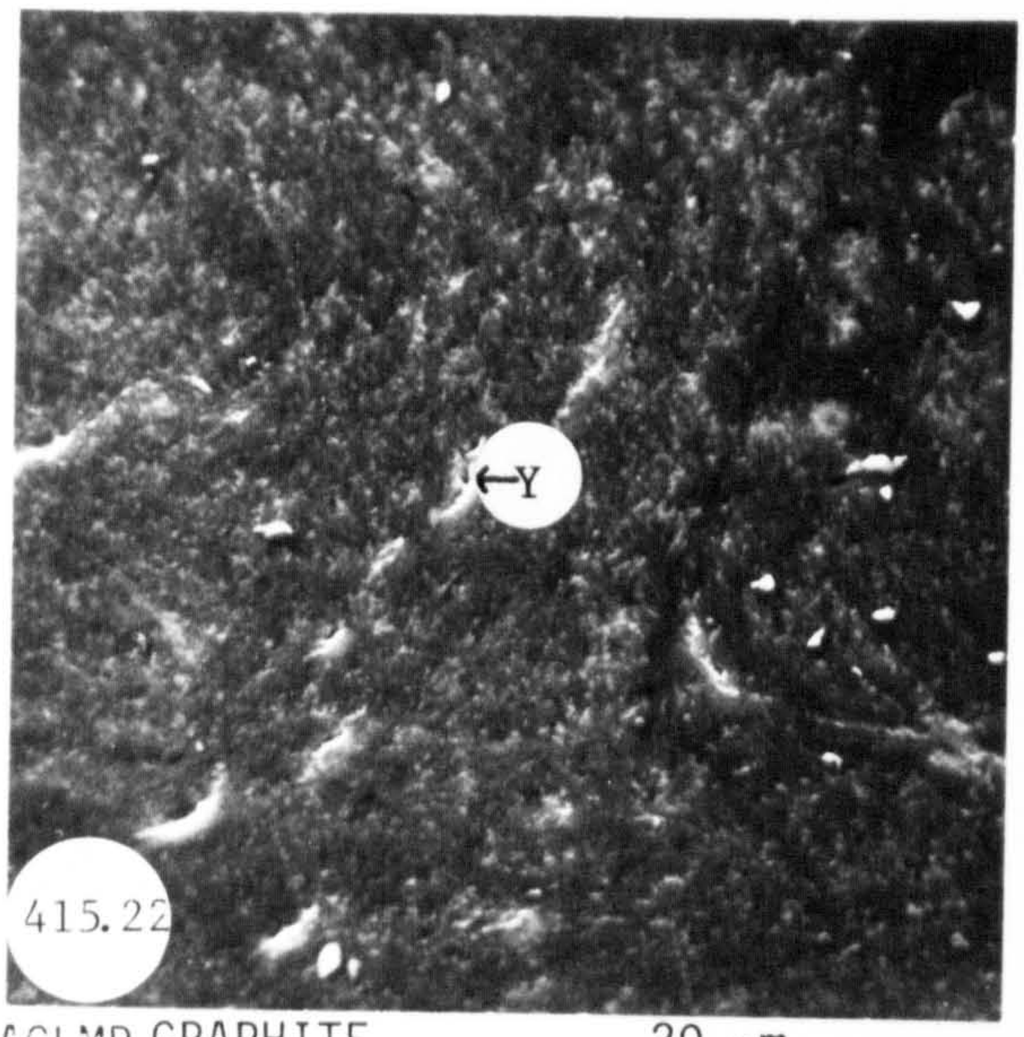






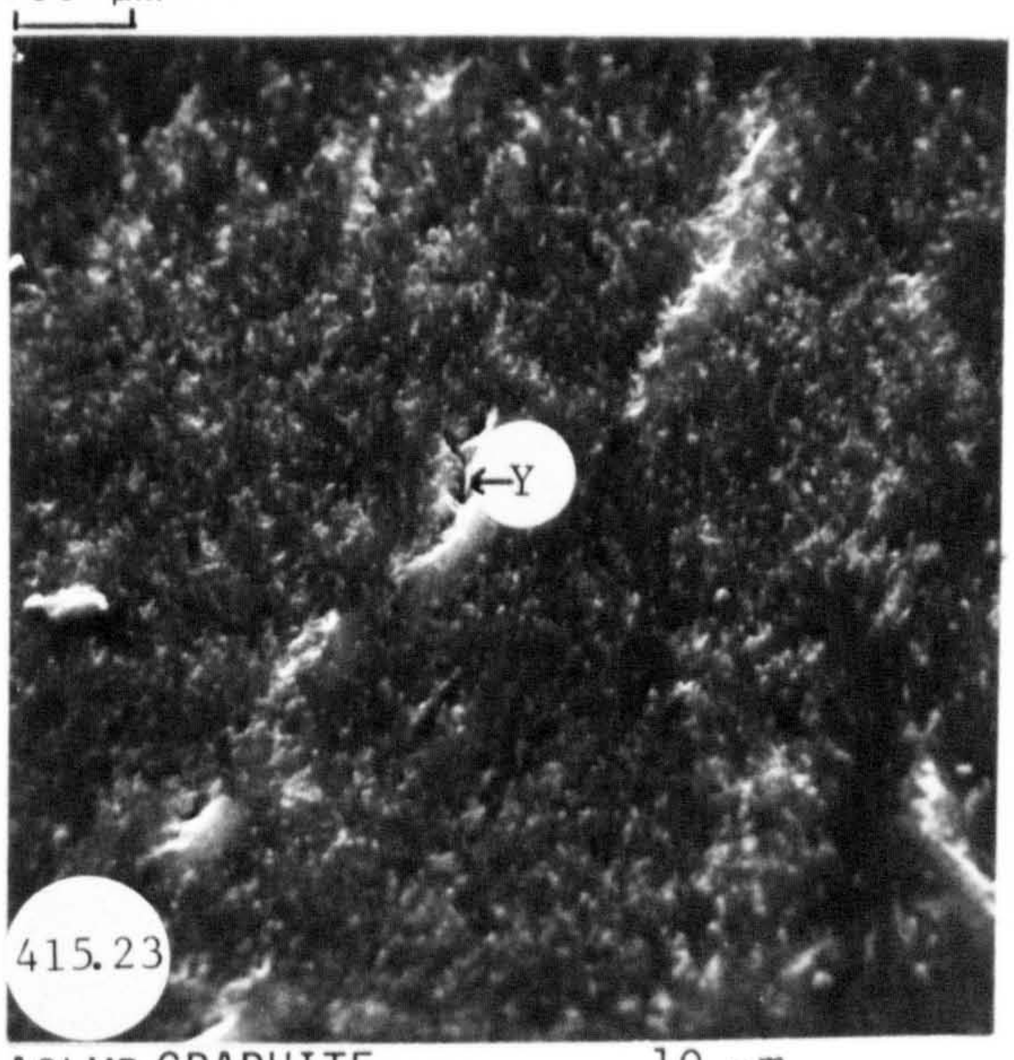
Figures 415.16 to 415.20. Scanning electron micrographs (stereoscan) of AGLMP Graphite (AG11) after gasification in carbon dioxide at 913 K for 16 hours. Weight loss 0.42%.

AGLMP GRAPHITE

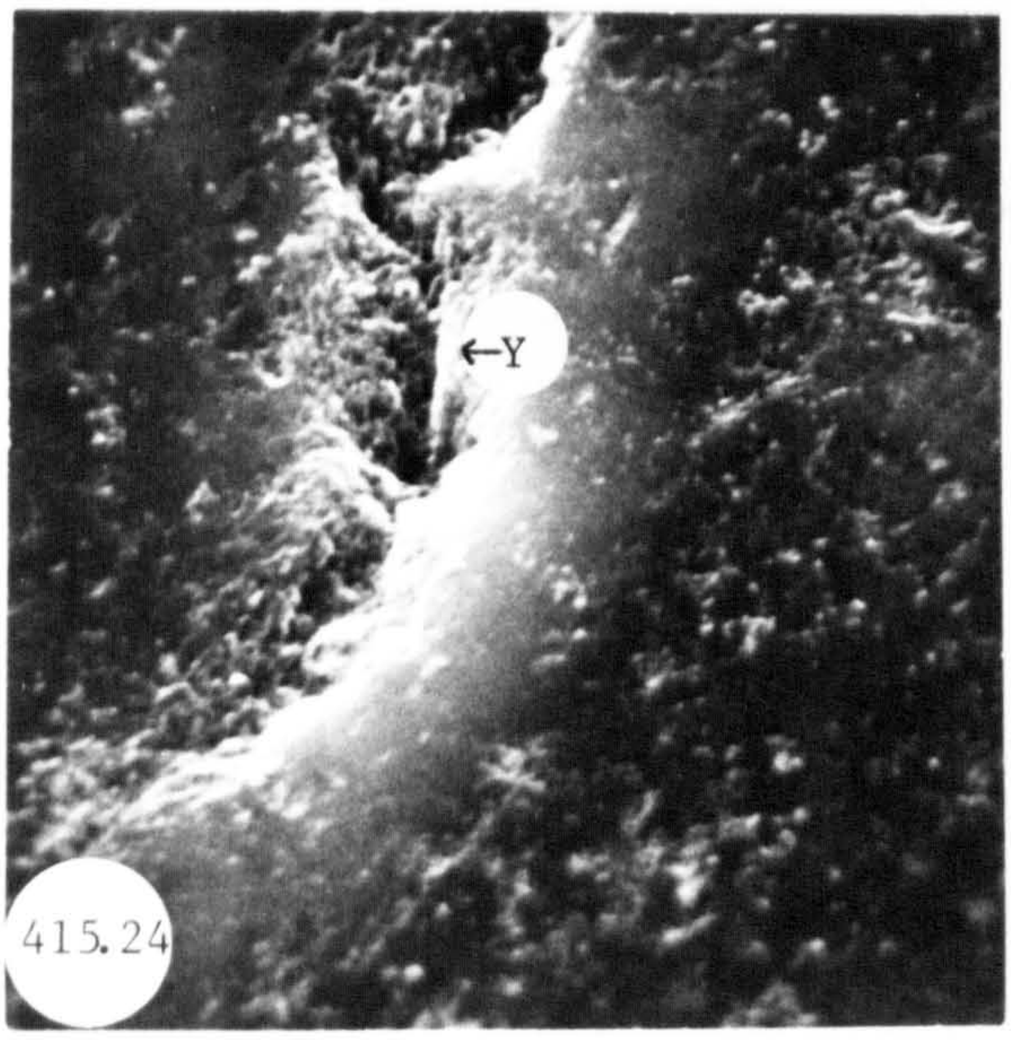


AGLMP GRAPHITE 20 μm

100 μm



AGLMP GRAPHITE 10 μm

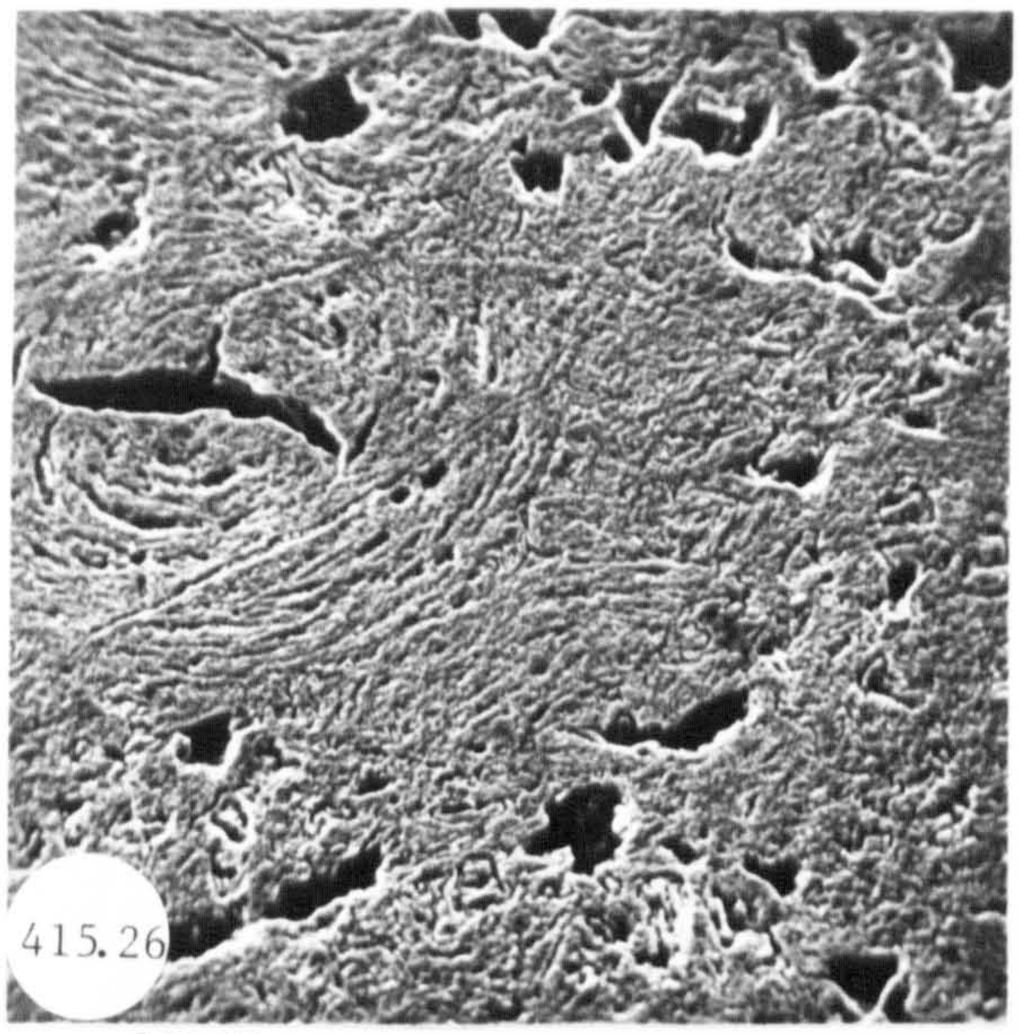


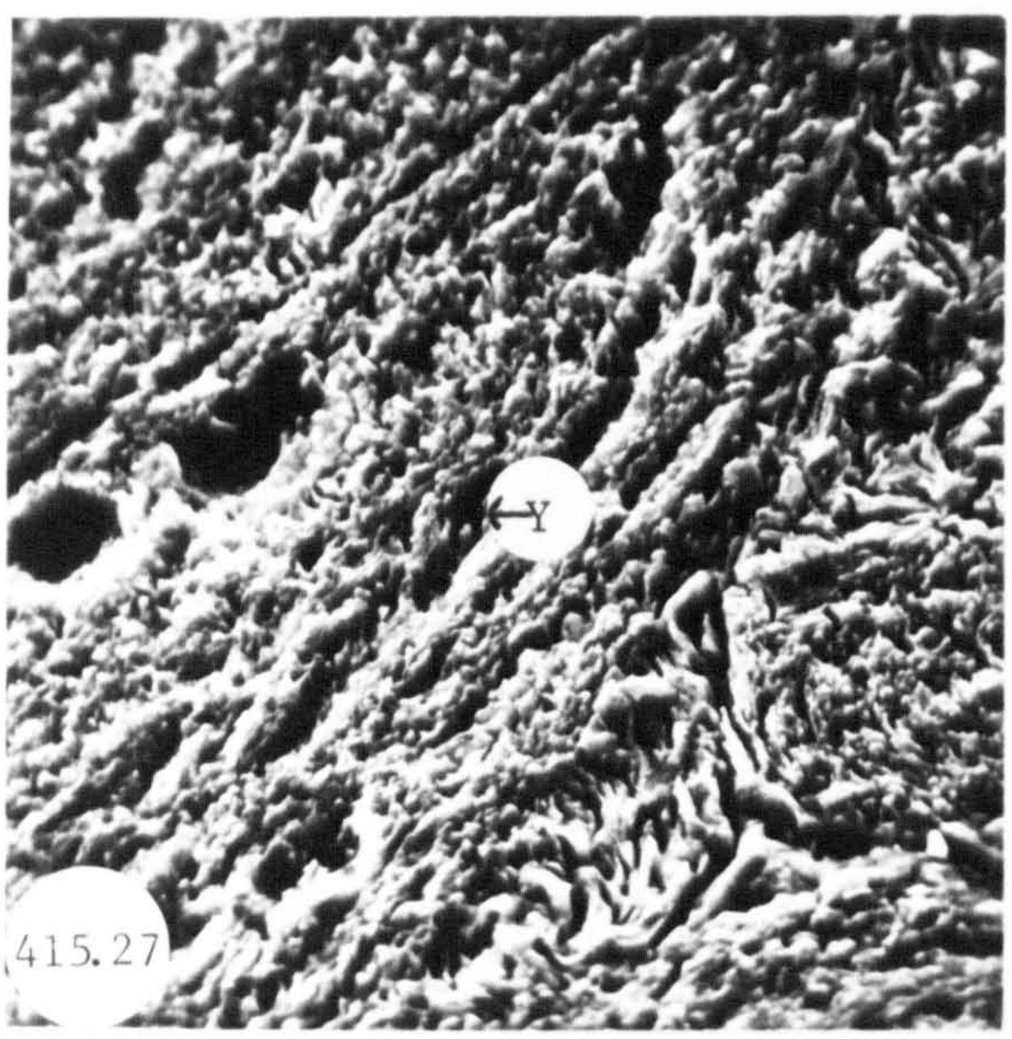
AGLMP GRAPHITE 2 μm

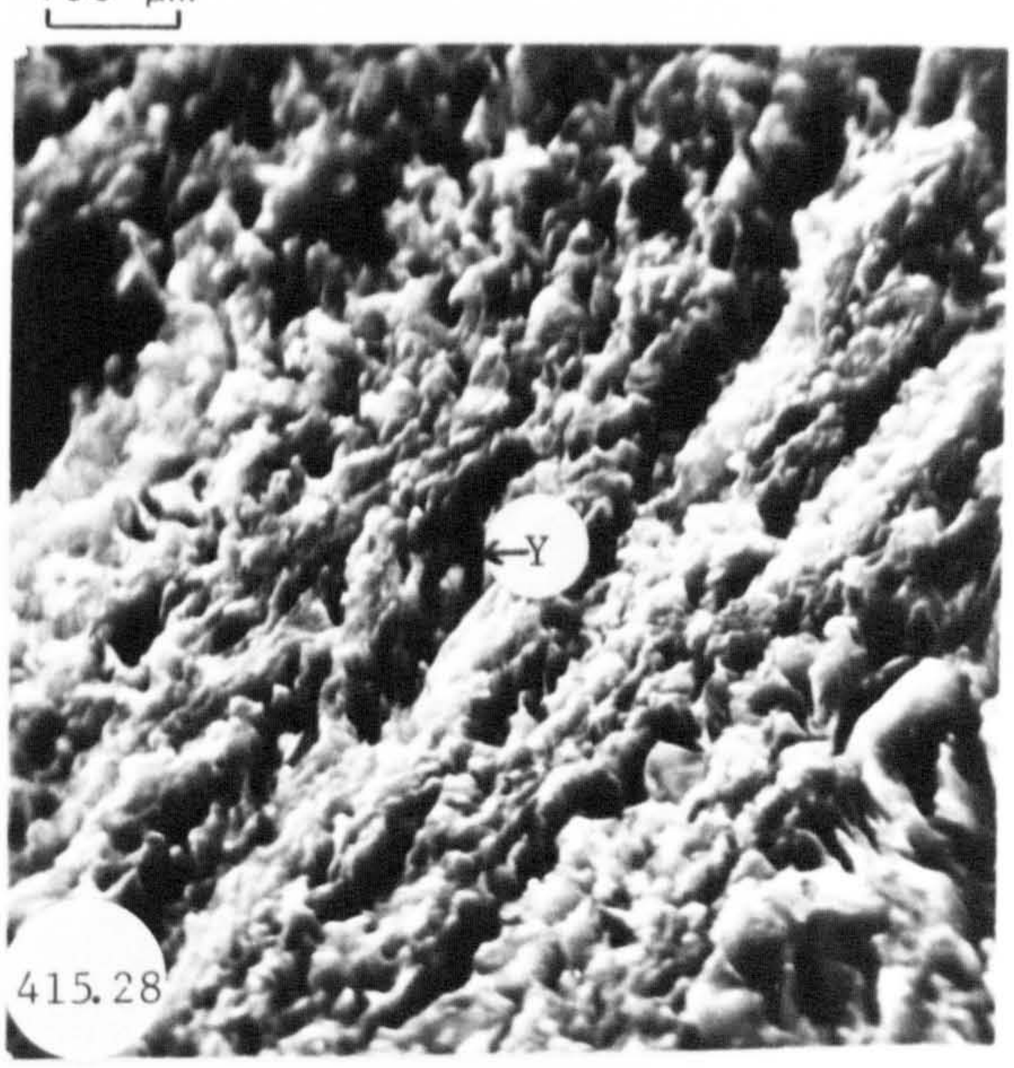


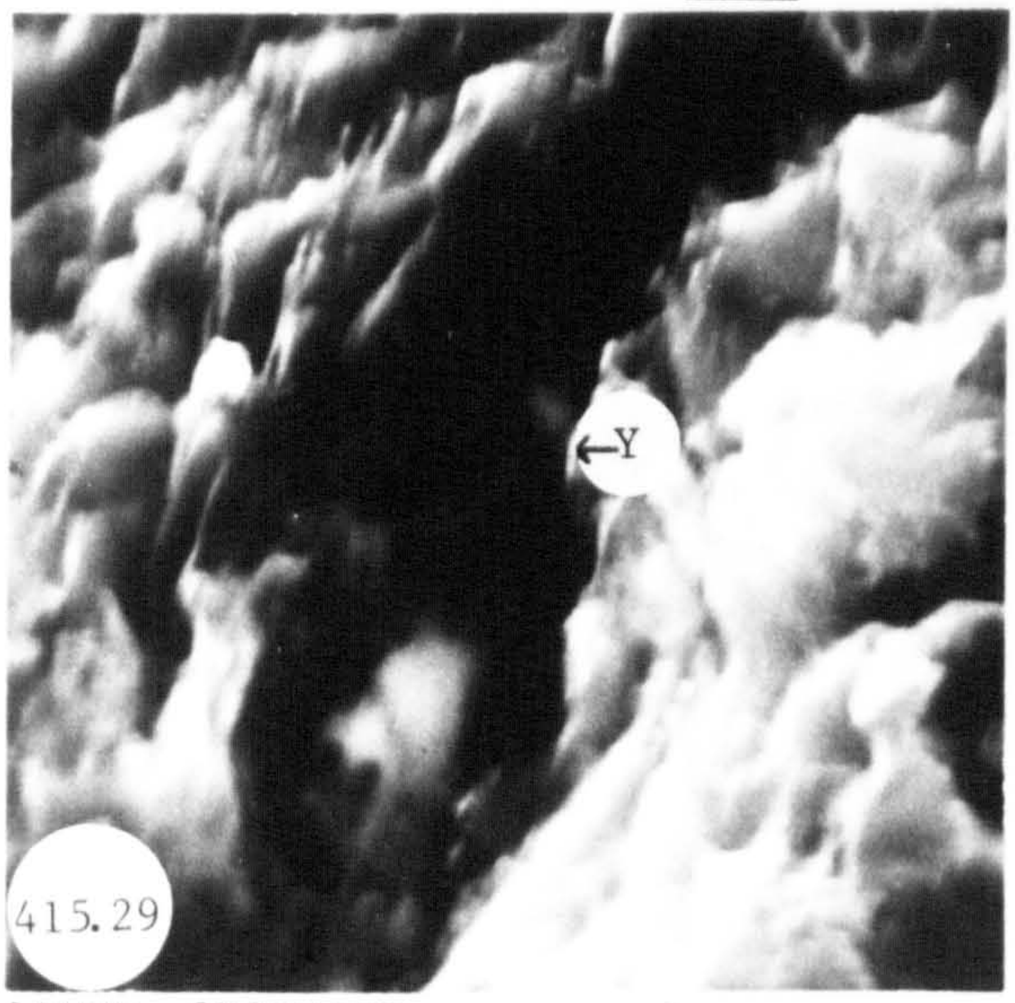
AGLMP GRAPHITE 5 μm

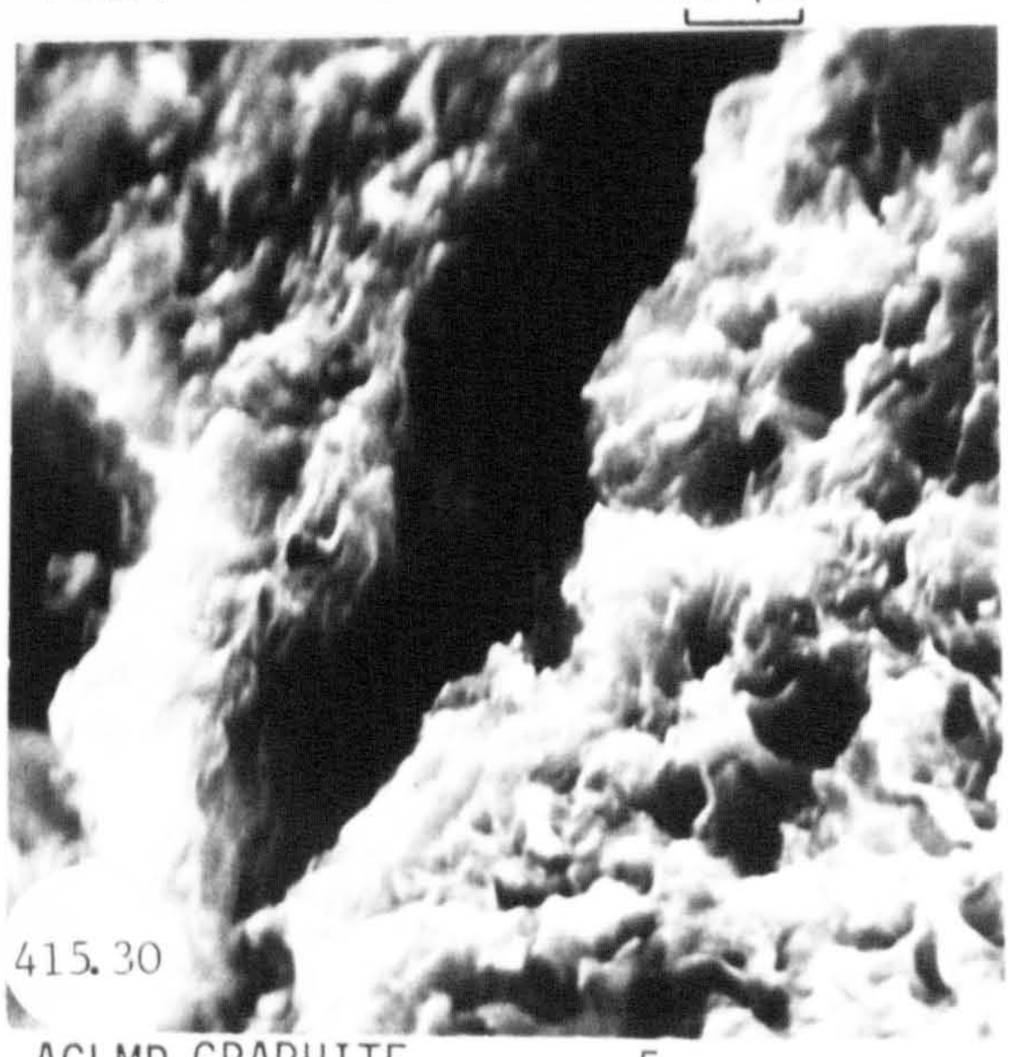
Figures 415.21 to 415.25. Scanning electron micrographs (stereoscan) of AGLMP Graphite (AG12) before gasification.











Figures 415.26 to 415.30. Scanning electron micrographs (stereoscan) of AGLMP Graphite (AG12) after gasification in carbon dioxide at 1073 K for 16 hours. Weight loss 1.13%.

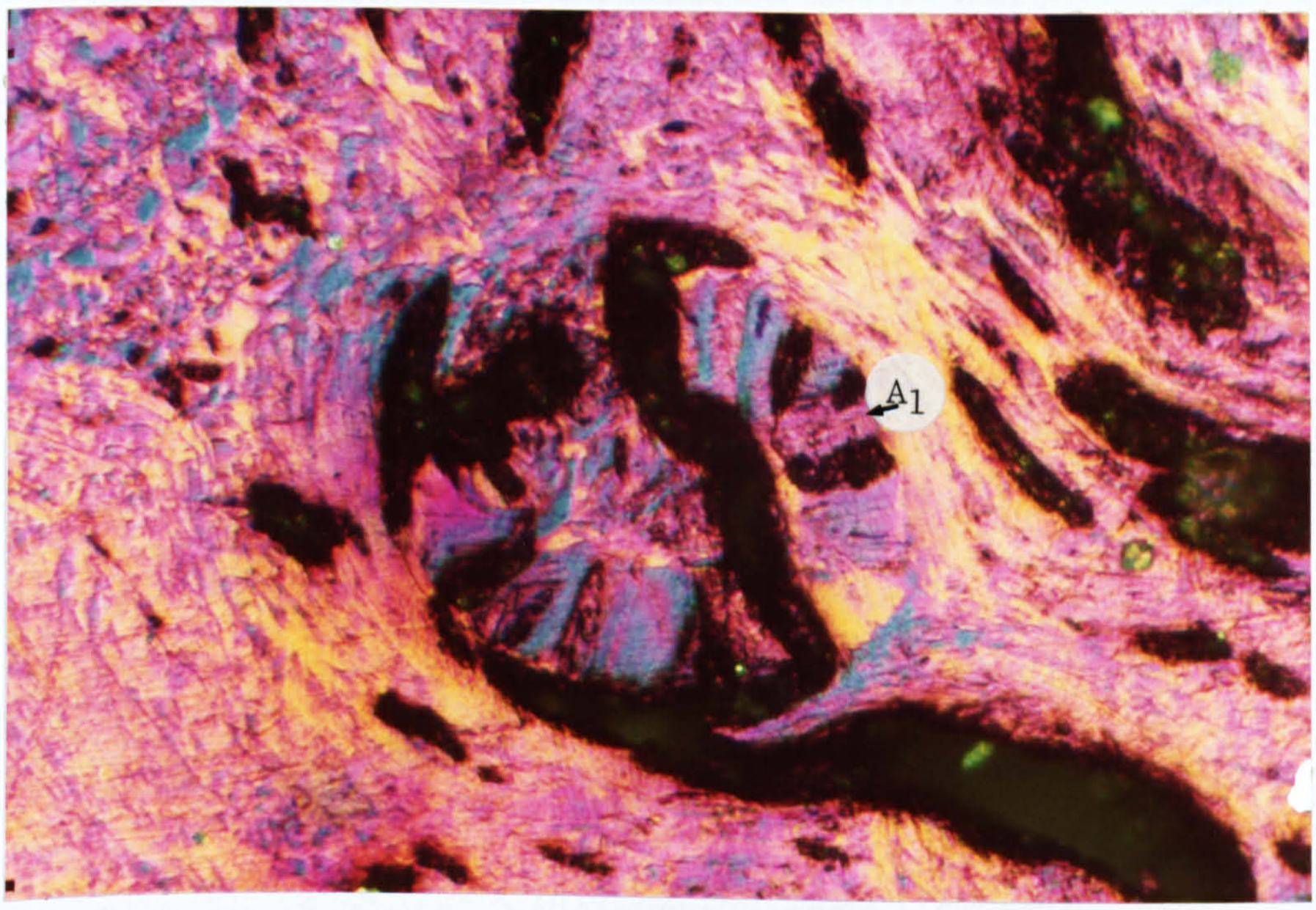
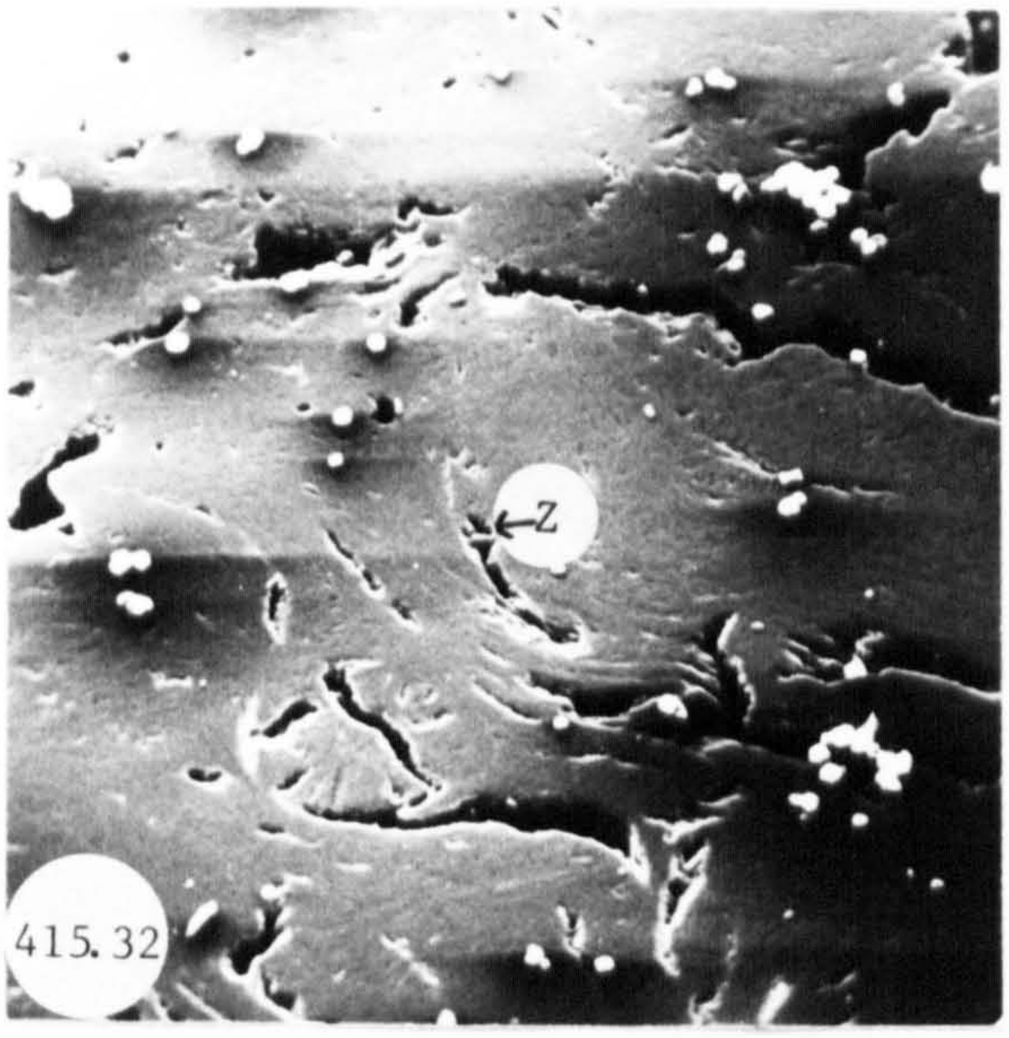
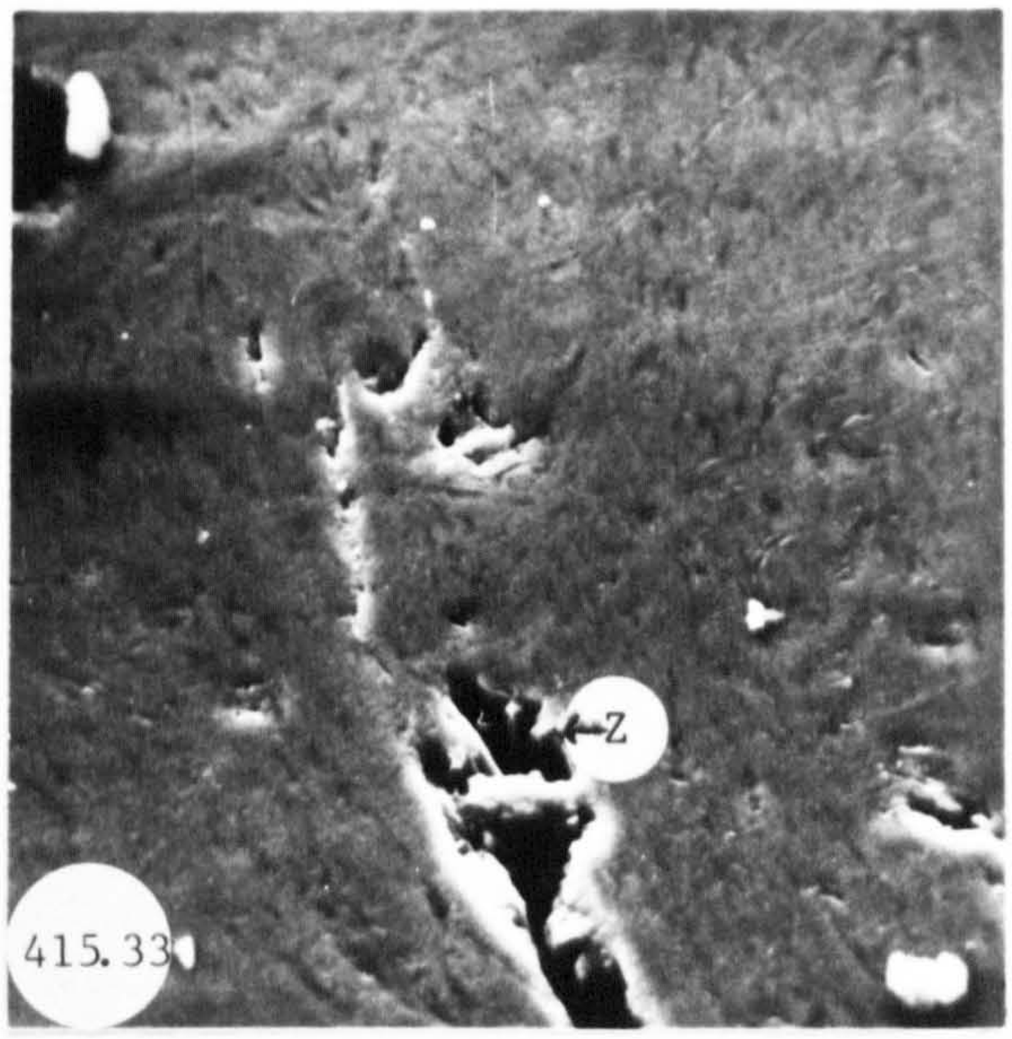


Figure 415.31. Optical micrograph of Lima Graphite (LG20) before gasification.



LIMA GRAPHITE 100 µm



LIMA GRAPHITE 20 µm



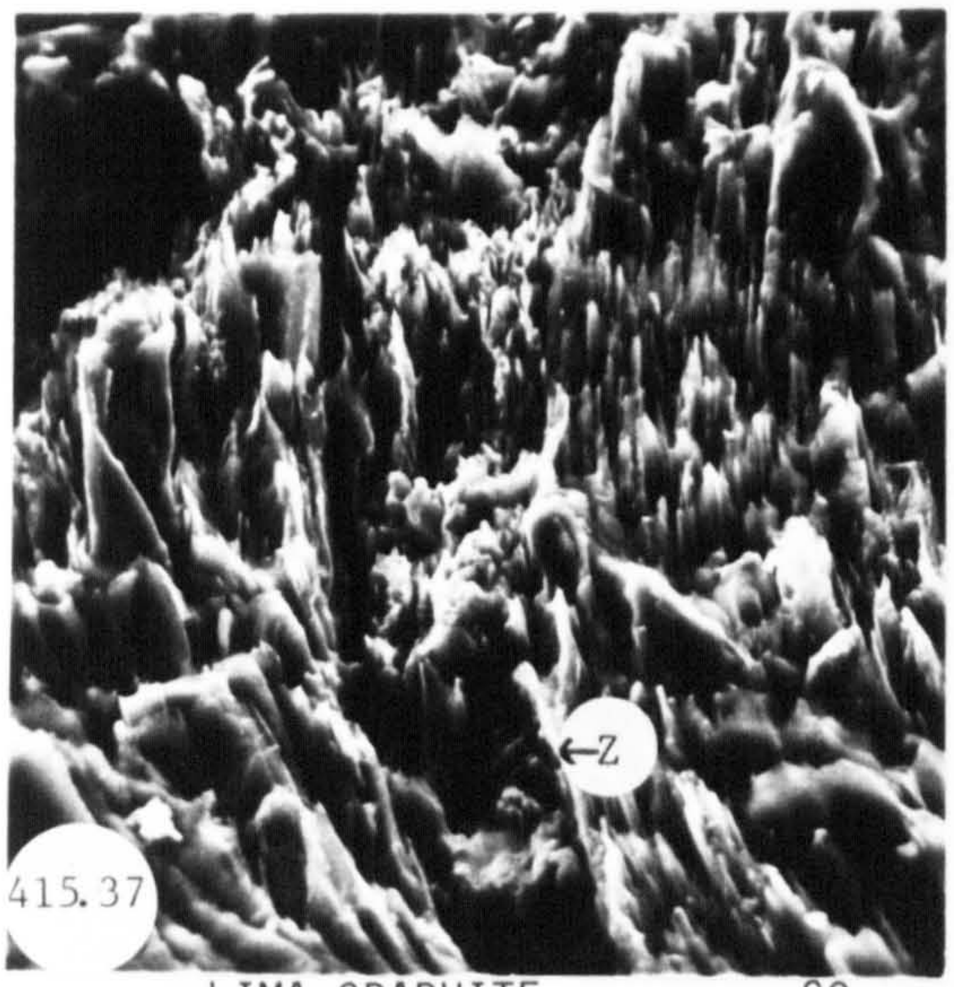
LIMA GRAPHITE 10 µm

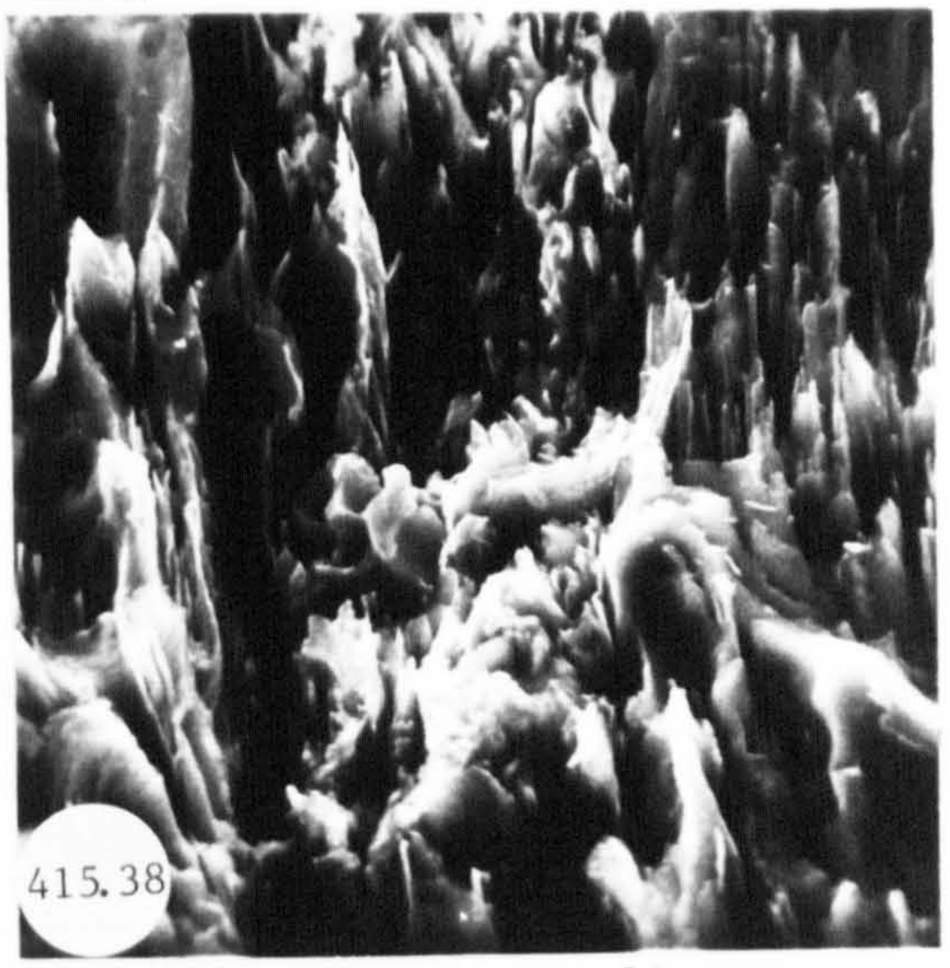


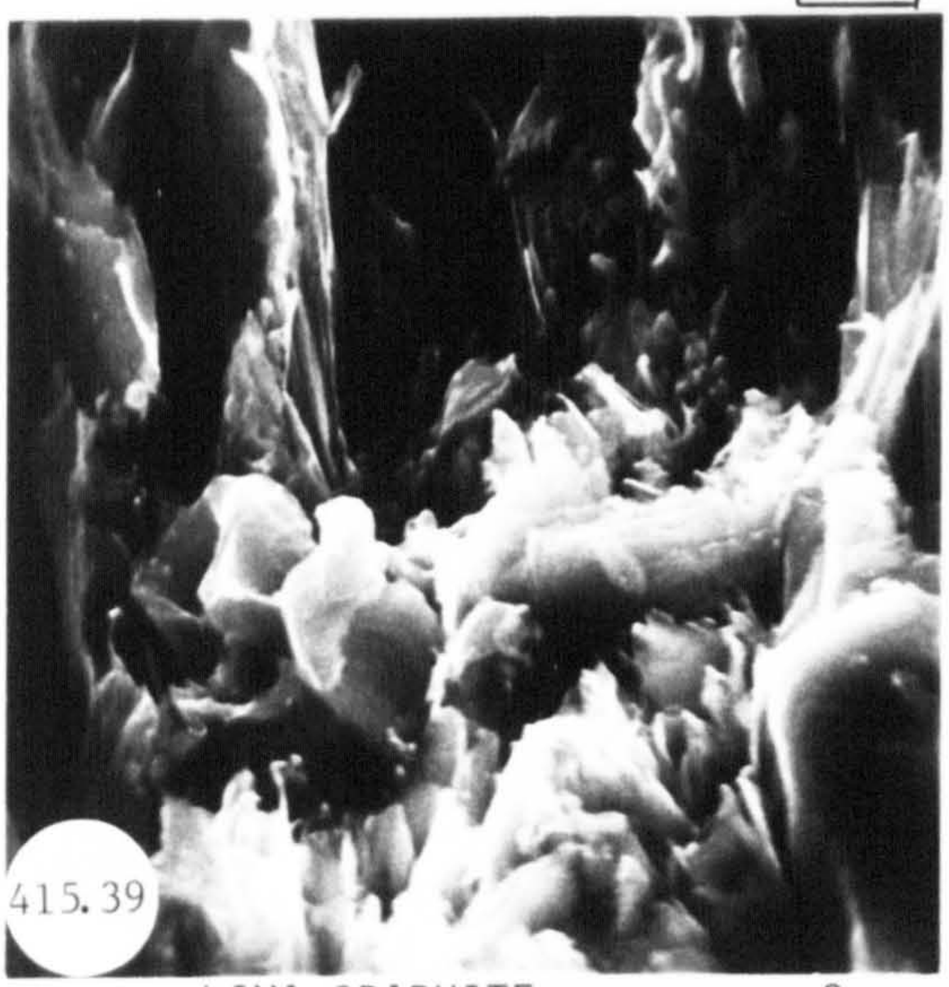
LIMA GRAPHITE 2 µm

Figures 415.32 to 415.35. Scanning electron micrographs (stereoscan) of Lima Graphite (LG20) before gasification.







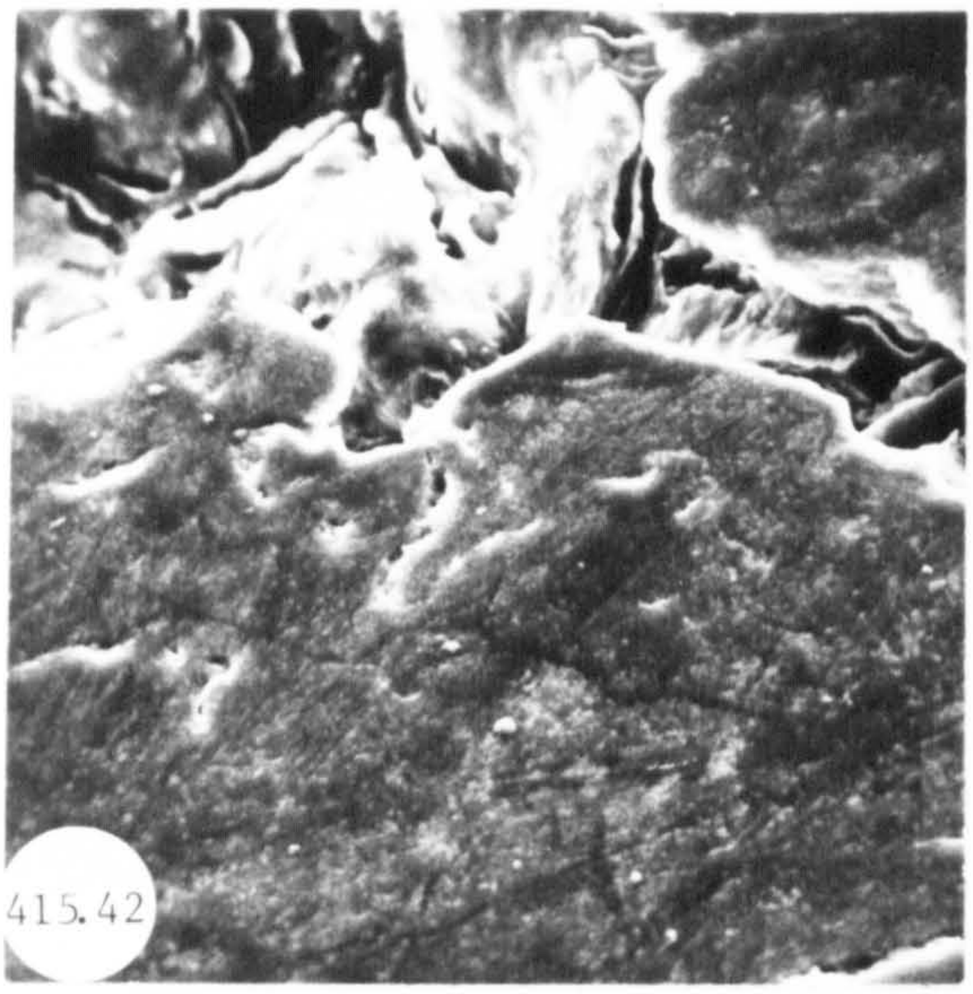




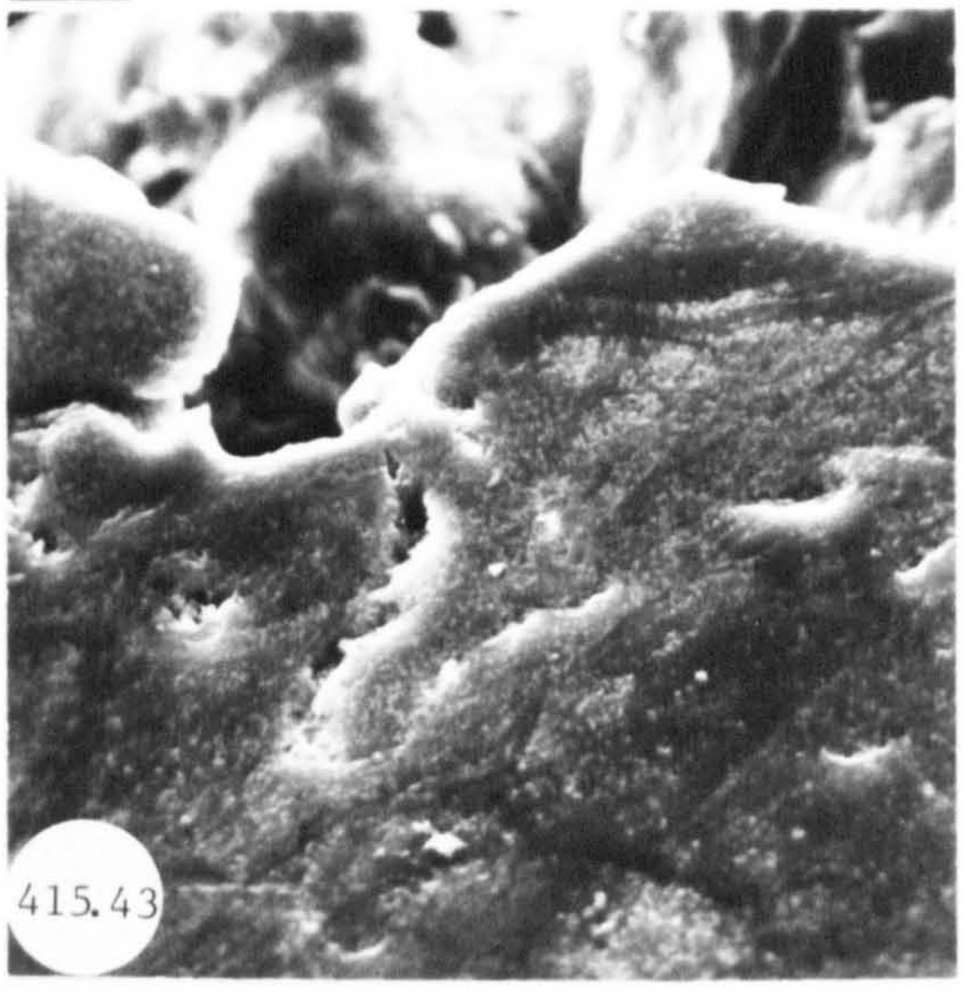
Figures 415.36 to 415.40. Scanning electron micrographs (stereoscan) of Lima Graphite (LG20) after gasification in carbon dioxide at 1173 K for 16 hours. Weight loss 6.78%.



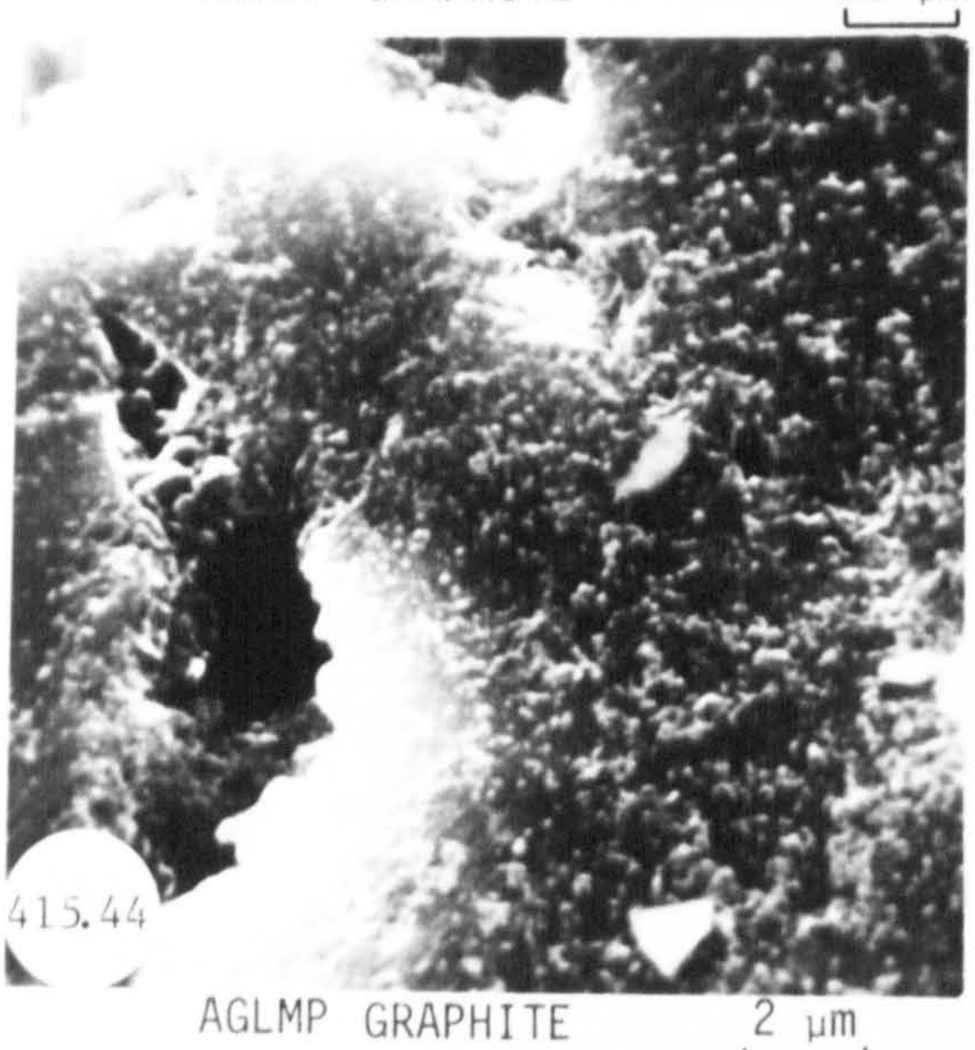
AGLMP GRAPHITE 100 µm



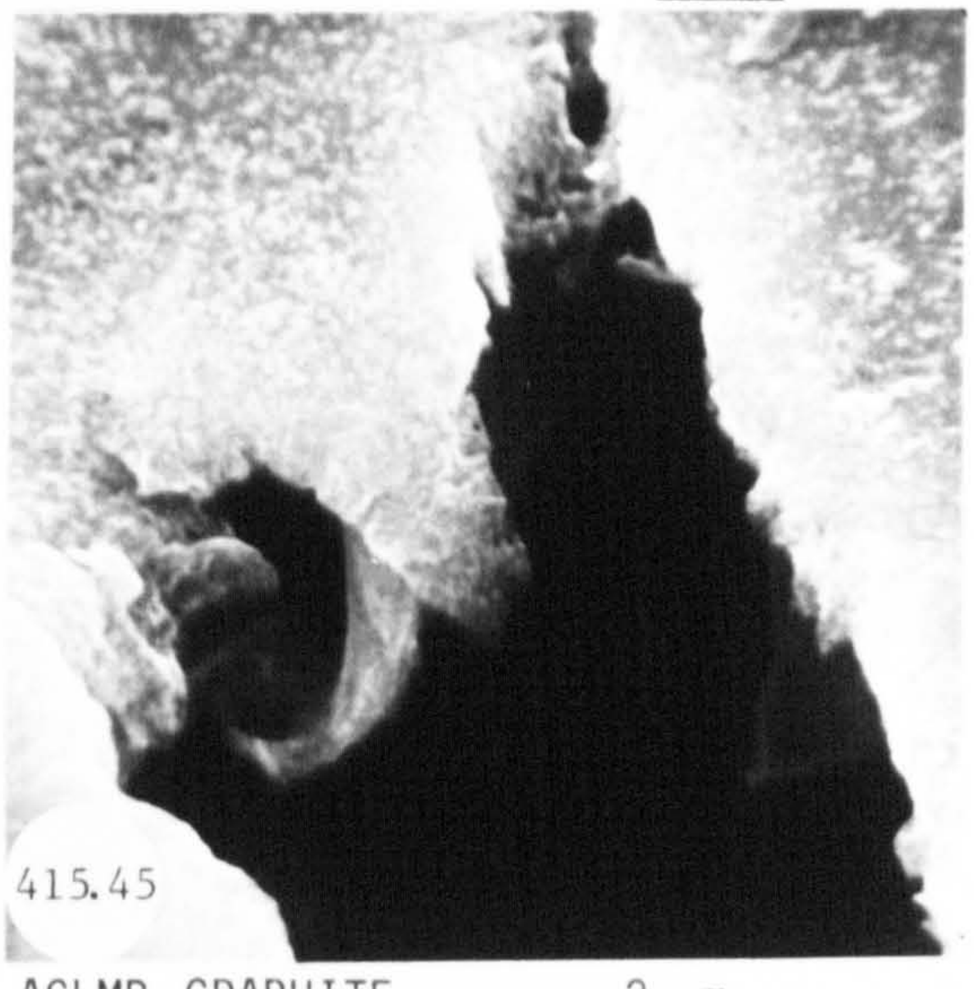
AGLMP GRAPHITE 20 µm



AGLMP GRAPHITE 10 µm

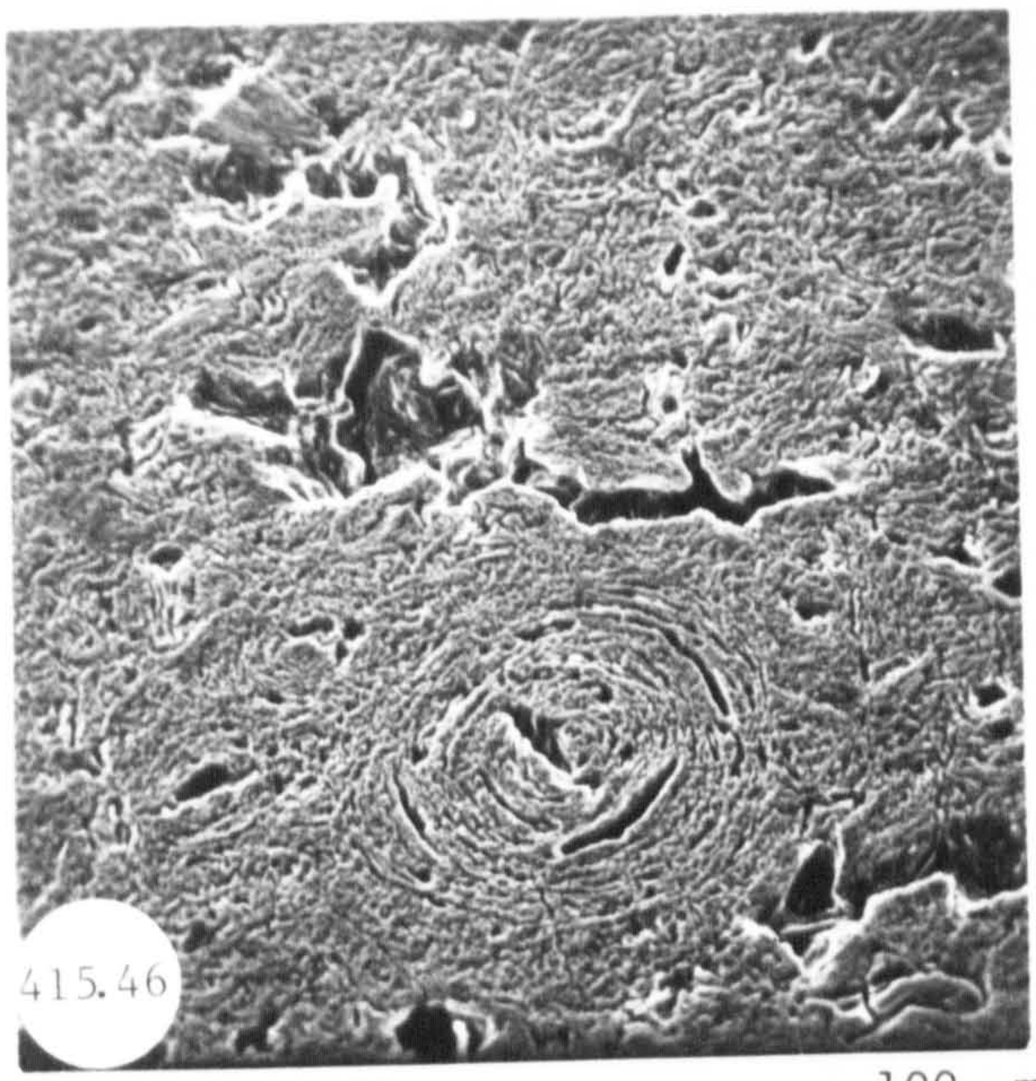


AGLMP GRAPHITE 2 µm

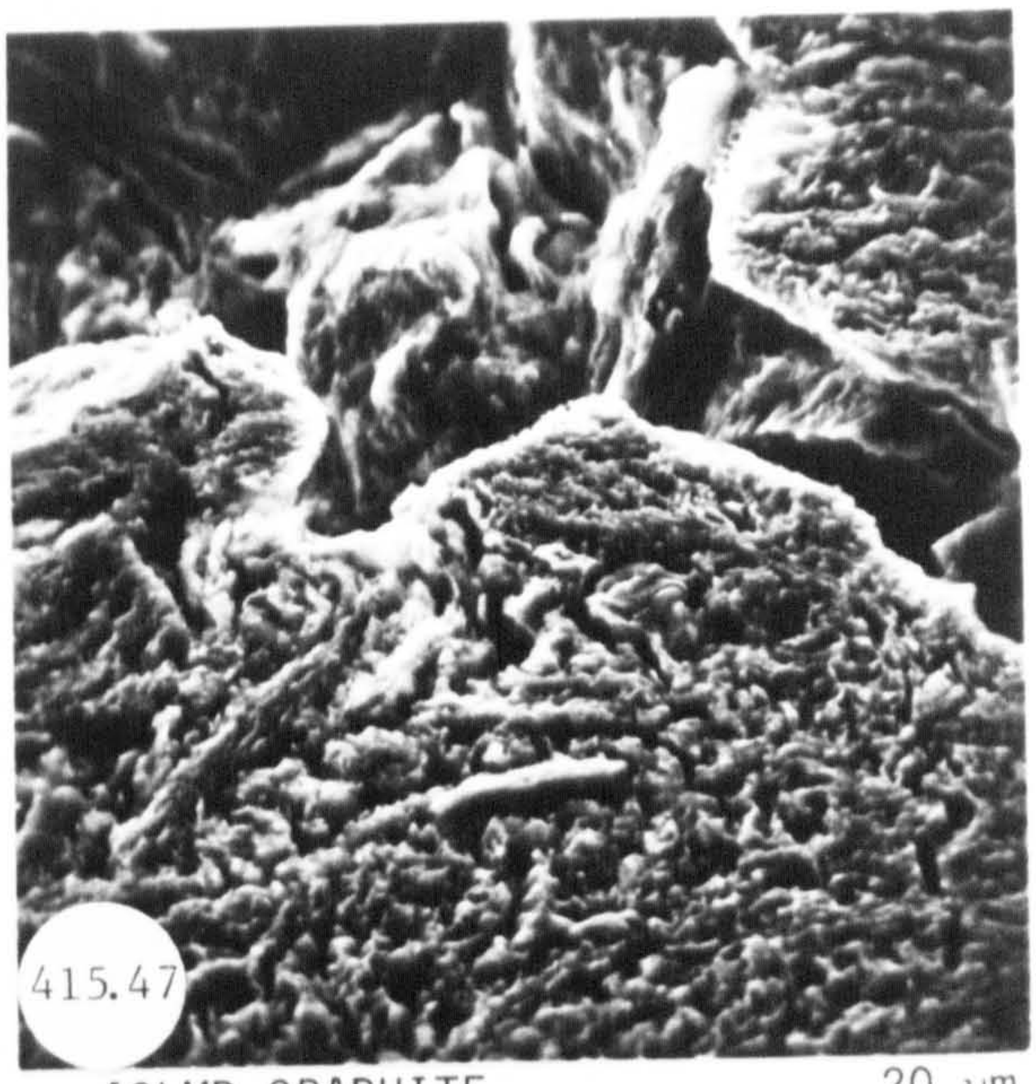


AGLMP GRAPHITE 2 µm

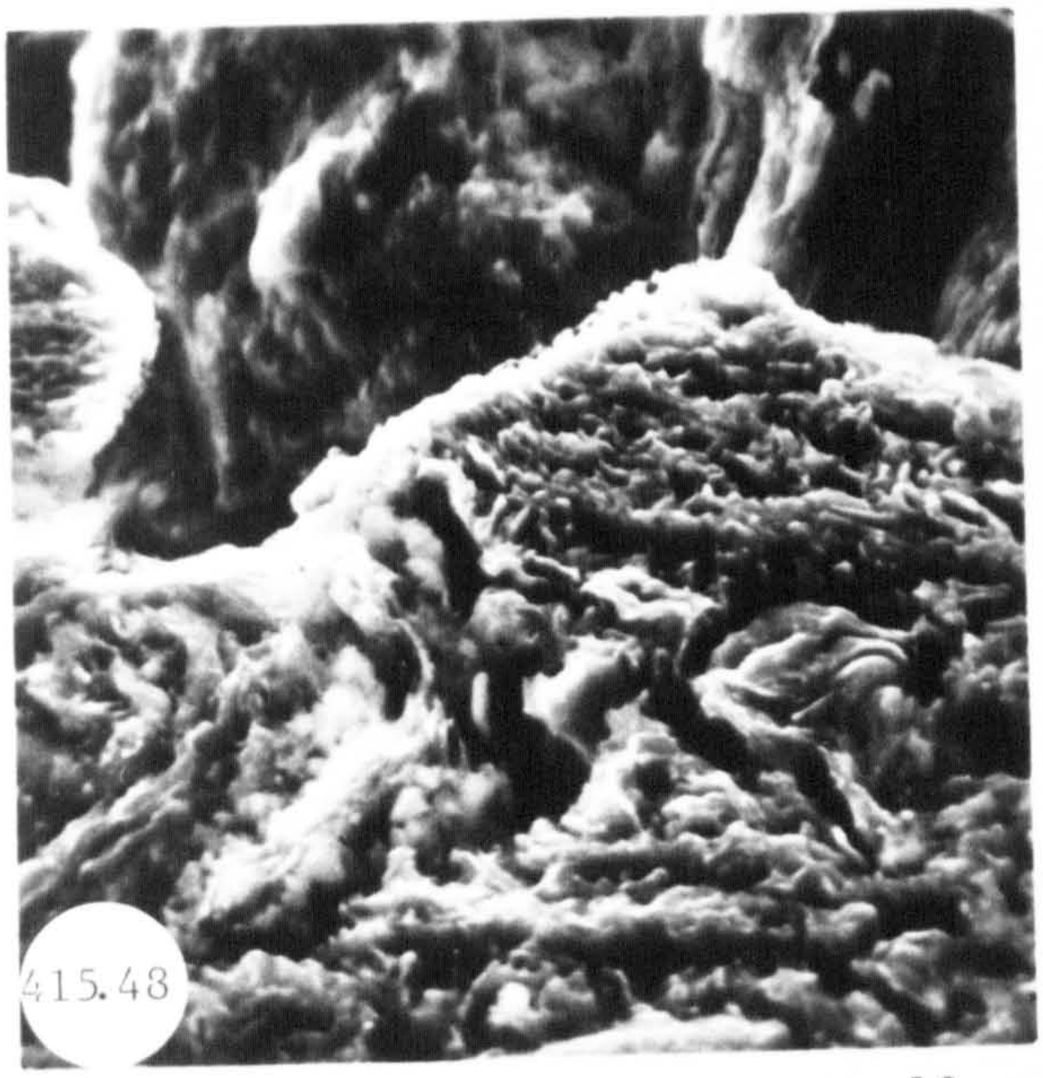
Figures 415.41 to 415.45. Scanning electron micrographs (stereoscan) of AGLMP Graphite (AG13) before gasification.



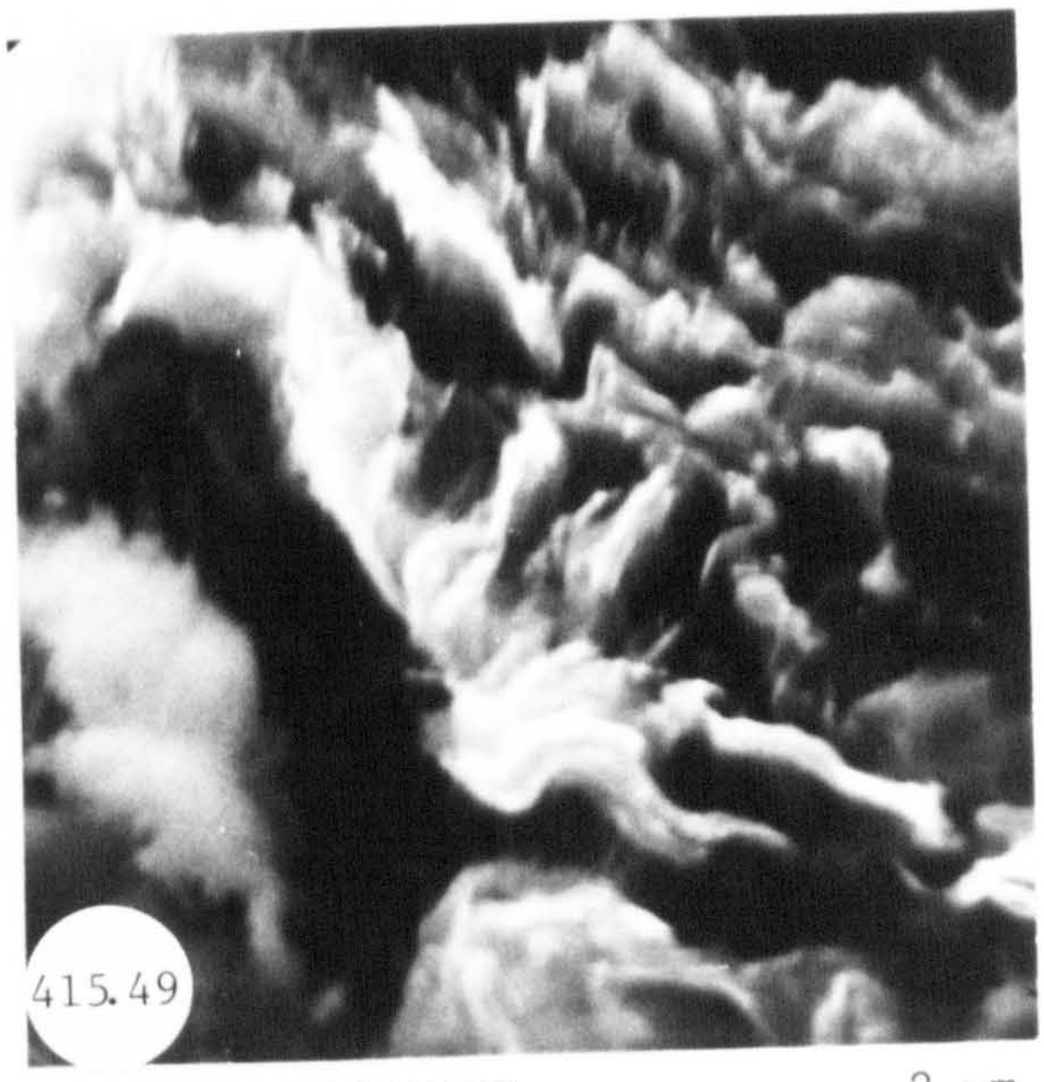
AGLMP GRAPHITE 100 µm



AGLMP GRAPHITE 20 µm



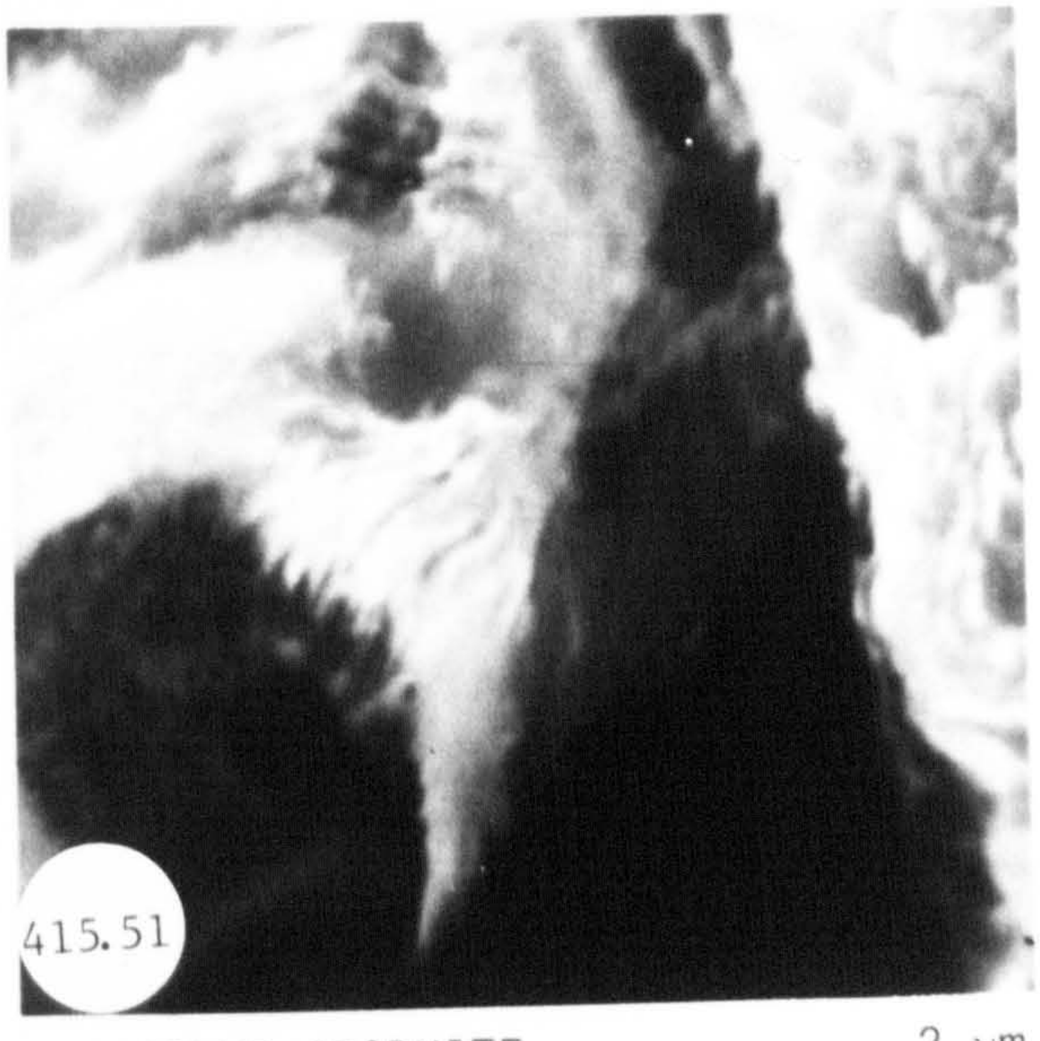
AGLMP GRAPHITE 10 µm



AGLMP GRAPHITE 2 µm



AGLMP GRAPHITE 5 µm



AGLMP GRAPHITE 2 µm

Figures 415.46 to 415.51. Scanning electron micrographs (stereoscan) of AGLMP Graphite (AG13) after gasification in carbon dioxide at 1173K for 16 hours. Weight loss 3.68%.

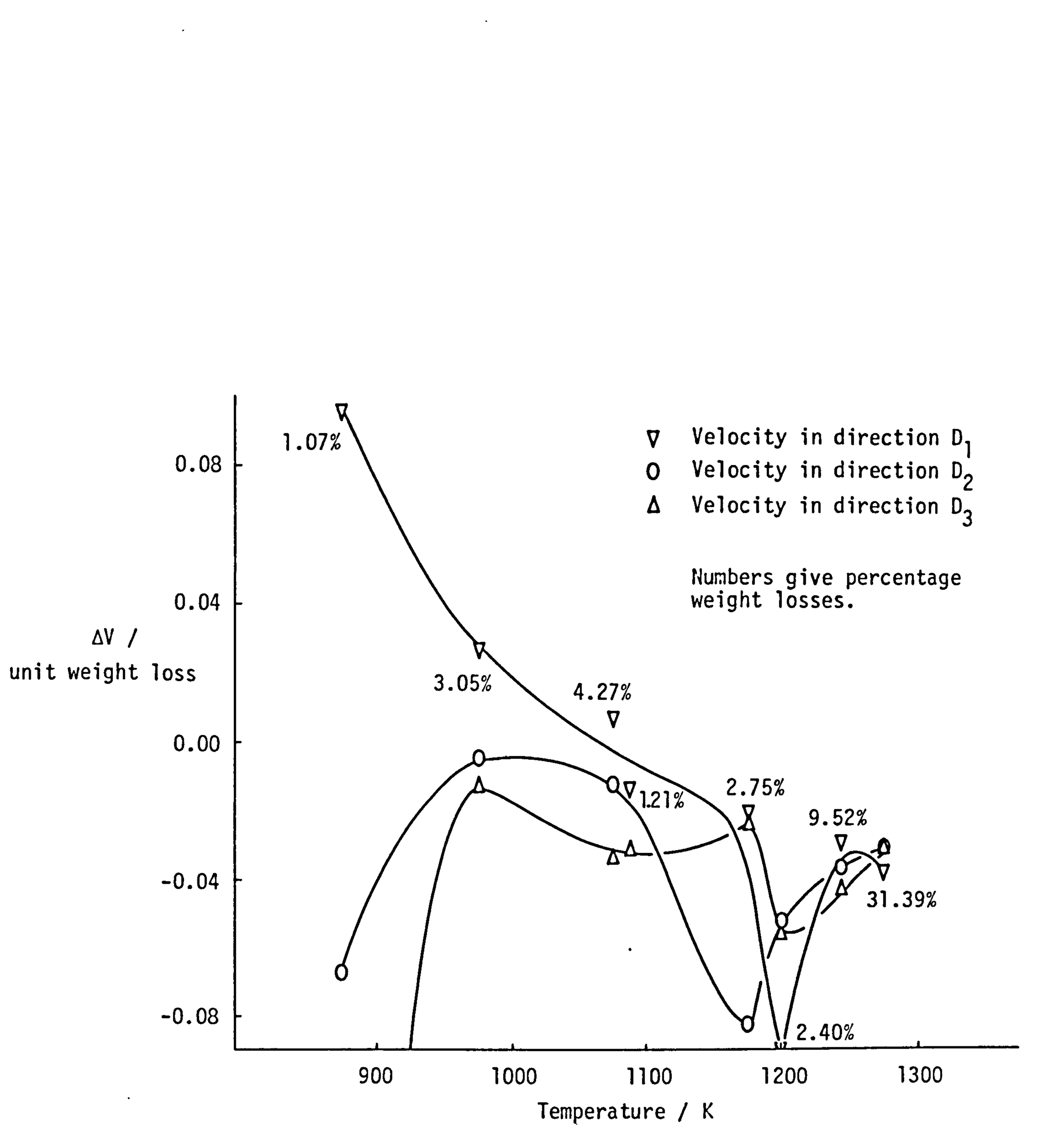


Figure 416. Ultrasonic testing of Lima graphite gasified in carbon dioxide.

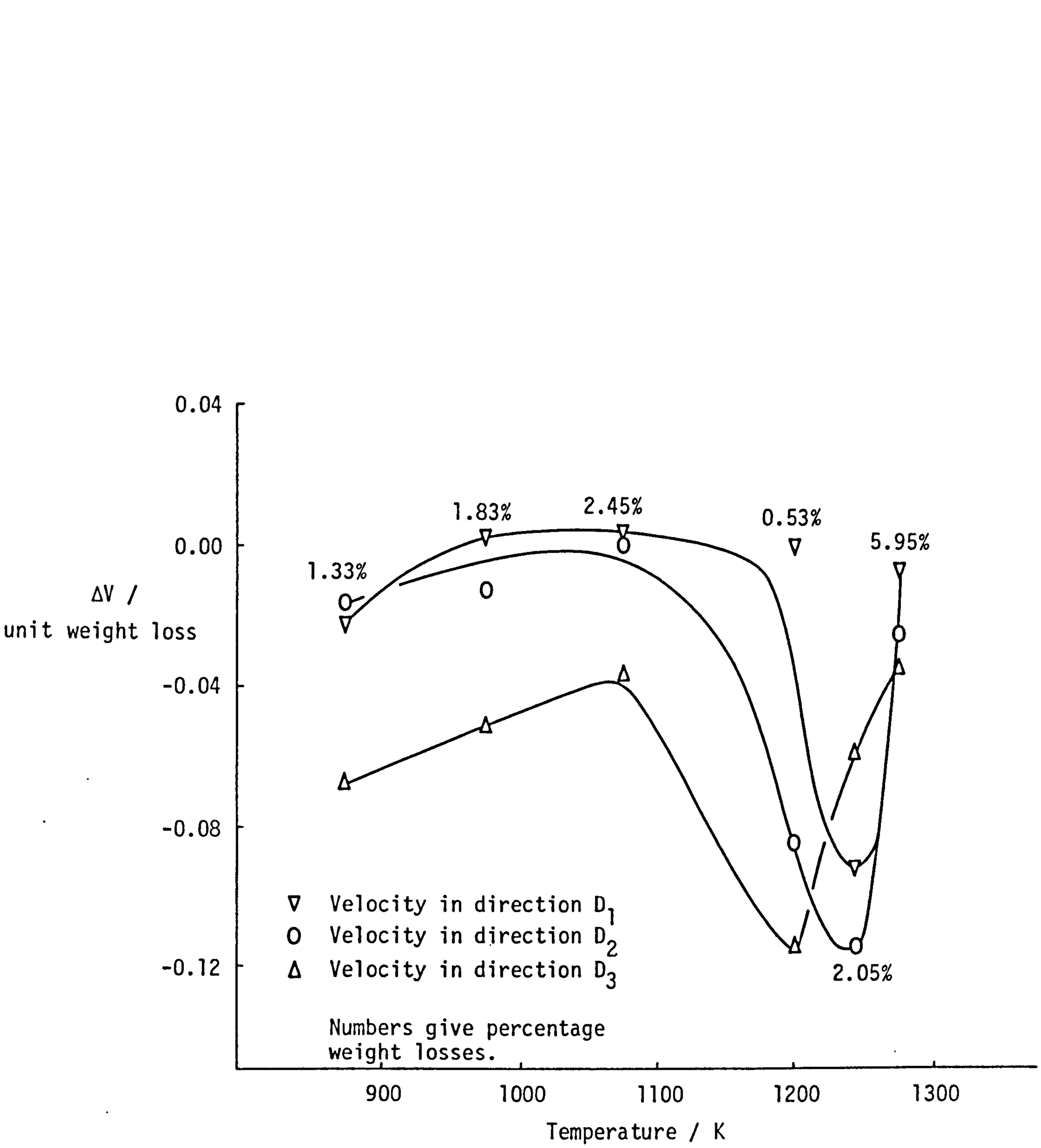


Figure 417. Ultrasonic testing of Morgans EYC 9106 graphite gasified in carbon dioxide.

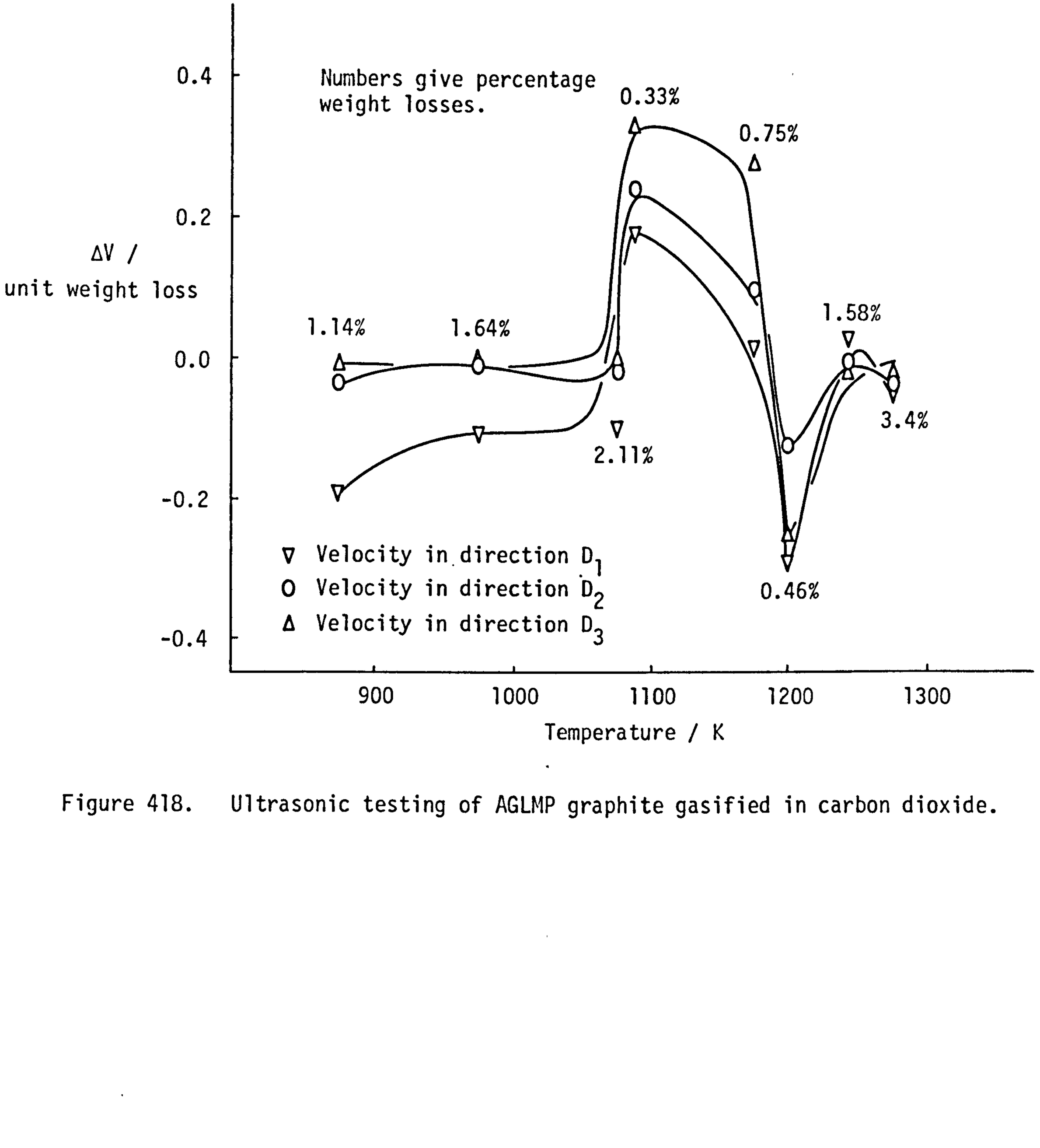


Figure 418. Ultrasonic testing of AGLMP graphite gasified in carbon dioxide.

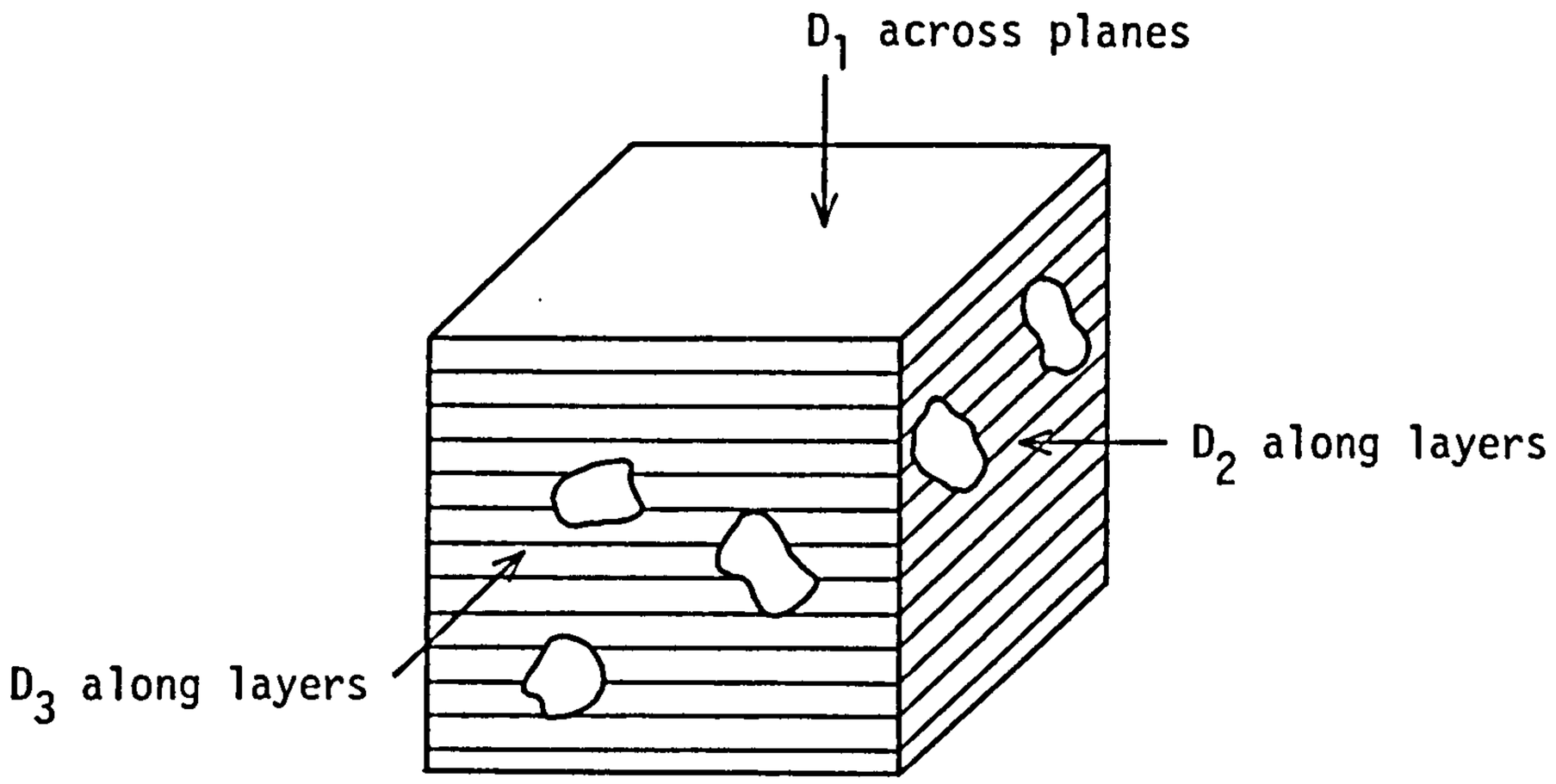
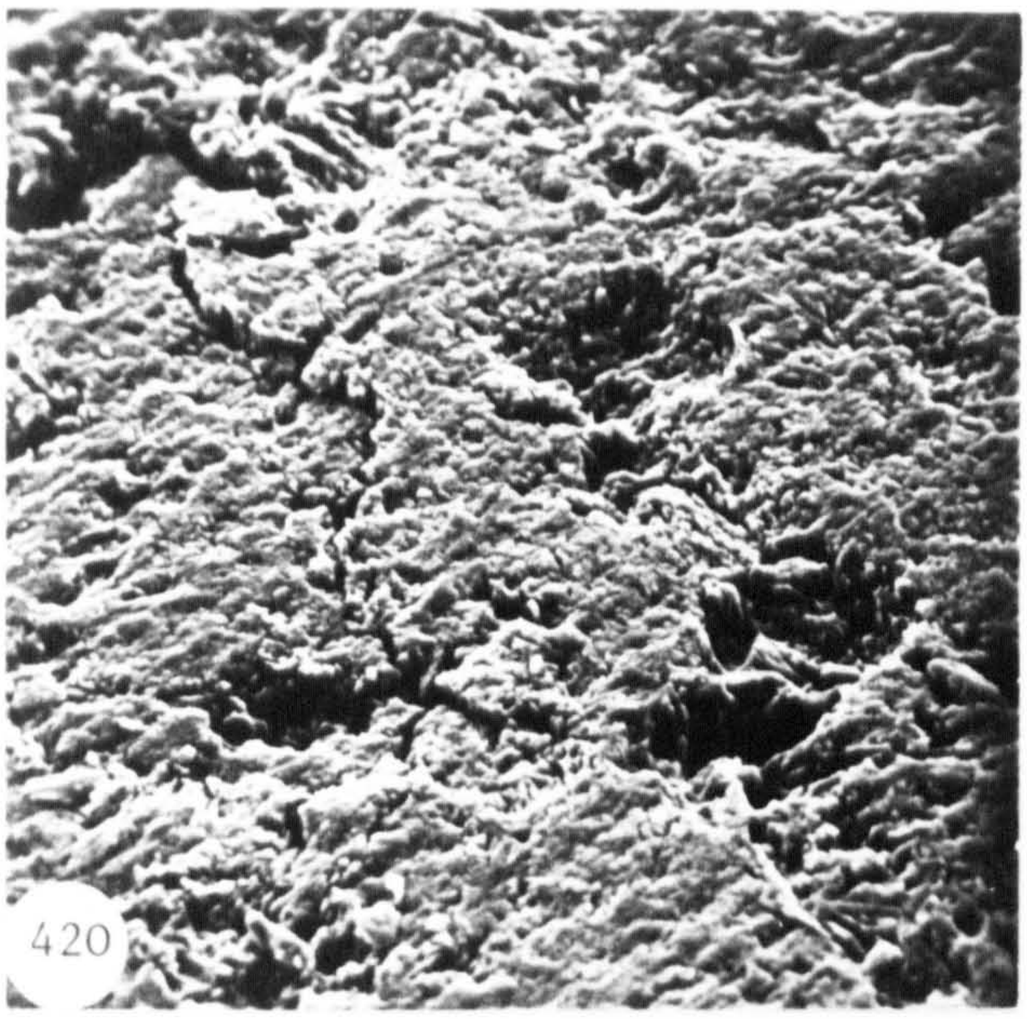
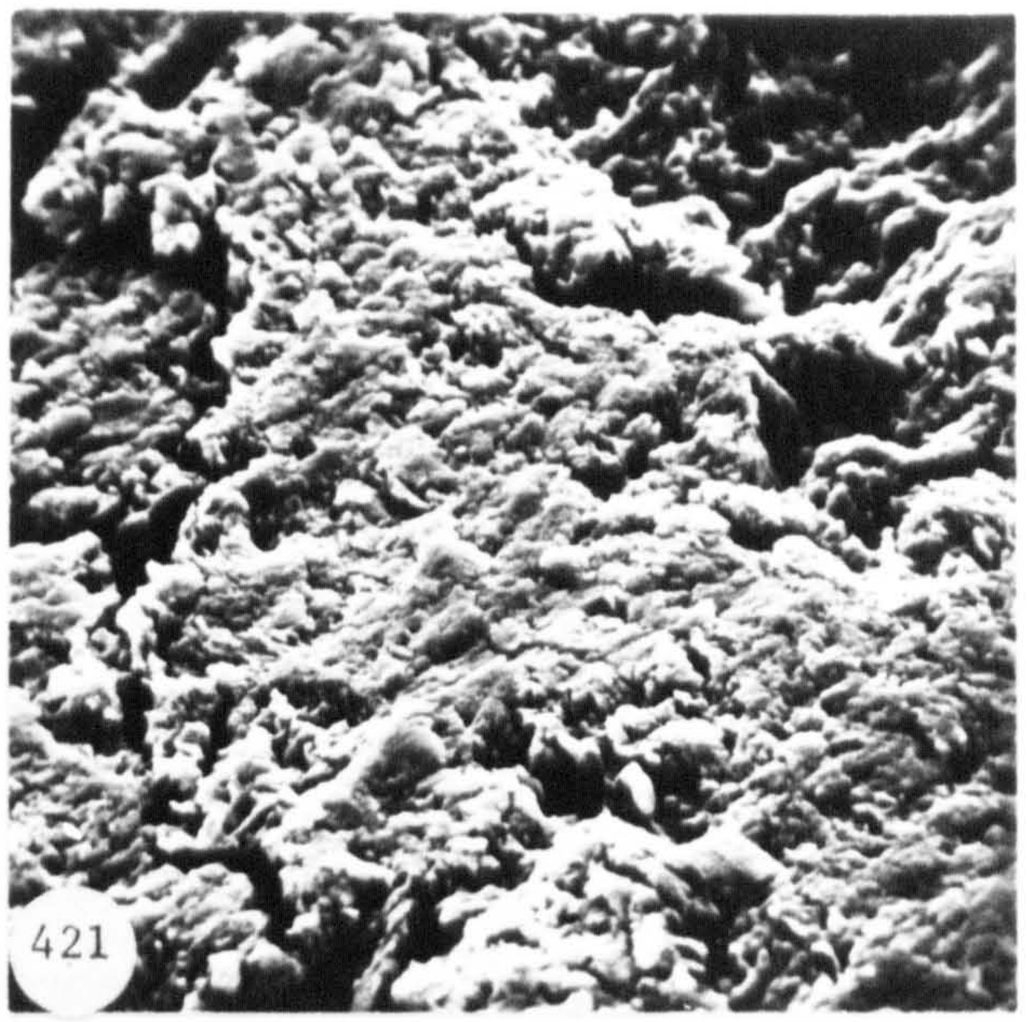


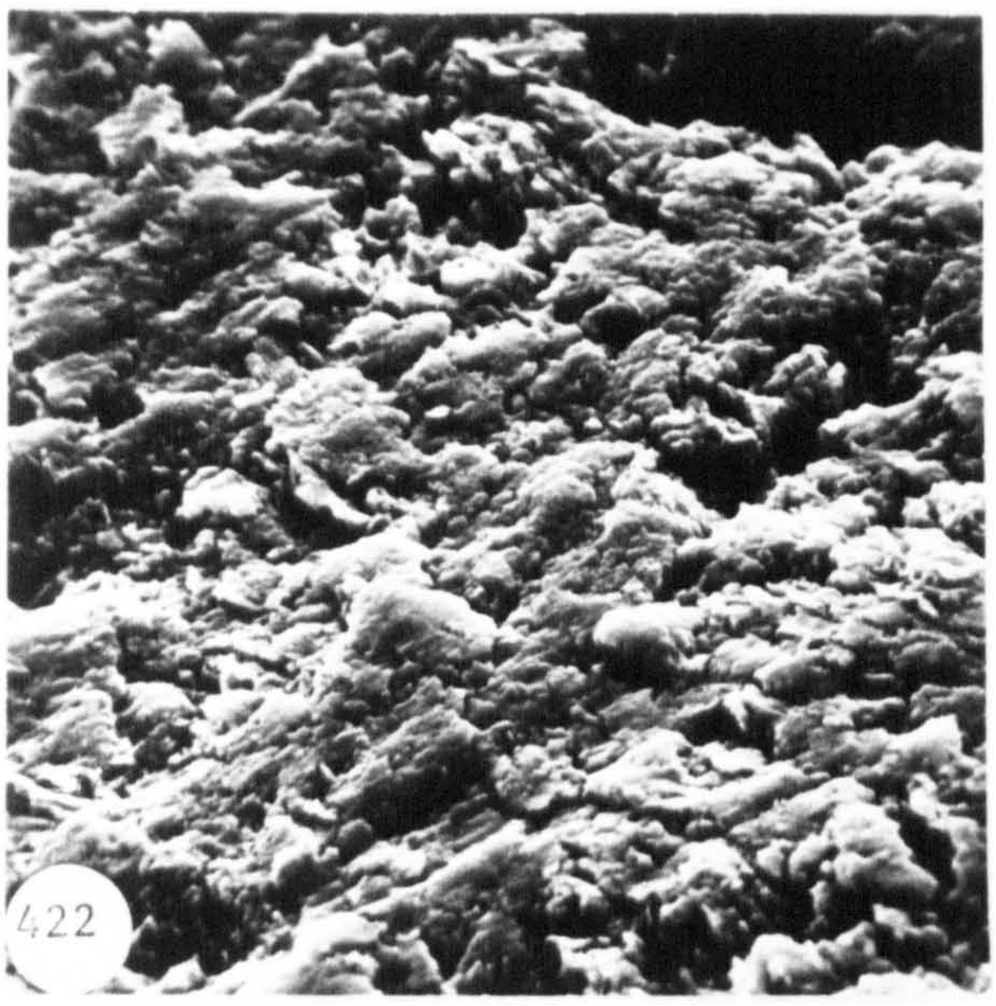
Figure 419. Model illustrating ultrasonic velocities through graphite in three directions.



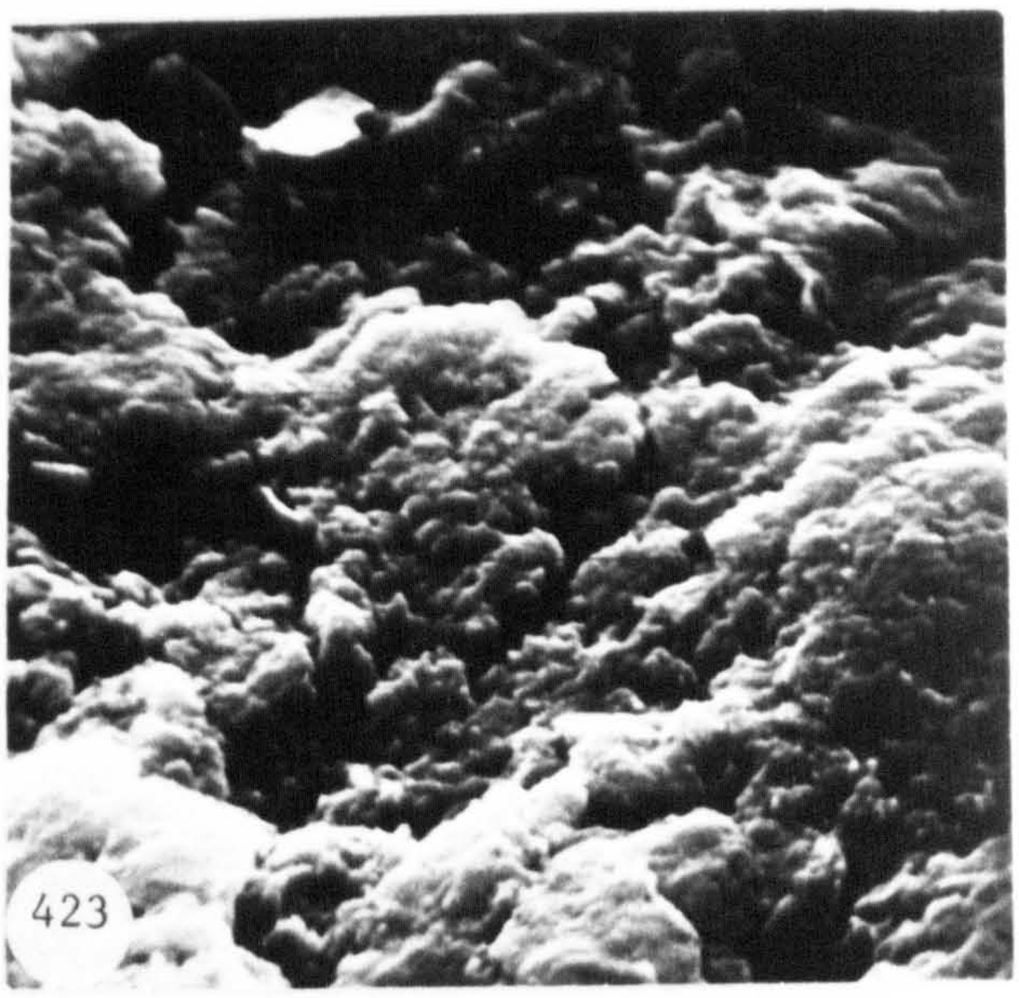
PITCH COKE GRAPHITE 50 µm



PITCH COKE GRAPHITE 20 µm

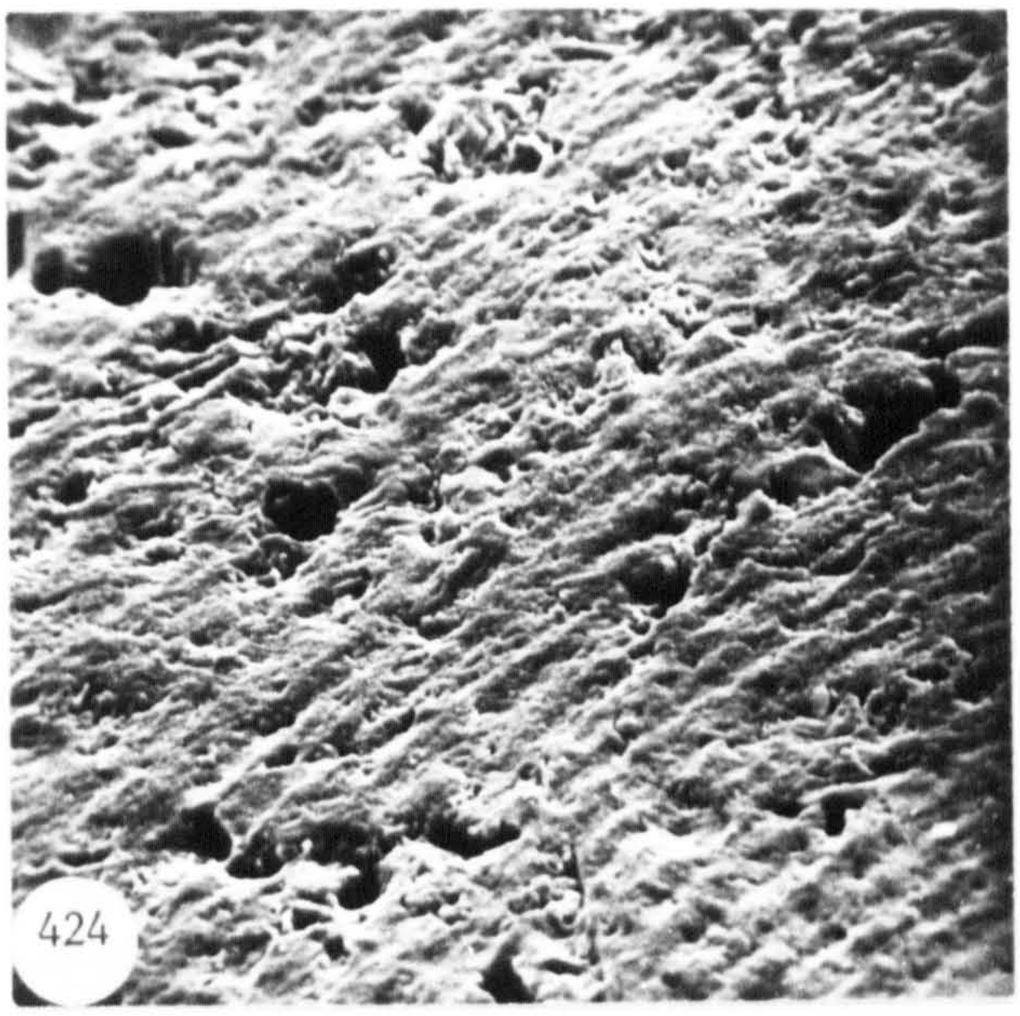


PITCH COKE GRAPHITE 10 µm

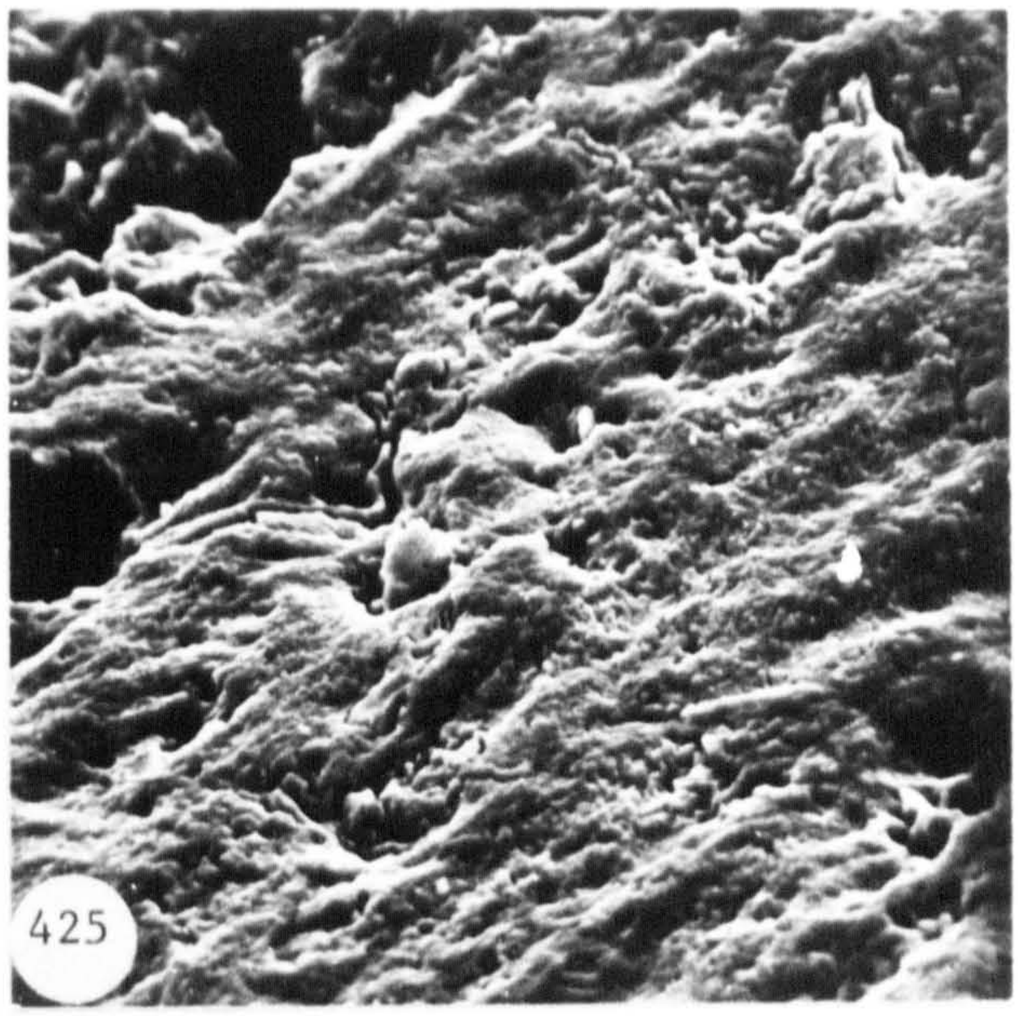


PITCH COKE GRAPHITE 2 µm

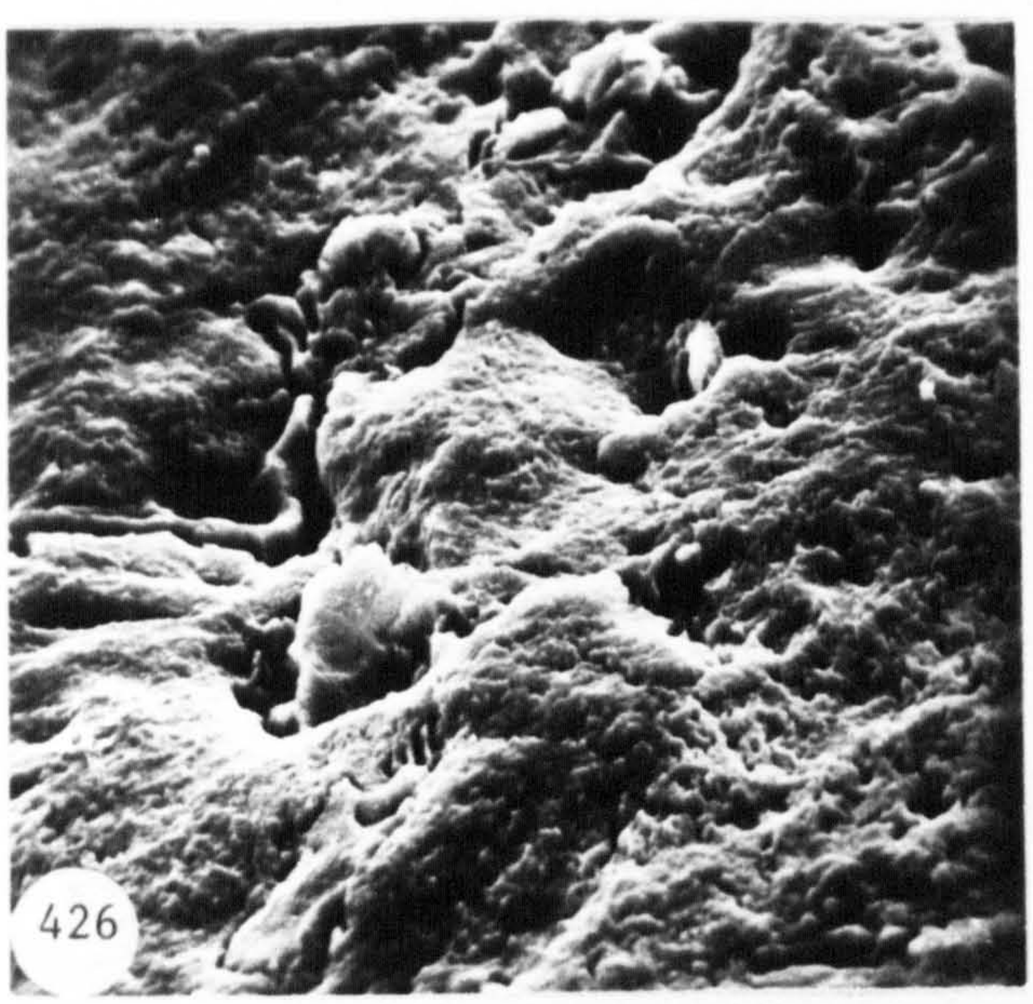
Figures 420 to 423. Scanning electron micrographs (stereoscan) of BAEL Pitch Coke Graphite Q4/1 (control for H.24).



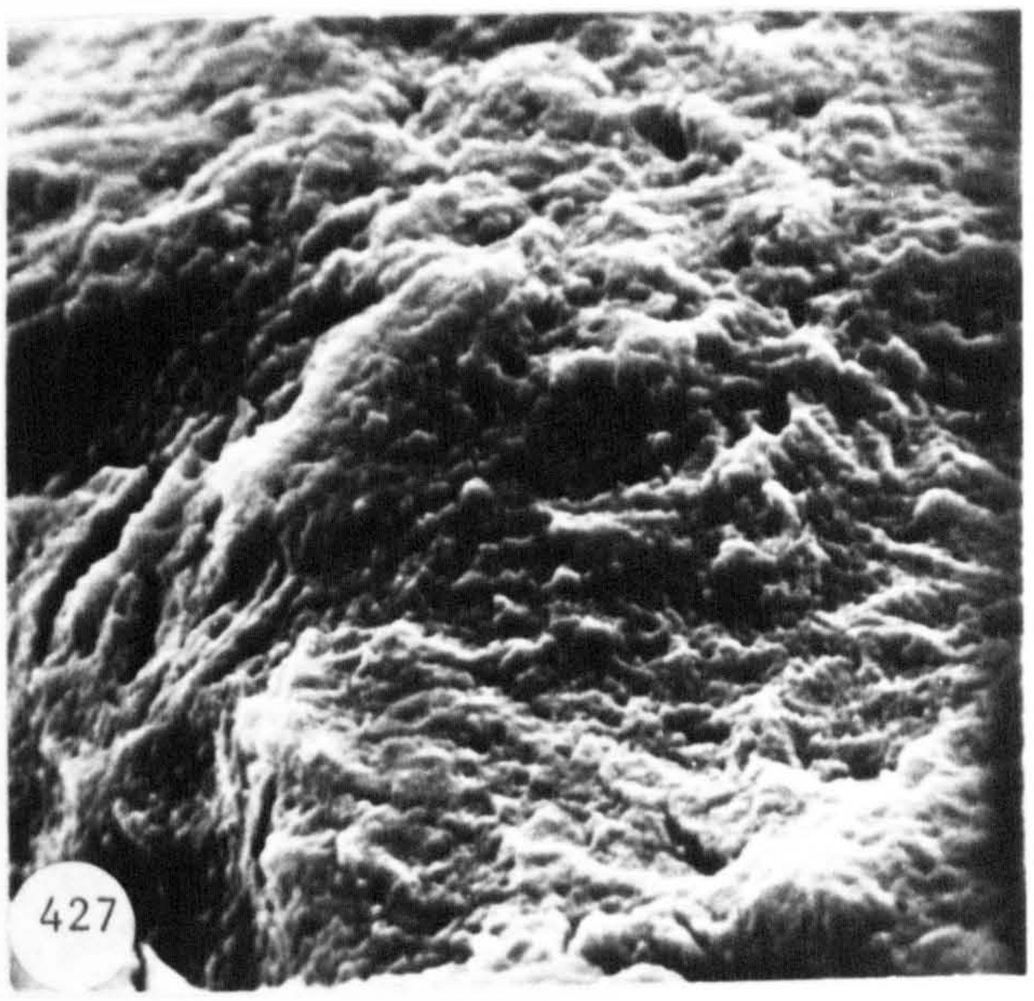
PITCH COKE GRAPHITE 50 µm



PITCH COKE GRAPHITE 20 µm

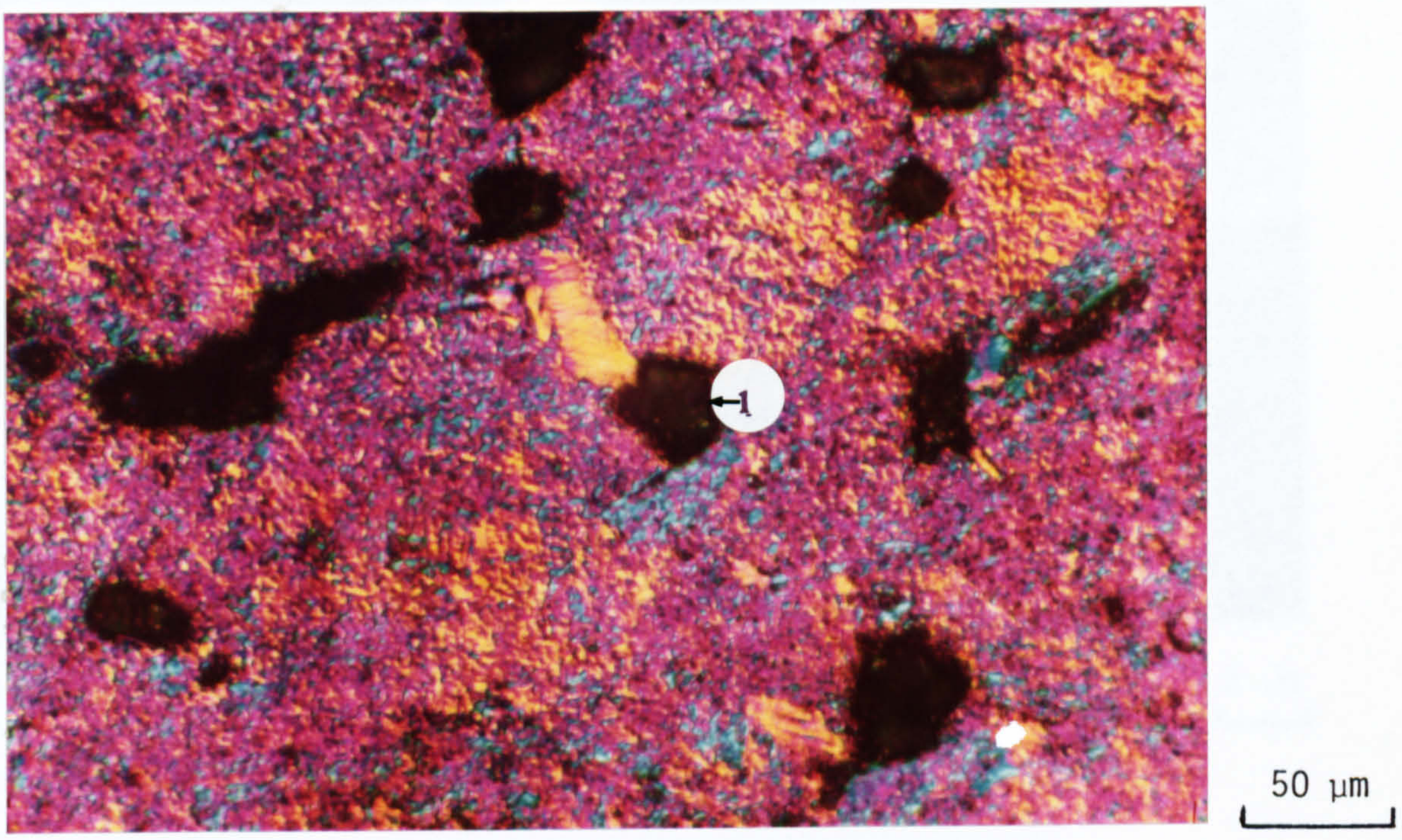


PITCH COKE GRAPHITE 10 µm



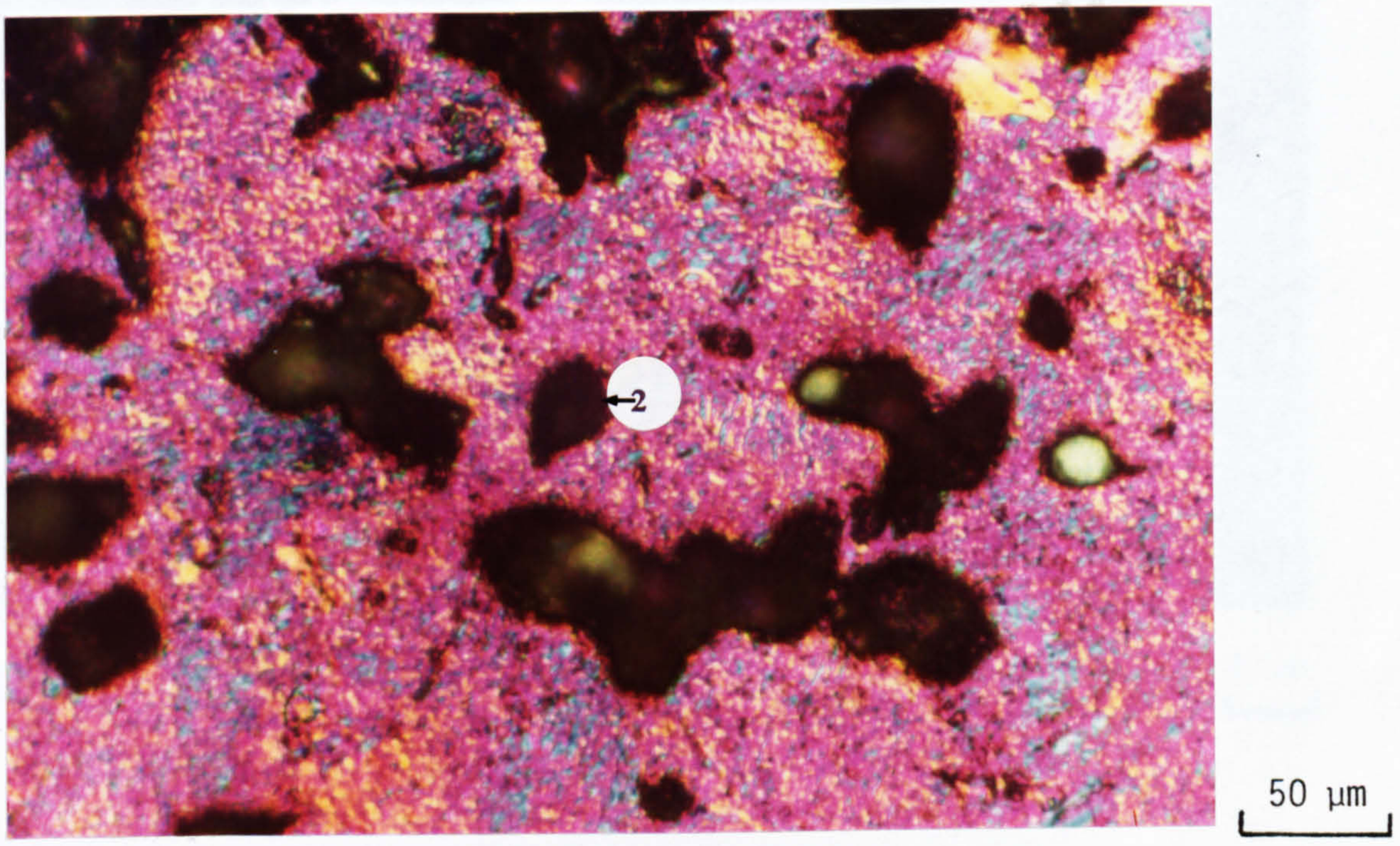
PITCH COKE GRAPHITE 2 µm

Figures 424 to 427. Scanning electron micrographs (stereoscan) of BAEL Pitch Coke Graphite H24, radiolytically oxidised in carbon dioxide. Weight loss 8.8%.



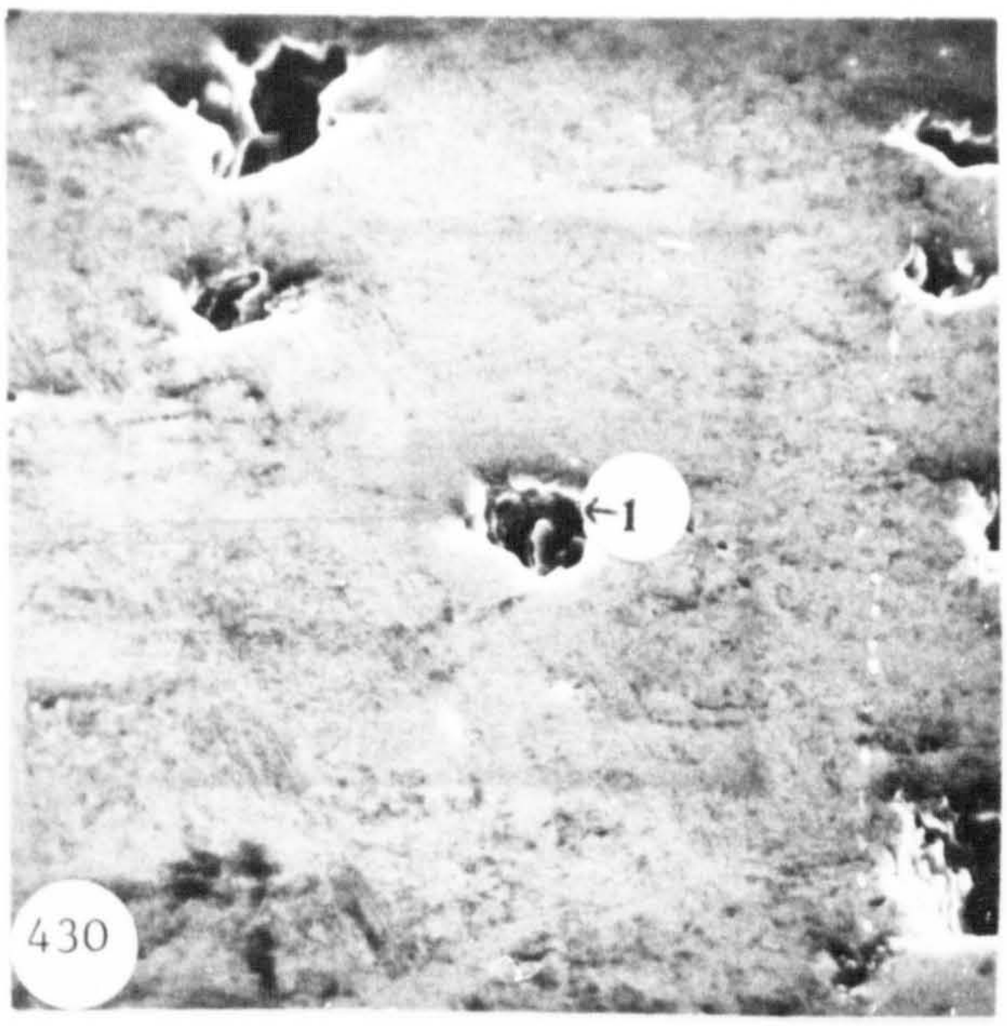
PITCH COKE GRAPHITE

Figure 428. Optical micrograph of BAEL Pitch Coke Graphite Q4/1 (Control for H24).

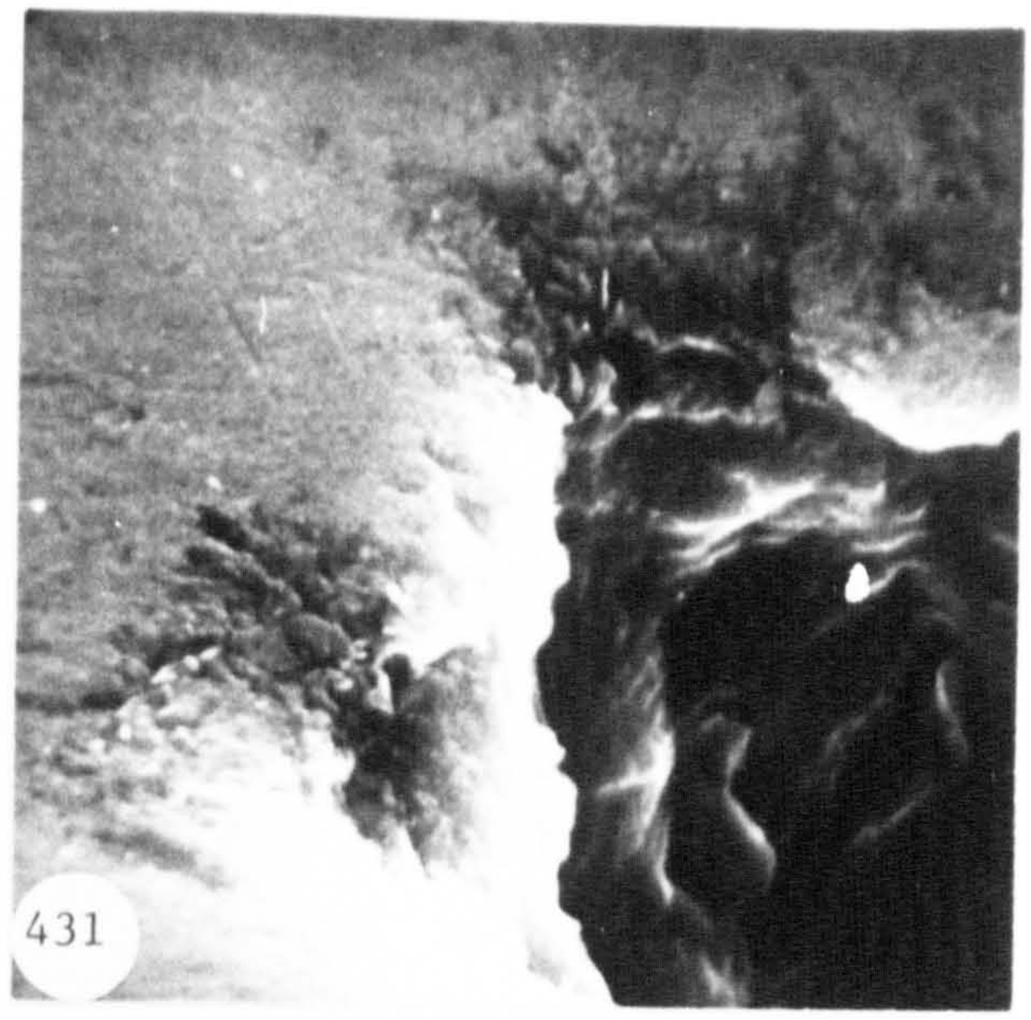


PITCH COKE GRAPHITE

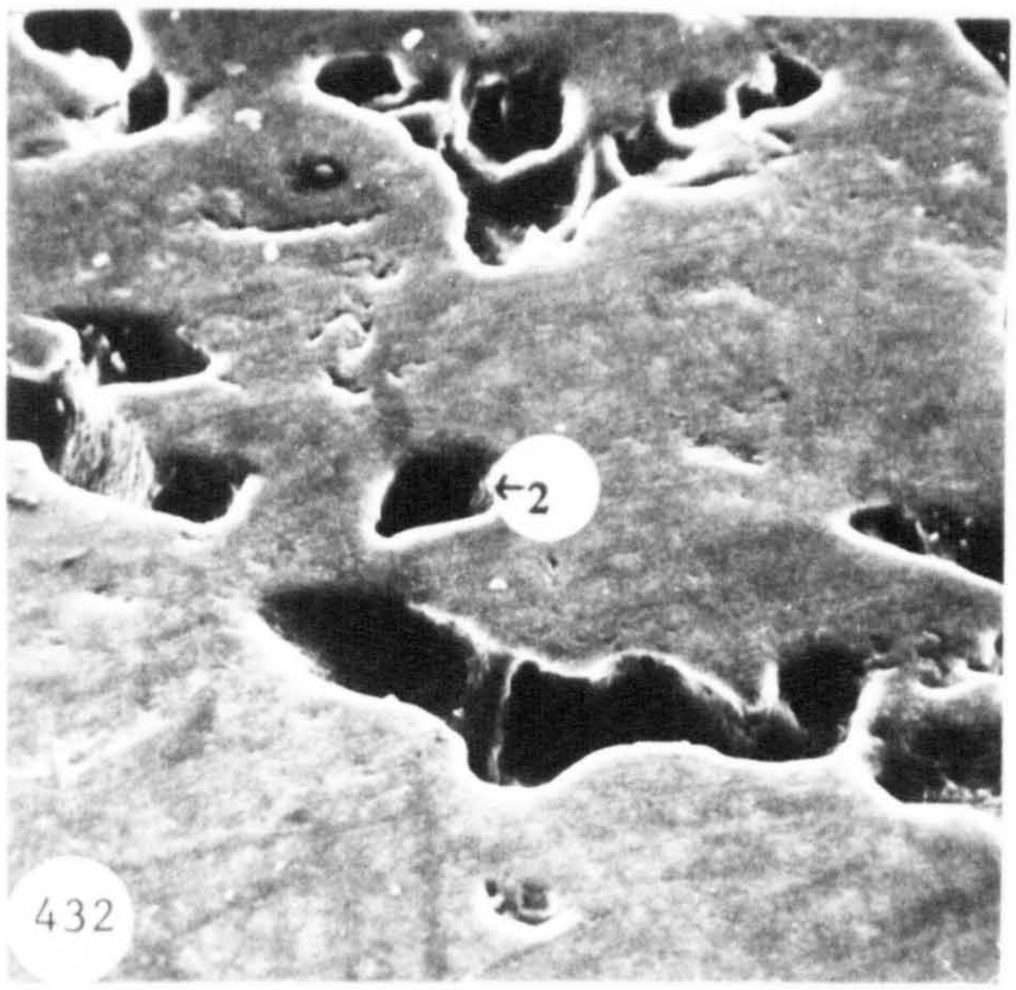
Figure 429. Optical micrograph of BAEL Pitch Coke Graphite H24, radiolytically oxidised in carbon dioxide.
Weight loss 8.8%.



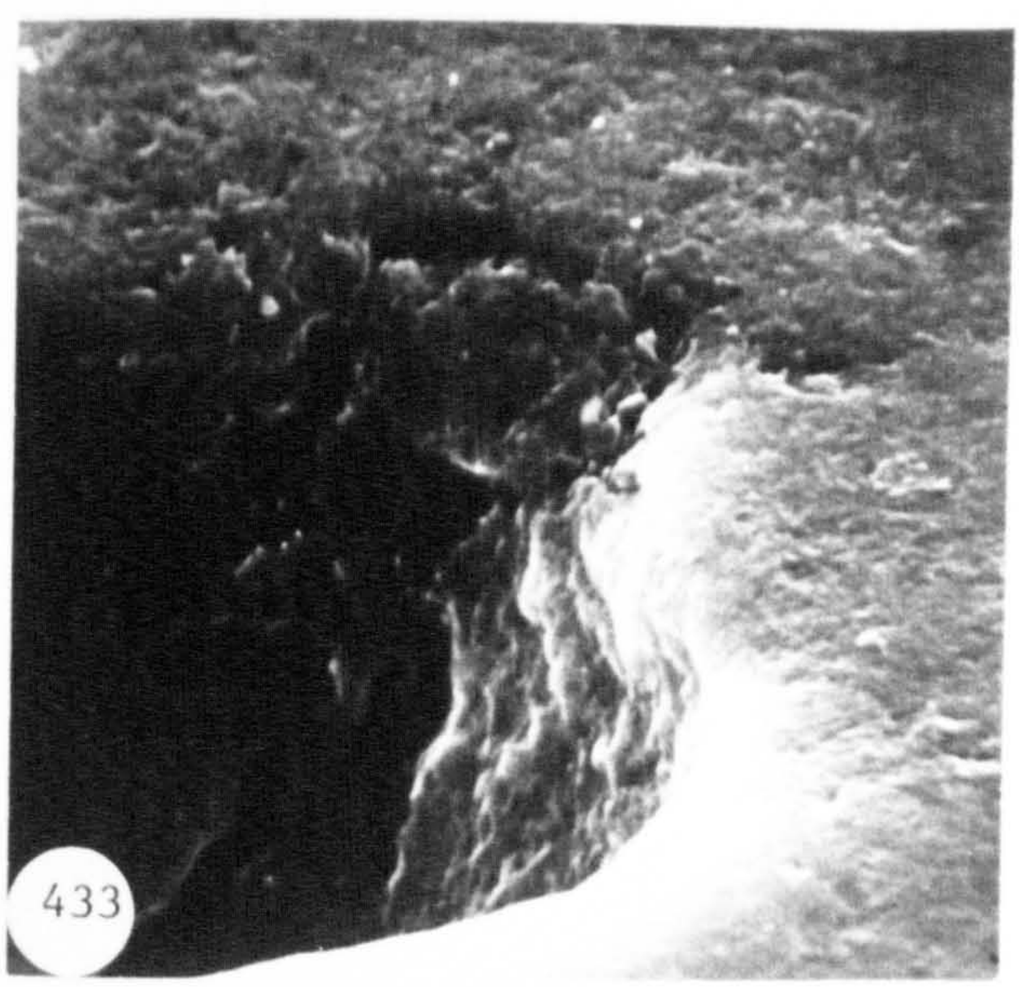
PITCH COKE GRAPHITE 40 μm



PITCH COKE GRAPHITE 2 μm

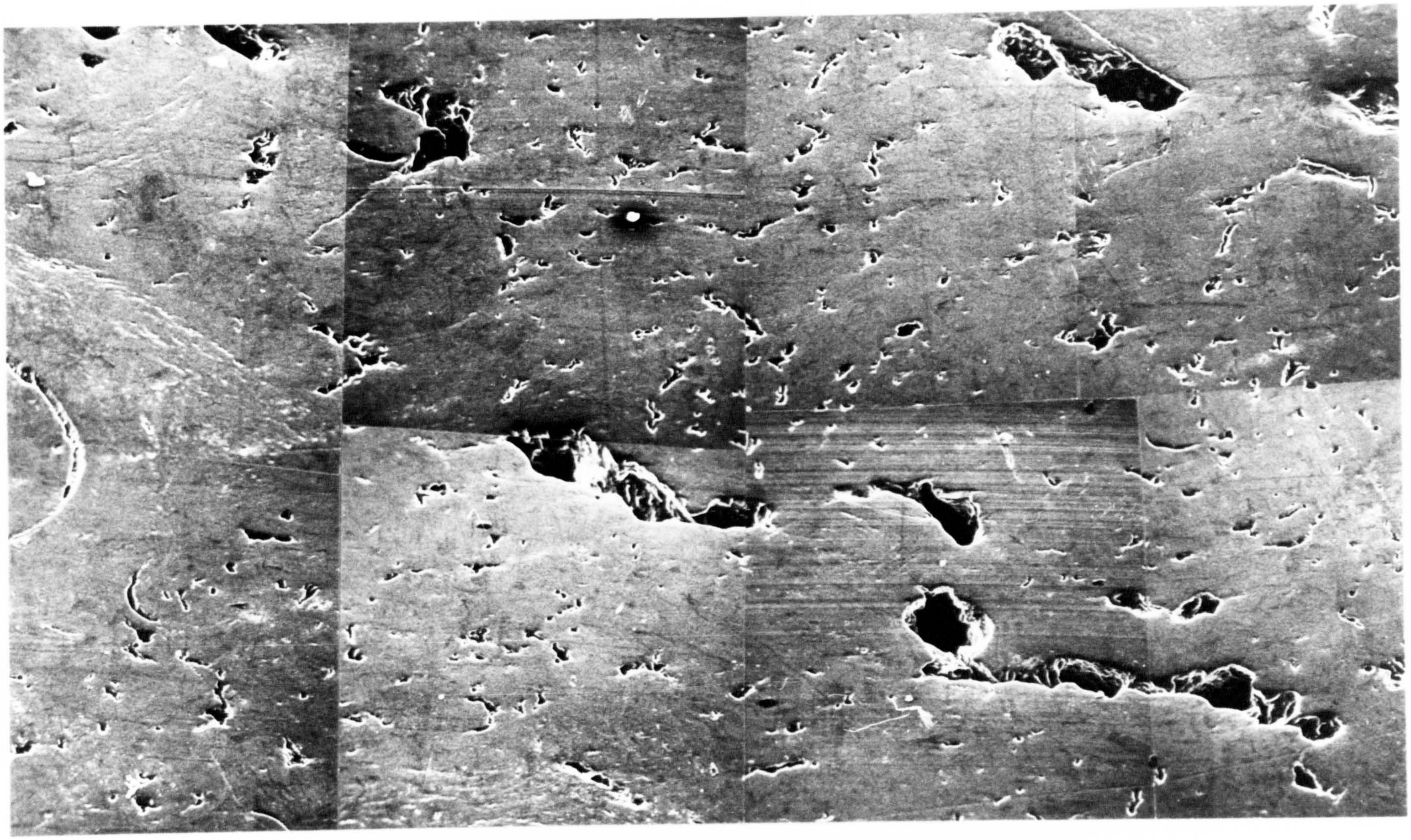


PITCH COKE GRAPHITE 40 μm



PITCH COKE GRAPHITE 2 μm

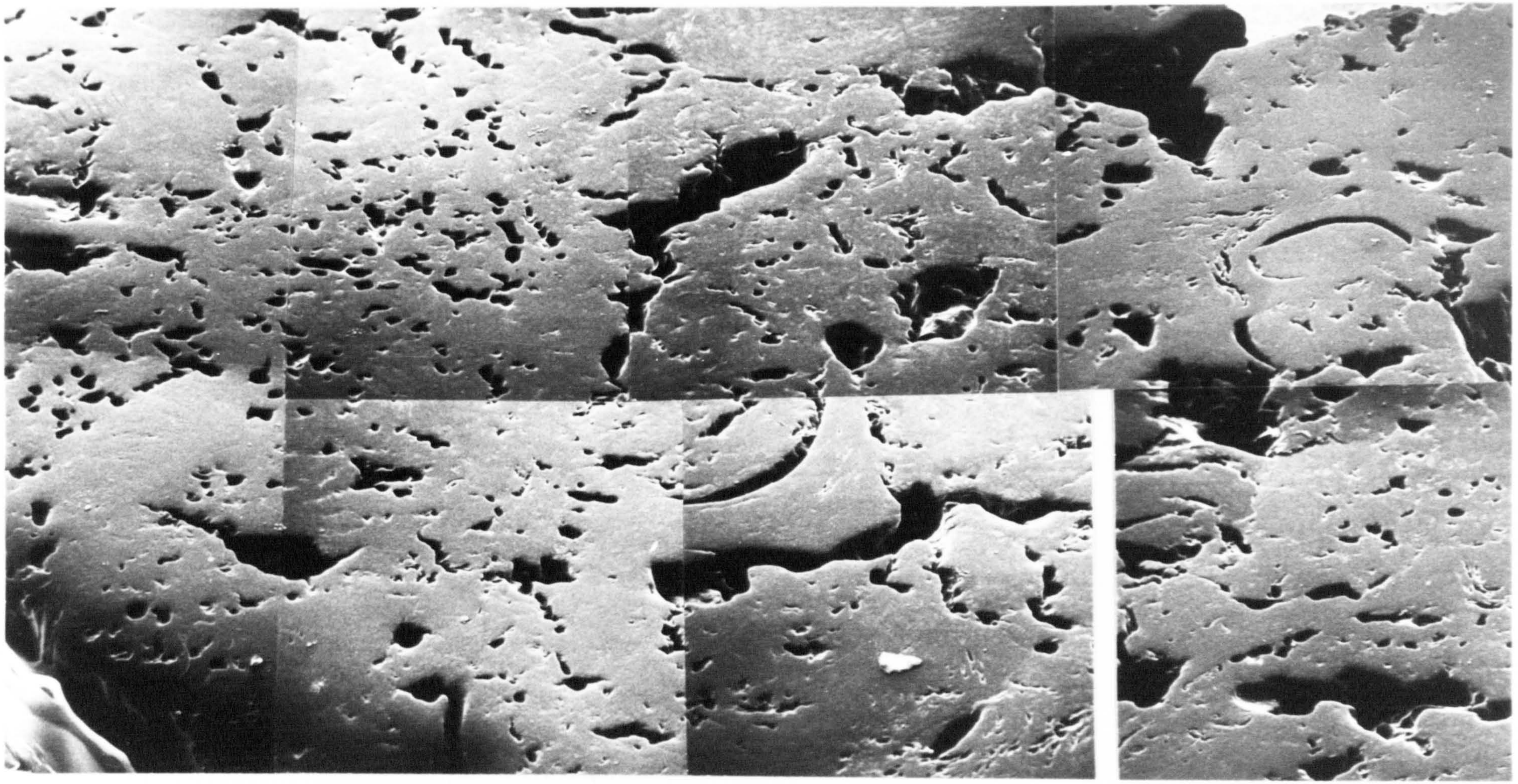
Figures 430 to 433. Scanning electron micrographs (stereoscan) of BAEL Pitch Coke Graphite Q4/1 (Figures 430 and 431) and H24 (Figures 432 and 433), radiolytically oxidised in carbon dioxide. Weight loss 8.8%.



PITCH COKE GRAPHITE

100 µm

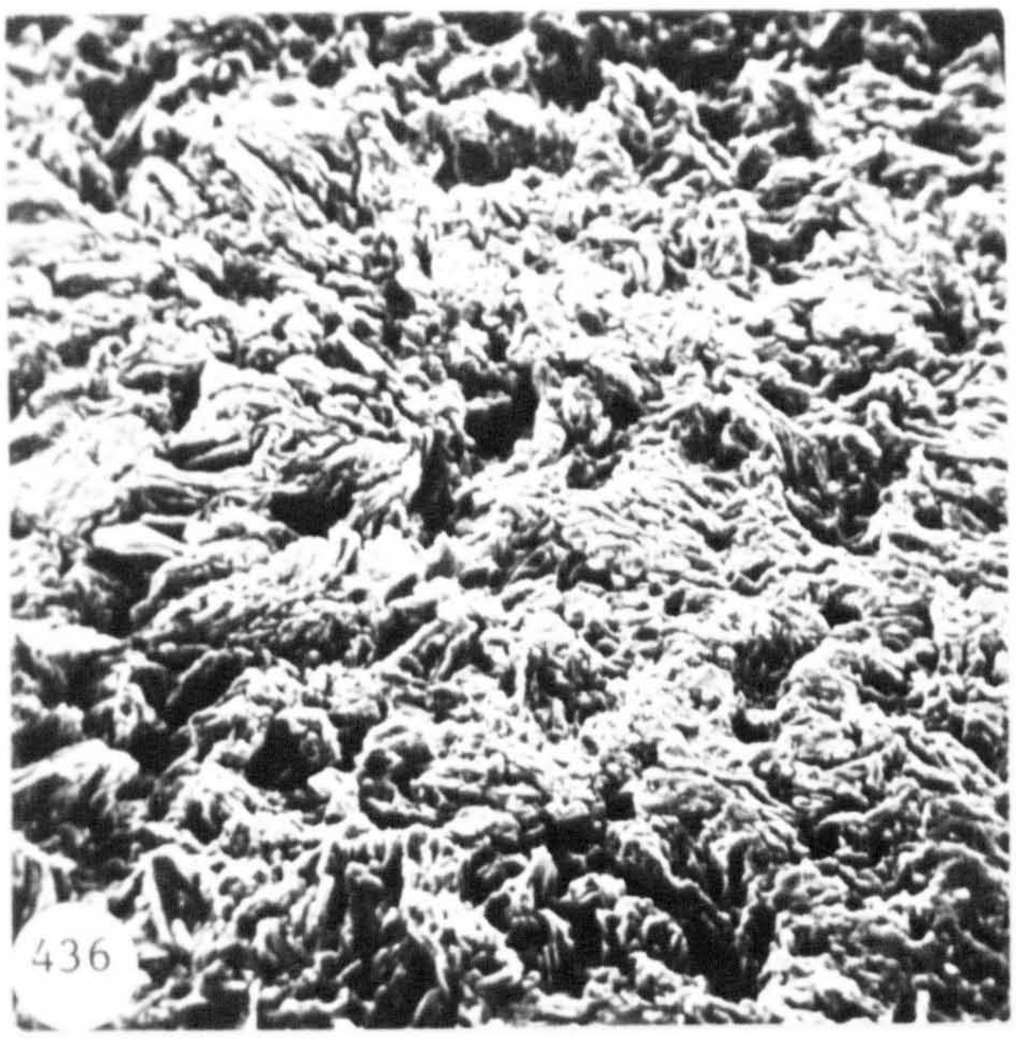
Figure 434. Photo-montage of BAEL Pitch Coke Graphite Q4/1 (Control for H.24)



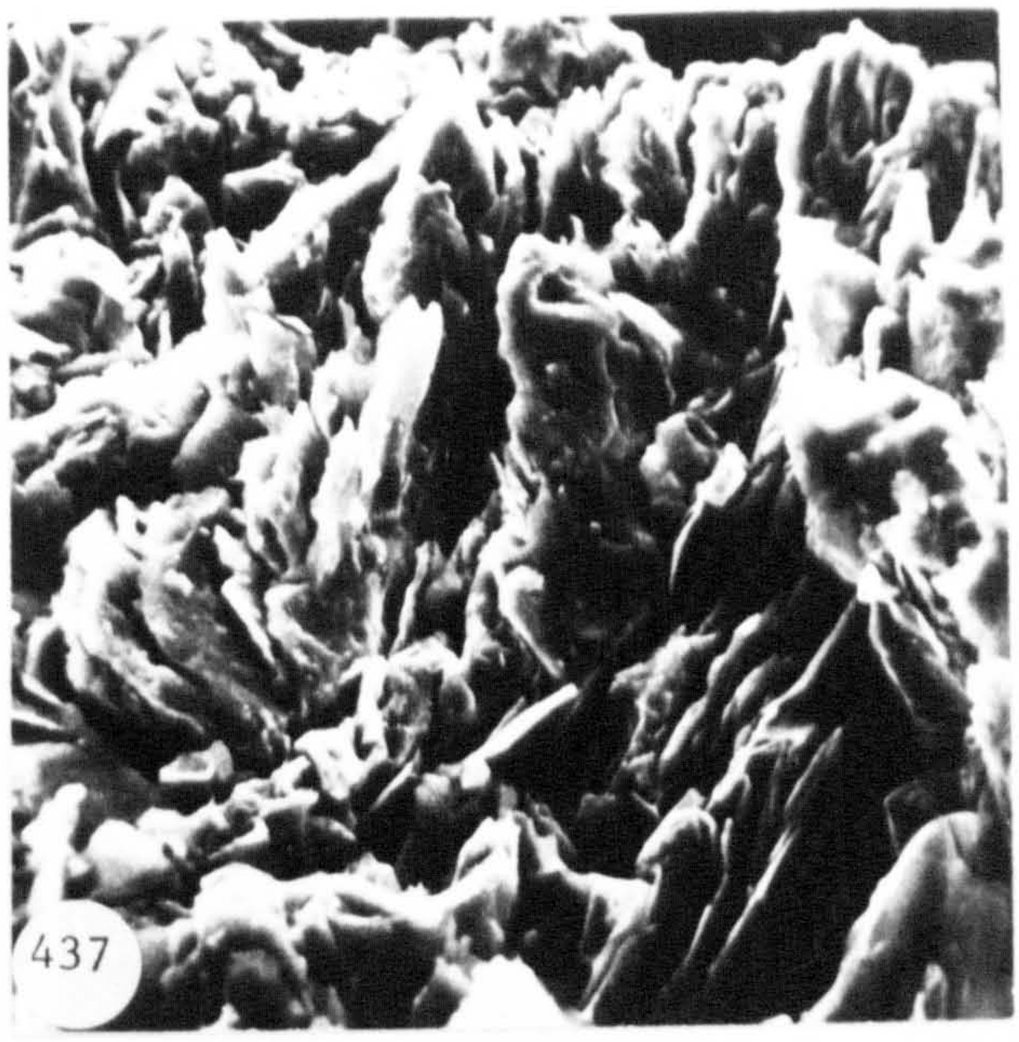
PITCH COKE GRAPHITE

100 μm

Figure 435. Photo-montage of BAEL Pitch Coke Graphite H24, radiolytically oxidised in carbon dioxide. Weight loss 8.8%.



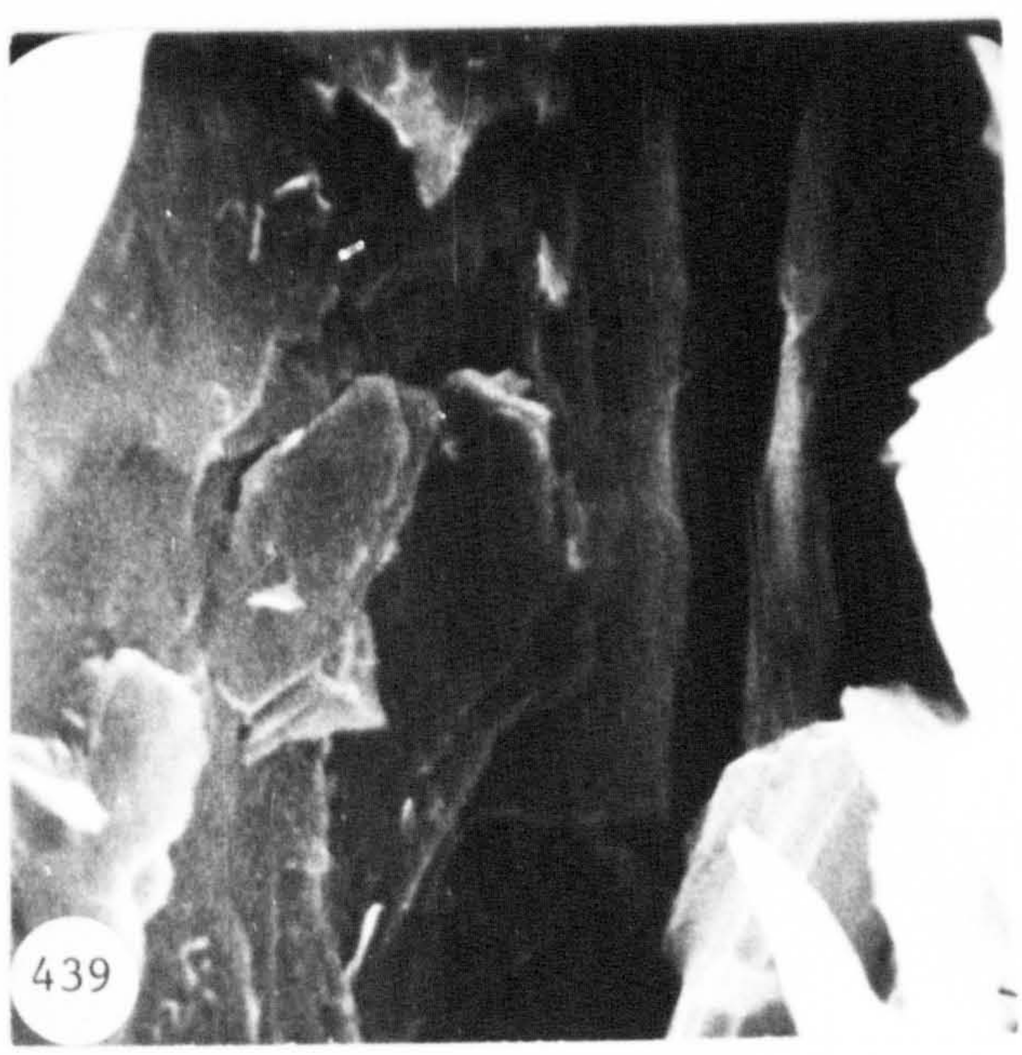
PGA GRAPHITE 100 µm



PGA GRAPHITE 20 µm

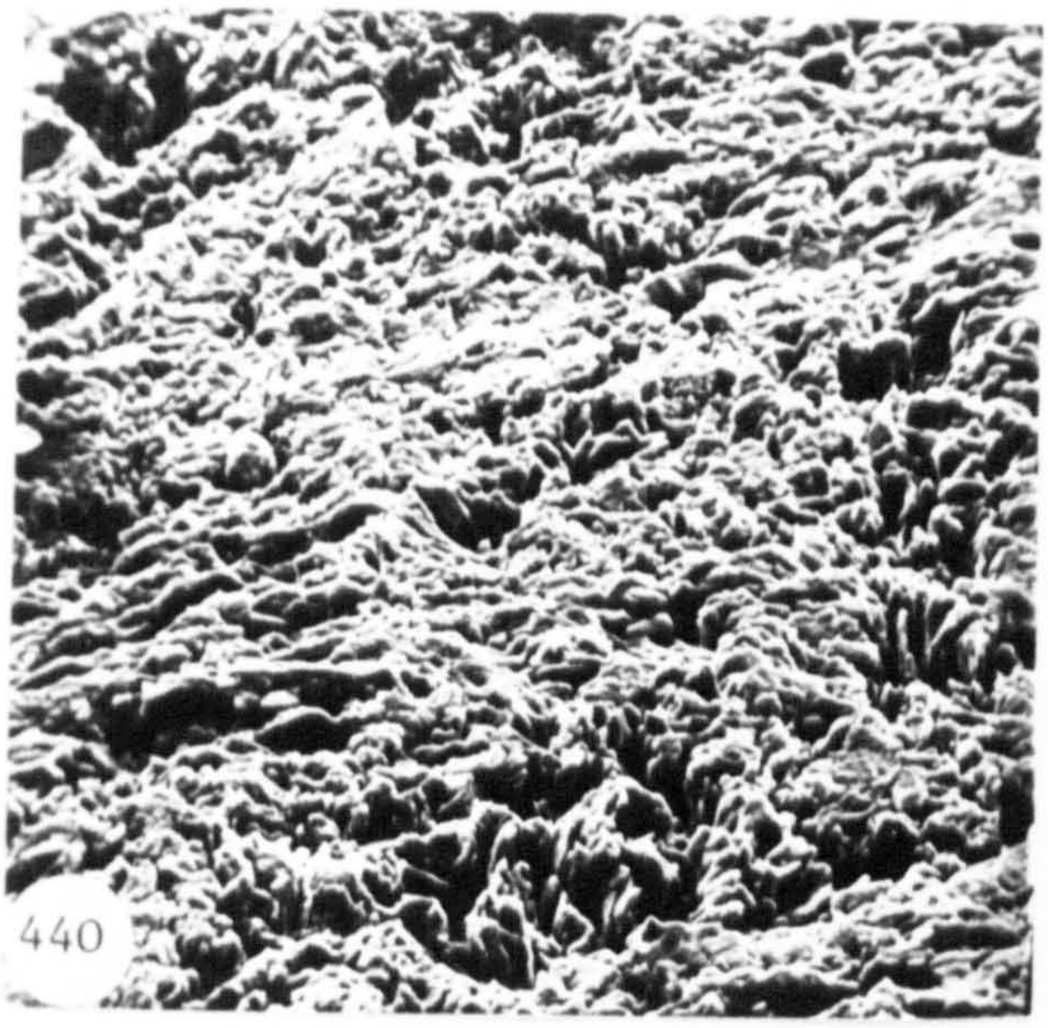


PGA GRAPHITE 10 µm

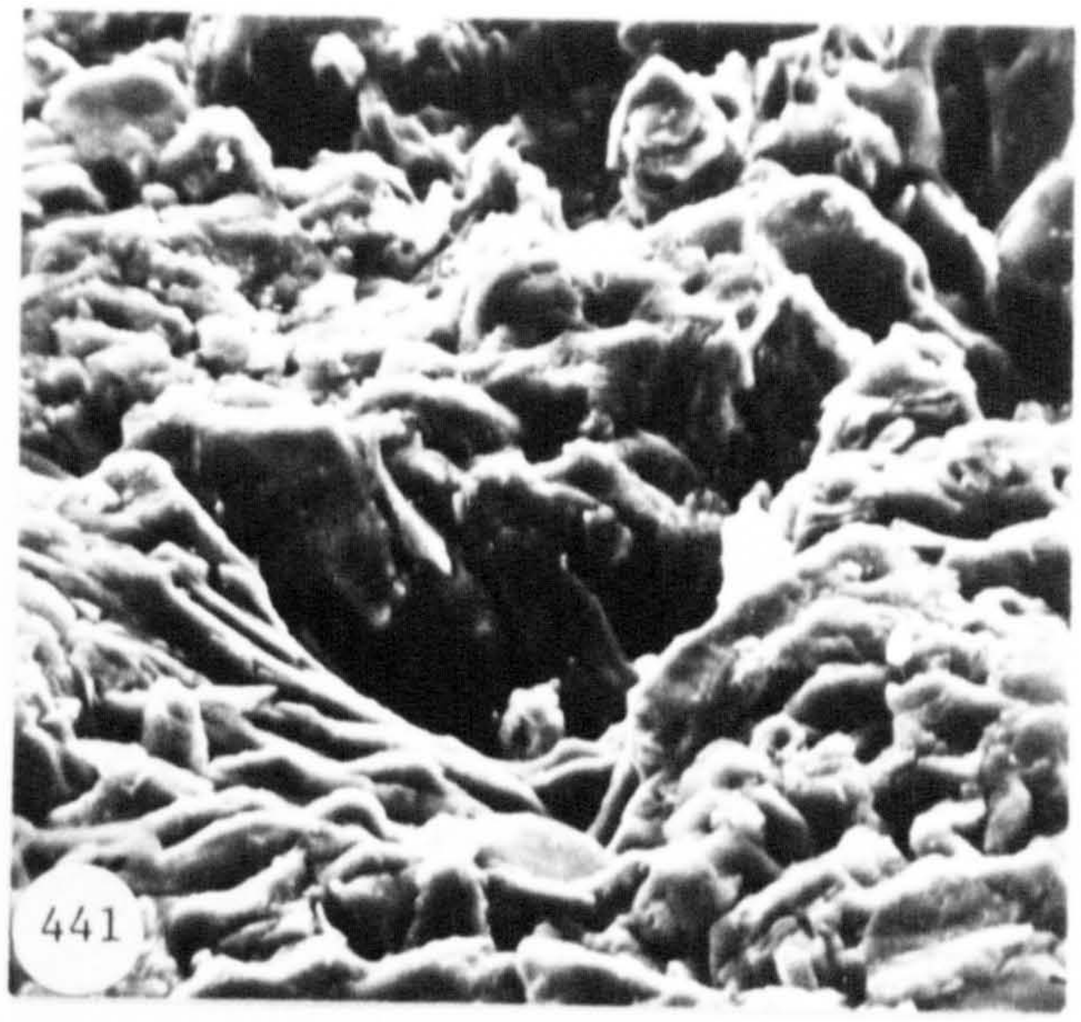


PGA GRAPHITE 2 µm

Figures 436 to 439. Scanning electron micrographs (stereoscan) of PGA Graphite C7/1 (Control for C79).



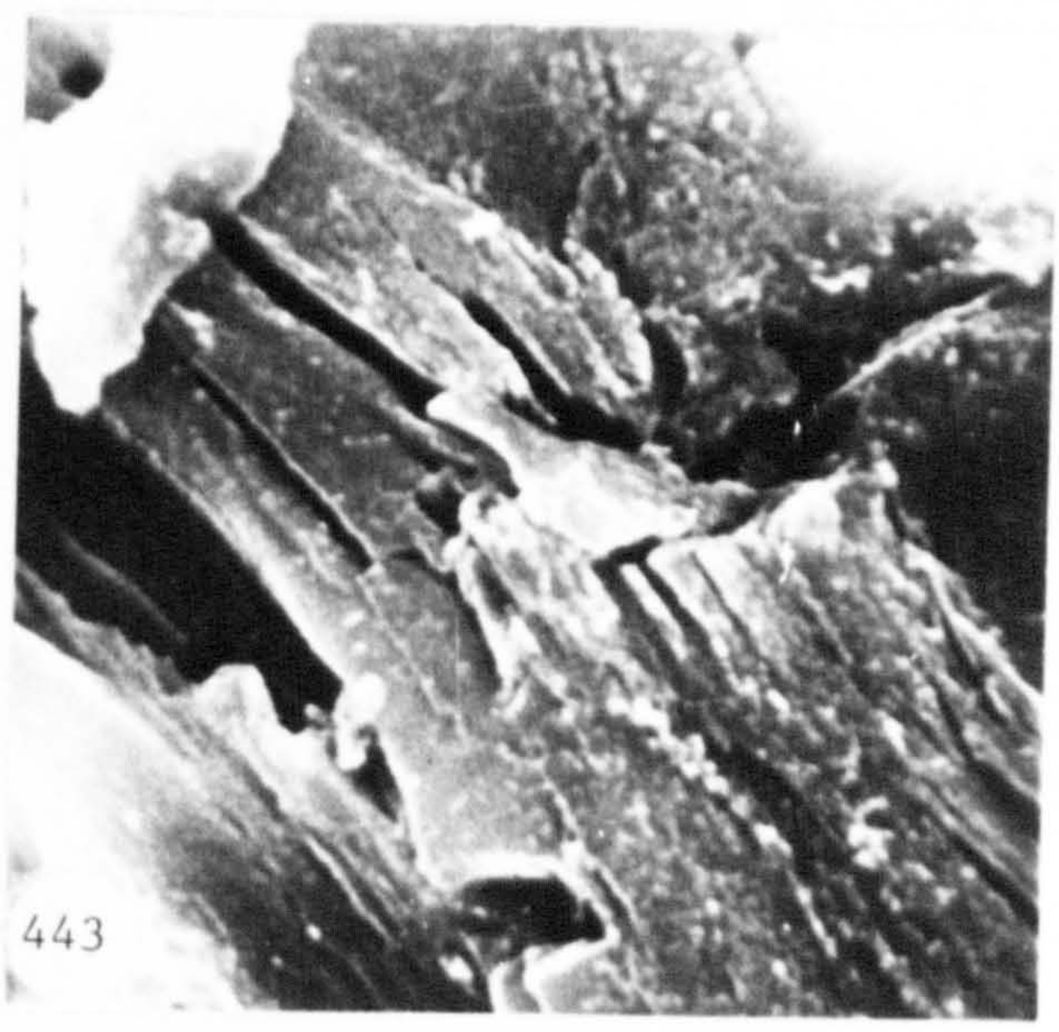
PGA GRAPHITE 100 µm



PGA GRAPHITE 20 µm

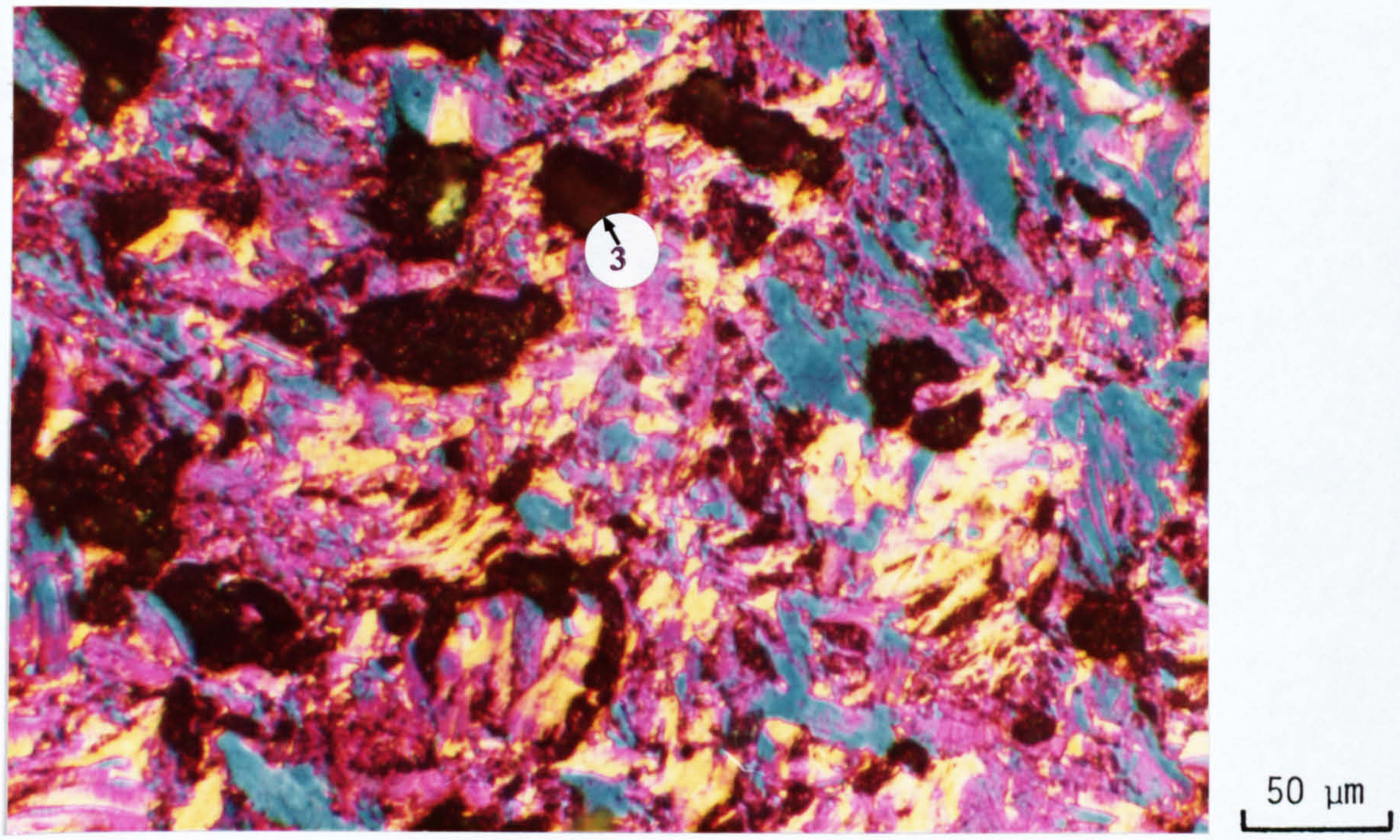


PGA GRAPHITE 5 µm



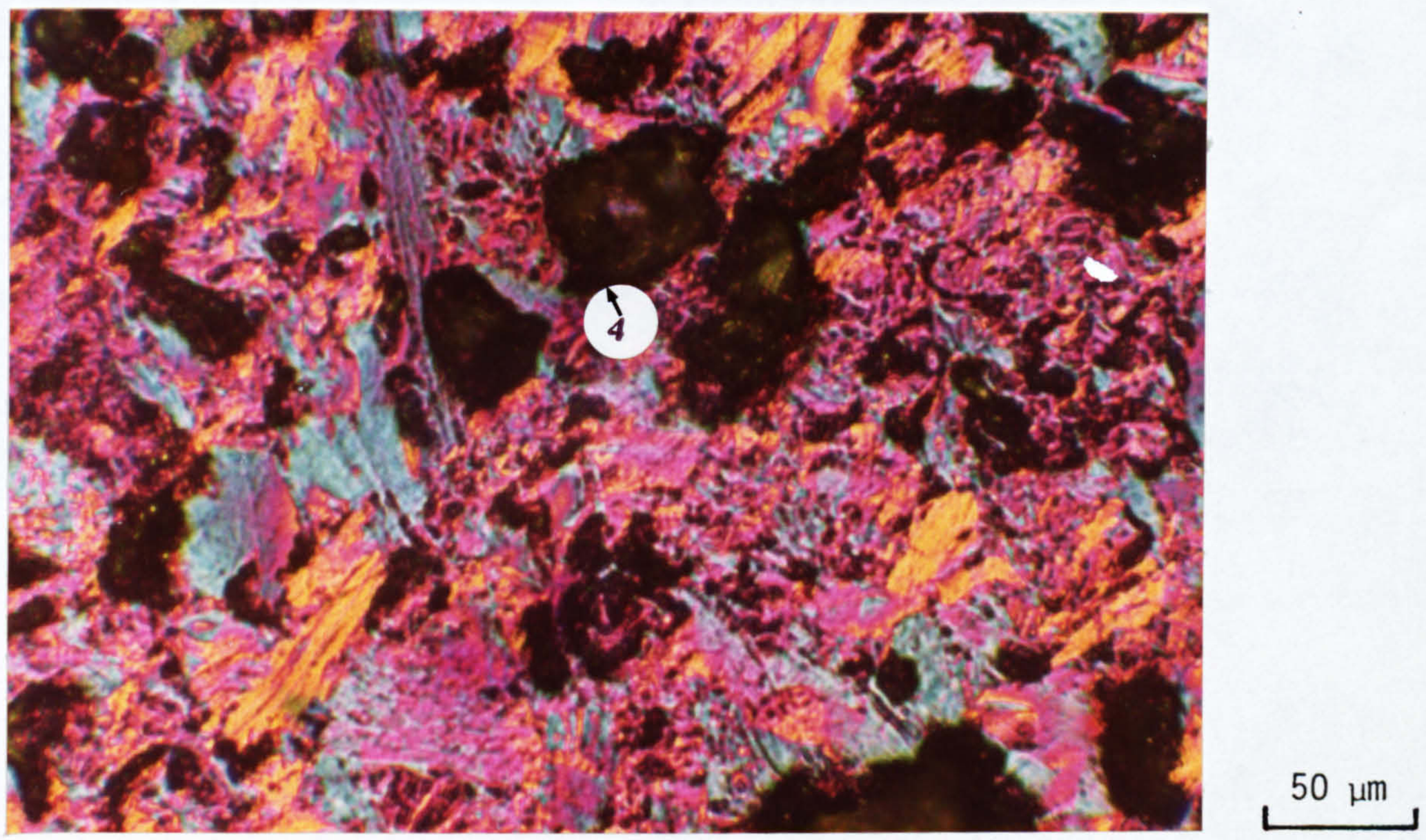
PGA GRAPHITE 2 µm

Figures 440 to 443. Scanning electron micrographs (stereoscan) of PGA Graphite C79, radiolytically oxidised in carbon dioxide. Weight loss 6.2%.



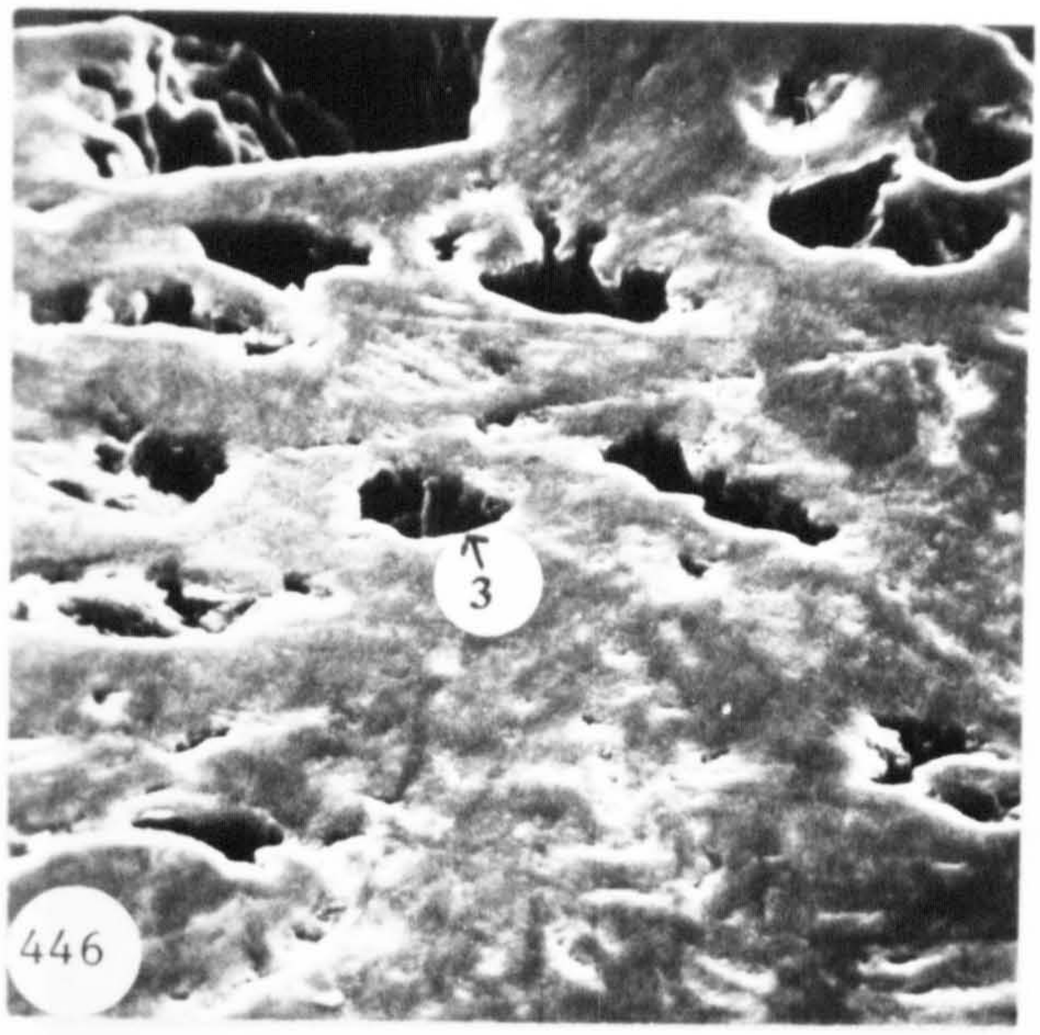
PGA GRAPHITE

Figure 444. Optical micrograph of PGA Graphite C7/1 (Control for C79).

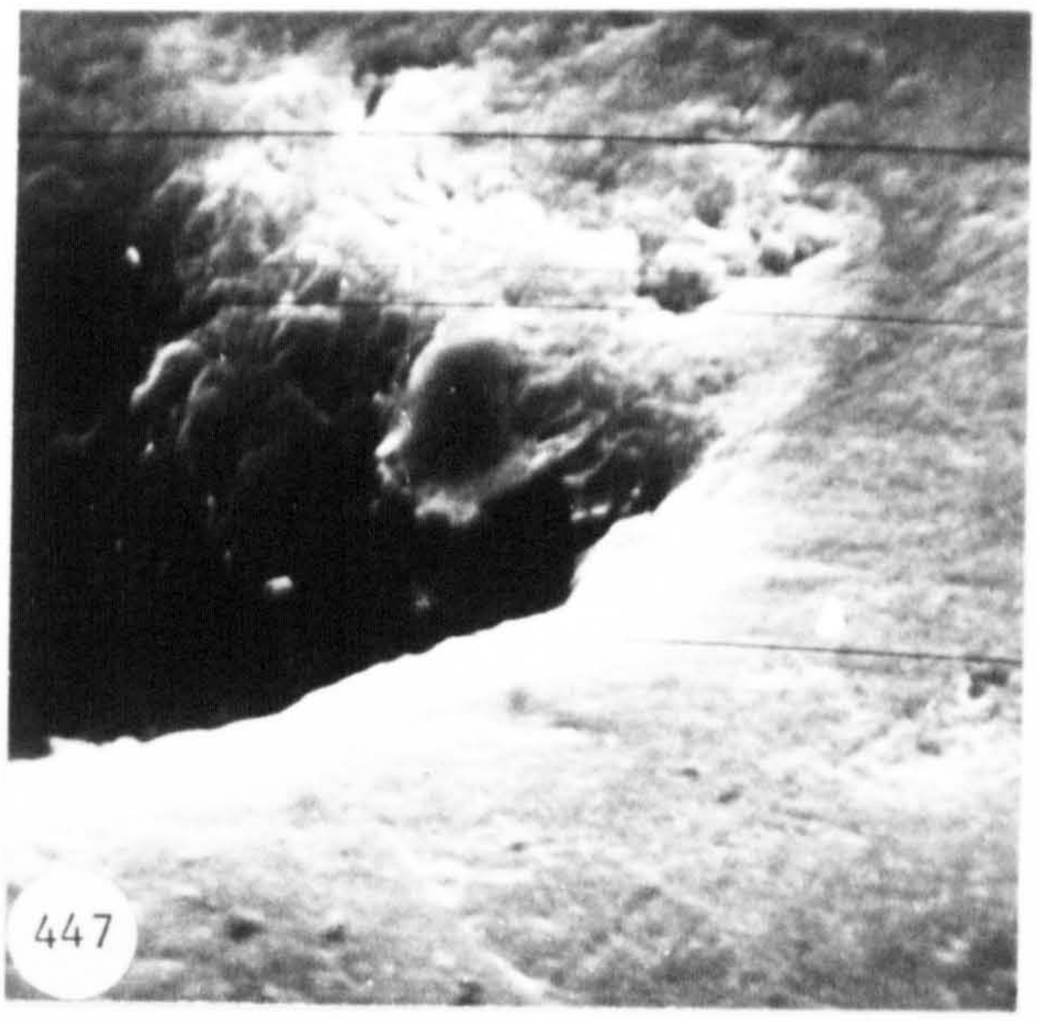


PGA GRAPHITE

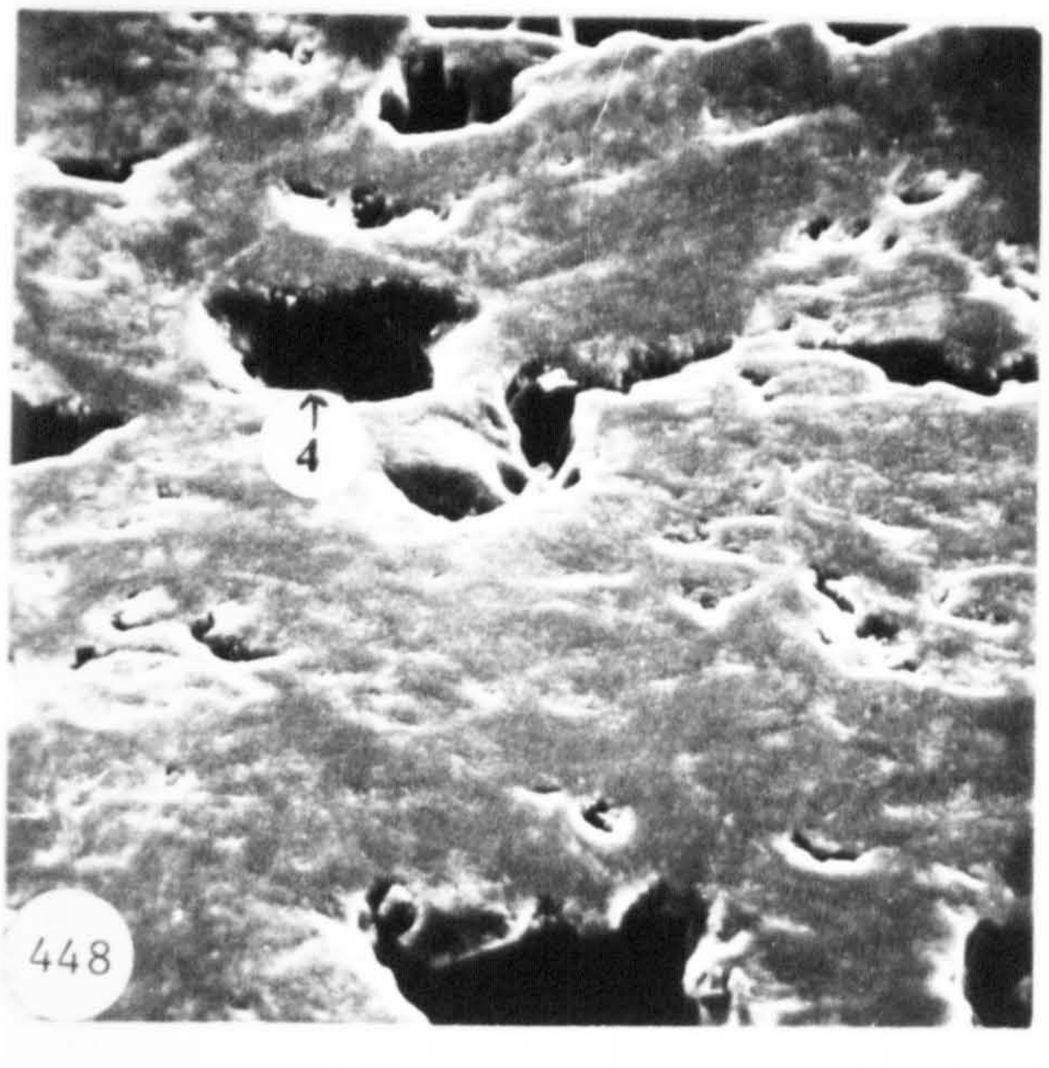
Figure 445. Optical micrograph of PGA Graphite C79, radiolytically oxidised in carbon dioxide. Weight loss 6.2%.



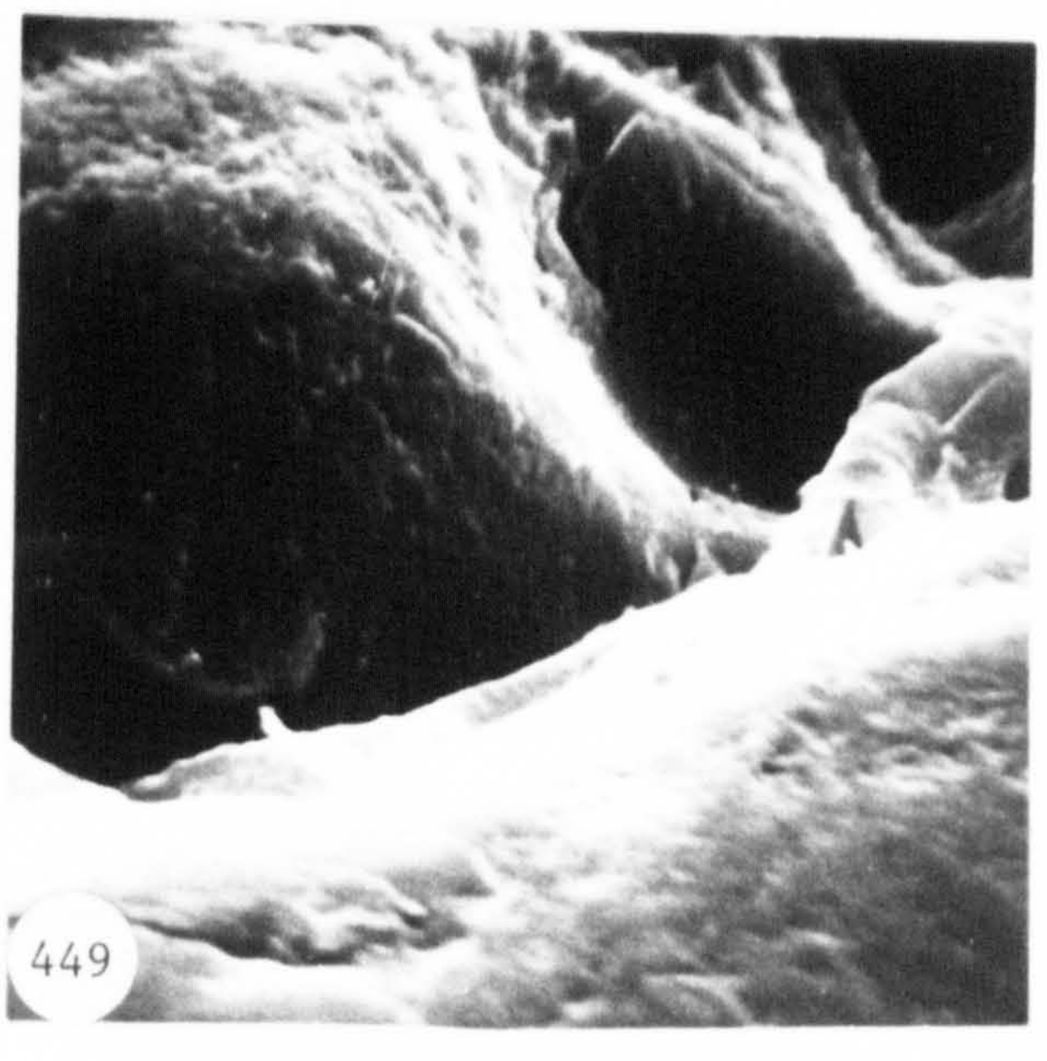
PGA GRAPHITE 40 μm



PGA GRAPHITE 2 μm

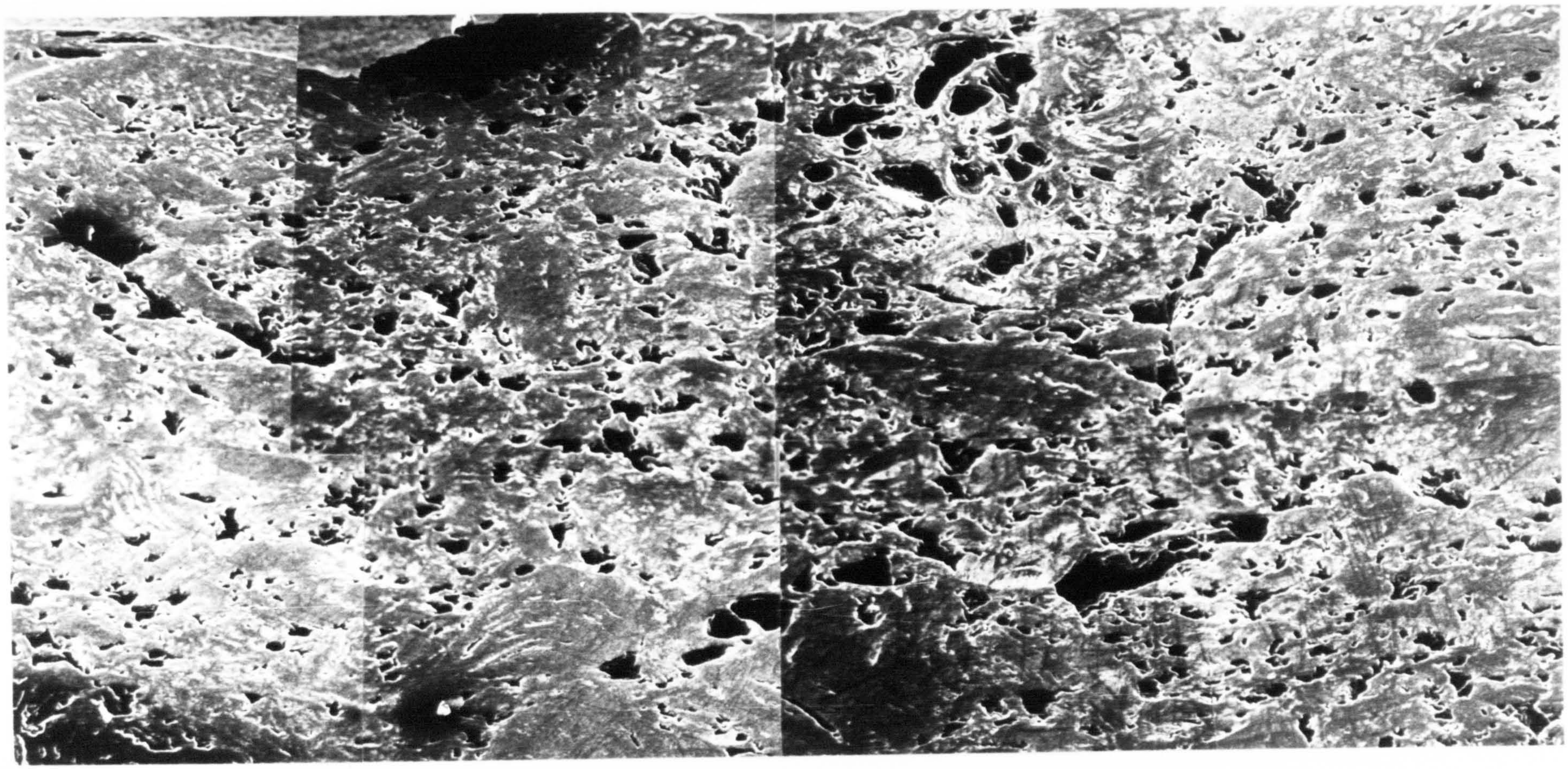


PGA GRAPHITE 40 μm



PGA GRAPHITE 2 μm

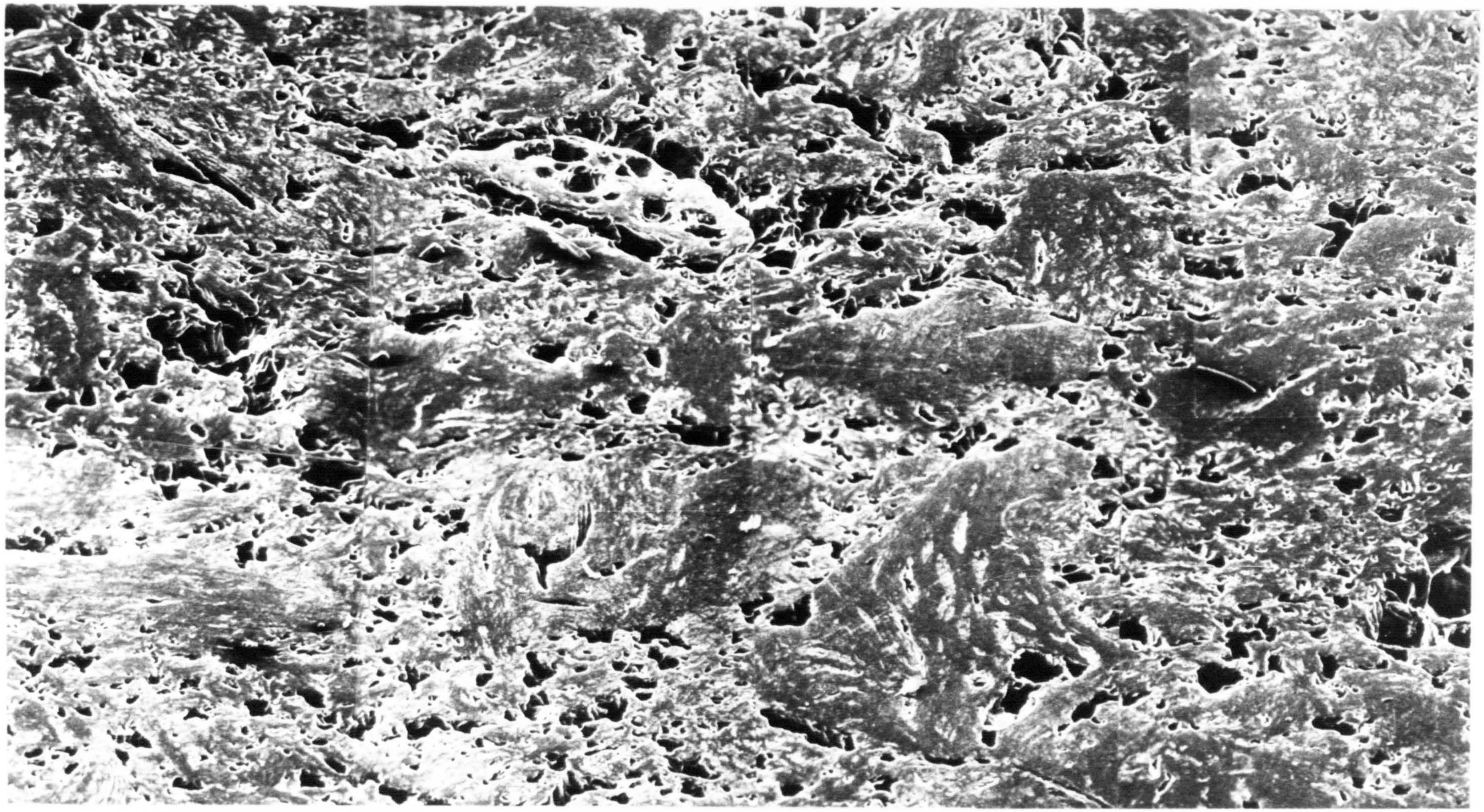
Figures 446 to 449. Scanning electron micrographs (stereoscan) of PGA Graphite C7/1 (Figures 446 and 447) and C79 (Figures 448 and 449), radiolytically oxidised in carbon dioxide. Weight loss 6.2%.



PGA GRAPHITE

100 μm

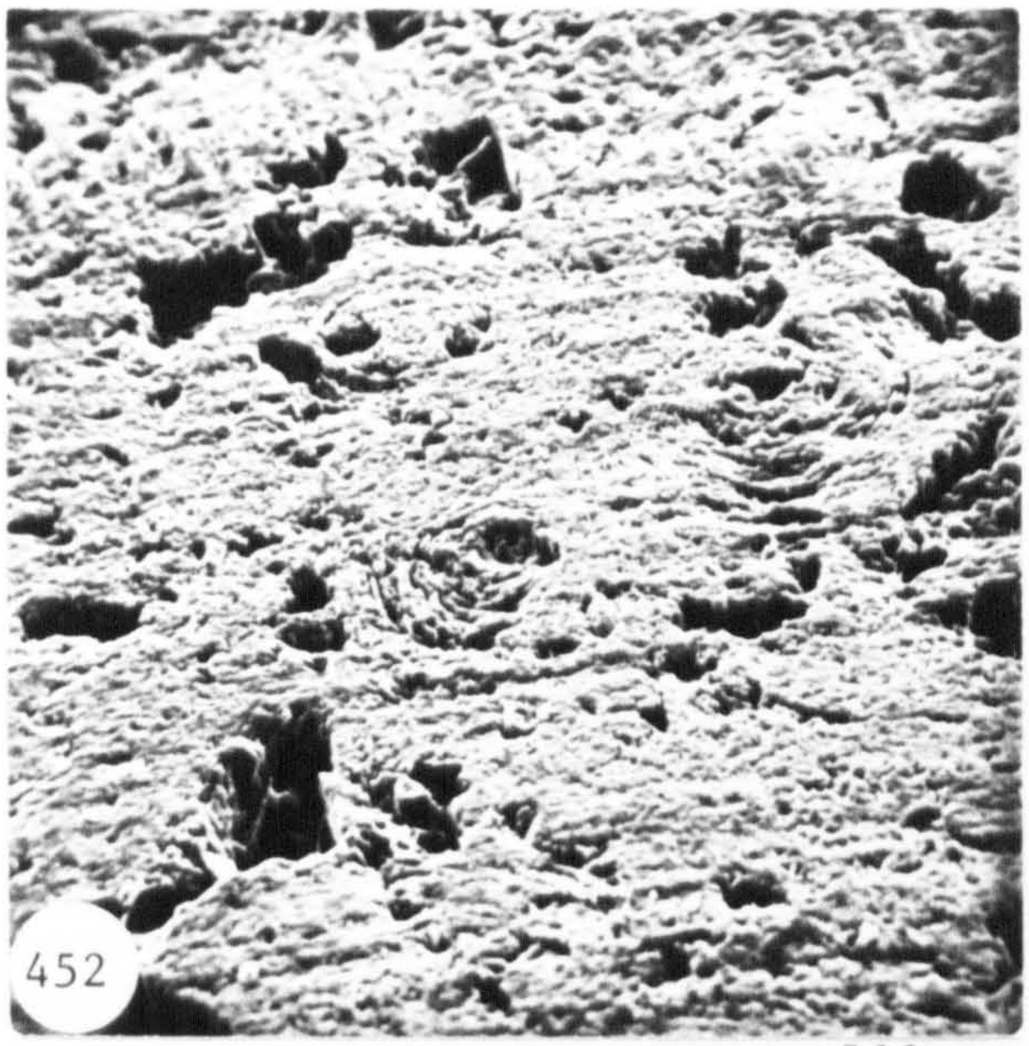
Figure 450. Photo-montage of PGA Graphite C7/1 (Control for C79).



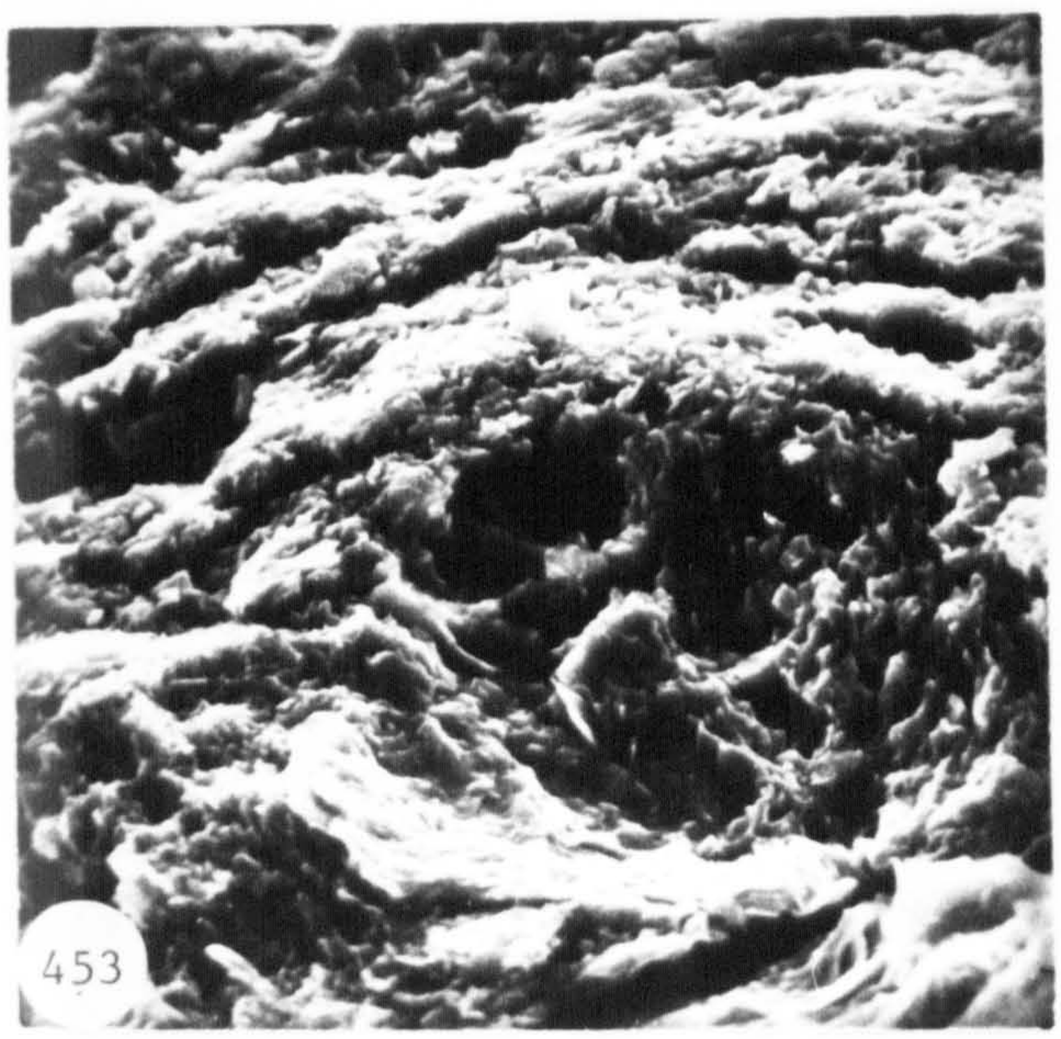
PGA GRAPHITE.

100 μm

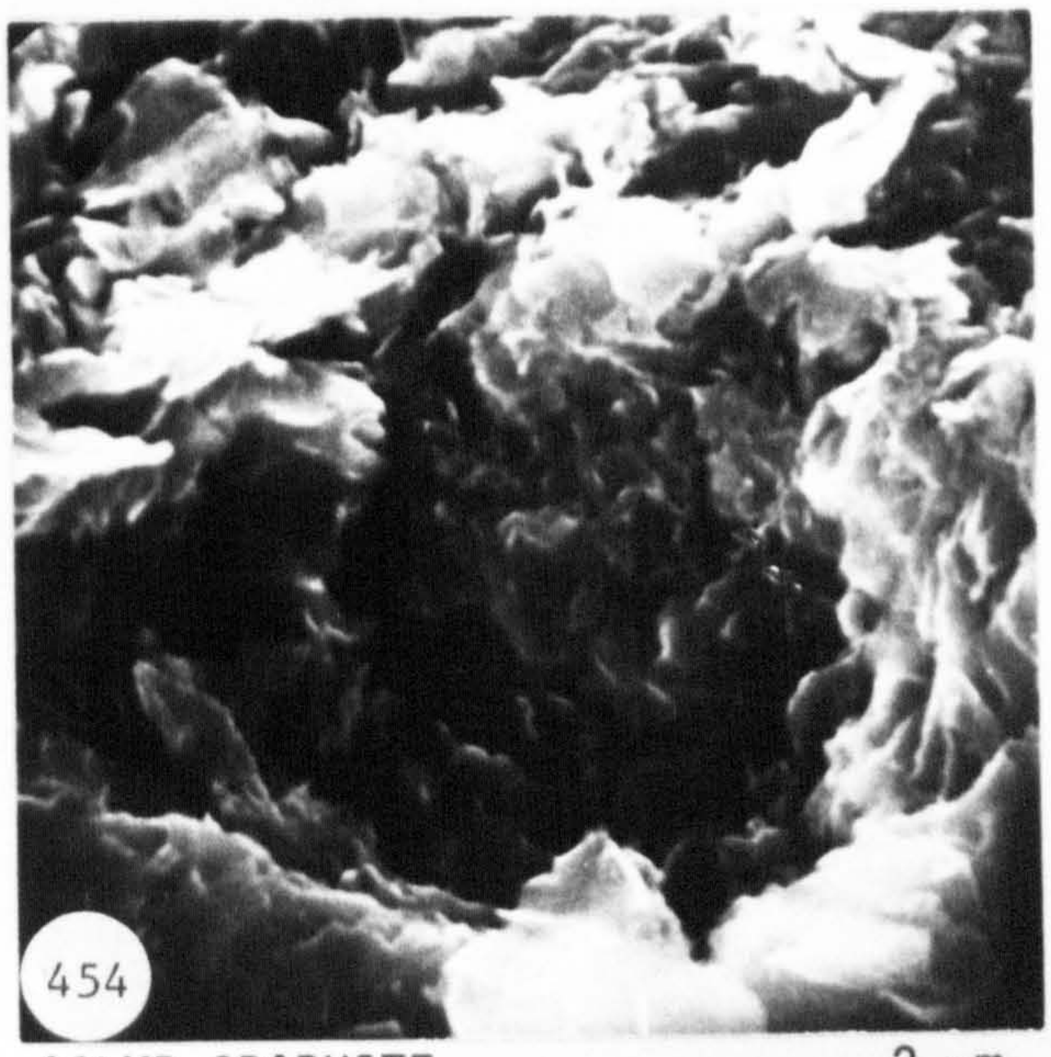
Figure 451. Photo-montage of PGA Graphite C79, radiolytically oxidised in carbon dioxide. Weight loss 6.6%.



AGLMP GRAPHITE 100 µm



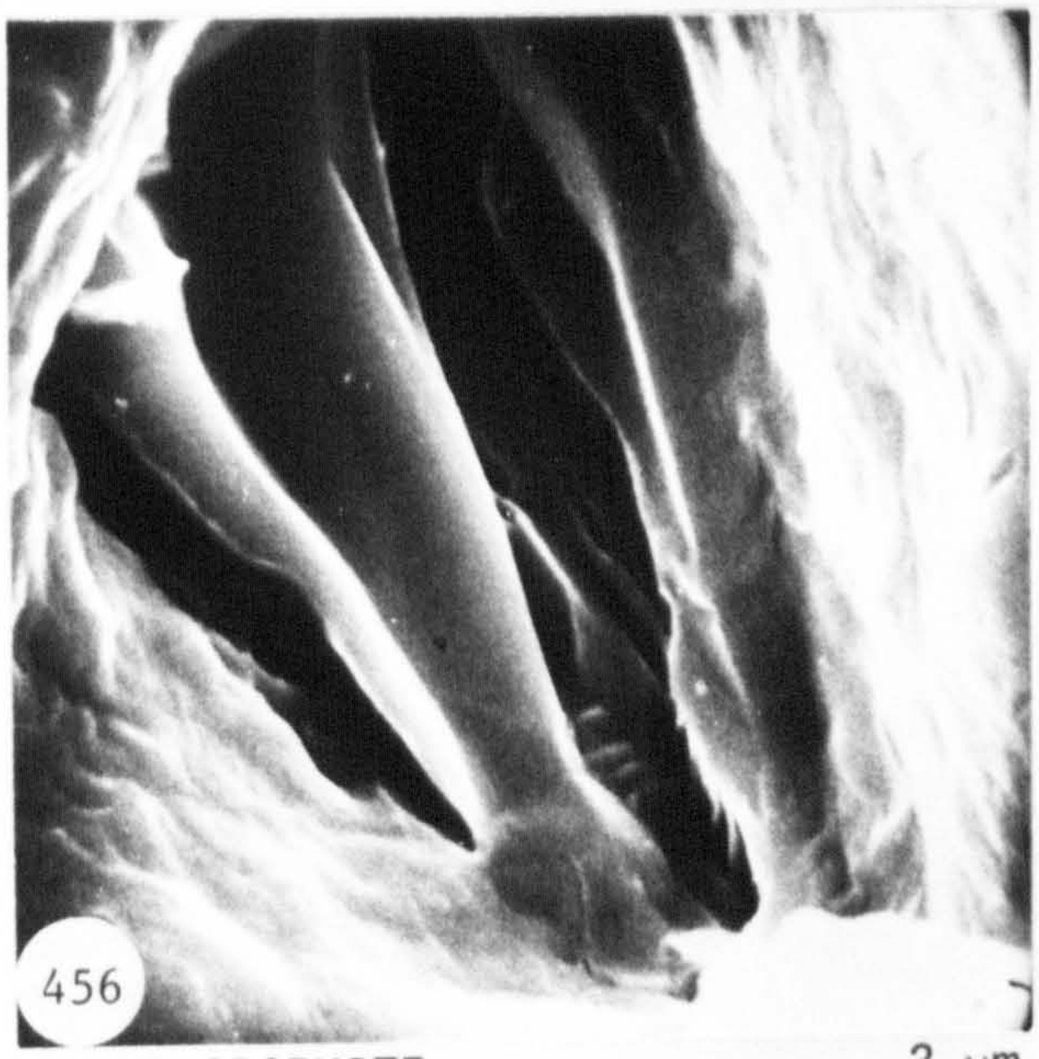
AGLMP GRAPHITE 10 µm



AGLMP GRAPHITE 2 µm

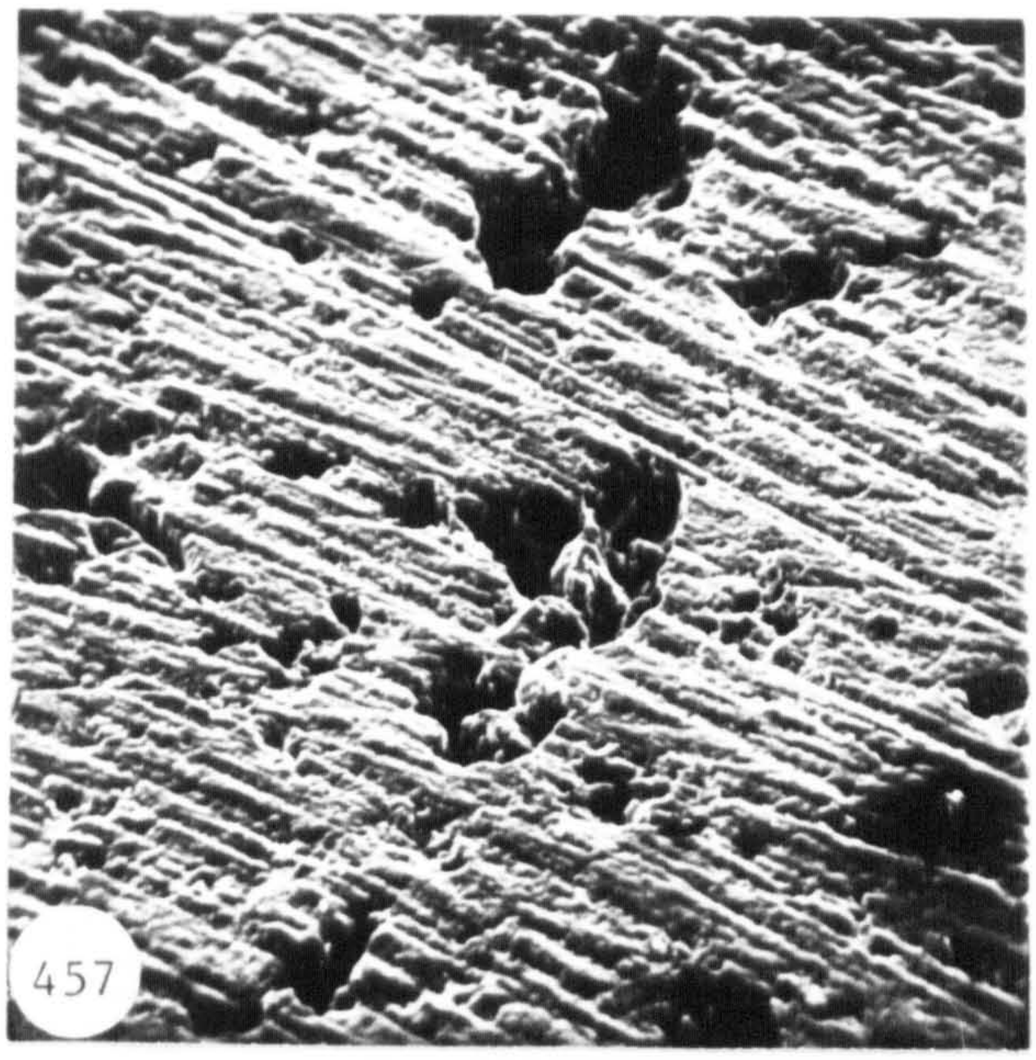


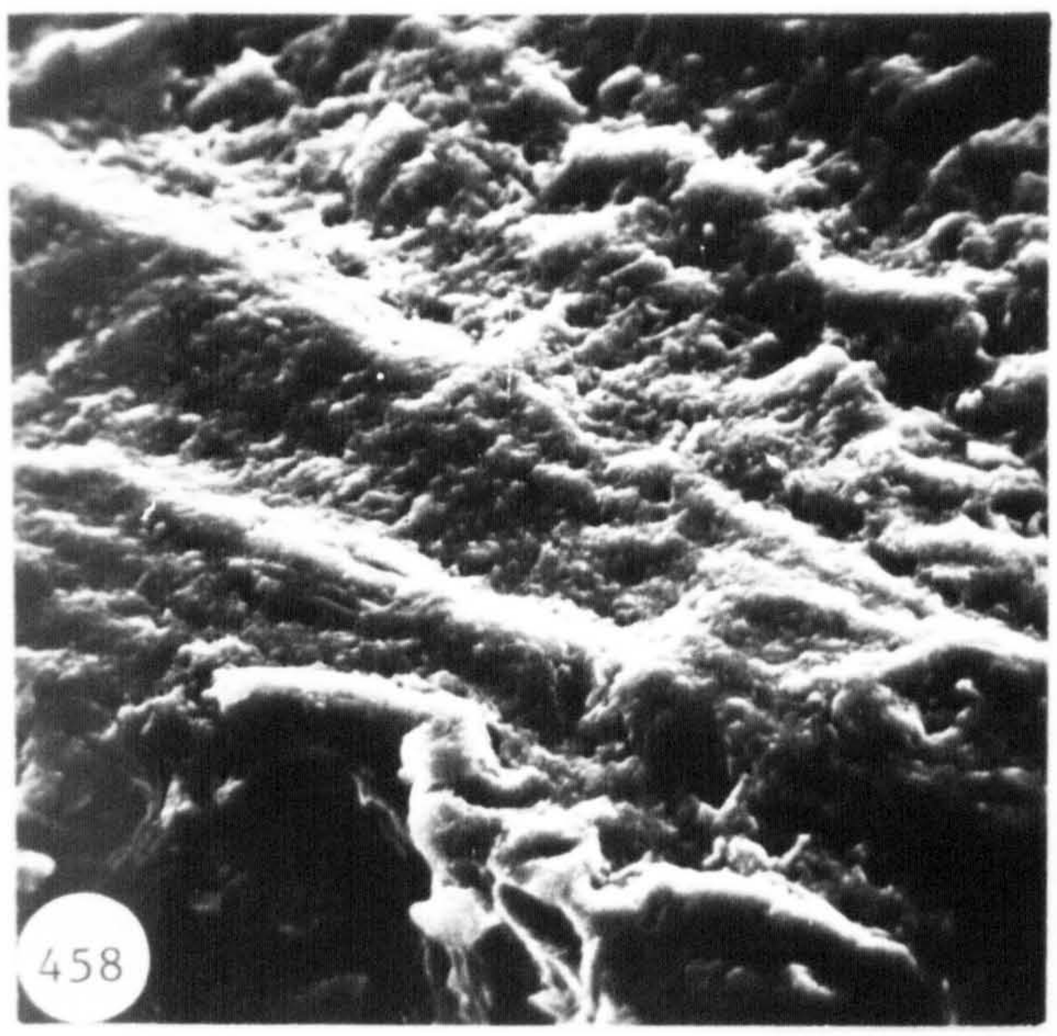
AGLMP GRAPHITE 20 µm

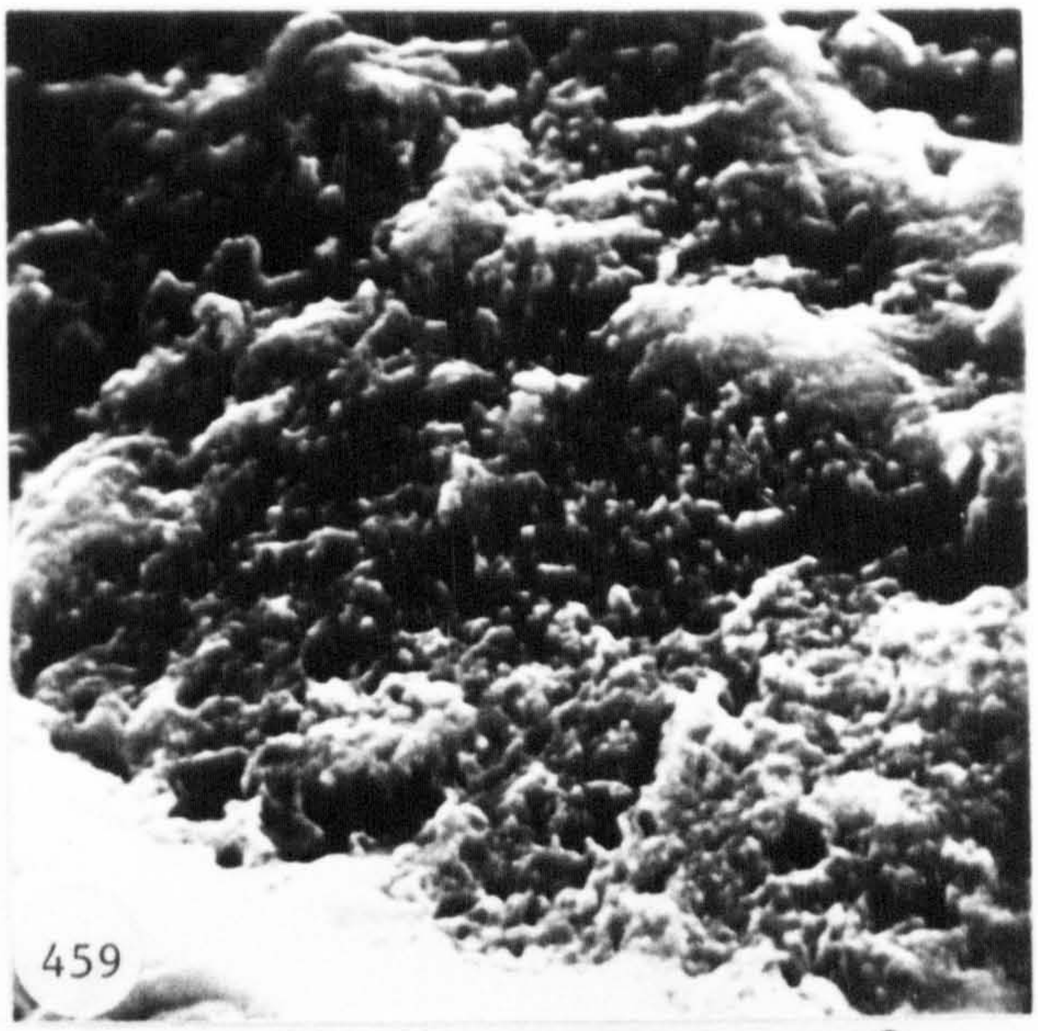


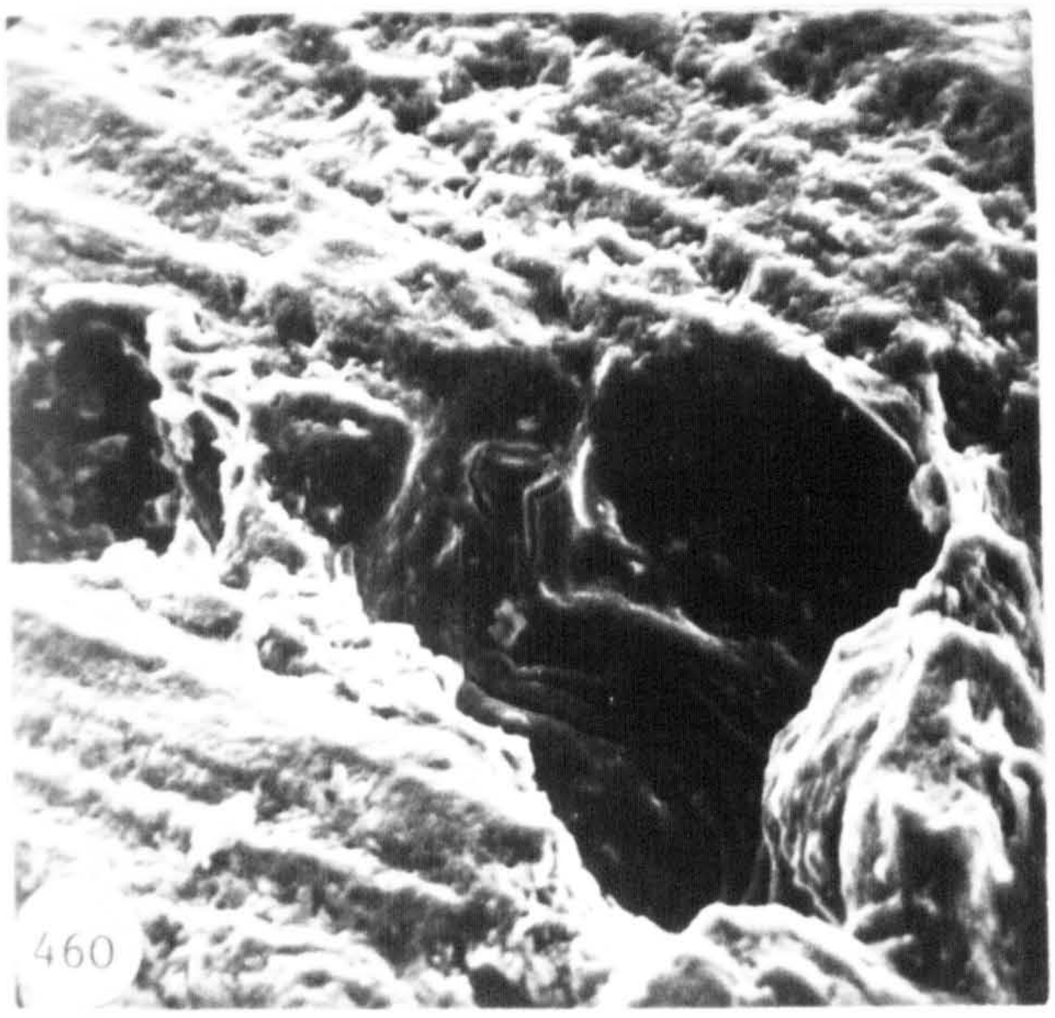
AGLMP GRAPHITE 2 µm

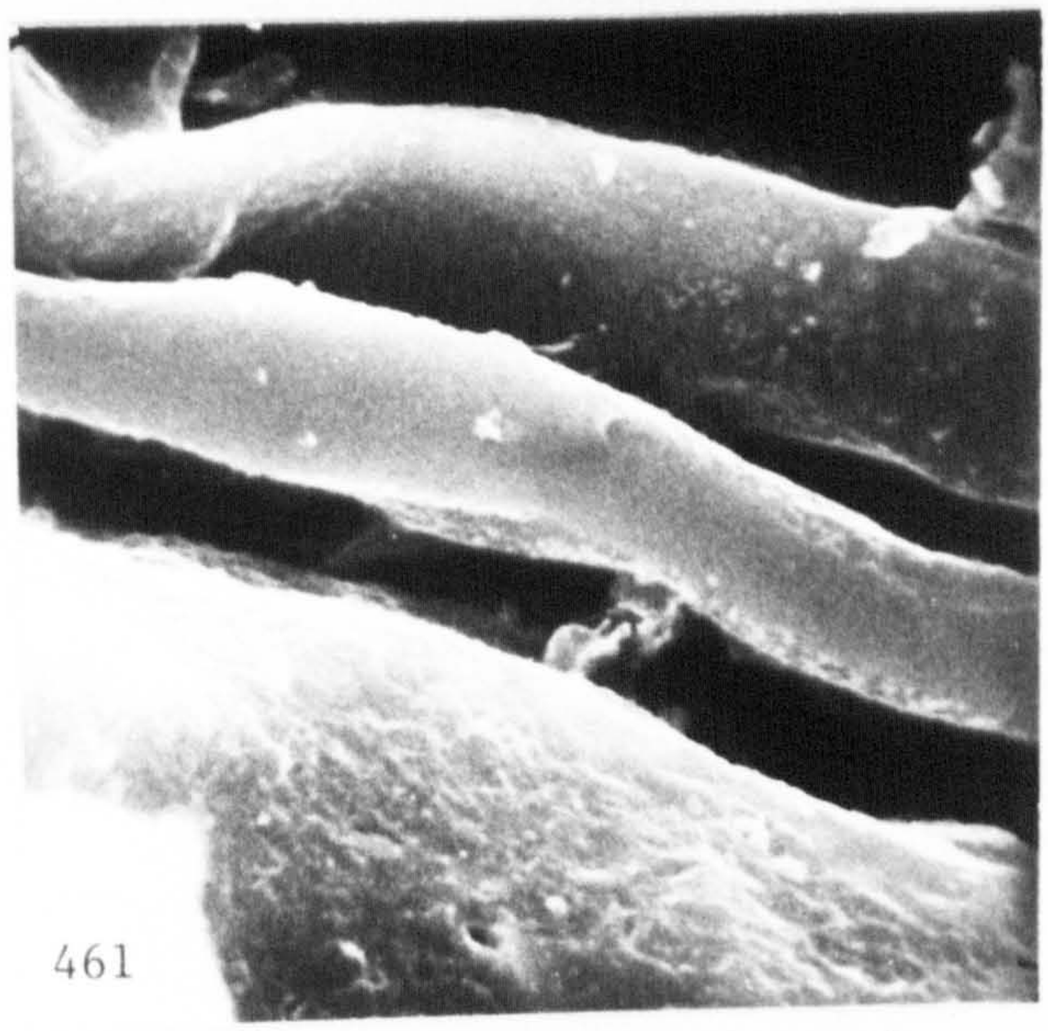
Figures 452 to 456. Scanning electron micrographs (stereoscan) of AGLMP Graphite 10F49 (control for M38).



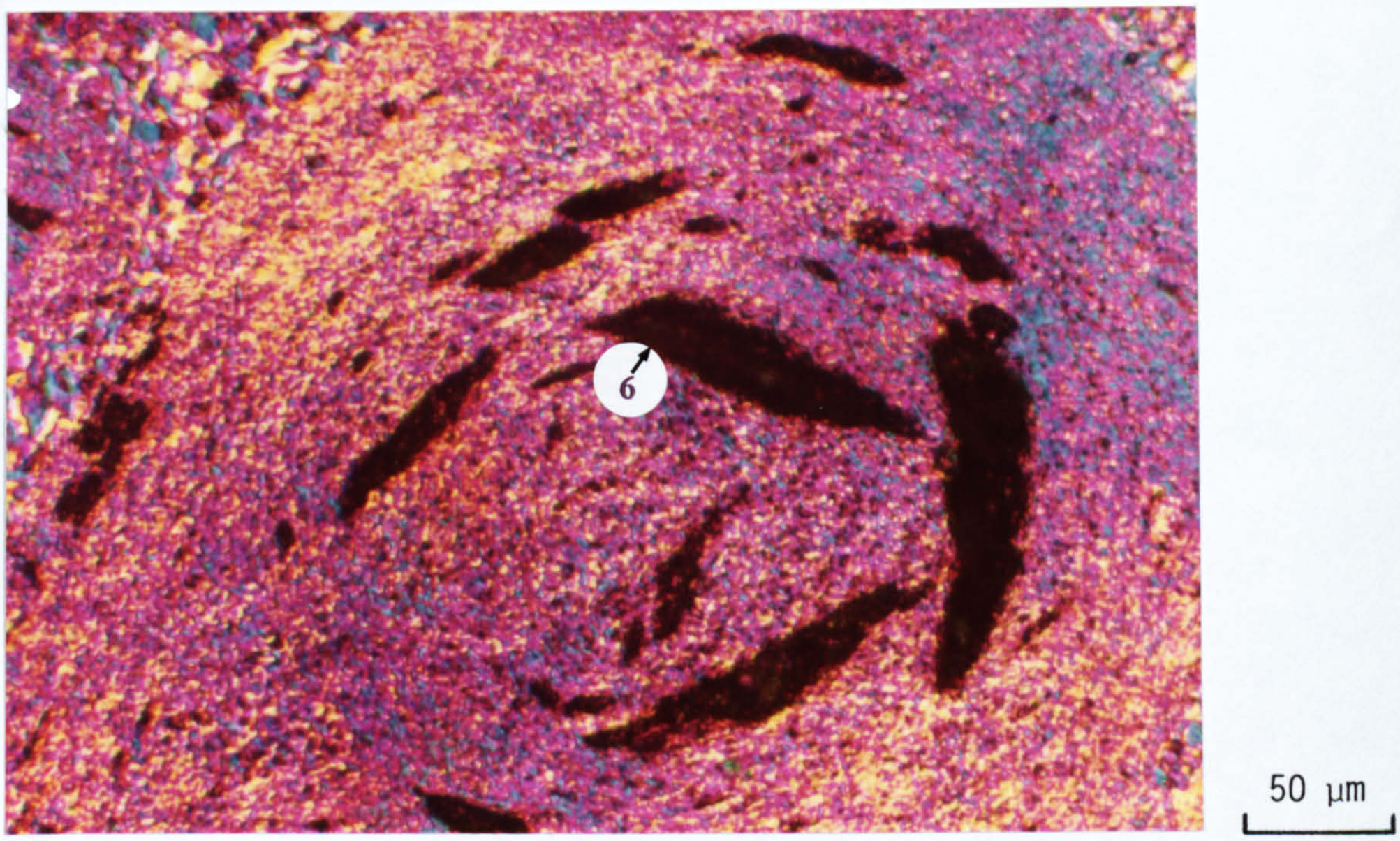






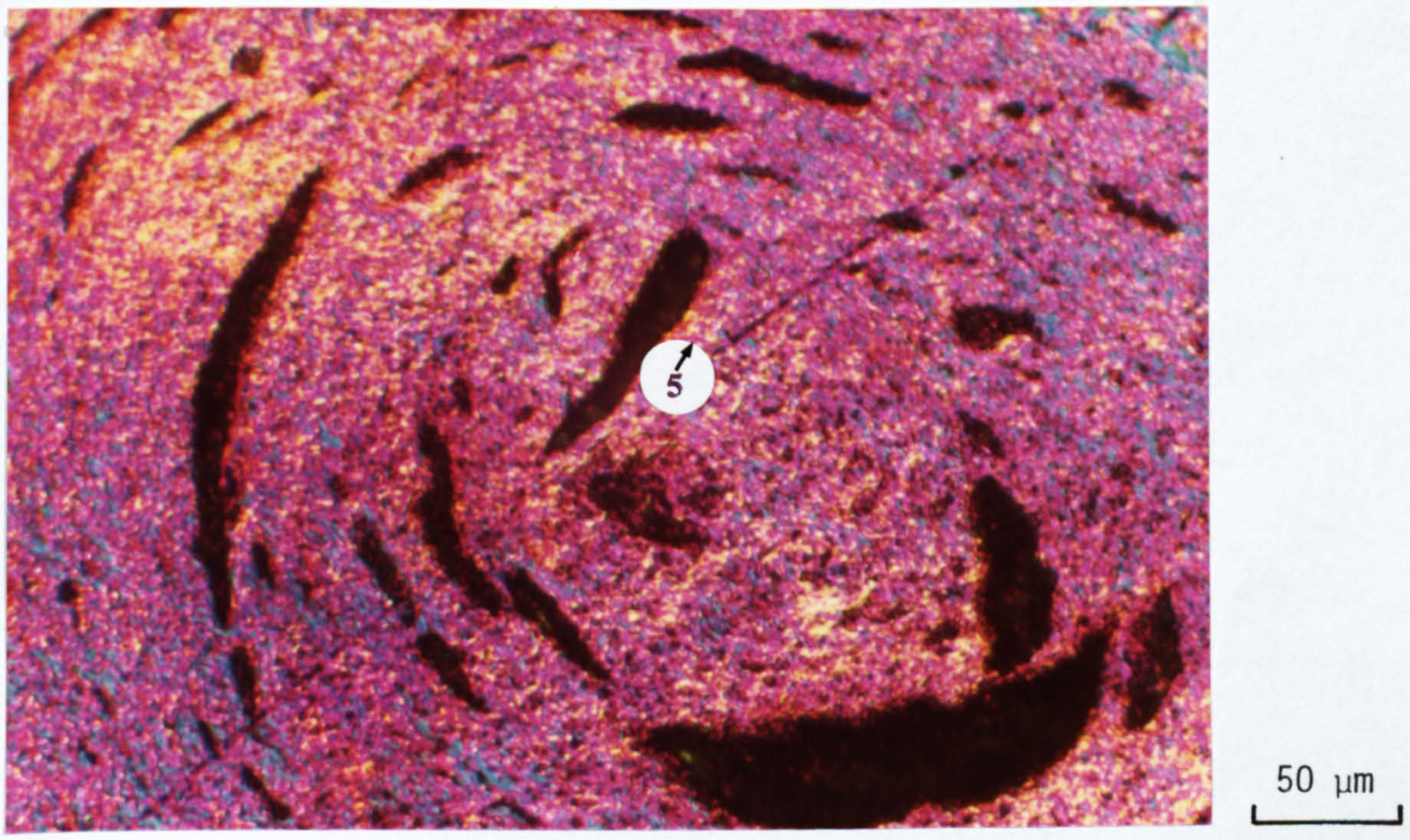


Figures 457 to 461. Scanning electron micrographs (stereoscan) of AGLMP Graphite M38, radiolytically oxidised in carbon dioxide. Weight loss 3.7%.



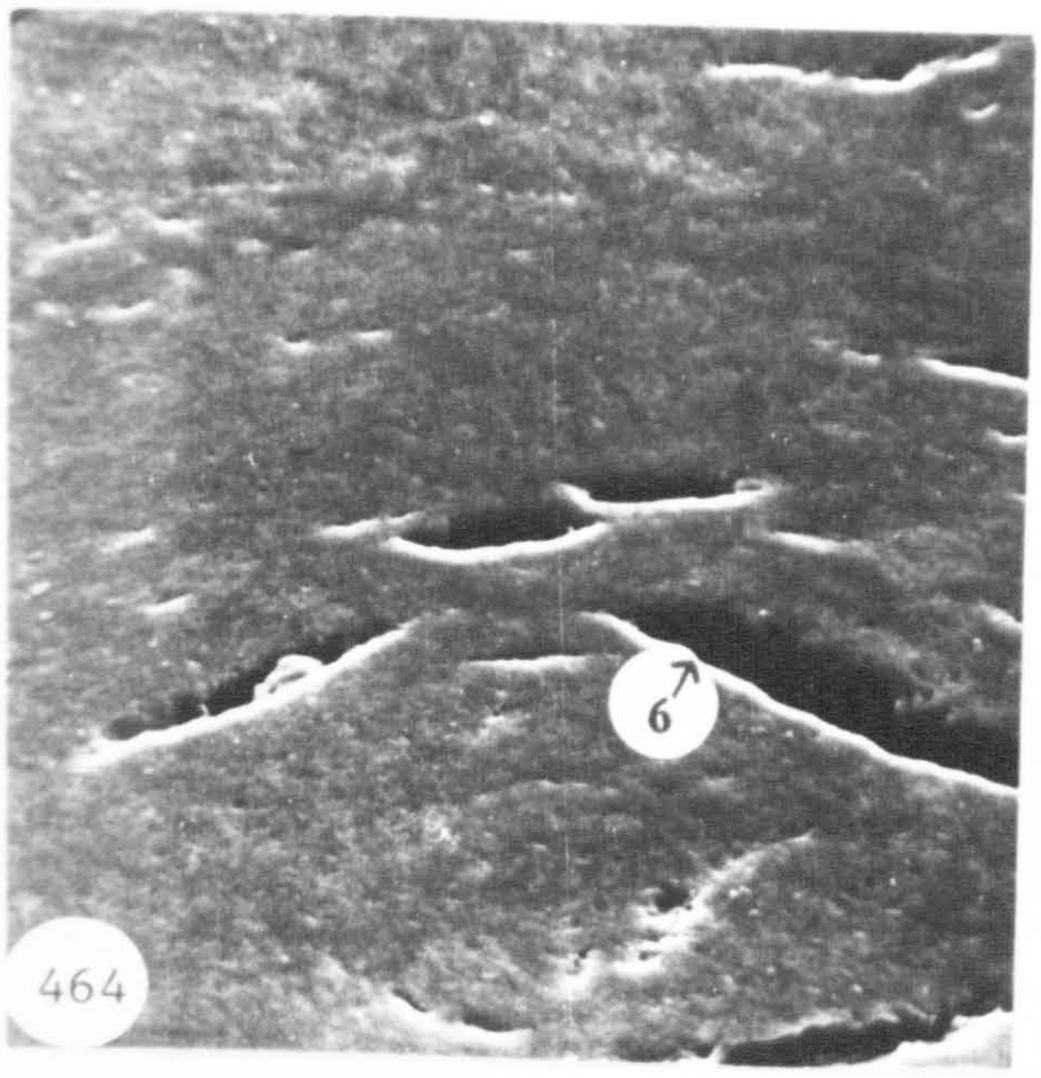
AGLMP GRAPHITE

Figure 462. Optical micrograph of AGLMP Graphite 10F49 (control for M38).

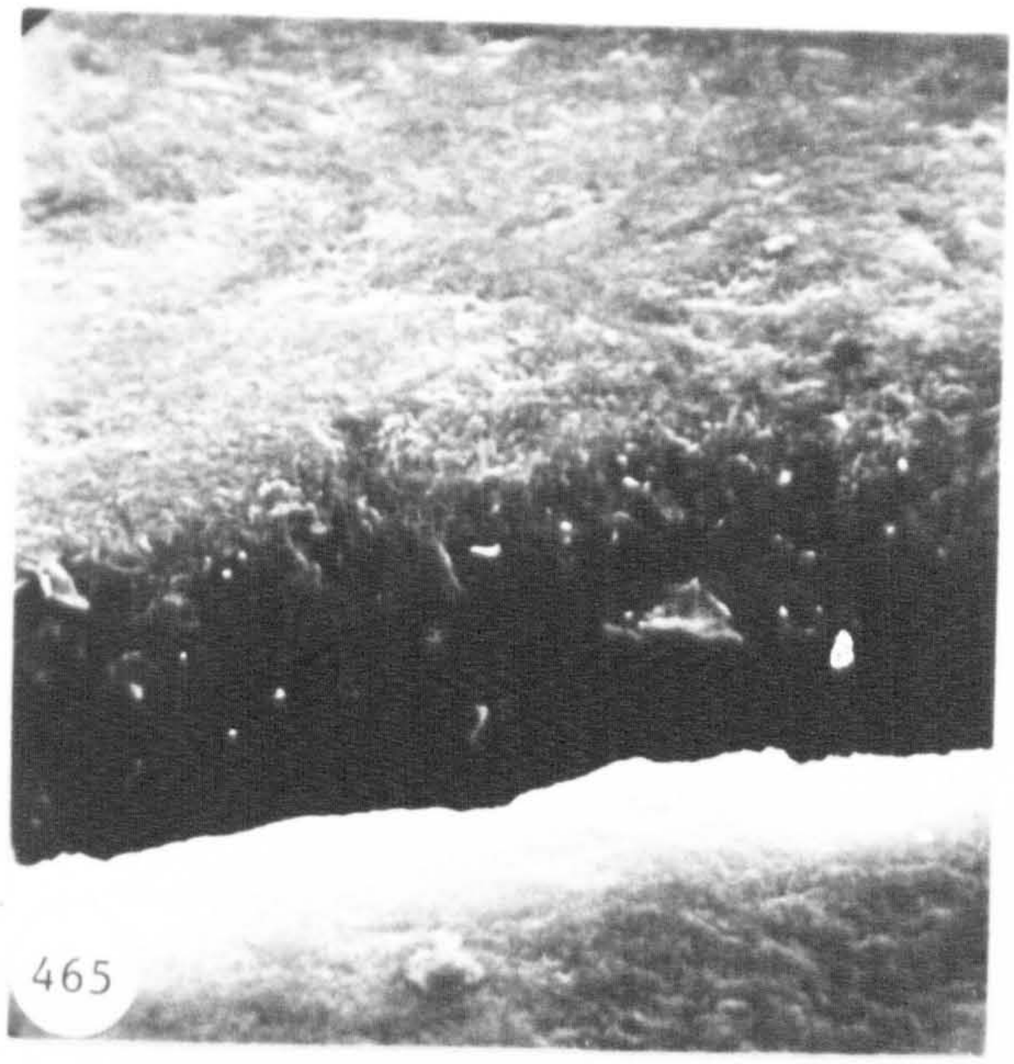


AGLMP GRAPHITE

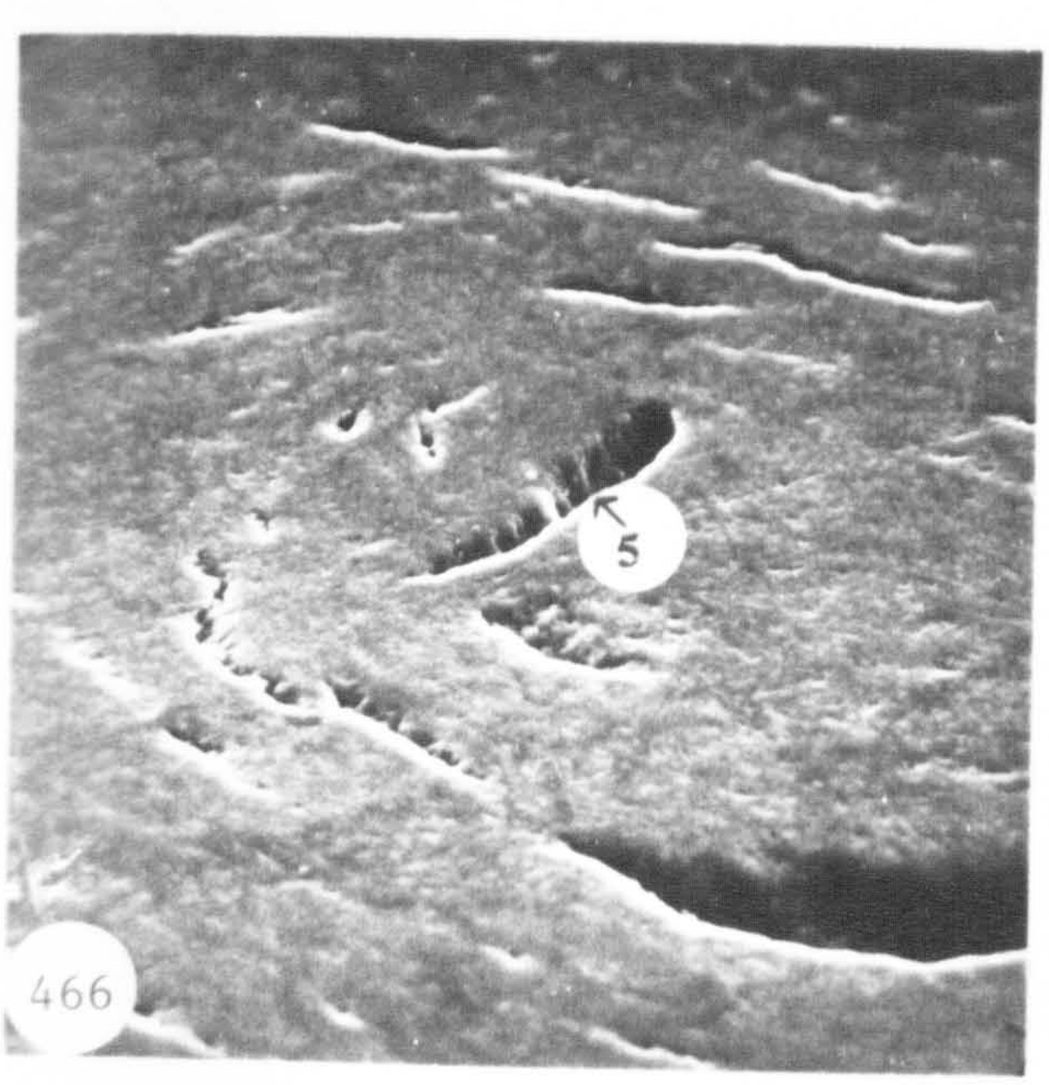
Figure 463. Optical micrograph of AGLMP Graphite M38, radiolytically oxidised in carbon dioxide. Weight loss 3.7%.



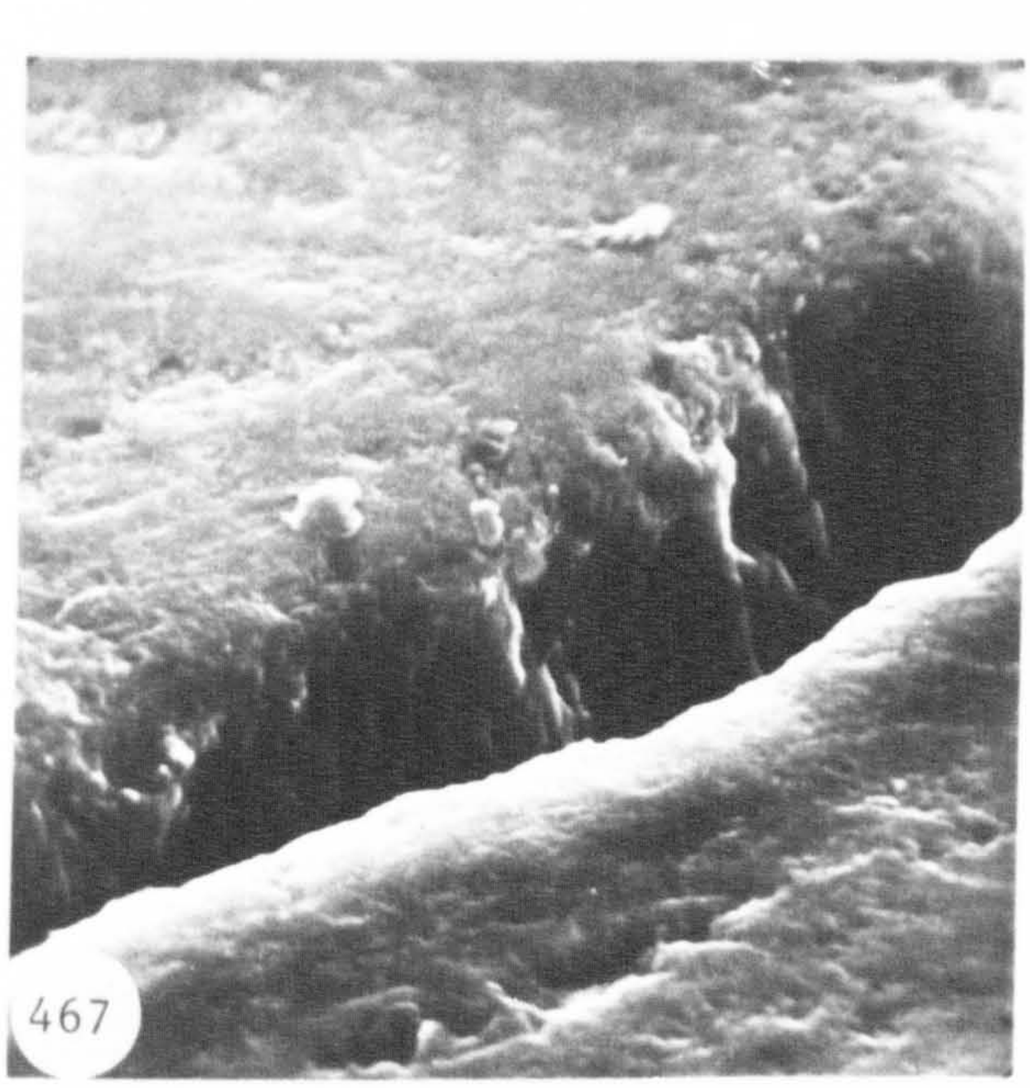
AGLMP GRAPHITE 40 μm



AGLMP GRAPHITE 2 μm

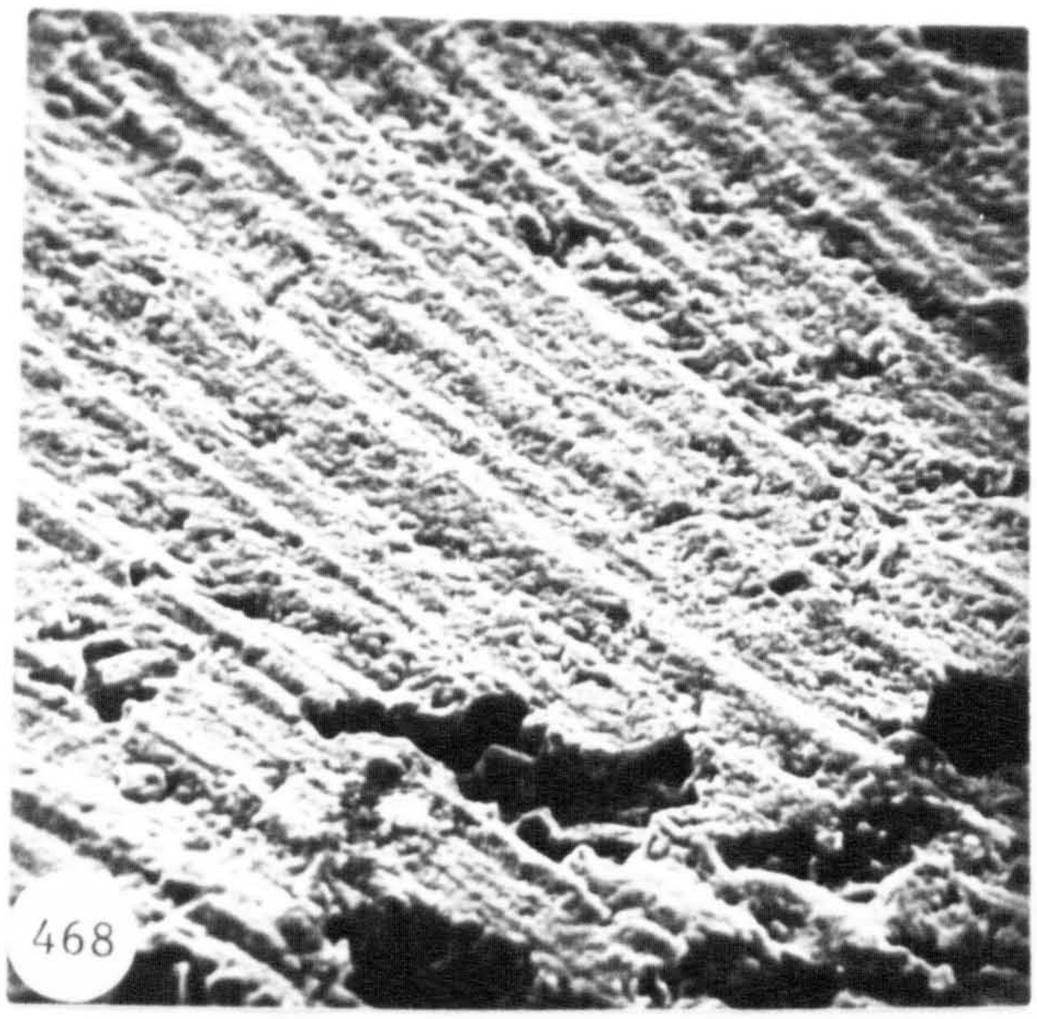


AGLMP GRAPHITE 40 μm

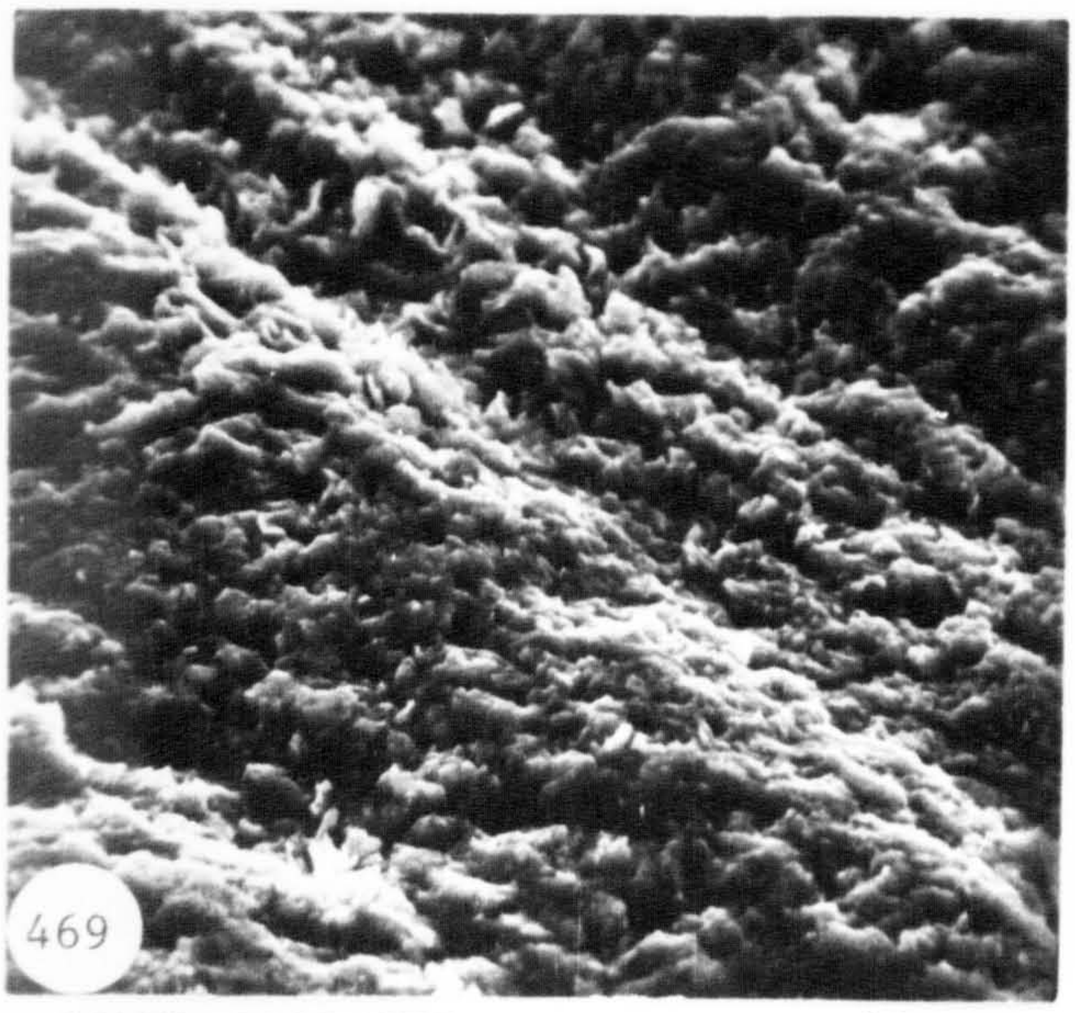


AGLMP GRAPHITE 2 μm

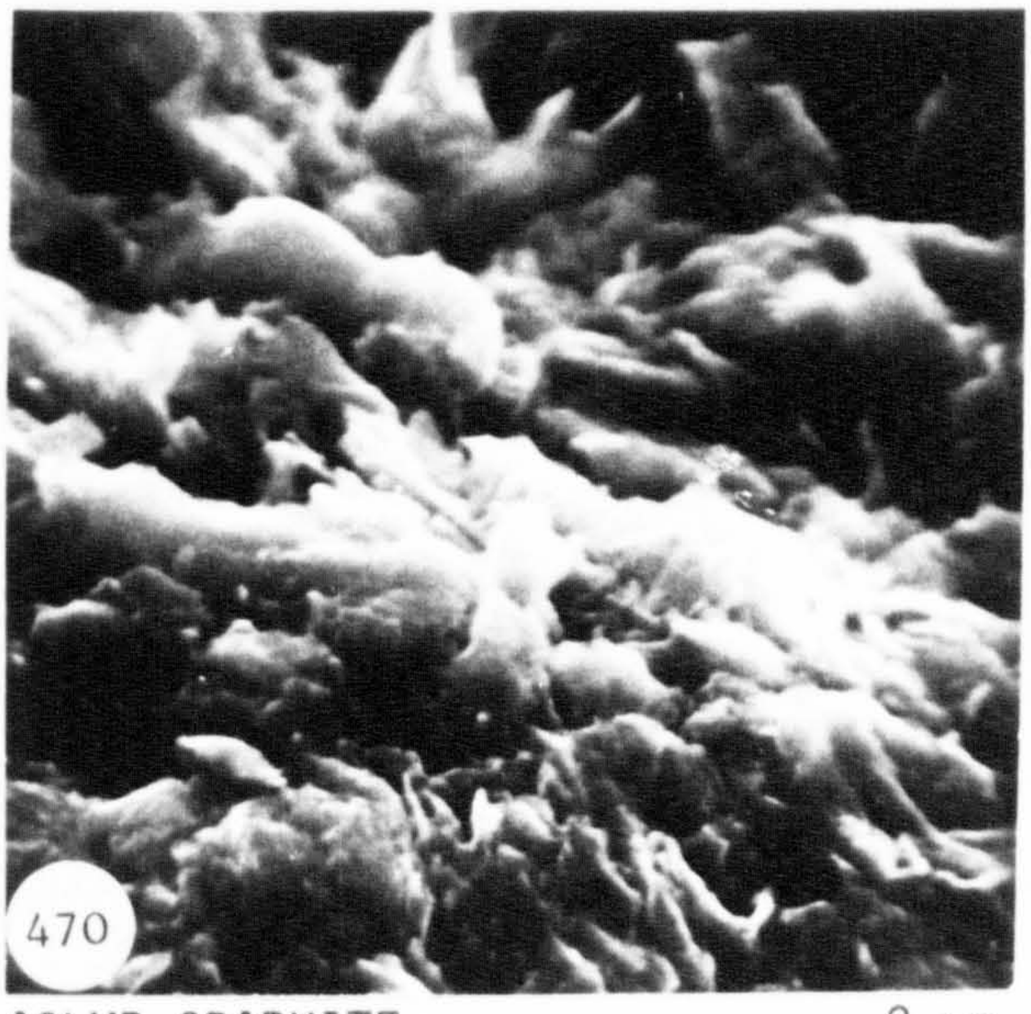
Figures 464 to 467. Scanning electron micrographs (stereoscan) of AGLMP Graphite 10F49 (Figures 464 and 465) and M38 (Figures 466 and 467), radiolytically oxidised in carbon dioxide. Weight loss 3.7%.



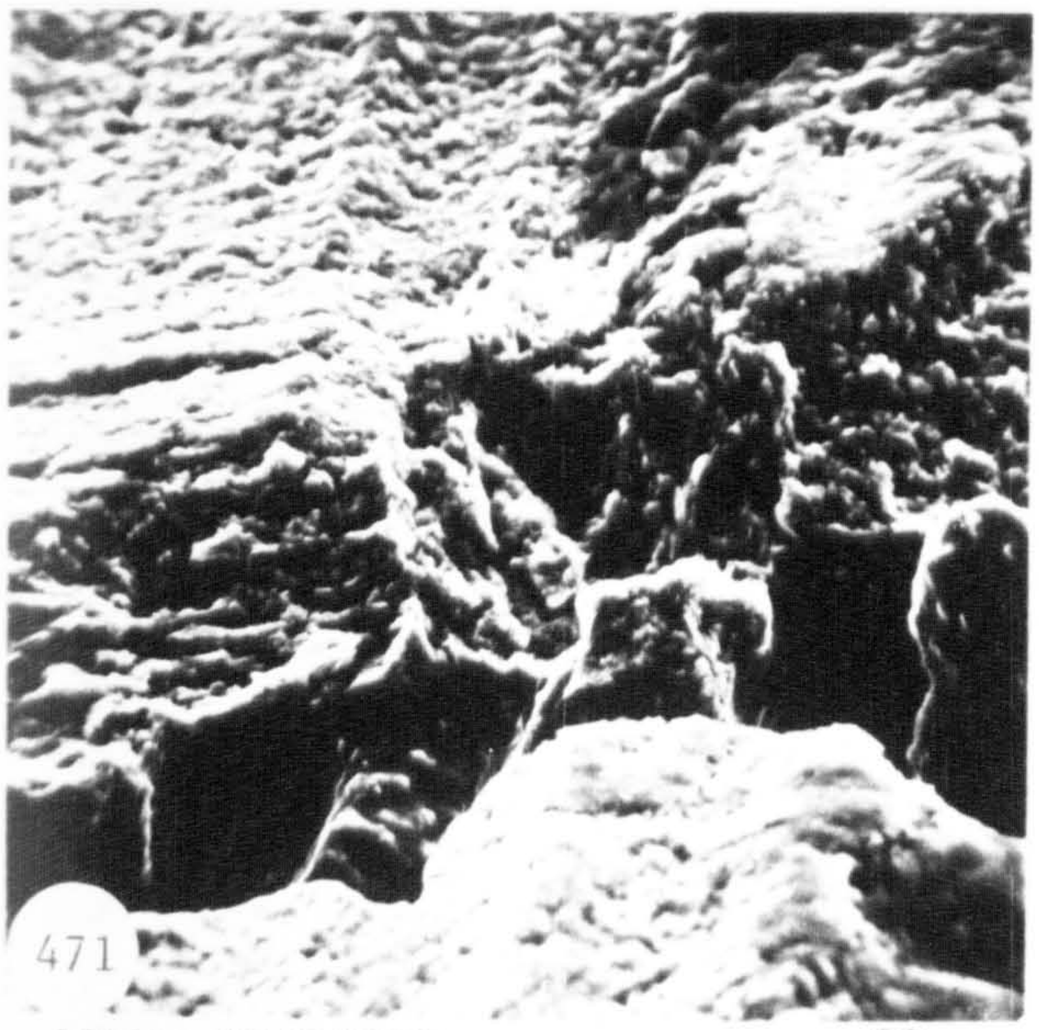
AGLMP GRAPHITE 50 μm



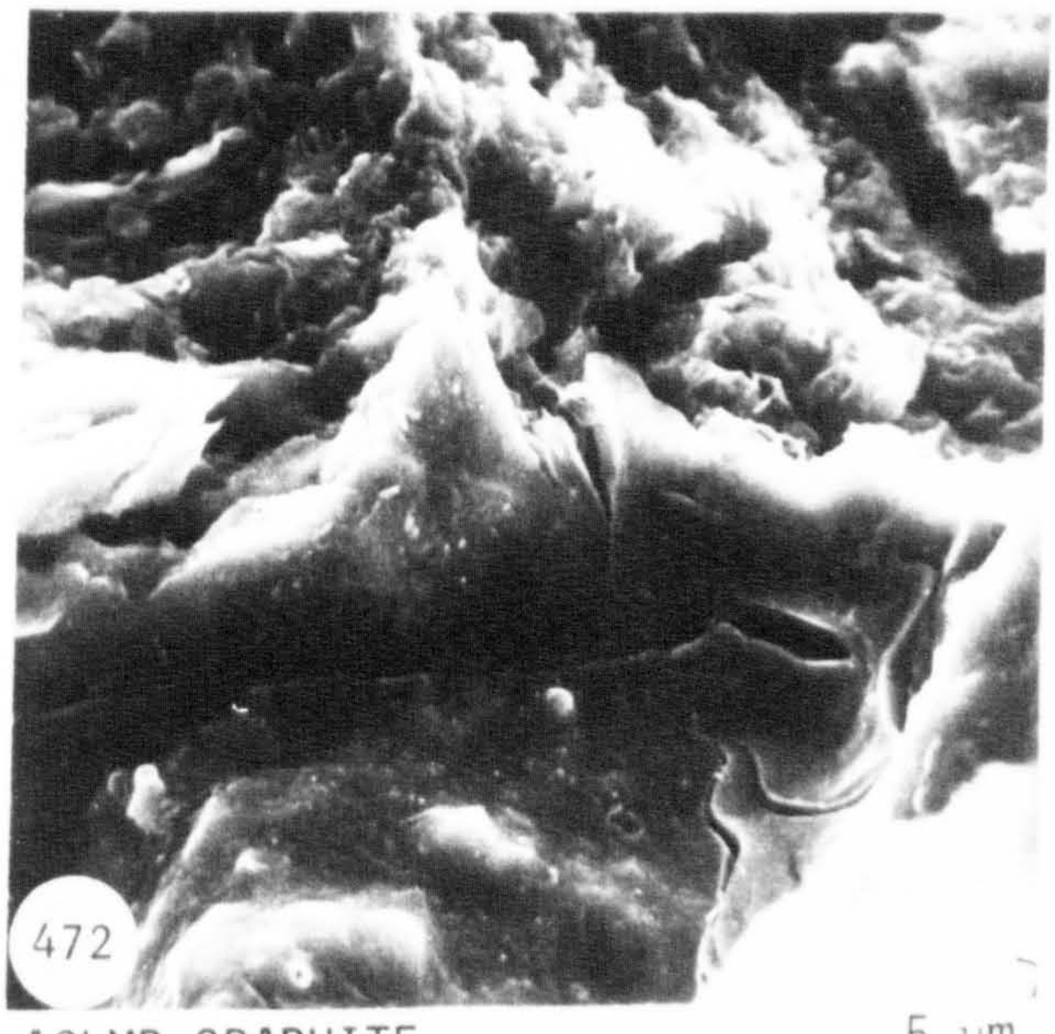
AGLMP GRAPHITE 10 μm



AGLMP GRAPHITE 2 μm

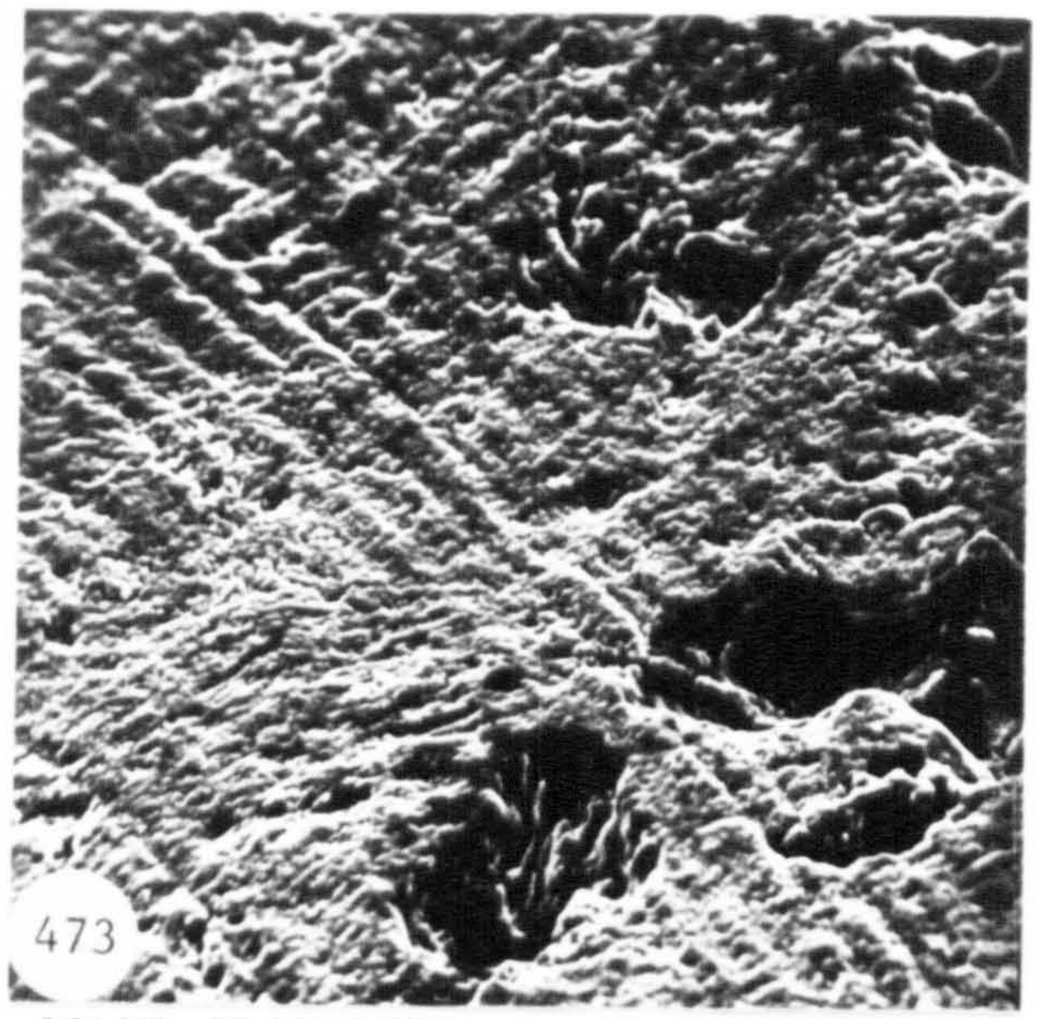


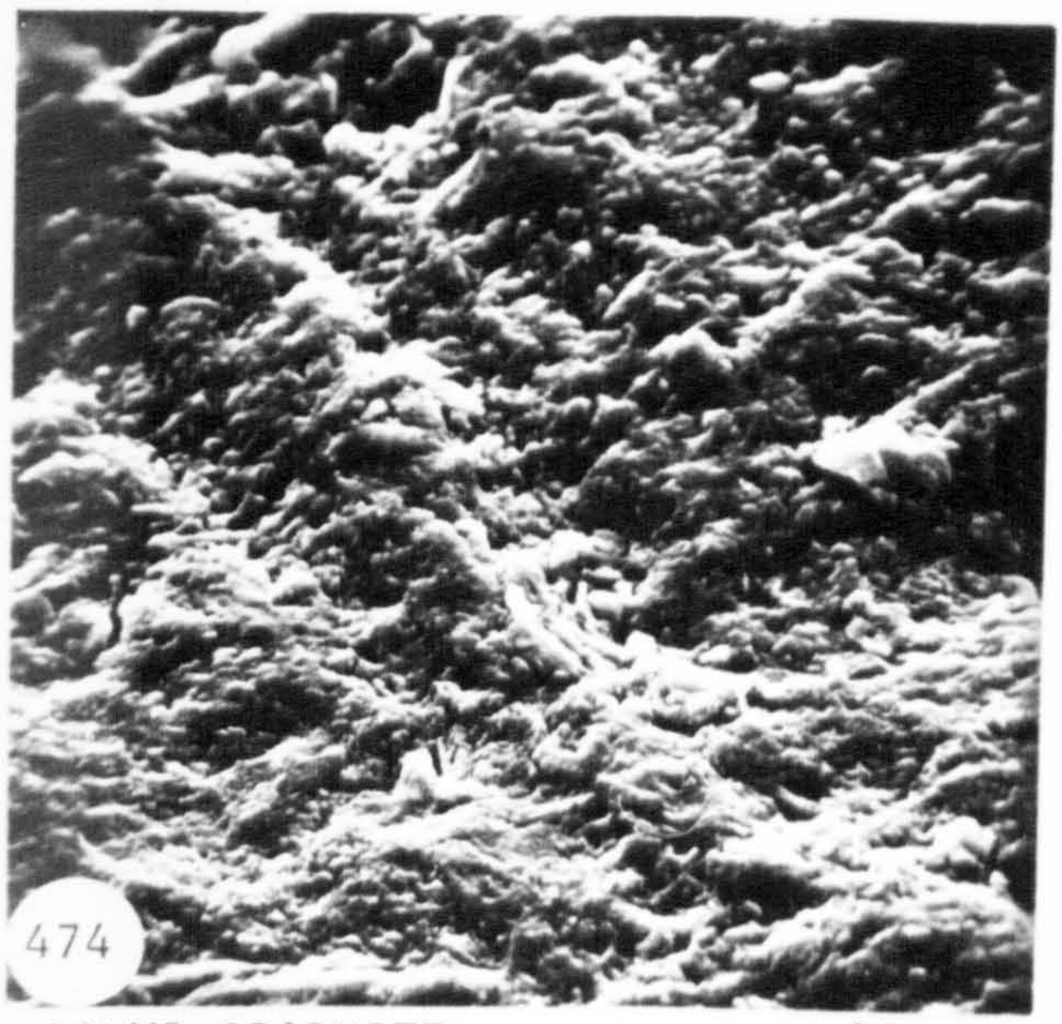
AGLMP GRAPHITE 20 μm

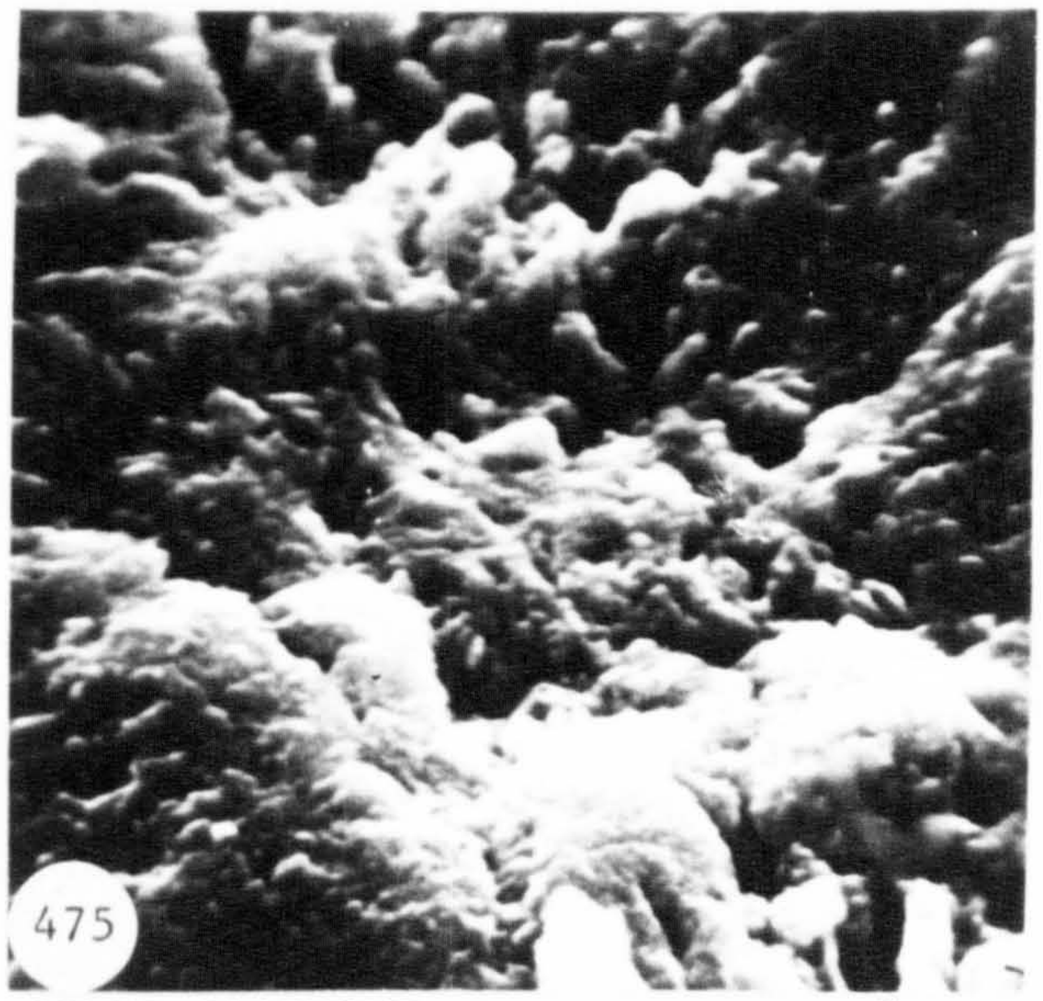


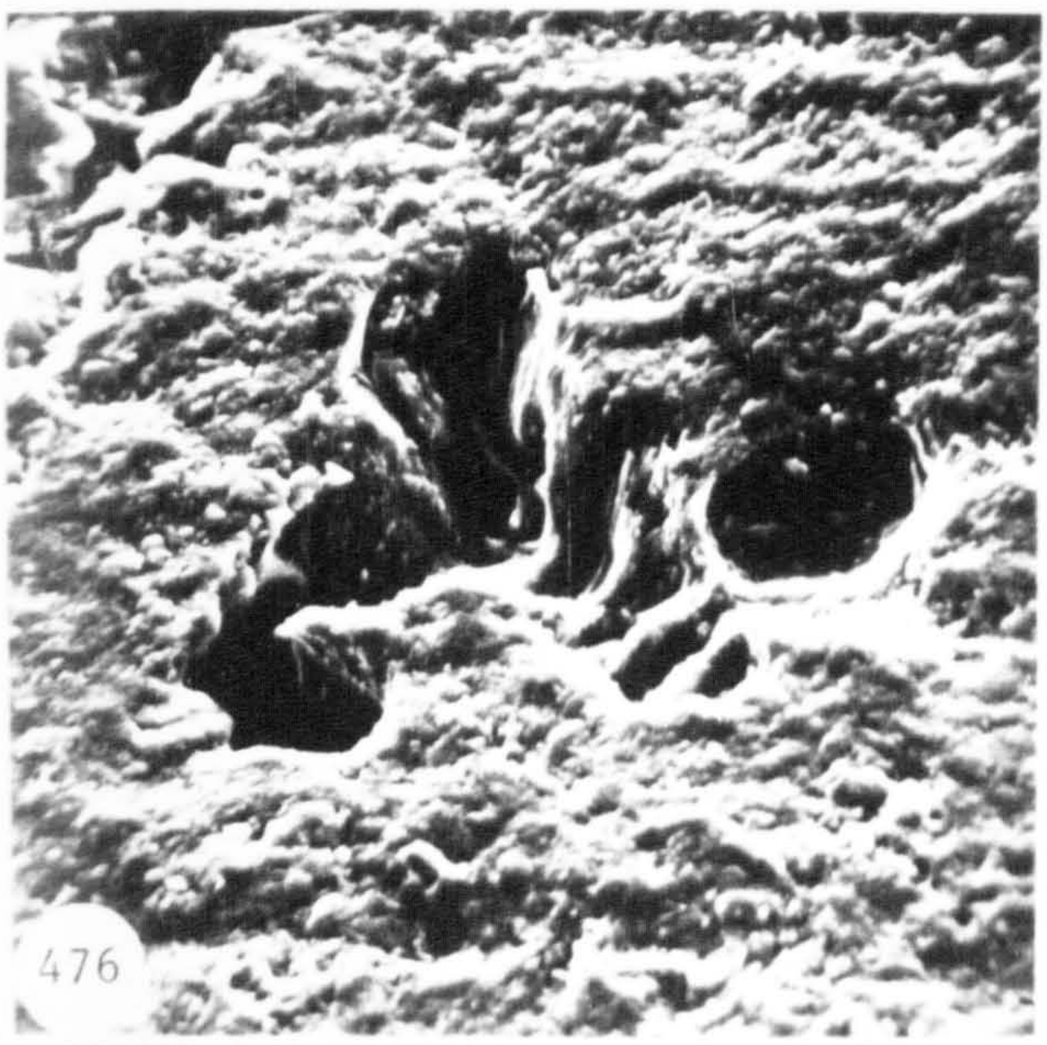
AGLMP GRAPHITE 5 μm

Figures 468 to 472. Scanning electron micrographs (stereoscan) of AGLMP Graphite 584/195 (control for M28).



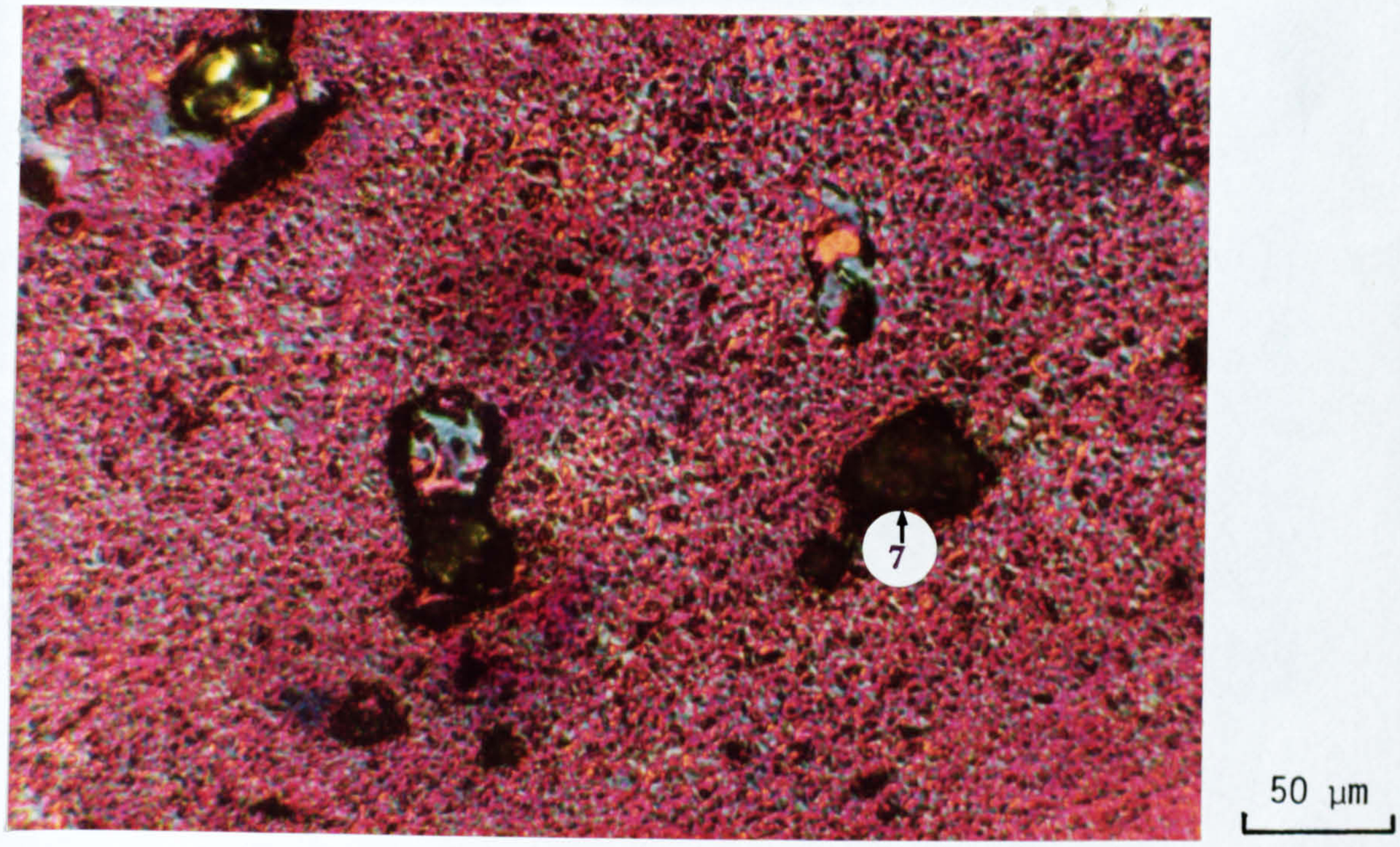






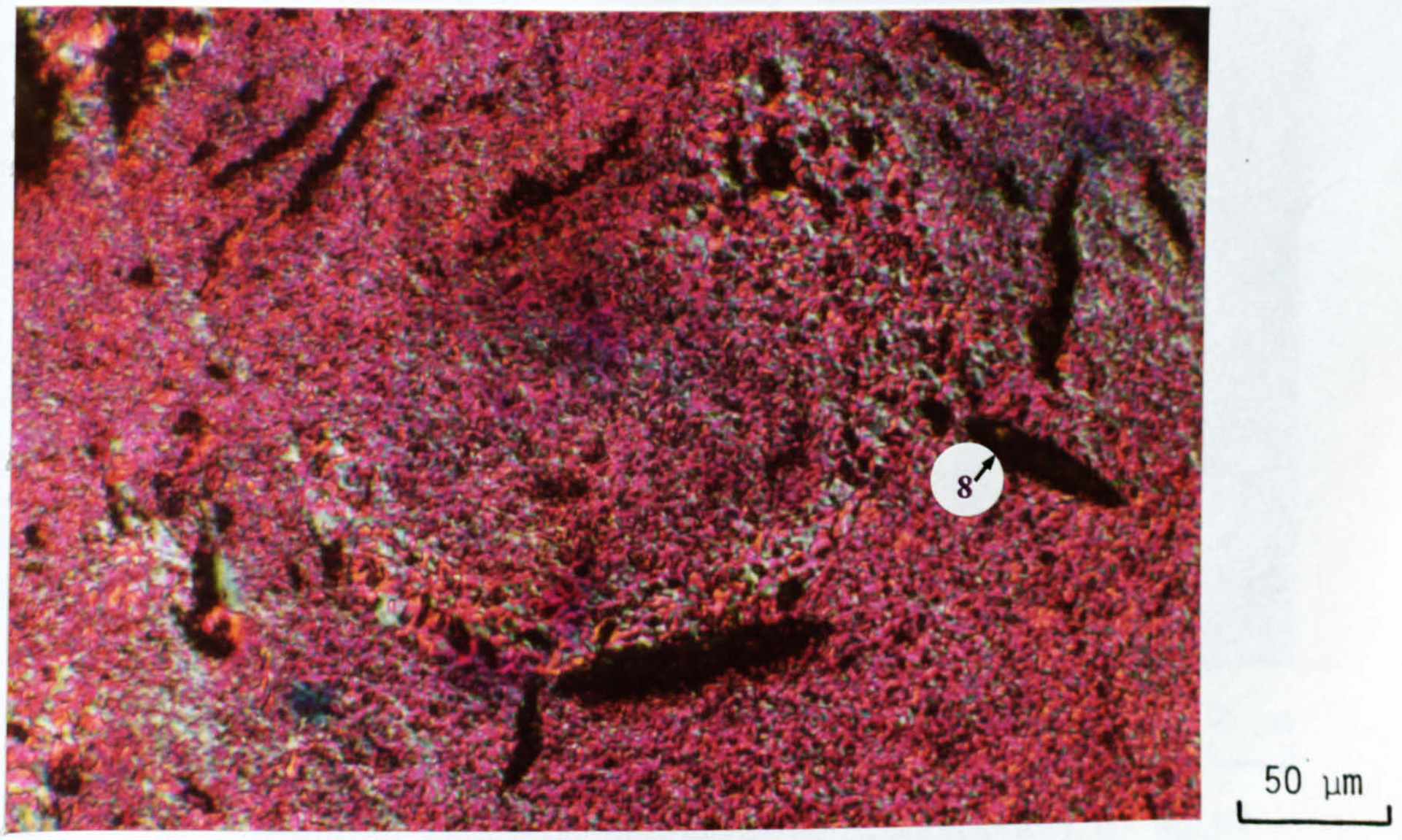


Figures 473 to 477. Scanning electron micrographs (stereoscan) of AGLMP Graphite M28, radiolytically-oxidised in carbon dioxide. Weight loss 3.5%.



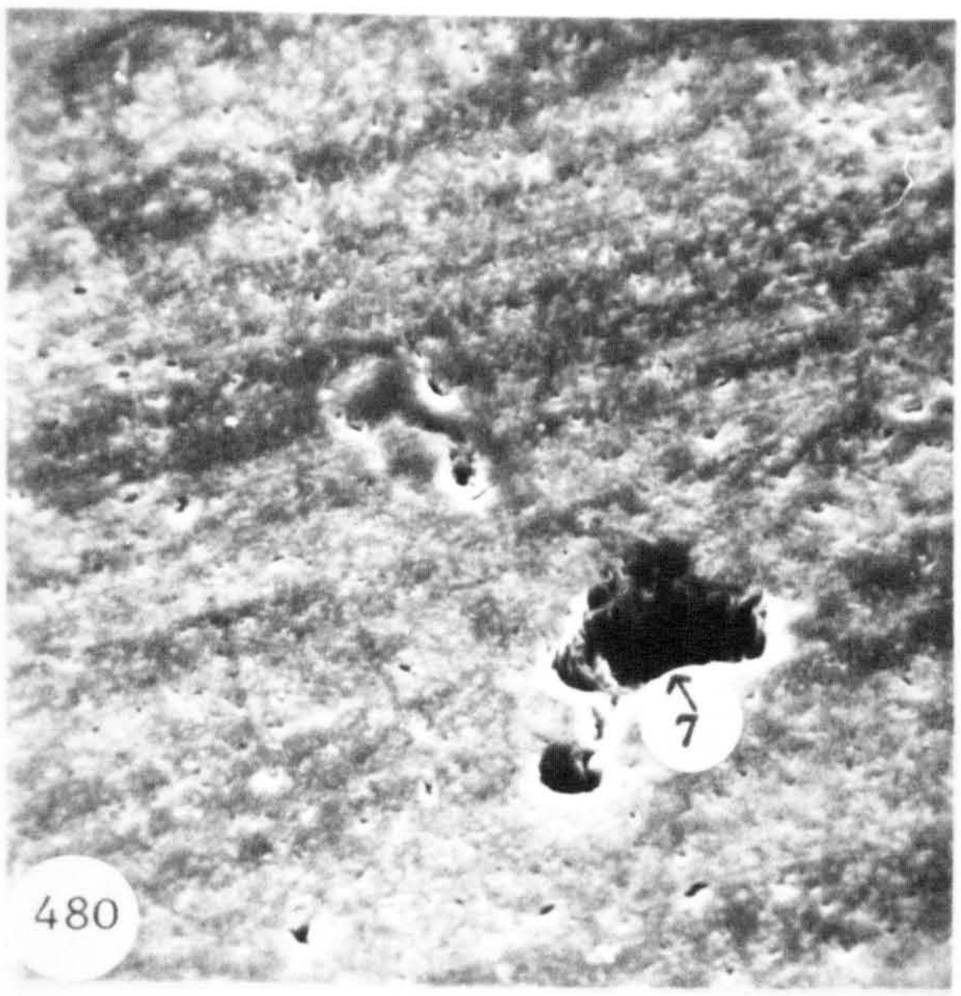
AGLMP GRAPHITE

Figure 478. Optical micrograph of AGLMP Graphite 584/195 (control for M28)

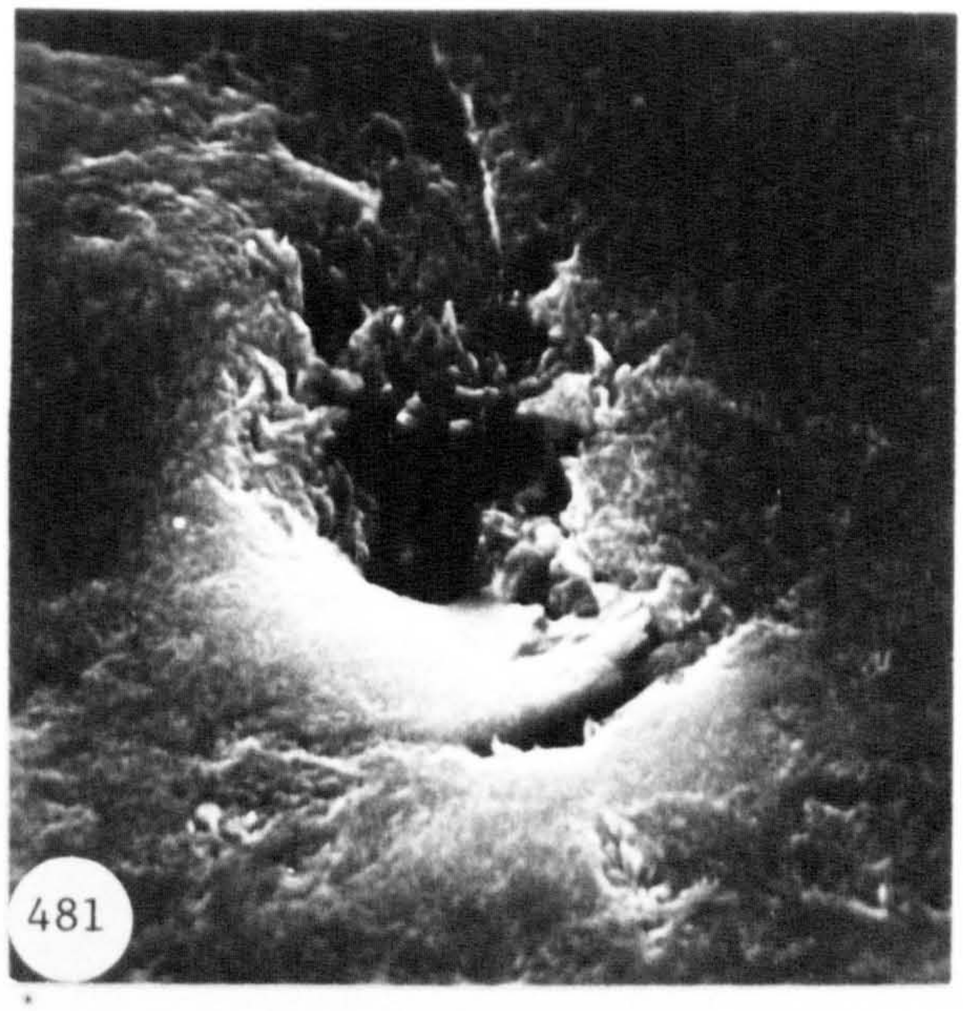


AGLMP GRAPHITE

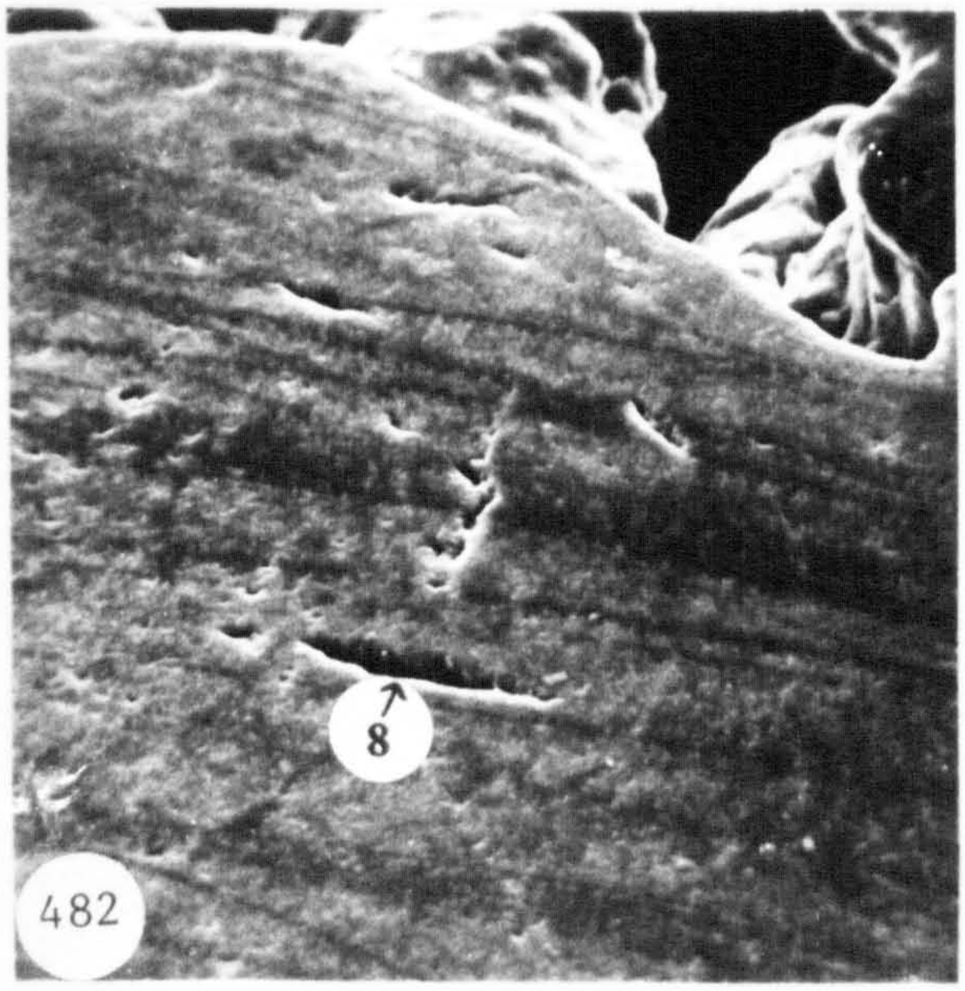
Figure 479. Optical micrograph of AGLMP Graphite M28, radiolytically oxidised in carbon dioxide. Weight loss 3.5%.



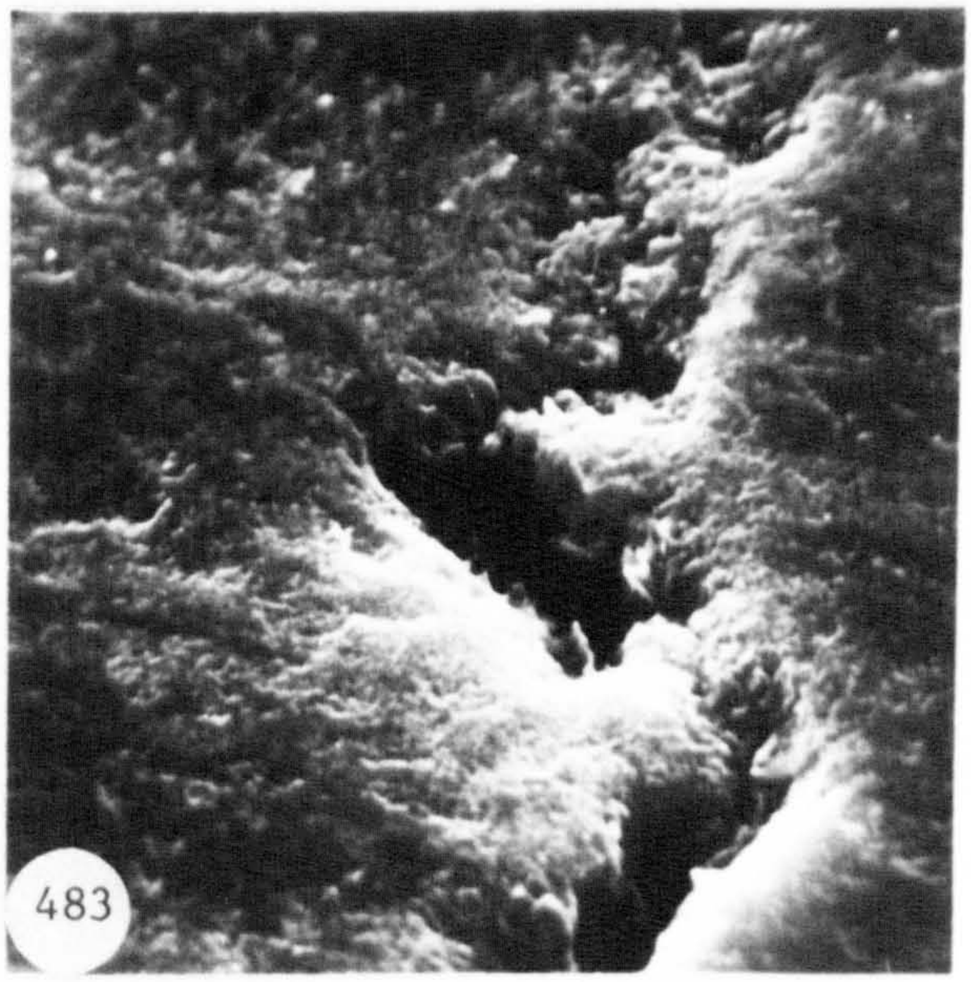
AGLMP GRAPHITE 40 μm



AGLMP GRAPHITE 2 μm

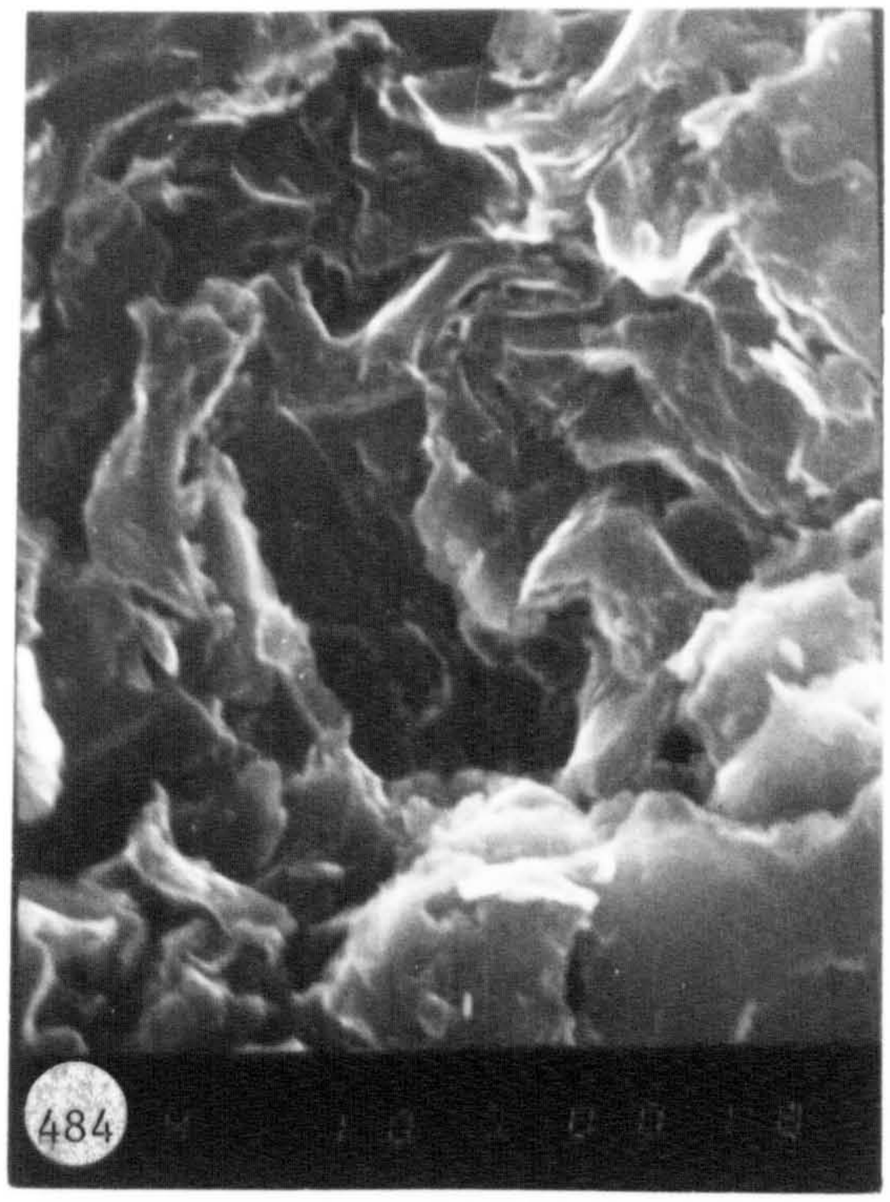


AGLMP GRAPHITE 40 μm

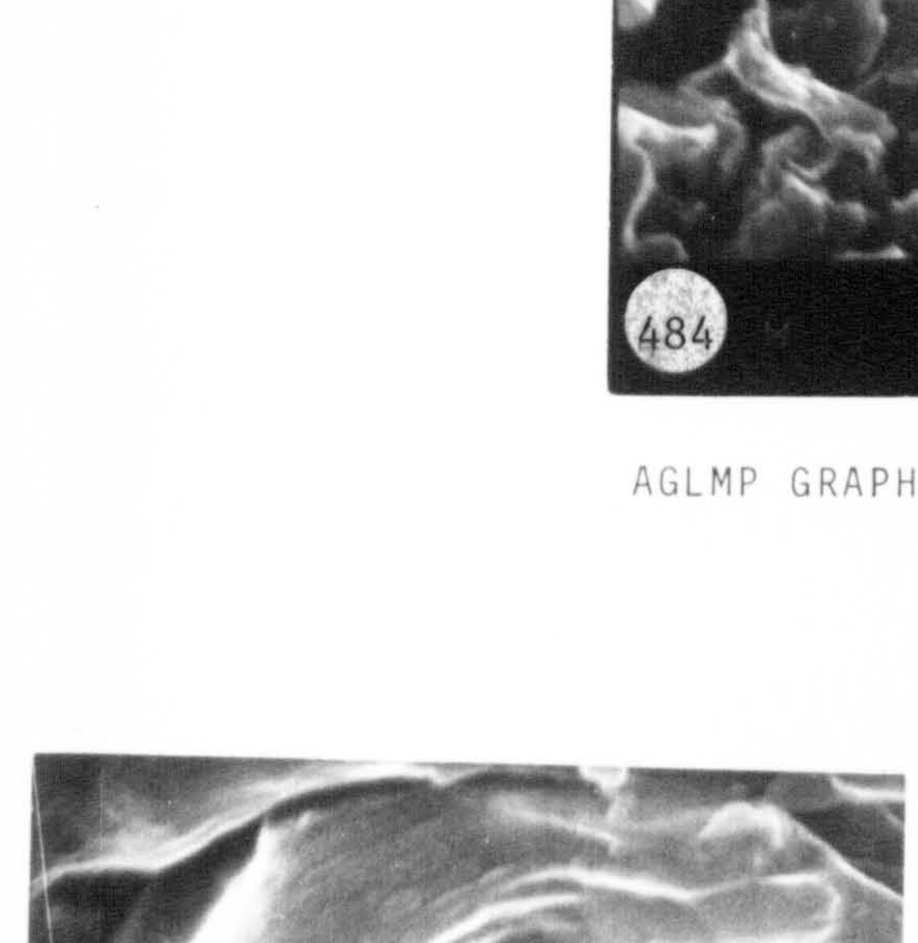


AGLMP GRAPHITE 2 μm

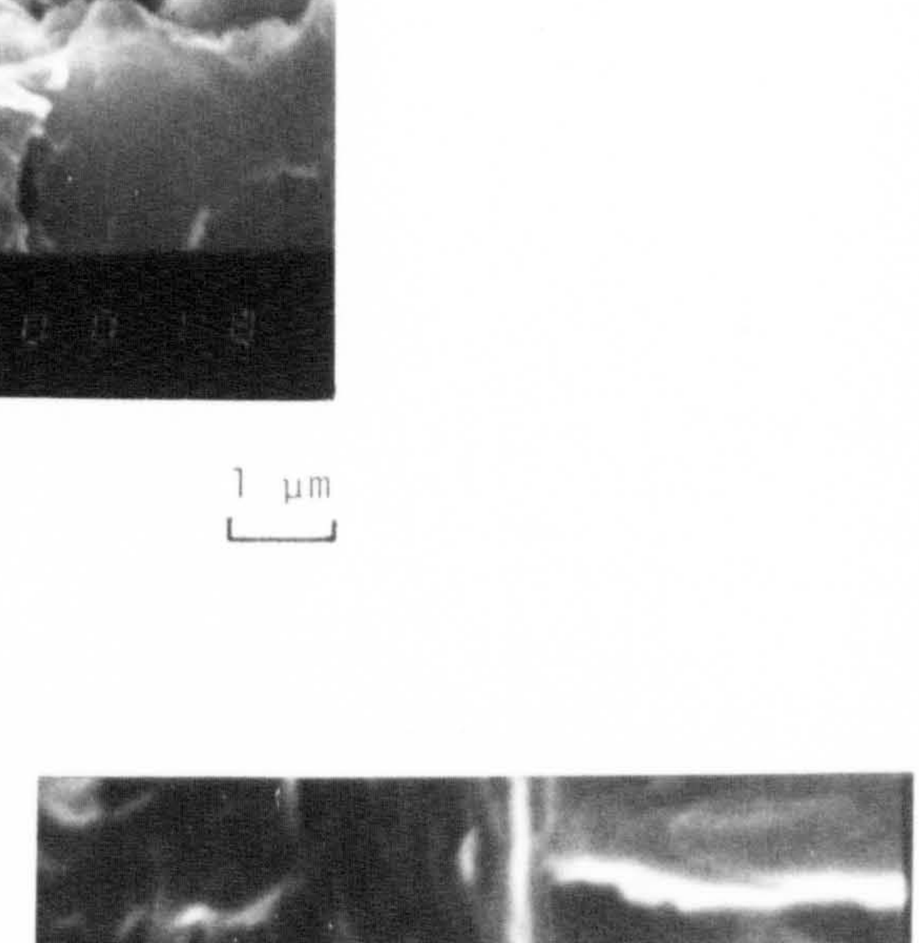
Figures 480 to 483. Scanning electron micrographs (stereoscan) of AGLMP Graphite 584/195 (Figures 480 and 481) and M28 (Figures 482 and 483), radiolytically oxidised in carbon dioxide. Weight loss 3.5%.



AGLMP GRAPHITE. 1 µm

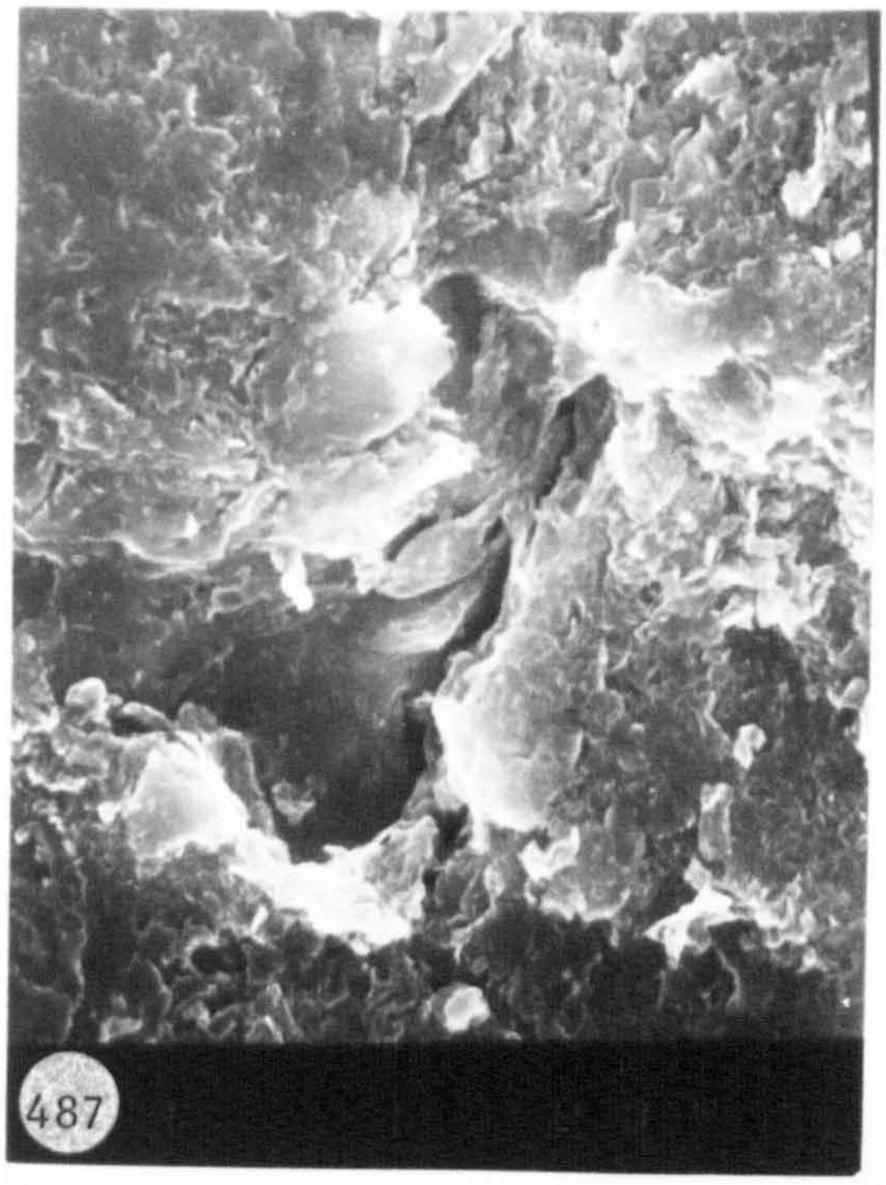


AGLMP GRAPHITE. 200 nm



AGLMP GRAPHITE. 100 nm

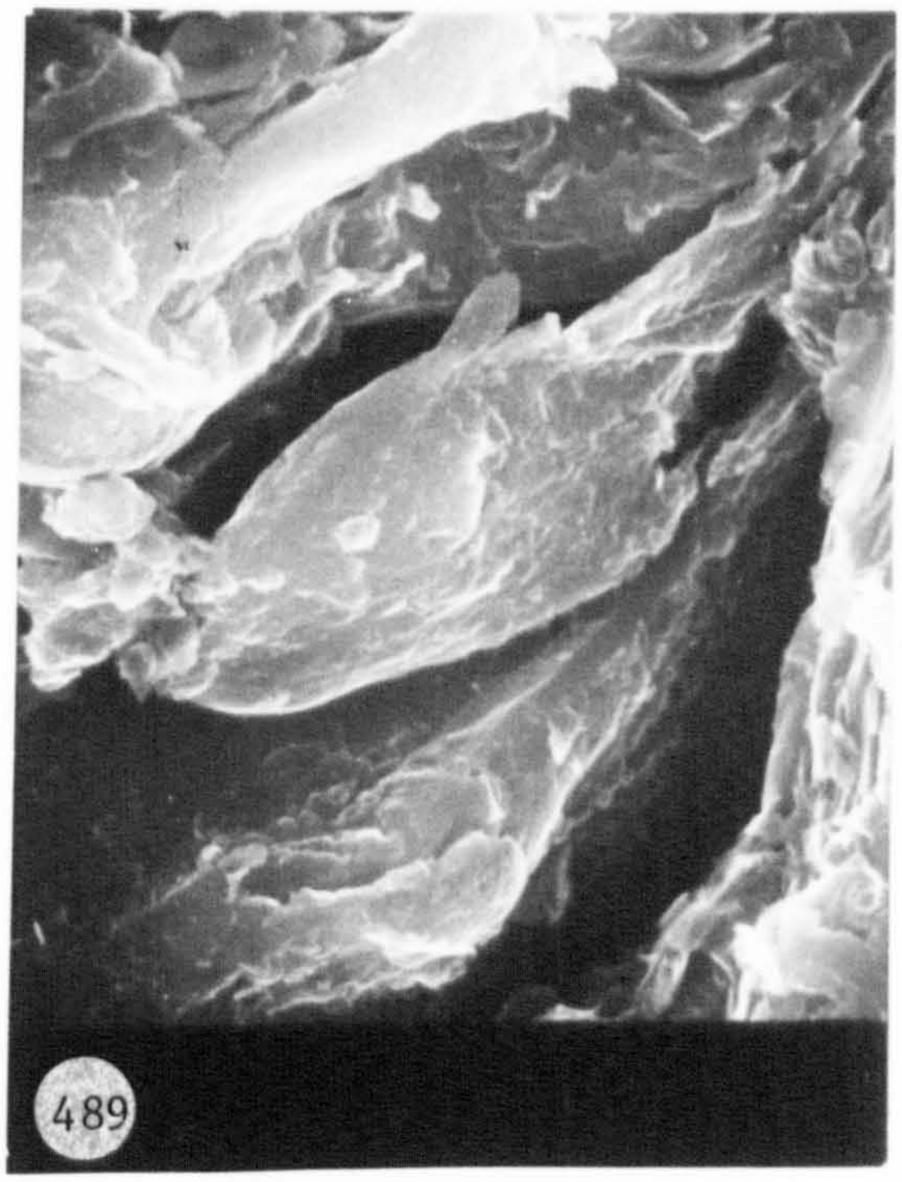
Figures 484 to 486 Scanning electron micrographs (JEOL 100C - ASID-4D) of AGLMP graphite (M28), radiolytically oxidised to 3.5% weight loss.



AGLMP GRAPHITE. 10 µm

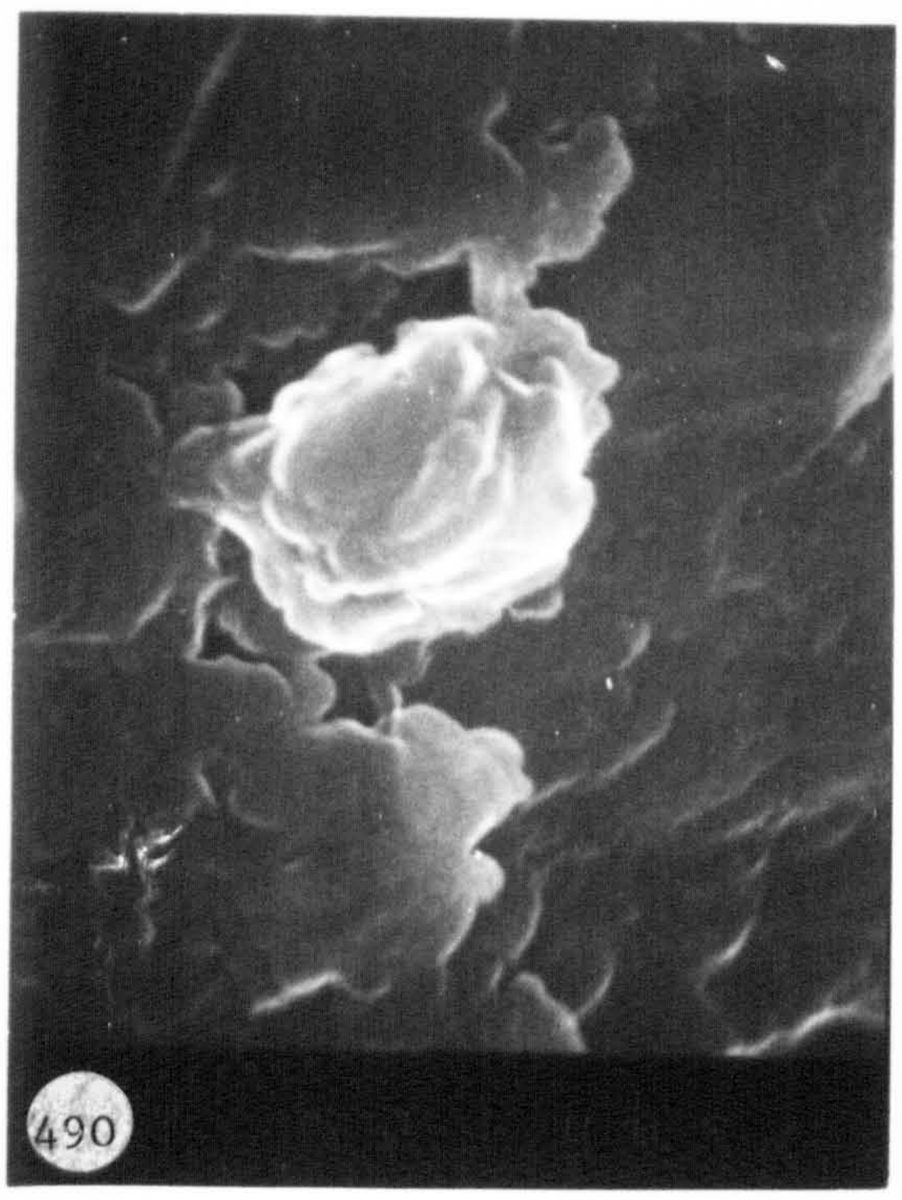


AGLMP GRAPHITE. 10 µm

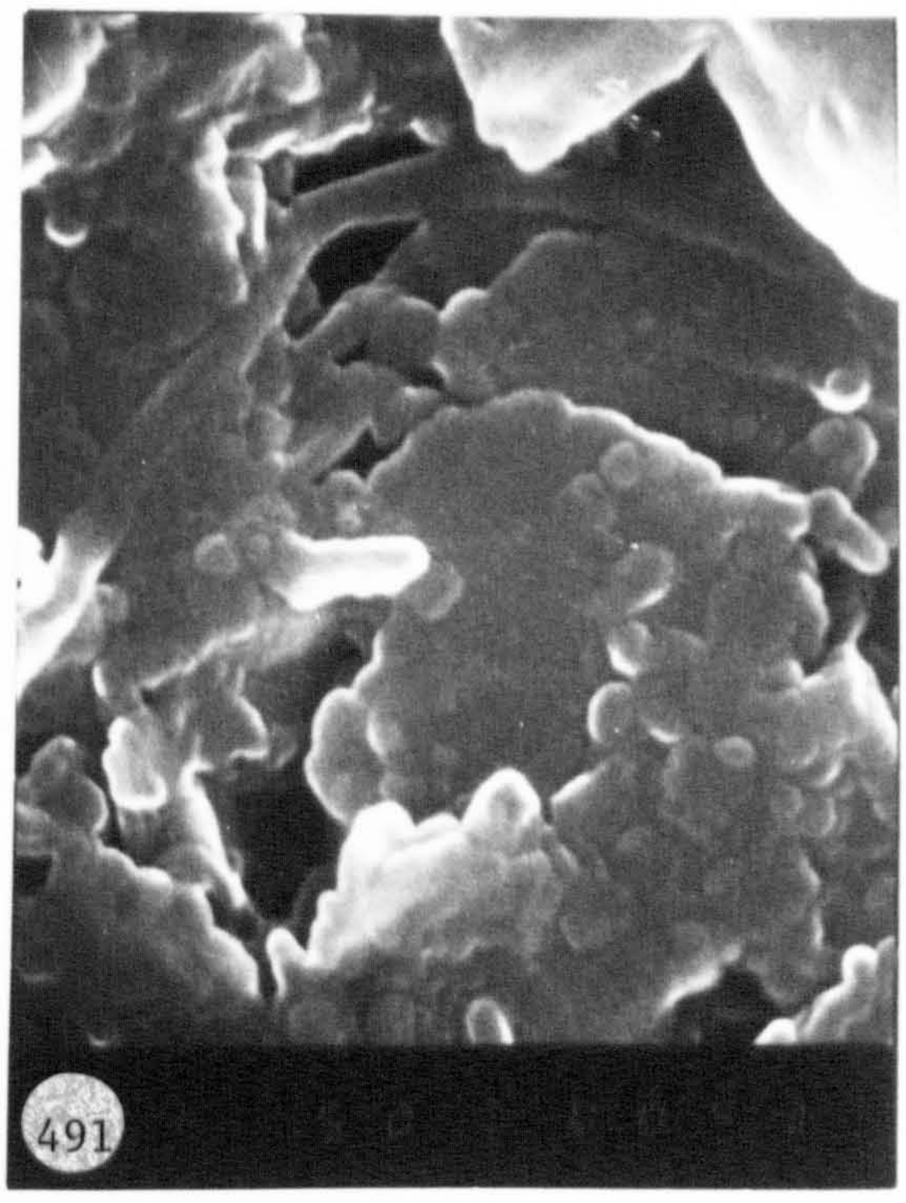


AGLMP GRAPHITE. 2 µm

Figures 487 to 489 Scanning electron micrographs (JEOL 100C - ASID-4D) of AGLMP graphite (M28), radiolytically oxidised to 3.5% weight loss.

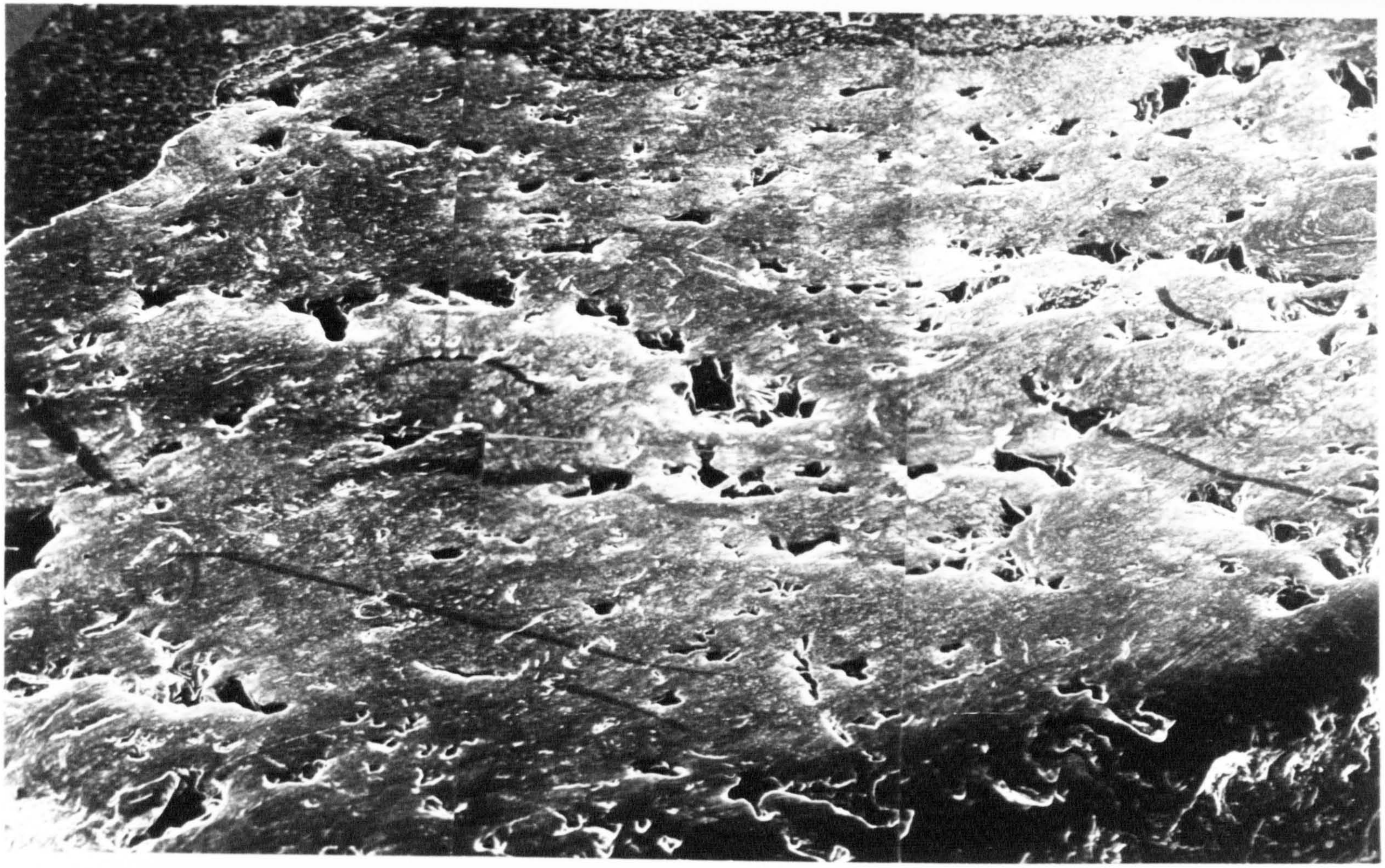


AGLMP GRAPHITE. 200 nm



AGLMP GRAPHITE. 200 nm

Figures 490 and 491 Scanning electron micrographs (JEOL 100C - ASID-4D) of AGLMP graphite (M28), radiolytically oxidised to 3.5% weight loss.



AGLMP GRAPHITE

100 μm

Figure 492. Photo-montage of AGLMP Graphite 584/195, (control for M28).

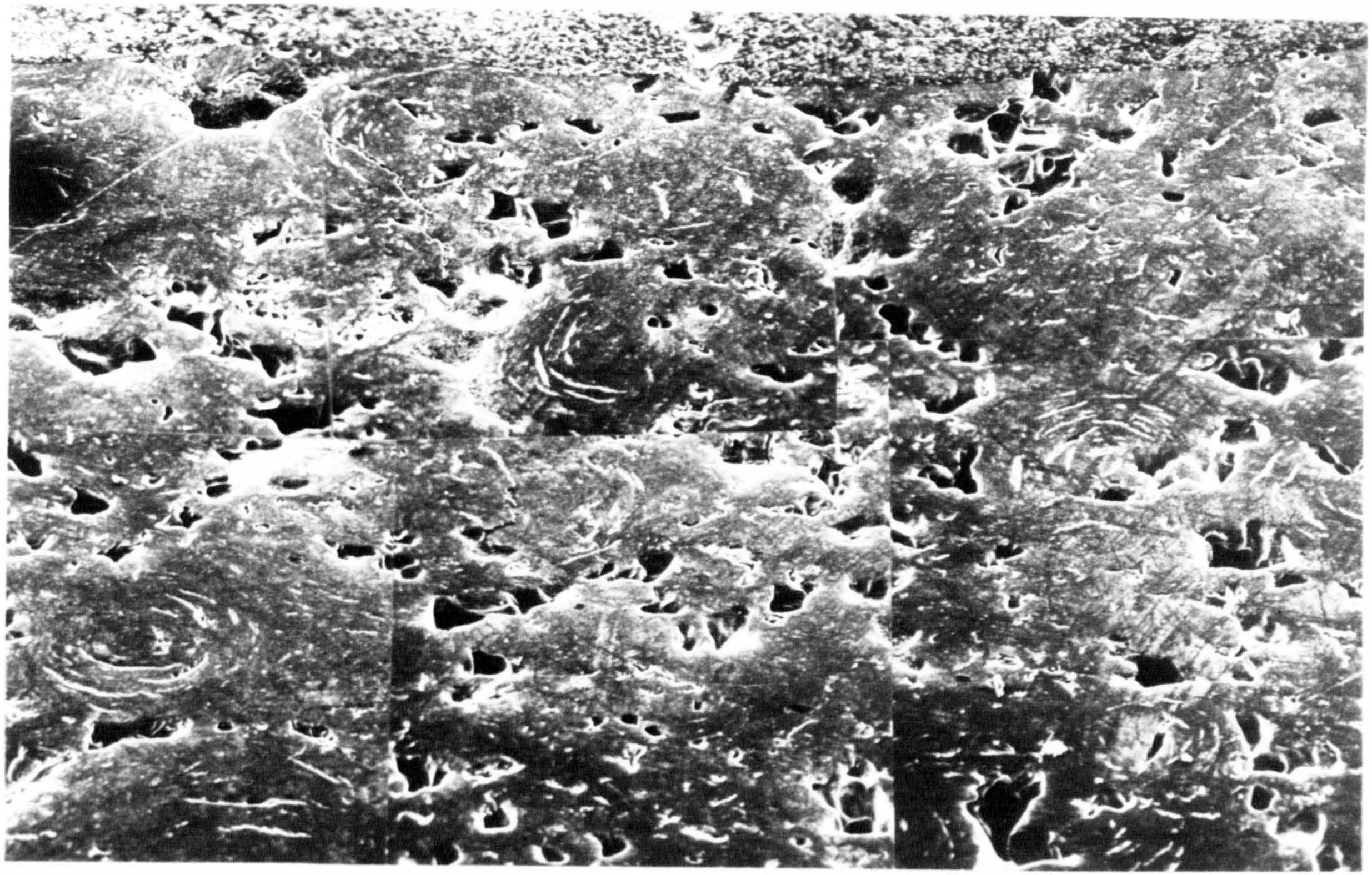
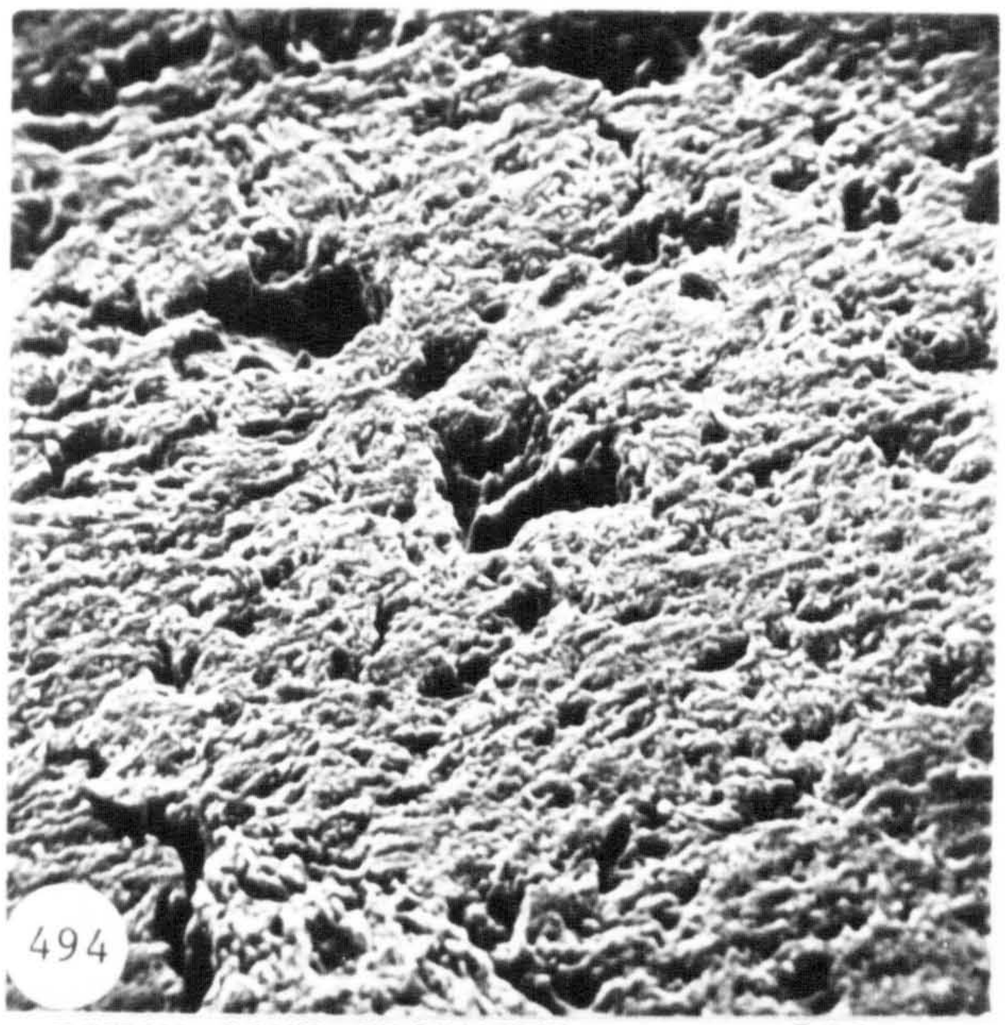
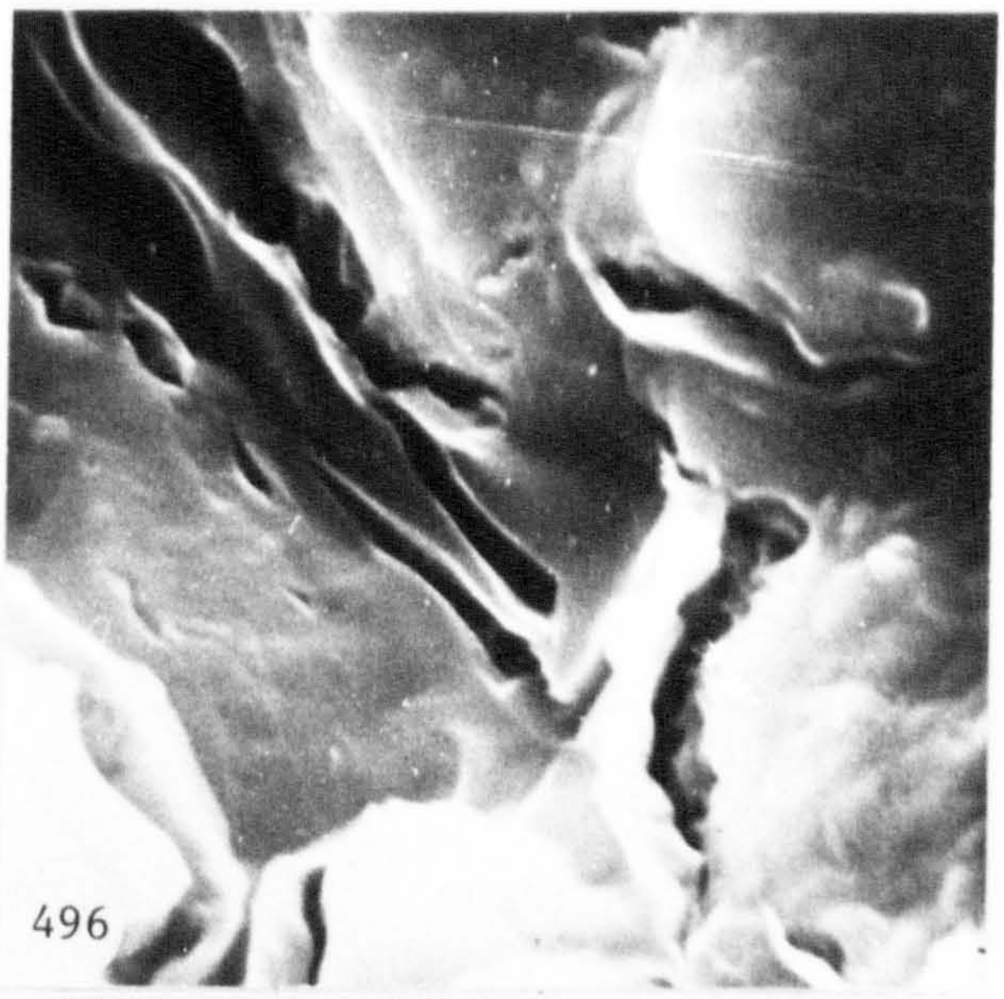
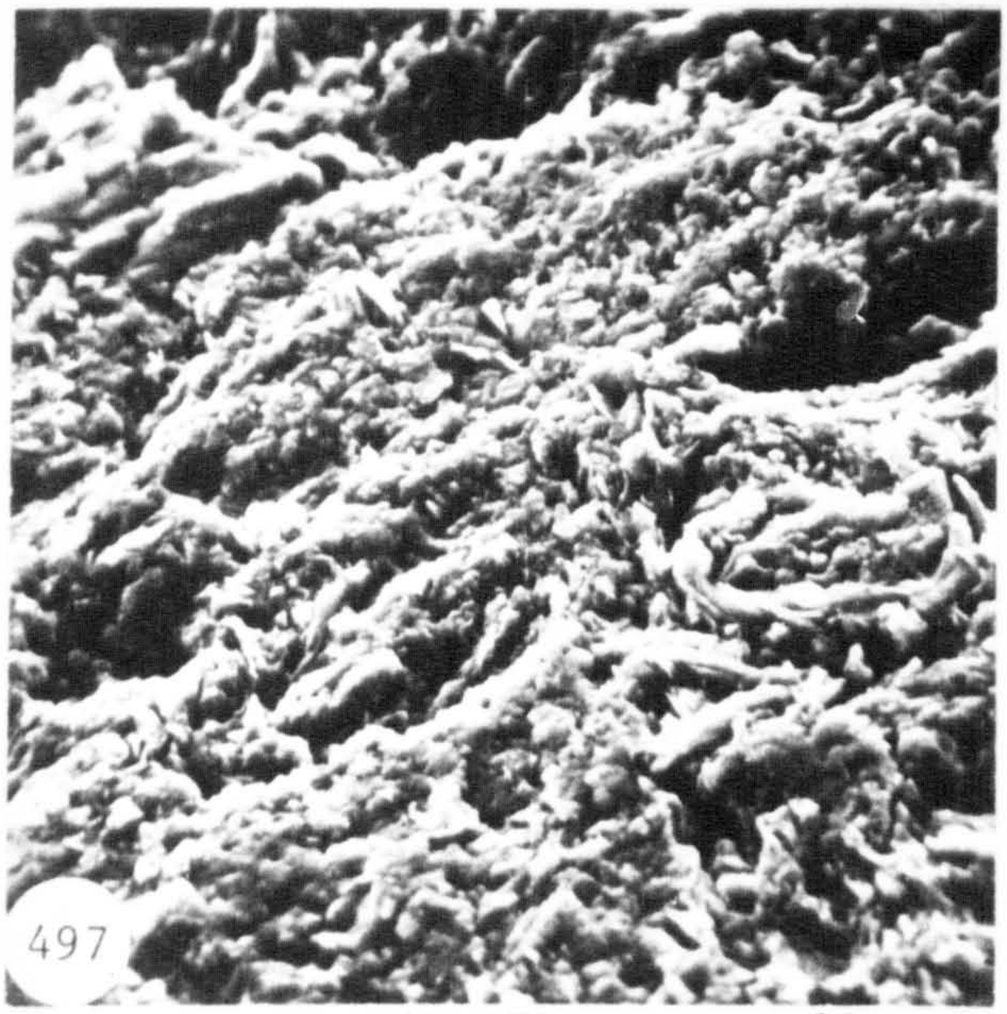


Figure 493. Photo-montage of AGLMP Graphite M28, radiolytically oxidised in carbon dioxide. Weight loss 3.5%.



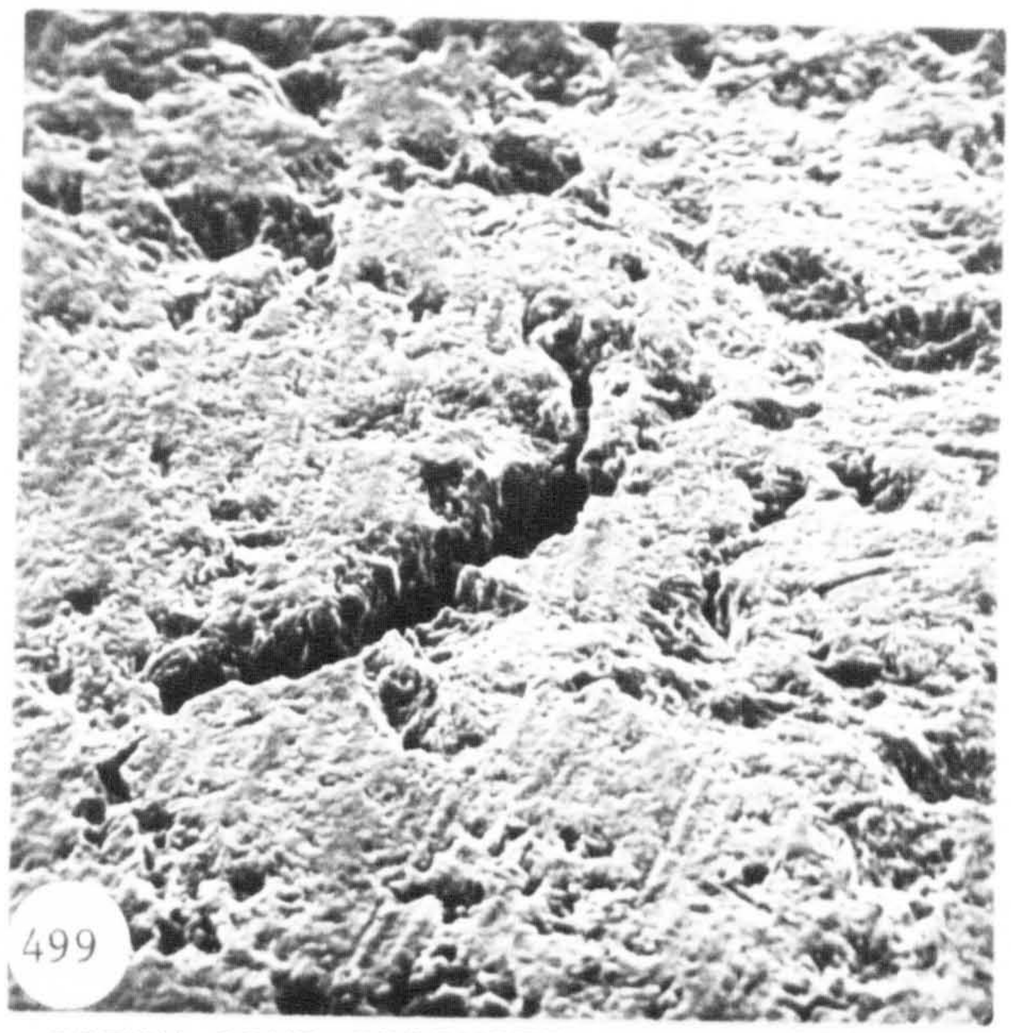


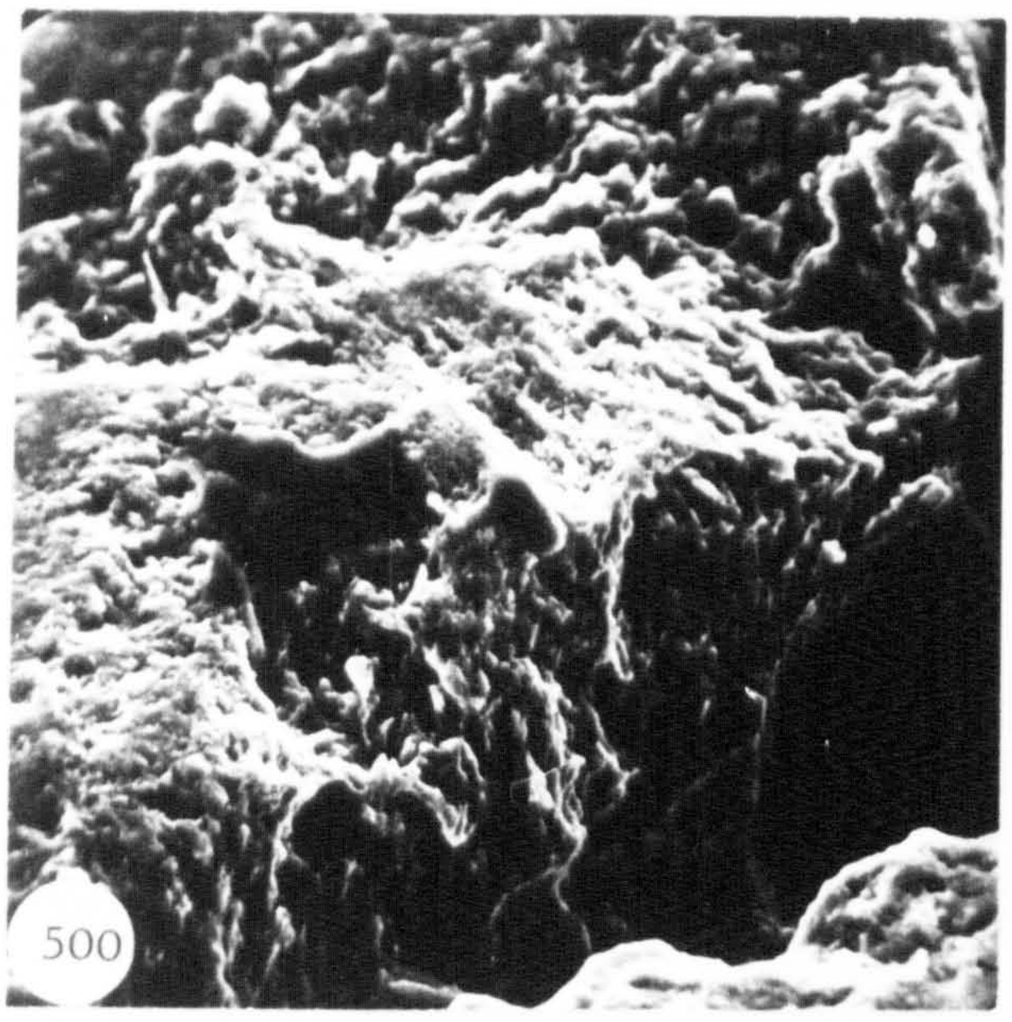


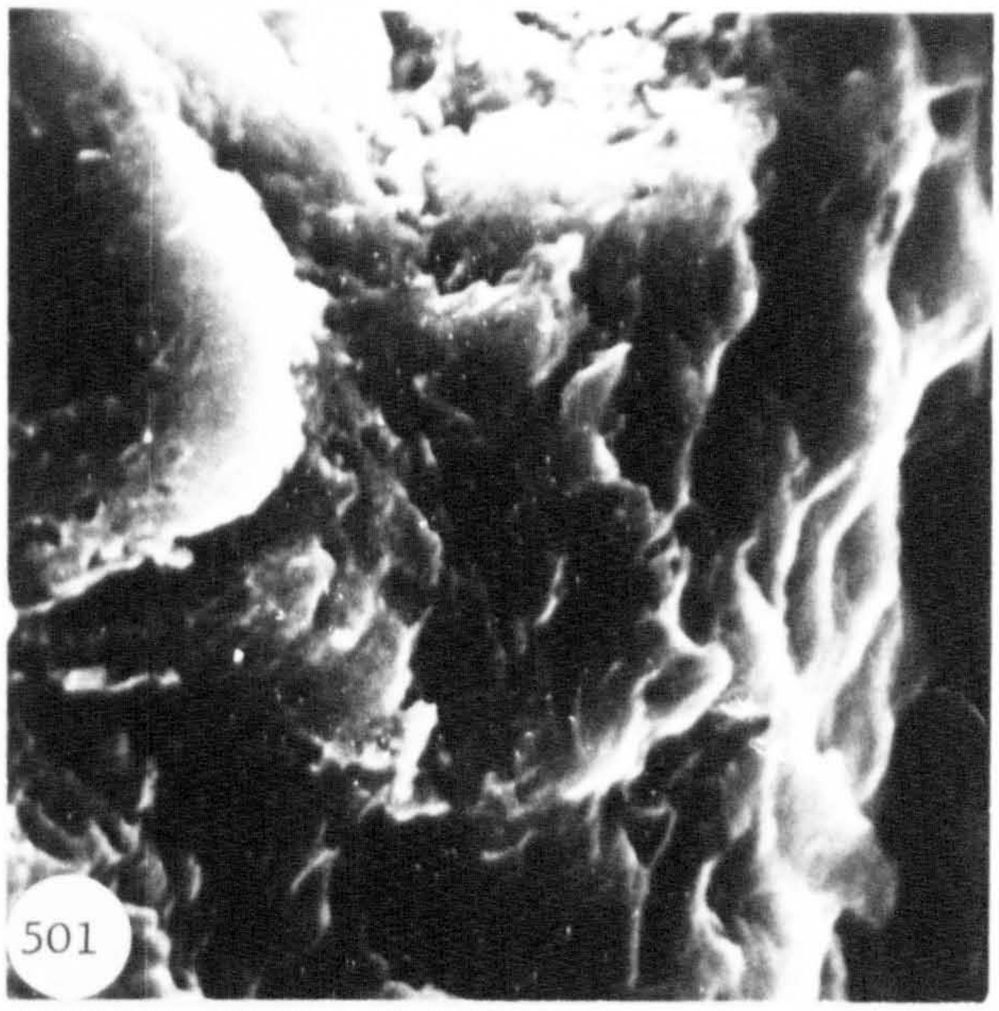


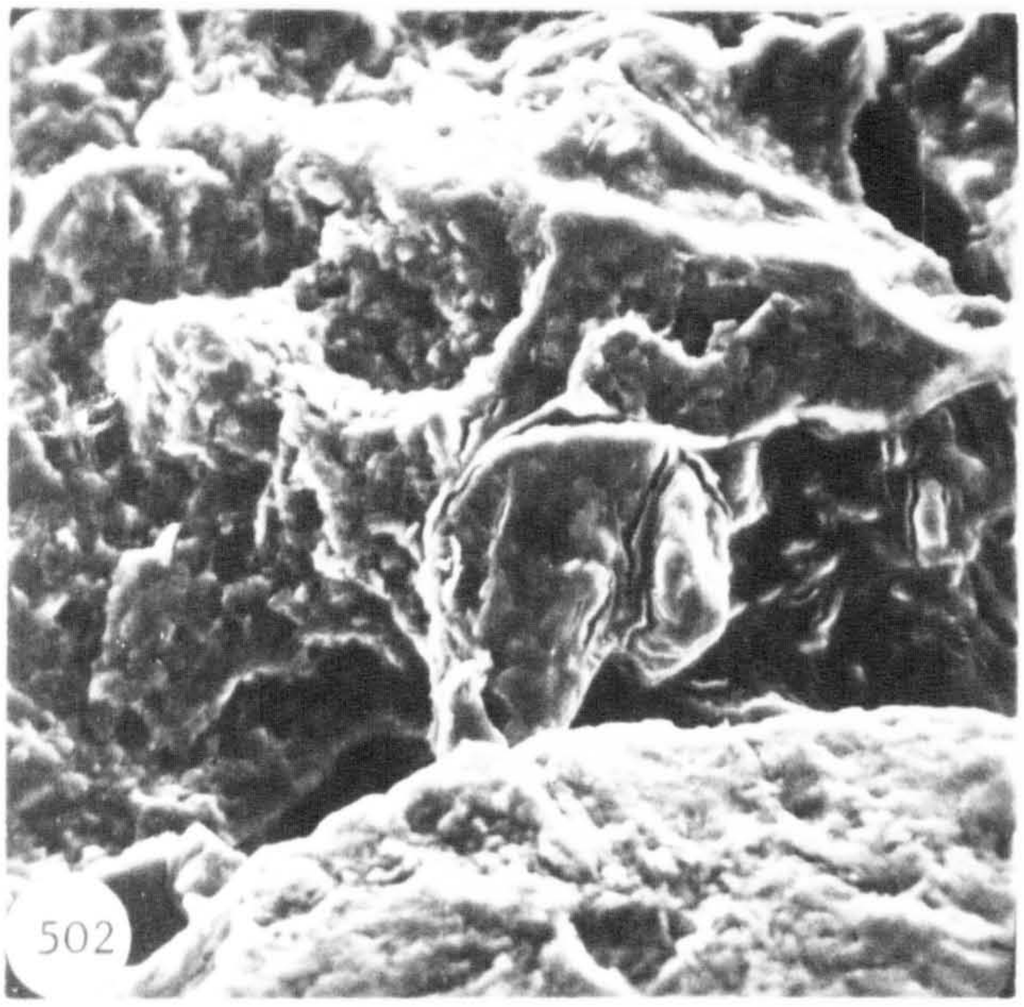


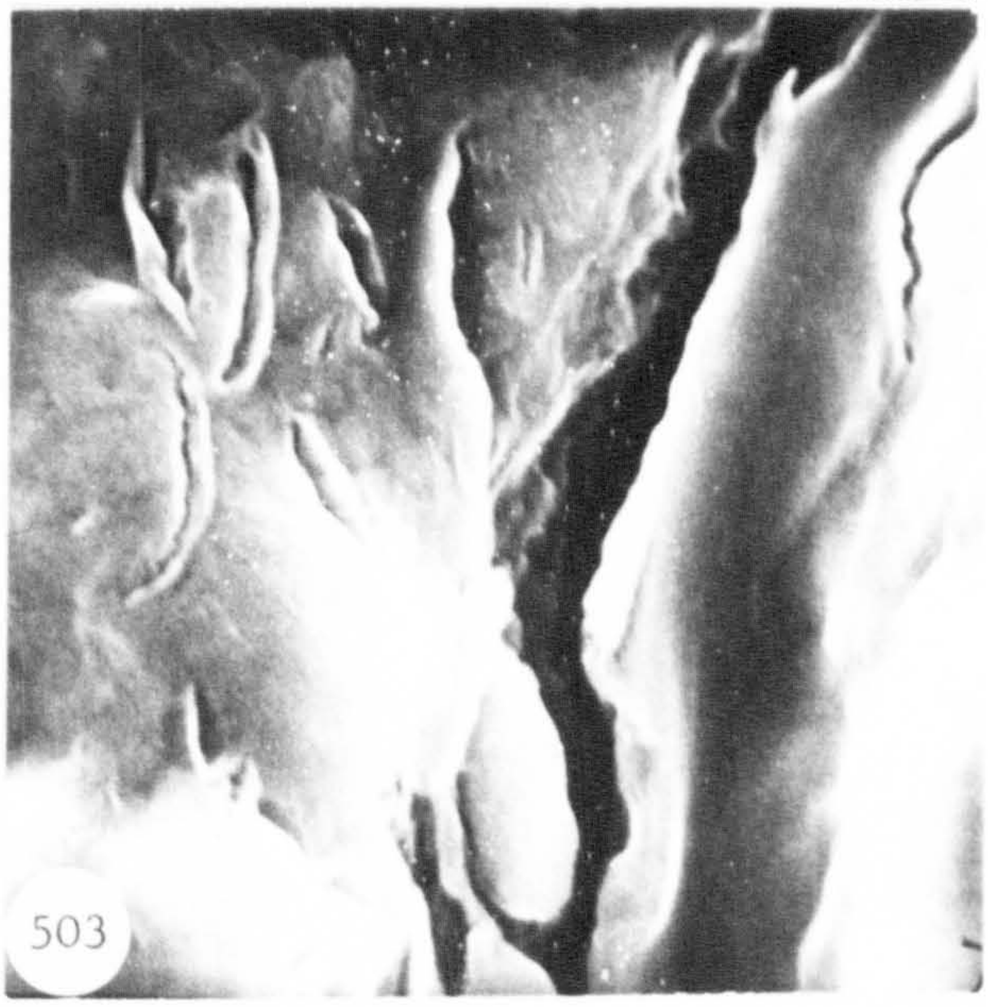
Figures 494 to 498. Scanning *electron* micrographs (stereoscan) of BAEL Pitch Coke Graphite Q6/1 (*control for* H30).



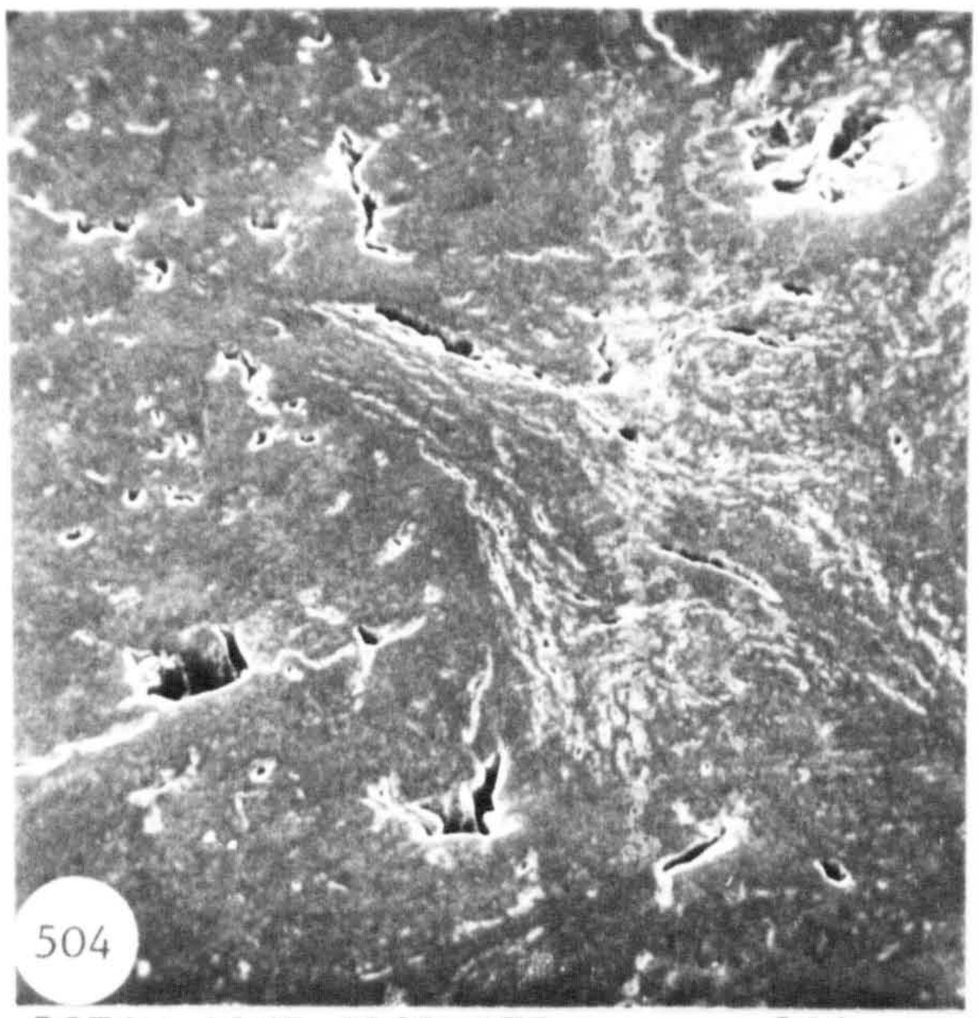


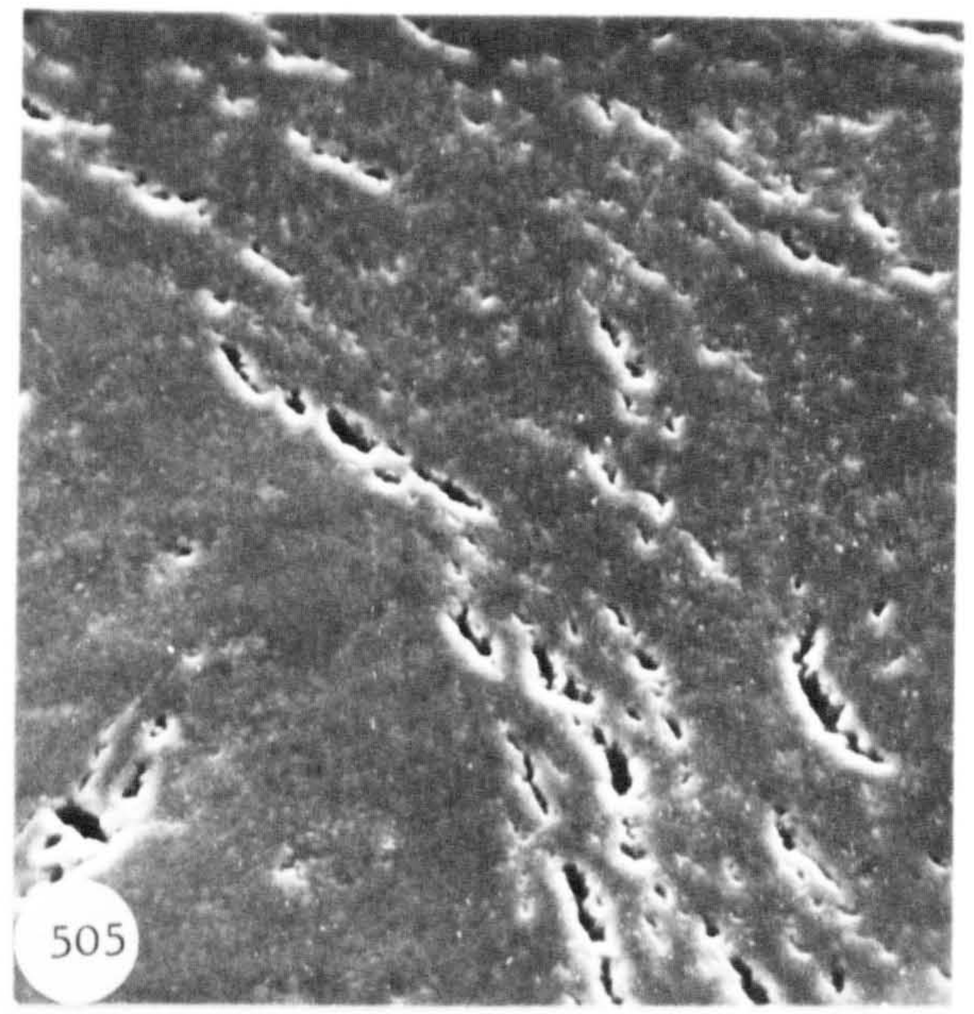


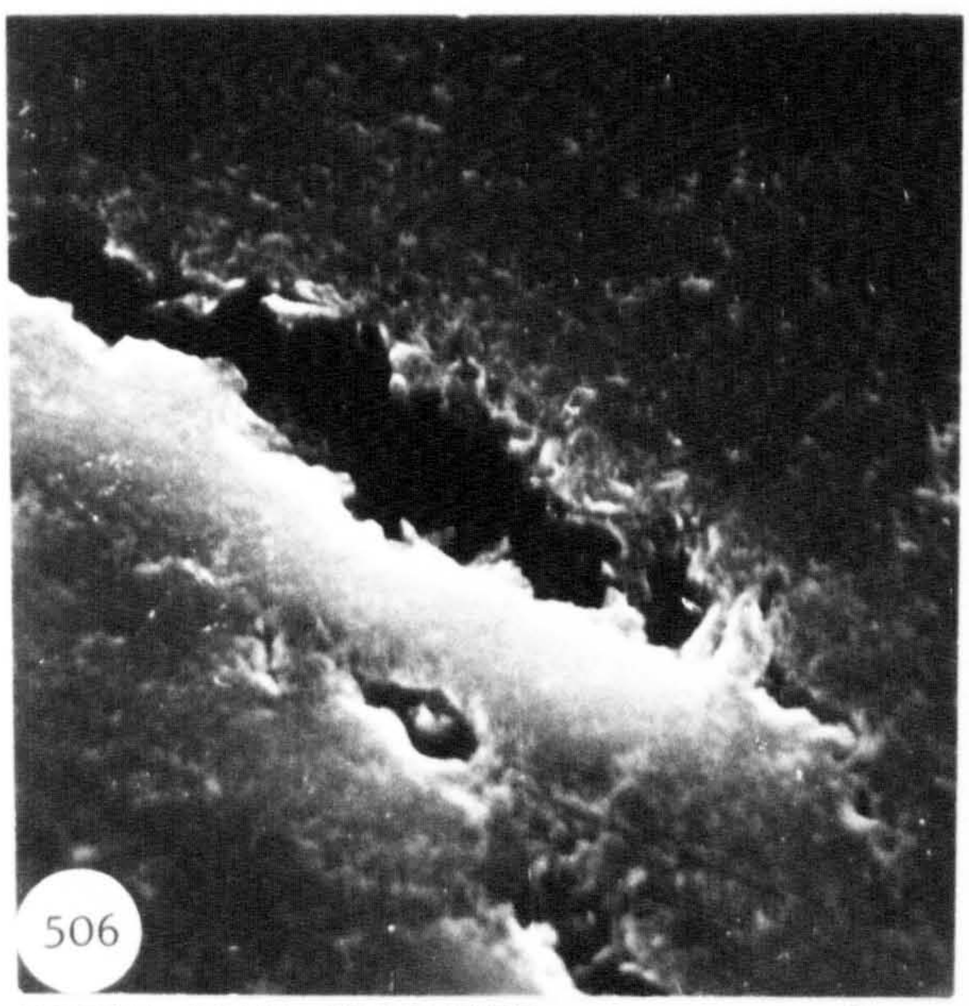


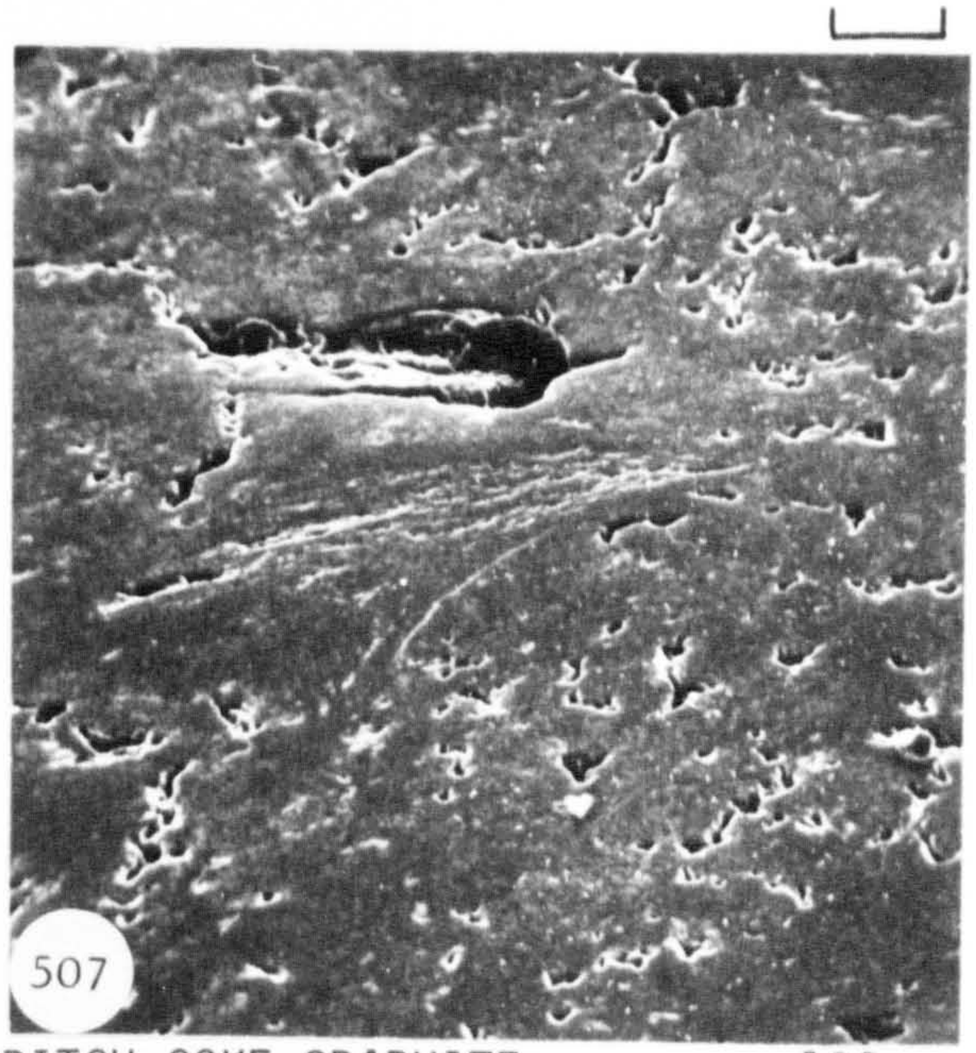


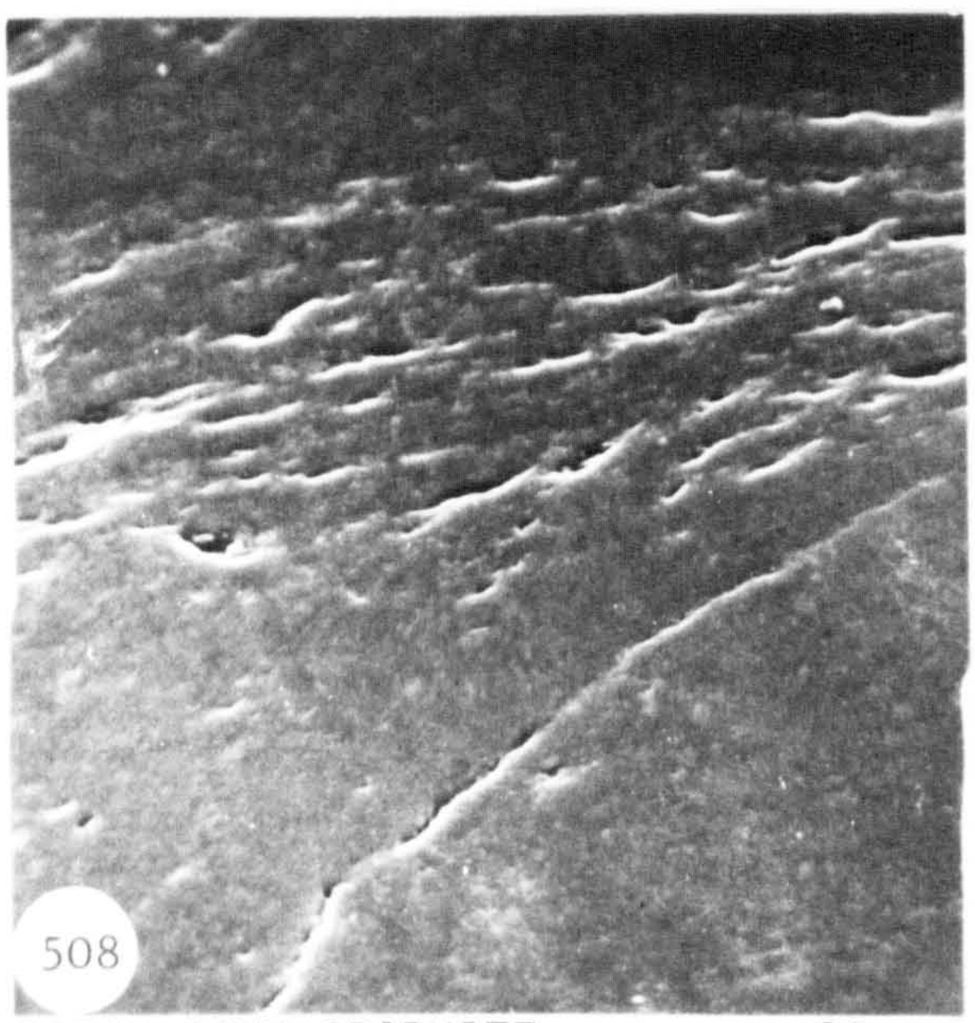
Figures 499 to 503. Scanning electron micrographs (stereoscan) of BAEL Pitch Coke Graphite H30, radiolytically oxidised in carbon dioxide. Weight loss 0.6%.

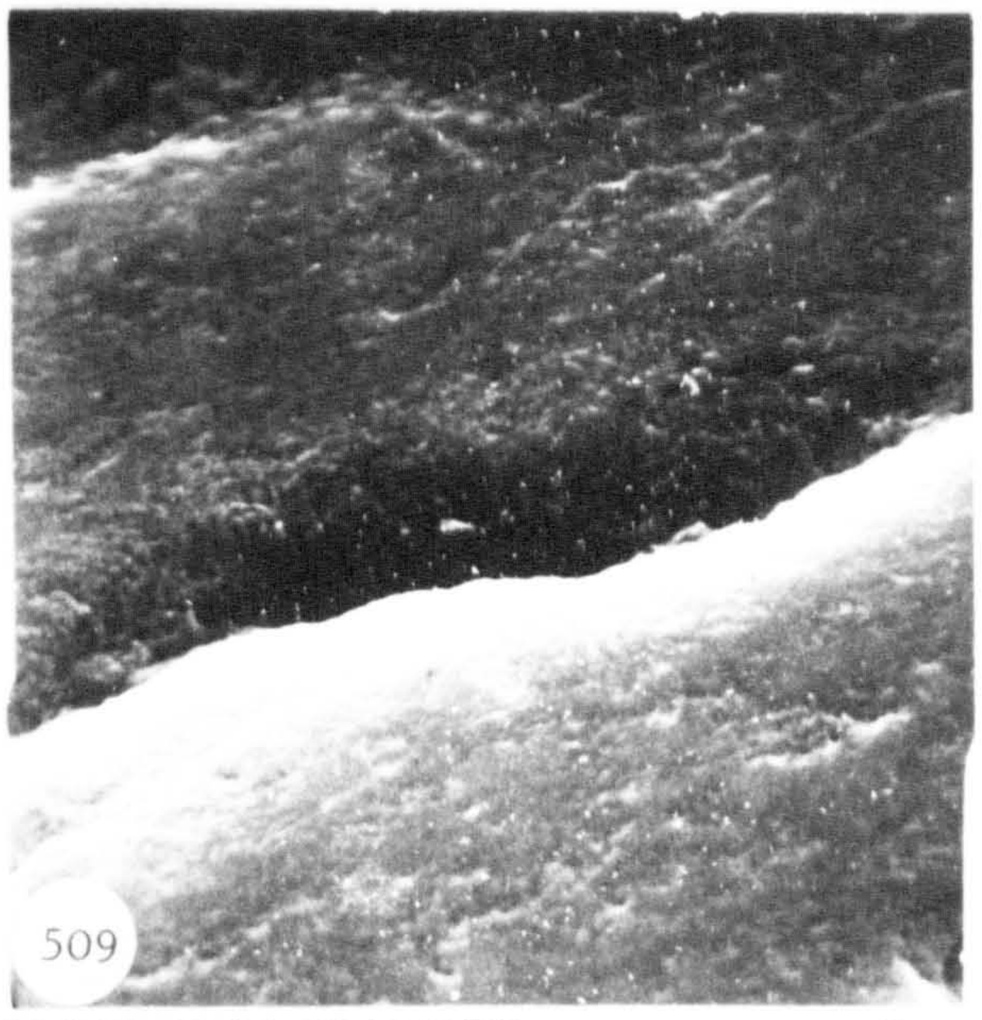












Figures 504 to 509. Scanning electron micrographs (stereoscan) of BAEL Pitch Coke Graphite Q6/1 (Figures 504 to 506) and H30 (Figures 507 to 509), radiolytically oxidised in carbon dioxide. Weight loss 0.6%.

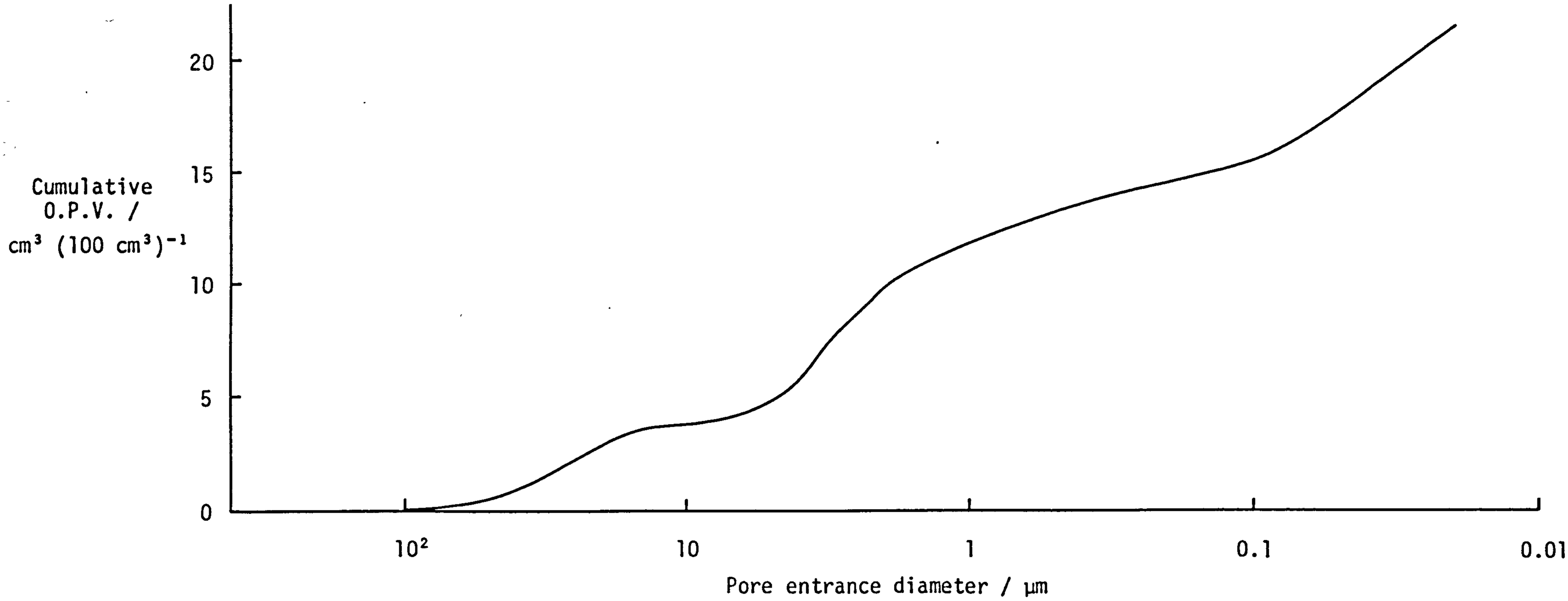


Figure 510. Mercury pore size distribution of virgin Lima graphite. Variation of cumulative open pore volume with pore entrance diameter.

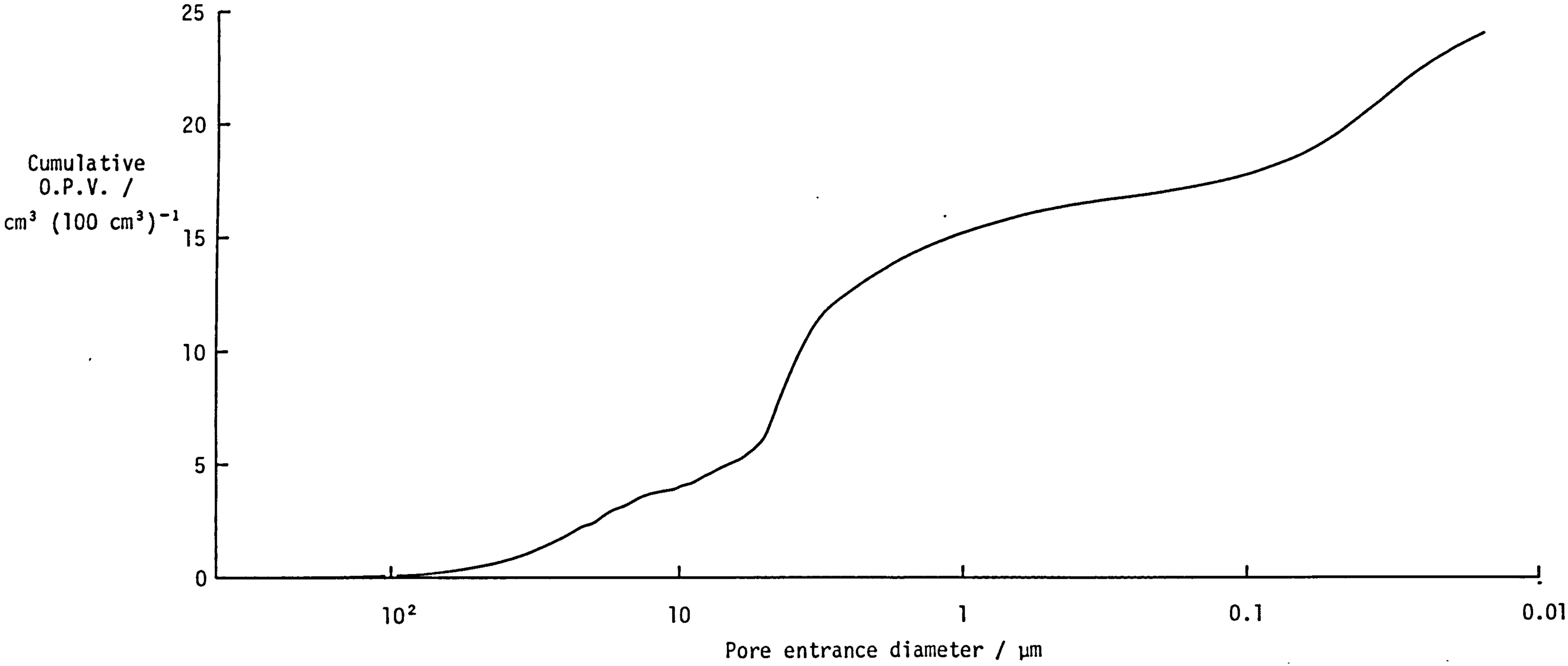


Figure 511. Mercury pore size distribution of Lima graphite radiolytically oxidised to 1.26% weight loss. Variation of cumulative open pore volume with pore entrance diameter.

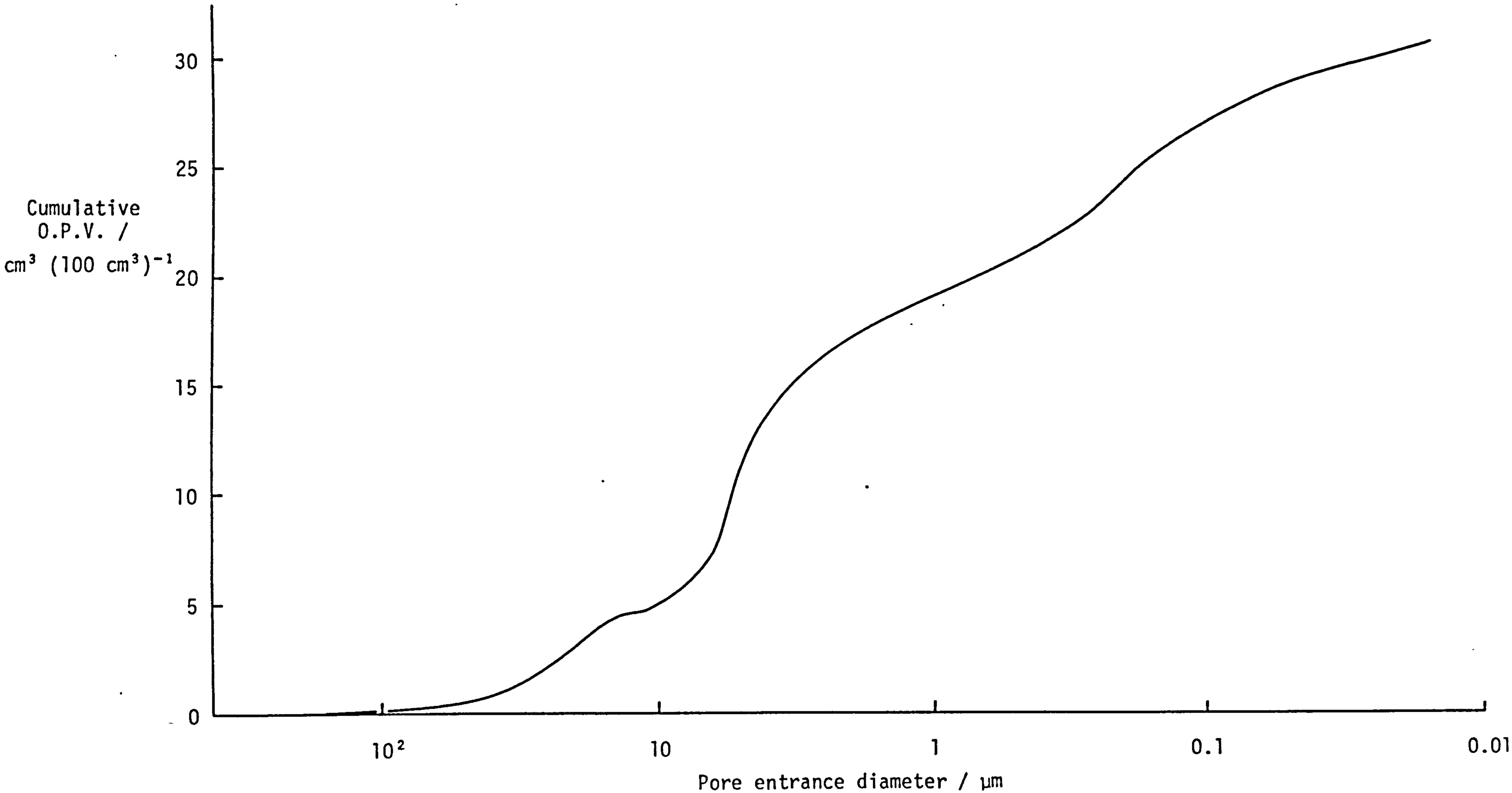


Figure 512. Mercury pore size distribution of Lima graphite radiolytically oxidised to 9.48% weight loss. Variation of cumulative open pore volume with pore entrance diameter.

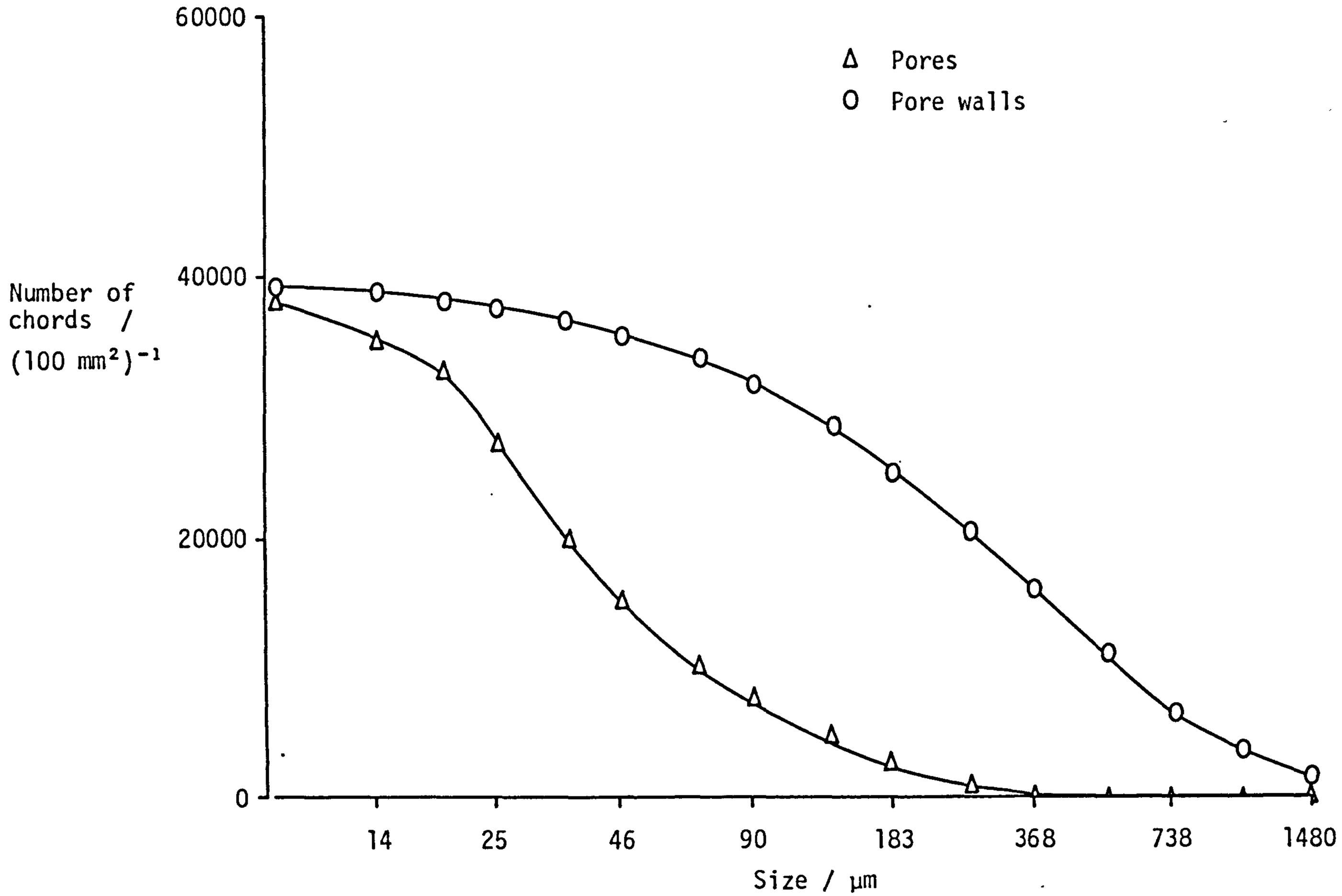


Figure 513. Distribution of number of chords present in BAEL pitch-coke graphite Q4/1 (control for H24).

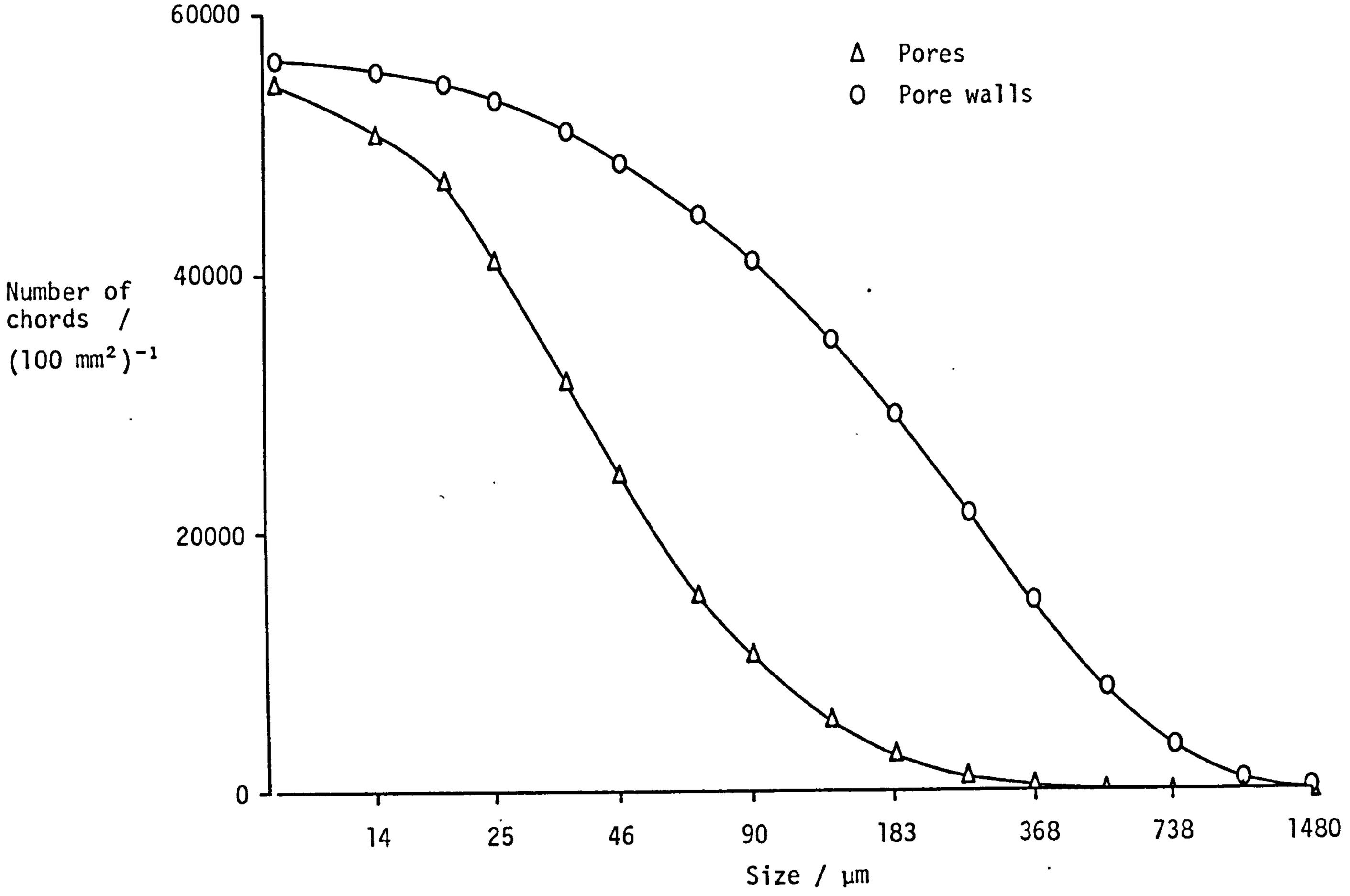


Figure 514. Distribution of number of chords present in BAEL pitch-coke graphite H24 radiolytically oxidised to 8.8% weight loss.

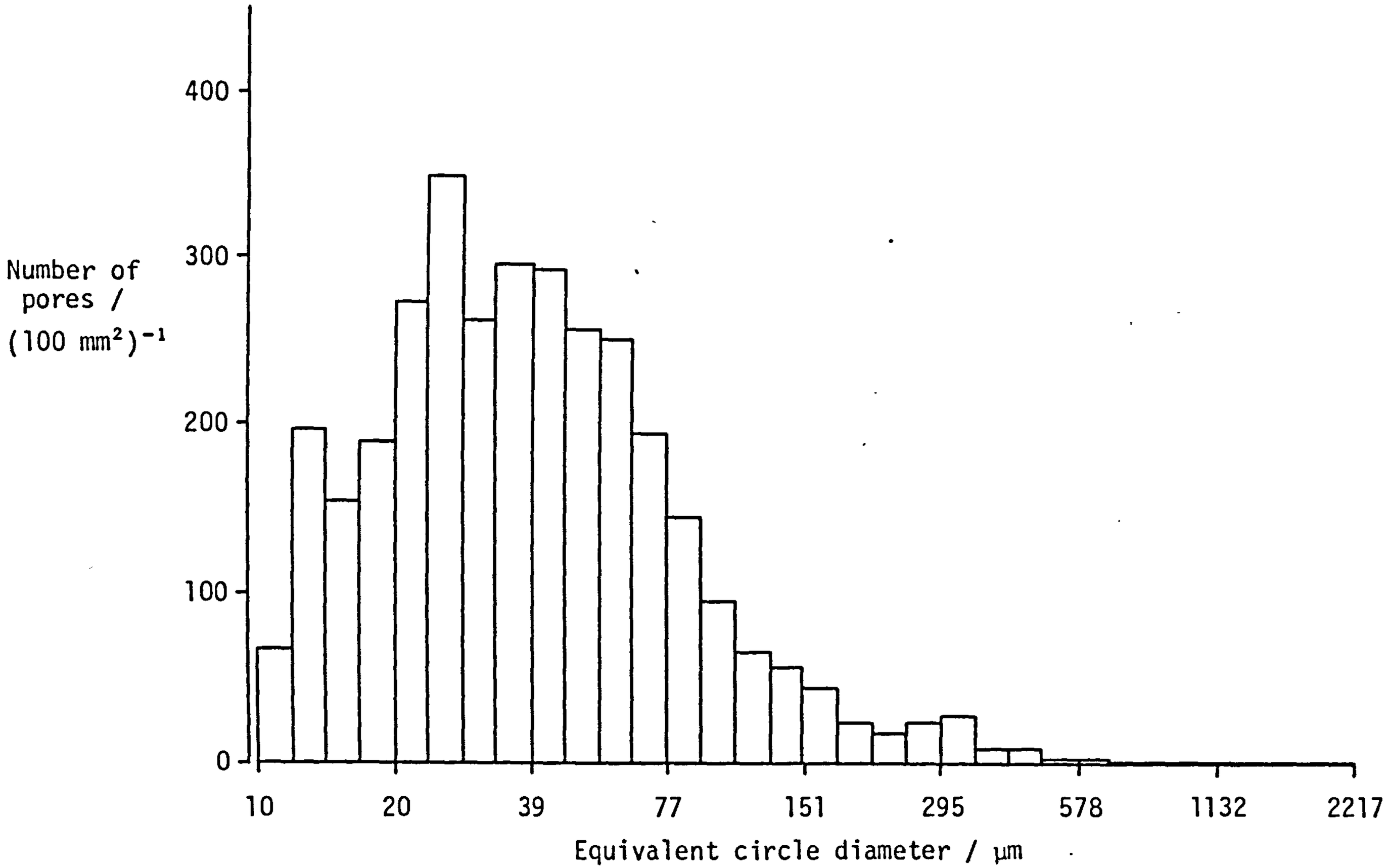


Figure 515. Corrected distribution of areas of pores in BAEL pitch-coke graphite Q4/1 (control for H24).

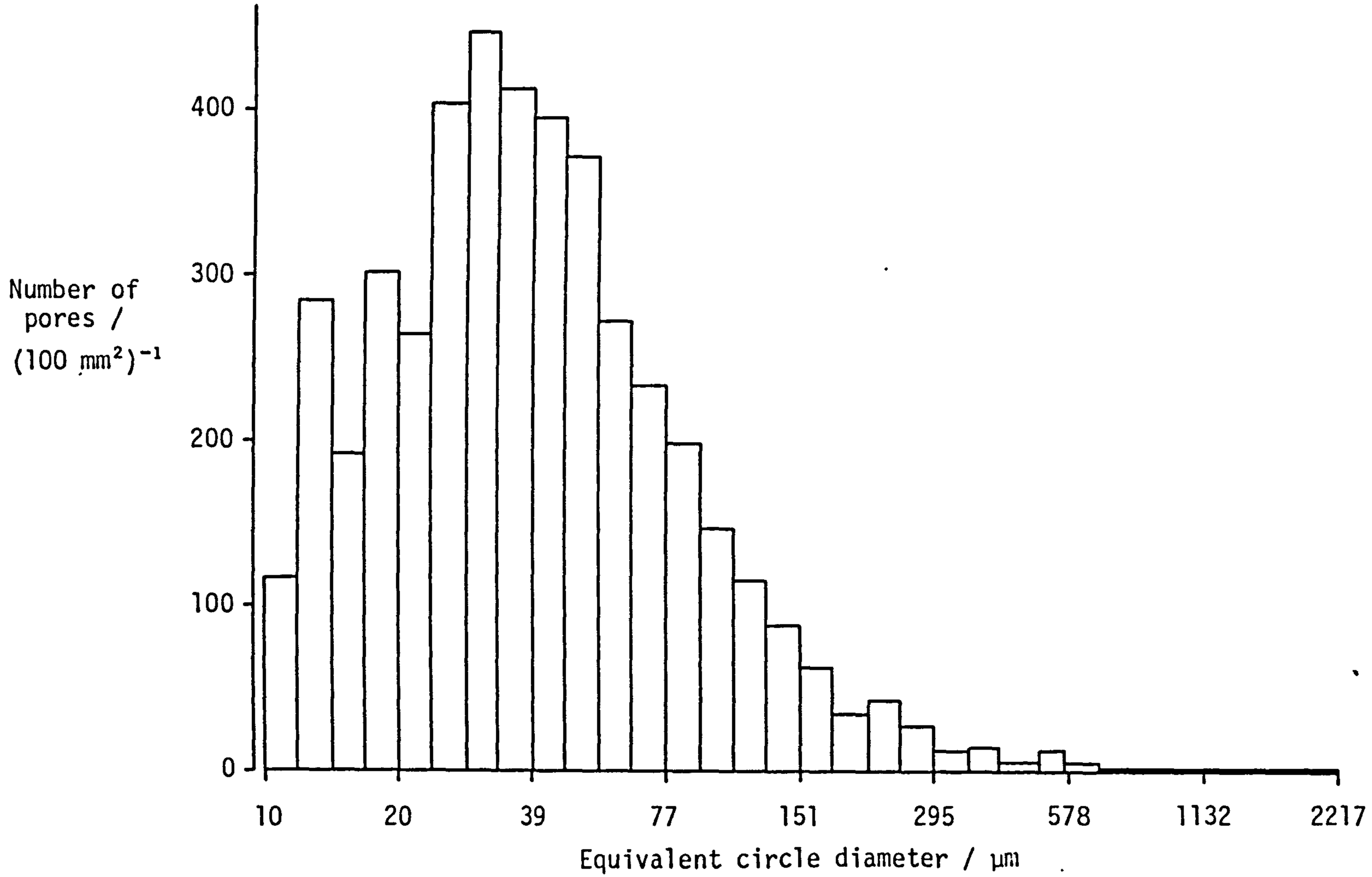


Figure 516. Corrected distribution of areas of pores in BAEL pitch-coke graphite H24 radiolytically oxidised to 8.8% weight loss.

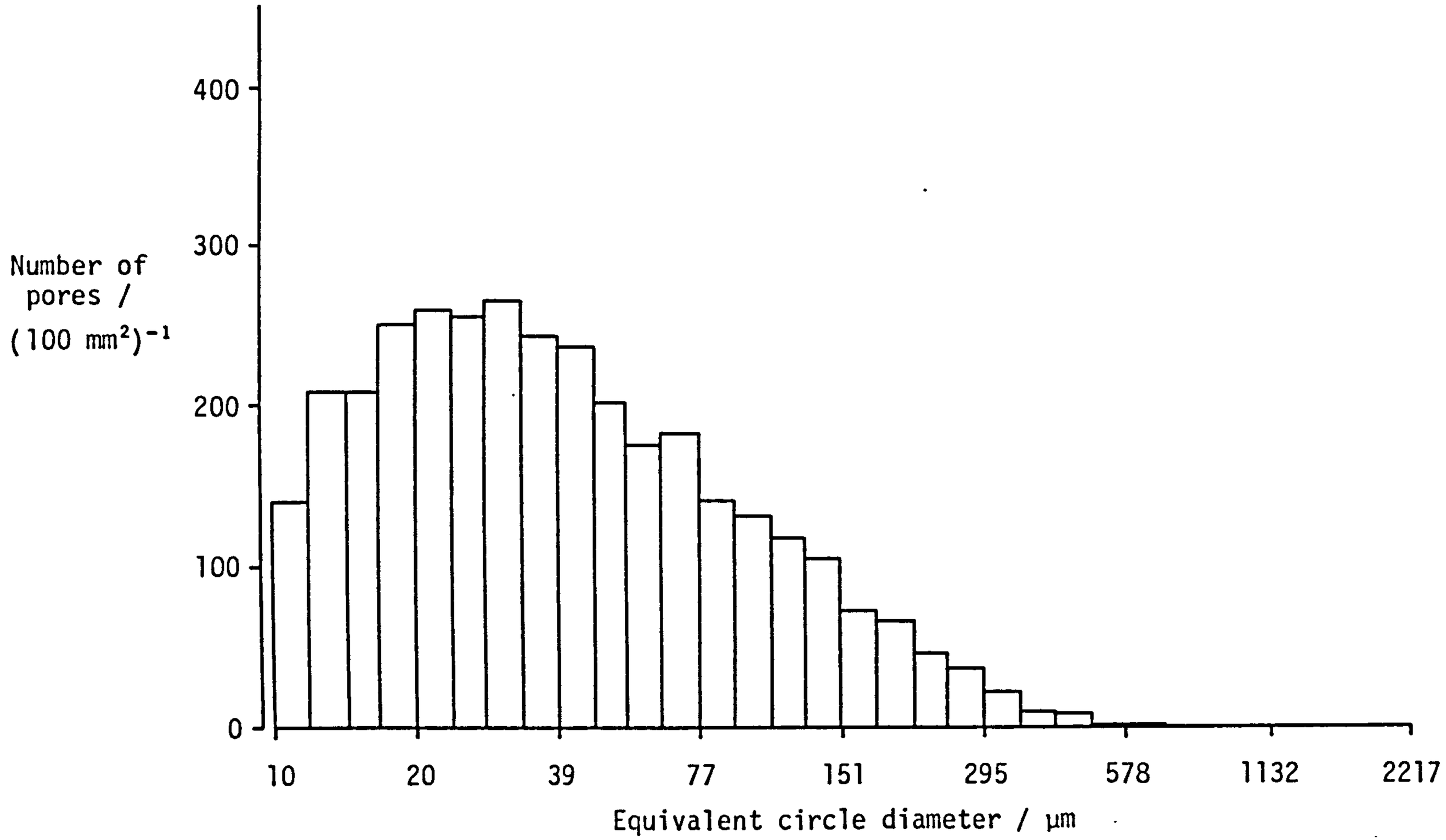


Figure 517. Corrected distribution of areas of pores in AGLMP graphite thermally oxidised to 3.1% weight loss.

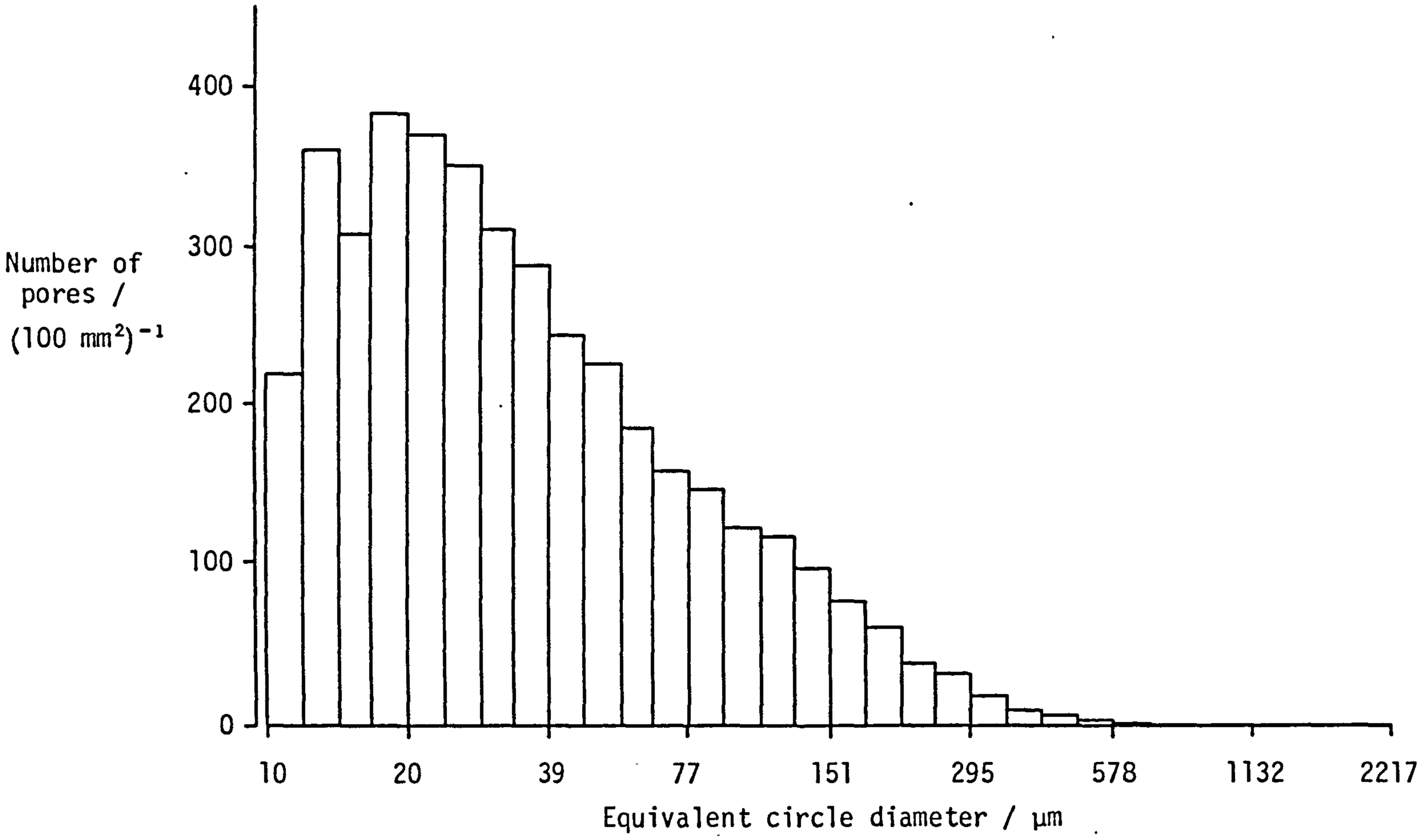


Figure 518. Corrected distribution of areas of pores in AGLMP graphite thermally oxidised to 5.4% weight loss.

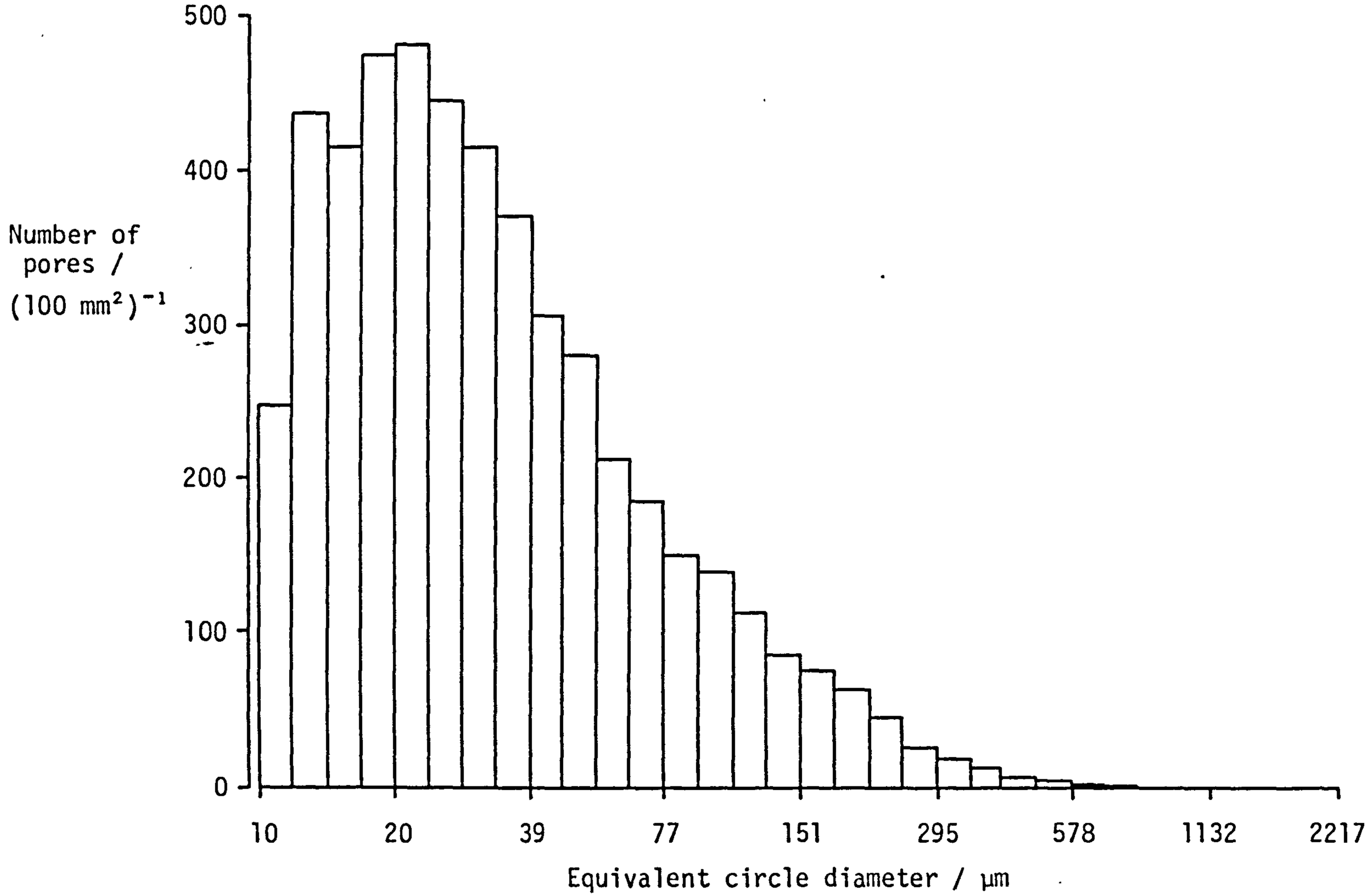
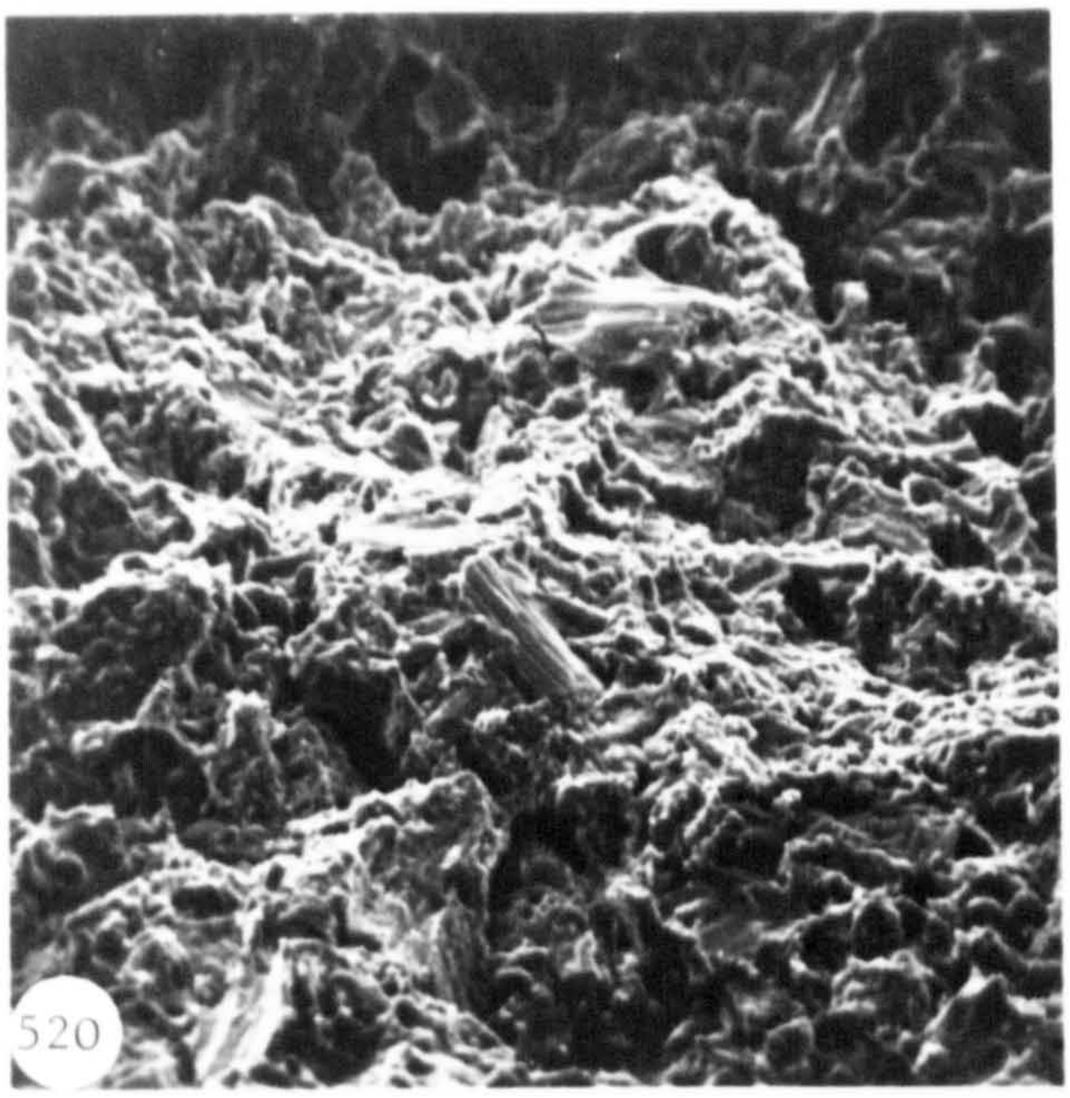
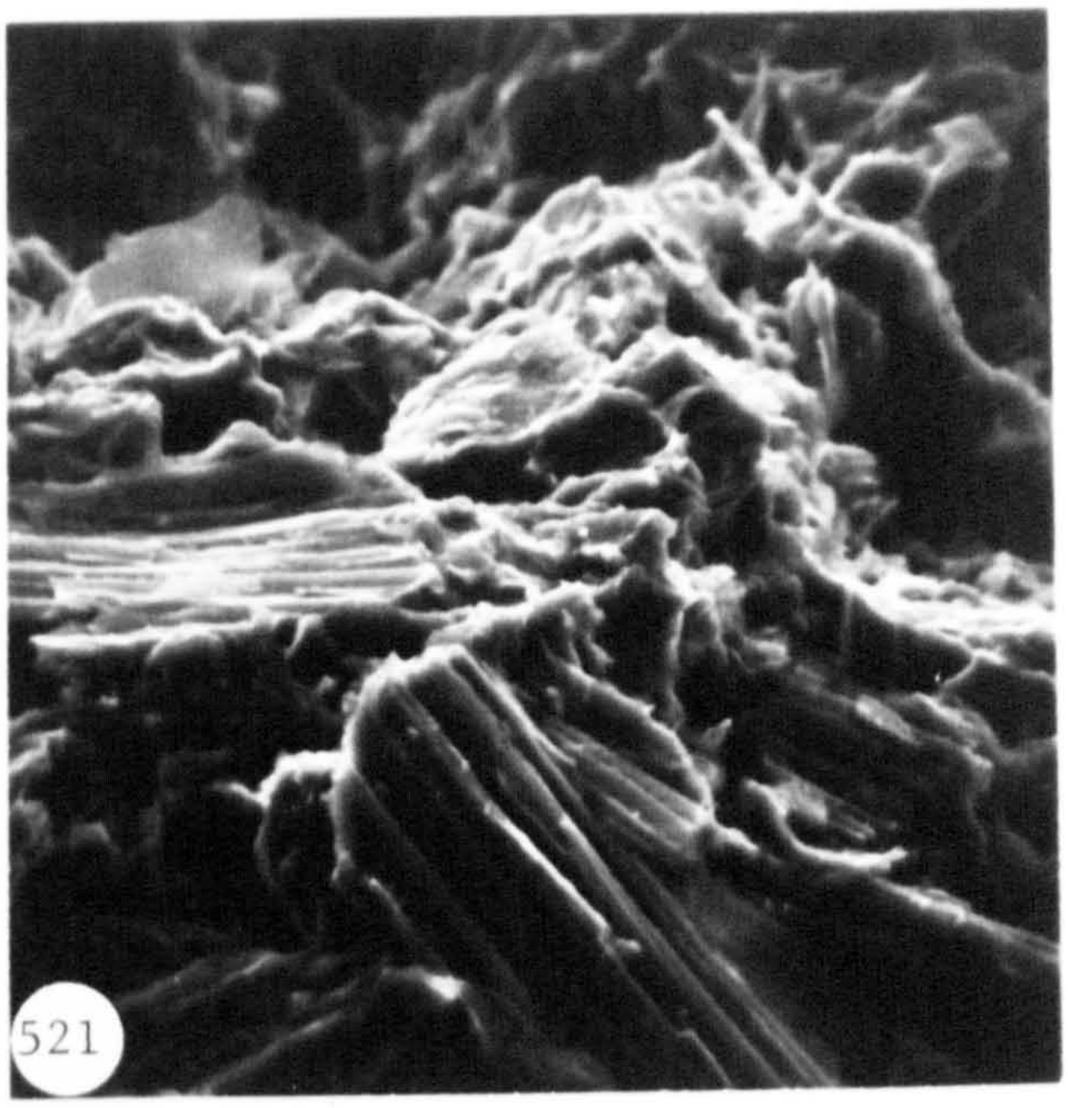


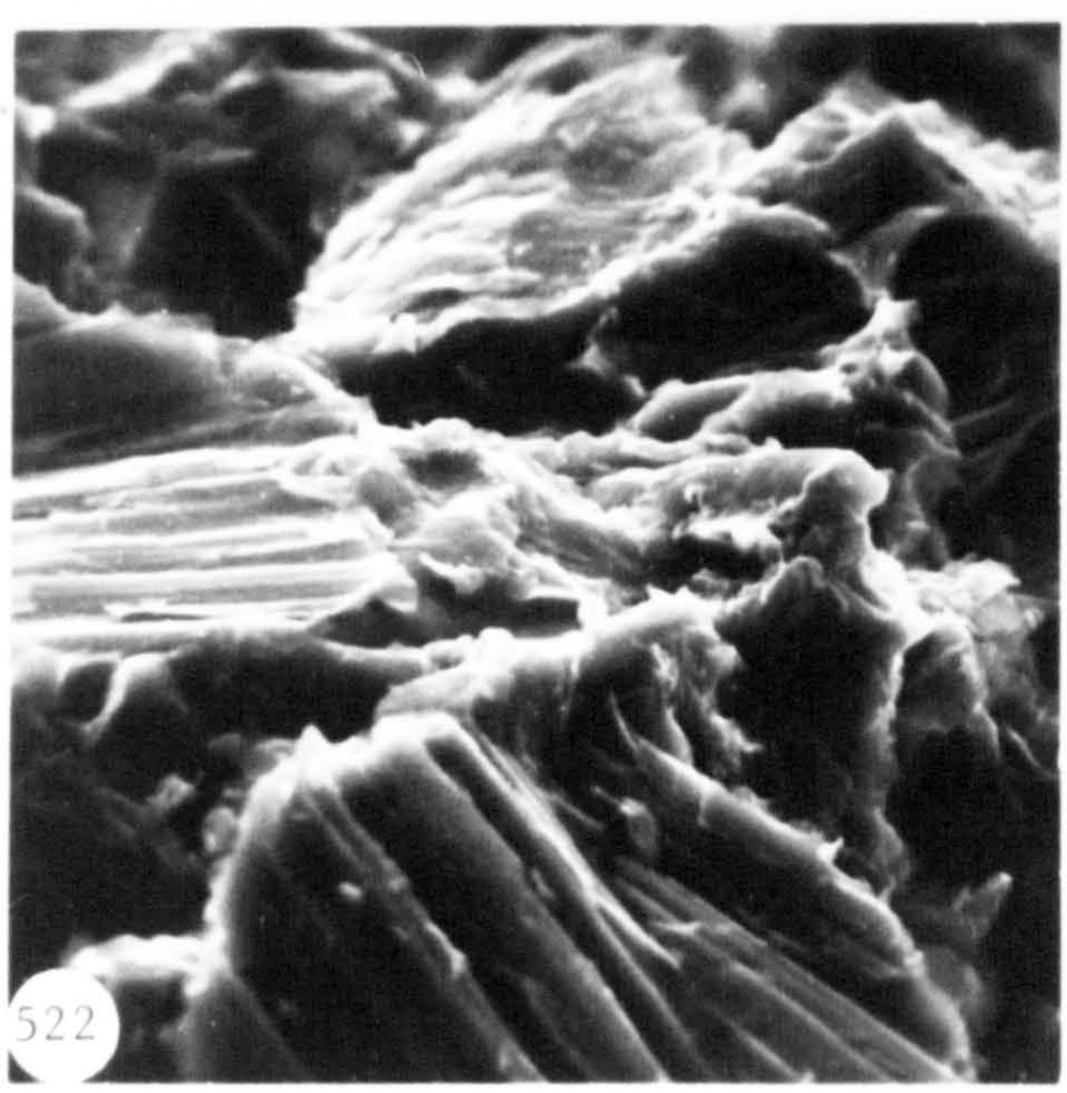
Figure 519. Corrected distribution of areas of pores in AGLMP graphite thermally oxidised to 10.5% weight loss.



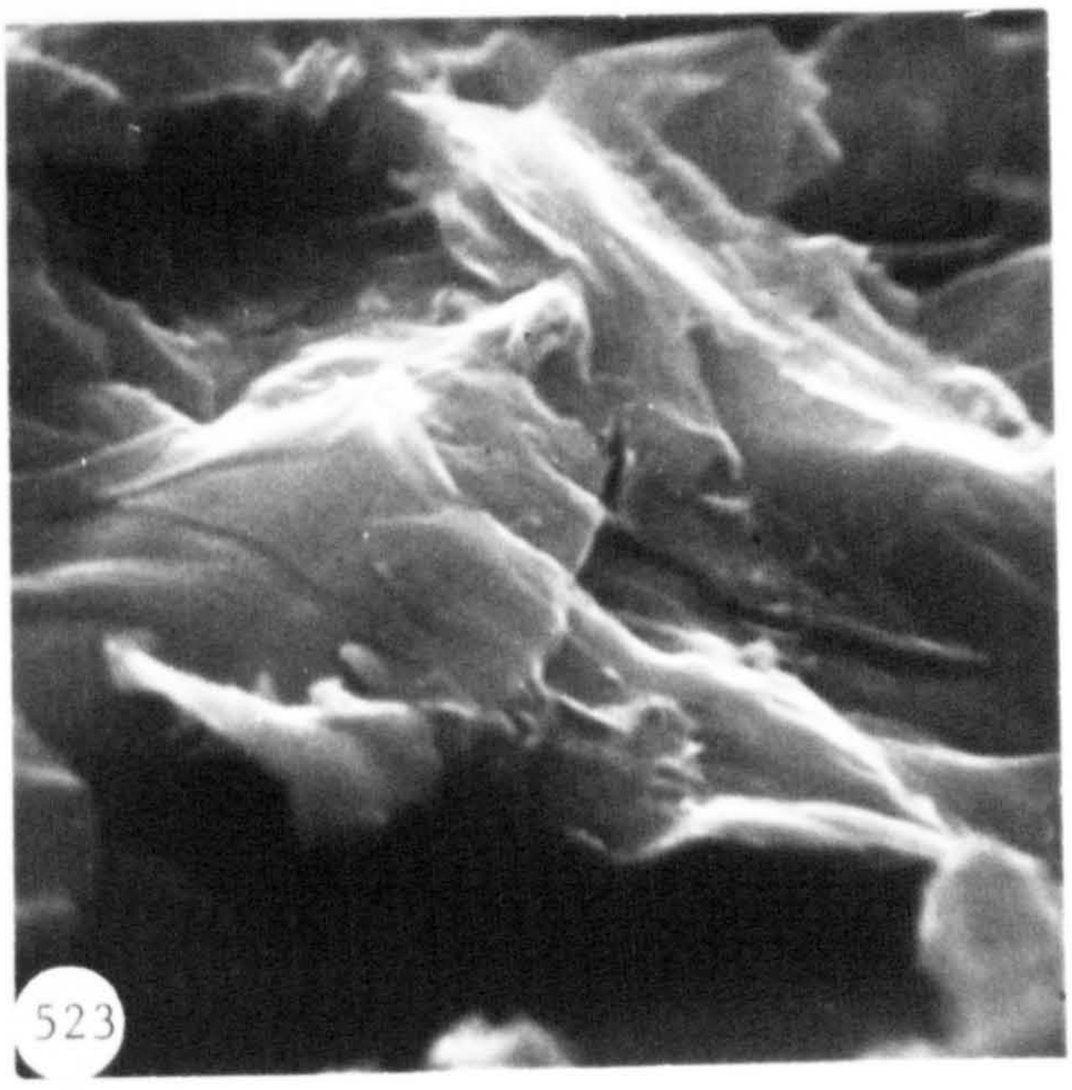
LIMA GRAPHITE 100 µm



LIMA GRAPHITE 20 µm

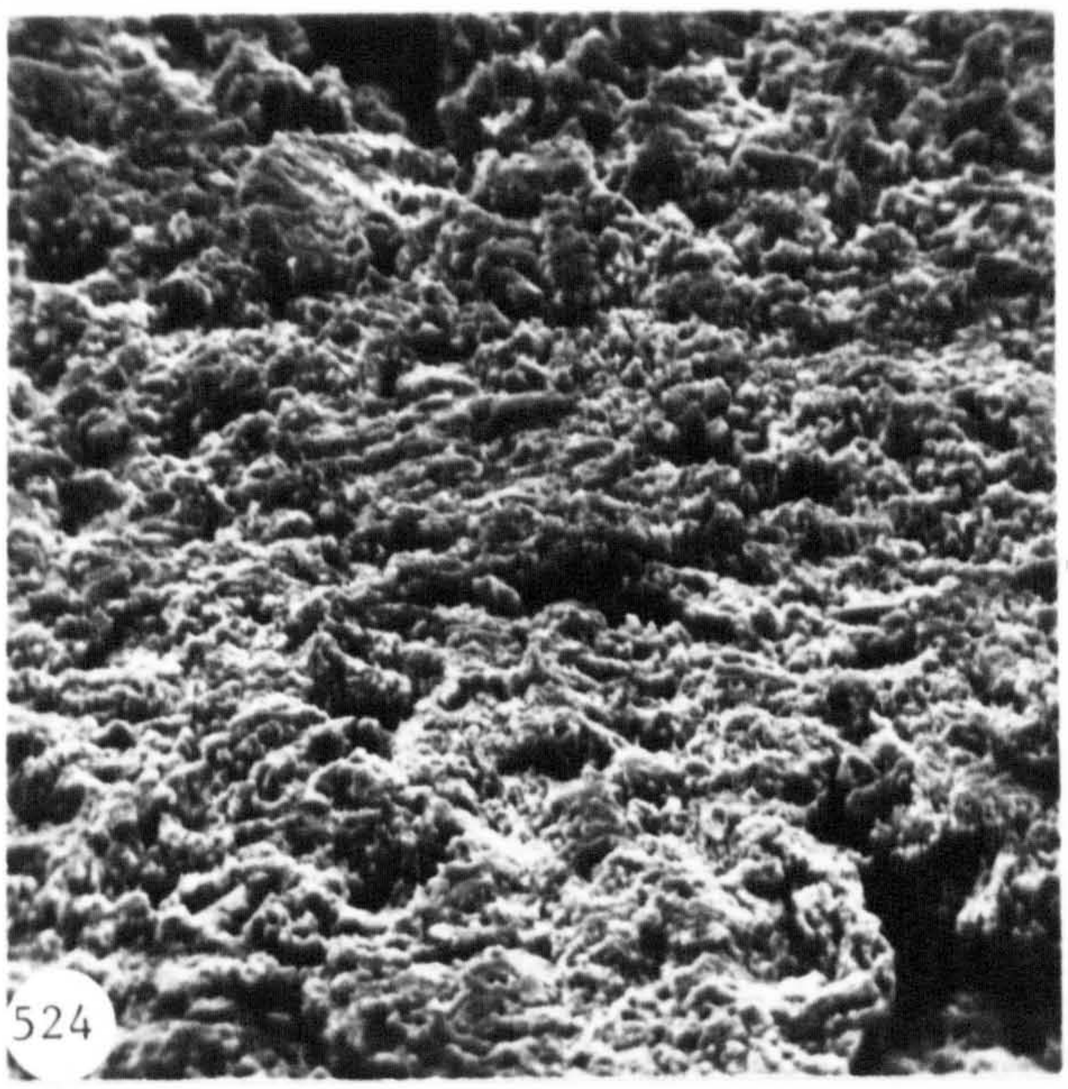


LIMA GRAPHITE 10 µm

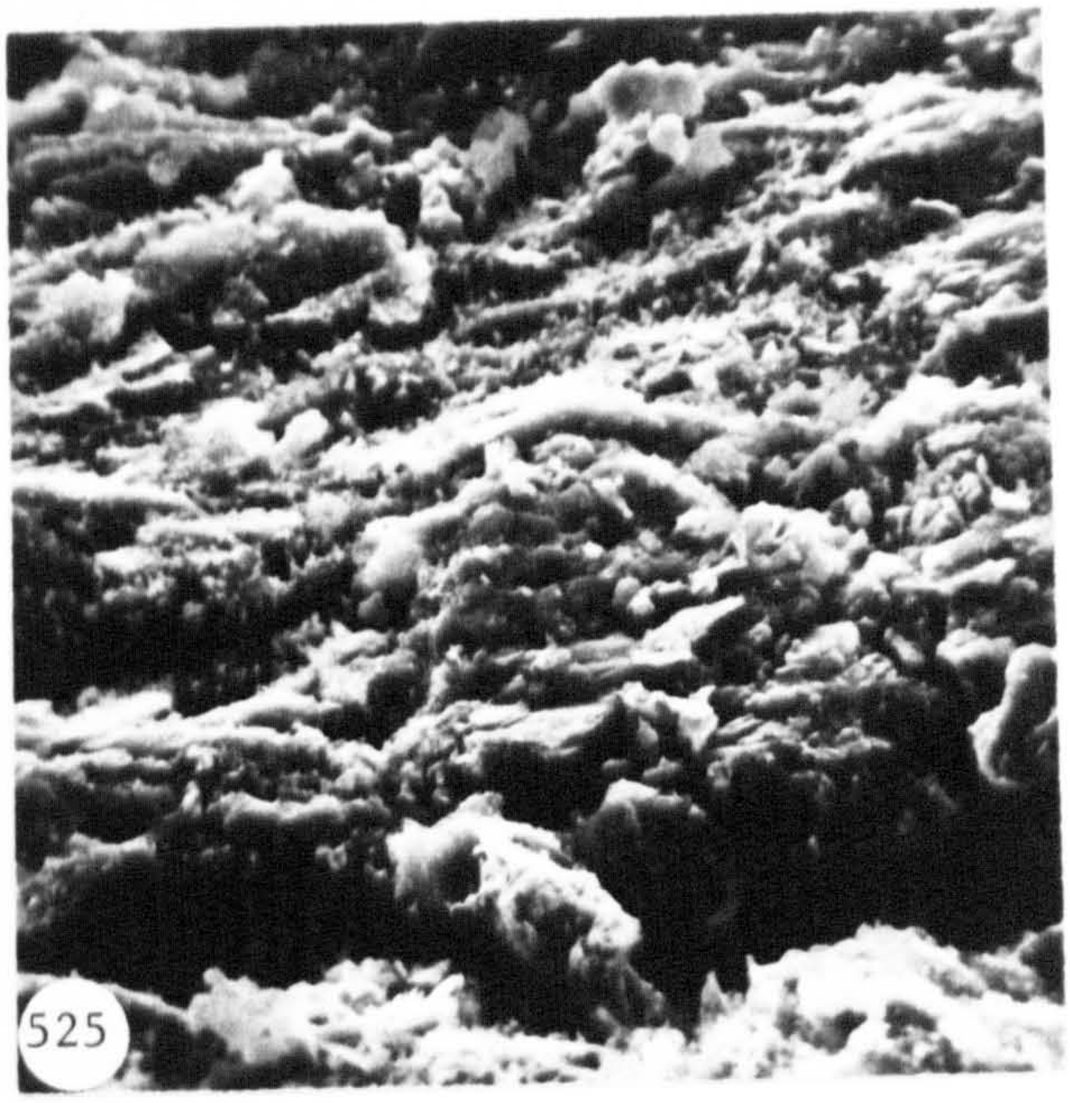


LIMA GRAPHITE 2 µm

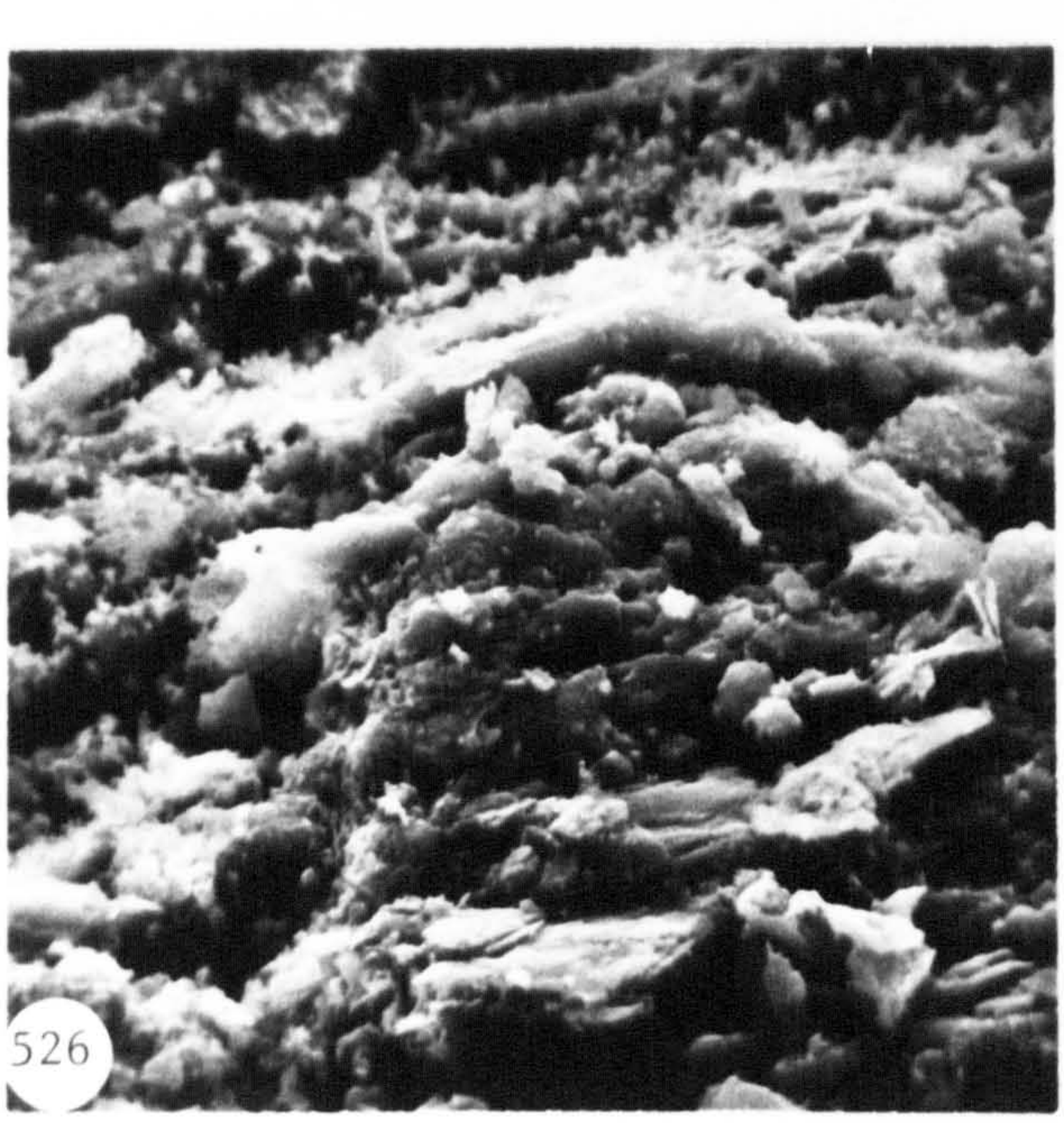
Figures 520 to 523. Scanning electron micrographs (stereoscan) of virgin Lima Graphite.



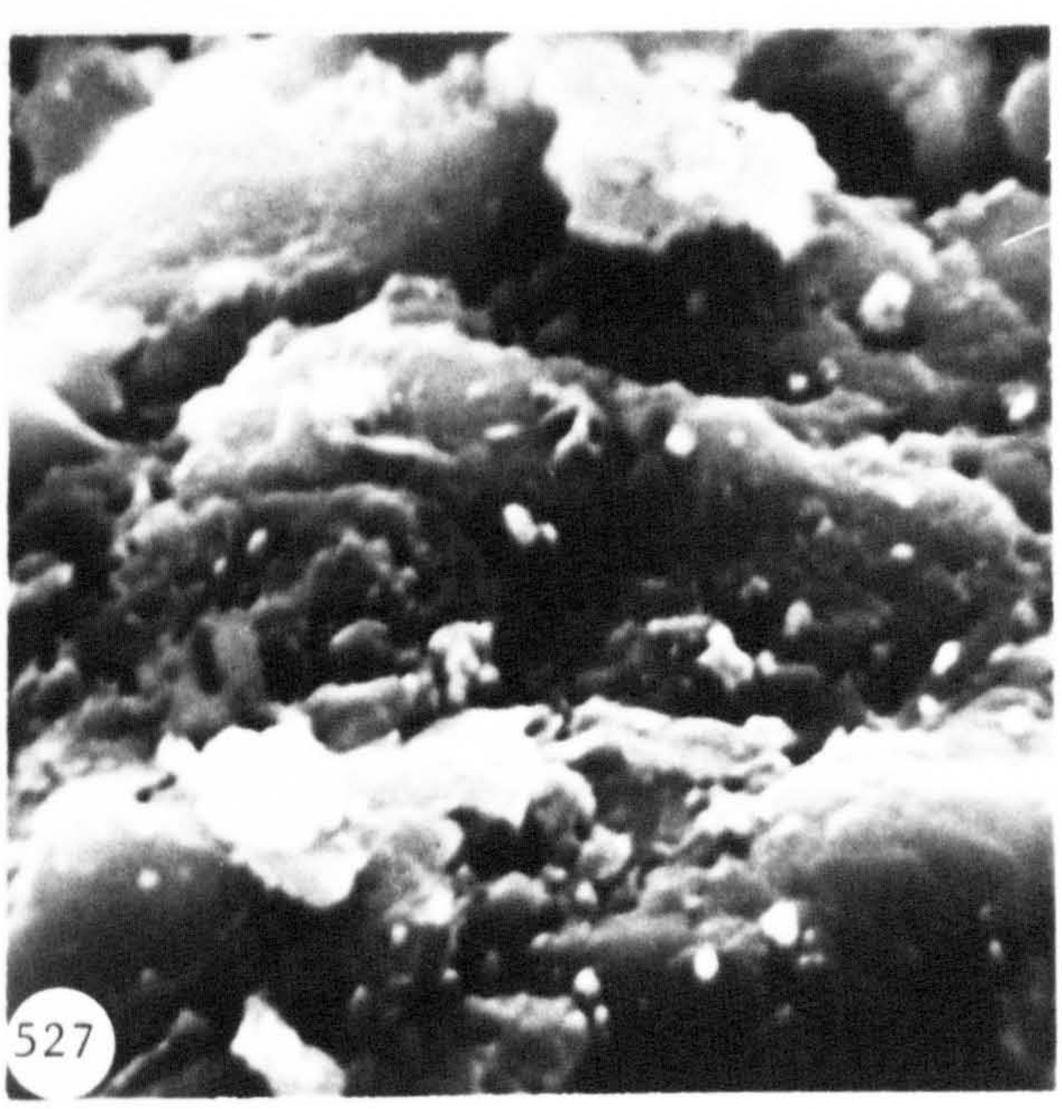
LIMA GRAPHITE 100 µm



LIMA GRAPHITE 20 µm

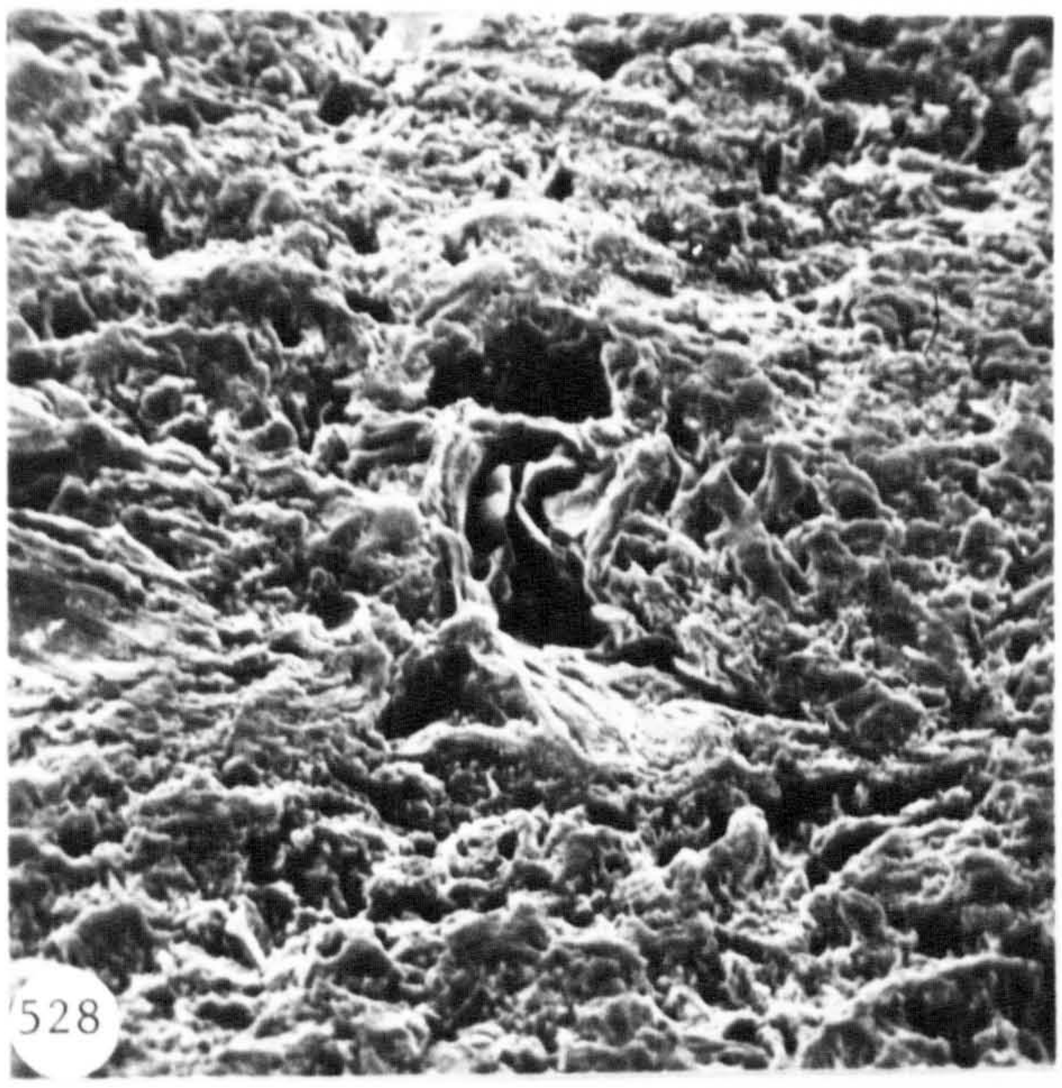


LIMA GRAPHITE 10 µm



LIMA GRAPHITE 2 µm

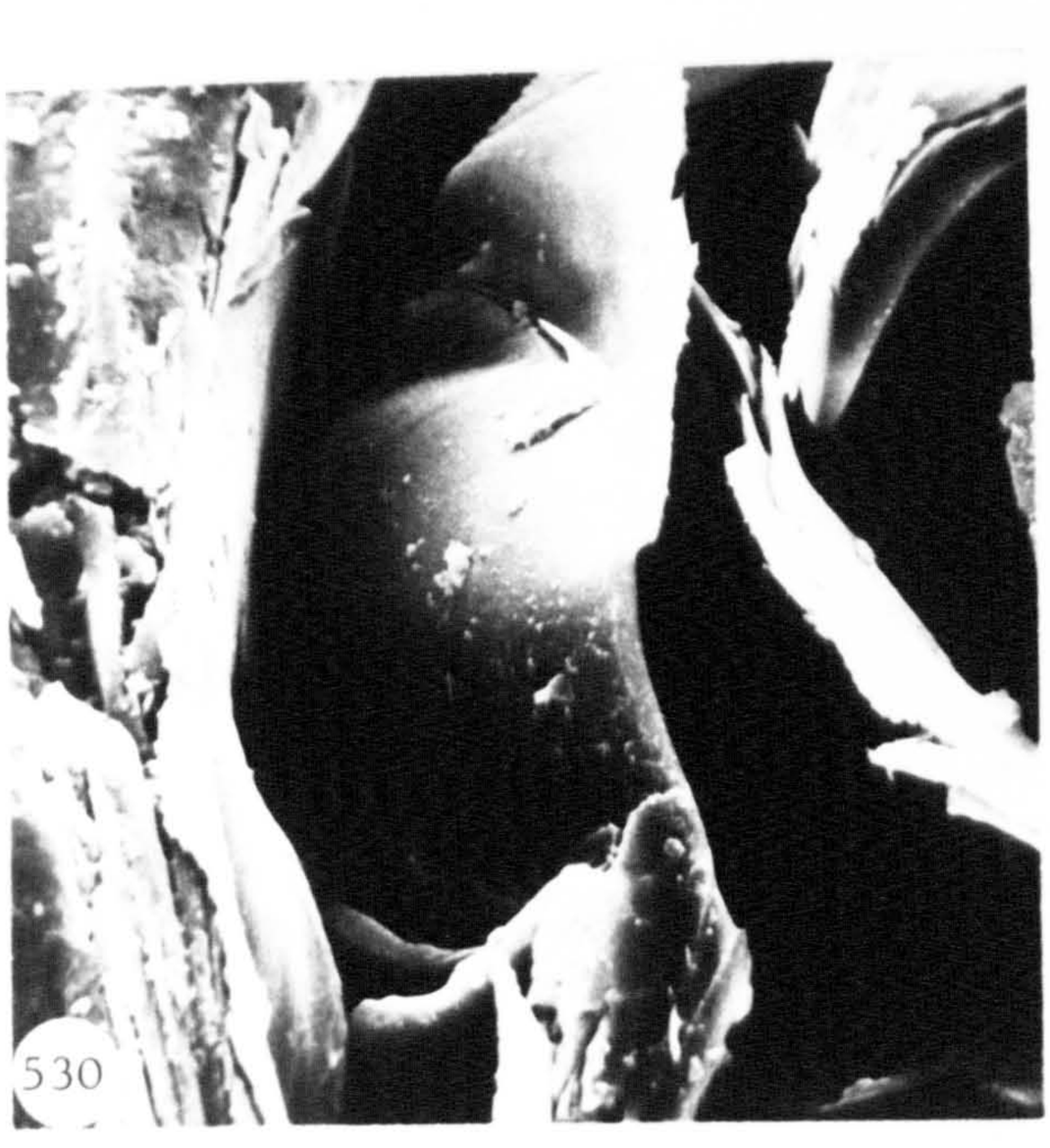
Figures 524 to 527. Scanning electron micrographs (stereoscan) of Lima Graphite radiolytically oxidised to 1.26% weight loss (inside surface).



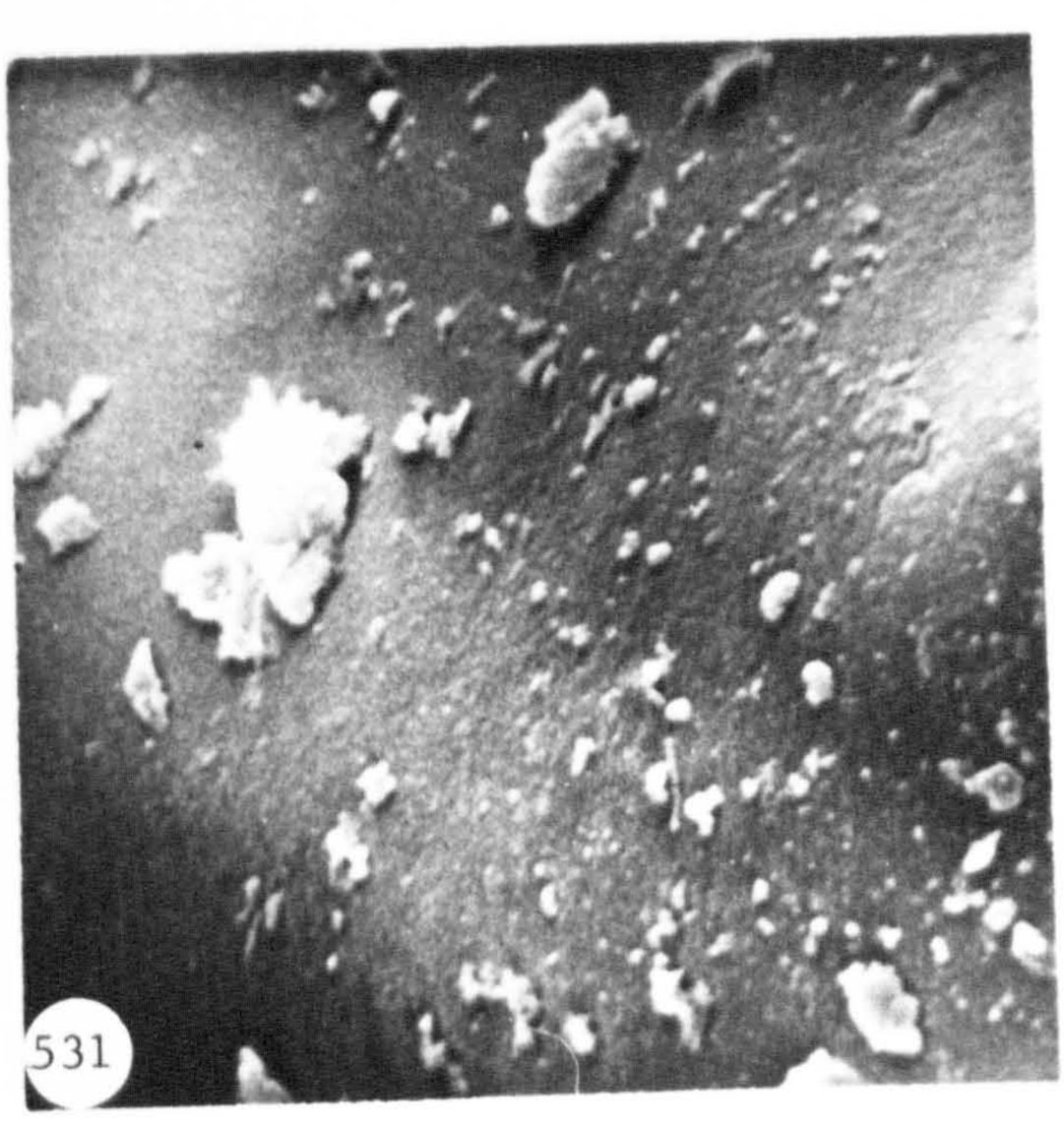
LIMA GRAPHITE 100 µm



LIMA GRAPHITE 20 µm

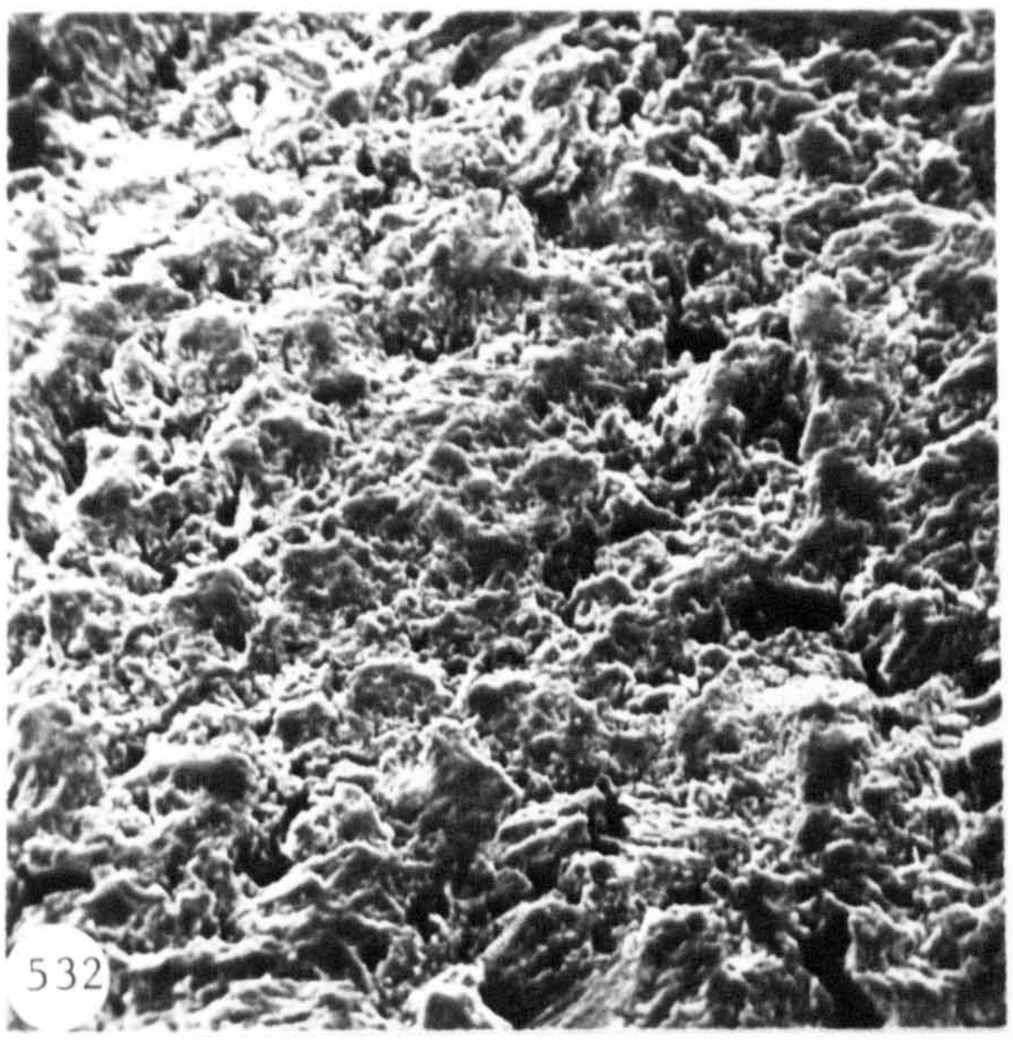


LIMA GRAPHITE 10 µm

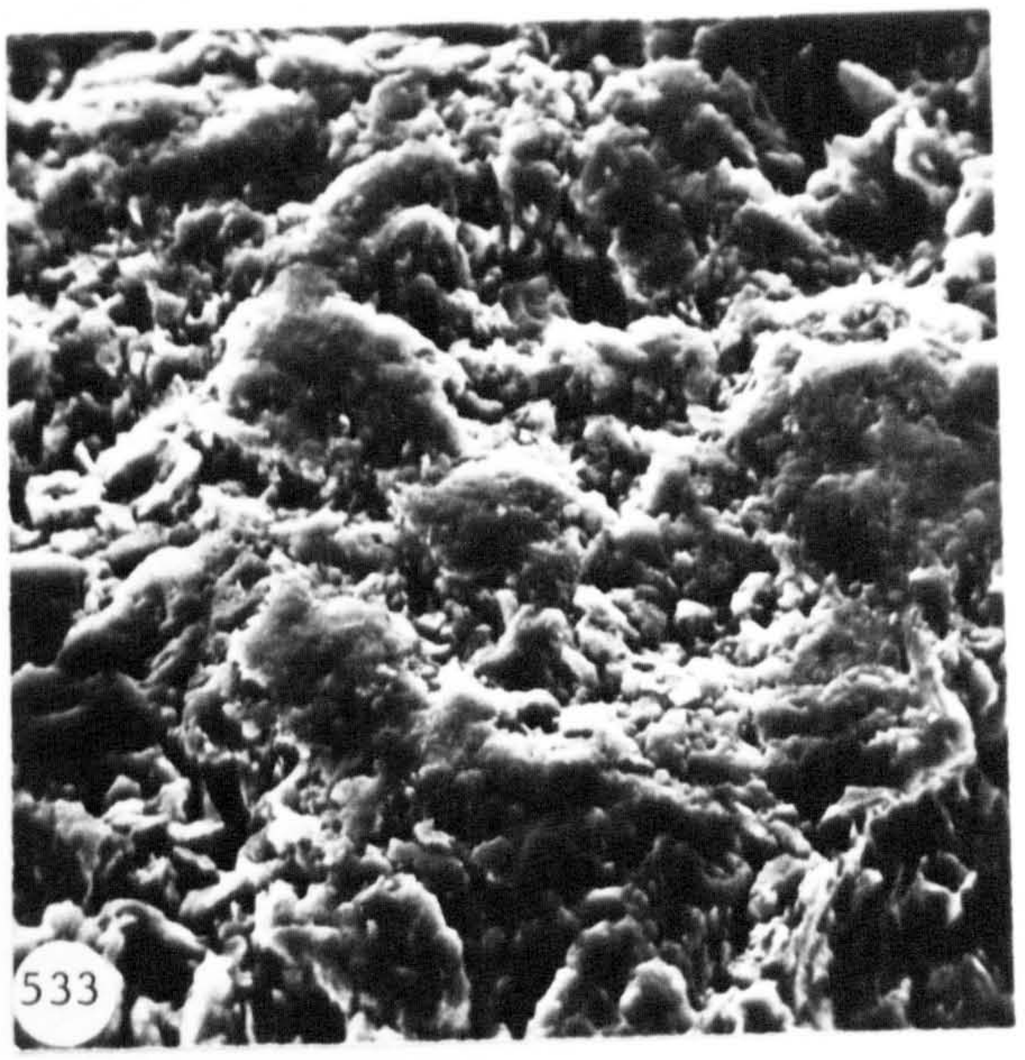


LIMA GRAPHITE 2 µm

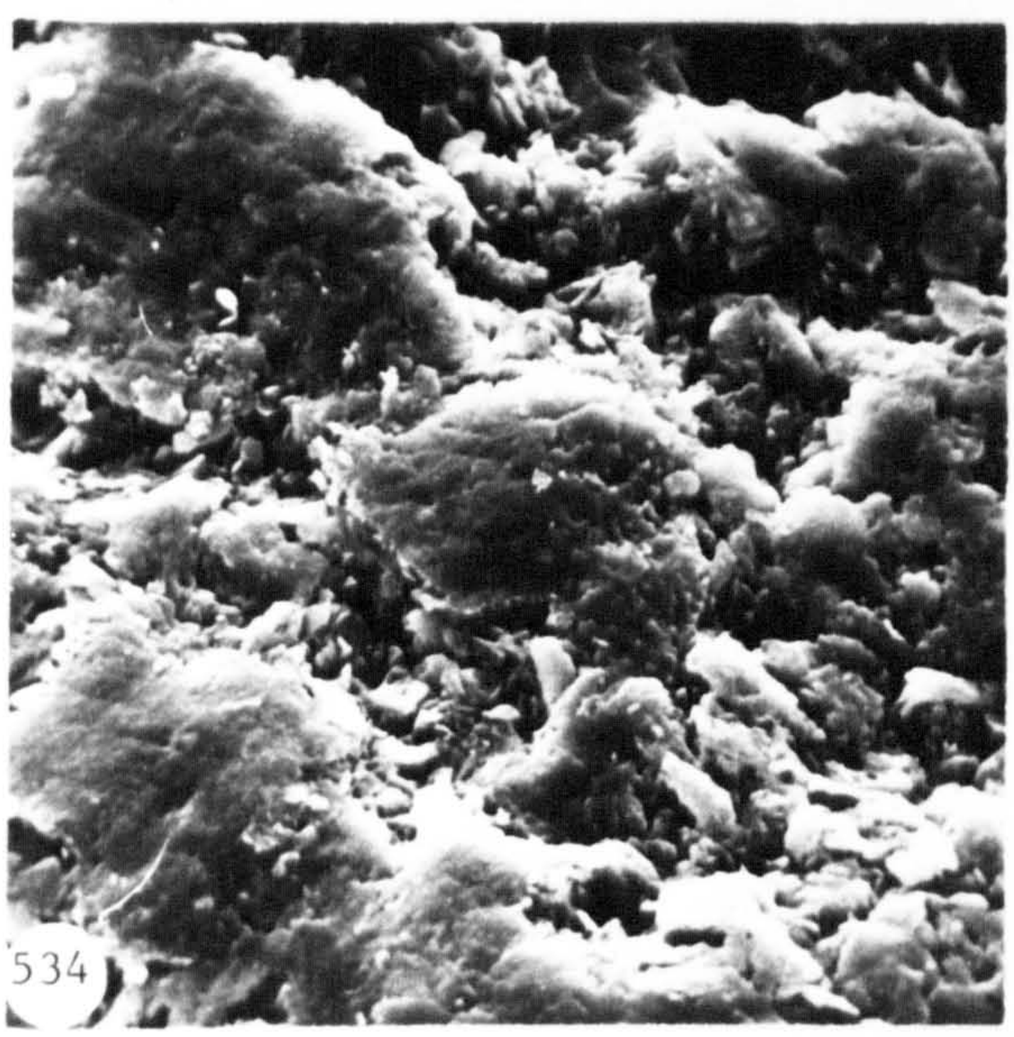
Figures 528 to 531. Scanning electron micrographs (stereoscan) of Lima Graphite radiolytically oxidised to 1.26% weight loss (outside surface).



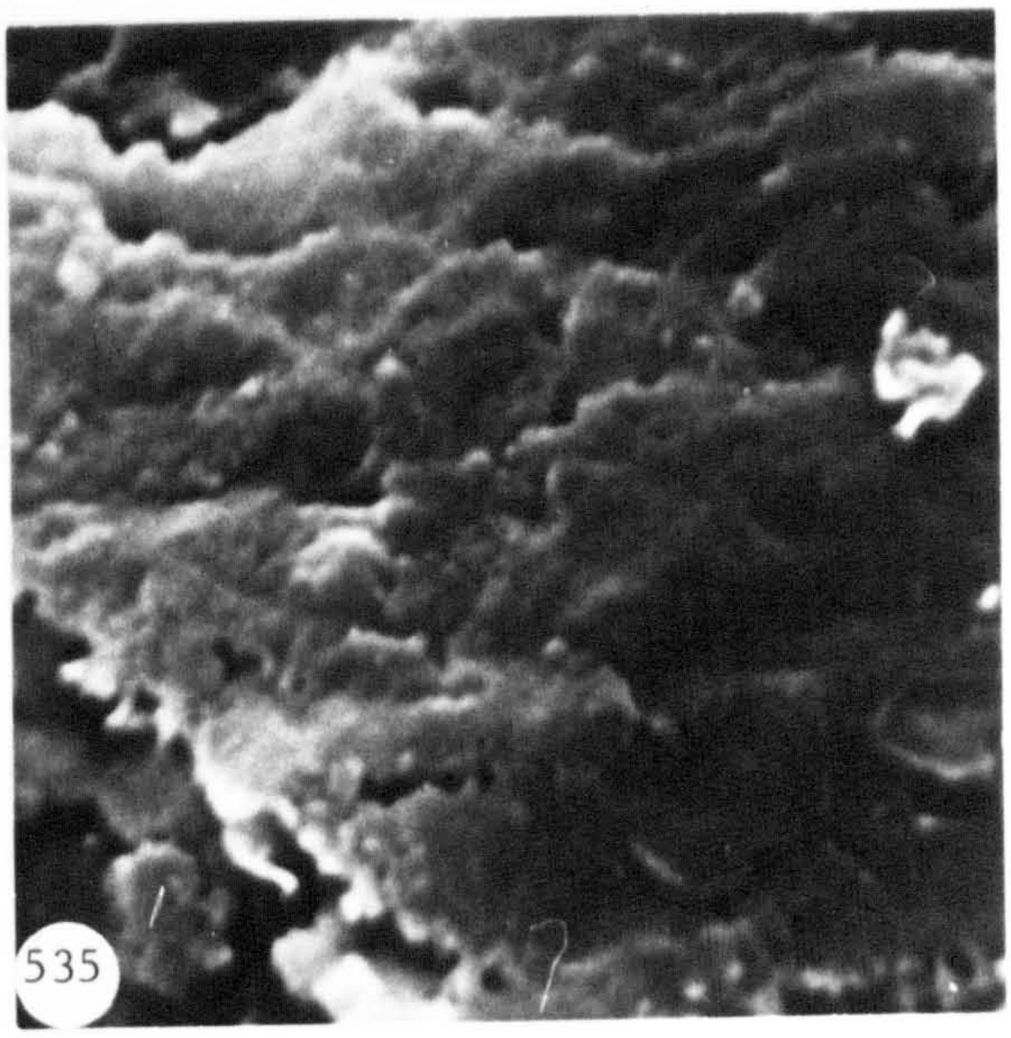
LIMA GRAPHITE 100 µm



LIMA GRAPHITE 20 µm

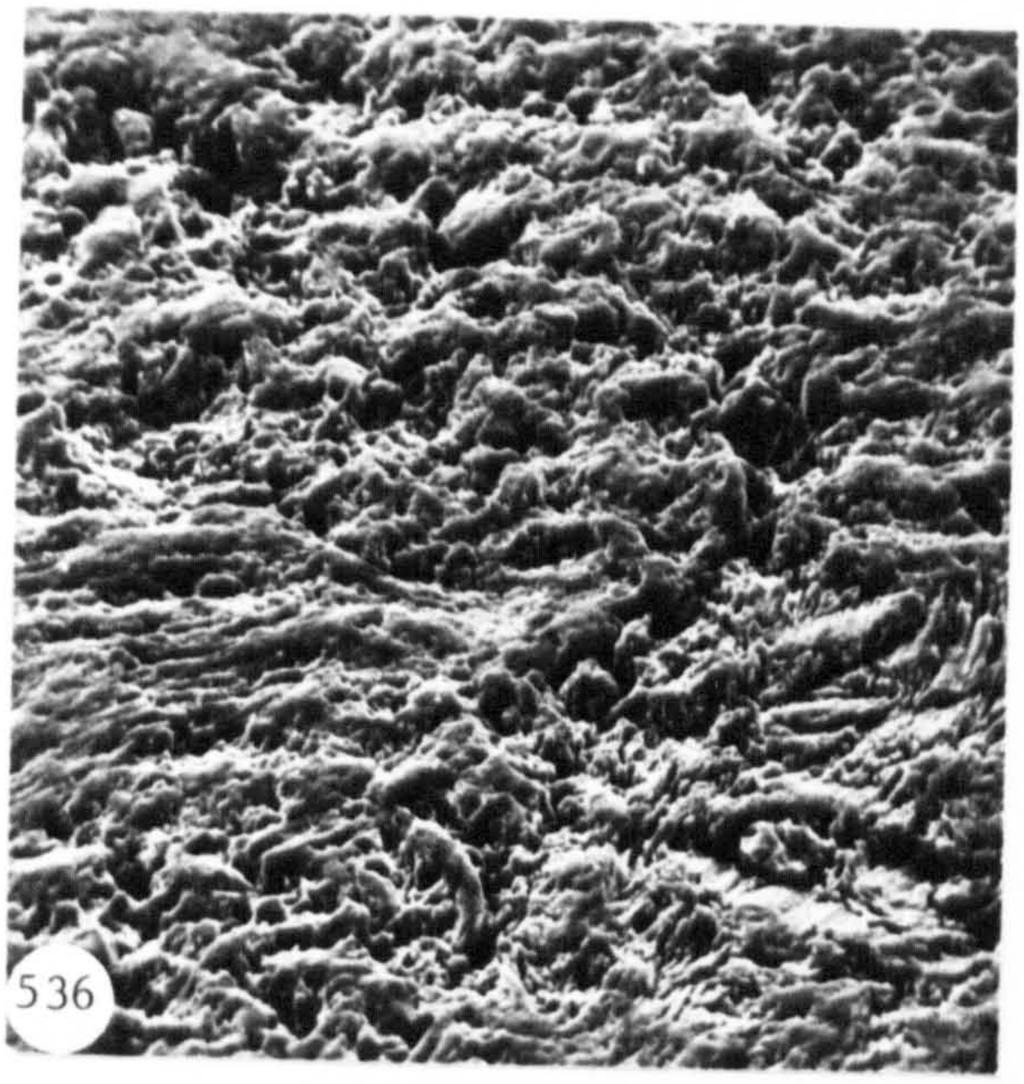


LIMA GRAPHITE 10 µm

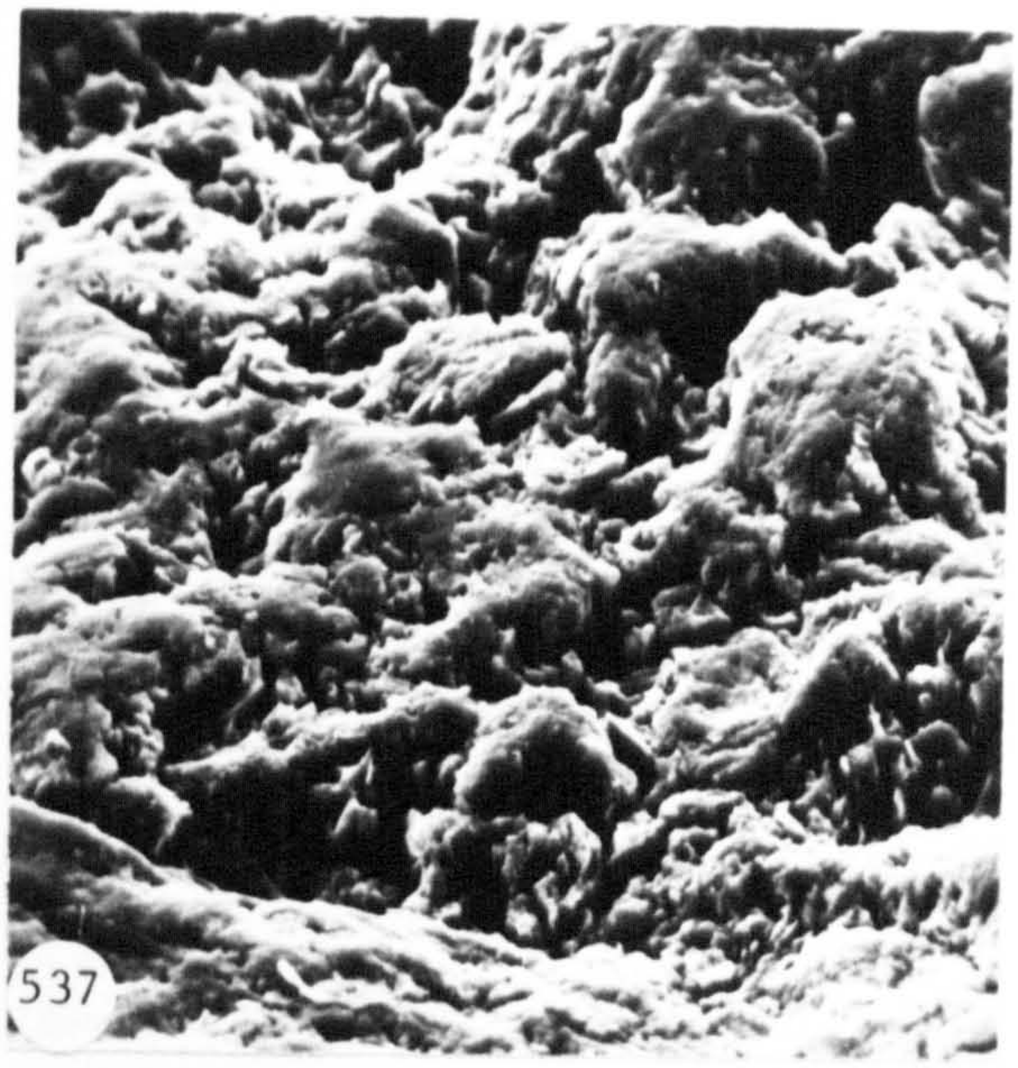


LIMA GRAPHITE 2 µm

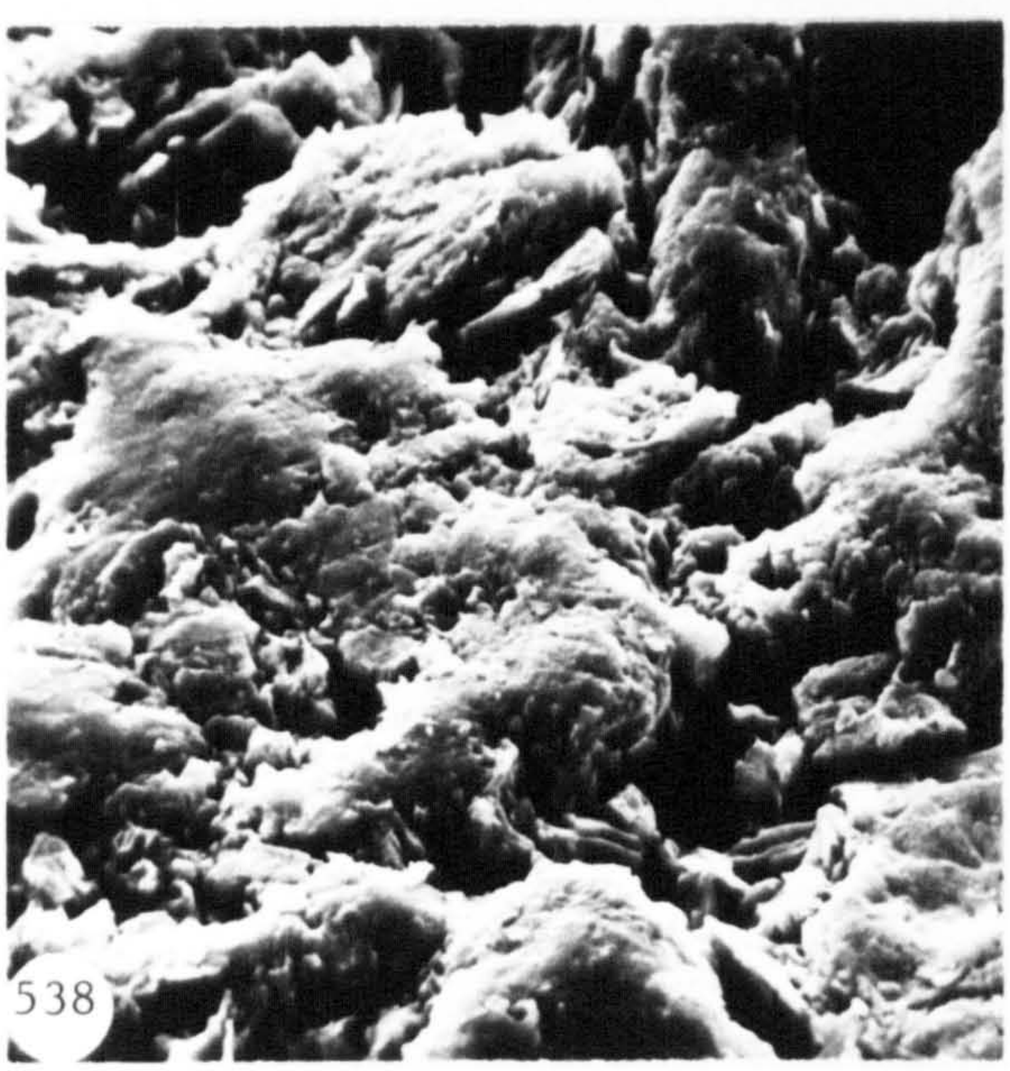
Figures 532 to 535. Scanning electron micrographs (stereoscan) of Lima Graphite radiolytically oxidised to 1.26% weight loss (outside surface).



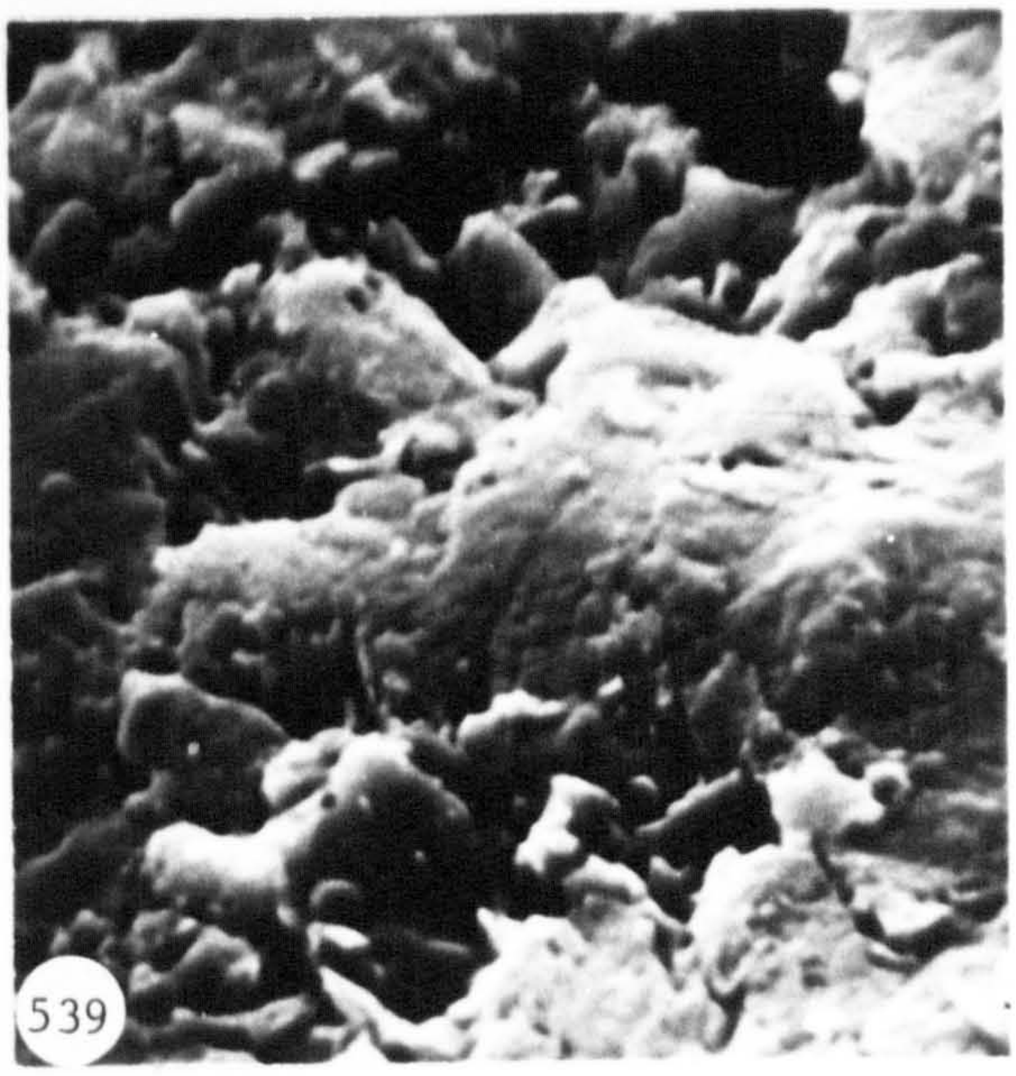
LIMA GRAPHITE 100 µm



LIMA GRAPHITE 20 µm

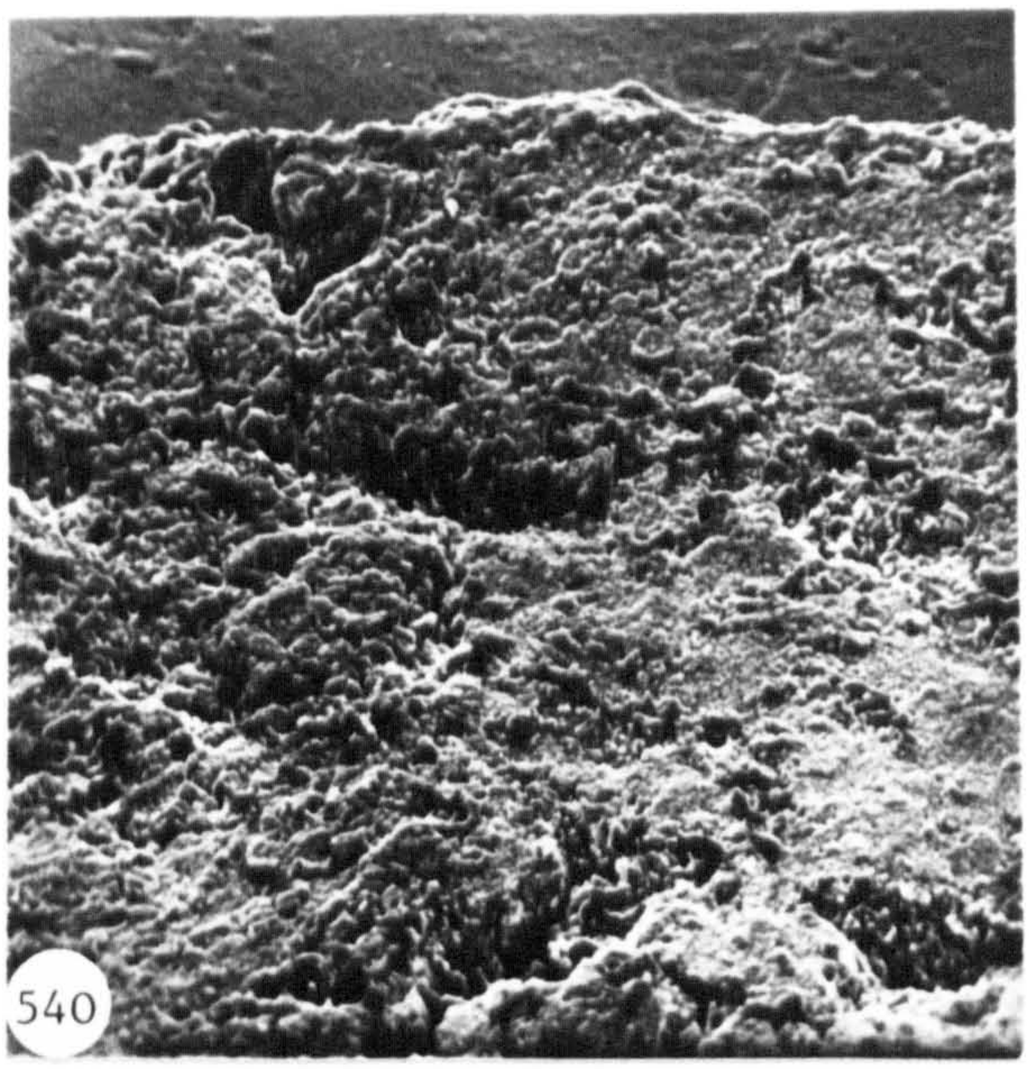


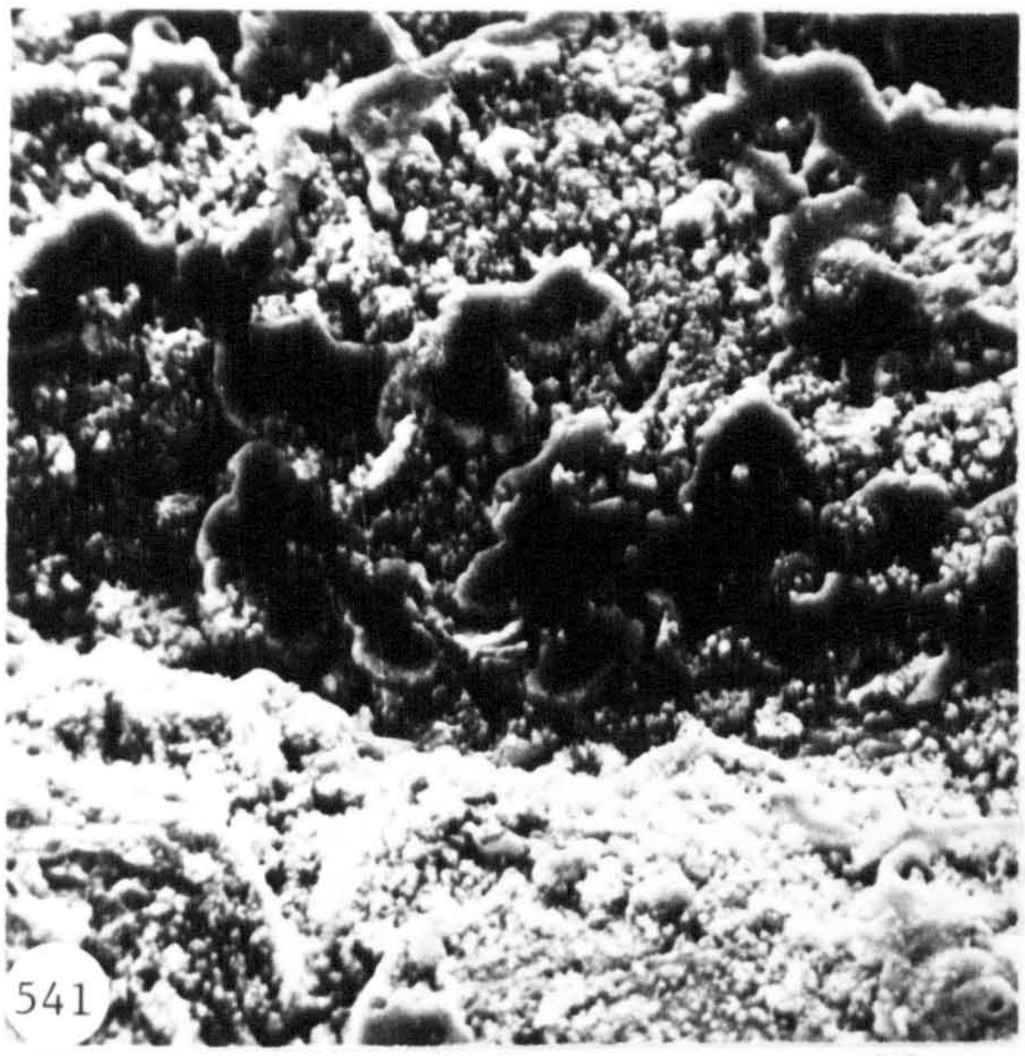
LIMA GRAPHITE 10 µm

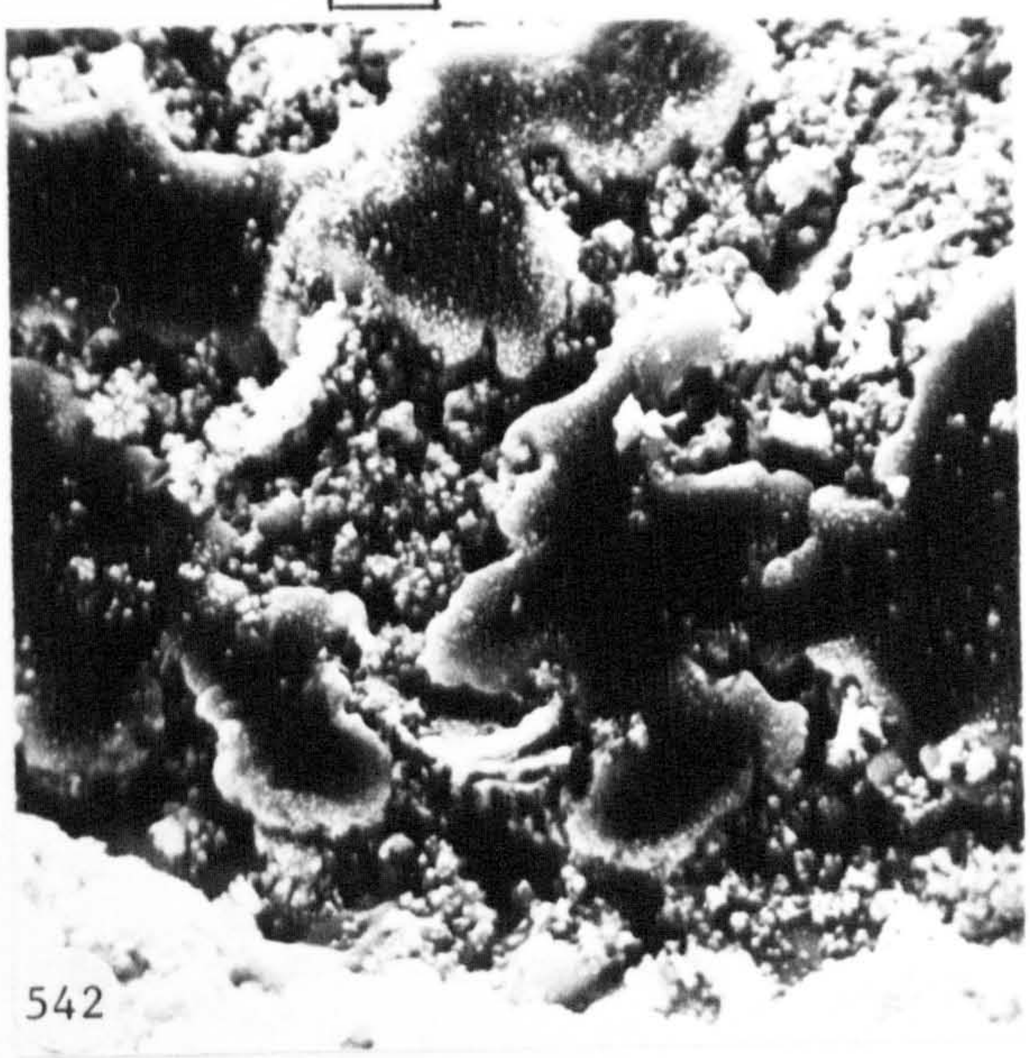


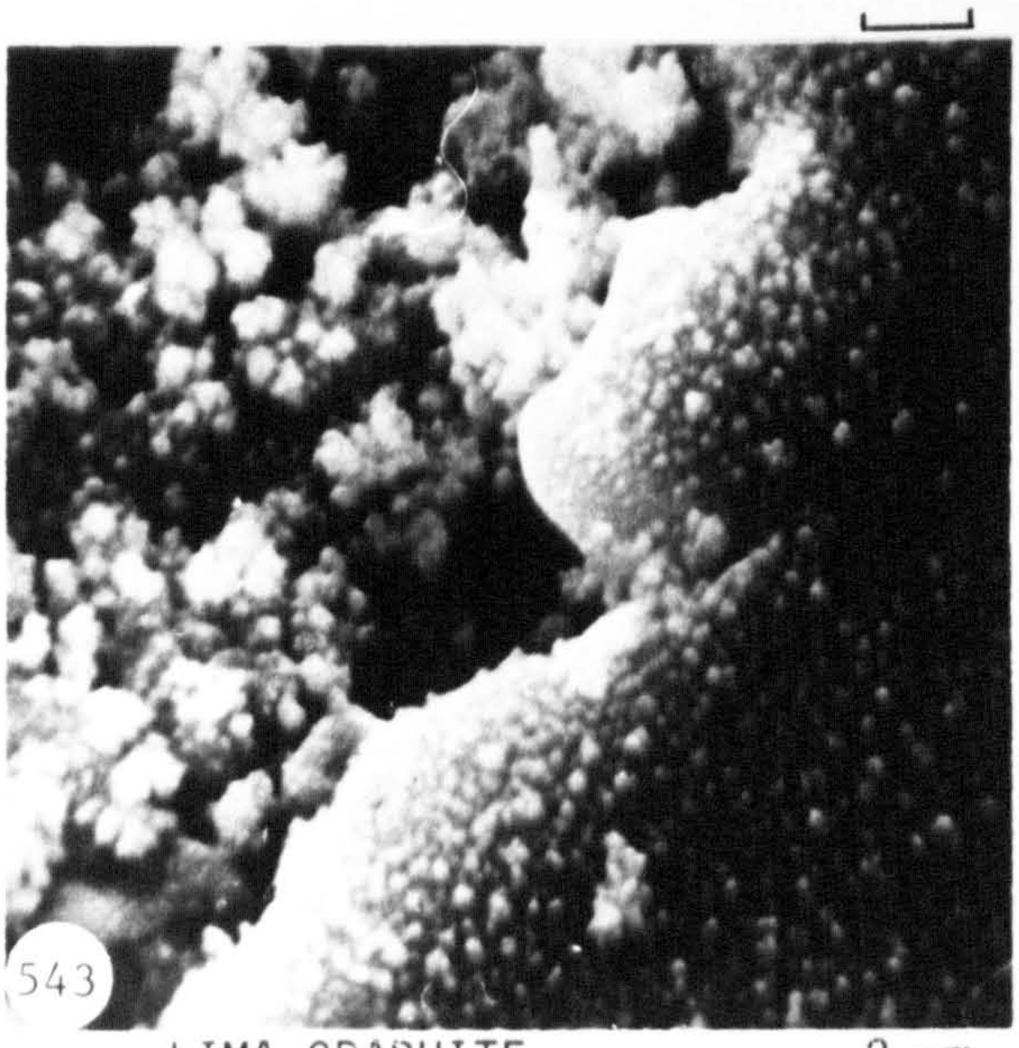
LIMA GRAPHITE 2 µm

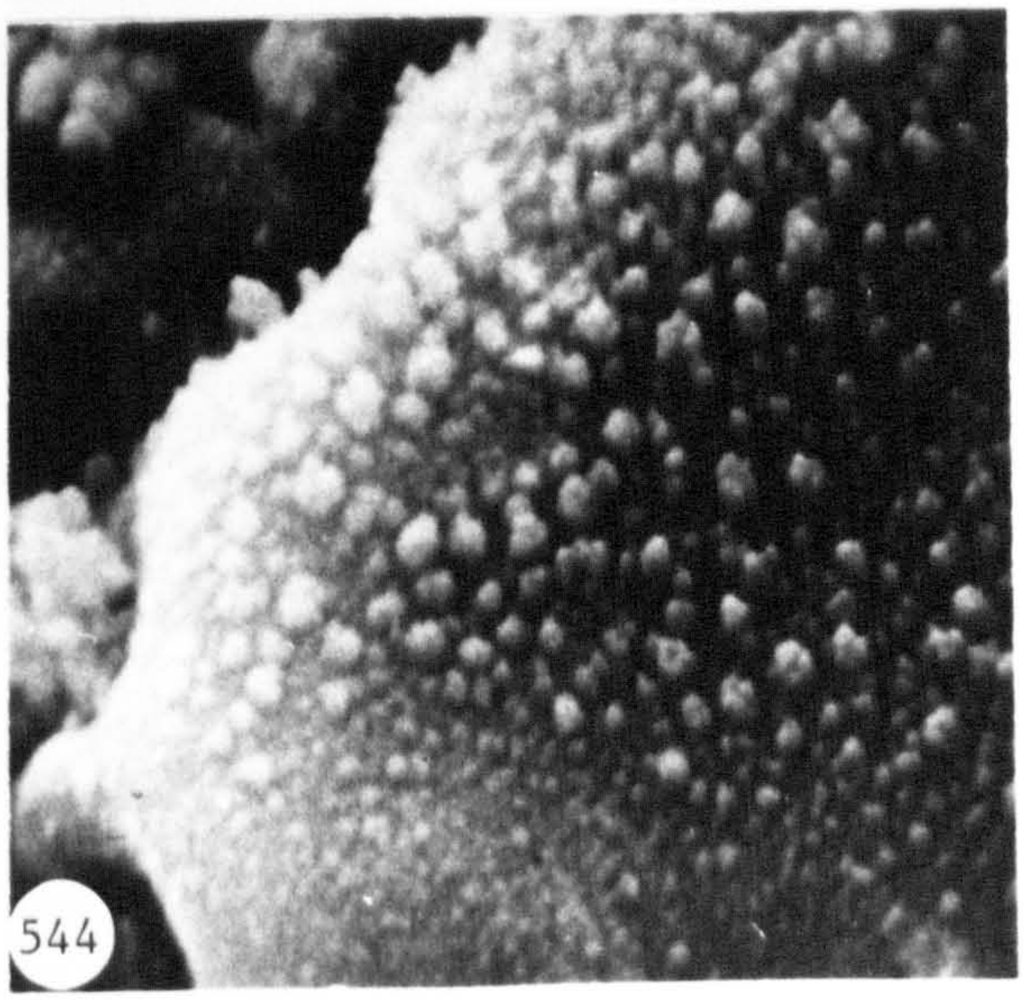
Figures 536 to 539. Scanning electron micrographs (stereoscan) of Lima Graphite radiolytically oxidised to 9.48% weight loss (outside surface).



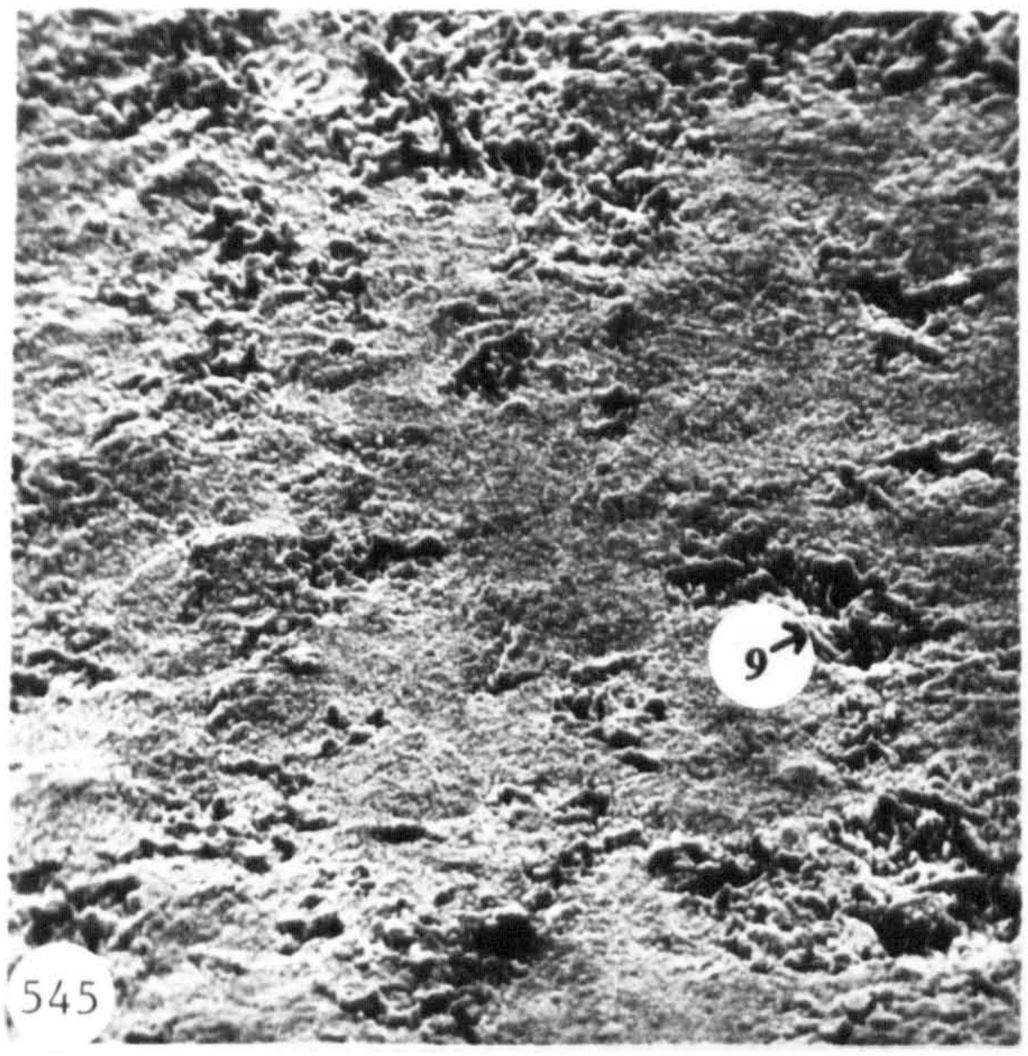




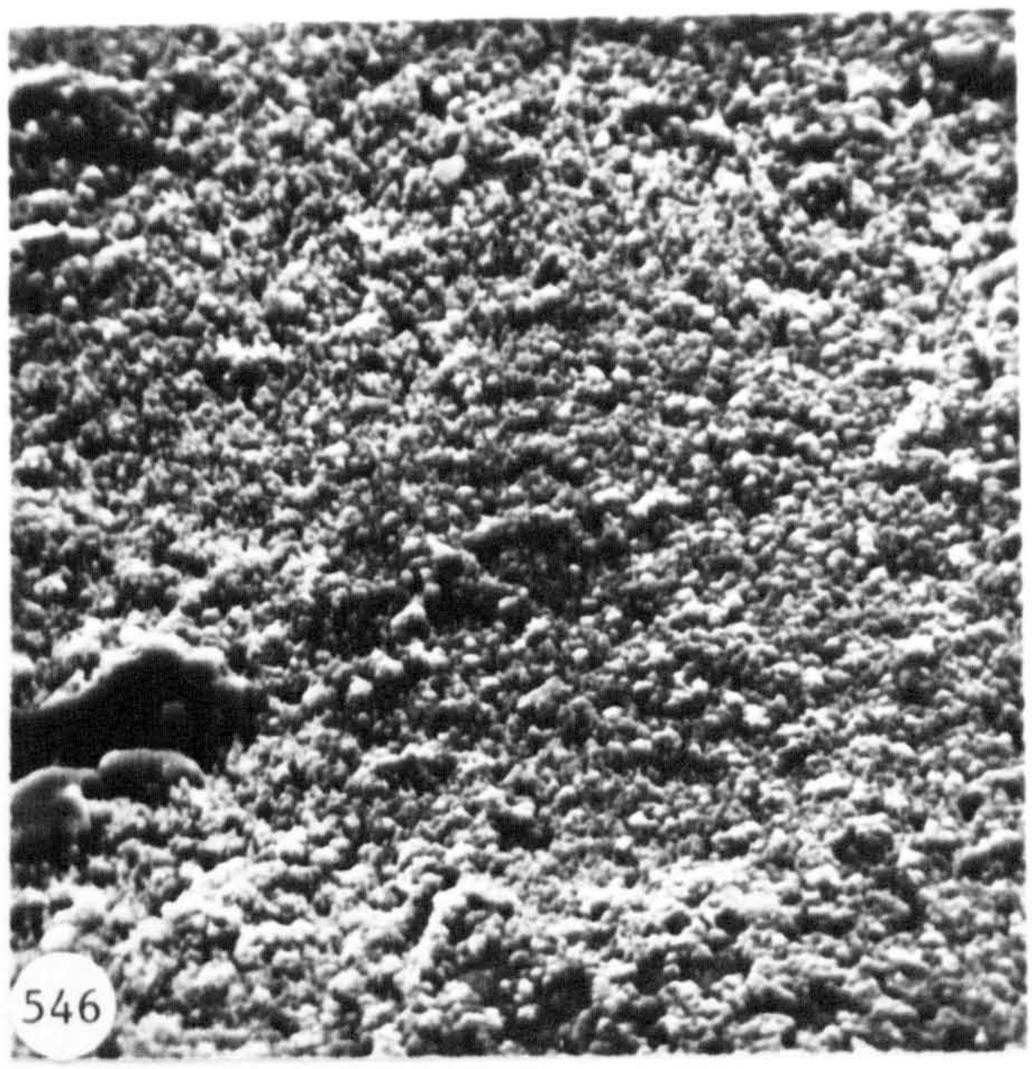




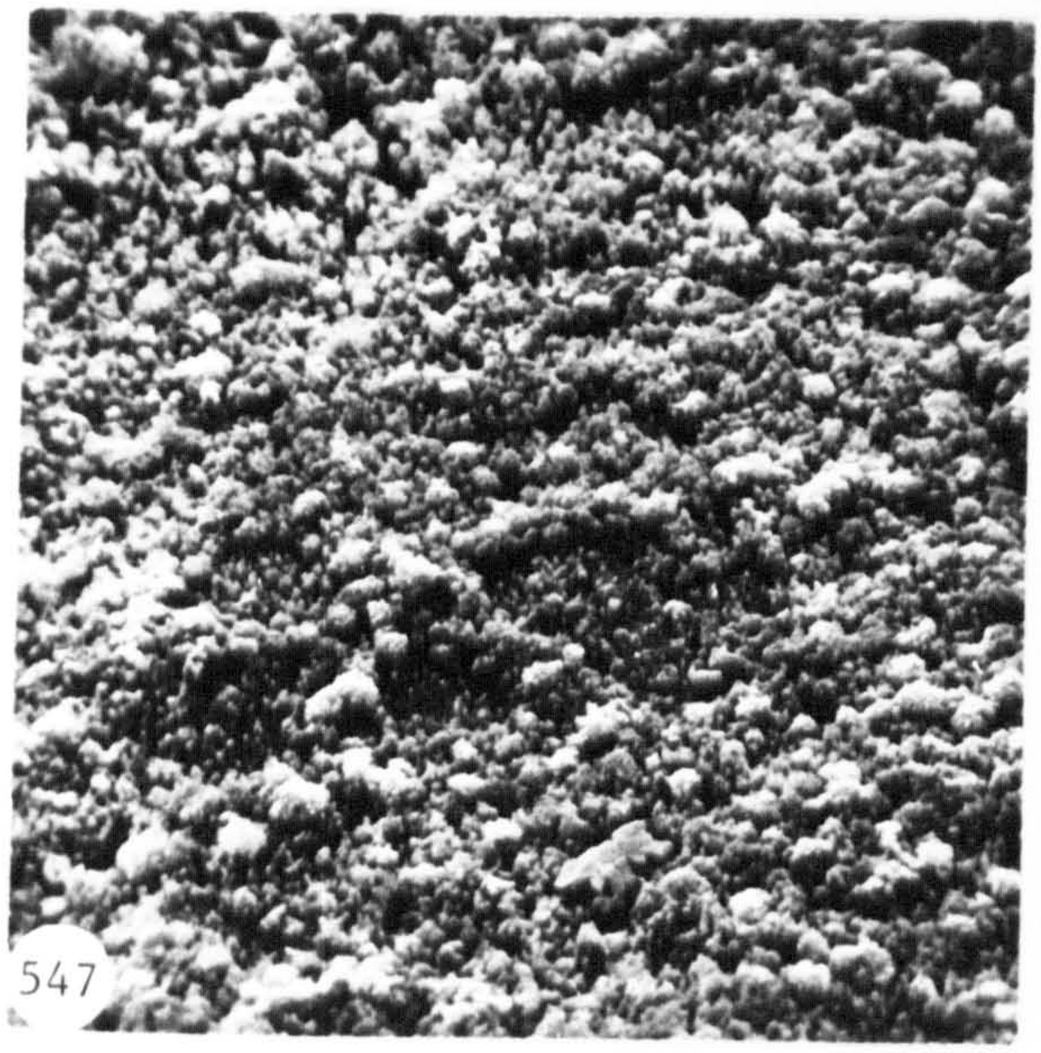
Figures 540 to 544. Scanning electron micrographs (stereoscan) of Lima Graphite radiolytically oxidised to 22.6% weight loss (inside surface).



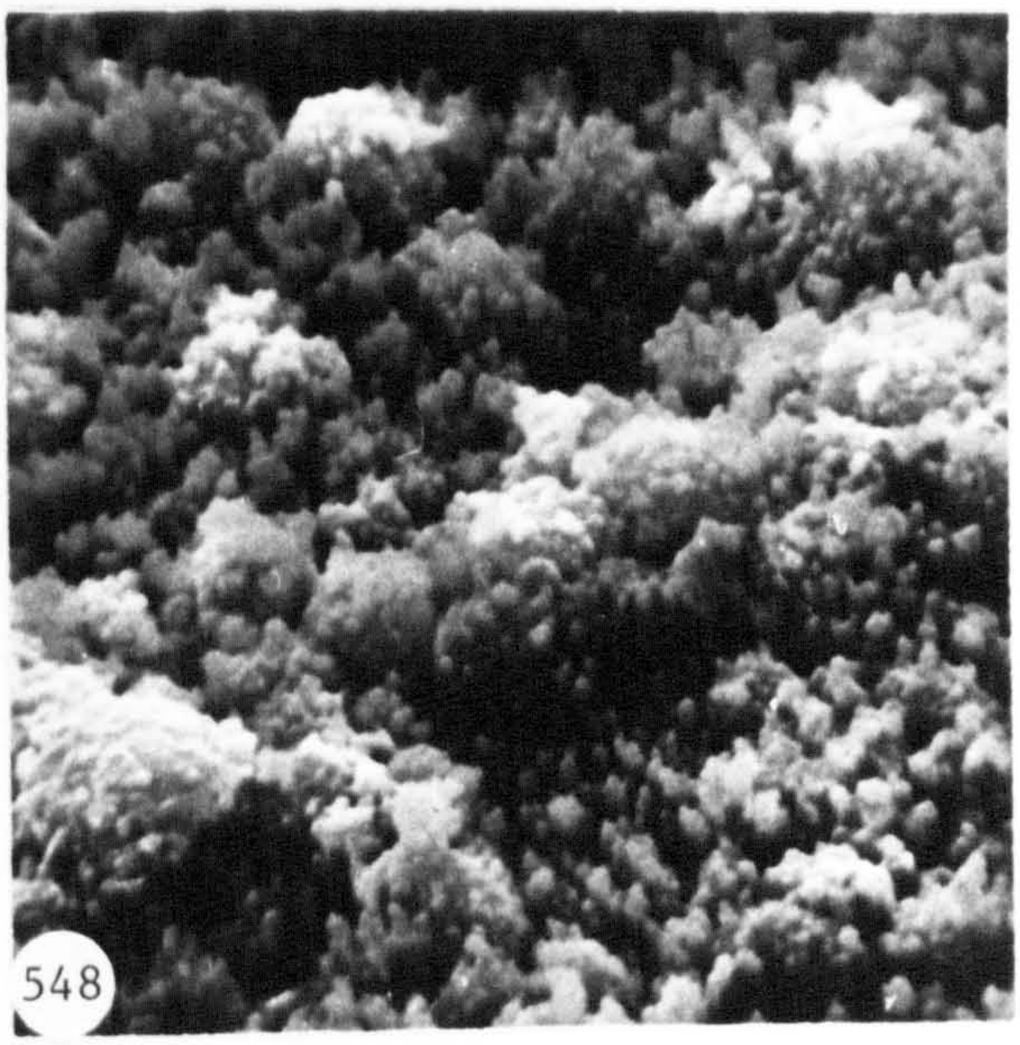
LIMA GRAPHITE 100 µm



LIMA GRAPHITE 20 µm

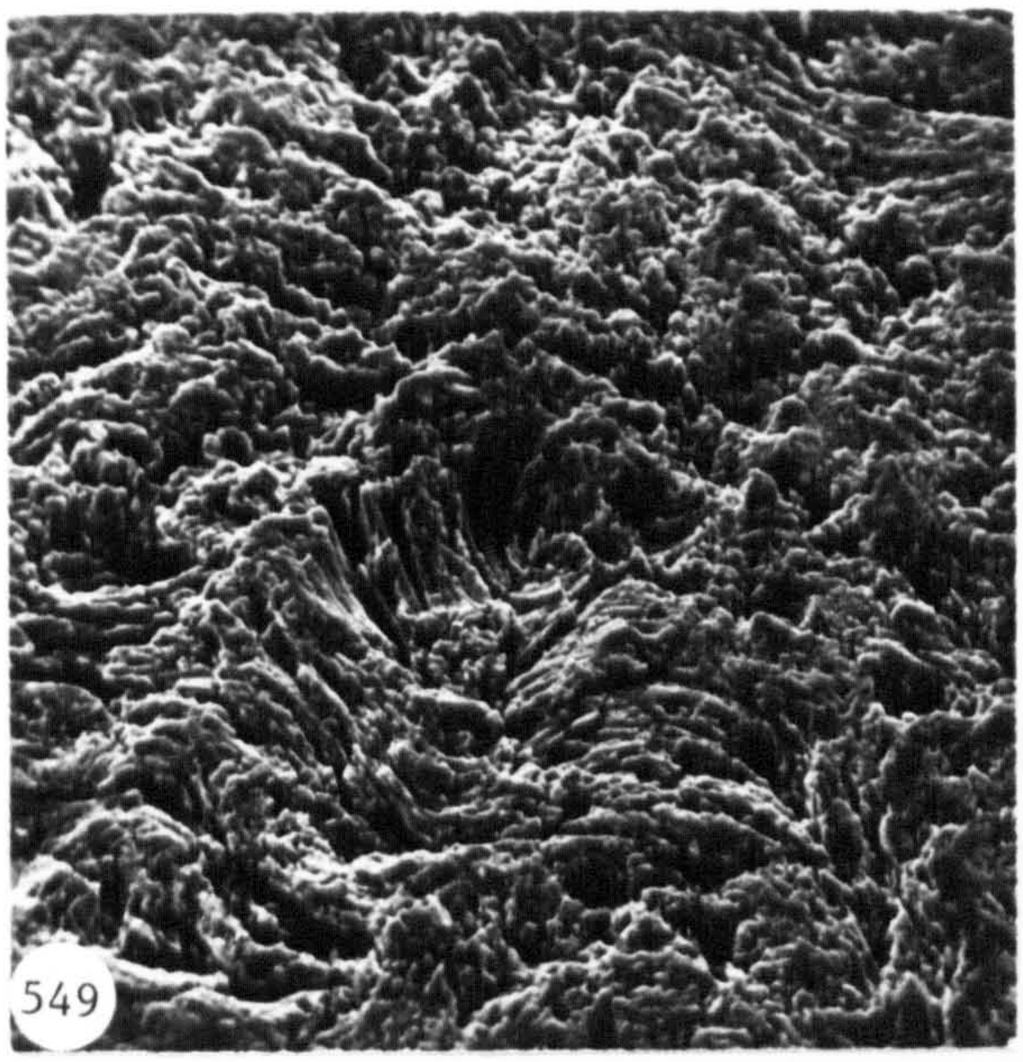


LIMA GRAPHITE 10 µm



LIMA GRAPHITE 2 µm

Figures 545 to 548. Scanning electron micrographs (stereoscan) of Lima Graphite radiolytically oxidised to 22.6% weight loss (inside surface).



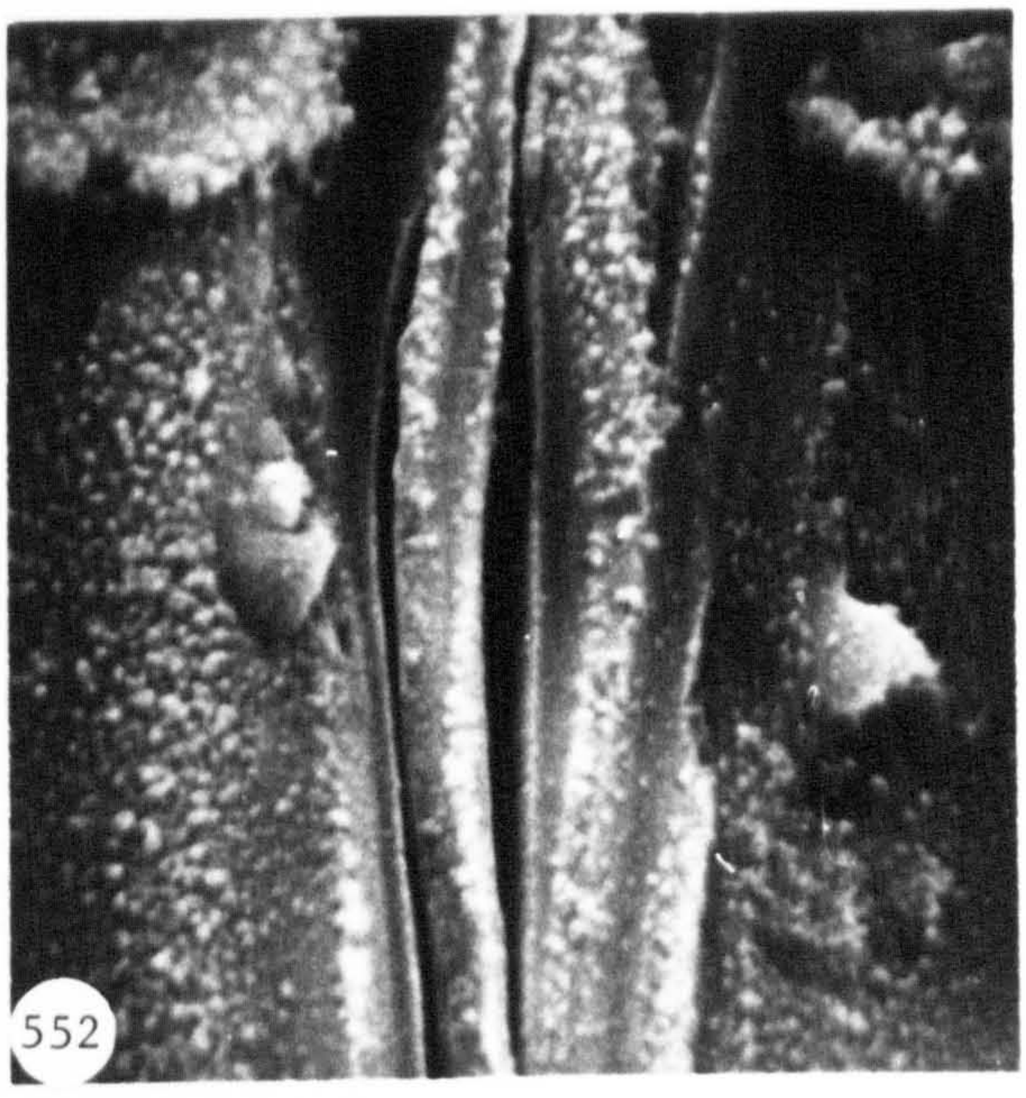
LIMA GRAPHITE 100 µm



LIMA GRAPHITE 20 µm

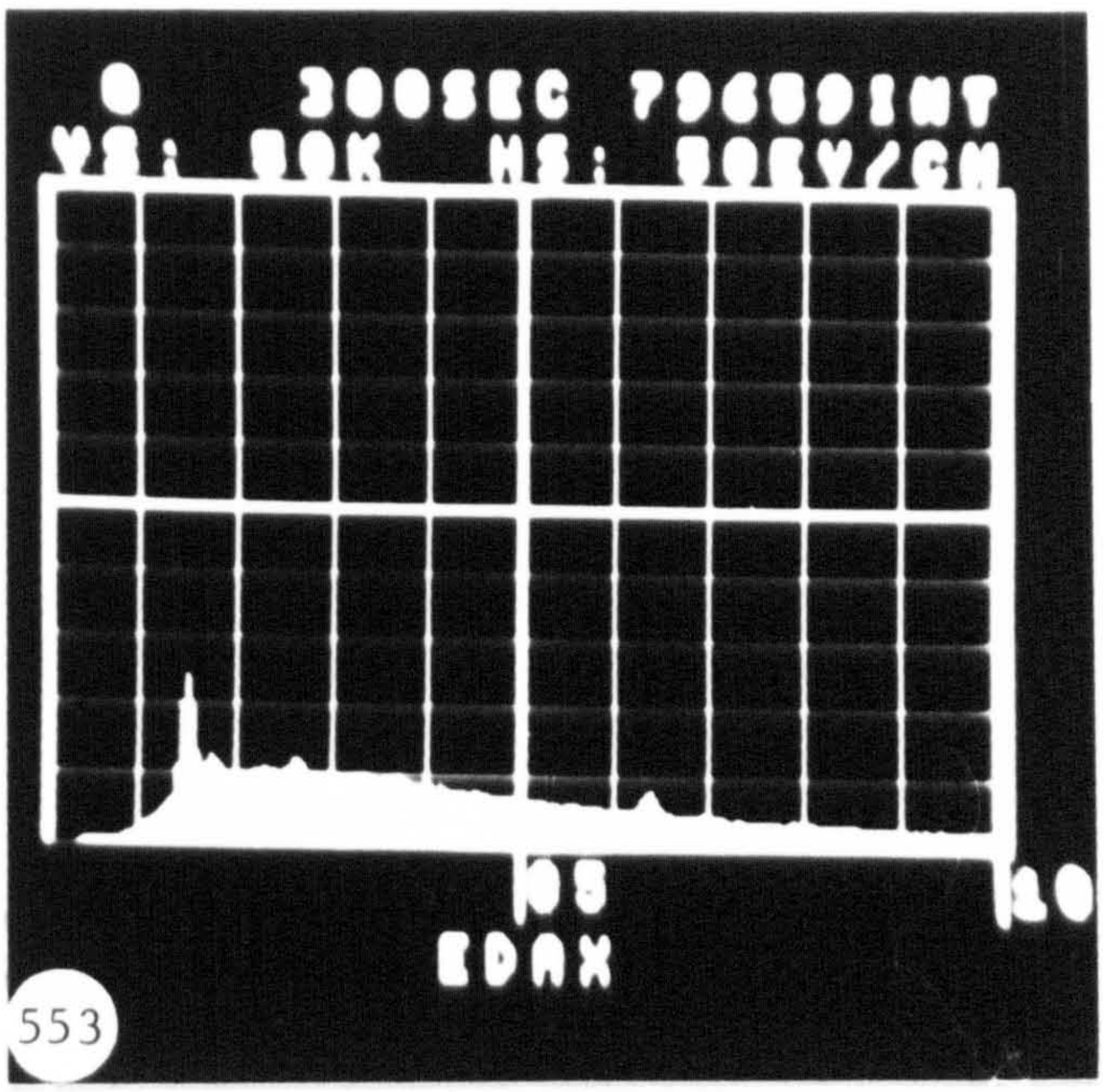


LIMA GRAPHITE 10 µm

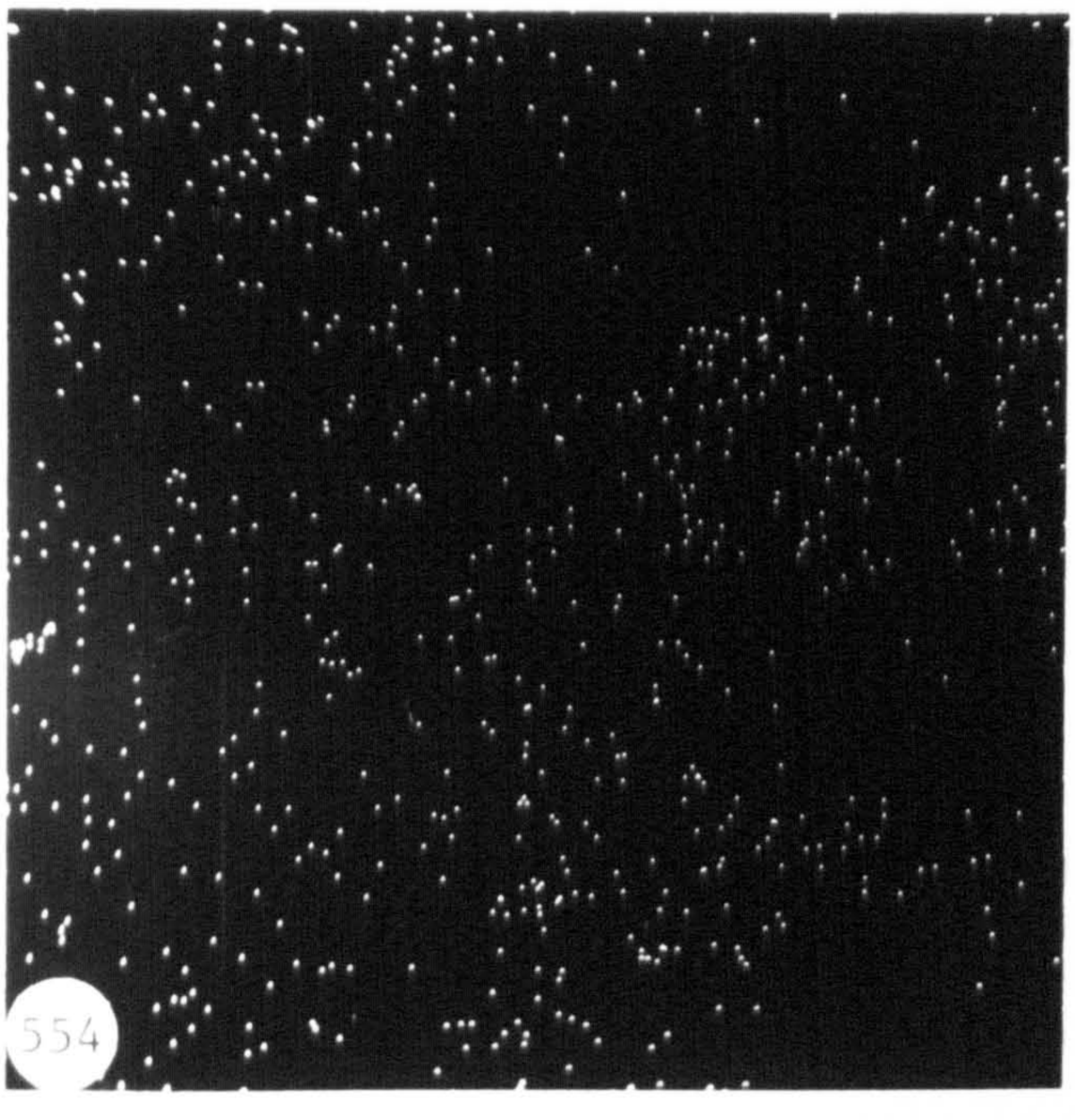


LIMA GRAPHITE 2 µm

Figures 549 to 552. Scanning electron micrographs (stereoscan) of Lima Graphite radiolytically oxidised to 22.6% weight loss (outside surface).



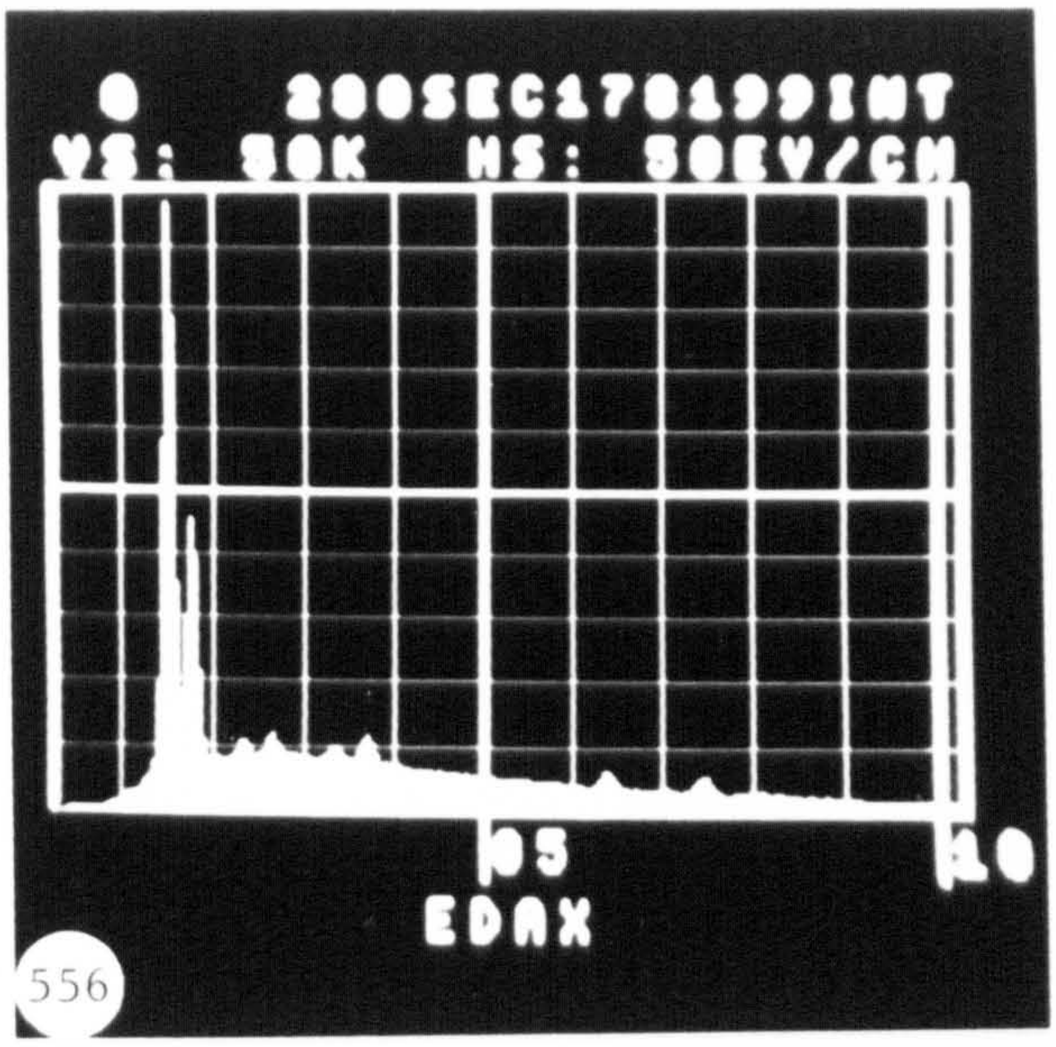
X-ray Spectrum



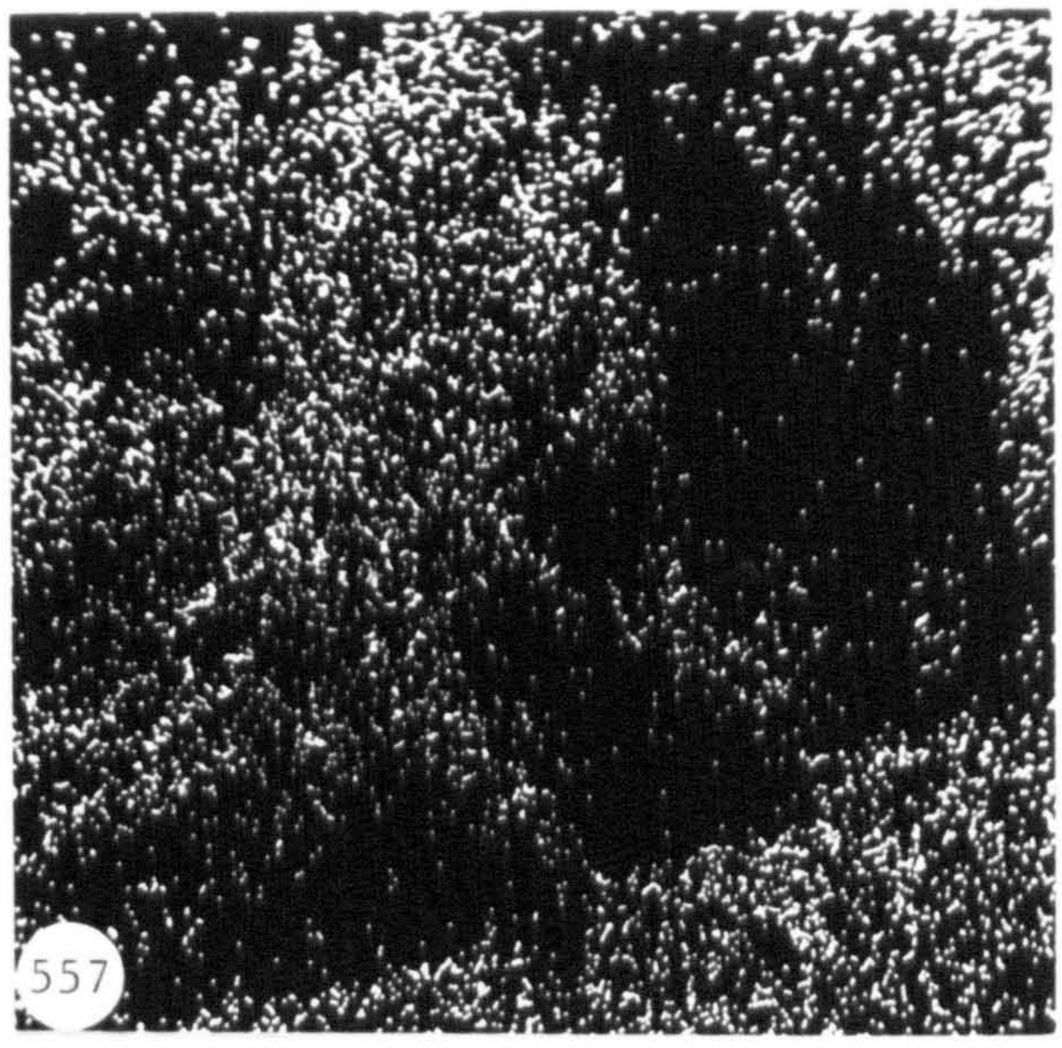


Silicon X-ray analysis Area Analysed 20 µm

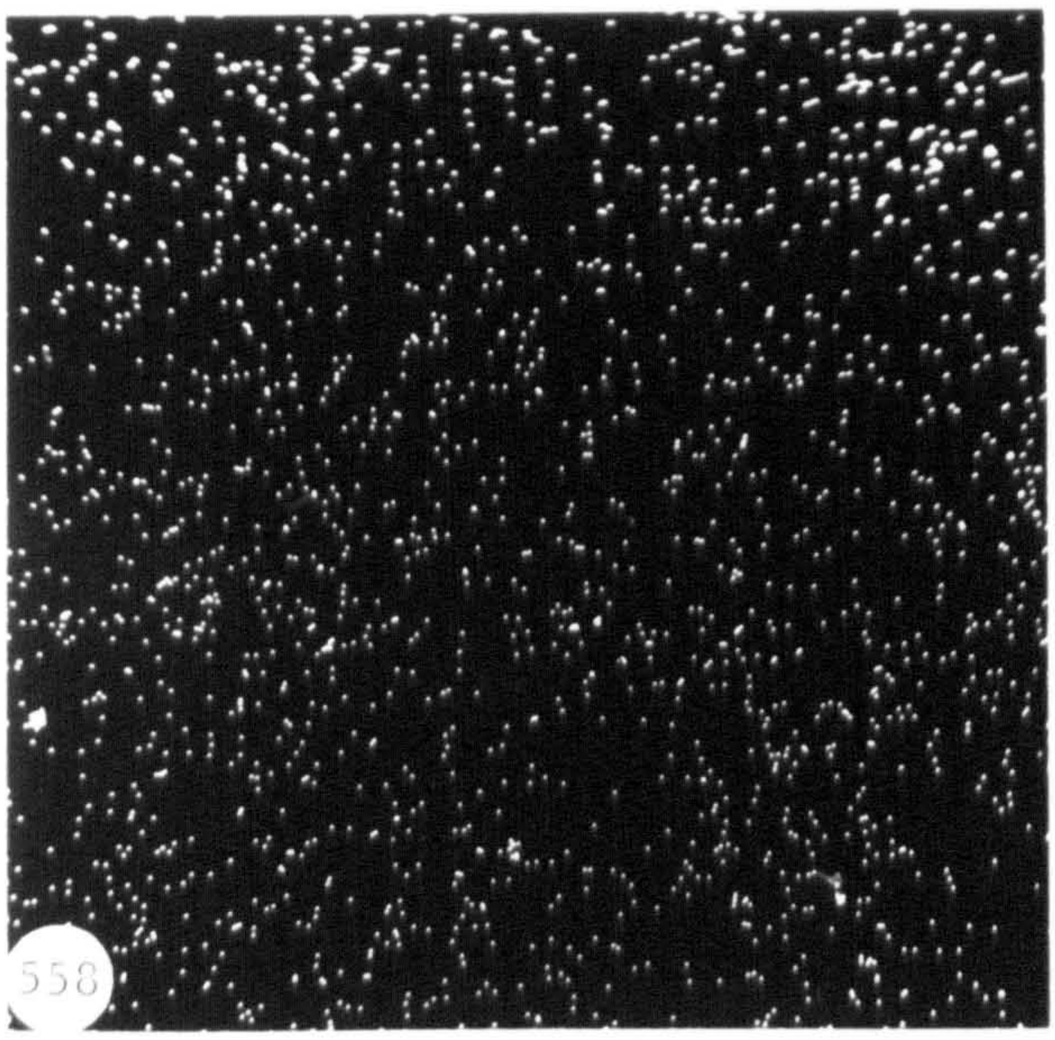
Figures 553 to 555. X-ray analysis of virgin Lima Graphite (control).



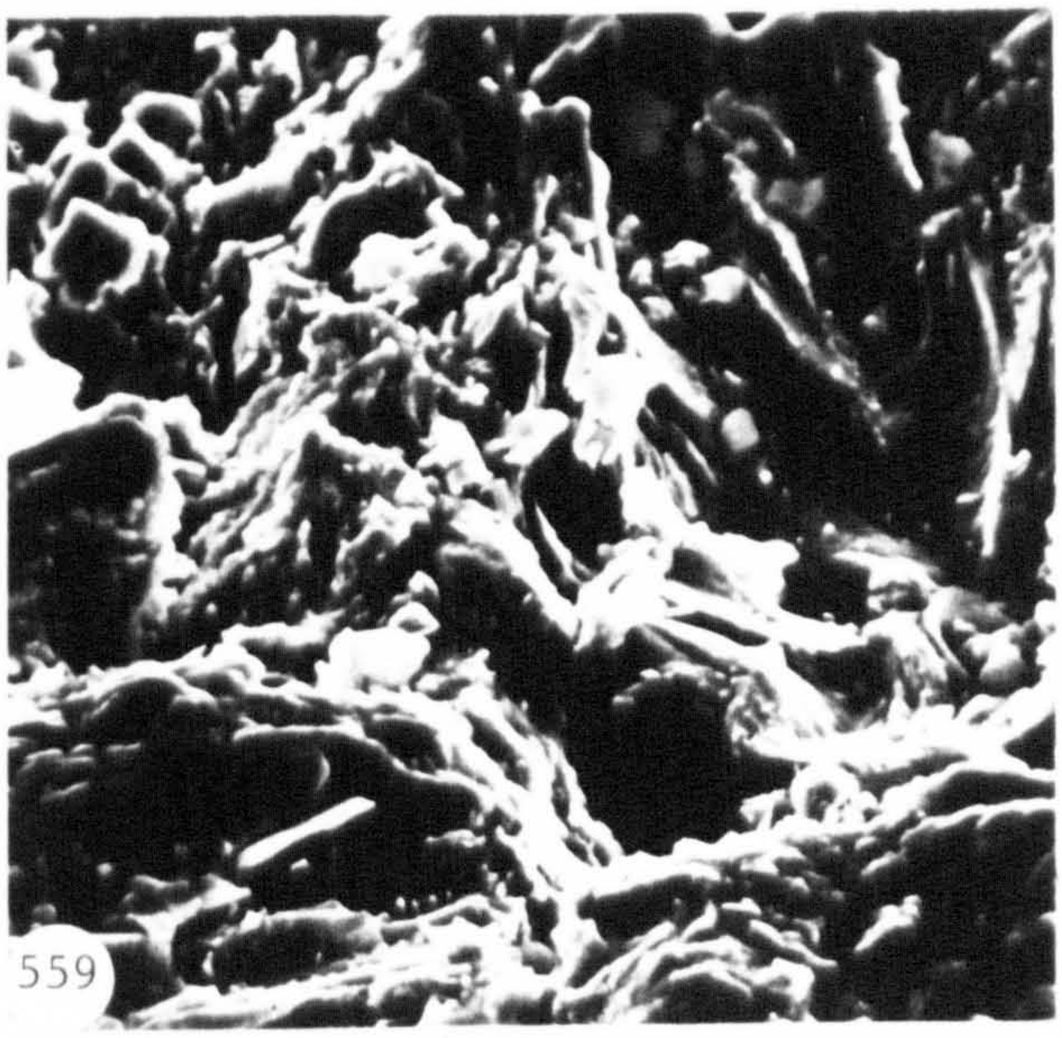
X-ray Spectrum



Silicon X-ray analysis

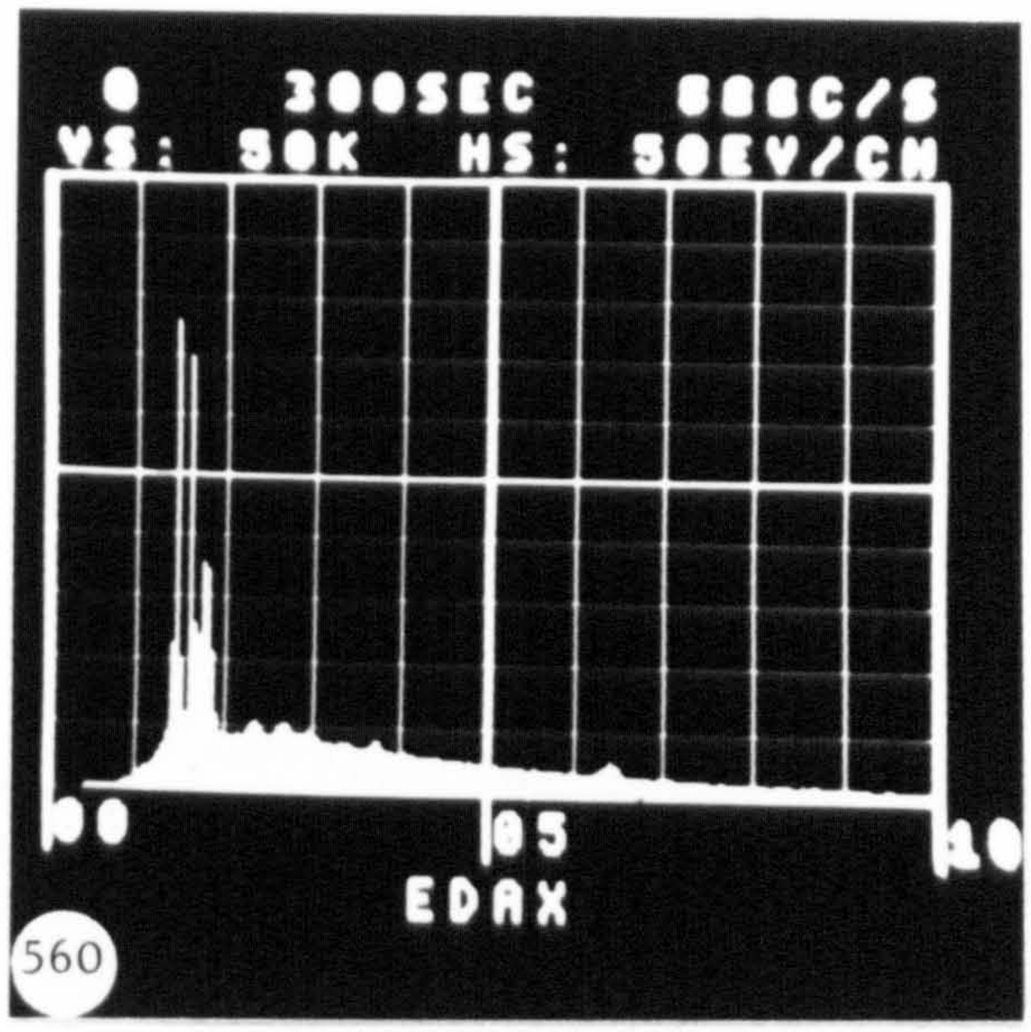


Nickel X-ray analysis

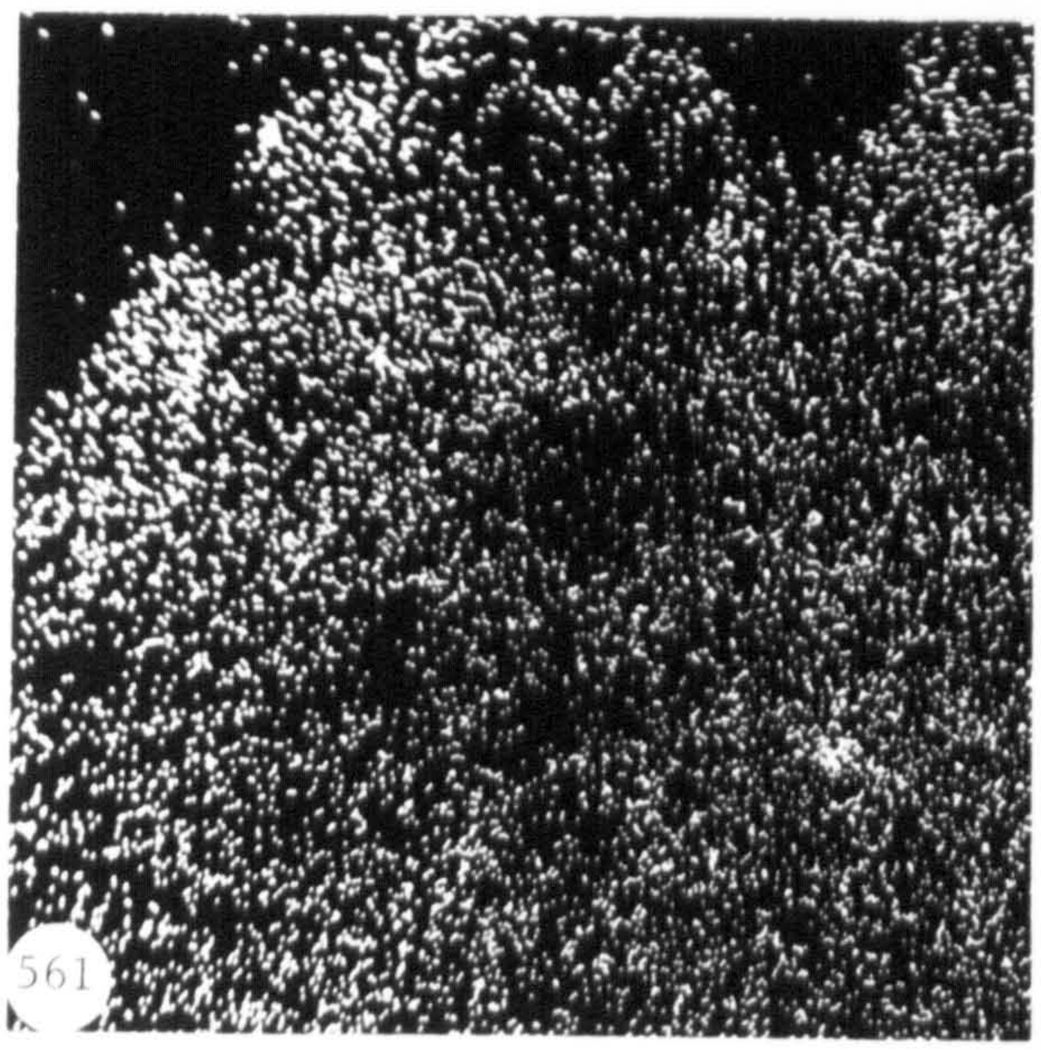


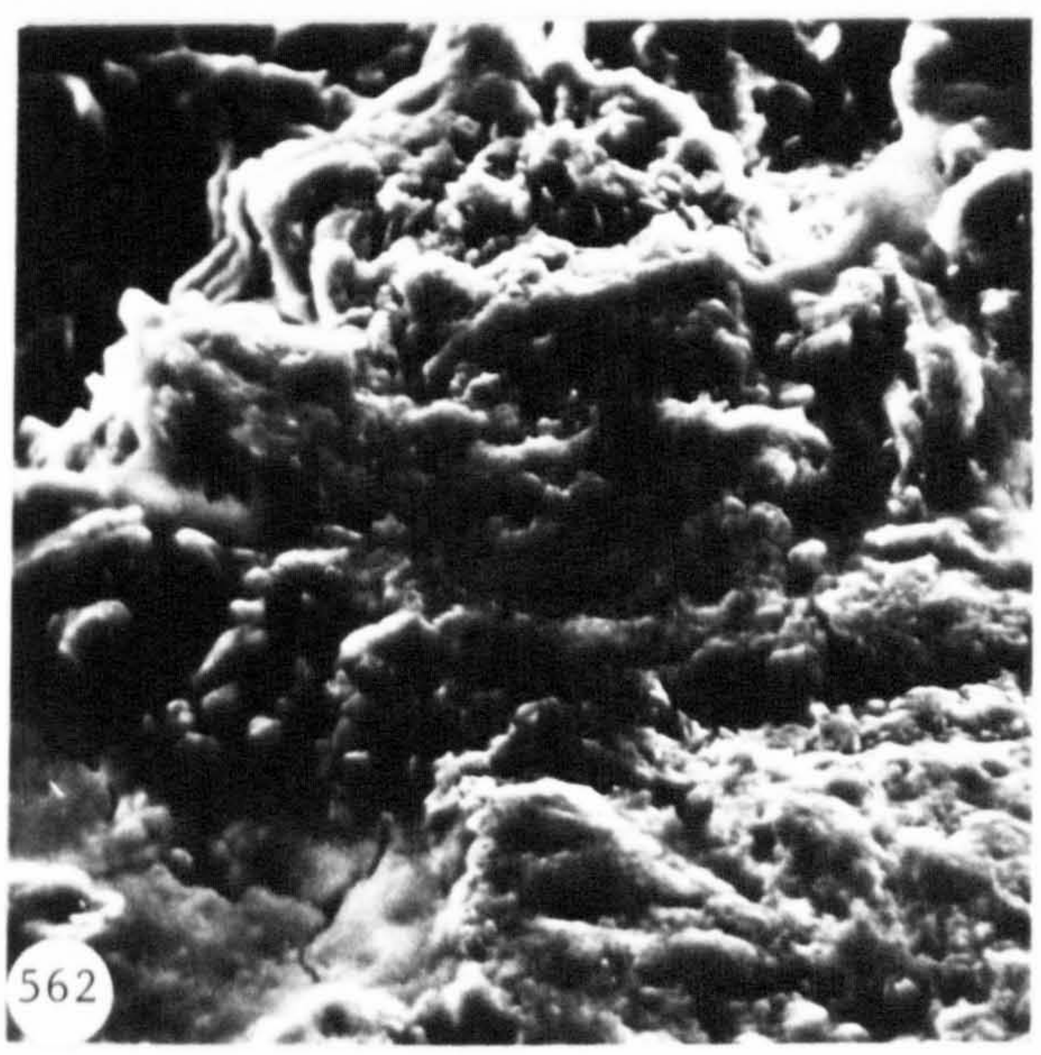
Area analysed 20 µm

Figures 556 to 559. X-ray analysis of Lima Graphite radiolytically oxidised to 1.26% weight loss (inside surface).



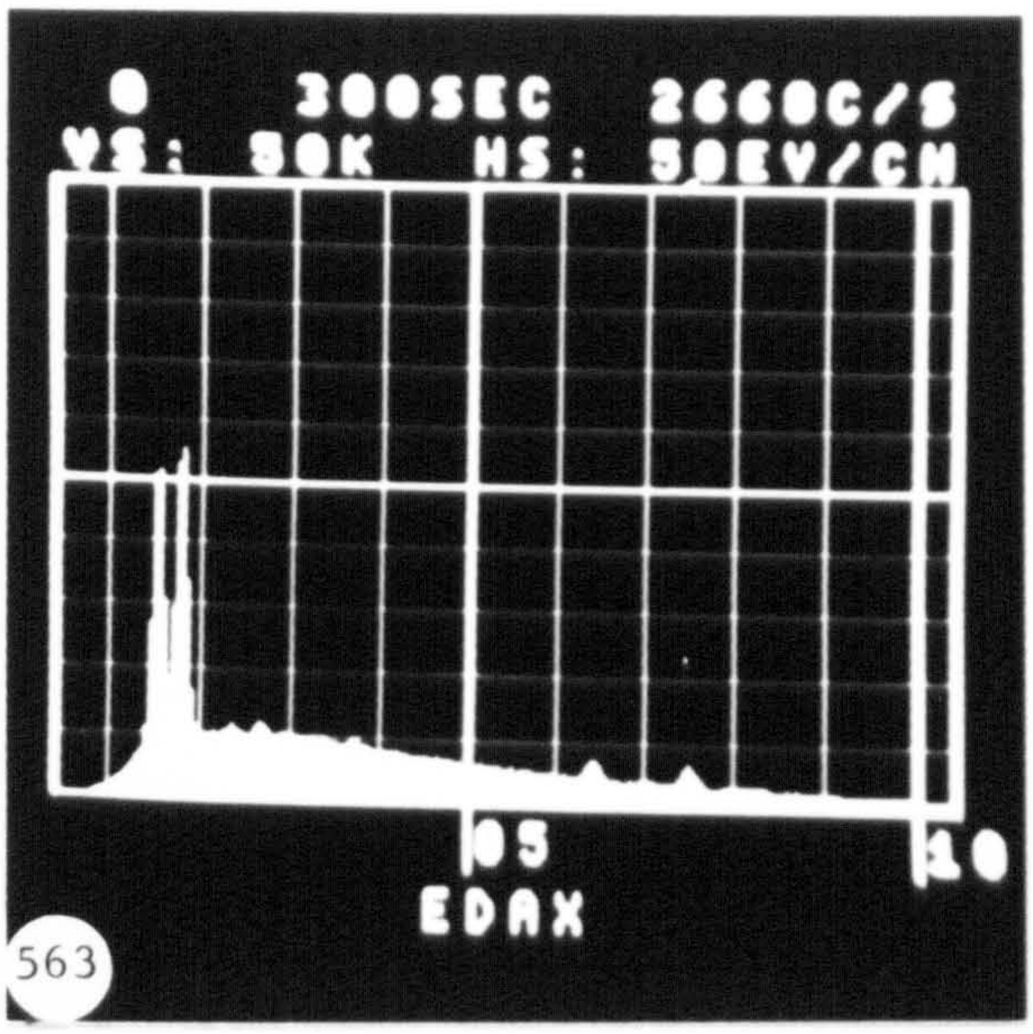
X-ray Spectrum



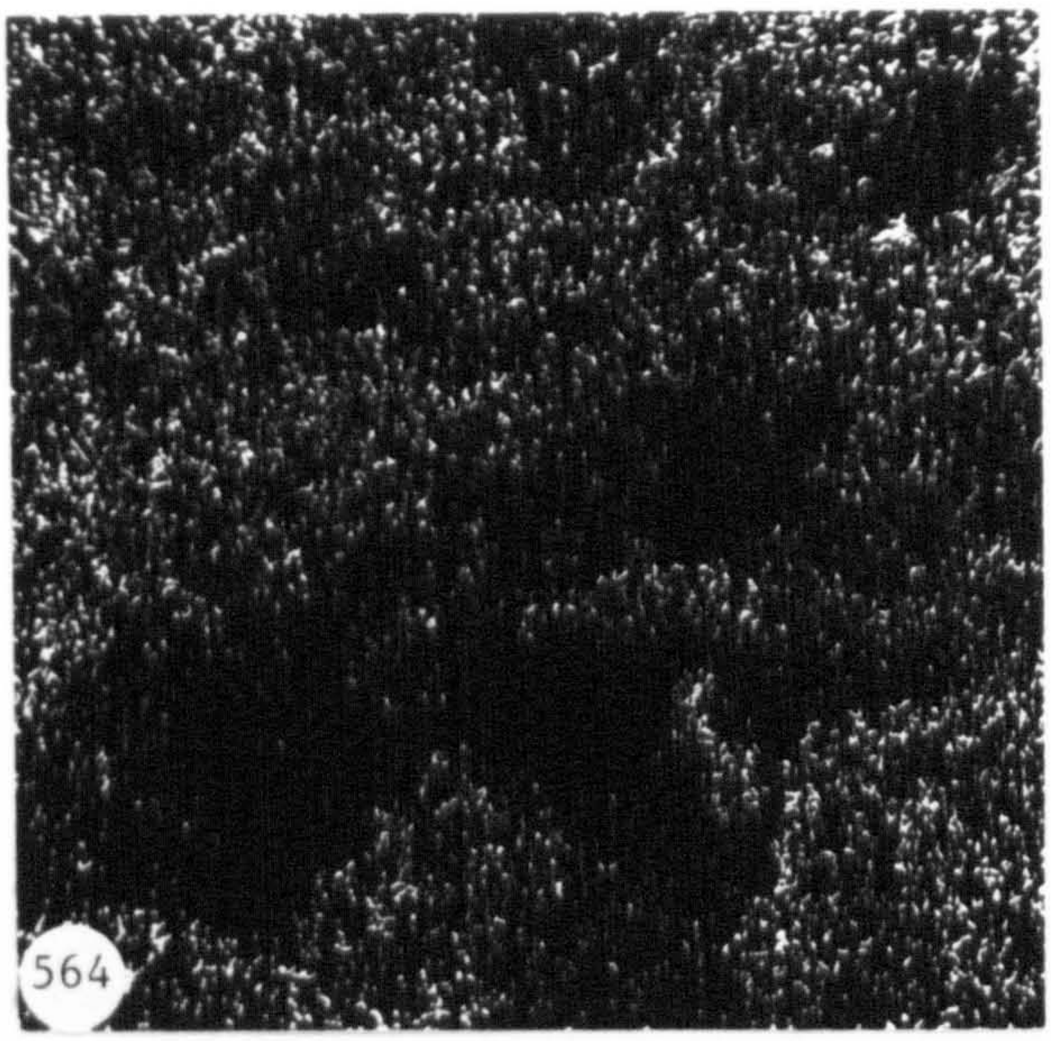


Silicon X-ray analysis Area analysed 20 µm

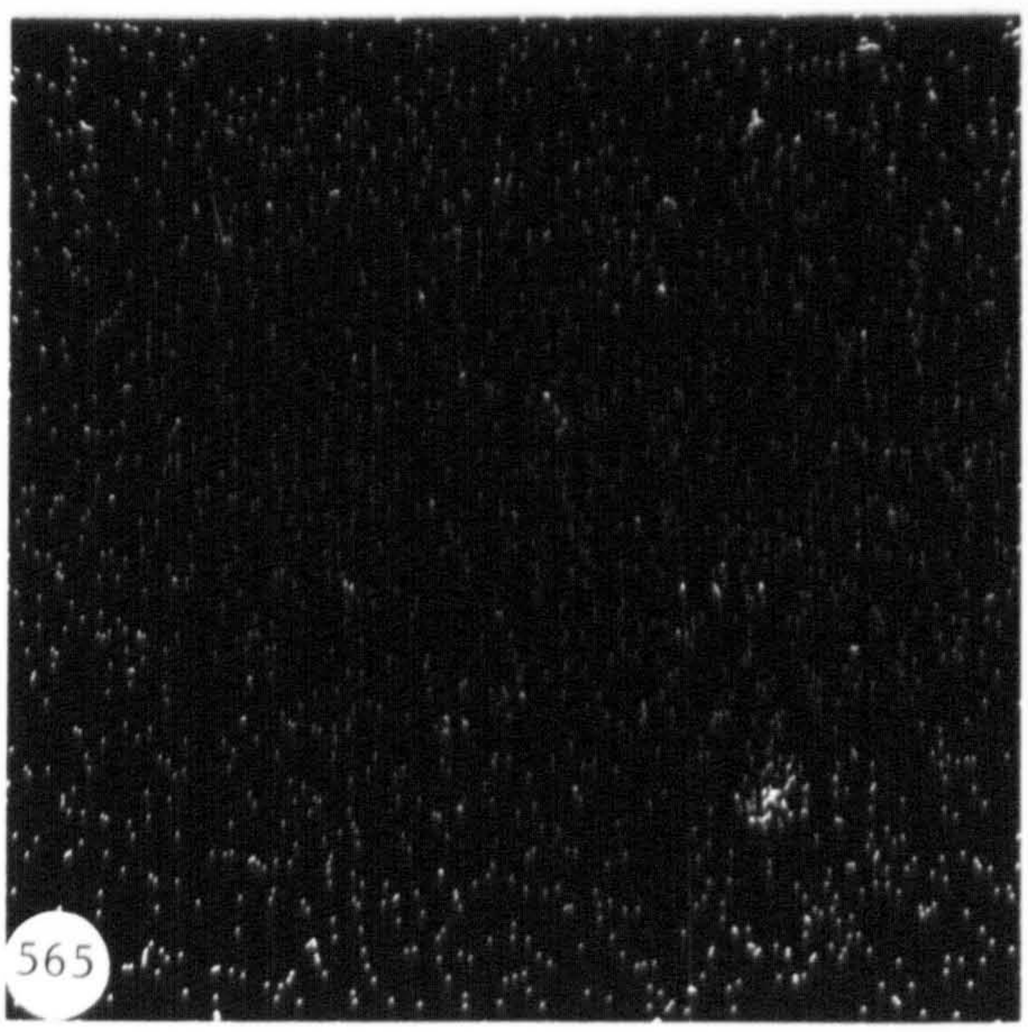
Figures 560 to 562. X-ray analysis of Lima Graphite radiolytically oxidised to 1.26% weight loss (outside surface).



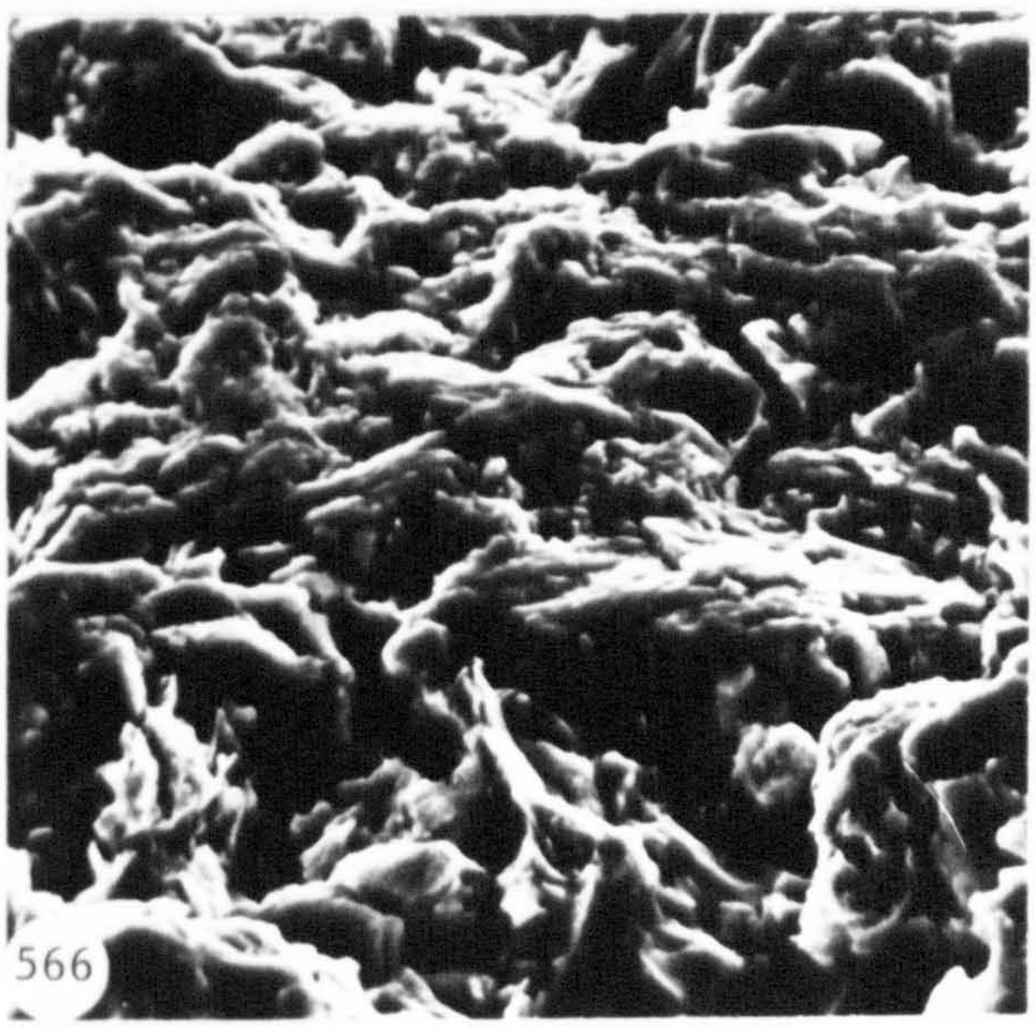
X-ray Spectrum



Silicon X-ray analysis

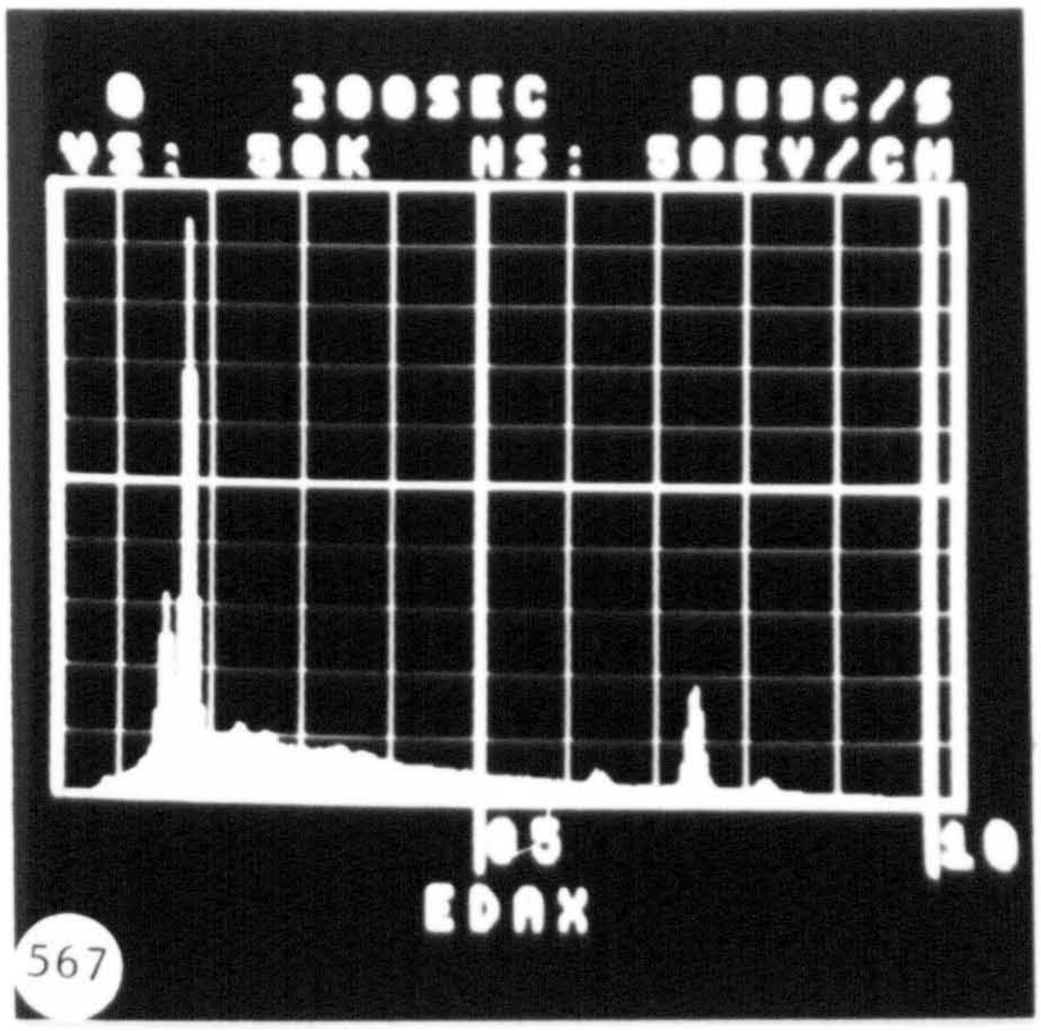


Nickel X-ray analysis

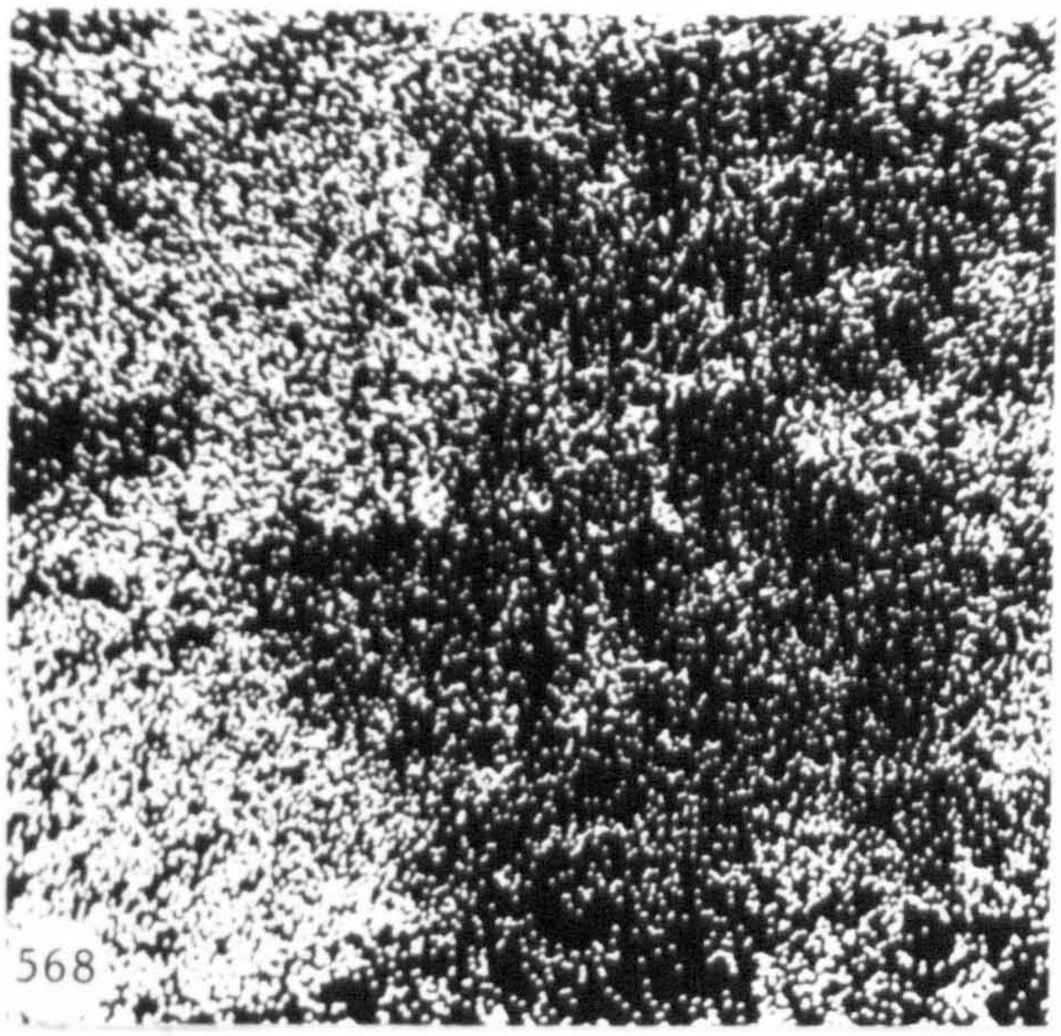


Area analysed 20 µm

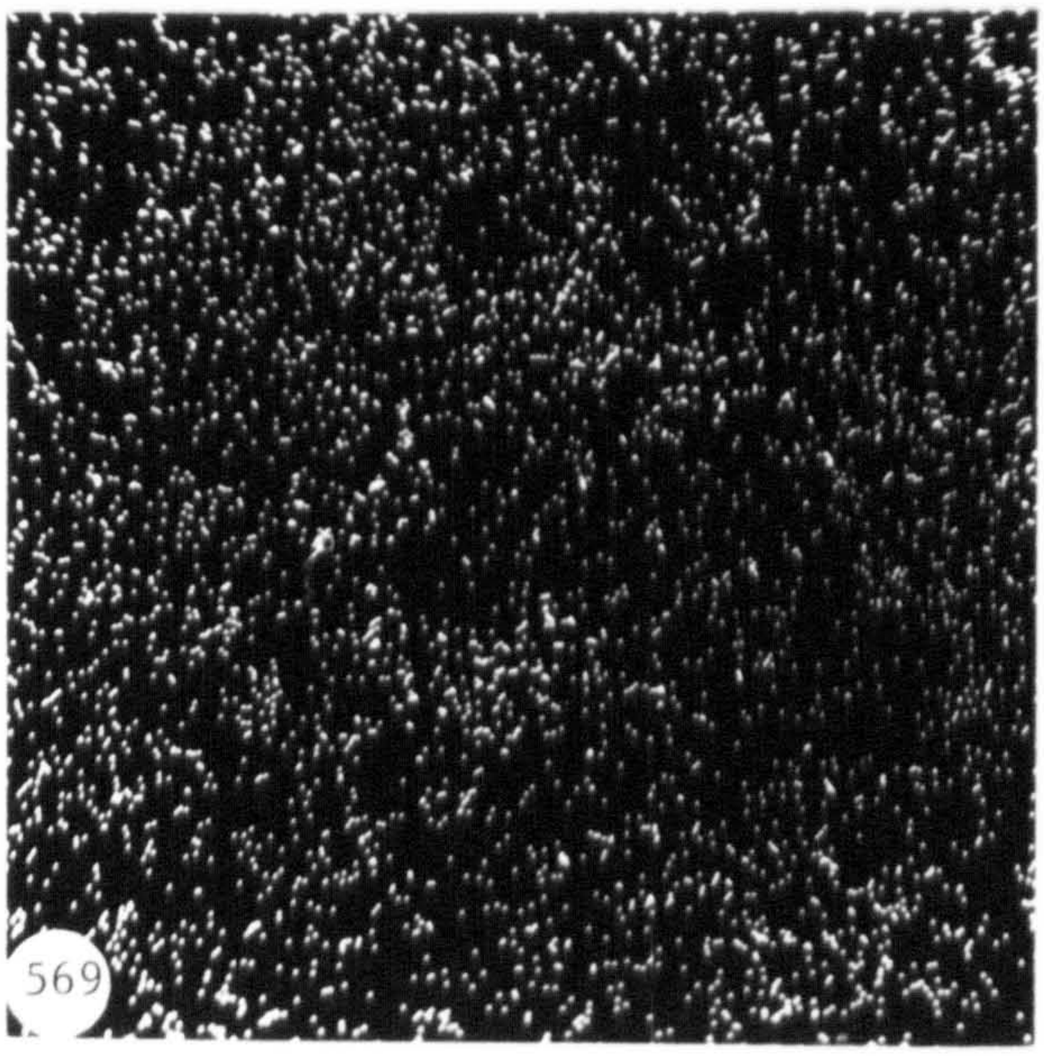
Figures 563 to 566. X-ray analysis of Lima Graphite radiolytically oxidised to 9.48% weight loss (outside surface).



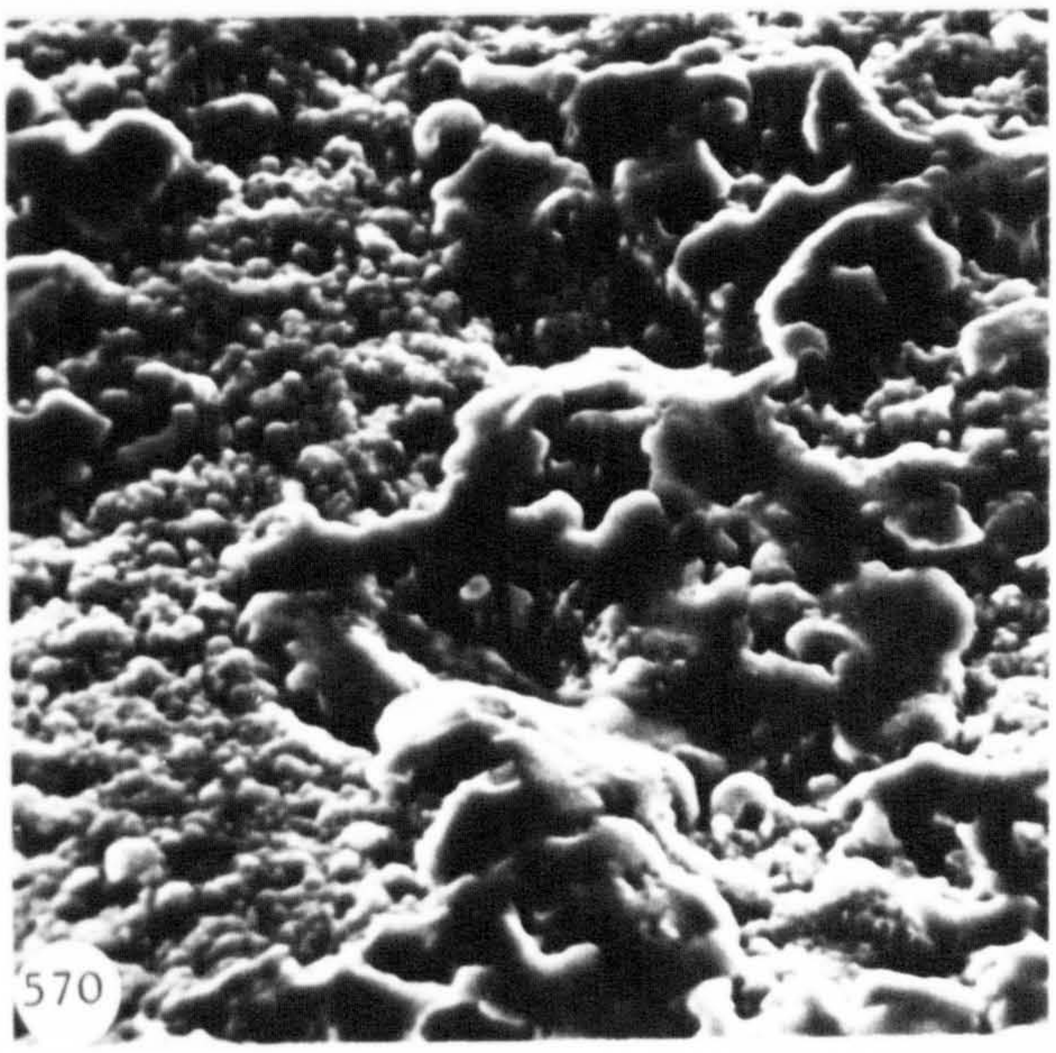
X-ray Spectrum



Silicon X-ray analysis

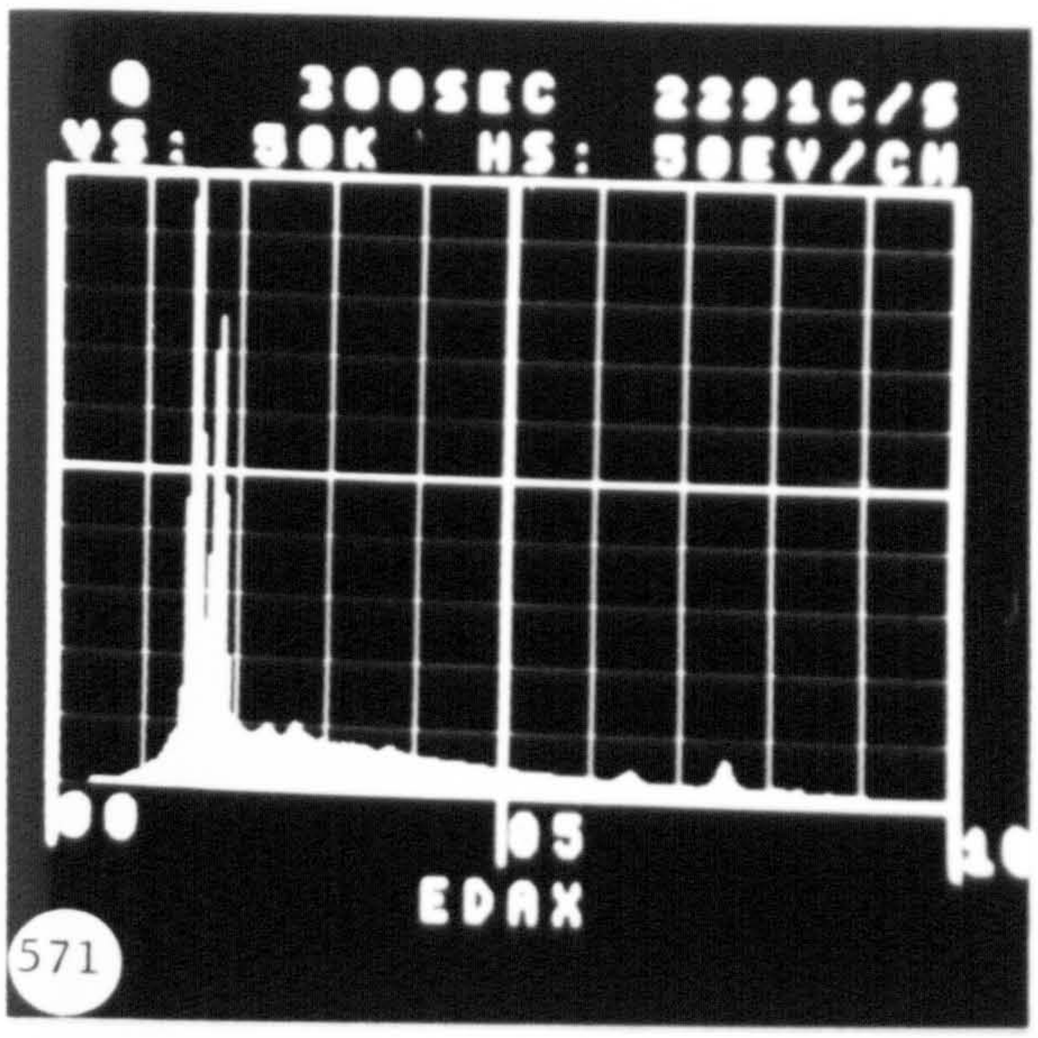


Nickel X-ray analysis

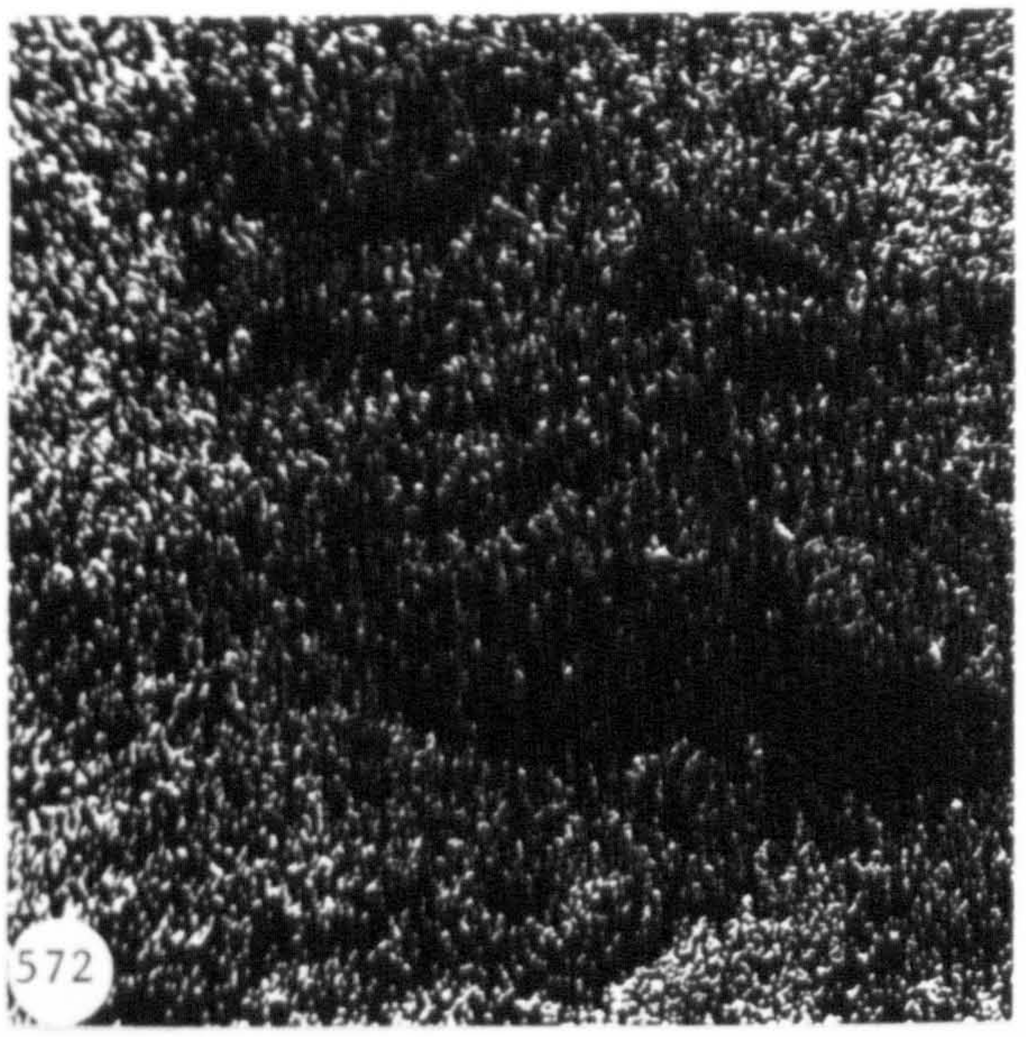


Area analysed 20 µm

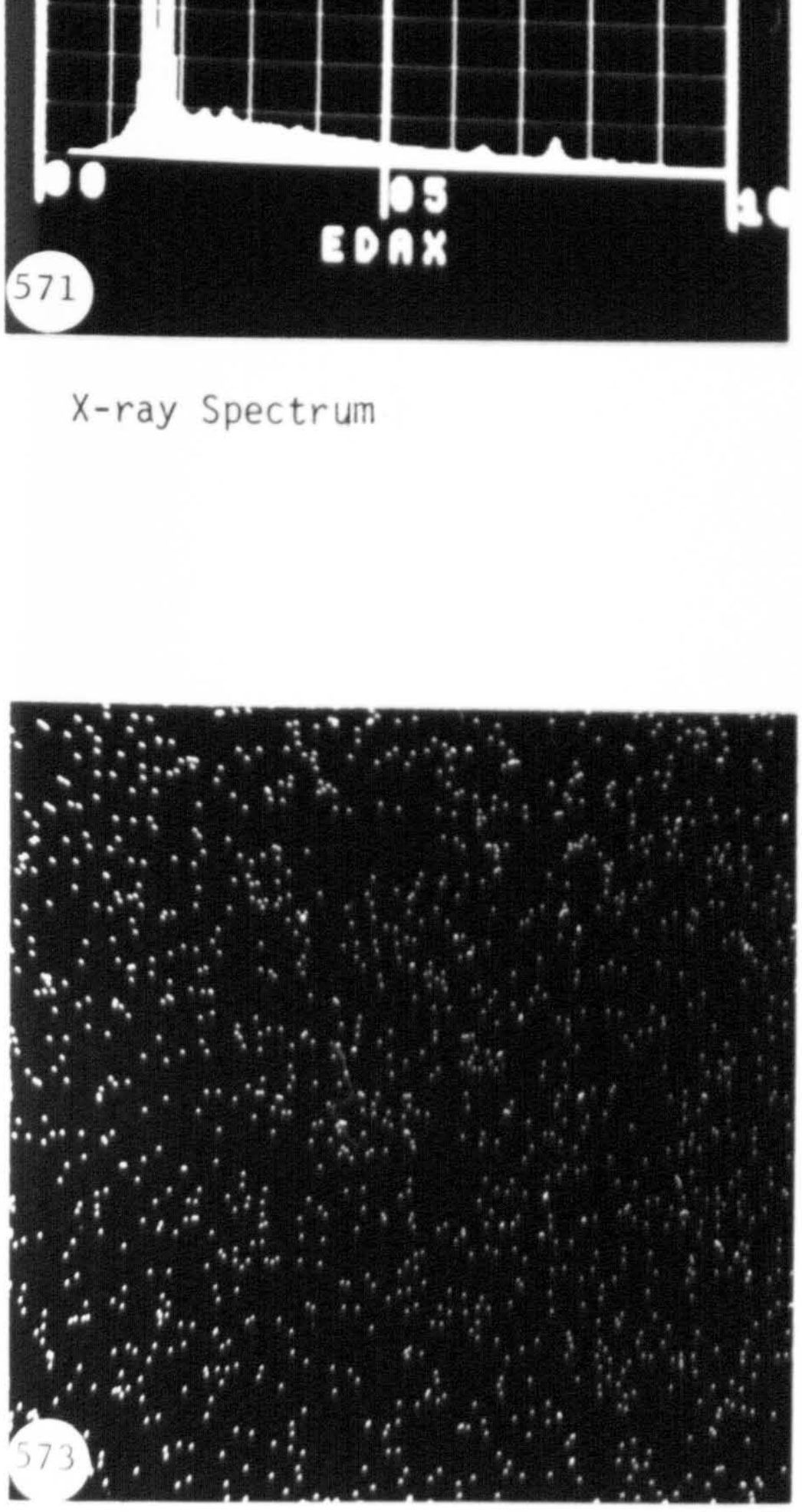
Figures 567 to 570. X-ray analysis of Lima Graphite radiolytically oxidised to 22.6% weight loss (inside surface).



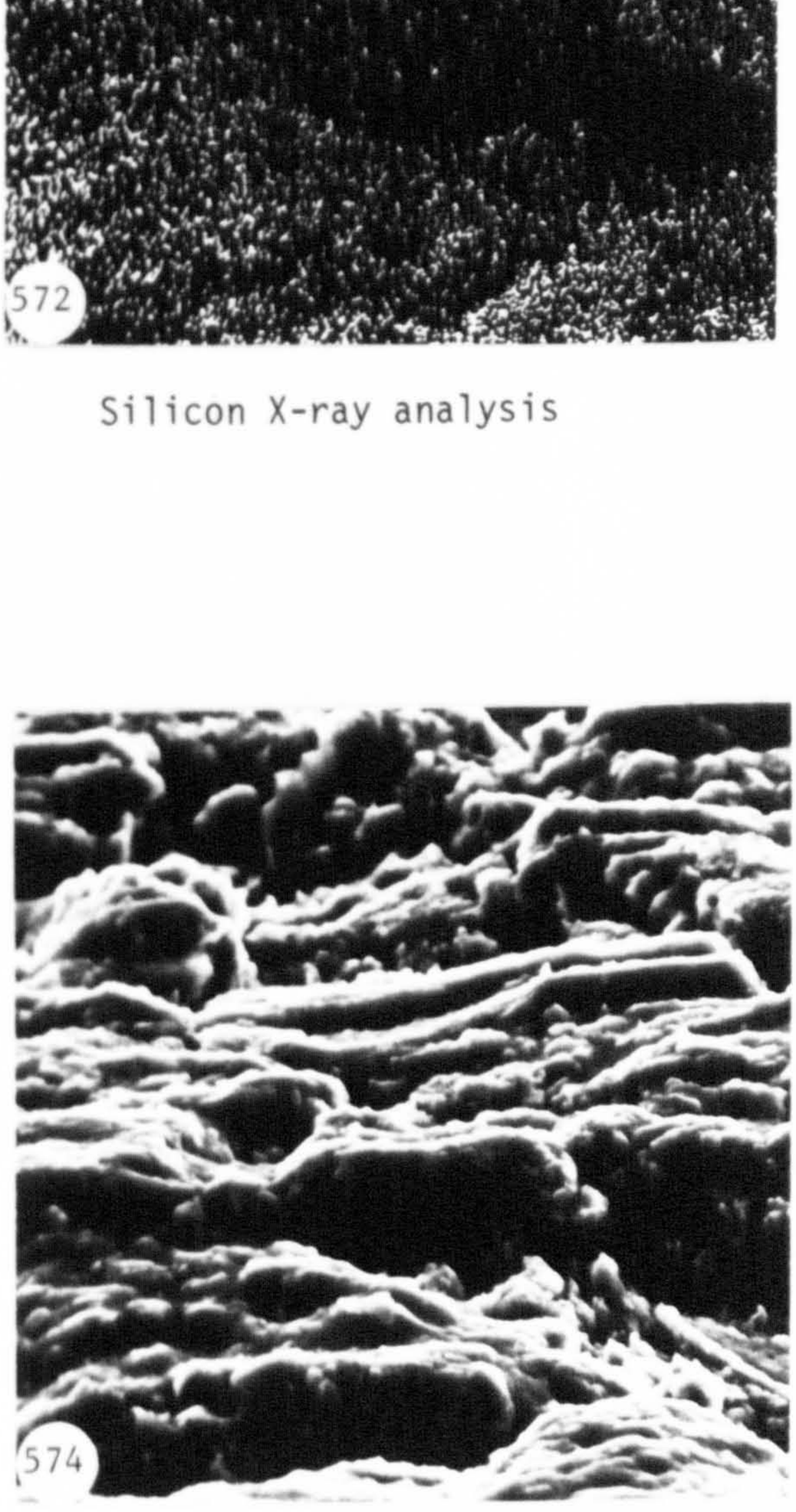
X-ray Spectrum



Silicon X-ray analysis



Nickel X-ray analysis



Area analysed

20 µm

Figures 571 to 574. X-ray analysis of Lima Graphite radiolytically oxidised to 22.6% weight loss (outside surface).

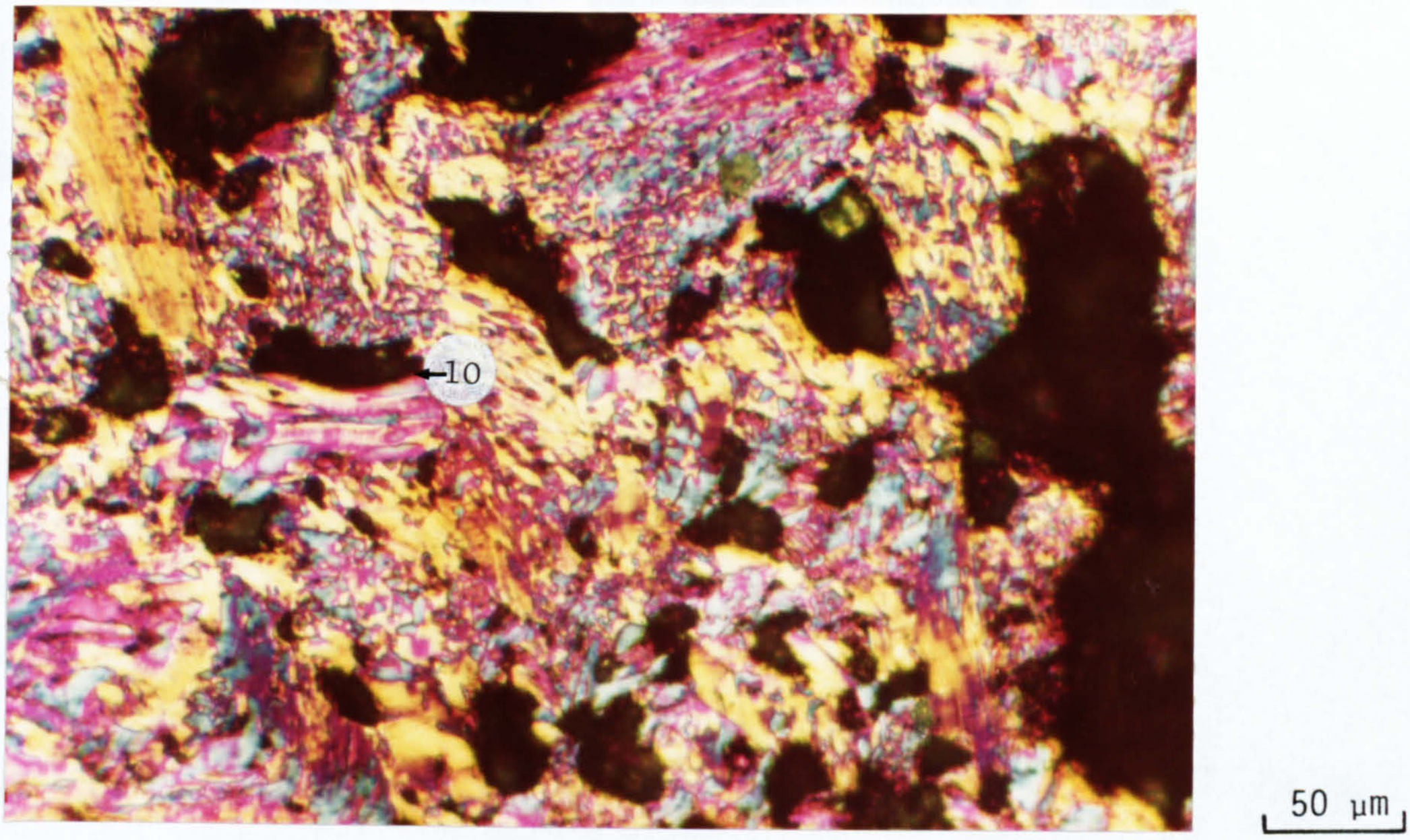


Figure 575. Optical micrograph of virgin Lima Graphite.

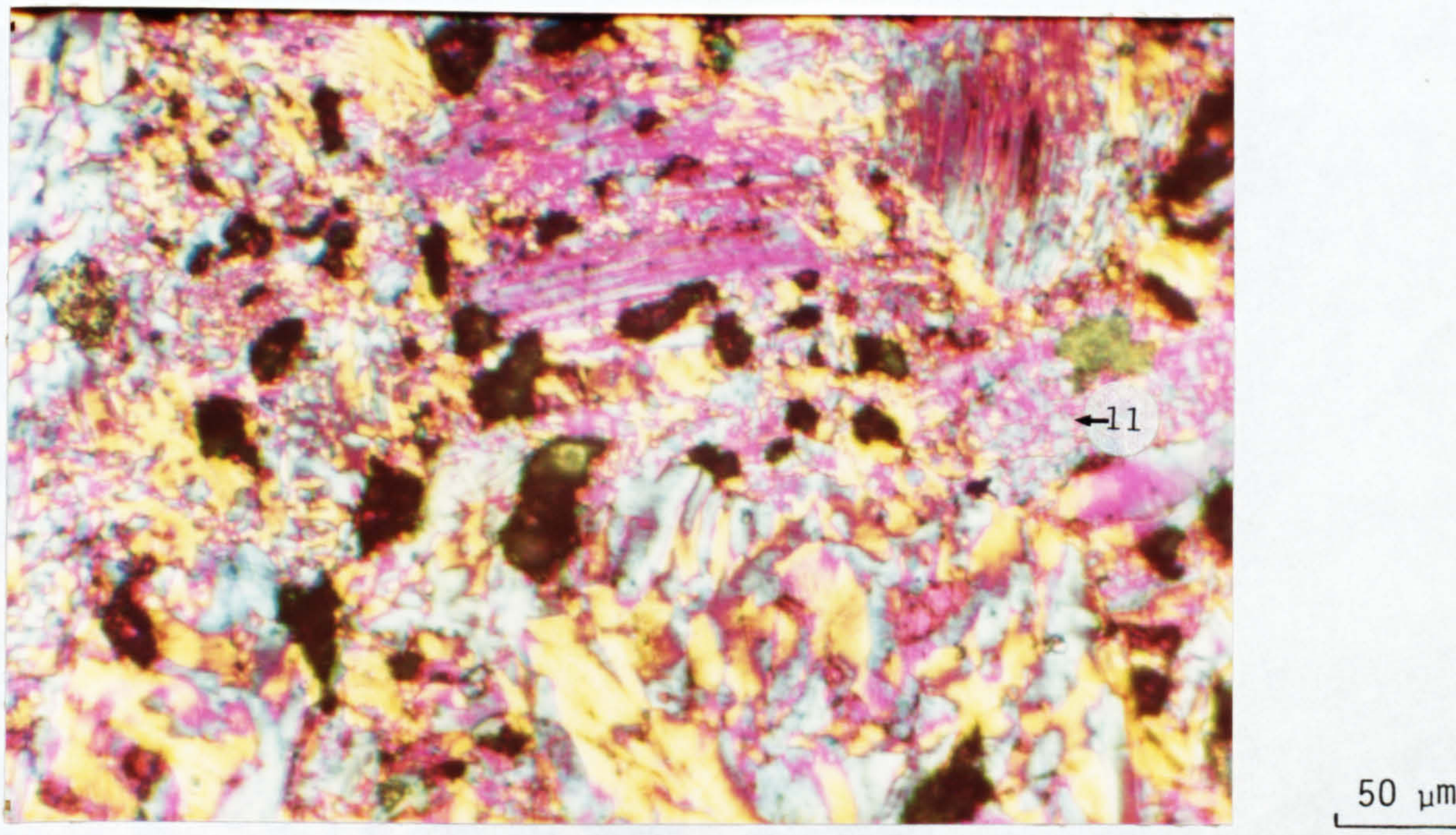


Figure 576. Optical micrograph of Lima Graphite radiolytically oxidised to 1.26% weight loss.

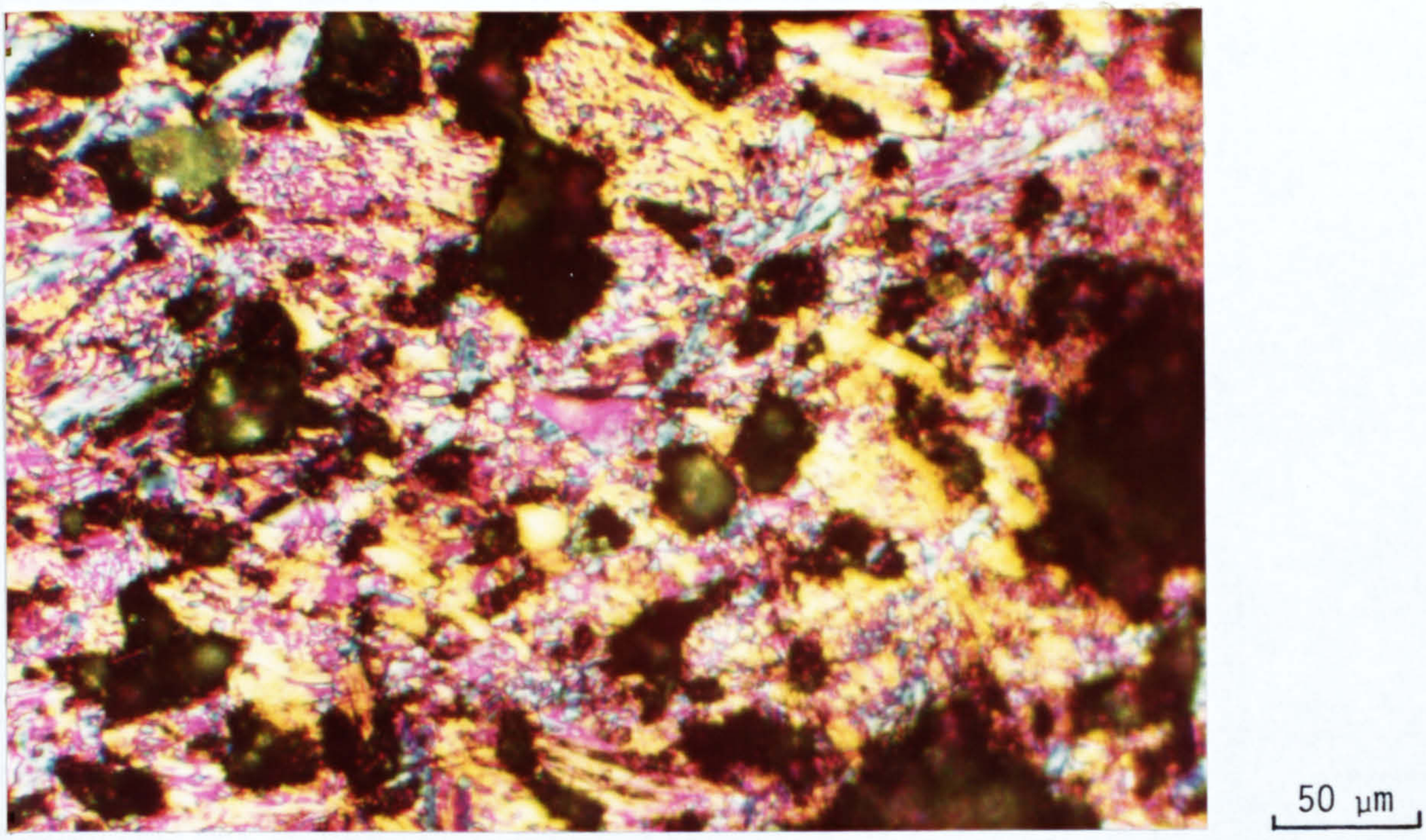


Figure 577. Optical micrograph of Lima Graphite radiolytically oxidised to 9.48% weight loss.

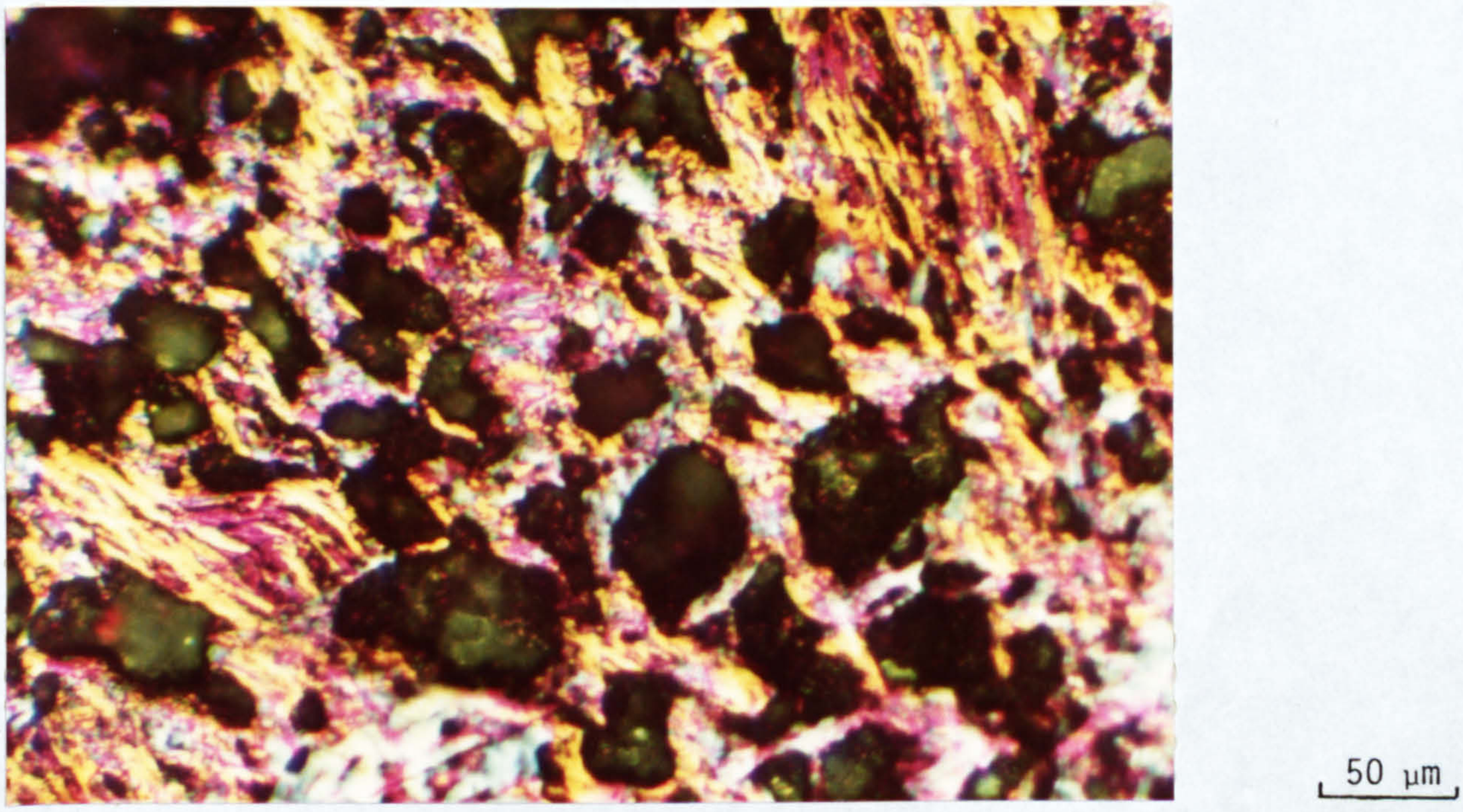


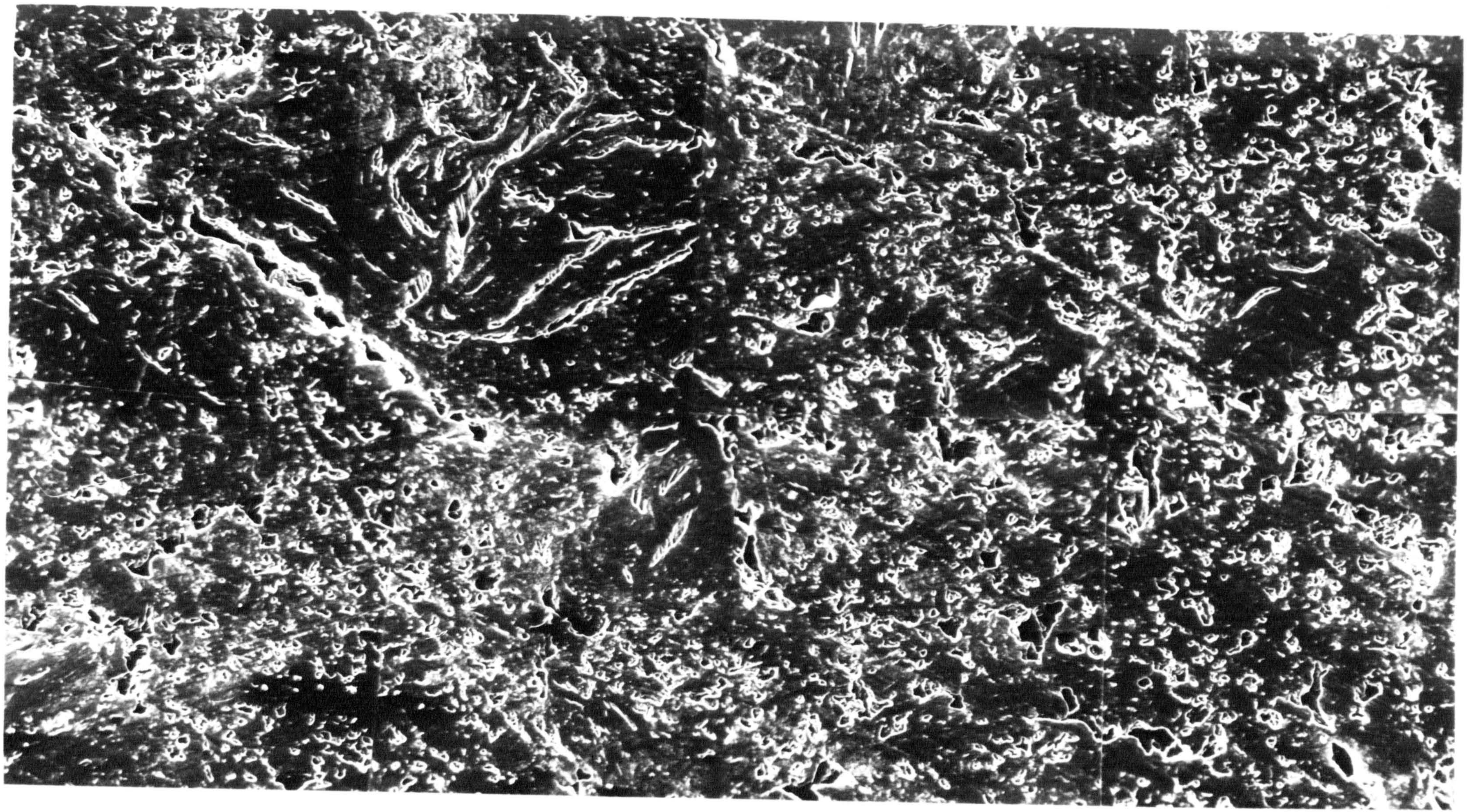
Figure 578. Optical micrograph of Lima Graphite radiolytically oxidised to 22.6% weight loss.



LIMA GRAPHITE

200 µm

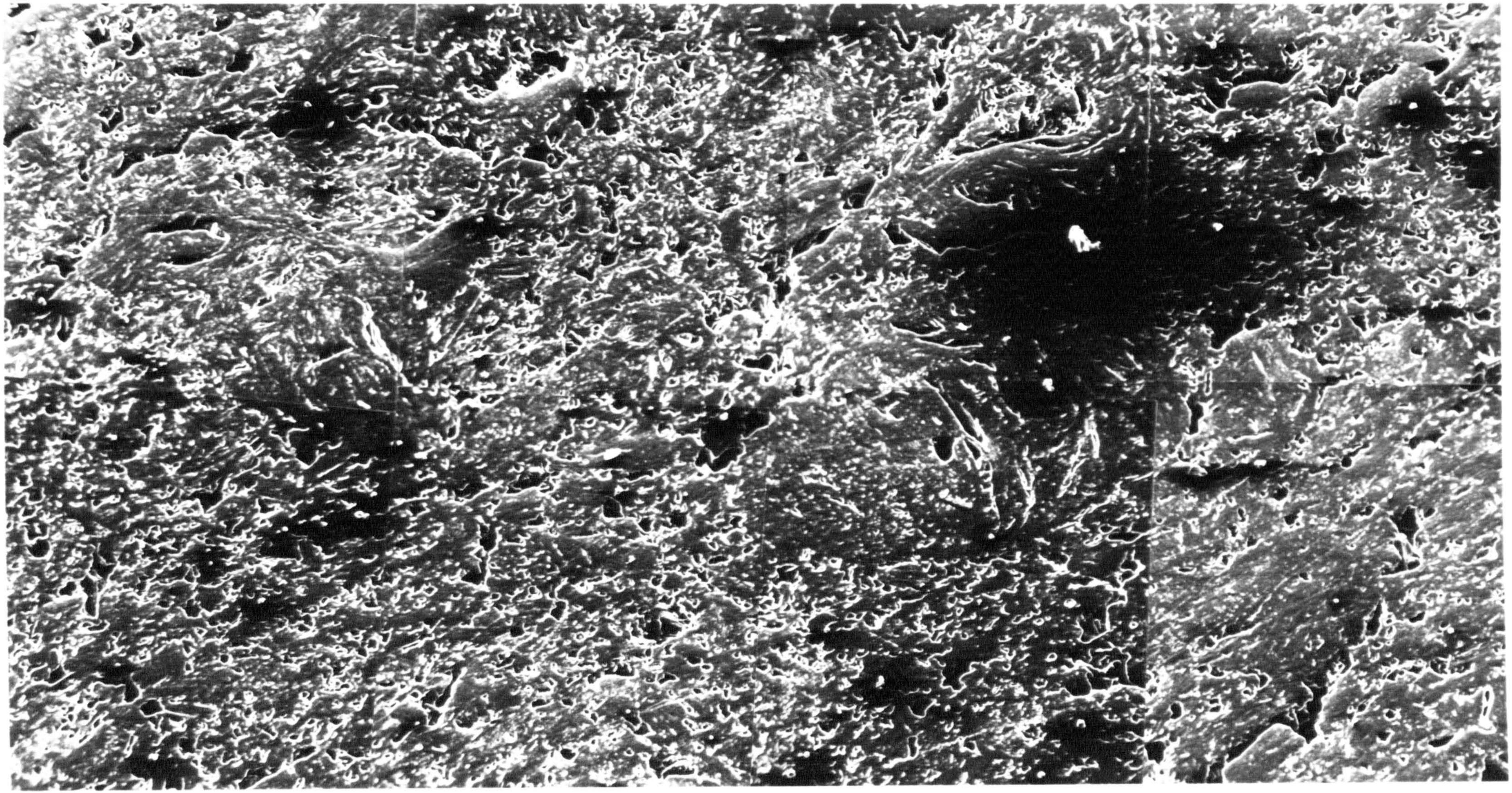
Figure 579. Photo-montage of virgin Lima Graphite



LIMA GRAPHITE

200 µm

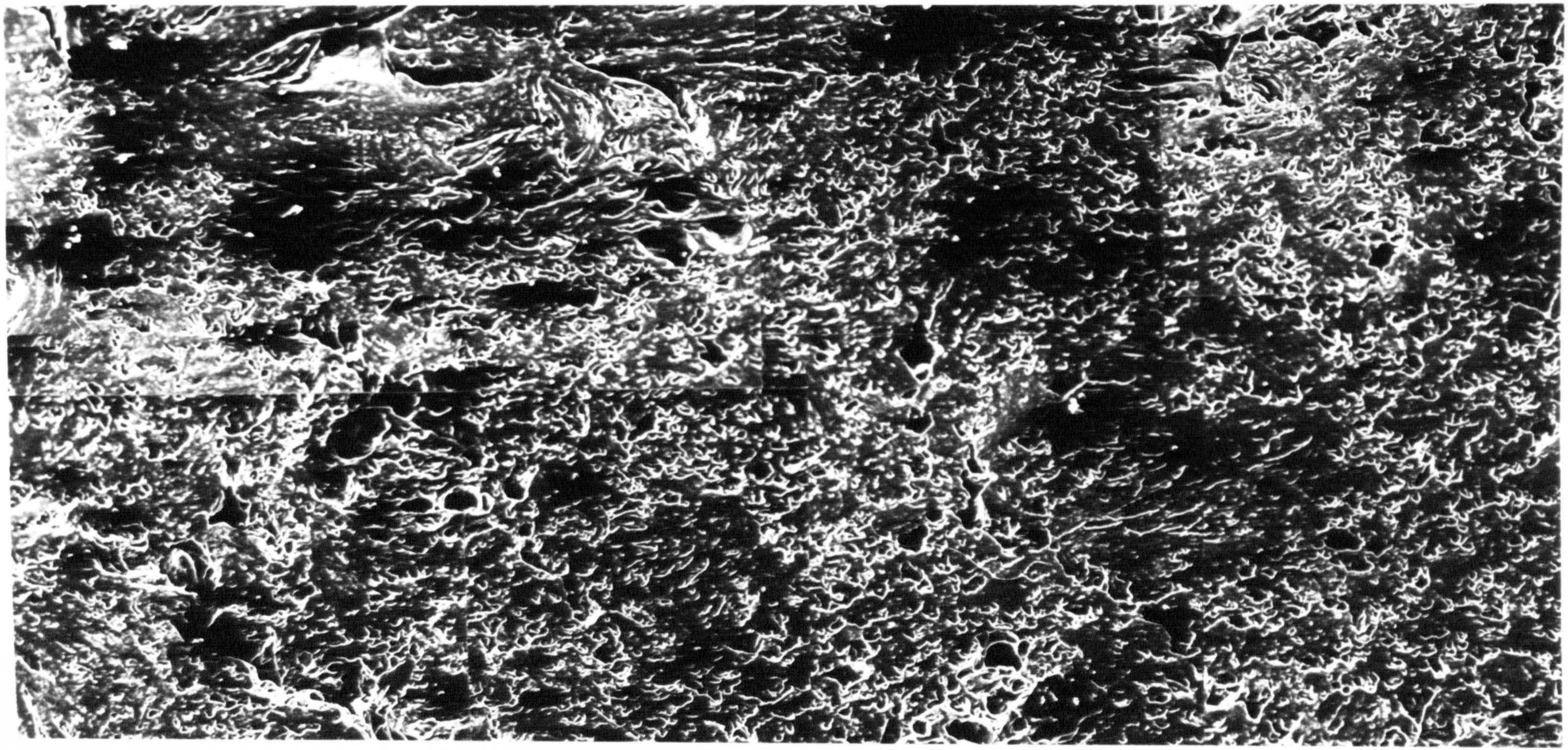
Figure 580. Photo-montage of Lima Graphite radiolytically oxidised to 1.26% weight loss.



LIMA GRAPHITE

200 μm

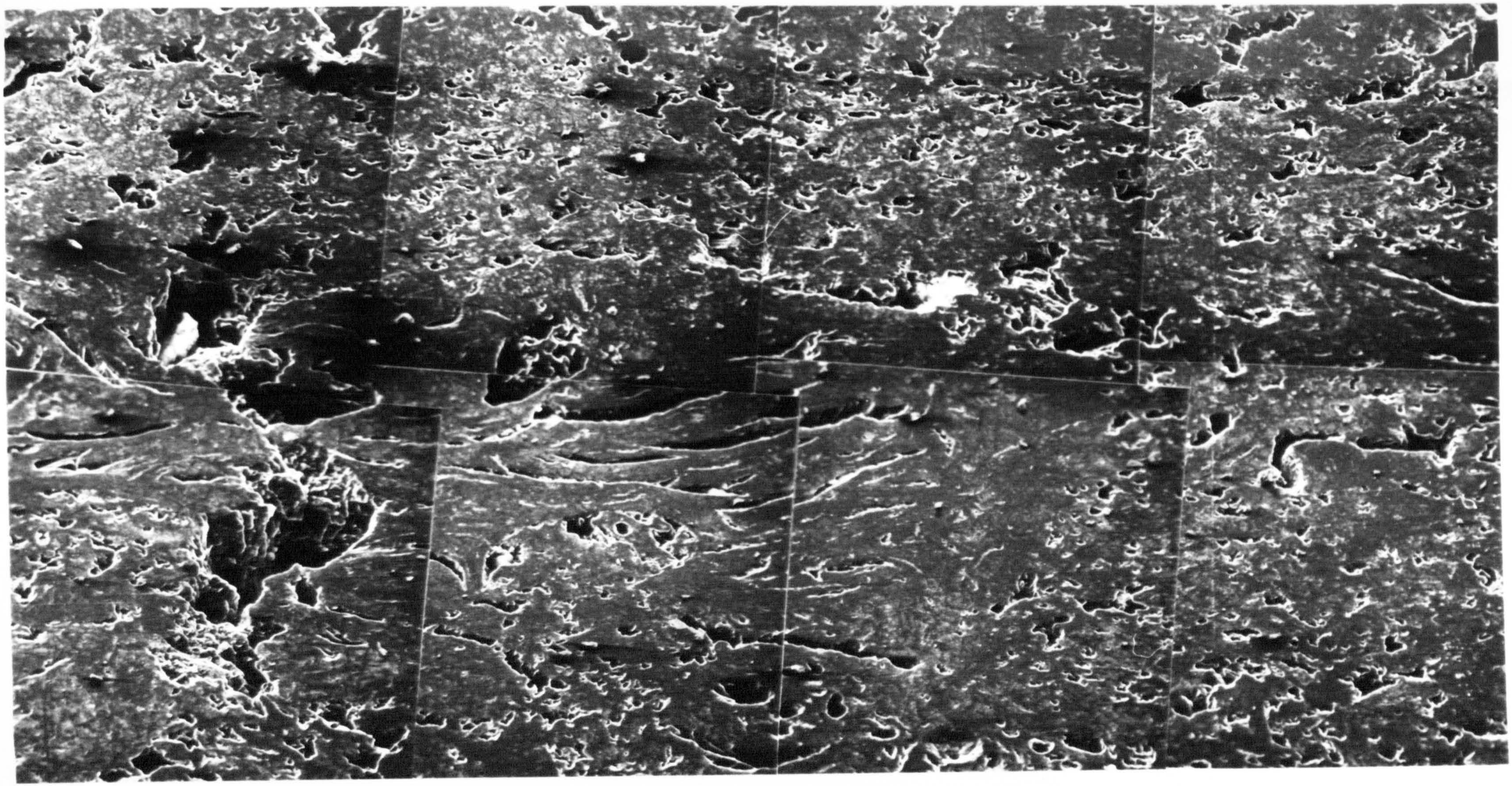
Figure 581. Photo-montage of Lima Graphite radiolytically oxidised to 9.48% weight loss.



LIMA GRAPHITE

200 µm

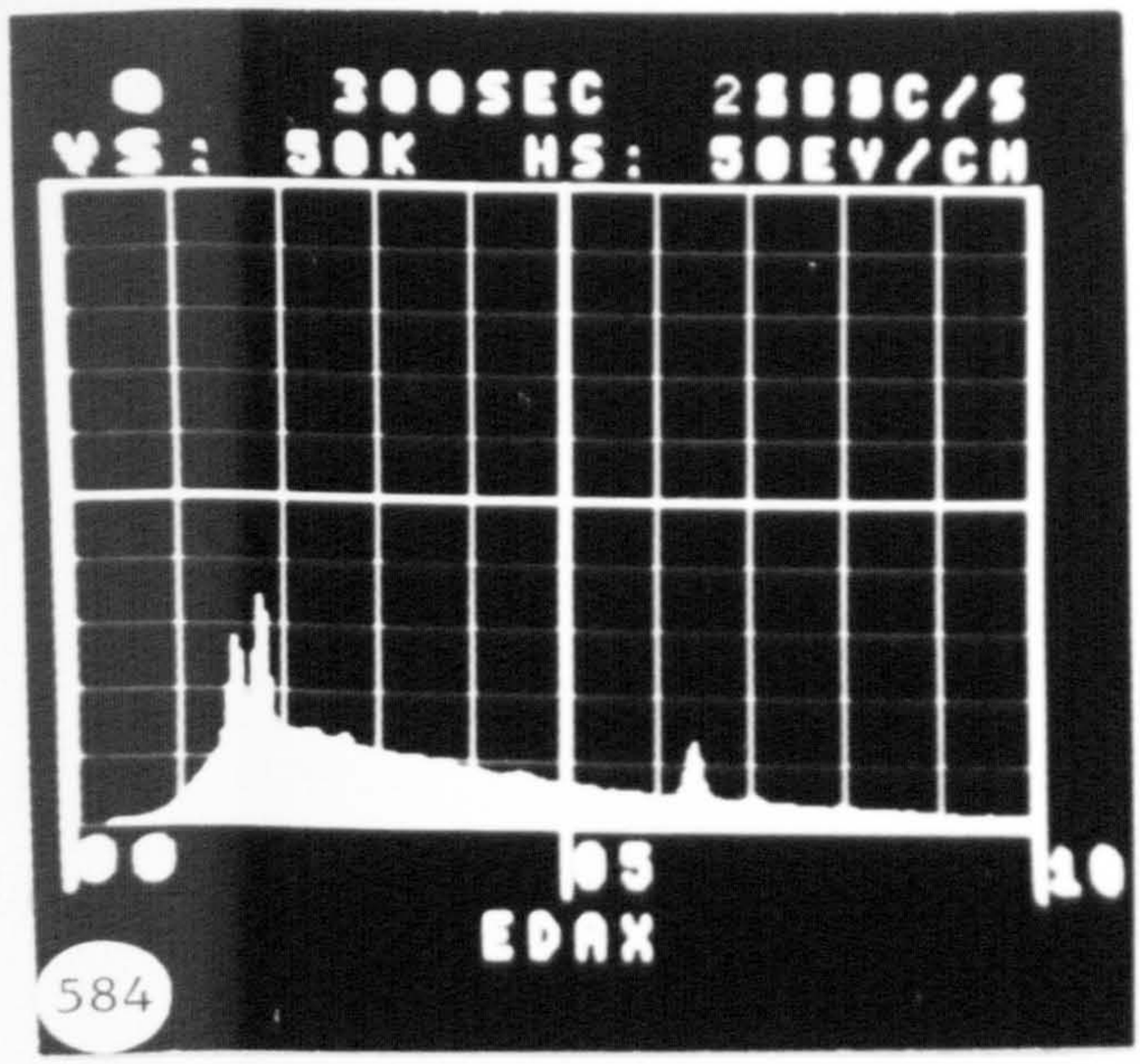
Figure 582. Photo-montage of Lima Graphite radiolytically oxidised to 22.6% weight loss.

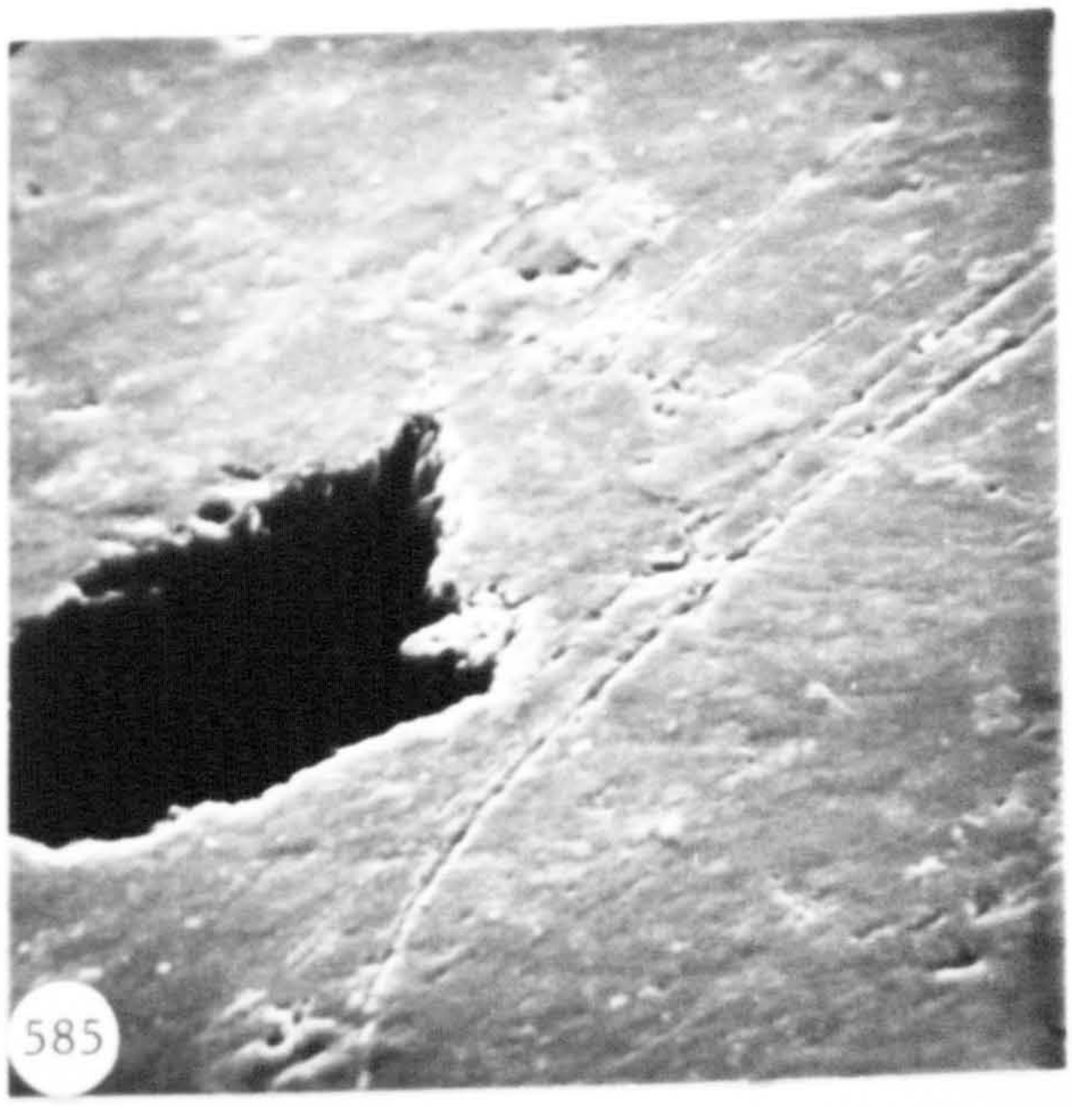


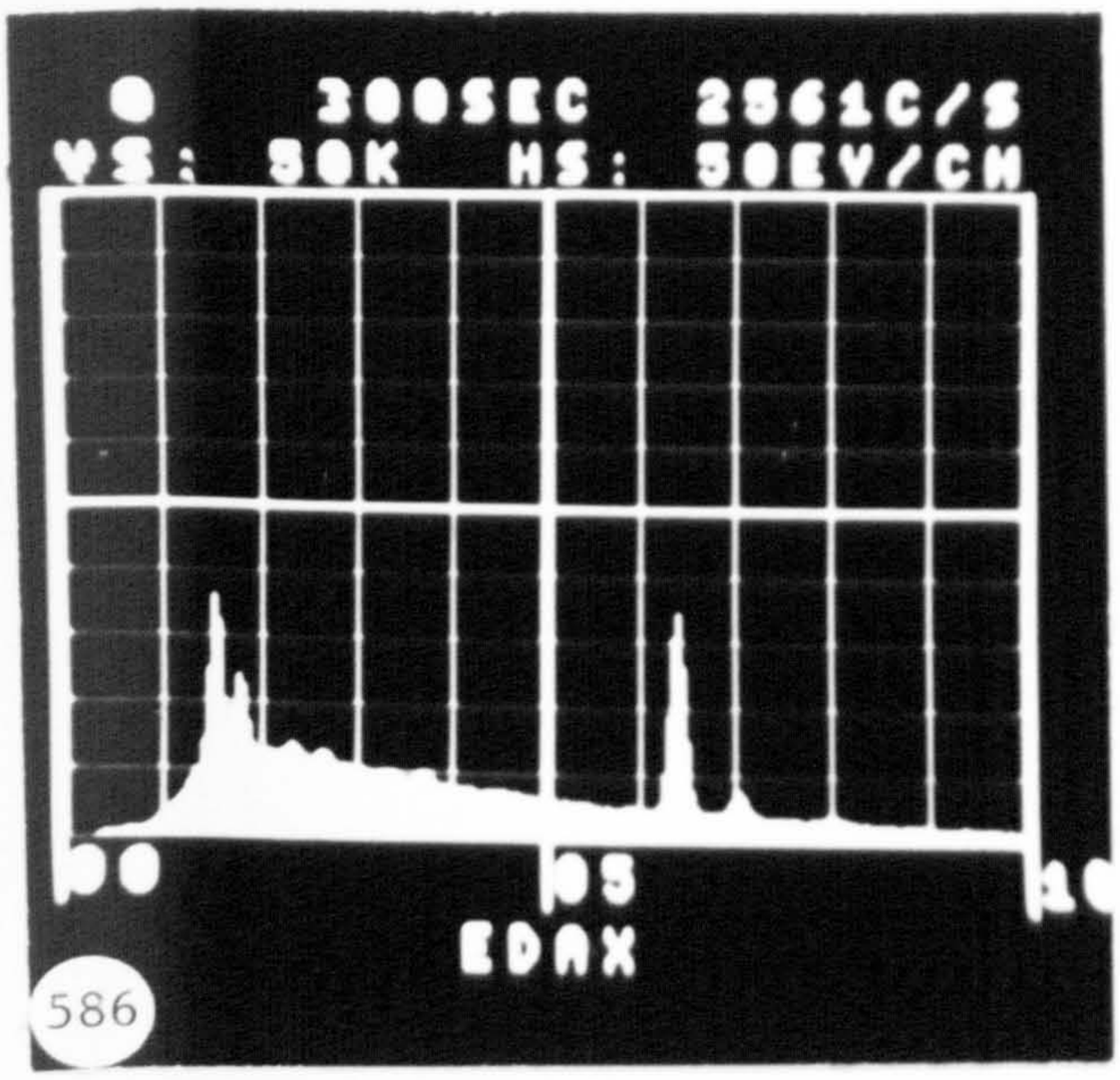
200 µm

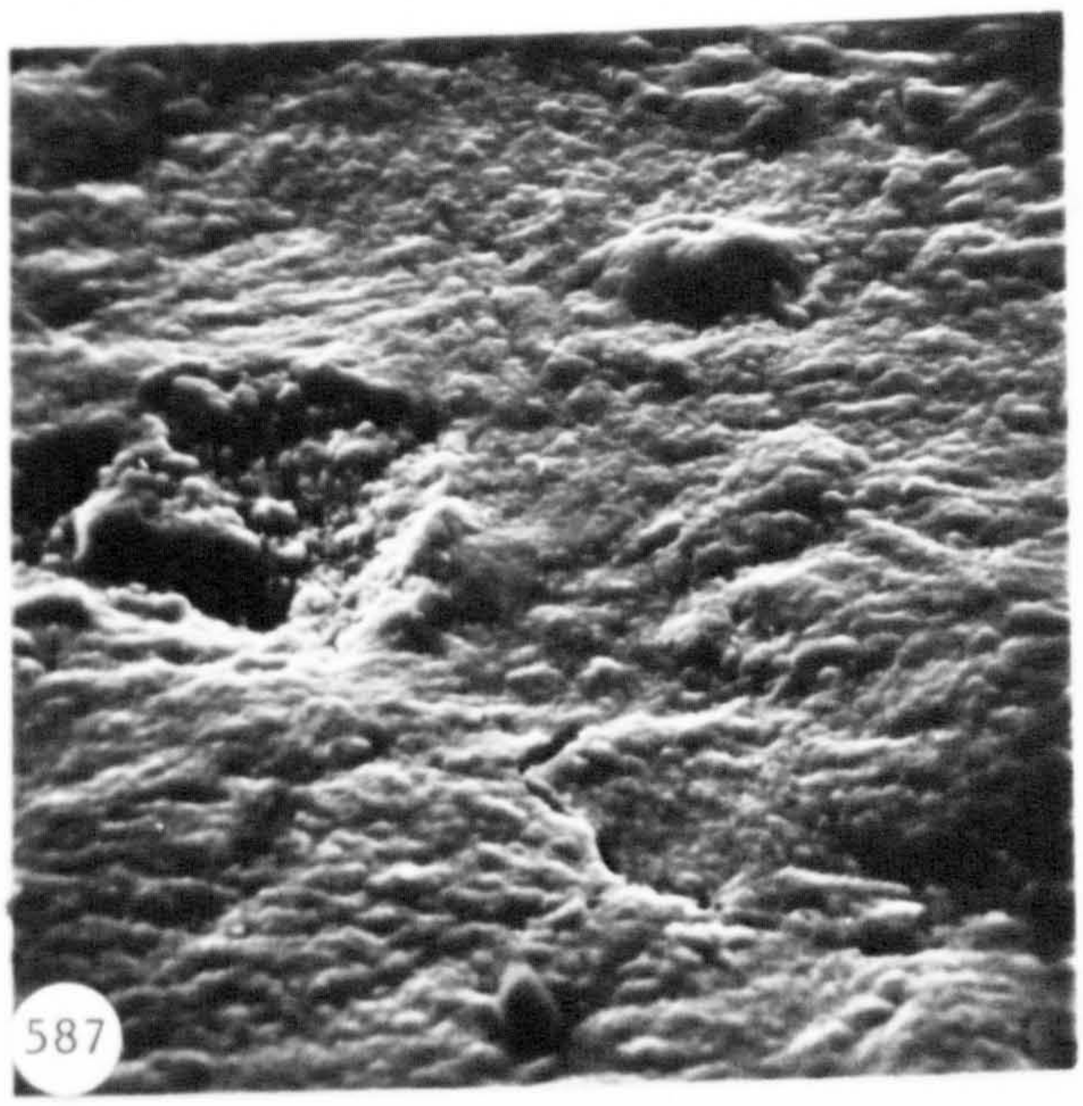
LIMA GRAPHITE

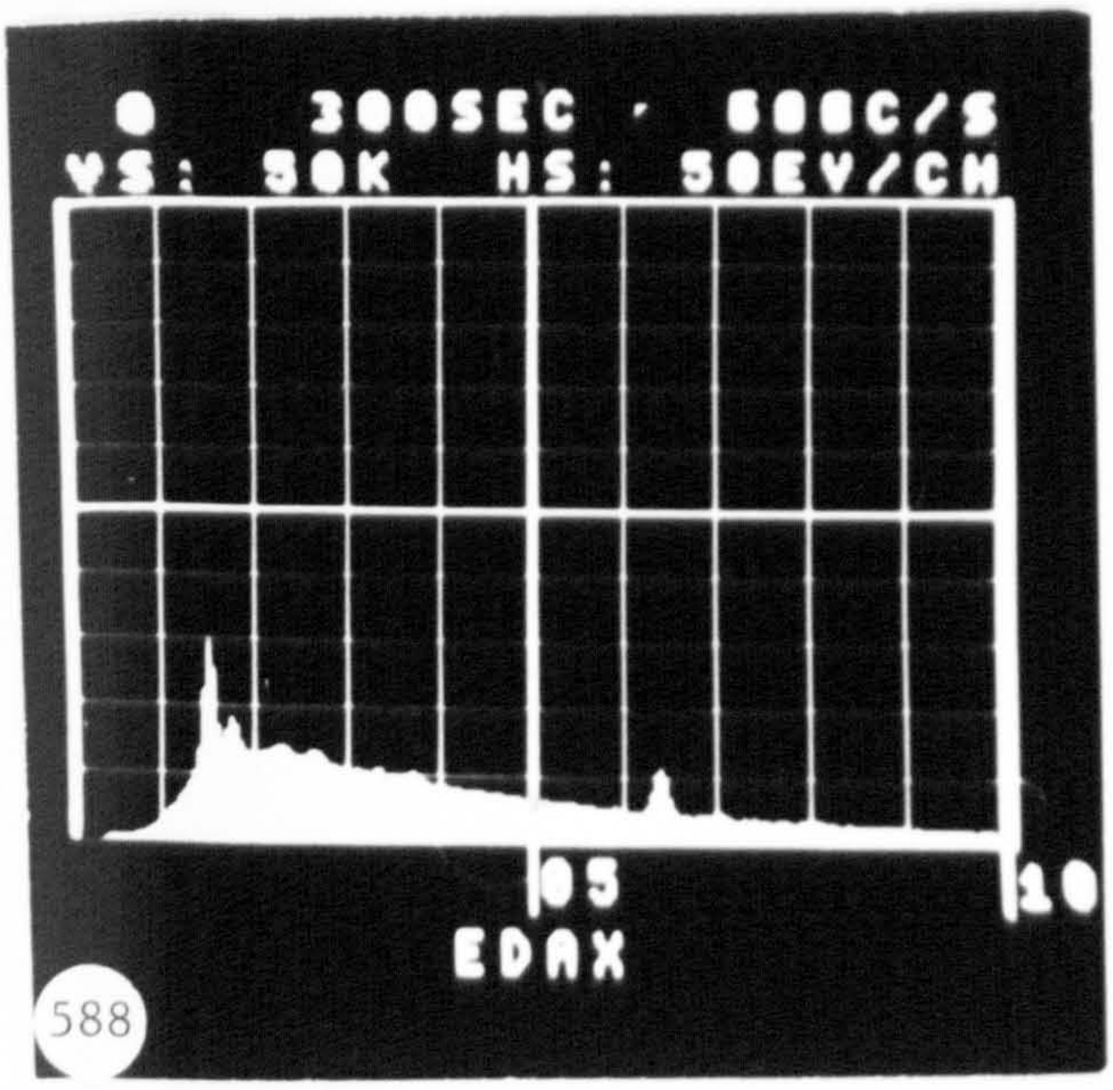
Figure 583. Photo-montage of Lima Graphite thermally gasified in carbon dioxide to 9.2% weight loss.

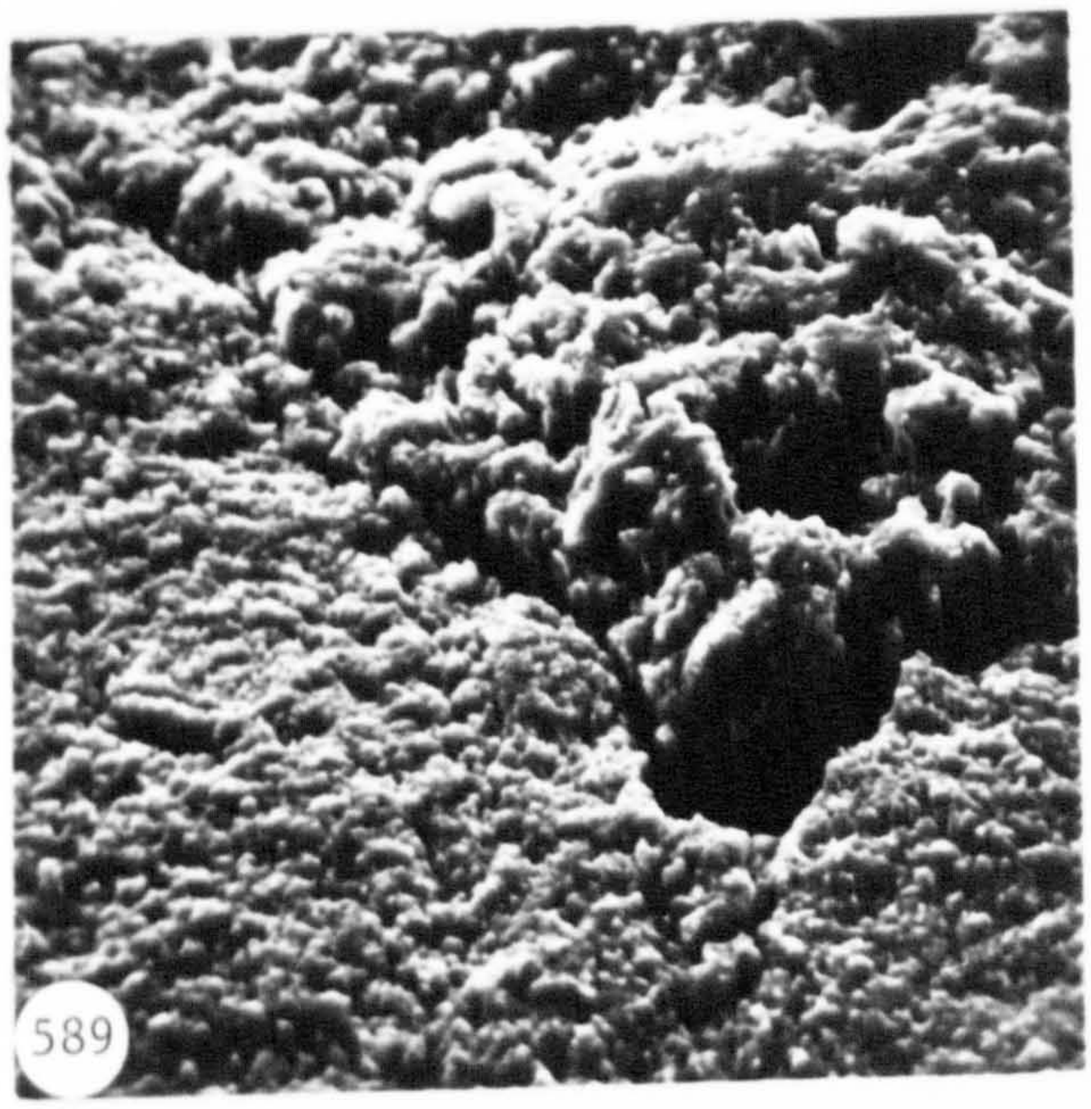










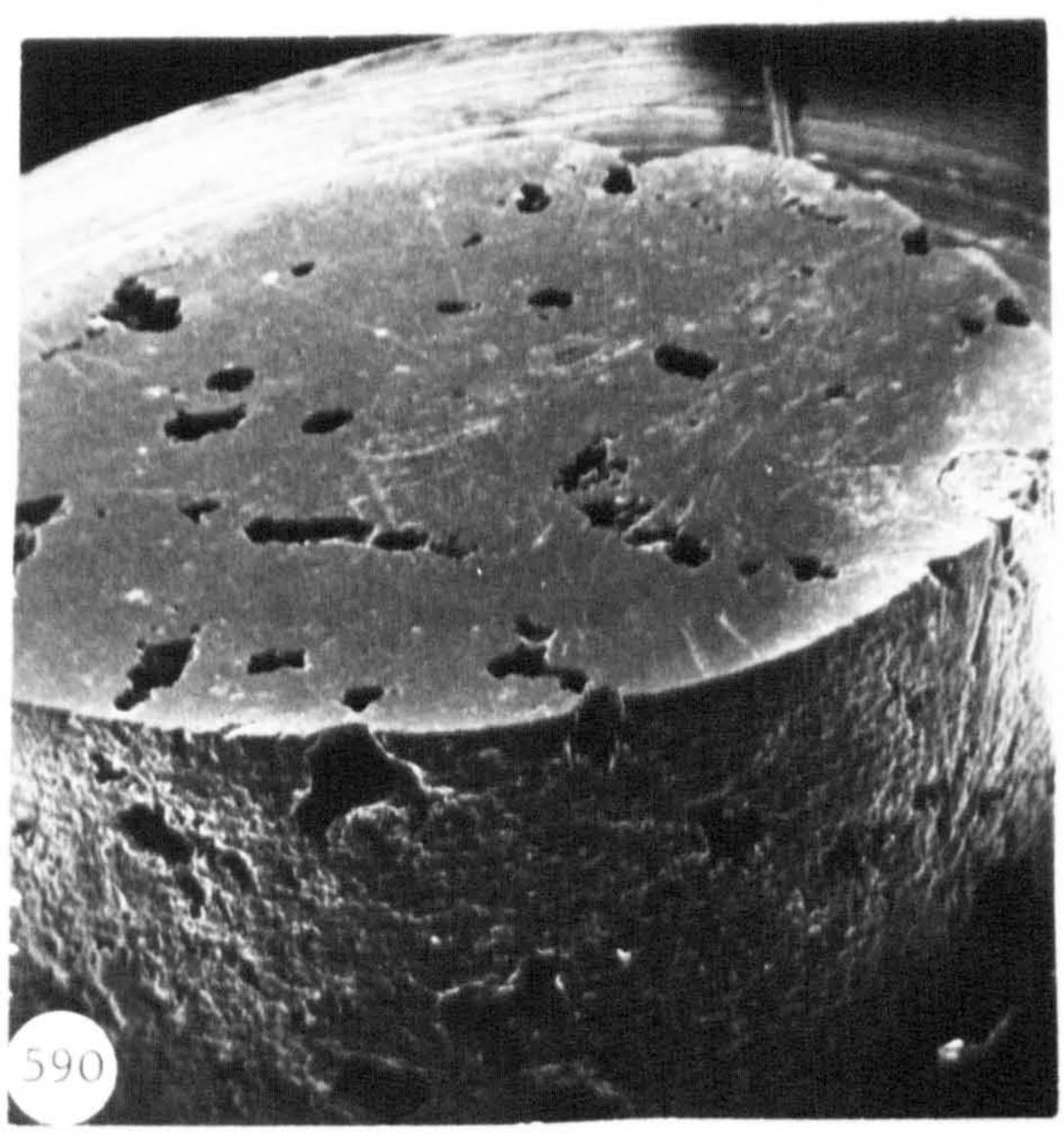


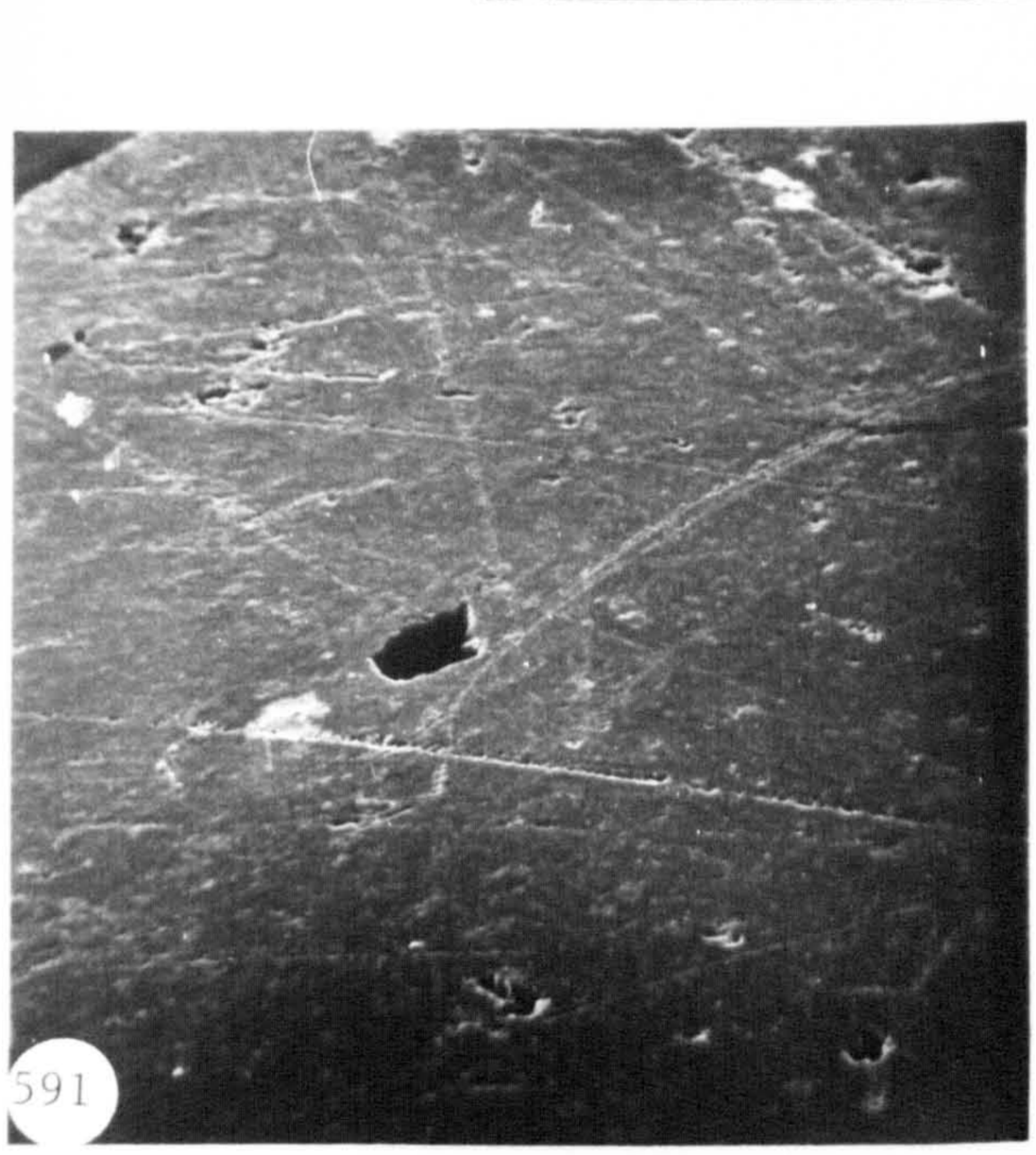
X-RAY SPECTRA

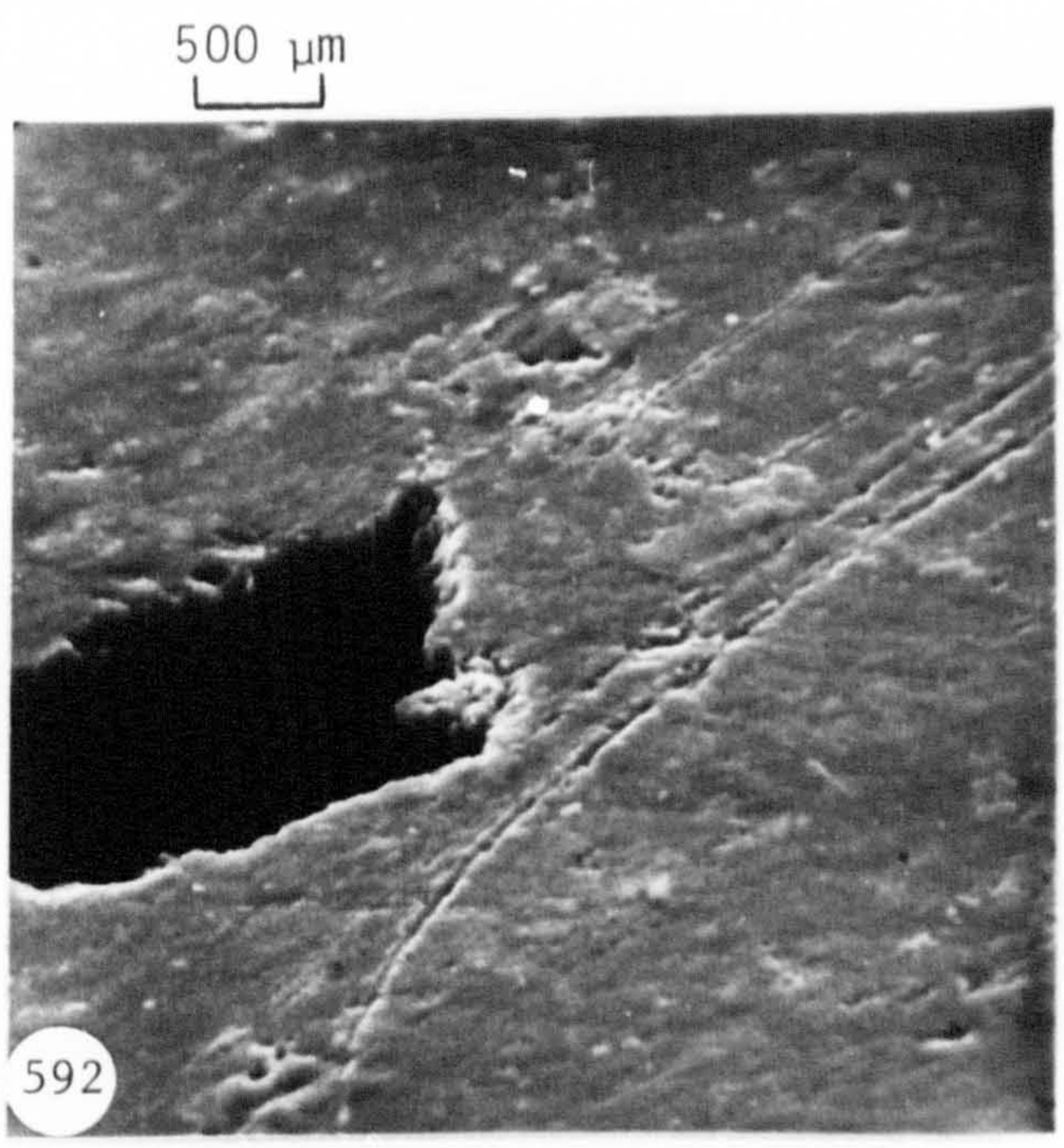
AREA ANALYSED

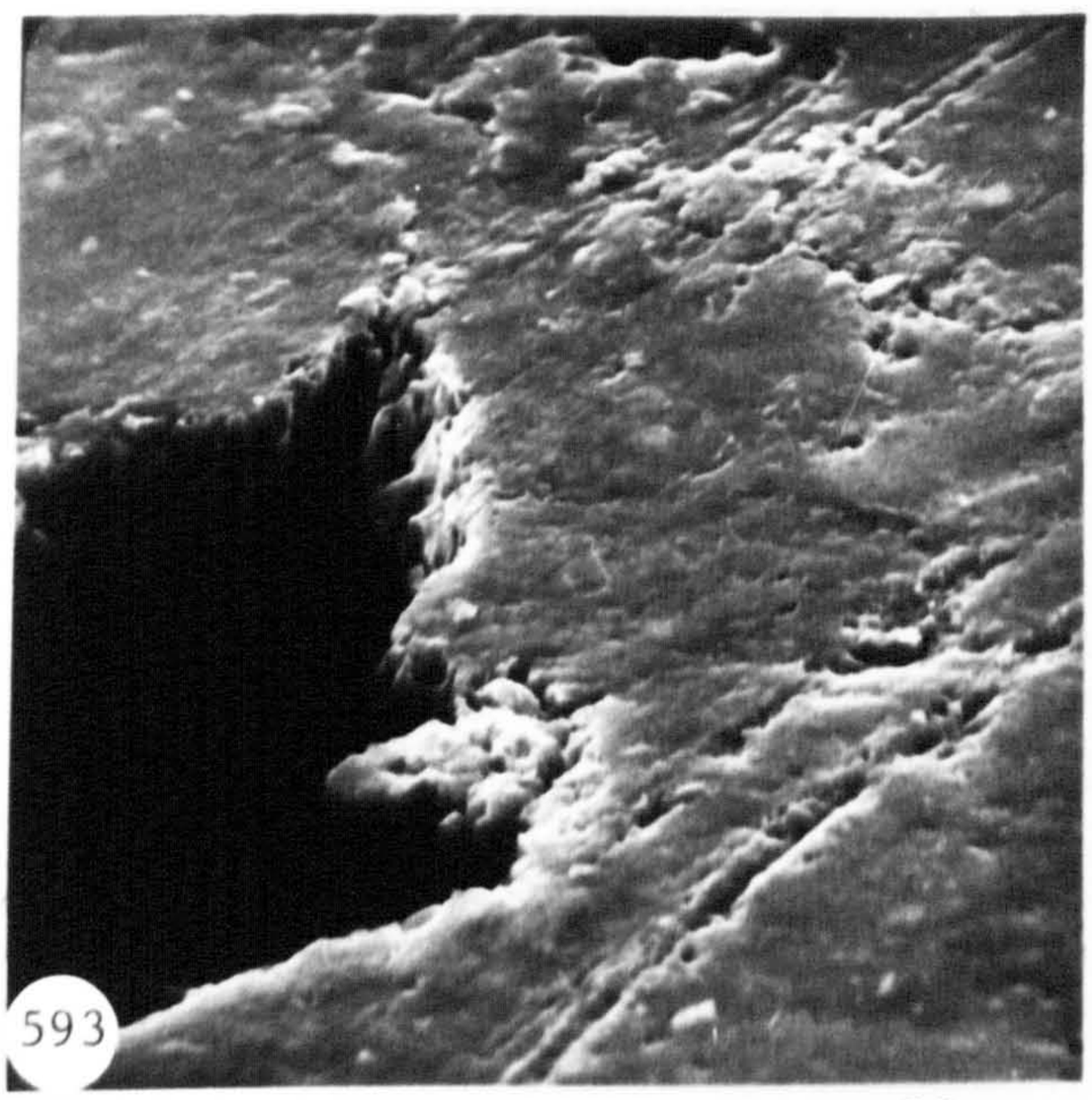
20 µm

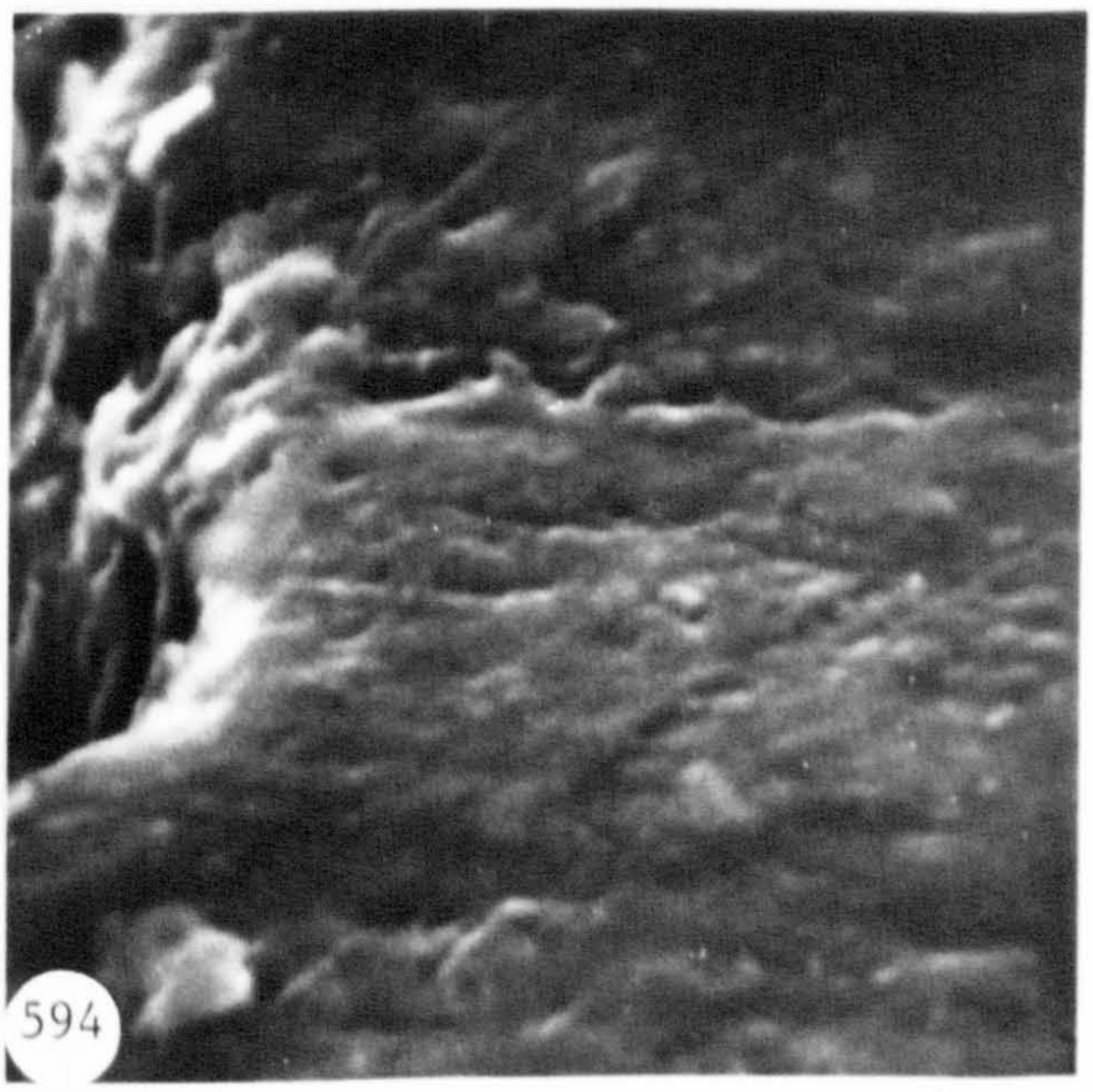
Figures 584 to 589. X-ray spectra of VQMB Pitch-coke Graphite; control (Figures 584 and 585), LZAA (Figures 586 and 587) and SBO (Figures 588 and 589).



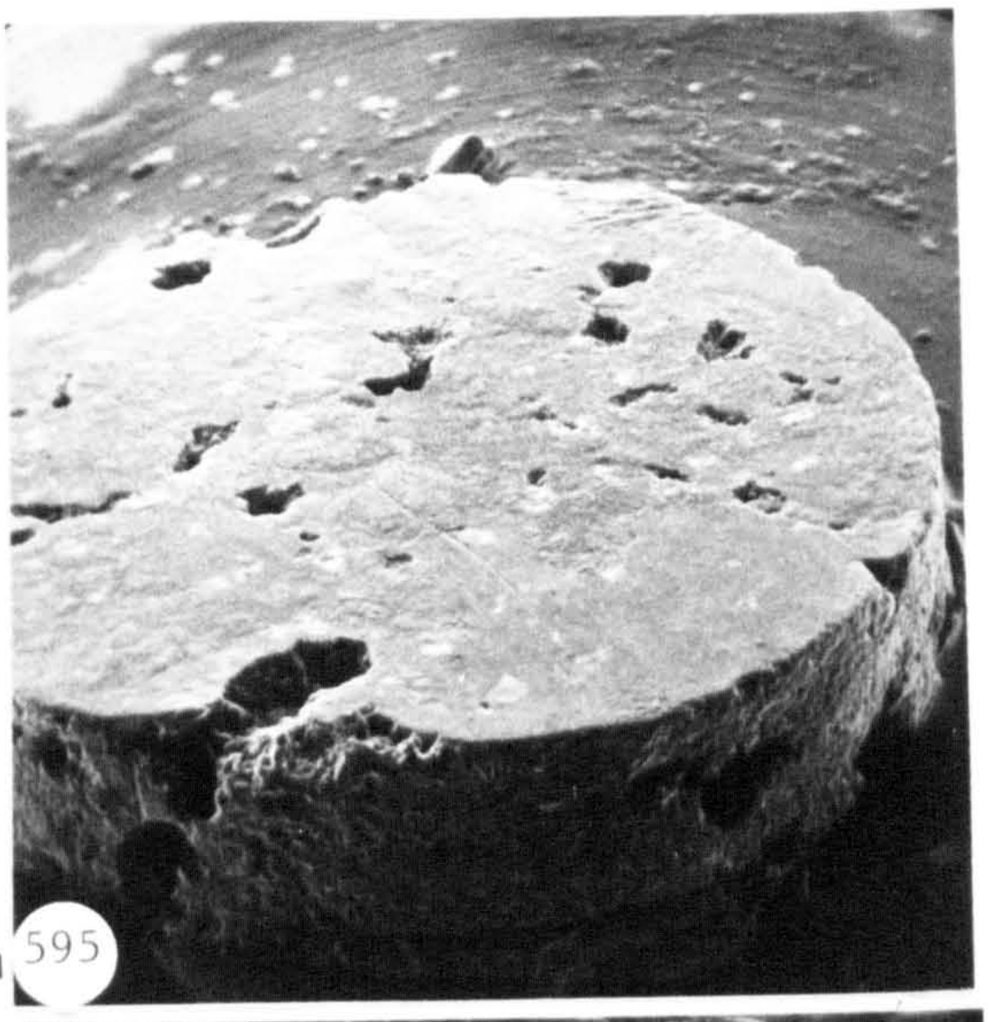


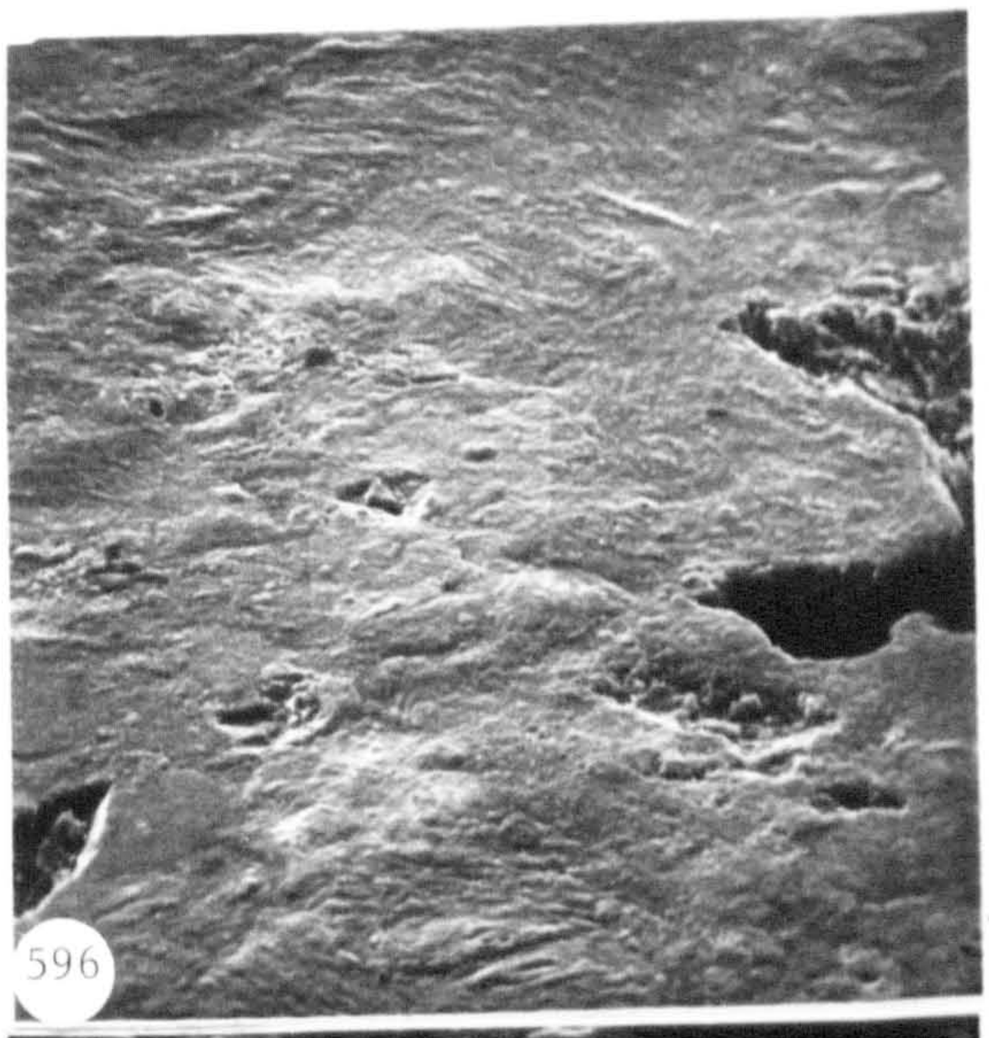


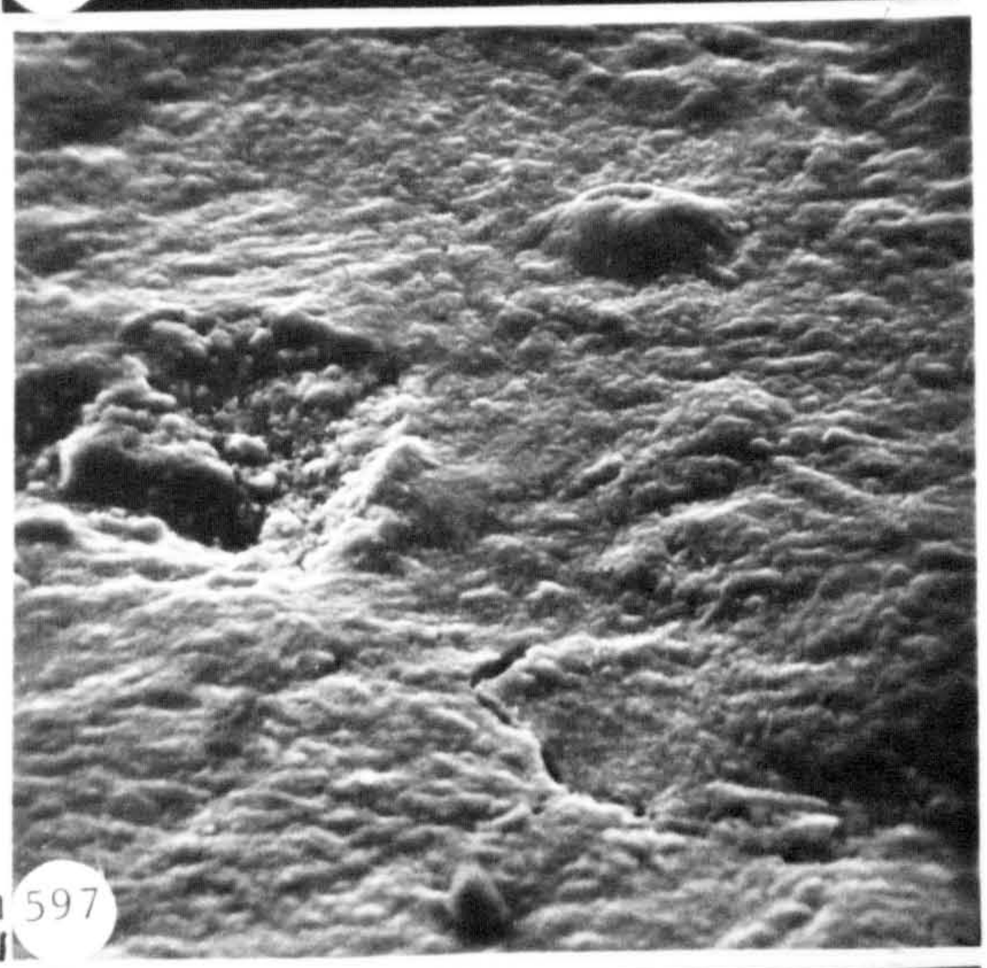


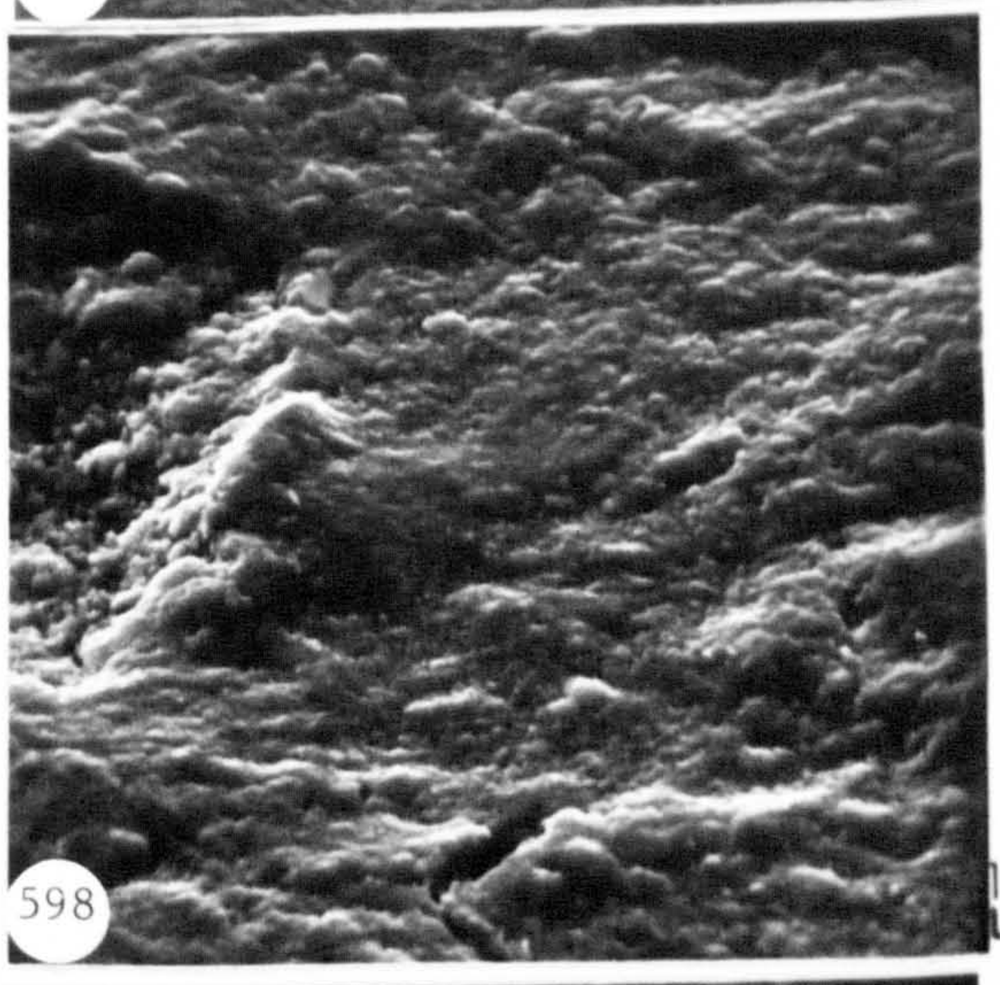


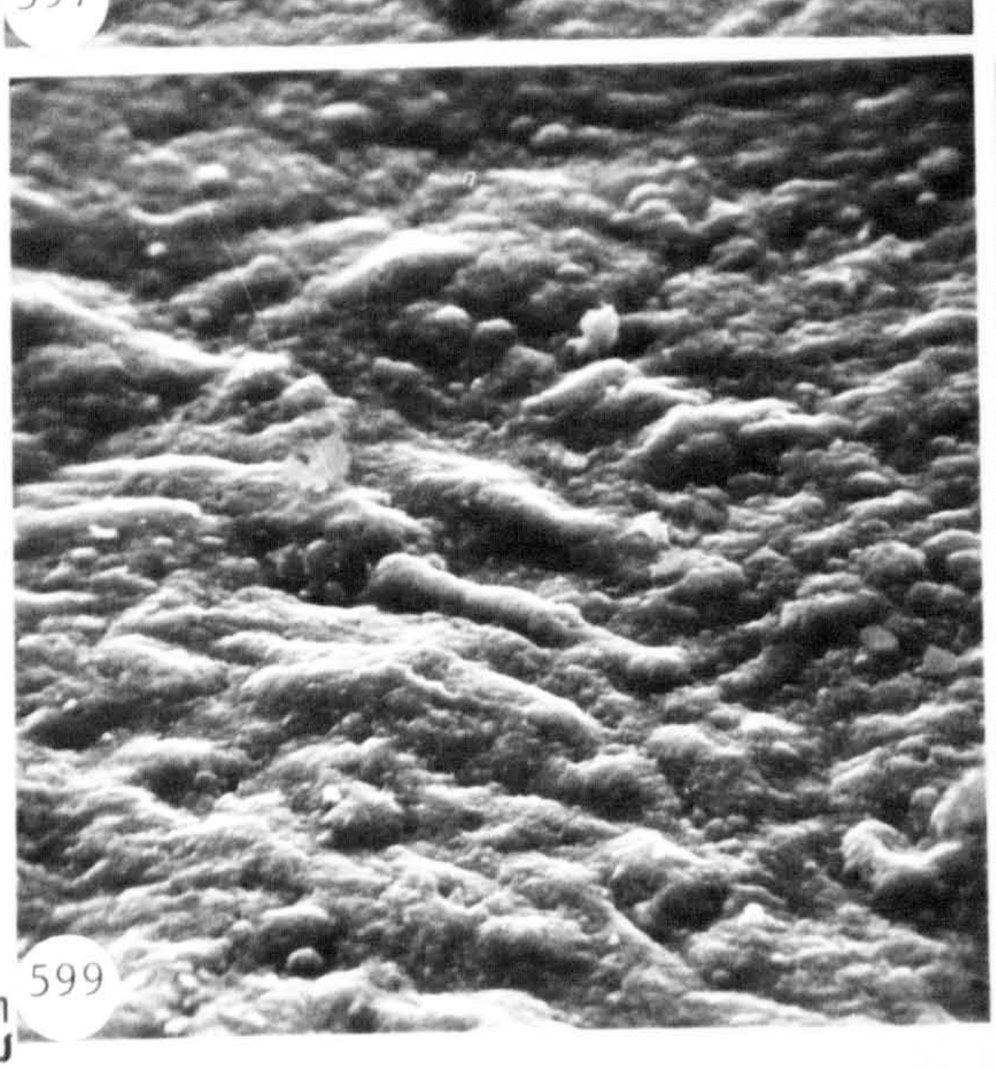
Figures 590 to 594. Scanning electron micrographs of VQMB Pitch-coke Graphite.

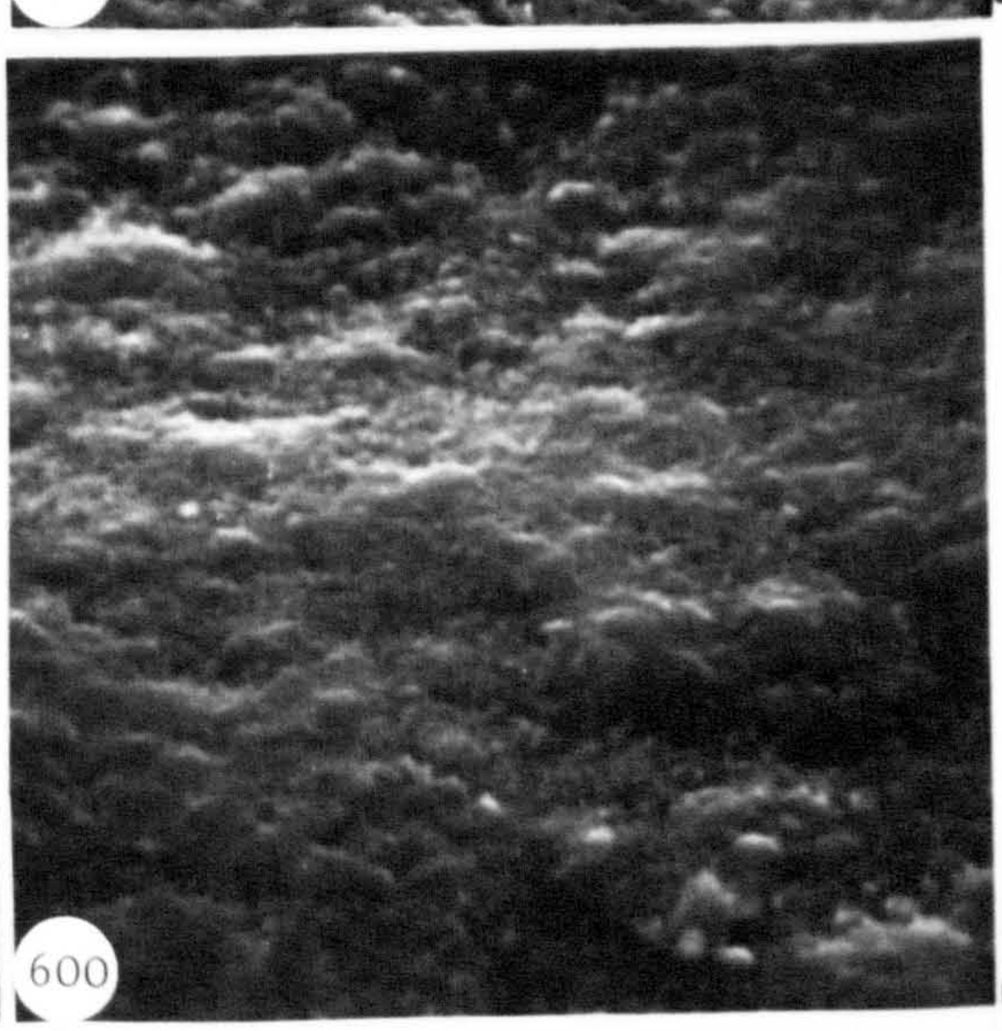


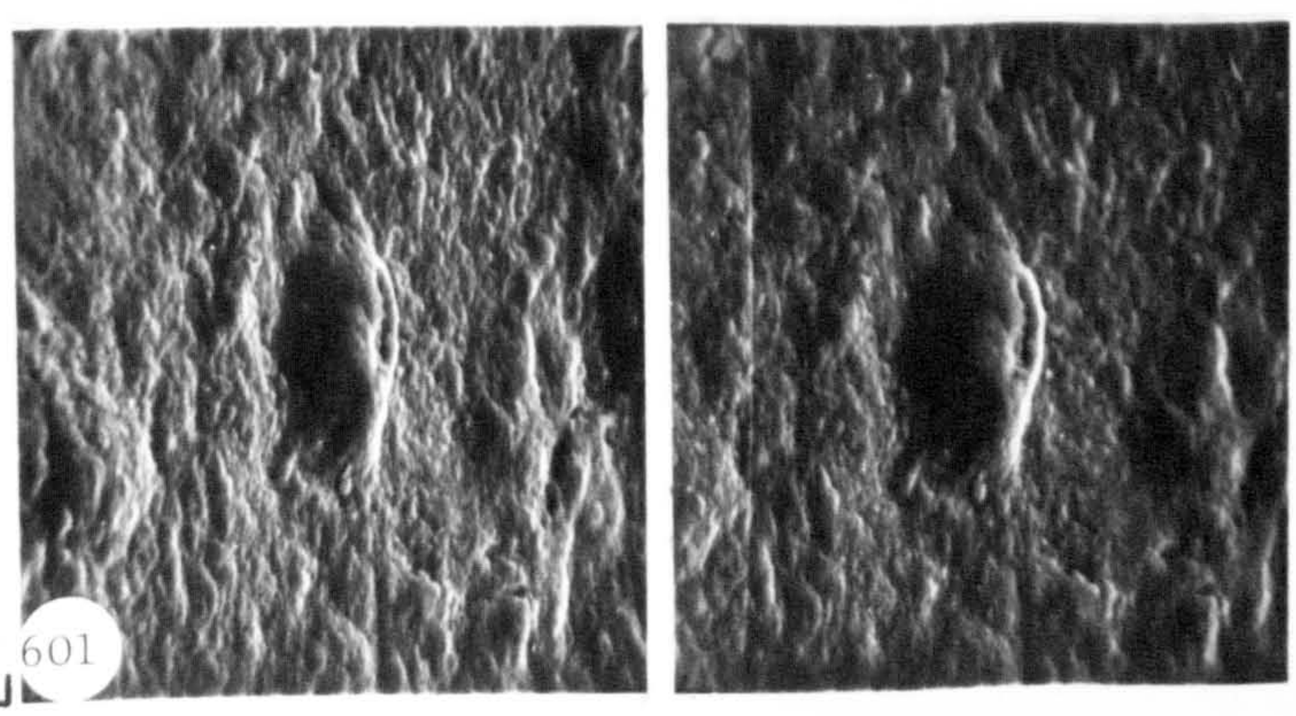




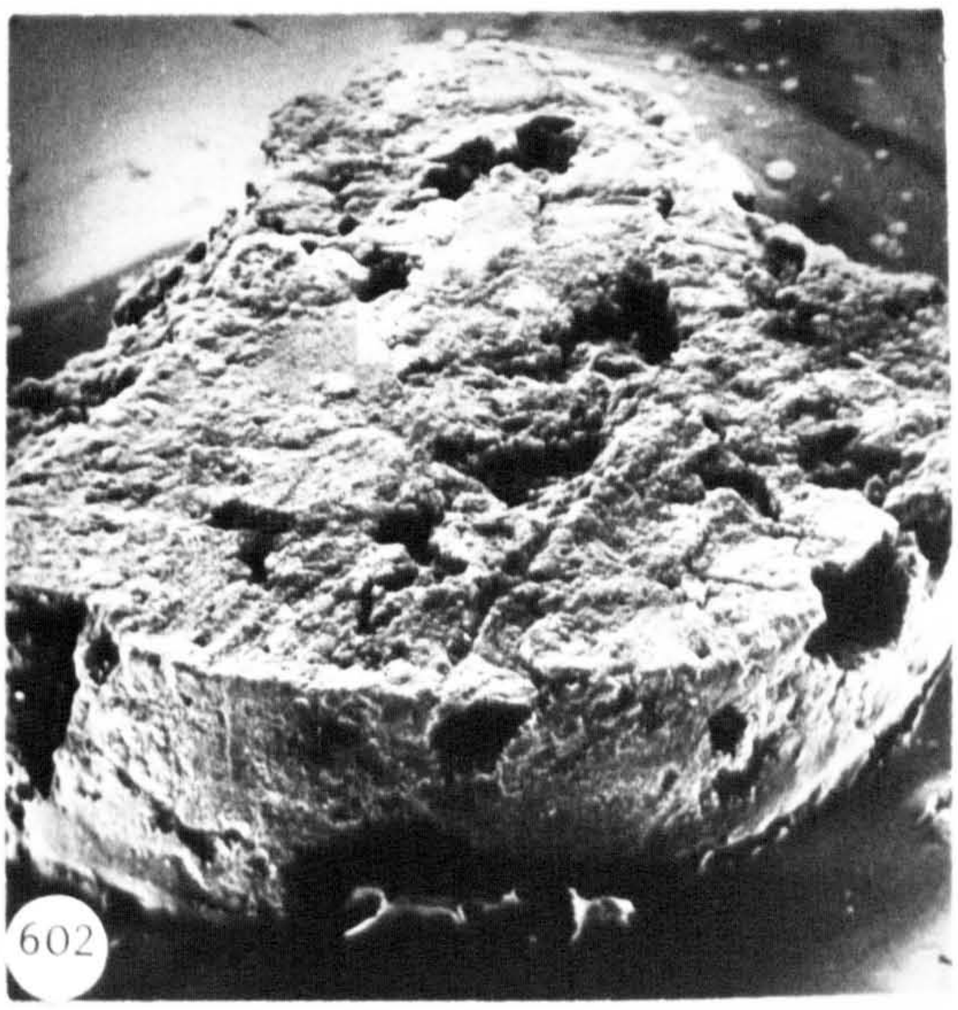


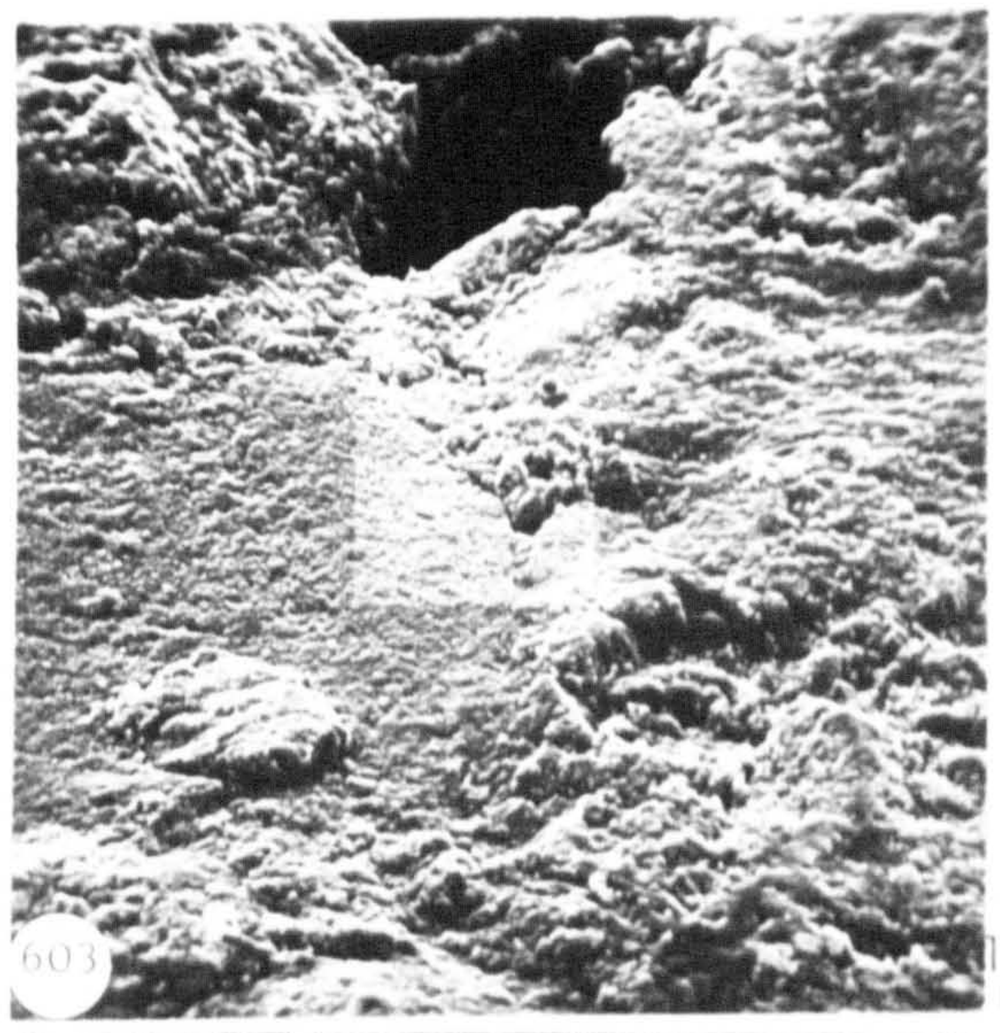




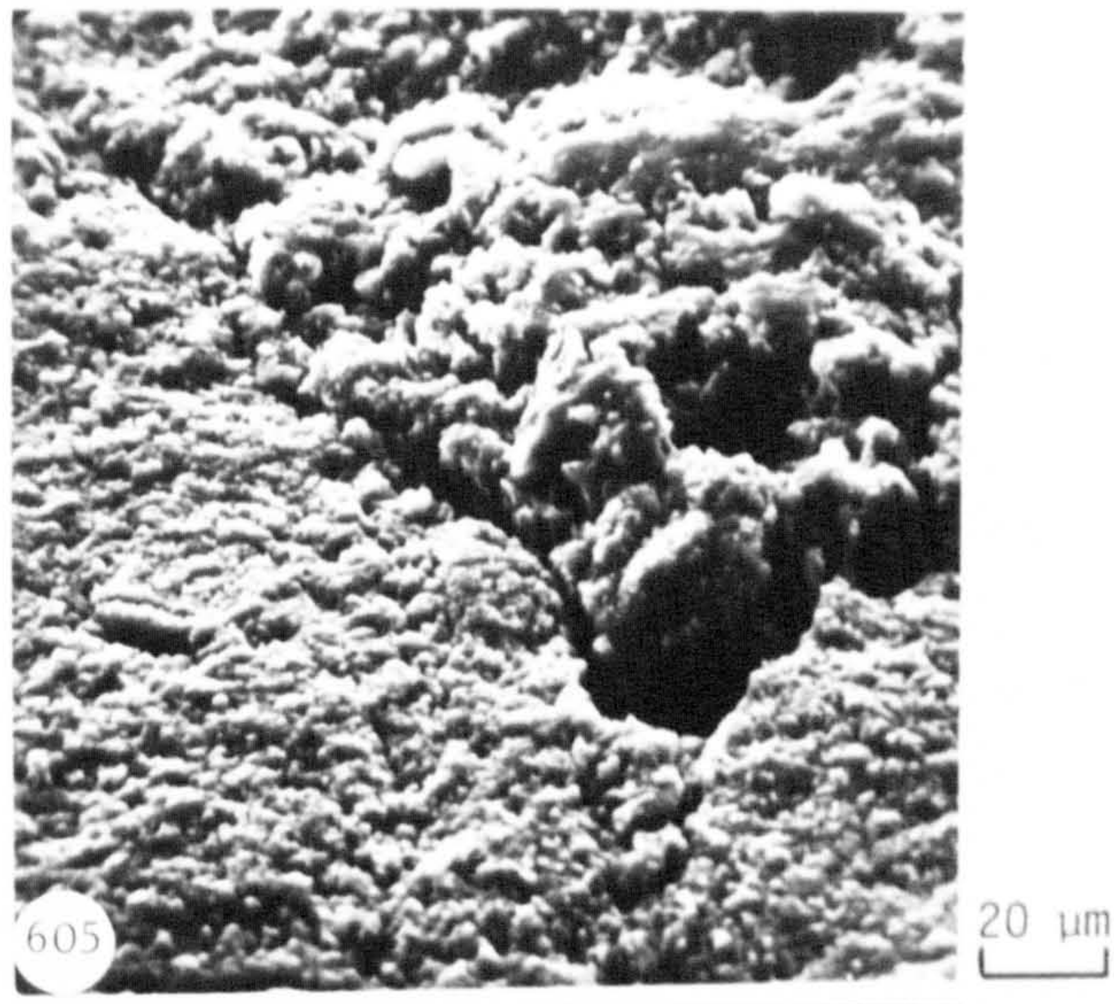


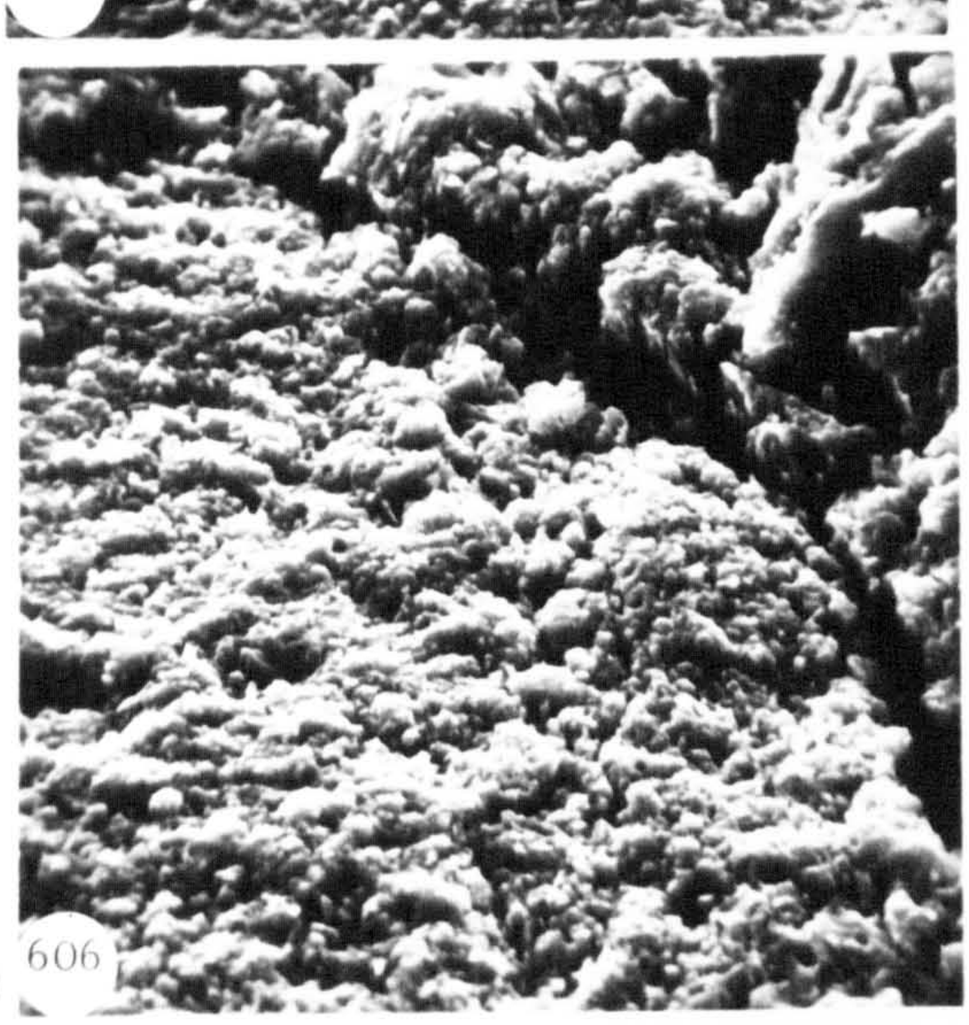
Figures 595 to 601.
Scanning electron micrographs of Pitch-coke Graphite (LZAA) after neutron irradiation, (-1.99% linear growth).

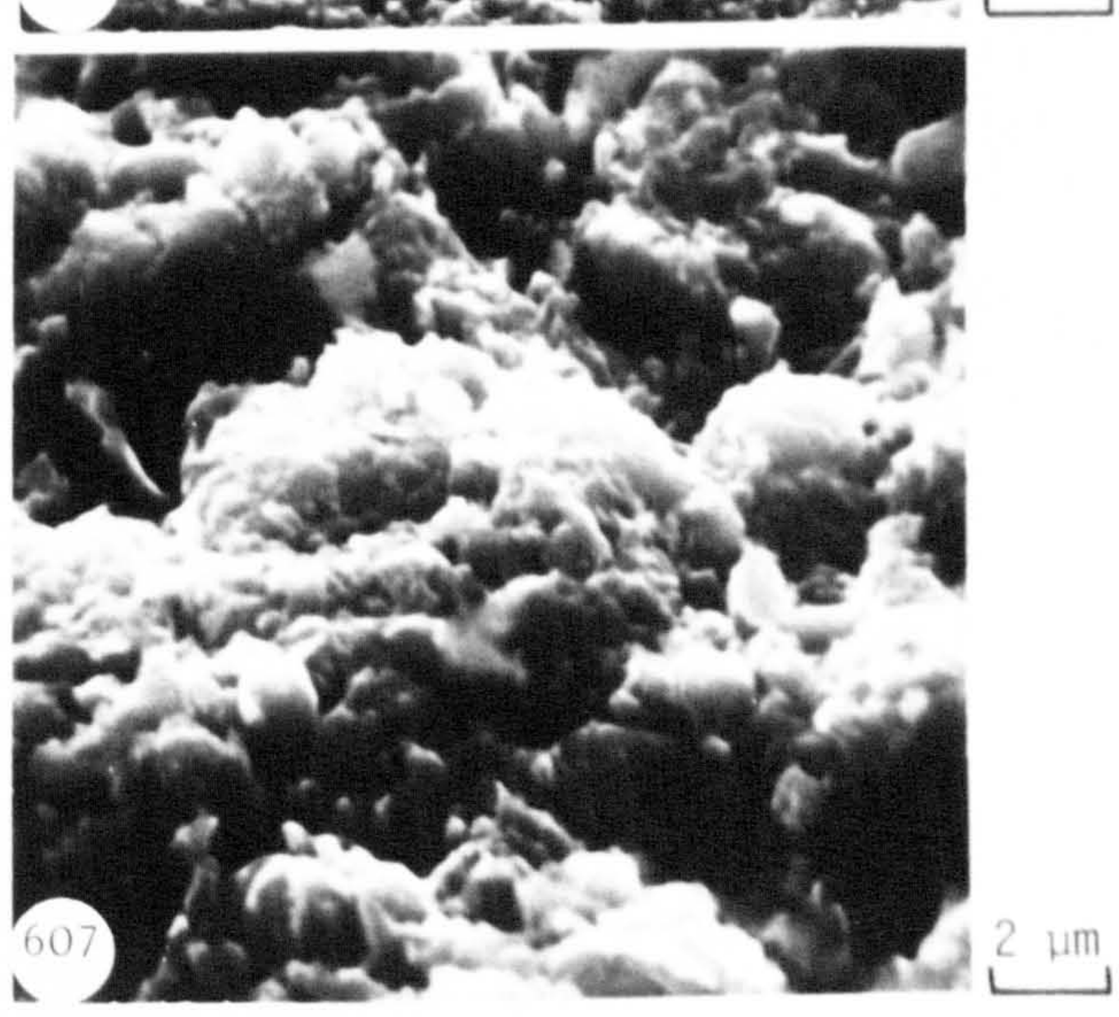


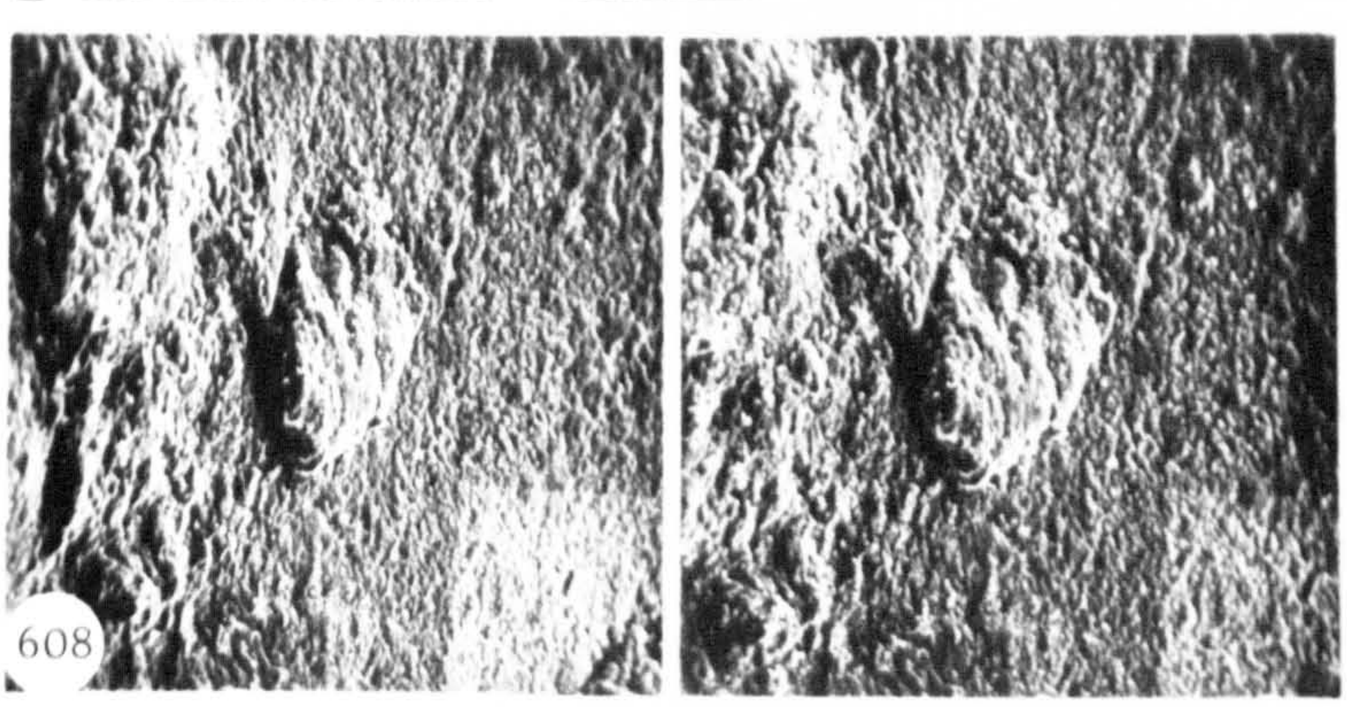




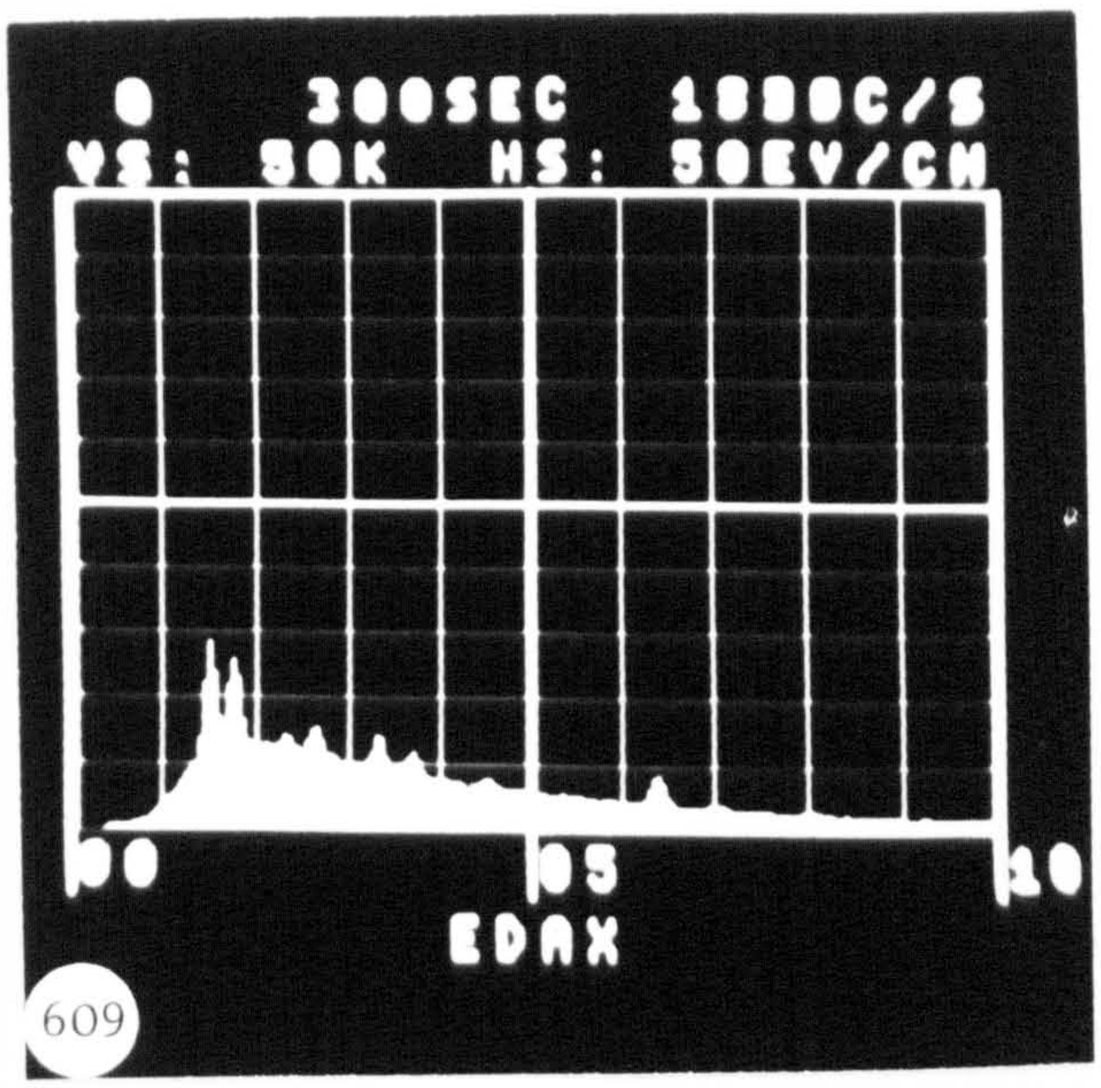




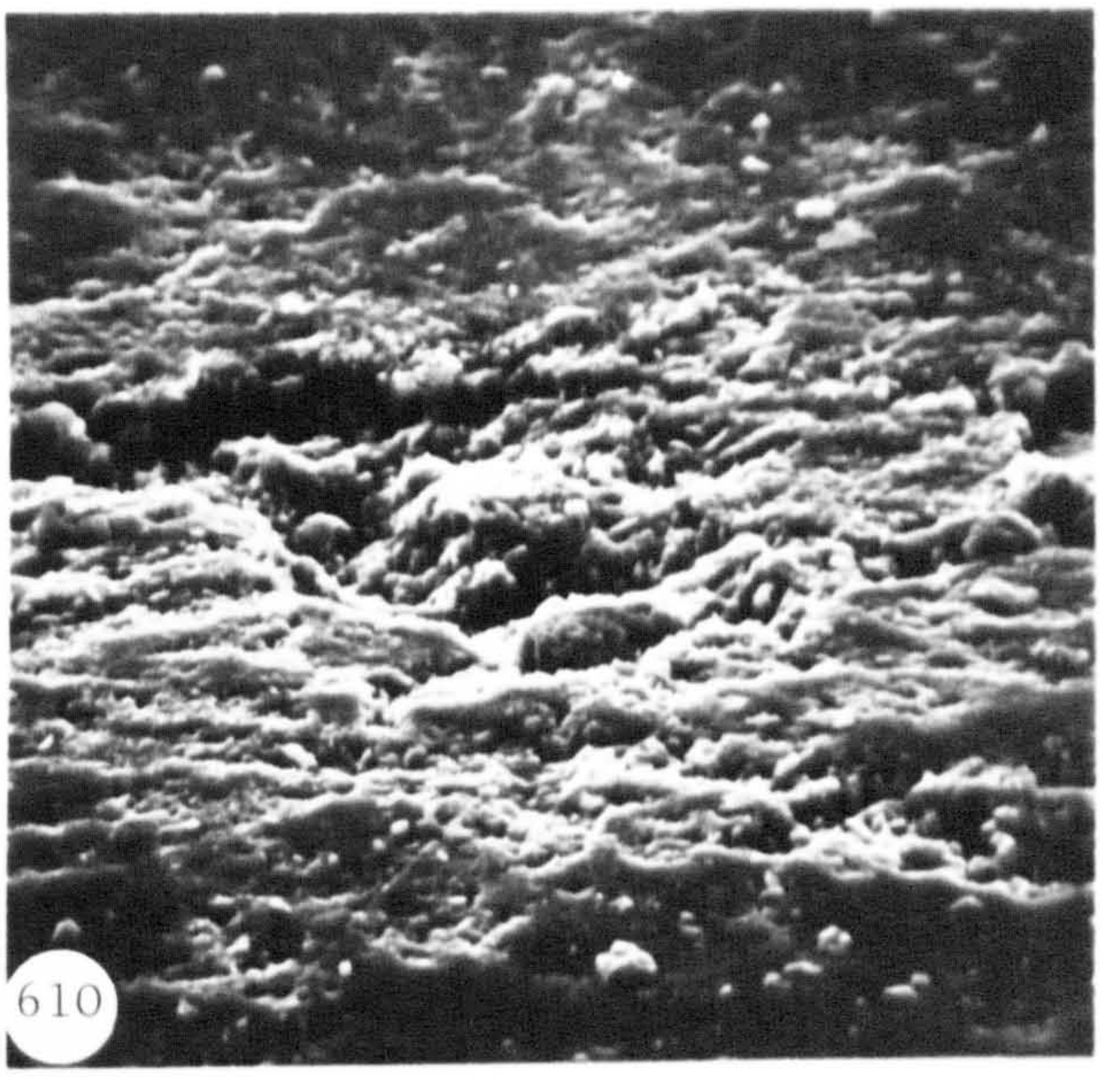




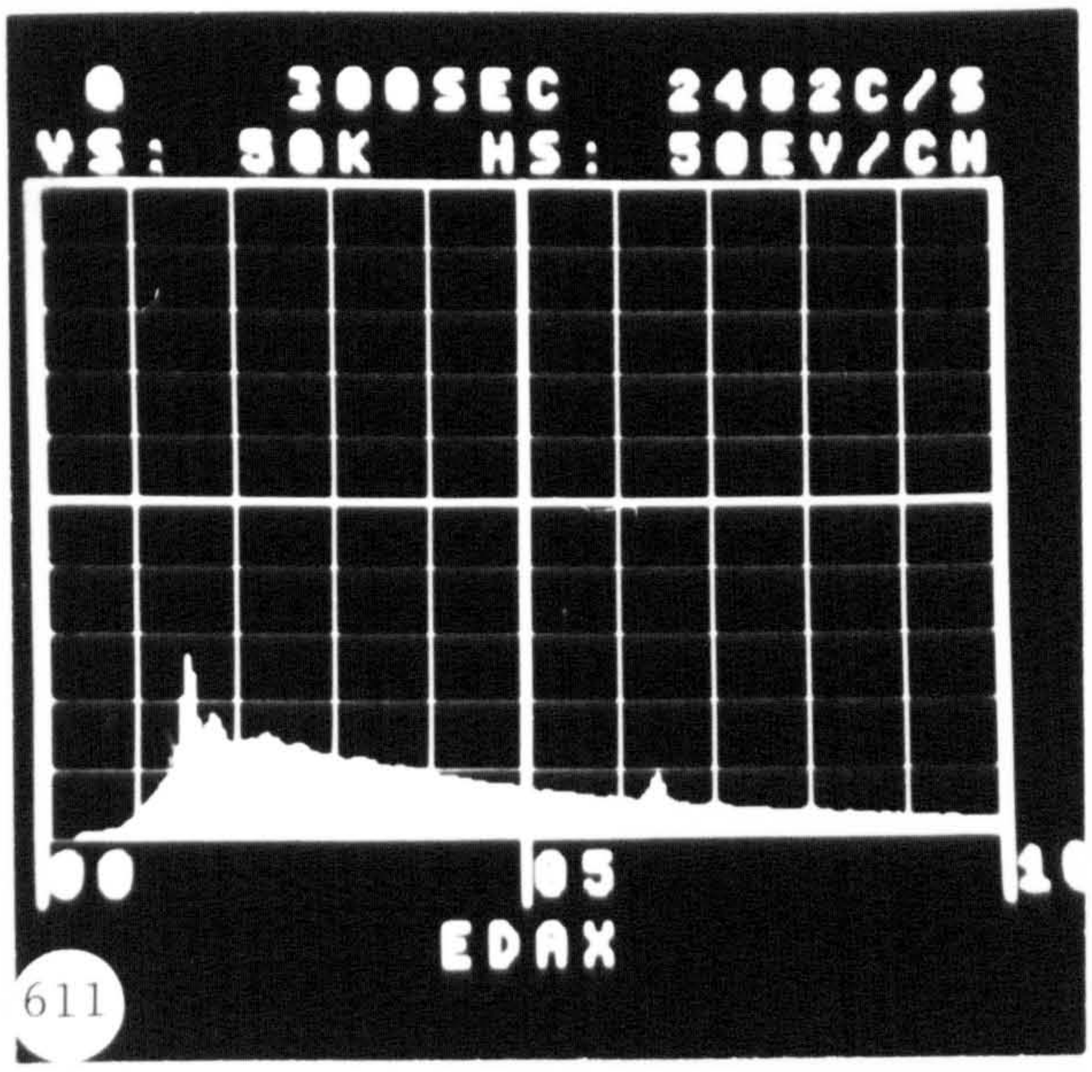
Figures 602 to 608.
Scanning electron micrographs of Pitch-coke Graphite (SBO) after neutron irradiation, (+3.99% linear growth).



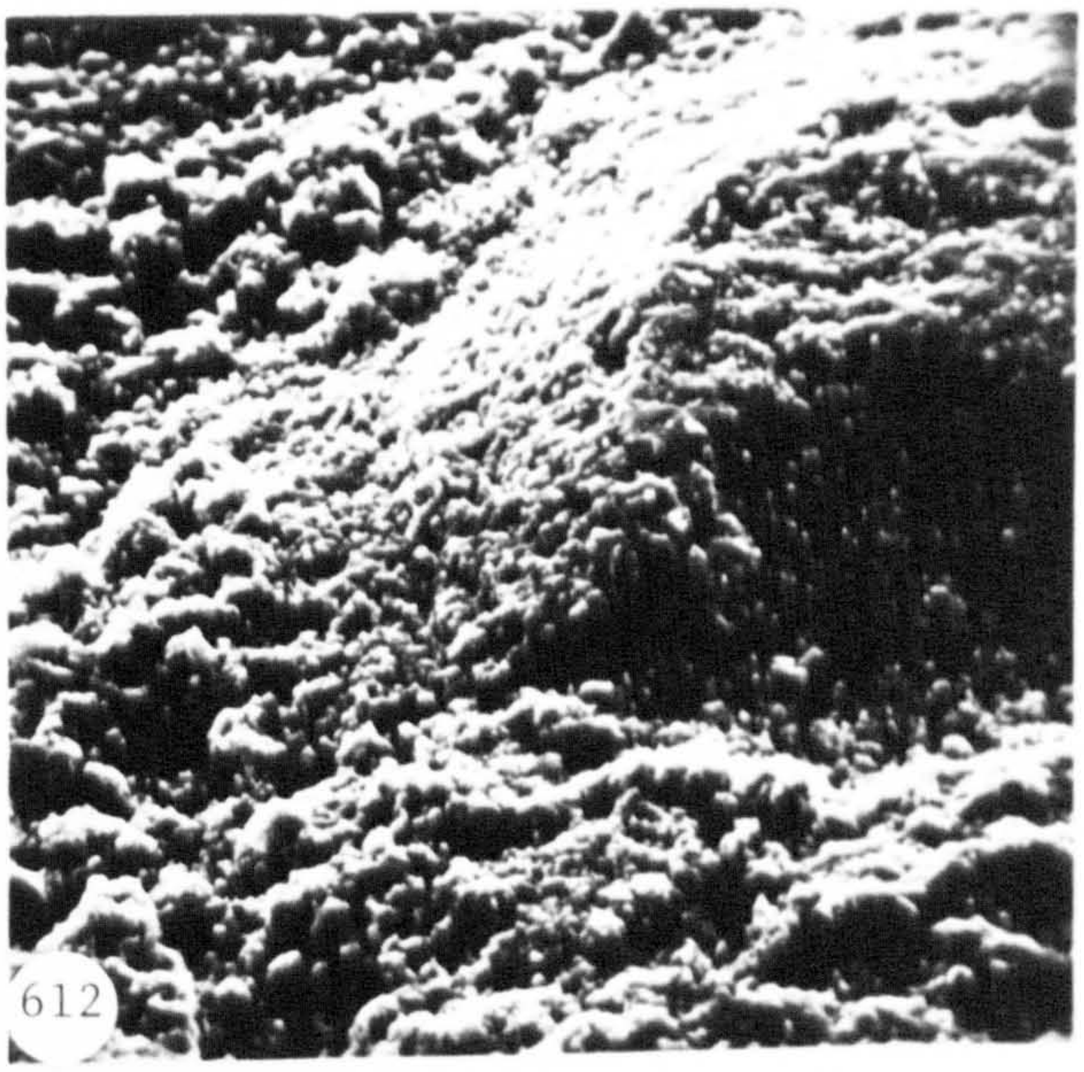
609



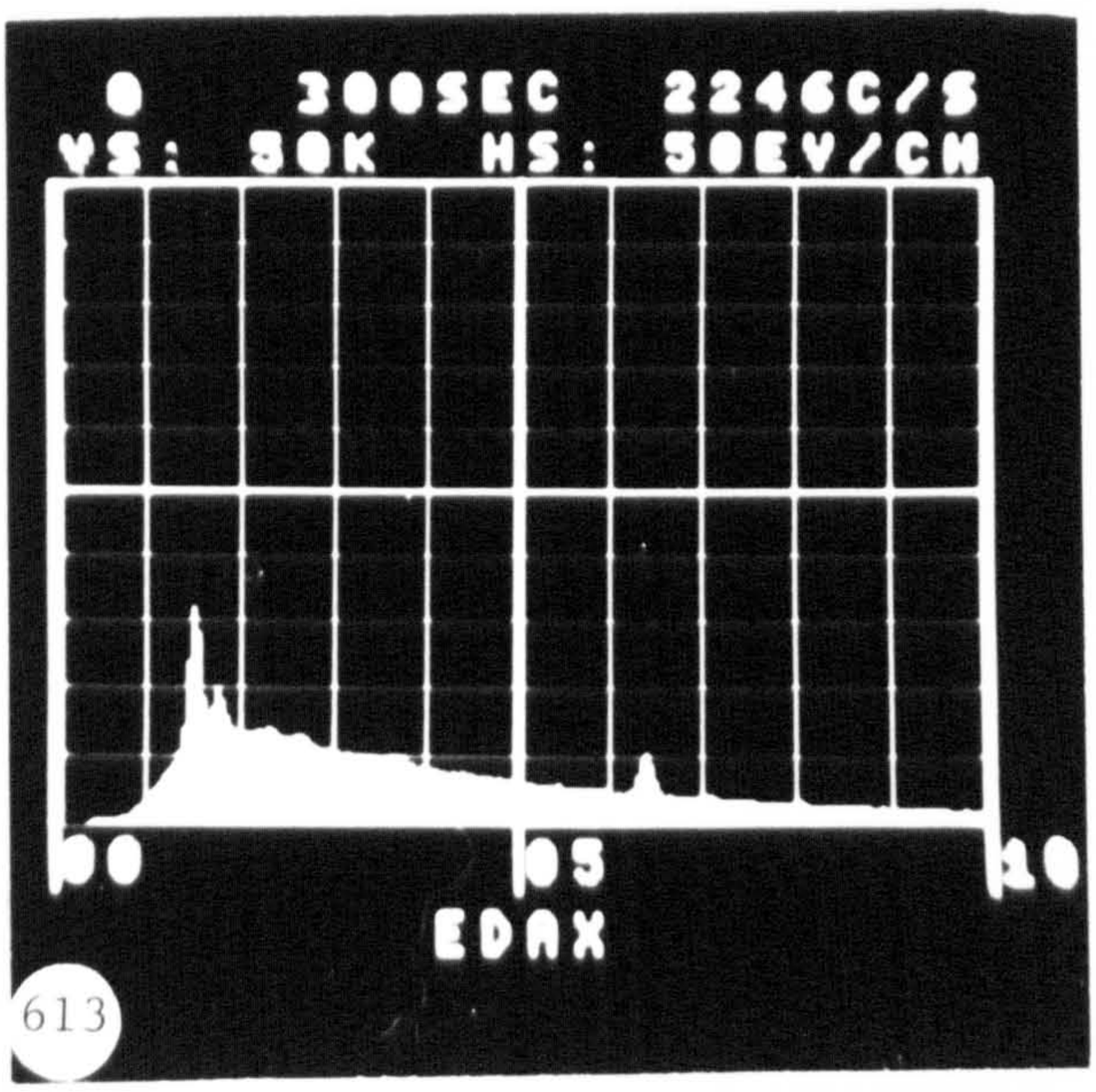
610



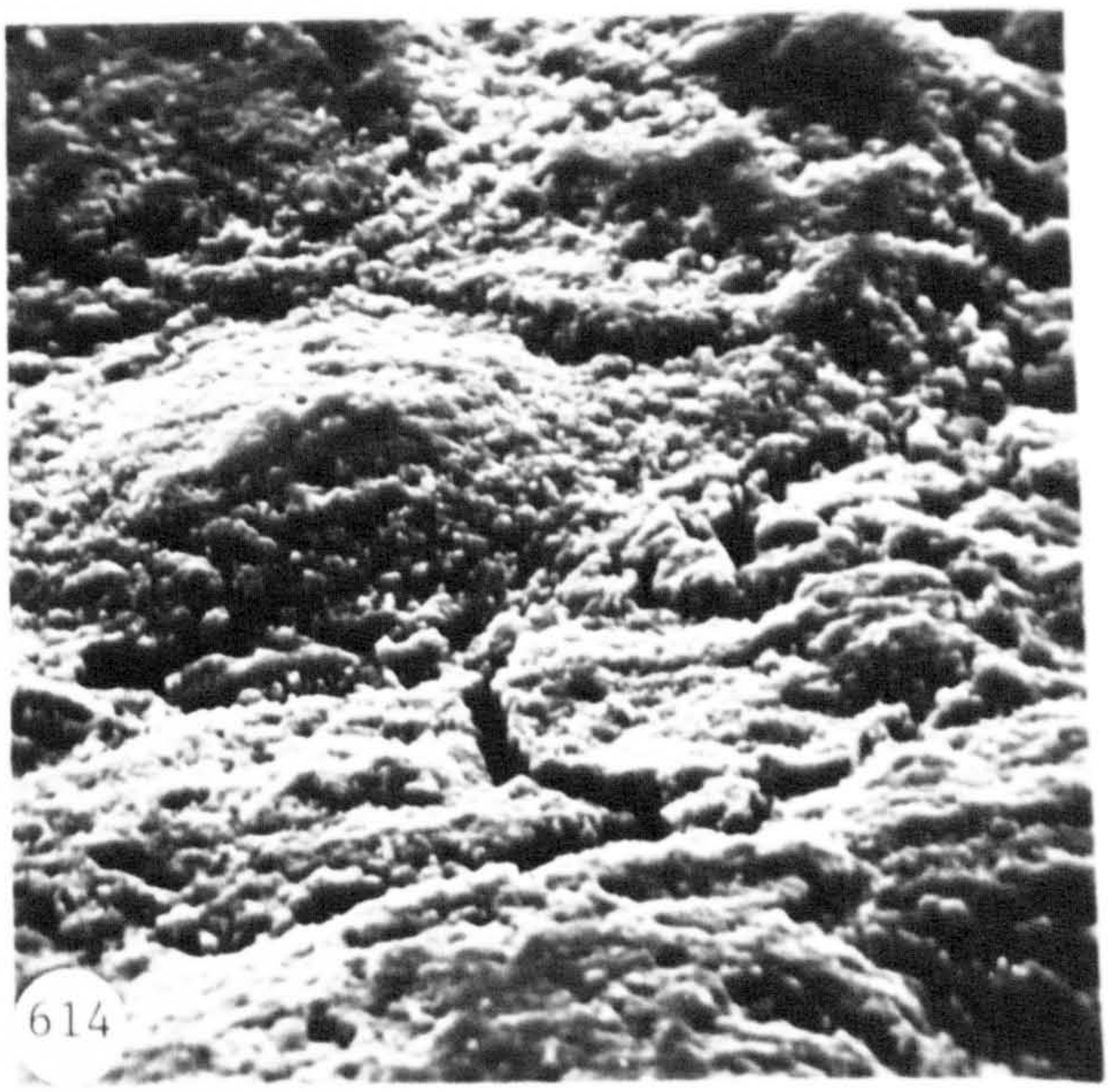
611



612



613



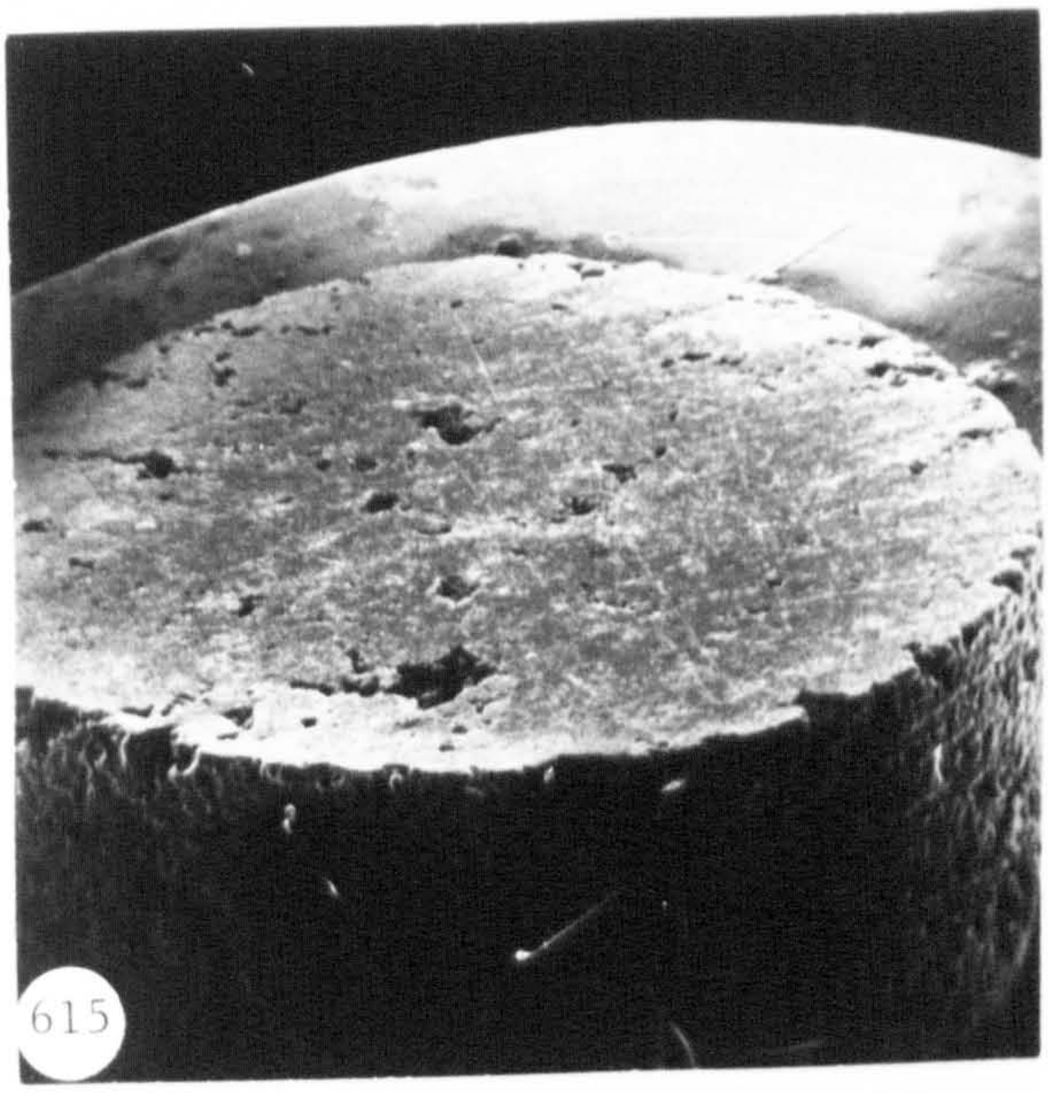
614

X-RAY SPECTRA

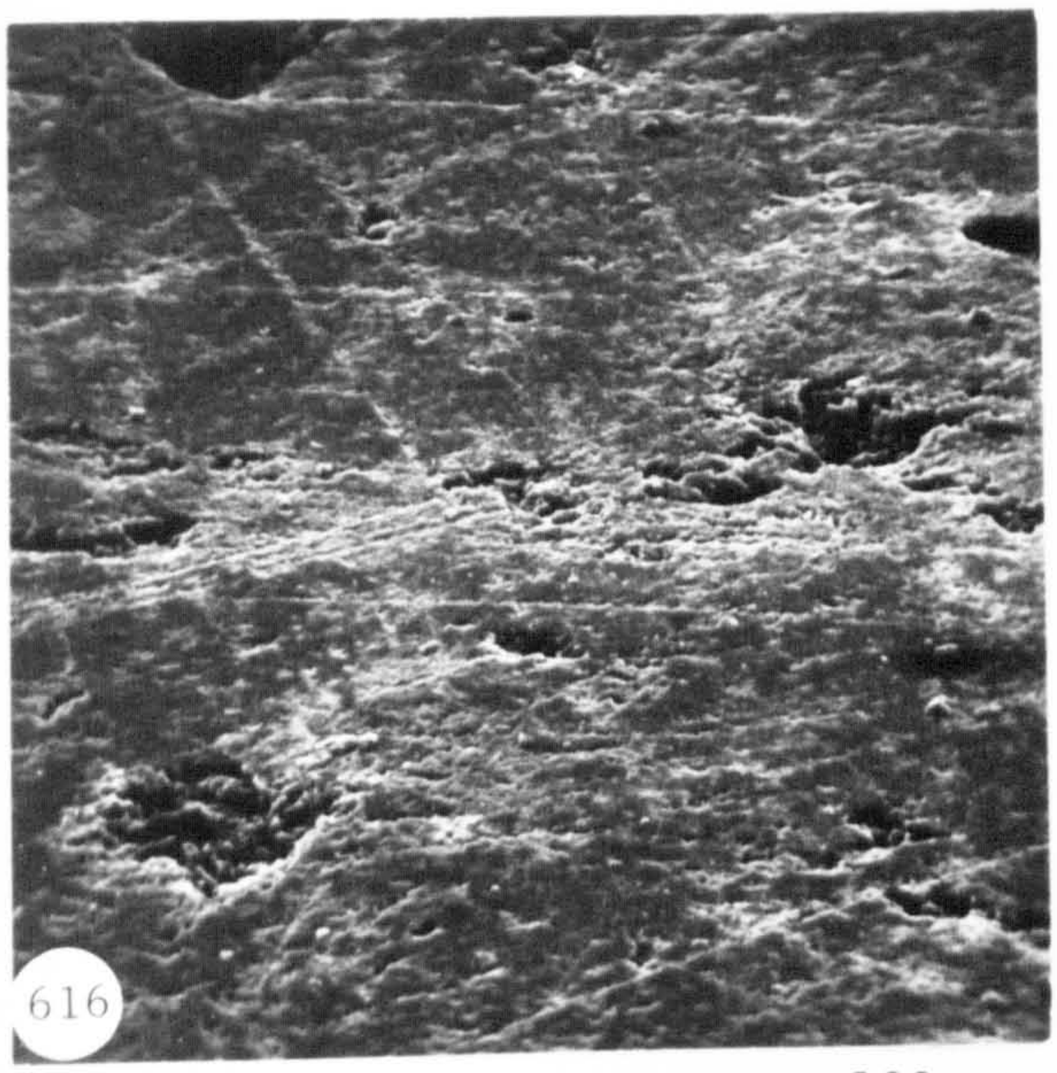
AREA ANALYSED

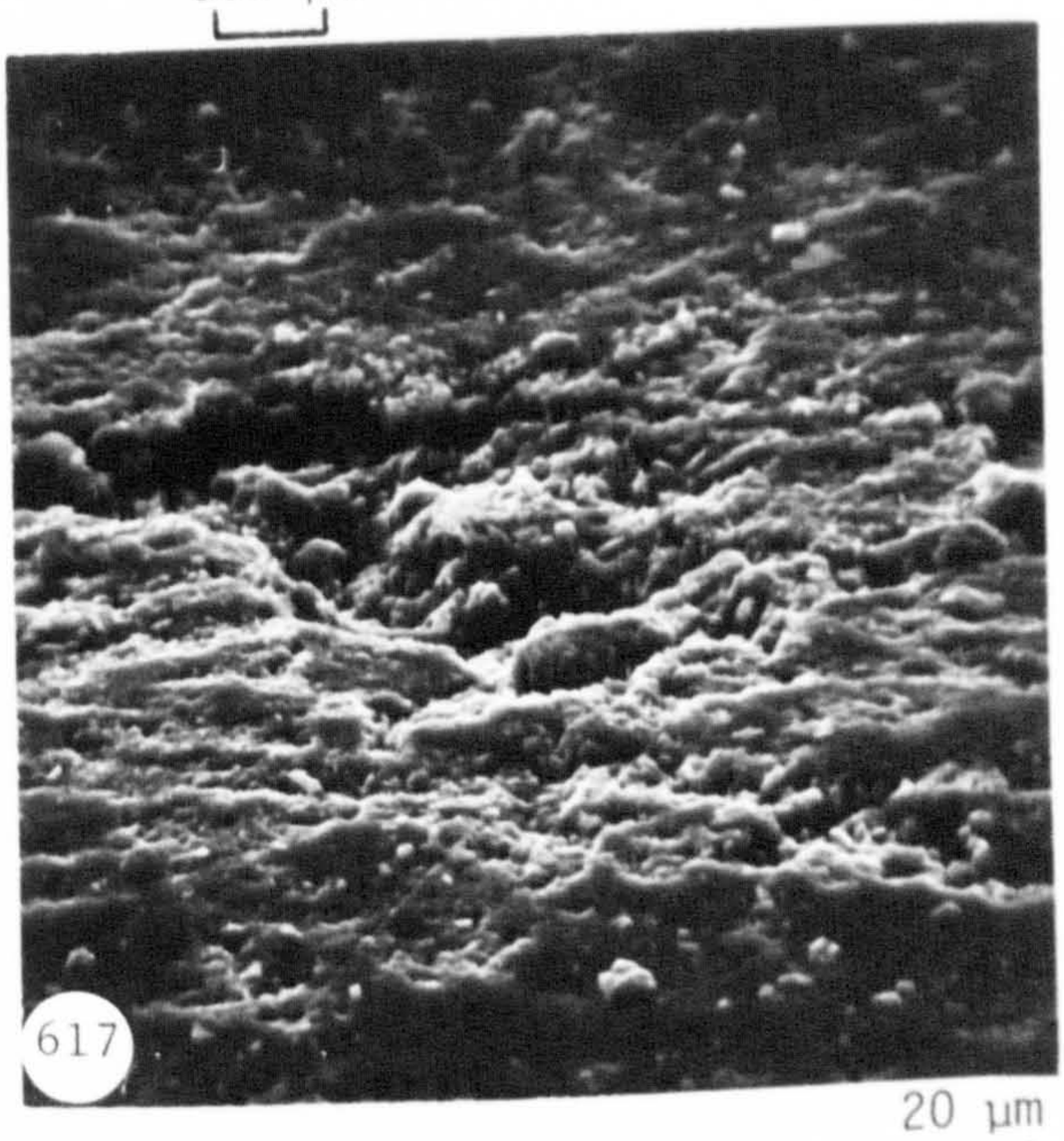
20 µm

Figures 609 to 614. X-ray spectra of Gilso-carbon Graphite (NA); control (Figures 609 and 610), FRC (Figures 611 and 612) and HAB (Figures 613 and 614).



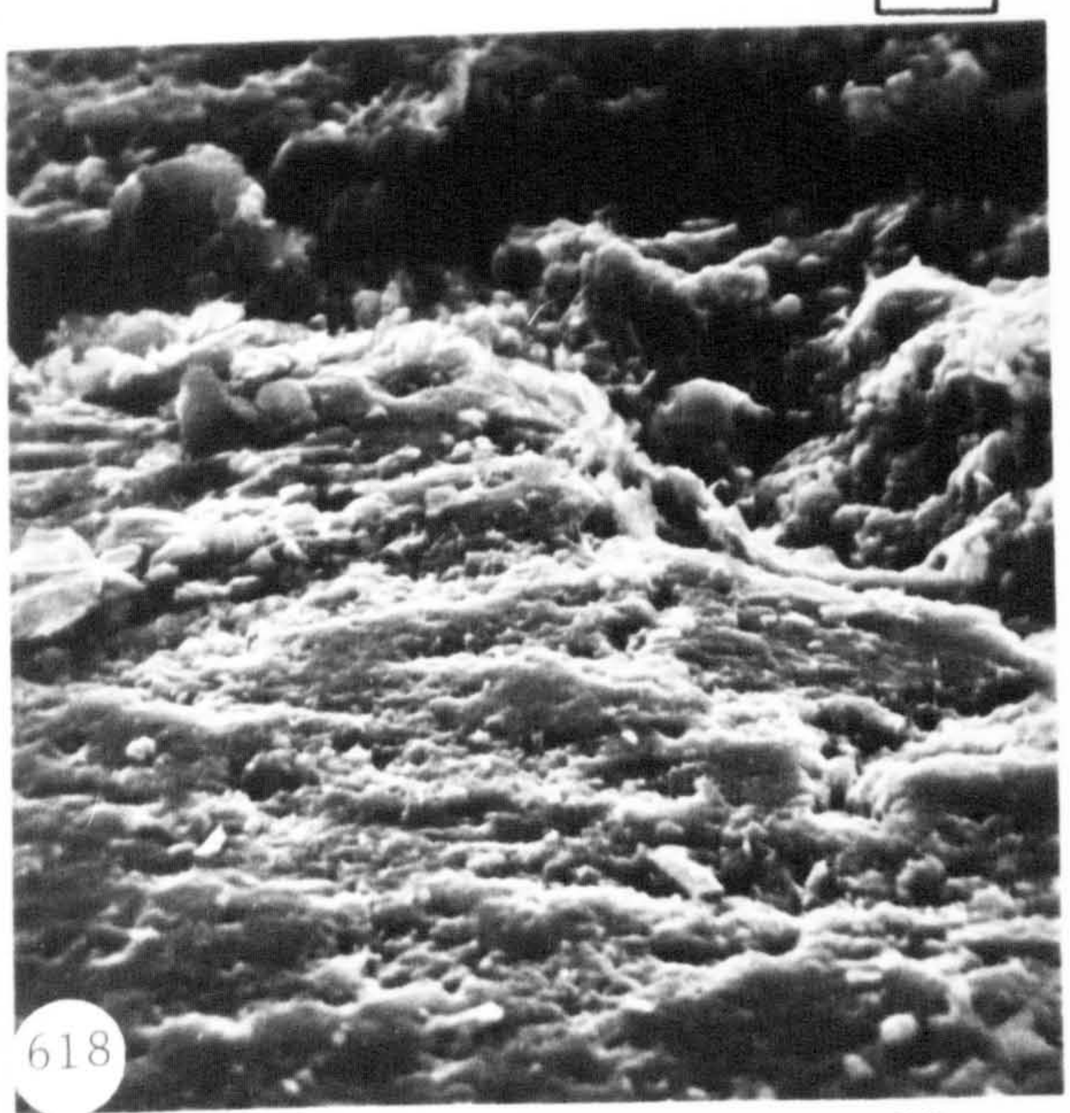
500 µm

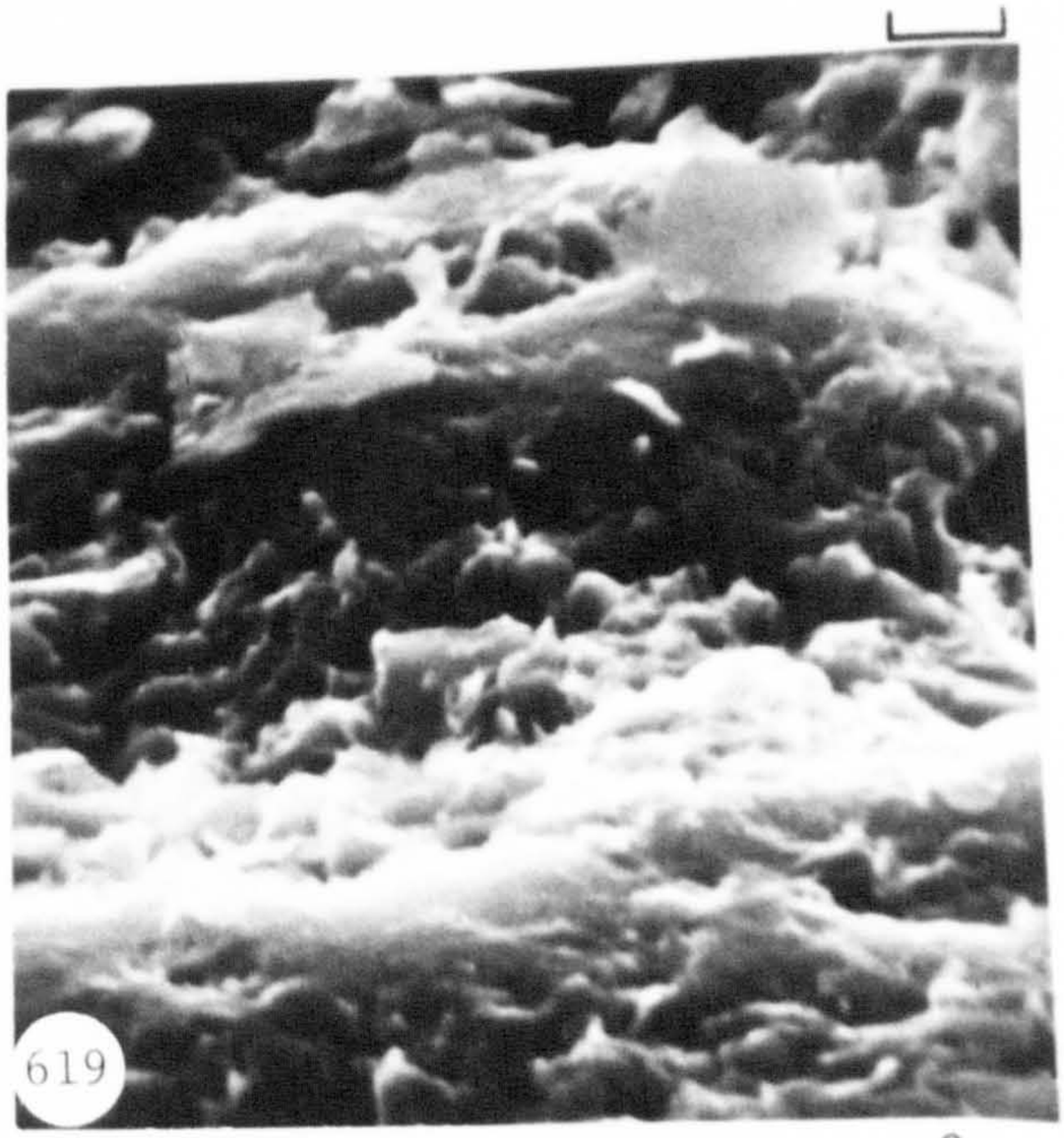




100 µm

20 µm

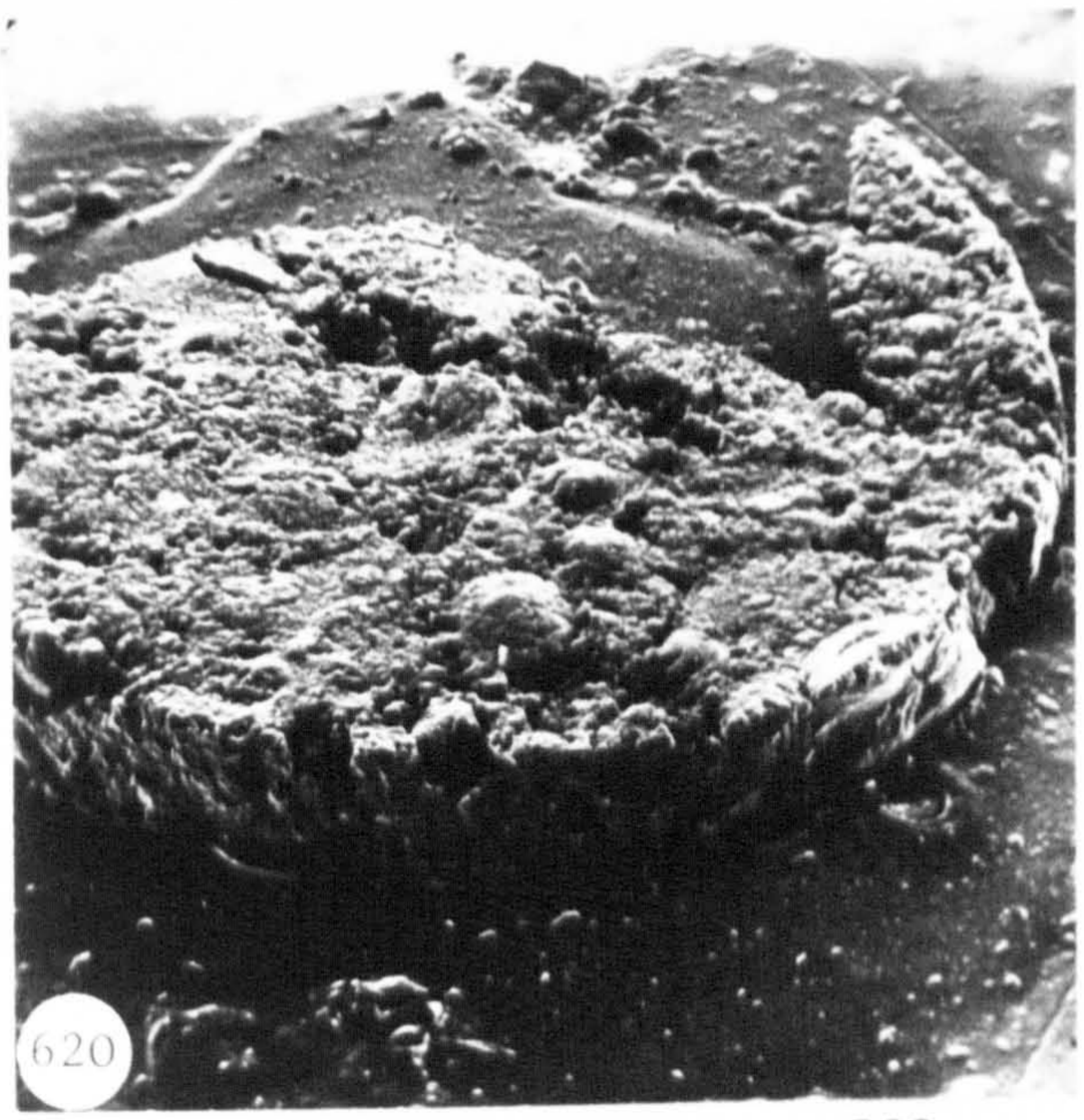




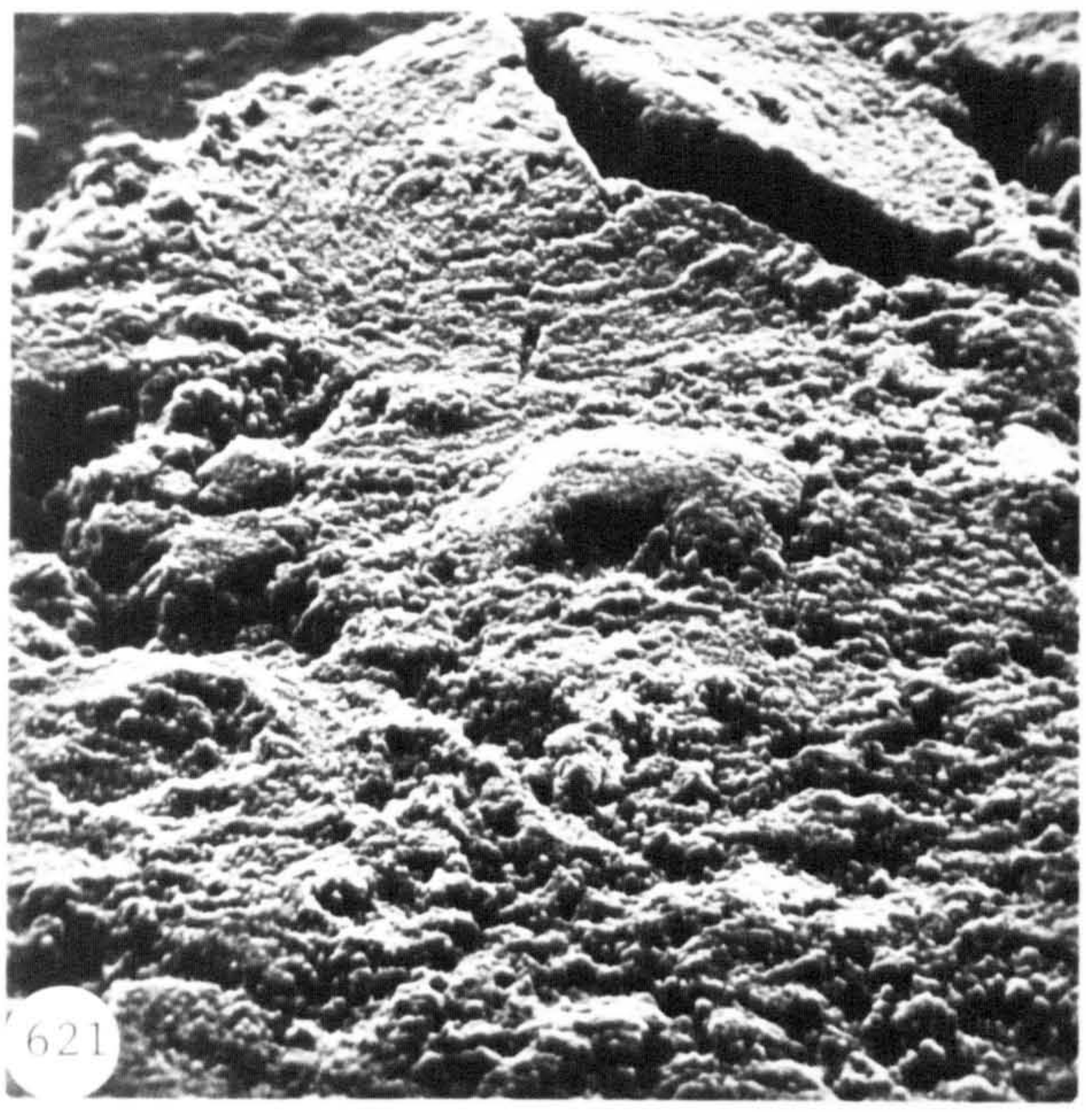
10 µm

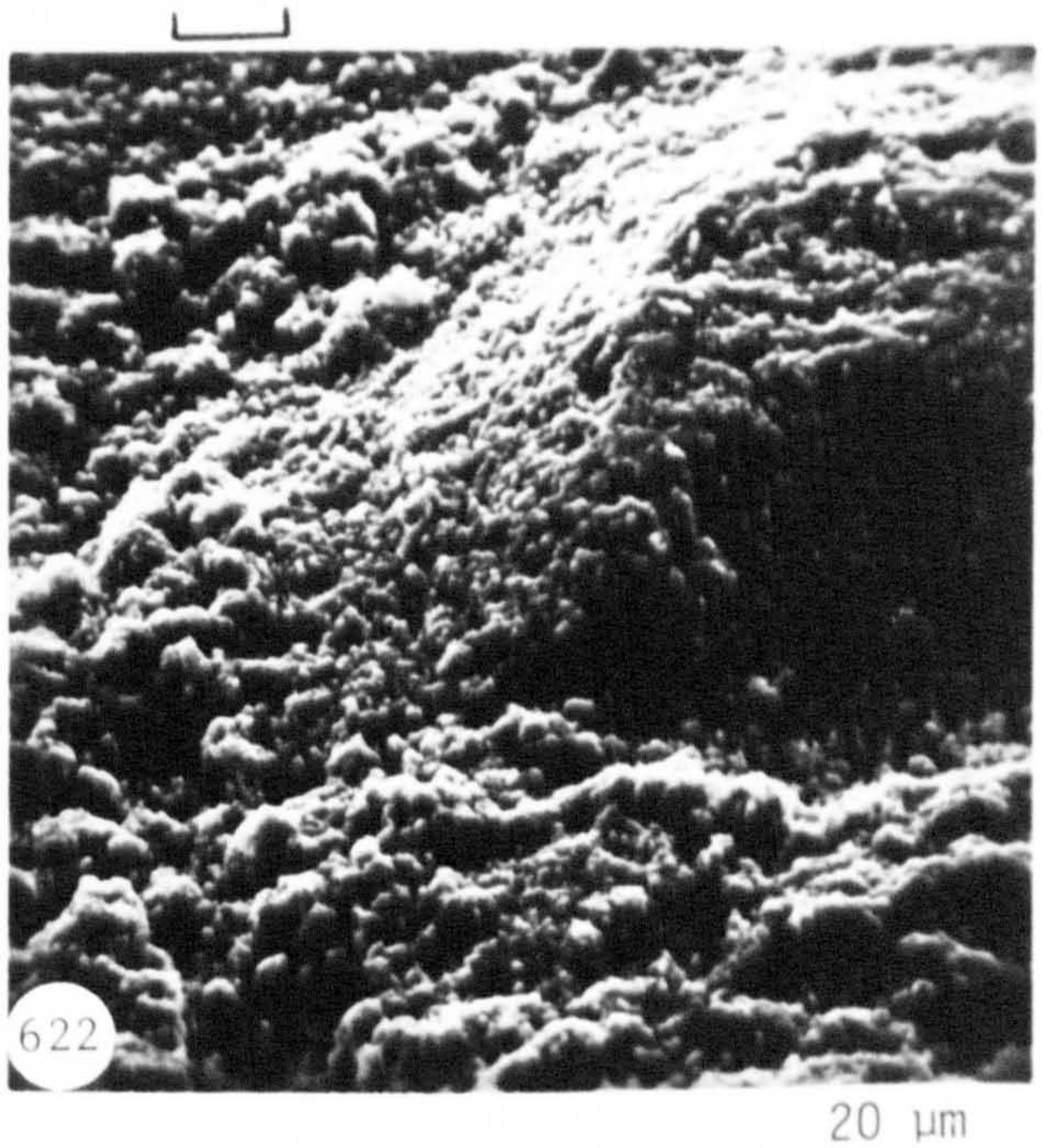
2 µm

Figures 615 to 619. Scanning electron micrographs of Gilso-carbon Graphite (NA).



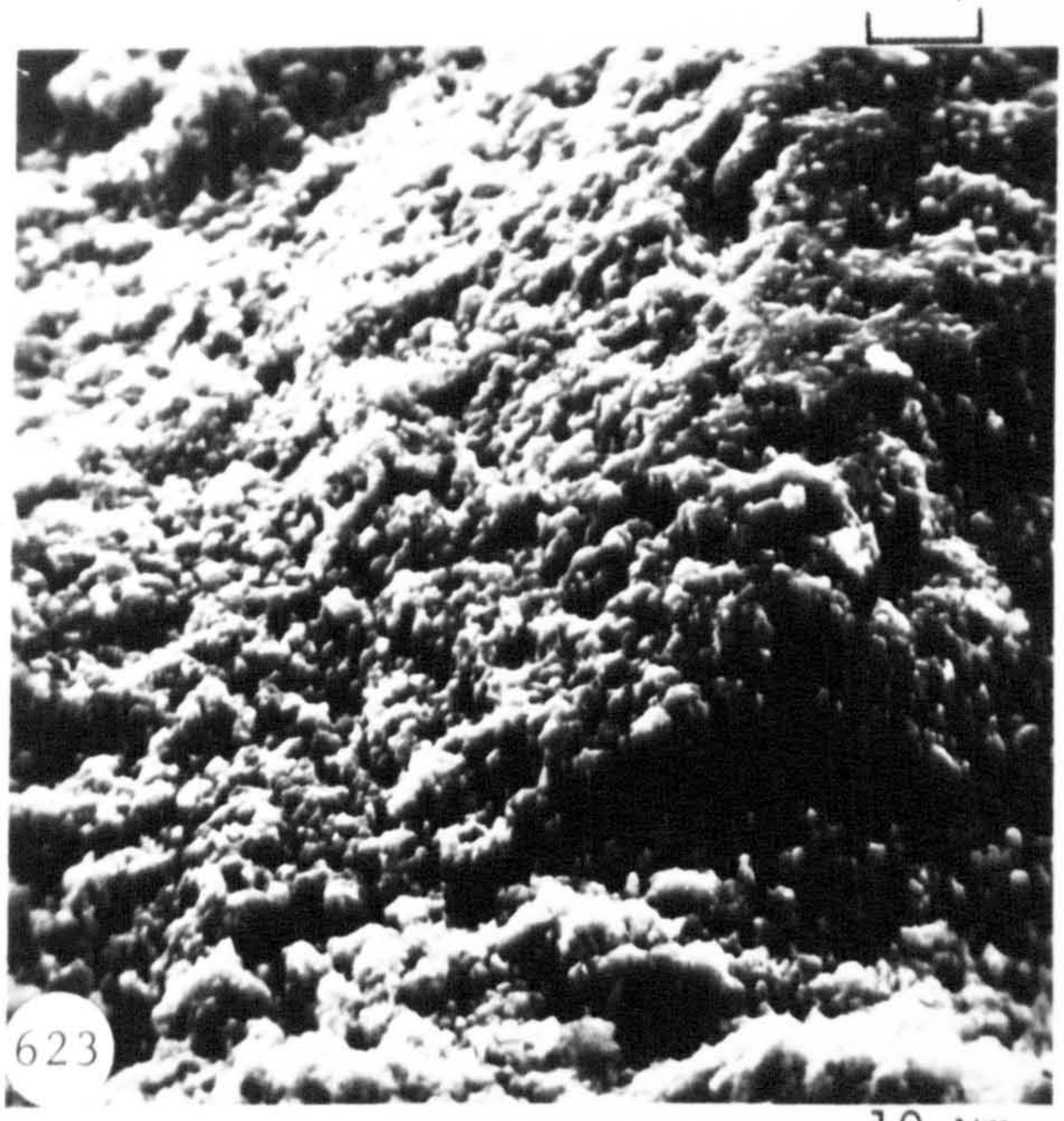
500 µm

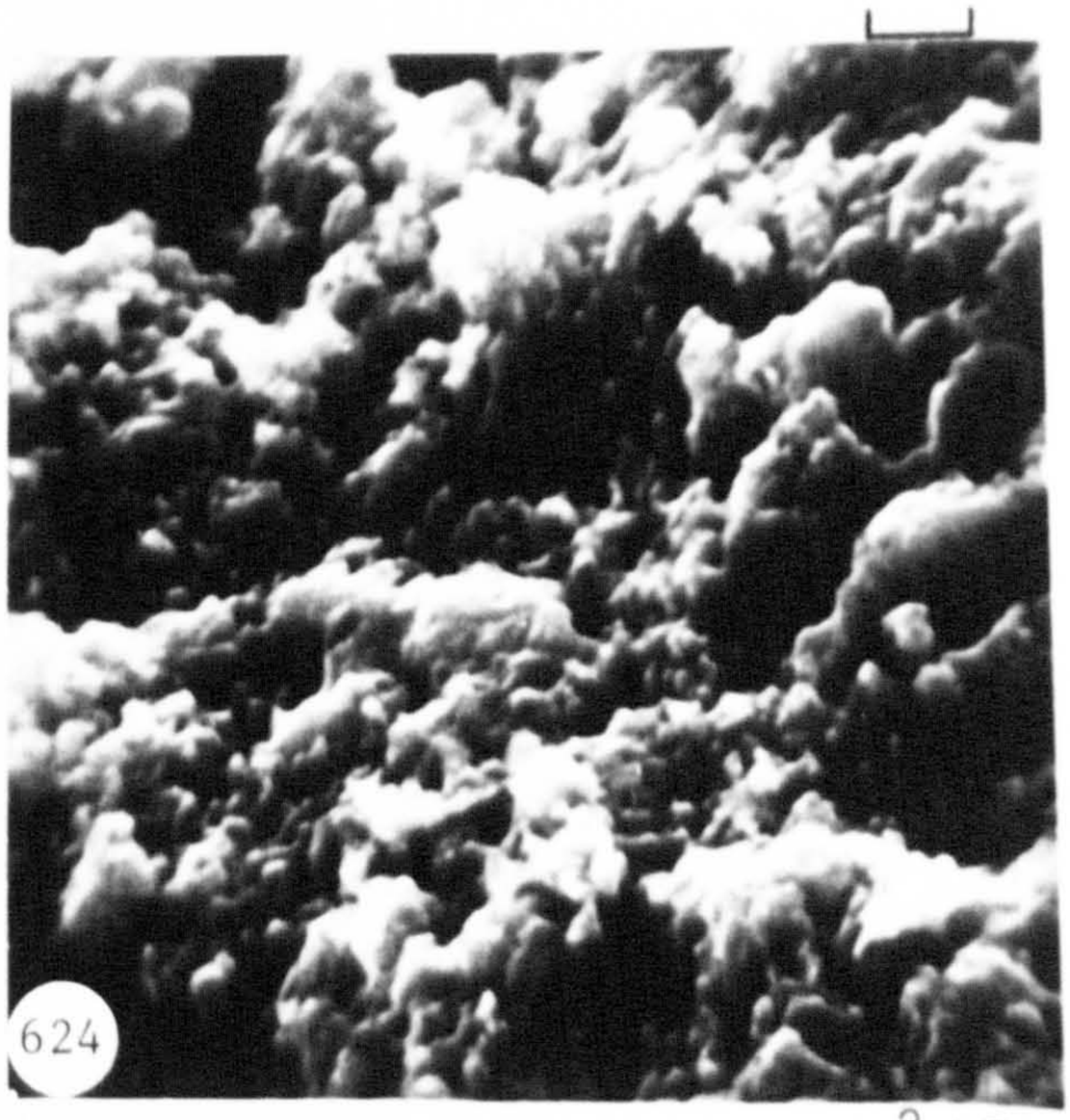




100 µm

20 µm

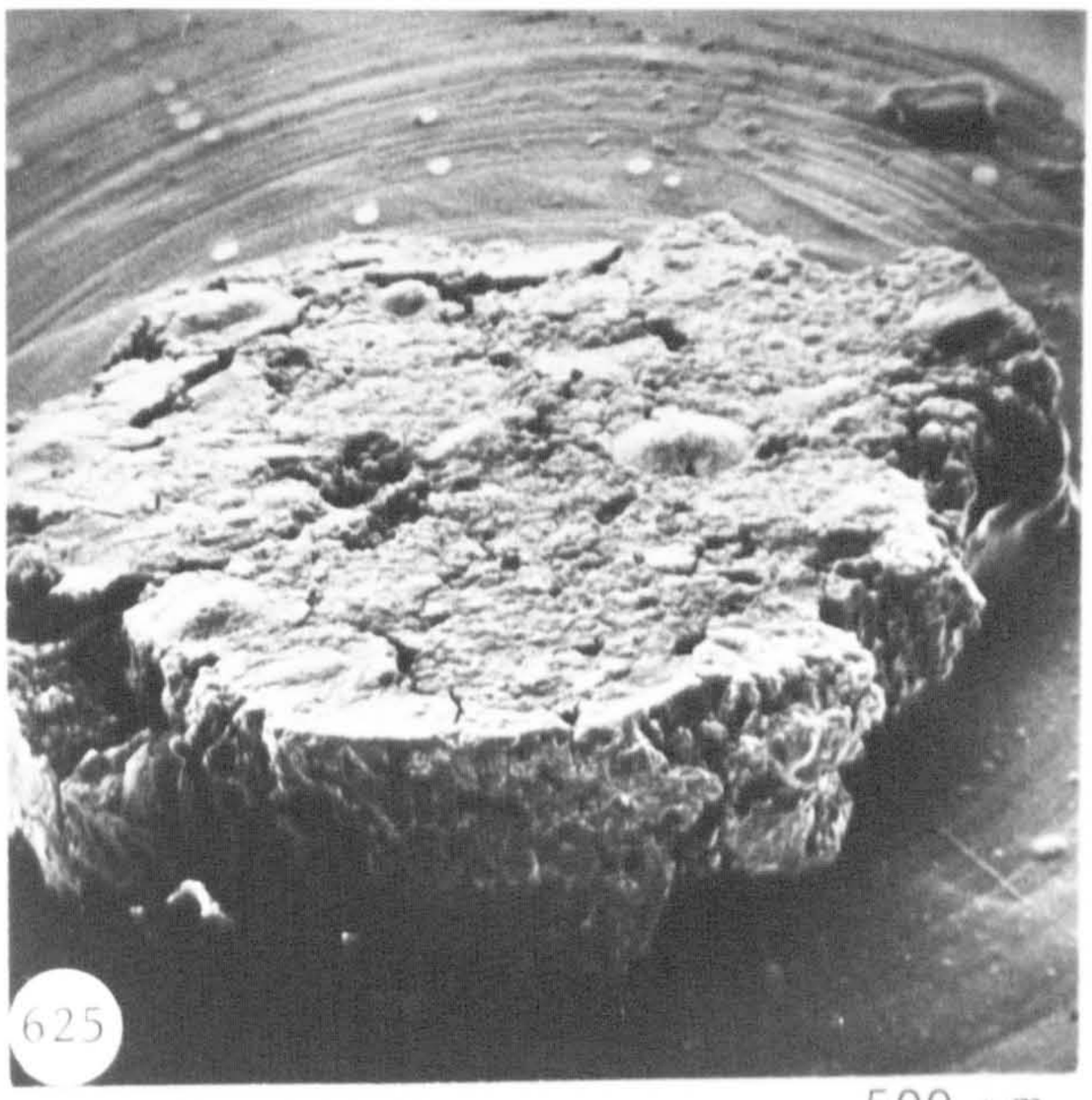


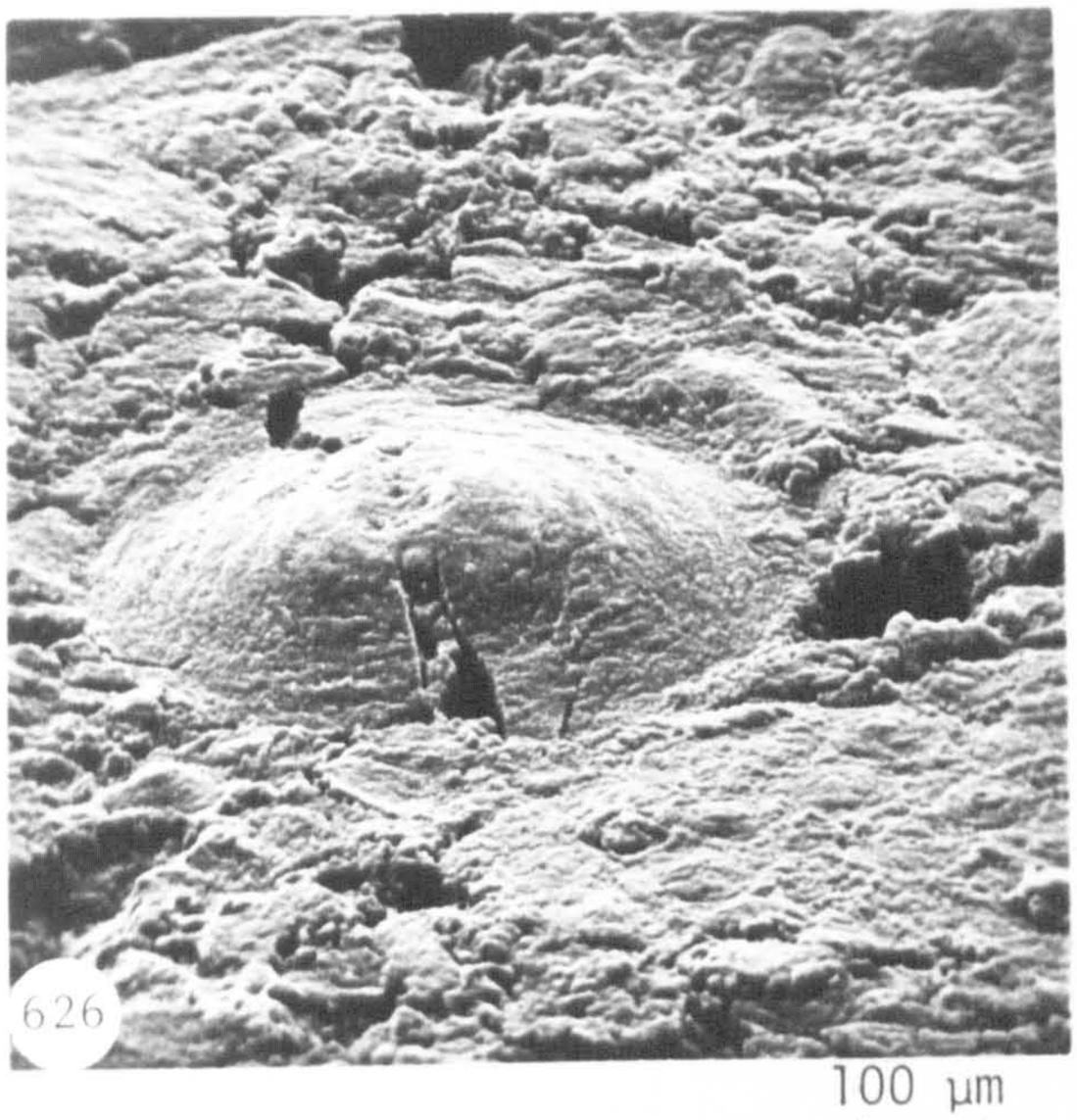


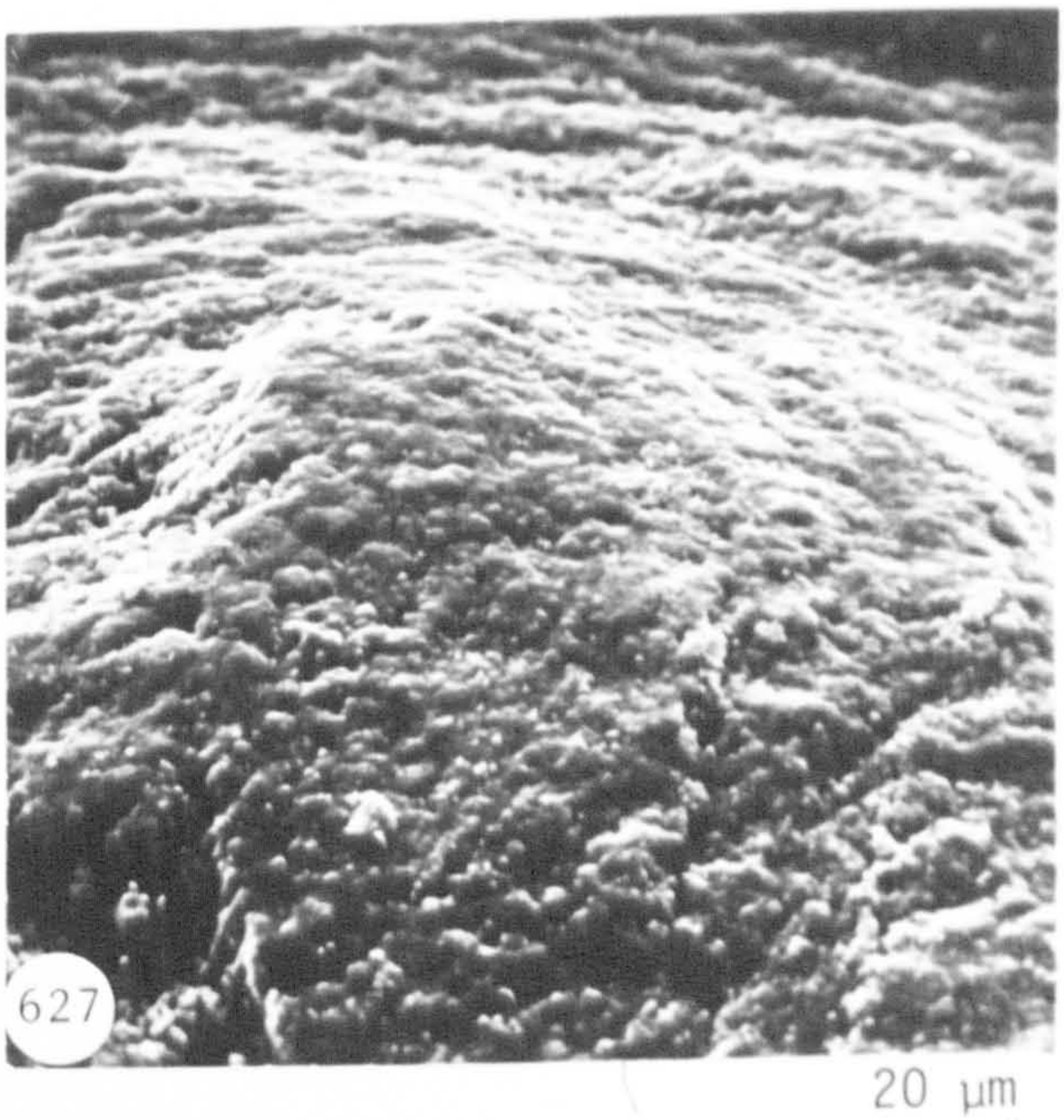
10 µm

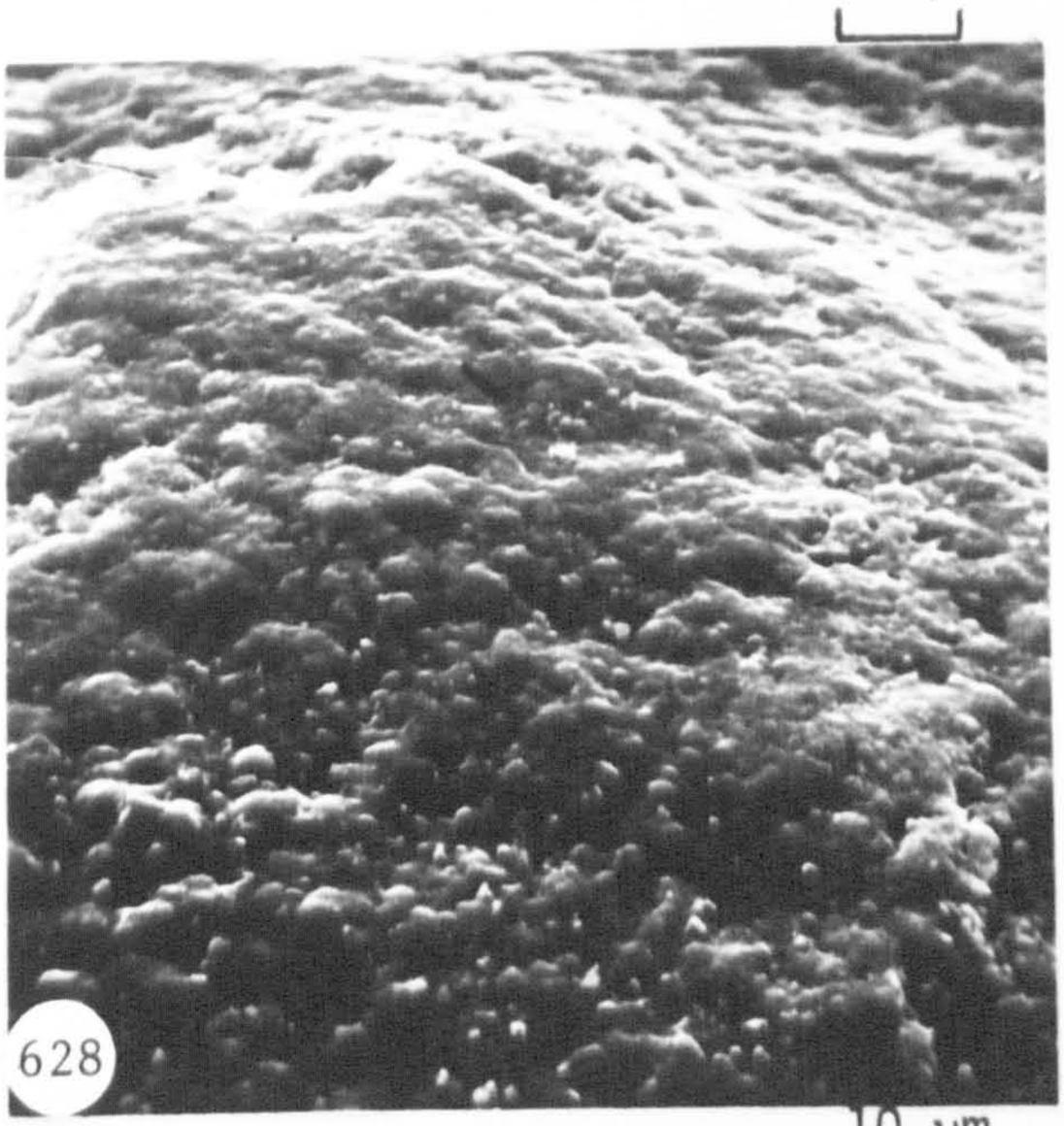
2 µm

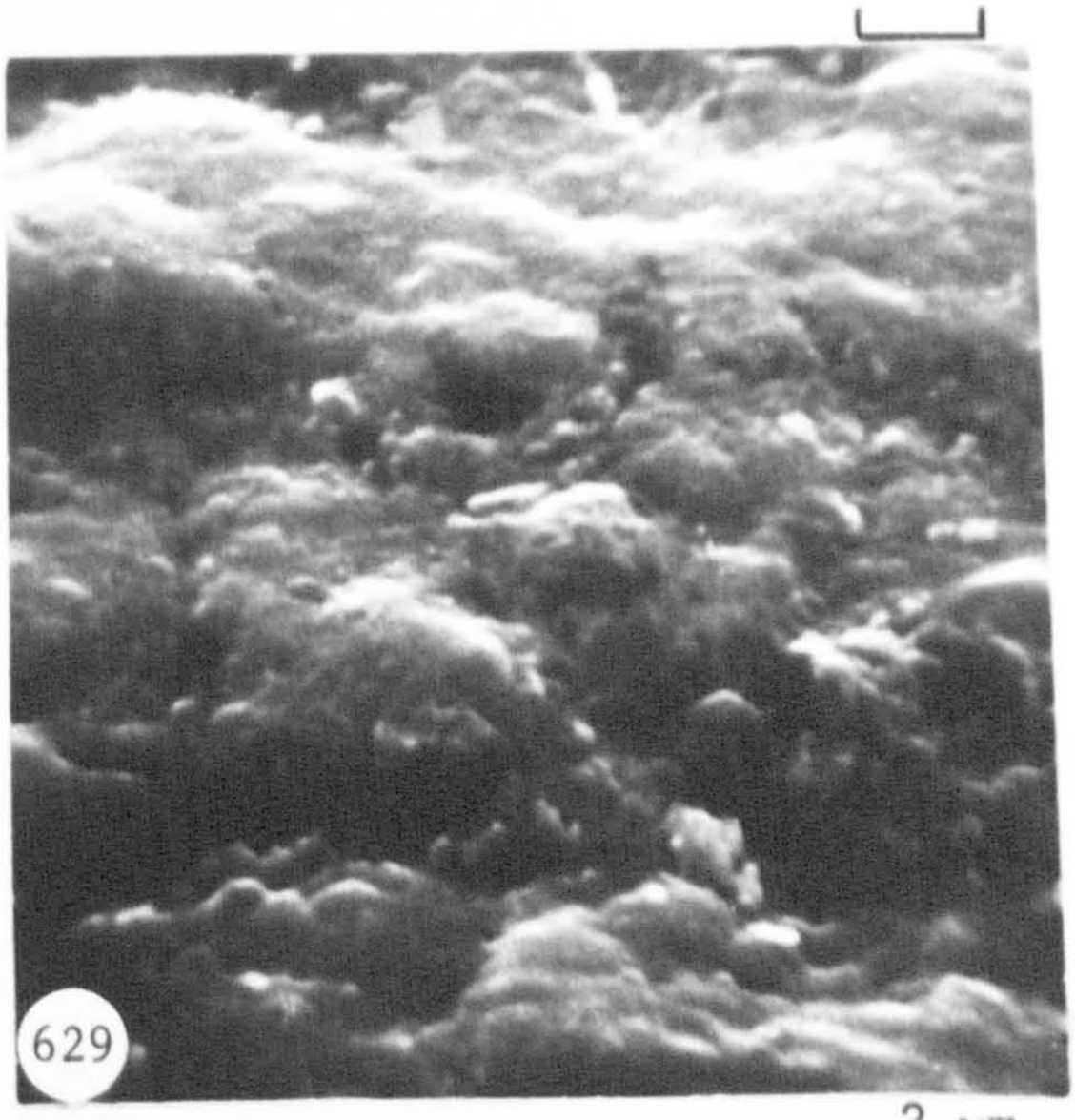
Figures 620 to 624. Scanning electron micrographs of Gilso-carbon Graphite (FRC) after neutron irradiation (-0.00% linear growth).



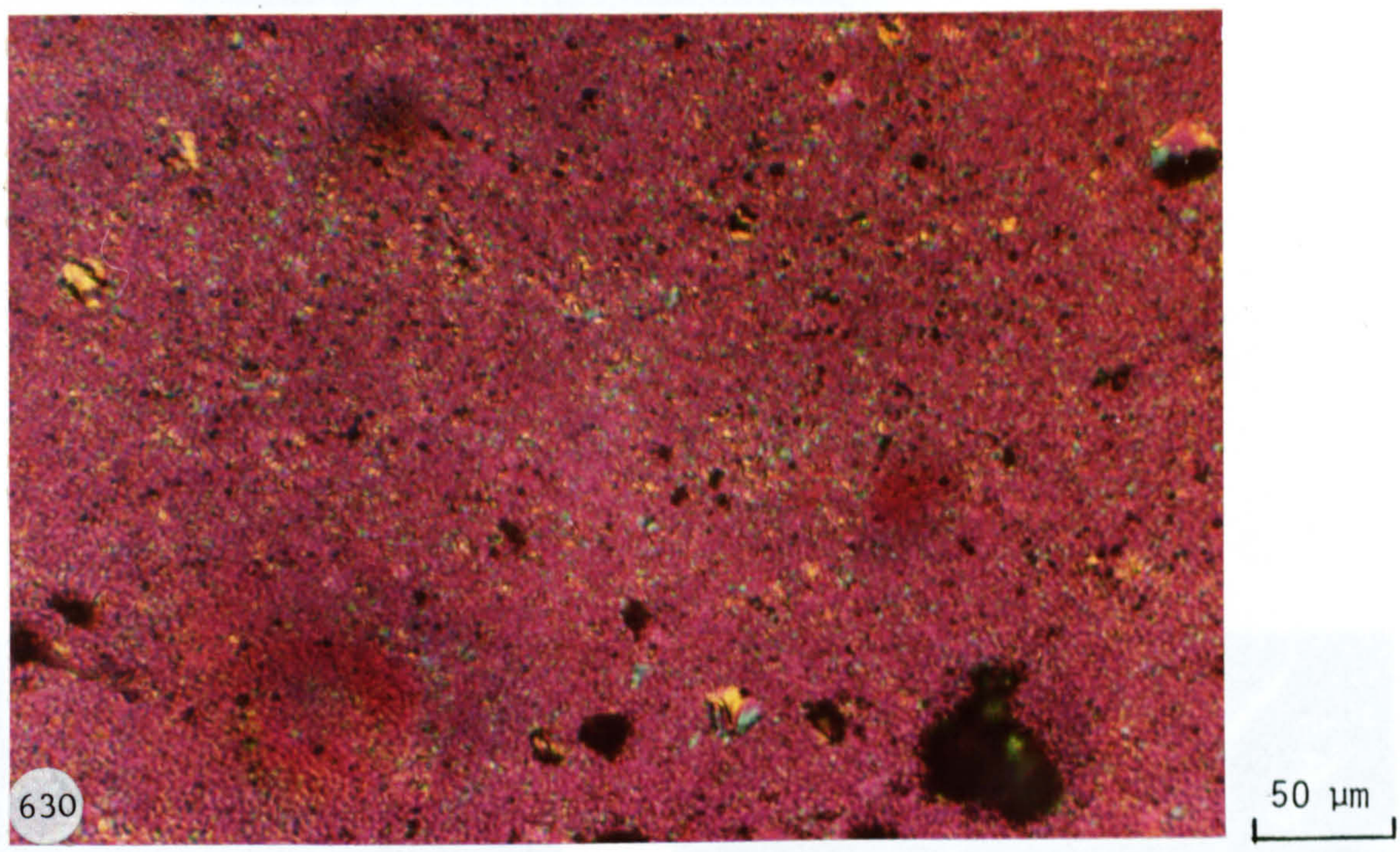


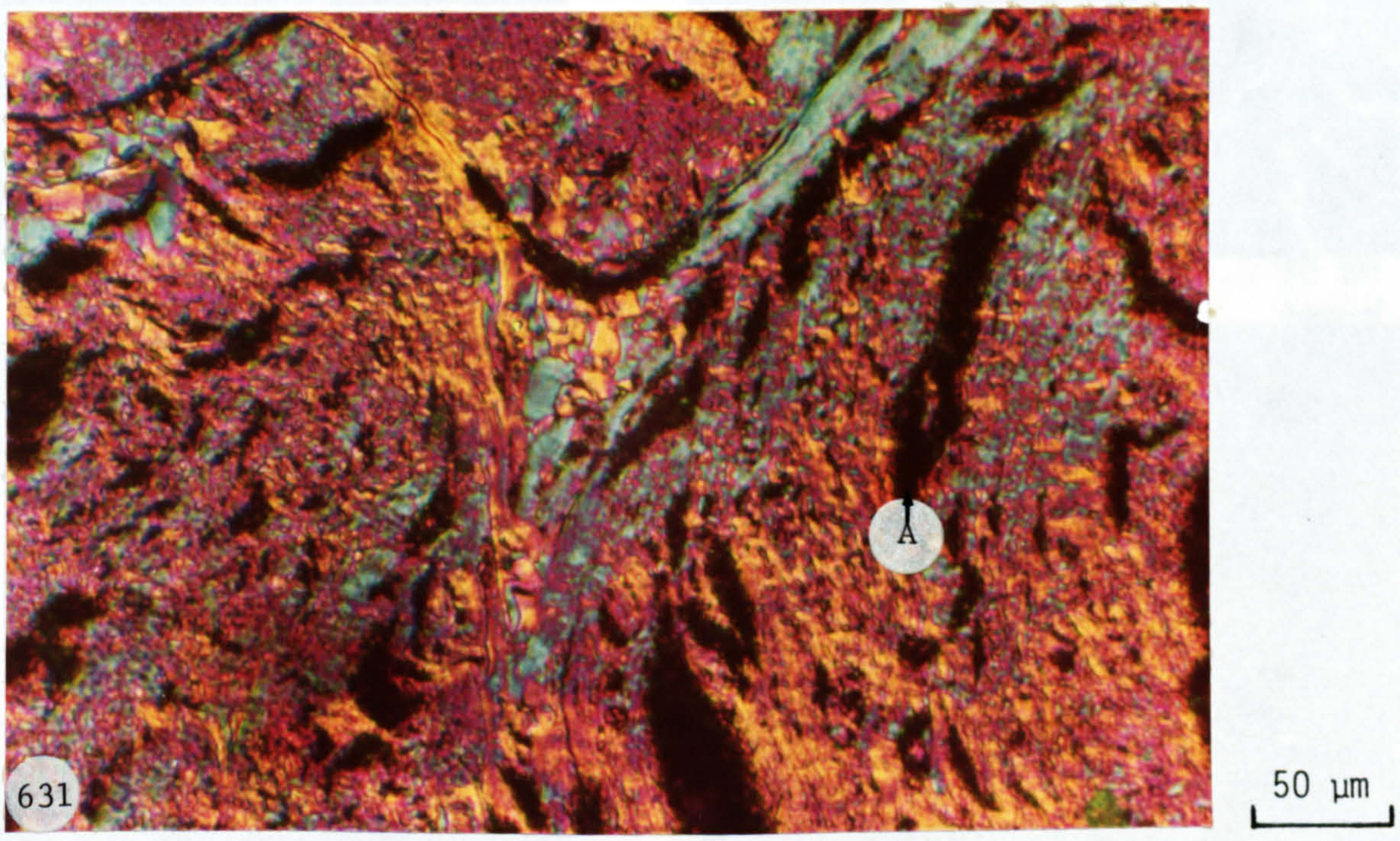




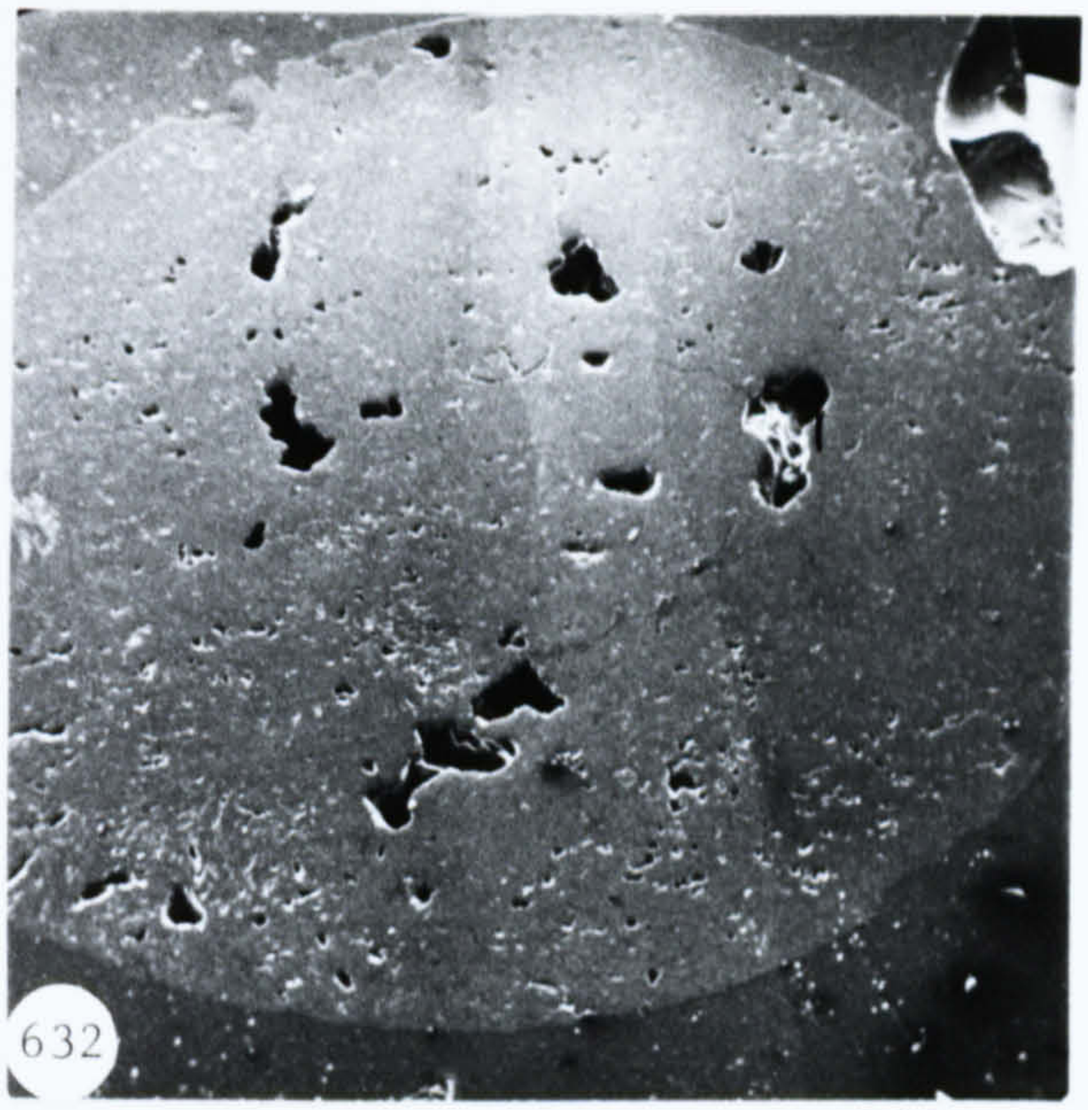


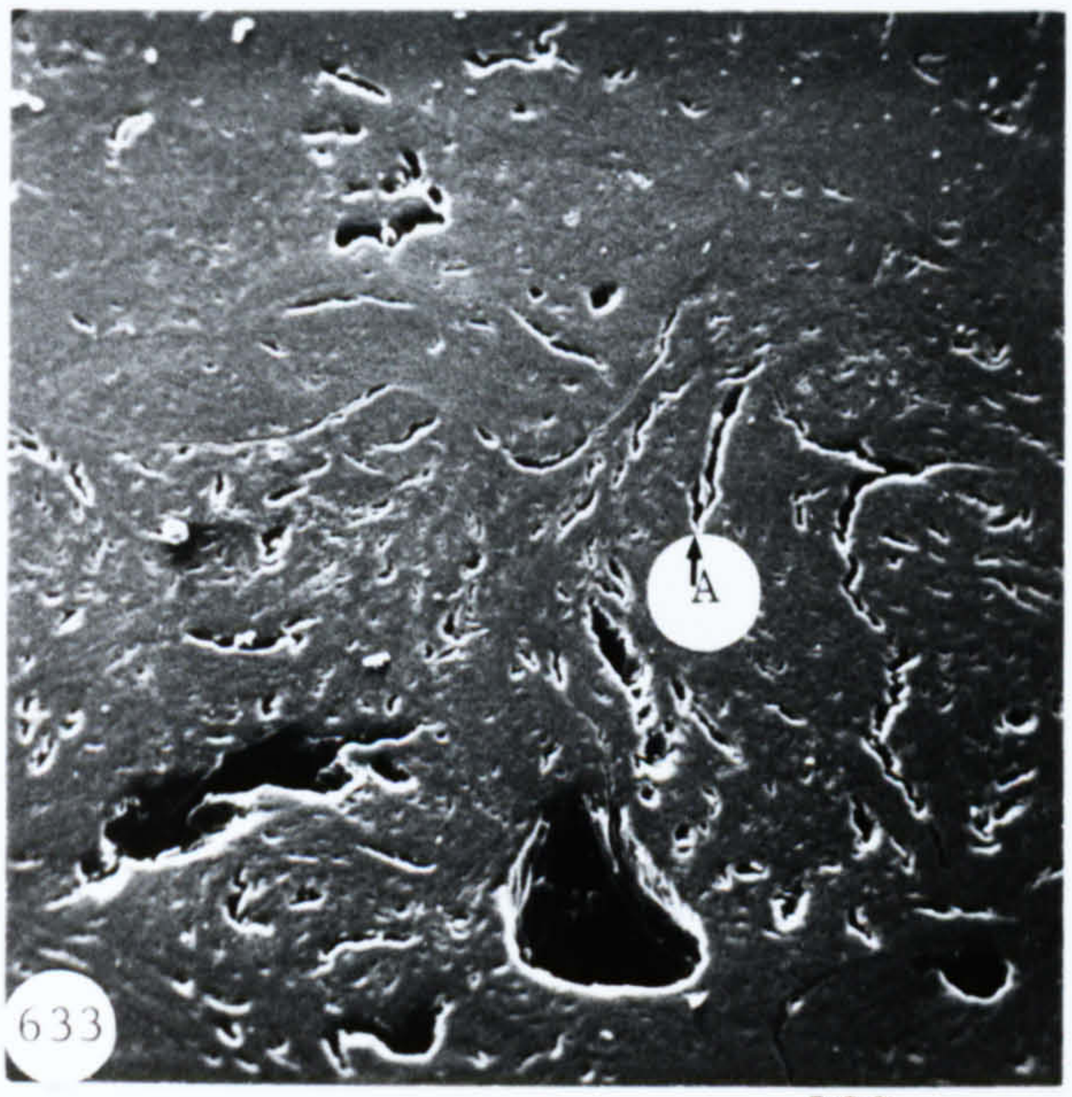
Figures 625 to 629. Scanning electron micrographs of Gilso-carbon Graphite (HAB) after neutron irradiation (+4.0% linear growth).

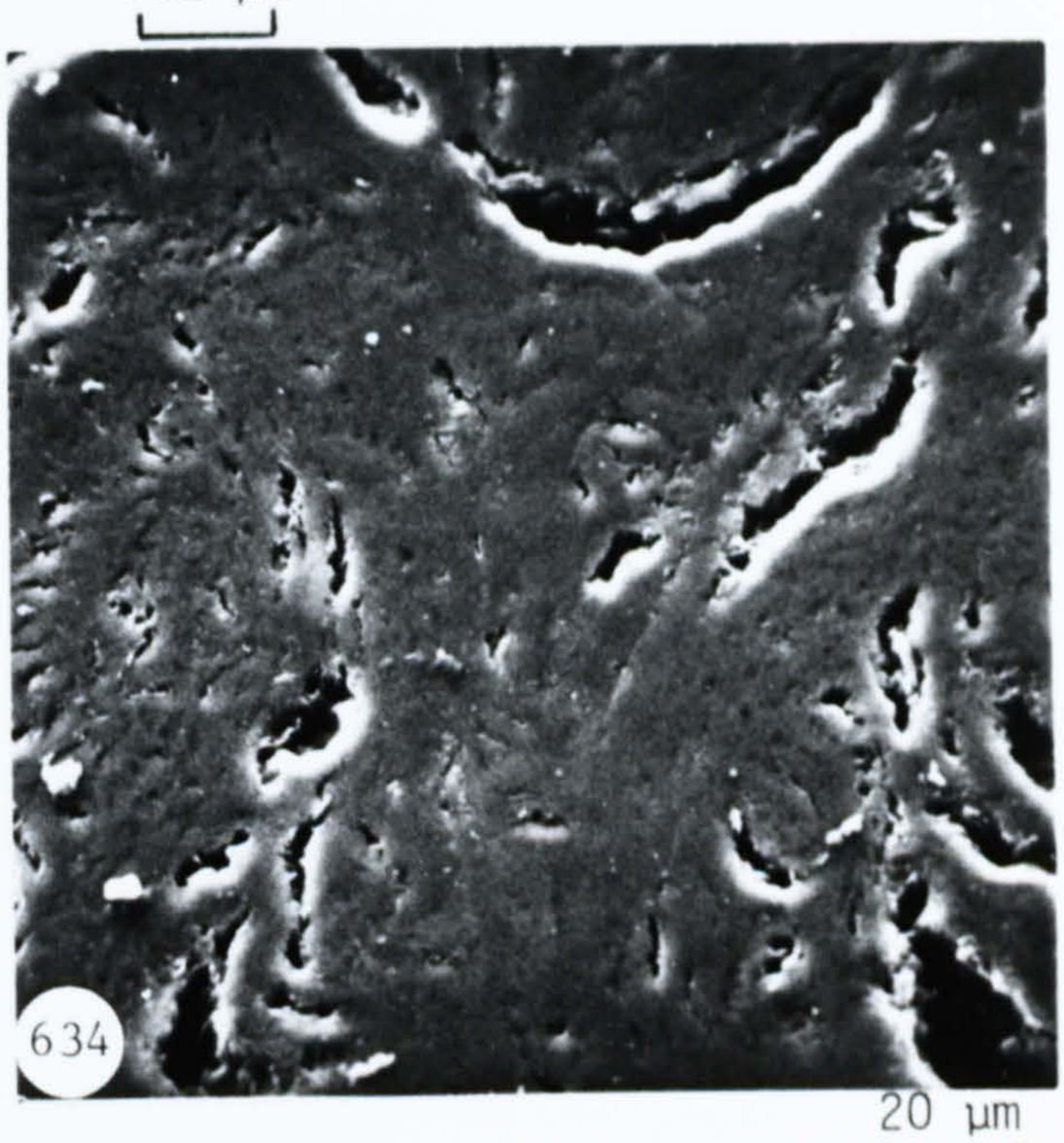


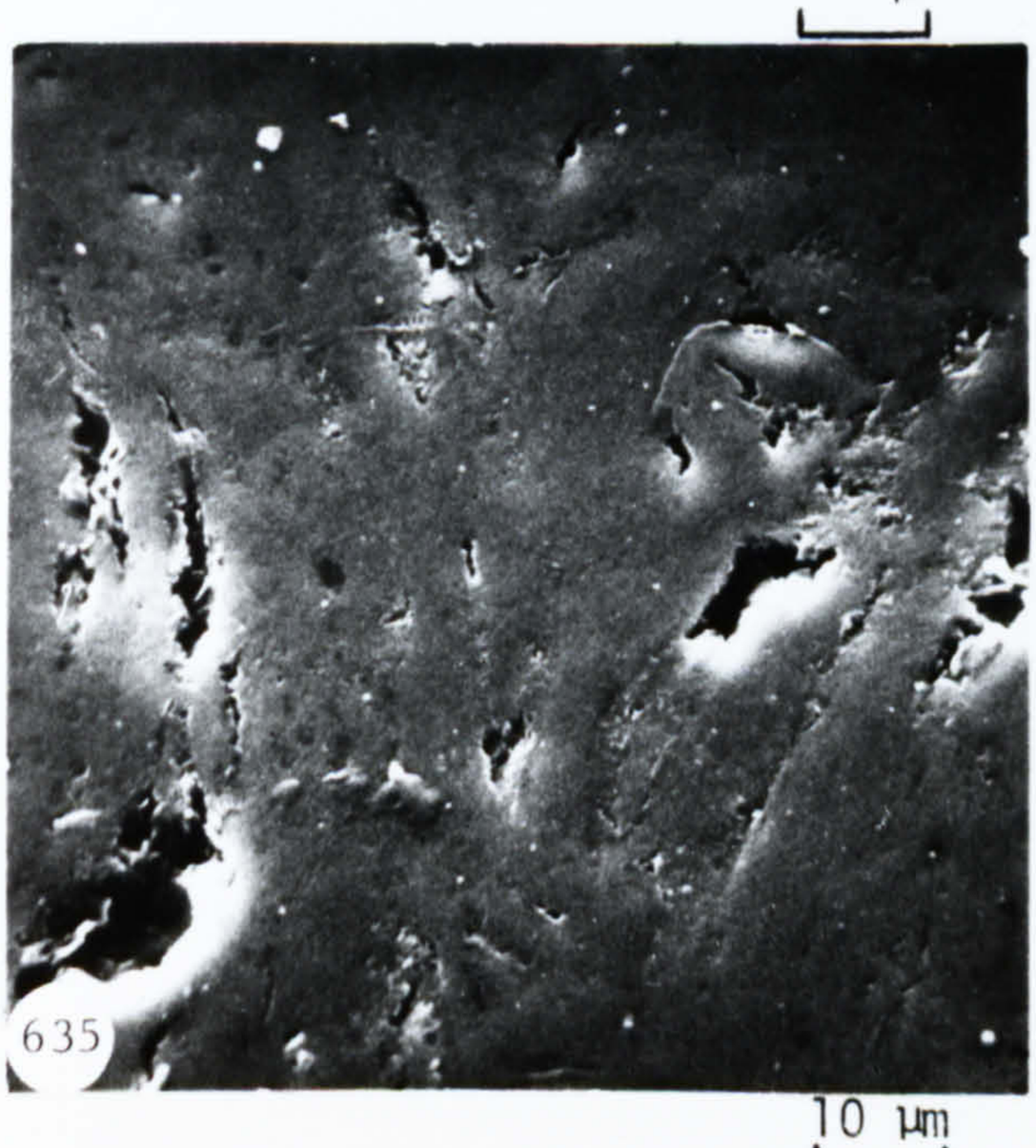


Figures 630 and 631. Optical micrographs of VQMB Pitch-coke graphite.



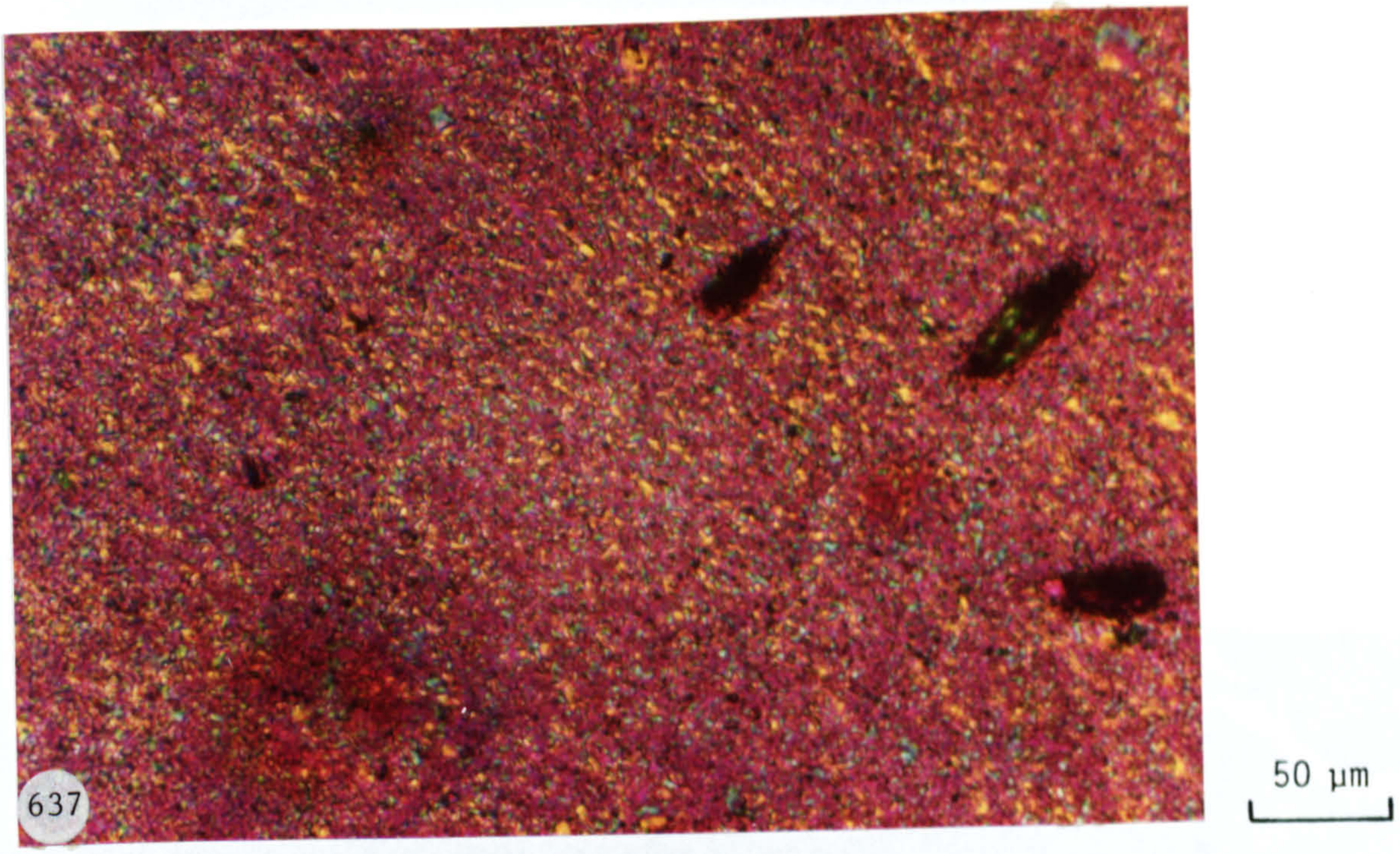


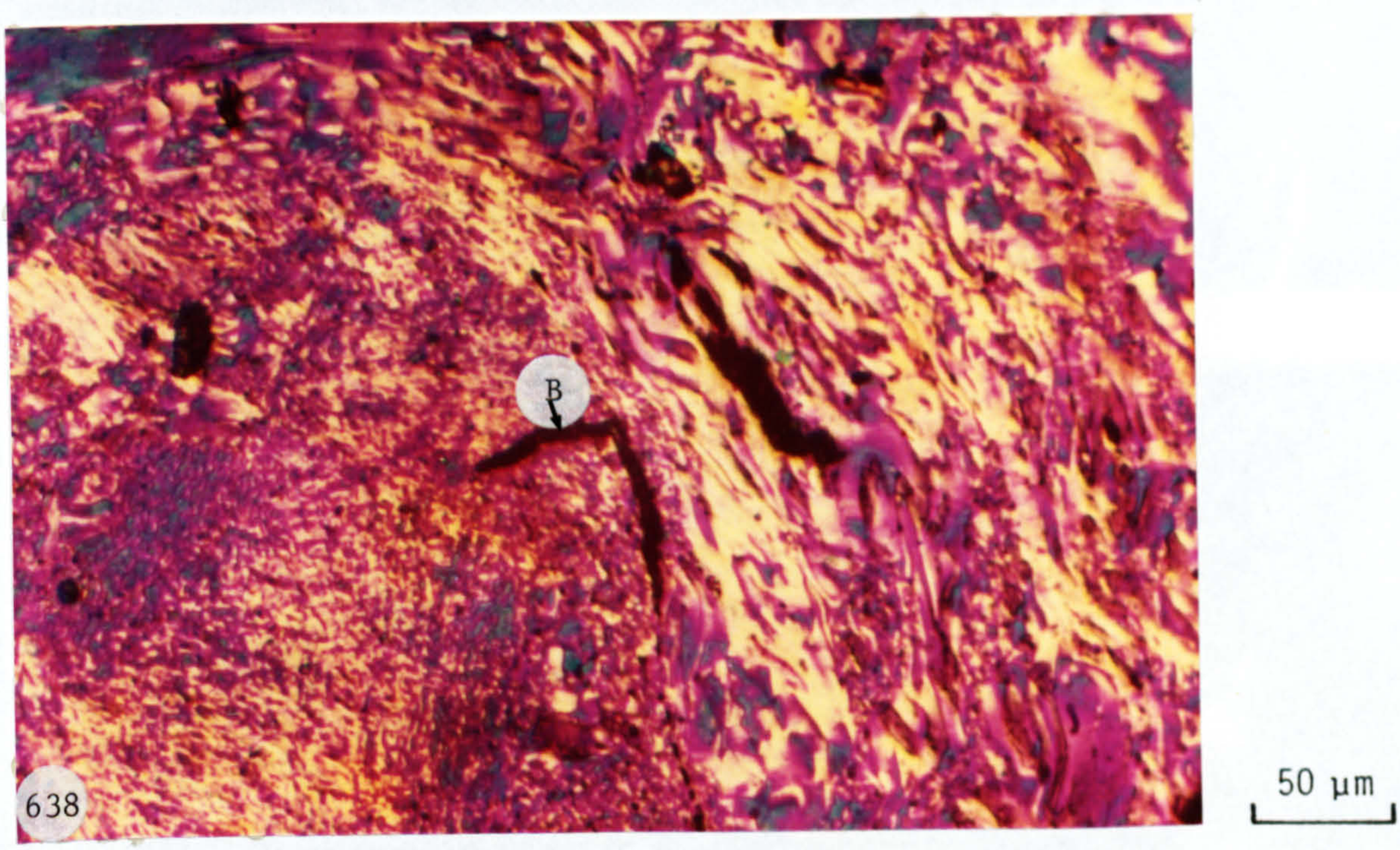




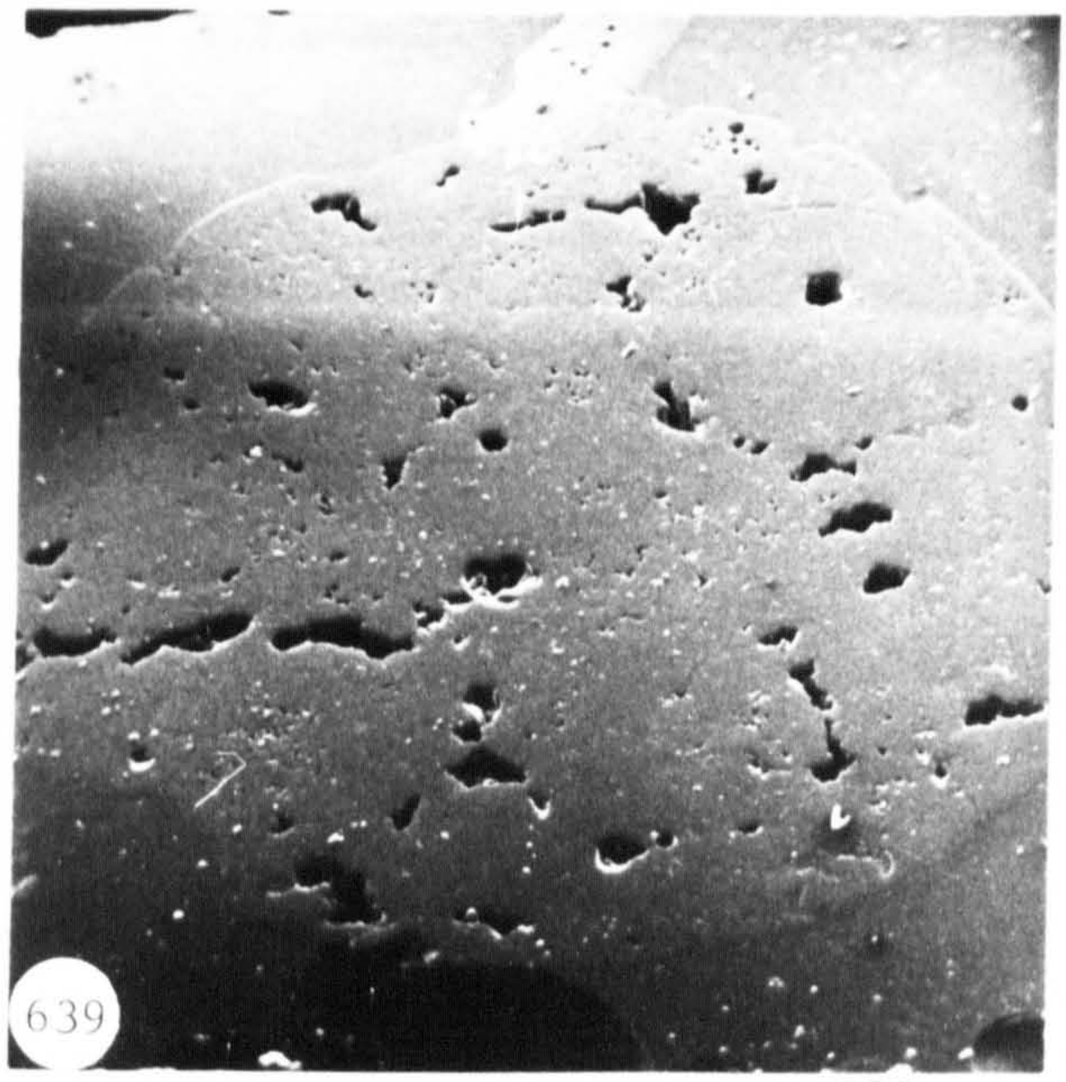


Figures 632 to 636. Scanning electron micrographs of VQMB Pitch-coke Graphite.

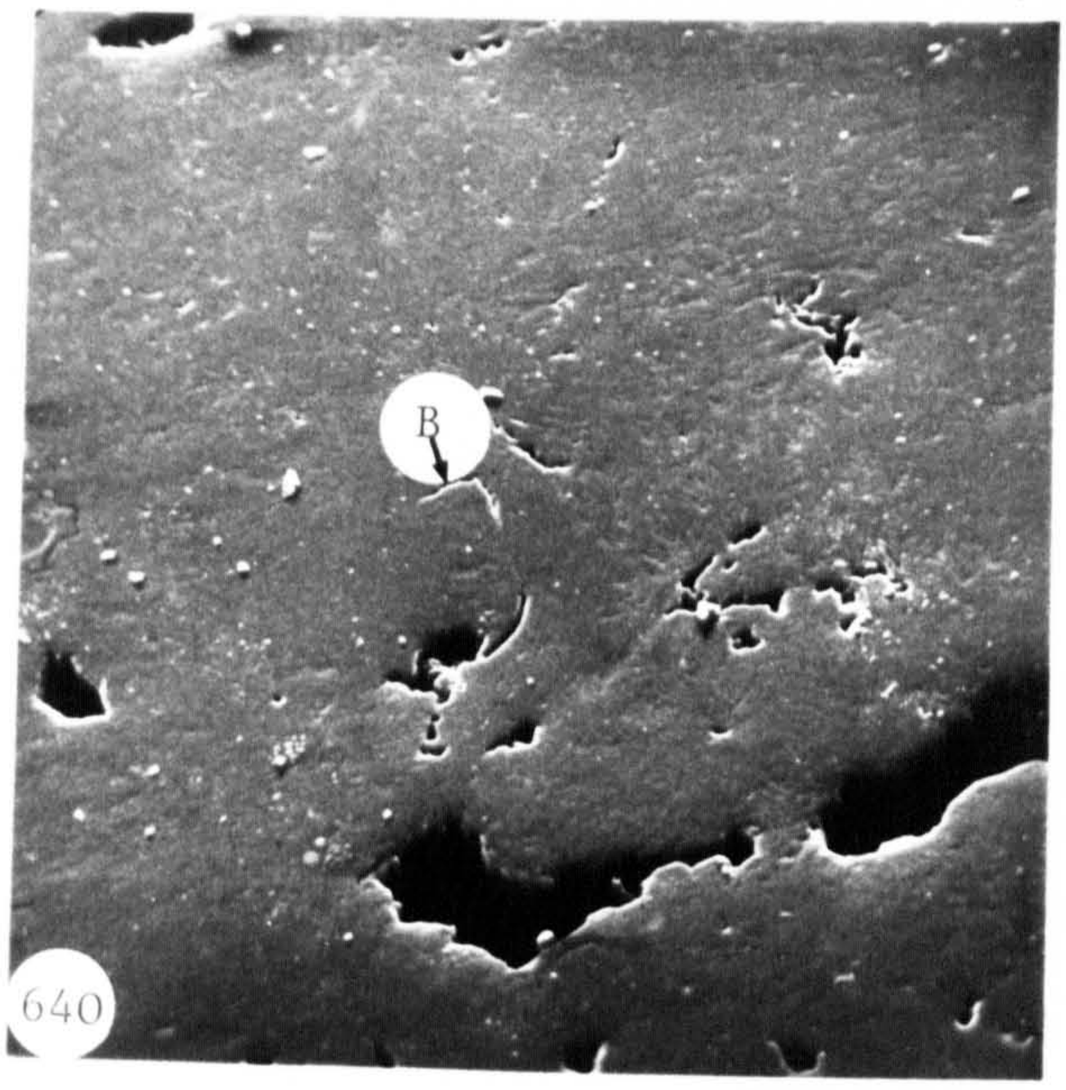




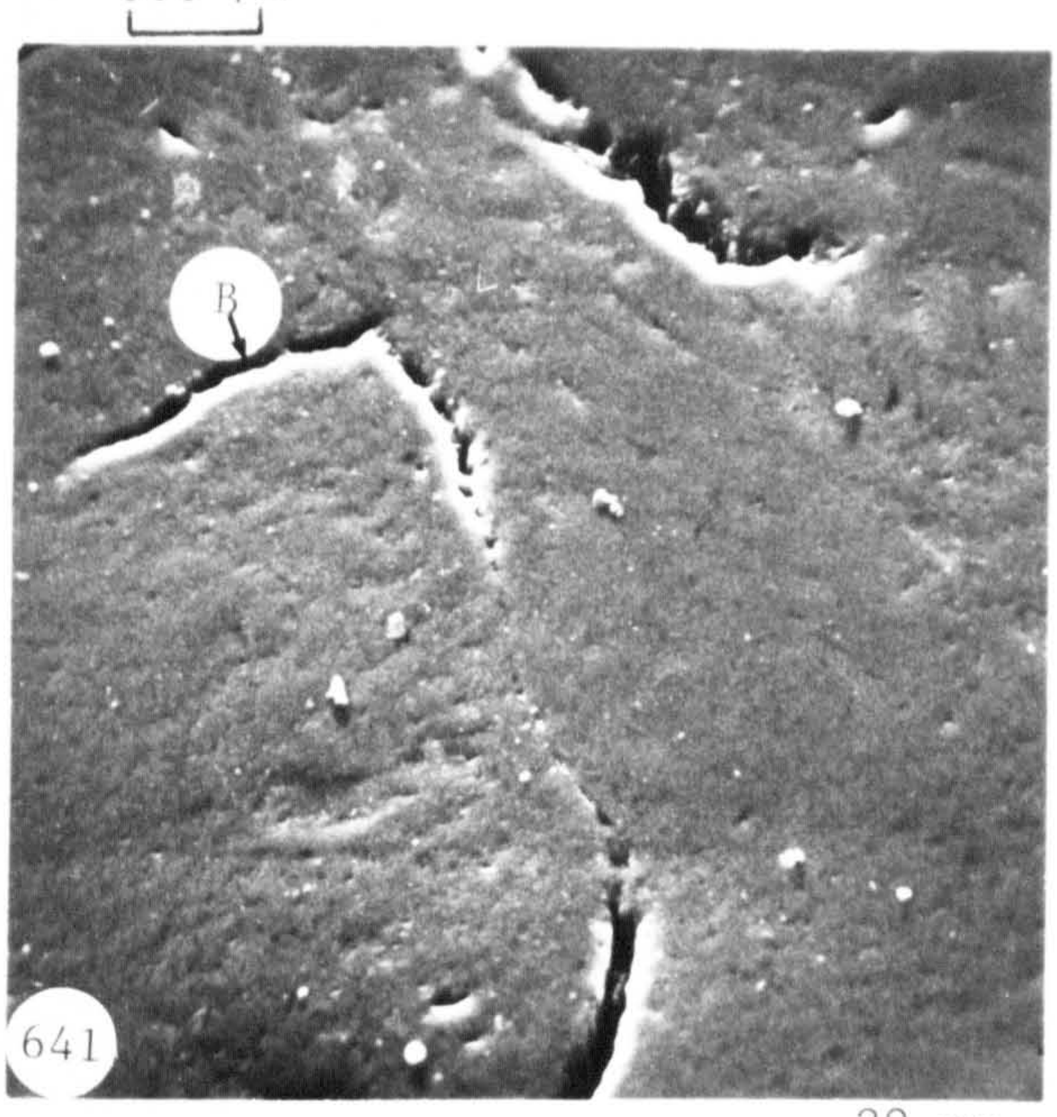
Figures 637 and 638. Optical micrographs of Pitch-coke graphite (LZAA) after neutron irradiation (-1.99% linear growth).



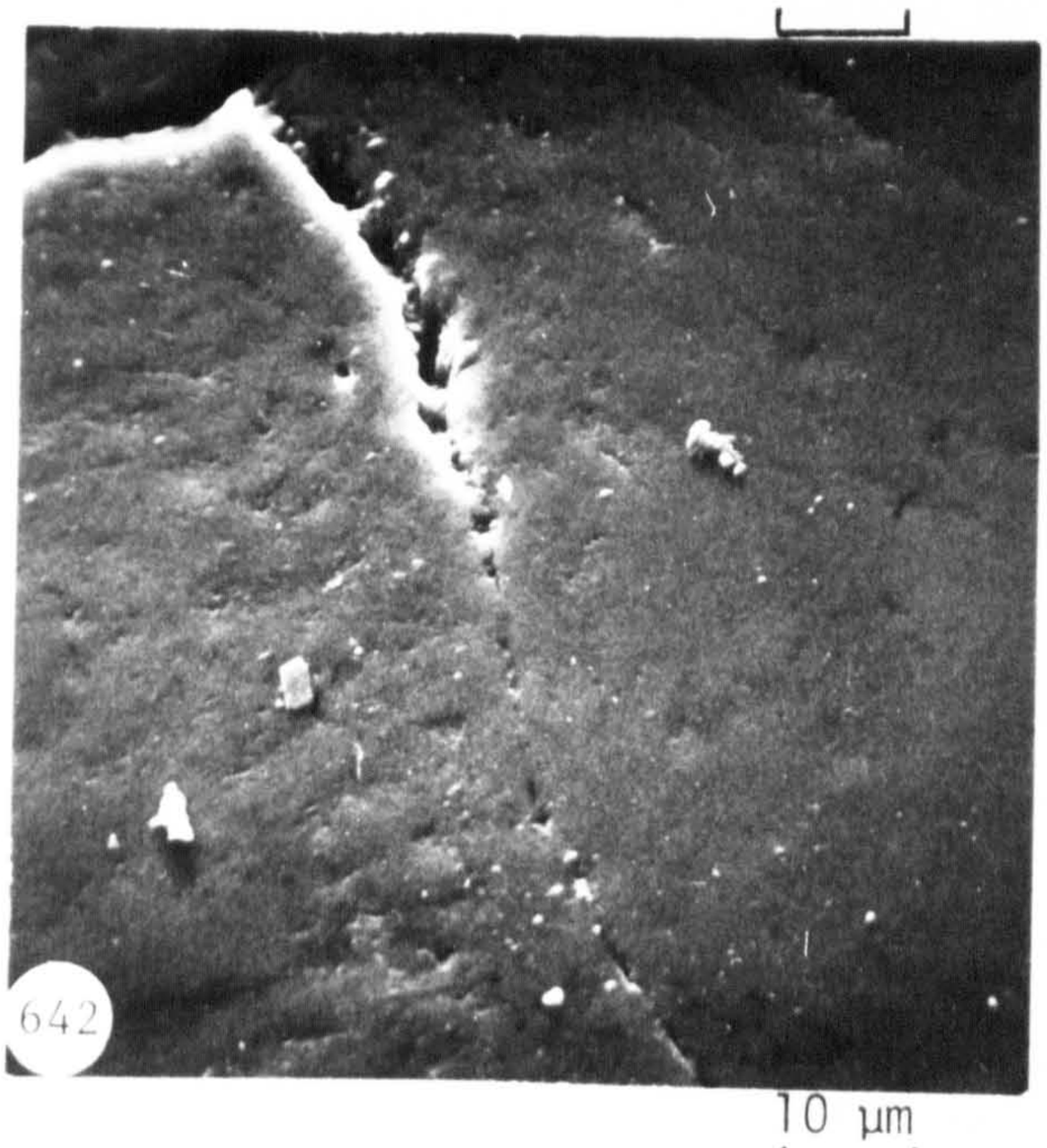
500 µm



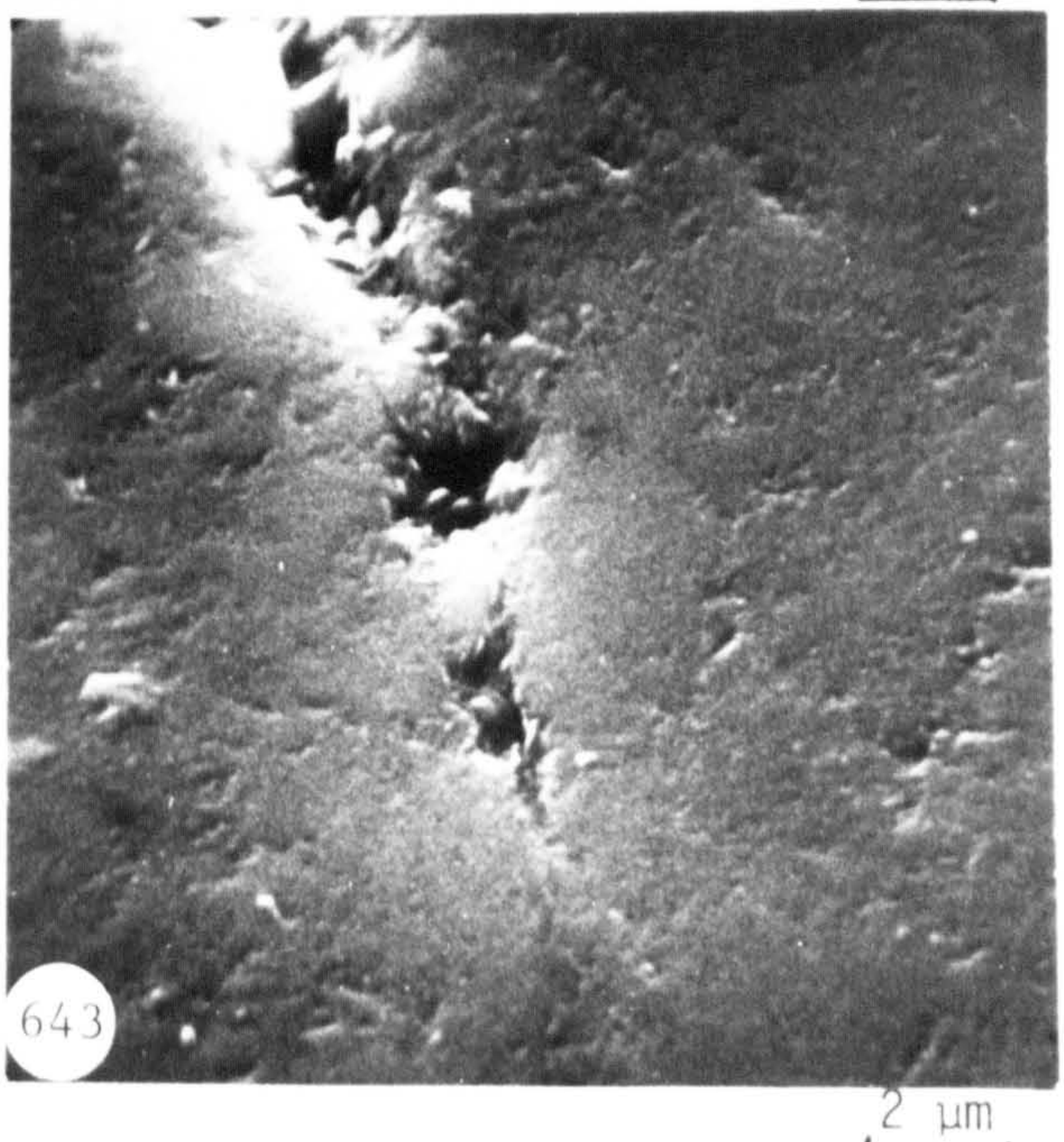
100 µm



20 µm

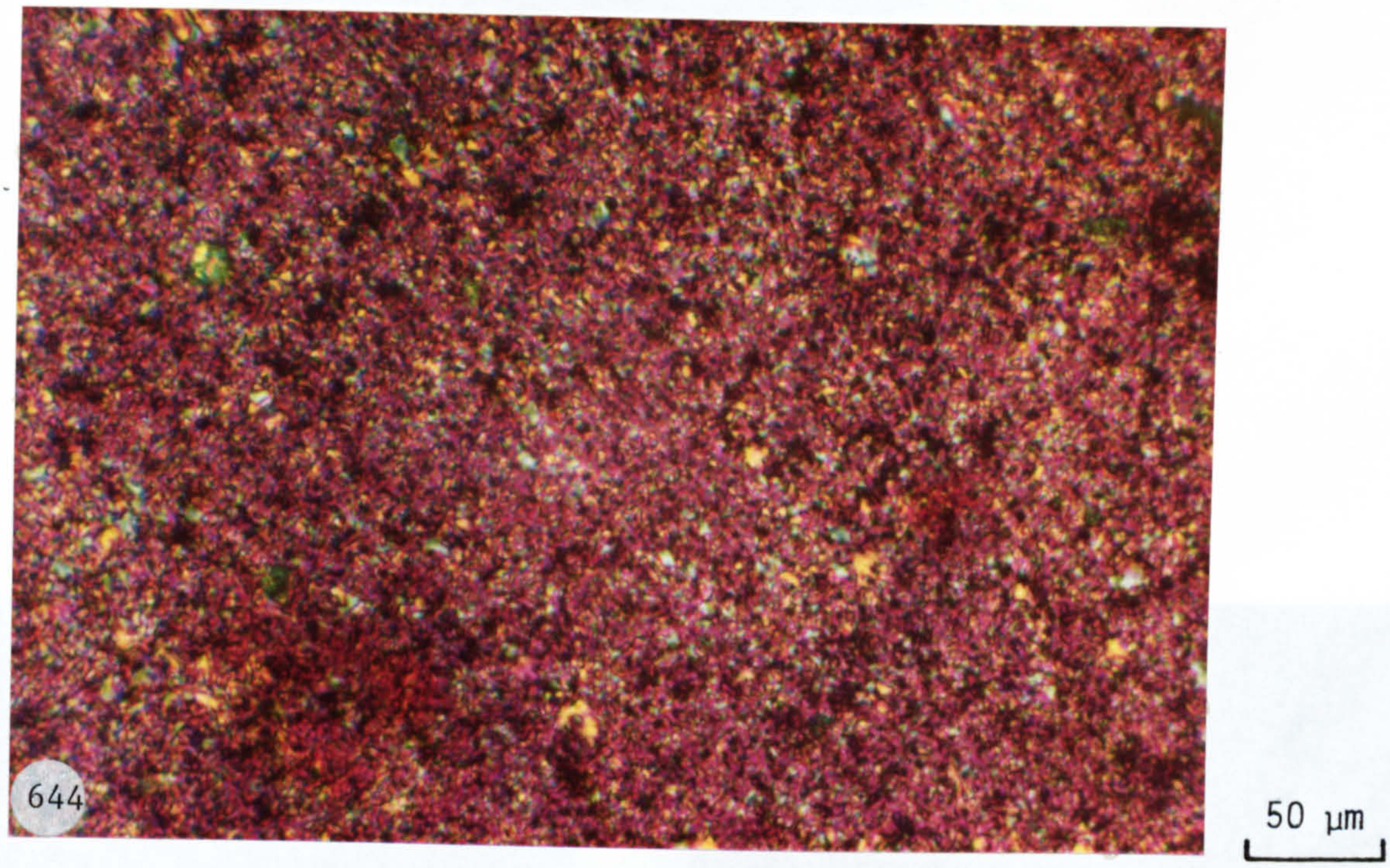


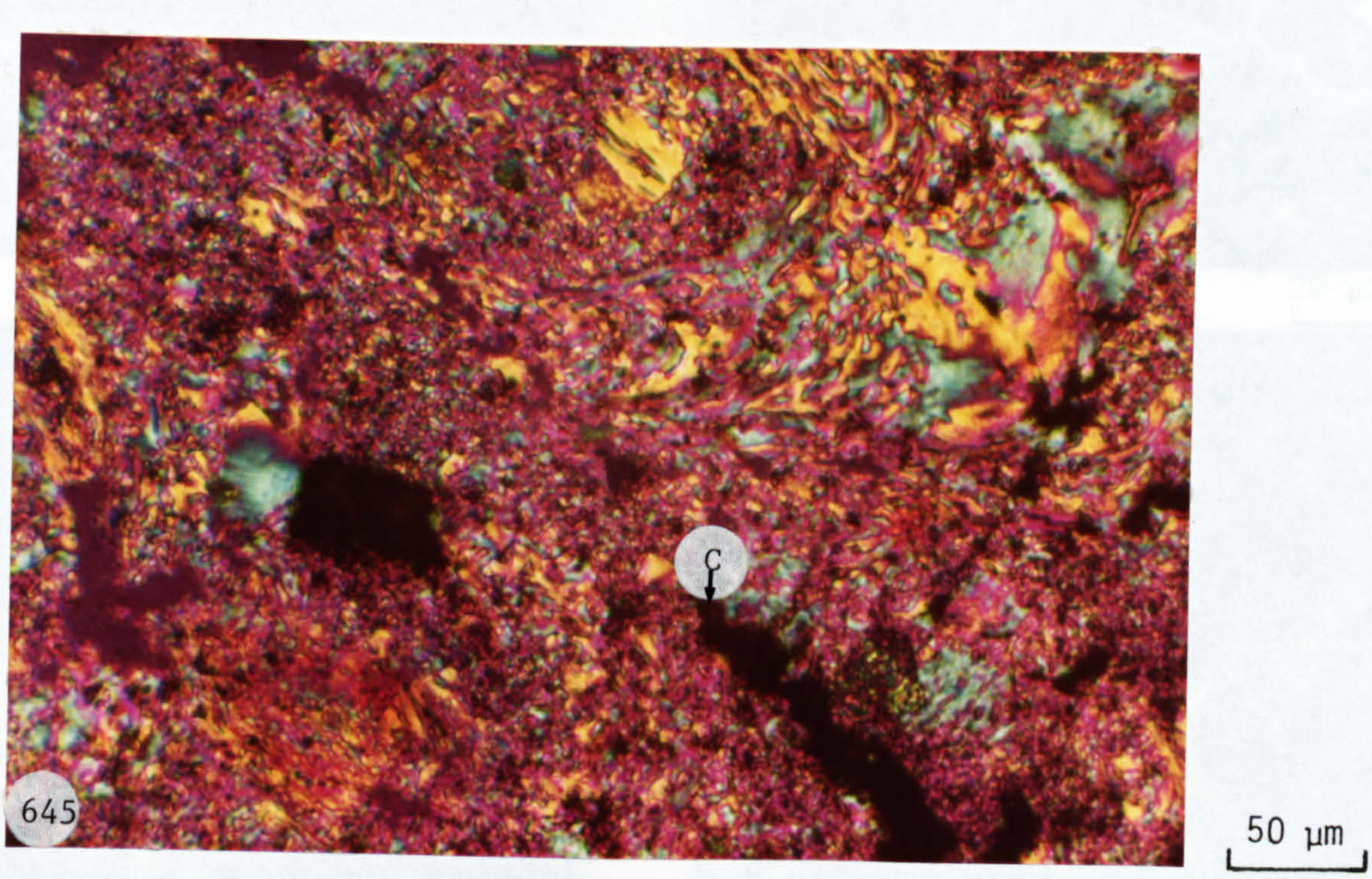
10 µm



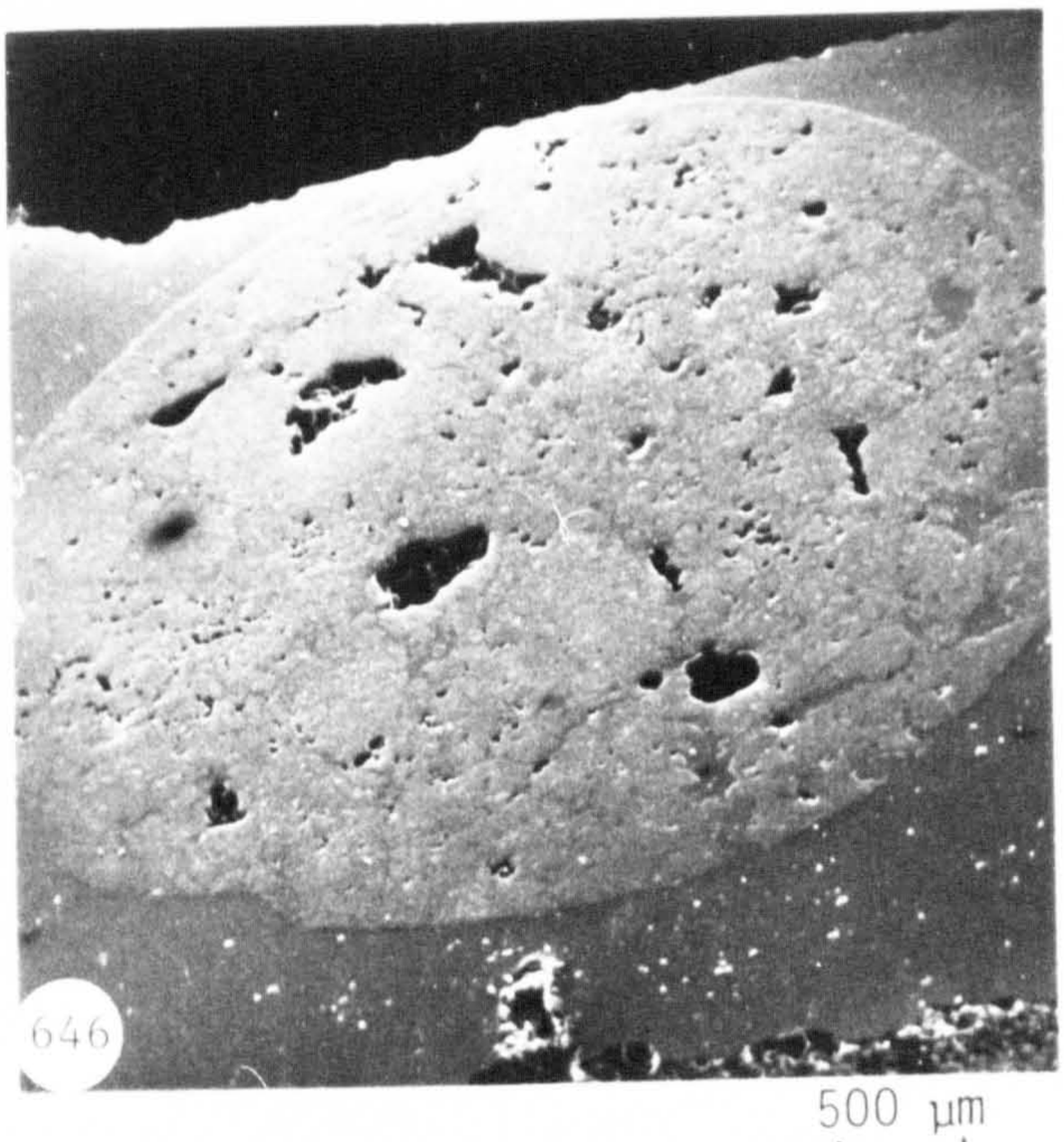
2 µm

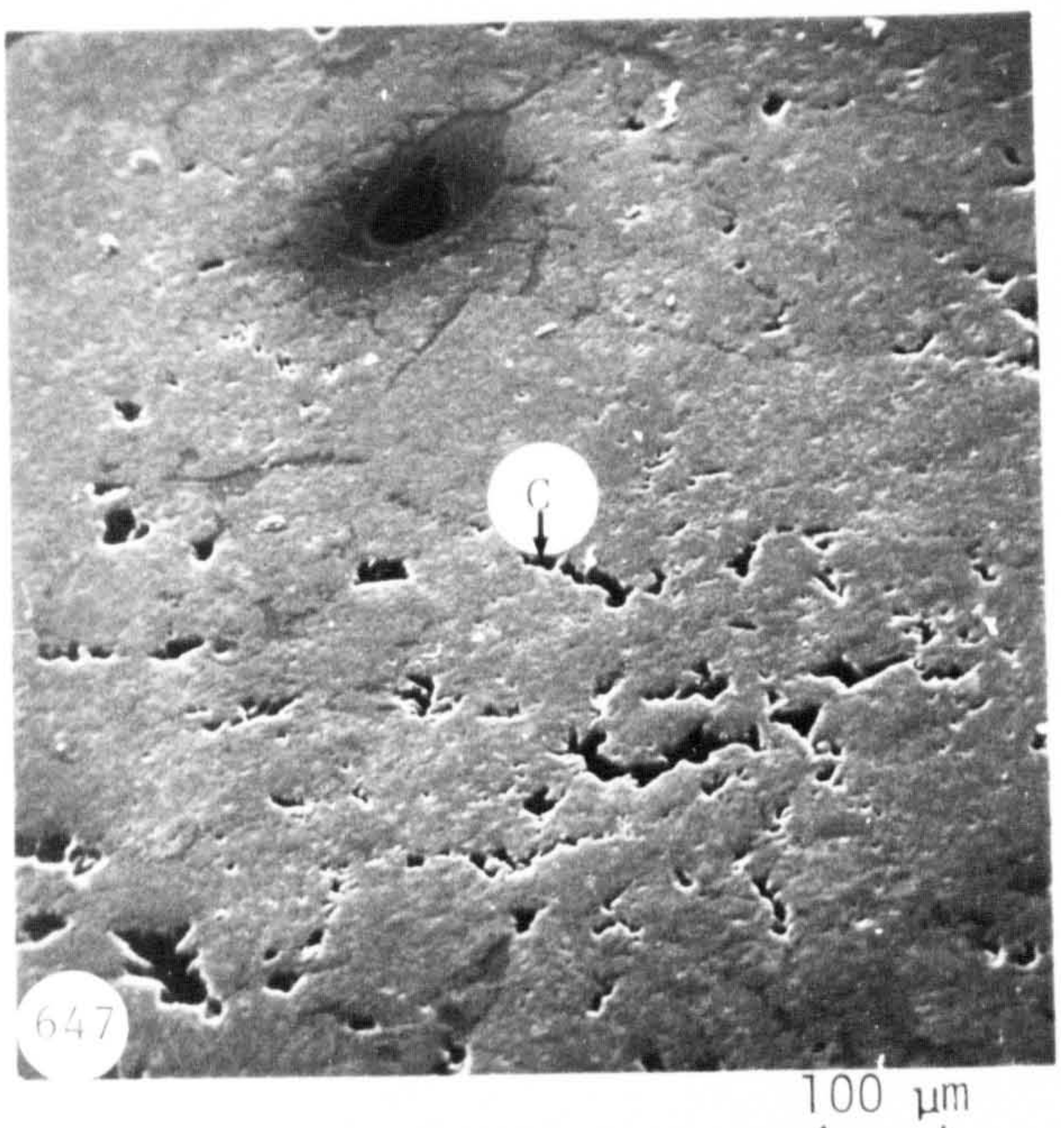
Figures 639 to 643. Scanning electron micrographs of Pitch-coke Graphite (LZAA) after neutron irradiation (-1.99% linear growth).

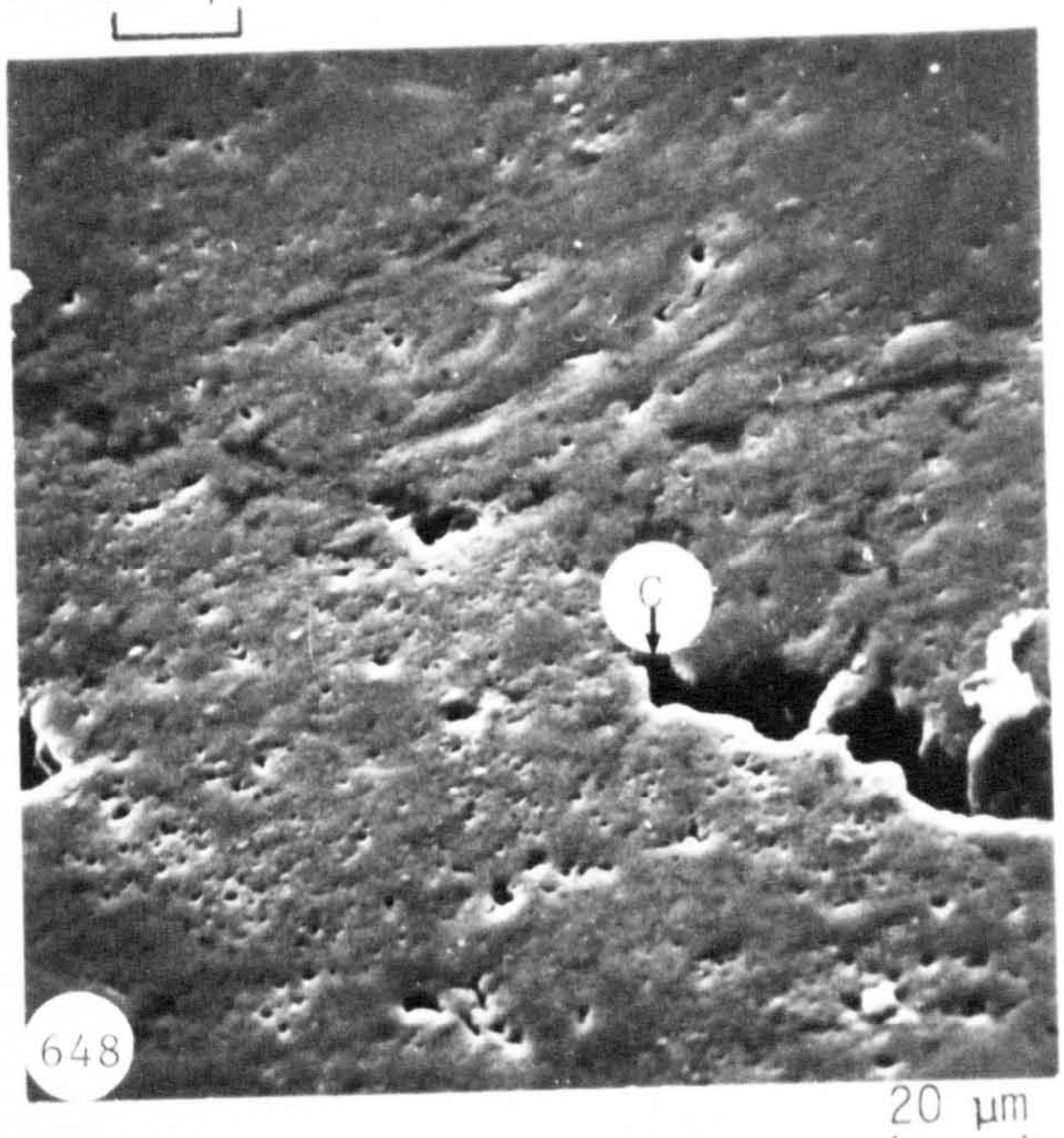


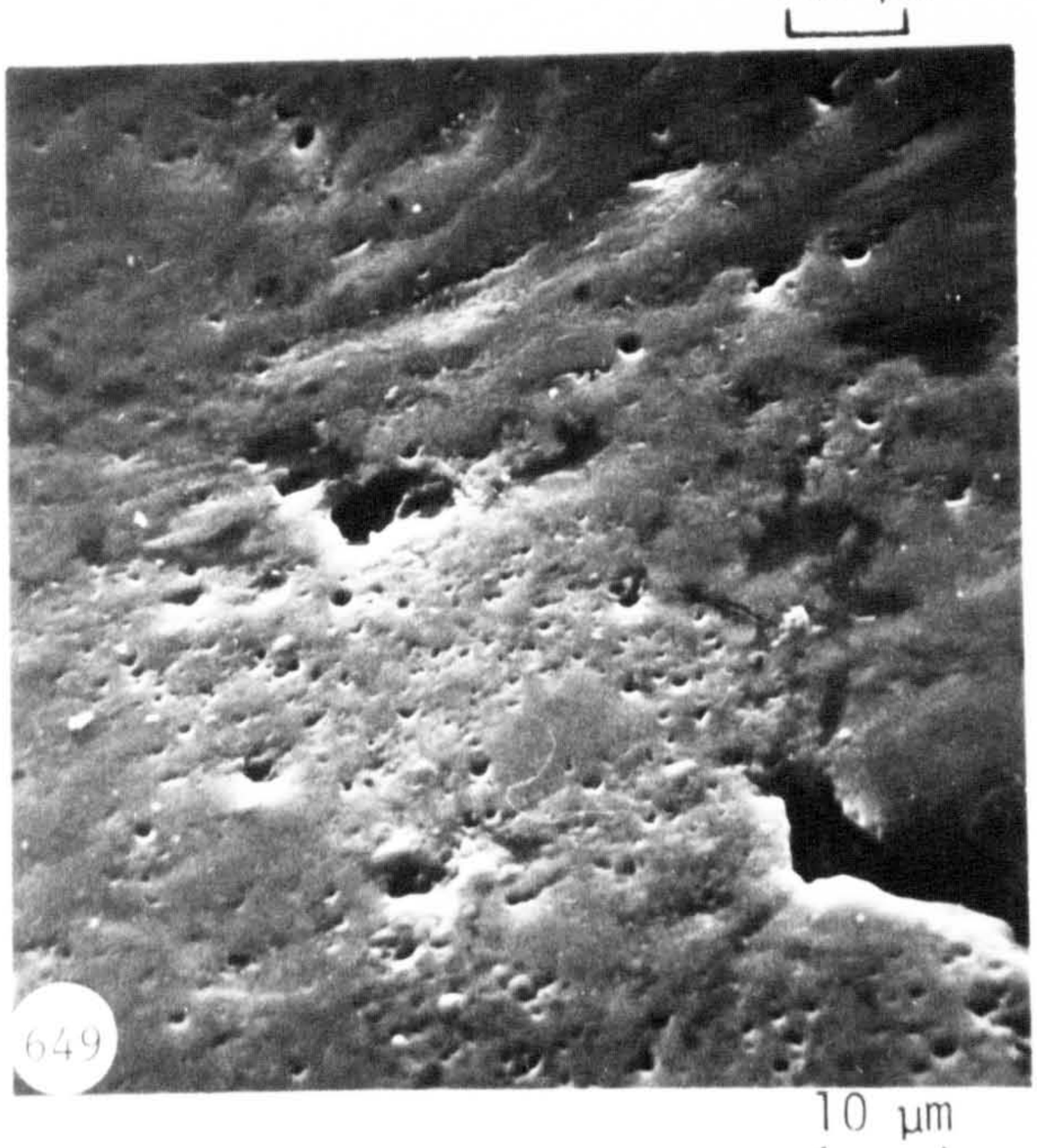


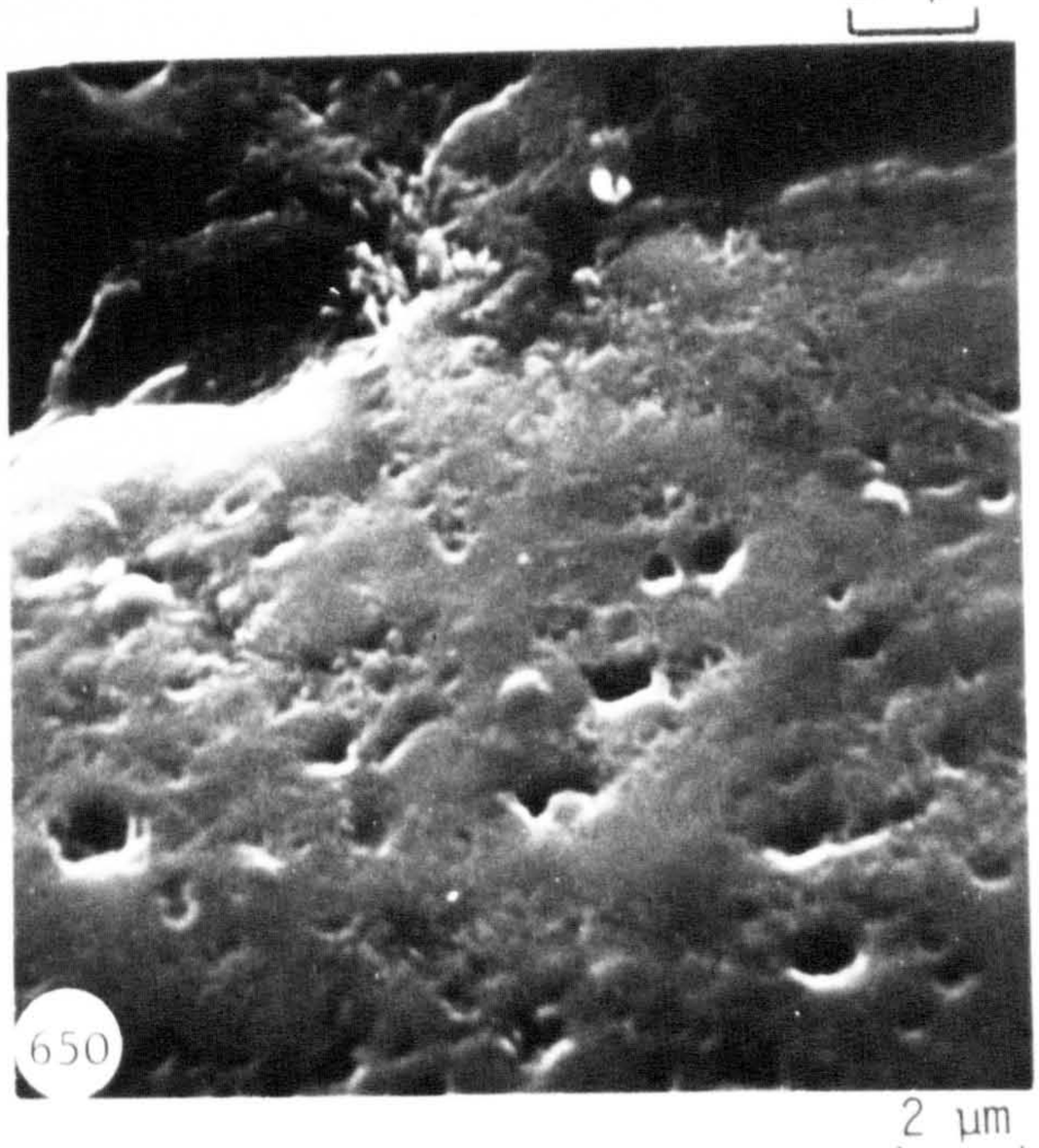
Figures 644 and 645. Optical micrographs of Pitch-coke graphite (SBO) after neutron irradiation (+3.01% linear growth).



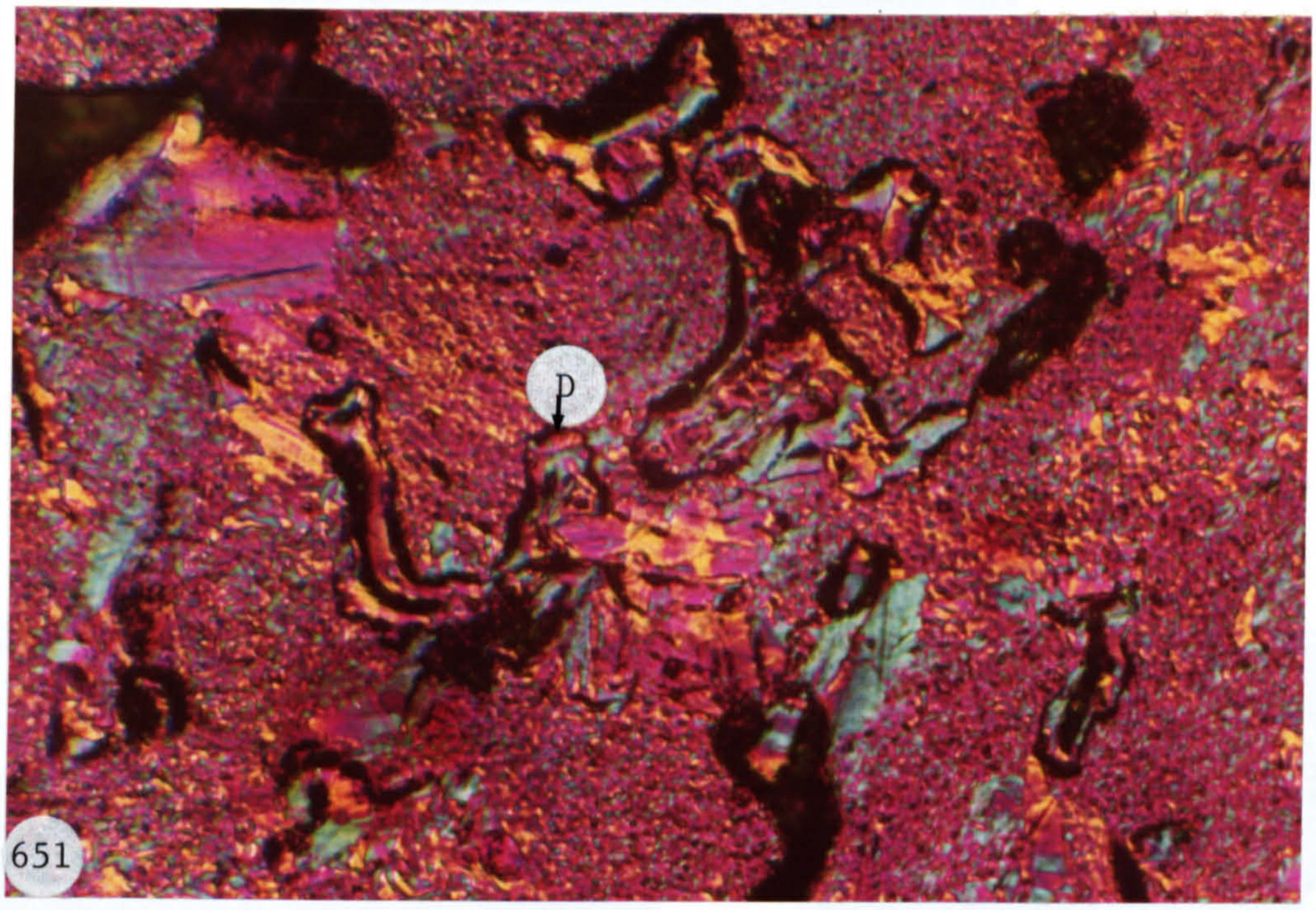


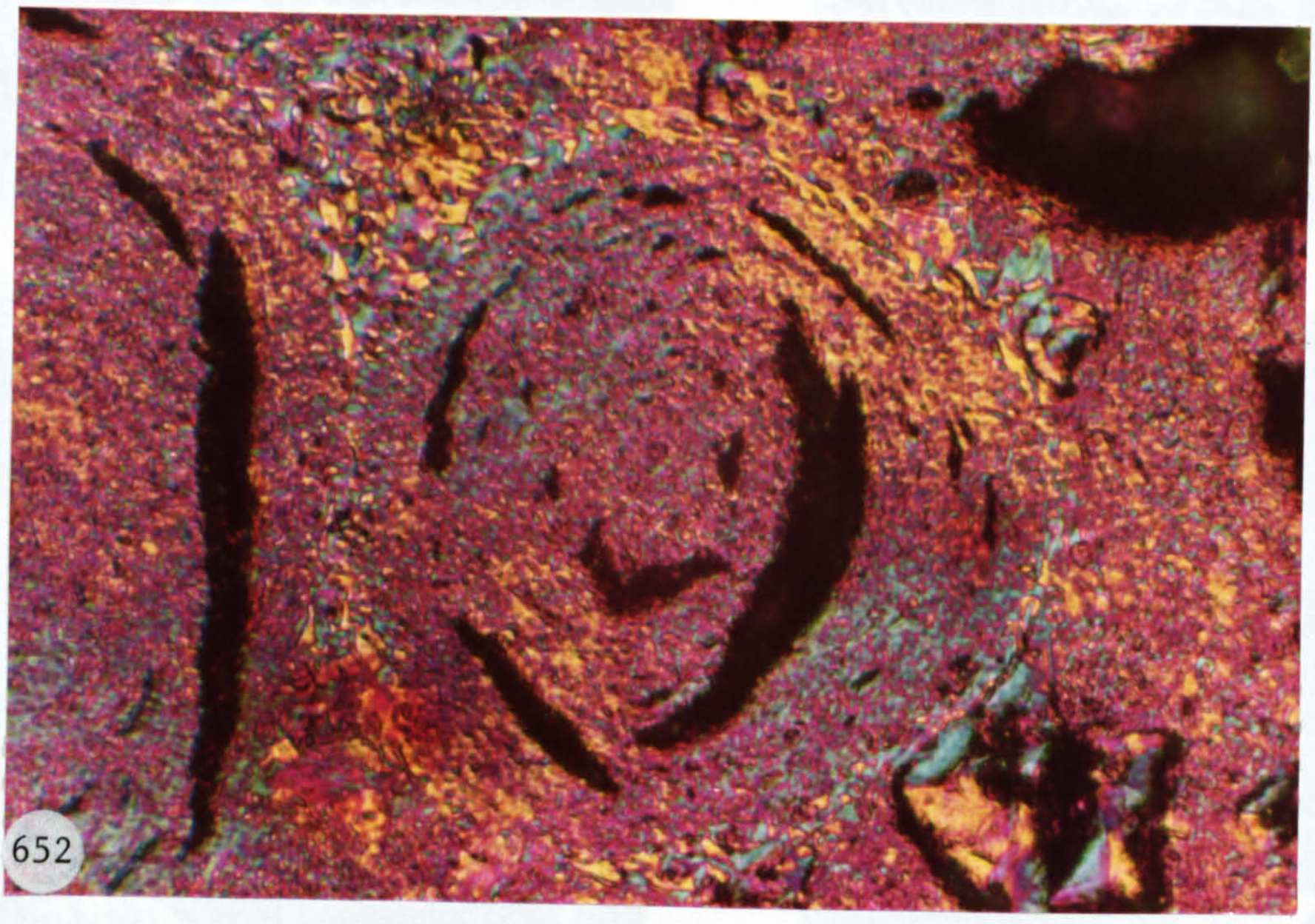




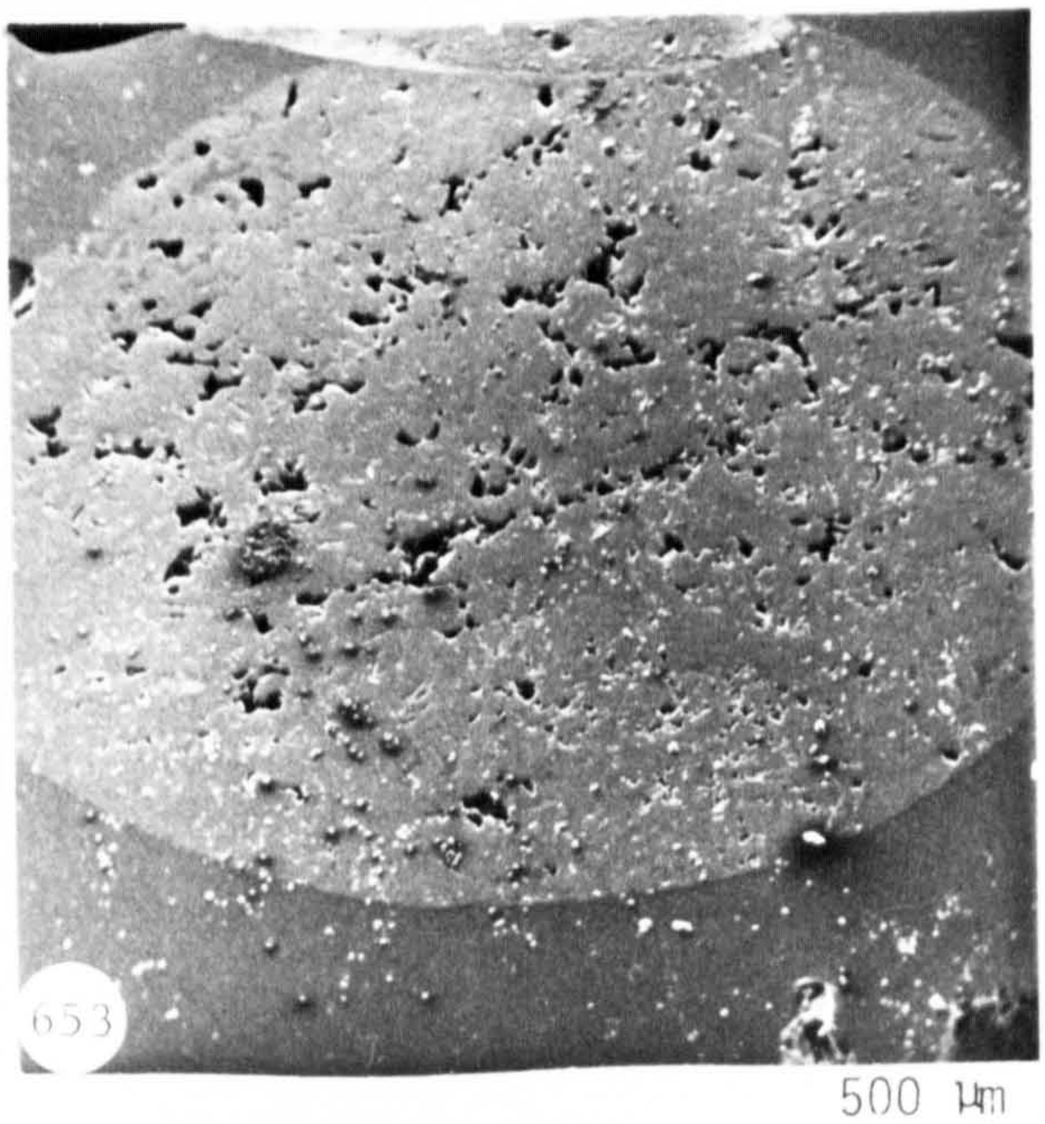


Figures 646 to 650. Scanning electron micrographs of Pitch-coke Graphite (SBO) after neutron irradiation (+3.01% linear growth).

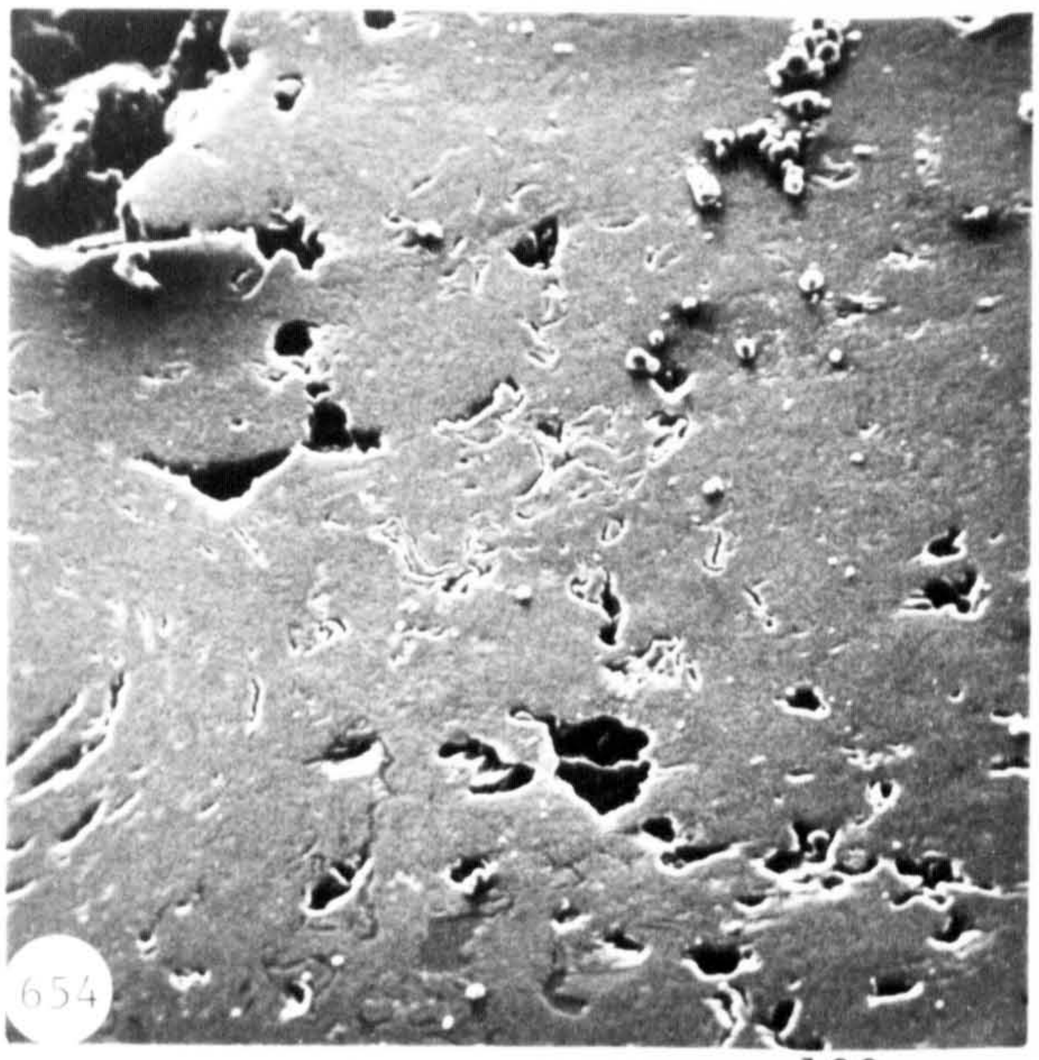




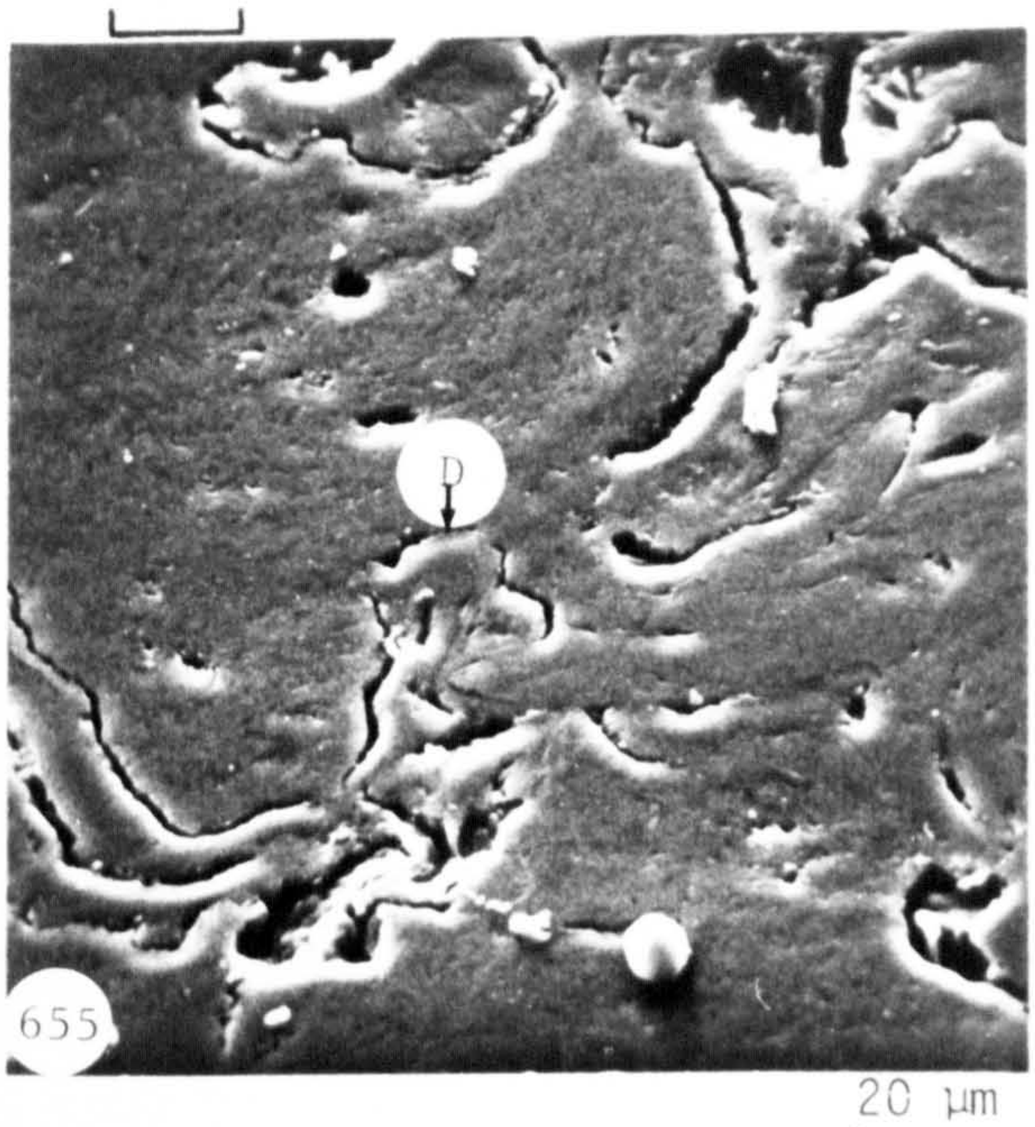
Figures 651 and 652. Optical micrographs of Gilso-carbon graphite (NA).



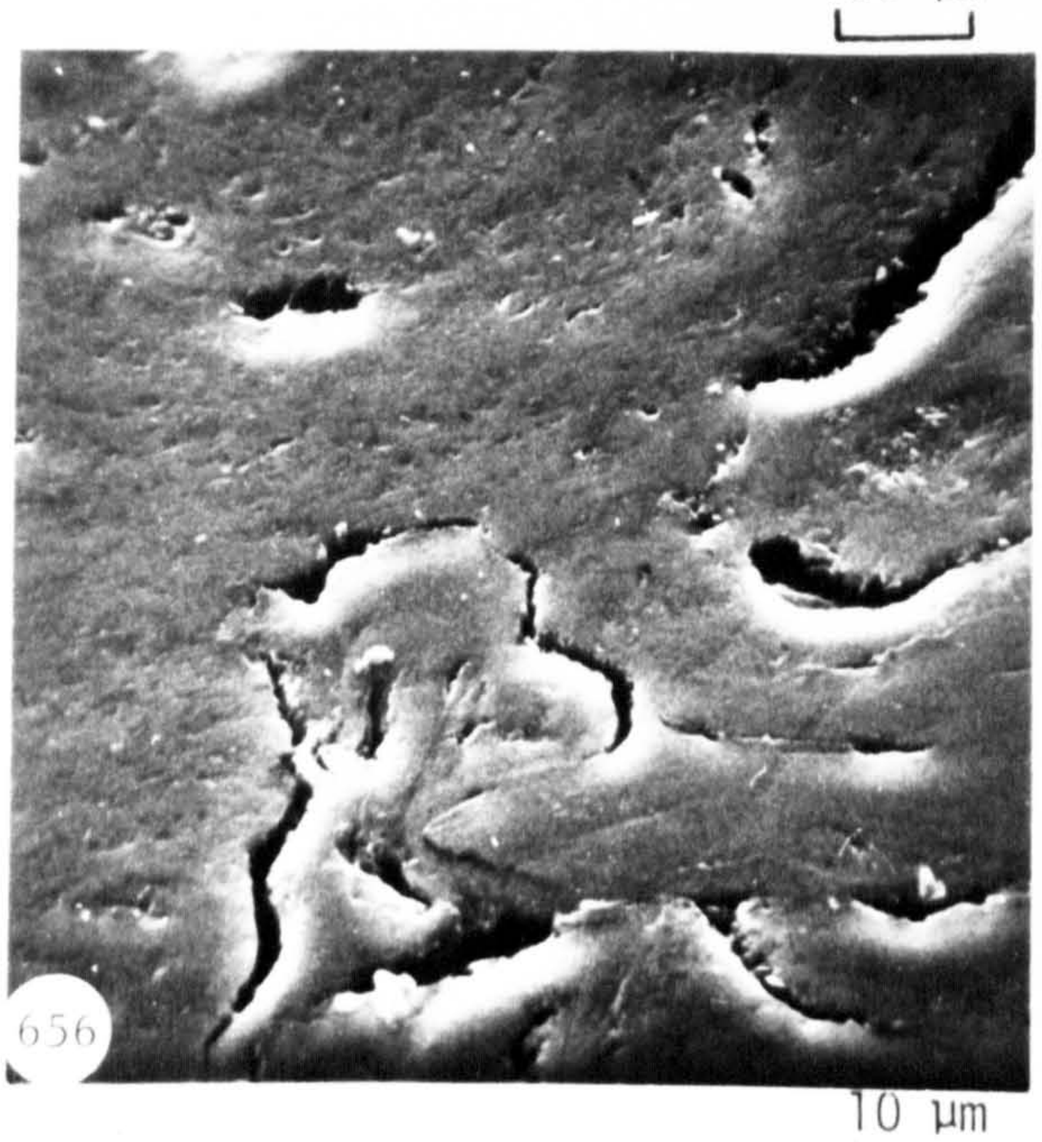
500 µm



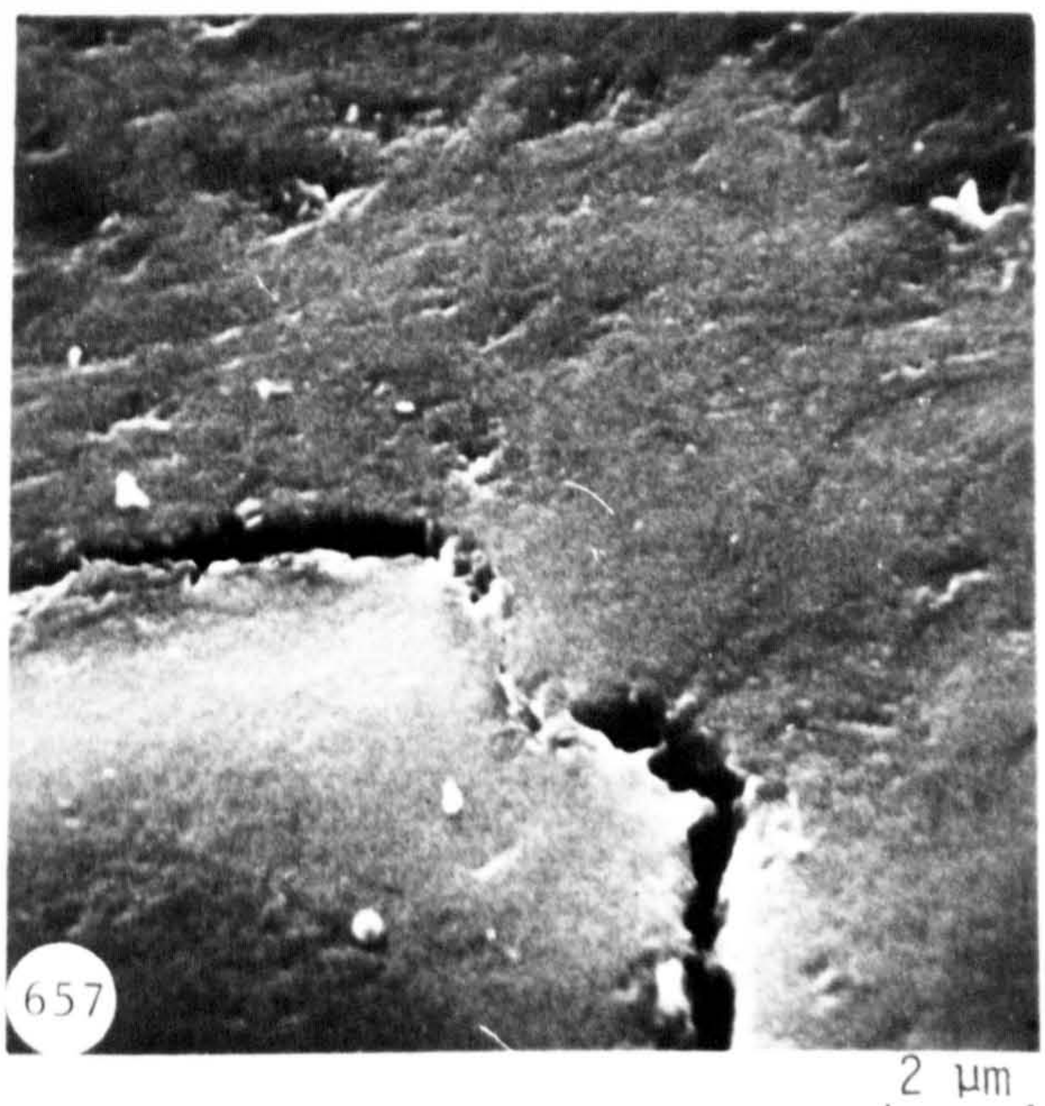
100 µm



20 µm



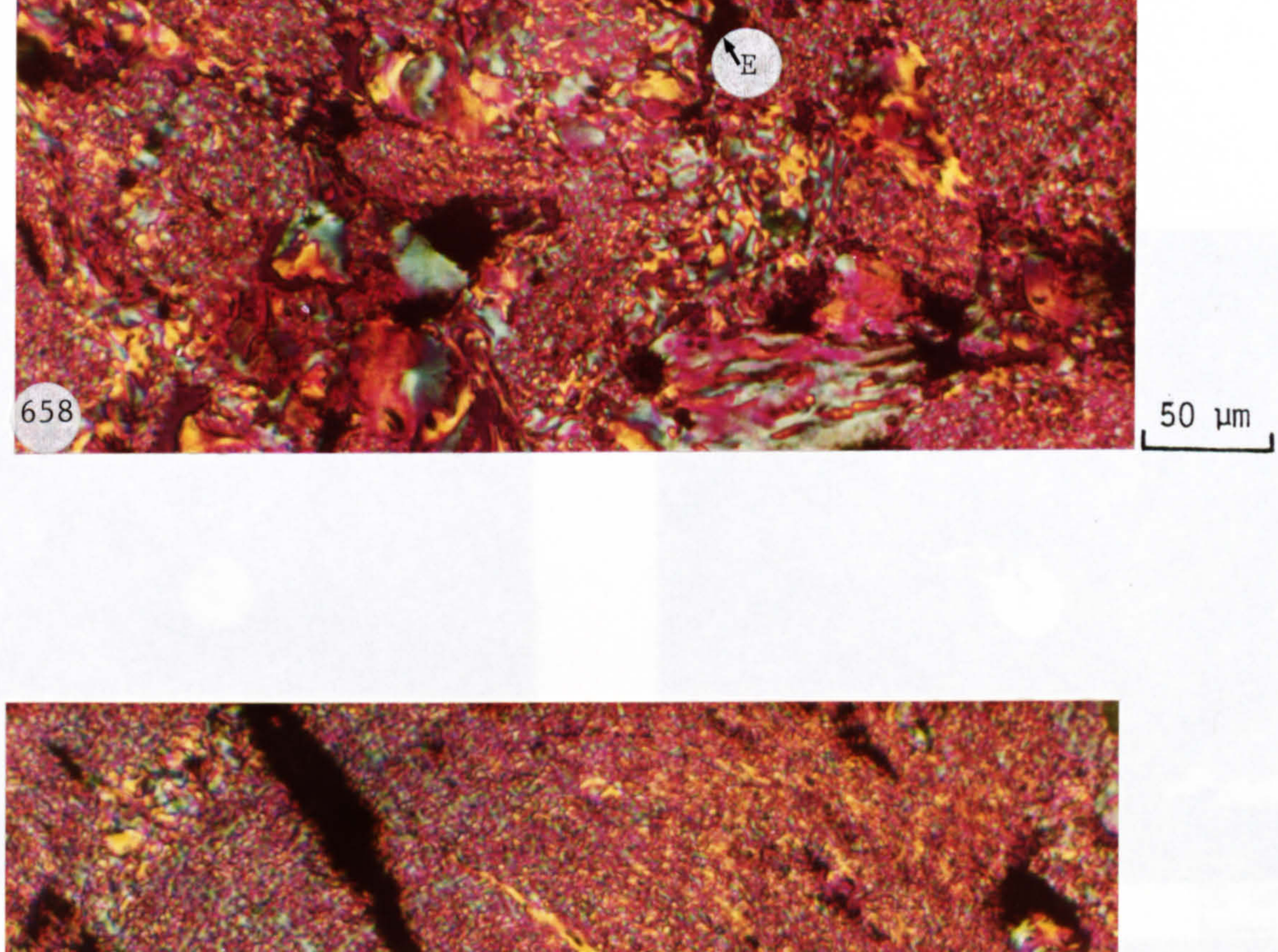
10 µm



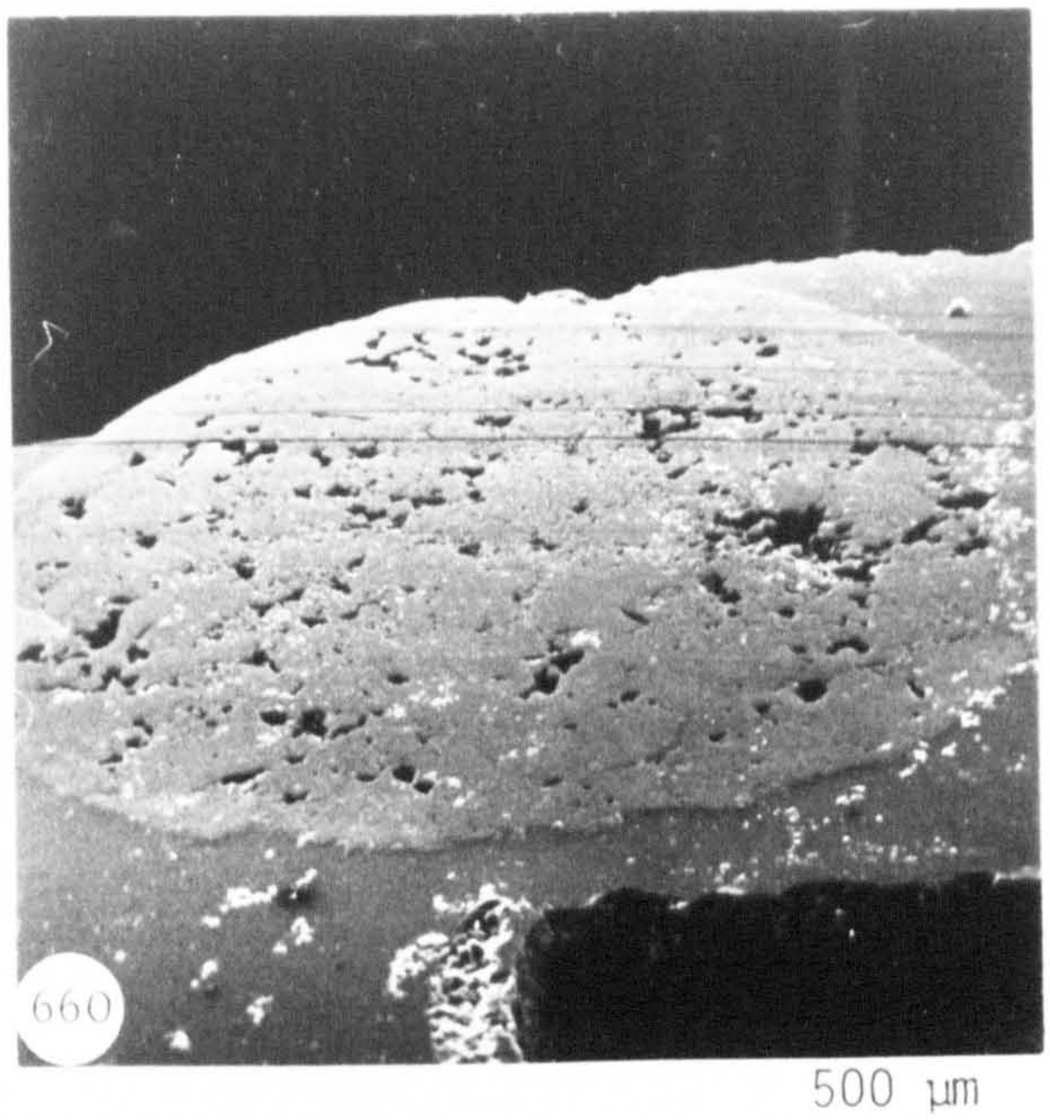
2 µm

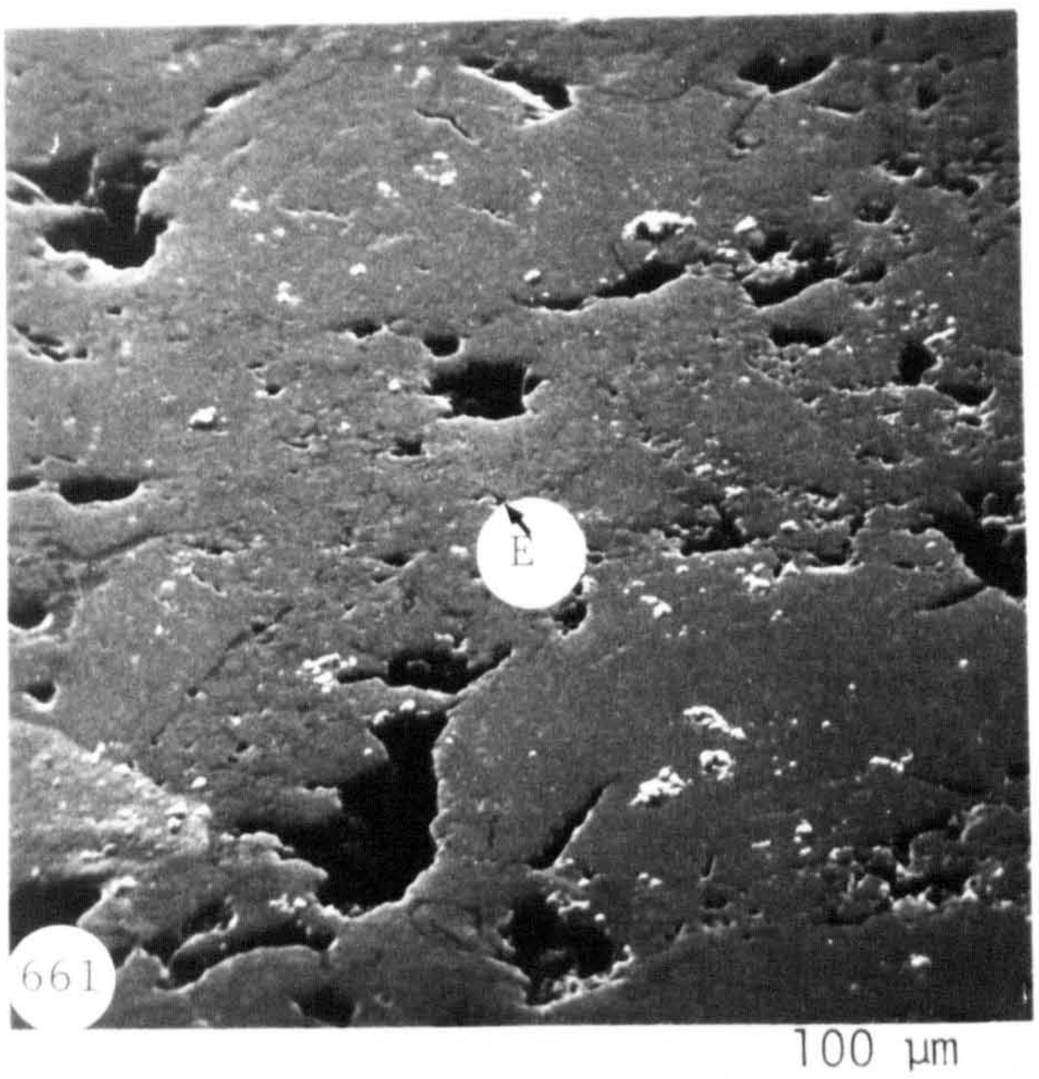
Figures 653 to 657. Scanning electron micrographs of Gilso-carbon Graphite (NA)

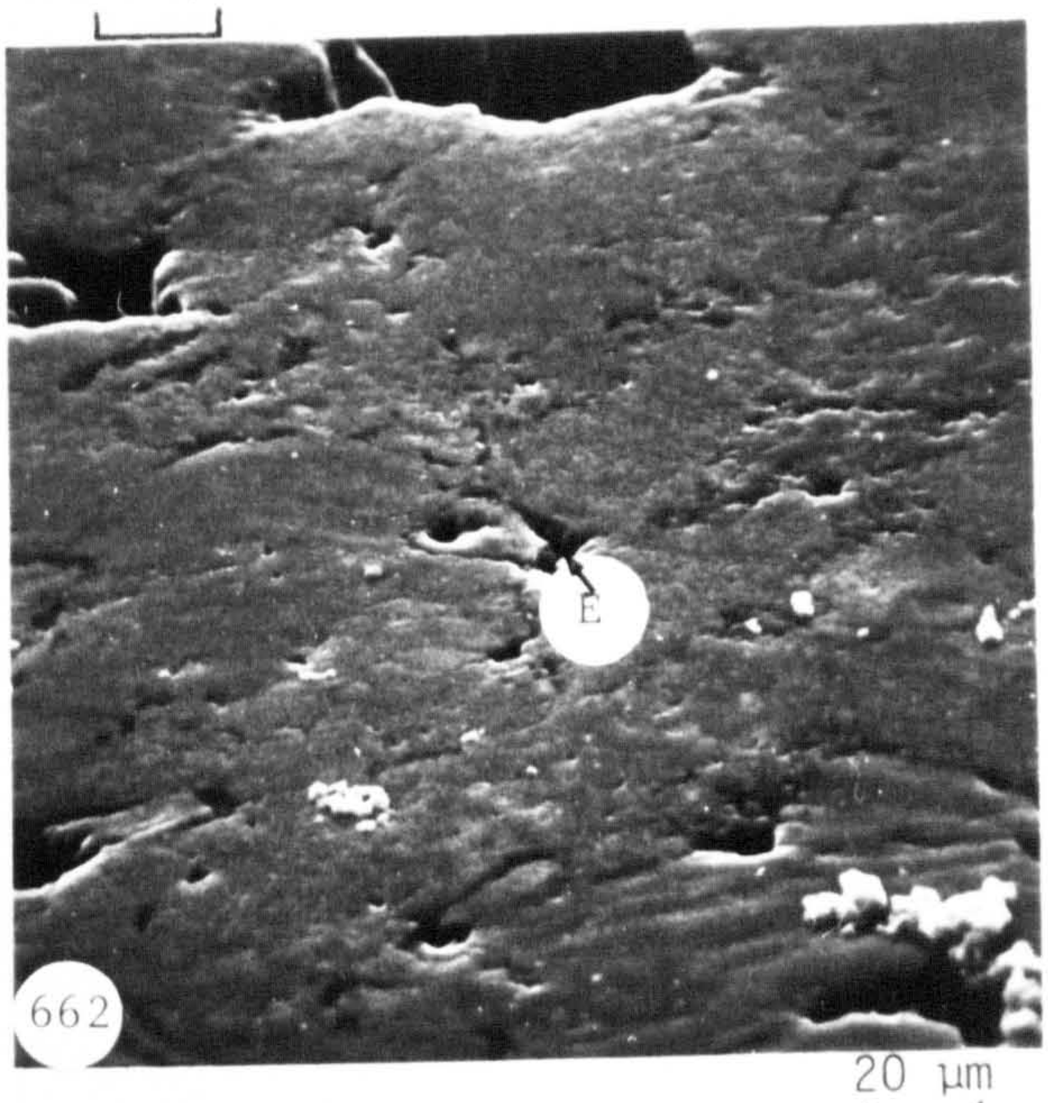


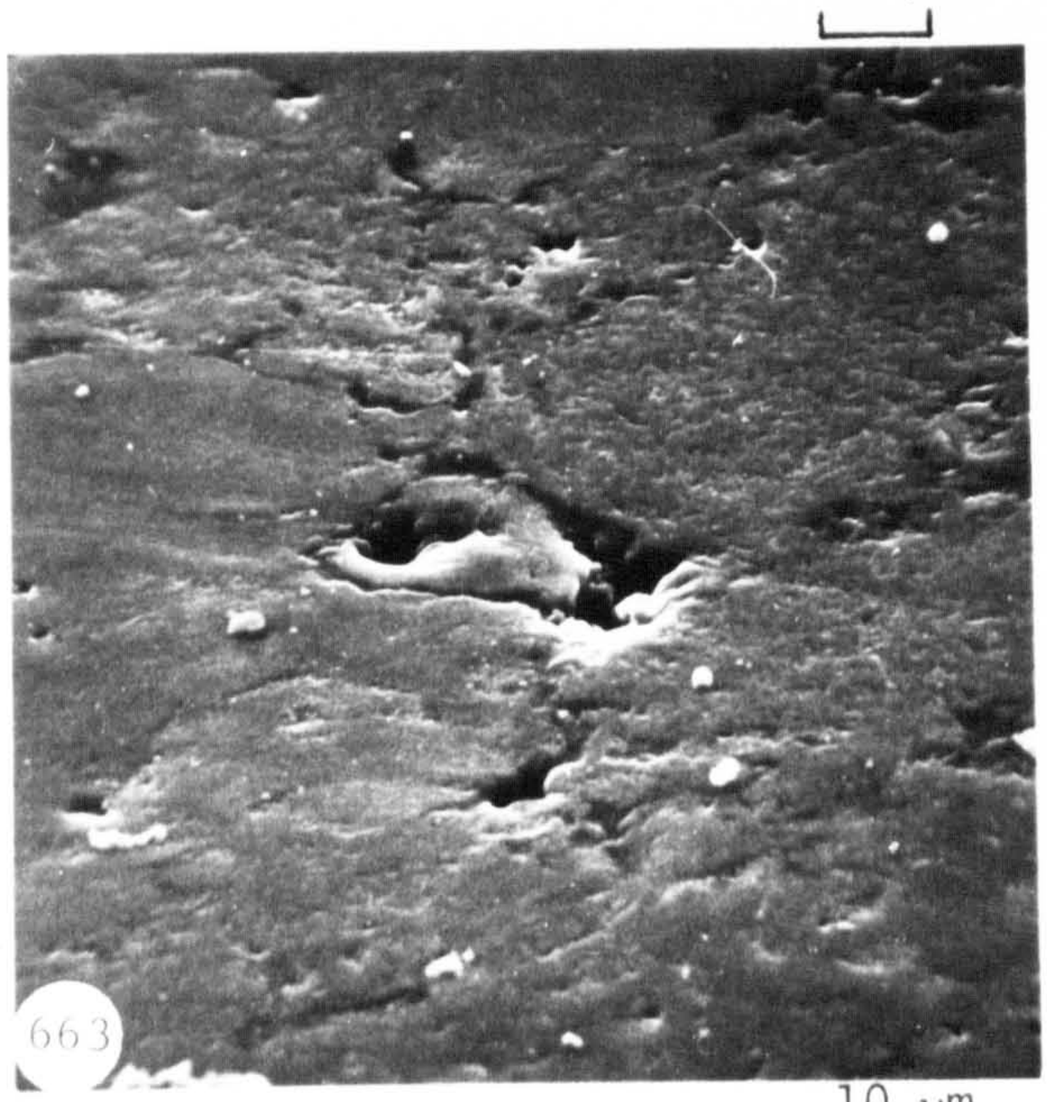


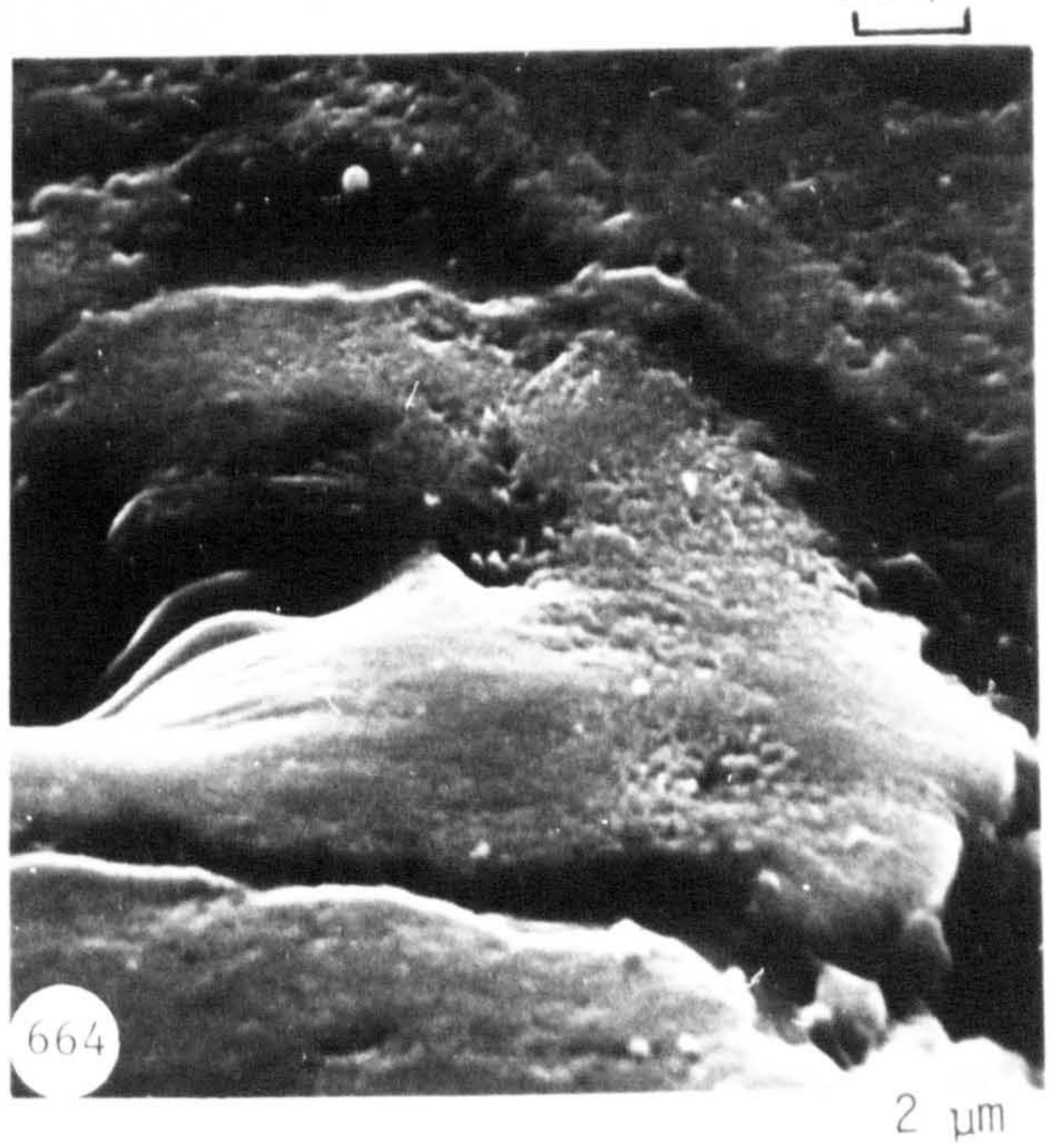
Figures 658 and 659. Optical micrographs of Gilso-carbon graphite (FRC) after neutron irradiation (-0.00% linear growth).



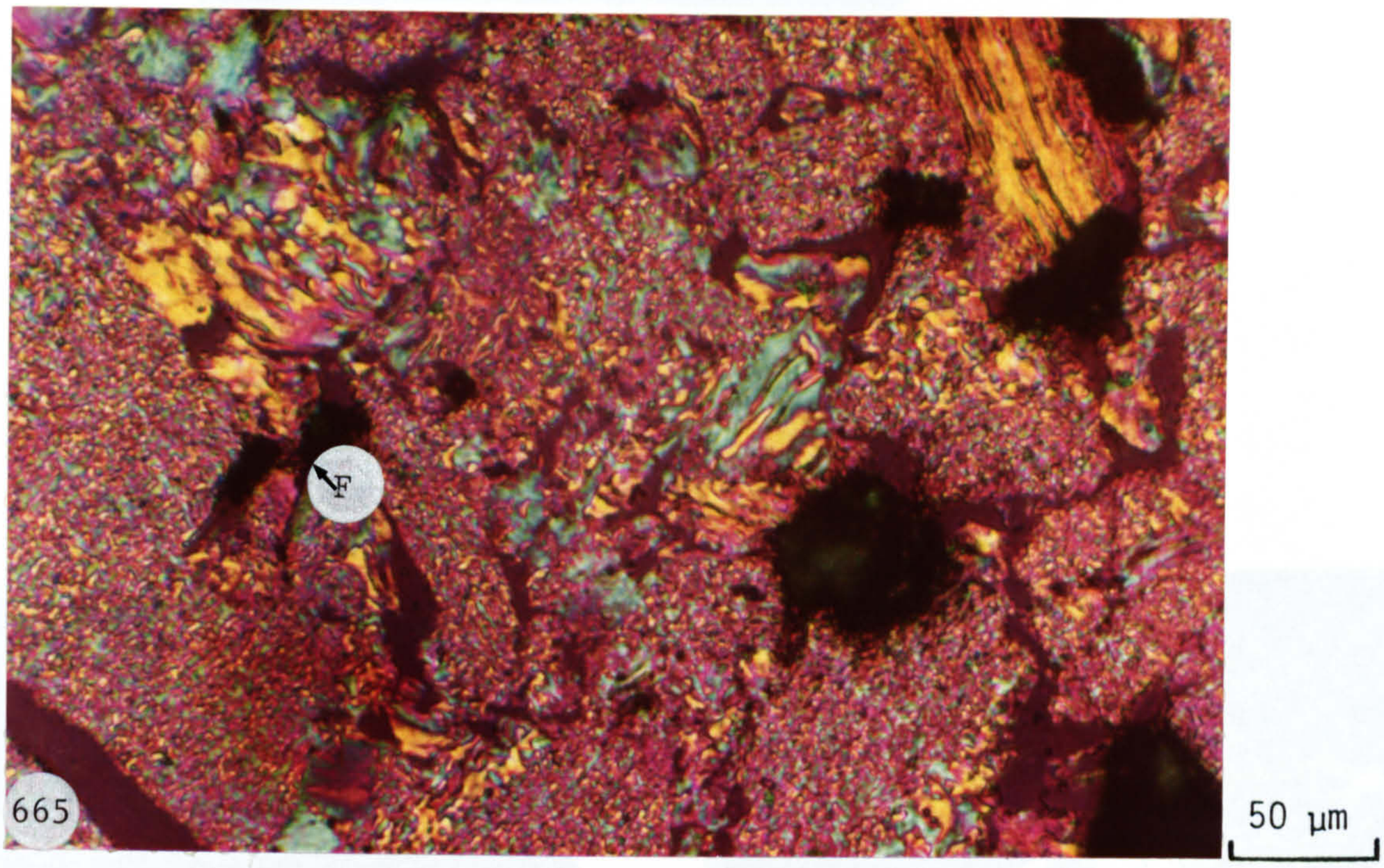


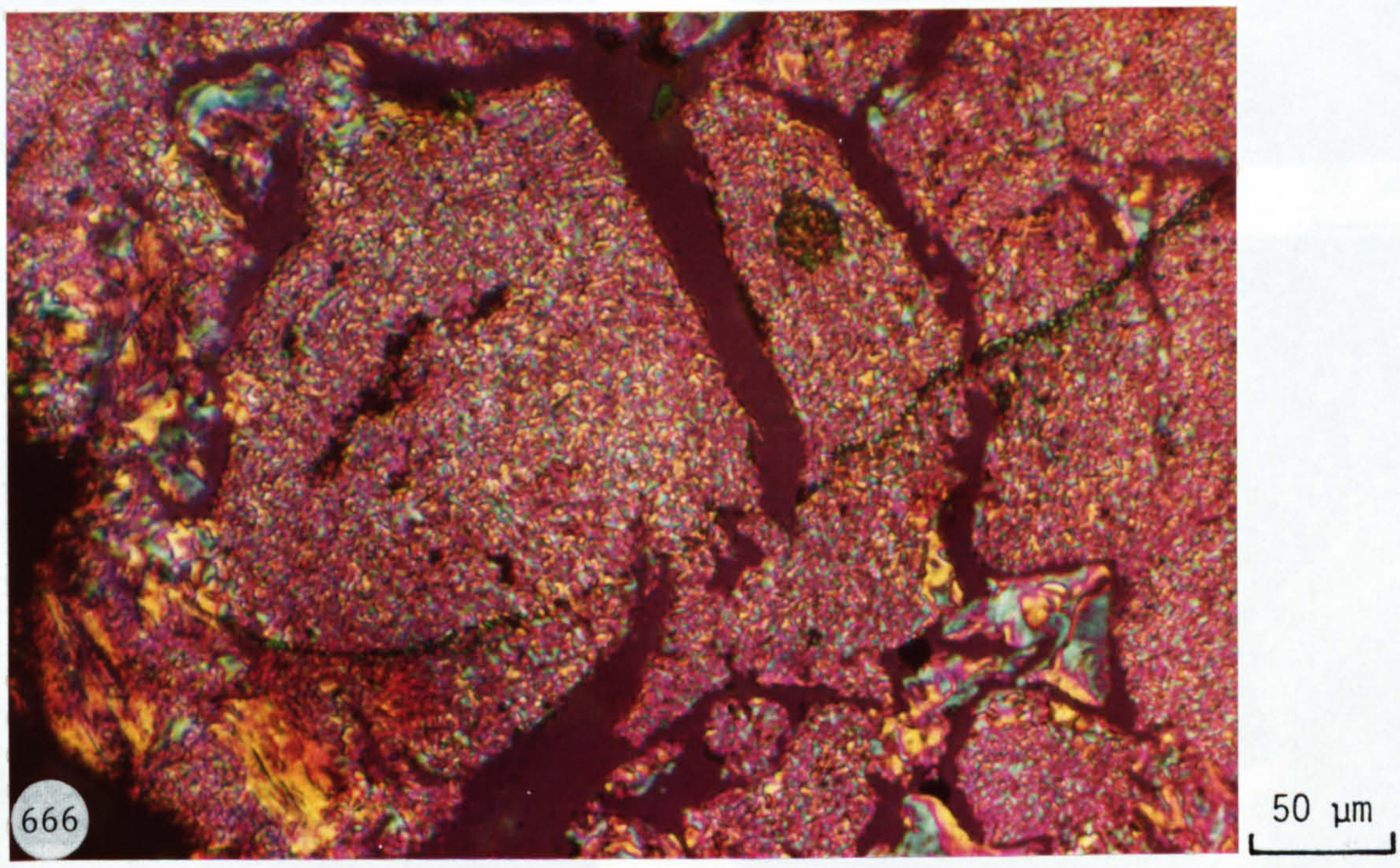




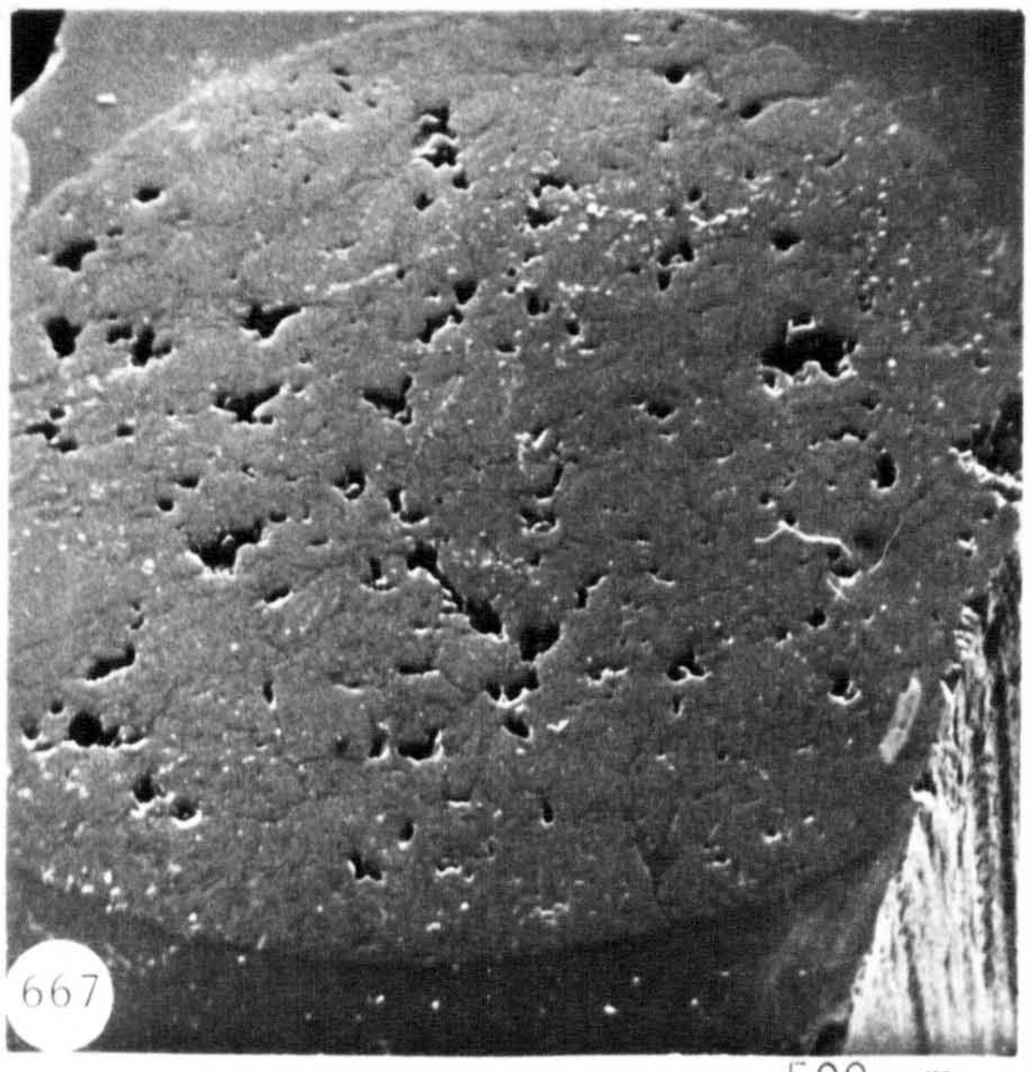


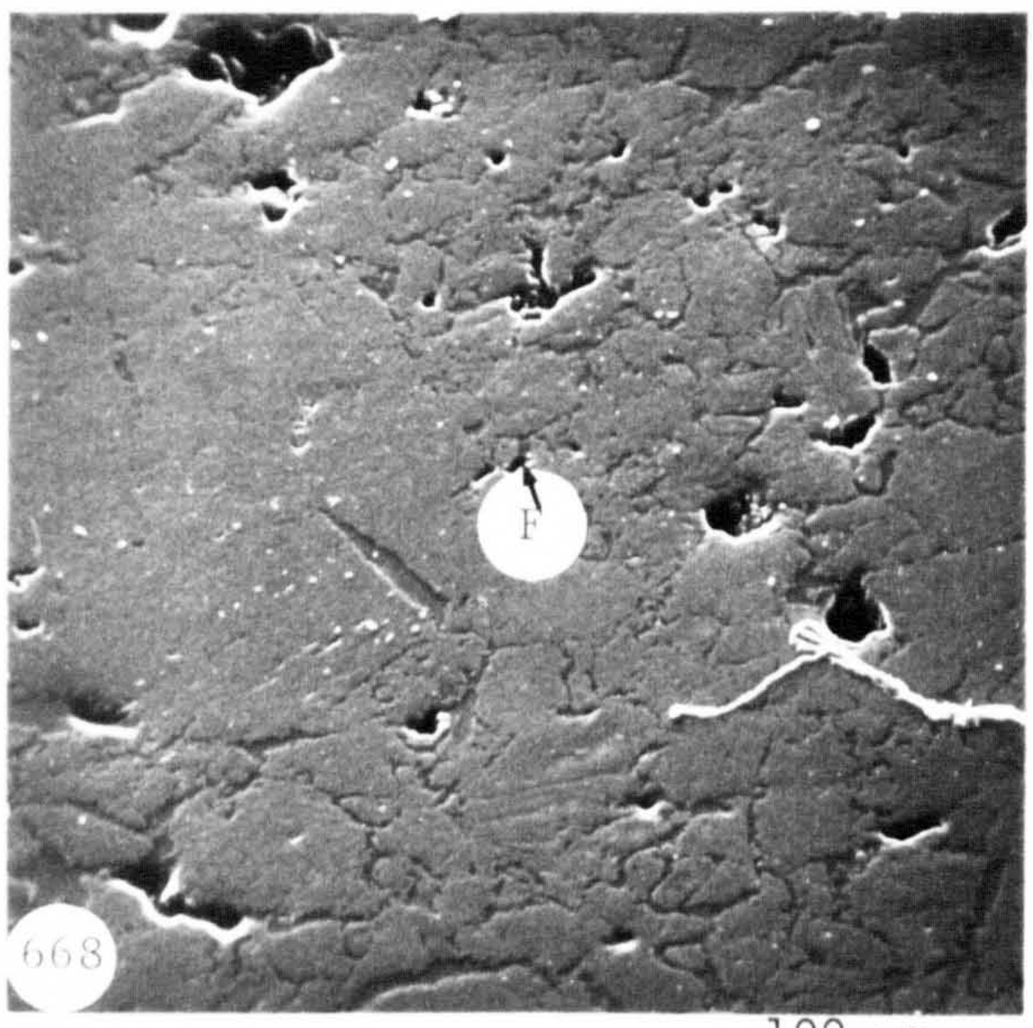
Figures 660 to 664. Scanning electron micrographs of Gilso-carbon Graphite (FRC) after neutron irradiation (-0.00% linear growth).

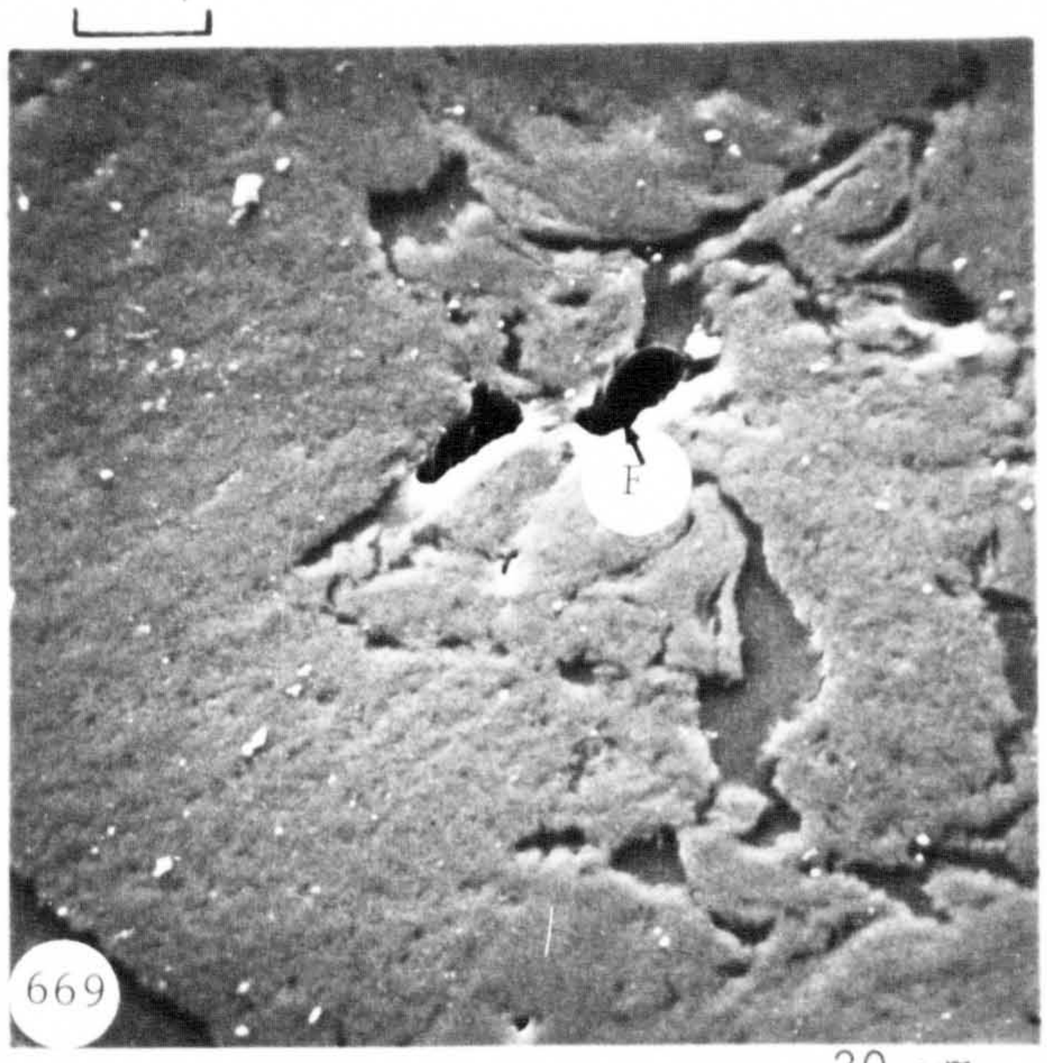


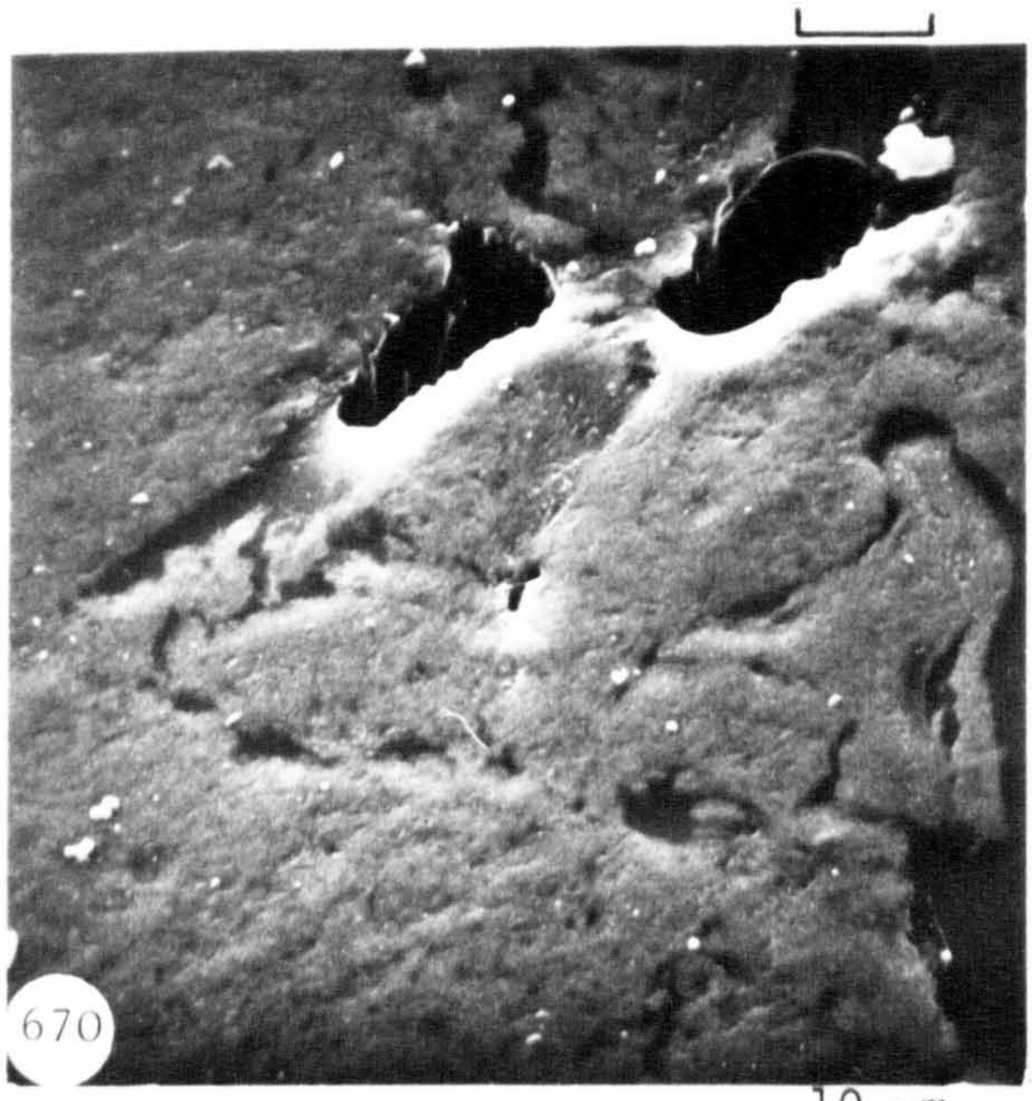


Figures 665 and 666. Optical micrographs of Gilso-carbon graphite (HAB) after neutron irradiation (+4.0% linear growth).











Figures 667 to 671. Scanning electron micrographs of Gilso-carbon Graphite (HAB) after neutron irradiation (+4.0% linear growth).

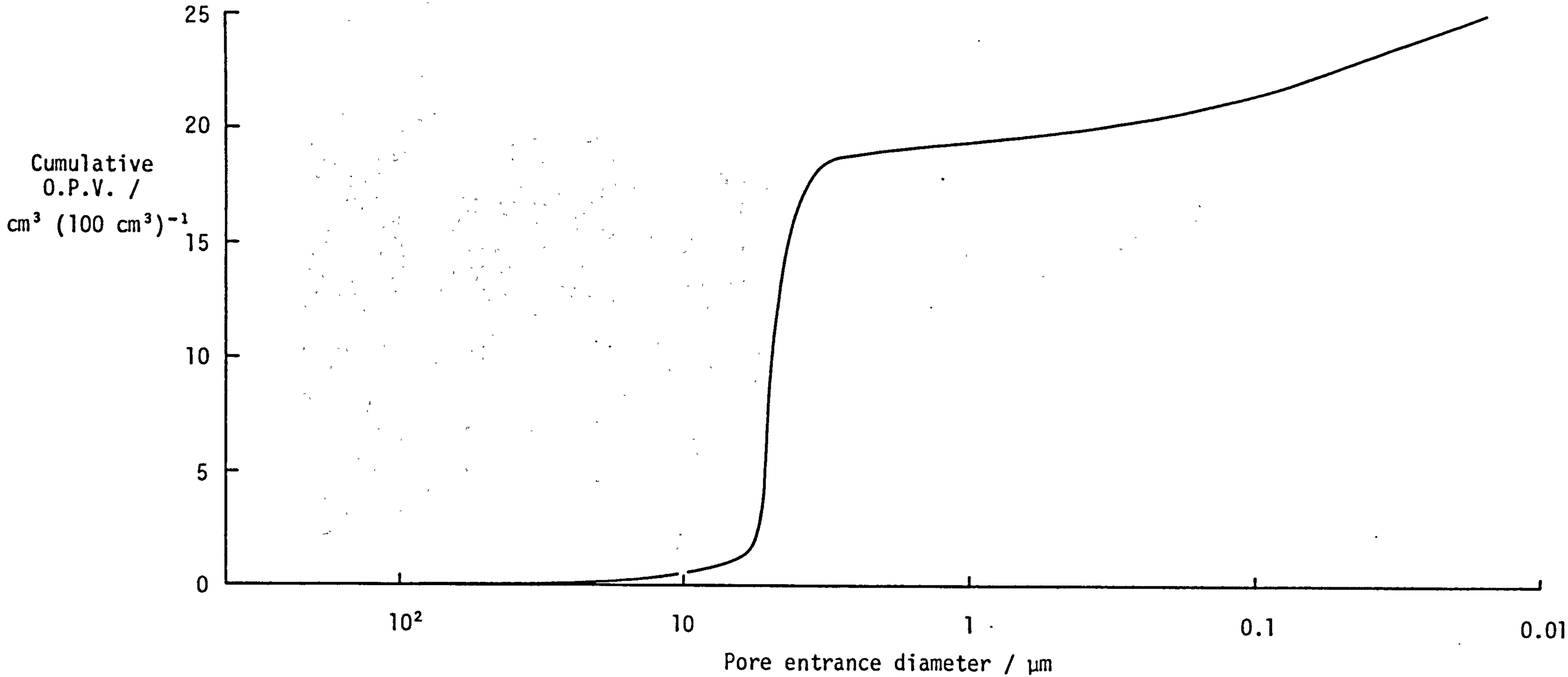
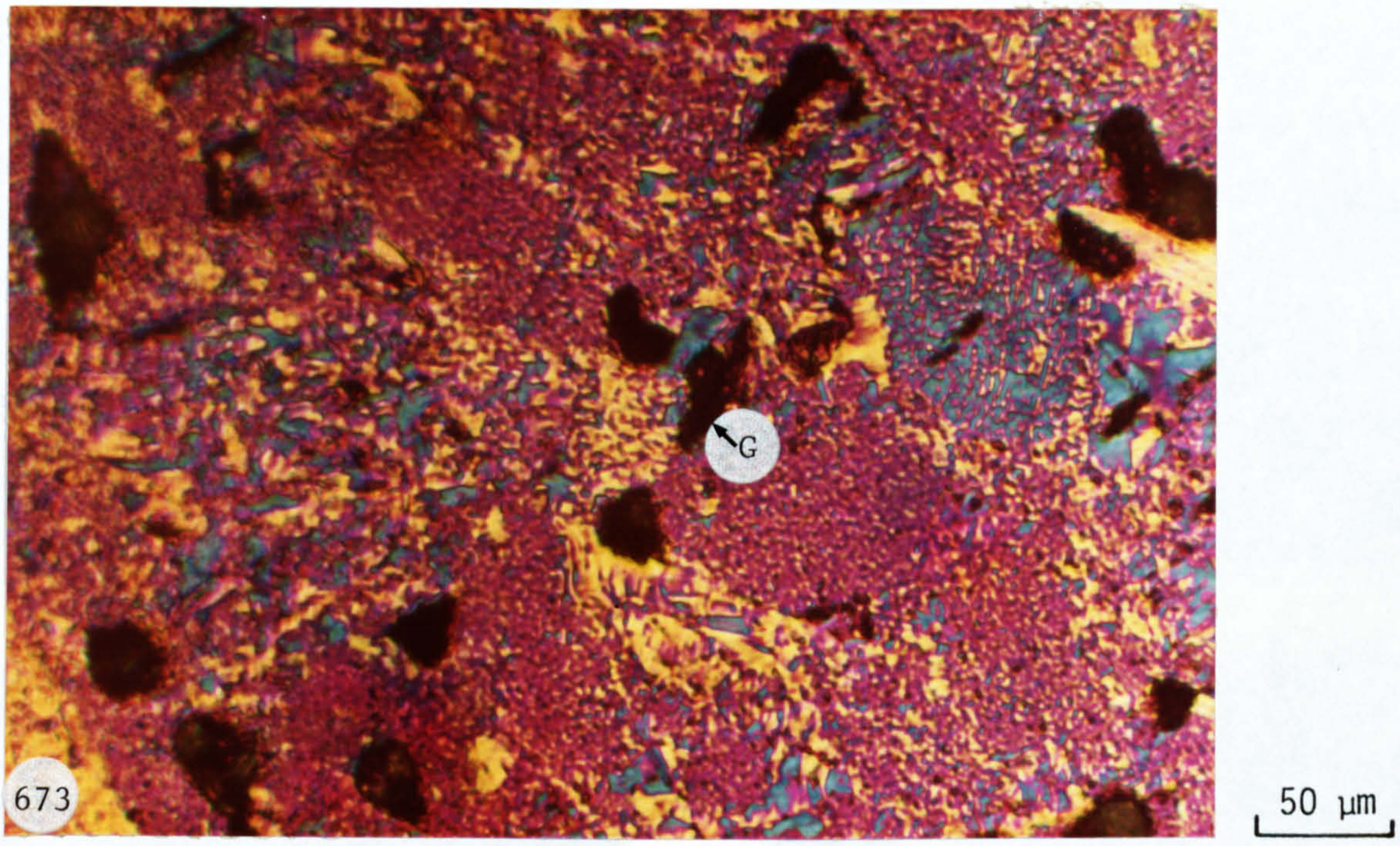
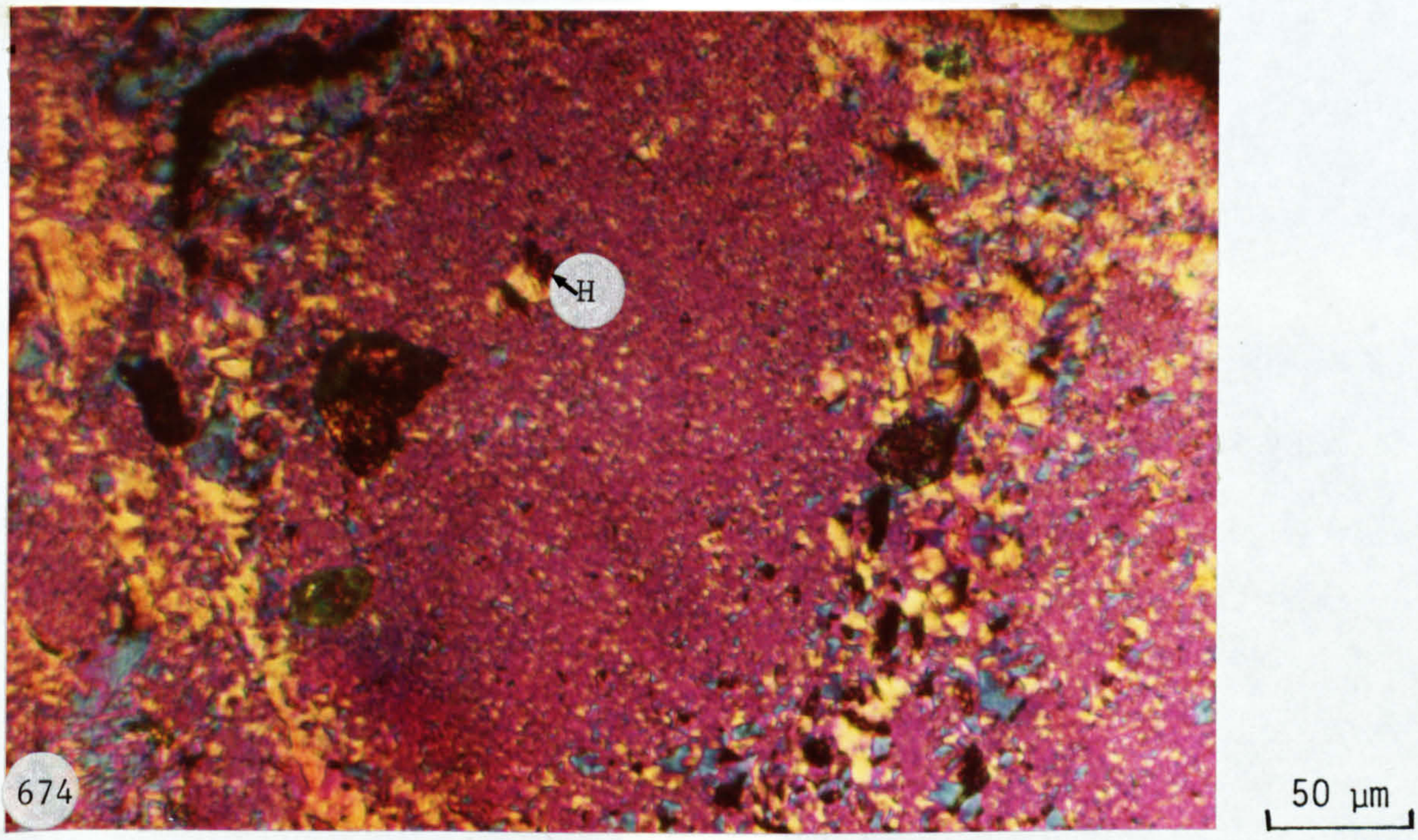
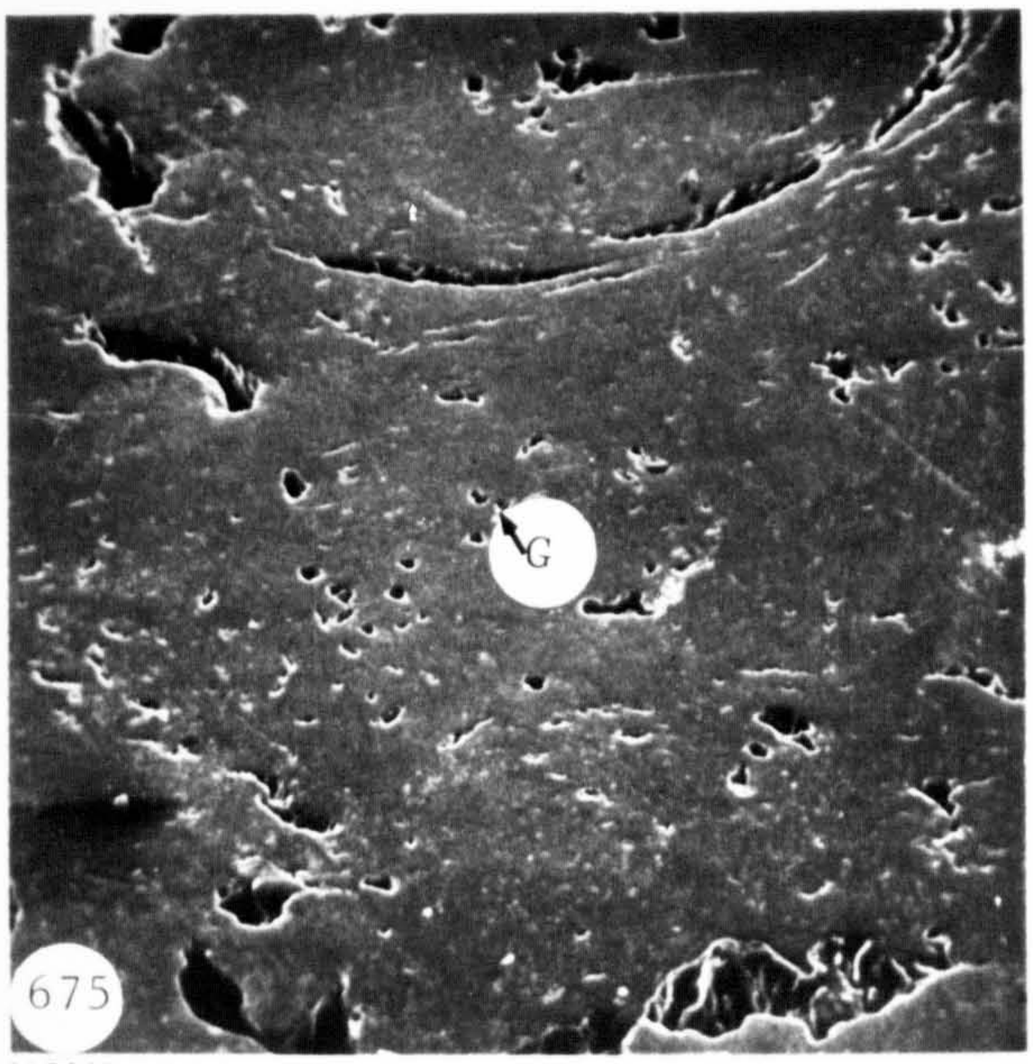


Figure 672. Mercury pore size distribution of virgin AGLCP graphite. Variation of cumulative open pore volume with pore entrance diameter.

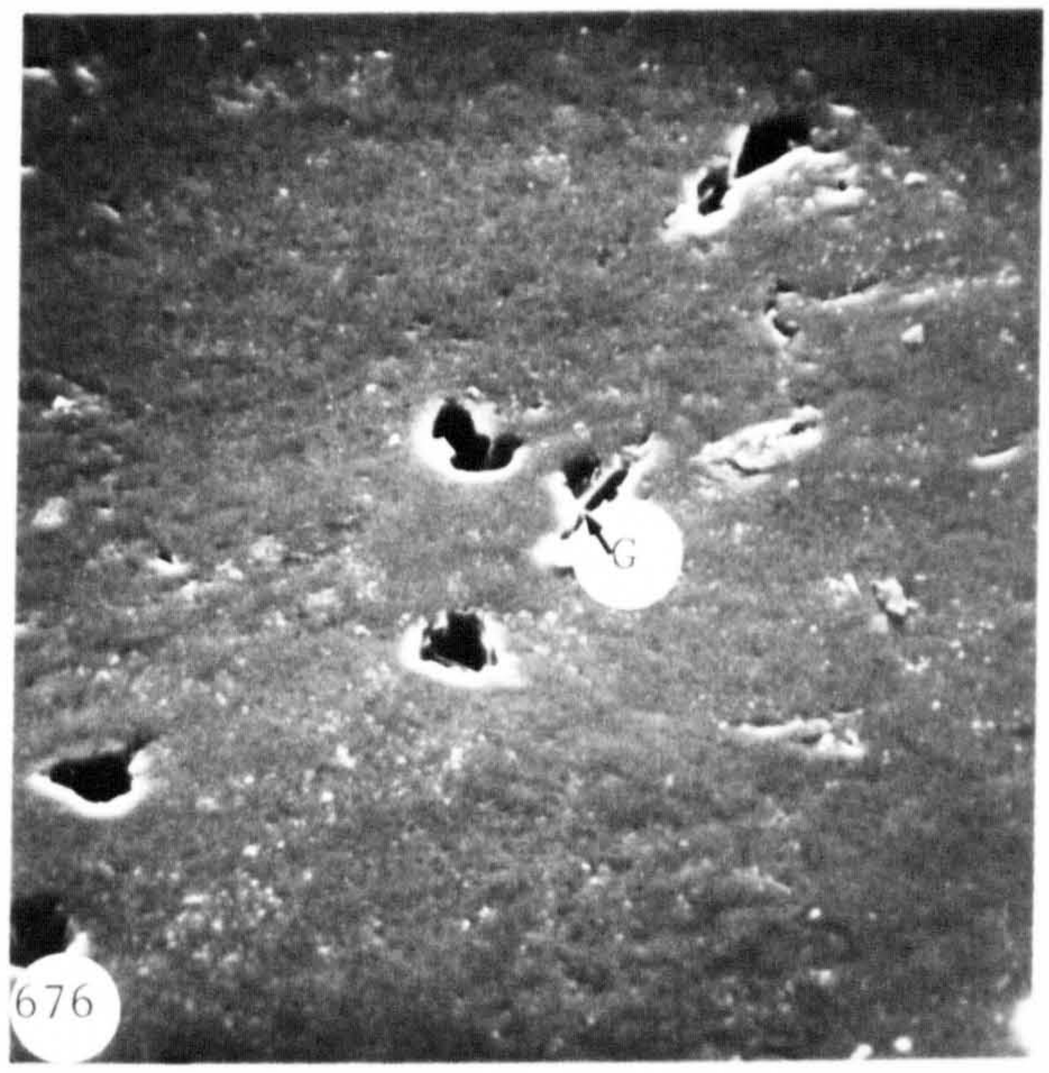




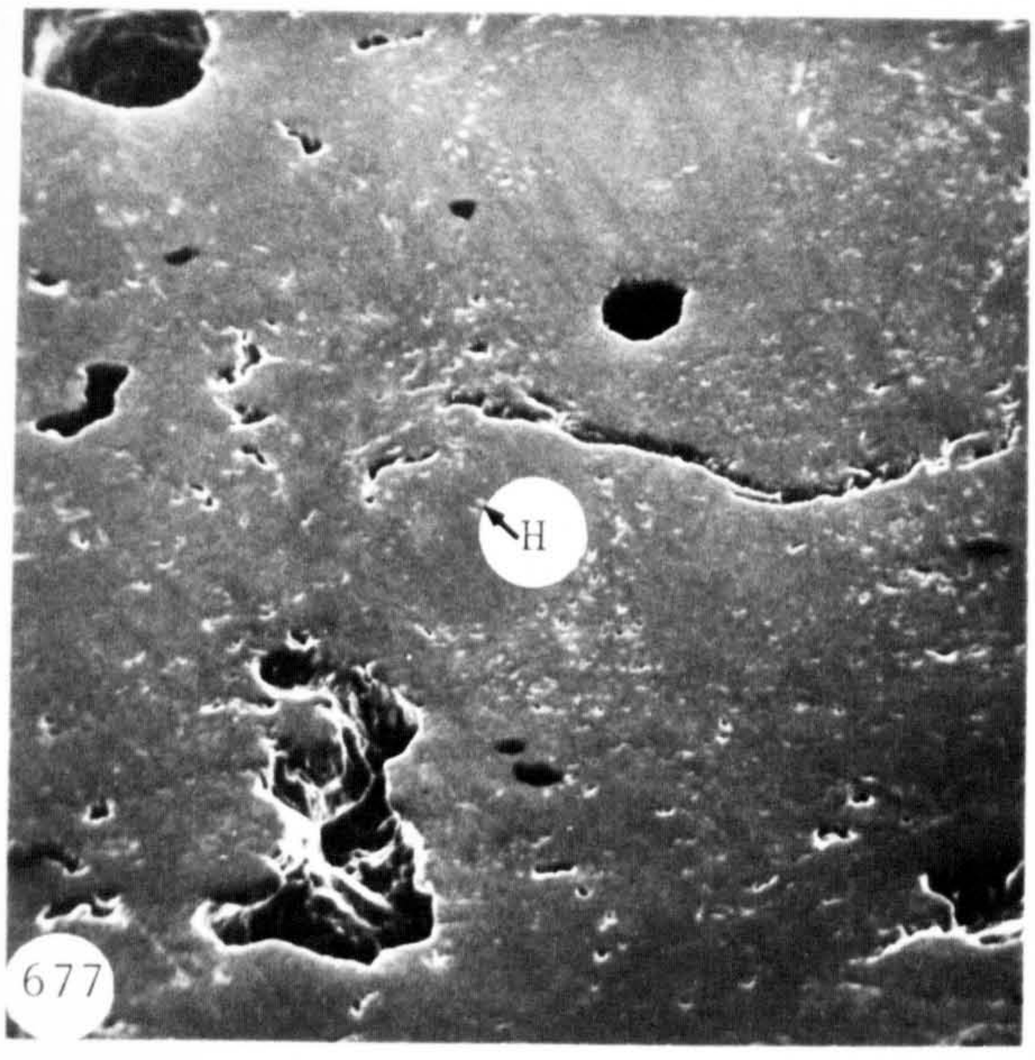
Figures 673 and 674. Optical micrographs of virgin VQMB Graphite.



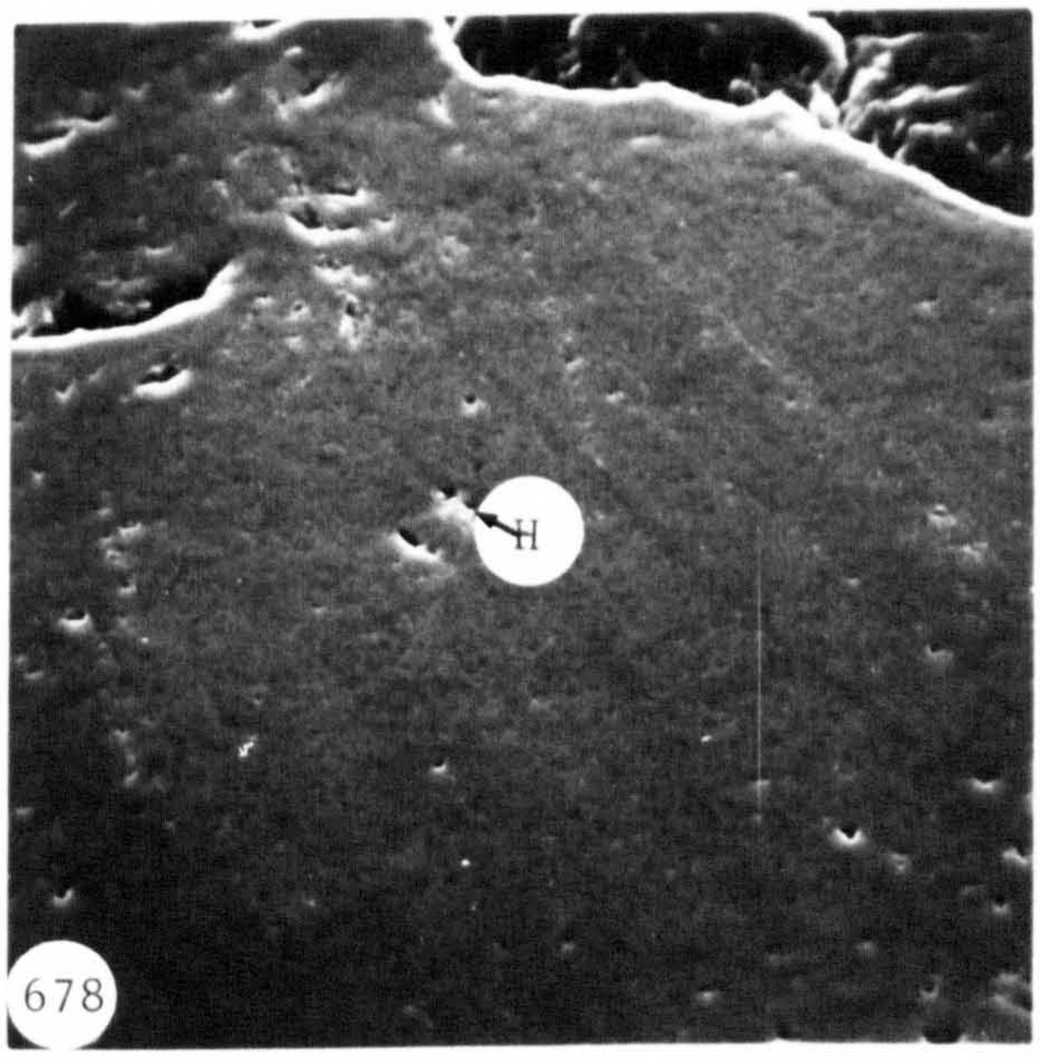
VQMB GRAPHITE 100 µm



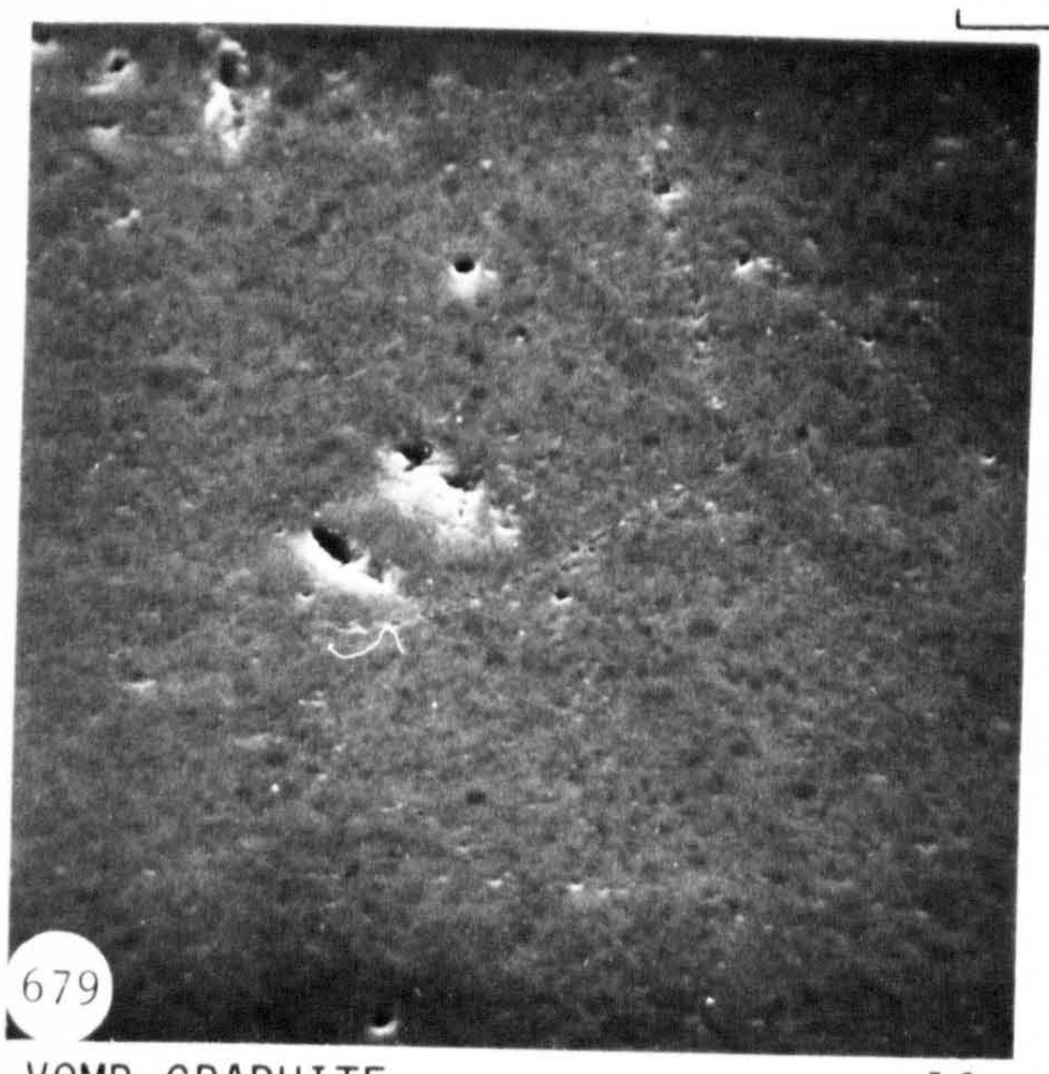
VQMB GRAPHITE 20 µm



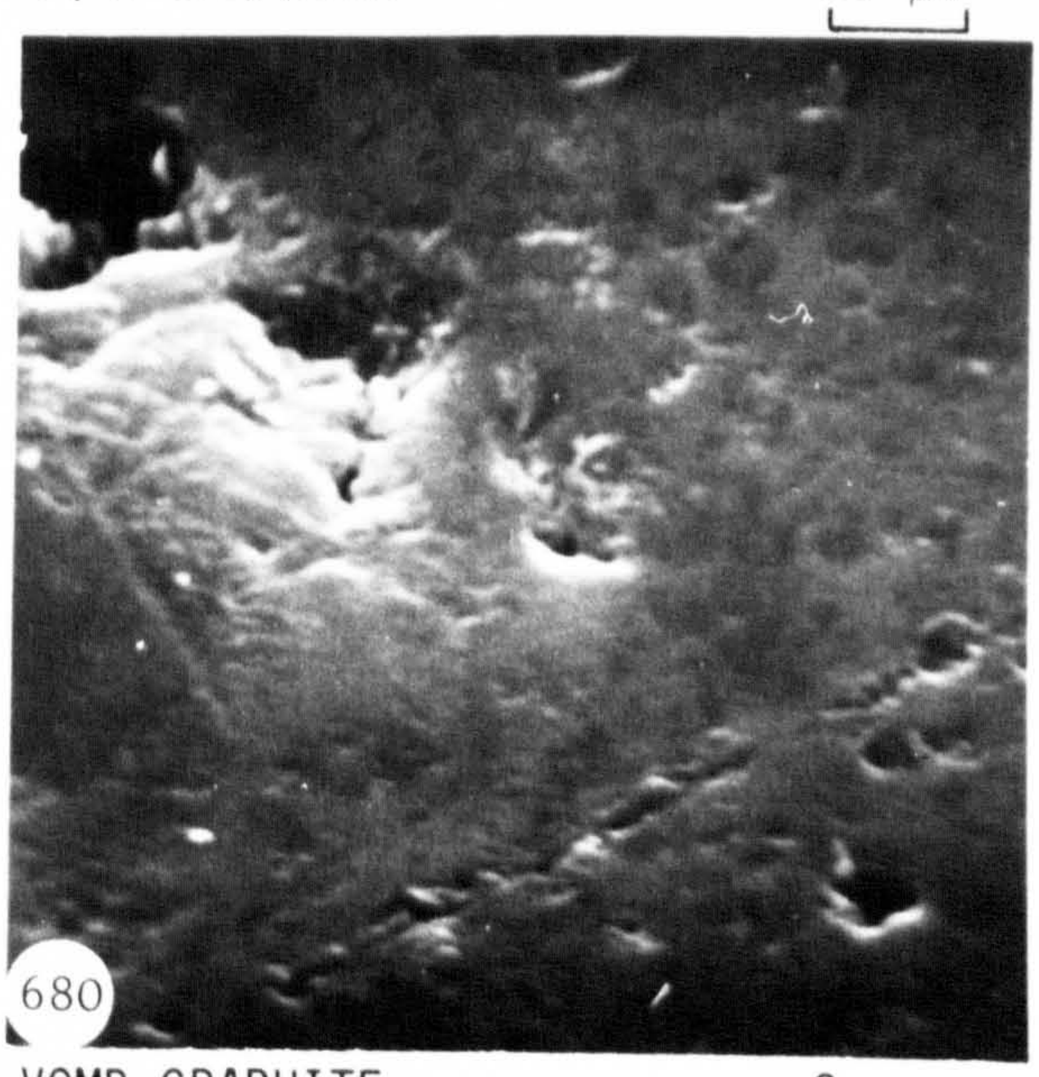
VQMB GRAPHITE 100 µm



VQMB GRAPHITE 20 µm

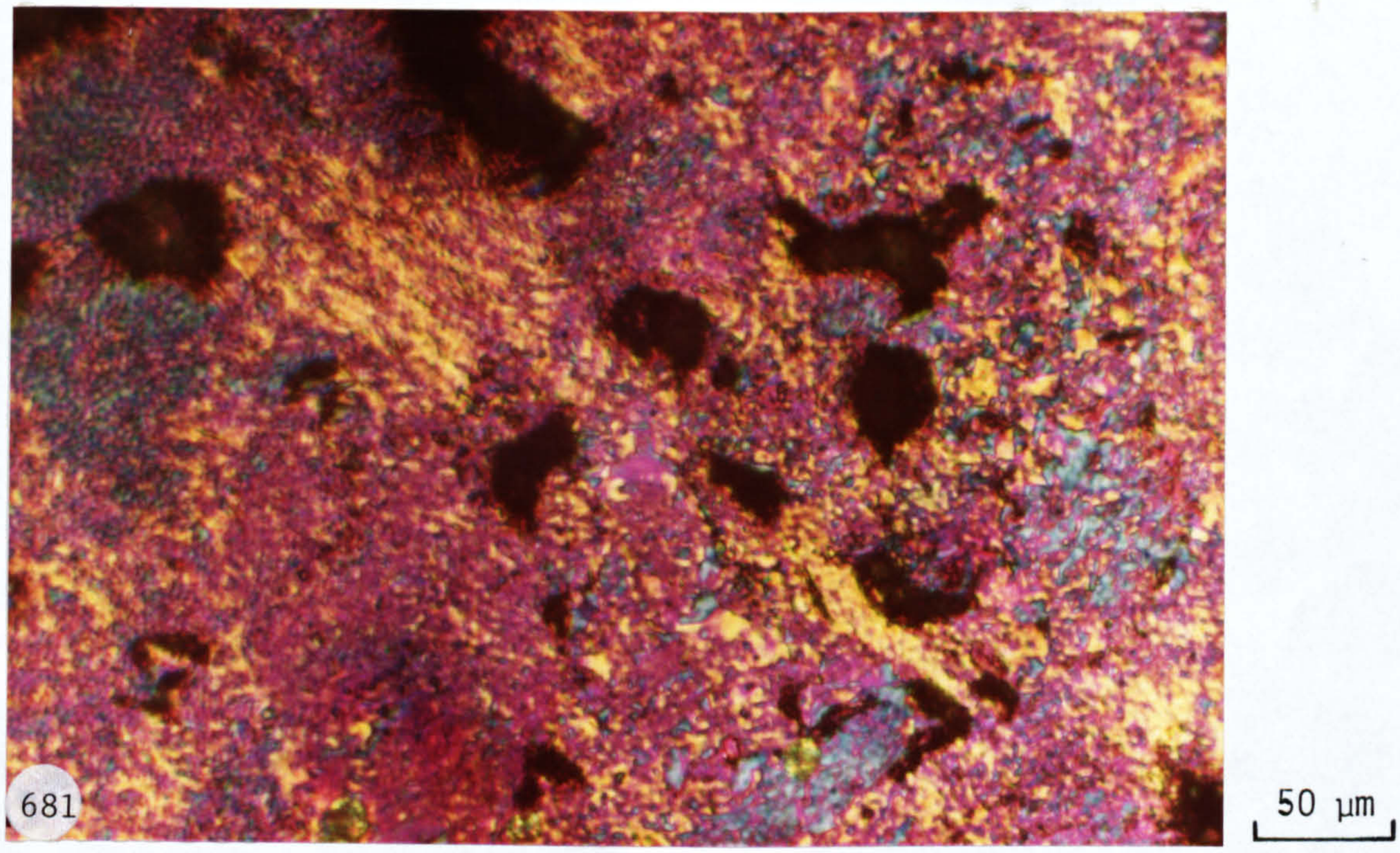


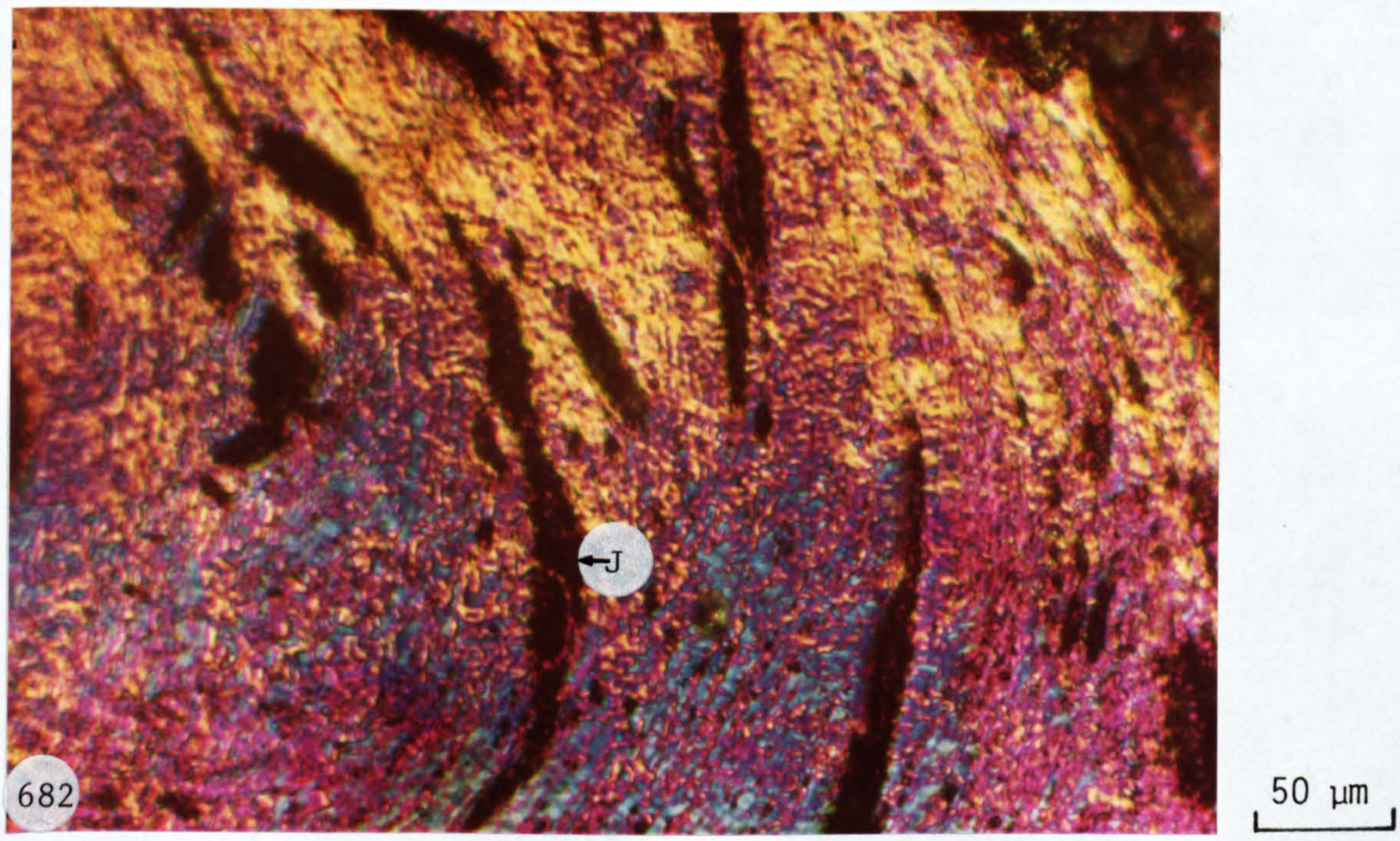
VQMB GRAPHITE 10 µm



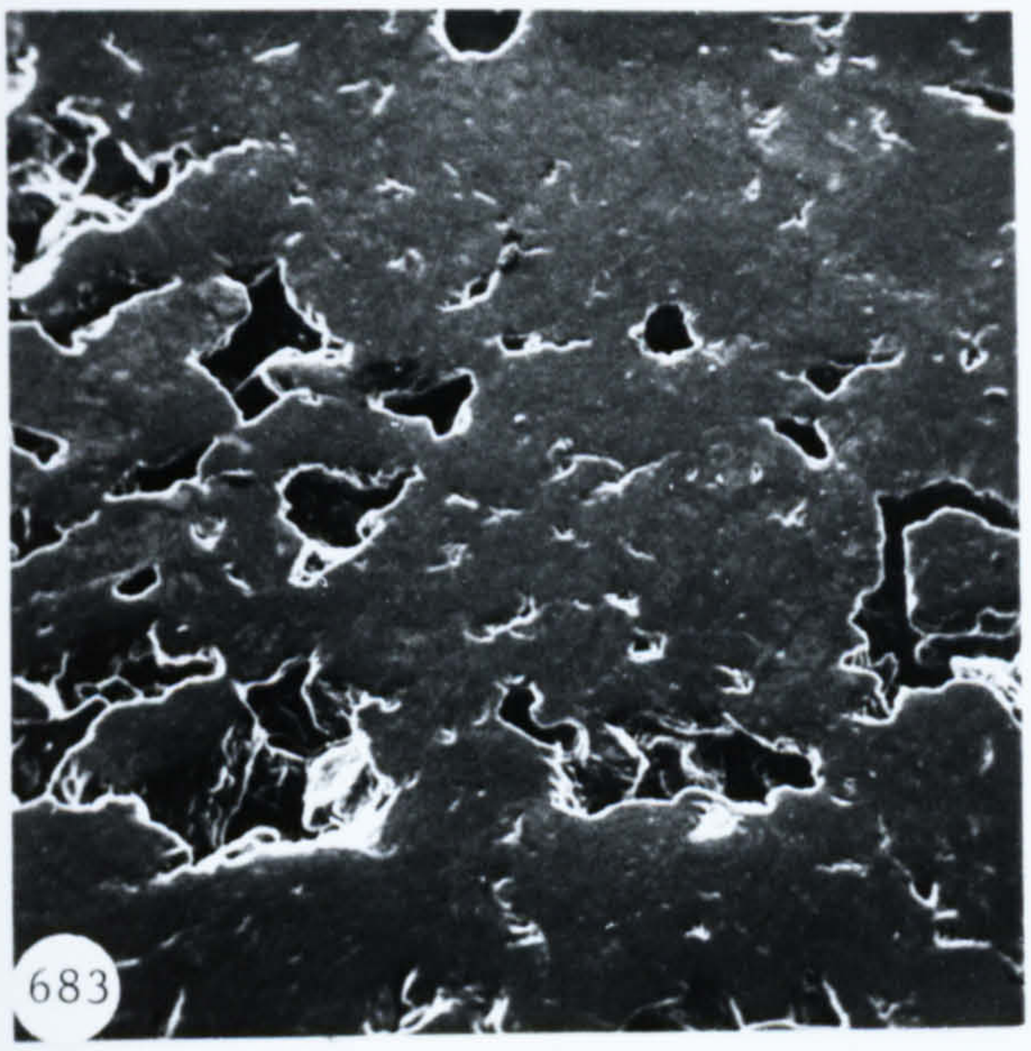
VQMB GRAPHITE 2 µm

Figures 675 to 680. Scanning electron micrographs (stereoscan) of virgin VQMB Graphite.

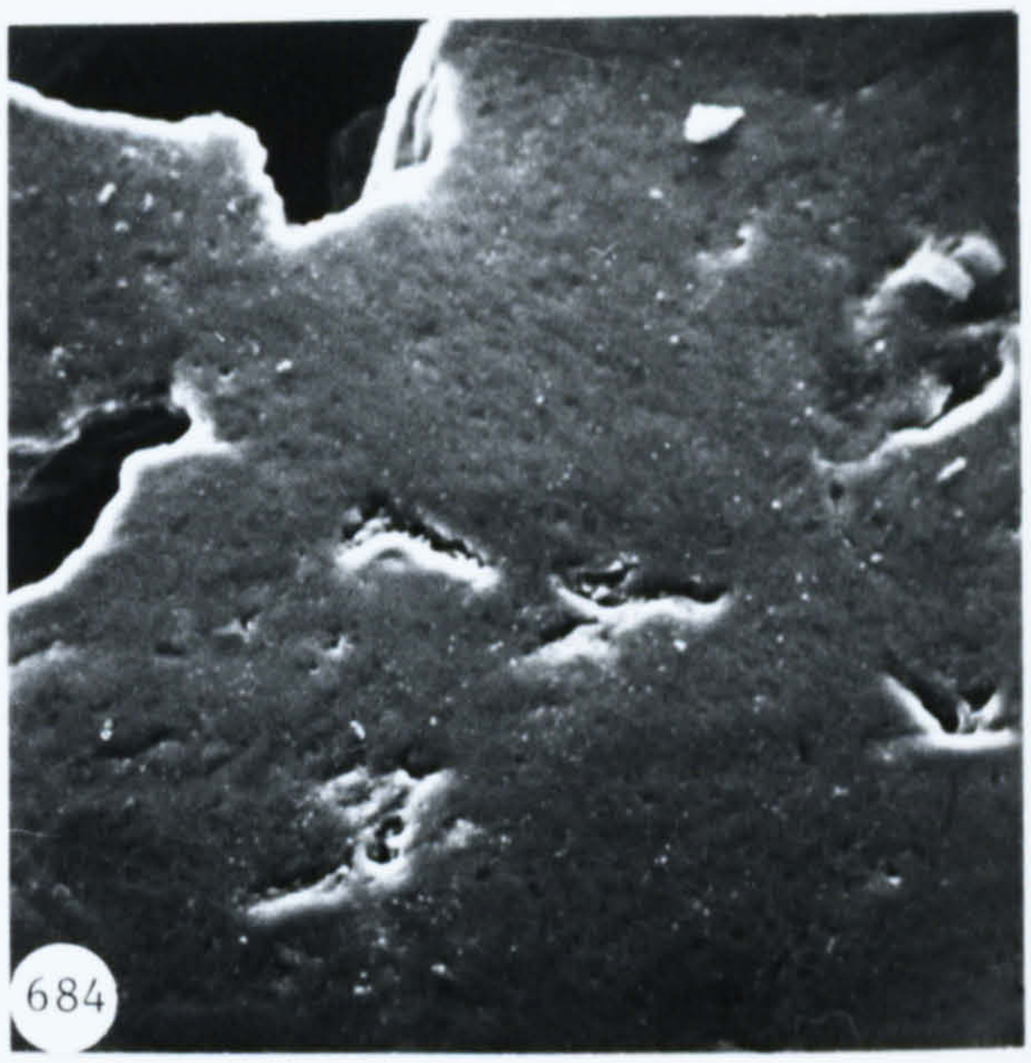




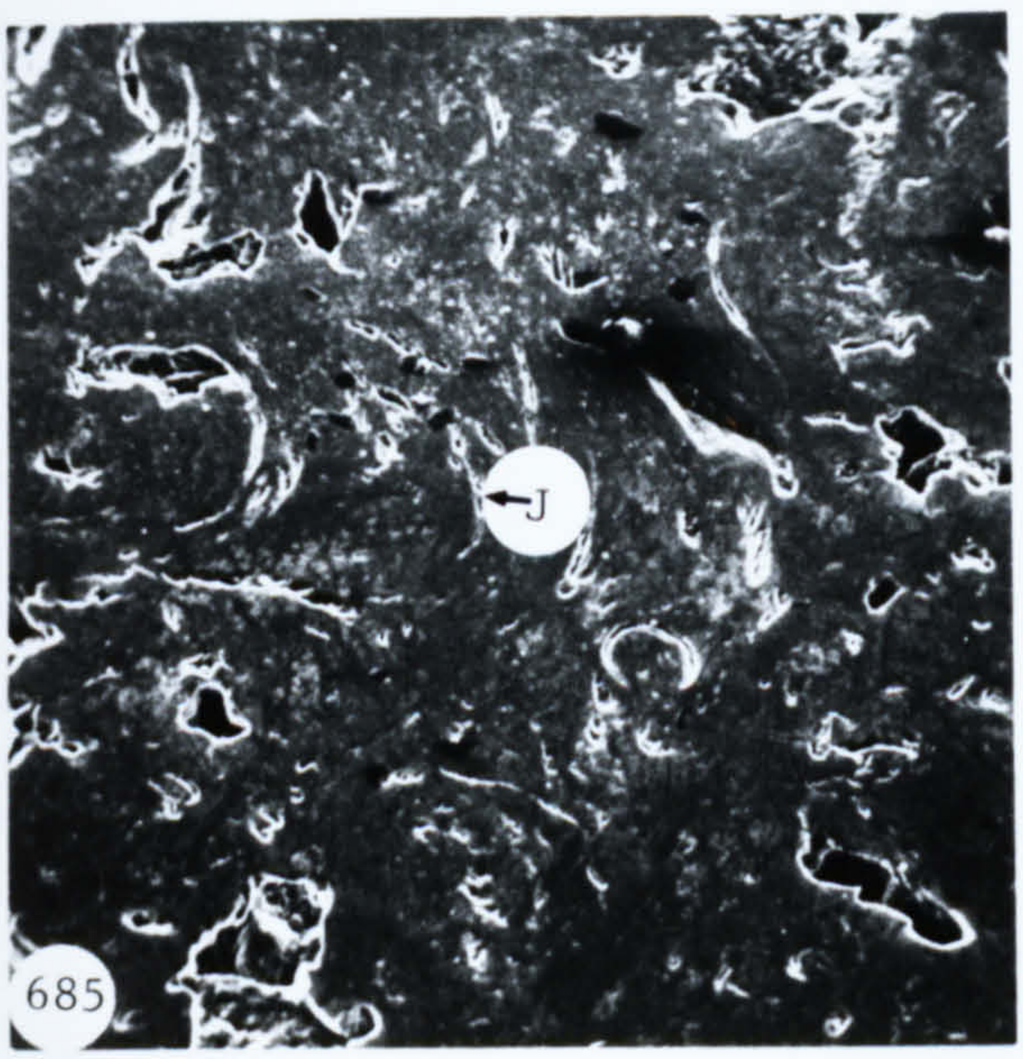
Figures 681 and 682. Optical micrographs of virgin VNMC Graphite.



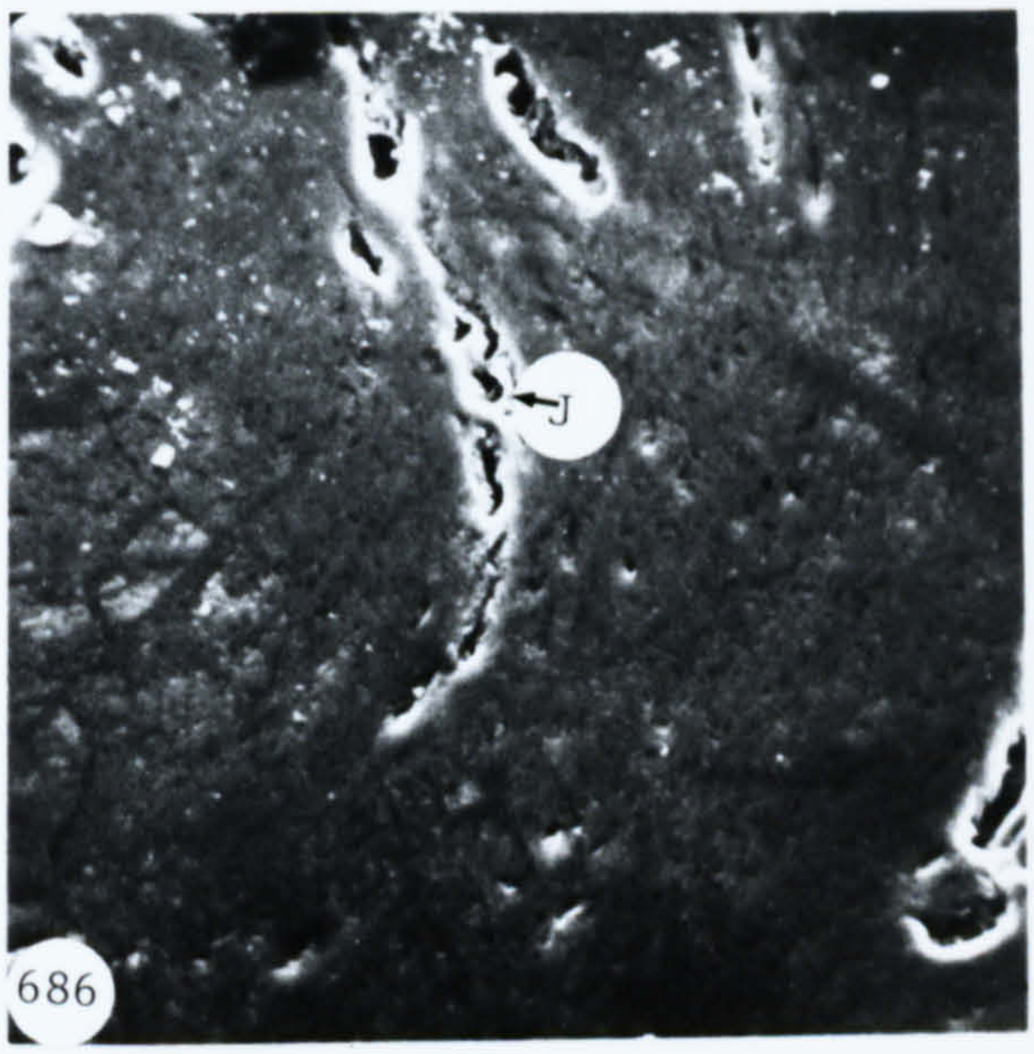
VNMC GRAPHITE 100 µm



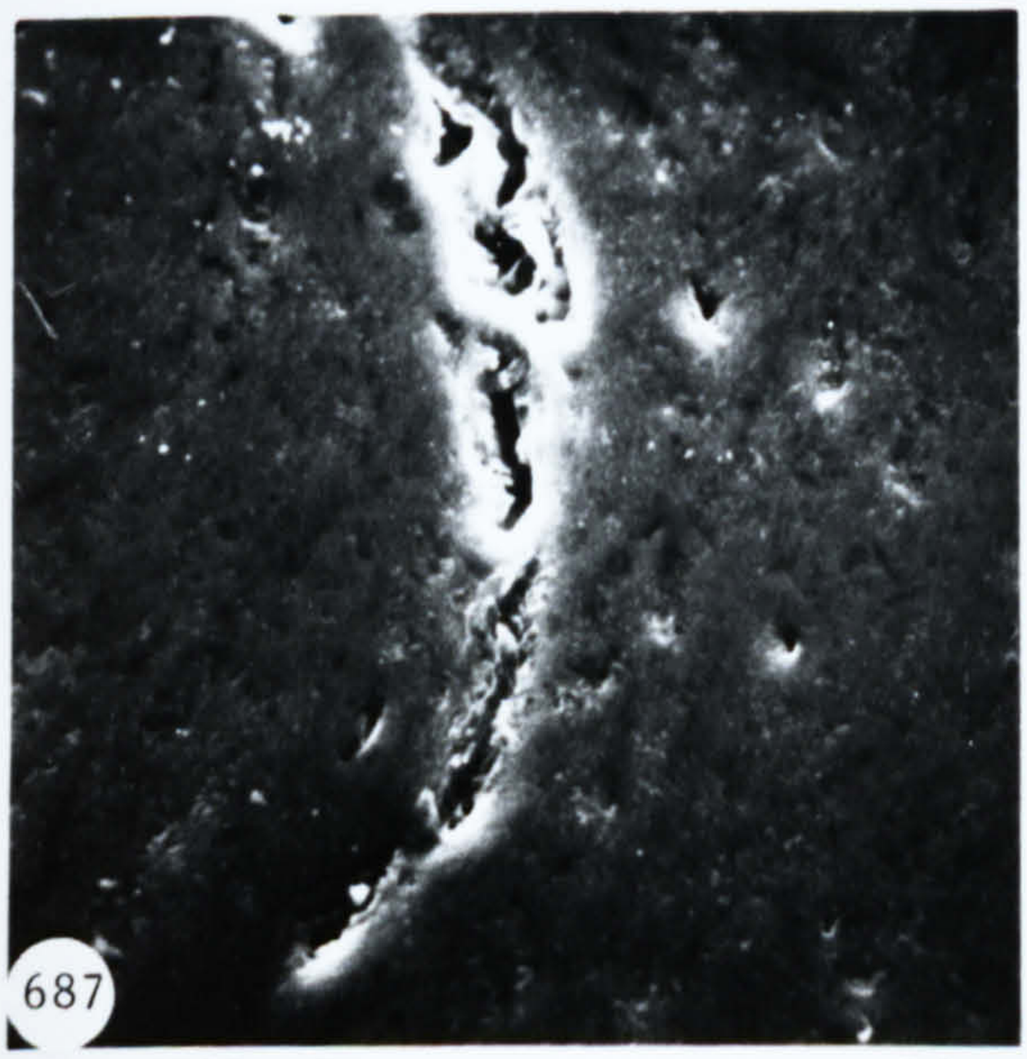
VNMC GRAPHITE 20 µm



VNMC GRAPHITE 100 µm



VNMC GRAPHITE 20 µm

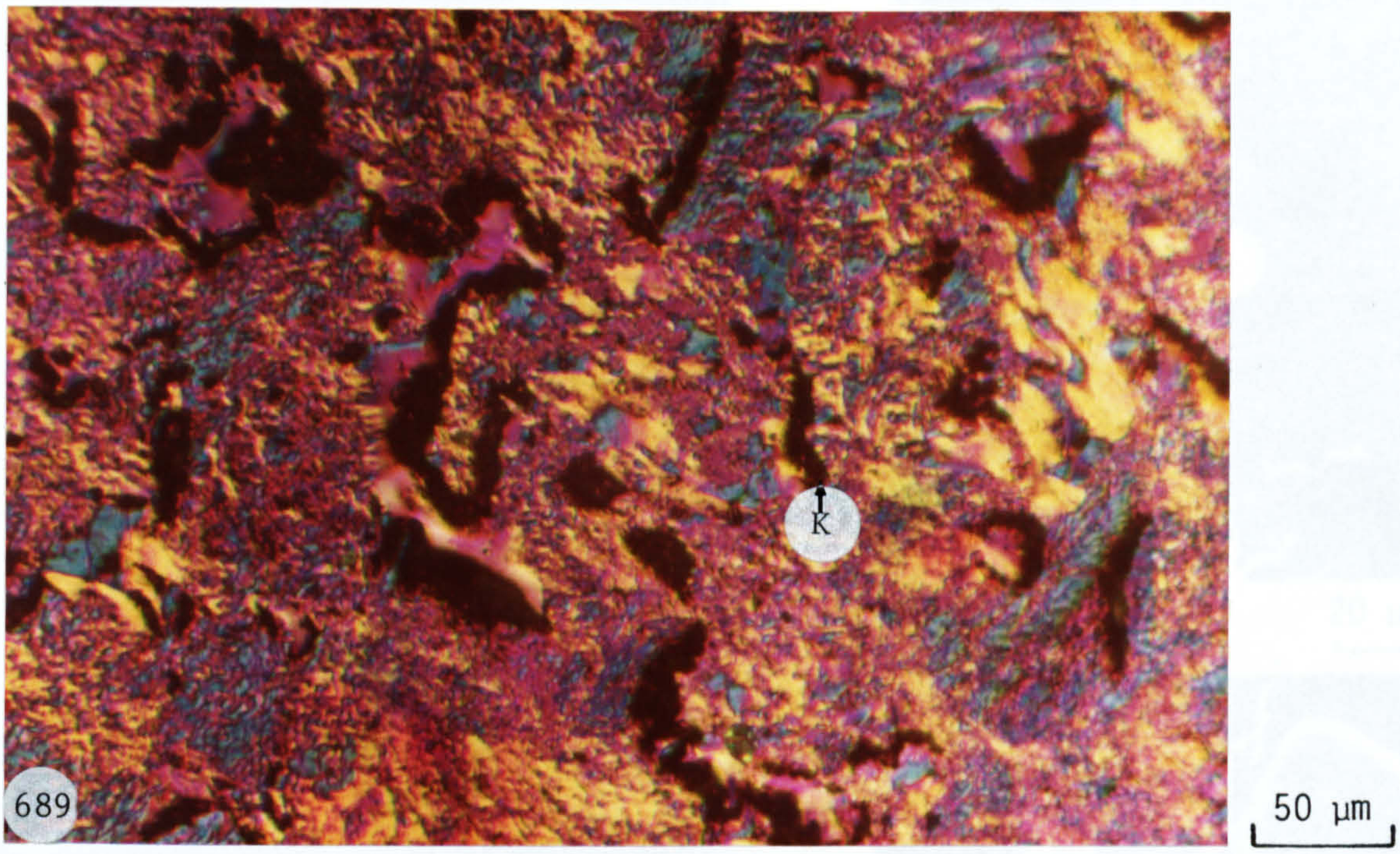


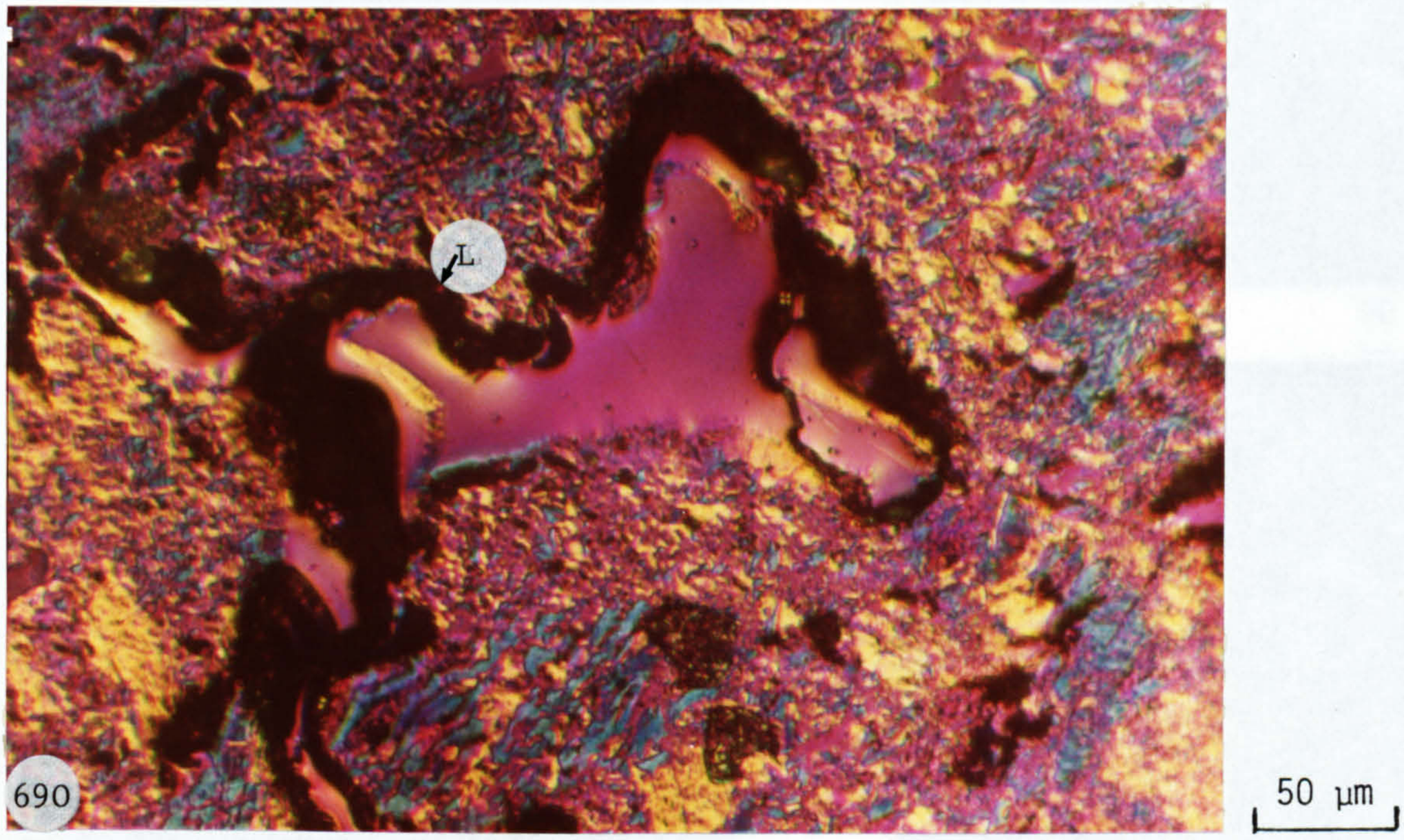
VNMC GRAPHITE 10 µm



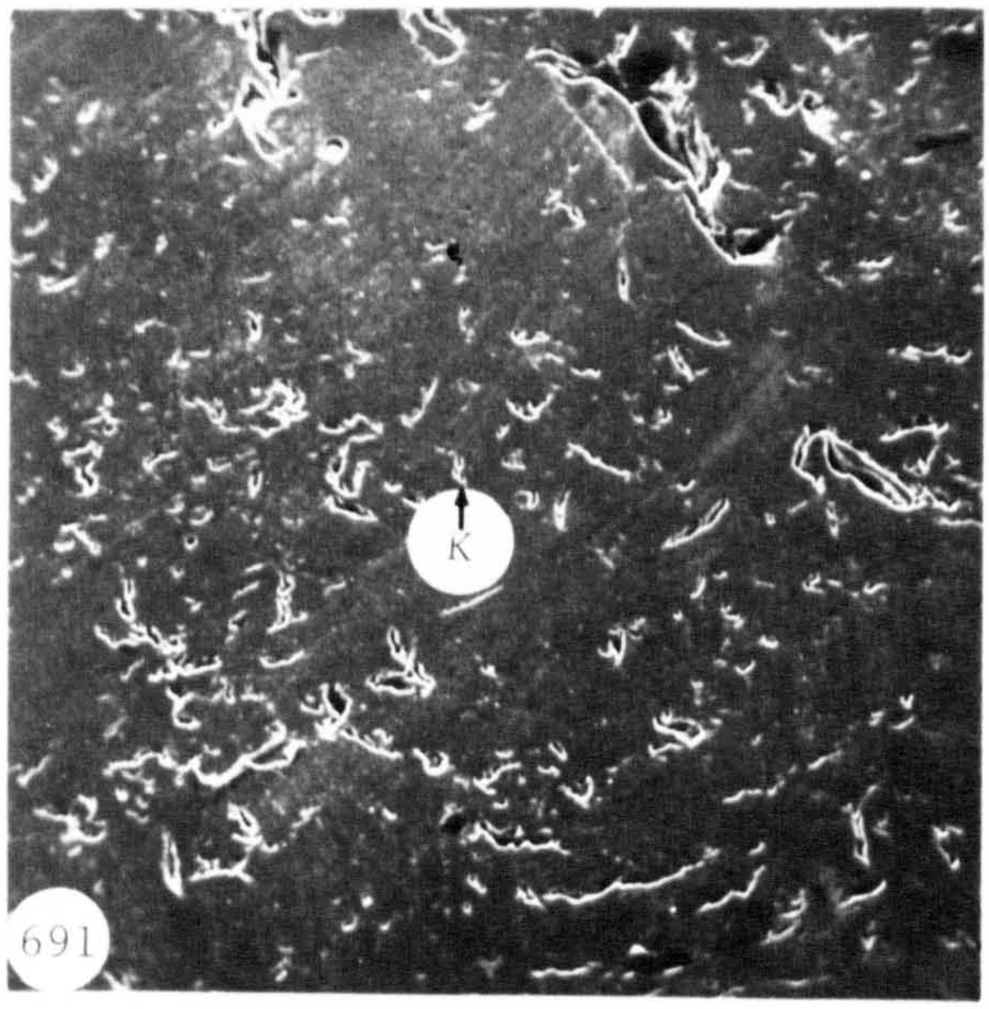
VNMC GRAPHITE 2 µm

Figures 683 to 688. Scanning electron micrographs (stereoscan) of virgin VNMC Graphite.

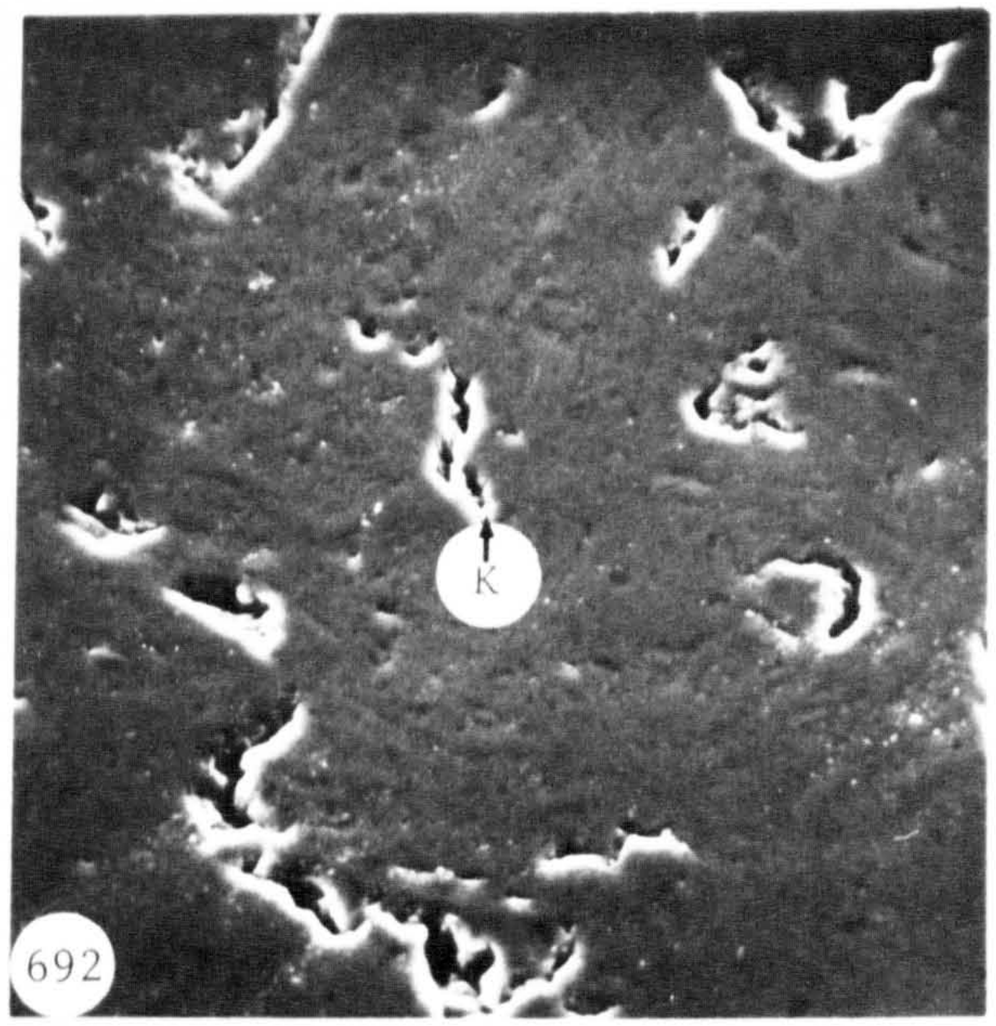




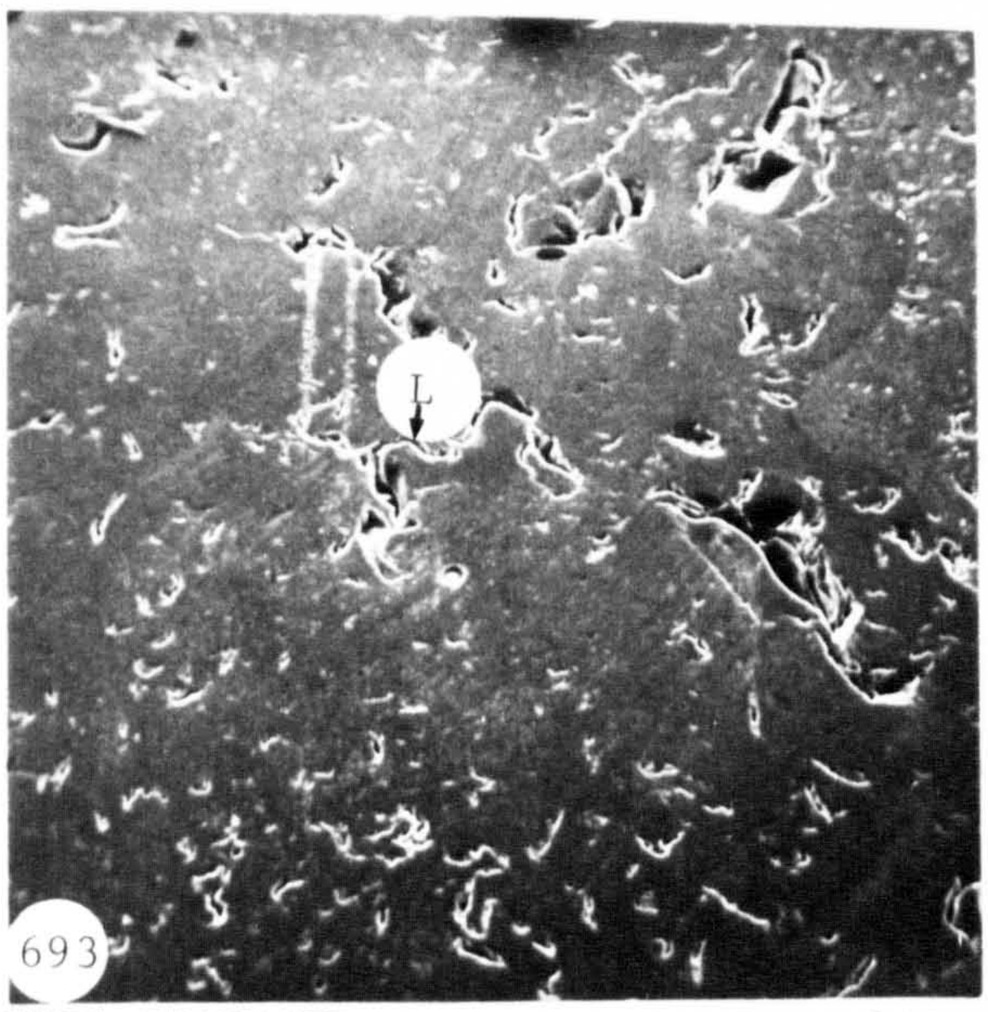
Figures 689 and 690. Optical micrographs of virgin VNEA Graphite.



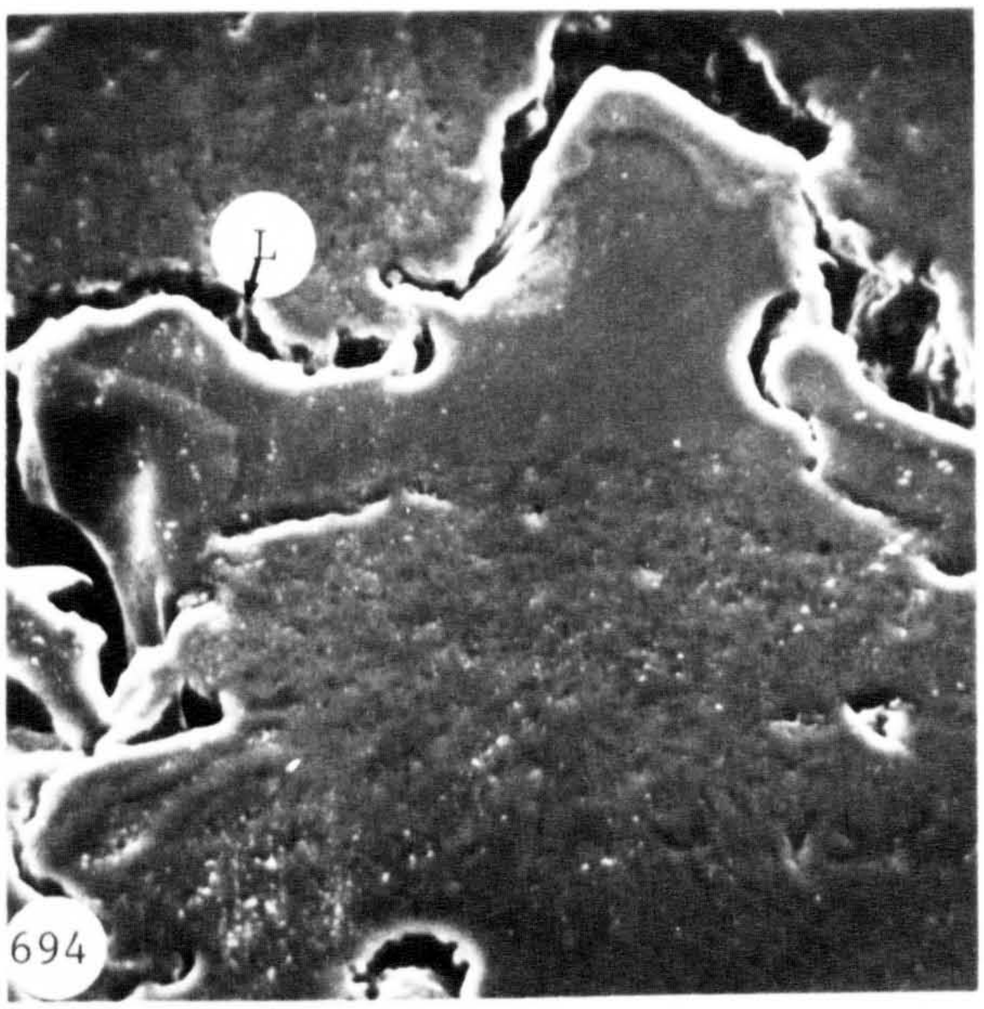
VNEA GRAPHITE 100 µm



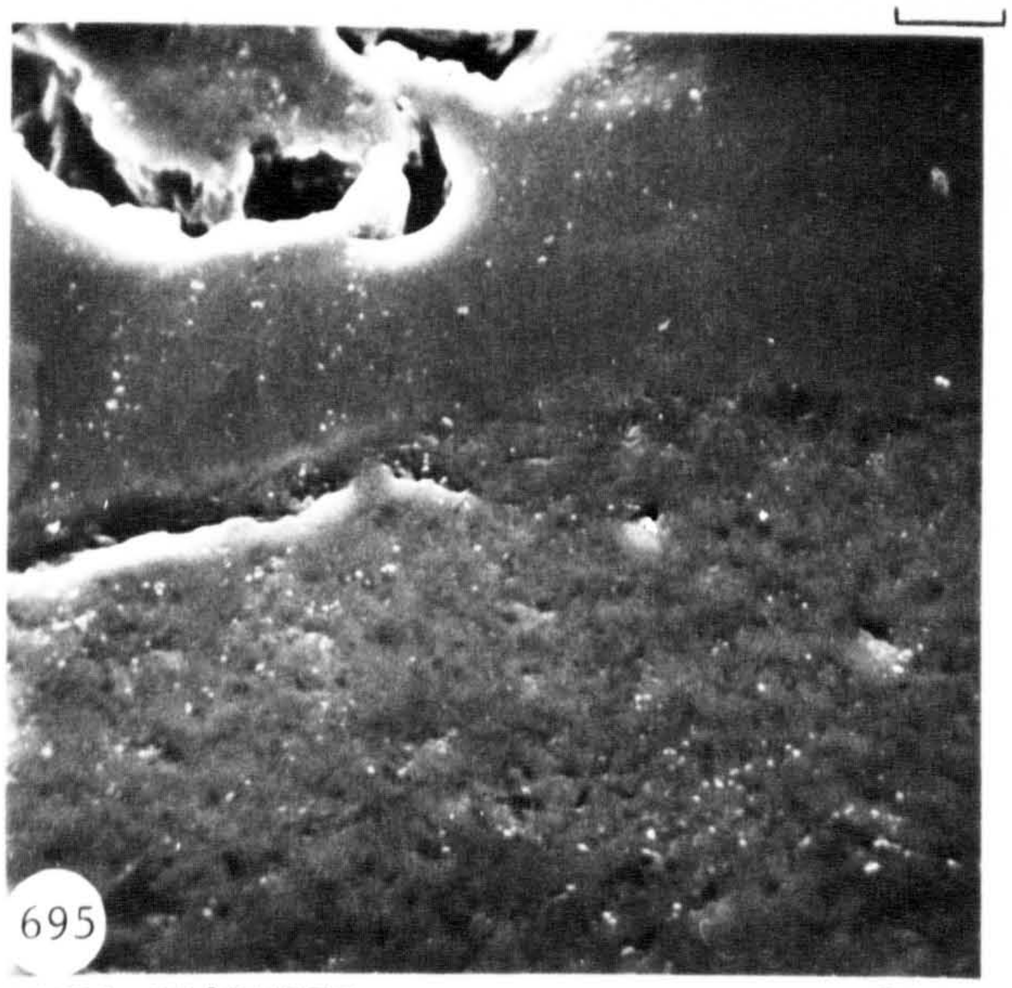
VNEA GRAPHITE 20 µm



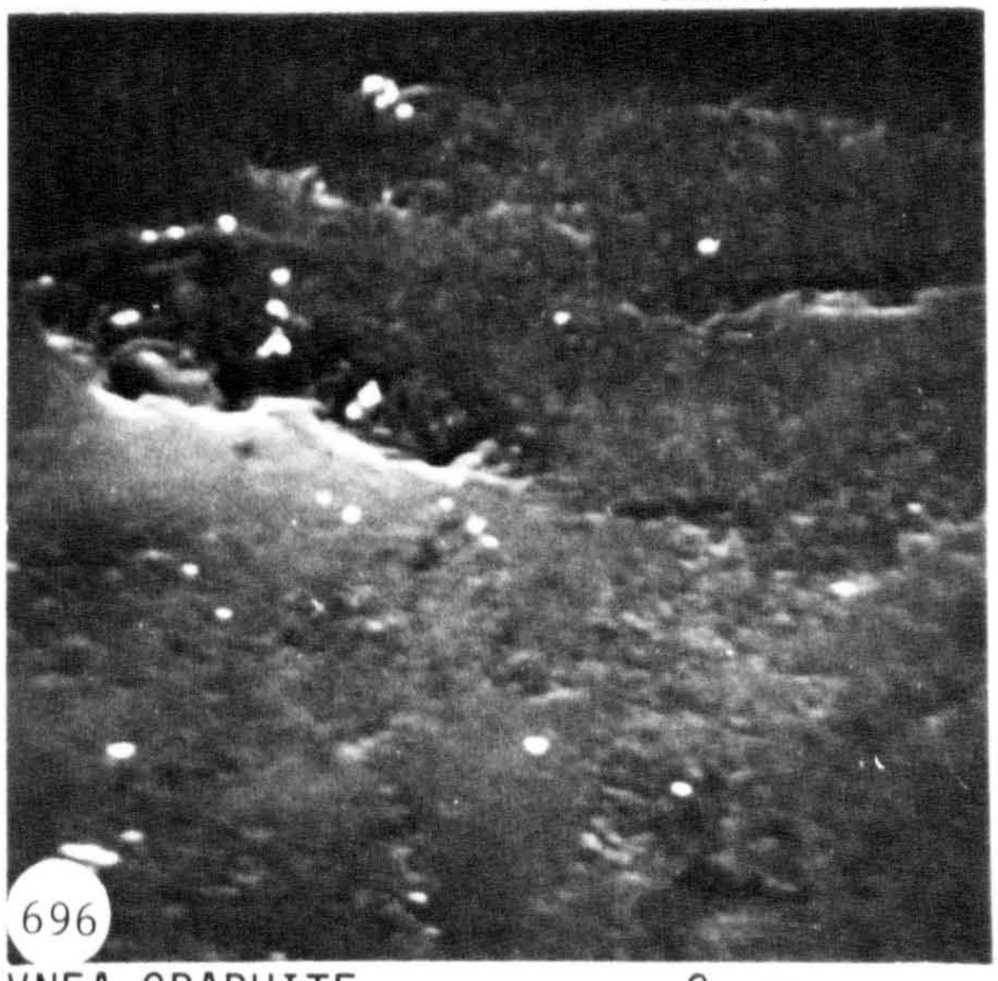
VNEA GRAPHITE 100 µm



VNEA GRAPHITE 20 µm



VNEA GRAPHITE 10 µm



VNEA GRAPHITE 2 µm

Figures 691 to 696. Scanning electron micrographs (stereoscan) of virgin VNEA Graphite.

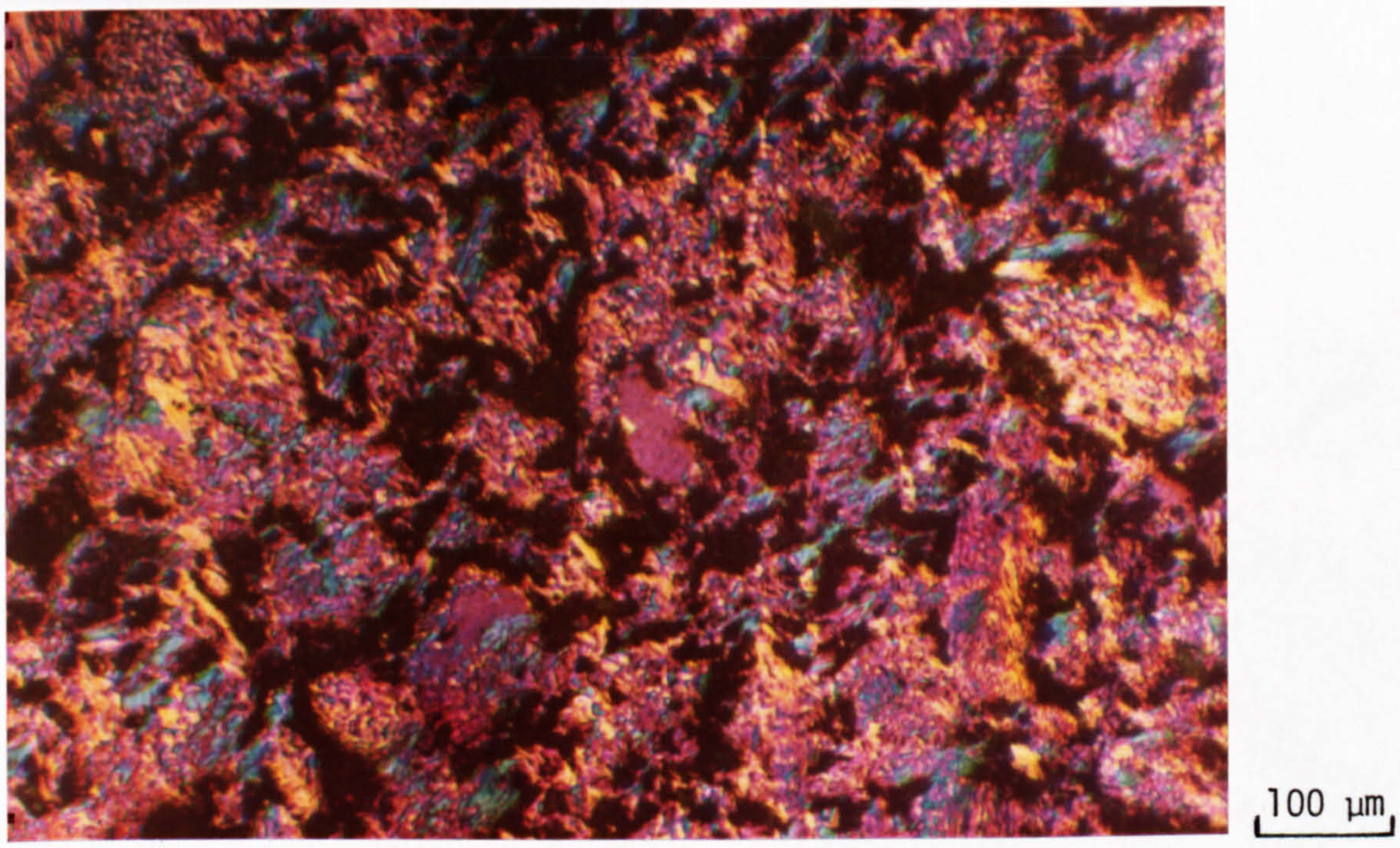
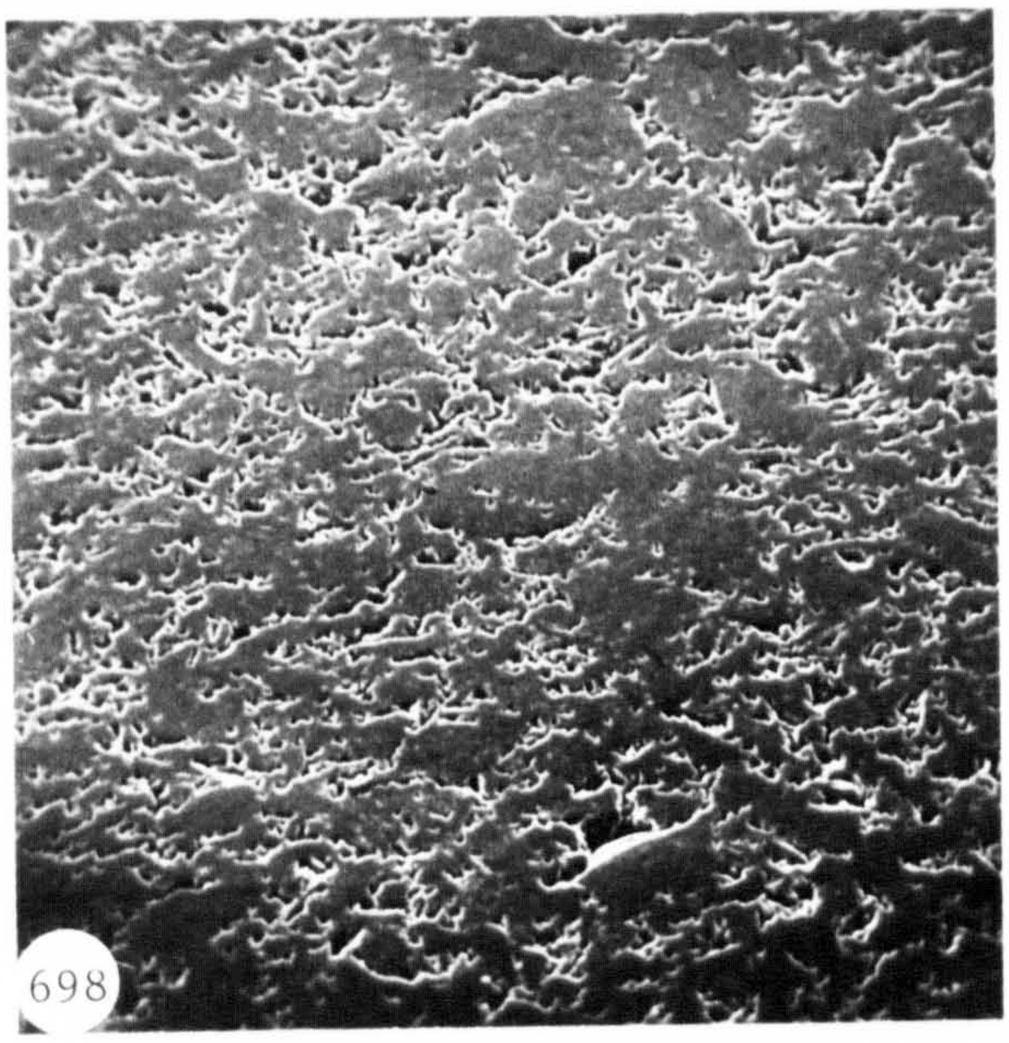
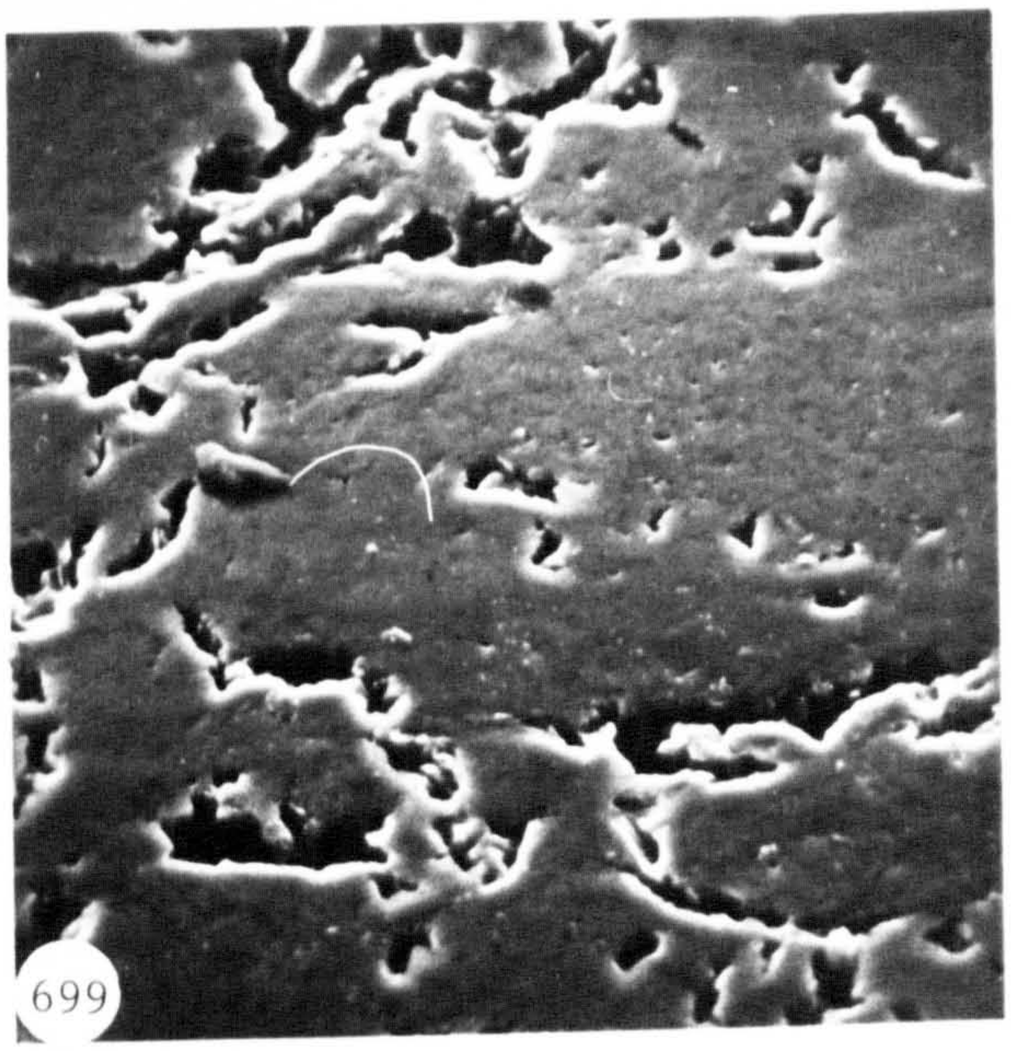


Figure 697. Optical micrograph of virgin AGLCP Graphite.



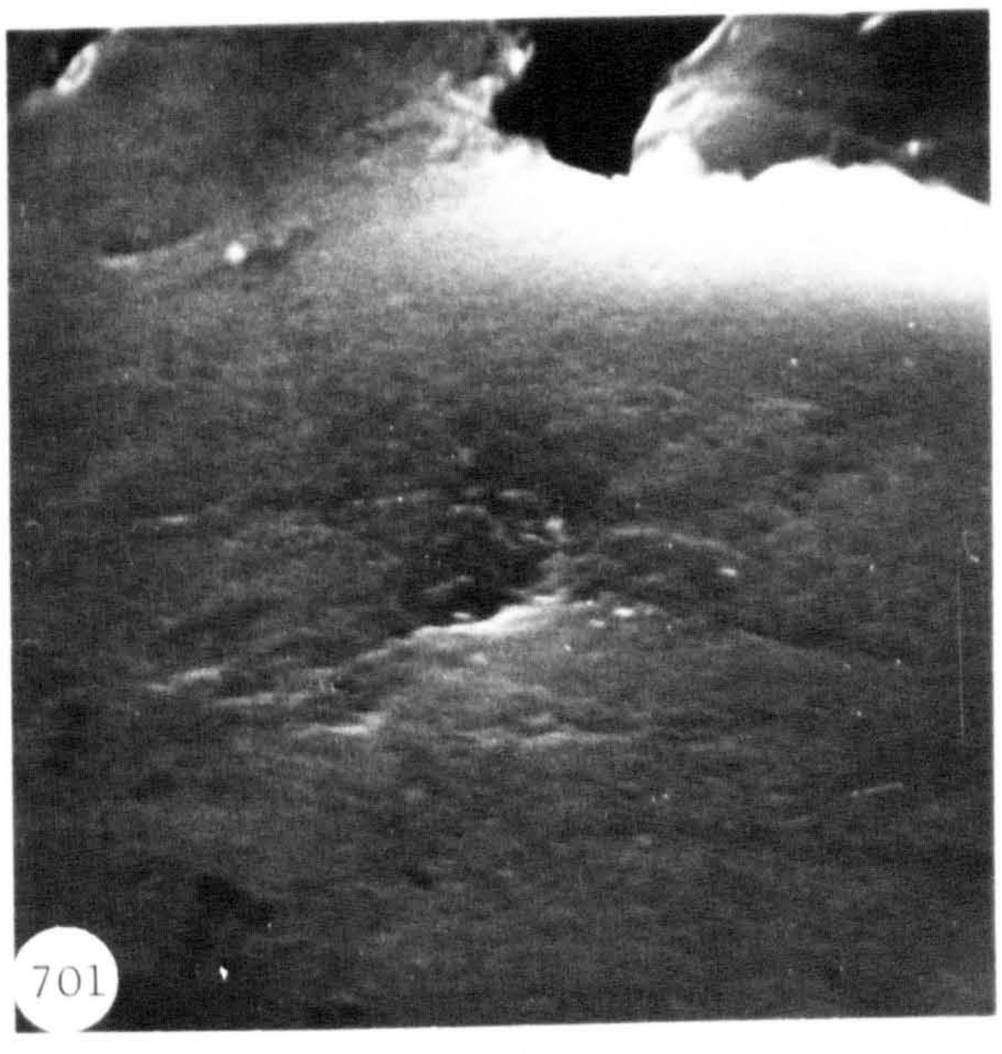
AGLCP GRAPHITE 100 µm



AGLCP GRAPHITE 20µm



AGLCP GRAPHITE 10 µm



AGLCP GRAPHITE 2 µm

Figures 698 to 701. Scanning electron micrographs (stereoscan) of AGLCP Graphite.

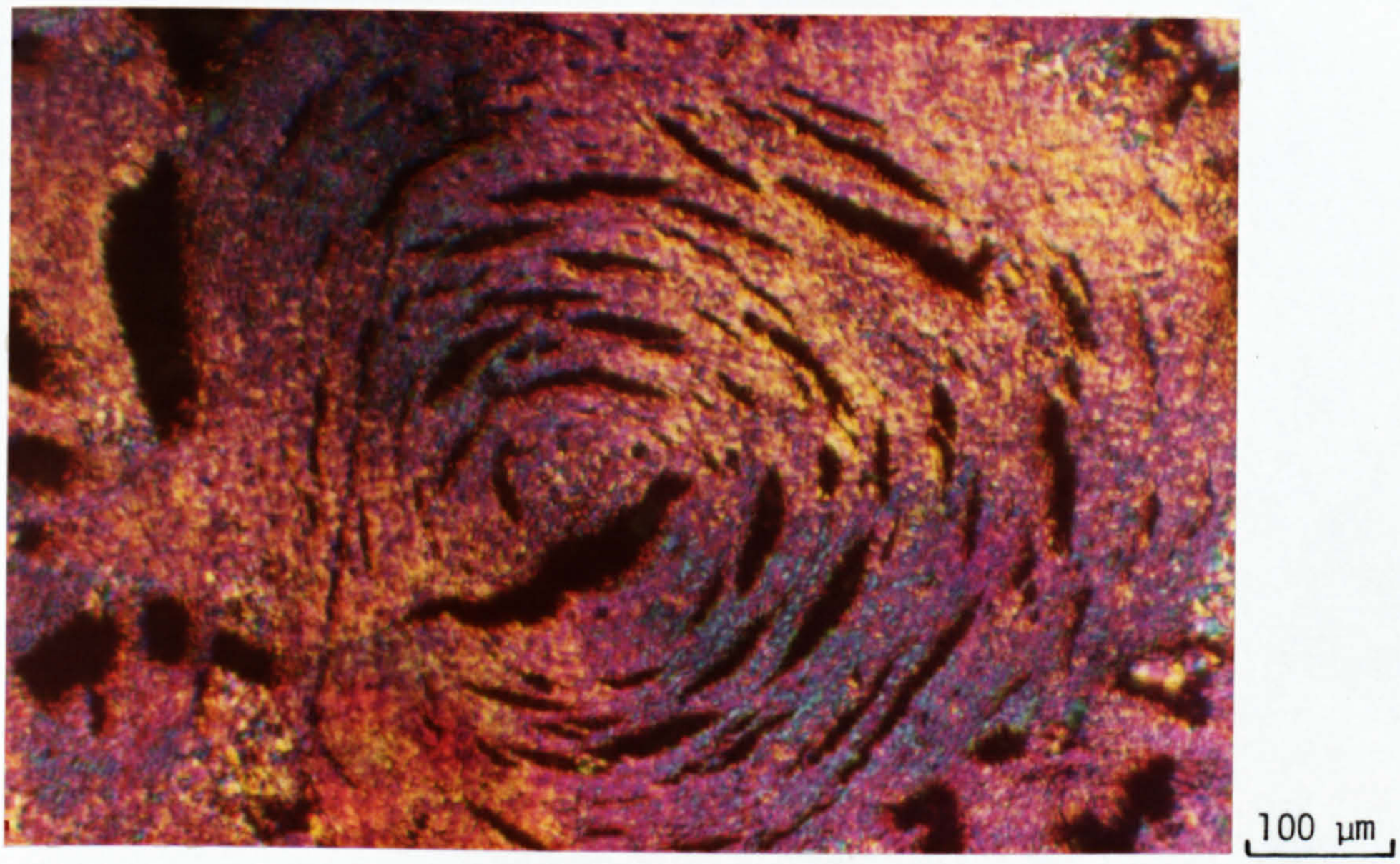
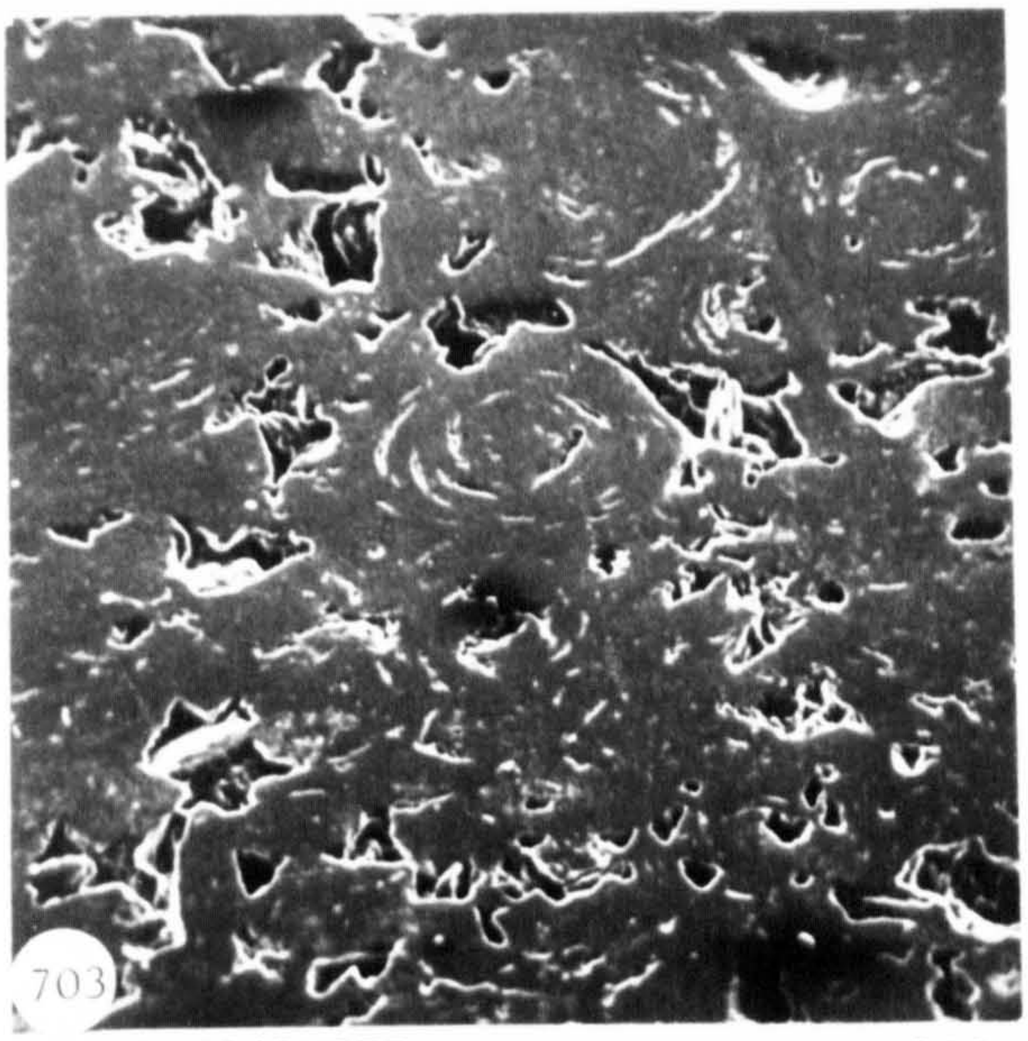
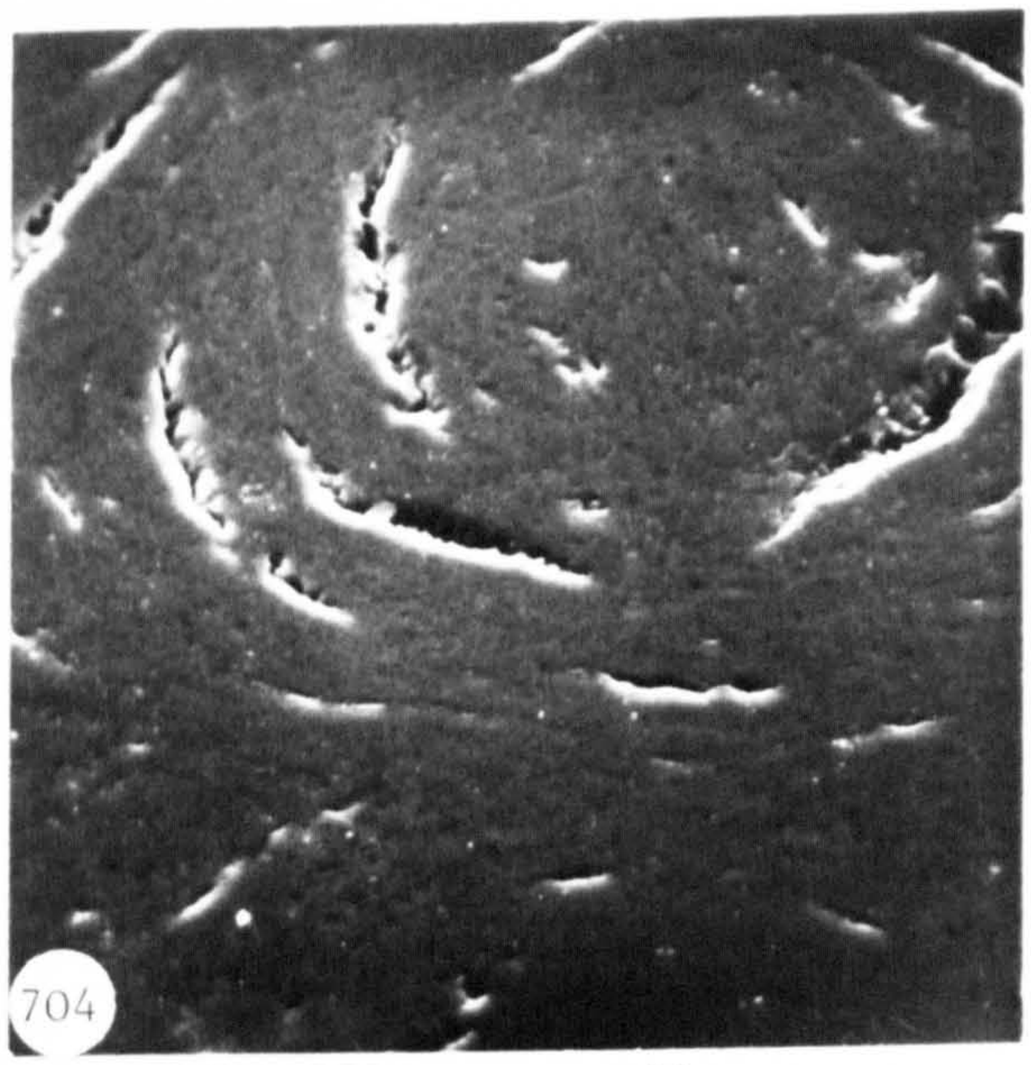


Figure 702. Optical micrograph of virgin UMP, unimpregnated AGLMP Graphite.



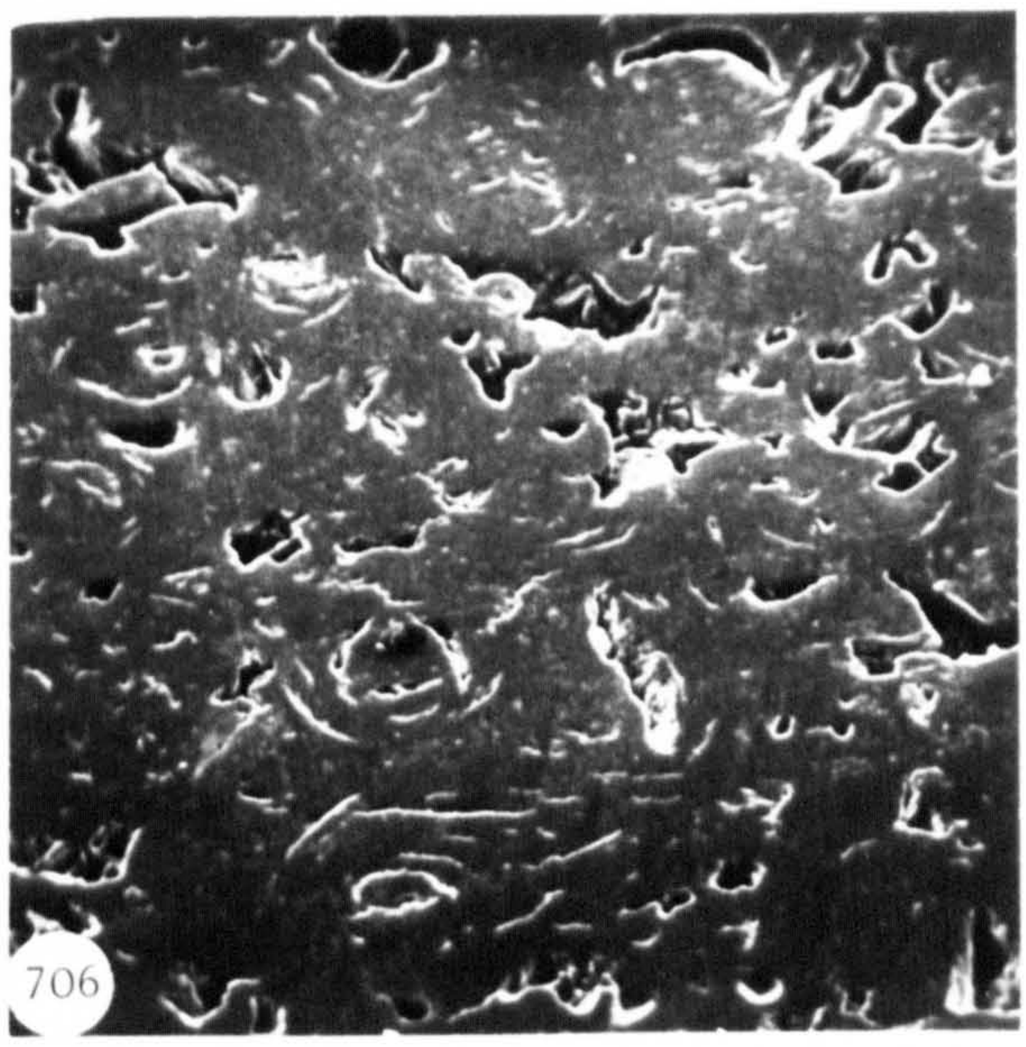
UMP GRAPHITE 100 µm



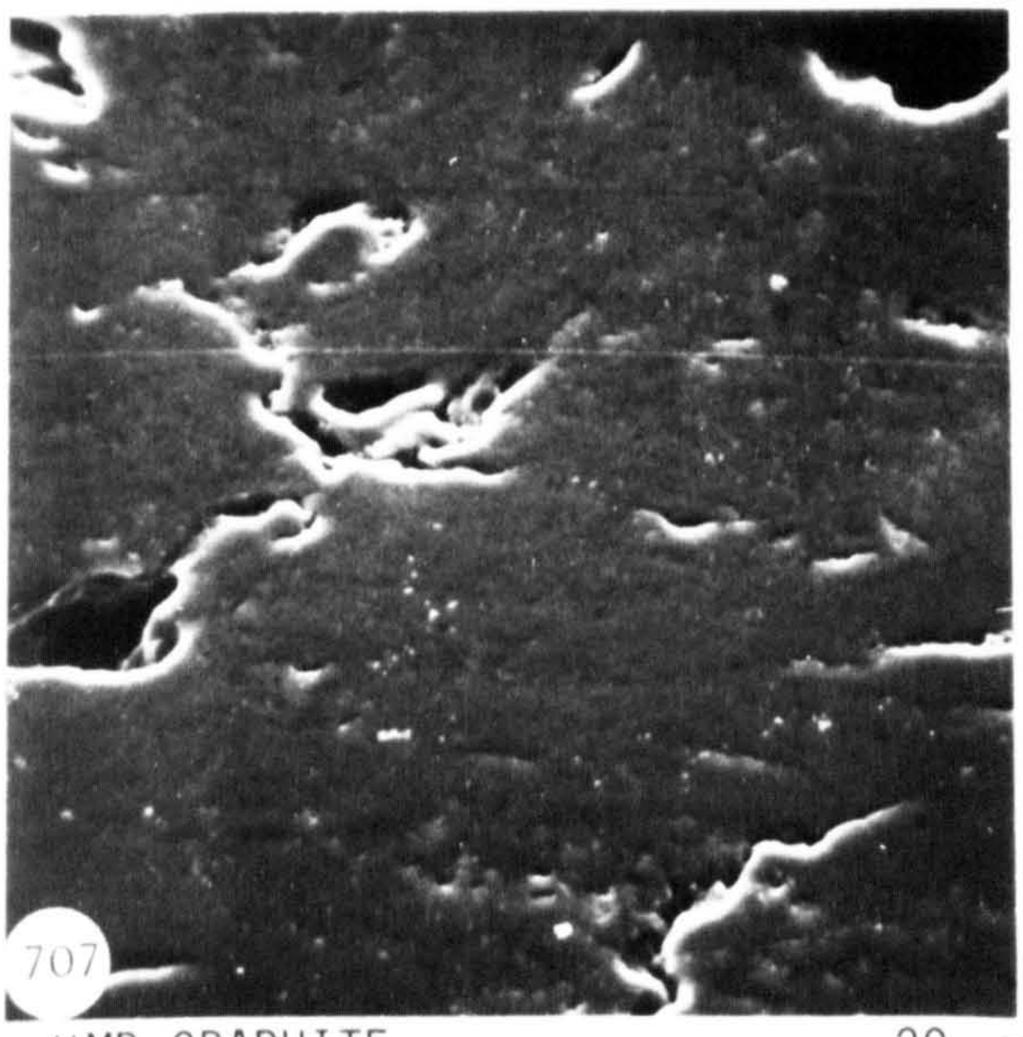
UMP GRAPHITE 20 µm



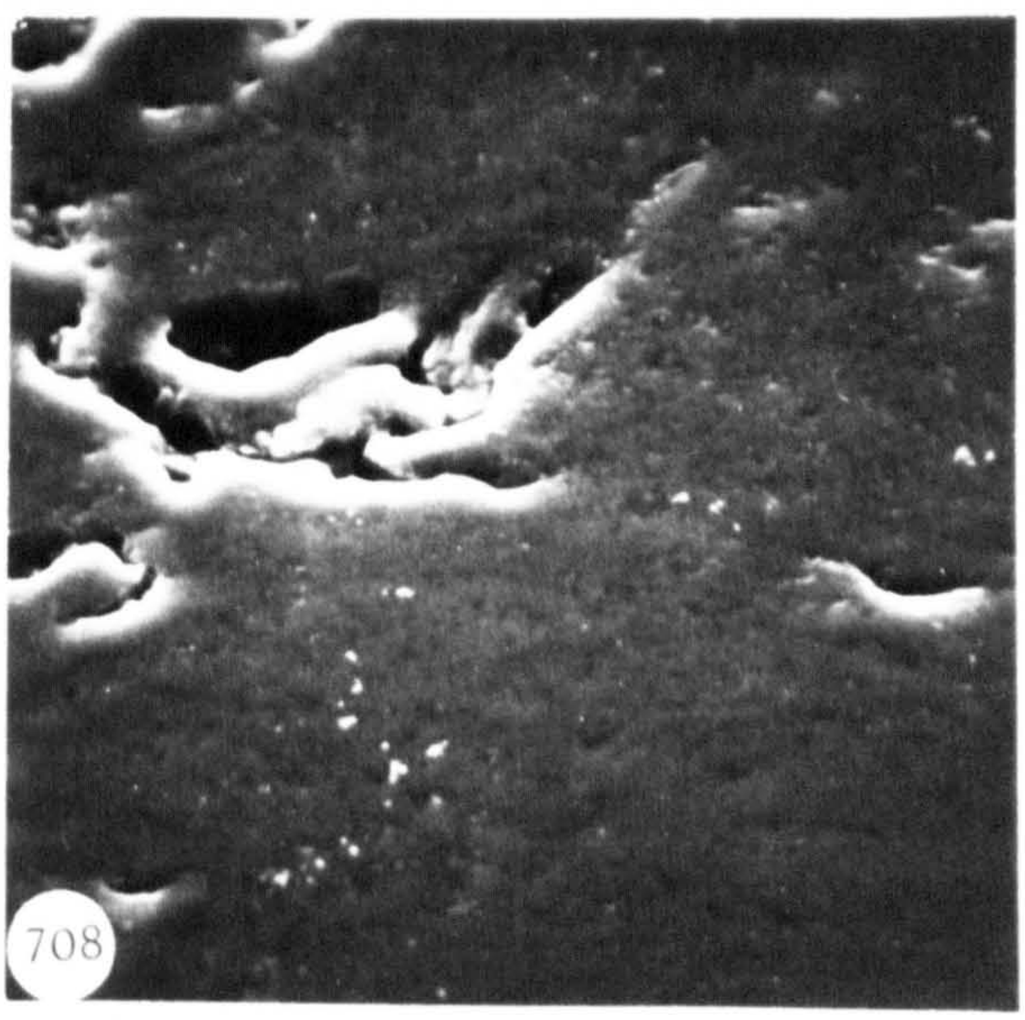
UMP GRAPHITE 200 µm



UMP GRAPHITE 100 µm



UMP GRAPHITE 20 µm



UMP GRAPHITE 10 µm

Figures 703 to 708. Scanning electron micrographs (stereoscan) of virgin UMP, unimpregnated AGLMP Graphite.

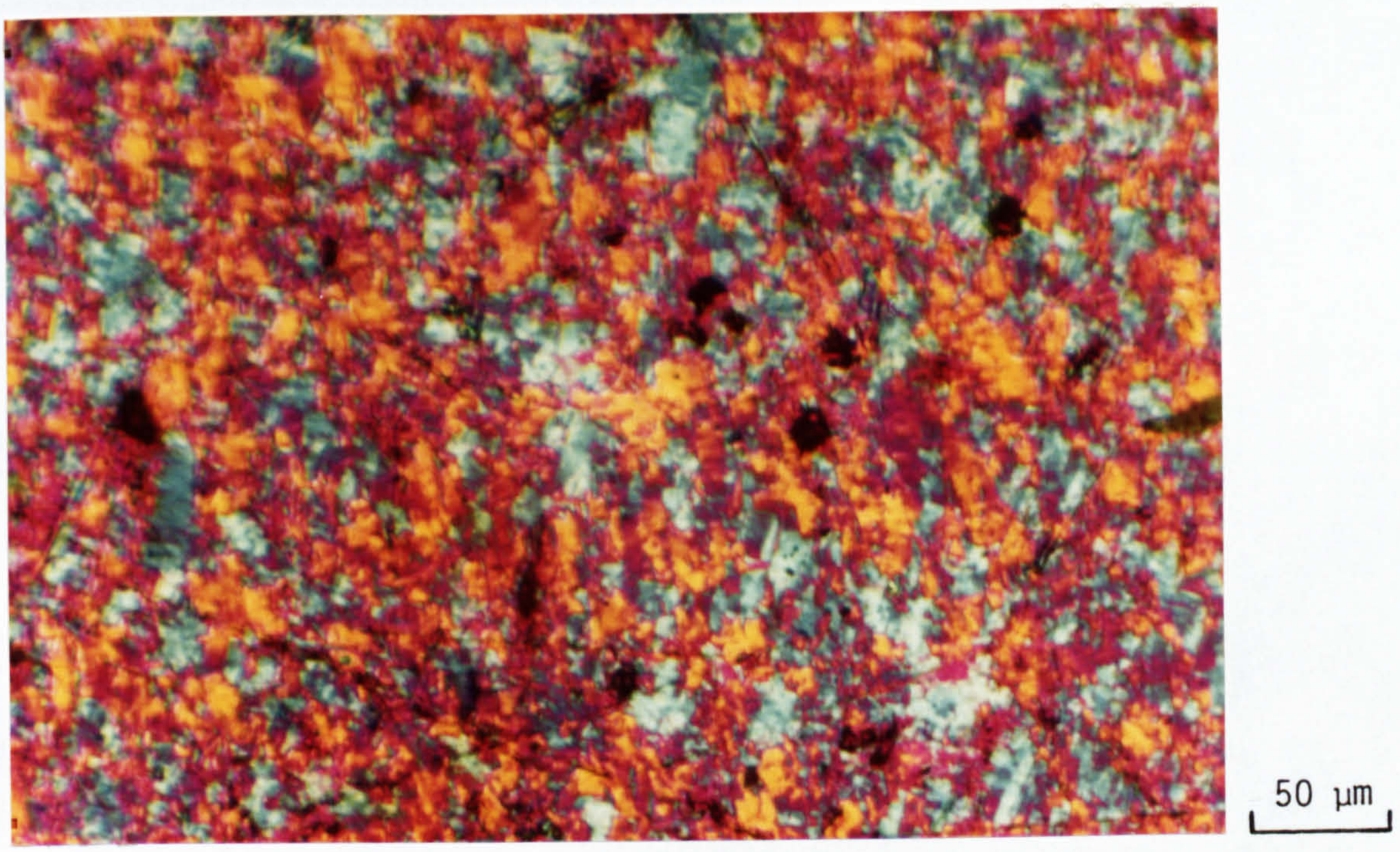


Figure 709. Optical micrograph of GG, a German Natural Graphite.

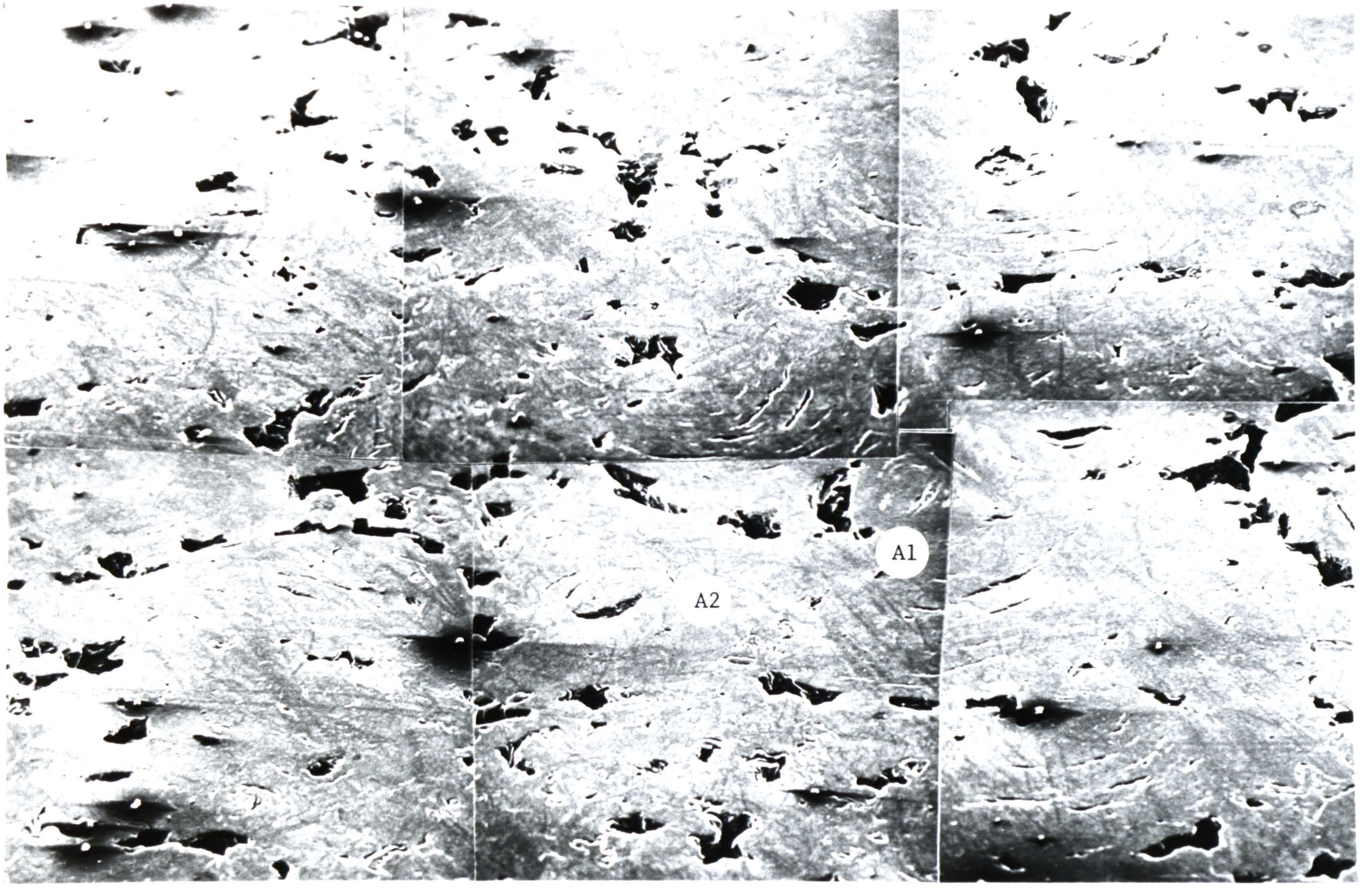


Figure 710. Photo-montage of AGLMP Graphite after the first polish.

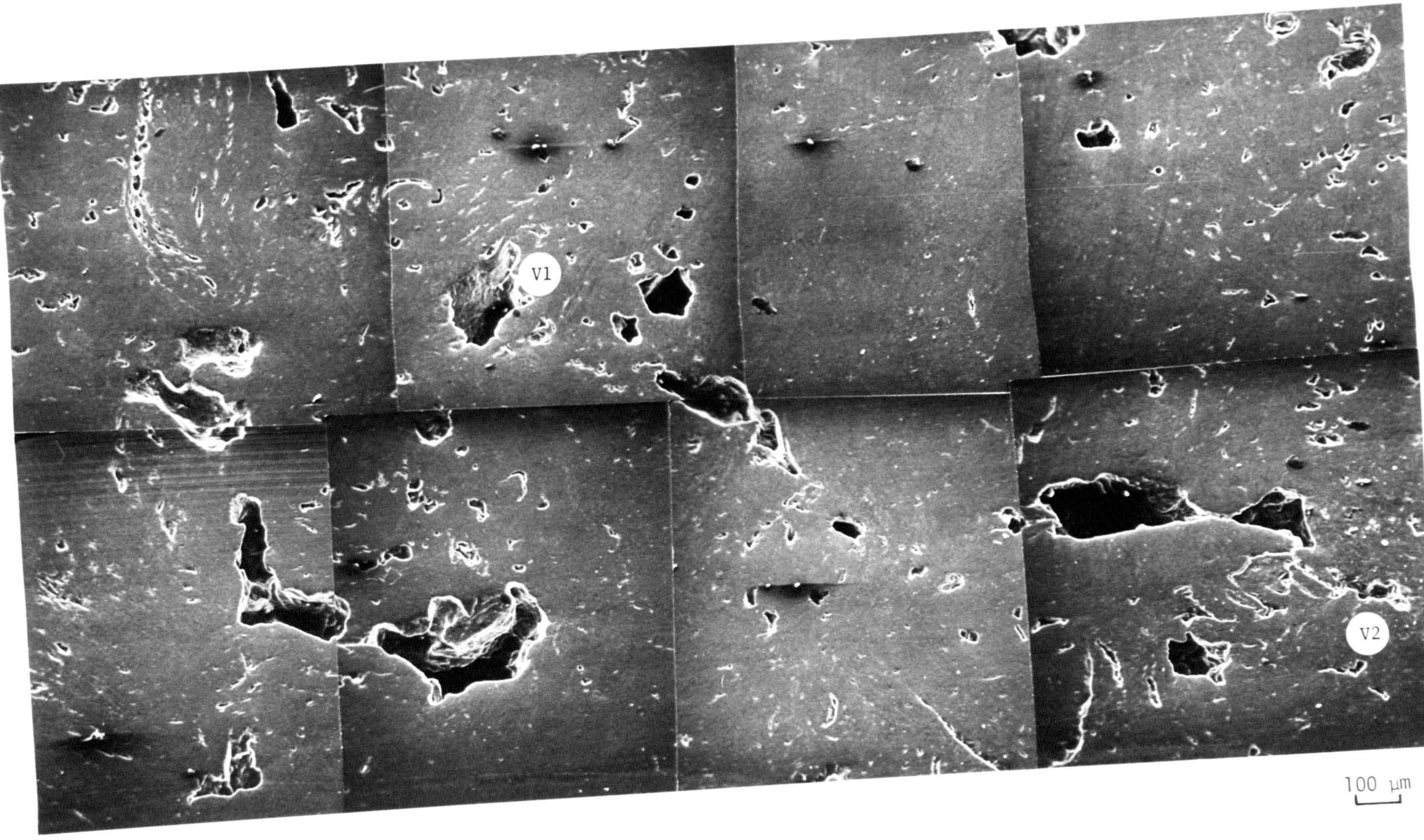


Figure 711. Photo—montage of VQMB Graphite after the first polish.



Overlay for Figure 712.1.

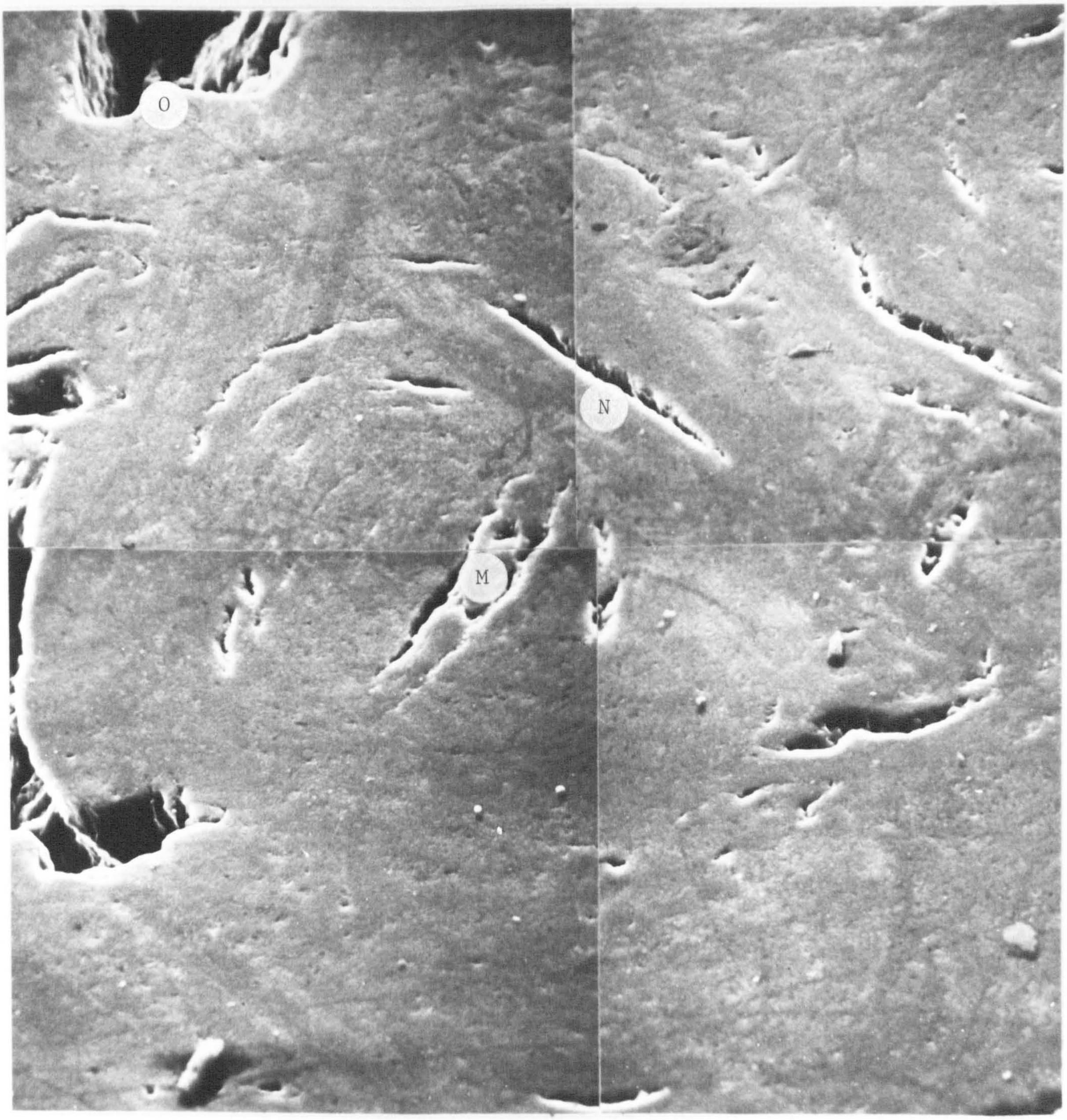


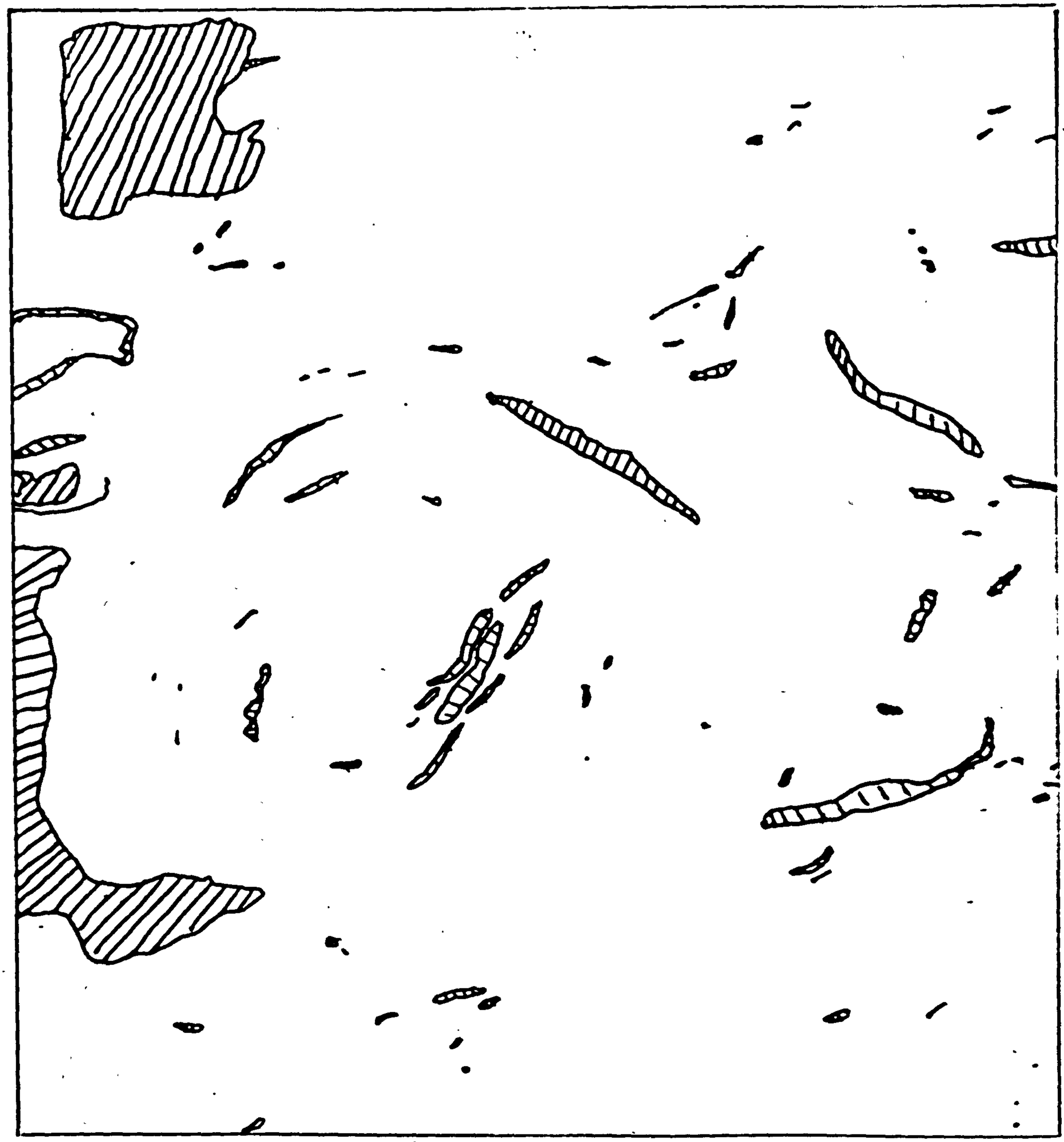
Figure 712.1. Photo-montage of AGLMP Graphite after the first polish.



20 μm

Overlay for Figure 712.1.

Figure 712.1. Photo-montage of AGLMP Graphite after the first polish.



Overlay for Figure 712.2.

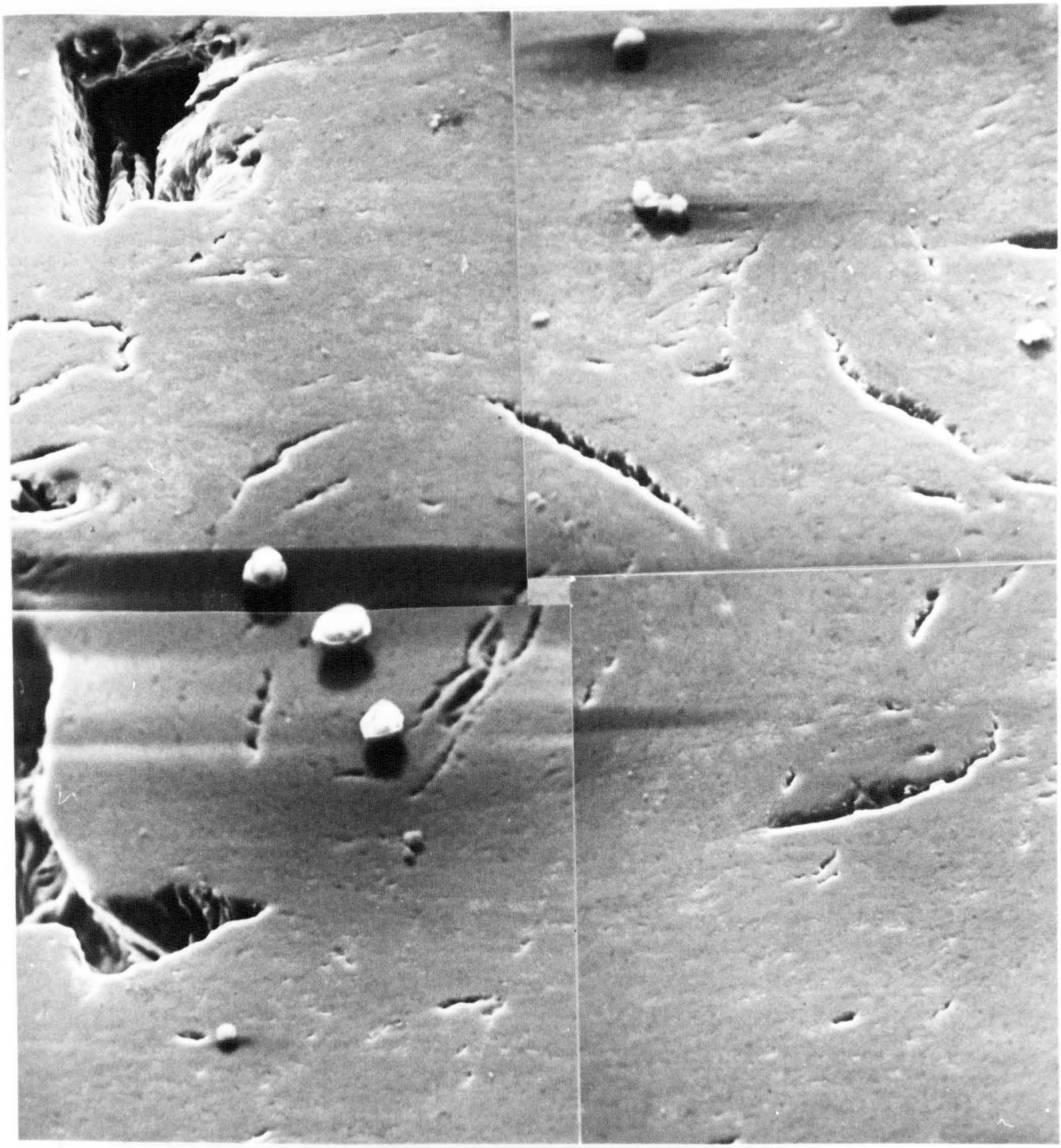
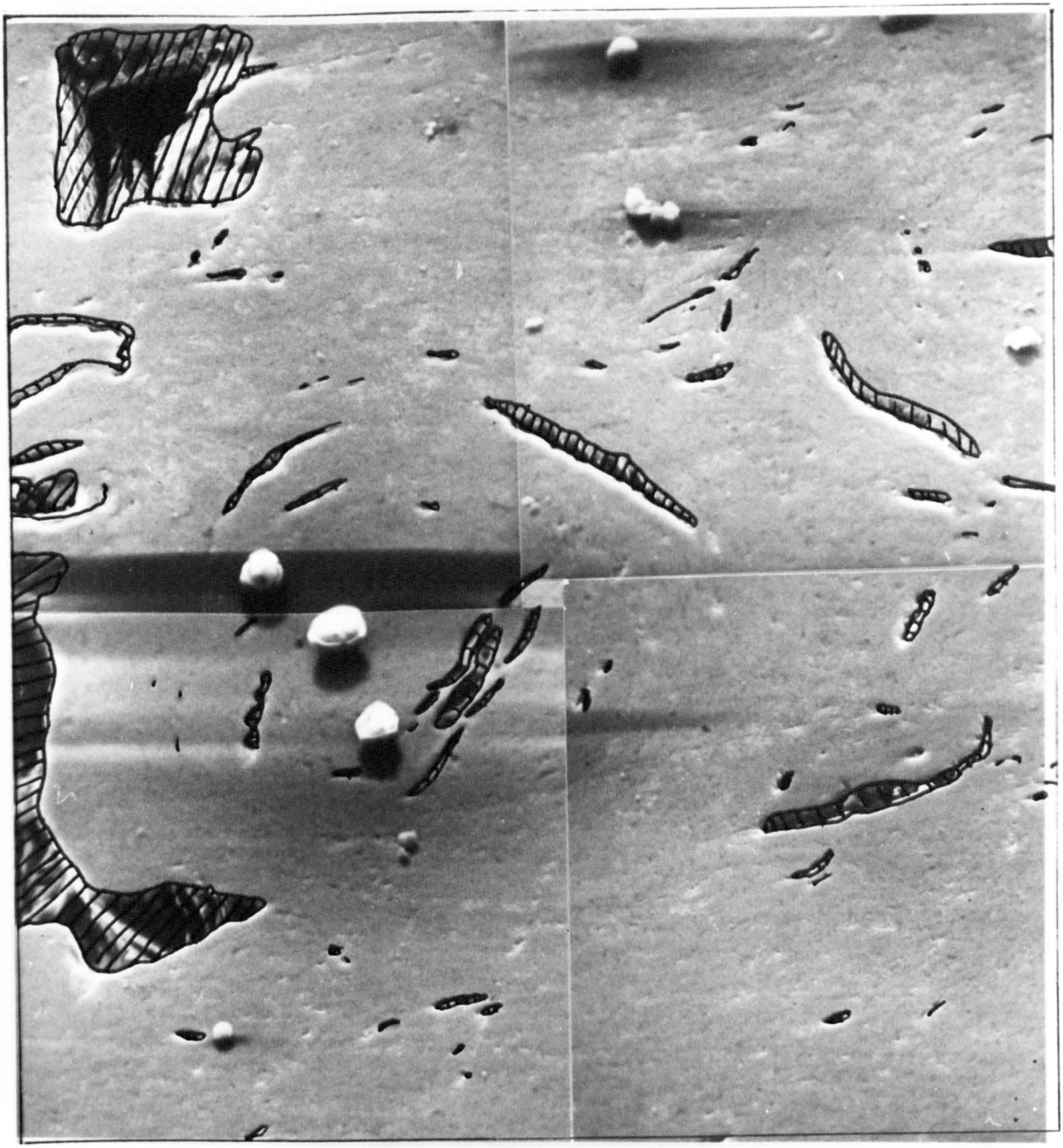


Figure 712.2. Photo-montage of AGLMP Graphite after the second polish.



Overlay for Figure 712.2.

Figure 712.2. Photo-montage of AGLMP Graphite after the second polish.



Overlay for Figure 712.3.

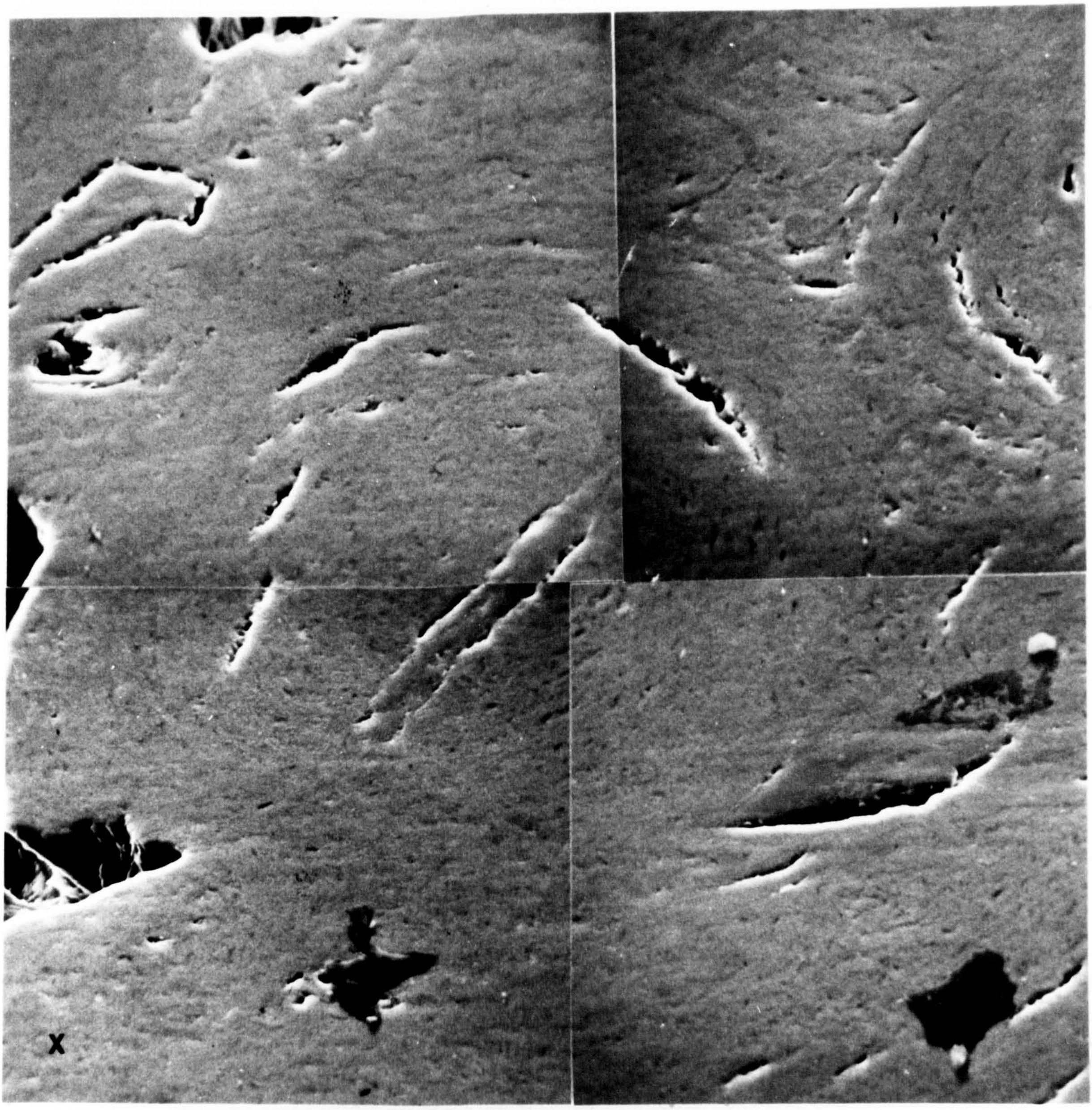
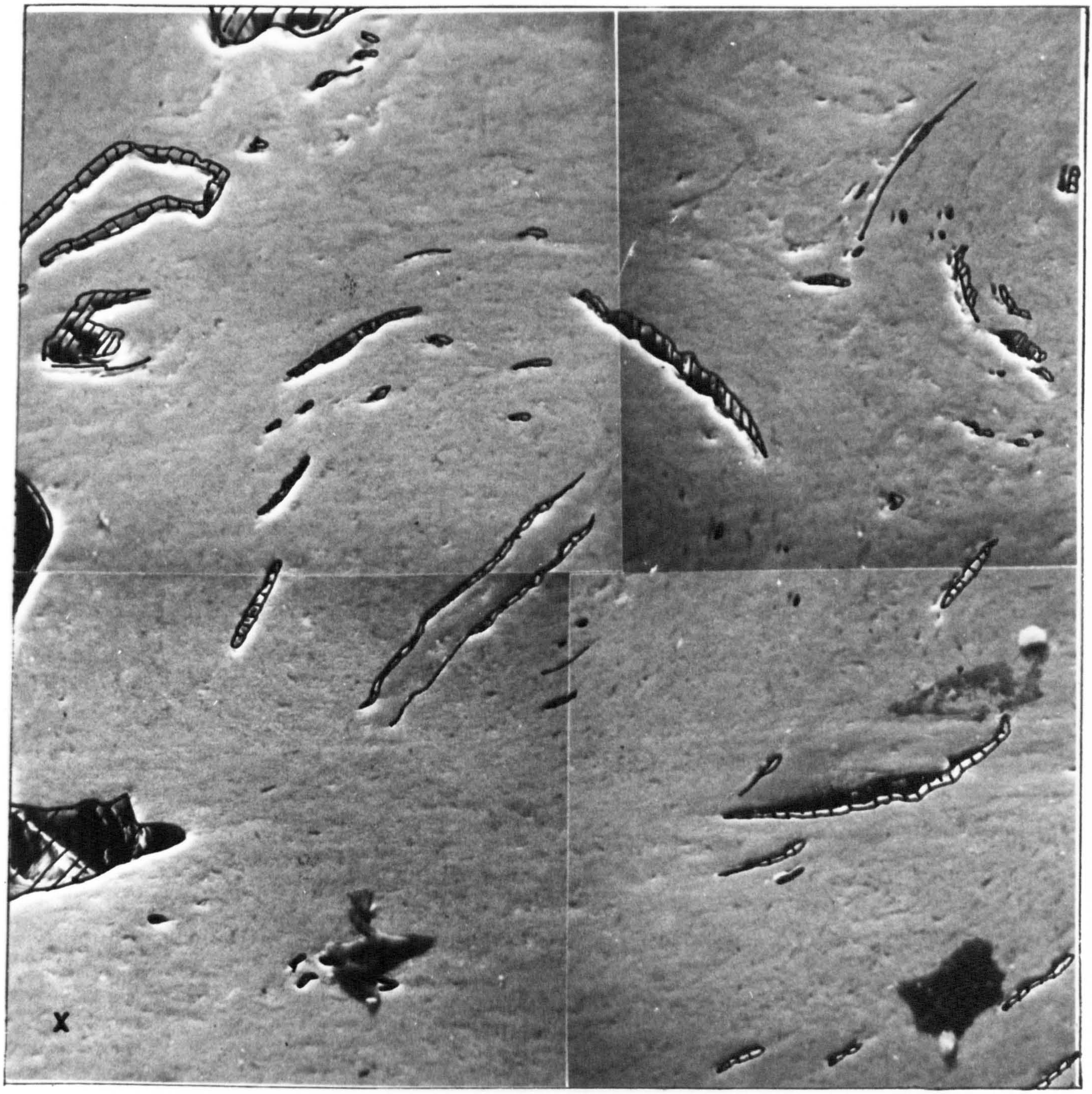
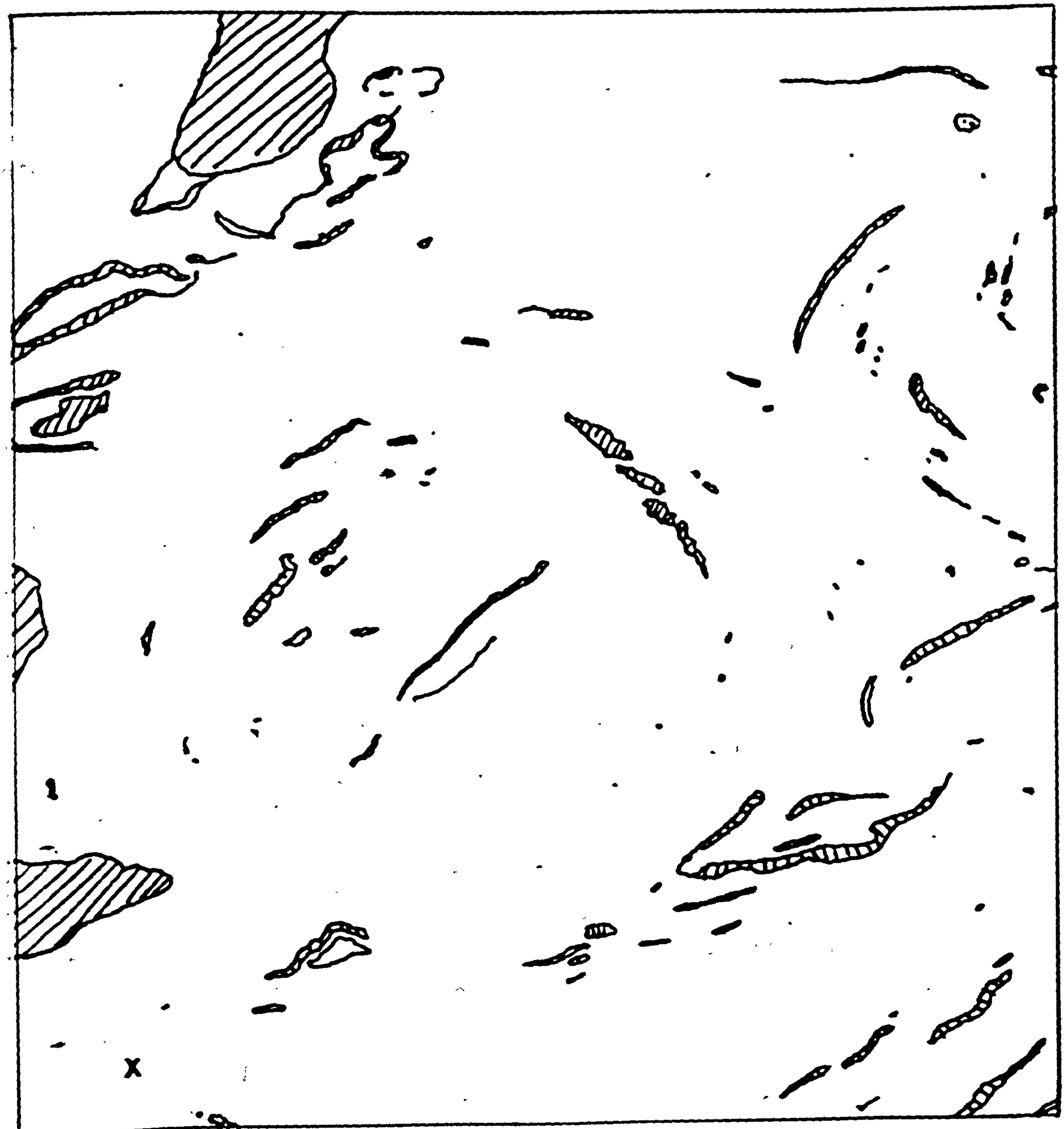


Figure 712.3. Photo-montage of AGLMP Graphite after the third polish.



Overlay for Figure 712.3.

Figure 712.3. Photo-montage of AGLMP Graphite after the third polish.



Overlay for Figure 712.4.

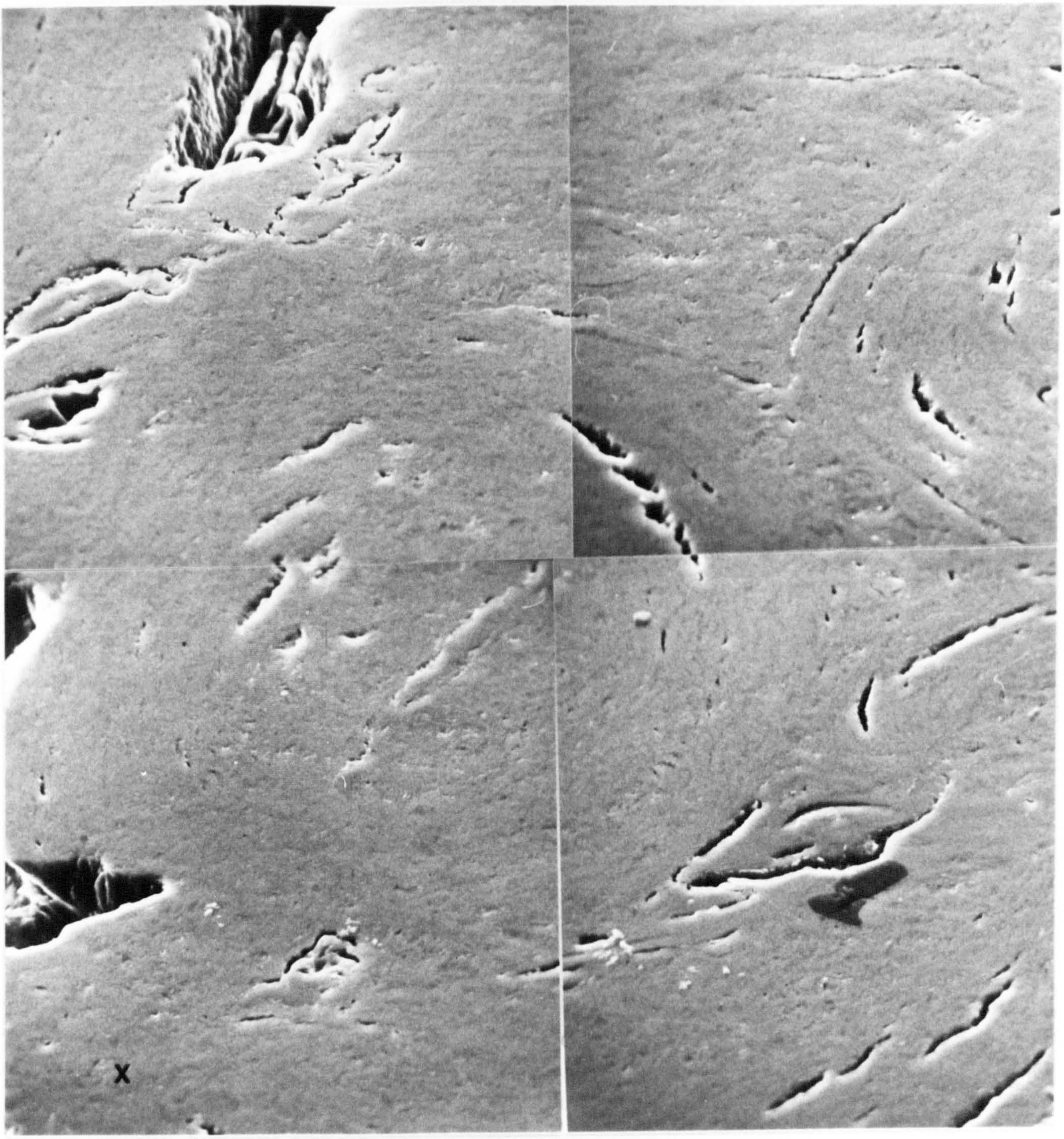
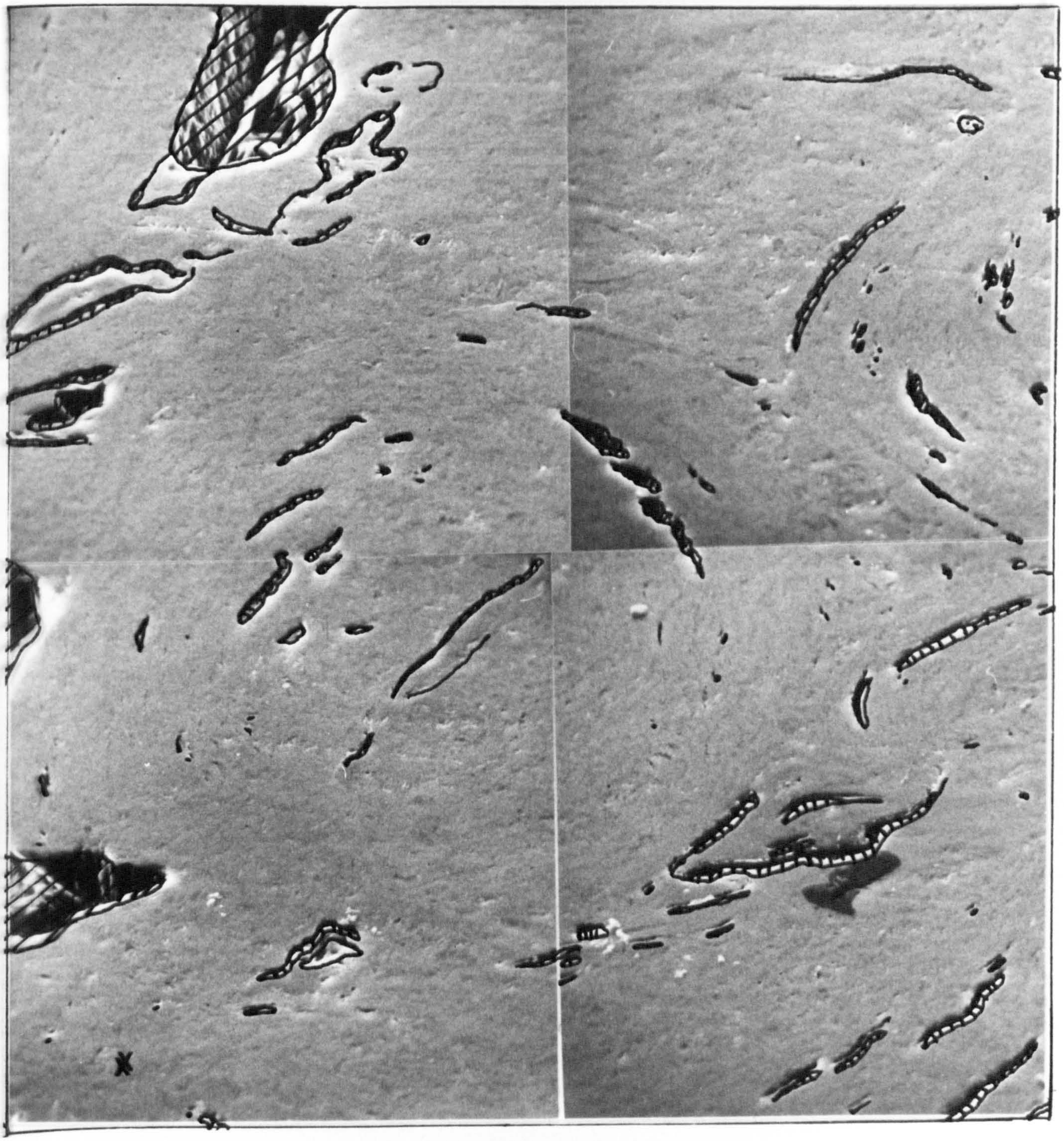


Figure 712.4. Photo-montage of AGLMP Graphite after the fourth polish.



Overlay for Figure 712.4.
Figure 712.4. Photo-montage of AGLMP Graphite after the fourth polish.



Overlay for 712.5.

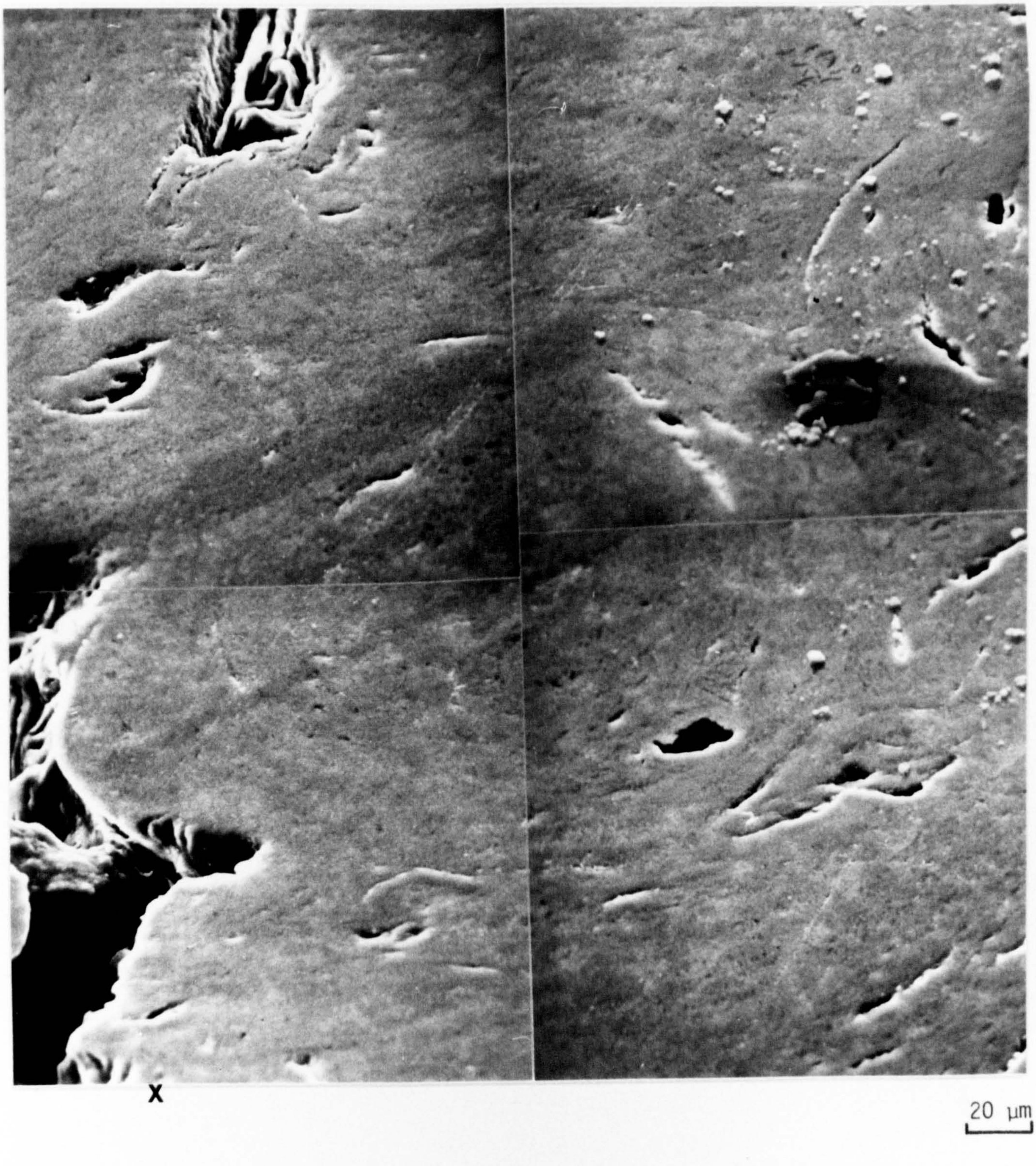
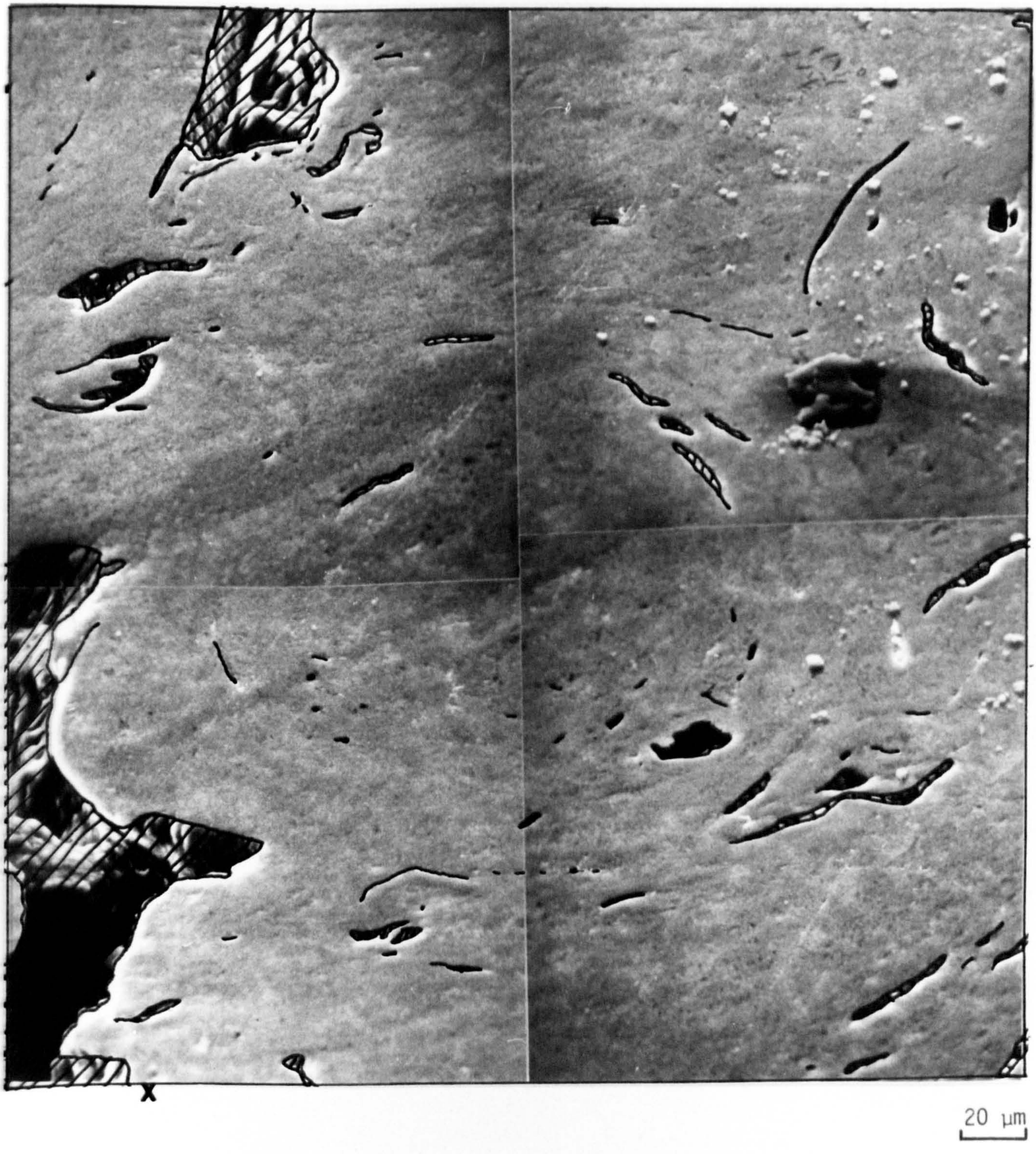


Figure 712.5. Photo-montage of AGLMP Graphite after the fifth polish.



Overlay for 712.5.

Figure 712.5. Photo-montage of AGLMP Graphite after the fifth polish.



X

Overlay for Figure 712.6.

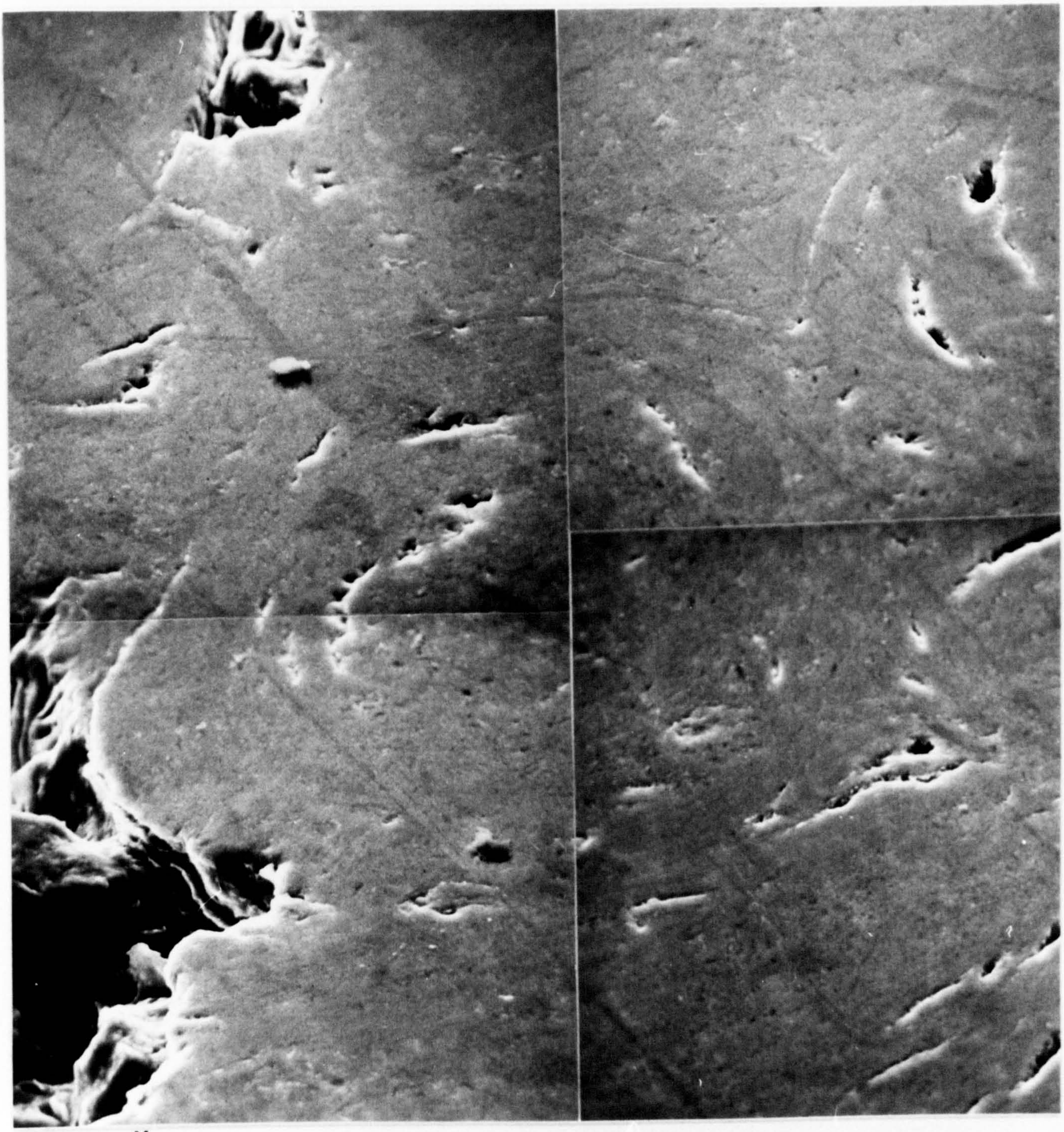
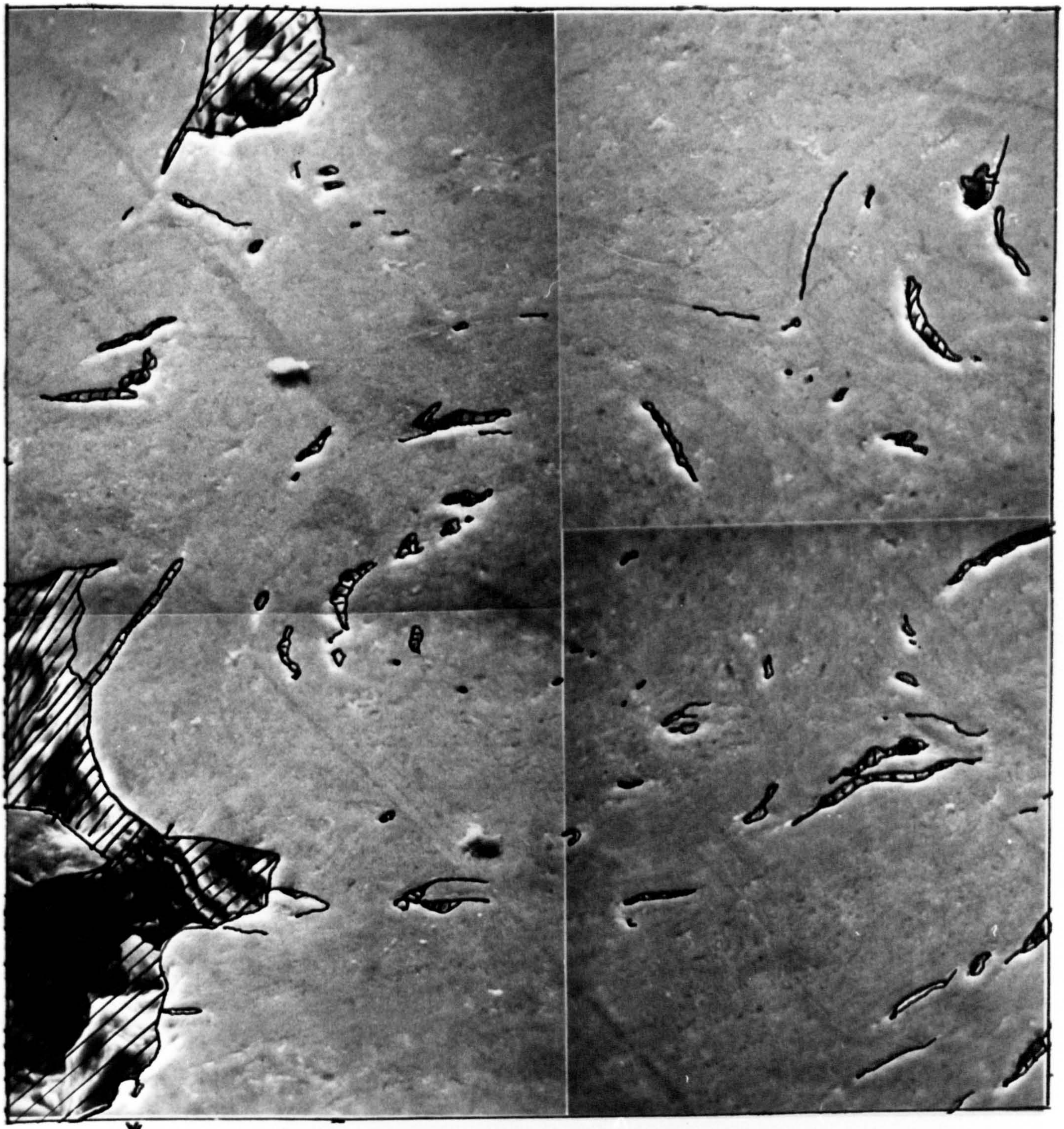


Figure 712.6. Photo-montage of AGLMP Graphite after the sixth polish.



Overlay for Figure 712.6.

Figure 712.6. Photo-montage of AGLMP Graphite after the sixth polish.



Overlay for Figure 712.7.

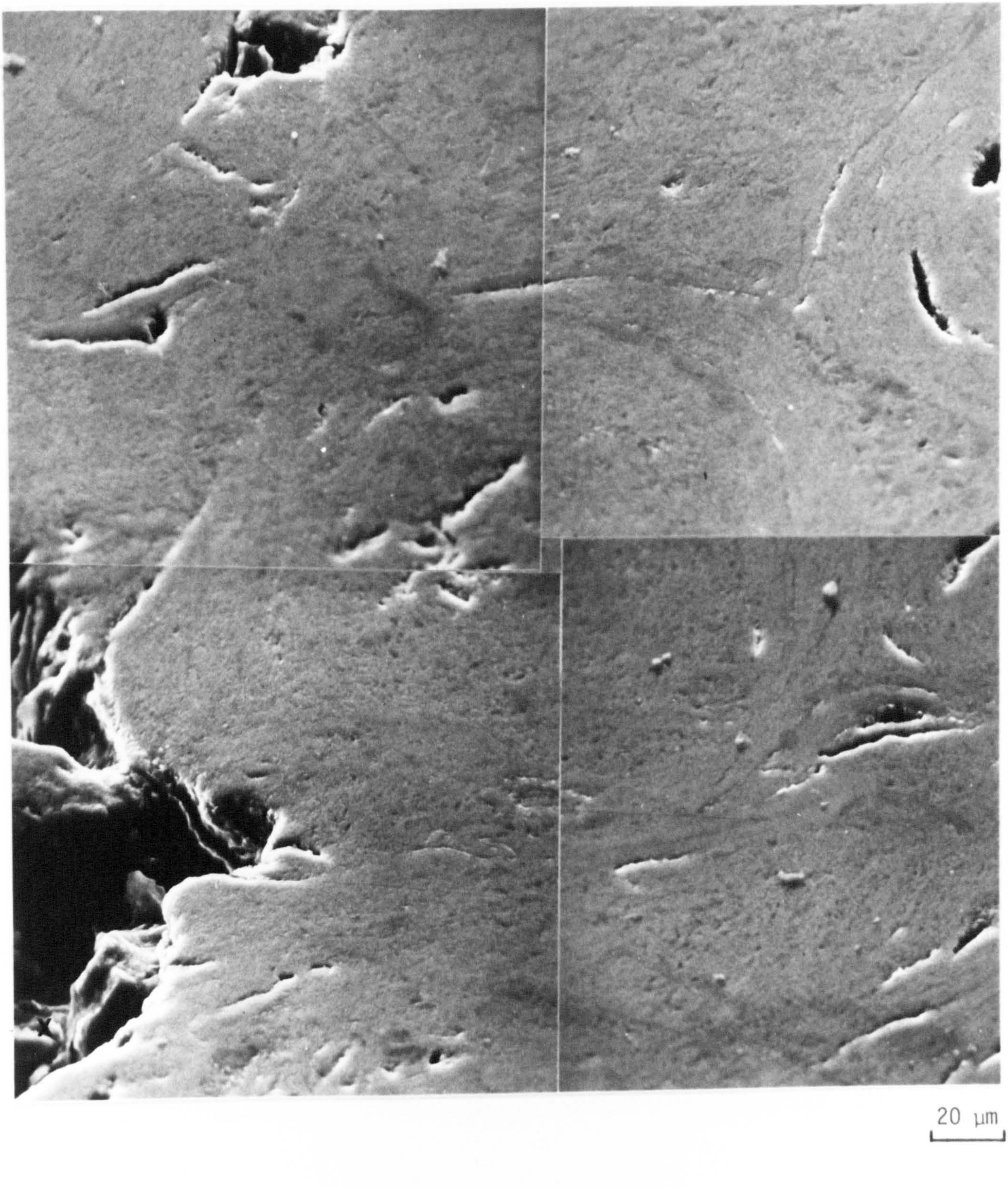
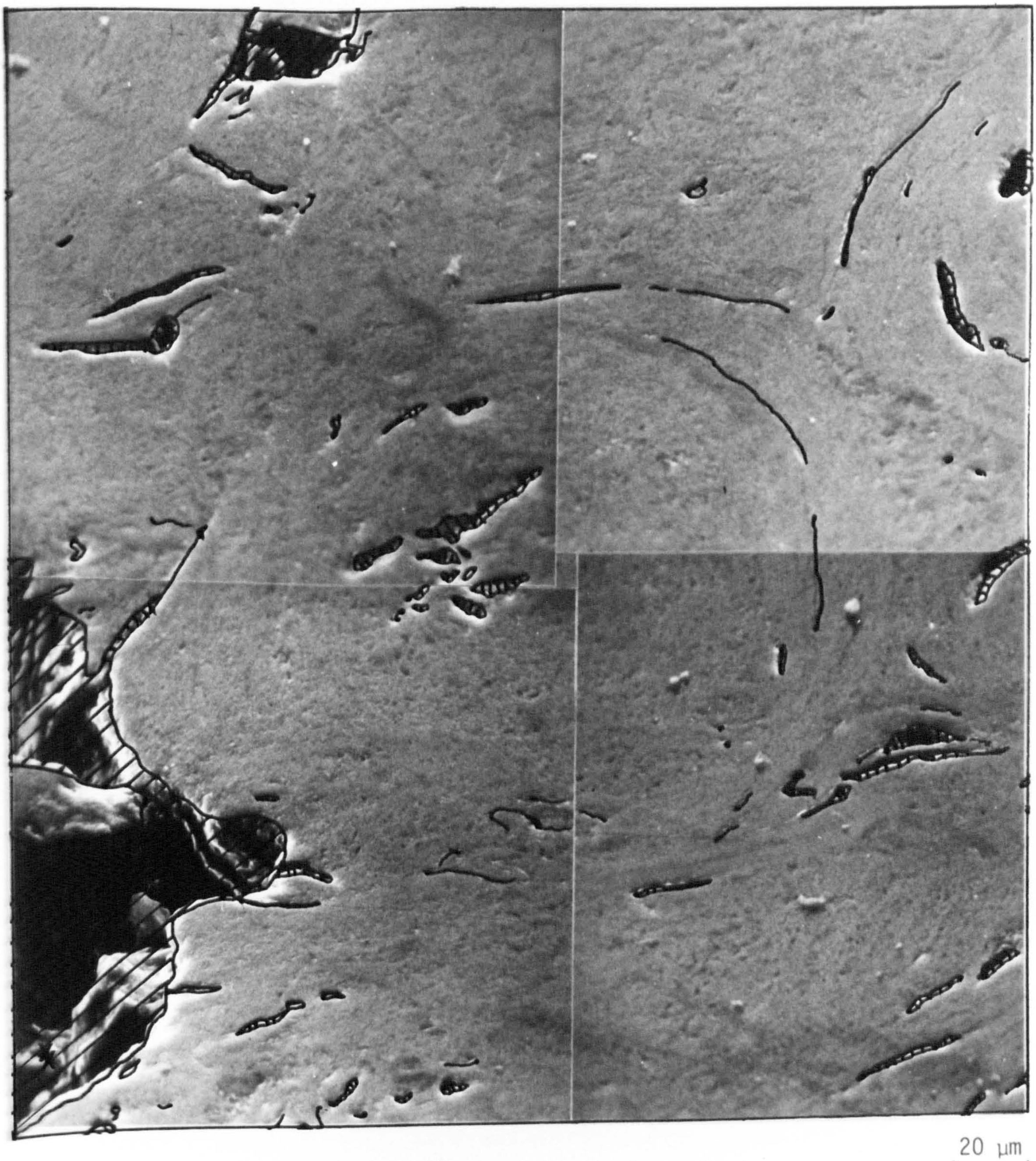


Figure 712.7. Photo-montage of AGLMP Graphite after the seventh polish.



Overlay for Figure 712.7.

Figure 712.7. Photo-montage of AGLMP Graphite after the seventh polish.



Overlay for Figure 712.8.

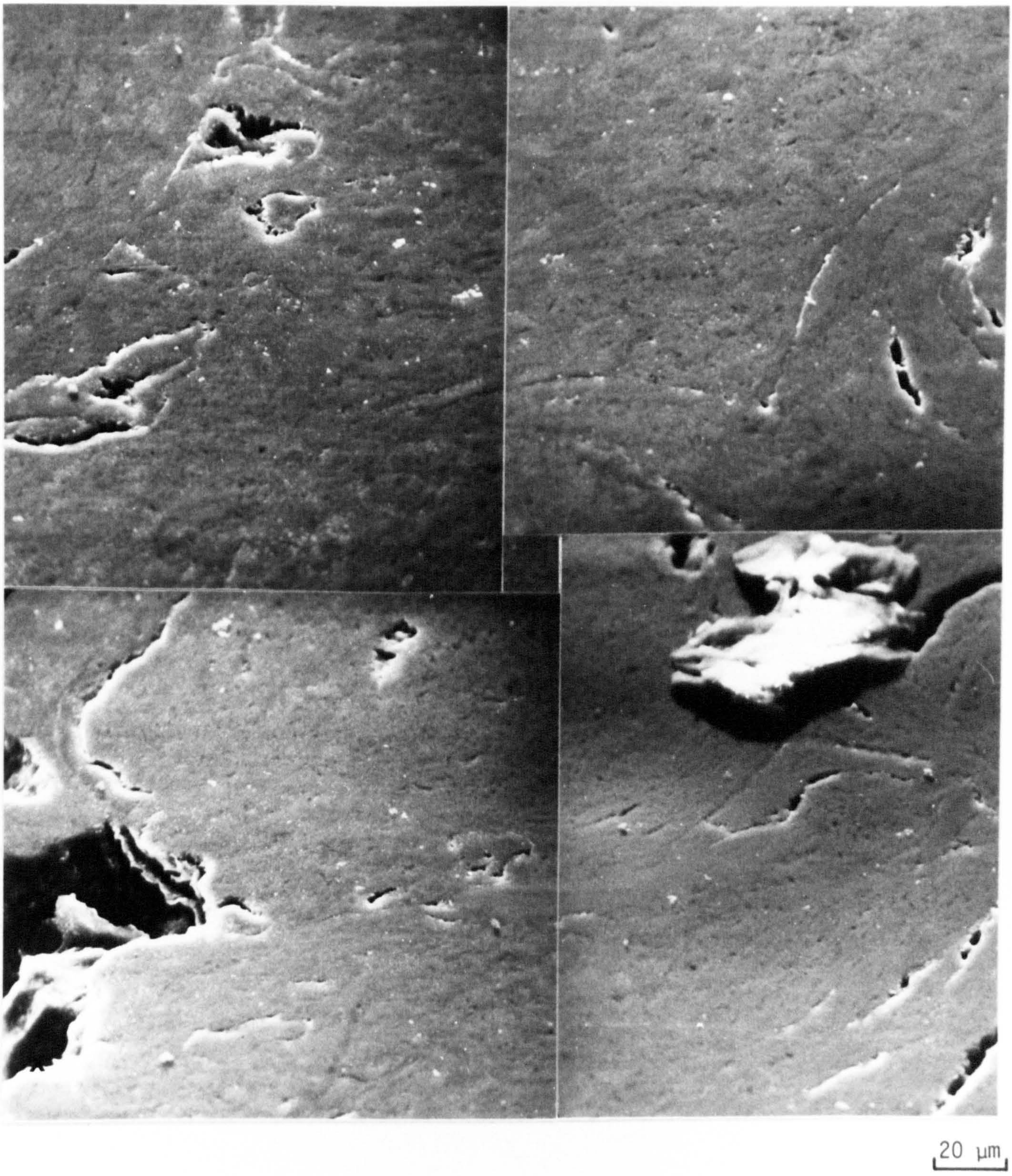
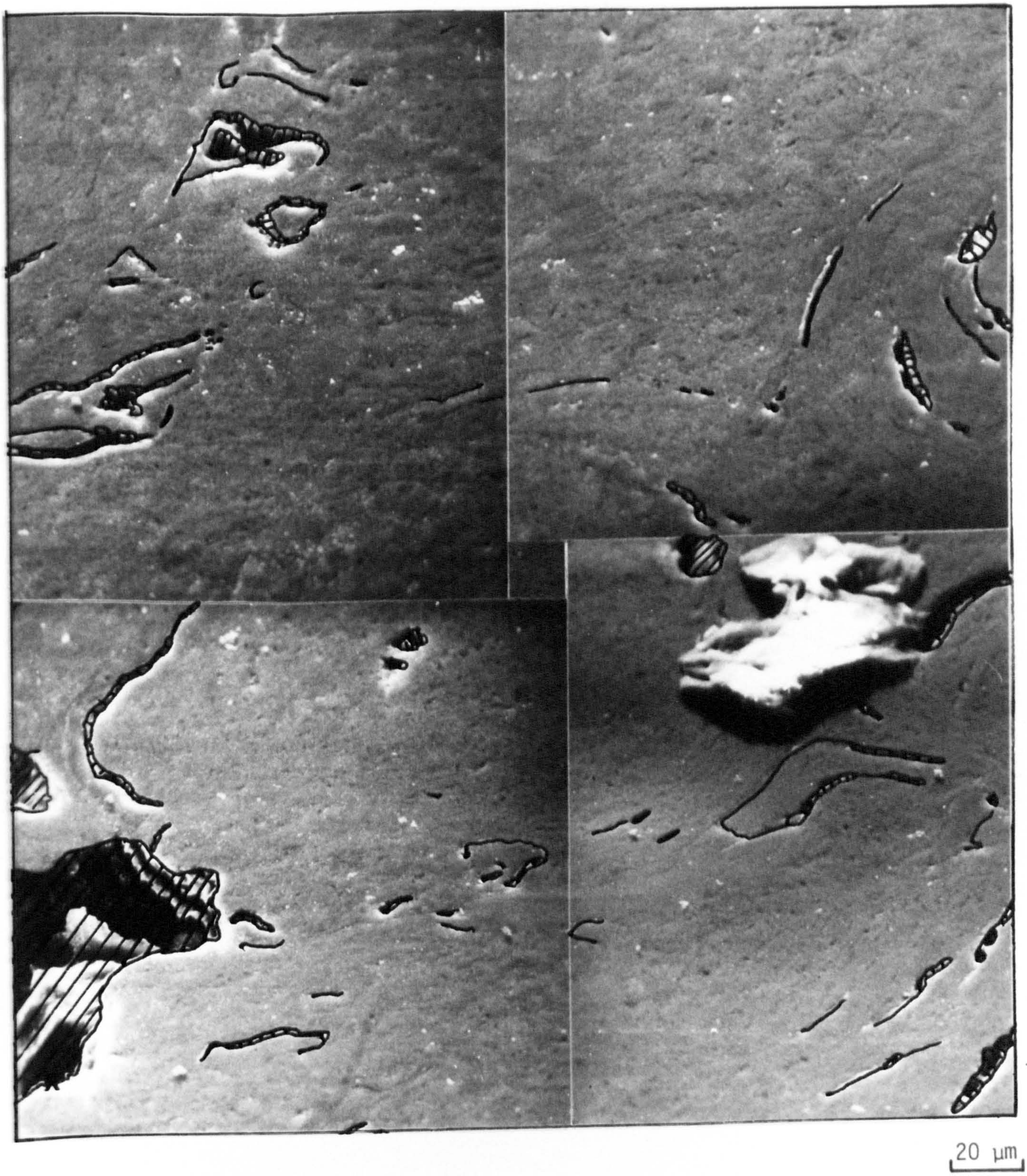


Figure 712.8. Photo-montage of Aglmp Graphite after the eighth polish.



Overlay for Figure 712.8.

Figure 712.8. Photo-montage of Aglmp Graphite after the eighth polish.



Overlay for Figure 712.9.

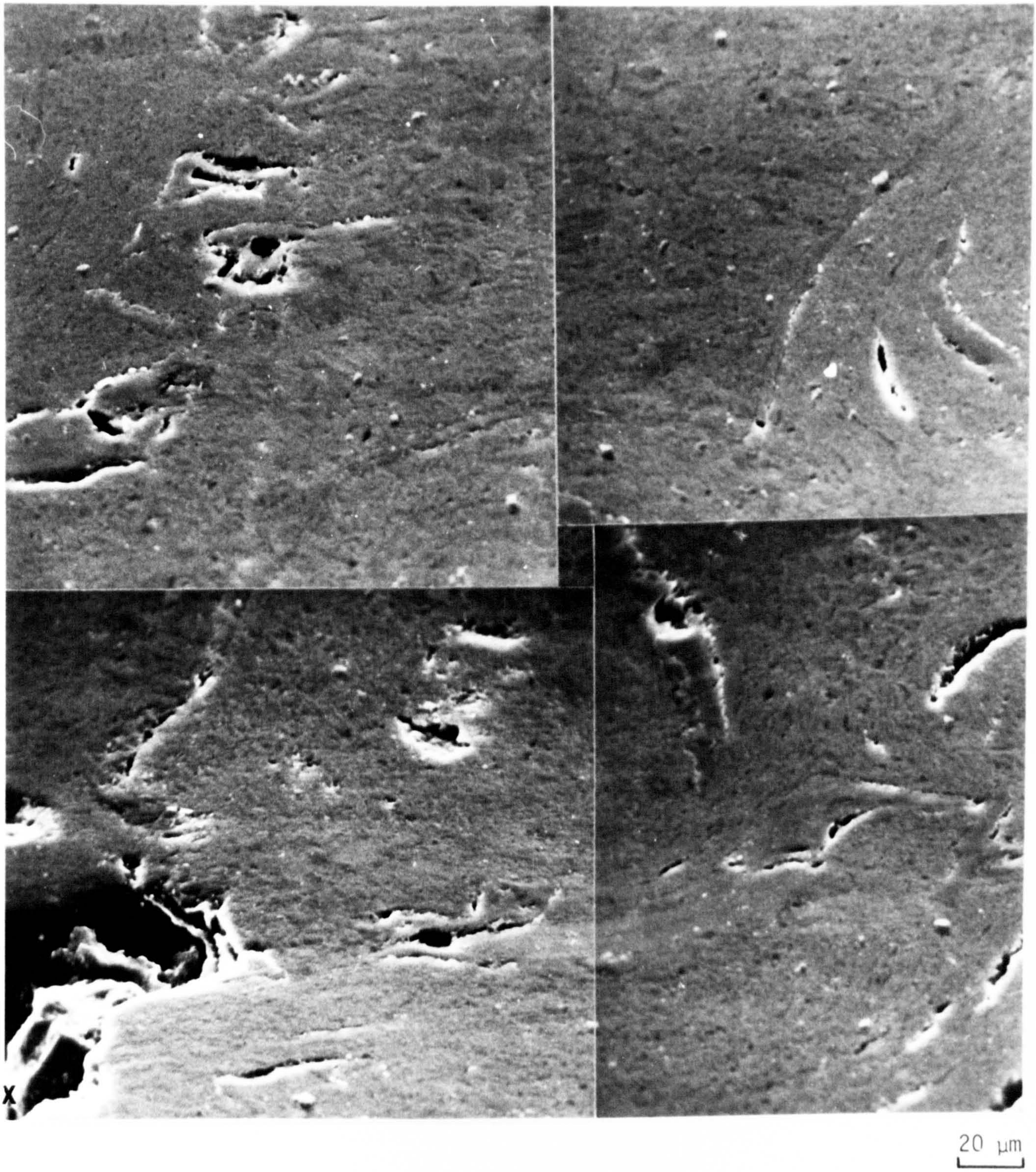
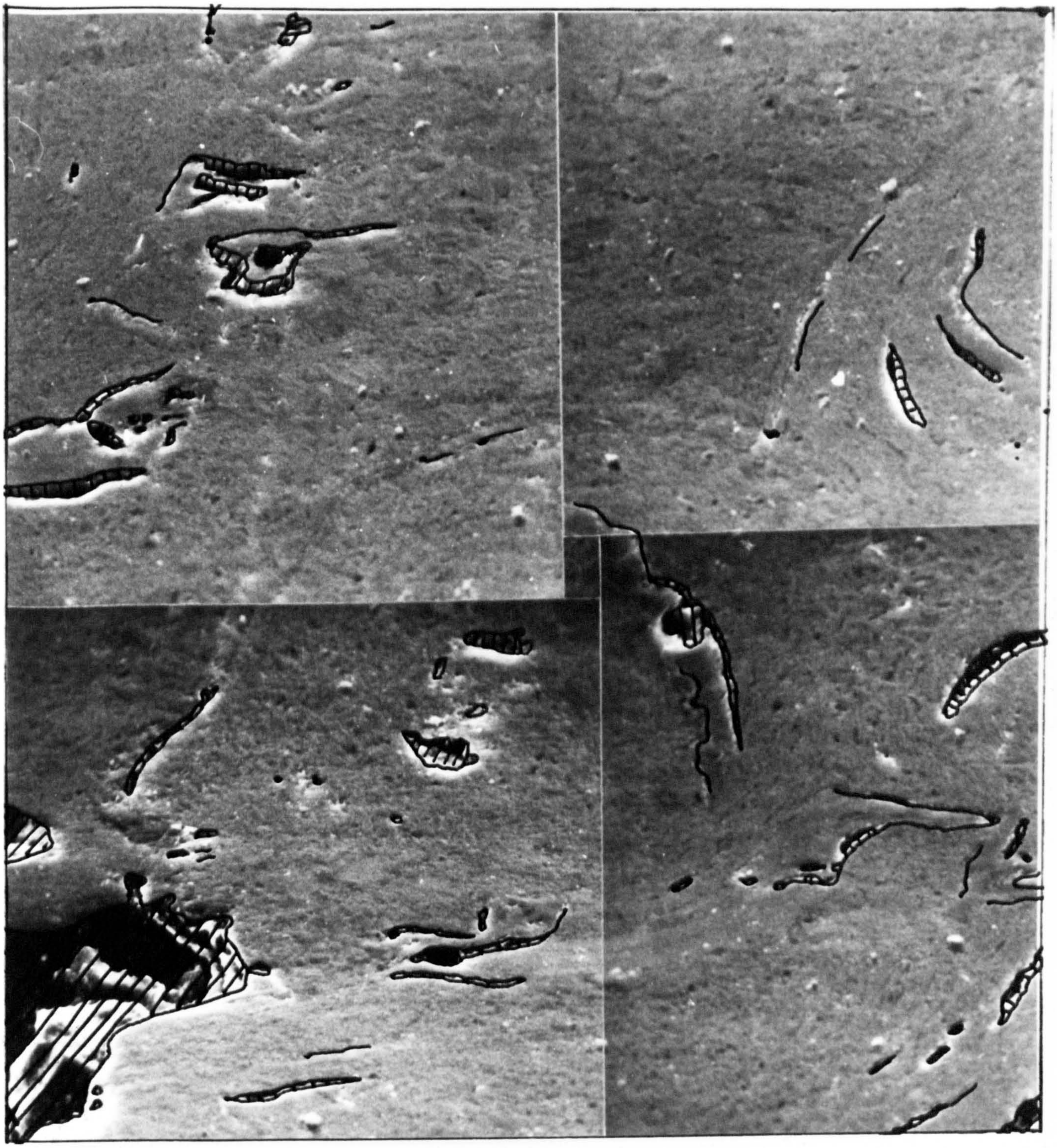
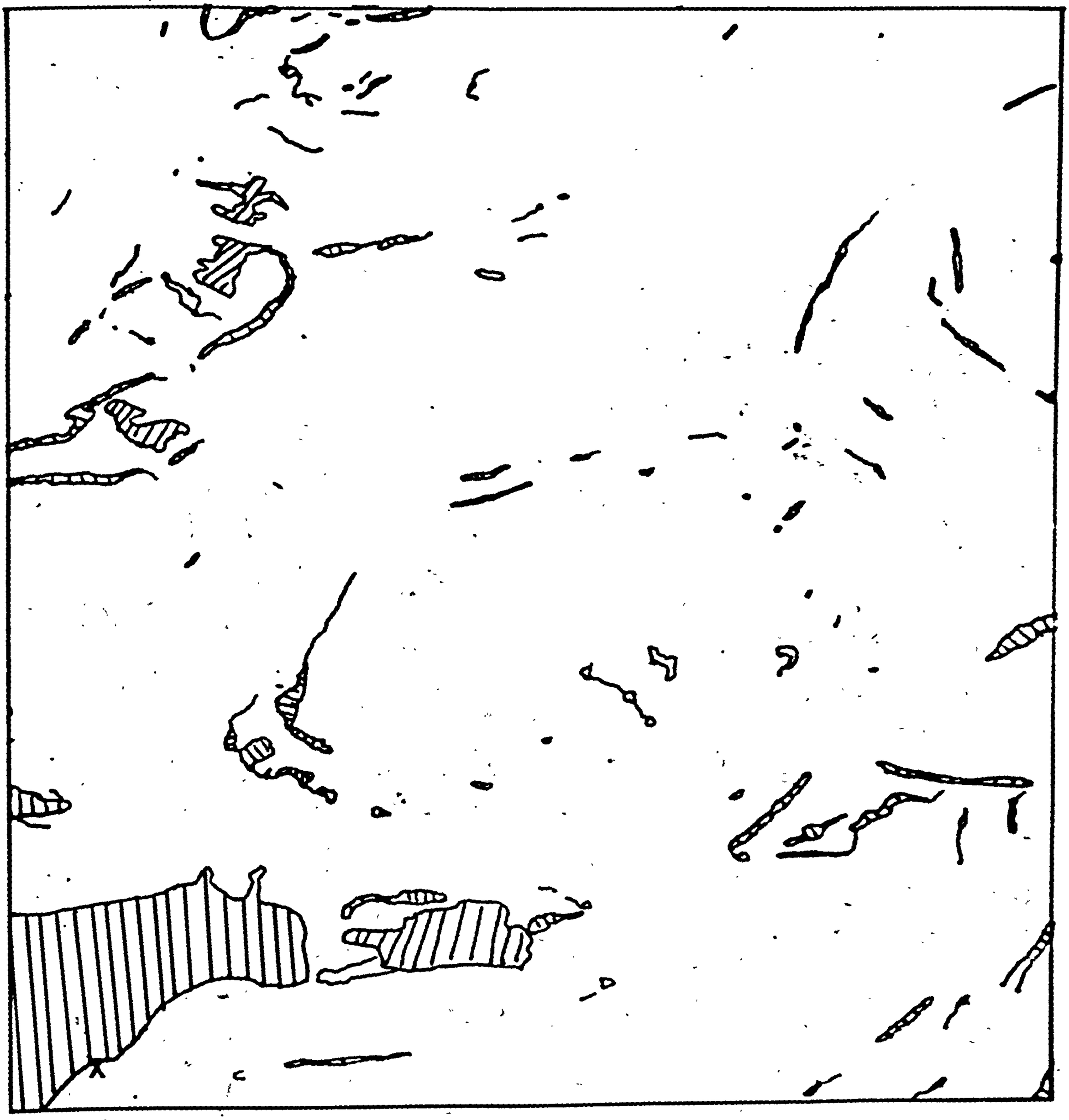


Figure 712.9. Photo-montage of AGLMP Graphite after the ninth polish.



Overlay for Figure 712.9.

Figure 712.9. Photo-montage of AGLMP Graphite after the ninth polish.



Overlay for Figure 712.10.

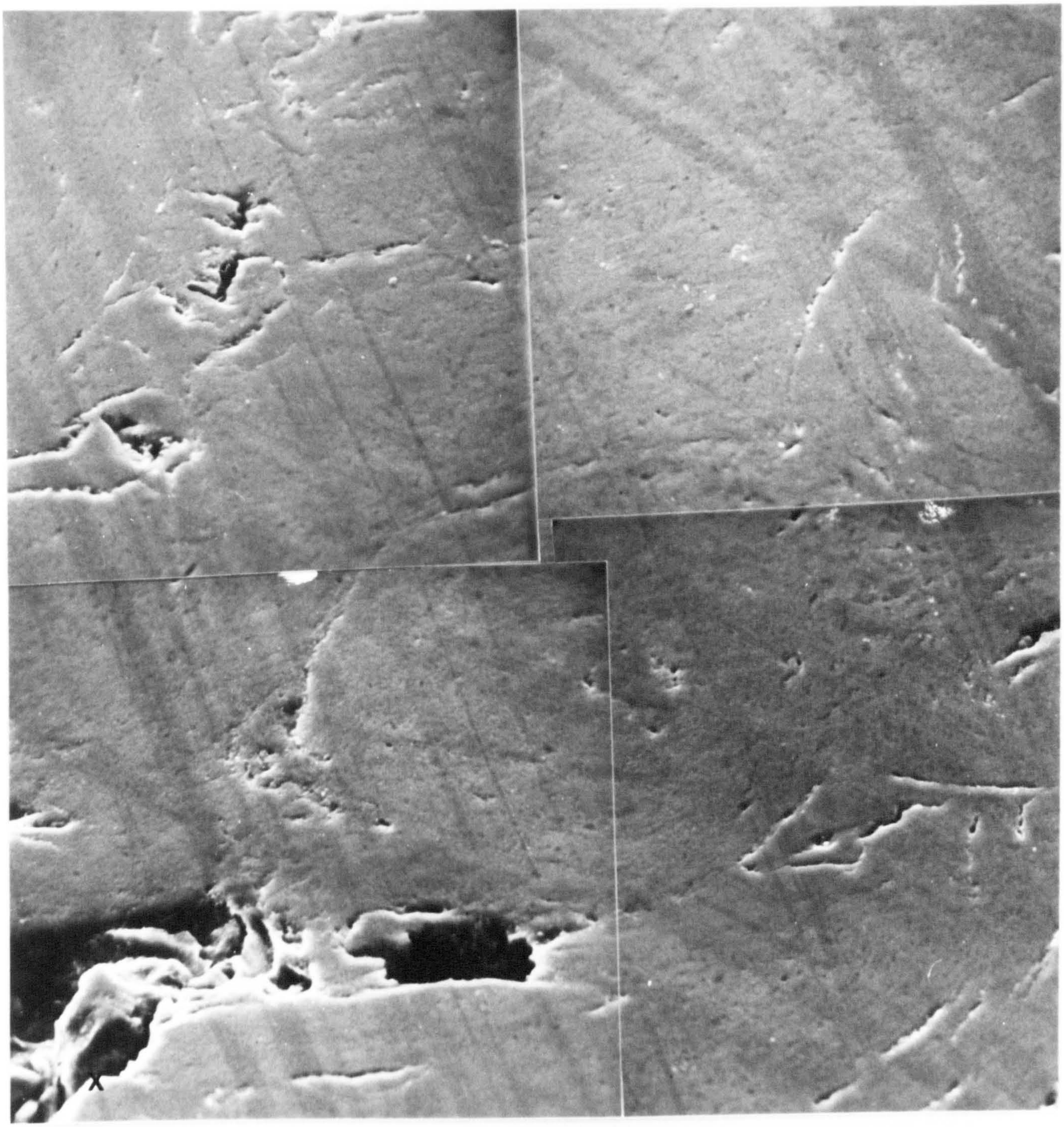
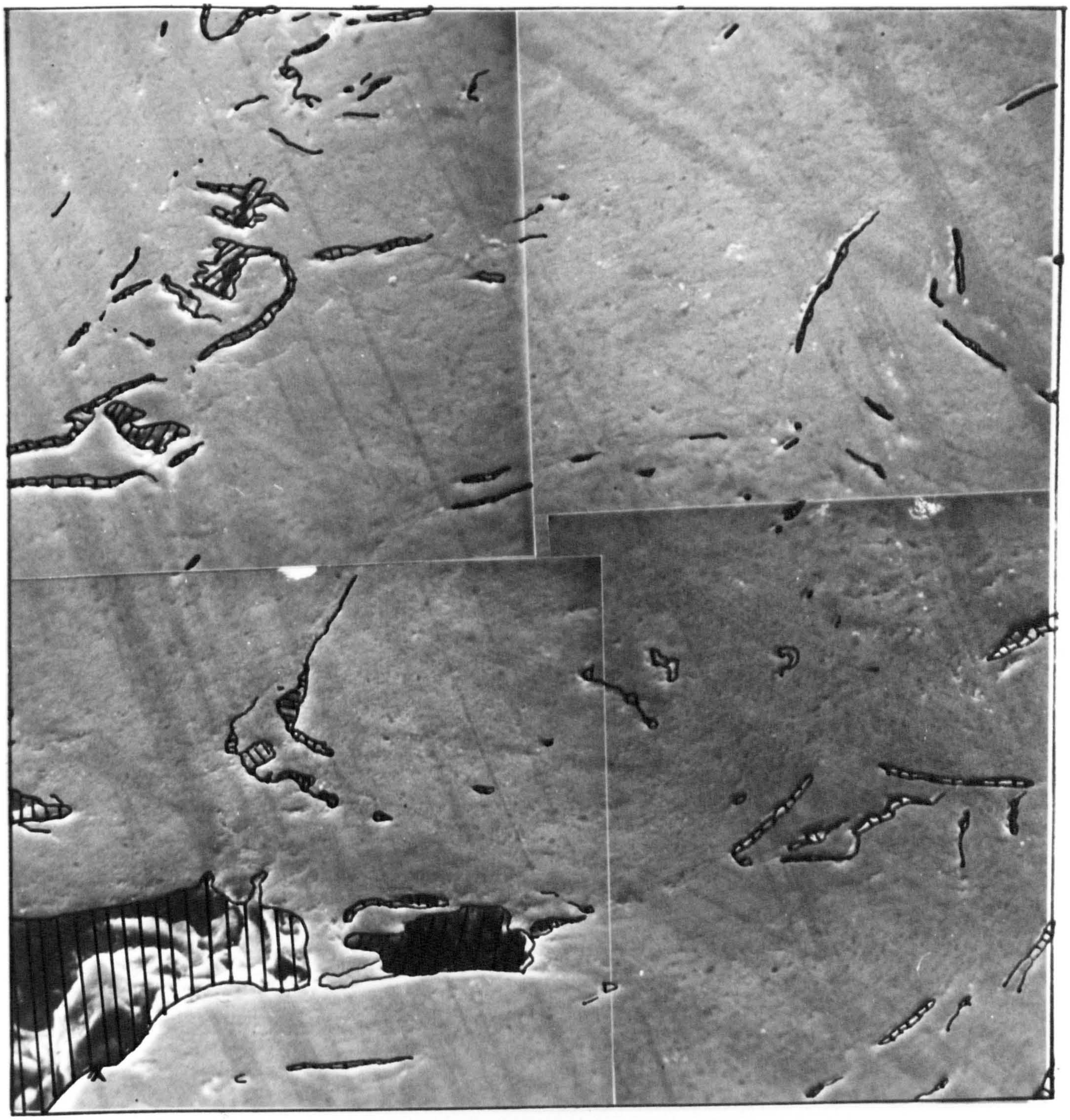


Figure 712.10. Photo-montage of AGLMP Graphite after the tenth polish.



Overlay for Figure 712.10.

Figure 712.10. Photo-montage of AGLMP Graphite after the tenth polish.

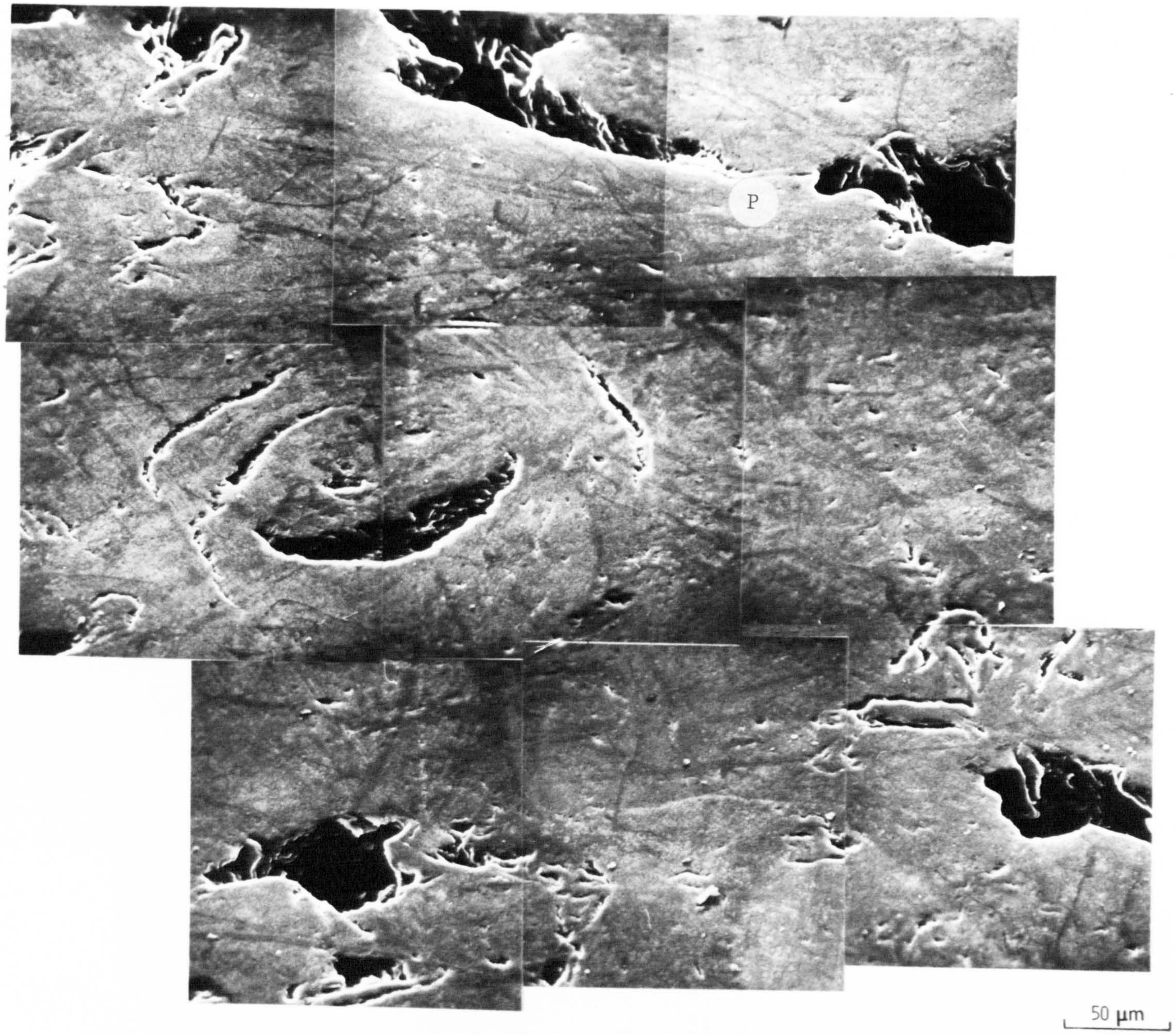


FIGURE 713.1. PHOTO-MONTAGE OF AGLMP GRAPHITE AFTER THE FIRST POLISH.

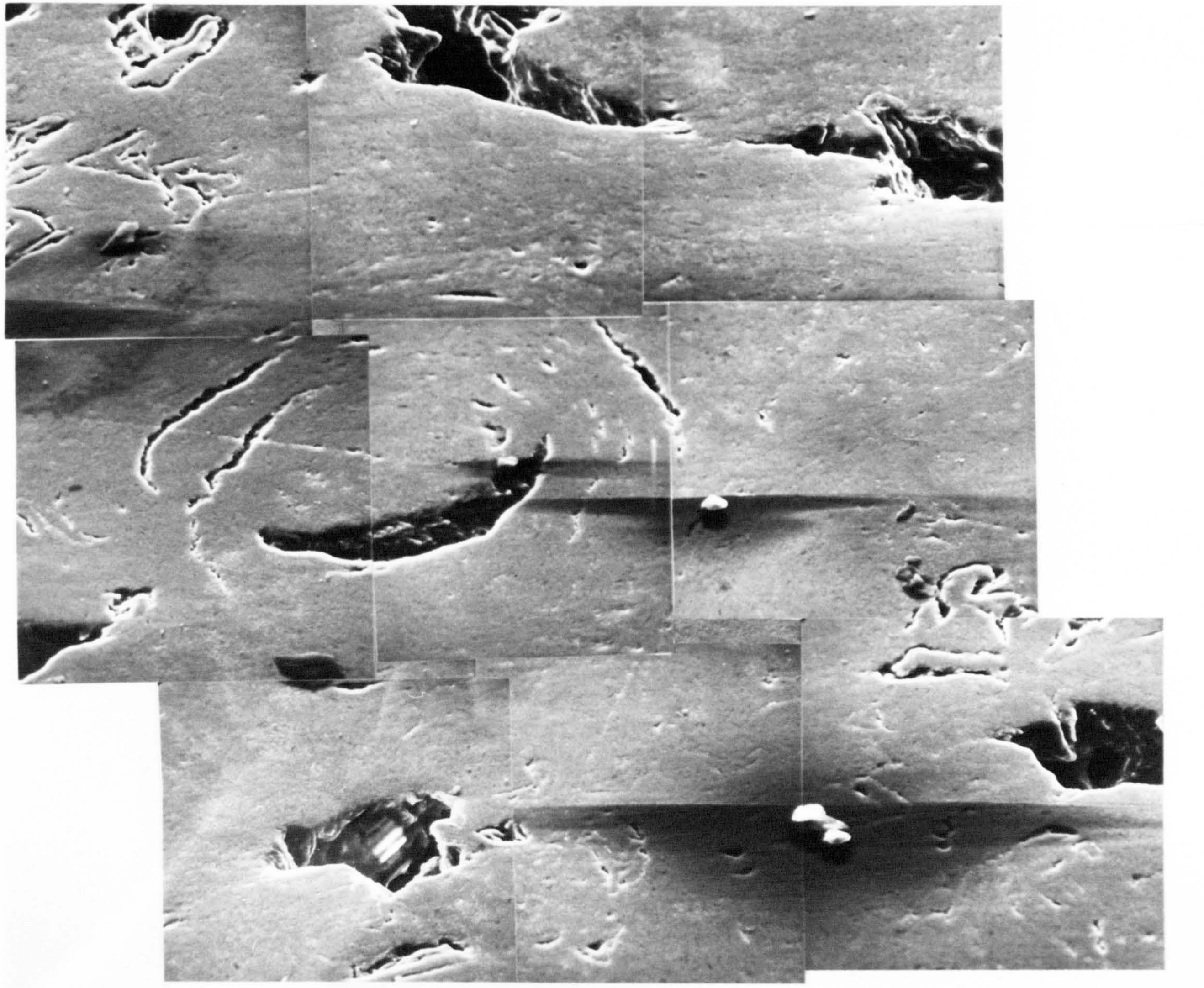


FIGURE 713.2. PHOTO-MONTAGE OF AGLMP GRAPHITE AFTER THE SECOND POLISH.

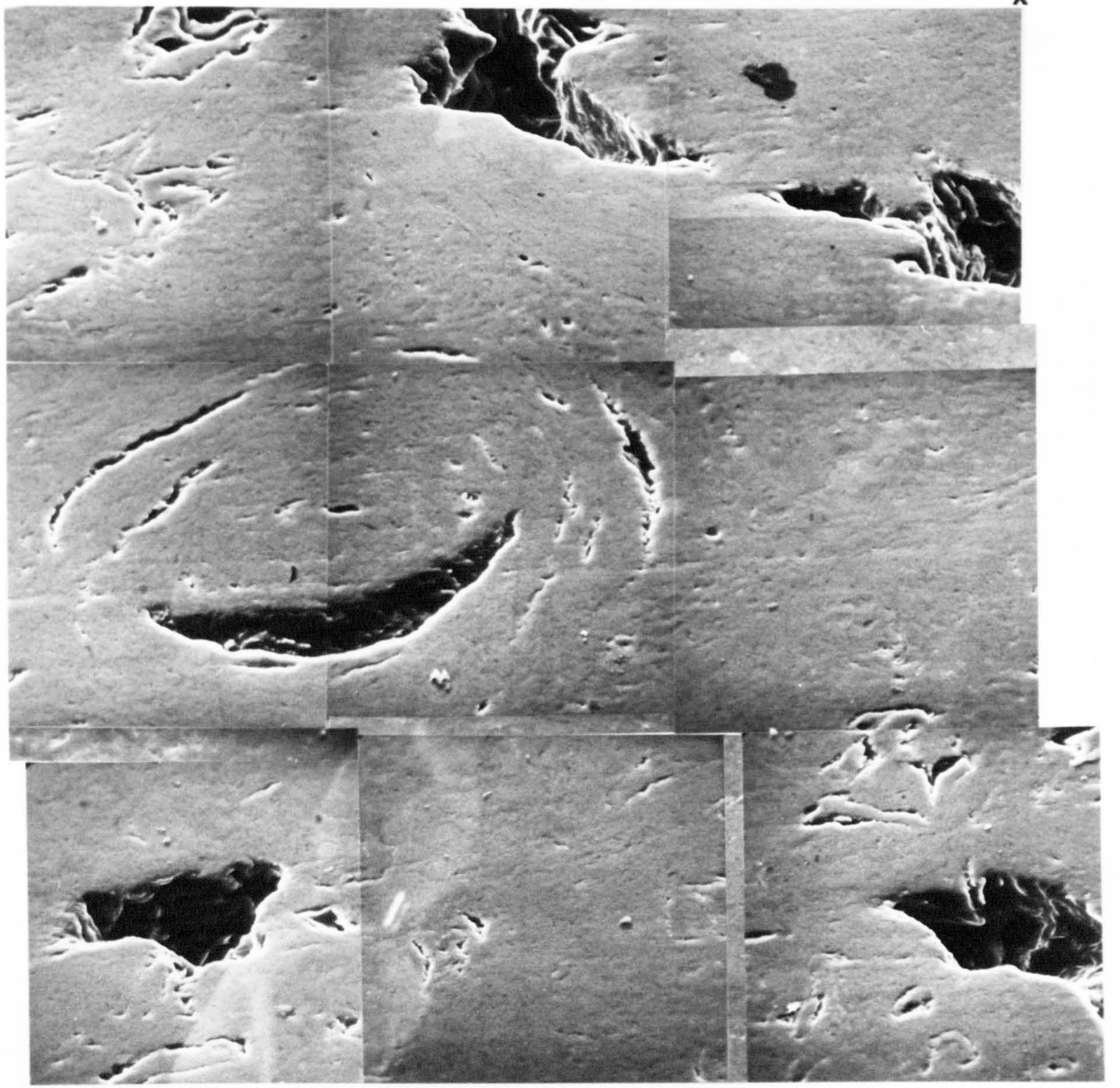


FIGURE 713.3. PHOTO-MONTAGE OF AGLMP GRAPHITE AFTER THE THIRD POLISH.

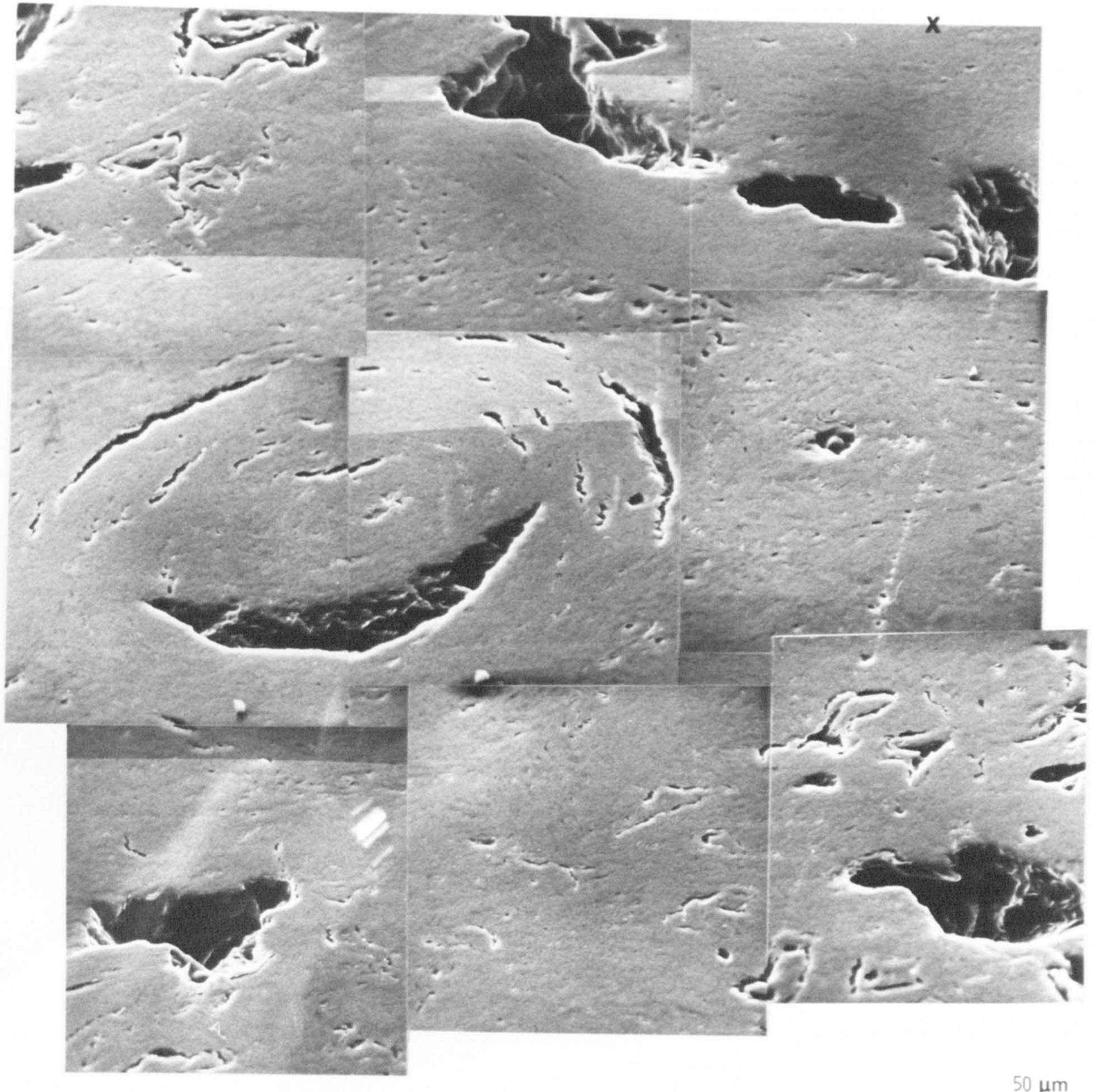


FIGURE 713.4. PHOTO-MONTAGE OF AGLMP GRAPHITE AFTER THE FOURTH POLISH.

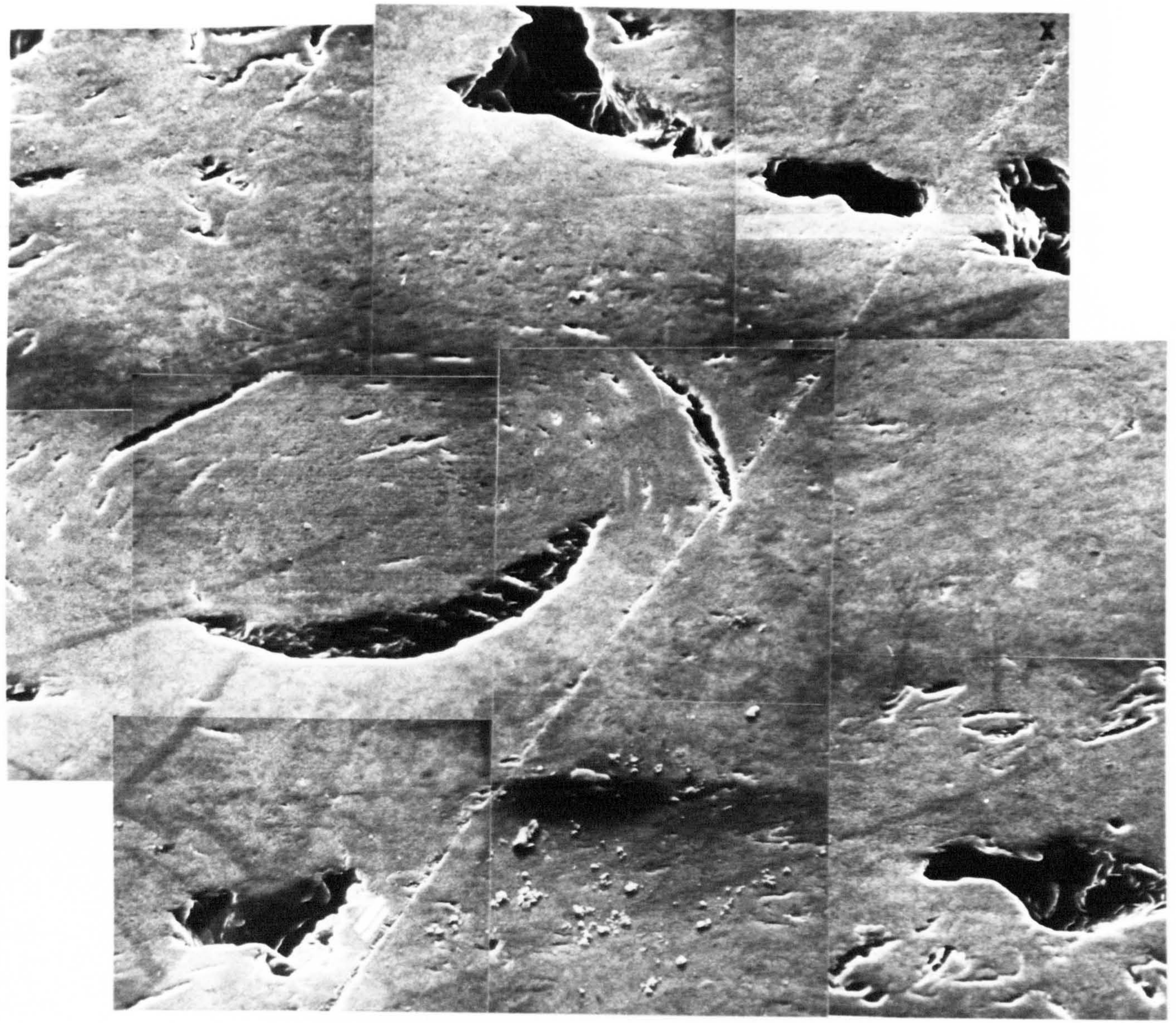


FIGURE 713.5. PHOTO-MONTAGE OF AGLMP GRAPHITE AFTER THE FIFTH POLISH.

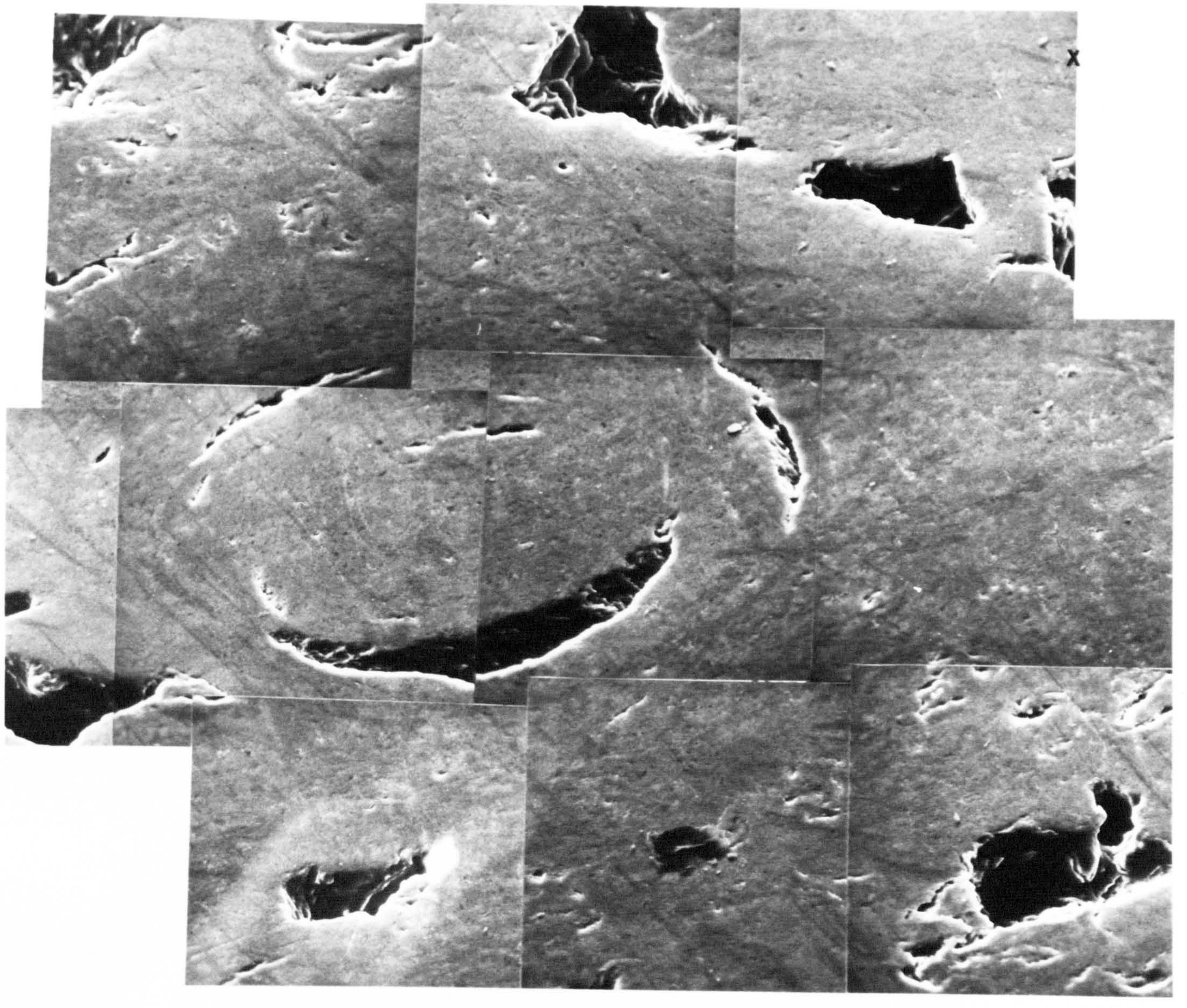


FIGURE 713.6. PHOTO-MONTAGE OF AGLMP GRAPHITE AFTER THE SIXTH POLISH.

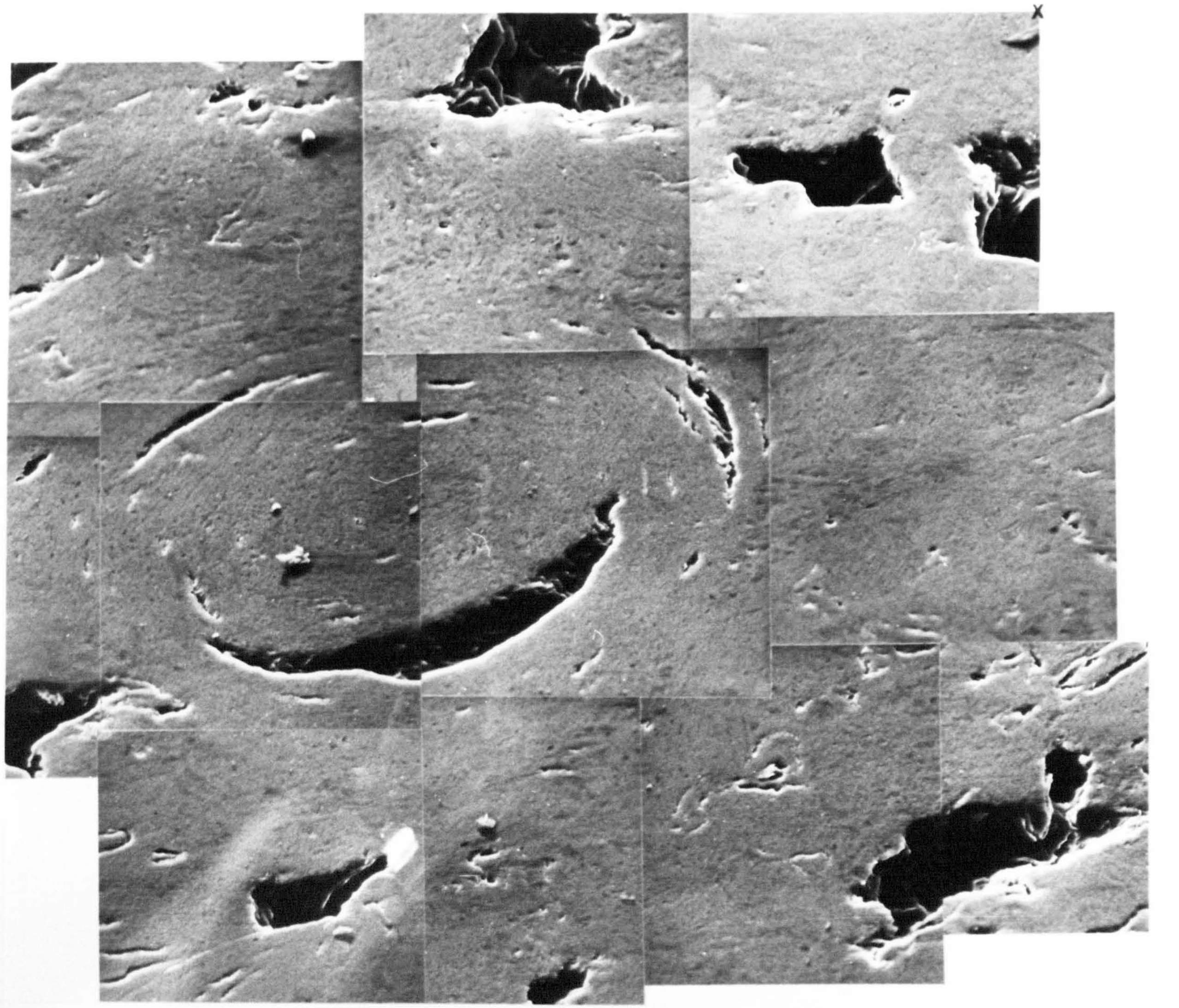


FIGURE 713.7. PHOTO-MONTAGE OF AGLMP GRAPHITE AFTER THE SEVENTH POLISH.

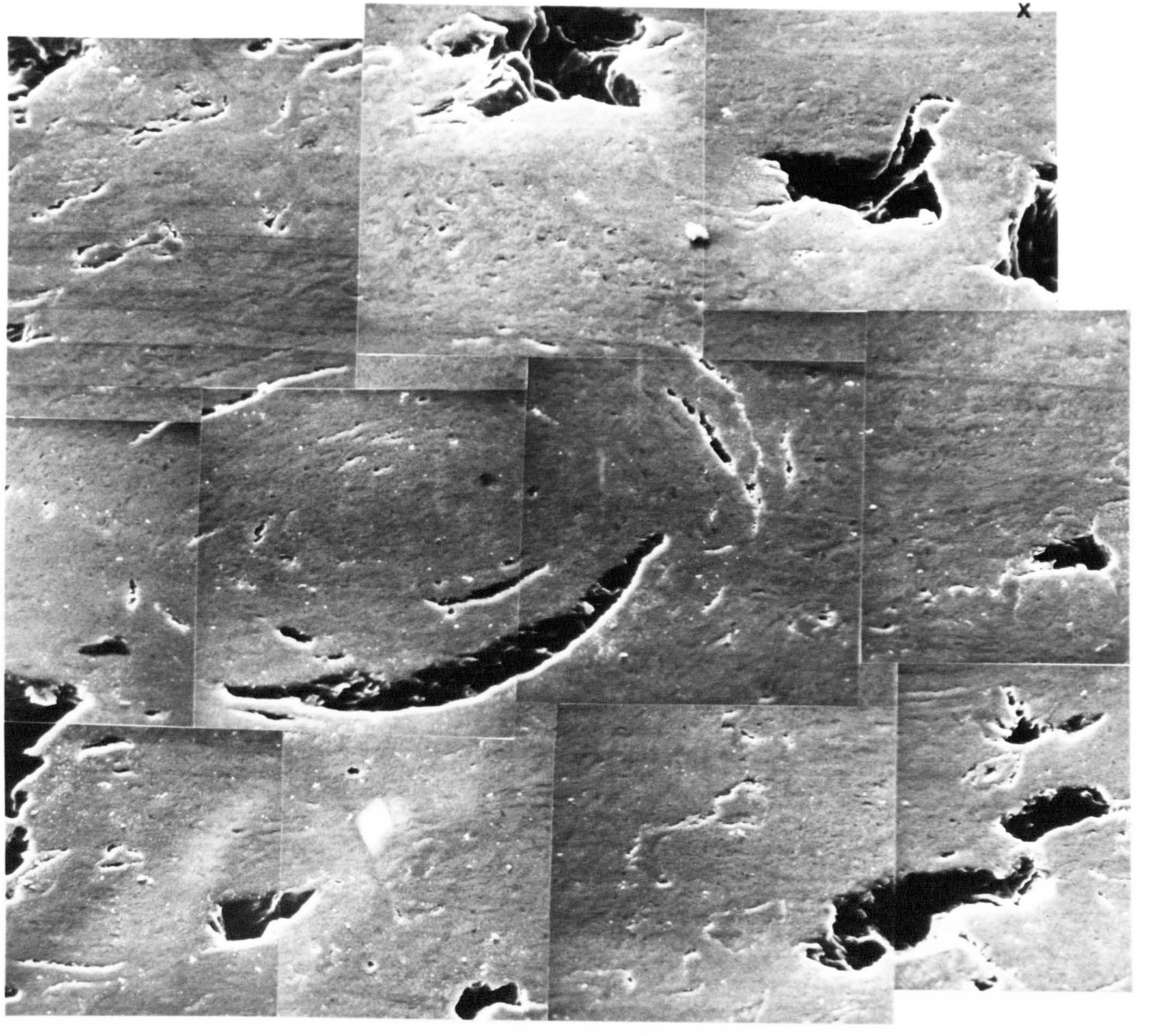


FIGURE 713.8. PHOTO-MONTAGE OF AGLMP GRAPHITE AFTER THE EIGHTH POLISH.

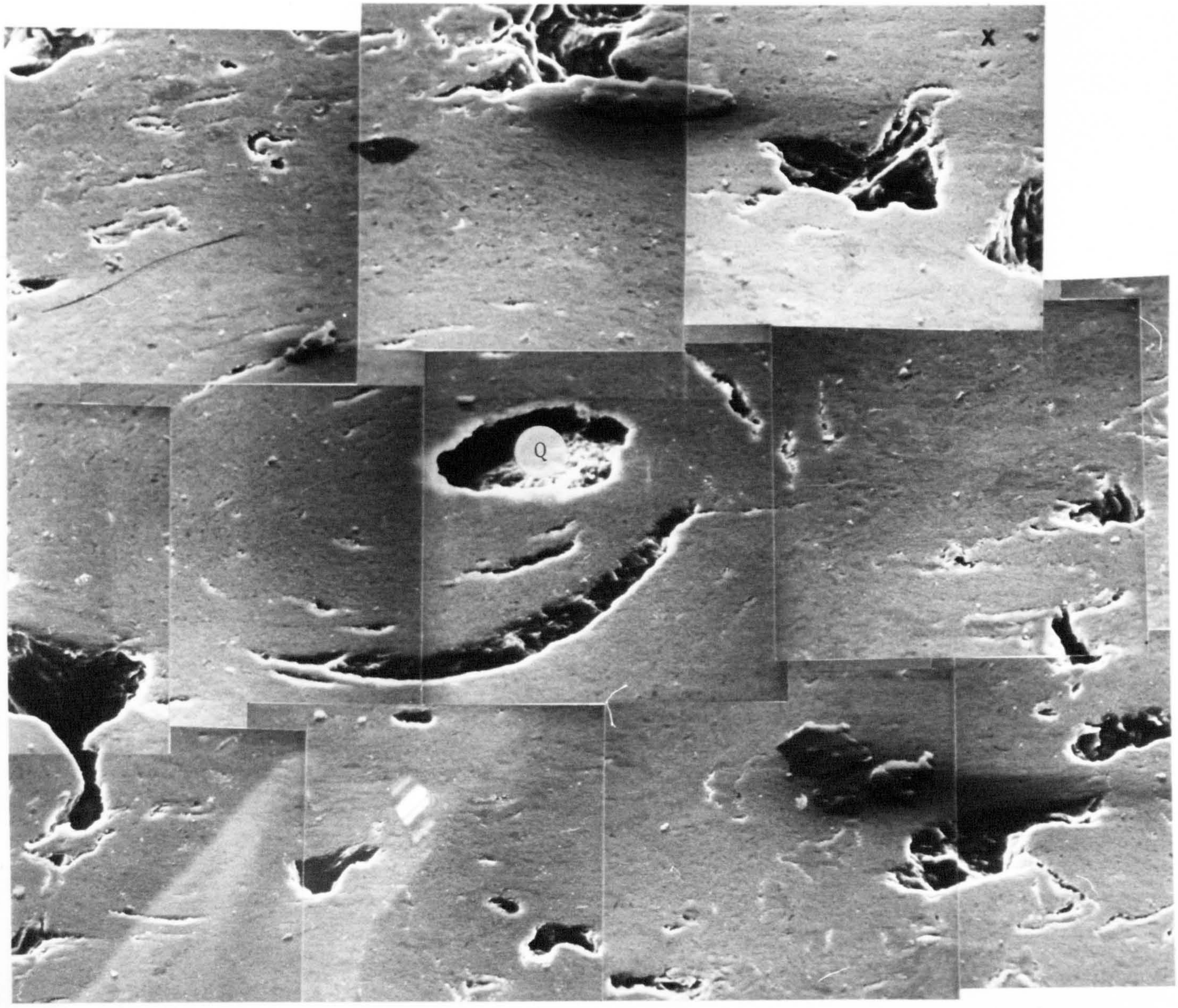


FIGURE 713.9. PHOTO-MONTAGE OF AGLMP GRAPHITE AFTER THE NINTH POLISH.

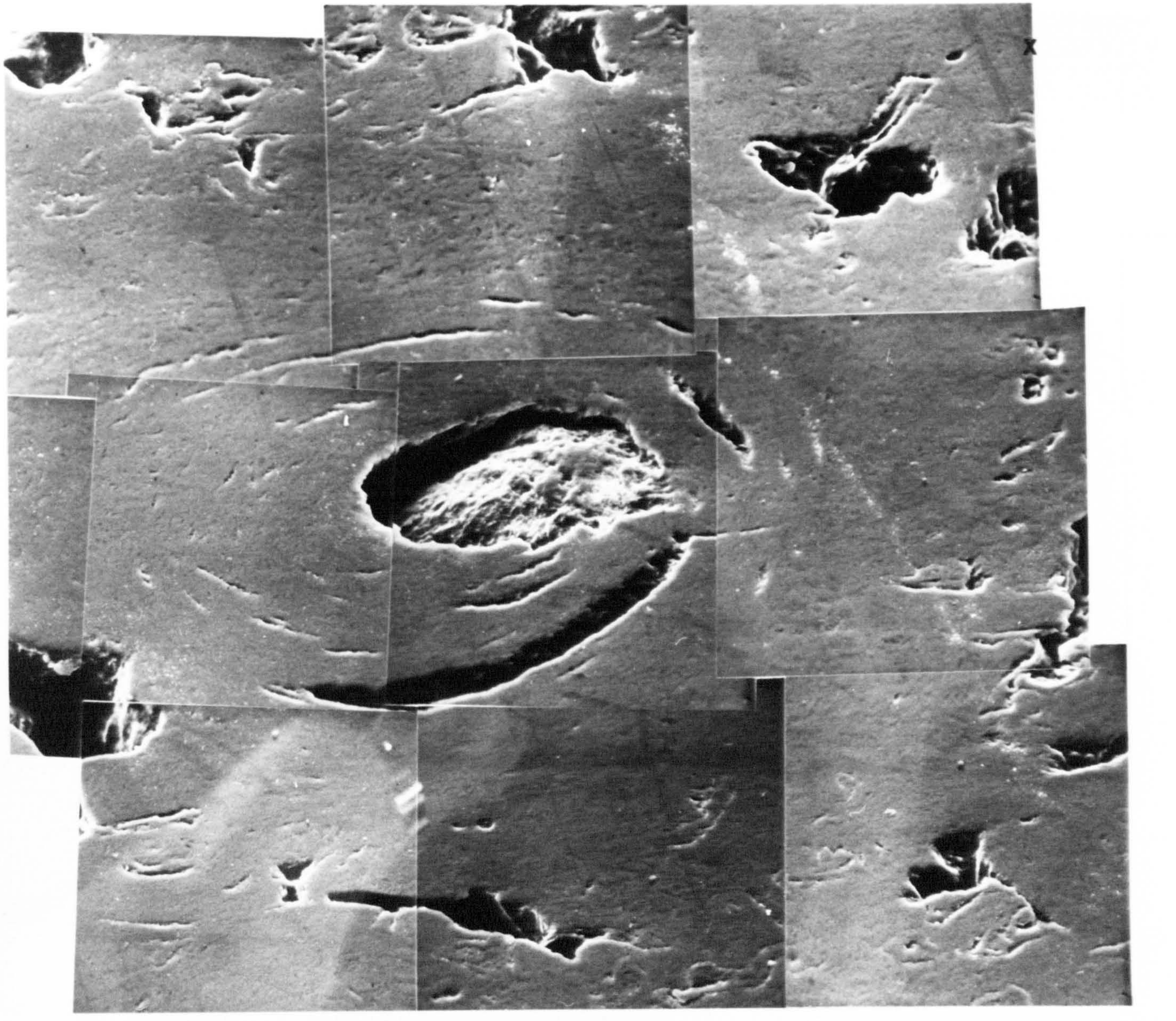


FIGURE 713.10. PHOTO-MONTAGE OF AGLMP GRAPHITE AFTER THE TENTH POLISH.



FIGURE 714.1. PHOTO-MONTAGE OF VQMB GRAPHITE AFTER THE FIRST POLISH.

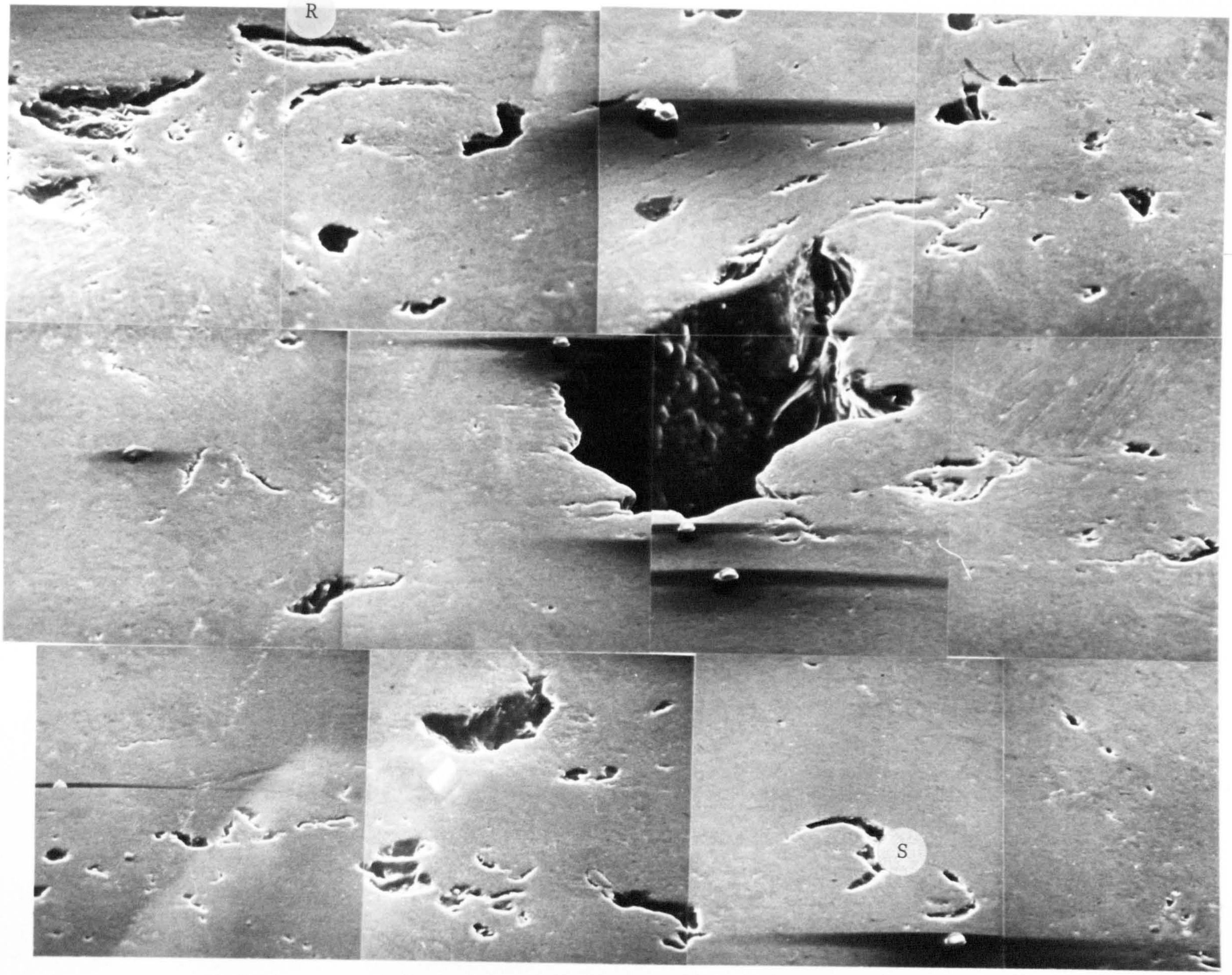


FIGURE 714.2. PHOTO-MONTAGE OF VQMB GRAPHITE AFTER THE SECOND POLISH.

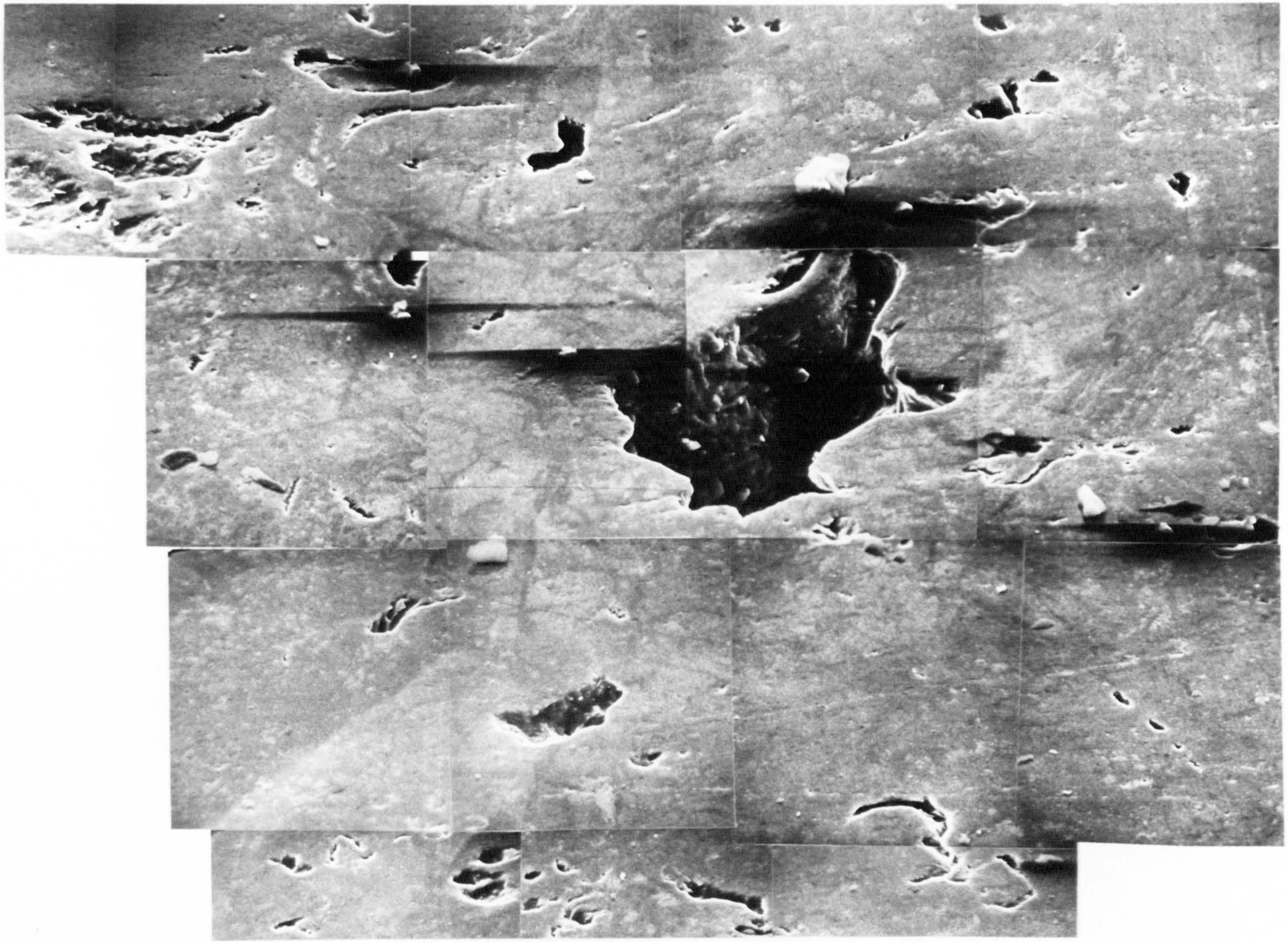


FIGURE 714.3. PHOTO-MONTAGE OF VQMB GRAPHITE AFTER THE THIRD POLISH.

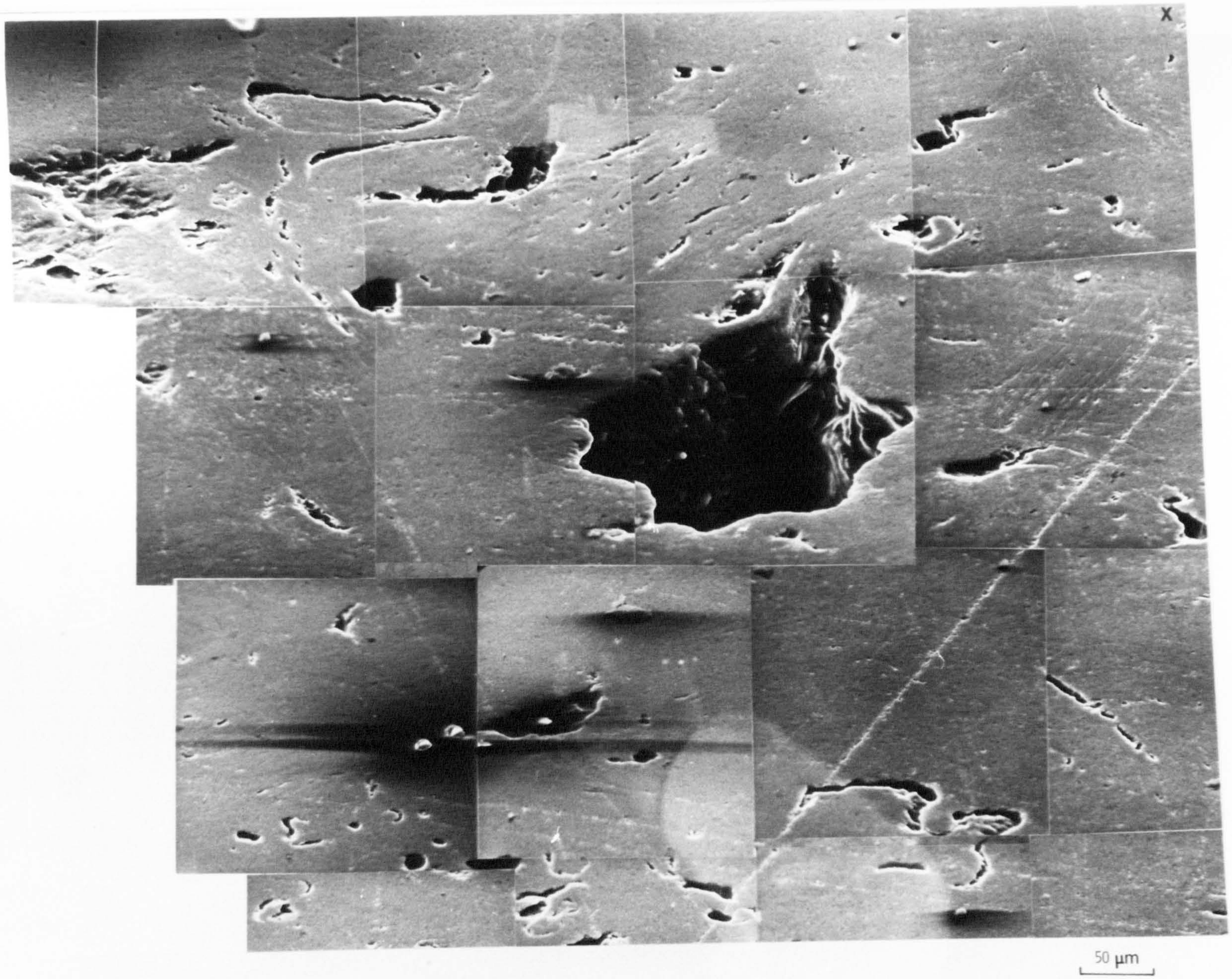


FIGURE 714.4. PHOTO-MONTAGE OF VQMB GRAPHITE AFTER THE FOURTH POLISH.

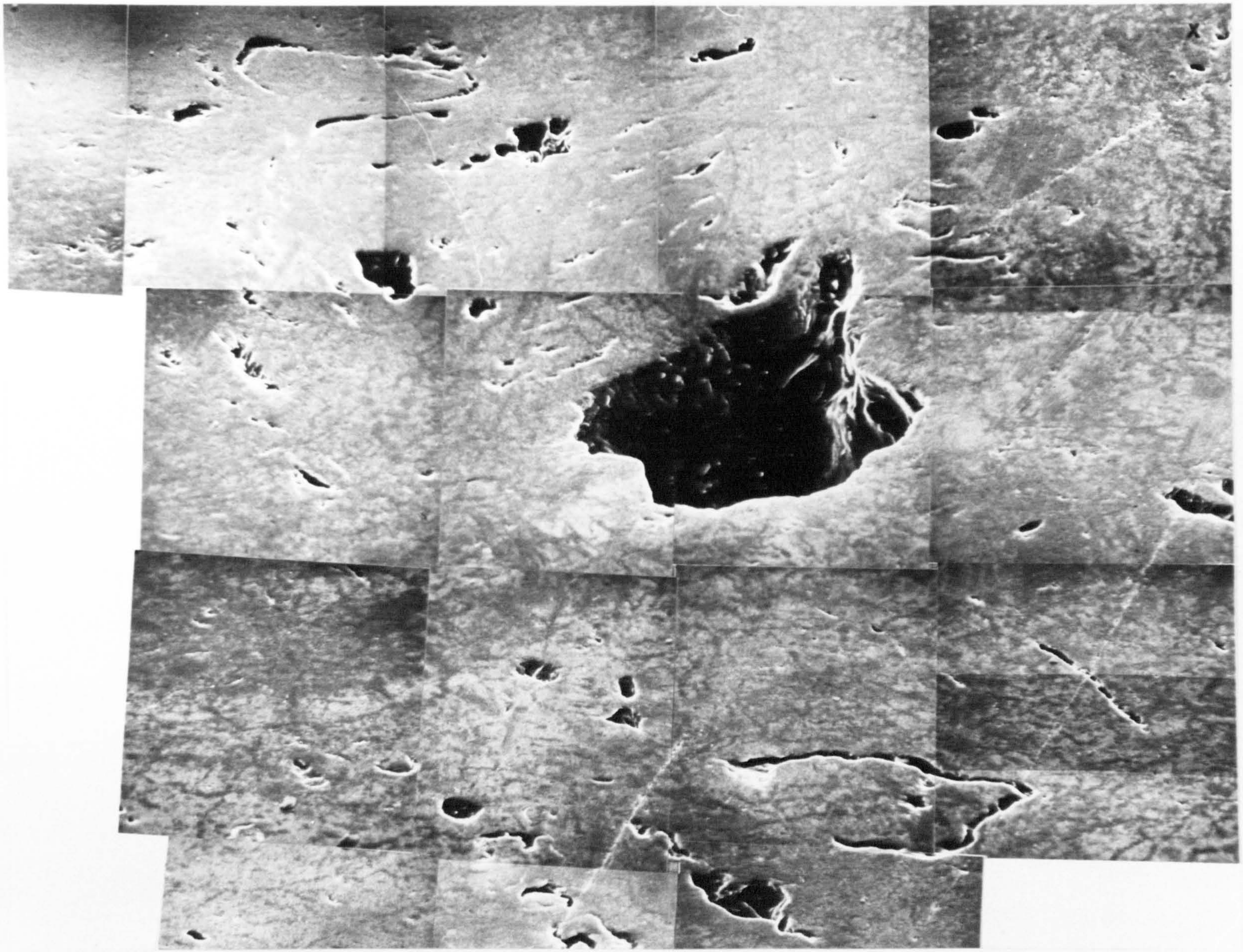


FIGURE 714.5. PHOTO-MONTAGE OF VQMB GRAPHITE AFTER THE FIFTH POLISH.

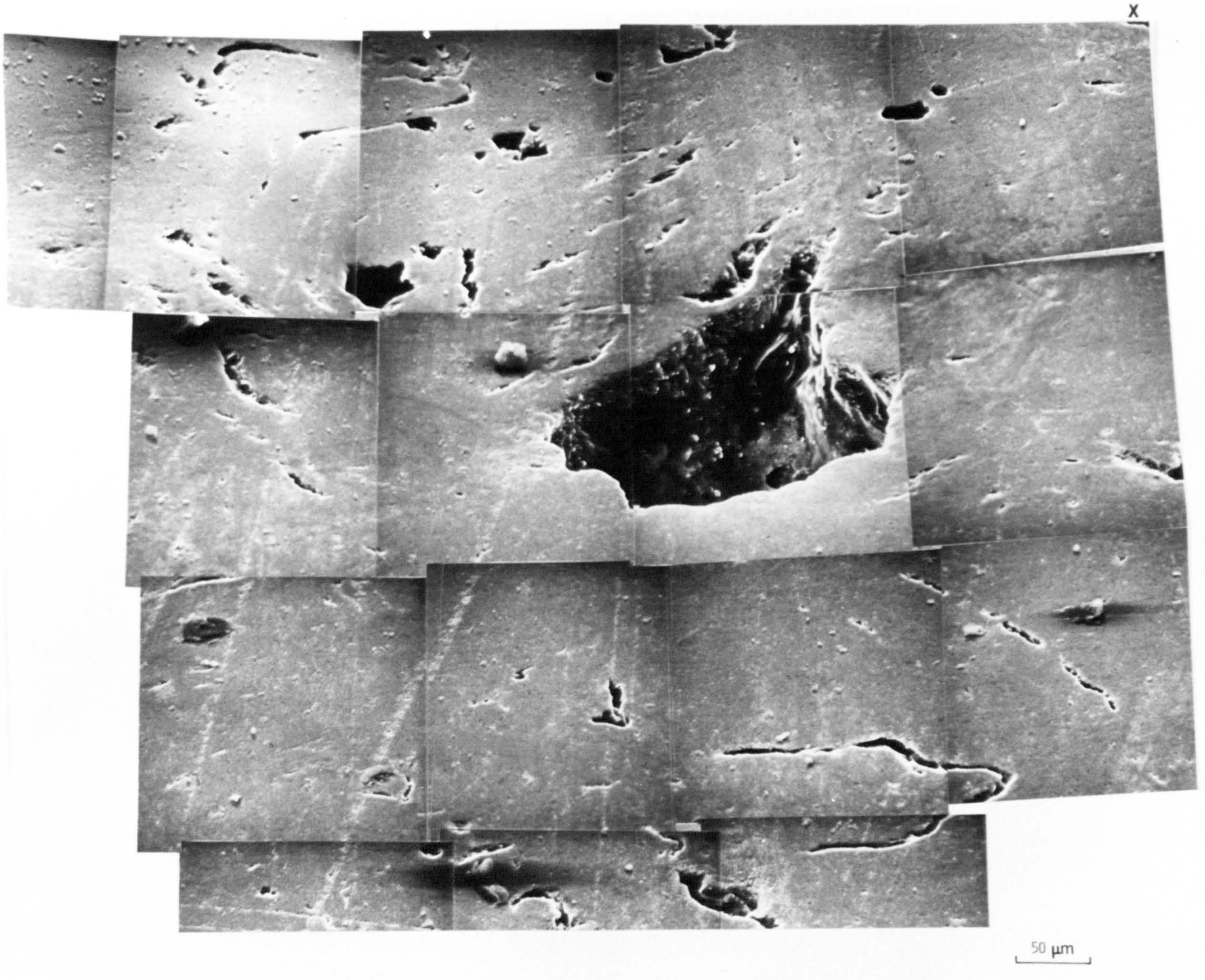


FIGURE 714.6. PHOTO-MONTAGE OF VQMB GRAPHITE AFTER THE SIXTH POLISH.

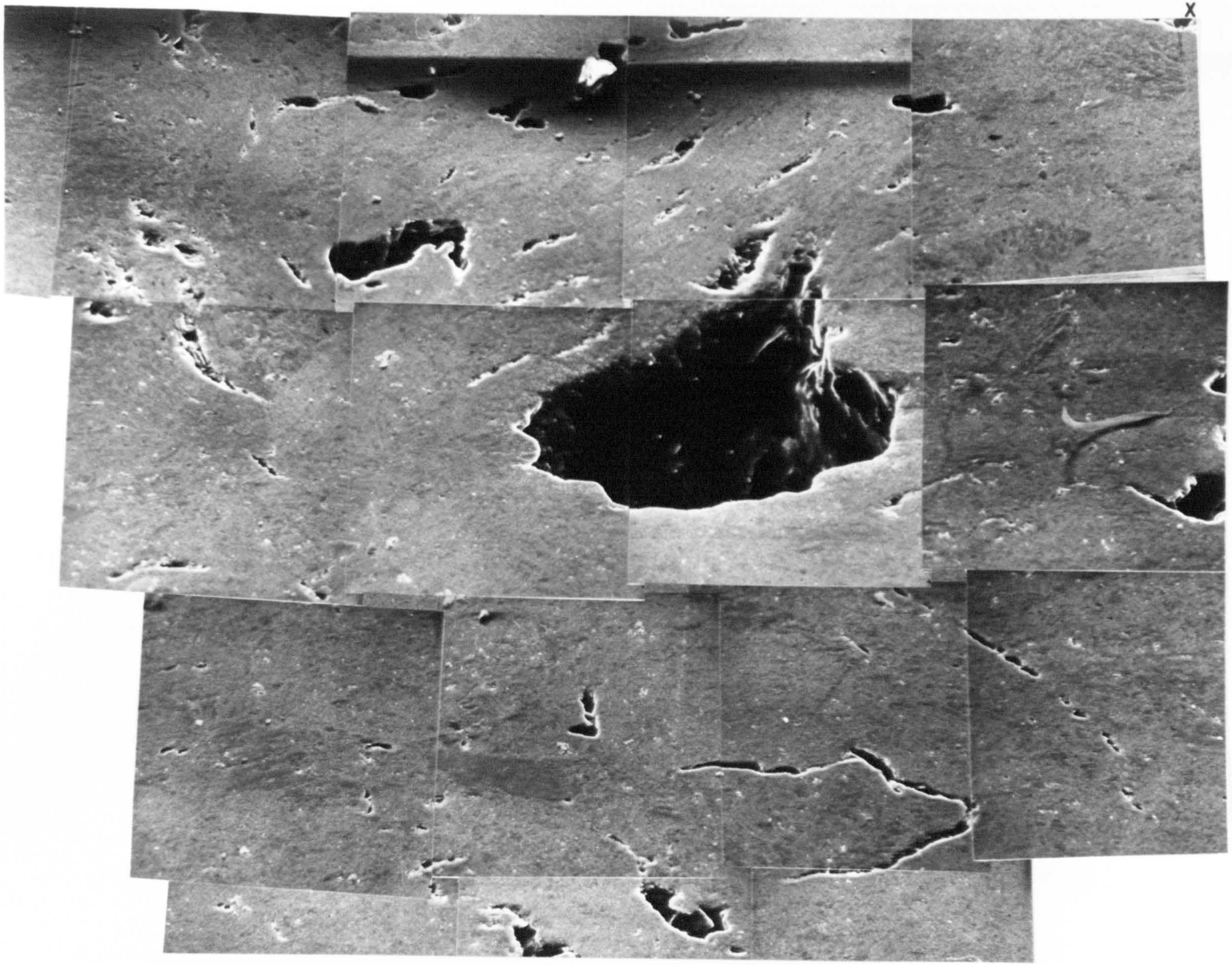


FIGURE 714.7. PHOTO-MONTAGE OF VQMB GRAPHITE AFTER THE SEVENTH POLISH.

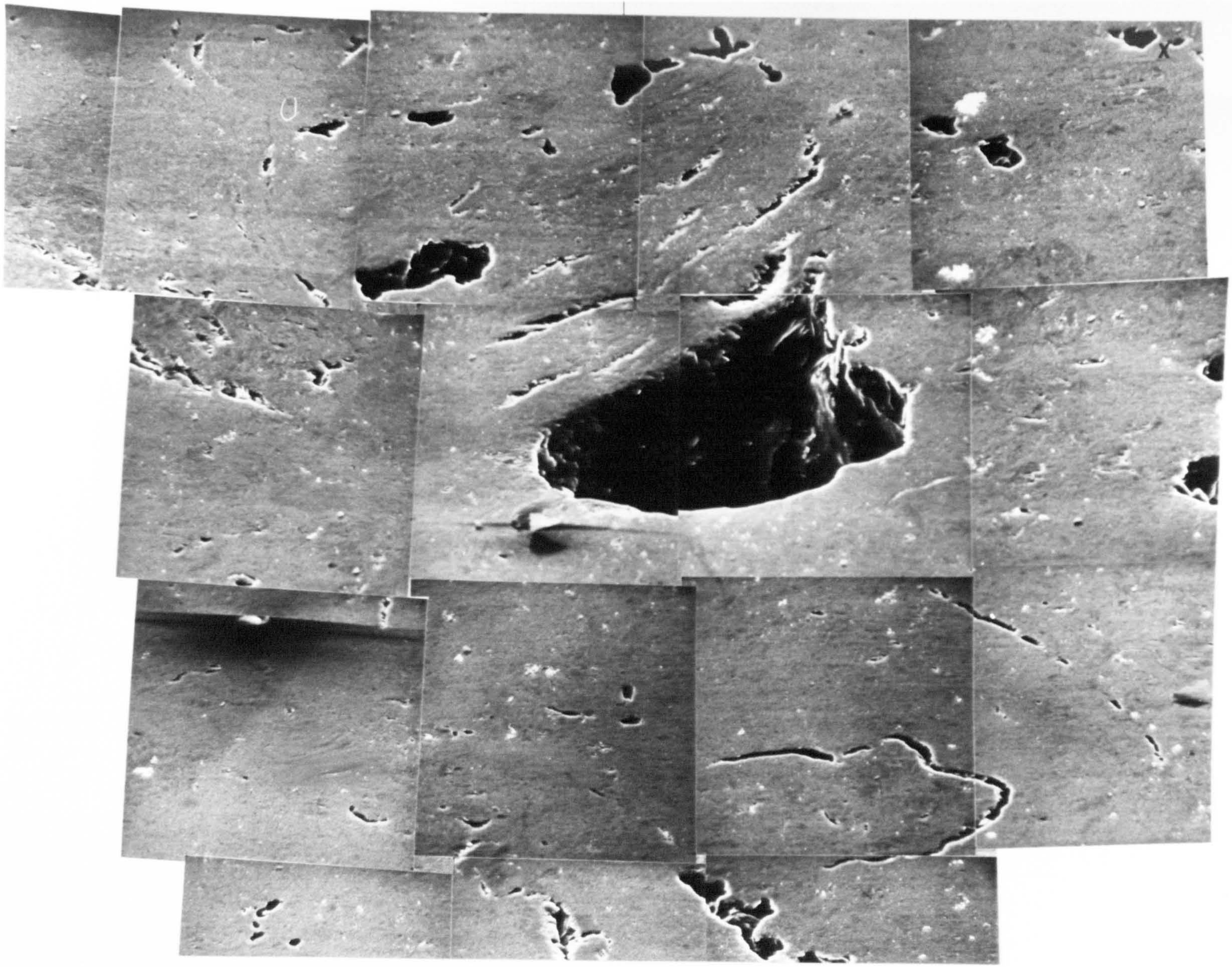


FIGURE 714.8. PHOTO-MONTAGE OF VQMB GRAPHITE AFTER THE EIGHTH POLISH.

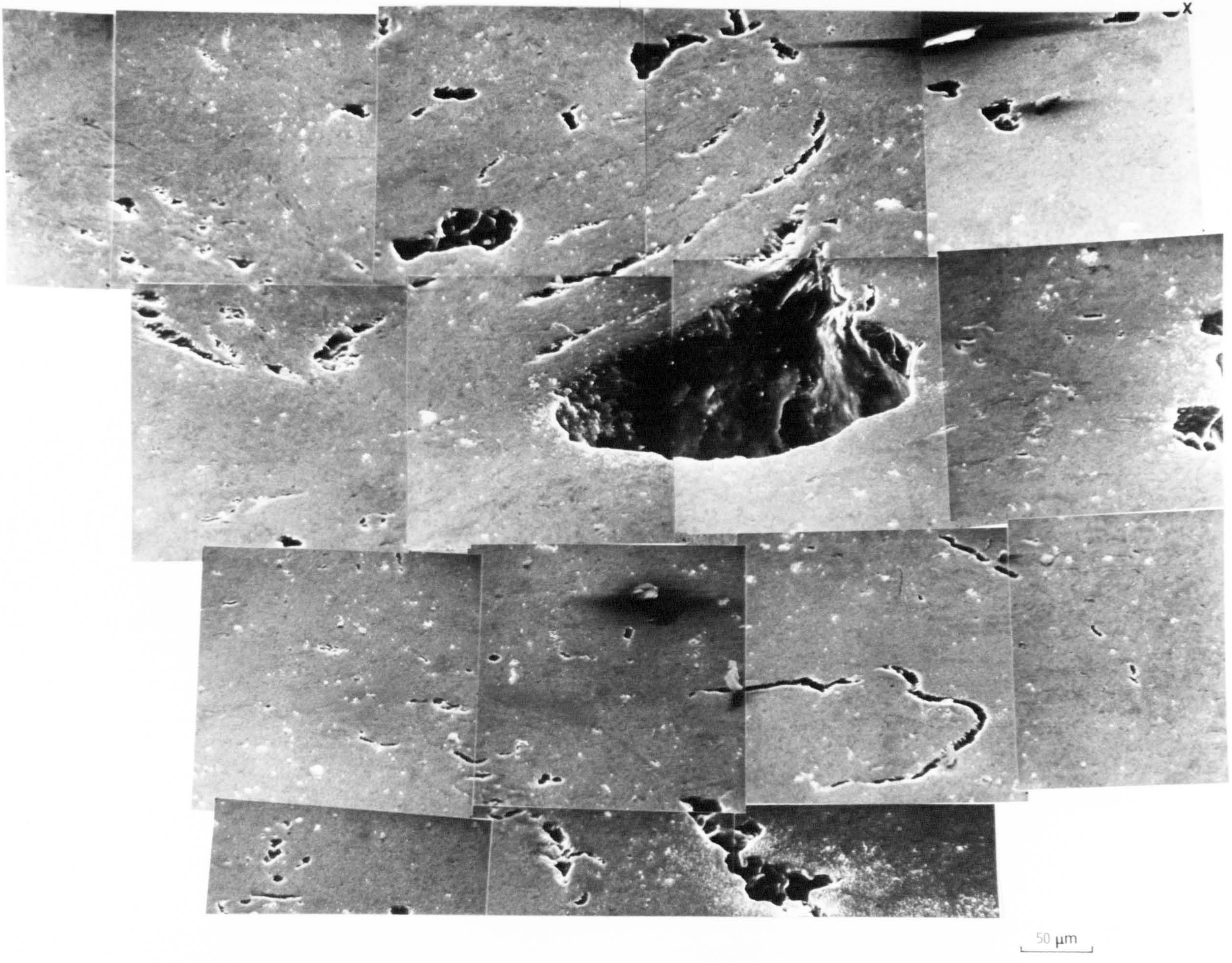


FIGURE 714.9. PHOTO-MONTAGE OF VQMB GRAPHITE AFTER THE NINTH POLISH.

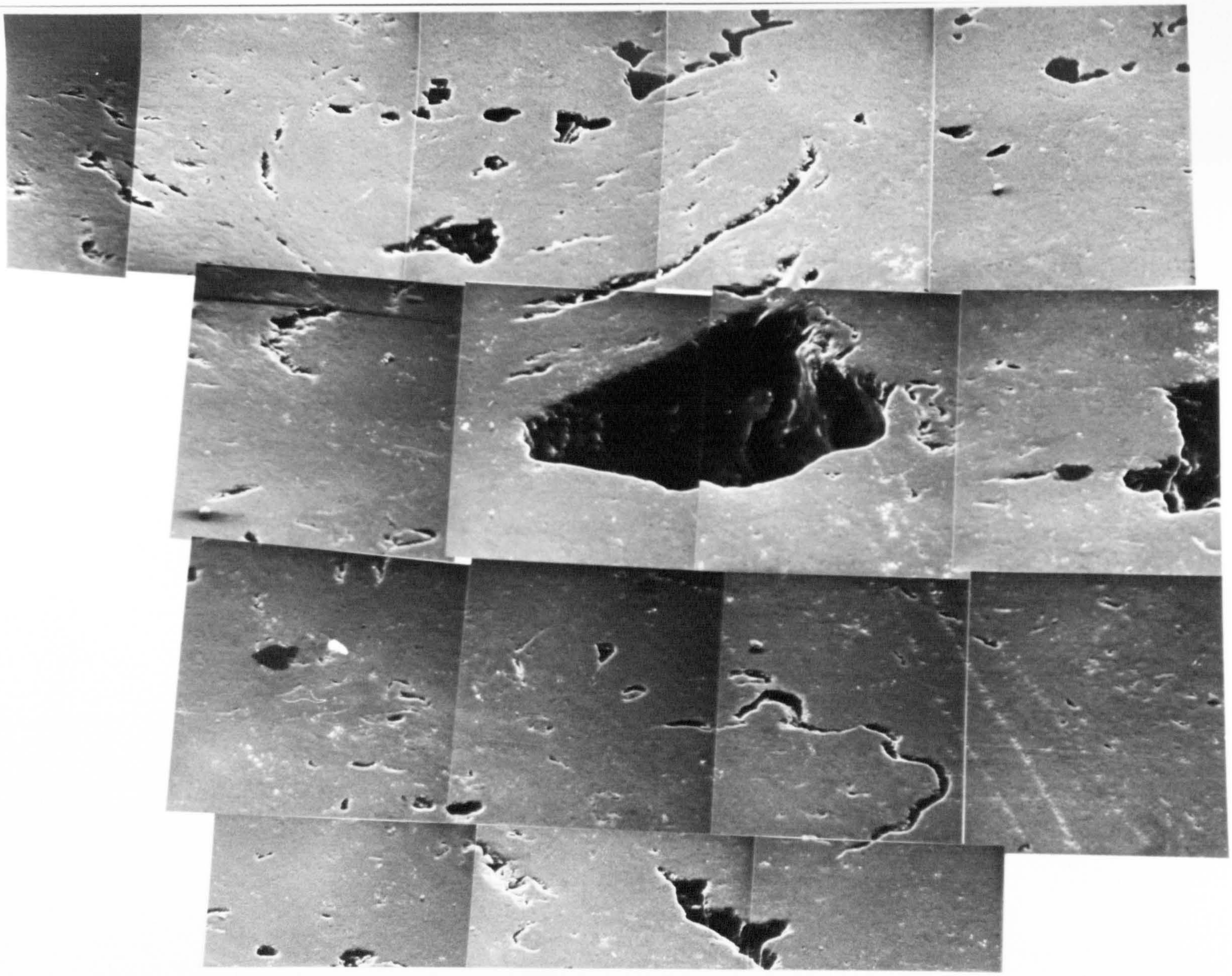


FIGURE 714.10. PHOTO-MONTAGE OF VQMB GRAPHITE AFTER THE TENTH POLISH.

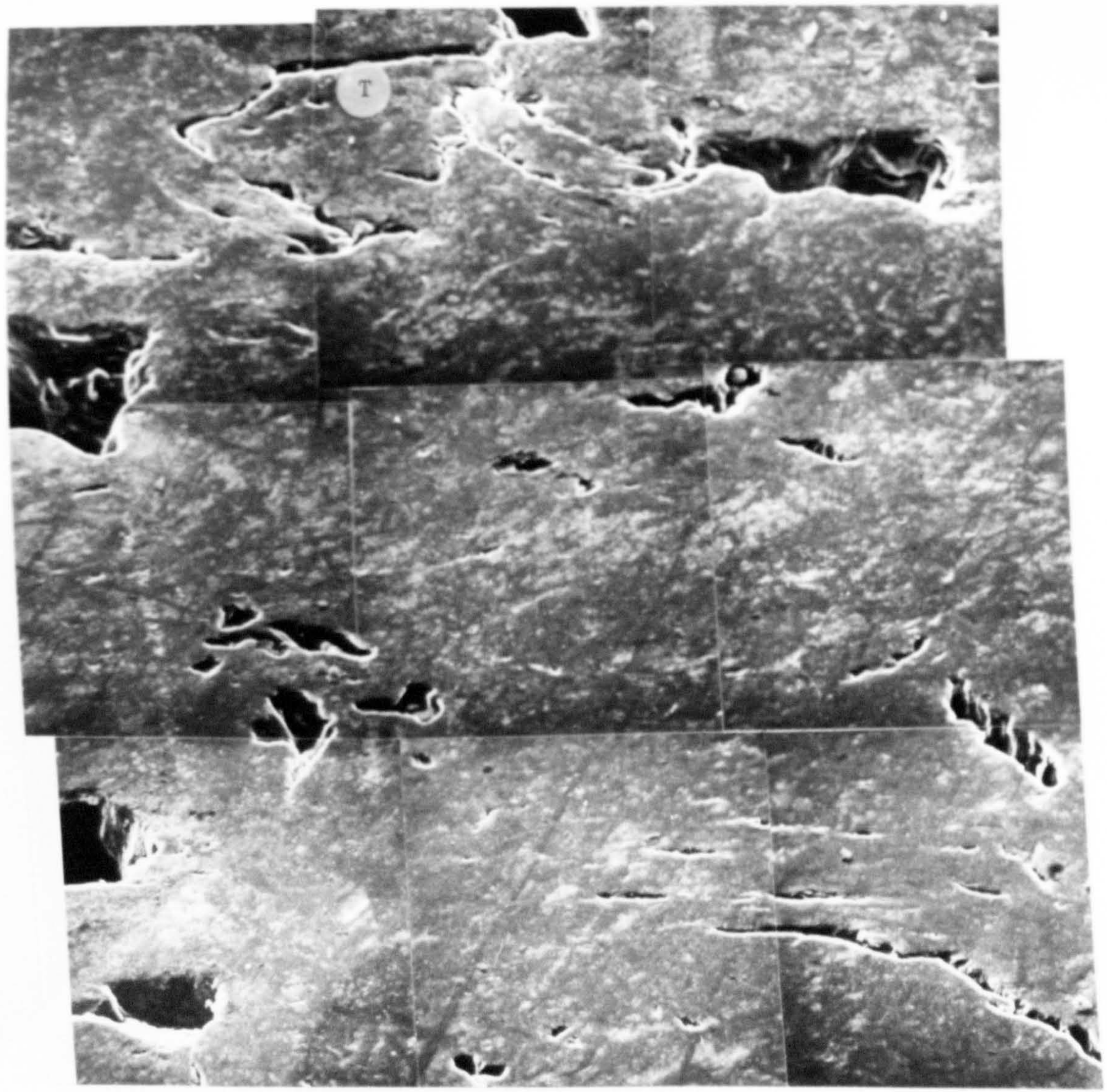


FIGURE 715.1. PHOTO-MONTAGE OF VQMB GRAPHITE AFTER THE FIRST POLISH.

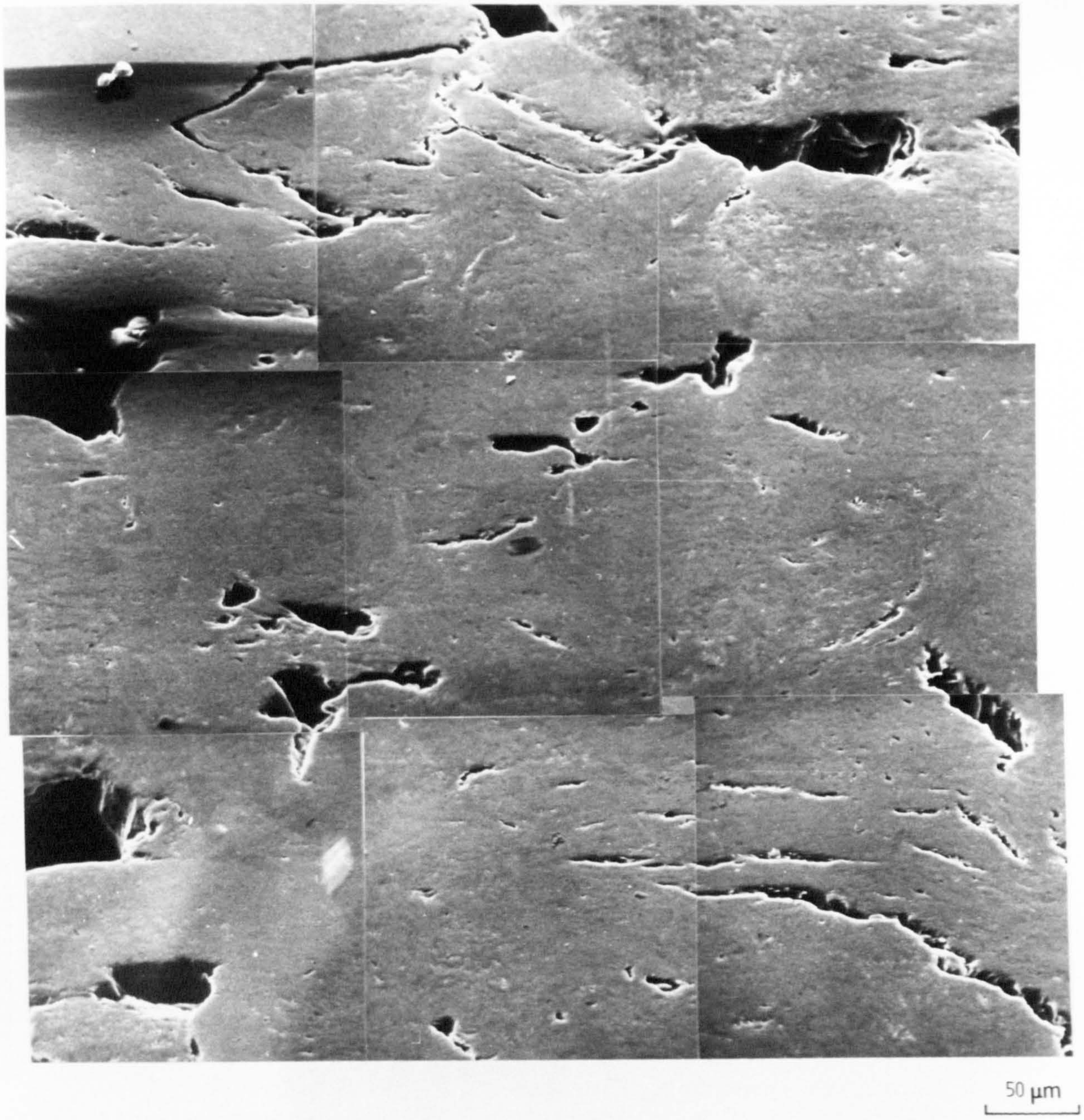


FIGURE 715.2. PHOTO-MONTAGE OF VQMB GRAPHITE AFTER THE SECOND POLISH.

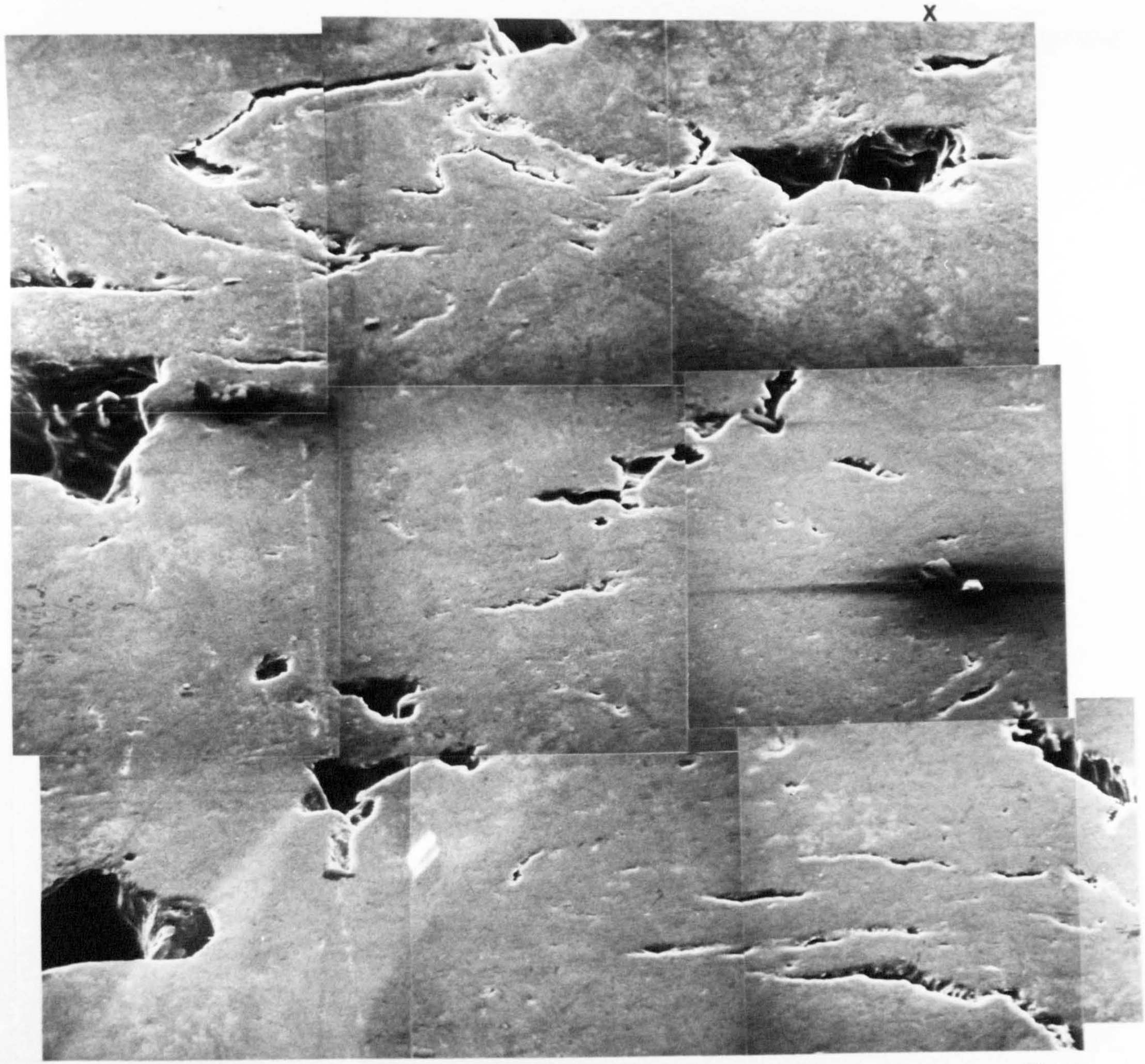


FIGURE 715.3. PHOTO-MONTAGE OF VQMB GRAPHITE AFTER THE THIRD POLISH.

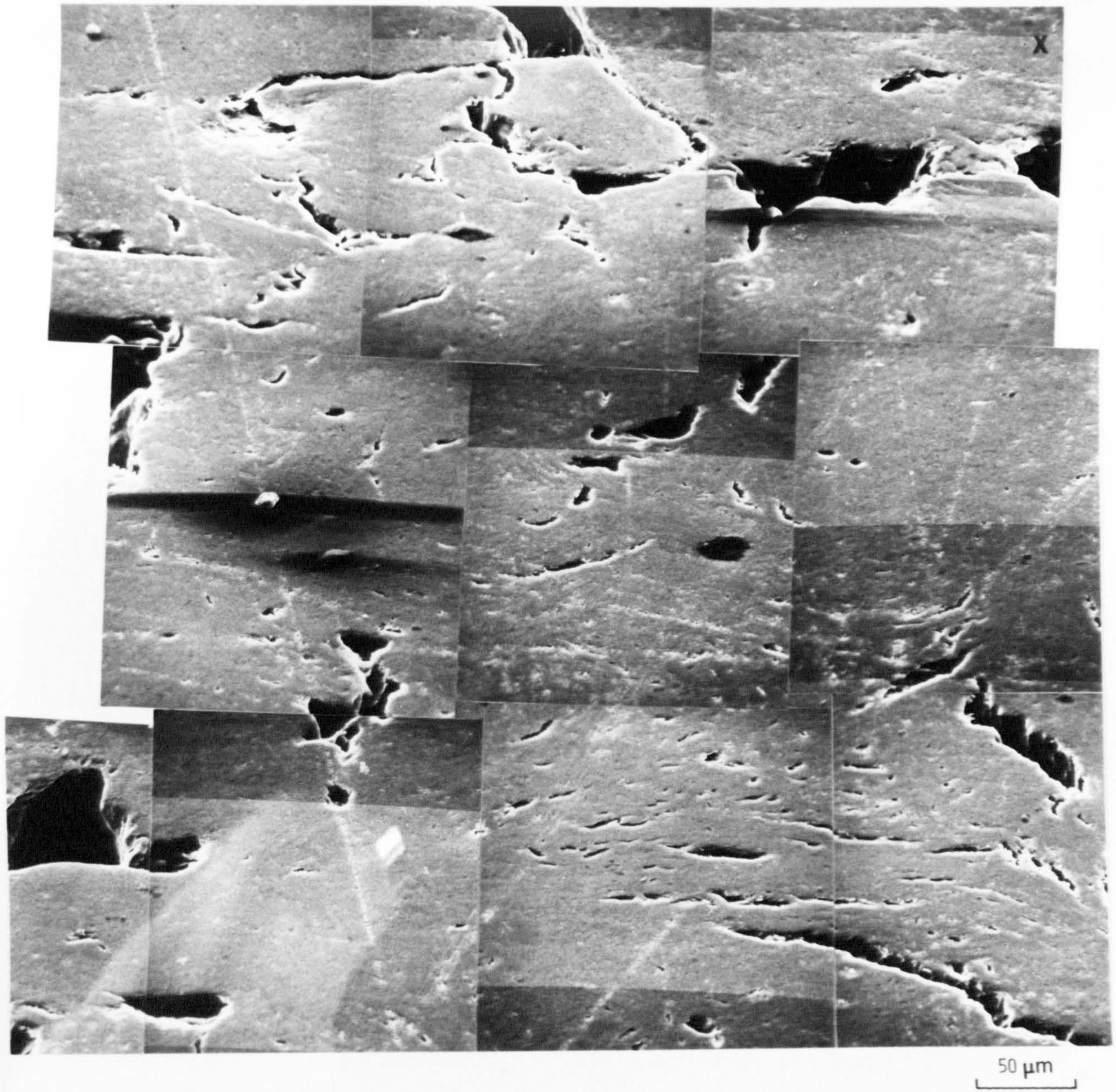


FIGURE 715.4. PHOTO-MONTAGE OF VQMB GRAPHITE AFTER THE FOURTH POLISH.

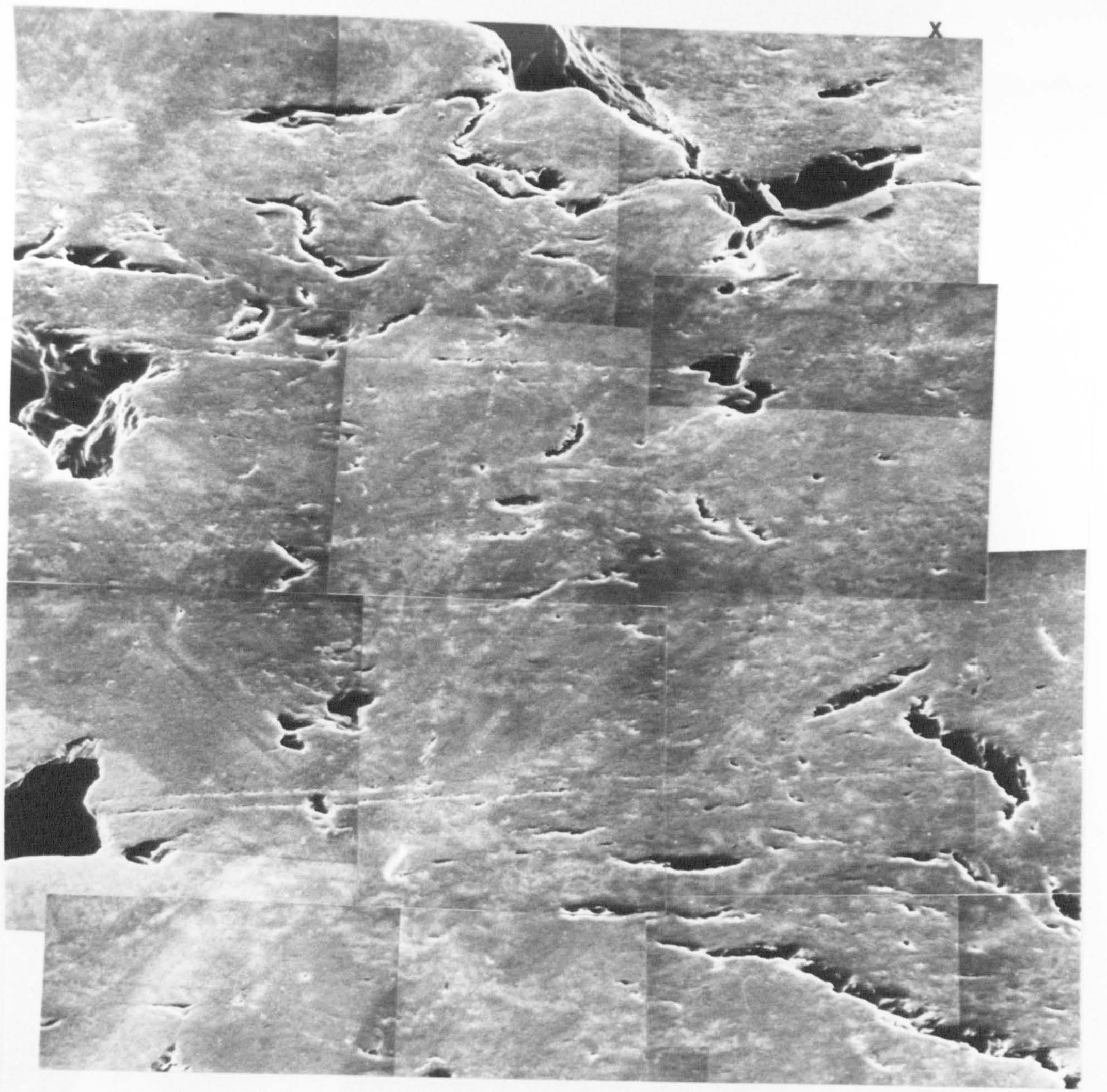


FIGURE 715.5. PHOTO-MONTAGE OF VQMB GRAPHITE AFTER THE FIFTH POLISH.

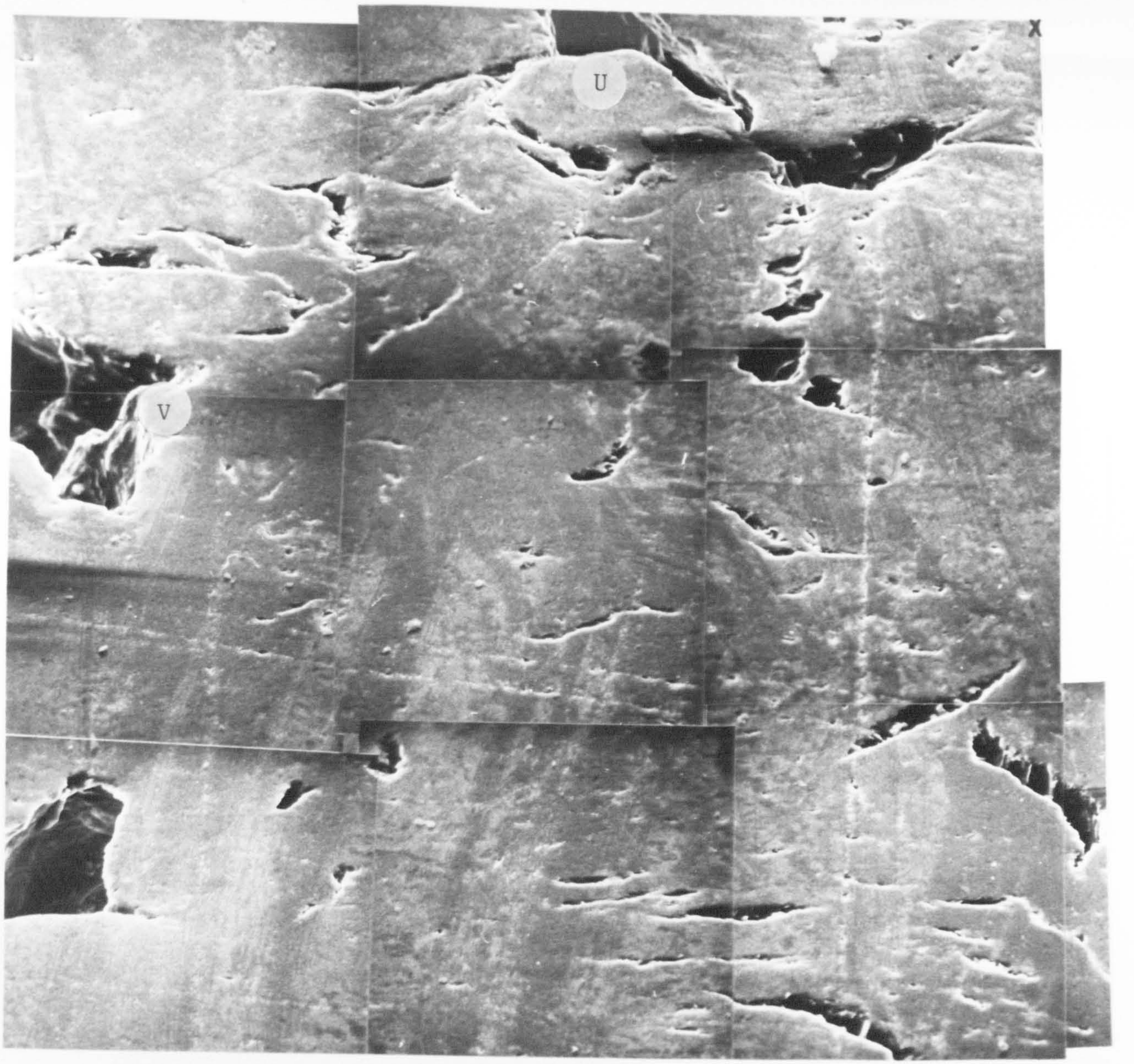


FIGURE 715.6. PHOTO-MONTAGE OF VQMB GRAPHITE AFTER THE SIXTH POLISH.

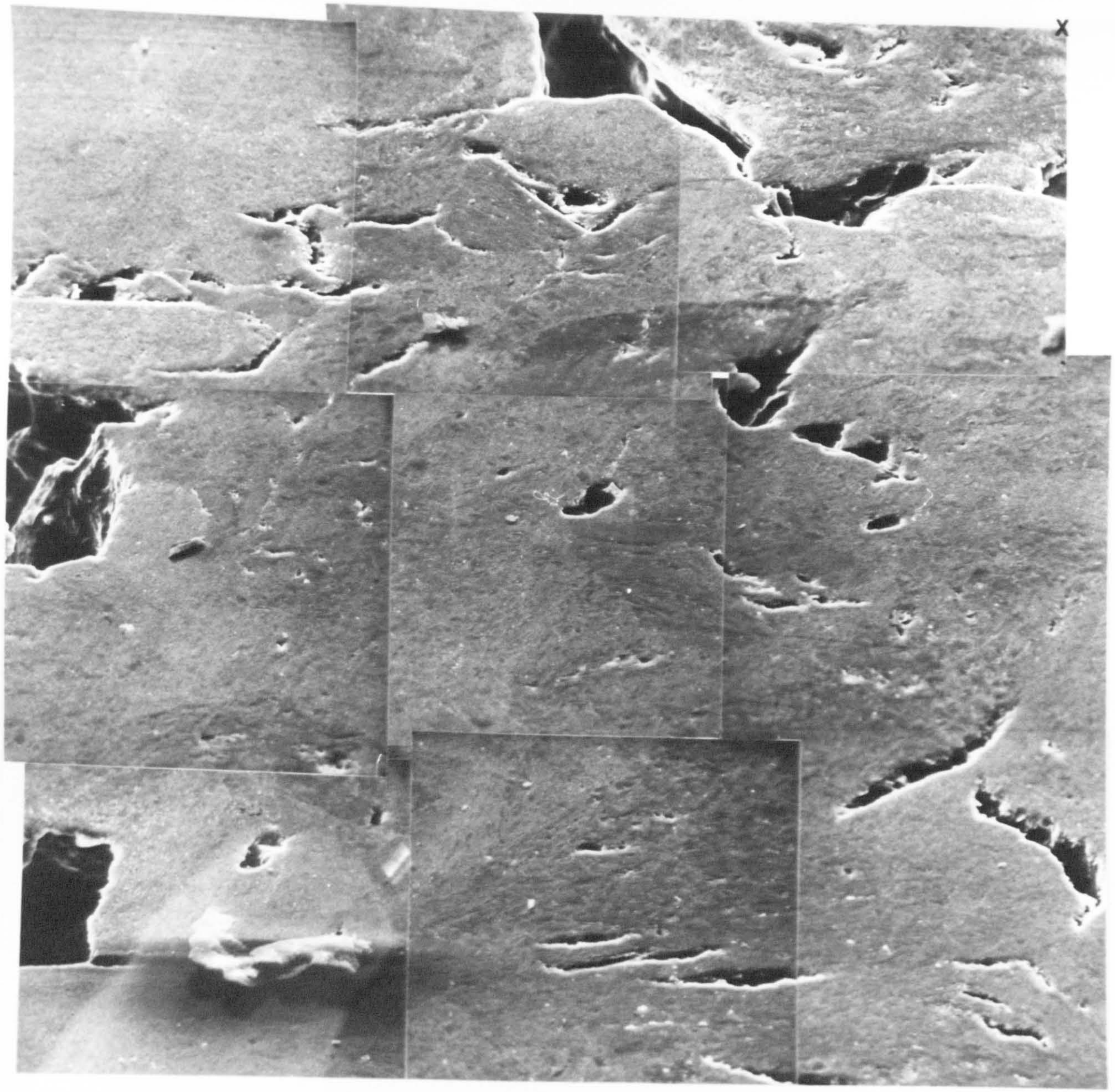


FIGURE 715.7. PHOTO-MONTAGE OF VQMB GRAPHITE AFTER THE SEVENTH POLISH.

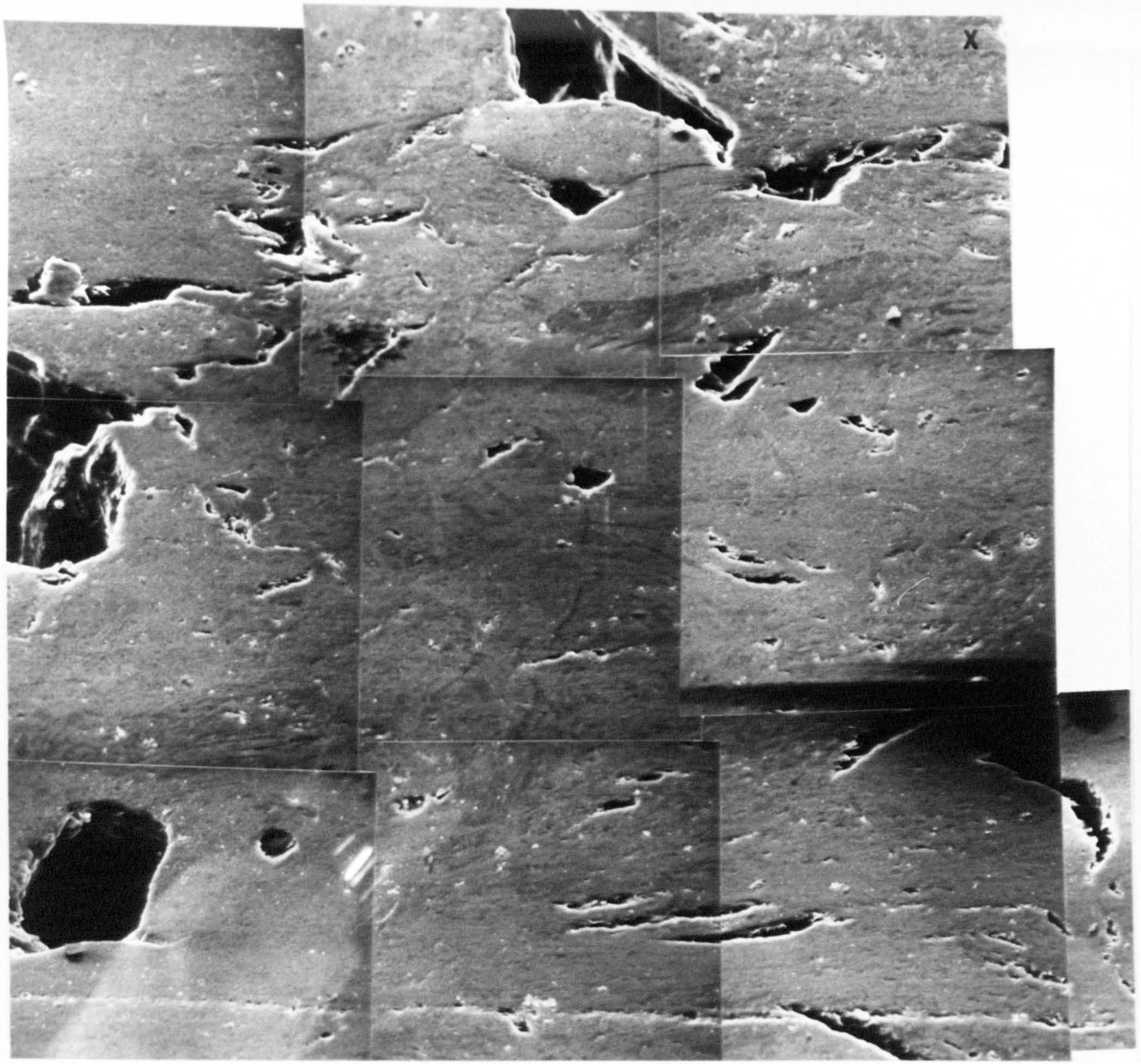


FIGURE 715.8. PHOTO-MONTAGE OF VQMB GRAPHITE AFTER THE EIGHTH POLISH.

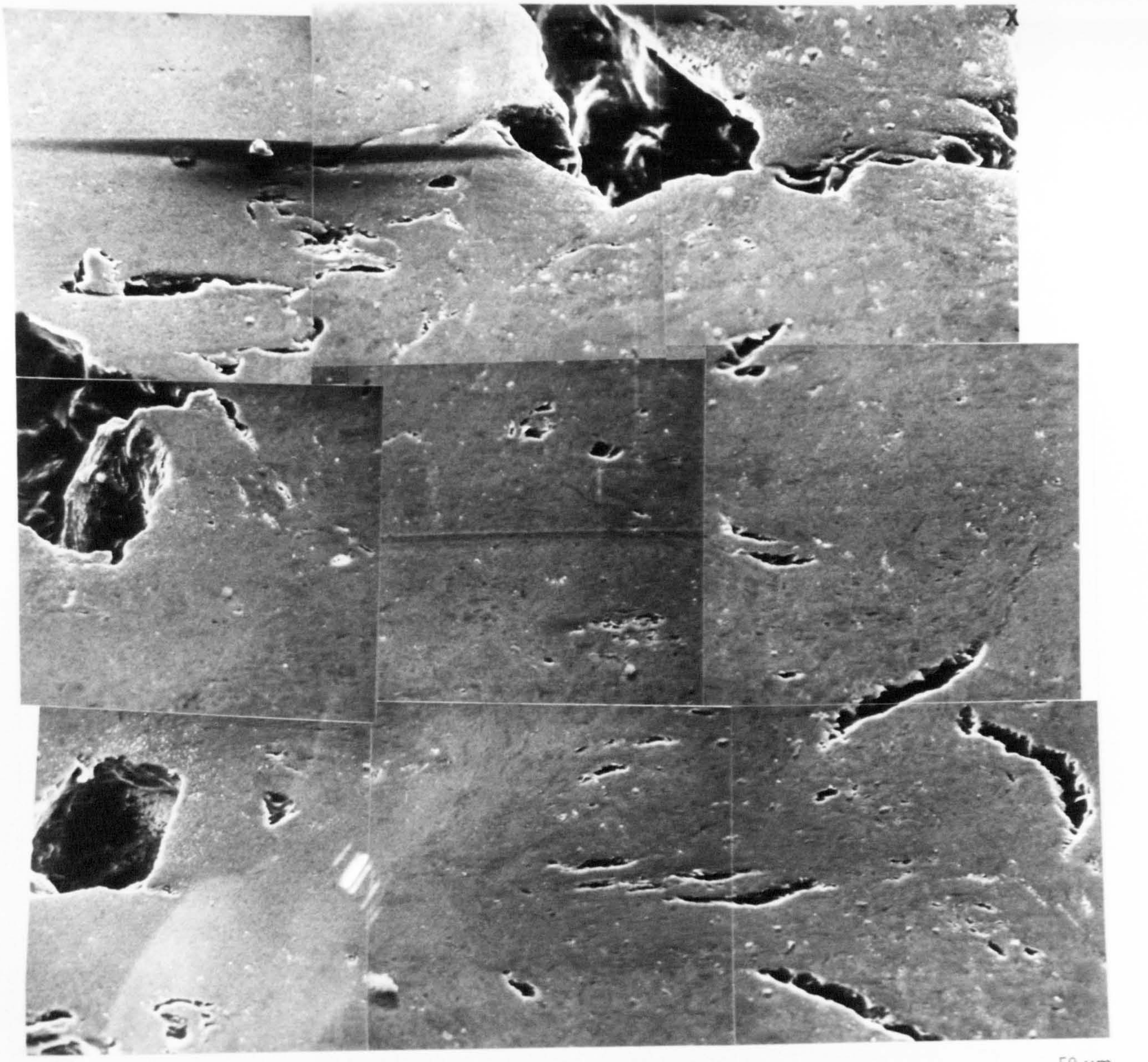


FIGURE 715.9. PHOTO-MONTAGE OF VQMB GRAPHITE AFTER THE NINTH POLISH.

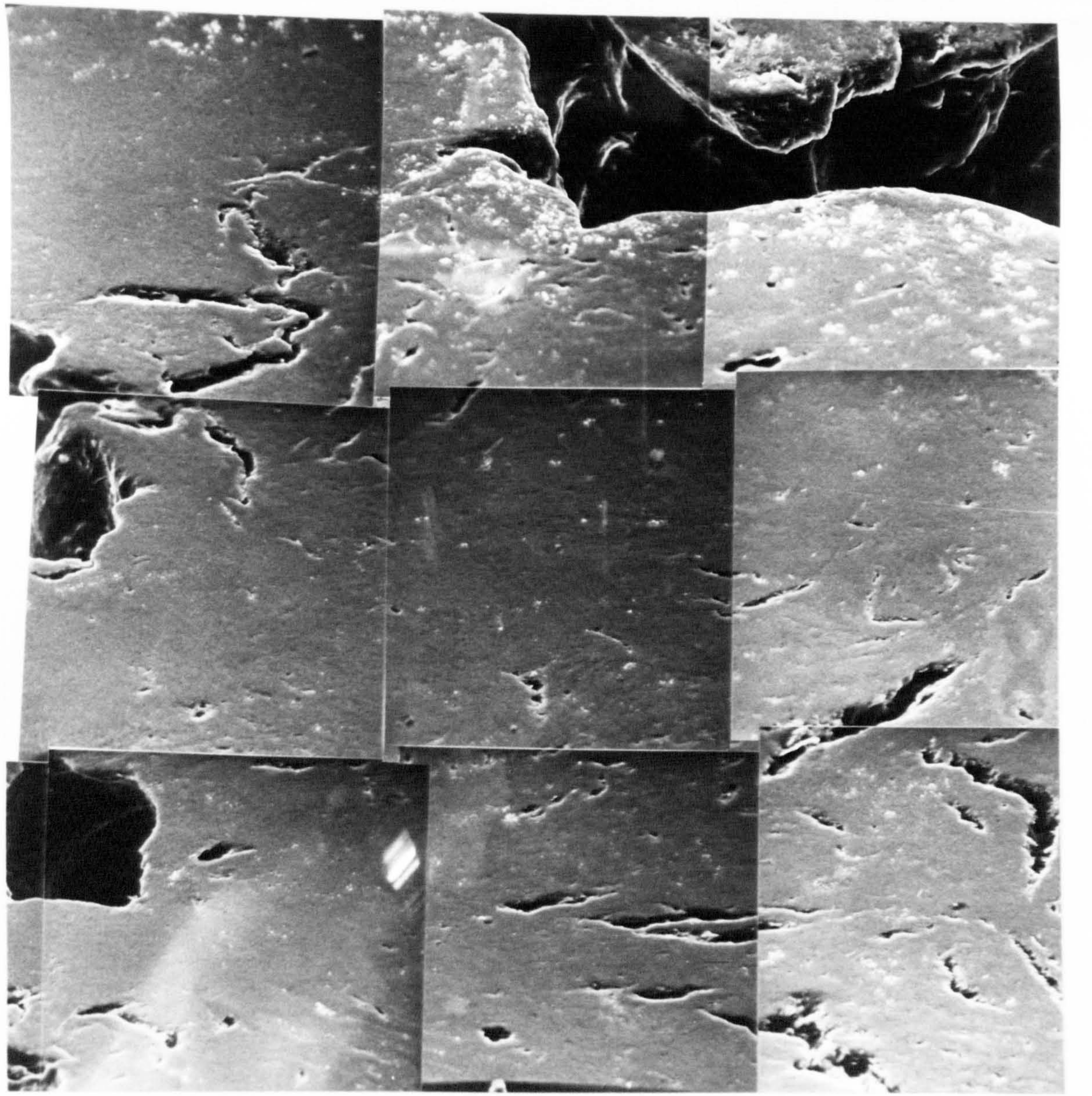


FIGURE 715.10. PHOTO-MONTAGE OF VQMB GRAPHITE AFTER THE TENTH POLISH.

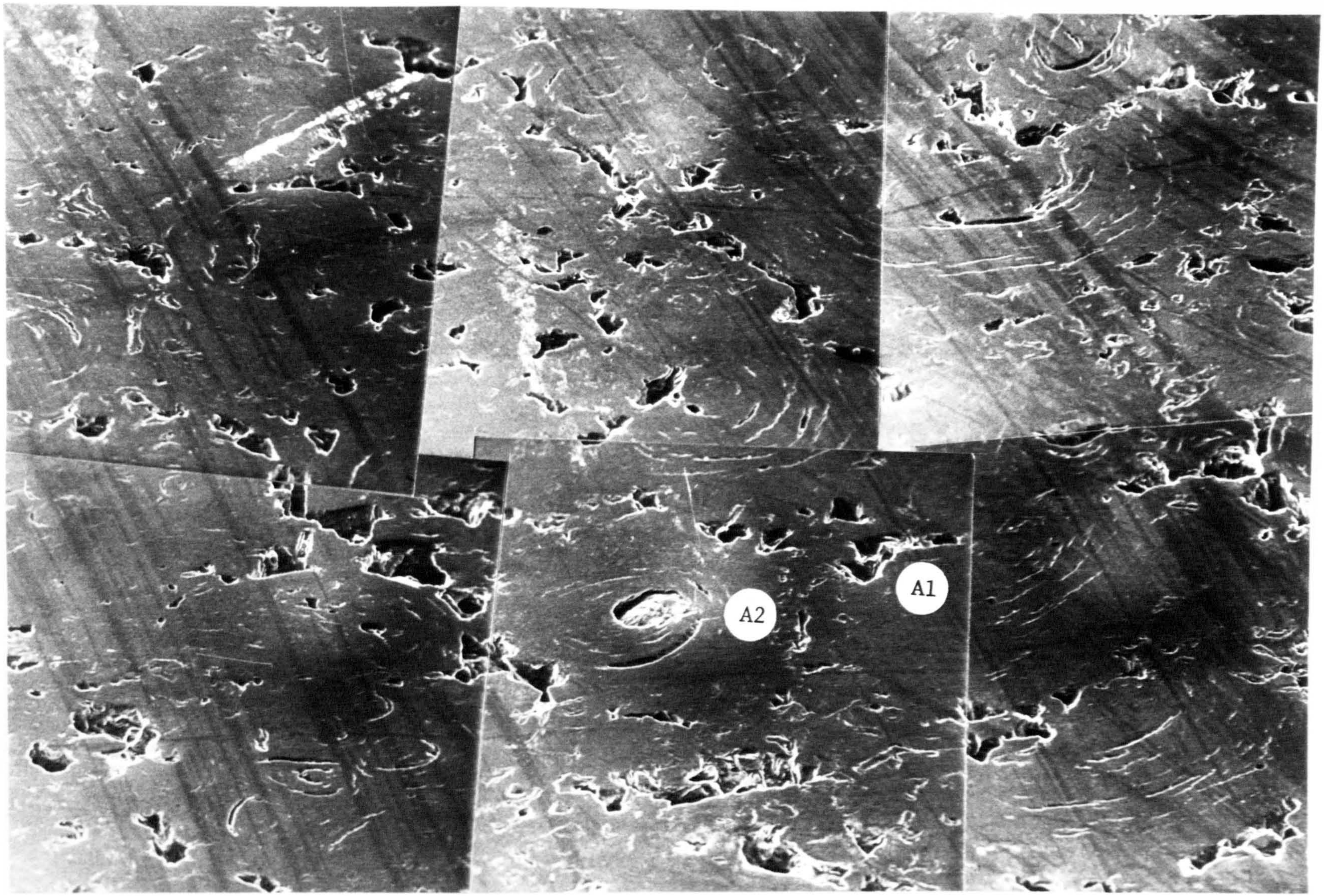


Figure 716. Photo-montage of AGLMP Graphite after the final polish

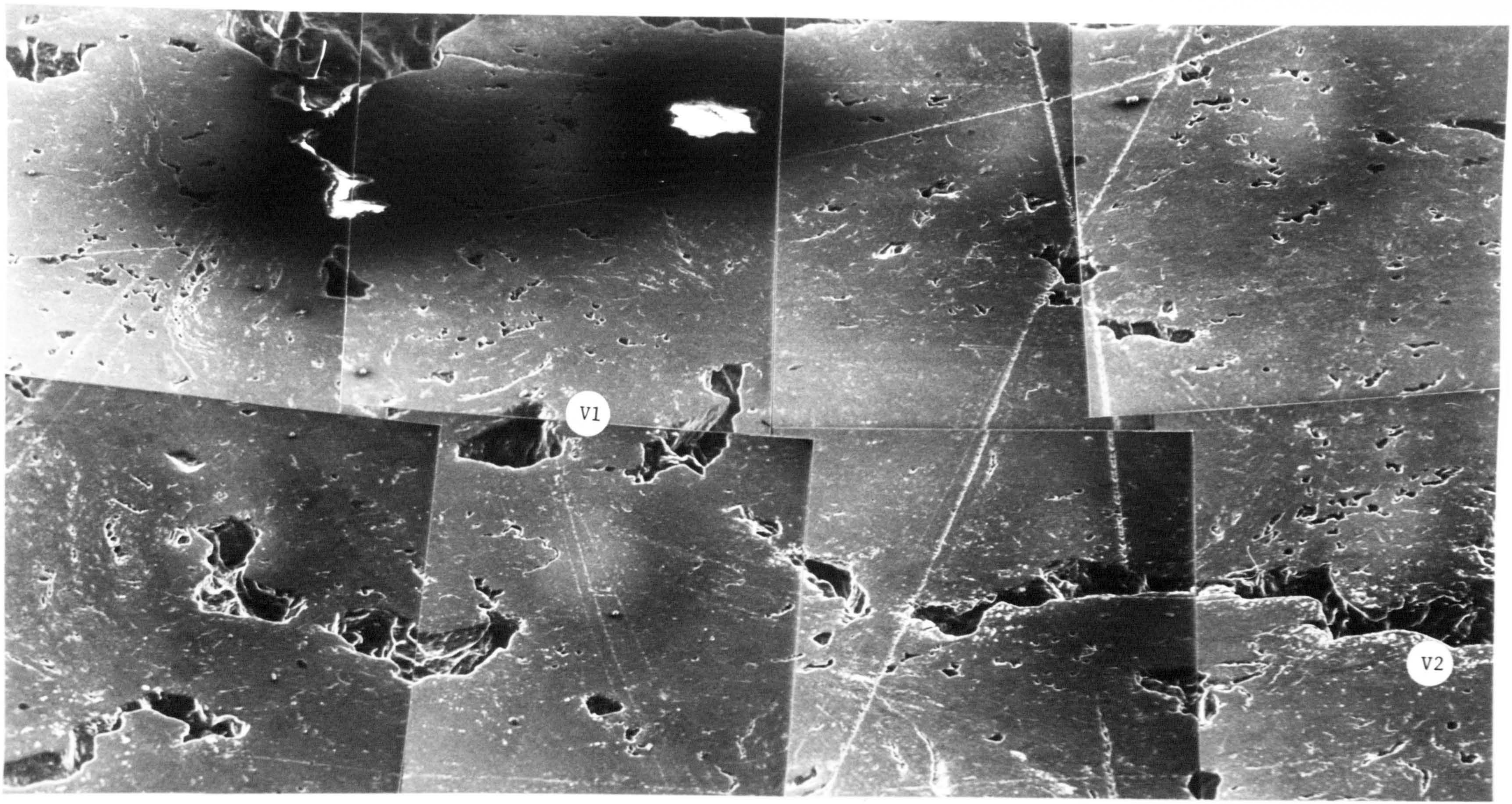


Figure 717. Photo-montage of VQMB Graphite after the final polish.

100 µm

APPENDIX I

Raw Data from the Quantimet

The raw data from the Quantimet refered to in Chapter 8, Section 8.4.2. and 8.5.2. are given in the following pages.

Size/ µm	Distribution of maximum Feret's diameters	Distribution of mean Feret's diameters
10.0	1	0
12.0	0	0
14.4	0	0
17.3	0	0
20.8	0	1
25.0	0	0
30.0	1	0
36.1	0	0
43.3	0	0
52.1	0	0
62.5	0	0
75.1	0	0
90.2	0	0
108.4	0	0
130.2	0	1
156.4	0	7
187.9	9	34
225.7	24	40
271.1	33	42
325.6	41	33
391.1	38	25
469.8	22	14
564.3	15	9
677.9	14	8
814.3	4	5
978.1	8	3
1174.9	2	4
1411.3	4	0
1695.2	1	1
2036.3	0	0
2446.0	0	0
2938.2	0	0
3529.3	0	0

Distribution of Feret's Diameters in PGA Graphite C7/1 (control for C79).

Size/ μm	Distribution of maximum Feret's diameters	Distribution of mean Feret's diameters
10.0	3	0
12.0	0	0
14.4	0	1
17.3	0	0
20.8	1	0
25.0	0	2
30.0	2	1
36.1	0	2
43.3	2	2
52.1	1	1
62.5	3	0
75.1	0	0
90.2	0	2
108.4	0	0
130.2	0	1
156.4	2	9
187.9	9	31
225.7	30	46
271.1	42	29
325.6	33	34
391.1	28	16
469.8	23	12
564.3	5	9
677.9	12	6
814.3	6	3
978.1	8	2
1174.9	3	1
1411.3	1	2
1695.2	1	0
2032.3	0	0
2446.0	0	0
2938.2	0	0
3529.3	0	0

Distribution of Feret's Diameters in PGA Graphite C79
Radiolytically Oxidised to 6.2% Weight Loss.

Size/ μm	Distribution of maximum Ferert's diameters	Distribution of mean Feret's diameters
10.0	2	0
12.0	0	0
14.4	0	1
17.3	0	0
20.8	1	0
25.0	0	0
30.0	0	0
36.1	0	0
43.3	0	0
52.1	0	0
62.5	0	0
75.1	0	0
90.2	0	0
108.4	0	1
130.2	0	3
156.4	5	30
187.9	40	53
225.7	38	55
271.1	54	36
325.6	30	17
391.1	22	9
469.8	14	6
564.3	8	4
677.9	3	1
814.3	1	0
978.1	0	0
1174.9	0	0
1411.3	0	0
1695.2	0	0
2036.3	0	0
2446.0	0	0
2938.2	0	0
3529.3	0	0

Distribution of Feret's Diameters in AGLMP Graphite 10F49 (control for M38).

Size/ μm	Distribution of maximum Feret's diameters	Distribution of mean Feret's diameters
10.0	1	0
12.0	0	0
14.4	0	0
17.3	0	0
20.8	0	0
25.0	0	0
30.0	0	0
36.1	0	0
43.3	0	0
52.1	0	0
62.5	0	0
75.1	0	0
90.2	0	0
108.4	0	0
13o.2	0	0
156.4	4	17
187.9	16	36
225.7	33	54
271.1	47	28
325.6	27	25
391.1	27	14
469.8	14	6
564.3	9	3
677.9	6	0
814.3	0	1
978.1	0	0
1174.9	1	0
1411.3	0	0
1695.2	0	0
2036.3	0	0
2446.0	0	0
2938.2	0	0
3529.3	0	0

Distribution of Feret's Diameters in AGLMP Graphite M38
Radiolytically Oxidised to 3.7% Weight Loss.

Size/ μm	Distribution of maximum Feret's diameters	Distribution of mean Feret's diameters
10.0	0	0
12.0	0	0
14.4	0	1
17.3	0	0
20.8	1	0
25.0	0	0
30.0	0	0
36.1	0	0
43.3	0	0
52.1	0	0
62.5	0	0
75.1	0	0
90.2	0	0
108.4	0	0
130.2	0	0
156.4	5	17
187.9	10	22
225.7	22	21
271.1	25	14
325.6	13	18
391.1	17	13
469.8	8	7
564.3	11	4
677.9	4	4
814.3	3	0
978.1	1	1
1174.9	2	0
1411.3	0	0
1695.2	0	0
2036.3	0	0
2446.0	0	0
2938.2	0	0
3529.3	0	0

Distribution of Feret's Diameters in AGLMP Graphite 584/195 (control for M28).

Size/ μm	Distribution of maximum Feret's diameters	Distribution of mean Feret's diameters
10.0	0	0
12.0	0	1
14.4	1	0
17.3	0	0
20.8	0	0
25.0	0	0
30.0	0	0
36.1	0	0
43.3	0	0
52.1	0	0
62.5	0	0
75.1	0	0
90.2	0	0
108.4	0	0
130.2	0	0
156.4	5	20
187.9	21	45
225.7	30	34
271.1	35	24
325.6	25	18
391.1	18	20
469.8	21	8
564.3	11	4
677.9	6	2
814.3	2	1
978.1	2	0
1174.9	0	1
1411.3	1	0
1695.2	0	0
2036.3	0	0
2446.0	0	0
2938.2	0	0
3529.3	0	0

Distribution of Feret's Diameters in AGLMP Graphite M28
Radiolytically Oxidised to 3.5% Weight Loss.

Size/ μm	Distribution of maximum Feret's diameters	Distribution of mean Feret's diameters
10.0	0	0
12.0	0	0
14.4	0	0
17.3	0	0
20.8	0	0
25.0	0	0
30.0	0	0
36.1	0	0
43.3	0	0
52.1	0	0
62.5	0	0
75.1	0	0
90.2	0	0
108.4	0	0
130.2	0	0
156.4	3	7
187.9	8	15
225.7	9	18
271.1	14	11
325.6	17	11
391.1	13	11
469.8	6	1
564.3	4	2
677.9	1	0
814.3	1	0
978.1	0	0
1174.9	0	0
1411.3	0	0
1695.2	0	0
2036.3	0	0
2446.0	0	0
2938.2	0	0
3529.3	0	0

Distribution of Feret's Diameters in BAEL Pitch-Coke Graphite Q6/1 (control for H30).

Size/ μm	Distribution of maximum Feret's diameters	Distribution of mean Feret's diameters
10.0	0	0
12.0	0	0
14.4	0	0
17.3	0	0
20.8	0	0
25.0	0	0
30.0	0	0
36.1	0	0
43.3	0	0
52.1	0	0
62.5	0	0
75.1	0	0
90.2	0	0
108.4	0	0
130.2	0	0
156.4	1	9
187.9	6	12
225.7	11	14
271.1	15	13
325.6	16	14
391.1	10	7
469.8	9	3
564.3	3	2
677.9	3	1
814.3	0	0
978.1	1	0
1174.9	0	0
1411.3	0	0
1695.2	0	0
2036.3	0	0
2446.0	0	0
2938.2	0	0
3529.3	0	0

Distribution of Feret's Diameters in BAEL Pitch-Coke Graphite H30 Radiolytically Oxidised to 0.6% Weight Loss.

Size/ μm	Distribution of maximum Feret's diameters	Distribution of mean Feret's diameters
10.0	4	2
12.0	0	0
14.4	1	2
17.3	0	0
20.8	2	2
25.0	0	5
30.0	5	1
36.1	0	0
43.3	2	1
52.1	2	1
62.5	1	1
75.1	1	0
90.2	0	1
108.4	0	0
130.2	0	0
156.4	12	96
187.9	103	246
225.7	210	224
271.1	209	153
325.6	167	95
391.1	107	54
469.8	49	34
564.3	45	19
677.9	17	12
814.3	14	6
978.1	7	2
1174.9	2	0
1411.3	0	0
1695.2	0	0
2036.3	0	0
2446.0	0	0

Distribution of Feret's Diameters in Virgin AGLMP Graphite.

Size/ μm	Distribution of maximum Feret's diameters	Distribution of mean Feret's diameters
10.0	4	0
12.0	0	0
14.4	0	0
17.3	0	0
20.8	0	1
25.0	0	1
30.0	1	0
36.1	0	0
43.3	1	0
52.1	0	0
62.5	0	0
75.1	0	0
90.2	0	0
108.4	0	0
130.2	0	0
156.4	4	44
187.9	50	105
225.7	87	106
271.1	100	76
325.6	87	58
391.1	61	34
469.8	27	25
564.3	27	9
677.9	13	8
814.3	7	4
978.1	4	2
1174.9	2	0
1411.3	2	0
1695.2	0	0
2036.3	0	0
2446.0	0	0
2938.2	0	0
3529.3	0	0

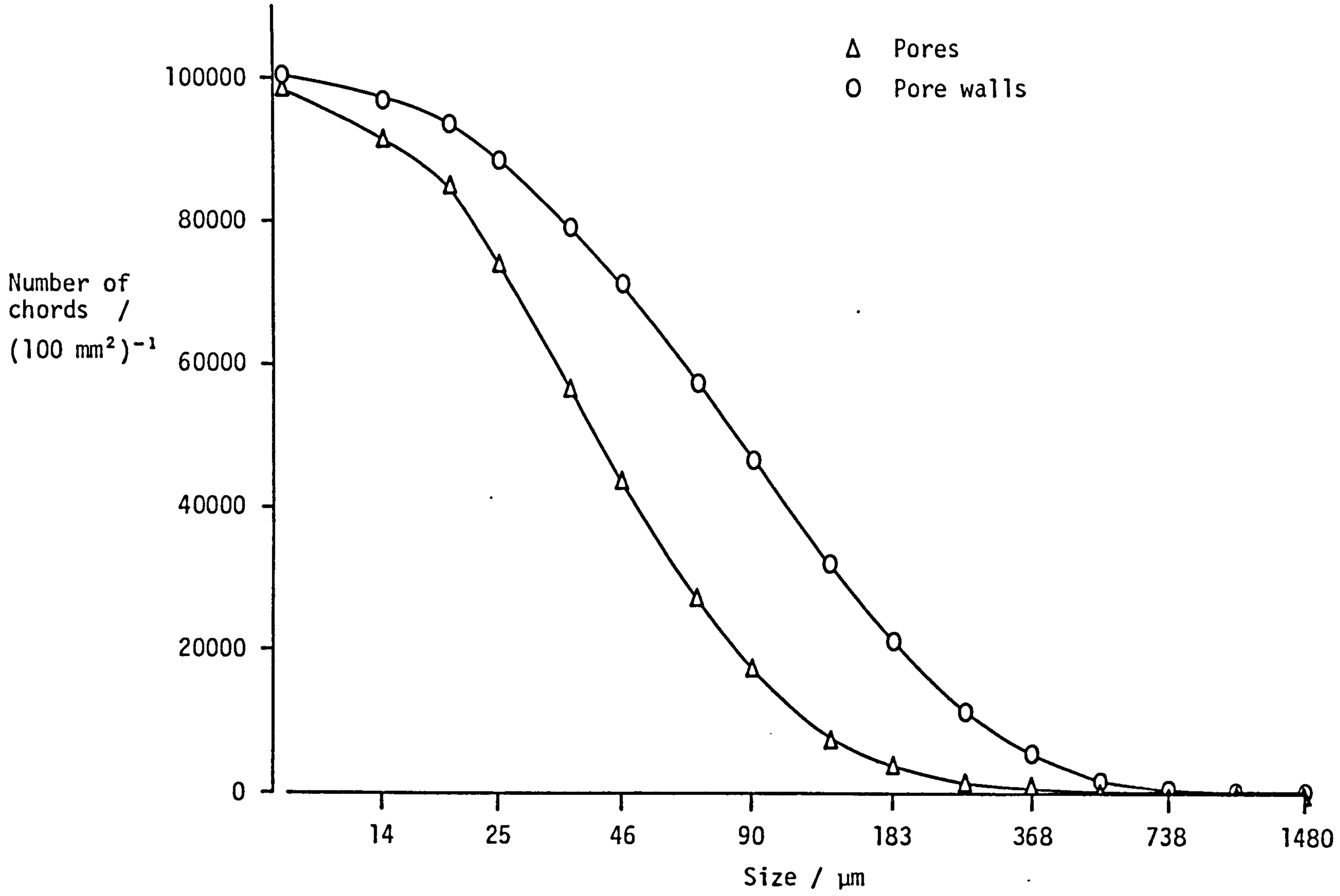
Distribution of Feret's Diameters in AGLMP Graphite Thermally Oxidised to 3.1% Weight Loss.

Size/ μm	Distribution of maximum Feret's diameters	Distribution of mean Feret's diameters
10.0	6	2
12.0	0	1
14.4	0	1
17.3	0	2
20.8	4	3
25.0	0	0
30.0	2	1
36.1	0	2
43.3	3	0
52.1	0	0
62.5	0	0
75.1	0	0
90.2	0	0
108.4	1	0
130.2	0	2
156.4	13	68
187.9	89	178
225.7	149	171
271.1	161	109
325.6	106	81
391.1	86	60
469.8	54	29
564.3	37	21
677.9	21	9
814.3	12	6
978.1	5	1
1174.9	2	1
1411.3	1	1
1695.2	0	0
2036.3	1	0
2446.0	0	0
2938.2	0	0
3529.3	0	0

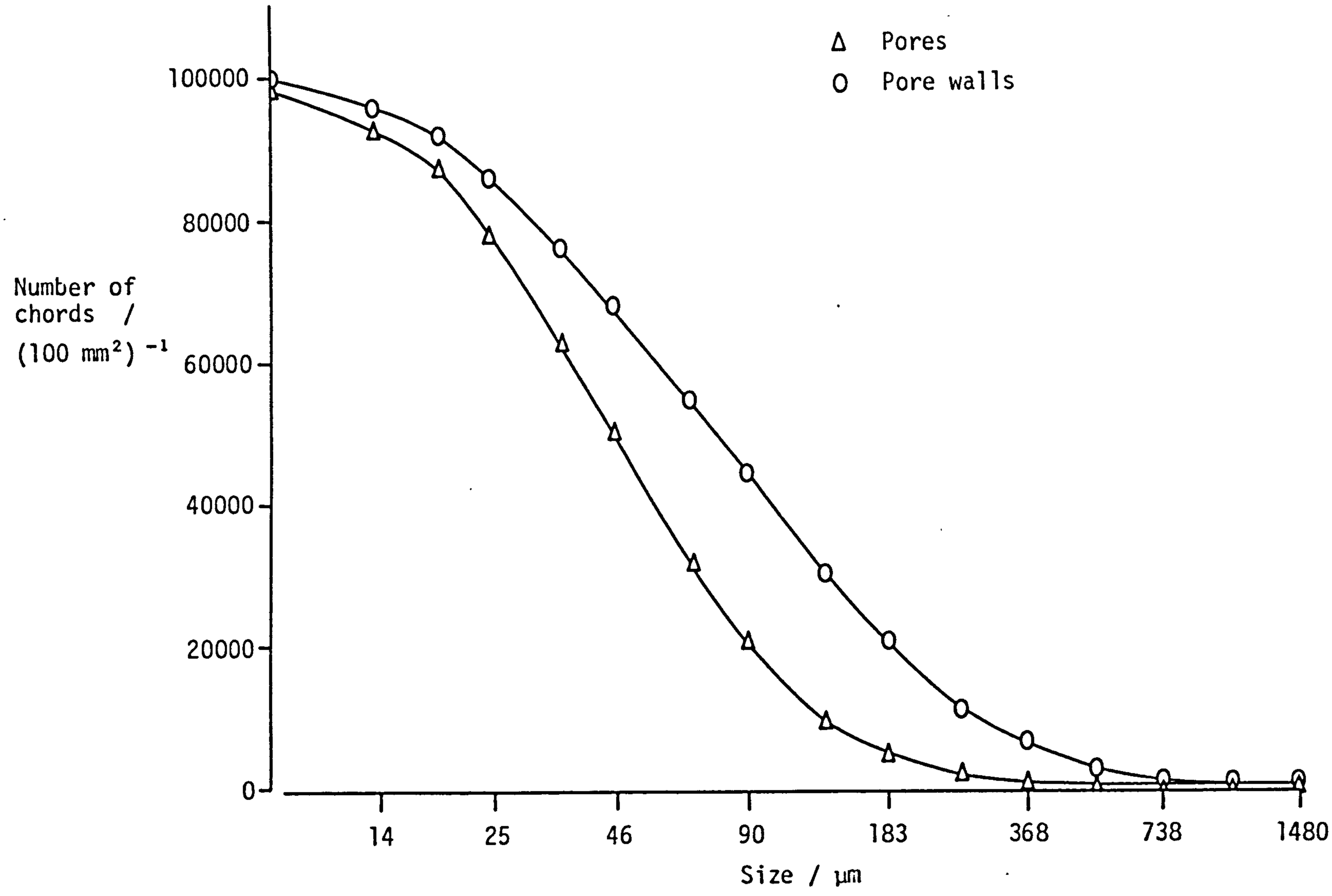
Distribution of Feret's Diameters in AGLMP Graphite Thermally Oxidised to 5.4% Weight Loss.

Size/ μm	Distribution of maximum Feret's diameters	Distribution of mean Feret's diameters
10.0	9	2
12.0	0	0
14.4	0	2
17.3	0	0
20.8	2	0
25.0	0	1
30.0	1	0
36.1	0	1
43.3	0	1
52.1	2	0
62.5	0	0
75.1	0	0
90.2	0	1
108.4	1	0
130.2	0	1
156.4	9	54
187.9	65	187
225.7	165	135
271.1	137	131
325.6	105	65
391.1	84	48
469.8	50	43
564.3	42	22
677.9	28	13
814.3	15	9
978.1	9	2
1174.9	1	2
1411.3	1	0
1695.2	1	0
2036.3	0	0
2446.0	0	0
2938.2	0	0
3529.3	0	0

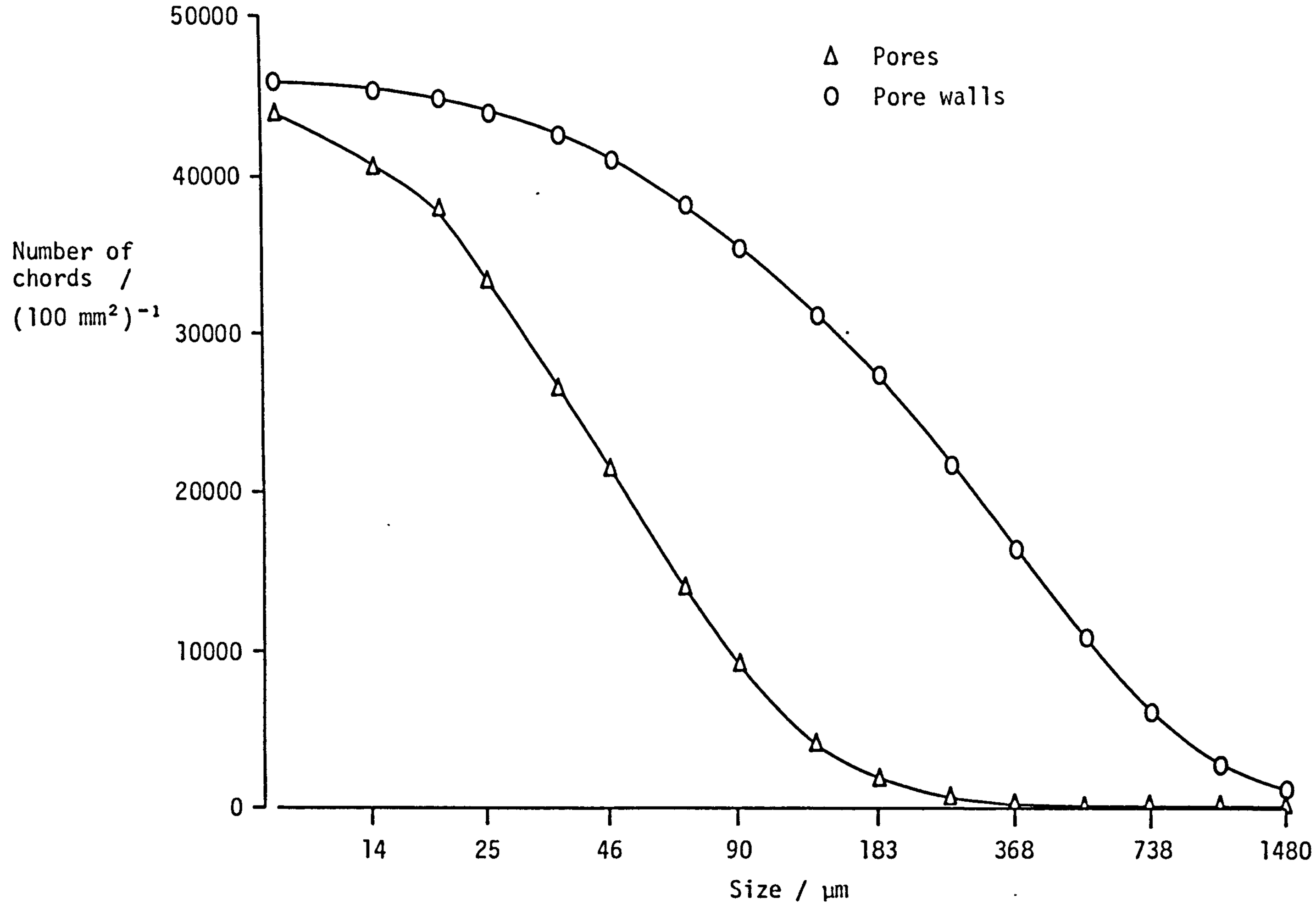
Distribution of Feret's Diameters in AGLMP Graphite Thermally Oxidised to 10.5% Weight Loss.



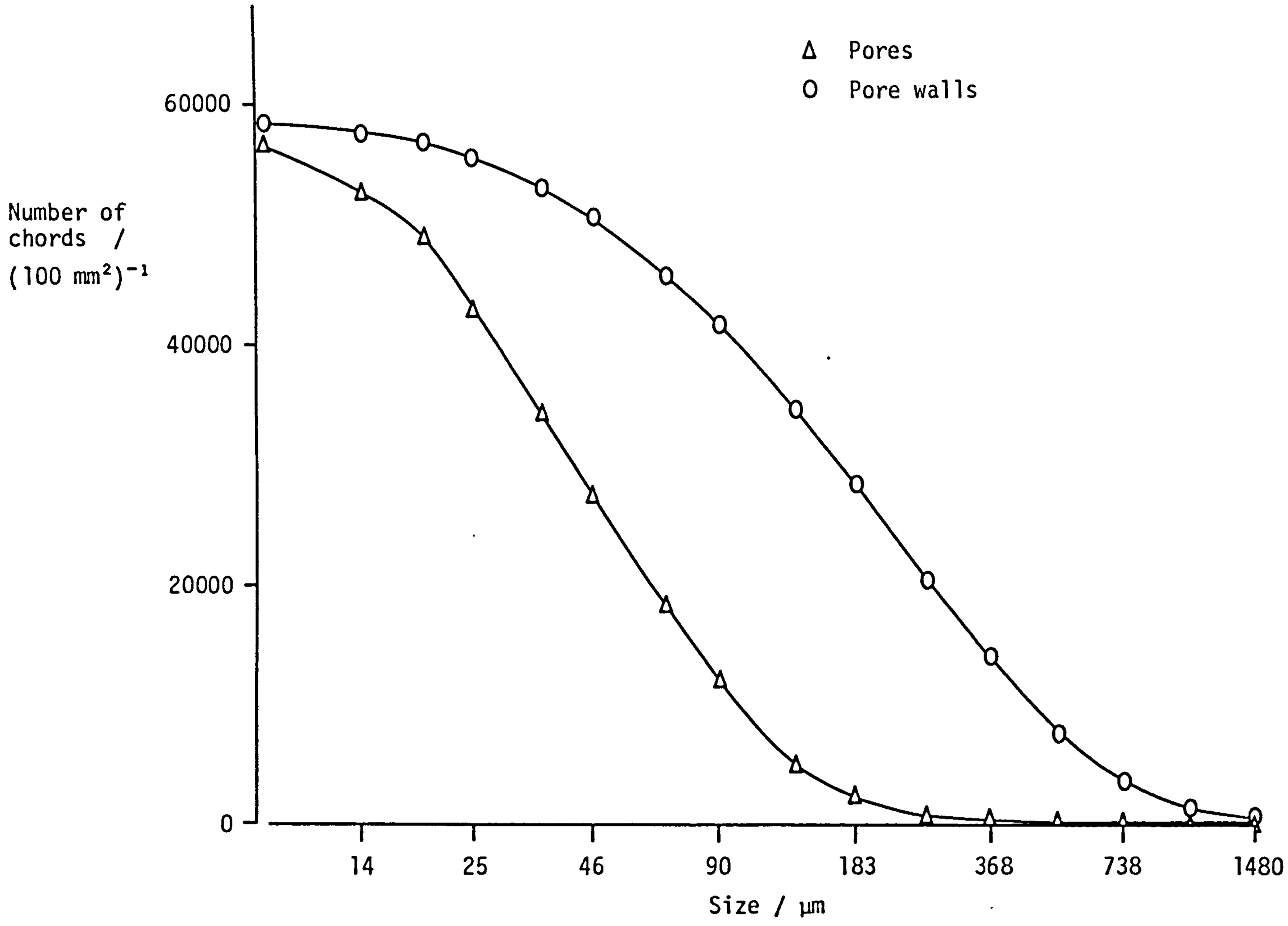
Distribution of number of chords present in PGA graphite C7/1 (control for C79).



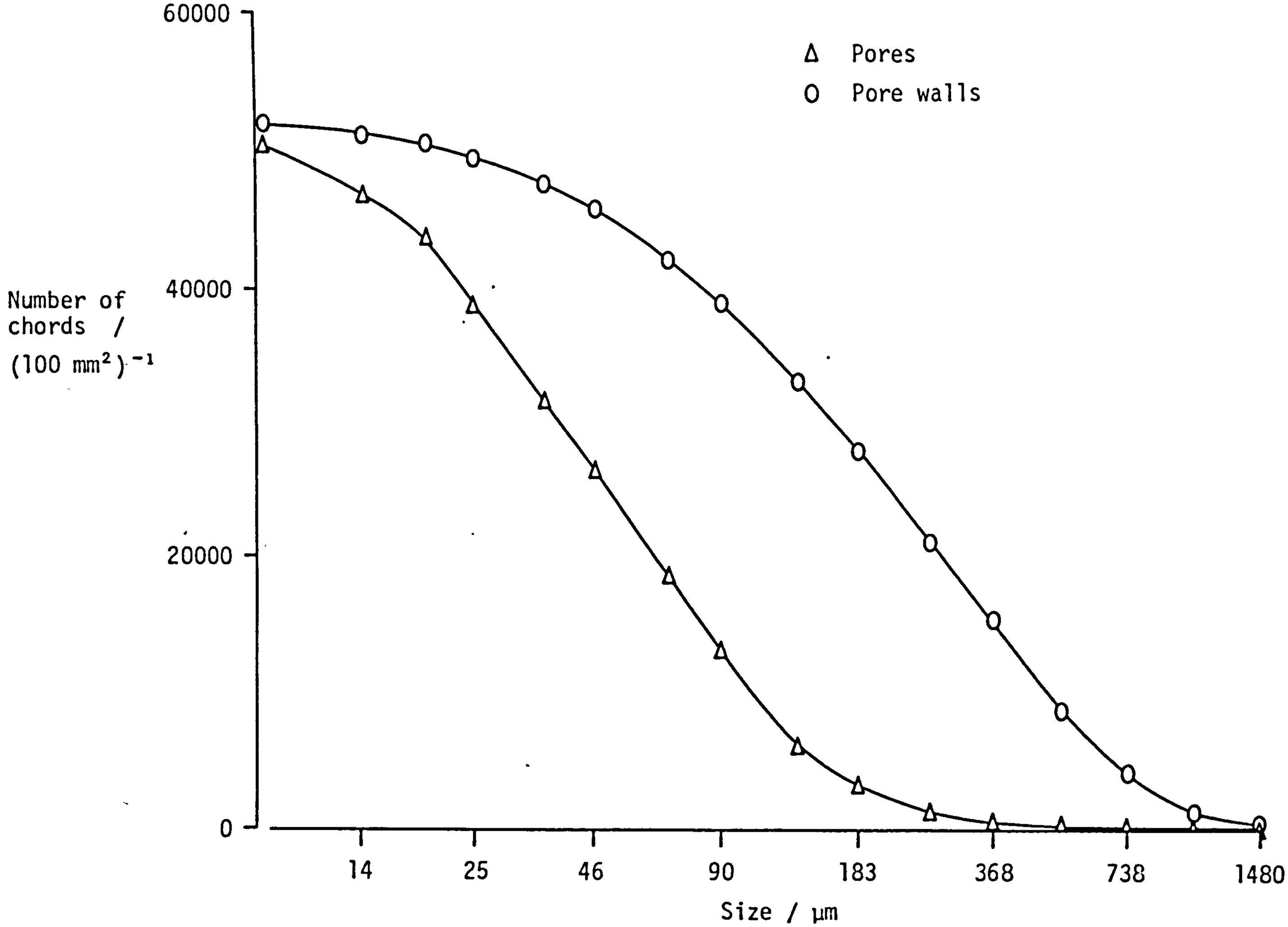
Distribution of number of chords present in PGA graphite C79 radiolytically oxidised to 6.2% weight loss.



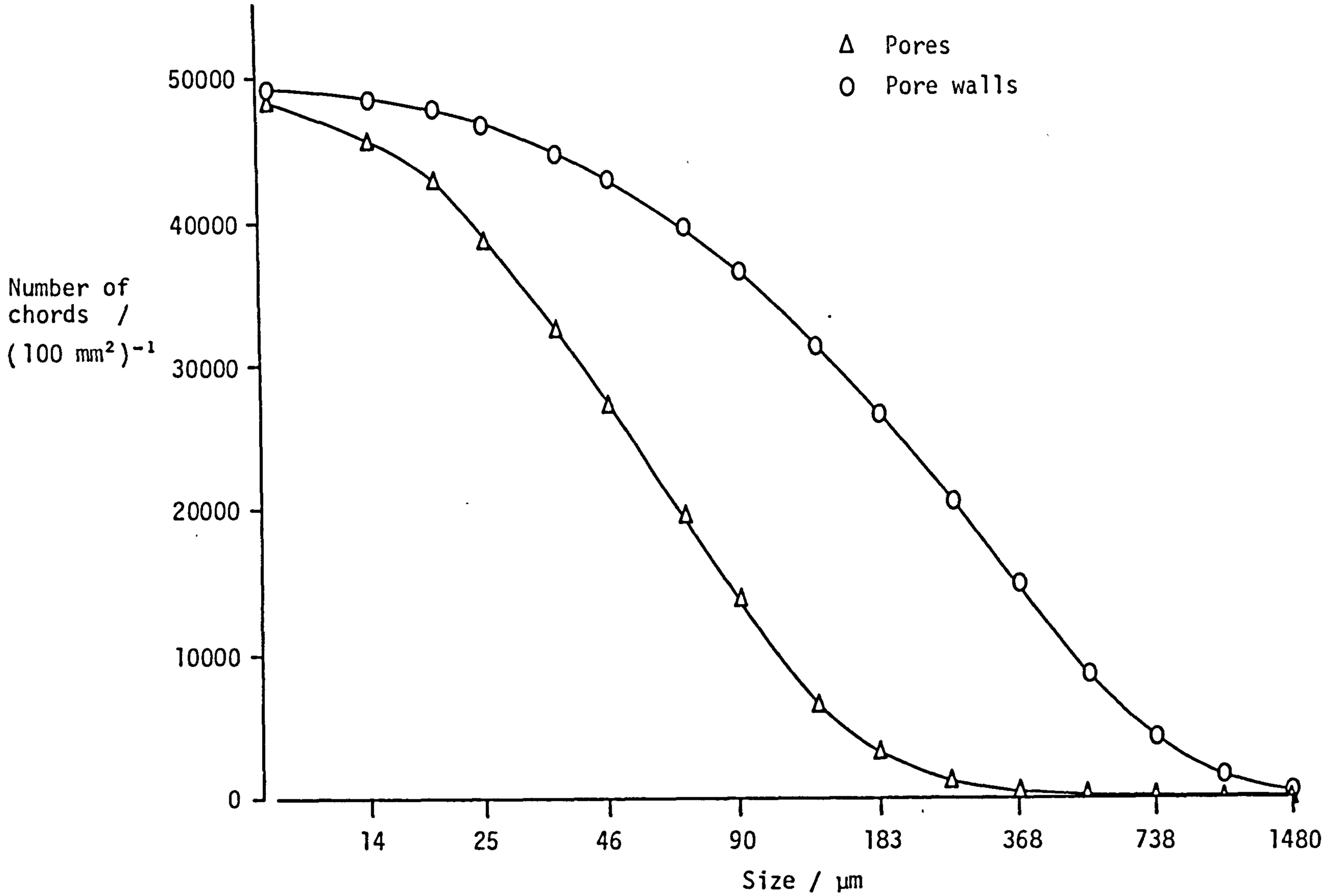
Distribution of number of chords present in AGLMP graphite 10F49 (control for M38).



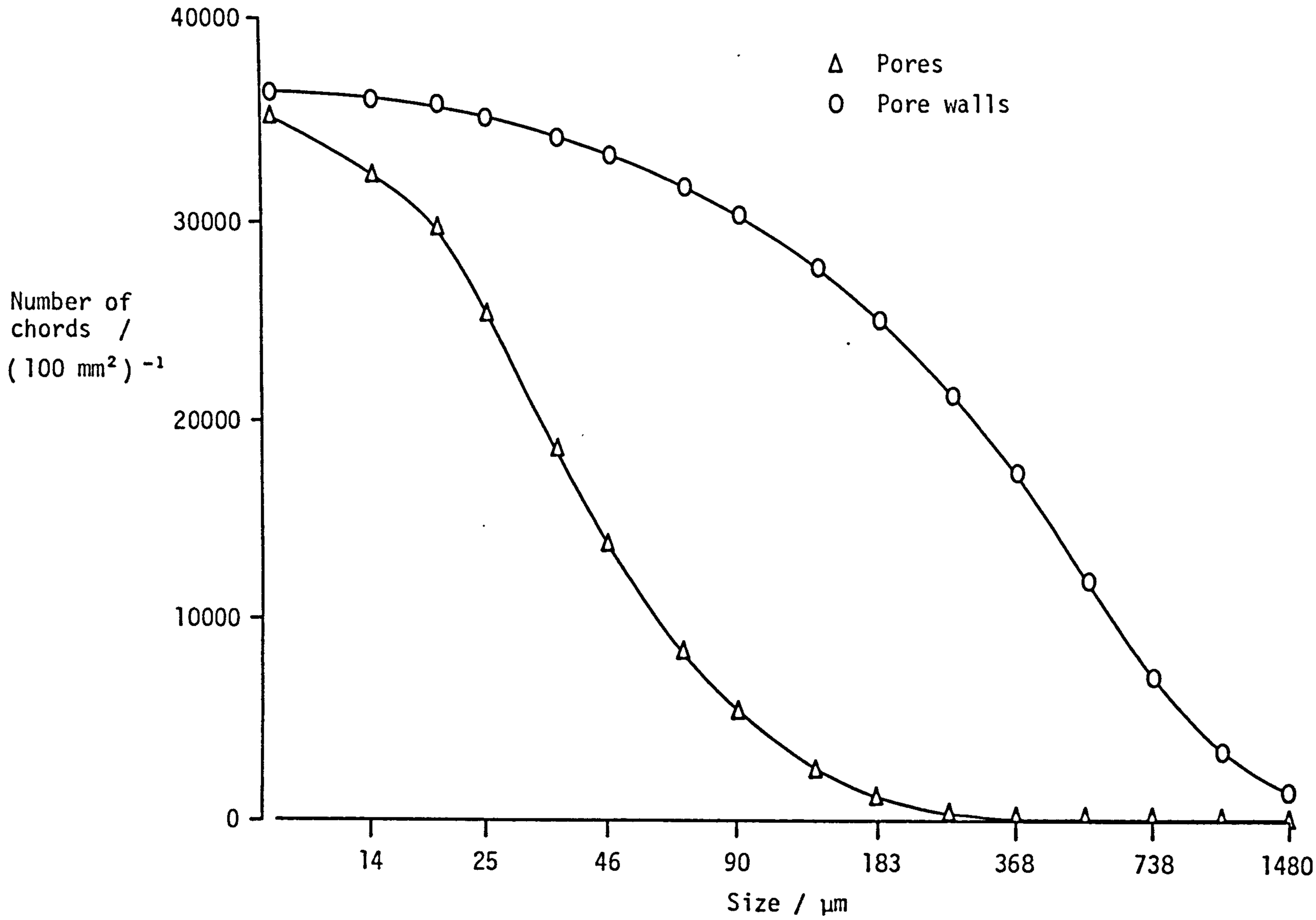
Distribution of number of chords present in AGLMP graphite M38 radiolytically oxidised to 3.7% weight loss.



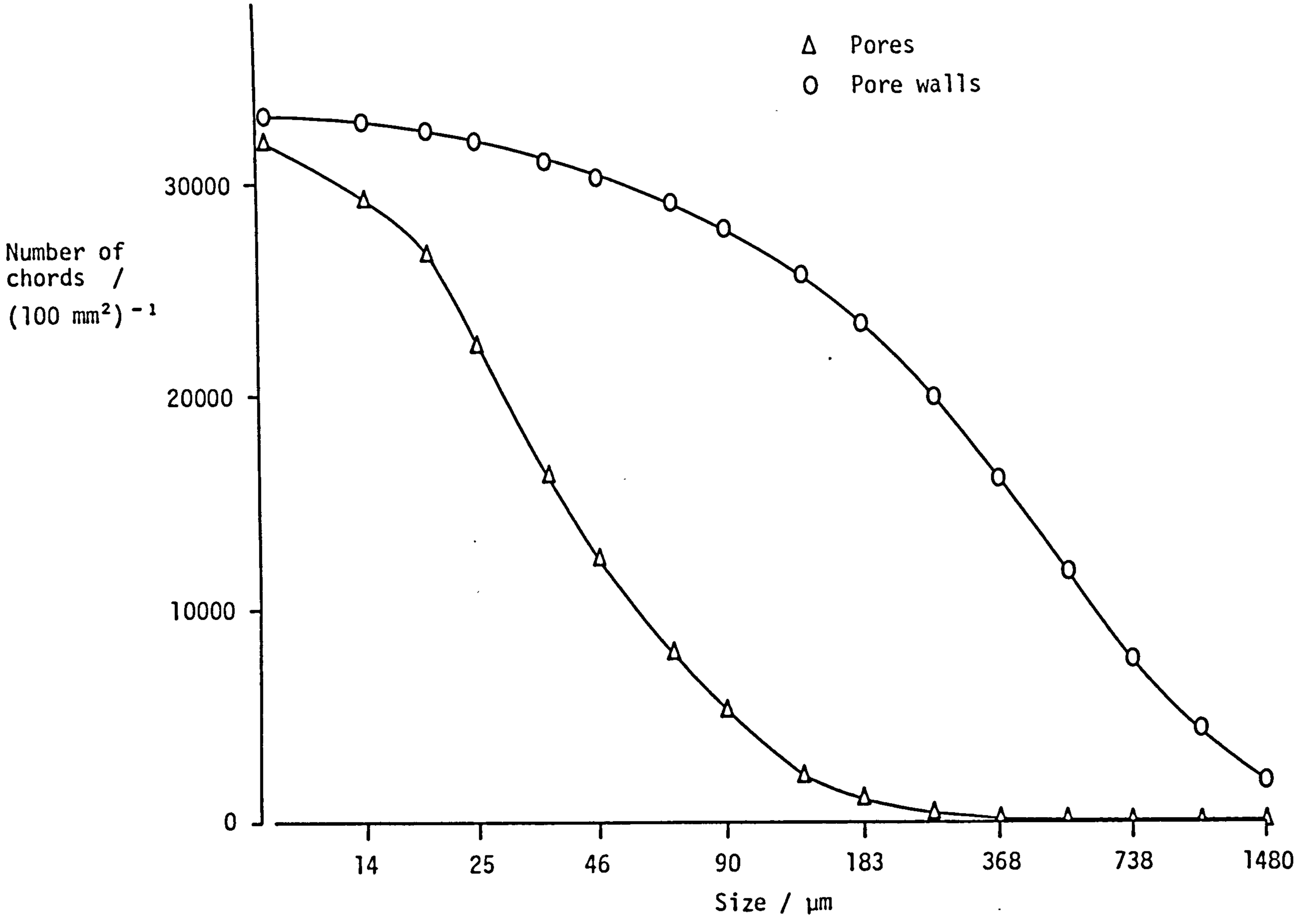
Distribution of number of chords present in AGLMP graphite 584/195 (control for M28).



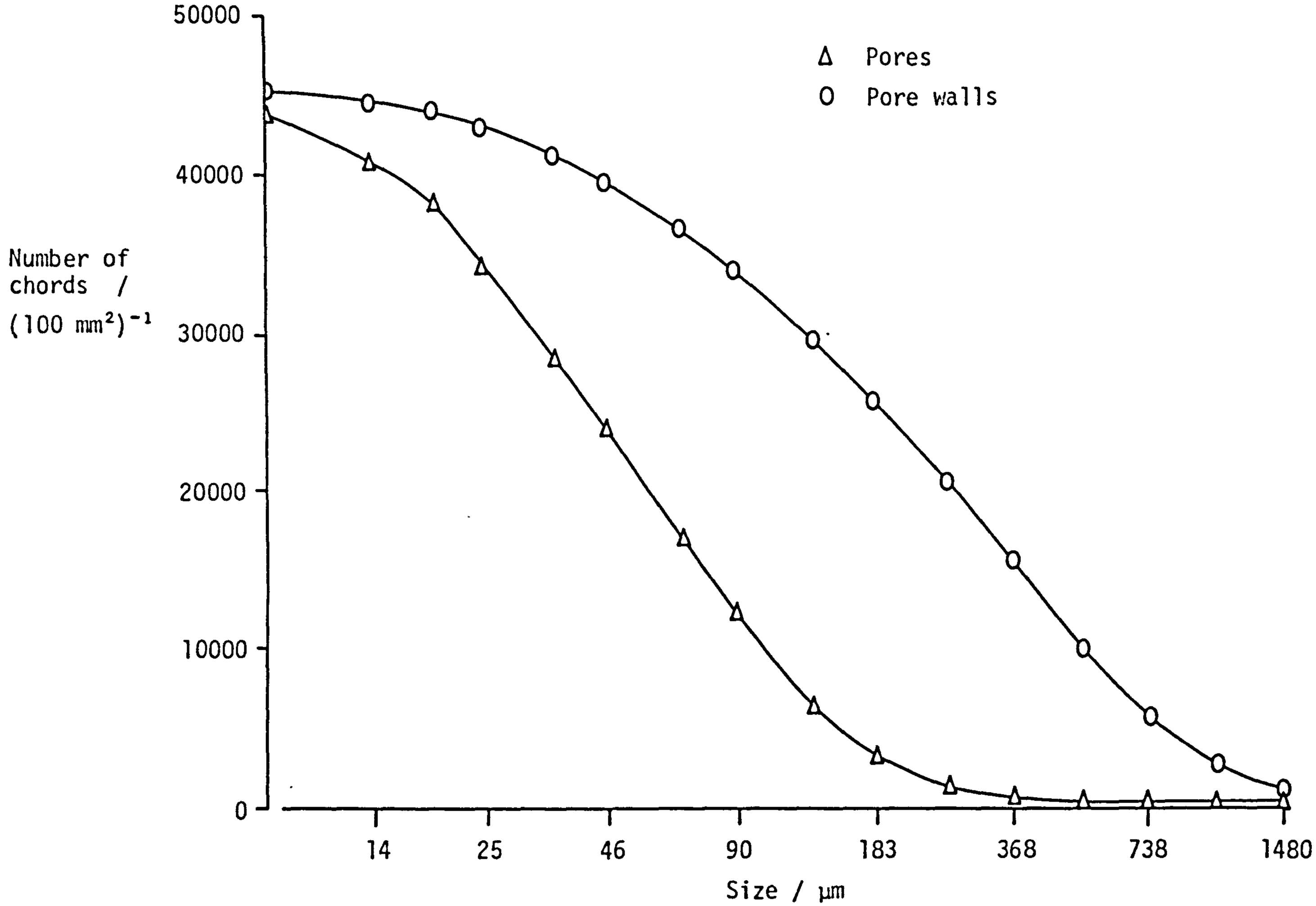
Distribution of number of chords present in AGLMP graphite M28 radiolytically oxidised to 3.5% weight loss.



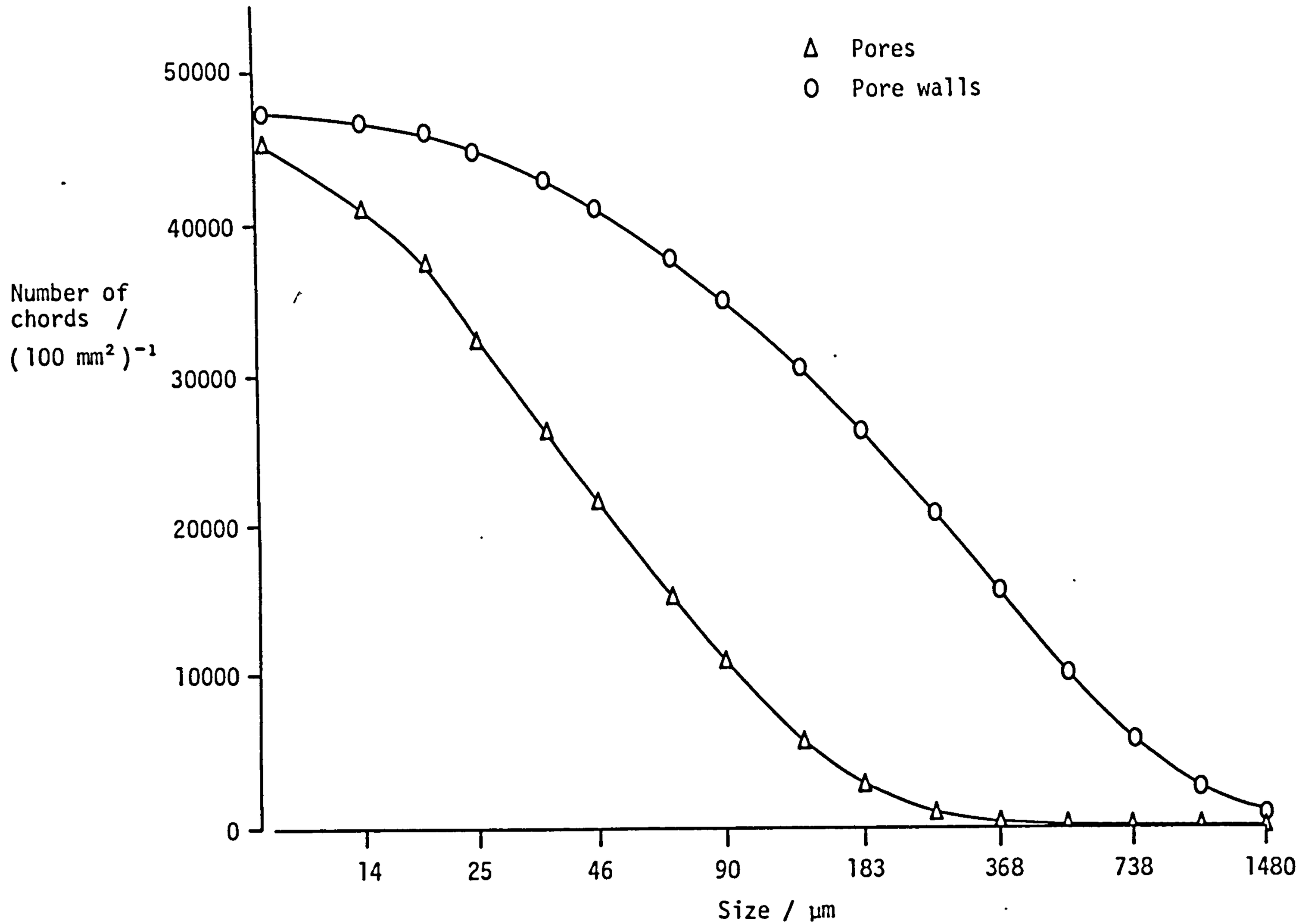
Distribution of number of chords present in BAEL pitch-coke graphite Q6/1 (control for H30).



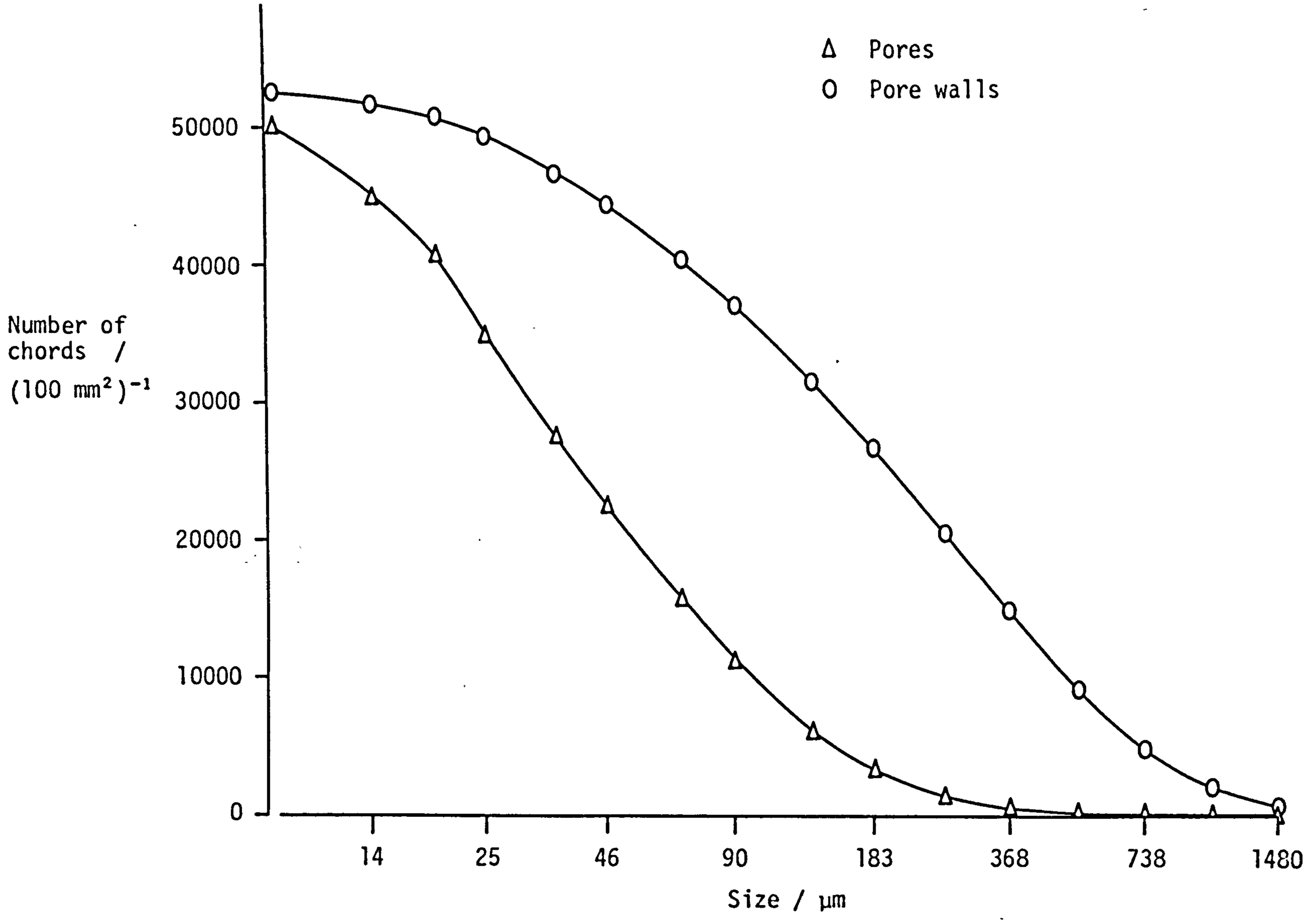
Distribution of number of chords present in BAEL pitch-coke graphite H30 radiolytically oxidised to 0.6% weight loss.



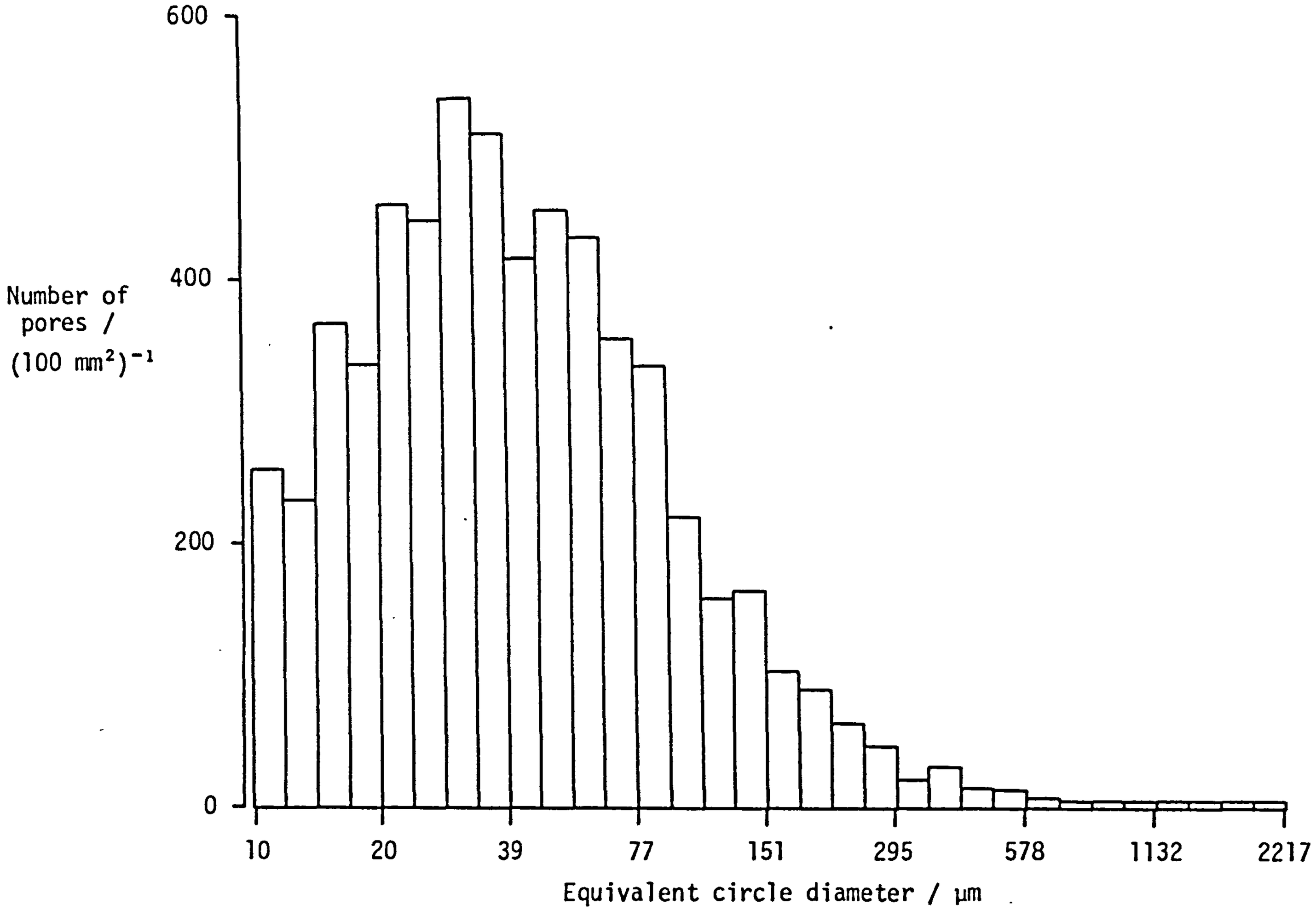
Distribution of number of chords present in AGLMP graphite thermally oxidised to 3.1% weight loss.



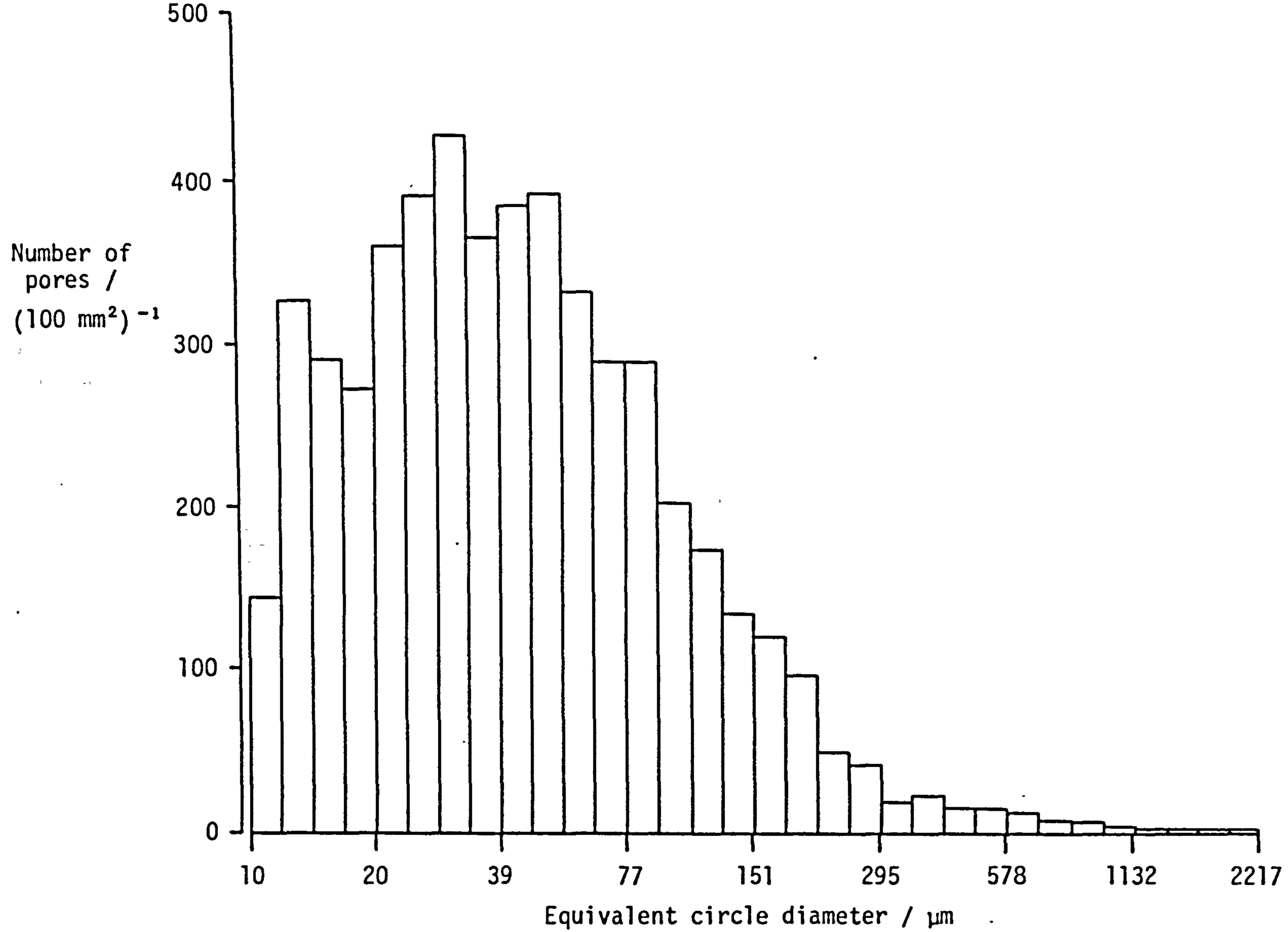
Distribution of number of chords present in AGLMP graphite thermally oxidised to 5.4% weight loss.



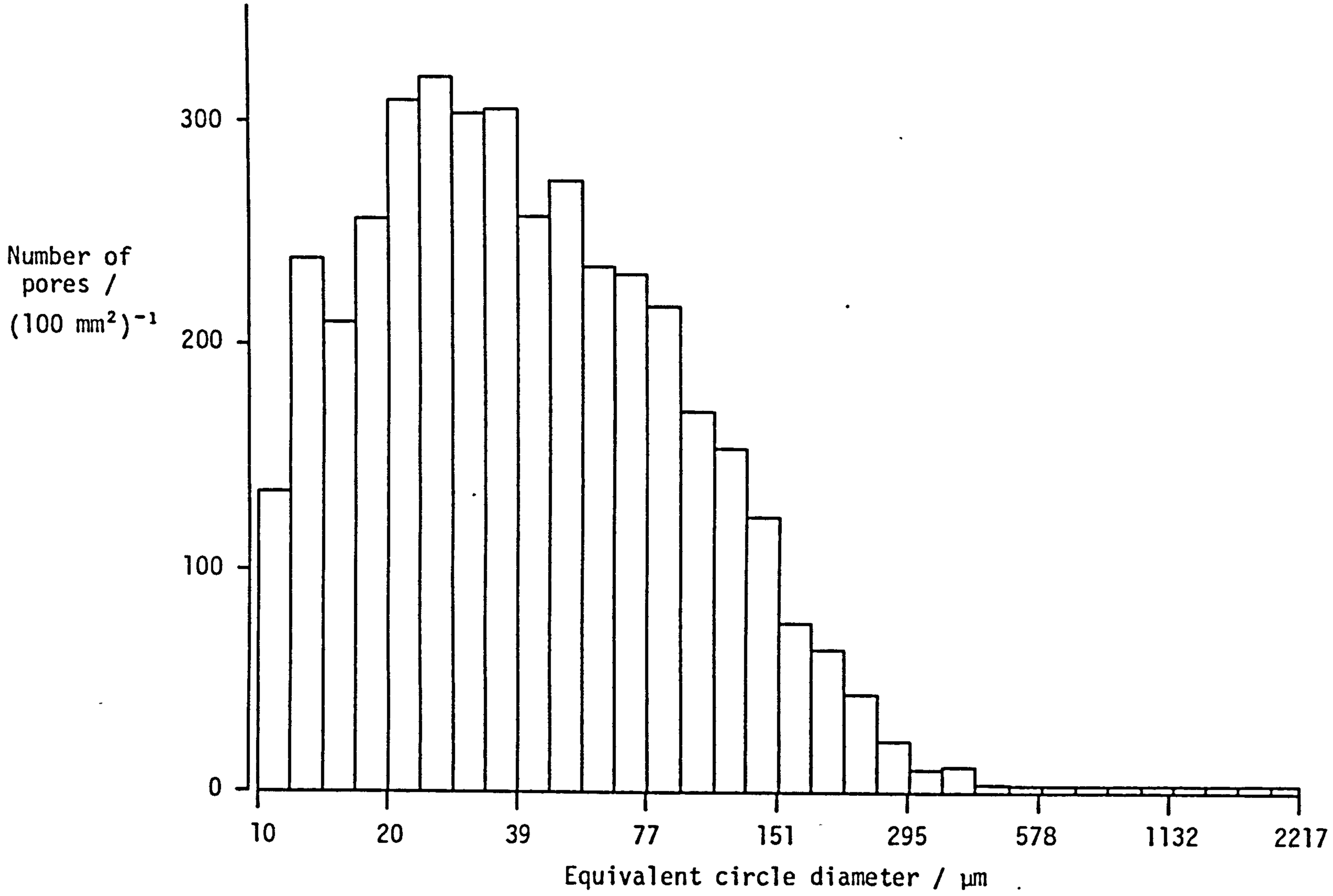
Distribution of number of chords present in AGLMP graphite thermally oxidised to 10.5% weight loss.



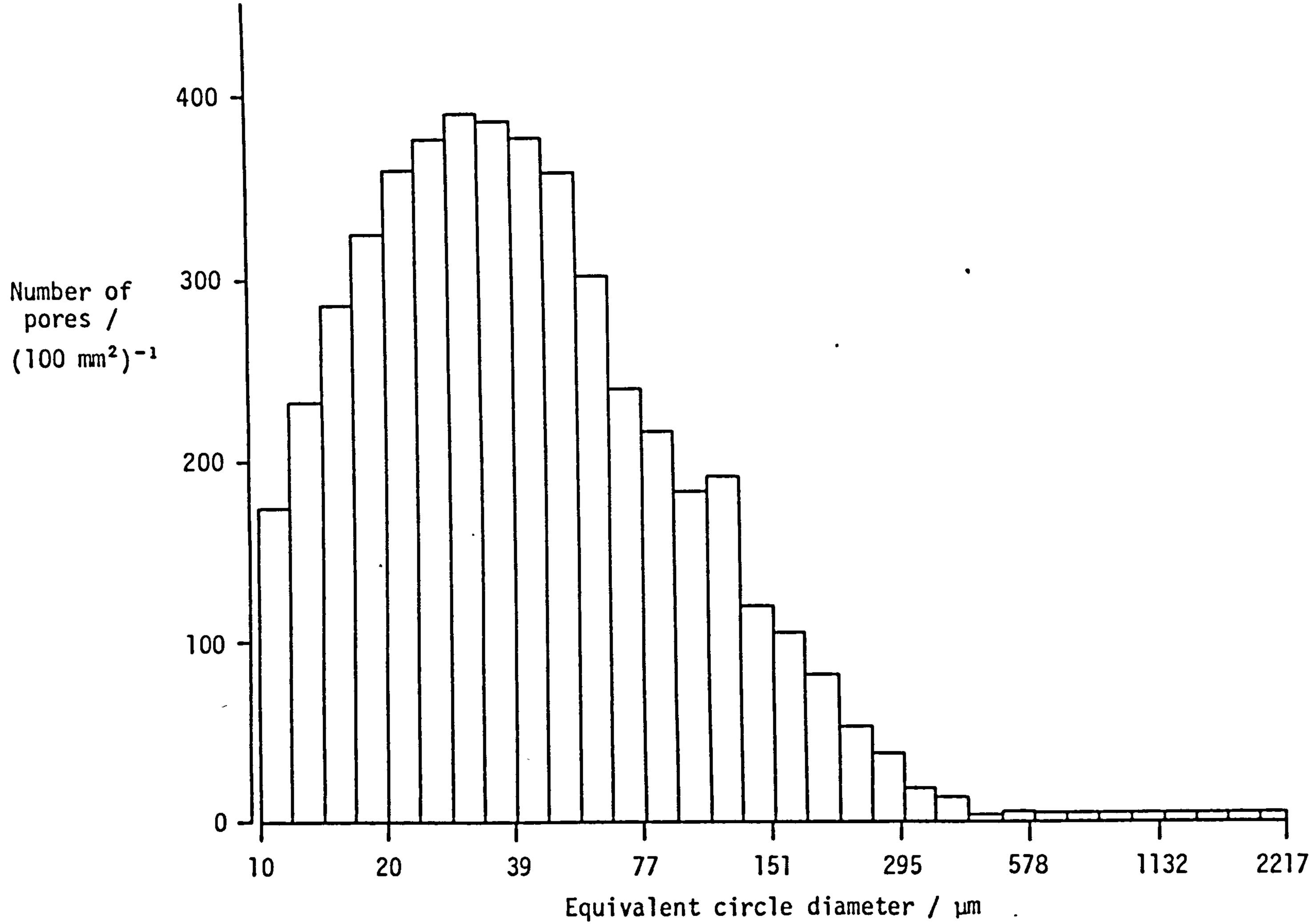
Corrected distribution of areas of pores in PGA graphite C7/1 (control for C79).



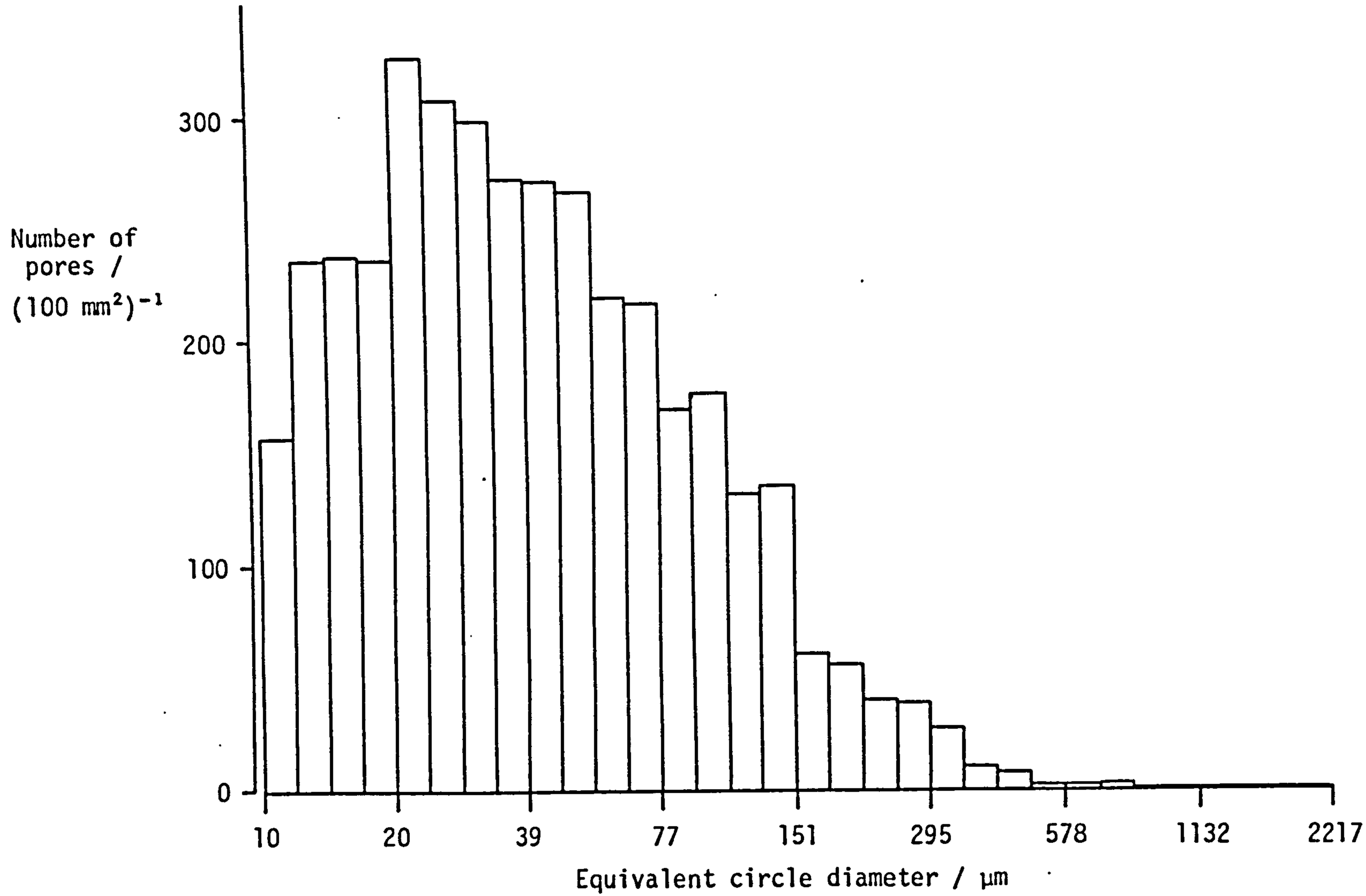
Corrected distribution of areas of pores in PGA graphite C79 radiolytically oxidised to 6.2% weight loss.



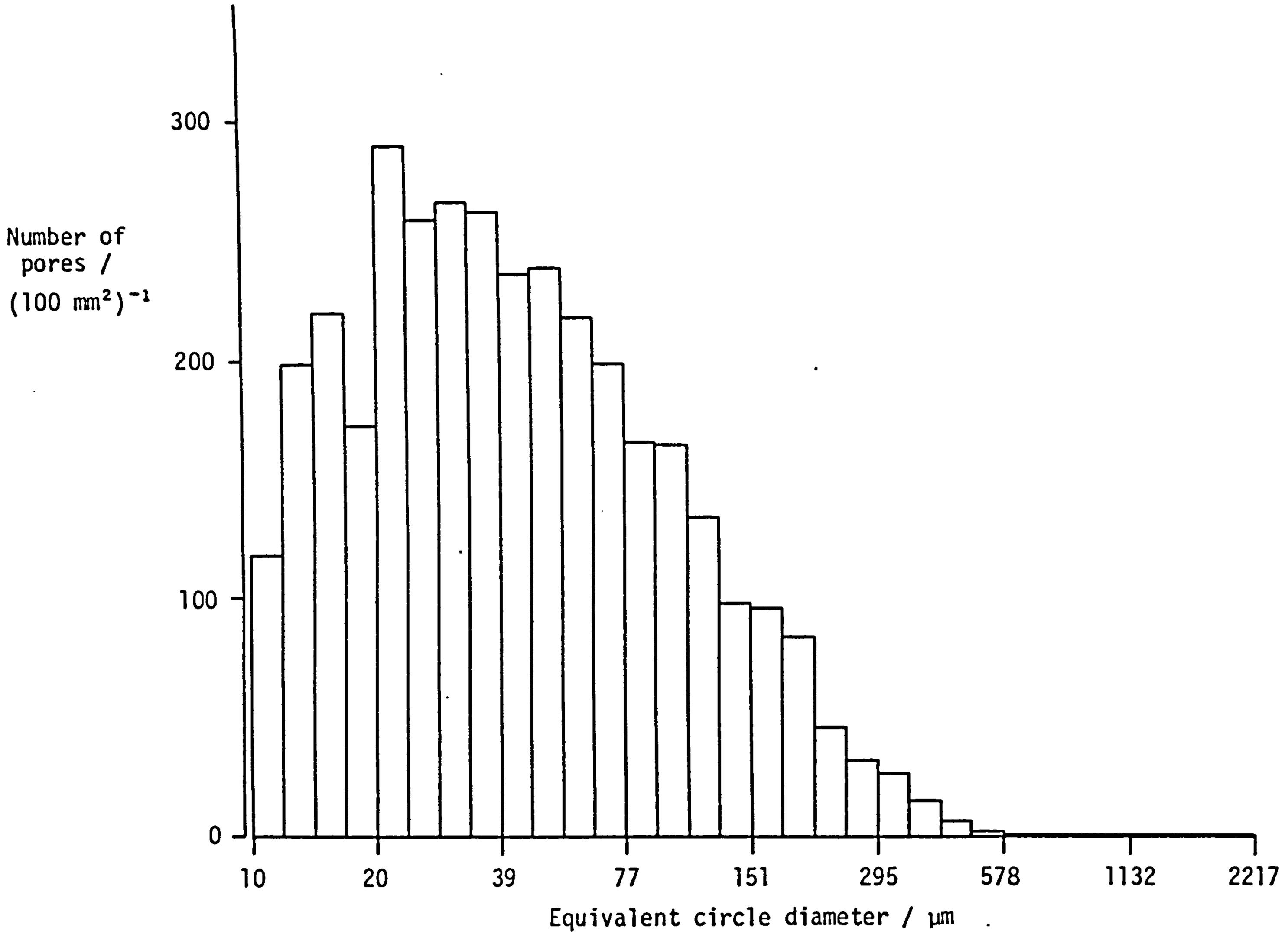
Corrected distribution of areas of pores in AGLMP graphite 10F49 (control for M38).



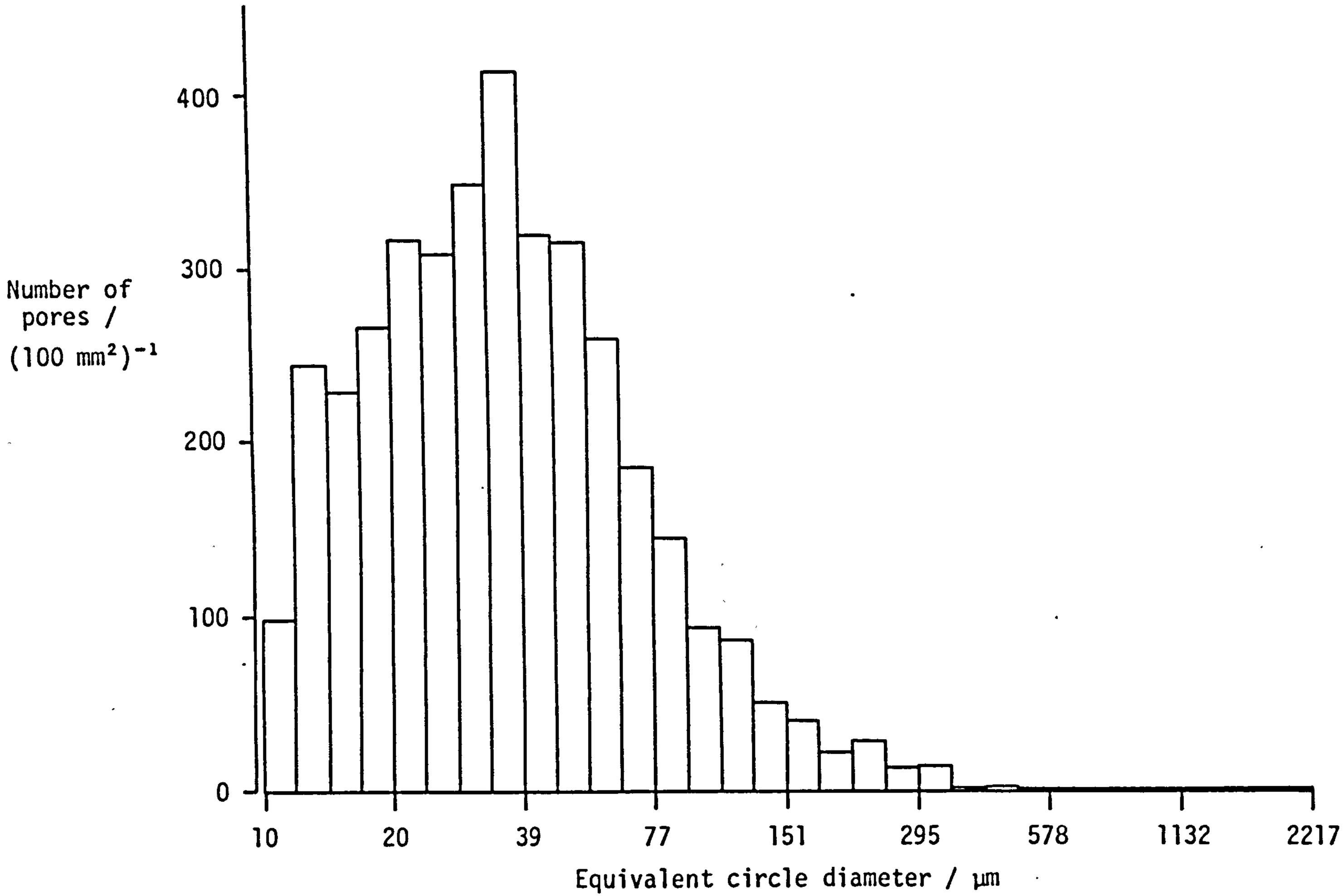
Corrected distribution of areas of pores in AGLMP graphite M38 radiolytically oxidised to 3.7% weight loss.



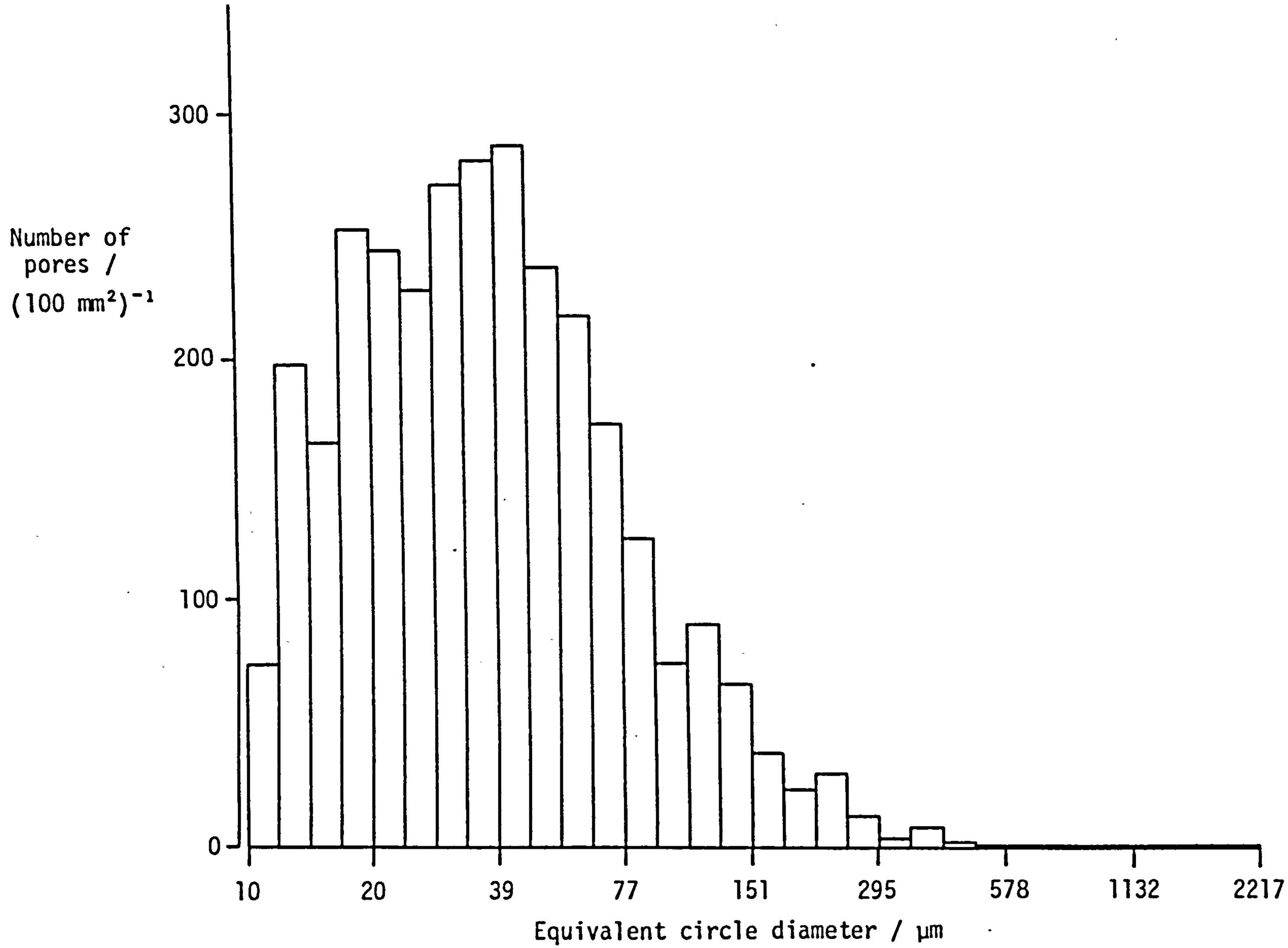
Corrected distribution of areas of pores in AGLMP graphite 584/195 (control for M28).



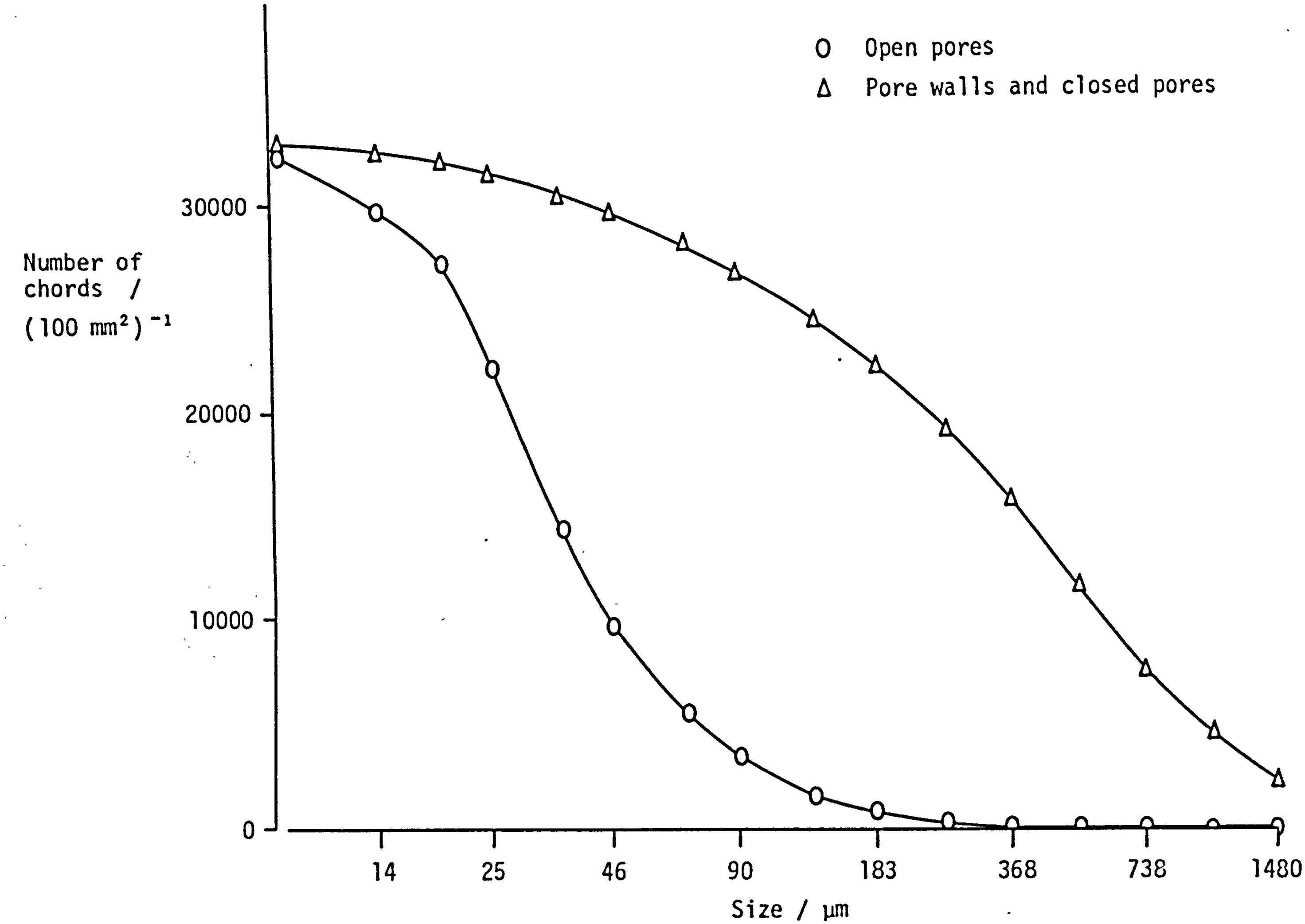
Corrected distribution of areas of pores in AGLMP graphite M28 radiolytically oxidised to 3.5% weight loss.



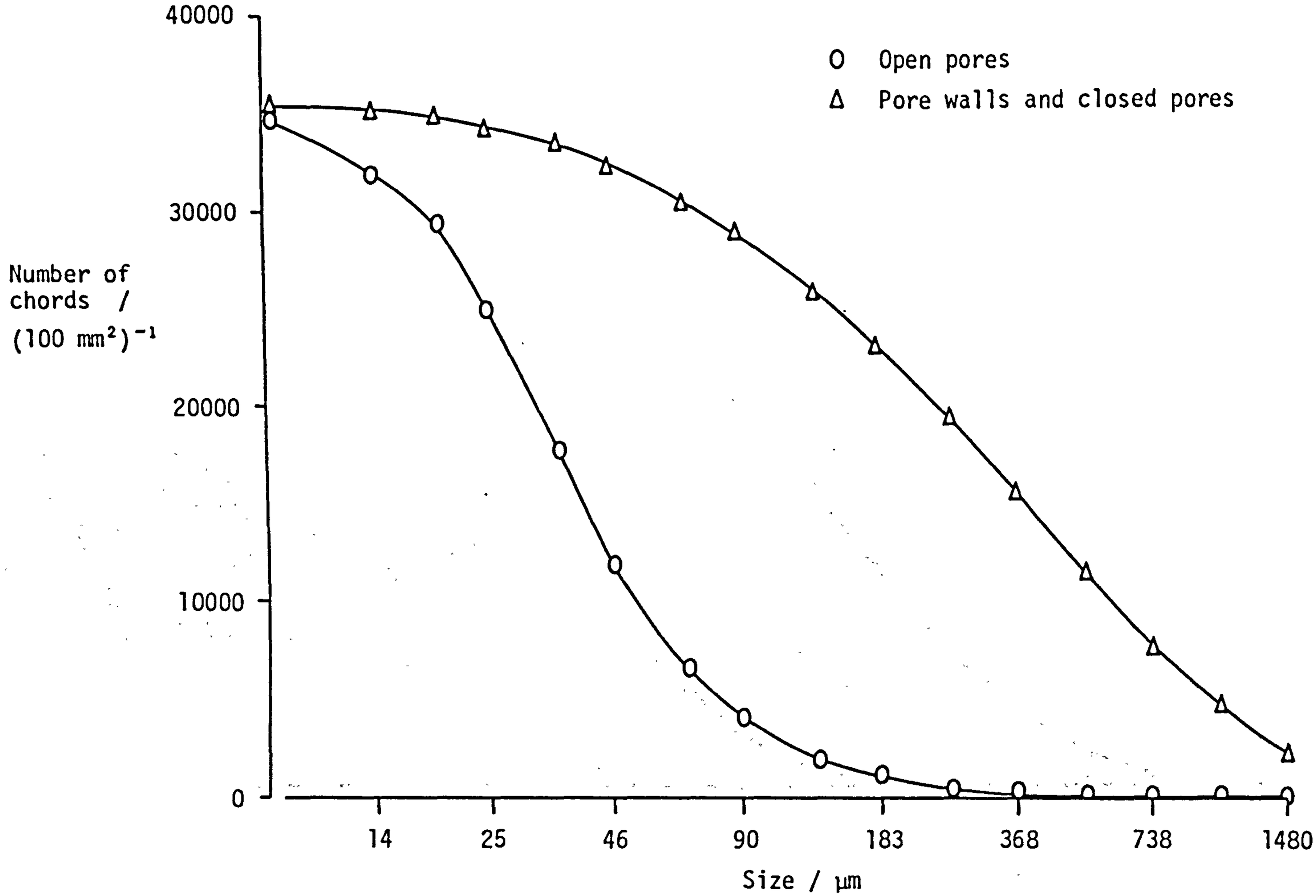
Corrected distribution of areas of pores in BAEL pitch-coke graphite Q6/1 (control for H30).



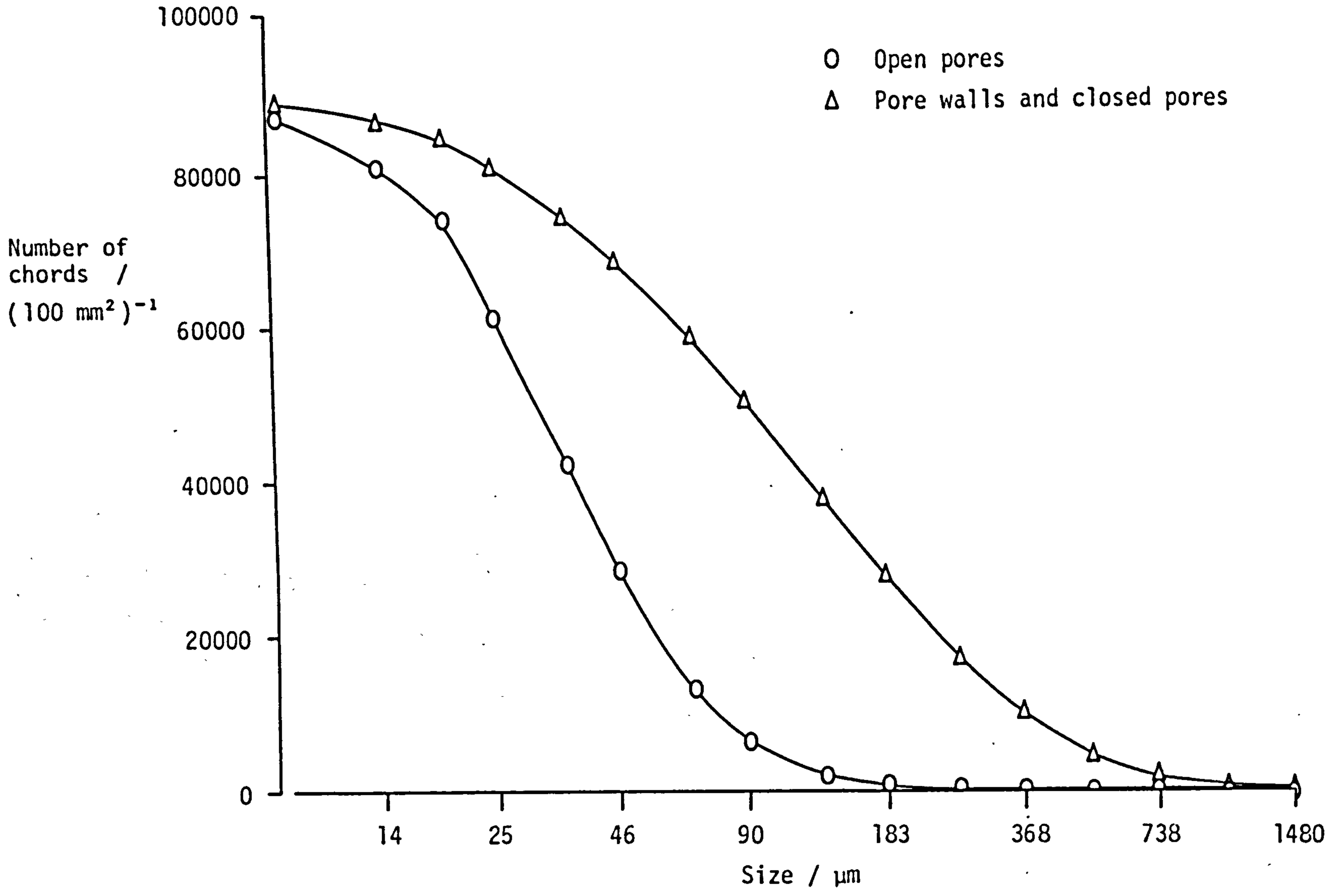
Corrected distribution of areas of pores in BAEL pitch-coke graphite H30 radiolytically oxidised to 0.6% weight loss.



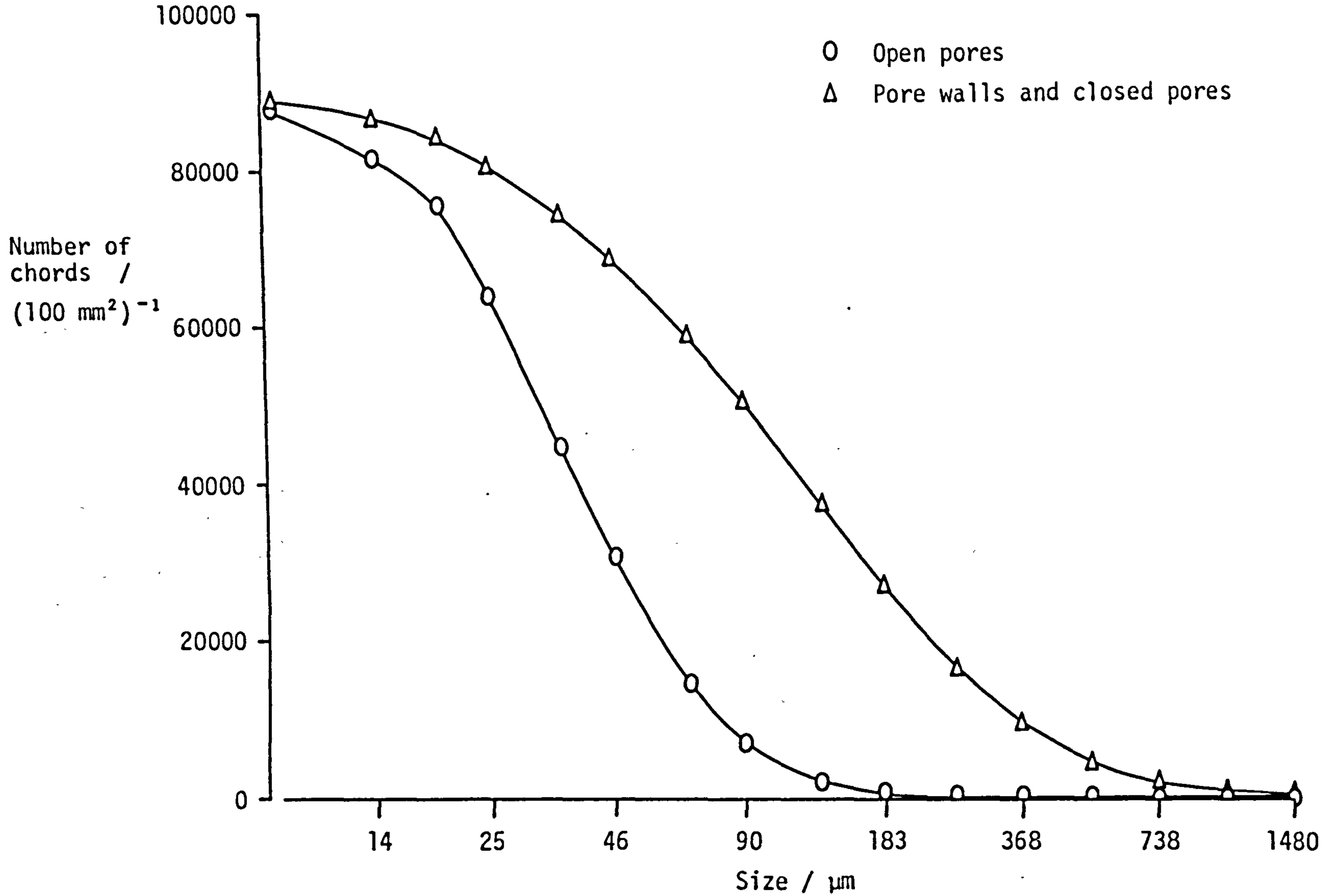
Distribution of number of chords present in gold impregnated BAEL pitch-coke graphite Q5/4 (control for H24).



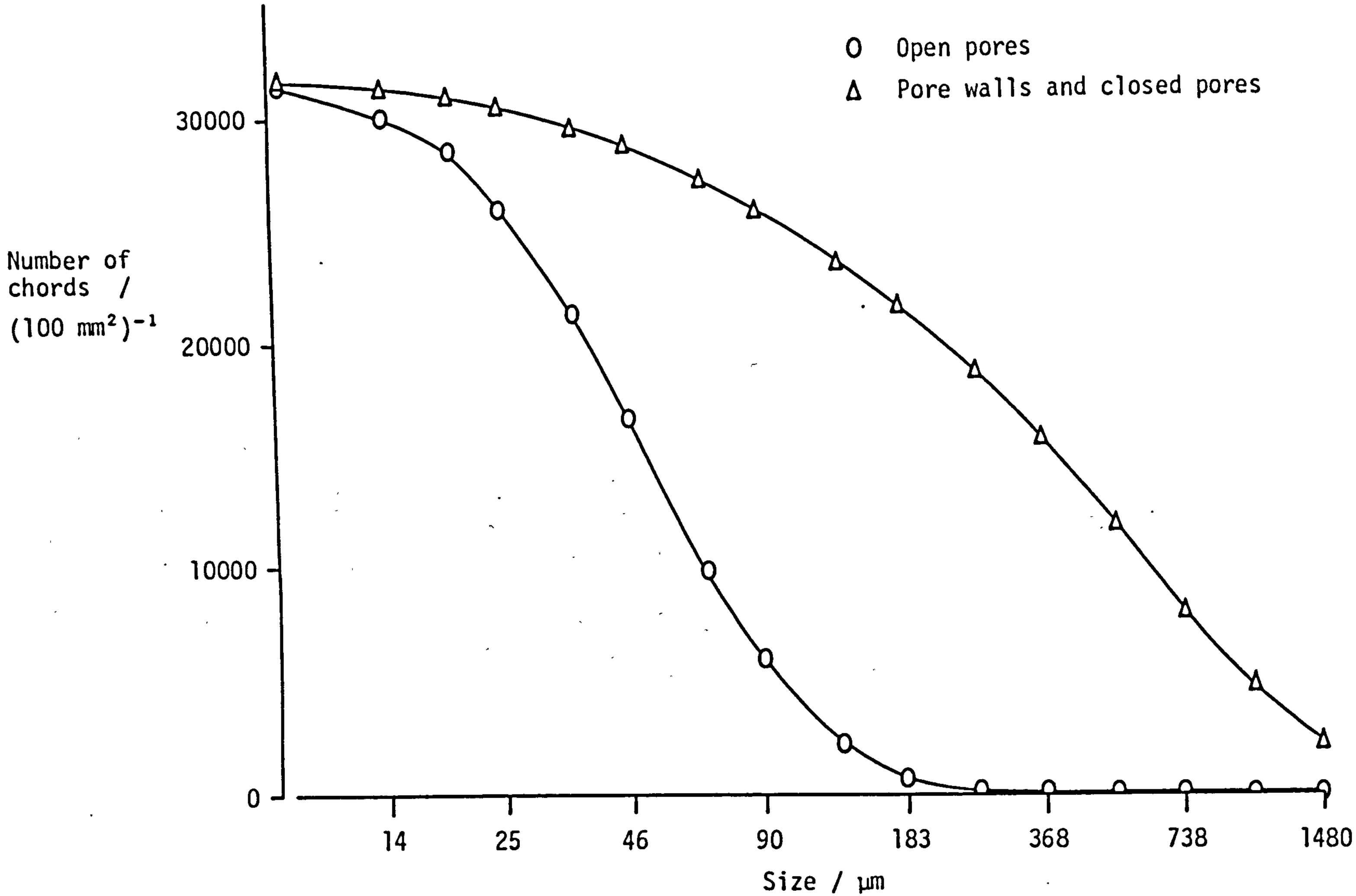
Distribution of number of chords present in gold impregnated BAEL pitch-coke graphite H24 radiolytically oxidised to 8.8% weight loss.



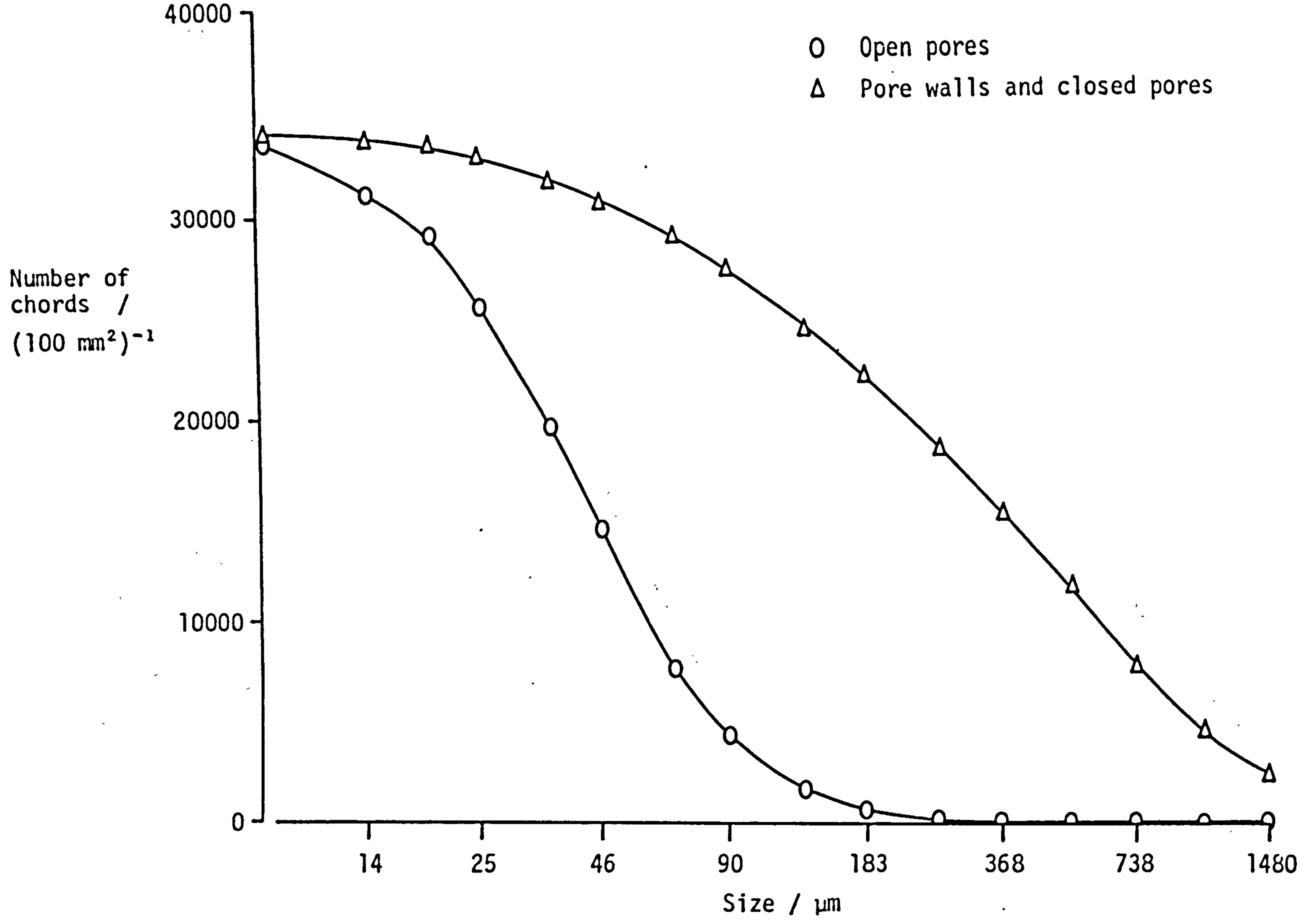
Distribution of number of chords present in gold impregnated PGA graphite C6/3 (control for C79).



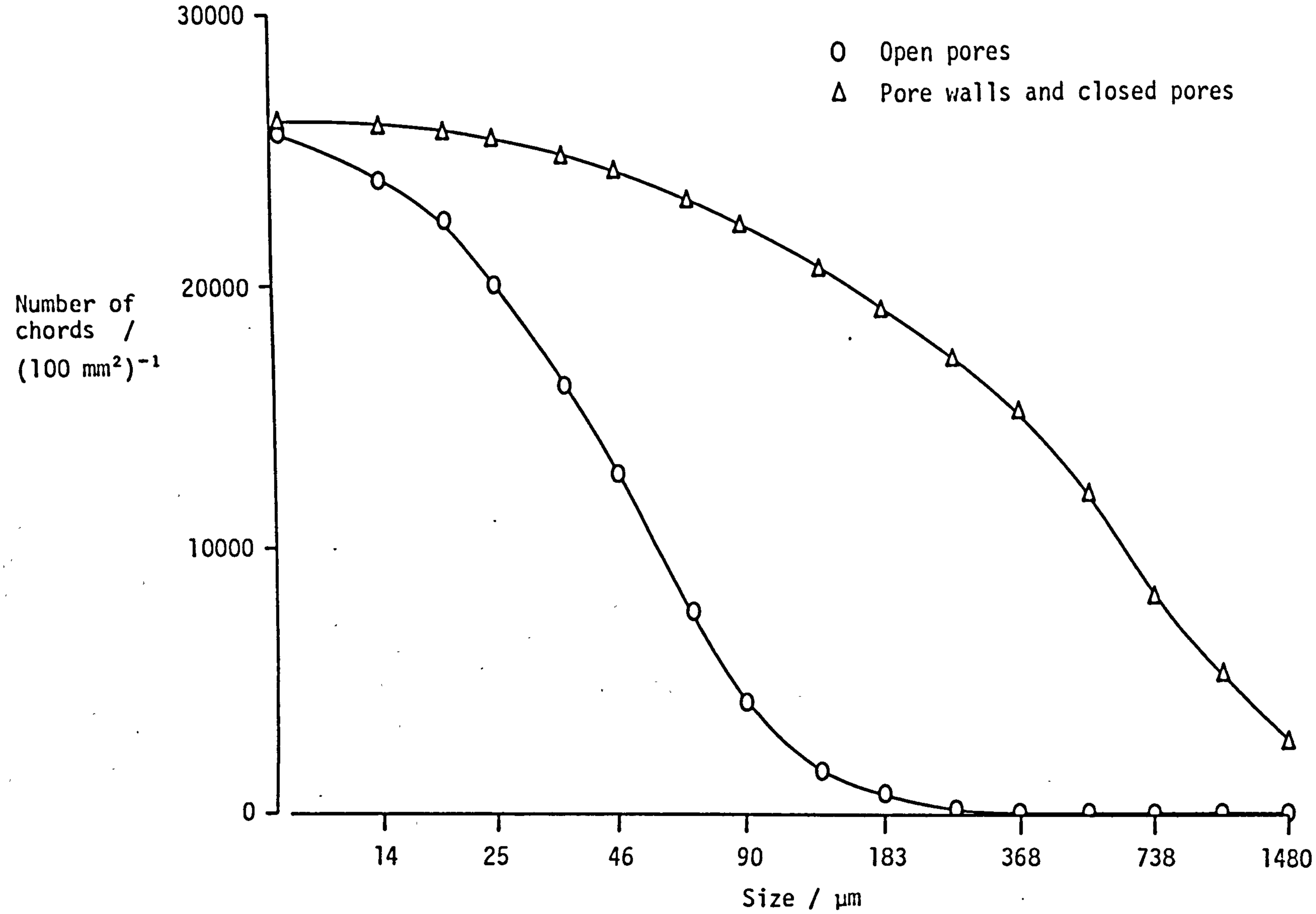
Distribution of number of chords present in gold impregnated PGA graphite C79 radiolytically oxidised to 6.2% weight loss.



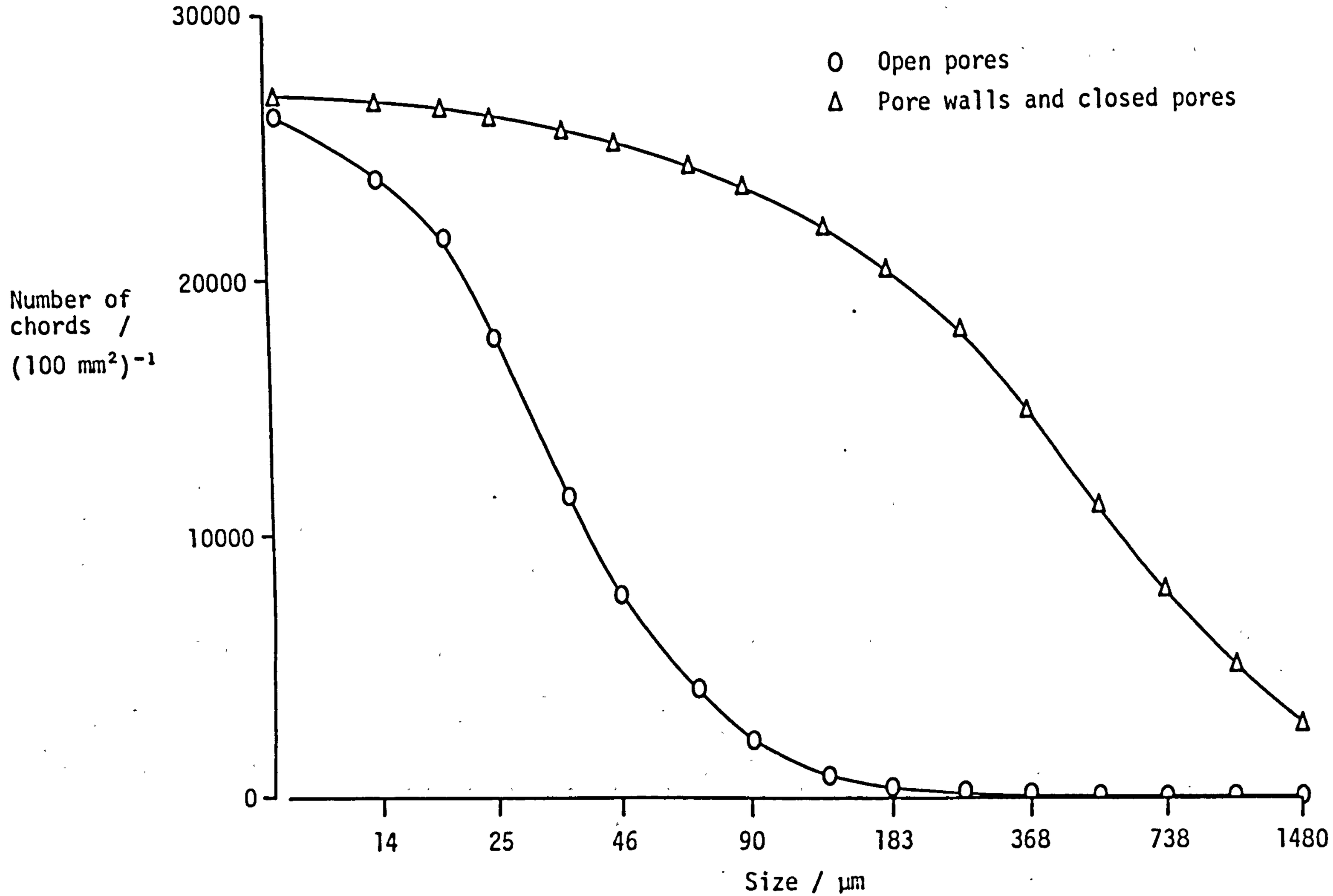
Distribution of number of chords present in gold impregnated AGLMP graphite 10F49 (control for M38).



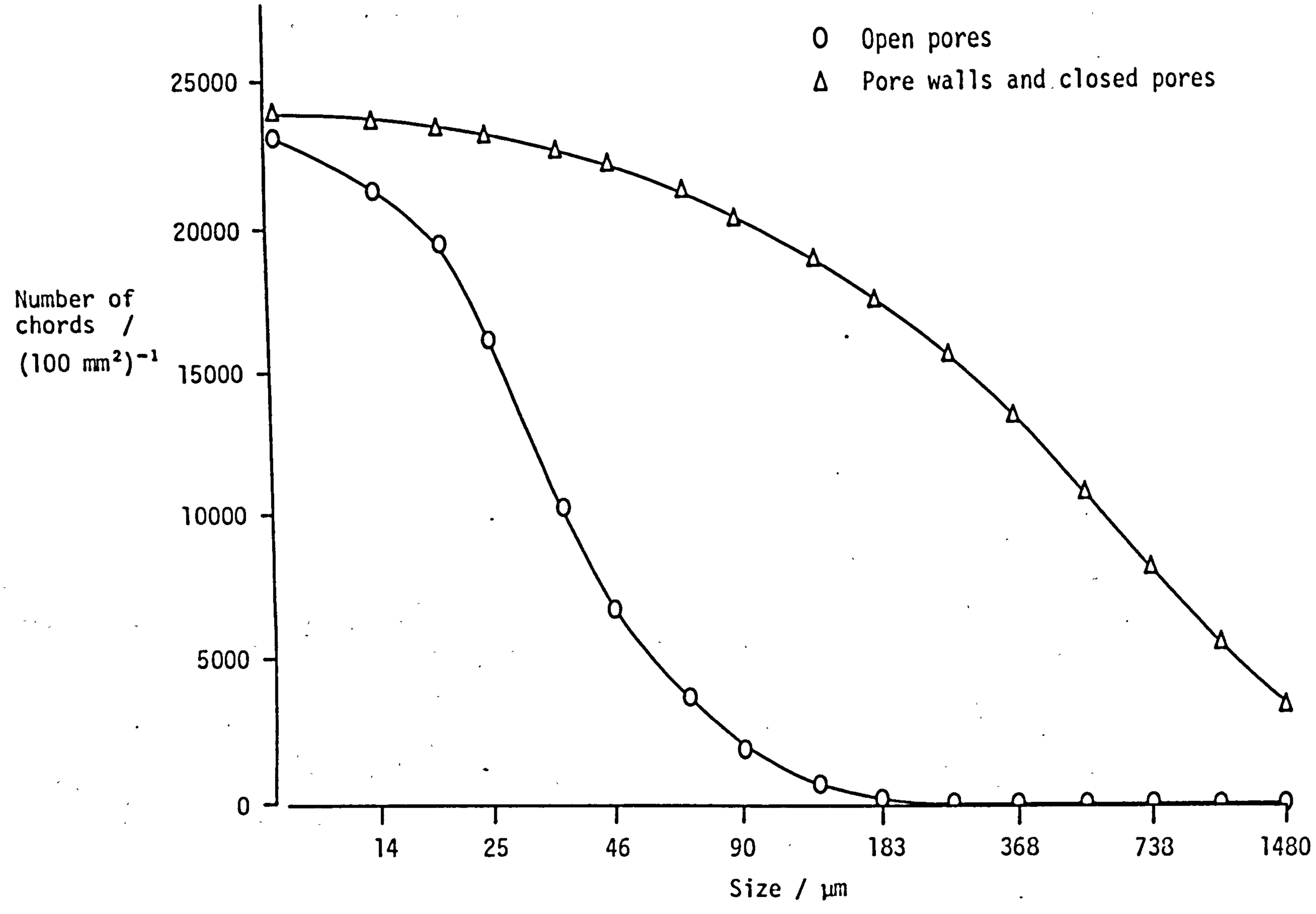
Distribution of number of chords present in gold impregnated AGLMP graphite M38 radiolytically oxidised to 3.7% weight loss.



Distribution of number of chords present in gold impregnated AGLMP graphite M28 radiolytically oxidised to 3.5% weight loss.



Distribution of number of chords present in gold impregnated BAEL pitch-coke graphite Q6/1 (control for H30).



Distribution of number of chords present in gold impregnated BAEL pitch-coke graphite H30 radiolytically oxidised to 0.6% weight loss.

APPENDIX II

Negative Numbers of Micrographs

Figure	Negative	Figure	Negative
3	A 5	77	CR10/8
4	B 4	78	CR10/10
5	B 14	79	CR10/240
6	B 17	80	CR10/241
7	A 13	81	CR10/242
8	B 11	82	CR9/137
9	CR8/462	83	CR9/140
10	CR8/465	84	CR9/146
11	CR8/463,464	85	CR9/158
12	CR9/475	86	CR9/156
13	CR10/23	87	CR9/161
14	CR9/528	88(a)	C 21
15	CR10/67	88(b)	C 16
16	CR9/530	89(a)	C 19
17	CR9/469	89(b)	C 17
18	CR9/466	90(a)	C 20
19	CR9/466,467	90(b)	C 18
20	CR10/71	91	CR9/506
21	CR10/72	92	CR9/511
22	CR9/451	93	CR9/522
23	CR9/452	94	CR9/509
24	CR9/452,453	95	CR9/517
25	CR9/454	96	CR9/528
26	CR10/64	97	CR9/509,510
27	CR9/444	98	CR9/514,515
28	CR9/447	99	CR9/523,524
29	CR9/445,446	100	CR8/498
30	CR9/448	101	CR8/499
31	CR10/63	102	CR9/477
32	CR9/545	103	CR8/500
33	CR9/542	104	CR8/503
34	CR9/542,543	105	CR8/504
35	CR10/61	106	CR9/480
36	CR10/243	107	CR8/506
37	CR9/456	108	CR9/487
38	CR9/461	109	CR9/496
39	CR9/458,459	110	CR9/489.490
40	CR9/460	111	CR9/492
41	CR10/73	112	CR9/499
42-49	H.V.E.M.Rotherham	113	CR9/504
50-67	JEOL 100C ASID-4D (Polaroid)	114	CR9/502,503
		115	CR9/501
68	C 8	116	CR9/304
69	C 9	117	CR9/339
70	A 8	118	CR9/339,340
71	B 20	119	CR9/339
72	CR10/12	120	CR9/147
73	CR10/16	121	CR9/149,150
74	CR10/17	122	CR9/149
75	CR10/15	122a	CR9/153
76	CR10/6	123	CR9/228

Figure	Negative
124	CR9/235
125	CR9/229,230
126	CR9/238
127	CR8/133,134
128	EM3/596,597
130	CR9/533
131	CR10/29
132	CR9/534,535
133	CR10/30,31
134	CR10/21
135	CR10/27
136	CR9/550
137	CR10/53
138	CR9/550,551
139	CR10/53,54
140	CR9/554
141	CR10/59
153	Polaroid
154	CR10/220
155	CR10/219
156	CR10/222
157	4 6
158	4 7
159	CR10/477
160	CR10/478
161	CR10/479
162	CR10/480
163	14 6A
164	15 8
165	CR11/104
166	CR11/105
167	CR11/106
168	CR11/107
169	CR11/158
170	CR11/159
171	CR11/160
172	CR11/161
173	CR11/169
174	CR11/170
175	CR11/168
176	CR11/167
177	CR11/166
178	CR11/171
179	6 16A
180	6 17A
181	8 9A
182	8 10A
183	4 12
184	CR11/177
185	CR11/178
186	CR11/180
187	CR11/179
188	7 0A
189	8 13A

Figure	Negative
190	13 4
191	13 16
192	CR11/80
193	CR11/81
194	CR11/82
195	CR11/83
196	4 15
197	4 16
198	CR10/496
199	CR10/497
200	CR10/498
201	CR10/499
202-210	JEOL 100C ASID-4D (Polaroid)
211	9 4
212	11 6A
213	CR10/527
214	CR10/529
215	CR10/528
216	4 20
217	CR10/489
218	CR11/172
219	CR11/175
220	CR11/173
221	9 12
222	11 15A
223	12 2
224	16 0
225	CR11/339
226	CR11/344
227	CR11/346
228	CR11/343
229	CR13/268
230	CR13/265
231	CR13/264
232	CR13/263
233	5 10
234	CR10/470
235	CR10/471
236	CR10/472
237-242	JEOL 100C ASID-4D (Polaroid)
243	14 13A
244	16 6
245	CR11/98
246	CR11/99
247	CR11/100
248	CR11/151
249	CR11/152
250	CR11/153
251	8 2A
252	8 4A
253	12 11
254	12 14

Figure	Negative
255	CR11/95
256	CR11/96
257	CR11/97
258	5 20
259	10 15A
260	CR10/510
261	CR10/512
262	CR10/511
263	24 20A
264	28 9
265	CR13/204
266	CR13/202
267	CR13/201
268	CR13/280
269	CR13/278
270	CR13/277
271	25 19
272	29 4A
273	CR13/163
274	CR13/162
275	CR13/275
276	CR13/274
277	17 12
278	19 15
279	CR11/364
280	CR11/367
281	CR11/365
282	CR13/137
283	CR13/140
284	CR13/138
285	CR13/254
286	CR13/252
287	CR13/251,253
288	CR13/251
289	CR13/250
290	28 2
291	CR12/506
292	CR12/504
293	CR13/191
294	CR13/189
295	CR13/283
296	CR13/281
297	23 15
298	26 .3
299	CR13/236
300	CR13/234
301	CR13/233
302	CR13/288
303	CR13/286
304	CR13/285
305	19 11
306	27 6A
307	28 no number
308	CR12/23

Figure	Negative
309	CR12/21
310	CR13/195
311	CR13/193
312	CR13/418
313	CR13/416
314	23 1
315	27 17A
316	CR12/554
317	CR12/552
318	CR13/227
319	CR13/225
320	CR13/422
321	CR13/420
322	24 16
323	27 5A
324	CR13/148
325	CR13/147
326	CR13/146
327	CR13/145
328	CR13/223
329	CR13/221
330	CR13/443
331	CR13/442
332	CR13/441
333	CR13/440
334	19 5
335	27 11A
336	CR12/15
337	CR12/13
338	CR12/128
339	CR12/130
340	CR13/411
341	CR13/409
342	26 13
343	27 16A
344	CR12/133
345	CR12/134
346	CR12/136
347	CR13/245
348	CR13/244
349	CR13/242
350	CR13/476
351	CR13/475
352	25 15
353	27 2A
354	CR13/159
355	CR13/157
356	CR13/240
357	CR13/239
358	CR13/479
359	CR13/477
360	24 11
361	28 7
362	CR13/155

Figure	Negative
363	CR13/153
364	CR13/237
365	CR13/238
366	CR13/483
367	CR13/481
368	23 7
369	27 0A
370	CR12/498
371	CR12/496
372	CR12/546
373	CR12/544
374	23 12
375	25 6
376	CR12/530
377	CR12/528
378	CR13/261
379	CR13/259
380	24 3
381	25 11
382	CR12/510
383	CR12/508
384	CR13/257
385	CR13/255
386	23 20
387	28 11
388	28 20
389	CR13/212
390	CR13/211
391	CR13/210
392	CR13/209
393	CR13/333
394	CR13/331
395	CR13/400
396	CR13/399
397	CR13/426
398	CR13/424
399	CR13/459
400	CR13/461
401	26 17
402	28 17
403	28 19
404	CR13/216
405	CR13/215
406	CR13/214
407	CR13/213
408	CR13/345
409	CR13/343
410	CR13/407
411	CR13/405
412	CR13/434
413	CR13/432
414	CR13/464
415	CR13/463
415.1	CR14/132
415.2	CR14/131
415.3	CR14/130
415.4	CR14/129
415.5	CR14/133
415.6	CR14/178
415.7	CR14/177
415.8	CR14/176
415.9	CR14/175
415.10	CR14/179
415.11	CR14/122
415.12	CR14/121
415.13	CR14/120
415.14	CR14/119
415.15	CR14/123
415.16	CR14/190
415.17	CR14/189
415.18	CR14/192
415.19	CR14/187
415.20	CR14/191
415.21	CR14/76
415.22	CR14/75
415.23	CR14/74
415.24	CR14/73
415.25	CR14/77
415.26	CR14/145
415.27	CR14/144
415.28	CR14/143
415.29	CR14/142
415.30	CR14/146
415.31	32 6A
415.32	CR14/58
415.33	CR14/57
415.34	CR14/56
415.35	CR14/55
415.36	CR14/196
415.37	CR14/195
415.38	CR14/194
415.39	CR14/193
415.40	CR14/197
415.41	CR14/66
415.42	CR14/65
415.43	CR14/64
415.44	CR14/63
415.45	CR14/68
415.46	CR14/155
415.47	CR14/154
415.48	CR14/153
415.49	CR14/152
415.50	CR14/158
415.51	CR14/157
420	CR11/528
421	CR11/527
422	CR11/526
423	CR11/525

Figure	Negative
424	CR11/516
425	CR11/515
426	CR11/514
427	CR11/513
428	21 14
429	21 4
430	CR12/159
431	CR12/157
432	CR12/148
433	CR12/146
434	CR12/329-336
435	CR12/321-328
436	CR11/183
437	CR11/184
438	CR11/185
439	CR11/186
440	CR11/147
441	CR11/148
442	CR11/149
443	CR11/150
444	22 6
445	20 19
446	CR12/182
447	CR12/180
448	CR12/172
449	CR12/170
450	CR12/349-356
451	CR12/337-344
452	CR11/274
453	CR11/276
454	CR11/277
455	CR11/280
456	CR11/282
457	CR11/290
458	CR11/286
459	CR11/285
460	CR11/291
461	CR11/293
462	22 10
463	22 14
464	CR12/270
465	CR12/268
466	CR12/426
467	CR12/424
468	CR12/1
469	CR11/599
470	CR11/598
471	CR11/136
472	CR11/137
473	CR11/579
474	CR11/577
475	CR11/576
476	CR11/127
477	CR11/128

Figure	Negative
478	20 12
479	20 5
480	CR12/292
481	CR12/290
482	CR12/286
483	CR12/284
484-491	JEOL 100C ASID-4D (Polaroid)
492	CR12/381,383,385-388
493	CR12/360,362-366
494	CR11/216
495	CR11/215
496	CR11/213
497	CR11/218
498	CR11/219
499	CR11/197
500	CR11/198
501	CR11/200
502	CR11/206
503	CR11/207
504	CR12/314
505	CR12/313
506	CR12/311
507	CR12/304
508	CR12/303
509	CR12/301
520	CR15/146
521	CR15/145
522	CR15/144
523	CR15/143
524	CR14/22
525	CR14/21
526	CR14/20
527	CR14/19
528	CR14/30
529	CR14/29
530	CR14/28
531	CR14/27
532	CR14/34
533	CR14/33
534	CR14/32
535	CR14/31
536	CR13/593
537	CR13/592
538	CR13/591
539	CR13/590
540	CR14/1
541	CR13/600
542	CR13/599
543	CR13/598
544	CR14/2
545	CR13/597
546	CR13/596
547	CR13/595

Figure	Negative
548	CR13/594
549	CR14/10
550	CR14/9
551	CR14/8
552	CR14/7
553	CR15/133
554	CR15/97
555	CR15/95
556	CR14/257
557	CR14/261
558	CR14/264
559	CR14/262
560	CR14/258
561	CR14/265
562	CR14/270
563	CR14/259
564	CR14/271
565	CR14/274
566	CR14/276
567	CR14/240
568	CR14/236
569	CR14/237
570	CR14/238
571	CR14/260
572	CR14/277
573	CR14/280
574	CR14/282
575	36 15
576	36 5
577	36 12
578	36 7
579	CR13/576-583
580	CR13/566-573
581	CR13/557-564
582	CR13/546-553
583	CR15/301-308
584	CR14/332
585	CR14/308
586	CR14/333
587	CR14/323
588	CR14/427
589	CR14/390
590	CR14/383
591	CR14/311
592	CR14/308
593	CR14/310
594	CR14/309
595	CR14/329
596	CR14/326
597	CR14/323
598	CR14/325
599	CR14/330
600	CR14/324
601	CR14/327,328

Figure	Negative
602	CR14/394
603	CR14/393
604	CR14/395
605	CR14/390
606	CR14/392
607	CR14/391
608	CR14/396,397
609	CR14/428
610	CR14/405
611	CR15/1
612	CR14/567
613	CR14/429
614	CR14/426
615	CR14/409
616	CR14/408
617	CR14/405
618	CR14/407
619	CR14/406
620	CR14/571
621	CR14/570
622	CR14/567
623	CR14/569
624	CR14/568
625	CR14/419
626	CR14/414
627	CR14/413
628	CR14/412
629	CR14/411
630	34 19
631	34 20
632	CR14/579
633	CR14/578
634	CR14/577
635	CR14/576
636	CR14/575
637	34 21
638	36 1
639	CR14/584
640	CR15/10
641	CR15/9
642	CR15/8
643	CR15/7
644	34 23
645	34 24
646	CR14/589
647	CR14/588
648	CR14/587
649	CR14/586
650	CR14/585
651	34 10
652	34 11
653	CR14/595
654	CR14/594
655	CR14/593

Figure	Negative
656	CR14/592
657	CR14/591
658	34 18
659	34 17
660	CR15/6
661	CR15/5
662	CR15/4
663	CR15/3
664	CR15/2
665	34 12
666	34 13
667	CR14/600
668	CR14/599
669	CR14/598
670	CR14/597
671	CR14/596
673	30 3
674	30 1
675	CR15/132
676	CR15/131
677	CR15/128
678	CR15/127
679	CR15/126
680	CR15/125
681	30 7
682	30 5
683	CR15/116
684	CR15/115
685	CR15/112
686	CR15/111
687	CR15/110
688	CR15/109
689	30 11
690	30 19
691	CR15/124
692	CR15/123
693	CR15/120
694	CR15/119
695	CR15/118
696	CR15/117
697	30 8
698	CR15/108
699	CR15/107
700	CR15/106
701	CR15/105
702	30 14
703	CR15/137
704	CR15/136
705	CR15/142
706	CR15/141
707	CR15/140
708	CR15/139
709	36 22
710	CR15/50-55

Figure	Negative
711	CR15/210-217
712.1	CR16/56-59
712.2	CR16/93-96
712.3	CR16/146-149
712.4	CR16/219-222
712.5	CR16/269-272
712.6	CR16/331-334
712.7	CR16/372-376
712.8	CR16/412-415
712.9	CR16/500-503
712.10	CR16/539-542
713.1	CR16/41-49
713.2	CR16/84-92
713.3	CR16/137-145
713.4	CR16/210-218
713.5	CR16/259-268
713.6	CR16/321-330
713.7	CR16/361-371
713.8	CR16/401-411
713.9	CR16/488-499
713.10	CR16/529-538
714.1	CR15/337-345
714.2	CR16/75-83
714.3	CR16/184-193
714.4	CR16/240-249
714.5	CR16/289-301
714.6	CR16/351-360
714.7	CR16/392-400
714.8	CR16/432-441
714.9	CR16/520-528
714.10	CR16/559-567
715.1	CR15/325-336
715.2	CR16/63-74
715.3	CR16/168-183
715.4	CR16/223-239
715.5	CR16/273-288
715.6	CR16/335-350
715.7	CR16/376-391
715.8	CR16/416-431
715.9	CR16/504-519
715.10	CR16/543-558
716	CR16/580-585
717	CR16/586-593